LBL-20200 c.2

RECEIVED
LAWRENCE
BERKELEY LABORATORY
JUL 12 1988
LIBRARY AND
DOCUMENTS SECTION

Annual Report

FY 1985

Applied Science Division

September 1986

Lawrence Berkeley Laboratory
University of California

LBL-20200 c.2

Prepared for the U.S. Department of Energy under Contract DE-AC03-76SF00098

DISCLAIMER

This document was prepared as an account of work sponsored by the United States Government. While this document is believed to contain correct information, neither the United States Government nor any agency thereof, nor the Regents of the University of California, nor any of their employees, makes any warranty, express or implied, or assumes any legal responsibility for the accuracy, completeness, or usefulness of any information, apparatus, product, or process disclosed, or represents that its use would not infringe privately owned rights. Reference herein to any specific commercial product, process, or service by its trade name, trademark, manufacturer, or otherwise, does not necessarily constitute or imply its endorsement, recommendation, or favoring by the United States Government or any agency thereof, or the Regents of the University of California. The views and opinions of authors expressed herein do not necessarily state or reflect those of the United States Government or any agency thereof or the Regents of the University of California.

LBL-20200

APPLIED SCIENCE DIVISION ANNUAL REPORT FY 1985

Elton J. Cairns

Head, Applied Science Division
and
Associate Director, LBL

Applied Science Division
Lawrence Berkeley Laboratory
University of California
Berkeley, California 94720

Prepared for the U.S. Department of Energy under Contract No. DE-AC03-76SF00098

FOREWORD

The mission of the Applied Science Division is to perform research on the complex energy issues that confront our nation. The research base is broad and is organized into five major programs: Chemical Process Research and Development, Solar Energy, Energy Efficient Buildings, Environmental Research, and Energy Analysis. The goal of these programs is to make key contributions to the solution of the critical problem of providing environmentally acceptable energy options for the future. Although researchers in each program use special expertise to conduct their studies, they are increasingly joining forces with the staff of other programs in the Division to investigate particular aspects of related problems. For example, the Windows and Daylighting Group in the Energy Efficient Buildings Program and the Passive Analysis and Design Group in the Solar Energy Program are jointly studying the effects of natural lighting on energy consumption in buildings.

The Chemical Process R&D Program is investigating five major research areas: (1) energy-related organometallic chemistry, (2) coal-related processes, (3) fuels from biomass by biochemical processes, (4) electrochemical energy storage, and (5) advanced thermal energy storage. Each of these projects focuses on transport-process principles, chemical kinetics, thermodynamics, separation processes, and organic and physical chemistry.

The objective of the Solar Energy Program is to advance the development and application of solar energy as a supplement to traditional, nonrenewable enegy resources, thus decreasing the rate at which these resources are depleted. The Solar Program consists of a number of applied and basic research projects, including (1) active solar cooling of buildings, (2) passive solar heating, cooling, and lighting of buildings, (3) advanced aperture materials, (4) solar energy conservation using microstructured materials, and (5) the photochemical conversion of sunlight to chemical and electrical energy.

The efficient use of energy in buildings is the emphasis of the Energy Efficient Buildings Program, which comprises the following related research areas: (1) energy performance of buildings (2) building ventilation and indoor air quality, (3) windows and daylighting, (4) lighting systems research, (5) buildings energy data compilation and analysis, and (6) building energy simulation using the DOE-2 computer model.

The objective of the Environmental Research Program is to study the hazardous effects of energy generation and use. The program is divided into seven major research areas that encompass transport and transformation, impacts, characterization, and abatement. These major areas are (1) atmospheric aerosols, (2) applied physics and laser spectroscopy, (3) oil shale, (4) combustion, (5) scrubber chemistry, (6) toxicology studies of biological systems, and (7) trace element analysis.

The Energy Analysis Program assesses economic and public policies and their relevance to the critical issues affecting national and regional energy supply and demand. The program is organized into three major areas: (1) building energy analysis, (2) economic studies, and (3) international energy studies. Virtually all of the program's research and analysis is quantitative, and much of the research staff is engaged in developing and applying mathematical models.

The Applied Science Division has close ties with several departments at the University of California, Berkeley, in particular the Mechanical Engineering and Chemical Engineering departments and the multidisciplinary Energy and Resources Group.

LAWRENCE BERKELEY LABORATORY
UNIVERSITY OF CALIFORNIA
APPLIED SCIENCE DIVISION

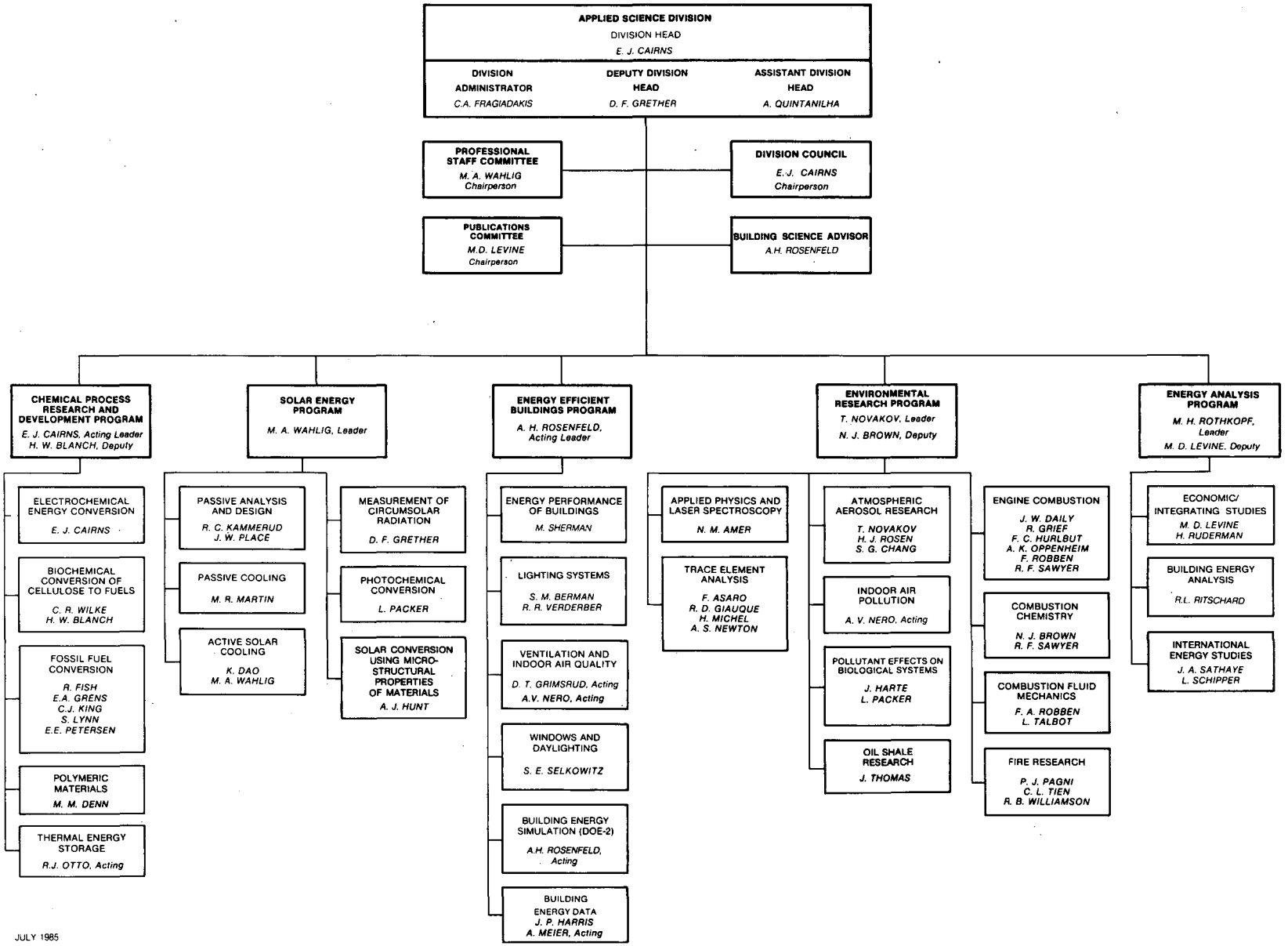

JULY 1985

APPLIED SCIENCE DIVISION

Elton J. Cairns

Division Head

Cheryl Fragiadakis

Division Administrator

Donald F. Grether

Deputy Division Head

Alex Quintanilha

Assistant Division Head

DIVISION OFFICE STAFF

Lily Cheng
Bruce Coolahan
Eric Essman
Helen Leung
Sandra Mocco
Maria Ossa
Rebecca Palmer
Susan Petersen
Janet Smith
Angela Smothers
Richard Wiebe
Zenaida Yuson

CHEMICAL PROCESS RESEARCH AND DEVELOPMENT PROGRAM STAFF

Elton Cairns, Program Leader
Harvey Blanch, Deputy Program Leader

Thomas Adler
Daniel Arenson
Jacki Ayer
Myra Baker
Vincent Battaglia
Wyn Bennett
Paul Berdahl
Douglas Bousfield
Garth Burns
Van Carey
Yew Khoy Chuah
Thomas Colson
Daniel Crean
Ayesha Daniels
Morton Denn
Minh Do
Jesse Dobson
Gregory Dow
Jean Dupon
Rachelle Edmond
Richard Fish
John Fitch
Gad Friedman*
Terry Grant
Edward Grens
Donald Hanson
Richard Hix
Arlon Hunt
Mark Isaacson
Alejandro Izquierdo
Rajiv Jain
Aviezer Kertes
Tae-Jeong Kim
C. Judson King
Kim Kinoshita
John Komlenic
Susan Lauer
Phillip Lessner
Scott Lynn
Giuseppe Marrucci
Frank McLarnon
Kenneth Miller
Riley Moore
Curtis Munson
Stewart Naftel
Joann Nakamura
Dan Neumann
Rollie Otto
Loree Pool
Mark Prausnitz
Robert Price
William Rixey
Ricardo San Martin
Michael Schuh
Aldo Sciamanna
Steve Sciamanna
John Senetar
Michael Smith
Craig Stevens
Kathy Striebel
Jon Sundquist
Janet Tamada
Raja Tannous
Rodney Thompson
Arne Thormodsen
Kent Udell†
Dale Wiley
Charles Wilke
Richard Williams
Jack Winnick*

*Participating guest.
†Earth Sciences Division.

SOLAR ENERGY PROGRAM STAFF

Michael A. Wahlig, Program Leader

Mari Adegran
Patrick Albrand
Hashem Akbari
Brandt Andersson
Rollin Armer*
Jacqueline Ayer
Fred Bauman
Shimshon Belkin
Paul Berdahl
Peter Brothers
Rodney Browning
William Carroll
J. Pascal Coutier
Kim Dao*
Bernard Fleury
Ian Fry
Karen Ghaffari
Donald Grether
Jeffrey Herz
Eva Hrabeta
Margaret Huflejt
Patricia Hull
Arlon Hunt
Marion Jenkins
Ronald Kammerud
Carl Lampert†
Jonathan Lieber
Kevin Lofftus
Marlo Martin
Ralph McLaughlin
Rolf Mehlhorn
Atila Mertol
Fletcher Miller
Joannis Mohrman
Jon Noring
Roland Otto
Lester Packer
Gunter Peschek
J. Wayne Place
Cindy Polansky
John Randolph
Joseph Rasson*
Arthur Robinson
Michael Rubin
Richard Russo
Fenwick Salter
Stephen Selkowitz
Louie Shaffer
Arthur Shavit
Deborah deSilveira
Susan Spath
Charlotte Standish
Haider Taha
Elisha Tel-Or
Param Tewari
Tsu-Chin Tsao
Mashuri Warren
Thomas Webster
Kevin Whitley
Walter Yuen
Sheng Hua Zhu

*Engineering Division.
†Materials and Molecular Research Division.

ENERGY EFFICIENT BUILDINGS PROGRAM STAFF

Arthur Rosenfeld, Program Leader

ADMINISTRATION

Debbie Giallombardo
Mary Hart
Theresa Lessard
Lynne Sherman
Nancy Wishner

ENERGY PERFORMANCE OF BUILDINGS

Jorn Brunsell*
Peter Cleary
Richard Diamond
Darryl Dickerhoff
Bruce Dickinson
Helmut Feustel
Dariush Hekmat
Rudiger Kulpman*
Leszek Lewicki
Mark Modera
Max Sherman†
Brian Smith
Carol Stoker
Cynthia Sverrisson
Richard Szydlowski

BUILDING VENTILATION AND INDOOR AIR QUALITY

Richard Allen
Michael Apte
Jehuda Binenboym
John Brown
Steve Brown
Andrew Carruthers
Lloyd Davis
Suzanne Doyle
William Fisk
Dennis Froehlich
John Girman
David Grimsrud†
Jed Harrison
Alfred Hodgson
Laura Horn
Falah Abu-Jarad*
Hossein Kaboli
Karl Koshlap
Joyce McCann
Gayle Milligan
Barbara Moed
Nancy Morrison
William Nazaroff
Anthony Nero†
Francis Offermann
Brian Pedersen
Richard Prill
Kenneth Revzan
Alan Robb
Ellen Saegebarth
Sandra Sampson
Mary Beth Schwehr
Richard Sextro
Harvey Sokol
Greg Traynor
Bradley Turk
Stephen Uno
Rodger Young

WINDOWS AND DAYLIGHTING

Dariush Arasteh
Erica Atkin
Deborah Connell
Craig Conner
Dennis DiBartolomeo
Patrice Dinhut
Martyn Dodd
Jean Ferrari
Edward Gleason
Mary Lou Hinman
Arlon Hunt
Richard Johnson
Harry Keller
Guy Kelly
Jeff Kessel
Jong Jin Kim
Joseph Klems
Carl Lampert
Jonathan Lieber
Kevin Lofftus
Moya Melody
Lino Monge
Mojtaba Navvab
Eliyahu Ne'eman
Shirley Nozaki
Thomas Omstead
Konstantinos Papamichael
Amy Rakley
Mike Rubin
Stephen Selkowitz†
Mark Spitzglas
Robert Sullivan
Glenn Sweitzer
Kimberlee Taylor
Param Tewari
John Thornton
Ning Wen
Michael Wilde
Ruth Williams
Mehrangiz Yazdanian
Phillip Yu

*Participating guest, †Group Leader.

LIGHTING SYSTEMS RESEARCH

Erica Atkin
Sam Berman†
Robert Clear
Charles Dumm‡
Jean Ferrari
Ellen Gailing
Chuck Green‡
Donald Hollister
Donald Levy
Fuzi Li*
Moya Melody
Oliver Morse‡
Francis Rubinstein
Michael Siminovitch
Kimberlee Taylor
Rudy Verderber
Gregory Ward
Ruth Williams
Tai-Ming Zhou*

BUILDINGS ENERGY DATA

Hashem Akbari
John Busch
Deborah Connell
Craig Conner
Olivier de la Moriniere*
Joseph Eto
Denise Flora
Betsy Gardiner
Charles Goldman
Kathy Greely
Steven Greenberg
Jeff Harris†
John Hartman
Patrick LeConiac*
Margaret Meal
Alan Meier
Alan Mitchell
Mary Ann Piette
Rosemary Riley
Arthur Rosenfeld
Jeana Traynor
Tony Usibelli
Leonard Wall*

BUILDING ENERGY SIMULATION

Bruce Birdsall
Fred Buhl
Joe Clarke*
Deborah Connell
Kathy Ellington
Ender Erdem
James Hirsch
Deborah Hopkins
Lan-Chieh Huang*
Karen Olson
Edward Sowell*
Frederick Winkelmann

*Participating guest, †Group Leader, ‡Engineering & Technical Services Division.

ENVIRONMENTAL RESEARCH PROGRAM STAFF

Tihomir Novakov, Program Leader
Nancy Brown, Deputy Program Leader

ATMOSPHERIC AEROSOL RESEARCH

William Benner
Mirke Bizjak*
Ray Dod
Lara Gundel
Anthony Hansen
Vida Hudnik*
Samuel Markowitz
Fred Mowrer
Tihomir Novakov†
Roland Otto
Cass Parker
Carolyn Pryor
Hal Rosen
Richard Schmidt
Wenzhi Song*
Wei-Han Su*
Linda Wroth
Quipeng Zhang*

APPLIED PHYSICS AND LASER SPECTROSCOPY RESEARCH

Nabil Amer†
Helmut Dersch
Robert Gerlach
William Imler
Marjorie Olmstead
Andrew Skumanich

OIL SHALE RESEARCH

Ernest Blatchley
Christian Daughton‡
Gloria Harris
Joseph Healy, Jr.
Leon Hunter
Bonnie Jones
Gregg Langlois
Frank Mandola
Carl Martin
Peter Persoff
Rick Sakaji
Robert Selleck‡
Jerome Thomas†

COMBUSTION RESEARCH

James Ang
Diana Brehob
Mark Brosmer
Nancy Brown†
John Cavolowsky
Robert Cheng
Peck Cho§
Derek Dunn-Rankin
Christopher Edwards
Janet Ellzey
Michael Forsha
Iskander Gokalp*
Ralph Greif
Jean Hertzberg
Kenneth Hom
Wei-Ming Huang
Gary Hubbard
Frank Hurlbut
Eileen Javar
Chung Lau§
Kwi Lee
Russell Lewis
Trudy Lionel
Donald Lucas
Richard Martin
Mehdi Namazian‡
Clement Okoh
Antoni Oppenheim
Patrick Pagni
Terry Parker
Richard Peterson
Maciej Pindera
Ahmed Rashed
Ola Rashed
Frank Robben
Robert Sawyer
Ian Shepherd‡
Pauline Sherman*
Horton Stewart‡
Lawrence Talbot
R. Brady Williamson

SCRUBBER CHEMISTRY RESEARCH

Kevin Brodbeck‡
Shih-Ger Chang†
Elizabeth Griffiths
Ke-Yuan Hu*
David Littlejohn
David Liu
Minduan Tu*
Abbey Wizansky
Steven Wolfgang

*Participating guest, †Group Leader, ‡University of California Berkeley, §University of California Davis.

TOXICOLOGY STUDIES OF BIOLOGICAL SYSTEMS

Charles Blanchard
Ian Fry
John Harte
Johanna Lang
John Maguire
Rolf Mehlhorn
Harvey Michaels
Lester Packer
Richard Schneider

TRACE ELEMENT ANALYSIS

Frank Asaro
Robert Giauque
Helen Michel
Amos Newton
Linda Sindelar
Fred Stross*
Rafael Zamora

ADMINISTRATIVE SUPPORT

Rachelle Edmond
Gloria Gill

*Participating guest.

ENERGY ANALYSIS PROGRAM STAFF

Michael Rothkopf, Program Leader
Mark Levine, Deputy Program Leader

Patrick Albrand
Sarita Bartlett
Betty Bratton
Jim Bull
Stephen Byrne
Quinsan Cao
Peter Chan
Fu Rong Chang
Alan Comnes
Paul Craig*
Rick Diamond
Joe Eto
David Foley
Andre Ghirardi
Peter Goering
Steve Gold
Charles Goldman
Kathy Greely
Jordi Gual
Mel Guerrero
James Harrigan
Diane Hawk
John Henly
Chean Yok Hsui
Joe Huang
Adam Kahane†
Edward Kahn
Andrea Ketoff
Jonathan Koomey
Stanislaus Lwakabamba‡
James McMahon
Stephen Meyers
Evan Mills
Oystein Olsen‡
Samuel Oren
Christopher Pignone
Imelda Reyes
Ronald Ritschard
Giancarlo Rizzo‡
Henry Ruderman
Jayant Sathaye
Lee Schipper
Nancy Schorn
Renee Slonek
Robert Sullivan
Thomas Teisberg
Isaac Turiel
Dorothy Turner
Edward Vine
Debbie Wilson
David Wood
Winifred Yen-Wood

*University of California Davis, †Affiliated staff, ‡Participating guest.

CONTENTS

CHEMICAL PROCESS RESEARCH AND DEVELOPMENT PROGRAM

Introduction 1-1

ENERGY-RELATED ORGANOMETALLIC CHEMISTRY

Synthesis of Dimetalla-azacyclobutenes via Reaction of Polynuclear Heteroaromatic Nitrogen Compounds with Triruthenium Dodecacarbonyl: Reactivity and Structural Elucidation
Richard H. Fish, Tae-Jeong Kim, Joanne L. Stewart, John H. Bushweller, Robert K. Rosen, and Jean Wisner Dupon 1-2

Hydrodenitrogenation Chemistry: Cleavage of Alkylcarbon-Nitrogen Bonds, Ammonia and Methane Formation in the HDN Reaction of 1,2,3,4-Tetrahydroquinoline with a Nickel Oxide Catalyst Supported on Silica
R.H. Fish, A.D. Thormodsen, R.S. Moore, D.L. Perry, J. Michaels, and H. Heinemann 1-6

Polymer Pendant Ligand Chemistry 2: Reactions of Vanadyl and Nickel Acetylacetonates with Catechol Ligands Bonded to Polystyrene-Divinylbenzene Resins
R.H. Fish, A. Izquierdo, Gad Friedman, and Robert Price 1-12

Carbon Oxygen Bond Cleavage Reactions of Model Coal Compounds Using Inorganic Electron Transfer Reagents
R.H. Fish and J.W. Dupon 1-14

COAL-RELATED RESEARCH

Processing of Condensate Waters from Coal Gasification
C.J. King, J.J. Senetar, T.M. Grant, L.J. Poole, and R.E. Thompson .. 1-15

Separations of Polar Organics from Aqueous Solutions by Processes Based upon Reversible Chemical Complexation
C.J. King, A.S. Kertes, D. Arenson, and J. Tamada 1-18

Jet Breakup Enhanced by an Initial Pulse
D.W. Bousfield and M.M. Denn 1-21

Removal of H_2S from Coal-Derived Synthesis Gas
R. Hix, S. Lynn, D. Neumann, S. Sciamanna, and C. Stevens 1-25

FUELS FROM BIOMASS BY BIOCHEMICAL PROCESSES

Production of Sugars from Cellulose: the Kinetics of Endoglucanase in Cellulose Hydrolysis
B. Eluzfon, D. Wiley, H. Blanch, C. Wilke, and A. Sciamanna 1-30

Production of Sugars from Cellulose: Cellulase Production by *T. Reesei* in Continuous Culture in Lactose Medium
F. Castillo, H. Blanch, and C. Wilke 1-35

ELECTROCHEMICAL ENERGY STORAGE RESEARCH

Technology Base Research Project for Electrochemical Energy Storage
E.J. Cairns, K. Kinoshita, and F.R. McLarnon 1-40

Battery Electrode Studies
E.J. Cairns, F.R. McLarnon, T.C. Adler, M.J. Isaacson, R. Jain, P.M. Lessner, K.G. Miller, S.A. Naftel, M.L. Smith, K.A. Striebel, and J. Winnick 1-43

ADVANCED THERMAL ENERGY STORAGE RESEARCH

Solid-State Radiative Heat Pump
P. Berdahl, K. Ghaffari, G. Ng, and L. Shaffer 1-50

Thermochemical Energy Conversion and Storage by Direct Solar Heating
A.J. Hunt, J. Ayer, and R. Otto 1-52

Constant-Volume Three-Phase Thermal Storage Module
V.P. Carey 1-56

SOLAR ENERGY PROGRAM

Introduction 2-1

Passive Research and Development
R.C. Kammerud, J.W. Place, M.R. Martin, M. Adegran, H. Akbari, P. Albrand, B. Andersson, F.S. Bauman, C. Benard, P.H. Berdahl, W.L. Carroll, J.P. Coutier, B. Fleury, P. LeConiac, A. Mertol, J.T. Thornton, T. Webster, K. Whitley, and Z. Yilmaz 2-3

Optical Materials Studies
S. Selkowitz, A.J. Hunt, C. Lampert, J.G. Lieber, K.D. Lofftus, M. Rubin, and P. Tewari 2-12

Active Solar Cooling
M. Wahlig, J. Rasson, M. Warren, K. Dao, R. Armer, P. Brothers, and P.L. Chen 2-19

Biological Oxidations and Bioenergetic Studies on the Photochemical Conversion of Solar Energy
L. Packer, R.J. Mehlhorn, I.V. Fry, A.E. Robinson, S. Belkin, E. Hrabeta, M. Huflejt, S. Spath, E. Tel-Or, and G.A. Peschek 2-26

LBL Building 71 Solar Cooling Project
F. Salter 2-31

Solar Energy Conversion Using Microstructured Materials: Direct Radiant Heating of Small Particle Suspensions
A.J. Hunt, J. Ayer, P. Hull, R. McLaughlin, F. Miller, J.E. Noring, R. Russo, and W. Yuen 2-33

High Temperature Ceramics Development Using the Sol-Gel Process
A. Hunt, J. Lieber, K. Lofftus, and P. Tewari 2-37

ENERGY EFFICIENT BUILDINGS PROGRAM

Introduction 3-1

Energy Performance of Buildings
M.H. Sherman, J.T. Brunsell, P.G. Cleary, R.C. Diamond, D.J. Dickerhoff, J.B. Dickinson, H.E. Feustel, D. Hekmat, R.B. Kuelpmann, L.L. Lewicki, M.P. Modera, B.V. Smith, and R.F. Szydlowski 3-8

Building Ventilation and Indoor Air Quality
D.T. Grimsrud, A.V. Nero, Jr., F. Abu-Jarad, R. Allen, M. Apte, J. Brown, S.R. Brown, J. Binenboym, W.J. Fisk, D. Froehlich, J.R. Girman, J. Harrison, A.T. Hodgson, K. Koshlap, J. McCann, B.A. Moed, R. Mowris, W.W. Nazaroff, T. Nuzum, B.S. Pedersen, R. Prill, K.L. Revzan, A. Robb, E. Saegebarth, G. Schiller, M. Schwehr, R.G. Sextro, H. Sokol, G.W. Traynor, B.H. Turk, S. Uno, and R. Young 3-18

Windows and Daylighting
S.E. Selkowitz, D. Arasteh, C. Conner, D.L. DiBartolomeo, A.J. Hunt, R.L. Johnson, H. Keller, J.D. Kessel, J.H. Klems, C.M. Lampert, J.G. Lieber, K.D. Lofftus, M. Navvab, E. Ne'eman, S. Nozaki, M.D. Rubin, M. Spitzglas, R. Sullivan, P. Tewari, N. Wen, and G.M. Wilde 3-49

Lighting Systems Research
S.M. Berman, R.R. Verderber, R.D. Clear, D.D. Hollister, F. Li, D.J. Levy, O.C. Morse, F.M. Rubinstein, M.J. Siminovitch, G.J. Ward, and T.M. Zhou 3-74

Buildings Energy Data
J. Harris, A. Meier, H. Akbari, J. Busch, P. le Coniac, C. Conner, D. Connell, J. Eto, D. Flora, B. Gardiner, C. Goldman, K. Greely, S. Greenberg, M. Meal, E. Mills, A. Mitchell, O. de la Moriniere, M. Piette, R. Riley, A.H. Rosenfeld, D. Stein, A. Usibelli, and L. Wall 3-82

Building Energy Simulation
J.J. Hirsch, B.E. Birdsall, W.F. Buhl, D.J. Connell, A.E. Erdem, D.J. Hopkins, K.H. Olson, and F.C. Winkelmann 3-92

Publications List 3-105

ENVIRONMENTAL RESEARCH PROGRAM

Introduction 4-1

ATMOSPHERIC AEROSOL RESEARCH

Estimates of Springtime Soot and Sulfur Fluxes Into the Arctic Troposphere: Implications to Source Regions
H. Rosen and A.D.A. Hansen 4-3

Horizontal Inhomogeneities in the Particulate Carbon Component of the Arctic Haze
A.D.A. Hansen and H. Rosen 4-6

Primary Oxidants—Results from Laboratory and Field Experiments
W.H. Benner and T. Novakov 4-10

Empirical Evidence for Heterogeneous SO_2 Oxidation in Ljubljana, Yugoslavia
M. Bizjak, V. Hudnik, A.D.A. Hansen, and T. Novakov 4-13

Kinetics of Soot-Cayalyzed SO_2 Oxidation in Aqueous Systems
L.A. Gundel, W.H. Benner, and T. Novakov 4-16

Sulfate and Carbonaceous Aerosols in Beijing, China
R.L. Dod, R.D. Giauque, T. Novakov, W.H. Su, Q.P. Zhang, and W.Z. Song 4-20

Size Fractionation of Black and Organic Particulate Carbon from Fires
R.L. Dod, F. Mowrer, L.A. Gundel, R.B. Williamson, and T. Novakov 4-22

APPLIED PHYSICS AND LASER SPECTROSCOPY RESEARCH

N.M. Amer, S.-H. Chen, H. Dersch, A. Frova, R.W. Gerlach, W. Imler, M. Olstead, A. Skumanich, D. Wei, and Z. Yasa

Laser Photothermal Measurements and Characterization 4-26

Surfaces and Interfaces 4-34

Amorphous Photovoltaic Semiconductors 4-37

Liquid Crystal Research 4-41

OIL SHALE RESEARCH

Treatment of an Oil Shale Retort Water by Stationary Fixed Biofilm
J.B. Healy, Jr., G.W. Langlois, R.H. Sakaji, J.F. Thomas, and C.G. Daughton 4-43

Effect of Oil Shale Retort Water on Biooxidation of Aromatic Amines
J.B. Healy, Jr., G.W. Langlois, J.F. Thomas, and C.G. Daughton 4-47

Sunlight Reactions of Volatile Organonitrogen Emissions from Oil Shale Wastewaters
E.R. Blatchley III, J.F. Thomas, and C.G. Daughton 4-52

Diffusivity of Nitrogen Heterocycles in Simulated Codisposed Oil Shale Wastes
P. Persoff, J.F. Thomas, and C.G. Daughton 4-55

COMBUSTION RESEARCH

Flame Structure in Reacting Turbulent Boundary Layers
R.K. Cheng, F. Robben, and L. Talbot 4-62

Intermittency and Conditional Velocity Statistics in Premixed Conical Turbulent Flames
R.K. Cheng, I.G. Shepherd, F. Robben, and L. Talbot 4-64

Spectral Behavior of Velocity Fluctuations in Premixed Turbulent Flames
I. Gokalp, I.G. Shepherd, and R.K. Cheng 4-67

Structure and Propagation of Turbulent Premixed Flames Stabilized in a Stagnation Flow
P. Cho, C.K. Law, J.R. Hertzberg, and R.K. Cheng 4-69

Premixed Flame Stabilization on a Bluff Body
J.R. Hertzberg and L. Talbot 4-71

Fluid Dynamic Considerations in the Numerical Modeling of Flames
M.Z. Pindera and L. Talbot 4-73

Linear Array for Rayleigh Scattering (LARS)
I.G. Sheperd, G.L. Hubbard, W. Walker, III, F. Robben, and L. Talbot 4-75

Theoretical Combustion Kinetics and Ignition Chemistry
Nancy J. Brown, Ola Rashed, and Donald Lucas 4-77

The Interaction of a Laminar Flame with its Self-Generated Flow During Constant Volume Combustion
D. Dunn-Rankin and R.F. Sawyer 4-81

Compression Ignition of Coal Slurry Fuels
D.D. Brehob and R.F. Sawyer 4-84

Controlled Combustion
N.J. Brown, J.A. Cavolowsky, C.F. Edwards, K. Hom, D. Lucas, A.K. Oppenheim, T.E. Parker, D.A. Rotman, R.F. Sawyer, and H.E. Stewart 4-88

SCRUBBER CHEMISTRY RESEARCH

Reaction of Nitric Oxide with Ferrous Cysteine in Aqueous Solutions
M.D. Tu and S.G. Chang 4-92

Kinetics and Thermodynamics of the Reaction Between Cystine and Hydrogen Sulfide Ion
D.K. Liu and S.G. Chang 4-95

Kinetics of the Reaction of Nitric Oxide with Sulfite and Bisulfite Ions in Aqueous Solution
D. Littlejohn, K.Y. Hu, and S.G. Chang 4-98

The Kinetics of Acid Hydrolysis of Nitridotrisulfate Ion
David Littlejohn, Abigail R. Wizansky, and S.G. Chang 4-101

Determination of Nitrogen-Sulfur Compounds by Ion Chromatography
D. Littlejohn and S.G. Chang 4-103

Investigation of the Reaction of Oxygen with Bisulfite Ion in Aqueous Solutions Using a High-Pressure Stopped-Flow Technique
D. Littlejohn, K.Y. Hu, and S.G. Chang 4-106

TOXICOLOGY STUDIES OF BIOLOGICAL SYSTEMS

Assymetry of the Inner Mitochondrial Membrane
R. Mehlhorn, J. Maguire, J. Lang, and L. Packer 4-109

TRACE ELEMENT ANALYSIS

Impacts of Large Extraterrestrial Bodies and Mass Extinctions
F. Asaro, Helen V. Michel, W. Alvarez, and L.W. Alvarez 4-114

Studies of Source of Lithic Artifacts and Trade Routes by Elemental Analysis
F.H. Stross, F. Asaro, and H.V. Michel 4-115

ENERGY ANALYSIS PROGRAM

Introduction 5-1

BUILDING ENERGY ANALYSIS

Simplified Calculations of Energy Use in Residences
R. Ritschard, Y. Huang, and J. Bull 5-2

Survey of Low-Rise Multi-Family Building Practices
P. Albrand, I. Turiel, R. Ritschard, and D. Wilson 5-6

Energy and Economic Analysis of Conservation Measures for Low Rise Multi-Family Housing
I. Turiel, P. Albrand, and R. Ritschard 5-10

Potential for Wind Induced Ventilation in Residences
S.J. Byrne, R.L. Ritschard, and D.M. Foley 5-13

Residential Prototype Loads Comparisons
R. Sullivan, Y.J. Huang, R. Ritschard, I. Turiel, and J. Bull 5-18

Federally-Assisted Housing: Plans and Preliminary Analysis
R. Ritschard, C. Goldman, E. Vine, R. Diamond, E. Mills, and K. Greely 5-23

Measured Energy Savings from Conservation Retrofits in Public Housing Projects
C. Goldman, K. Greely, and R. Ritschard 5-25

Impact of HUD Subsidy Policy on Retrofit Savings for Public Housing Authorities
E. Mills and R. Ritschard 5-28

Analysis of Occupant Behavior and Energy and Hot Water Consumption in Public Housing
E. Vine and R. Diamond 5-30

Home Energy Rating Tool: Follow-On Analysis
R. Ritschard, C. Hsui, and Y.J. Huang 5-34

Performance of Daylighting Systems in Commercial Buildings in Hot Climates: Singapore Case Study
M. Levine and I. Turiel 5-37

Estimation of Energy Intensity by End Use for Commercial Buildings Using Conditional Demand Analysis
I. Turiel, P. Craig, M. Levine, J. McMahon, G. McCollister, and B. Hesterberg 5-41

ECONOMIC STUDIES

The LBL Residential Energy Demand Forecasting Model
J.E. McMahon and P. Chan 5-44

Economic Impacts of Residential Conservation Programs on Electric Utilities
E. Kahn, C. Pignone, J. Eto, J. McMahon, and M.D. Levine 5-48

Regional Analysis of the Economic and Institutional Environment for New and Enhanced Utility Programs
W. Yen-Wood, E. Kahn, and M. Levine 5-51

Energy Efficiency Choice in the Purchase of Residential Appliances
H. Ruderman, M.D. Levine, and J.E. McMahon 5-60

An Investigation of the Reasons for the Rapid Market Penetration of Electric Heat Pumps in the Residential Sector
Mark D. Levine 5-63

Validation of the LBL Residential Hourly Demand Model
H. Ruderman, G. Verzhbinsky, and M.D. Levine 5-67

Market Share Elasticities of Home Heating and Cooling Systems
David Wood, Henry Ruderman, and James E. McMahon 5-71

Utility Load Shape Impacts of Residential Energy Conservation Measures
H. Ruderman, P. Chan, and M.D. Levine 5-75

Impacts of Proposed Changes in the Federal Tax Code on Renewable Energy and Cogeneration Projects
E. Kahn and C. Goldman 5-80

A Decade of U.S. Energy Policy
M. Levine and P. Craig 5-83

Analysis of Federal Energy Efficiency Standards for Appliances
M.D. Levine, P. Chan, J.E. McMahon, and H. Ruderman 5-89

Modeling the Demand for Household Appliances and Energy
H. Ruderman 5-93

Planning for Oil Overcharge Funds: The California Experience
E. Vine, J. Sathaye, and A. Rosenfeld 5-97

Policy Analysis of Natural Resource Sale Mechanisms
M. Rothkopf, D. Wood, and C. Bart McGuire 5-102

A Natural Gas Policy Model
T.J. Teisberg, B.A. Miller, and M.H. Rothkopf 5-107

INTERNATIONAL ENERGY STUDIES

Residential Energy Use in Industrialized Countries
Lee Schipper, Andrea Ketoff, Stephen Meyers, Peter Goering, and Dianne Hawk 5-109

Energy Use in the Service Sector: An International Perspective
Lee Schipper, Steven Meyers, and Andrea N. Ketoff 5-113

Energy Consumption and Structure of the U.S. Residential Sector
S. Meyers 5-116

Residential Demand for Natural Gas: A Dynamic, Discrete-Continuous Choice Approach
Oystein Olsen and Sarita Bartlett 5-119

Changes in the Patterns of Oil Use in Latin America
Andre Ghirardi, Peter Goering, and Andrea Ketoff 5-120

Outlook for Oil and Energy Demand in Asia
Jayant A. Sathaye and Melchor Guererro 5-124

Changing Energy Use Patterns in Mexico
Andrea N. Ketoff, Andre Ghirardi, and Peter Goering 5-127

Residential Energy Use in LDCs: Guidelines for the Analysis of Low-Income African Countries
Gianfranco Rizzo, Andrea Ketoff, and Andre Ghirardi 5-131

Transport Energy Use in Cities of the Less Developed Countries
Jayant Sathaye and Stephen Meyers 5-134

Energy Conservation Measures and Policies for Commercial Buildings for the Association of Southeast Asian Nations (ASEAN)
M. Levine and I. Turiel 5-137

CHEMICAL PROCESS RESEARCH AND DEVELOPMENT PROGRAM

INTRODUCTION

The Chemical Process Research and Development Program has five main projects applying chemistry and chemical engineering to problems in the production of new fuels, their environmental impact, and energy storage. These projects are:

(1) Energy-related organometallic chemistry
(2) Processing of effluent gases and liquids resulting from synthetic-fuel production, to provide acceptable waste or recycle streams
(3) Production of liquid fuels from biomass
(4) Electrochemical energy storage
(5) Thermal energy storage

Each of these projects focuses on transport-process principles, chemical kinetics, thermodynamics, separation processes, and organic and physical chemistry.

The first project involves studies on the use of heterogeneous metal cataysts to remove nitrogen from model coal compounds and to synthesize organometallic compounds that are models for metal mediated carbon-nitrogen bond cleavage reactions. Another aspect involves the use of alkali metals and crown ethers to study the cleavage reactions of compounds such as ethers and esters that have carbon-oxygen bonds and that model the linkages in coal. In addition, the isolation and molecular characterization of trace metal compounds in fossil materials is being studied, and innovative methods of removing these trace metal compounds are being developed. This includes the use of polymer-pendant catechol ligands to remove characterized arsenic, vanadium, and nickel compounds from solution and eventually from complex matrices.

The second project involves the development of novel and improved methods for processing synfuel condensate waters to make them suitable for recycle, thereby minimizing process-water requirements. The main emphasis is on physiochemical methods, particularly solvent extraction and stripping, to remove organics. Identification of the contaminating organics is difficult, but necessary to permit development of appropriate solvents for their removal. LBL studies have successfully examined simultaneous solvent extraction in removal of ammonia and acid gases by stripping.

The conversion of biomass to liquid fuels has been an area of considerable research and development within the Chemical Process Program over the past several years. The biological conversion of wood and agricultural residues to ethanol has been examined. An enzymatic hydrolysis of these cellulosic materials has been developed to yield monomeric hexose and pentose sugars. These can be subsequently fermented to produce ethanol. Various high-rate fermentation processes have been developed, and novel processes for ethanol recovery that are less energy intensive than conventional processes are being studied.

The electrochemical energy storage program provides research to develop advanced battery systems for electric vehicle and stationary energy storage applications. Topics include identification of new electrochemical couples for advanced batteries, improvements in battery components and materials, establishment of engineering principles applicable to electrochemical energy storage and conversion, and the development of metal/air cells and fuel cells for transportation. Major emphasis is on applied research that will lead to superior performance and lower life-cycle costs.

The fifth project is a series of research and development efforts in thermal energy storage. This project focuses on new and innovative approaches that have a broad range of applications and on the utilization of solar energy.

Synthesis of Dimetalla-azacyclobutenes via Reaction of Polynuclear Heteroaromatic Nitrogen Compounds with Triruthenium Dodecacarbonyl: Reactivity and Structural Elucidation*

Richard H. Fish, Tae-Jeong Kim, Joanne L. Stewart, John H. Bushweller, Robert K. Rosen, and Jean Wisner Dupon

We, as well as others, have found that a wide variety of transition metal compounds[1a–g] catalyze the homogeneous, regiospecific hydrogenation of polynuclear heteroaromatic nitrogen and sulfur compounds. The mechanism of hydrogenation of the nitrogen heterocyclic ring encompasses a prior coordination of the nitrogen compound to the catalytic metal center using either rhodium or ruthenium complexes.[1b,d] These rhodium and ruthenium complexes were either mono or tetranuclear, and thus it would be of interest to more clearly define the coordination of the polynuclear heteroaromatic nitrogen compounds to catalyst metal centers. We chose to study a ruthenium cluster, $Ru_3(CO)_{12}$, where several ruthenium metal centers were available for bonding to the nitrogen ring. Recently, several groups have reported on the reactions of polynuclear heteroaromatic nitrogen compounds with metal clusters. These include the studies of Yin and Deeming[2] with the triosmium cluster, $Os_3(CO)_{12}$, and polynuclear heteroaromatic compounds such as pyridines and quinolines. The resultant substituted clusters have been characterized spectroscopically as a triangle of osmium atoms with the nitrogen and the 2-carbon atoms. More recently, Laine *et al.*[3] substantiated the structure of both mono- and disubstituted quinoline-triosmium clusters by x-ray analysis and extended the examples to saturated nitrogen heterocyclic compounds such as piperidines and 1,2,3,4-tetrahydroquinoline. An excellent review of cyclometallated complexes with heterocyclic ligands, covering many other examples, was recently published by Constable.[4]

While our present study on the triruthenium cluster, $Ru_3(CO)_{12}$, reactions with quinoline, 1,2,3,4-tetrahydroquinoline, phenanthridine, and 9,10-dihydrophenanthridine was under way, Laine *et al.*[3] and Lewis *et al.*[5] both reported the quinoline-triruthenium complex. Our present results extend the knowledge in the synthesis and reactivity of dimetalla-azacyclobutene compounds of ruthenium with the above-mentioned nitrogen ligands. In addition, we also report the x-ray crystal structure of the phenanthridine-triruthenium derivative, $Ru_3(\mu\text{-}H)(\mu\text{-}C_{13}H_8N)(CO)_{10}$, **5**, as well as the reactions of the quinoline and phenanthridine-triruthenium complexes, **1**, **5**, with hydrogen gas, hydride reagents, and trifluoroacetic acid.

ACCOMPLISHMENTS DURING FY 1985

The Reaction of Quinoline with Triruthenium Dodecacarbonyl ($Ru_3(CO)_{12}$)

The reaction of triruthenium dodecacarbonyl ($Ru_3(CO)_{12}$) with excess quinoline only provided the mono-substituted four membered ring dimetalla-azacyclobutene complex, **1**, (Eq. 1).

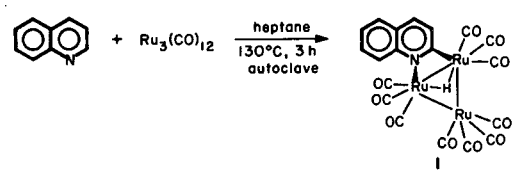

(1)

The reaction was performed in a sealed autoclave, in order to prevent decomposition from loss of CO, in heptane solvent at 130°C for 2–3 hours under argon. This result is in contrast to the recently reported result of Laine *et al.*[3] where they obtain the mono and bis quinoline-ruthenium complex in a 1:2 ratio under similar conditions, but using methylcyclohexane as the solvent. The orange to red complex has been formulated from its ^1H, ^{13}C, and IR spectra as well as by elemental and mass spectral analysis and was consistent with the reported parameters.[3] The 200 MHz ^1H NMR spectrum of **1** showed the

*This work was supported by the Assistant Secretary for Fossil Energy, Office of Technical Coordination of the U.S. Department of Energy through the Pittsburgh Energy Technology Center under Contract No. DE-AC03-76SF00098.

absence of the 2-carbon proton, which appears as a doublet of doublets in the spectrum of free quinoline at 8.81 ppm. The proton of the 8-carbon atom remains evident in the spectrum of the quinoline derivative. As expected, all of the signals due to the remaining aromatic protons shift upfield upon coordination to the triruthenium cluster. The bridging hydride signal of the quinoline complex, a singlet, occurs at −14.01 ppm. This value is normal for hydrides bridging one face of a triruthenium cluster, e.g., $Ru_3(\mu\text{-}H)(\mu\text{-}0{=}C(Me))(CO)_{10}$ at −13.88 ppm and $NEt_4Ru_3(\mu\text{-}H)(\mu\text{-}CO)(CO)_{10}$ at −12.76 ppm.

The Reaction of Complex 1 with Hydrogen Gas

In order to determine the utility of the dimetalla-azacyclobutenes as potential model intermediates in catalytic hydrogenation reactions, we studied complex **1** with hydrogen gas (500 psi at 85°C in toluene) and found that quinoline was formed along with $H_4Ru_4(CO)_{12}$ (Eq. 2).

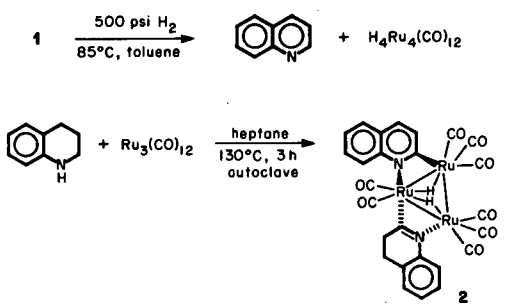

(2)

Apparently, the ligand is released as the cluster reacts with H_2 to form $H_4Ru_4(CO)_{12}$, a catalyst we studied in the hydrogenation of polynuclear heteroaromatic nitrogen compounds including quinoline.[1a,c]

The Reaction of Complex 1 with Hydride Reagents

Complex **1** was reacted with both $LiAlH_4$ and $LiBEt_3H$; however, **1** does appear to react even under forcing conditions, i.e., 60°C for several hrs in THF. Apparently, the carbon-nitrogen double bond is not reduced in the complex, while in the free ligand it is readily reduced. These results infer that the nitrogen ligand is not the site of reaction with hydride or H_2 reactants for reasons that are not clear as yet.

The Reaction of 1,2,3,4-Tetrahydroquinoline with $Ru_3(CO)_{12}$

$Ru_3(CO)_{12}$ reacts with 1,2,3,4-tetrahydroquinoline, under similar conditions as described above in the synthesis of the quinoline derivative, to form several different products. The major product was a novel triruthenium cluster[2] containing one molecule of quinoline and one of 3,4-dihydroquinoline. The proposed structure (Eq. 3) is based on ^1H, ^{13}C NMR, and infrared and mass spectroscopic evidence.

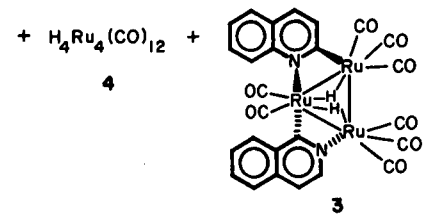

(3)

In the 200 MHz ^1H NMR spectrum, the region from 7.4 to 8.0 ppm strongly resembles that of the monosubstituted quinoline derivative, complex **1**. The 6.9 to 7.3 ppm region of the same NMR spectrum can therefore be interpreted as signals due to the 3,4-dihydroquinoline aromatic protons. Two triplets due to the methylene protons are located at 3.18 and 2.62 ppm. Signals for the two bridging hydrides were found at −14.01 and −17.64 ppm. The EIMS had prominent fragment ions at m/e 687 ($M^{+\cdot}$−Ru), 658 ($M^{+\cdot}$−quinoline), 657 ($M^{+\cdot}$−3,4-dihydroquinoline), and a sequence of ions that show a loss of CO from the m/e 658 and 657 ions to eventually give the ions at m/e 433 and 432 ($M^{+\cdot}$−8CO-quinoline or 3,4-dihydroquinoline). Additionally, the solution IR spectrum shows twelve CO stretches from 2104 to 1970 cm^{-1}. Complex **2** appears to disproportionate readily in cold (−30°C) acetone over several days to afford $H_4Ru_4(CO)_{12}$ and quinoline. The other minor products in the THQ reaction with $Ru_3(CO)_{12}$ are the bis quinoline complex, **3** (Ref. 3), and $H_4Ru_4(CO)_{12}$, **4**.

The Reaction of Phenanthridine and Dihydrophenanthridine $Ru_3(CO)_{12}$

The reaction of either phenanthridine or 9,10-dihydrophenanthridine with $Ru_3(CO)_{12}$ provided the same compound, **5** (Eq. 4). The NMR spectrum was conclusive for **5** with the absence of the C-9 proton at ~ 9.3 ppm, while the other signals were found between 8.4 and 7.61 ppm in the correct ratios and the bridging hydride at −13.73 ppm. The solution

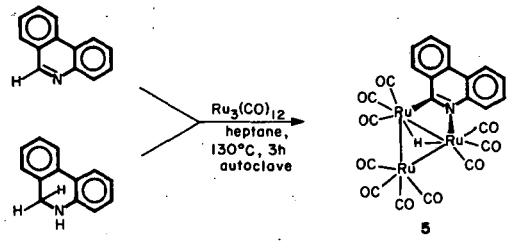

(4)

IR showed eight CO stretches between 2106 and 1991 cm, while the EIMS had prominent ions at m/e 706 ($M^{+\cdot}-2CO$), 594 ($M^{+\cdot}-6CO$), and 482 ($M^{+\cdot}-10CO$).

The X-Ray Crystal Structure of $Ru_3(\mu\text{-}H)(\mu\text{-}C_{13}H_8N)(CO)_{10}$, 5

In order to more clearly define the structure of **5** and compare the results to the recently reported x-ray crystal data of the quinoline-triosmium complex,[3] we obtained the single crystal x-ray analysis of **5**, as shown in Fig. 1. The molecule contains an isosceles triangle of ruthenium atoms with a hydride atom and the phenanthridine ligand bridging one edge. The Ru(2)-Ru(3) bond (2.866(1) Å), spanned by the two bridging ligands, is significantly longer than the other two Ru-Ru bonds (2.851(1), 2.844(1) Å). In fact, this bond is longer than the average Ru-Ru bond length in $Ru_3(CO)_{12}$ (2.854(7) Å).[6] It has

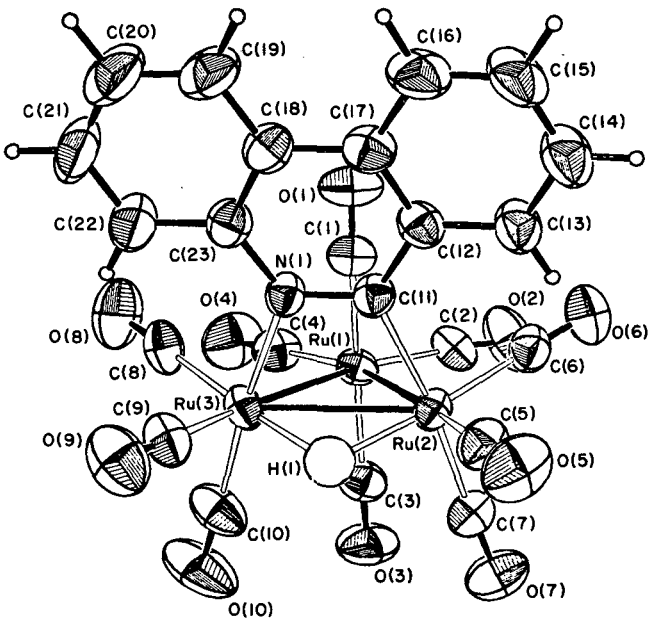

Figure 1. ORTEP diagram of $Ru_3(\mu\text{-}H)(N\text{-}C_{13}H_8N)(CO)_{10}$, **5** showing 50% probability ellipsoids. (XBL 859-4023)

been noted previously, by Churchill, DeBoer, and Rotella, that a single, unsupported hydride bridging two or more metal atoms causes a lengthening of the metal-metal bond.[7] However, those metal-metal bonds bridged by a hydride and another ligand generally shortened relative to the metal-metal bond in the unsubstituted compound. Bruce has suggested that the metal-metal bond length is a measure of the donor and pi-acceptor capacity of the bridging ligand.[8] For example, if the bridging group is a good pi-acceptor, a counterbalancing shortening effect on the metal-metal bond is noted: e.g., $HRu_3(CO)_{10}(COCH_3)$, 2.803 Å;[9] $HRu_3(CO)_{10}(C_2But)$, 2.792 Å.[10] In this case, because the bond is lengthened, we conclude that the phenanthridine is only weakly bound to the cluster and does not seem to be involved in any sort of delocalized backbonding with the metals.

The phenanthridine ligand is nearly planar; the maximum deviations being those of atom C(14), 0.024 Å and C(22) −0.043 Å, from the best weighted least-squares plane. The heterocyclic ligand is nearly perpendicular to the triangle of ruthenium atoms, with a dihedral angle of 106.7° between the two planes. The angle between the plane of metal atoms and the plane consisting of Ru(2), Ru(3), and H(1) is 32.5°. The dihedral angle between the plane of the phenanthridine ligand and the Ru(2)-Ru(3)-H(1) plane is 74.2°, probably due to the steric congestion of the carbonyl ligands and the bulk of the phenanthridine. In comparison with the bond parameters of free phenanthridine, the C(11)-N bond is lengthened by 0.021 Å (1.312 Å vs 1.291 Å).[11] This type of effect has been noted previously in the case of coordination of alkenes and alkynes to Pt(II) and Pt(0) where the C-C bond lengthens by 0.015−0.02 Å.[12] The length of the C(11)-N bond of this study is somewhat shorter than those reported for similar osmium clusters with coordinated heterocycles, e.g., $HOs_3(C_9H_6N)(CO)_{10}$, 1.329(35) Å; $H_2Os_3(C_9H_6N)_2(CO)_8$, 1.367−1.383 Å.[3] Other osmium clusters with bridging C-N bonds have bond lengths in the range 1.21 Å to 1.403 Å.[13] Nubel, Wilson, and Brown have reported a dinuclear bridged pyridine complex, $(\mu\text{-}H)Re_2(CO)_8(\mu\text{-}NC_5H_4)$, with a C-N bond length of 1.372(9)Å.[14]

The Reaction of Complex 5 with Hydrogen Gas

The hydrogenation of complex **5**, under longer reaction times than studied for complex **1**, again provided the ligand and $H_4Ru_4(CO)_{12}$ as well as some of the reduced ligand 9,10-dihydrophenanthridine. This result is not to surprising, since the hydride, **4**,

was active as a catalyst in the hydrogenation of polynuclear heteroaromatic nitrogen compounds.[1a,c]

PLANNED ACTIVITIES FOR FY 1986

We carried out several reactions with complexes **1** and **5** with the theme that they would allow insight in the interaction of reagents such H_2 gas, hydrides, and protons with the nitrogen ligands bonded to the triangle of ruthenium atoms. The hydrogenation reaction with complex **1** gave quinoline and $H_4Ru_4(CO)_{12}$ as the only products. The hydrogen attacks the ruthenium cluster liberating the nitrogen ligand, while a similar reaction occurs with complex **5**. The hydrogenation is complicated by the formation of $H_4Ru_4(CO)_{12}$, a catalyst we used to regioselectively reduce the nitrogen ring in compounds such as quinoline and phenanthridine.[1a] The next reaction studied was that of hydride reagents with **1**, **5**. To our disappointment, neither compound appeared to react with either $LiAlH_4$ or $LiBEt_3H$. These hydride results with complexes **1**, **5** are in contrast to similar reactions of these hydrides with the free ligands. For example, quinoline and phenanthridine react with $LiAlH_4$ to reduce the carbon-nitrogen double bond. This result clearly points out that the dimetalla-azacyclobutenes are not good models for the study of carbon-nitrogen bond cleavage reactions with nucleophilic reagents, since it appears that the ruthenium cluster rather than the complexed nitrogen ligand is the site of reaction. Thus, we will attempt to study the reactions of dimetalla-azacyclopropanes, and in FY 86 we will direct our attention to the synthesis of these compounds.

REFERENCES

1. (a) Fish, R.H., Thormodsen, A.D., and Cremer, G.A. (1982), *J. Amer. Chem. Soc. 104,* p. 5234.
   (b) Fish, R.H., Tan, J.L., and Thormodsen, A.D. (1984), *J. Org. Chem. 49,* p. 4500.
   (c) Fish, R.H. (1983), *Ann. N.Y. Acad. Sci. 415,* p. 292.
   (d) Fish, R.H., Tan, J.L., and Thormodsen, A.D. (1985), *Organometallics 4,* p. 1743.
   (e) Fish, R.H., Thormodsen, and A.D., Heinemann, H. (1985), *J. Mol. Catal. 31,* p. 191.
   (f) Lynch, *et al.* (1982), *J. Mol. Catal. 17,* p. 109.
   (g) Lynch, T.J., Banah, M., Kaesz, H.D., and Porter, C.R. (1984), *J. Org. Chem. 49,* p. 1266.
2. Yin, C.C. and Deeming, A.J. (1975), *J. Chem. Soc. Dalton Trans.,* p. 2091.
3. Eisenstadt, A., Giandomenico, C.M., Frederick, M.F., and Laine, R.M. (1985), *Organometallics 4,* p. 2033.
4. Constable, E.C. (1984), *Polyhedron 3,* p. 1037.
5. Foulds, G.A., Johnson, B.F., and Lewis, J. (1985), *J. Organomet. Chem. 294,* p. 123.
6. Churchill, M.R., Hollander, F.J., and Hutchinson, J.P. (1977), *Inorg. Chem. 16,* p. 2655.
7. Churchill, M.R., DeBoer, B.G., and Rotella, F.J. (1976), *Inorg. Chem. 15,* p. 1843.
8. Bruce, M.I. (1982), in *Comprehensive Organometallic Chemistry,* Chap. 32.5, G. Wilkinson, F.G.A. Stone, E.W. Abel, Eds. Pergamon Press, Oxford.
9. Johnson, B.F.G., *et al.* (1979), *J. Organomet. Chem. 173,* p. 187.
10. Catti, M., Gervasio, G., and Mason, S.A. (1977), *J. Chem. Soc. Dalton Trans.,* p. 2260.
11. Roychowdhury, P. (1973), *Acta Crystallogr., Sect. B. 29B,* p. 1362.
12. Ittel, S.D., and Ibers, J.A. (1976), *Adv. Organomet. Chem. 14,* p. 33.
13. (a) Adams, R.D., Dawoodi, Z., Foust, D.F., and Segmuller, B.E. (1983), *J. Amer. Chem. Soc. 105,* p. 831.
    (b) Adams, R.D. and Dawoodi, Z. (1981), *J. Amer. Chem. Soc. 103,* p. 6510.
    (c) Dawoodi, Z., Mays, M.J., and Raithby, P.R. (1981), *J. Organomet. Chem. 219,* p. 103.
14. Nubel, P.O., Wilson, S.R., and Brown, T.L. (1983), *Organometallics 2,* p. 515.

Hydrodenitrogenation Chemistry: Cleavage of Alkylcarbon-Nitrogen Bonds, Ammonia and Methane Formation in the HDN Reaction of 1,2,3,4-Tetrahydroquinoline with a Nickel Oxide Catalyst Supported on Silica*

R.H. Fish, A.D. Thormodsen, R.S. Moore, D.L. Perry, J. Michaels, and H. Heinemann

As serious attention has been given to the use of shale oil and coal derived liquids as refinery feedstocks, several unique processing problems associated with these materials have been identified. One of the most important is the removal of nitrogen, an undesired component in the final fuels to be made from these synthetic oils. While petroleum contains typically less than 0.3 wt% nitrogen, coal derived liquids can contain up to 0.8 wt%[1] and shale oils can have up to a 2.2 wt% nitrogen content.[2]

The existing process for nitrogen removal, hydrodenitrogenation (HDN), involves the catalytic reduction and cleavage of carbon-nitrogen bonds to remove the nitrogen as ammonia. The processing conditions are quite severe, 300 to 400°C, 1000 psi hydrogen. Typical catalysts are $NiMo/Al_2O_3$ or $CoMo/Al_2O_3$. Under these conditions any aromatic structures are fully reduced before nitrogen removal takes place. This represents an unnecessary and excessive consumption of hydrogen, especially in the case of highly aromatic coal derived liquids.

We have recently demonstrated the ability of transition metal complex catalysts to selectively reduce only the nitrogen containing ring in several polynuclear nitrogen-containing heteroaromatics.[3–7] We have now turned our attention to possible means of cleaving the reduced carbon-nitrogen bonds produced by these transition metal catalysts. By combining a selective reduction with a selective bond cleavage we hope to avoid the wasteful use of hydrogen in the conventional HDN process.

We have investigated the use of heterogeneous catalysts, and especially highly loaded supported nickel catalysts, for C-N bond cleavage in the selectively reduced nitrogen heterocycle, 1,2,3,4-tetrahydroquinoline. While the use of this particular reduced compound as an HDN substrate has not received a great deal of attention prior to this study, the fully saturated compound, decahydroquinoline, has been investigated by Katzer *et al.*,[8] who found that catalysts containing both metal and acidic support sites were apparently necessary to cause HDN. Our use of highly loaded supported catalysts was suggested in part by studies conducted by Maier *et al.*[9] In that study it was found that 40% Pt on SiO_2 was very effective as an HDN catalyst for quinoline under relatively mild conditions (1 atm. H_2, 150–200°C), and that the high metal loading was crucial in this application. In this report, we detail our accomplishments with highly loaded supported catalysts in the HDN reaction with nitrogen heterocyclic substrates.

ACCOMPLISHMENTS DURING FY 1985

Survey of Catalysts

A quick examination was made of the use of a variety of compounds as catalysts for C-N bond cleavage in 1,2,3,4-tetrahydroquinoline, as shown in Table 1. Various bulk metals and metal oxides, as well as a fluid catalytic cracking catalyst, were found to either be entirely inactive or to catalyze the undesired dehydrogenation of tetrahydroquinoline to quinoline.

Several supported nickel catalysts, and one supported rhodium catalyst, all showed the desired C-N bond cleavage activity to varying degrees. Two of these, a 30% Ni/SiO_2 catalyst prepared in our laboratory and a 50% Ni/SiO_2 catalyst supplied as a gift by United Catalyst (C46-7-03), showed the highest activity and were singled out for more detailed studies.

30% Ni Catalyst Results

Table 2 presents the results obtained with a 30% Ni on silica catalyst prepared in our laboratory. The compound, 1,2,3,4-tetrahydroquinoline, was converted at 320°C into a variety of products, the principal ones being quinoline (34.0%), aniline (27.5%), benzene (8.4%), 2-methylaniline (7.2%), and indole (6.5%). The aniline and benzene derivatives are formed via the cleavage of C-N bonds in 1,2,3,4-tetrahydroquinoline and are thus the desired products. Quinoline, formed by dehydrogenation of 1,2,3,4-tetrahydroquinoline, and the side-product indole, are unwanted. At a higher temperature, 360°C, the relative amounts of quinoline and ben-

*This work was supported by the Assistant Secretary for Fossil Energy, Office of Technical Coordination of the U.S. Department of Energy through the Pittsburgh Energy Technology Center under Contract No. DE-AC03-76SF00098.

Table 1. Summary of heterogeneous catalyst results using 1,2,3,4-tetrahydroquinoline as substrate.[a]

Catalyst	Results
Bulk nickel (powder)	Inactive
Bulk manganese (powder)	Inactive
Cr_2O_3 (powder)	Inactive
ZrO_2 (powder)	Inactive
Zeolite (fluid cat. cracking)	Inactive
Bulk copper (granules)	Dehydrogenation[b]
8% Cu, 8% Ni/SiO_2[d]	Dehydrogenation
5% Ni/SiO_2[d]	Dehydrogenation, C-N cleavage[c]
5% Rh/SiO_2[e]	Dehydrogenation, C-N cleavage
30% Ni/SiO_2[d]	C-N cleavage, dehydrogenation
50% Ni/SiO_2[f]	C-N cleavage, dehydrogenation
60% Ni/Al_2O_3[f]	Dehydrogenation, C-N cleavage

[a]Conditions: Approximately 1 cc each catalyst, T = 250°C–350°C, 0.14 cc/hr 1,2,3,4-tetrahydroquinoline, 30 cc/min H_2 at 1 atm. Analysis by capillary gas chromatography.

[b]Formation of quinoline

[c]Formation of alkyl anilines and alkyl benzenes.

[d]Prepared as described in experimental section.

[e]Donated by Dr. A. Bell's research group (UC Berkeley).

[f]Donated by United Catalyst.

zene increased, while the relative amount of aniline derivatives in the product mixture decreased. Importantly, little reduction of the 5,6,7,8 ring of 1,2,3,4-tetrahydroquinoline was observed, indicating the higher selectivity of this system towards bond cleavage as compared to hydrogenation.

The compounds 2-propylaniline and propylbenzene, both plausible intermediates in the HDN of 1,2,3,4-tetrahydroquinoline, were also investigated as substrates. In addition to the expected products of C-N bond cleavage (benzenes) and propyl chain cleavage (anilines), both 1,2,3,4-tetrahydroquinoline and 2-methylindole were formed with 2-propylaniline. Apparently, a catalyzed or free radical mechanism may lead to ring closure of 2-propylaniline to form these two latter products. Since ring opening of 1,2,3,4-tetrahydroquinoline to form 2-propylaniline may be the first step in the HDN of 1,2,3,4-tetrahydroquinoline, the potential reversibility of this ring opening is of great interest.

When propylbenzene was used as a substrate, no condensible products were formed, except for a trace of benzene and toluene. The very high activity of the catalyst towards this material is probably a result of the lack of any basic nitrogen compounds (quinoline or aniline derivatives) in this reaction. These materials are known to be strong catalyst poisons, and in this particular case when they are present they apparently moderate the activity of the catalyst, preventing it from completely reducing and/or cleaving substrates. In the absence of these nitrogen bases, complete hydrogenolysis of the substrate (to methane, see below) or conversion to coke must occur, resulting in no condensible products being observed.

Some of the gas generated during the HDN of 1,2,3,4-tetrahydroquinoline at 320°C was trapped in a water trough (eliminating ammonia) and analyzed by gas chromatography. It was found to be almost entirely methane (99.5%), with traces of ethane, propane, and butane. Much of this methane is presumably formed by the partial or complete hydrogenolysis of only the saturated 1,2,3,4 ring in tetrahydroquinoline. Some may as well result from the entire hydrogenolysis of 1,2,3,4-tetrahydroquinoline, the results of a mass balance with the 50% Ni catalyst (see below) indicate that this total hydrogenolysis may be an important reaction.

50% Ni Catalyst Results

The results for the 50% nickel catalyst, shown in Table 3, are quite similar to those discussed above. The primary difference between the two catalysts is the degree of activity. At temperatures 100°C lower, and with one third as much catalyst, the 50% Ni material exhibited the same overall conversion of 1,2,3,4-tetrahydroquinoline as the 30% catalyst. Additionally, the 50% Ni catalyst was more efficient in catalyzing the C-N bond cleavage reaction, relative to dehydrogenation to form quinoline.

The major products formed from the HDN of 1,2,3,4-tetrahydroquinoline using this 50% Ni catalyst at 250°C were 2-methylaniline (14.3%), quinoline (14.3%), 5,6,7,8-THQ (1.41%), aniline (0.4%), benzene (9.2%), and 2-ethylaniline (8.6%). Relative to the 30% nickel catalyst more aniline and benzene derivatives and less quinoline are produced by this catalyst. Combined with the higher overall activity of this catalyst, this result indicates that the 50% Ni material is more suitable than the 30% Ni material for the HDN of 1,2,3,4-tetrahydroquinoline. This situation is improved further at the slightly higher reaction temperature of 260°C, with the relative amounts of benzenes and anilines increasing, and the amount of quinoline and 5,6,7,8-tetrahydroquinoline decreasing.

Table 2. Results using 30% Ni/SiO_2 catalyst.[a]

Substrate: Temperature: Products (mol%)[b]	1,2,3,4-THQ (320°C)	1,2,3,4-THQ (360°C)	2-Propylaniline (320°C)	Propylbenzene (320°C)
Benzene	8.4%	12.2%	19.3%	trace
Toluene	1.4%	1.8%	2.9%	trace
Ethylbenzene	trace	trace	trace	0.0%
Propylbenzene	trace	trace	5.3%	0.0%
Aniline	27.5%	18.9%	9.3%	0.0%
2-Methylaniline	7.2%	2.7%	5.7%	0.0%
2-Ethylaniline	trace	trace	trace	0.0%
2-Propylaniline	trace	trace	37.0%	0.0%
Quinoline	34.0%	44.5%	0.0%	0.0%
5,6,7,8-THQ	trace	trace	0.0%	0.0%
1,2,3,4-THQ	5.3%	3.5%	5.8%	0.0%
Indole	6.5%	9.1%	trace	0.0%
2-Methylindole	2.1%	0.9%	2.3%	0.0%
Unidentified	7.6%	6.4%	12.4%	0.0%

[a]Conditions: 0.86 g catalyst, 0.14 cc/hr substrate, 30 cc/min H_2 at 1 atm. Products identified by GCMS and verified by comparison with standards (except 2-methylaniline and 2-ethylaniline).

[b]Not included in the product normalization is the amount of gaseous products obtained. For a 340°C 1,2,3,4-tetrahydroquinoline run the hydrocarbon gases produced were analyzed by gas chromatography to give 99.5% CH_4, e.g., 0.1% C_2H_6, 0.4% C_3H_8, e.g., 0.02% C_4H_{10}. Ammonia was also produced.

We observed less cyclization when 2-propylaniline was reacted over the 50% Ni catalyst, as compared to the 30% Ni case. Only traces of 1,2,3,4-tetrahydroquinoline and indoles were produced. The primary products were benzene and propylbenzene, with surprisingly small amounts of toluene and ethylbenzene being formed. Aniline derivatives were also formed in this reaction. As with the 30% Ni catalyst, reaction of propylbenzene over the 50% Ni catalyst provided only trace amounts of benzene and toluene as products. In the absence of the moderating effects of nitrogen bases, the catalyst seems to be extremely active towards total hydrogenolysis.

An analysis of the gas formed during the HDN of tetrahydroquinoline with the 50% Ni catalyst showed that it was almost entirely methane (99.8%). Other gases, if present, were below the detection limit of the gas chromatograph. A mass balance on the liquid products revealed that about 70% of the 1,2,3,4-tetrahydroquinoline was converted to the identified products in the tables, and about 10% of the reactant is converted to unidentified liquids. The 20% that remains cannot be accounted for in the condensible products and presumably is converted to methane (although some may be converted to coke as well). Our apparatus does not trap all of the gases formed, thus a mass balance on the non-condensible products could not be performed.

Additional experiments were done with the 50% nickel on silica catalyst in which quinoline was used as the substrate. The results of these runs, at three different temperatures, are shown in Table 4. In this case the nitrogen-containing ring in quinoline must

Table 3. Results using 50% Ni/SiO_2 catalyst (United Catalyst C46-7-03).[a]

Substrate: Temperature: Products (mol%)[b]	1,2,3,4-THQ (250°C)	1,2,3,4-THQ (260°C)	2-Propylaniline (250°C)	Propylbenzene (250°C)
Benzene	9.2%	15.8%	29.9%	trace
Toluene	1.8%	2.8%	4.3%	trace
Ethylbenzene	trace	trace	trace	0.0%
Propylbenzene	trace	trace	20.8%	0.0%
Aniline	9.4%	16.7%	6.0%	0.0%
2-Methylaniline	14.3%	20.0%	5.4%	0.0%
2-Ethylaniline	8.6%	8.6%	1.4%	0.0%
2-Propylaniline	2.0%	1.6%	21.5%	0.0%
Quinoline	14.3%	9.8%	0.0%	0.0%
5,6,7,8-THQ	14.1%	5.9%	0.0%	0.0%
1,2,3,4-THQ	4.7%	1.6%	trace	0.0%
Indole	2.7%	3.1%	trace	0.0%
2-Methylindole	5.0%	4.5%	trace	0.0%
Unidentified	13.9%	9.6%	10.7%	0.0%

[a]Conditions: 0.26 g catalyst, 0.14 cc/hr substrate, 30 cc/min H_2 at 1 atm. Products identified by GCMS and verified by comparison with standards (except 2-methylaniline and 2-ethylaniline).

[b]Not included in the product normalization is the amount of gaseous products obtained. For the 1,2,3,4-tetrahydroquinoline runs the hydrocarbon gases produced were analyzed by gas chromatography to give at least 99.8% CH_4; other hydrocarbons (if present) were below the detection threshold of the instrument. Ammonia was also produced.

presumably be reduced prior to any cleavage of C-N bonds. At the highest temperature, 280°C, the overall HDN of quinoline was more efficient than that of 1,2,3,4-tetrahydroquinoline, while at 250°C less HDN of quinoline took place. However, for all three of these runs mass balances reveal that a considerable amount of the quinoline is converted to noncondensible products, ranging from approximately 50% at 250°C to 70% at 280°C. This is clearly not a desired reaction, and in this regard the results with 1,2,3,4-tetrahydroquinoline, in which only 20% was "lost" in this way, are superior to those with quinoline.

General Hydrodenitrogenation Scheme

Figure 1 is a schematic representation of the kinds of reactions we propose to account for the products observed in the various reactions described above. The compound, 1,2,3,4-tetrahydroquinoline, may either be ring opened to form 2-propylaniline or dehydrogenated/hydrogenated to form quinoline and 5,6,7,8-tetrahydroquinoline.

The compound, 2-propylaniline, may undergo cyclizations to form indoles, or reform 1,2,3,4-tetrahydroquinoline. Instead, propylaniline can have the nitrogen atom cleaved to form various derivatives of benzene, or have carbon atoms hydrogenolyzed on the propyl group to form other anilines. These anilines may in turn be converted to benzene derivatives.

The path that leads from quinoline to 1,2,3,4-tetrahydroquinoline to propylaniline and finally to

Table 4. Results using 50% Ni/SiO_2 catalyst.[a]

Substrate Temperature Products (mol%)	Quinoline (250°C)	Quinoline (260°C)	Quinoline (280°C)
Benzene	0.6	3.2	21
Toluene	0.7	1.6	5
Ethylbenzene	trace	trace	trace
Propylbenzene	0.1	0.24	trace
Aniline	6	12	20
2-Methylaniline	12	16	15
2-Ethylaniline	8	6.5	2.7
2-Propylaniline	2	1.2	trace
Quinoline	26	26	19
5,6,7,8-THQ	15	7	1.2
1,2,3,4-THQ	9	5	1
Indole	1.5	2	1.6
2-Methylindole	5	5	3
Unidentified	15	14	10.5

[a]Conditions: 0.26 g catalyst, 0.14 cc/hr substrate, 30 cc/min H_2 at 1 atm. Products identified by GCMS and verified by comparison with standards (except 2-methylaniline and 2-ethylaniline).

the benzenes and anilines is the desired course of hydrodenitrogenation. The other paths shown, and the partial reversibility of the above path, are reactions that we wish to avoid. By understanding the nature of these catalysts, we will hopefully be able to control these different types of reactions in a more reasonable fashion.

Characterization of Catalysts

Figure 2 shows a transmission electron micrograph of a used sample of the 30% Ni catalyst. A bimodal distribution of nickel crystallites is apparent here, with many small crystallites in the 200 angstrom size range and a few larger crystals in the 2000 angstrom range. Although not visible in this picture, coke deposits were also found on the surface. A chemical analysis of this same catalyst sample showed a 0.13% carbon content.

A preliminary x-ray photoelectron spectroscopy (XPS) study of this same catalyst has revealed the presence of primarily metallic nickel on the surface, with small amounts of nickel oxide.

An XPS study of the 50% nickel catalyst (Fig. 3) shows a very different spectrum than that found with the 30% nickel catalyst. This spectrum, showing here the nickel $2P_{3/2,1/2}$ lines, indicated that the nickel is present as a tertiary oxide, with nickel ions

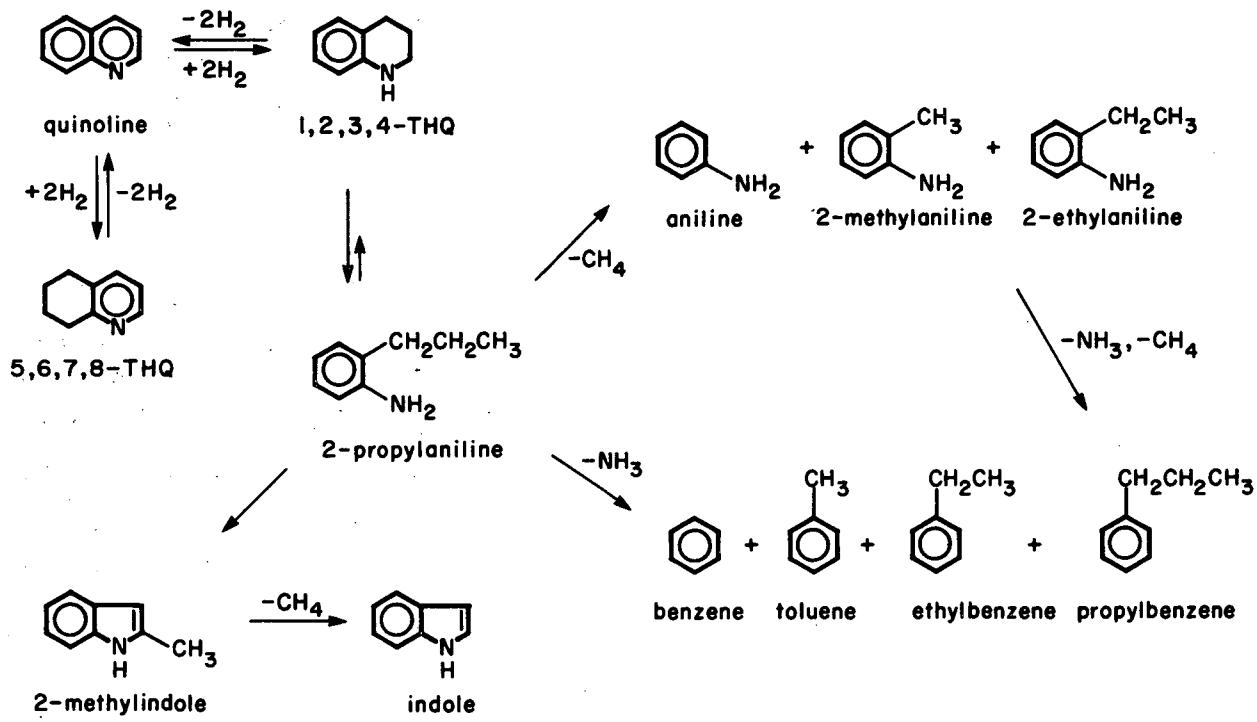

Figure 1. Proposed reaction network for HDN using supported nickel catalyst. (XBL 862-563)

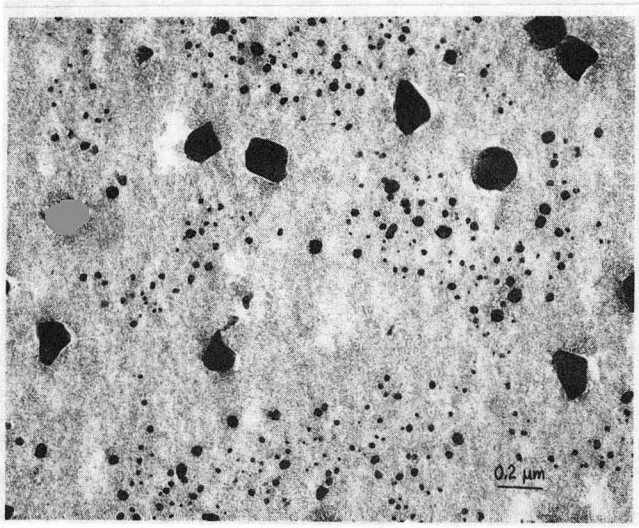

Figure 2. Transmission electron micrograph of 30% Ni/SO_2 catalyst. (XBB 8511-9385)

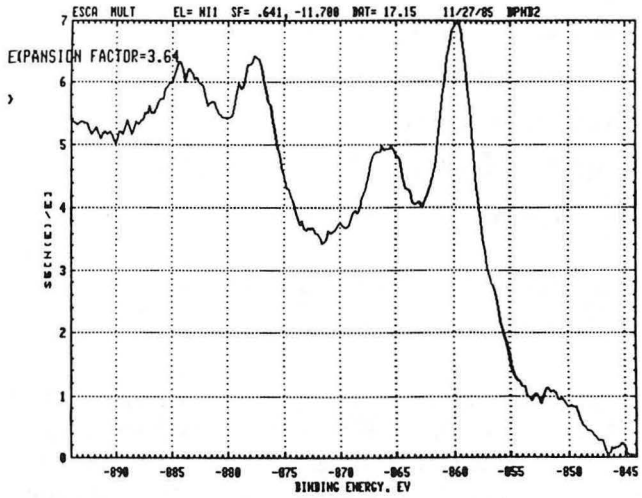

Figure 3. XPS spectrum of Ni $2P_{3/2,\,1/2}$ lines in used 50% Ni/SiO_2 catalyst. (XBL 862-564)

and support ions in a mixture. Aluminum was also found to be present in this catalyst, allowing for the possibility of nickel aluminate, as well as nickel silicate.

The differences we see between the two nickel catalysts may thus in part be explained by the difference in the state of the nickel on the surface of the catalyst. We are planning further morphological examination of both nickel catalysts in an effort to resolve this issue.

PLANNED ACTIVITIES FOR FY 1986

We plan to use an advanced XYTEL unit to better evaluate the catalysts found to be effective in the studies described above. This device allows for semi-continuous monitoring of the products of reaction by on-line gas chromatography, and should provide accurate kinetic data.

We also plan to probe the structure of the various catalysts using several techniques, including scanning and transmission electron microscopy, x-ray photoelectron spectroscopy, and various surface absorption techniques. By gaining an understanding of the morphological features of the catalysts in relation to their chemical activity, we hope to identify those catalyst features that are essential for the desired C-N bond cleavage activity.

REFERENCES

1. Gorbaty, M.L. and Harney, B.M. (1979), "Refining of Synthetic Crudes," *Advances in Chemistry Series 179,* ACS, Washington, D.C., Chap. 1.
2. Ibid., Chap. 3.
3. Fish, R.H., Thormodsen, A.D., and Cremer, G.A. (1982), *J. Amer. Chem. Soc. 104,* p. 5234.
4. Fish, R.H., Tan, J.L., and Thormodsen, A.D. (1984), *J. Org. Chem. 49,* p. 4500.
5. Fish, R.H. (1983), *Ann. N.Y. Acad. Sci. 415,* p. 292.
6. Fish, R.H., Thormodsen, A.D., and Heinemann, H. (1985), *J. Mol. Catal. 31,* p. 191.
7. Fish, R.H., Tan, J.L., and Thormodsen, A.D. (1985), *Organometallics 4,* p. 1743.
8. Katzer, J.R., Stiles, A.B., and Kwart, H. (1980), *Development of Unique Catalysts for Hydrodenitrogenation of Coal Derived Liquids,* DOE/ET/03297-1.
9. Maier, W.F. and Guttieri, M.J. (1984), *J. Org. Chem. 49,* p. 2875.

Polymer Pendant Ligand Chemistry 2: Reactions of Vanadyl and Nickel Acetylacetonates with Catechol Ligands Bonded to Polystyrene-Divinylbenzene Resins*

R.H. Fish, A. Izquierdo, Gad Friedman, and Robert Price

The use of polymer-supported pendant ligands for metal ion removal is a well-developed field.[1a,b] We have recently reported on the use of polymer-supported catechol ligands for removal of organoarsonic acids and arsenate from solution.[2] We have also discovered a facile regeneration reaction that removes the arsenic compounds, while providing the catechol ligand site for reuse.[2]

In this report, we will describe our results on the reactions of vanadyl and nickel acetylacetonates with the catecholated resins (20% cross-linked) to provide evidence for a ligand exchange, i.e., formation of vanadyl and nickel catechol compounds on the resin with the release of acetylacetone.

ACCOMPLISHMENTS DURING FY 1985

The reaction of the 20% cross-linked catecholated resins with vanadyl acetylacetonate was studied. Table 1 shows the results of this type of ligand exchange reaction with evidence that removal of vanadyl ion is rapid and is enhanced by both a temperature increase and by the addition of a bidentate ligand, 2,2′-bipyridine. The rates of removal can be seen in Fig. 1 and show the rapid uptake that takes place (less than 1 hour), as well as the effect of temperature on the concentration of vanadyl ion removed.

In another experiment, we reacted nickel acetylacetonate with the catecholated resin at 64°C in meOH (1:1 ratio Ni/catechol) and found a 32% removal of nickel from solution.

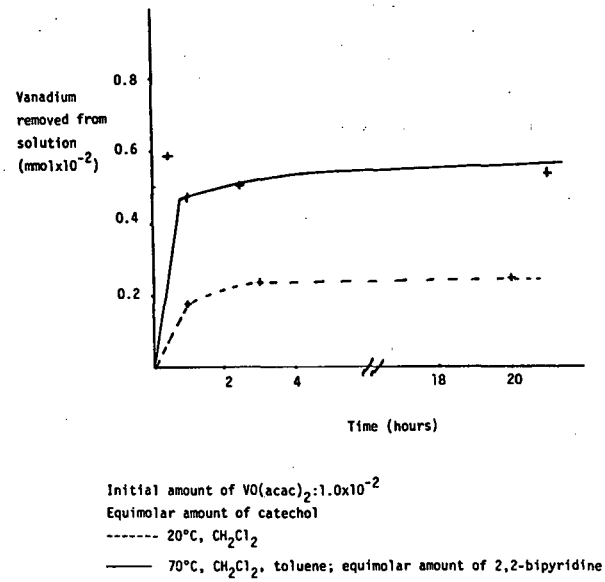

Figure 1. (XBL 862-566)

We also found that Fourier Transform infrared spectroscopy was a powerful tool to ascertain the structure of vanadyl complexes on the beads (Eq. 1).

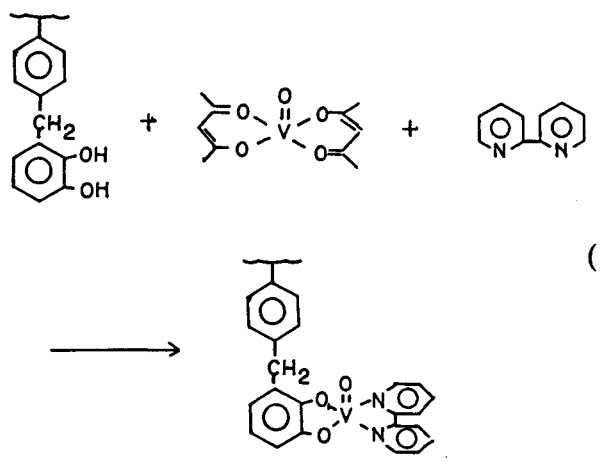

(1)

*This work was supported by the Assistant Secretary for Fossil Energy, Office of Oil, Gas and Shale Technology of the U.S. Department of Energy through the Bartlesville Project Office under Contract No. DE-AC03-76SF00098.

Table 1. Initial amount of $VO(acac)_2$: 1.00×10^{-2} mmol.[a]

Exp No.	Temperature (°C)	Cathecol (mmol × 10^2)	2,2-Bipyridine (mmol × 10^{-2})	Vanadium removed from solution m(mol × 10^{-2})
1	20[b]	1.16	—	0.26
2	20[b]	2.30	—	0.51
3	20[b]	0.98	1.04	0.47
4	70[c]	1.00	—	0.38
5	70[c]	0.95	1.04	0.60
6	80[c]	1.04	—	0.45
7	80[c]	2.30	2.26	0.68

[a]Conditions: 5.92% by weight of catechol ligand in the 20% cross-linked polymer.

[b]Solvent: CH_2Cl_2.

[c]Solvent: CH_2Cl_2-toluene.

PLANNED ACTIVITIES FOR FY 1986

We are continuing the polymer-pendant ligand chemistry to more clearly define the rates of removal of vanadyl and nickel compounds from solution and to use Fourier Transform infrared spectroscopy for determination of vanadyl and nickel catecholate structures on the resins.[3]

REFERENCES

1. (a) Frechet, J.M. and Farrall, M.J. (1977), *Chemistry and Properties of Cross-Linked Polymers,* S.S. Labana, Ed., Academic Press, New York. (b) Blasius, E. and Brazio, B. (1967), *Chelating Ion Exchange Resins in Chelates in Analytical Chemistry,* H.A. Flaschlia, and J.A. Barnard, Eds., Marcel Dekker.
2. Fish, R.H. and Tannous, R.S. (1985), *Inorg. Chem. 24,* p. 4456.
3. Fish, R.H., Izquierdo, A., Friedman, G., and Price, R. (to be submitted for publication).

Carbon Oxygen Bond Cleavage Reactions of Model Coal Compounds Using Inorganic Electron Transfer Reagents*

R.H. Fish and J.W. Dupon

Aryl ethers and esters are currently accepted models for the postulated structure of coal. As with coal, rigorous conditions are usually necessary to effect any cleavage of the strong C-O bond.

We have investigated the cleavage of the C-O bonds in aryl ether and ester compounds as models for coal. We have observed efficient and selective cleavage in the presence of M(Ln) compounds where M = alkali metal and Ln = multidentate ligands, such as ethylenediamine and crown ethers. A mechanism involving electron transfer from the oxidation of the metal to a phenyl ring of the ether is proposed.

ACCOMPLISHMENTS DURING FY 1985

Earlier cyclic voltammograms in the literature, on the reductive carbon-oxygen bond cleavage of diaryl ethers, indicate that these compounds can be reduced electrochemically to their radical anion at high negative potential, e.g., −3.05 v *vs* SCE for diphenyl ether.[1] Therefore, in order to accomplish this objective chemically, strong reducing agents were deemed necessary. Mejer *et al.*[2] utilized a five-fold excess of lithium metal and ethylenediamine to cleave benzyl phenyl and diphenyl ethers. The first step of the eventual C-O bond cleavage is believed to be the addition of an electron to a phenyl ring of the ether.

We have studied the reaction of potassium/crown ether complexes with diaryl ethers and esters. A stable solution of electrons is generated at 0°C by the ready oxidation of the metal (Eq. 1).

$$K^{o} + CE \xrightarrow{THF} K^{+} \rightarrow CE + e^{-}\ (\text{solvated}), \qquad (1)$$

$$CE \equiv 18\ \text{Crown}\ 6\ \text{Ether}.$$

As benzyl phenyl ether was added to the deep blue solution of the potassium/18-crown-6 reagent, the color changed within fifteen minutes to a yellow-orange. The reaction was complete in twenty hours, producing toluene and phenol as the only products in a 1:1 ratio.

Reaction with dibenzyl ether was not as clean. Under the same reaction conditions, bibenzyl and benzaldehyde were produced in addition to toluene and benzyl alcohol. Bibenzyl can result from the coupling of two relatively stable benzyl radicals.

PLANNED ACTIVITIES FOR FY 1986

A survey of the reductive cleavage reactions of various aryl ethers and esters will be utilized to discern relative rates of cleavage. In addition, lithium/12-crown-4 will be used as a reducing agent and compared to the studies with potassium metal. We also intend to synthesize and examine the crown ether complexes of alkali metals with the macrocyclic ethers attached to a polymeric backbone. Immobilization of the crown ether on polyvinyl sytrene would provide enhanced stability and reactivity toward reductive cleavage of the aryl ethers.

REFERENCES

1. Woolsey, N.F. and Bartak, D.E. (1984), *Quantitation of the Reductive Cleavage of Aryl Ethers of SRC and Coals,* Final Report DOE/PC/30227-T3 (DE840 1206).
2. Mejer, S., Ganiecka, K., and Jablonski, L. (1977), *Rosz. Chem. 51,* p. 2477.

*This work was supported by the Electric Power Research Institute through the U.S. Department of Energy under Contract No. DE-AC03-76SF00098.

Processing of Condensate Waters from Coal Gasification*

C.J. King, J.J. Senetar, T.M. Grant, L.J. Poole, and R.E. Thompson

Large volumes of condensate water are formed when reactor effluents from coal gasification are cooled. Water streams from lower-temperature gasification processes contain large concentrations of ammonia, acid gases, and dissolved organics—notably, phenolic compounds. For both economic and environmental reasons, it is necessary to process these waters sufficiently to allow recycling, probably as make-up to a cooling-tower system.

The principal objective of this project is to provide basic understanding enabling development of improved physicochemical processing methods for condensate waters formed during coal-gasification processes. Particular attention is given to solvent-extraction, adsorption, and stripping processes. Other aspects of the project have dealt with chemical characterization of condensate waters, so as to provide a sound basis for research on processing alternatives, and characterization of the mechanism and kinetics of hydantoin compounds, which are formed in the quench-water circuit and tend to concentrate in the blowdowns of cooling towers to which condensate waters would logically be recycled.

Current research focuses upon 1) extraction with both conventional and novel chemically associating solvents which enable effective removal of organic contaminants with promise of low energy consumption, 2) fractionation and removal of organic contaminants by regenerated adsorption and other solid-sorption processes, 3) combining extraction of ammonia with stripping of acid gases in an innovative process which can recover ammonia as an isolated product, and 4) combining Items #1 and/or #2 with Item #3 synergistically.

*This work was supported by the Morgantown Energy Technology Center, Morgantown, WV, through the Assistant Secretary for Fossil Energy, Office of Surface Coal Gasification, Advanced Process Research Program of the U.S. Department of Energy under Contract No. DE-AC03-76SF00098.

ACCOMPLISHMENTS DURING FY 1985

Characterization of Condensate Waters

Analytical results obtained in previous years are described in a recently published paper.[1] The most significant results of the past year have been identification and quantification of thiocyanate and polysulfides, which account for most of the remaining unidentified Chemical Oxygen Demand (COD), organic nitrogen, and organic sulfur in condensate water from Run 101 of the Morgantown Energy Technology Center (METC) gasifier. The full results are shown in Table 1.[2] Our analysis of this water now accounts for 95–96% of the measured COD, 100% of the measured Total Organic Carbon (TOC), 85–100% of the measured organic sulfur, and 94% of the measured organic nitrogen. The uncertainties are associated with polysulfides. For these, only the zero-valent sulfur portion responds to the analysis, and the average number of zero-valent S atoms per mole of divalent sulfur in the polysulfide is unknown.

Analyses of various compositional properties were made for a sample of condensate water supplied from the Great Plains Gasification Associtess demonstration plant. These results were compared with analyses supplied by METC from Argonne National Laboratory and the University of Illinois. Differences were explored and interpreted.

Formation of Hydantoin Compounds

Measurements of the rate of formation of 5,5-dimethyl hydantoin in the presence and absence of various reactants, with various proportions among the reactants, and at various temperatures, revealed 1) that the formation reaction involves, simultaneously, acetone, cyanide, ammonia, and carbon dioxide; 2) that the kinetics are first order in each of these substances; 3) that a "sink" for cyanide exists but is not fully explained; and 4) that there is a strong temperature sensitivity to the reaction. Cyanide is the limiting reagent for the formation of hydantoins in most or all condensate waters. Differences in amounts of hydantoin formation can be interpreted in terms of a) the amount of cyanide formed in the gasifier system, and b) the time, temperature, and mixing conditions within the quench-water circuit.

Table 1. Analysis of METC run-101 condensate water.

	Concentration (mg/L)	COD (%)	TOC (%)
Hydroxybenzenes:		85.7	93.7
Phenol	1,380		
Cresols	1,990		
Xylenols	840		
Dihydroxybenzenes:		2.4	2.8
Catechol	40		
4-methyl catechol	40		
Resorcinol	65		
Hydroquinone	4		
Naphthols	37	0.8	0.9
5,5-dimethyl hydantoin	20	0.2	0.3
Low-MW organic compounds:		1.5	1.6
Acetone	60		
Acetone cyanohydrin	ND[a]		
Acetonitrile	65		
Acetic acid	ND		
Methanol	0		
*Thiocyanate	209 [370][b]	1.9	1.4
*Polysulfide sulfur	[104]	3.0[c]	0.0
Identified COD/TOC (%)		95.8	100.7
Measured COD/TOC (mg/L)		12,250	3,490
Organic nitrogen (mg/L)[d]	120 (94% identified)		
Organic sulfur (mg/L)[d]	404 (100% identified)[c]		

[a]ND: Not determined.
[b]Values in brackets are for a nonacidified sample that had aged.
[c]Assuming polysulfides are in the form SS^{2-}.
[d]Nitrogen and sulfur balances are based on nonacidified samples that had aged.

Extraction of Phenols

Previous work on the use of tri-n-octyl phosphine oxide (TOPO) as an extractant for phenols has now been published.[3]

Distribution coefficients were measured for various condensate-water components extracted into various solvents, including methyl isobutyl ketone (MIBK), benzophenone, tri-n-butyl phosphate (TBP), tributyrin, furan, and 4-methyl cyclohexanone.[2] From an analysis of these results, TBP, a common reagent in the hydrometallurgical and nuclear-processing industries, appears to offer significant potential advantages for removal of organics by solvent extraction. It is a high-boiling solvent, thereby lessening the energy requirement for distillation. Phenol and alkylated phenols can readily be recovered from TBP by distillation. Some means must be provided for removal of higher-boiling phenols from the solvent. Back-extraction into an aqueous base is a possibility for that purpose. Explorations of aqueous ammonia for regeneration of TBP revealed that it should be suitable for those phenols having a forward equilibrium distribution coefficient in the range of 10 to 20. Diluents, such as alcohols, can be used to control the magnitude of the forward distribution coefficient. TBP is also one of the more effective solvents for hydantoins.

Removal of Thiocyanate

Ion-exchange methods for removing thiocyanate have been investigated. Strong-base exchangers effectively remove thiocyanate but are difficult to regenerate. Weak-base exchangers afford a better and effective compromise between capacity and regenerability. Regeneration with aqueous ammonia and other bases has been investigated, and aqueous ammonium carbonate/bicarbonate solution has been identified as a potentially attractive regenerant.

Adsorption of Phenols

Research with adsorbents and polymeric sorbents is directed toward processes which would enable either bulk removal and recovery of organics, or final clean-up following other physicochemical processing methods. Full regenerability with a low energy requirement is a goal. Sorbents considered include conventional activated carbons, chemically treated carbons, and various types of synthetic polymeric resins, in both macroreticular and gel forms. We have initiated studies on the regenerability of phenols from activated carbons, on which there is conflicting information.

Isolation and Recovery of Ammonia

Removal of ammonia by stripping is energy intensive, because of the low pH (about 8.5) resulting from the simultaneous presence of carbon dioxide and hydrogen sulfide in condensate waters. We have been carrying out research on an innovative approach to this problem, wherein ammonia is extracted from condensate water while the acid gases, carbon dioxide and hydrogen sulfide, are simultaneously stripped. This greatly reduces the steam requirement for stripping and serves to isolate the ammonia as a product.

For this purpose, various liquid cation exchangers are being explored. In research so far, we have given the most attention to di-2-ethylhexyl phosphoric acid (D2EHPA) as extractant. Experiments include measurement of equilibrium distribution coefficients, water solubilities of extractants and complexes, phase-settling characteristics, regenerability, and degradation tendencies due to temperature and other chemical constituents. A recent publication describes this work.[4]

Phosphinic-acid extractants have lower acidity and potentially greater thermal stability than the organic phosphoric acids. These properties should make phosphinic acids more effective extractants for ammonia. Cyanex-272 (American Cyanamid Company) is a phosphinic acid extractant developed for the hydrometallurgical industry, where it has excellent properties for cobalt/nickel separation. This material, as supplied, contains substantial amounts of impurities which affect its extraction behavior. A purification method has been developed and utilized for large batches of Cyanex-272. Extraction experiments with Cyanex-272 have confirmed that it possesses near-optimal acidity for regenerable extraction of ammonia. This is evidenced by a sharp rise in the equilibrium distribution coefficient for ammonia at values of pH just below the values (8.0–9.5) typical of condensate waters.

PLANNED ACTIVITIES FOR FY 1986

After an initial literature survey, appropriate experiments will be carried out to reveal the factors determining the degree of reversibility of adsorption of phenol and phenolics on conventional activated carbons. On the basis of the results obtained, surface-treatment methods for carbons will be conceived and pursued. These will have the potential of enhancing the regenerability of phenol-laden carbons, while maintaining satisfactory adsorption capacity.

A literature survey will be made to determine functional groups capable of interacting specifically with phenols, with the interaction being strong enough to give good adsorption capacity, while being weak enough to allow facile regeneration. Polymeric sorbents having these groups will be obtained and/or synthesized and will be tested for their capability of giving regenerable bulk removal of phenolic solutes and/or regenerable final cleanup of condensate waters.

In situ equilibrium distribution coefficients will be measured for extraction of the compounds present in condensate water by means of MIBK and TBP as solvents. These will reveal complexation, micellization, adsorption onto suspended solids, or other complicating factors within the waters.

The properties of the phosphinic acid extractant, Cyanex-272, for extraction of ammonia will continue to be explored. The immediate concern is the thermal stability, as measured by the phosphorous content of an equilibrium aqueous phase, formation of degradation products, and/or loss of extraction ability. Necessary regeneration conditions will be the next item for attention.

Another possibility is to combine the extraction-based method for recovery and isolation of ammonia, on the one hand, with organics removal by means of the same extraction system. This potentially important synergism will be examined through experiments and process calculations.

Computer simulations of ammonia and acid-gas stripping will also be initiated, to give insight into other avenues that may be effective in reducing the energy requirement for removal and isolation of ammonia.

REFERENCES

1. Mohr, D.H. and King, C.J. (1985), "Identification of Polar Organic Compounds in Coal-Gasification Condensate Water by Gas Chromatography–Mass Spectrometry Analysis of High-Performance Liquid Chromatography Fractions," *Environ. Sci. & Technol. 19,* p. 929.
2. Senetar, J.J. and King, C.J. (1986), *Characterization and Treatment of Coal-Gasification Condensate Waters,* LBL-20988.
3. MacGlashan, J.D., Bixby, J.L., and King, C.J. (1985), "Separation of Phenols from Dilute Aqueous Solution by Use of Tri-n-Octyl Phosphine Oxide as Extractant," *Solvent Extraction & Ion Exchange 3,* p. 1.
4. Mackenzie, P.D. and King, C.J. (1985), "Combined Solvent Extraction and Stripping for Removal and Isolation of Ammonia from Sour Waters," *Ind. Eng. Chem. Process & Devel. 24,* p. 1192.

Separations of Polar Organics from Aqueous Solutions by Processes Based upon Reversible Chemical Complexation*

C.J. King, A.S. Kertes, D. Arenson, and J. Tamada

Separations for recovery of various polar organic substances from aqueous solution consume a large amount of energy industrially. Examples include the recovery of ethanol, butanol, acetic acid, glycols, phenols, adipic acid, sugars, and cornstarch products. The need for recovery of such substances will increase still further with the advent of bioprocessing technology, since most of the methods for production of chemicals from biomass generate the product(s) in dilute aqueous solution.

For the most part, these separations are presently accomplished by distillation and evaporation. Reversible chemical complexation provides a low-energy alternative to distillation and evaporation and should be particularly attractive for those solutes which are less volatile than (or comparably volatile to) water. This category includes all the solutes mentioned above. The use of reversible chemical complexation for separation trades upon selective and reversible chemical interaction between functional groups of the solute and the extractant. Many of these are of the Lewis acid–Lewis base (electron acceptor-donor) class.[1]

This project pursues development of chemical and engineering knowledge to enable rational interpretation and modeling of phase-equilibrium and transport mechanisms for such separations. On the basis of this knowledge, further goals are to develop rational criteria for complexation reagents, to develop suitable methods for regeneration and process integration, and to define the most likely applications.

Solutes of particular interest are carboxylic acids, alcohols, and multifunctional compounds containing the -COOH and -OH groups. Carboxylic acids are chosen because of their importance as fermentation products and because it is already known that association with tertiary amines or phosphoryl compounds can provide an effective means of separation. Alcohols, glycols, and related solutes containing -OH groups are chosen because they account for a large fraction of U.S. energy expended for separations and recovery of polar organics from water, and because of their future importance.

The initial phases of the project have dealt with (1) a literature survey of pertinent chemical information for extraction of carboxylic acids and alcohols, (2) measurement and chemical modeling of phase-equilibrium behavior for extraction of carboxylic acids by amine extractants in various diluents, and (3) exploratory measurements designed to identify classes of reagents which may be most attractive for association with alcohols.

*This work was supported by the Assistant Secretary for Conservation and Renewable Energy, Office of Energy Systems Research, Energy Conservation and Utilization Technologies Division of the U.S. Department of Energy under Contract No. DE-AC03-76SF00098.

ACCOMPLISHMENTS DURING FY 1985

Extraction of Carboxylic Acids

A critical survey has been made of the literature covering the chemistry of extraction of carboxylic acids from aqueous solution.[2] This survey covers the acids involved in the pyruvic/tricarboxylic cycle of glucose fermentation, and includes lactic, succinic, tartaric, propionic, citric, pyruvic, fumaric, maleic, malic, and itaconic acids. It includes extraction with hydrocarbon and carbon-oxygen solvents, phosphoryl extractants, and amines.

Experimental measurements have focussed upon the extraction of succinic acid by Alamine 336 (Henkel Corporation—a tertiary amine mixture, with 8 to 10 carbon alkyl groups) in various diluents. Figure 1 shows data for the concentration-based equilibrium distribution coefficient of succinic acid, extracted from water into a solvent mixture of Alamine 336 and methyl isobutyl ketone (MIBK). These equilibrium distribution coefficients are high enough to be of considerable potential industrial interest.

As is evidenced by Fig. 1, the extraction behavior is complex. The pertinent effects appear to include (1) complexation between the amine and the acid, (2) complexation of the first complex with additional acid molecules, facilitating the extraction further, and (3) solvation of these acid-amine complexes by the diluent (MIBK).

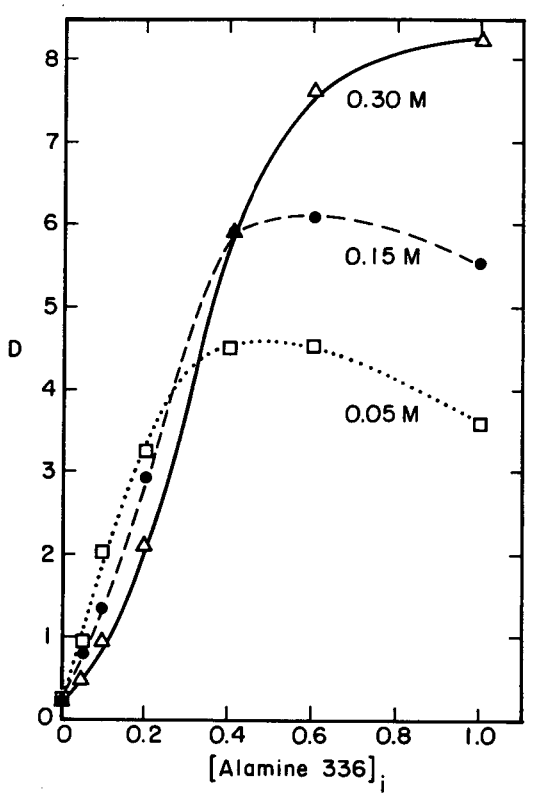

Figure 1. (XBL 862-714)

Similar data obtained with chloroform as diluent show much higher distribution coefficients, probably resulting from stronger solvation of the complexes by the Lewis acid, chloroform.

Experiments carried out for extraction of succinic acid by tri-n-octyl phosphine oxide (TOPO) in MIBK diluent gave much lower values of the equilibrium distribution coefficient, increasing from 0.5 to 1.85 as the molar ratio of TOPO to succinic acid was increased from 1.25 to 5 with a solvent composed of 0.346 molar TOPO in MIBK. TOPO is a strong hydrogen bonding Lewis base. It appears that the ability of the tertiary amines to form an ion pair is an important factor causing them to be more effective extractants than TOPO for succinic acid.

Extraction of Alcohols

A critical and thorough literature survey has been made of the extraction chemistry and solution properties of the lower aliphatic alcohols (methanol, ethanol, propanol, isopropanol, and the four butanols). This study reveals a number of subtle and complex interactions in both aqueous and organic solutions, which can form the basis for generation of improved methods of extraction. Preliminary results of this survey were presented at a DOE conference in October 1985,[3] and the full manuscript is being readied for publication.

From this review and from previous explorations made in our group,[4] the higher alcohols and carboxylic acids have been found to give more attractive combinations of distribution coefficient and selectivity for extraction of ethanol from water than do other common solvents. Extending the resulting concept of strong hydrogen-donor solvents, we have investigated the various isomers of cresol, in various diluents, as extractants for ethanol.

Cresol isomers have been found to give weight-fraction-based equilibrium distribution coefficients around 2.0, which is a very encouraging result. None of the other common solvents gives equilibrium distribution coefficients above 1.0.[4] Noninteracting diluents reduce the equilibrium distribution coefficient in rough proportion to cresol concentration. However, chloroform as a diluent is synergistic, giving distribution coefficients that remain high for solvent mixtures composed of m-cresol and chloroform. Apparently the electron-acceptor characteristic of chloroform serves to solvate the cresol-ethanol complex and/or encourage its formation.

Another strong acid, di-2-ethylhexyl phosphoric acid (D2EHPA) in an alkane diluent, gave rather low equilibrium distribution coefficients for extraction of ethanol. Presumably, the effectiveness of this extractant is hampered by extensive dimerization of the acid in the organic phase. Furthermore, hydrogen-bonding ability is probably a more important form of acidity than is proton ionization for interaction with the alcohol group.

PLANNED ACTIVITIES FOR FY 1986

Extraction of Carboxylic Acids

Chemical modeling is being used for interpretation of the data for extraction of succinic acid by tertiary amine extractants in various diluents. Computer approaches are being implemented for determining the most important complexes and for fitting chemical parameters to experimental data. These methods will be used for our earlier data on extraction of acetic acid by amine-containing solvent mixtures, as well, in order to provide a basis for comparison.

Methods of regeneration of acid-amine extracts will also be explored.

Extraction of Alcohols

Experiments with phenolic extractants will be continued, with different diluents, including chemically active ones. The aims are to determine the most effective phenolic extractants, to establish effective diluents, to assess necessary regeneration conditions, to determine the effect of temperature on the equilibrium, and to interpret experimental results through chemical modeling.

The review of extraction chemistry of alcohols revealed that there are significant effects of isomeric alcohol structures. So as to provide more information on this effect, a series of measurements will be made to determine phase equilibria for extraction of the four isomeric butanols from aqueous solution by means of cresol in an alkane diluent. These results will be interpreted in terms of aqueous and organic phase effects, individually.

Adsorption

Chemical complexation can also be used in separations carried out by adsorption, through the inclusion of specific functional groups on the adsorbent surface, or within a penetrable polymeric sorbent. Preliminary studies will be made of the attractiveness of this approach for recovery of carboxylic acids, alcohols, and glycols from aqueous solution. As an initial step, the efficacy of polymeric resins containing the phenolic -OH group for sorption of alcohols will be examined.

REFERENCES

1. King, C.J. (1986), "Separation Processes Based upon Reversible Chemical Complexation," plenary lecture at Tenth Interamerican Congress of Chemical Engineering, Santiago, Chile, November 1983; *Handbook of Separation Process Technology*, R.W. Rousseau, Ed., Wiley, New York, in press.
2. Kertes, A.S. and King, C.J. (1985), "Extraction Chemistry of Fermentation-Product Carboxylic Acids," presented at 189th Amer. Chem. Soc. Natl. Mtg., Miami, FL, April 1985; *Biotechnol. Bioeng.*, February 1986.
3. King, C.J., Munson, C.L., and Kertes, A.S. (1985), "Extraction of Ethanol from Aqueous Solutions," presented at DOE/ORNL Conference on Separation Science and Technology for Energy Applications, Knoxville, TN, October 1985.
4. Munson, C.L. and King, C.J. (1983), *Ind. Eng. Chem. Process Des. & Devel. 23*, p. 109.

Jet Breakup Enhanced by an Initial Pulse*

D.W. Bousfield and M.M. Denn

The breakup of a liquid jet following an initial finite periodic disturbance of the nozzle exit velocity was analyzed using a nonlinear thin filament theory. Breakup occurs over two distinct time scales, the second of which is characterized by the growth rate calculated from linear stability theory. An approximate analysis of the kinematics during the first time scale enables an analytical prediction of the breakup time.

The surface tension–driven breakup of a filament into droplets was first analyzed by Rayleigh,[1] who calculated the growth rate of an infinitesmal disturbance in the absence of viscosity; the growth of disturbances on Newtonian liquid filaments has subsequently been reviewed by Bogy[2] and McCarthy and Molloy.[3] The growth rate of an infinitesmal disturbance on a viscoelastic liquid filament was computed by Goldin *et al.*[4] and Middleman.[5] Bousfield and coworkers[6,7] have used both one-dimensional asymptotic analysis and a transient finite element method to analyze the growth and ultimate breakup of disturbances that attain finite size on Newtonian and viscoelastic liquid filaments, showing good agreement with experiments; these analyses follow in the tradition established by Rayleigh and subsequent workers, in that the frame of reference is imbedded in the moving filament and temporal growth of an initially small disturbance is studied without regard to possible flow rearrangement associated with the exit from a nozzle.

There is some interest in analyzing filament breakup and droplet formation following the imposition of a large periodic axial velocity at the nozzle; a large velocity pulse using a positive displacement device has been proposed, for example, as a means of controlling droplet size and breakup time in a Kraft recovery furnace for efficient combustion of black liquor.[8] The one-dimensional asymptotic analysis formulated by Bousfield *et al.*[6,7] is well suited for studying this problem, since any initial conditions can be accommodated. In contrast to the usual studies of disturbance growth, we assume here that the filament is of constant radius R_o at time $t = 0$, but is subjected to an initial mean axial velocity

$$(z,o) = v_o \sin(\pi z/L) \quad , \tag{1}$$

where L is the half-wavelength of the induced velocity and v_o is the magnitude of the velocity pulse relative to the mass average exit velocity of the jet. The following parameters appear in the analysis for a Newtonian fluid:

$$\alpha = \frac{R_o}{L} \quad , \tag{2a}$$

$$\beta = \frac{\rho\sigma L^2}{\eta^2 R_o} \quad , \tag{2b}$$

$$U_o = \frac{v_o \eta R_o}{\sigma L} \quad , \tag{2c}$$

where η is the viscosity, ρ is the density, and σ is the surface tension of the Newtonian liquid. $U_o\beta = v_o\rho L/\eta$ is a Reynolds number based on the maximum pulse velocity and disturbance half length. Dilute polymer solutions are further characterized by a polymer relaxation time λ_p and a solution retardation time λ_r, which appear in two additional dimensionless groups:

$$\phi = \frac{\lambda_p \sigma}{\eta R_o} \quad , \tag{2d}$$

$$\Lambda = \frac{\lambda_r}{\lambda_p} \quad , \tag{2e}$$

ACCOMPLISHMENTS DURING FY 1985

Breakup Characteristics

The thin filament analysis is described in detail elsewhere[7] and only results are presented here. The calculations shown on different time scales in Figs. 1 and 2 are typical of all cases studied for Newtonian liquids; the parameters here are $\alpha = 0.16$, $\beta = 1.8$, and $U_o = 1.67$, corresponding to $R_o = 0.5$ mm, $L = 3.14$ mm, and $v_o = 0.47$ m/s, with fluid properties $\eta = 0.67$Pa s, $\rho = 1350$ Kg/m^3, and $\sigma = 0.03$ N/m. There is a very rapid decrease in the minimum radius R_{min}, followed by an approach to a straight line on a semi-logarithmic plot of $(R_o - R_{min})/R_o$. As we shall show subsequently, the

*This work was supported by the U.S. Army, ARRADCOM, under Agreement No. 3311-1412 through the U.S. Department of Energy under Contract No. DE-AC03-76SF00098.

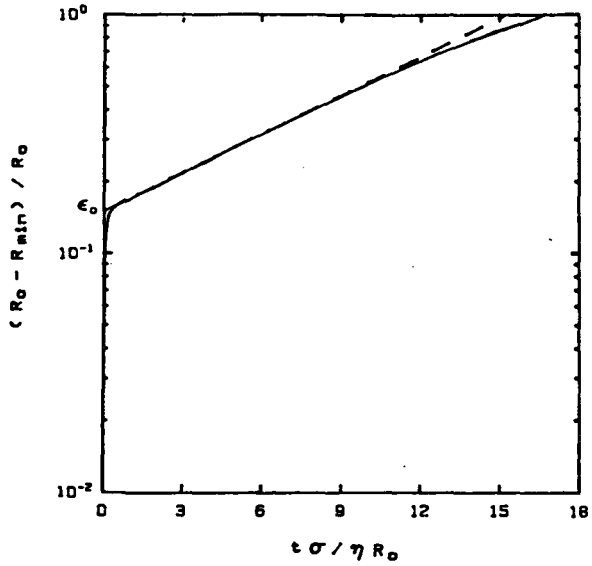

Figure 1. Disturbance growth for $\alpha = 1.8$, $\beta = 1.8$, and $U_0 = 1.67$. The slope of the dashed line is the growth rate from linear stability theory. (XBL 862-715)

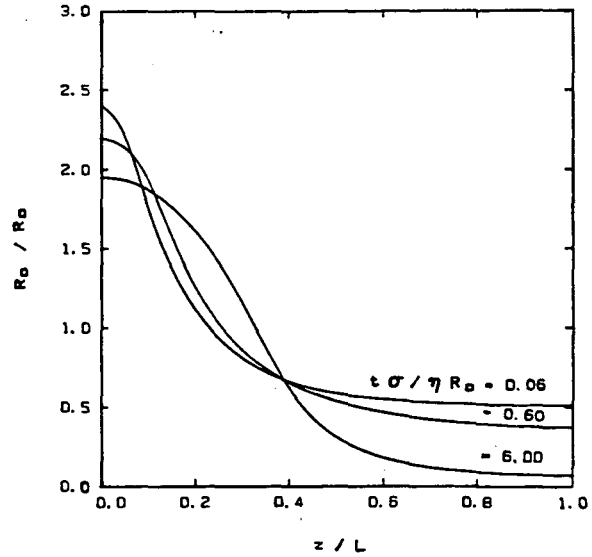

Figure 3. Radius profiles for the calculations of Figs. 1 and 2. (XBL 862-717)

response in this first region is inertially determined and independent of surface tension; the relevant time scale is therefore that appropriate to viscous transport over a length L: $\rho L^2/\eta$. The slope of the dashed straight line is the growth rate given by the linear stability theory for surface tension-driven growth of infinitesmal disturbances, which is close to 0.07 for these values of α and β; the relevant time scale here is $\eta R_0/\sigma$. It is remarkable that the growth rate of this nonlinear process is given so accurately after the initial transient by a linear growth rate. Breakup occurs when $(R_0 - R_{min})/R_0$ reaches unity; deviation from the linear solution is small even approaching breakup. The shape profiles for this case are shown in Fig. 3, where it is obvious that the disturbance relative to the undeformed cylinder ($R = R_0$) is large.

When inertia is an important factor in the sur-

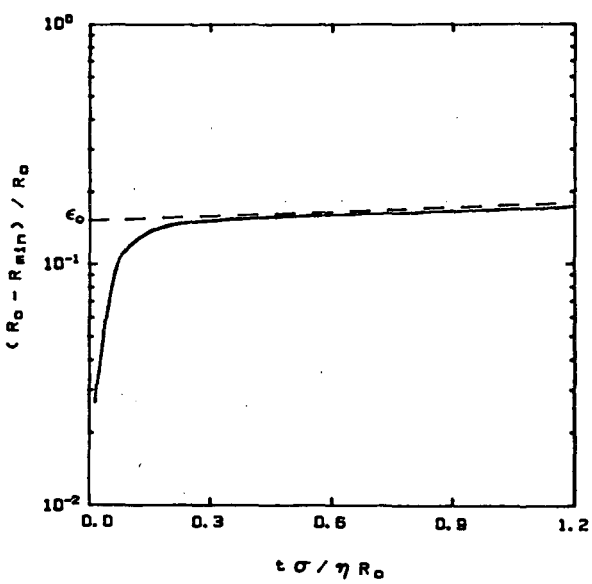

Figure 2. Same as Fig. 1, but over a fifteen-fold longer time scale. Breakup occurs when $(R_0 - R_{min})/R_0$ equals unity. (XBL 862-716)

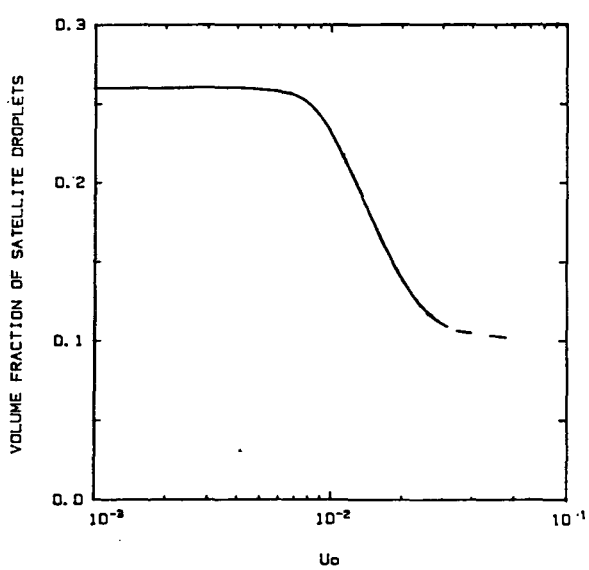

Figure 4. Volume fraction of satellite drop as a function of pulse velocity; $\alpha = 0.08$, $\beta = 1890$. (XBL 862-718)

face tension-driven breakup process (large β), the filament breaks up into primary and satellite droplets. The asymptotic thin filament theory predicts the experimentally observed primary and satellite droplet sizes for small disturbances very well as a function of imposed disturbance wavelength.[7] According to the theory, a large initial velocity ($\beta u_o \sim 10$) supresses the formation of satellite droplets relative to the primary droplet when α is small. A typical calculation is shown in Fig. 4 for $\alpha = 0.08$, $\beta = 1890$; these are parameter values typical of experiments on glycerol-water jets. The satellite droplet size at high values of U_o is not well-characterized because of the difficulty in representing a highly distorted filament with finite differences, but the effect is clear.

The response of a viscoelastic fluid is similar to that of a Newtonian fluid, in that there are responses over two distinct time scales. A typical response is shown in Fig. 5, where the parameters are the same as those in Figs. 1 through 3, except that $\phi = 0.18$ and $\Lambda = 0$ (a "Maxwell fluid"). The response over the time scale $\rho L^2/\eta$ now includes a damped oscillation; as discussed below, this is the typical inertial response of an underdamped viscoelastic material. Following the initial short-time response, the response over the time scale of order $\eta R_o/\sigma$ follows the linear theory for a viscoelastic liquid.[4,5] The linear theory approximates the disturbance growth until breakup for parameter values studied in this work, but it is known[7] that for sufficiently large values of ϕ (depending on Λ) the breakup is

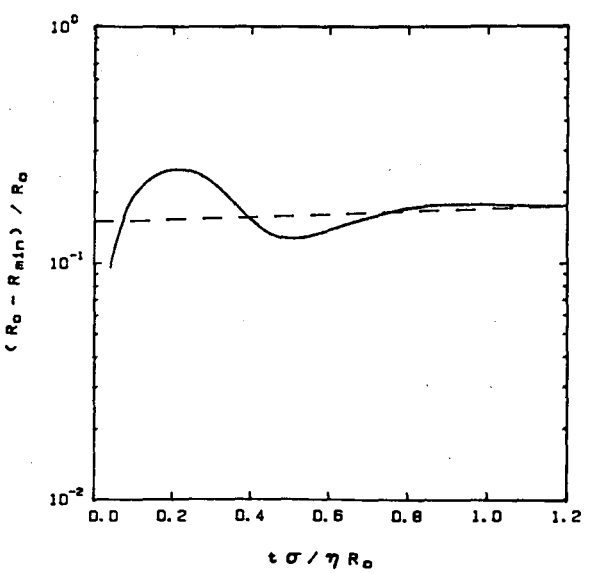

Figure 5. Disturbance growth for a viscoelastic liquid for the conditions in Fig. 1, but with $\phi = 0.18$ and $\Lambda = 0$. (XBL 862-719)

governed at long times by viscoelastic nonlinearities and that the breakup time can be of a different order of magnitude from that computed by linear theory.

Analytical Estimates

The computed results suggest an approximation procedure that can enable analytical solutions for the breakup time. Following the initial transient, the disturbance growth is closely approximated by linear theory until breakup. The linear growth rate is known analytically. If it were possible to estimate the intercept (denoted ϵ_o in Figs. 1 and 2), then the time (or time-of-flight) to breakup could be estimated analytically in terms of geometry, fluid properties, and the maximum velocity v_o and half wavelength L of the positive displacement device.

A rough estimate of ϵ_o, which is surprisingly accurate for Newtonian liquids, can be obtained in the following way. The velocity perturbation imposed at time $t = 0$ will initially die out because of viscous dissipation; the interaction of inertial and viscous stresses occurs on a time scale $\rho L^2/\eta$, which is usually much less than the time scale $\eta R_o/\sigma$ for surface tension–driven flows. Linear stability theory would predict the axial velocity decay to occur as

$$v(z,t) = -\, v_o \sin(\pi z/L) \exp(-3\pi^2\eta t/\rho L^2) \ . \quad (3)$$

The area-averaged continuity equation expressed in terms of the radius R(z,t) is

$$\frac{\partial R}{\partial t} = -\frac{R}{2}\frac{\partial v}{\partial z} - v\frac{\partial R}{\partial z} \ . \quad (4)$$

Equation (4) can be solved exactly if we take Eq. (3) as the expression for the velocity. The solution so obtained remains finite only at $z = L$ (the minimum) or $z = 0$ (the maximum), but not both, and it is inconsistent with the assumed uniform initial radius. It nevertheless appears to give a reasonable description of the short-time response in the neighborhood of the minimum, $z = L$. The solution that is finite at $z = L$ is

$$R(z,t) = \frac{\text{constant}}{(1 - \cos \pi z/L)^{1/2}} \exp\left[-\frac{\beta U_o}{6\pi} + \frac{\beta U_o}{6\pi}\exp(-3\eta\pi^2 t/\rho L^2)\right] . \quad (5)$$

This function approaches a limit for $t \gg \rho L^2/3\pi^2\eta$; we thus obtain

$$\epsilon_o = 1 - \frac{R(z,\infty)}{R(z,0)} = 1 - \exp(-\beta U_o/6\pi) \quad . \quad (6)$$

Equation (6) is plotted in Fig. 6, together with the values of ϵ_o obtained by extrapolating the semi-logarithmic region of the growth curve to $t = 0$ for $\alpha = 0.16$, $\beta = 1.8$ (the conditions shown in Figs. 1–3 for $U_o = 1.67$). Agreement is quite good up to a predicted initial perturbation of 0.4, and probably adequate at still higher pulsing velocities. Since the linear theory of surface tension-driven instabilities predicts the breakup time quite well for given initial perturbation ϵ_o, a completely analytical estimate of the breakup time or time-of-flight is thus available.

The equivalent result for a dilute polymer solution is obtained by replacing the coefficient of time, $-3\pi^2\eta/\rho L^2$, in Eqs. (3) and (5) with $-\gamma$, where γ is the root of

$$\frac{\gamma(1 + \lambda_p\gamma)}{1 + \Lambda\lambda_p\gamma} = -\frac{3\pi^2\eta}{\rho L^2} \quad . \quad (7)$$

This quadratic equation will have complex roots whenever the discriminant

$$\text{dis} = \frac{12\eta\pi^2\lambda_p}{\rho L^2} - \left[1 + \frac{3\eta\pi^2\Lambda\lambda_p}{\rho L^2}\right]^2 \quad (8)$$

is positive, with a period of oscillation given by

$$T = 4\pi\lambda_p/(\text{dis})^{1/2} \quad . \quad (9)$$

This short-time behavior is seen in the complete thin filament calculations in Fig. 5. The damped oscillatory response to an initial deformation is characteristic of the inertial response of viscoelastic liquids; see the squeeze flow analysis of Lee et al.[9] for example.

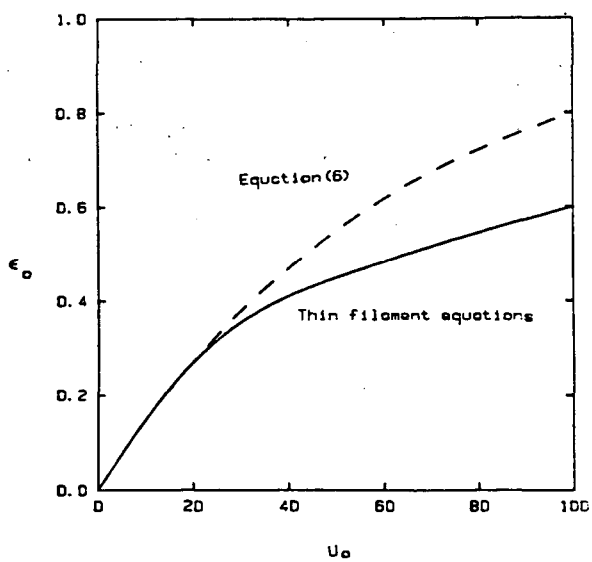

Figure 6. ϵ_o as a function of U_o. The broken line is the analytical estimate from Eq. (6). (XBL 862-720)

Conclusion

The observation that the disturbance following a finite pulse grows over two distinct time scales, and that the second of these is characterized by the linear growth rate for a surface tension-driven disturbance, enables an analytical estimate of the breakup time or time-of-flight. Together with Eq. (6), we therefore have a closed form algebraic design equation for the breakup length of jets in which the finite initial disturbance is imposed by an oscillating positive displacement device.

PLANNED ACTIVITIES FOR FY 1986

Work in FY 1986 will focus on the use of transient finite element methods for analyzing the growth and deformation of inviscid inclusions in polymeric liquids in which the far field is extensional.

ACKNOWLEDGEMENT

This problem was first brought to our attention by I.H. Stockel. We have had helpful conversations with G. Marrucci.

NOTATIONS

L	half wavelength of disturbance
R	filament radius
R_o	initial filament radius
t	time
T	period of oscillation
U_o	dimensionless peak velocity
v	averaged axial velocity
v_o	initial axial peak velocity
z	axial coordinate
α	dimensionless geometric parameter
β	dimensionless fluid properties
γ	linear analysis growth factor
ϵ	dimensionless disturbance magnitude
ϵ_o	effective initial disturbance
η	fluid viscosity
Λ	ratio of relaxation and retardation times
λ_p	polymer relaxation time
λ_r	retardation time
ρ	fluid density
σ	surface tension
ϕ	dimensionless relaxation time

REFERENCES

1. Rayleigh, Lord (1879), "On the Capillary Phenomena of Jets," *Proc. Royal Soc. Lond. A29*, p. 71.
2. Bogy, D.B. (1979), "Drop Formation in a Circular Liquid Jet," *Ann. Rev. Fluid Mech. 11*, p. 207.
3. McCarthy, M.J. and Molloy, N.A. (1974), "Review of Stability of Liquid Jets and the Influence of Nozzle Design," *Chem. Eng. J. 7*, p. 1.
4. Goldin, M., Yerushalmi, J., Pfeffer, R., and Shinnar, R. (1969), "Breakup of a Laminar Capillary Jet of a Viscoelastic Fluid," *J. Fluid Mech. 38*, p. 689.
5. Middleman, S. (1965), "Stability of a Viscoelastic Jet," *Chem. Engng. Sci. 20*, p. 1037.
6. Bousfield, D.W., Marrucci, G., and Denn, M.M. (1984), "Dynamics of Liquid Filament Breakup," *Proc. IX Intl. Congress on Rheology 2*, p. 239.
7. Bousfield, D.W., Keunings, R., Marrucci, G., and Denn, M.M. (1986), "Nonlinear Analysis of the Surface Tension-Driven Breakup of Viscoelastic Filaments," *J. Non-Newtonian Fluid Mech. 21*, p. 79.
8. Stockel, I.H. (1985), "Research on Droplet Formation for application to Kraft Black Liquors," DOE technical report DOE/CE/40626-T1.
9. Lee, S.J., *et al.* (1984), "Compressive Flow Between Parallel Disks: II. Oscillatory Behavior of Viscoelastic Materials Under a Constant Load," *J. Non-Newtonian Fluid Mech. 14*, p. 301.

Removal of H_2S from Coal-Derived Synthesis Gas*

R. Hix, S. Lynn, D. Neumann, S. Sciamanna, and C. Stevens

When coal is gasified, most of the organic sulfur is converted to hydrogen sulfide and must be removed before the gas can be utilized either as a fuel or as synthesis gas. Similarly, most sources of natural gas contain H_2S, as do many refinery gases. The problem of removing the hydrogen sulfide varies with the nature of the gas that has been produced and with the purpose to which the gas is to be put. In some cases one wishes to remove only hydrogen sulfide, in others one wishes to remove carbon dioxide as well, and in still others there are hydrocarbons that can profitably be recovered as separate products. The UC Berkeley Sulfur Recovery Process (UCBSRP) is a new approach to this problem being developed at the Lawrence Berkeley Laboratory that consists of

- absorbing the hydrogen sulfide in a polar organic solvent;
- converting the dissolved hydrogen sulfide to sulfur by reacting it with an equivalent amount of sulfur dioxide dissolved in the same solvent;
- recovering co-absorbed gases from the solvent by stripping;
- recovering elemental sulfur from the solvent by crystallization; and
- generating the sulfur dioxide for the process by burning hydrogen sulfide or sulfur, recovering heat from the combustion gas in a waste-heat boiler, and recovering SO_2 by scrubbing the gas with cooled solvent from the crystallization step.

The overall objectives of this project are to obtain the physical and chemical data needed to design process configurations that utilize the steps enumerated above, and to evaluate these process configurations to determine their economic potential. The work to meet these objectives has been subdivided into the following tasks:

- To determine the solubilities of H_2S, SO_2, CO_2, CH_4 and other hydrocarbon gases, water, and sulfur in the organic solvent as functions of pressure, temperature, and solvent composition;
- To determine the effects of temperature and solvent composition on reaction kinetics;
- To investigate the suitability of steel and other materials of construction for this system;
- To determine the parameters controlling

*This work was supported by the Assistant Secretary for Fossil Energy, Office of Coal Utilization, Division of Surface Coal Gasification, of the U.S. Department of Energy under Contract No. DE-AC03-76SF00098.

the crystal size distribution of sulfur so that crystals of 100 microns or greater will be formed in the process;

- To determine the parameters controlling reactive absorption of hydrogen sulfide by solutions containing sulfur dioxide;
- To set up a computer model of this process to aid in its evaluation and evolution; and
- To compare the anticipated costs of this process with those of conventional technology.

ACCOMPLISHMENTS DURING FY 1985

The gases of interest in the UCBSRP are SO_2, H_2S, CO_2, propane, and butane. The solvents of interest are characterized by low vapor pressure, miscibility with water, and good solvating power for these gases. The following polyglycol ethers are currently under investigation:

- Diglyme: Diethylene glycol dimethyl ether,
- Triglyme: Triethylene glycol dimethyl ether,
- Tetraglyme: Tetraethylene glycol dimethyl ether,
- Dowanol DM: Diethylene glycol methyl ether,
- Dowanol TBH: Triethylene glycol butyl ether.

Also of interest is the effect of water on the solubilities of gases in these solvents.

The solubility of SO_2 in these solvents was determined first, and a paper based on this work was published recently.[1] The results obtained for H_2S, CO_2, and propane to date are given in Table 1. As seen from the uncertainties on the coefficients, the experimental technique is quite reproducible. For comparison purposes Table 2 shows Henry's Law values for these three gases at 25°C expressed on a weight fraction basis. The lower glymes have a slightly higher capacity for dissolved gases than do the higher glymes. The diethers are generally better than the monoethers as solvents for these gases. The effect of temperature on solubility is such that at 100°C Dowanol DM (a monoether) is slightly better than tetraglyme (a diether). Also, the selectivity for H_2S relative to CO_2 is greater at 25°C than at 100°C for all of the solvents. Propane solubility is somewhat higher than carbon dioxide solubility in these solvents. In Dowanol TBH, the tert-butyl ether of diethylene glycol, the solubility of propane is almost double that of CO_2 because of the increased aliphatic character of this solvent.

Table 1. Constants for Henry's law correlation for H_2S and CO_2 in organic solvents. $H = \exp [A/T + B]$.[a]

	H_2S	
Solvent	A	B
Diglyme	−2095.9 ± 1.8%	13.483 ± 0.8%
Triglyme	−2147.2 ± 3.4%	13.443 ± 1.5%
Tetraglyme	−2257.1 ± 0.4%	13.616 ± 0.2%
Dowanol DM	−1943.2 ± 1.0%	13.255 ± 0.4%
Dowanol TBH	−1817.2 ± 1.7%	12.500 ± 0.7%
	CO_2	
Solvent	A	B
Diglyme	−1378.0 ± 1.7%	12.829 ± 0.6%
Triglyme	−1370.7 ± 0.2%	12.729 ± 0.1%
Tetraglyme	−1363.7 ± 4.0%	12.581 ± 1.0%
Dowanol DM	−1250.8 ± 2.5%	12.971 ± 0.6%
	Propane	
Solvent	A	B
Triglyme	−1325.2 ± 1.14%	12.130 ± 0.44%
Tetraglyme	−1238.6 ± 2.01%	11.824 ± 0.43%
Dowanol DM	−1135.1 ± 0.02%	12.465 ± 0.48%
Dowanol TBH	−1414.3 ± 0.19%	12.342 ± 0.20%

[a]H = kPa/mole fraction, T = Kelvin.

Table 2. Henry's law values at 25°C for gases in organic solvents (MPa/Wt. fraction).

Solvent	H_2S	CO_2
Diglyme	2.50	11.18
Triglyme	2.69	13.77
Tetraglyme	2.75	15.16
Dowanol DM	2.97	17.67
Dowanol TBH	4.10	19.48

A detailed study of the catalysis of the reaction between H_2S and SO_2 by N,N-dimethyl aniline (DMA) in polyglycol ethers was reported at the ACS meeting in Philadelphia in August, 1984, and will be published shortly.[2] The reaction is first-order with respect to both reactants. The reaction-rate constant exceeds 10 liters/mole-s at ambient temperature when the DMA content is 10 wt%, so that reaction is substantially complete in less than 10 seconds. A study now in progress shows that the same rate constant is found at the 1-wt% level for many heterocyclic nitrogen compounds.

A computer program that simulates the complete process is nearing completion. The program subroutines for each of the unit operations work well; the remaining programming effort will determine the most effective method for linking the subroutines for a complete simulation. The program is currently being used to test alternative process configurations. It utilizes all of the physical and chemical data that have been obtained to date and will be expanded to use new results as they are obtained.

A comparative study is being made of one application of the UCBSRP. The gas to be treated is the recycle stream from a high-pressure (2000 psia) hydrodesulfurization plant (Fig. 1). It is primarily hydrogen but also contains light hydrocarbons as well as H_2S. The flowsheet for this application is shown in Fig. 2. Co-absorbed gases are compressed and sweetened for delivery to the refinery's fuel gas system. The stack gas from the process is to contain about 10 ppm SO_2. The scale of operation is 100 long tons of sulfur per day. The flowsheet for conventional technology to accomplish the same treatment is shown in Fig. 3. A diethanol amine absorber-stripper operation feeds H_2S to a Claus plant that is followed by a SCOT tail-gas clean-up unit.

Comparison of the two flowsheets shows that there are significantly fewer unit operations in the UCBSRP. The capital costs for the two processes were estimated from the purchased costs of the major items of equipment. The capital for the UCBSRP is about 60% that for the conventional technology. The energy equivalent of the electricity and low-pressure steam for the UCBSRP will be less than the energy in the high-pressure steam produced, whereas the conventional process is a substantial net energy consumer.

The process configuration for the UCBSRP will vary with process conditions. Different flowsheets would be used in the treatment of gas streams at pressures of 100 to 600 psia and at near-atmospheric pressure. Examples of these are being developed with the aid of the computer model.

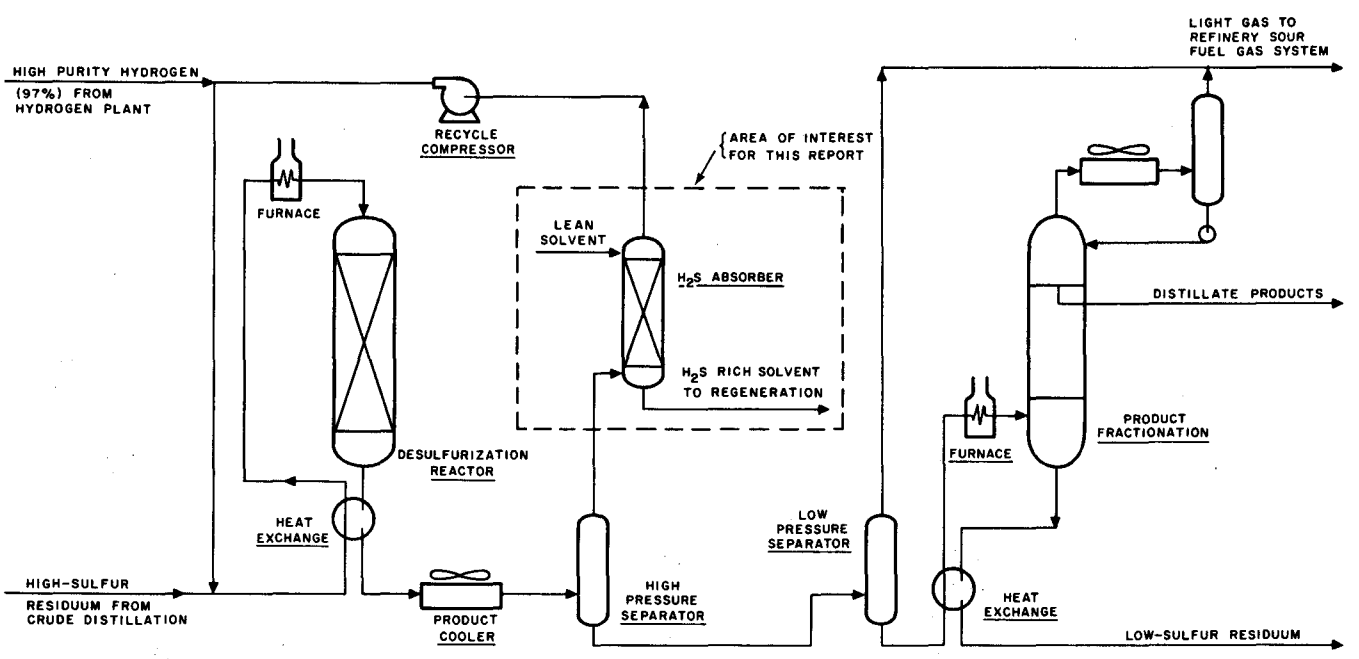

Figure 1. Simplified process flow diagram, residuum desulfurization process. (XBL 861-340)

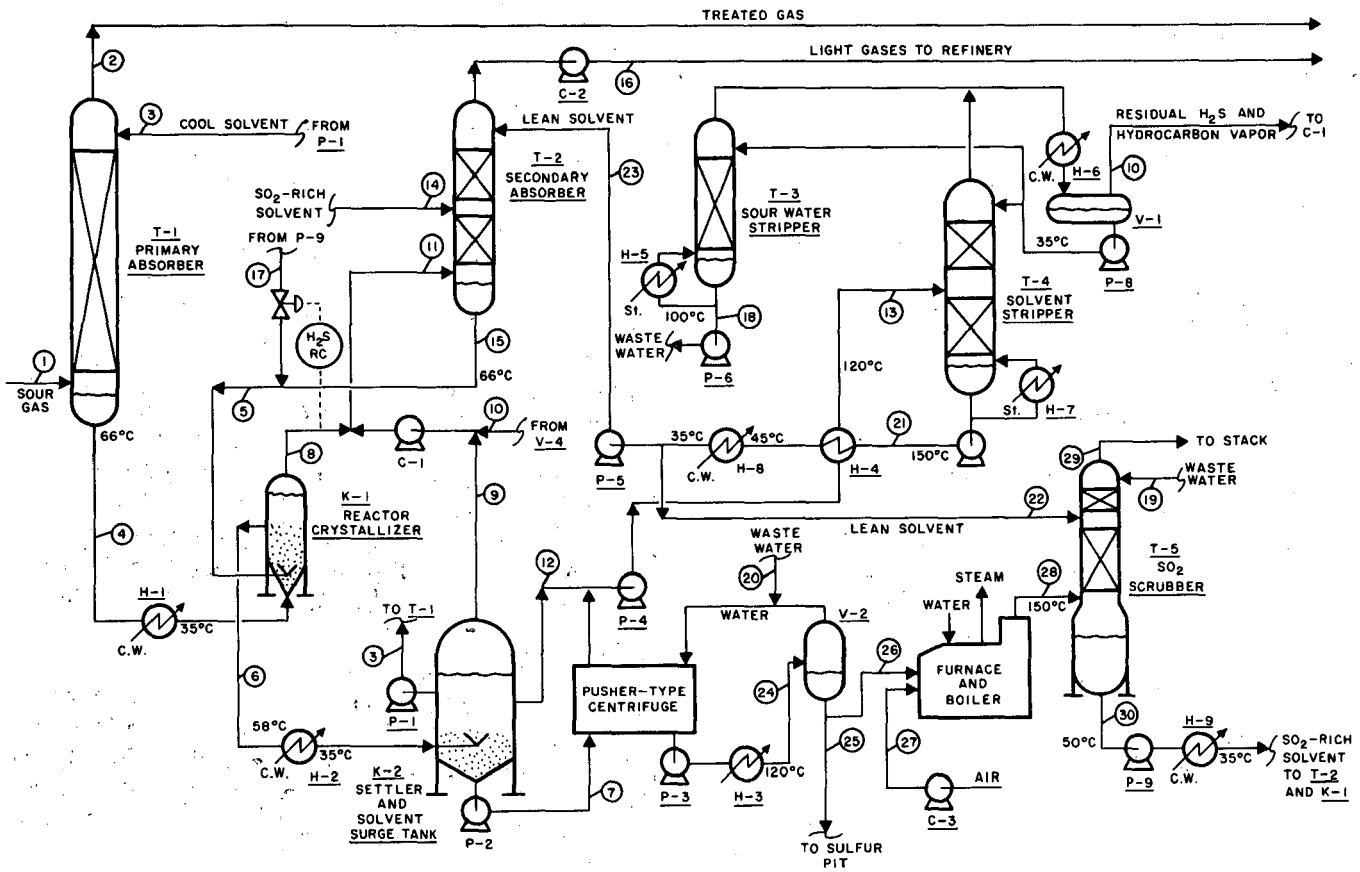

Figure 2. Process flow diagram, UCB sulfur recovery process. (XBL 861-341)

PLANNED ACTIVITIES FOR FY 1986

The determination of gas solubilities is nearly completed. The final solute gas will be butane. Determining the effect of water on the solubilities of H_2S, SO_2, and propane in one monoether and one diether will complete the study.

The study of reaction kinetics at ambient temperature will be completed in the first half of the current fiscal year. New equipment and a different experimental procedure are needed to study the reaction at elevated temperatures and in very dilute solutions. Work on this project is just starting.

Short-term corrosion studies have found no perceptible attack on any of the metals tested. Long-term studies at elevated temperatures are now being prepared.

The equipment for studying the factors controlling crystal size distribution has been assembled, and experimentation will start in January, 1986.

The theory for modeling absorption with chemical reaction when both reactants are volatile is being developed. It will be used in the interpretation of the experiments that will also start in January.

Computer modeling and cost analysis of the UCBSRP will continue during the fiscal year.

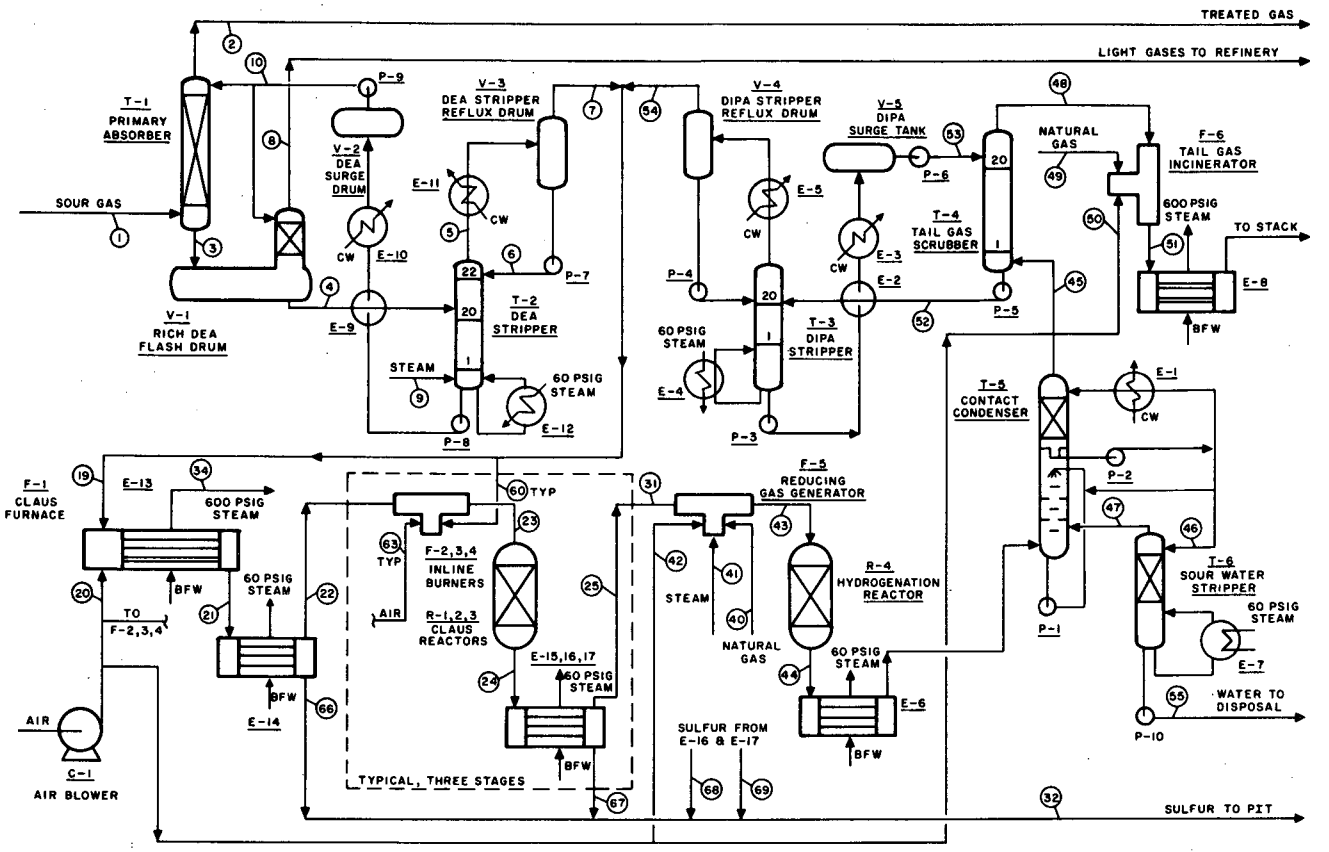

Figure 3. Process flow diagram, conventional processing. (XBL 861-342)

REFERENCES

1. Demyanovich, R.J. and Lynn, S. (1985), "Use of a Polar Organic Solvent to Control Emissions from a Sulfuric Acid Plant," in *Processing and Utilization of High Sulfur Coals*, Y.A. Attia, Ed., Elsevier Science Publishers, Amsterdam.
2. Neumann, D.W. and Lynn, S. (1986), "The Kinetics of the Reaction of Hydrogen Sulfide and Sulfur Dioxide in Organic Solvents," *I&EC Process Design and Development 25* (in press).

Production of Sugars from Cellulose: The Kinetics of Endoglucanase in Cellulose Hydrolysis*

(This article has been reprinted from the FY 1984 Annual Report.)

B. Elzufon, D. Wiley, H. Blanch, C. Wilke, and A. Sciamanna

The research of the Biochemical Process Group has focused on the hydrolysis of lignocellulosic materials to sugars and their subsequent fermentation by yeast to ethanol and other fuel-grade chemicals. Various studies have examined the kinetics of enzymatic hydrolysis of cellulose and hemicellulose fractions for optimal sugar production, the physical and chemical nature of the raw materials, the optimal production and recovery of enzymes, and the use of new organisms for converting polymeric pentosans and hexosans to sugars.

Cellulase is composed of three individual enzymes that function synergistically to break down cellulose. An overall kinetic model of cellulase behavior is being developed based on models of the behavior of the individual enzymes. In this article, an effort to develop a kinetic model of endoglucanase, one of the three cellulase enzymes, is reported.

ACCOMPLISHMENTS DURING FY 1984

A modified viscometric technique was developed to assay endoglucanase activity and was used to determine its kinetic parameters. Endoglucanase was found to be more active in its pure form than as part of the cellulase system. This may be due to the accumulation of cellobiose, a product of cellobiohydrolase, which inhibits endoglucanase. The influence on endoglucanase activity of cellobiose and glucose, known inhibitors of cellulase, was also studied. Cellobiose was found to inhibit endoglucanase via partial mixed-type inhibition. Glucose, however, was found to be a nonessential activator of endoglucanase.

An analytical technique was developed to measure enzyme activity that takes advantage of the polymeric characteristics of cellulose. Once developed, this technique was used to study endoglucanase behavior. A kinetic model was then developed based on experimentally determined kinetic parameters. An additional model based on these inhibition and activation mechanisms was developed and was successful in predicting endoglucanase behavior.

A typical single polymeric carbohydrate component from biomass contains molecules of many different chain lengths. A molecular weight measure will therefore yield only an average value. There are three methods of averaging the molecular weight of different polymer chains in a mixture: (1) a molecule-number average molecular weight, M_n; (2) a weight average molecular weight, M_w; and (3) a viscosity average molecular weight, M_v.

M_n is determined by counting the number of molecules in a sample of a given weight and determining the average weight on the basis of the number of molecules at each weight. Molecular weights can be measured by determining the number of molecules in a sample of known weight by chemically reacting the end groups with some compound so that they can be distinguished from the other monomer units. An example is the colorimetric reaction.[1] This method of molecular weight determination is also the basis for the reducing sugar assay. M_n is usually the most probable molecular weight and lies near the peak of a molecular weight distribution curve, as shown in Fig. 1.

M_w determines average molecular weight by the weight percent of each molecule present. The ratio of M_w to M_n is a measure of the range of the molecular weight distribution and is called the polydispersity; for carboxymethyl cellulose (CMC), polydispersity is assumed to be two.[2]

M_v is determined by relating molecular weight to solution viscosity and is the simplest experimental method for measuring the molecular weight of a polymer. It lies between M_n and M_w and is usually closer to M_w, as shown in Fig. 1. Since M_v is close to M_w it is approximately equal to M_w; therefore, $M_v \approx M_w \approx 2M_n$. Thus the viscosity method for assaying endoglucanase activity is also the basis for measuring the molecular weight of a polymer.

*This work was supported by the Office of Energy Research, Office of Basic Energy Sciences, Chemical Sciences Division of the U.S. Department of Energy under Contract No. DE-AC03-76SF00098 and by the Solar Energy Research Institute under Contract No. DX-4-04059-1.

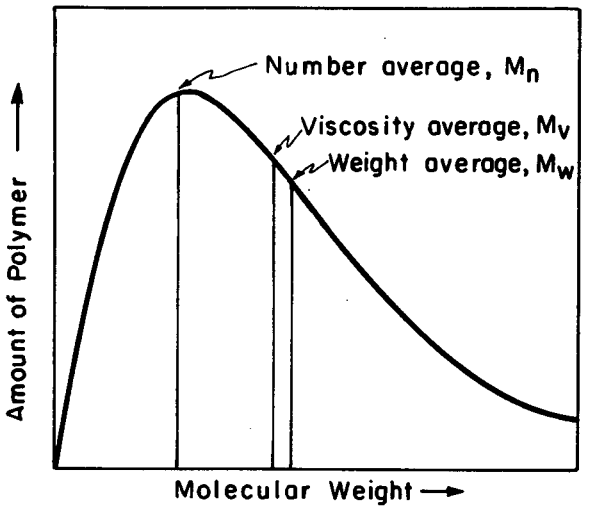

Figure 1. Molecular weight distribution of a typical polymer.[3] (XBL 839-6385)

M_v is related to the intrinsic viscosity of a polymer by the Mark-Houwink equation:

$$[\eta] = H(M_v)^x \quad , \tag{1}$$

where H and x are constants and $[\eta]$ is the intrinsic viscosity.[3] Intrinsic viscosity is a physical property of the polymer and is defined as a measure of the polymer's ability to increase the viscosity of a solvent in the absence of polymer-polymer interaction or at infinite dilution.[2] The relationship between viscosity and concentration that is most suited to CMC is the Baker relation:

$$\frac{\eta}{\eta_s} = \left(1 + \frac{[\eta]}{C_s}\right)^8, \tag{2}$$

where η_s is the solvent viscosity and η is the solution viscosity.[2] The Baker relationship is only valid for polymer solutions of low concentration.

This method of molecular weight determination is applied to the viscometric assay by measuring the viscosity change in a dilute solution with time once the enzyme has been added. Viscosity is related to M_n by the relation:

$$\eta \overset{(a)}{\text{———}} [\eta] \overset{(b)}{\text{———}} M_v \overset{(c)}{\text{———}} M_n \quad ,$$

where (*a*) is Eq. (2), (*b*) is Eq. (1), and (*c*) is the polydispersity.

CMC was used as a substrate for all the kinetic experiments; it is a cellulose ether produced by reacting alkali cellulose with sodium monochloracetate. Its structure is close to that of cellulose except that, on some of the monomer units, a carboxymethyl group ($-OCH_2COO^-$) is substituted for the hydroxyl group attached to the sixth carbon. While structurally similar to cellulose, CMC is water soluble. Therefore, it can be used to examine the kinetic behavior of endoglucanase or cellulase on long polymer chains.

The CMC used was medium viscosity; obtained from Sigma Chemical (No. C-4888), it had a reported viscosity average molecular weight of 250,000 daltons, an average degree of polymerization of 1100, and a degree or substitution of 0.7. The molecular weight of this lot of CMC ranged from 130,000 to 250,000 daltons as determined viscometrically. The CMC was dissolved in 0.05 M sodium acetate buffered to a pH of 5.0. The polydispersity was assumed to be two, and the Mark-Houwink constants from Eq. (1) were $H = 2.17 \times 10^{-5}$ and $x = 0.83$ (Ref. 2).

At low concentrations, CMC solutions are Newtonian fluids, but, at higher concentrations, they exhibit power-law behavior. For the kinetic experiments done in this study, the solution concentrations ranged from 10 to 30 g/L. The rheological behavior of CMC in this range is summarized in Table 1. In the concentration range used, CMC behaved as a power-law fluid. For the inhibition experiments, glucose and cellobiose were also added to the solutions, which did not affect the rheological behavior of the solution.

The mutant strain of *Trichoderma reesei*, Rutgers-C30, produced the cellulase enzyme used in this study. Endoglucanase and cellobiohydrolase are extracellular enzymes, while β-glucosidase is primarily cell-bound.[4] The fermentation broth was ultrafiltered with 0.005 M ammonium carbonate and concentrated to 238 grams of soluble protein per liter.[5] The raw cellulase had specific endoglucanase

Table 1. Rheology of concentrated, medium-viscosity CMC.

M_v (dalton)	CMC (g/L)	K^a (P/sec)	n^a	$\eta_{app}{}^b$ (cp)
280,000	10	0.816	0.87	37.4
250,000	30	41.7	0.65	512
	20	5.54	0.78	148
	10	0.424	0.89	21.9
130,000	30	5.47	0.80	165
	20	1.18	0.86	51.0

[a] $\tau = K(D)^n$, where τ is shear stress and D is shear rate.

[b] $\eta_{app} = K(D)^{n-1}$ for $D = 400\ sec^{-1}$.

activity of 6.0 units per mg of soluble protein and a specific β-glucosidase activity of 2.6 units per mg. A unit of activity is the micromoles of bonds broken or micromoles of reducing sugars produced per minute when an appropriate substrate is enzymatically reacted.

The cellulase was fractionated using ion exchange chromatography,[5] and seven separate peaks were collected. The results of the typical ion exchange are shown in Table 2. Fractions II and V showed significant endoglucanase activity. Fraction II was a low molecular weight protein that also had β-glucosidase activity. Fraction V was a high molecular weight protein with a very low β-glucosidase activity, approximately 96% pure endoglucanase, used in this study. Gel electrophoresis showed it to have two components. The major component had a molecular weight of approximately 66,000, and the minor component had a molecular weight of approximately 29,000. Each enzyme component obtained in the ion exchange was purified further by gel permeation chromatography (GPC). Fraction V-A was shown to be pure protein via gel electrophoresis, and it had a specific endoglucanase activity of 25.4 U/mg. The other peak, V-B, was also high in endoglucanase activity with a specific activity of 10.2 U/mg.

In order to correlate viscosity with intrinsic viscosity, and thus with molecular weight, it was necessary to obtain samples covering a range of molecular weights typical of those found over the assay reaction period. This was done by adding varying amounts of cellulase to a polymer solution and allowing the reaction to take place at 40°C for 5 minutes. The reaction was quenched by increasing the pH of the solution to 10, temporarily deactivating the enzyme. The cellulase was then denatured by heating the solution to 90°C for about 5 minutes, and the solution was returned to its original pH of 5.

Samples of different molecular weights were prepared this way, and the apparent viscosity of each sample was determined at the high substrate concentrations. Each sample was then diluted and its intrinsic viscosity measured. Correlation curves were developed in this manner for 10, 20, and 30 g/L CMC solutions. The relationships developed were used to correlate viscosity, η, to intrinsic viscosity, $[\eta]$, and were of the form,

$$[\eta] = a + b\eta \quad . \tag{3}$$

The values of a and b that were determined are listed in Table 3. These correlations are considered valid for CMC solutions of number average molecular weights ranging from 50,000 to 130,000.

A Couette viscometer was used to measure the rheology of the concentrated solutions, and a capillary viscometer was used to measure the viscosity of the dilute solutions. The assay, when performed in a Couette viscometer, was at a constant shear rate for the entire reaction period. The original viscosity of the CMC solution was measured, cellulase or endoglucanase was added to the solution, and the solution was returned to the viscometer. Viscosity change was measured with respect to time by measuring the change in torque with respect to time at a constant shear rate. A typical degradation curve is shown in Fig. 2. The reaction progress was recorded in this manner for approximately 5 minutes or until the viscosity change became very small. All assays were

Table 2. Cellulase enzyme description.

Cellulase fraction	Wt.% of total soluble protein	β-Glucosidase activity (U/mg)		Endoglucanase activity (U/mg)	
		ion exch.	gel perm.	ion exch.	gel perm.
Total cellulase	100.0	2.6		6.0	
I-A	10.1	27	146.0	0.32	1.0
I-B			7.3		0.4
II	31.0	4.2	0.2	16.0	27.2
III	17.3	0.03	0.05	1.3	3.7
IV	8.0	0.03	0.03	0.74	0.78
V-A	8.3	0.04	0.04	24.8	25.4
V-B	0.3		0.03		10.2
VI	11.4	0.05	0.09	1.6	5.0
VII	13.9	0.01	0.0	0.53	0.29

Source: Ref. 5.

Table 3. Parameters for viscosity–intrinsic viscosity correlation for medium viscosity carboxymethylcellulose.

CMC (g/L)	a[a]	b[a]
10	0.251	1.40×10^{-2}
20	0.254	2.51×10^{-3}
30	0.257	6.04×10^{-4}

[a]Parameters fitting Eq. (3).

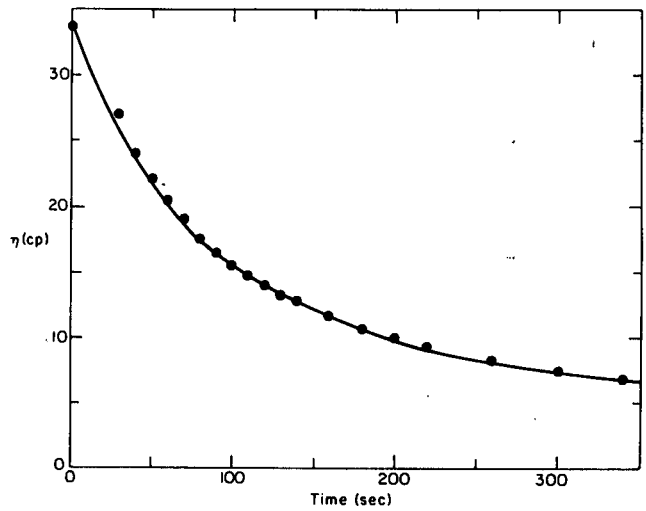

Figure 2. Effect of enzymatic degradation on solution viscosity. (XBL 839-6388)

performed at 40°C, which is near the optimum temperature of 45°C for cellulase activity and is consistent with kinetic experiments carried out by others.[2] Activity was determined from the slope of the linear portion of a plot of $1/M_n$ versus time according to Eq. (1). A typical plot is shown in Fig. 3. Activity was measured as a function of substrate concentration for different enzyme concentrations, and inhibition parameters were then determined for cellulase and endoglucanase. At a constant enzyme concentration, activity was measured at different cellobiose concentrations; these experiments were repeated using glucose. In order to determine the type of inhibition present, experiments were performed in which both glucose and cellobiose were added to the reaction mixture.

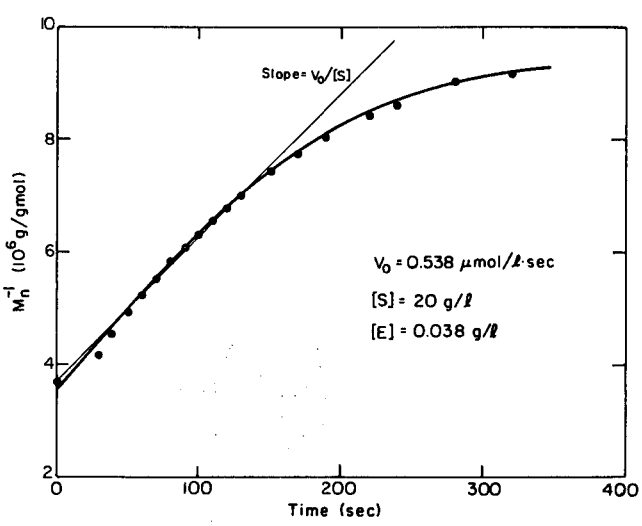

Figure 3. Activity determination for endoglucanase. (XBL 839-6389)

The kinetic parameters describing the behavior of endoglucanase were determined from experimental data. First, the effect of enzyme concentration on reaction velocity, v_o, was examined. Second, the role of glucose in endoglucanase regulation along with the effect of cellobiose on endoglucanase activity was considered. Third, the behavior of purified endoglucanase was compared to the behavior of endoglucanase in the presence of the other cellulolytic enzymes. Using initial rate models for activation and inhibition, kinetic parameters were fit to the data and incorporated into an overall model of endoglucanase behavior.

An assumption of Michaelis-Menten kinetics[6] is that the reaction velocity is directly proportional to the concentration of the enzyme substrate complex,

$$v_o = k_p[ES] \quad . \tag{4}$$

It then follows that the maximum reaction velocity is proportional to the total enzyme concentration,

$$V_{\max} = k_p[E_t] \quad , \tag{5}$$

where k_p is the rate constant for the product-forming step. Lineweaver-Burk plots were prepared for various enzyme concentrations, and $V_{\max}$ was determined at each concentration for both cellulase and endoglucanase. In the range of enzyme concentrations tested, $V_{\max}$ was a linear function of E_t as can be seen in Figs. 4 and 5.

The advantages of the Couette viscometric technique are that it can measure initial rates and allows the use of higher enzyme and substrate concentrations. On the basis of the consistency of the results of the kinetic studies, it is an effective method for studying initial rate kinetics. However, it is limited for the study of reaction progress versus time because the molecular weight distribution and how it changes with time is not known. If the initial value of the polydispersity can be determined exactly, then the assay can measure absolute activities rather than relative values.

While the $V_{\max}$ values may be slightly inaccurate, the values of the Michaelis constant and the inhibition and activation parameters will not be affected by a change in the value used for k. A serious limitation of the assay is that the dependence of the molecular weight distribution on time must be determined concurrently, such as with GPC.

Endoglucanase activity was evaluated assuming that Michaelis-Menten kinetics could be applied

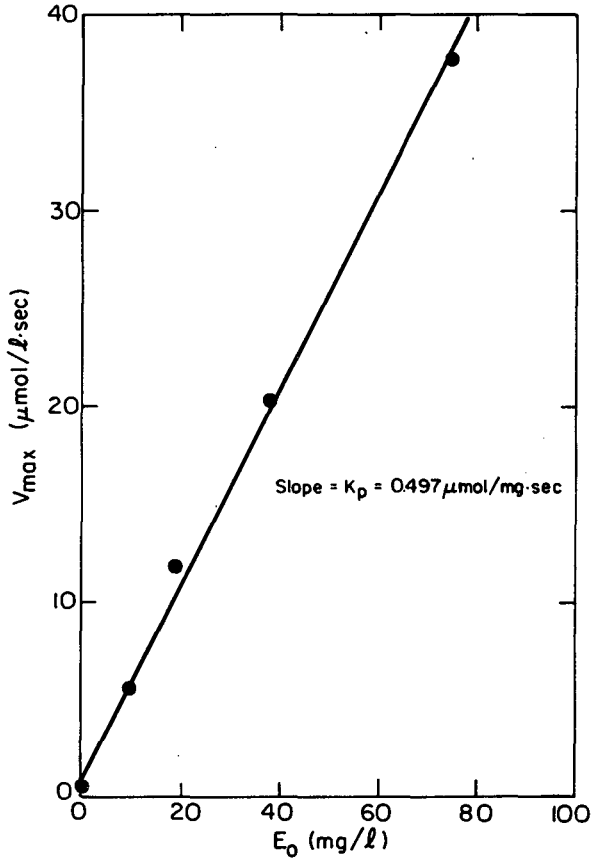

Figure 4. Determination of k_p for cellulase. (XBL 839-6390)

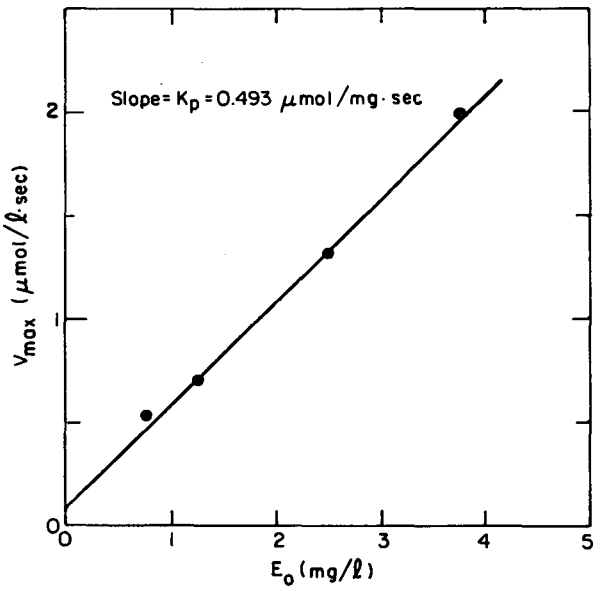

Figure 5. Determination of k_p for endoglucanase. (XBL 839-6391)

under the given experimental conditions. The assumptions on which the Michaelis-Menten model are based appear to be reasonable for the experimental conditions in this study. One of these assumptions is that V_{max} is directly proportional to the total enzyme concentration. As can be seen in Figs. 4 and 5, a linear enzyme dilution curve was obtained. Glucose and cellobiose have been identified as inhibitors of the cellulase system. Their effect on endoglucanase was studied. Cellobiose was found to inhibit endoglucanase via a partial mixed-type inhibition mechanism. Glucose, on the other hand, was found to be a nonessential activator of endoglucanase. The overall model of endoglucanase behavior can be represented schematically by Fig. 6. This is a model of a nonessential activator in competition with a partial mixed inhibitor. The values of the kinetic parameters for this model are summarized in Table 4.

PLANNED ACTIVITIES FOR FY 1985

The results reported here will be incorporated into an overall model for the cellulase system of enzymes derived from the *T. reesei* mutant strain Rut-C30.

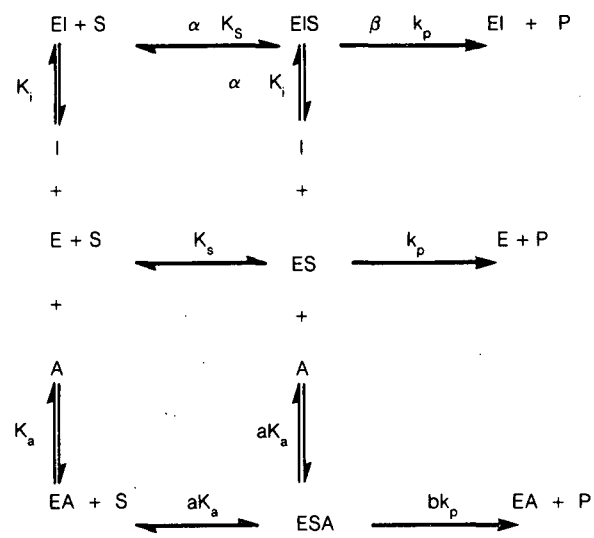

Figure 6. Schematic model of endoglucanase behavior: A nonessential activator in competition with a partial mixed-type inhibitor. (XBL 8311-4474)

Table 4. Kinetic parameters for endoglucanase activity.

	Cellulase	Endoglucanase
K_m	0.030	0.028
K_i	0.012	0.004
α	1.26	1.70
β	0.572	0.606
K_a	2.00	0.250
a	0.468	0.470
b	2.21	1.15

REFERENCES

1. Orichowskyj, S.T. (1982), "Recovery of Cellulase Enzymes by Countercurrent Adsorption," M.S. Thesis, University of California, Berkeley.
2. Almin, K.E., and Eriksson, K.E. (1967), "Enzymic Degradation of Polymers (I), Viscometric Determination of Enzymic Activity," *Biochim. Biophys. Acta. 139*, p. 248.
3. Billingham, N.C. (1977), in *Molar Mass Measurement in Polymer Science,* Wiley and Sons, New York.
4. Ghose, T.K. (1977), in *Advances in Biochemical Engineering,* Vol. 6, p. 39, T.K. Ghose, A. Fiechter, and N. Blakebrough, Eds., Springer-Verlag, Berlin.
5. Wiley, D. (1985), *Mechanism and Kinetics of Cellulose Hydrolysis,* Ph.D. Thesis, University of California, Berkeley.
6. Segel, I.H. (1975), in *Enzyme Kinetics,* Chapters 3–5, Wiley and Sons, New York.

Production of Sugars from Cellulose: Cellulase Production by *T. Reesei* in Continuous Culture in Lactose Medium*

(This article has been reprinted from the FY 1984 Annual Report.)

F. Castillo, H. Blanch, and C. Wilke

In the process of cellulose utilization, perhaps the most obvious area for major improvement is the production of cellulase enzyme for hydrolysis of wood and agricultural residues that can then be fermented into ethanol fuel. Nearly 50% of the cost of producing glucose from cellulosic material is attributed to enzyme production alone. Improvements in this step would therefore have dramatic impact and are important if economical hydrolysis processes are to be realized.

The first major thrust in this area has been the development of improved mutant strains of the filamentous fungus *Trichoderma reesei*, free from catabolite repression and capable of constitutive cellulase production. One such hyperproducing mutant, developed at Rutgers University (Rut-C30) and isolated,[1] presents an interesting potential for the development of processes aimed at the commercial production of cellulases.

Lactose is utilized by this microorganism; when it grows on this disaccharide, the enzymes of the cellulase complex are induced. This fact suggests that milk or cheese whey may be used as a medium to grow Rut-C30 and produce the enzymes. This procedure may also be an efficient method of whey treatment, reducing its high biological oxygen demand (BOD).[2,3] Additional advantages of whey utilization are its solubility and ease of handling as a fermentation medium compared to insoluble cellulose and its rich composition in nutrients[4,5] that may require only a few economical supplementations.

ACCOMPLISHMENTS DURING FY 1984

The objectives of this work are twofold: (1) to obtain information on the regulatory controls operating on the synthesis of the cellulases and (2) to study the effects of environmental variables on the production of the enzymes.

Rut-C30 strain was used throughout the experiments. The fermentation medium consisted of a double concentration of salt solution modified from that of Ryu *et al.*[6] to insure lactose limitation. It contained per liter: 25 g lactose, 4 g $(NH_4)_2(SO_4)$, 2 g KH_2PO_4, 0.3 g $MgSO_4 \cdot 7\ H_2O$, 0.15 g $CaCl_2 \cdot 2H_2O$, and 0.2 mL surfactant (Tween 80). For foam control, General Electric silicon AF-60 at 0.05 to 0.1

*This work was supported by the Assistant Secretary for Conservation and Renewable Energy of the U.S. Department of Energy under Contract No. DE-AC03-76SF00098 and by the Solar Energy Research Institute under Contract No. DR-0-9058-1.

v/v% was used. For continuous culture, a Chemap 20 L fermentor was used, with a 5 L reactor vessel (2.5 to 2.8 L working volume). Regulation of pH was carried out by automatic addition of 2 *N* ammonium hydroxide.

After samples were withdrawn aseptically from the reactor vessel, they were divided into two fractions: one was frozen whole while the second was filtered through 0.45 micrometer polycarbonate membranes, with the filtrate frozen until it was assayed. Assays for enzyme activities included determinations of filter paper activity, endoglucanase (CMCase), and cellobiohydrolase (cotton activity) by methods described previously[7]; cellobiase (β-glucosidase) and lactase (β-galactosidase) were assayed with p-nitrophenyl glucopyranoside (p-NPG) and o-nitrophenyl galactopyranoside as substrates, respectively, at 5 m*M* final concentrations. Activities of both enzymes as functions of temperature and pH indicated that, for cellobiase activity determined with p-NPG, the optimum pH was 4.6 and the optimum temperatures were 73°–75°C. For lactase activity, they were 4.6 and 62°–65°C, respectively.

The organism is a complete prototroph and grew well in this simple medium. Dry weight, intra- and extracellular protein, and total biomass (dry weight and extracellular protein) as functions of dilution rate are shown in Figs. 1 and 2. As can be seen, reduction of antifoam concentration from 0.1 to 0.05% produced slight increases in the cellular protein. In this medium, the maximum yield obtained was 0.486 g total biomass/per gram lactose utilized, and the maintenance coefficient was calculated at 6 mg lactose per gram of total biomass per hour. Maximum specific growth rate was 0.12 per hour, and the saturation constant for lactose was estimated at 0.763 g/L (0.77 m*M*).

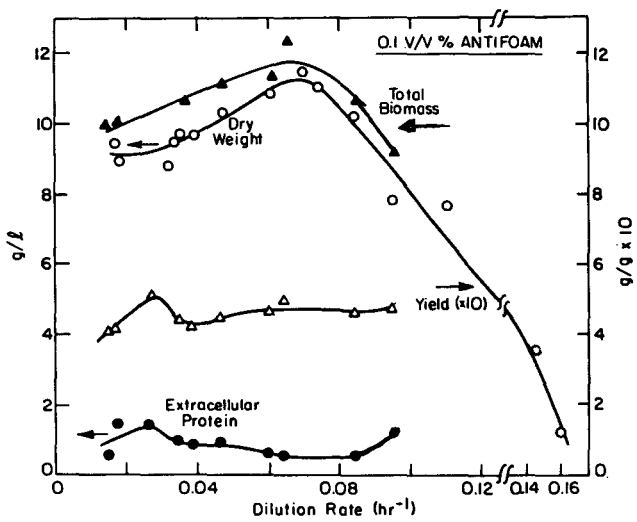

Figure 1. Various parameters of Rut-C30 growth in submerged culture vs. substrate (lactose) dilution rate in the presence of 0.1 v/v% antifoam. (XBL 8311-6604)

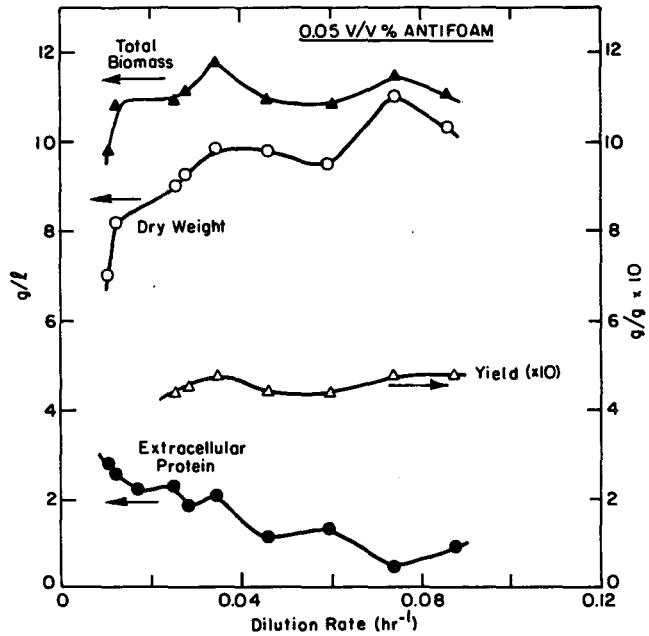

Figure 2. Various parameters of Rut-C30 growth in submerged culture vs. lactose dilution rate in the presence of 0.05 v/v% antifoam. (XBL 8311-6605)

The profiles of enzyme production and specific activities as functions of dilution rate when the medium contained 0.1% antifoam are shown in Figs. 3 and 4. In subsequent experiments, antifoam was not added and the foam was easily kept under control by reducing the aeration rate. The profiles obtained for production of the enzyme (Fig. 3) indicate the presence of dual regulatory mechanisms for the synthesis of the enzymes, their induction, and catabolite repression.[8]

The organism was found to produce a lactase, and the activity of this enzyme was assayed only in the filtrates. Although the enzyme was present outside of the cell, no significant levels of glucose were detected in the medium even at high dilution rates. This lactase may be excreted by the organism along with the other enzymes, or its presence in the medium may result from cell lysis or fragmentation caused by the high-speed agitation, or both.

To study the effects of temperature and pH on the production of the enzymes, the dilution rate was fixed. One parameter was varied at a time, and the

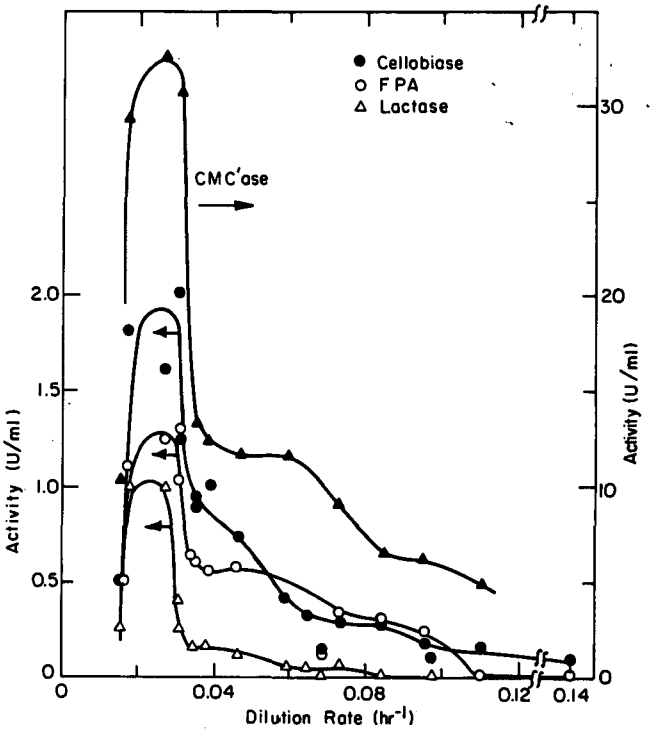

Figure 3. Growth profiles of enzyme components vs. dilution rate in the presence of 0.1 v/v% antifoam. (XBL 8311-6606)

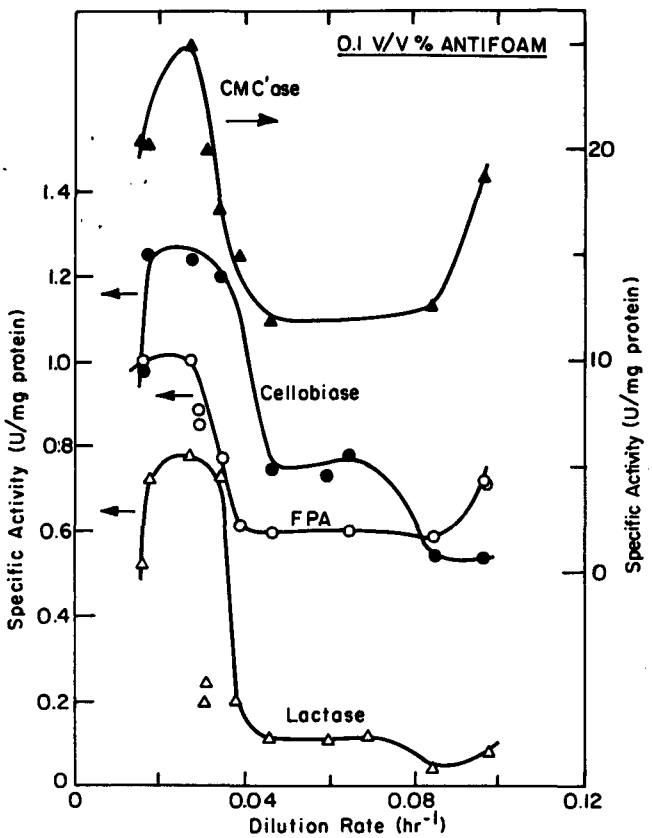

Figure 4. Specific growth profiles of enzyme components vs. dilution rate in the presence of 0.1 v/v% antifoam. (XBL 8311-6607)

new steady states were allowed to stabilize after each variation. Figures 5, 6, 7, and 8 show the steady-state values for biomass, protein, and enzymes as functions of temperature and pH.

For the next set of experiments, 26°C and pH 5 were selected and maintained. To study the effects of nutrient addition, pulses (equivalent to 1% of working volume) were added to the reactor vessel and the responses studied with respect to time. Addition of a yeast nitrogen base (YNB) pulse at 50 times the standard concentration produced increases in all of the enzymes (Fig. 9). When pulses of glucose or lactose were applied, transient decreases in the levels of all five enzymes were observed, such as would occur in catabolite repression. When the different groups of nutrients from YNB were tested separately, none induced the observed increase in enzyme productivity as when whole YNB was used.

Addition of the surfactant Tween 80 did increase the levels of the enzymes. Other nutrients and compounds used in the past, such as urea, proteose peptone, or corn-steep liquor, did not enhance enzyme levels. When the medium was shifted to 2 times the standard concentration, the original transient decrease in all enzymes was followed by an increase to new high levels.

PLANNED ACTIVITIES FOR FY 1985

Capital and energy costs concentrate in the enzyme production step of the biomass hydrolysis process. When steam-exploded wood is used as the cellulose source, in the overall process, about 12% of the total input is used in enzyme production. Process economic evaluation indicates that the use of delignified or soluble carbon sources such as lactose in whey is favorable in fed-batch or continuous cultivation, respectively. The optimum conditions for the initial batch period using this substrate will be determined. The effect of feeding regimes and aeration conditions on enzyme production will be studied. Experiments in which application of pulses with combinations of different groups of nutrients and use of a more concentrated medium are contemplated.

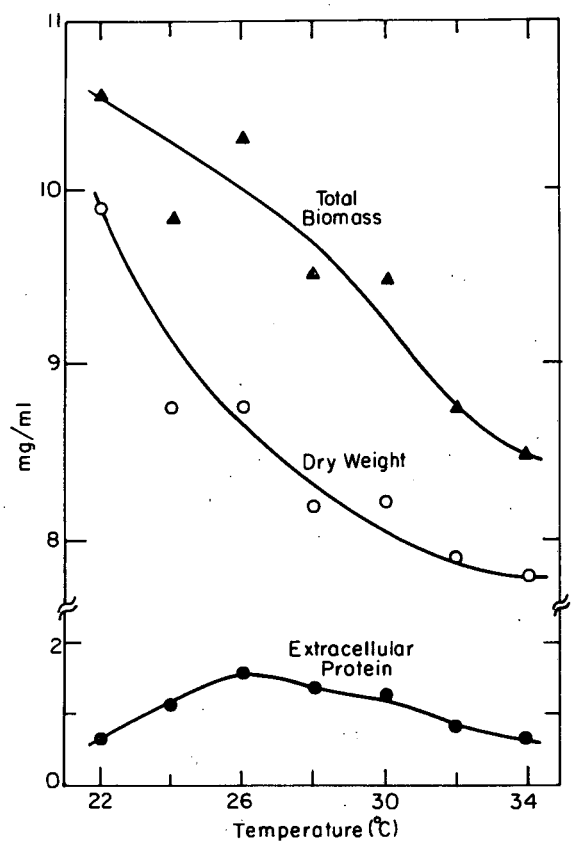

Figure 5. Steady-state growth of Rut-C30 vs. temperature. (XBL 8311-6608)

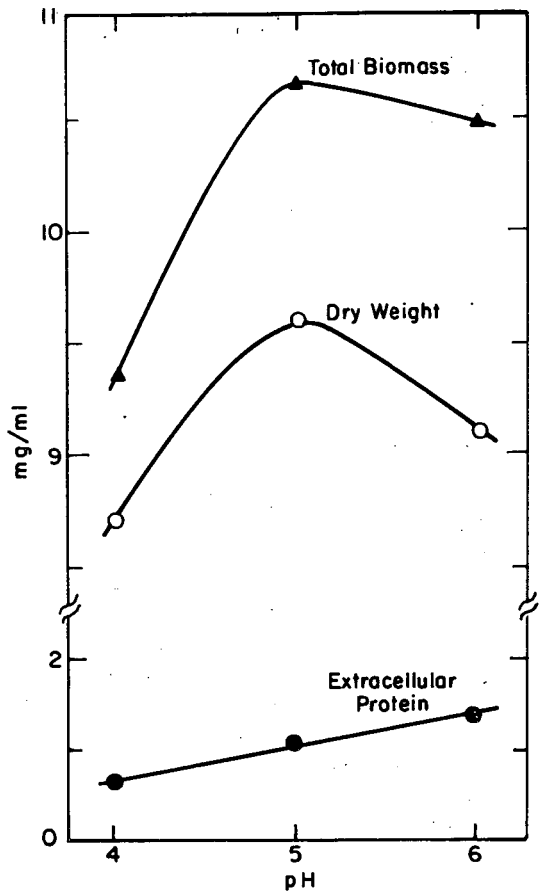

Figure 7. Steady-state growth of Rut-C30 vs. pH. (XBL 8311-6610)

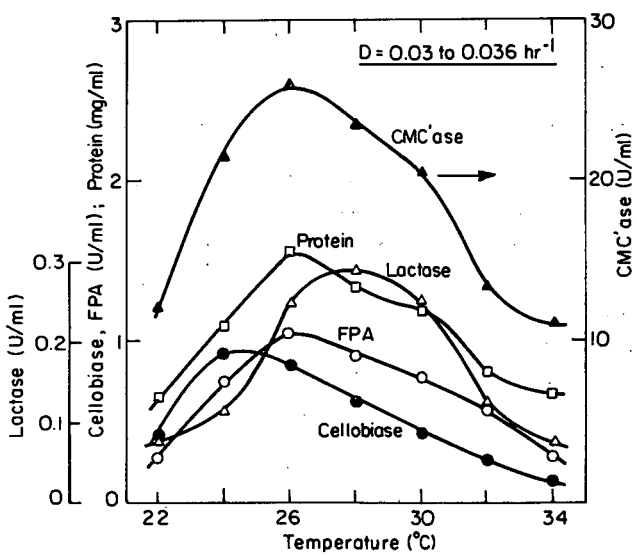

Figure 6. Growth profiles of enzyme components vs. temperature at dilution rates of 0.03 to 0.036 hr^{-1}. (XBL 8311-6609)

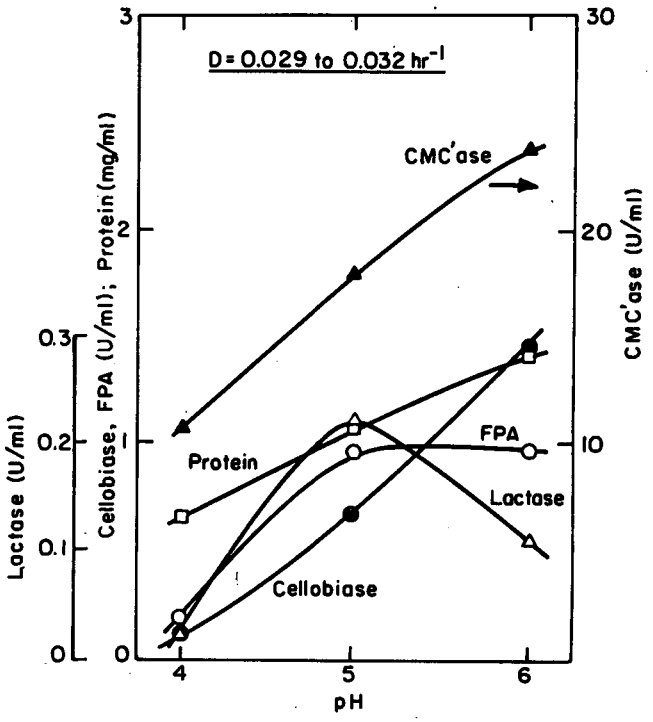

Figure 8. Growth profiles of enzyme components vs. pH at dilution rates of 0.029 to 0.032 hr^{-1}. (XBL 8311-6611)

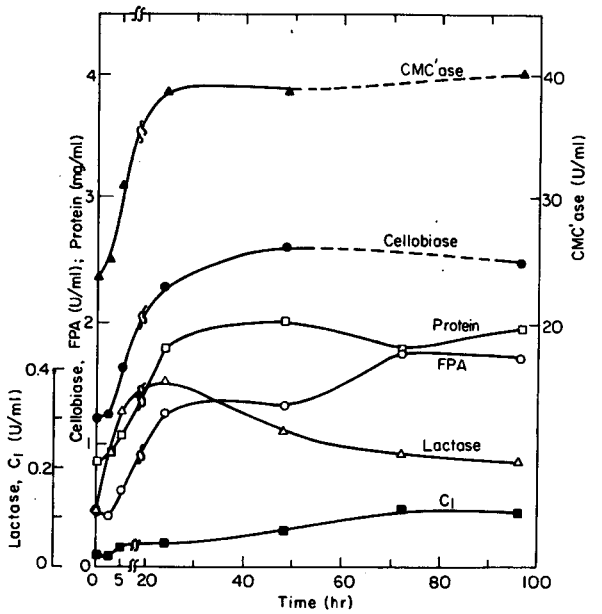

Figure 9. Growth of enzyme components over time with added yeast nitrogen base, 30 mL, 50× standard concentration. (XBL 8311-6612)

REFERENCES

1. Montenecourt, B.S. and Eveleigh, D.E. (1977), "Preparation of Mutants of *T. reesei* with Enhanced Cellulase Production," *Appl. Environ. Microbial. 34*, p. 777.
2. Kosikowski, F.V. (1977), *Cheese and Fermented Milk Foods,* Edward Brothers, Inc., Ann Arbor, Michigan.
3. Wix, P. and Woodbine, M. (1958), "The Disposal and Utilization of Whey; a Review," *Dairy Sci. Abstracts 20*, p. 537, Part 1; p. 621, Part 2.
4. Mairopoulou, I.P. and Kosikowski, F.V. (1972), "Composition, Solubility and Stability of Whey Powders; Free Amino Acids and Soluble Peptides of Whey Powders," *J. Dairy Sci. 56*, p. 1128, Part 1; p. 1135, Part 2.
5. Glass, L. and Hedrick, T.I. (1977), "Nutritional Composition and Major Factors Including Amino Acids in Sweet and Acid Type Dry Wheys; Vitamins, Mineral and Calorie Contents of Dry Wheys," *J. Dairy Sci. 60*, p. 185, Part 1; p. 190, Part 2.
6. Ryu, D., Andreotti, R., Mandels, M., Gallo, B., and Reese, E.T. (1979), "Studies on Quantitative Physiology of *Trichoderma reesei* with Two-Stage Continuous Culture for Cellulase Production," *Biotechnol. Bioeng. 21*, p. 1887.
7. Wilke, C.R. and Blanch, H.W. (1981), *Bioconversion of Cellulose,* LBL-14219.
8. Toda, K. (1981), "Induction and Repression of Enzymes in Microbial Culture," *J. Chem. Tech. Biotechnol. 31*, p. 775.

ELECTROCHEMICAL ENERGY STORAGE RESEARCH

Technology Base Research Project for Electrochemical Energy Storage*

E.J. Cairns, K. Kinoshita, and F.R. McLarnon

The Lawrence Berkeley Laboratory (LBL) is lead center for management of the Technology Base Research (TBR) Project, which is supported by the Electrochemical Branch of DOE's Office of Energy Storage and Distribution. The purpose of this project is to provide the research base to support DOE efforts to develop electrochemical energy conversion systems for electric vehicle and stationary energy storage applications. The specific goal is to identify the most promising electrochemical technologies and transfer them to industry and/or another DOE program for further development and scale-up.

The TBR project is divided into three major elements: Exploratory Research, Applied Science Research, and Air Systems Research. The generic research topics included in each of these elements are listed in Table 1.

The general research areas addressed by the TBR Project include identification of new electrochemical couples for advanced batteries, determination of technical feasibility of the new couples, improvements in battery components and materials, establishment of engineering principles applicable to electrochemical energy storage and conversion, and the investigation of fuel cell and metal/air systems for transportation applications. Major emphasis of the project is given to applied research that will lead to superior performance and lower life-cycle costs.

The LBL scientists who participate in the program are E.J. Cairns, K. Kinoshita, and F.R. McLarnon of the Applied Science Division, and L.C. DeJonghe, J.W. Evans, R.H. Muller, J.S. Newman, P.N. Ross, and C.W. Tobias of the Materials and Molecular Research Division.

Table 1. Topics covered by the Technology Base Research Project for Electrochemical Energy Storage.

I. EXPLORATORY RESEARCH
- New Rechargeable Electrochemical Cells
- Thermally Regenerative Cells

II. APPLIED SCIENCE RESEARCH

A. Engineering-Science Research
- Electrode Morphological Studies, Chemical/Structural Analysis
- Transport Phenomena, Electrocatalysis, Electrode Kinetics,and Cell Thermodynamics
- Modeling of Electrochemical Cells and Battery Systems
- Advanced Physicochemical Methods for Electrochemical Research

B. Materials Research
- Ceramic, Molten-Salt, Glass, and Polymeric Electrolytes
- Corrosion Problems in Electrochemical Storage Devices
- Novel Electrode Structures
- New Component Fabrication Techniques
- Battery Separators

III. AIR SYSTEMS RESEARCH
- Air Electrodes
- Metal/Air Cells
- Fuel Cells
- New Electrolytes
- New Electrocatalysts

ACCOMPLISHMENTS DURING FY 1985

LBL conducted a vigorous in-house research program and monitored 30 subcontracts during FY 1985. A description of the research projects conducted by the subcontractors can be found in the recent annual report, *Technology Base Research Project for Electrochemical Energy Storage* (LBL-19545), and the in-house work, "Electrochemical Energy Storage," is summarized in the next article and in the *Materials and Molecular Research Division 1985 Annual Report* (LBL-20230). Highlights of the subcontracted work follow.

*This work was supported by the Assistant Secretary for Conservation and Renewable Energy, Office of Energy Storage and Distribution of the U.S. Department of Energy under Contract No. DE-AC03-76SF00098.

Exploratory Research

- Duracell has continued their investigation of a novel rechargeable $Li/LiAlCl_4-SO_2/C$ cell that offers attractive specific energy (524 Wh/kg theoretical), stability of the lithium electrode, and the ability to withstand limited overcharge. All of these are attractive characteristics for a secondary lithium cell. Duracell has now achieved 60–90 cycles (100% depth-of-discharge) to 2.6 V cutoff in small cells (0.5 Ah). A gradual loss in capacity of about 1% per cycle is observed, which is attributed to the poor mechanical structure of the positive electrode, and electrolyte starvation on deep discharge.
- Experimental measurements at the University of Pennsylvania demonstrated that divalent cations (Mg^{2+} and Pb^{2+}) can be ionic conductors in poly(ethylene oxide); this result is contrary to early predictions. This study could lead to new classes of secondary batteries using polymeric electrolytes.
- Dow Chemical completed their investigation of a new high-temperature Na/S cell that uses a glassy electrolyte. They recently found that the corrosion of glasses D406 ($Na_2O-2\ B_2O_3-0.2\ SiO_2-0.16\ NaCl$) and T806 ($Na_2O-1.1\ B_2O_3-1.3\ SiO_2$) by sulfur at 400°C is virtually stopped by the addition of 0.5 wt% of a hydrocarbon polymer (poly(4-methyl-1-pentene)) to sulfur.

Applied Science Research

- Argonne National Laboratory (ANL) has achieved over 375 cycles (3500 hour) at 397°C with a small prismatic cell (25 Ah) with a dense upper-plateau FeS_2 electrode, a Li-Al negative electrode, and LiCl-LiBr-KBr electrolyte (m.p. 310°C). Cell data indicate a 50% increase in specific energy and specific power (versus a standard two-plateau cell), and utilization is about 85% with virtually no loss in capacity after more than 375 cycles. If comparable performance is achieved with realistic cell hardware, this cell chemistry could lead to a very high-performance battery (>200 W/kg, >180 Wh/kg).
- Experimental studies at Rockwell International, Inc. indicate that ZrO_2-toughened β''-alumina should contain between 10–15 vol% ZrO_2 to obtain the optimum strength and ionic conductivity. Ceramatec, Inc., is now investigating techniques to process this new material into practical electrolyte tubes.
- ANL has identified a glass composition (42 mol% Na_2O–8 mol% Al_2O_3–5 mol% ZrO_2–45 mol% SiO_2) that has chemical stability (at 400°C in Na, Na_2S_3, Na_2S_4, and S) on a par with other candidate solid electrolytes, β''-alumina and DOW glass, for use in high-temperature Na/S cells.
- A family of glasses with composition analogous to NASIGLAS ($Na_{1+x}Zr_{2-x}/3Si_3P_{3-x}O_{12-2x}/3$) has been synthesized by the Massachusetts Institute of Technology. The conductivity at 350°C for several of the sodium-based glasses is as high as 10^{-4} $ohm^{-1}cm^{-1}$.
- Brookhaven National Laboratory (BNL) has continued their investigation of the kinetics of Zn deposition in Zn/halogen cell environments. Measurements at BNL show that the presence of Ca on a Zn surface does not inhibit layer growth, but it does accelerate the kinetics for Zn deposition in acid electrolytes. On the other hand Cd on Zn surfaces appears to inhibit layer growth and accelerate nucleation.
- Lawrence Livermore National Laboratory (LLNL) has extended their measurements of mutual diffusion coefficients for aqueous, high-purity $ZnCl_2$ systems at 25.00 ± 0.005°C. Measurements have been completed for 2.4999 M $ZnCl_2$–1.25 M KCl and 2.5001 M $ZnCl_2$–4.0002 M KCl.
- Raman spectroscopy studies at ANL of Zn^{2+} in concentrated KOH show conclusively that there is only one dominant Zn^{2+} coordination environment; Zn^{2+} ions are probably present in an octahedral or tetrahedral complex with Zn^{2+} to hydroxyl linkages.

Air Systems Research

- Energy Research Corporation has demonstrated that perovskite-catalyzed bifunctional air electrodes can operate for >800 cycles at 10/20 mA/cm^2 (charge/discharge), with stable overpotentials of 600/−280 mV with respect to a Hg/HgO reference electrode. This performance is comparable

to prior Westinghouse technology, yet the catalyst composition is simpler, and corrosion of the perovskites does not appear to be a problem.

- Pinnacle Research Institute was selected for research on metal/air batteries on the basis of proposals received in response to a Request for Proposals (RFP) by LBL. Their program will involve research and development of particulate zinc electrodes for Zn/air batteries, with emphasis on optimizing the charge and discharge characteristics of these electrodes.
- ELTECH Systems, Inc., has continued their role as prime contractor for research and development of the Al/air battery. A 5-cell Al/air stack was assembled at ELTECH Systems Corp. and testing is under way. Performance using 99.999% aluminum anodes agrees with the values calculated from the performance of individual components.
- ELTECH Systems, Inc., is now testing aluminum alloys containing 0.1% In and 0.05% Ga that show a low corrosion rate (11 mA/cm^2 at open circuit and 7 mA/cm^2 at 600 mA/cm^2) and reasonable potentials (1.76 V open-circuit potential and 1.35 V at 600 mA/cm^2) in 4 N NaOH at 60°C.
- Los Alamos National Laboratory (LANL) has continued their role as Technology Center for fuel cell R & D. Studies at LANL on steam-reforming of methanol, which is the preferred portable fuel for fuel cells, suggest that rapid oxygen exchange occurs on the catalyst (Cu-ZnO) surface. Experimental evidence indicates that methanol adds to an oxide vacancy and reacts with lattice oxygen atoms to generate CO_2.
- United Technologies Corp. has found that the performance of iron TMPP supported on Black Pearls 2000 in a phosphoric acid fuel cell increases with the heat-treatment temperature of the catalyst. The O_2-reduction performance reaches a maximum with a catalyst that is heat-treated at 950°C.
- Experiments at the University of Virginia suggest that for Pt-Cr alloys, the composition range of greatest interest for fuel-cell applications is within the ordered solid-solution structure between 17 and 35 a/o Cr.

PROGRAM CHANGES IN 1985

Funding support for the following projects was initiated in 1985:

- Spectroscopic Studies of the Passive Film on Alkali and Alkaline Earth Metals in Non-Aqueous Solvents. A Surface Science Approach—Case Western Reserve University;
- Battery Separator Research—Sandia National Laboratory;
- Technology Base Research on Zinc/Air Battery Systems—Pinnacle Research Institute.

Funding support for the following projects ended in 1985:

- Research on Materials Relating to the Sodium Heat Engine—Ford Motor Company;
- Improve the Lifetime of the Hollow Fiber Sodium/Sulfur Cell—Dow Chemical Company;
- Reaction Profiles in Porous Electrodes—Lockheed Missiles & Space Company;
- Semiconductor Electrochemistry Approach to the Study of Oxide Films—SRI International;
- Research on Separators for Alkaline Zinc Batteries—Pinnacle Research Institute;
- Zinc/Nickel Oxide Battery Membrane Separator Studies—Brigham Young University;
- Development of Bifunctional Oxygen Electrodes for Alkaline Metal-Oxygen Rechargeable Cells—Energy Research Corporation.

PLANNED ACTIVITIES FOR FY 1986

New initiatives include the following:

- Selections will be made from proposals on research and development of novel concepts for rechargeable lithium cells submitted in response to a Request for Proposals (RFP) issued by the TBR Project.
- Applied research will be conducted on the characterization of components for secondary batteries.

Battery Electrode Studies*†

E.J. Cairns, F.R. McLarnon, T.C. Adler, M.J. Isaacson, R. Jain, P.M. Lessner, K.G. Miller, S.A. Naftel, M.L. Smith, K.A. Striebel, and J. Winnick‡

The purpose of this research is to study the behavior of electrodes used in secondary batteries and to investigate practical means for improving their performance and lifetime. Systems of current interest include ambient-temperature rechargeable cells with zinc electrodes [Zn/air, Zn/NiOOH, Zn/AgO, Zn/Cl_2, Zn/Br_2, and Zn/Fe $(CN)_6^{-3}$]; rechargeable high-temperature cells (Li/S, Li-Al/FeS_2, Li-Si/FeS_2, and Na/S); fuel cells; and liquid-junction photovoltaic cells. The approach used in this investigation is to study life- and performance-limiting phenomena under realistic cell operating conditions.

ACCOMPLISHMENTS DURING FY 1985

Measurement of Concentrations in Porous Zinc Electrodes Using Micro-electrodes

(M.J. Isaacson, F.R. McLarnon, and E.J. Cairns)

The purpose of this work is to develop reference micro-electrodes as useful analytical tools, and use them to measure species concentration changes in secondary porous zinc electrodes. Cadmium, zinc, and α-palladium reference micro-electrodes are currently being investigated. The use of cadmium electrodes was discontinued due to poor stability. Stable and reproducible Zn electrode potentials were measured at various hydroxide and zincate concentrations; the results shown in Fig. 1 agree with and supplement the work of Dirkse,[1] and Hampson, Herdman, and Taylor.[2] Some α-Pd potential measurements in zincate-containing alkaline electrolytes are shown in Fig. 2.

Electrochemical cells are currently being fabricated for the porous electrode experiments. The cell provides for as many as eleven Zn and α-Pd electrodes. A multiplexer controlled by a microcomputer monitors the micro-electrodes while the cell is being charged and discharged. Future work will emphasize the implementation and interpretation of the porous electrode experiments.

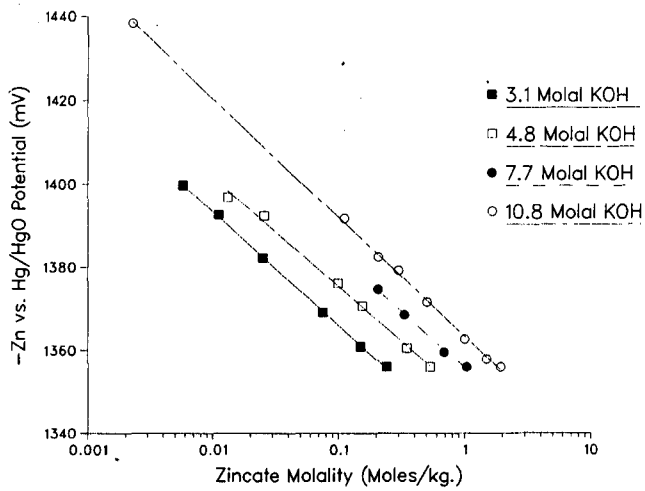

Figure 1. Variation of zinc electrode rest potential with $K_2Zn(OH)_4$ molality at constant hydroxyl-ion molality. Potentials are measured versus an Hg/HgO reference electrode in the same solution, and the temperature is 25°C. (XBL 861-242)

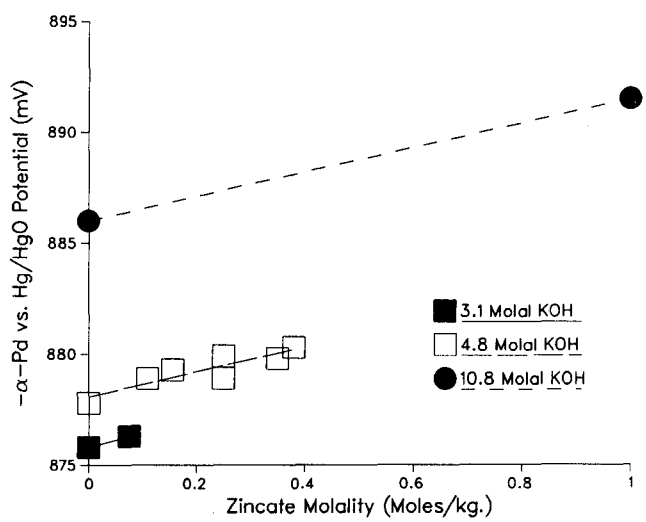

Figure 2. Variation of α-Pd electrode rest potential with $K_2Zn(OH)_4$ molality at constant hydroxyl-ion molality. Palladization is approximately 55 coulombs/cm^2, potentials are measured versus an Hg/HgO reference electrode in the same solution, and the temperature is 25°C. (XBL 861-243)

*This work was supported by the Assistant Secretary for Conservation and Renewable Energy, Office of Energy Storage and Distribution of the U.S. Department of Energy under Contract No. DE-AC03-76SF00098.

†This project is part of a larger effort, "Electrochemical Energy Storage," described in the Materials and Molecular Research Division 1985 Annual Report.

‡Department of Chemical Engineering, Georgia Institute of Technology, Atlanta, GA.

The Effect of Calcium Hydroxide on Secondary Zinc Electrodes

(R. Jain, F.R. McLarnon, and E.J. Cairns)

The aim of this research is to investigate the addition of calcium hydroxide to the zinc electrode as a practical means of reducing zinc species solubility in strong alkaline electrolytes. The reduced zinc solubility is expected to slow the rate of active material redistribution in the zinc electrode, thereby increasing its cycle life.

Identical pairs of zinc electrodes, containing 0%, 10%, 25%, and 40% $Ca(OH)_2$ by weight, were fabricated. Fabrication, cell assembly, and cycling procedures were similar to those used by J.T. Nichols, *et al.*[3] and M.H. Katz *et al.*[4] All negative electrodes had the same dry weight, so as more $Ca(OH)_2$ was added, less excess zinc was used. Two sintered nickel oxide positive electrodes were used in a cell, and the $Ca(OH)_2$-free zinc electrodes had 3.0 times the capacity of the NiOOH electrodes. The electrolyte was ZnO–saturated 31 wt% KOH-1 wt% LiOH. The 1.3-Ah cells were charged at a 5-hour rate and discharged at a 2.5-hour rate, limited by either the cell voltage or the zinc electrode potential.

The $Ca(OH)_2$-free electrode showed significant zinc redistribution after cycling. Many areas of the electrode were bare of zinc or showed very little material. The general direction of material movement was away from the center of the electrode, but some dense island regions of zinc remained in the central area. The material near to the electrode edges was also dense.

The 10%-$Ca(OH)_2$ electrodes also showed considerable zinc redistribution. Again, the general direction of material movement was away from the center of the electrode. However, unlike the $Ca(OH)_2$-free electrode, there were no bare areas and there remained a uniform "background" amount of zinc material over the electrode. KEVEX x-ray analysis showed that this material was a calcium-zinc compound. These electrodes also had dense island growths in the center and dense growths at the edges, and analysis showed these regions to be predominantly Zn. The overpotential of the negative electrode in the 10%-$Ca(OH)_2$ cell was slightly greater than that in the $Ca(OH)_2$-free cell.

The 25%-$Ca(OH)_2$ cells appeared to behave the best of the cells tested. Again, there was general zinc material movement toward the edges of the negative electrodes. However, for these electrodes there were fewer dense island regions and less thickening at the electrode edges. Also, there was significantly more background zinc material. Cells x-rayed at cycles 100 and 150 showed very few differences, implying that the background zinc material is fairly stable. The zinc-electrode overpotential in the 25%-$Ca(OH)_2$ cell was higher than that of the 10%-$Ca(OH)_2$ cell. Also, the current density during charge had to be decreased by 25% for the cell to function properly.

The 40%-$Ca(OH)_2$ cells operated for only a few cycles. They displayed high overpotentials, and their operation would have required charge currents which would have been too low to be practical.

Scanning Electron Micrographs were taken of various regions of the electrodes; KEVEX x-ray analysis, x-ray fluorescence analysis, atomic adsorption analysis, and powder x-ray diffraction studies were also performed, and zinc material balances were obtained.

The Effect of Pulse-Charging Regimes on the Cycle-Life Performance of Zinc/Nickel Oxide Cells

(T.C. Adler, F.R. McLarnon, and E.J. Cairns)

Previous studies of the effect of pulse charging on the cycle-life performance of Zn/NiOOH cells employed sheet current collectors[4] or were cycled at a low depth of discharge.[5] The purpose of this study is to evaluate promising pulse-charging regimes using mesh current collectors and a demanding (100% depth of discharge) cycling regimen.

Several pulse-charging modes were evaluated in which the frequency, peak current density (pcd), and on-time/off-time ratios were varied. A cell pulse-charged at a pcd of 15.7 mA/cm^2, 30 ms on/90 ms off, retained over two-thirds of its zinc-covered area when cycling was stopped at cycle 125. Comparison of SEM photographs of the discharged zinc electrodes for cells charged with constant current showed the pulse-charged zinc electrode to have a more densely textured surface than the constant-current charged electrode. This effect may be attributed to the larger number of nucleation sites generated during pulse-charging.

Mathematical Modeling of the Zinc Electrode

(K.G. Miller, F.R. McLarnon, and E.J. Cairns)

Factors limiting the cycle life of the zinc electrode are redistribution of active material over the face of the electrode[6,7] and passivation.[8] A one-dimensional, time-dependent model is being developed to predict the cause and extent of Zn

redistribution and passivation as the electrode is cycled. This model will take into account changes in current density, overpotential, and species concentration. The equations for the model are complete, and the appropriate computer program is being written.

Transient potential and current step experiments have been carried out to determine exchange current densities for the zinc electrode in electrolytes of various KOH and zincate concentrations. The 99.999% pure Zn disc electrodes were fabricated from 1-mm diameter wires polished with successive abrasives to a final polish with 0.3μ Al_2O_3. Zinc counter and reference electrodes were used, and the electrolyte solutions were deaerated. Preliminary results for experiments of 200 ms duration show exchange current densities in the 0.1–0.25 mA/cm^2 range. Subsequent experiments will employ 98% Zn–2% Pb electrodes, as well as pure Zn deposited onto a Pb substrate, in order to simulate the conditions expected in a working cell.

Mathematical Modeling of the Sodium/Sulfur Cell

(S.A. Naftel, F.R. McLarnon, and E.J. Cairns)

A set of equations has been developed to describe the behavior of the sulfur electrode in sodium/sulfur cells. The mathematical description takes into account the effects of diffusion, convection, and migration on the behavior of the electrode, unlike that of previous work.[9,10] An attempt will be made to measure ionic potentials throughout the cathode, in order to confirm the results of modeling. An additional experiment to measure the capillary pressure of sulfur and Na_2S_x in graphite felt has been designed in order to obtain data necessary for predicting convective and wicking effects.

Glass Electrolytes for Lithium/Sulfur Cells

(M.L. Smith, J. Winnick, F.R. McLarnon, and E.J. Cairns)

Novel Li/S cells, which employ a fast-lithium-ion conducting lithium chloroborate glass as the solid electrolyte, have been built and operated at 400°C. The composition of glass used for this study,[11] 7.3 mol% $(LiCl)_2$, 25.7 mol% Li_2O, and 67.0 mol% B_2O_3, had an ionic conductivity of 2.9×10^{-3} $(\Omega^{-1}\cdot cm^{-1})$ at 400°C, which was somewhat lower than those of other lithium chloroborate glasses,[12] which have shown ionic conductivities as high as 2×10^{-2} $(\Omega^{-1}\cdot cm^{-1})$.

The current-voltage characteristics of these cells were examined; they were found to be capable of supporting pseudo-steady-state current densities up to 15 mA/cm^2 for 15–20 hours. A limiting current was found to exist at approximately 23 mA/cm^2. These cells could be charged and discharged with approximately equal polarization in either direction. However, the accumulation of a crystalline reaction layer on the surface of the electrolyte during discharge caused the cells to fail before the completion of a full charge-discharge cycle.

These cells were also used to measure the the solubility of lithium (as a polysulfide) in sulfur. The solubility limit was found to occur at $0.04\ ^{+0.03}_{-0.01}$ mol% Li at 400°C. This is in agreement with the value reported by Sharma.[13]

Oxygen Reduction on Platinum in Fuel Cell Electrolytes

(K.A. Striebel, F.R. McLarnon, and E.J. Cairns)

Preliminary rotating ring–disk electrode (RRDE) studies of oxygen reduction in dilute Cs_2CO_3 and KOH showed that solutions with higher carbonate anion concentrations supported higher oxygen reduction currents.[14,15] These experiments have been supplemented by a series of RRDE experiments in mixed electrolytes (KOH, KCO_3 and KF) with the aim to identify the independent effects of ionic strength, pH, and carbonate anion concentration. At a constant ionic strength of 0.7M, both OH^- and $CO_3^=$ appear to have a positive effect on the kinetic current at 0.9 V vs Reference Hydrogen Electrode (RHE), with the highest kinetic currents observed when both of these ions are present. Peroxide is generated as an unwanted side product and is detected with the ring during a RRDE experiment. Carbonate ion appears to suppress peroxide formation while OH^- appears to increase peroxide formation.

Oxygen reduction experiments in K_2CO_3 and KOH have been completed at concentrations up to 1.0M. When results are adjusted for differences in oxygen solubility, kinetic currents (at 0.9 V vs RHE) are 2 to 2.5 times higher in K_2CO_3 than in KOH at the same concentration. However, lower oxygen solubilities in carbonate electrolytes may lead to higher mass transfer overpotentials in a fuel cell.

Two new all-PTFE cells have been designed and built to carry out measurements at elevated temperatures in more concentrated alkaline electrolytes, on both smooth platinum and supported-platinum gas-diffusion electrodes.

Engineering Analysis of Photoelectrochemical Cells

(P.M. Lessner, J. Winnick, F.R. McLarnon, and E.J. Cairns)

We are studying the electrochemistry of the aqueous polysulfide redox couple because of its potential application in energy conversion and storage devices such as photoelectrochemical cells and redox batteries.[16–18] Our efforts have concentrated on the fundamental measurement of kinetic and transport parameters by a transient potential step method, steady-state measurements on rotating disk electrodes, modifications of solution chemistry through addition of organic cosolvents, and construction and testing of porous electrodes.

The transient potential step method was used to obtain data on exchange current density and active species concentration.[19–21] The applicability of this technique in the low (linear) overpotential region has been well analyzed.[22,23] Cobalt was chosen as the electrocatalyst for most of the studies, but platinum and MoS_2 were also used. Experiments were performed over the temperature range of 25–80°C. The cell used for these experiments was constructed of a 1/2-inch nylon tube cross, wrapped in heating tape and insulation for operation at elevated temperature. Data were recorded on a digital storage oscilloscope over a time interval of several milliseconds. An attempt was made to fit (using nonlinear least squares)[24] each data set to an analytical expression for a current-time transient for a multistep redox reaction under kinetic-diffusion control.[23] At temperatures below about 48°C the fit was good, but as temperature increased the fit became poor. A fit to the short-time data at higher temperatures underestimated the experimental currents at longer times.

The overall reaction in the aqueous polysulfide electrolyte can be written:

$$1/3S_4^{2-} + 4/3H_2O + 2e^- \rightleftharpoons 4/3HS^- + 4/3OH^- \quad (1)$$

The points in Fig. 3 show a plot of the active species concentration versus temperature which was determined from the fitting procedure mentioned above. The bulk concentrations of the species in Reaction 1 are orders of magnitude higher than the concentration of the active species determined from the potential step measurements. The radical anion S_2^- (supersulfide) is in equilibrium with tetrasulfide:

$$S_4^{2-} \rightleftharpoons 2S_2^- \quad (2)$$

Its concentration was evaluated from published equilibrium data,[25] and the line in Fig. 3 shows the concentration of supersulfide as a function of temperature. There is good agreement between the calculated concentration of supersulfide and the experimentally obtained concentrations, which suggests that supersulfide is the electrochemically active species.

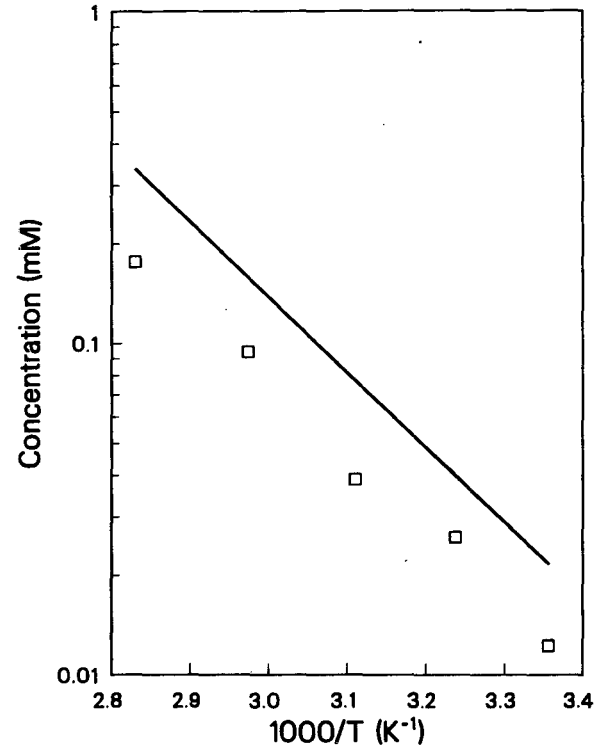

Figure 3. Active species concentration in 1M Na_2S_4 at pH = 12: □ calculated from diffusion parameter; ___ calculated from Ref. 25. (XCG 861-7035)

The deviations between the fit to the analytical form of the current-time transient and the experimental data can now be understood. At lower temperatures, and for the time scales considered here, very little conversion of tetrasulfide to supersulfide takes place (low rate of reaction and thin boundary layers), so it is the supersulfide initially present that determines the response. As the temperature increases, the forward rate of Reaction 2 becomes a significant factor, but at low overpotentials it is not the sole rate-determining step. One of the assumptions made in deriving the analytical form of the current time transient[23] is that there is only one rate-determining step; this assumption is violated here, which explains the deviation between experiment and theory.

The correct form of the material balances and boundary conditions for an electrode reaction with two steps that occur at comparable rates, at least one

of which is homogeneous, were formulated.[26] The nonlinear partial differential equations were solved numerically using a VAX 8600 computer, and comparison of experimental data and model predictions is shown in Fig. 4. The agreement is excellent, and the derived dimerization rate constant agrees with that determined for other radical anion reactions.[27] The exchange current densities are the order of 1 mA/cm^2 and are significantly higher than those previously reported.[28]

Steady-state data are needed to evaluate performance of candidate electrocatalysts. Before constructing a porous redox electrode we need to estimate the ratio of true to projected area needed and the appropriate hydrodynamic conditions for operation. The rotating disk electrode was chosen for these evaluations because it can be polished to a reproducible surface and can be operated under well-known hydrodynamic conditions. It was found that at 77°C a current of about 3 mA/cm^2 could be sustained on smooth cobalt electrode at 50 mV polarization and a rotation rate of 1000 rpm. Our preliminary design goals[19] should then require a ratio of true to projected area of about 4, under these hydrodynamic and temperature conditions.

In aprotic, organic solvents containing C=O, S=O and P=O structural units, the equilibrium of Reaction 2 is shifted to the right,[29,30] and the resulting increase in supersulfide concentration would be expected to improve electrode reaction rates. A previous study using N,N-dimethylformamide (DMF) showed that as it was added to an aqueous polysulfide solution, supersulfide was produced at the expense of tetrasulfide.[31] Current-voltage curves for a water-DMF and pure aqueous polysulfide solutions were recorded at cobalt and platinum electrodes. Figure 5 shows a comparison of the responses. Addition of DMF increases the current density by over 100% at the same temperature and total overpotential.[32,33]

Porous flow-through electrodes fabricated from screens could achieve the ratio of true to projected area and hydrodynamic boundary layer thicknesses with only small parasitic power losses. A cell and flow system for evaluating screen electrode performance has been constructed. We plan to test screens fabricated from several metals and metal sulfides as well as aqueous solutions containing organic cosolvents.

PLANNED ACTIVITIES FOR FY 1986

Continuing research efforts on secondary alkaline zinc electrodes will focus on the application of *in-situ*

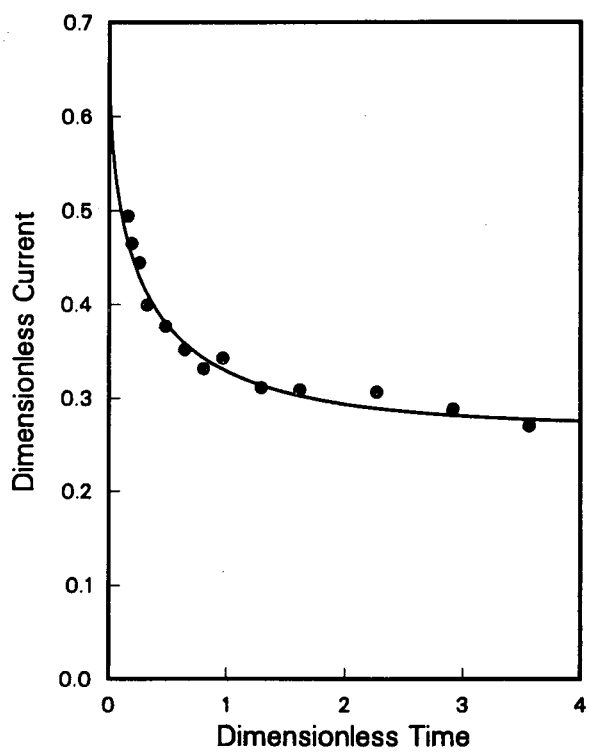

Figure 4. −20.1 mV step at 80.4 °C: • experimental data; —— calculated response with k_f = 0.15 sec^{-1}. (XCG 861-7036)

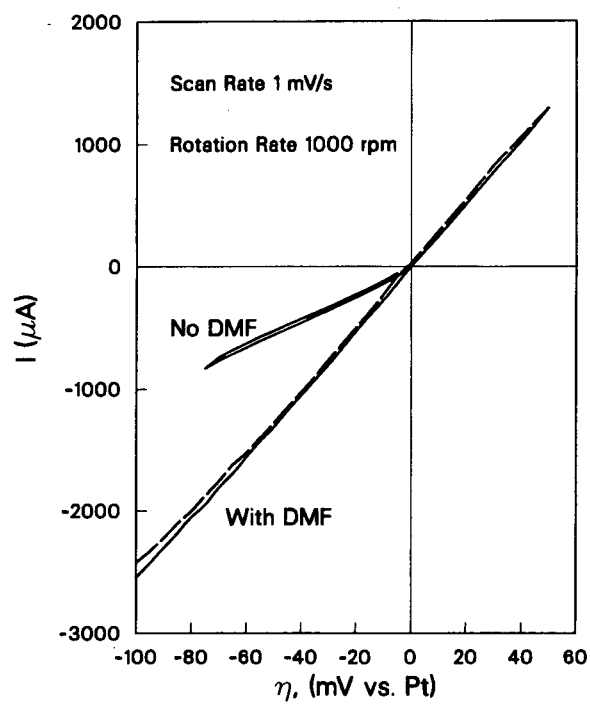

Figure 5. Addition of DMF to a 1M Na_2S_4 aqueous solution; response at a 0.2 cm^2 Co electrode, 77°C. (XCG 861-7037)

microelectrode potential measurements to determine electrolyte species concentrations in operating zinc electrodes; the development of a comprehensive mathematical model and complementary testing of Zn/NiOOH cells to verify the model; the performance of cycle-life experiments to complement mathematical analysis of zinc-electrode current collection; the evaluation of optimized pulsed-current charging regimes with electrolyte and electrode formulations that exhibit reduced zinc-species solubility; and the microscopic study of model zinc electrodes.

High-temperature alkali metal/sulfur cell studies will include measurement of capillary pressures in sulfur electrodes; mathematical modeling of the sulfur electrode and complementary operation of Na/S cells; and a thermodynamic stability analysis of solid electrolytes for use in Li/S cells.

Research on advanced electrolytes for fuel cells will include the fabrication of porous gas diffusion electrodes to test the performance of alkaline-carbonate electrolytes. Advanced electrocatalysts will be evaluated in sulfur/polysulfide redox electrolytes.

REFERENCES

1. Dirkse, T.P. (1954), "The Nature of the Zinc-Containing Ion in Strongly Alkaline Solutions," *J. Electrochem. Soc. 101*, p. 328.
2. Hampson, N.A., Herdman, G.A., and Taylor, R. (1970), "Some Kinetic and Thermodynamic Studies of the System Zn/Zn(II), OH^{2-}," *J. Electroanal. Chem. 25*, p. 9.
3. Nichols, J.T., McLarnon, F.R., and Cairns, E.J. (1985), "Zinc Electrode Cycle-Life Performance in Alkaline Electrolytes Having Reduced Zinc Species Solubility," *Chem. Eng. Commun. 37*, p. 355.
4. Katz, M.H., McLarnon, F.R., and Cairns, E.J. (1982), "Computer Control of Electrochemical Experiments with Application to Zinc/Nickel Oxide Cells," LBL-15546.
5. Wagner, O.C. and Almerini, A. (1984), *Proc. 31st Power Sources Symp.*, The Electrochemical Society, Pennington, NJ, p. 255.
6. McBreen, J. (1972), "Zinc Electrode Shape Change in Secondary Cells," *J. Electrochem. Soc. 119*, p. 1620.
7. Choi, K.W., Bennion, D.N., and Newman, J. (1976), "Engineering Analysis of Shape Change in Zinc Secondary Electrodes. I. Theoretical," *J. Electrochem. Soc. 123*, p. 1616; "Engineering Analysis of Shape Change in Zinc Secondary Cells. II. Experimental," *ibid.*, p. 1628.
8. Sunu, W.C. and Bennion, D.N. (1980), "Transient and Failure Analysis of the Porous Zinc Electrode. I. Theoretical," *J. Electrochem. Soc. 127*, p. 2007; "Transient and Failure Analyses of the Porous Zinc Electrode. II. Experimental," *ibid.*, p. 2017.
9. Jacquelin, J. and Pompon, J.P. (1979), "A Mathematical Model of the Behaviour of the Molten Sodium Polysulfide Electrode," in *Power Sources*, Vol. 7, p. 713, J. Thompson, Ed., Academic Press, London.
10. Breiter, M.W. and Dunn, B. (1979), "Potential Distribution Model for Rechargeable Sulphur-Electrodes in Sodium-Sulfur Cells," *J. Appl. Electrochem. 9*, p. 291.
11. Smith, M.L., McLarnon, F.R., and Cairns, E.J. (1985), "Investigation of a Vitreous Electrolyte for Use in Lithium/Sulfur Cells," LBL-20737.
12. Button, D.P., Tandon, R.P., Tuller, H.L., and Uhlmann, D.R. (1981), "Fast Lithium-Ion Conduction in Chloroborate Glasses. II. Diborates and Metaborates," *J. Solid State Ionics 5*, p. 655.
13. Sharma, R.A. (1972), "Equilibrium Phases in the Lithium-Sulfur System," *J. Electrochem. Soc. 119*, p. 1439.
14. Striebel, K.A., McLarnon, F.R., and Cairns, E.J. (1985), "The Effect of Carbonate Ions on the Reduction of Oxygen at Platinum Electrodes in Dilute Alkaline Electrolytes," 167th Meeting of the Electrochemical Society, Toronto, Canada, Paper No. 410.
15. Applied Science Division (1985), Annual Report for FY 1984, LBL-18750, pp. 1-40 to 1-44.
16. Ellis, A.B., Kaiser, S.W., Bolts, J.M., and Wrighton, M.S. (1977), "Study of n-type Semiconducting Cadmium Chalcogenide-Based Photoelectrochemical Cells Employing Polychalcogenide Electrolytes," *J. Am. Chem. Soc. 99*, p. 2839.
17. Russak, M.A. and Creter, C. (1984), "Vacuum Evaporated $CdSe_{1-x}Te_x$ Thin Films for Electrochemical Photovoltaic Cells," *J. Electrochem. Soc. 131*, p. 556.
18. Licht S., *et al.* (1985), "High Efficiency n-Cd(Se,Te)/$S^{=}$ Photoelectrochemical Cell Result- ing From Solution Chemistry Control," *Appl. Phys. Lett. 46*, p. 608.
19. Lessner, P., Winnick, J., McLarnon, F.R., and Cairns, E.J. (1985), "Porous Counterelectrodes For Aqueous Polysulfide Photoelectrochemical Cells," 167th Meeting of the Electrochemical

Society, Toronto, Canada, Paper #666.
20. Lessner, P., Winnick, J., McLarnon, F.R., and Cairns, E.J. (1985), "Electrode Kinetics in Aqueous Polysulfide Electrolytes: Transient Experiments," LBL-20603, submitted to The Electrochemical Society for the Boston, MA, Meeting, May 1986.
21. Lessner, P., Winnick, J., McLarnon, F.R., and Cairns, E.J. (1986), "Kinetics of Aqueous Polysulfide Solutions: Part II. Electrochemical Measurement of the Rates of Coupled Electrochemical and Chemical Reactions by the Potential Step Method," LBL-20990, submitted to *J. Electrochem. Soc.*
22. Nagy, Z. (1980), "On The Theory of the Potential and Voltage Step Relaxation Techniques for the Investigation of Fast Electrode Reactions," *Electrochim. Acta 25*, p. 575.
23. Nagy, Z. (1982), "Error Analysis of the Potential and Voltage Step Relaxation Technique for the Measurement of Kinetics of Electrode Reactions," *J. Electrochem. Soc. 129*, p. 1943.
24. More, J.J., Garbow, B.S., and Hillstrom, K.E. (1980), Argonne National Laboratory Report ANL-80-74.
25. Giggenbach, W. (1971), "The Blue Solutions of Sulfur in Water at Elevated Temperatures," *Inorg. Chem. 10*, p. 1306.
26. Lessner, P., Winnick, J., McLarnon, F.R., and Cairns, E.J. (1986), "Kinetics of Aqueous Polysulfide Solutions: Part I. Theory of Coupled Electrochemical and Chemical Reactions, Response to a Potential Step," LBL-20989, submitted to *J. Electrochem. Soc.*
27. O'Reilly, J.E. and Elving, P.J. (1971), "Electrochemical Reductions of Pyrimidine in Acetonitrile. Behavior of the Anion Free Radical," *J. Am. Chem. Soc. 93*, p. 1871.
28. Allen, P.L. and Hickling, A. (1957), "Electrochemistry of Sulfur: Part 1. Overpotential in the Discharge of the Sulfide Ion," *Trans. Faraday Soc. 53*, p. 1626.
29. Rauh, R.D., Shuker, F.S., Marston, J.M., and Brummer, S.B. (1977), "Formation of Lithium Polysulfides in Aprotic Media," *J. Inorg. Nucl. Chem. 39*, p. 1761.
30. Abraham, K.M., Rauh, R.D., and Brummer, S.B. (1978), "A Low Temperature Na-S Battery Incorporating a Soluble S Cathode," *Electrochim. Acta. 23*, p. 501.
31. Giggenbach, W. (1968), "On the Nature of the Blue Solutions of Sulfur," *J. Inorg. Nucl. Chem. 30*, p. 3189.
32. Lessner, P., Winnick, J., McLarnon, F.R., and Cairns, E.J. (1985), "Addition of DMF to Aqueous Polysulfide Electrolytes: Response at Co and Pt RDE," LBL-20604, submitted to The Electrochemical Society for Boston Meeting, May 1986.
33. Pfeiffer, C.R. (1985), "Improved Aqueous Polysulfide Redox System Utilizing an Organic Cosolvent—Philip M. Lessner, Frank R. McLarnon, Elton J. Cairns and Jack Winnick," DOE Case No. IB-620.

Solid-State Radiative Heat Pump*

P. Berdahl, K. Ghaffari, G. Ng, and L. Shaffer

The purpose of this research is to establish the research basis for the development of a new class of heat pump. This new heat pump would be a solid-state device that accepts input energy in the form of electricity and pumps infrared (heat) radiation across a thermally insulating gap. An important potential application is the cooling of buildings, in conjunction with thermal storage.

Semiconductor materials with direct narrow bandgaps in the range of 0.03–0.25 eV emit equilibrium thermal radiation which is in large part due to electron-hole recombination. An excess or deficit of infrared radiation, compared to the thermal equilibrium value, can be produced when the concentrations of electrons and holes are varied from their thermal equilibrium values by electrical means. Two techniques for varying the concentrations of electrons and holes are of special interest here: (1) electrical bias of a p-n junction to produce carrier injection or, for reverse bias, carrier extraction; (2) the magneto-concentration effect in which orthogonal electric and magnetic fields are used to enhance (or deplete) the concentrations of electrons and holes near the semiconductor's surface. The p-n junction technique seems particularly promising for the development of technologically mature devices, while the magneto-concentration effect offers the opportunity for the study of key recombination phenomena in a simpler experimental system.

ACCOMPLISHMENTS DURING FY 1985

The primary line of research was the construction of the Galvano-Magnetic Luminescence (GML) spectrometer, its first application to determine the GML spectrum of indium antimonide, and the theoretical interpretation of this data to give new measurements of the room temperature carrier lifetime of InSb. Also, experimental work was started toward the explicit demonstration of a continuous cooling effect.

The GML phenomenon is the departure from the equilibrium luminescence emitted by an object in the presence of mutually orthogonal electric and magnetic fields, both parallel to the emitting surface. The new instrument for GML measurements consists of an oscillator and power amplifier to produce an alternating electric field in the sample, a laboratory electromagnet for producing a static magnetic field, and a sensitive synchronous detection scheme to measure the quantity and spectrum of infrared radiation which varies in synchronism with the alternating electric field. The optical portion of the detection system consists of several mirrors, a grating monochromator, and a liquid nitrogen cooled $Hg_{1-x}Cd_xTe$ photoconductive infrared detector. The optical system is calibrated by replacing the sample by a heated blackbody source, modulated with a mechanical chopper. The GML spectrum of intrinsic (pure) InSb obtained with the new spectrometer is shown in Fig.1.[1] The solid dots are the experimental measurements; the theoretical curve will be discussed shortly. The integral of the spectrum is 3.5 W m^{-2} for the noted experimental conditions. This

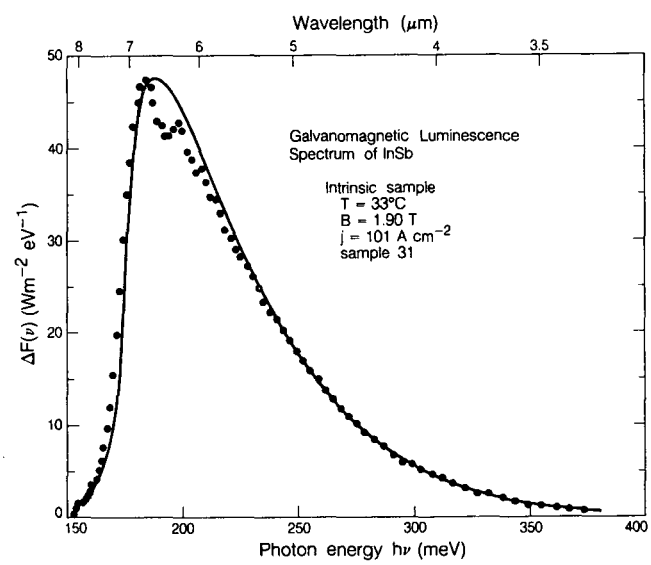

Figure 1. Measured and computed spectra of galvanomagnetic luminescence from intrinsic InSb. The sample thickness is 0.36 mm. The structure in the data near the peak is an artifact due to water vapor in the optical path. (XBL 854-9949)

*This work was supported by the Assistant Secretary for Conservation and Renewable Energy, Office of Energy Storage and Distribution of the U.S. Department of Energy under Contract No. DE-AC03-76SF00098.

radiant heat flow is pumped into and out of the sample alternately, at the 2 kHz frequency of the exciting field.

Prior observations of the GML phenomenon with InSb have been made in Russia[2,3] and Japan.[4] However our measurements have resolved the line shape under conditions of low excitation (carrier concentrations not greatly different from equilibrium values) and are calibrated in absolute units. These facts make it particularly interesting to compare the data with a theoretical calculation. This calculation[1] proceeds by solving the transport equations for electrons and holes in crossed electric and magnetic fields to determine the rate at which these carriers approach the free surface. The carriers accumulate at the surface and recombine radiatively (producing photons) or non-radiatively. Each emitted photon then has a certain probability to avoid reabsorption and reflection at the crystal surface and to emerge from the crystal. For the opposite polarity of the electric field, carriers are withdrawn from the crystal surface, producing a deficit of infrared emission (compared to thermal equilibrium conditions), a phenomenon sometimes termed negative luminescence. The theoretical result for the modulated radiant energy flux per unit photon energy is

$$\Delta F(\nu) = \frac{8N}{(N+1)^2}\,\tau\left(\frac{\pi b(\nu)}{L+\alpha^{-1}(\nu)}\right)\left(\frac{\mu_e\mu_h B}{\mu_e+\mu_h}\right)\left(\frac{j}{qn_o}\right), \quad (1)$$

where N is the index of refraction, τ is the excess carrier lifetime, $b(\nu)$ is the Planck blackbody spectrum per unit solid angle per unit photon energy, $\alpha(\nu)$ is the equilibrium optical absorption coefficient, L is the effective ambipolar diffusion length (a quantity known in terms of the other parameters),[1] μ_e and μ_h are the electron and hole mobilities, B is the magnetic field (z-direction), q is the electron charge, n_o is the intrinsic carrier concentration, and j is the current density (x-direction). The photon energy is $h\nu$, where h is Planck's constant. The crystal surface is in the y = 0 plane, and the emission occurs across this plane in the negative y-direction. Since all the parameters in Eq.(1) are known except the carrier lifetime τ, this lifetime can be determined by fitting the expression (1) to the data. This fit is shown as the continuous curve in Fig. 1. The resulting value of τ is 12 ns. Thus GML measurements provide a new technique for the determination of carrier lifetimes in semiconductors.

The GML measurements show directly how well a GML solid-state radiative heat pump works. However, the deduction of carrier lifetimes from the GML measurements makes it possible to evaluate materials also as parts of other types of solid-state radiative heat pumps, such as the large-area junction types which will require no magnetic field. For any radiant heat pump the quantum efficiency η_q, which is the probability that an excess electron-hole pair will produce a photon, is the key materials parameter. It is given by the relation $\eta_q = \tau/\tau_r$, where τ_r is the radiative lifetime, a quantity which can easily be computed from optical absorption data. For intrinsic InSb the radiative lifetime (at 33°C) is 580 ns; and, thus, the quantum efficiency is 2%. The eventual development of high efficiency heat pumps, with, say, 50% of the Carnot coefficient of performance, will require a correspondingly high efficiency for radiative recombination. GML spectroscopy accompanied by quantitative spectral analysis is a new tool for understanding how η_q varies with parameters such as temperature and doping and to identify materials which may have suitably high values of η_q.

GML measurements were also performed on p-type InSb. This material has cadmium (about 50 ppm) present as a dopant. The luminescence is qualitatively different from that of pure InSb. There is less luminescence at room temperature, but the intensity of the luminescence increases rapidly with increasing current (and, presumably, with increasing temperature). This behavior is not yet understood. Other features of the measurements, also different from pure InSb, are that the intensity is a nonlinear function of magnetic field, and that the spectrum of emission extends into the "forbidden" energy gap. This feature is of particular interest because of the relatively small number of materials with small energy gaps.

Another activity was experimental work designed to explicitly show a continuous (nonalternating) cooling effect in a vacuum, using a thin crystal in orthogonal electric and magnetic fields. A schematic diagram of the experimental device is shown in Fig. 2. Sample fabrication is proving to be challenging. One requires single crystals with an area of 1 cm^2 which are preferably only a few microns thick.

PLANNED ACTIVITIES FOR FY 1986

Successful completion of the continuous cooling experiment is a key goal. It is intended to produce a small (about 1 mW) cooling effect, to be detected by a thermocouple. This cooling effect may be masked by parasitic heating effects, in which case its existence will be demonstrated by showing that

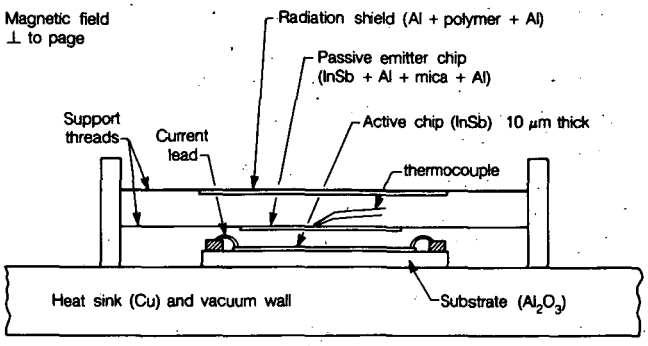

Figure 2. Diagram of the apparatus for the continuous cooling effect experiment. (XBL 859-10788)

reversal of a magnetic field, while maintaining constant electric power input, causes the thermocouple's temperature to decrease. Observation of this cooling effect will confirm the theoretical expectation that galvanomagnetic luminescent devices can function as cooling devices, and increase confidence that future p-n junction solid-state radiative heat pumps will also be capable of producing cooling.

The GML measurements will be continued on InSb, and extended to cover a larger range of temperature and doping concentrations. The preparation of thinner samples will enhance signal-to-noise levels because higher current densities can be employed. These measurements will culminate in a comprehensive paper on the galvanomagnetic luminescence of indium antimonide. Also, GML measurements will be initiated with one of the narrow-bandgap lead salts, probably $Pb_{1-x}Sn_xTe$. Due to qualitatively distinct band structure, the parasitic Auger recombination mechanism which shortens the carrier lifetimes in InSb may be less important. Finally, theoretical calculations in support of the experimental work will continue.

REFERENCES

1. Berdahl, P., and Shaffer, L. (1985), *Appl. Phys. Lett. 47*, p. 1330.
2. Ivanov-Omskii, V.I., Kolomiets, B.T., and Smirnov, V.A. (1965), *Sov. Phys. Dokl. 10*, p. 345.
3. Bolgov, S.S., Malyutenko, V.K., and Pipa, V.I. (1979), *Sov. Tech. Phys. Lett. 5*, p. 610.
4. Morimoto, T. and Chiba, M. (1981), *Phys. Lett. A85*, p. 395.

Thermochemical Energy Conversion and Storage by Direct Solar Heating*

A.J. Hunt, J. Ayer, and R. Otto

The objective of this research is to investigate the use of concentrated solar energy to drive the endothermic portion of a thermochemical energy storage cycle. A thermochemical cycle provides a means to store energy collected by a solar thermal power plant on clear days and to produce electricity during the night or on cloudy days. The cycle consists of two steps: (1) an endothermic step in which energy is supplied to dissociate the gas and (2) an exothermic step in which the products of decomposition are combined over a catalyst to release heat energy at high temperatures. The heat can be used to operate a turbine or for industrial processes.

In particular, we are investigating the decomposition reaction of gases adsorbed on the surface of small particles that act both as the solar absorber and catalyst. This is an application of the direct-flux small-particle solar reactor known as the STARR (Solar Thermally Activated Radiant Reactor), described in the Solar Energy Program chapter of the Annual Report. The STARR uses a suspension of small particles (diameter less than 1 μm) as the solar absorber, heat exchanger, and in this case, catalyst for the reaction. The advantages of using small particles for this application are: (1) they are excellent absorbers of sunlight, (2) only a small mass of particles is required, (3) the small particle size provides a large surface area per gram of material, which greatly enhances catalysis of a gas phase reaction, (4) small particles can rapidly heat the surrounding gas to a high temperature, (5) the overall system efficiency is high because direct absorption eliminates the need for conventional heat exchangers. and (6) if the particles act as photocatalytic sites the reaction can take place at temperatures below that required for equilibrium dissociation.

*This work was supported by the Assistant Secretary for Conservation and Renewable Energy, Office of Systems Research, Energy Storage Division of the U.S. Department of Energy under Contract No. DE-AC03-76SF00098.

ACCOMPLISHMENTS DURING FY 1985

The decomposition reaction of SO_3 was chosen to investigate the feasibility of the STARR concept for thermochemical energy storage for several reasons: SO_3 has a very large endothermic enthalpy of dissociation, both SO_3 and SO_2 (the product of the dissociation reaction) can be stored as liquids near ambient temperatures; the thermodynamic process of dissociation is well known;[1] and there are extensive evaluations of thermochemical storage cycles using this reaction.[2,3]

Hematite (Fe_2O_3) particles were chosen for the absorber and catalyst for the experimental research for several reasons. First, it is an established catalyst for SO_3 dissociation. Second, small particles of hematite are excellent solar absorbers. In addition to heating the gas and acting as a dissociation site, hematite also has the proper characteristics to initiate photocatalytic dissociation of SO_3.

Theory

Figure 1 illustrates the equilibrium fraction of SO_3 dissociated versus temperature at a total constant pressure of 1 atmosphere. Starting from pure SO_3, the percent of SO_3 dissociated cannot exceed the thermodynamic limit at that temperature and therefore must lie on or below the curve in the shaded region. The experimental results obtained by Rocket Research Co. using Fe_2O_3 are plotted in Fig. 1, and it can be seen that they fall below the equilibrium concentrations.[1] In the STARR concept, small particles of hematite are entrained in the SO_3 gas and injected into a reactor with a transparent window. The particles absorb sunlight and act as the sites for the catalytic decomposition. Because the particles are (1) hotter than the gas, and (2) the molecular transport to and from their surface is not hindered by a substrate, they should be more effective than conventional catalysts.

In addition to improved performance due to the nature of the heat and mass transfer processes in STARR, photo processes may also play a role. It is possible to photodissociate SO_3 at ambient temperatures using near UV light. In this case, the degree of dissociation may be maintained *above* the equilibrium value if the photon flux is sufficient to overcome the thermal reaction rates tending toward equilibrium (see Fig. 1). The SO_3 molecule absorbs a UV photon directly to initiate this process. Solar photons contain sufficient energy to dissociate SO_3 since the enthalpy of dissociation is 23 kcal/mole, or 1.0 eV/molecule, an energy well below the peak of the solar spectrum. However, SO_3 is not absorbing at most solar wavelengths. Photodissociation can occur if there is a way to transfer the energy from solar photons to the SO_3 molecule. If it can be accomplished, a degree of dissociation exceeding that of the equilibrium value at a given temperature can be

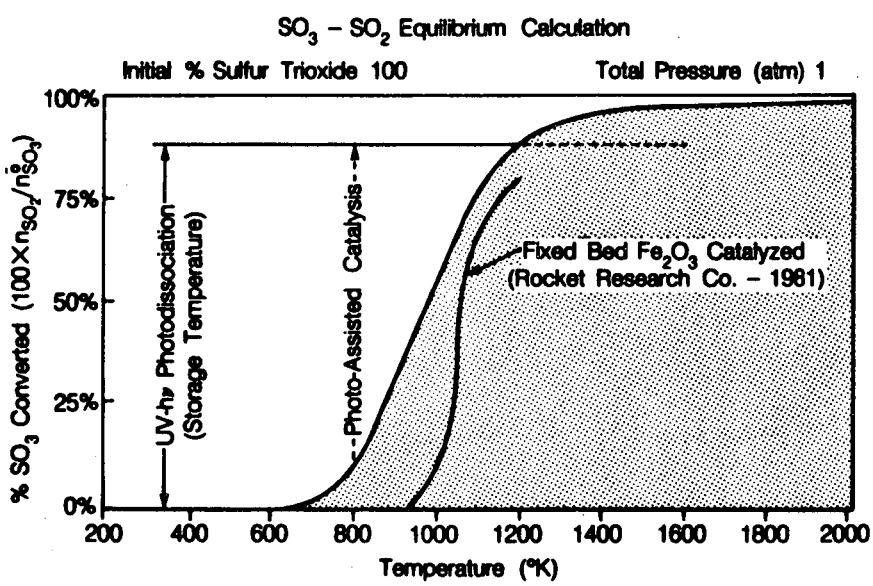

Figure 1. Equilibrium dissociation yields and photothermal pathways for SO_3 dissociation. (XBL 853-1888A)

achieved. Thus, a SO_2/SO_3 storage system directly utilizing solar photons can operate at a lower temperature and higher efficiency than one based on thermodynamic equilibrium.

Several mechanisms for photodissociation are possible because of the presence of the absorbing particles. Reduced sites may be produced on the surface of the Fe_2O_3 particles by photodissociation of the hematite as is illustrated in Fig. 2. Upon contact with SO_3, these sites regain the lost oxygen atom, thereby releasing SO_2. This mechanism is consistent with that proposed by Rocket Research.[1] Another coupling mechanism is the production of electron-hole pairs by photoabsorption in a semiconducting particle and their subsequent transport to the particle surface. The photoproduced charges reach the surface and react with adsorbed SO_3 molecules in a combined oxidation-reduction reaction to initiate dissociation. Hematite particles are good candidates for this process because they have semiconductor properties and a bandgap (2.2 eV) well within the solar spectrum.

Experimental System

An experimental system was designed and built to study the dissociation of SO_3 as a function of temperature and radiant flux density. The apparatus has

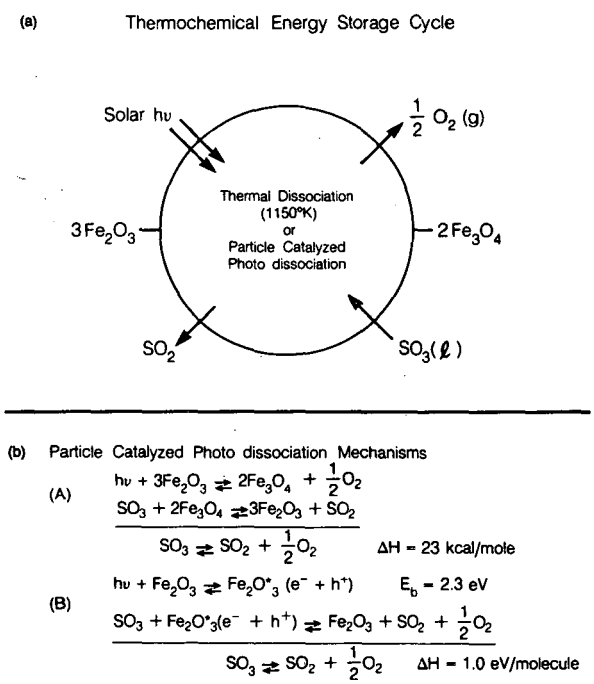

Figure 2. A conceptualization of a storage cycle for a solar thermally activated radiant receiver using small particles as heat exchanger and catalyst. (XBL 865-11120)

two principal components, the SO_3 transfer system and the radiant reactor. These components are described below.

Because SO_3 is an extremely reactive and toxic compound, great care was taken to build a transfer apparatus that is both safe and easy to use in a laboratory environment. Small containers of SO_3 (100 grams) were received in the form of sealed pyrex vials which, once opened, cannot be resealed. However, because only a small amount of SO_3 is required for each run, a method to transfer small quantities of SO_3 was developed. After opening, the glass SO_3 vial is placed in a resealable stainless steel container equipped with vacuum valve. The valve is attached to the transfer system and is hand controlled to allow small quantities of SO_3 vapor to be transferred into the reactor. The container is airtight to avoid contact of SO_3 with water vapor, since this will result in the rapid exothermic production of corrosive sulfuric acid. The design of the transfer system has several unique features. The apparatus was built completely from stainless steel, teflon, quartz, and pyrex because SO_3 does not react with these materials. The system is evacuated so that only pure SO_3 is transferred into the reacting chamber. Because SO_3 condenses at 41°C, the entire transfer system is maintained above this temperature to keep the SO_3 from condensing in the transfer lines. A schematic diagram of the apparatus is given in Fig. 3.

The function of the reactor is to provide an environment to study the dissociation of SO_3 under either isothermal conditions or when subjected to a combination of thermal heating and simulated concentrated solar flux. The reactor (Fig. 4) must be transparent to allow radiant energy to enter and interact with the gas and particles. It must hold a vacuum while connected to the transfer apparatus, and seal completely when removed from it. For the initial experiments the particles are not entrained in the gas but are distributed on a quartz disk suspended in the reaction zone. The particles are widely spaced to simulate a particle-gas suspension. The gas in the reaction zone can be sampled while the reaction is occurring by the use of an argon purge system.

The reaction temperature must be measured to determine the degree of dissociation of the SO_3. Accurate measurement of the temperature in the reaction zone is difficult for several reasons. Because of the corrosive environment, thermocouple wire may be corroded. Measuring temperatures in a radiant environment is difficult because a thermocouple will absorb incident radiation and heat, thus giving

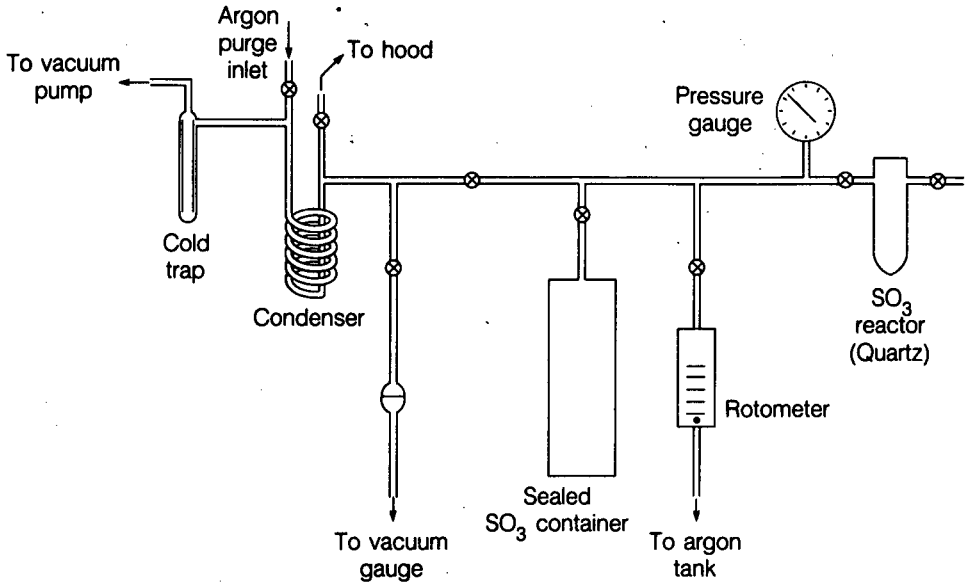

Figure 3. The SO_3 transfer system. (XBL 861-9707)

inaccurate results. Optical pyrometers will not give reliable measurements because of the intense radiant flux in the reactor zone. Given these limitations, it was decided that the temperature in the reactor would be measured with an insulated thermocouple separated from the reactor zone by a thin quartz plate. It is not subjected to the most intense radiant flux because it is beyond the focus and partly shielded by the particles on the quartz disk (see Fig. 4). The radiant source for this experiment is a 2.2 kW xenon arc lamp that provides a peak light intensity of 2600 kW/m^2 at the focus. The lamp has a spectrum similar to the solar spectrum and is filtered to remove the UV.

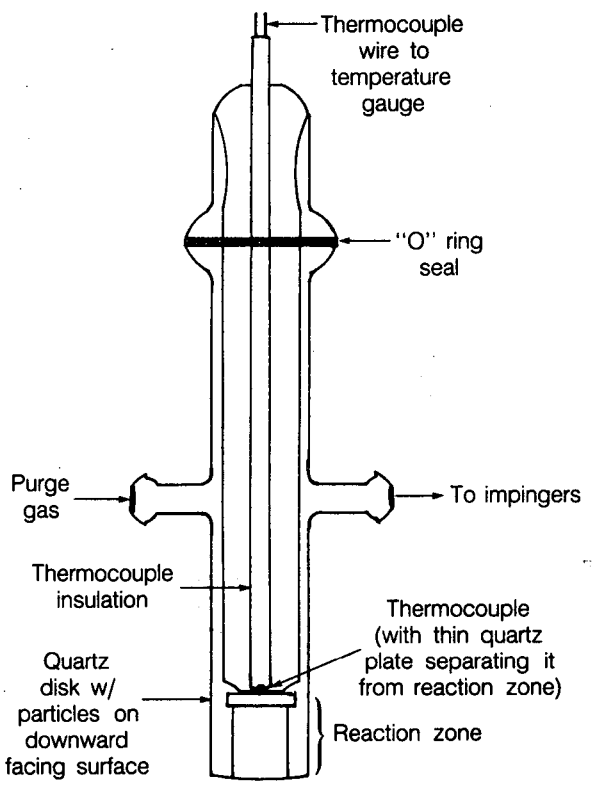

Figure 4. Conceptualization of a small particle radiant reactor. (XBL 861-9708)

PLANNED ACTIVITIES FOR FY 1986

During FY 1986, the SO_3 dissociation experiments will be carried out. There are two phases to each experiment. The first phase is the dark reaction. In this step, the reactor is held at temperature until equilibrium is attained, and a small amount of gas is sampled. In the second phase, known as the light-on phase, the lamp is turned maintained at the same temperature as before, and the gas is again sampled. The SO_2/SO_3 gas stream passes through an aqueous bubbler solution containing formaldehyde to quench the dissociation reaction and preserve the bisulfite ion. Relative amounts of SO_2 and SO_3 in the solution will be measured using ion chromatography, and the light reaction and dark reaction will be compared. If photoassisted catalysis occurs, the SO_2/SO_3 ratio will be greater in the light reaction than in the dark reaction at the same temperature.

REFERENCES

1. Schmidt, E.W., *et al.* (1980), *Development of a Long-Life High-Temperature Catalyst for the SO_2/SO_3 Energy Storage System,* Rocket Research Co. Report RRC-80-R-697.
2. Chubb, T.A. (1974), "Analysis of Gas Dissociation Solar Thermal Power System," *Solar Energy 17,* p. 129.
3. Dayan, J., Lynn, S., and Foss, A. (1979), "Evaluation of Sulfur Oxide Chemical Heat Storage Process for a Steam Solar Electric Plant," LBL-7864.

Constant-Volume Three-Phase Thermal Storage Module*

V.P. Carey

The overall objectives of this research are to demonstrate the feasibility of a new three-phase storage module concept and to experimentally examine the energy storage and heat transfer mechanisms of the module. This work will also aim to develop analytical models of the transport within the module. The results will be used to determine optimal module configurations, PCM materials, working fluids, and thermal control techniques for typical storage applications.

To assess the viability of the module concept and investigate thermal transport within it, a fully instrumented laboratory-scale module has been designed. In this prototype module, encapsulated Glauber's salt is used as the PCM, and R-11 fluorocarbon as the working fluid. This salt changes phase at 89°F. At this temperature, the vapor pressure of R-11 is about 19 psia, so the test module will operate at just above atmospheric pressure.

ACCOMPLISHMENTS DURING FY 1985

During 1985, the prototype thermal storage module was fabricated in the shop, instrumented, and testing was started. Compatibility studies indicated that the encapsulating resin used to make the pellets slowly breaks down when exposed to R-11. Consequently, testing with these pellets in the module could be conducted only for limited time periods.

Transient tests conducted in the spring of 1985 demonstrated the feasibility of the storage module concept. In addition to documenting the energy storage and retrieval modes, the heat transfer process during the heat input mode was studied in detail. The heat input process was observed to consist of three stages. During the initial stage of heat input, the temperature and pressure rise within the module, storing heat sensibly. When the temperature inside exceeds the melting temperature of the PCM by a slight amount, the PCM begins to melt and energy is stored in its latent heat. The temperature and pressure within the module remain about constant during this process. As initially hoped, this storage process is very efficient, requiring only a very small temperature difference to transfer the heat.

When the PCM is completely melted, the temperature and pressure in the module again begin to rise. An analytical model of the transient two-phase heat transfer during the input process when the PCM melts has also been developed. The predictions of this model agree well with the experimental results. This work is summarized in Ref. 1.

PLANNED ACTIVITIES FOR FY 1986

Further work is needed to experimentally determine the two-phase transport behavior during the heat extraction process, and to develop an analytical model for it. However, it appears that reduced funding support will make it impossible to achieve these objectives.

REFERENCES

1. Do, M.T. (1985), "An Experimental and Theoretical Study of Heat Transfer in a Constant-Volume Three-Phase Thermal Storage Module," M.S. Report, Department of Mechanical Engineering, Univ. of California at Berkeley.

*This work was supported by the Assistant Secretary for Conservation and Renewable Energy, Office of Energy Storage and Distribution of the U.S. Department of Energy under Contract No. DE-AC03-76SF00098.

SOLAR ENERGY PROGRAM

INTRODUCTION

During FY 1985, the Solar Energy Program at Lawrence Berkeley Laboratory (LBL) continued to focus on research extending the technology base for a broad range of solar energy applications and to explore new approaches to solar energy conversion.

Passive approaches to heating, cooling, and lighting of buildings are a major research topic. In these technologies, architectural design, construction materials, and natural energy flows between the interior and exterior environment are used to control a building's interior climate and reduce consumption of nonrenewable energy. In FY 1985, LBL examined the application of passive solar technologies to commercial buildings. Projects in both systems development and materials research were carried out.

In commercial buildings, cooling and lighting requirements, including both electric consumption and electric demand, typically dominate energy operating costs. For this reason, research in passive systems development was directed at daylighting and passive cooling. These activities were supported by system simulations and performance monitoring and evaluation.

In daylighting research, two areas of investigation were pursued: developing and refining innovative roof aperture systems and evaluating existing daylighting systems. A facility for measuring illumination levels and light quality of scale models was used in conjunction with detailed building energy analysis simulations to examine the total energy impacts of various roof aperture configurations on office, school, and other buildings. Evaluation of existing daylit buildings includes not only the energy benefits of daylighting but also the functional and aesthetic advantages of daylit spaces. The basis of energy savings in the technology and in occupants' response to it is the focus of the work.

Systems analyses of passive buildings concentrated in three areas: (1) the total energy impacts of advanced aperture materials, (2) energy characterization of passive opportunities in specific building types, and (3) detailed investigation of the energy impact of specific passive technologies. In FY 1985 aperture materials work focused on high insulation clear glazing and the implications of increased access to the solar resource, for both heat and daylight, without significant degradation of the thermal envelope. Energy characterization research studied both office buildings and schools. Detailed systems analysis was done for a variety of applications of thermal mass, to determine its effect on energy use, in particular on cooling and peak demand costs.

Research on advanced aperture materials also continued. This work is intended to identify and develop promising new optical materials for the next generation of high-performance glazings. Research focuses on four technical areas:

(1) Low-conductance, high-transmittance materials, e.g., durable low-emittance glazings and transparent aerogels.
(2) Optical-switching materials, e.g., electrochromic coatings.
(3) Angle-selective transmitting materials.
(4) Materials to enhance daylight utilization in buildings, e.g., light-guide systems.

The research includes technology assessment studies and multiyear research planning; materials synthesis; studies of optical, thermal, chemical, and structural characteristics; stability and durability studies; energy performance studies; and activities to transfer results of our work to appropriate industrial and other private-sector users.

LBL is also engaged in research on the active solar cooling of buildings. Thermodynamic cycles that have the potential for increasing the efficiency of solar-driven absorption air conditioners by at least a factor of 2, compared to the current state of the art, are being studied. The testing phase of the first of these advanced cycle machines, using the double-effect regenerative absorption cycle, was completed during FY 1985. Stable and efficient operation has been achieved, and design performance has essentially been attained. In parallel with the experimental work, simulations and analyses of solar cooling systems have been performed to establish the operating requirements and thermal performance of current and advanced space conditioning systems. This work is helping to determine future research needs for the DOE solar cooling program. Activities in FY 1985 concentrated on the effects of storage options on solar cooling system performance and on

the comparative performance of advanced absorption and desiccant solar cooling systems under the same operating conditions.

A 25-ton-capacity solar absorption air conditioning system had been installed in LBL Building 71 as part of the Solar in Federal Buildings Program. Repeated problems with the newly developed collectors used for this project, start-up and maintenance problems, and then a problem with the chiller, signaled an early end to this demonstration project.

Research continues to explore advanced concepts for using the microstructural properties of materials in conversion, control, and collection of sunlight. The goal is to find and develop solar applications for small-particle suspensions, aggregates, and diffractive structures through a balanced program of experimental and analytical studies. Previous successful solar testing of the Small Particle Heat Exchange Receiver (SPHER) has led to new research efforts to investigate direct radiant heating of particle suspensions for chemical process applications, for thermal energy storage, and for the detoxification of chemical wastes.

In related research, LBL is developing new materials formed from aggregates of small particles (aerogels), both for transparent insulating windows and as intermediate states in the fabrication of ceramic materials with superior properties.

Finally, one of our more basic research projects concerns biological energy conversion techniques, using one of the simplest and most stable biological energy converters known: the pigmented protein bacteriorhodopsin. This project is attempting to elucidate how the molecular structure of this protein uses sunlight to produce an electrical proton current across bacterial and artificial membranes. Such understanding should ultimately suggest ways to produce novel photoelectric cells and solar batteries.

Research is also underway on the bioenergetics of cyanobacteria (blue-green algae) organisms which carry out an O_2 evolving photosynthesis like higher plants, but which also can fix atmospheric N_2 into ammonia. The focus of these studies is to understand mechanisms of photooxidative damage with the objective of improving their efficiency in photosynthetic biomass and ammonia nitrogen production.

Passive Research and Development*

R.C. Kammerud, J.W. Place, M.R. Martin, M. Adegran, H. Akbari, P. Albrand, B. Andersson, F.S. Bauman, C. Benard, P.H. Berdahl, W.L. Carroll, J.P. Coutier, B. Fleury, P. LeConiac, A. Mertol, J.T. Thornton, T. Webster, K. Whitley, and Z. Yilmaz

The amount of conventional fuel used to heat, cool, and light buildings is determined by (1) the interaction of the building with its environment, (2) the thermal gains associated with the activities occurring within the structure, (3) the thermal storage characteristics of the building, and (4) the operating characteristics of the equipment used to convert conventional fuels to end-use energy. Traditionally, the building design process has not adequately accounted for the combined influence of these four factors on building energy consumption. To do so requires that the designer have access to techniques for properly controlling the interactions of the building with the environment and for managing the energy flow within the structure.

Passive heating, cooling, and lighting strategies integrate the energy control and management schemes into the building design. The design parameters are selected so that they enhance and control the coupling of the building to the environment, thereby reducing the requirements for auxiliary heating, cooling, and lighting energy. In this context, the Passive Program at LBL is directed at theoretical and experimental investigations of the energy performance implications of passive design strategies, with emphasis on natural lighting and passive and hybrid cooling of commercial buildings. The specific objectives of the program are the following:

(1) Develop analytic descriptions of the energy processes that occur within a building and between a building and the environment.
(2) Evaluate the effectiveness of passive systems in reducing energy consumption for space heating, space cooling, and lighting.
(3) Develop techniques for integrating effective passive technologies into conventional building systems and structures.
(4) Develop appropriate design tools as a mechanism for transferring newly gained knowledge on passive technologies to segments of the design and building communities.

The strategy used to meet these objectives consists of coordinated experimental and theoretical tasks leading to advanced energy analysis capabilities that can be used in passive system design and evaluation. The emphasis to date has been on improving our understanding of how energy is transferred within passive buildings, how that relates to energy savings exhibited by existing passive buildings, and how future passive systems can be integrated with the structure, mechanical systems, and functional requirements of buildings to improve their energy, functional, and economic performance. Accomplishments and plans in each of these areas are described below.

ACCOMPLISHMENTS DURING FY 1985

Experimental Buildings

Twenty-three passive commercial buildings have been designed and built with DOE support. These are experimental buildings which push the state-of-the-art design; they incorporate advanced conservation features and passive heating, cooling, and lighting strategies. These buildings are being used to examine the effectiveness of state-of-the-art passive strategies in commercial buildings, thereby better defining research needs in heat transfer, modeling, analysis, and design. The information gathered directly from these buildings is also valuable in confirming or providing a basis for modifying the occupancy and energy-related assumptions typically made during the design process.

The passive commercial experimental buildings program has completed the performance evaluation phase, in which studies have been made of: (1) occupancy effects on thermal performance and occupant satisfaction and (2) thermal/energy performance. Data have been collected on the design process and the designs themselves. In addition, performance data have been collected for a 12-month period after occupation; this consists of reports on occupancy schedules and occupant satisfaction as well as energy use data. In some projects, specialized automated monitoring and data acquisition systems have recorded hourly data.

The Passive Commercial Building Extended Analysis Project of the Passive Research and Development Group consists of two projects: (1) analysis of the effect of roof monitors on lighting, heating, and cooling, with special consideration

*This research was supported by the Assistant Secretary for Conservation and Renewable Energy, Office of Solar Heat Technologies, Solar Buildings Technology Division, of the U.S. Department of Energy under Contract No. DE-AC03-76SF00098.

given to lighting control strategies, both manual and automatic; and (2) analysis of the thermal effects resulting from variation in occupancy and occupant interaction with passive systems. In FY 1984, the major effort was to complete the first project and establish the parameters on the second. In FY 1985 the effort was put toward completion of the thermal effects portion of the project and a special supplement to the lighting effects study to evaluate the quality of lighting at one of the buildings.

The roof monitor portion of the study completed in FY 1984[1–3] resulted in unexpectedly high lighting energy savings with daylighting provided by roof apertures and with fully manual control of electric lighting, as shown in Fig. 1. The four bars represent the electricity consumption with manual control, on/off lighting controls, dimming lighting control, and with no daylighting provided (baseline). The difference between each of the first three and the fourth is the energy saved through daylighting. The study has provided considerable information to direct future research in a field which is still in the process of identifying the basic potentials of different daylighting approaches.

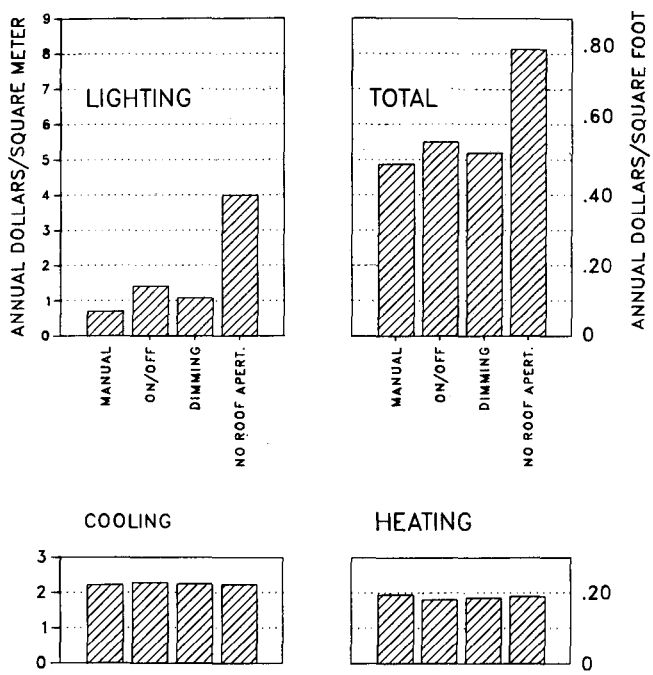

Figure 1. Annual energy costs are shown for the Mt. Airy (North Carolina) Library, broken into lighting, cooling, and heating costs. Dramatic savings could be achieved from daylighting with any of the control strategies tested, but the manual electric lighting control actually used in the building resulted in the greatest savings. (XBL 862-546)

During FY 1985 a supplemental study was completed.[4] The lighting quality in one of the buildings was studied in detail, to determine the effect of different electric lighting and daylighting configurations and combinations and the ability of occupants to read and perform other visual tasks, based on light levels, light distribution, glare, and contrast. Both the task surface and the rest of the visual field were observed. Situations leading to both successful and unsuccessful lighting environments were identified and analyzed.

Thermal analysis of other issues related to occupant comfort, satisfaction, and interaction with passive systems drew on the work of Min Kantrowitz, an LBL subcontractor, for identification of important occupant-related issues. Four areas were evaluated: (1) thermal mass: sensitivity of energy use and comfort to mass amount and exposure; (2) thermostat setback: its integration with mass and effect on comfort; (3) acoustics: its impact on energy use and competition for surface area with passive systems; and (4) shading: energy use sensitivity to variations in shading and shade control. The building energy analysis program BLAST† was used to simulate alternatives in each of these areas. Two to four buildings from the experimental program were simulated to provide a range of situations for each topic.

The results of these studies[1,5] indicated a counteractive relationship between thermal mass and thermostat setbacks strong enough to result in recommendations to eliminate setbacks if significant thermal mass is used and to use only modest levels of thermal mass if deep setbacks are planned to limit energy use during unoccupied hours. It was also found that although acoustic treatment in passive commercial buildings has typically been less effective than occupants desired; in each case methods were found to provide effective acoustic treatment with little or no degradation of the energy performance of the building.

Natural Lighting

In FY 1985, energy analyses on a prototypical, single-story office building outfitted with a variety of roof aperture configurations were continued.[6–9] A prototype building configuration for energy analysis of roof apertures in schools was also developed, and analyses begun. The emphasis in the office building studies was on assessing the effect of roof glazing area, orientation, and tilt in moderating the interac-

†BLAST (Building Loads Analysis and System Thermodynamics) is trademarked by the Construction Engineering Research Laboratory, U.S. Department of the Army, Champaign, Illinois.

tion of the building with the solar resource. In order to assess the implications of this moderating process, calculations were made of lighting electricity consumption, cooling electricity consumption, heating fuel consumption, peak electricity demand, and annual energy operating costs for the building in a range of U.S. climates. The following combinations of orientation and tilt have been examined:

- horizontal;
- south-facing vertical;
- south-facing tilted up sixty degrees from horizontal;
- north-facing vertical;
- north-facing tilted up forty-five degrees from horizontal;
- the combination of south-facing vertical and north-facing vertical;
- the combination of east-facing and west-facing, both tilted up sixty degrees from horizontal;
- the combination of southeast-facing and southwest-facing, both vertical;
- the combination of southeast-facing and southwest-facing, both tilted up sixty degrees from horizontal;
- the combination of north-facing, south-facing, east-facing, and west-facing, all vertical; and
- the combination of northeast-facing, northwest-facing, southeast-facing, and southwest-facing, all vertical.

For each of these glazing orientations and tilts, simulations were performed for a range of roof glazing areas between 0% and 10% of the building floor area, except for north-facing vertical glazing, where the weak collection of sunlight indicated the need to examine larger glazing areas.

Figures 2a–2d show the results of some of these simulations for linear roof apertures on the prototypical office building in Atlanta, GA. Typical Meteorological Year (TMY) data were used in these simulations. In Fig. 2a, annual lighting electricity consumption (at the site) is plotted versus the aperture ratio, defined as the ratio of total roof glazing area to building floor area. (The consumption of primary energy by the utility to generate power would be on the order of three to four times higher than consumption at the site, because of generating inefficiencies and electrical network losses.) Four curves are drawn in Fig. 2a, corresponding to roof glazing which is vertical facing south, vertical facing north, vertical facing both south and north (equally divided), and horizontal (skylights). At all aperture ratios, horizontal glazing has the lowest cooling electricity consumption, reflecting the highly effective annual collection of both diffuse skylight and beam sunlight. At all aperture ratios, the north-facing glazing has the highest lighting electricity consumption, reflecting the negligible collection of beam sunlight and the weaker collection of diffuse skylight resulting from the fact that the vertical glazing faces only half the skydome. Lying approximately halfway between the curves for horizontal and north-facing glazings is the curve for south-facing glazing. The relative positions for these curves are explained by the fact that vertical glazing facing south collects substantially more beam sunlight than vertical glazing facing north, but is substantially less effective than horizontal glazing in the annual collection of both diffuse skylight and beam sunlight. If lighting electricity reductions were the only impact of roof apertures, then horizontal would clearly be the preferred glazing orientation. However, the thermal impacts of roof apertures are also important.

In Fig. 2b, annual cooling electricity consumption at the site (fans plus direct expansion cooling unit) is plotted versus aperture ratio. For small aperture ratios, the cooling electricity consumption decrease with increasing aperture ratio, because all the admitted sunlight is being used to displace electric light of higher heat content. In fact, at small aperture ratios (around 1%), the glazing orientations which collect most effectively during the cooling season have the lowest cooling electricity consumption; i.e., horizontal glazing has the lowest cooling electricity consumption and vertical north-facing has the highest. At larger aperture ratios, the order of the curves is reversed, in the sense that the glazing orientations which collect most effectively during the cooling season produce the highest cooling electricity consumption. This result is explained by the fact that at larger aperture ratios, solar gains frequently exceed the illumination requirements of the building. These excess radiation gains create a thermal load which is not offset by reductions in heat from the electric lights. In general, the cooling electricity consumption curves suggest that horizontal is not the preferred orientation for the roof glazing. This is directly counter to the implications of the lighting electricity consumption results.

In Fig. 2c, boiler fuel consumption is plotted as a function of aperture ratio. In general, the curves tend to be fairly flat. Also, the cost per unit of heating fuel energy at the site is substantially lower than the cost per unit electrical energy at the site. Consequently, from an economic point of view, the variations in the boiler fuel consumption with aperture ratio are relatively inconsequential.

In Fig. 2d, annual operating energy cost is plotted as a function of aperture ratio. For small aperture ratios, all the curves decrease with increasing aperture ratio. The rate of decrease of the operating energy cost is largest for the glazings which collect sunlight most effectively. At larger aperture ratios, the cost curve for the horizontal glazing levels off and then starts to increase. This results from the fact that increases in cooling energy consumption and summertime peak demand offset the decrease in lighting electricity consumption. For all the vertical glazings, the costs continue to decrease with increasing aperture ratio up to the full 10%. However, all three curves for vertical glazing are essentially level at a 10% aperture ratio, suggesting that there is little benefit in going to larger ratios for this particular building type, glazing material, and electric lighting control system.

The results can be summarized as follows:

- For small apertures, horizontal glazing yields the greatest cost benefit.
- At larger glazing areas vertical glazing facing south or the combination of vertical glazings facing both south and north yields the greatest cost benefit.
- Vertical glazings facing south or both south and north produce the largest cost benefit per unit of building floor area.
- Horizontal glazing produces the largest cost benefit per unit of installed glazing area.

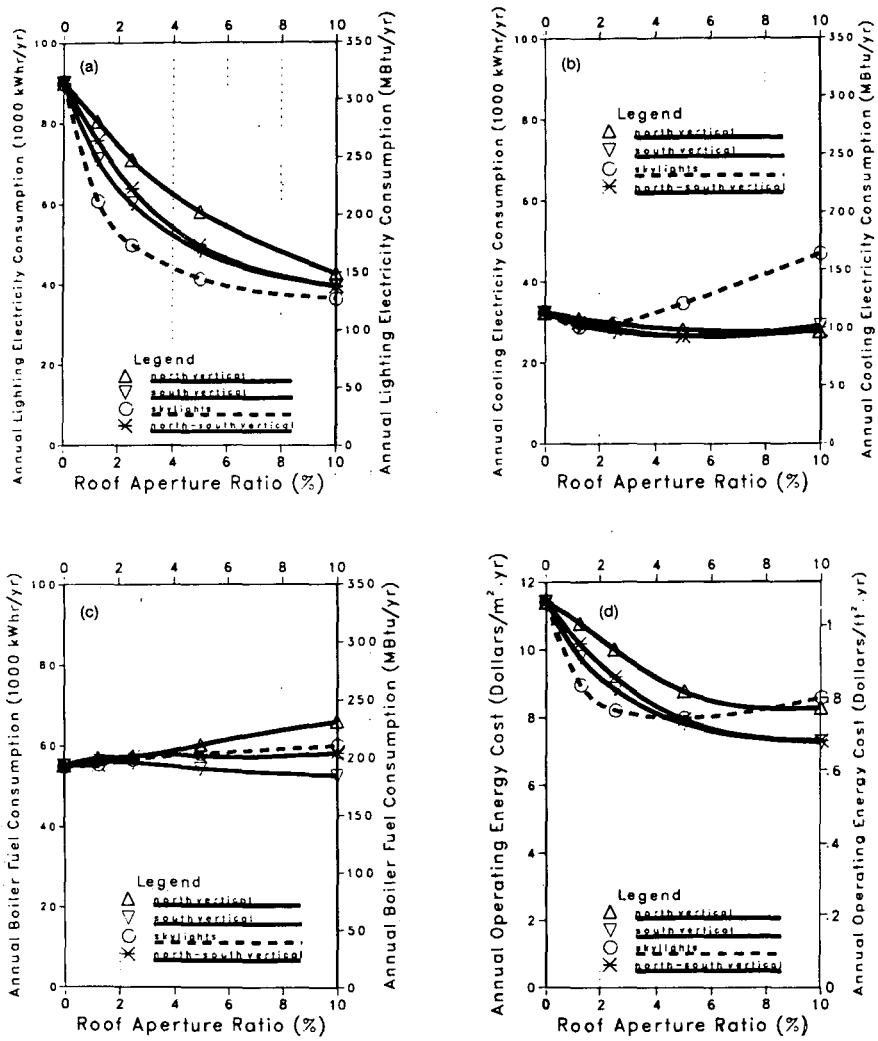

Figure 2. Results of simulations of linear roof apertures on a prototype office building in Atlanta, Georgia, showing the effect of roof aperture ratio on annual energy consumption and cost. Typical Meteorological Year data were used. (a) Lighting electricity consumption; (b) cooling electricity consumption; (c) boiler fuel consumption; and (d) operating energy cost. (XBL 848-3318A)

In general, the results indicate substantial potential benefits from fairly small glazing areas. For example, at a two percent aperture ratio, horizontal glazing produces an energy operating cost savings of about 20 dollars per square foot of glazing.

In addition to the parametric analysis of glazing area, orientation, and tilt, simulations were also performed to determine the sensitivity of the energy and cost predictions to various assumptions in the analysis. Among the factors examined were: thermal comfort conditions in the building, more sophisticated thermal controls of the building, glazing characteristics, obstruction of daylight by snow, dirt accumulation on the glazing, and variation of the internal surface treatments. Of particular significance was the detailed examination of thermal conditions in the prototype building. This study suggested that air temperature alone is not an adequate indicator of thermal comfort in buildings which aggressively utilize environmental resources to reduce energy consumption. In order to deal with nonuniform thermal environments, the Passive Research and Development Group has added a detailed thermal comfort analysis subroutine to BLAST, thereby facilitating a more accurate assessment of the thermal performance of passive buildings.

Design integration was studied in FY 1985. The emphasis in this work was on utilizing the analysis results in a design process examining the integration of the roof apertures with other building systems, such as the building structure, the electric lighting, interior design, the HVAC system, and other passive strategies. Concepts were generated for a variety of roof configurations, both light-weight and thermally massive. A folded-plate, wooden structure was studied in detail (Fig. 3). Structural and economic analyses indicate that there is significant potential for minimizing ceiling and roofing costs by integrating the daylighting apertures with the roofing system.[10] Analysis of integrated roof aperture configurations required the development of specialized measurement equipment. A particularly important development has been the integrating window pyranometer (IWP).[11] Figure 4 shows this instrument applied to a model of the sawtooth configuration in Fig. 3. It is able to measure the solar flux across an *area* of window, rather than just one point, as with other pyranometers. A flux meter of about 4 inches square is placed behind the area of the model to be measured and the back of the material is kept at a constant temperature by continuous flushing with ambient air. As many daylighting configurations are often partially shaded, the integrating effect of this instrument is critical to the analyses.

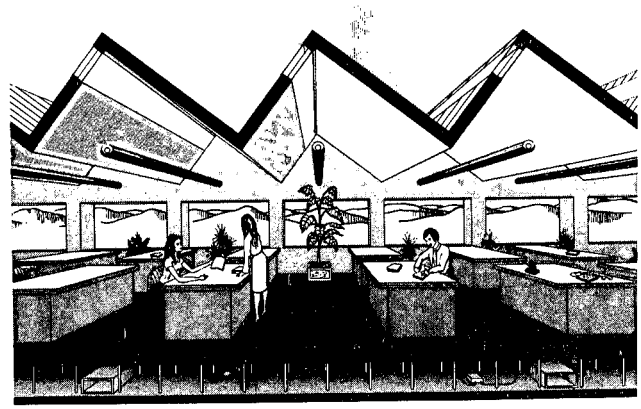

Figure 3. A linear roof aperture system with diffusing glazing tilted toward the south. (XBL 854-1953)

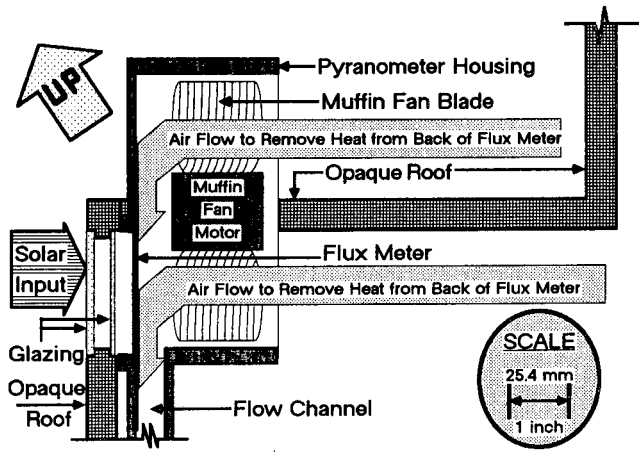

Figure 4. An Integrating Window Pyranometer (IWP) for scale-model measurement of the solar flux over the full glazing area. (XBL 862-547)

Initial efforts at developing design guidelines from both the analytical information resulting from examinations of roof aperture systems and the structural, economic, and design information from the design integration studies were begun in FY 1985.[12]

Residential Thermal Mass

A two-year effort[‡] to explore structural thermal mass on residential heating and cooling loads has been completed. The project had two major phases:

[‡]This research effort has been supported by the Assistant Secretary for Conservation and Renewable Energy, Office of Buildings and Community Systems, Building Systems Division of the U.S. Department of Energy under Oak Ridge National Laboratory Subcontract No. MPO 41X-70373V through Contract No. DE-AC03-76SF00098.

(1) a validation phase, in which simulation predictions were compared with measured data collected by other participants in the program, and (2) a parametric simulation phase, in which predictions of the effects of various thermal mass configurations in models representing realistic buildings were developed and analyzed. Last year's Annual Report described the results from the first phase. The project's second phase consisted of determinating, by simulation, the annual heating and cooling loads for an extensive set of parametric variations of wall thermal mass configurations for a typical residence.[13]

The general approach was to select a prototypical single-family detached residence that had average current practice thermal integrity, design, and use characteristics. The simulated energy performance of this prototypical building in a range of U.S. climates was used as a baseline reference. The baseline configuration was then modified to reflect the incorporation of thermal mass into the exterior walls in varying ways and amounts. The energy performance of these modified configurations was then simulated and compared to the baseline energy performance. Finally, a nonlinear empirical model that represents the energy use results in the data base as a function of wall thermal mass and thermal resistance was developed, and coefficient values for the model were determined by least-squares fits to the data.

All the energy performance simulations for both phases of the project used the building analysis computer program BLAST-3.0. BLAST is a computerized, comprehensive energy analysis simulation tool employing a detailed heat balance solution method with an hourly time increment that correctly accounts for the effects of structural thermal mass on the dynamics of building energy consumption.

The specific house design used for this effort was a 1200 ft^2 three-bedroom residence based on plans developed by the Tennessee Valley Authority (TVA) for a passive solar demonstration project. Choices for layout and materials were taken from detailed blueprints. The design's insulation levels and window thermal integrity were selected to satisfy the requirements of typical building energy performance standards for most U.S. locations. Typical occupant behavior, based on extensive surveys by others, was also assumed. Simulations were conducted for several different climatic conditions. Six cities were chosen to represent the full range of selected climatic parameters representing heating and cooling severity, humidity, and solar gains: Atlanta, Denver, Miami, Minneapolis, Phoenix, and Washington, D.C.

The parametric variations to the house design comprised systematic changes to the values of the thermophysical properties of the exterior walls. The basic wall configuration consisted either of two layers (a low-mass insulating layer and a thermally massive layer with varying thermophysical properties) or of just a massive layer alone. For the two-layer wall, variations also included placement of the insulating layer either external to or internal to the thermally massive layer. Parametric variations were performed separately for the different wall types by combining variations in each of the individual layers. Sufficient intermediate values were used for each parameter to allow the thermal mass and thermal resistance effects to be distinguished. Three hundred and thirteen simulations were performed for each climate, with each simulation yielding annual heating and cooling sensible loads.

The same pattern of load variations was observed for all generic wall types and for all climates, and depends on variations in both the wall thermal resistance and the thermal mass. In general, the data tended to form families of curves: data for one generic wall type in one climate would separate into a series of related curves, where each curve is produced by the data points at various thermal mass levels, for a particular thermal resistance. Several important aspects of behavior were observed in the data:

- For a particular value of wall thermal resistance, increasing the wall thermal mass always reduces both the heating and cooling loads.
- The relative sensitivity of changes to the loads due to incremental changes in the exterior wall's thermal resistance or thermal mass varies widely, and is dependent on the particular values for each, the load type, the wall type, and the climate.
- The relative importance of exterior wall mass for reducing heating loads, as opposed to cooling loads, is strongly dependent on climate.
- For other than massless walls, the loads for different generic wall types with the insulation layer position inverted, but with the same total resistance were different. It was generally true that the loads were lower when the insulation layer was outside the mass layer.

Using a heuristic approach a thermal mass characterization parameter μ for multilayer walls was found:

$$\mu = \sqrt{\sum_{i=1}^{N} t_i \rho_i c_i},$$

where t_i, ρ_i, and c_i are the thickness, density, and

specific heat, respectively, of the ith wall layer. μ is analogous to the thermal resistance of a massless wall.

The general shape of the heating and cooling load variation with μ was the same for the full range of resistances simulated. By trial and error the following analytical form was chosen as the nonlinear regression model:

$$L(\mu,R) = L_\infty(R) + \frac{(L_0(R) - L_\infty(R))}{\sqrt{\tfrac{1}{2}(\cosh(2\sqrt{\pi/24\beta\mu}) + \cos(2\sqrt{\pi/24\beta\mu}))}},$$

where

$$L_0(R) = a_0 + \frac{b_0}{c_0 + R},$$

$$L_\infty(R) = a_\infty + \frac{b_\infty}{c_\infty + R}.$$

Where a_0, b_0, c_0, a_∞, b_∞, c_∞, and β are seven regression coefficients and R is the thermal resistance of the wall. This model was then used in a series of least-square fits to the data. An entire family of data curves including the data for all simulated values of R for a generic wall type can be regressed simultaneously to determine the seven coefficients. The regression procedure was carried out separately for heating and cooling loads, for each of the generic wall types, in each climate.

In general, the agreement between the model predictions and the data is quite good, both qualitatively and quantitatively. The shapes of the curves are all accurately reproduced, including the complex behavior as a function of R at intermediate and high values of μ. The relative error ranges from a low of about 0.1% to a high of 3.7%, with overall averages of about 1% for both heating and cooling. Figure 5 shows the typical agreement that can be achieved between the BLAST simulation data base and the seven-parameter nonlinear model predictions, using the coefficients derived from the regression procedure. Graphical comparisons for other locations show the same general quality of agreement.

It is expected that the data base, and the model that has been developed to represent it, will ultimately lead to an increased, quantitative understanding of the effect of exterior wall thermal mass on the energy performance of residential buildings.

Climate Analysis

A project was undertaken in FY 1985 to develop an area of research looking into climate issues related to buildings. In the past, such issues have been investigated by building researchers primarily as necessary, but peripheral, undertakings to support the primary research goals of building energy analysis, including some previous climate work done in the solar program.[14] As a result, most of such research has been taken only so far as necessary to achieve the limited requirements of the building research and, being of secondary importance, is seldom published. Therefore, much repetition occurs and communication of results is very limited.

The intention of the project has been to develop a climate research program with two broad goals:

- Create an environment in which climate's relation to buildings is a primary topic of research; and
- Develop, collect, and disseminate information on the climate/building relationship.

During this initial effort, the primary technical task has been a study of the impact of refinements to wind data on energy analysis results.[15] Climate data used for building energy analysis are usually collected at airports or similar unobstructed sites, where there is minimal interference with the instrumentation, and the climate itself is not altered by local

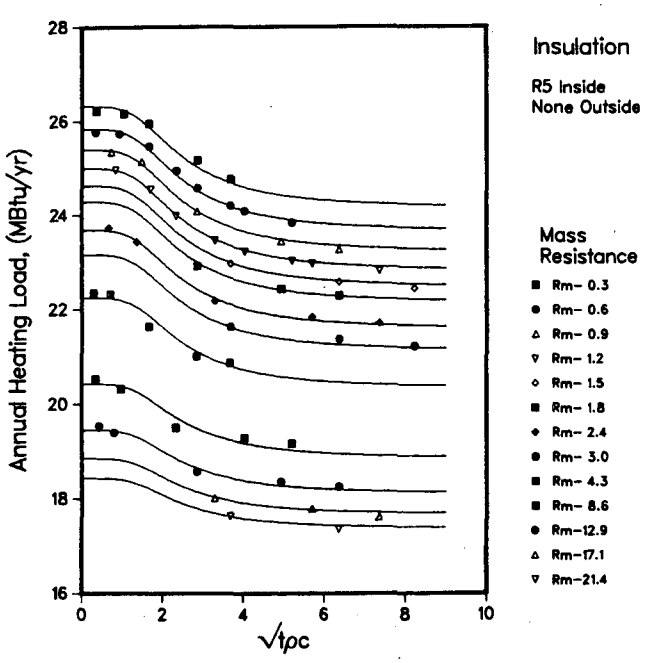

Figure 5. Comparison between BLAST simulation data and empirical model predictions: Atlanta, Heating, Rin=0, Rout=0. (XBL 862-548)

variations in terrain or nearby obstructions. Wind data are usually measured atop a mast, usually standardized now to 25 feet and/or 10 meters, but historically highly variable. Wind speeds around buildings, however, are rarely unobstructed, and the height of the winds of interest is usually much lower than that at which they are measured.

Despite this distinction between measured wind data and that which would better represent wind speeds *near the building*, nowhere in the usual chain of weather data measurement, manipulation, preparation for building analyses, or in the building analysis process itself, is the difference between measured airport data and wind activity around a building corrected.

Alternative algorithms which relate wind speed at different heights and with different obstructions within the same atmospheric wind regime exist. Two well-documented ones were chosen to test the sensitivity of building energy analyses to variations in the description of the wind data used. The first algorithm is part of a method used by Max Sherman and others to identify the actual wind behavior and effects around single-family residences. The second is used by Ed Arens for his program SITECLIMATE, which takes weather station data and adjusts it for use at a specific building site.

Comparisons were made for a standard situation: a one-story residence in a suburban setting in Nashville, with a three-story office building down the street. In all, five simulations were run:

- A constant, high wind (15 mph) superimposed on standard TMY climate data, to set an upper limit
- The base case, using standard TMY climate data
- TMY data with wind speed altered according to the Sherman algorithm
- TMY data with wind speed altered according to the Arens algorithm
- No wind (0 mph) superimposed on the TMY data, to set a lower limit

Each set was run with both DOE-2 and BLAST, in order to identify any program specific anomalies which might occur.

The results can be seen in the two figures showing heating and cooling loads (Fig. 6). In comparison with the base case, overall heating loads are down 19% (Sherman) to 34% (Arens). Cooling loads are up 7% (Sherman) to 17% (Arens). BLAST and DOE-2 show essentially identical effects. To a designer, the more important point might be to identify the total wind impact on his energy use. Starting at the level of no wind, wind adds 20%, 46%, or 81%,

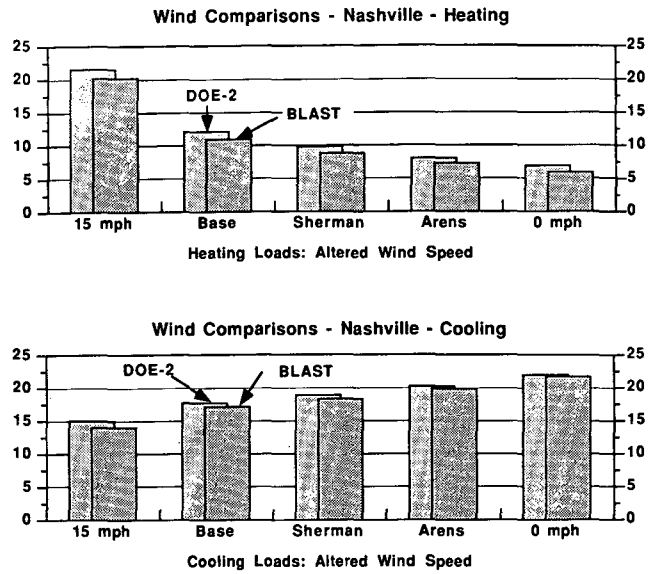

Figure 6. Modifications to wind data to better reflect actual wind conditions in the vicinity of the building can significantly alter the calculated heating and cooling requirements of a residence. (XBL 862-549)

respectively, to the heating load, depending on whether Arens, Sherman, or the base case is used. Likewise, wind lowers the cooling load 8%, 16%, or 21% for the same three cases.

Clearly, the wrong data can provide a false perception of how much energy is being used, and for what purpose. More significantly, those false perceptions can lead to design decisions which are not justified by the actual environment of the building. In new buildings, substantial costs might be incurred in order to solve wind-induced problems which do not warrant them, while more important aspects of the energy environment might be ignored. Likewise, infiltration may be an overemphasized retrofit option, the benefits of which may be considerably less than expected. These results argue strongly for an improved method of determining the actual wind speed in the vicinity of a specific building, and incorporating that into building energy analysis techniques, possibly into the data itself.

PLANNED ACTIVITIES FOR FY 1986

Experimental Buildings

A two-year program to develop a daylighting system evaluation methodology will begin, as part of the Passive Solar Federal Buildings Program. It will provide owners and designers of daylit buildings a method to determine the effectiveness of daylighting

to reduce electric consumption in their buildings. This work will be coordinated with a parallel effort by SERI to develop a methodology for thermal performance of passive buildings.

Natural Lighting

The work which has gone on to date will provide the basis for a set of design guidelines to be developed in FY 1986. These guidelines will cover the use of daylighting in office buildings through the use of roof apertures. The characterization of energy use in daylit commercial buildings will continue with investigations of school and retail buildings.

Climate Analysis

Investigation of climate patterns resulting in peak heating and cooling loads will begin in FY 1986. This work will be a preliminary step in determining the course of research toward better prediction of peak loads and more effective design of mechanical systems.

REFERENCES

1. Andersson, B., *et al.* (1983), "Thermal Effects Resulting from Occupant Behavior and Building Operation," in *Proceedings of the Passive and Hybrid Solar Energy Update*, Washington, DC, 26–28 September 1983, DOE, p. 121; LBL-16738.
2. Andersson, B., *et al.* (1984), "Total Building Impacts of South-Facing Roof Apertures," in *Proceedings of the Windows in Building Design and Maintenance,* Göteborg, Sweden, 13–15 June 1984, Swedish Council for Building Research, p. 209; LBL-17562.
3. Andersson, B. *et al.* (1985), "Effect of Daylighting Options on the Performance of Two Existing Passive Commercial Building," in *Proceedings of the Solar Buildings*, Washington, DC, 18–20 March 1985, DOE, p. 257; LBL-18069.
4. Adegran, M., Andersson, B., Place, W. (1985), *Mt. Airy Library, a Qualitative Study of Daylighting in a Passive Solar Building,* LBL-18527.
5. Andersson, B., *et al.* (1985), *Effects of Occupant Issues on the Energy Performance of Two Existing Passive Commercial Buildings,* LBL-18398.
6. Place, W., *et al.* (1985), "The Impact of Glazing Orientation and Tilt on the Energy Performance of Roof Apertures," *ASHRAE Transactions,* Vol. 91, No. 2A; LBL-18838.
7. Coutier, P., Place, W., and Fontoynont, M. (1984), *The Predicted Impact of Localized Roof Apertures on the Energy Performance of Office Buildings,* LBL-17724.
8. Place, W., *et al.* (1984), "The Predicted Impact on Roof Aperture Design on the Energy Performance of Office Buildings," *Energy and Buildings 6*, p. 361; LBL-14790.
9. Place, W., *et al.* (1983), "Predicted Impact of Linear Roof Apertures on the Energy Performance of Office Buildings," in *Proceedings of the Passive and Hybrid Solar Energy Update,* Washington, DC, 26–28 September 1983, DOE, p. 51; LBL-16738.
10. Bauman, F., *et al.* (1985), "The Experimentally Measured Performance of a Linear Roof Aperture Daylighting System," LBL-19590, submitted to *ASHRAE Transactions.*
11. Bauman, F., Place, W., Thornton, J., and Howard, T.C., (1985), "An Integrating Window Pyranometer for Beam Daylighting Measurement in Scale-Model Buildings," LBL-19494, submitted to *ASHRAE Transactions.*
12. Place, W., Andersson, B., Coutier, P., and Kammerud, R., (1985), *Design Guidelines for Roof Apertures in Non-residential Buildings,* LBL-19973 Abstract.
13. Carroll, W.L., Sullivan, R., and Mertol, A. (1985), *Thermal Mass: BLAST Residential Parametric Simulations,* LBL-19681.
14. Andersson, B., Carroll, W.L., and Martin, M. (1985), "Aggregation of U.S. Population Centers Using Climate Parameters Related to Building Energy Use," *ASHRAE Transactions,* Vol. 91, No. 2B; LBL-15230.
15. Andersson, B., *et al.* (1986), *The Importance of Refining Wind Data for Building Energy Analysis,* LBL-21036, in preparation.

Optical Materials Studies*

(This article, except for the section on Aerogels, has been reprinted from the FY 1984 Annual Report.)

S. Selkowitz, A.J. Hunt, C. Lampert, J.G. Lieber, K.D. Lofftus, M. Rubin, and P. Tewari

Significant reductions in energy consumed by the building sector will come not only from better building design strategies but also from the development and introduction of new glazing materials. Since the inception of our program in 1976, identification, characterization, and exploratory development of promising new fenestration materials have been major activities. Research on new optical materials and on modifications of existing glazing materials is intended to create a technology base to assist industry with developing the next generation of advanced fenestration systems.

In addition to the research projects described in the following sections, the overall Optical Materials effort at LBL includes development of a multiyear research plan and scientific coordination of related DOE-funded research projects at universities, private sector firms, and other national laboratories. Results of the DOE-supported program are made available to interested parties in the private sector. For example, an annual technical conference and industry forum is held each year in August in conjunction with a meeting of the International Society for Optical Engineering (SPIE). This meeting serves as a forum to review and discuss the direction of the overall DOE program as well as to report on recent technical progress. A joint international effort on glazing optical materials under the auspices of the International Energy Agency is being developed with our participation.

In 1976, when our program began, we identified the development of low-emittance ("low-E") coatings as a major program objective. DOE-supported research activities have helped the fenestration industry to accelerate market introduction of new high-performance window systems incorporating these coatings. Several small firms began offering commercial products in 1982, and in 1984 many of the largest glass and window manufacturers introduced "low-E" products. In the near term, the use of low-E coatings in a conventional double-glazed window provides better thermal performance than triple glazing and makes a lighter and more compact window. In the long term, this coating technology offers the potential to produce transparent windows having heat transfer values as low as those of insulating walls. On an annual basis, such windows should outperform the best-insulated wall, even for a north orientation in a cold climate, since diffuse solar gain will offset some conductive losses. We initiated planning in late 1984 for a Low-E Window Roundtable, to be co-sponsored with the National Fenestration Council. We believe that the positive impact of this DOE-supported effort can serve as a model for the transfer and development of research findings in other optical materials areas.

*This work was supported by the Assistant Secretary for Conservation and Renewable Energy, Office of Buildings Energy Research and Development, Building Systems Division; the Office of Solar Heat Technologies, Passive and Hybrid Solar Energy Division; and the Office of Energy Systems Research, Energy Conversion and Utilization Technology Program of the U.S. Department of Energy under Contract No. DE-AC03-76SF00098.

GLASS AND PLASTIC SUBSTRATES

Accomplishments During FY 1984

To predict the optical properties of complex window systems incorporating thin-film coatings, the optical properties of the glass and plastic substrates must be accurately known. These properties have not been available in a complete and self-consistent form even for the most common varieties of glass used in windows, hence the need for this measurement effort. This year, we completed work on standard clear glasses, glasses having absorbing additives, and high-purity glasses. Our results are summarized in a paper that includes a complete set of optical constants from the near ultraviolet through the little-studied far infrared for all common window glasses.[1] We also provide some spectrally and directionally averaged bulk properties for calculating solar and thermal radiative heat transfer through windows. Figure 1 shows the real and imaginary components of the complex index of refraction for a clear glass as determined by Kramers-Kronig analysis of reflection measured with a Fourier-transform spectrometer over the near-infrared and infrared spectrum.

Future measurements will be greatly simplified with our new spectrometer, which covers the ultraviolet to the near infrared. In addition to having optics that are far superior to those of our previous instrument, this system features completely automated operation and data collection. The instrument is installed and operating, although not all functions have been tested.

Planned Activities for FY 1985

We will collect, organize, and catalogue our low-emissivity samples. These samples will be com-

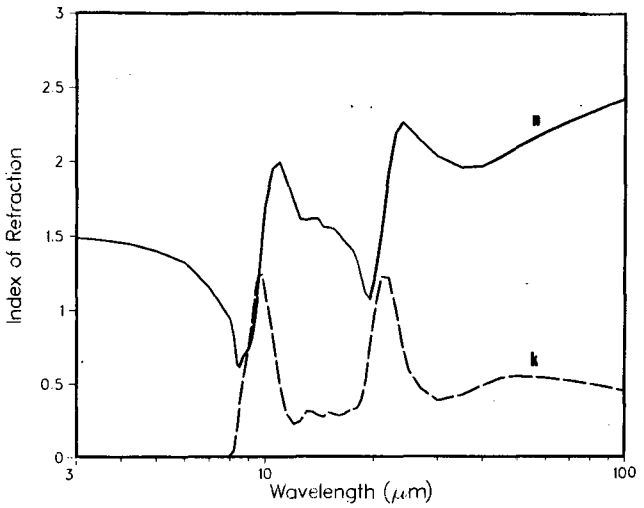

Figure 1. Real (n) and imaginary (k) parts of the complex index of refraction for soda-lime silica glass. (XBL 8412-5271)

pletely characterized as part of our participation in the Low-E Window Roundtable in August 1985. Our spectrometer will be fully functioning.

LOW-CONDUCTANCE, HIGH-TRANSMITTANCE GLAZINGS

An ideal glazing material for residences in cold climates would have good optical clarity, high solar transmittance to admit sunlight in winter, and low thermal conductance to reduce heating costs. Such windows would perform better than insulated walls on an annual basis, even in northern orientations in cold climates. Simulation results for a north-facing window in Madison, Wisconsin are shown in Fig. 2. Windows must have U-value and shading coefficient combinations that place them to the right of the "0" net heat transfer line if they are to provide net energy benefits. Two promising research activities are under way to develop the technical basis for such advanced windows.

LOW-EMITTANCE, GRADIENT-INDEX COATINGS

Accomplishments During FY 1984

Since 1976, we have contributed to the development of window coatings that transmit sunlight but reflect in the thermal infrared, thus suppressing radiative heat transfer. Commercially available coatings based on metal-dielectric multilayer films have satisfactory optical properties but are not sufficiently durable to be used in nonsealed glazings. By producing a film having a continuously varying index of refraction to reduce reflection in the solar spectrum, we could use materials that are inherently more durable but less transparent than the metal films. Our analytical studies suggest that a gradient-index coating could improve solar transmittance by 25% without reducing emittance or durability.

We have begun by studying the titanium oxynitride (TiN_xO_y) system, producing these gradient-index coatings by plasma-assisted chemical vapor deposition (CVD). Better compositional control and durability have been achieved in a limited number of samples deposited by magnetron sputtering. We installed a new sputtering system and completed the first tests for homogeneous coatings. The coatings are being characterized by electron microscopy, Auger electron spectroscopy (AES), and Rutherford

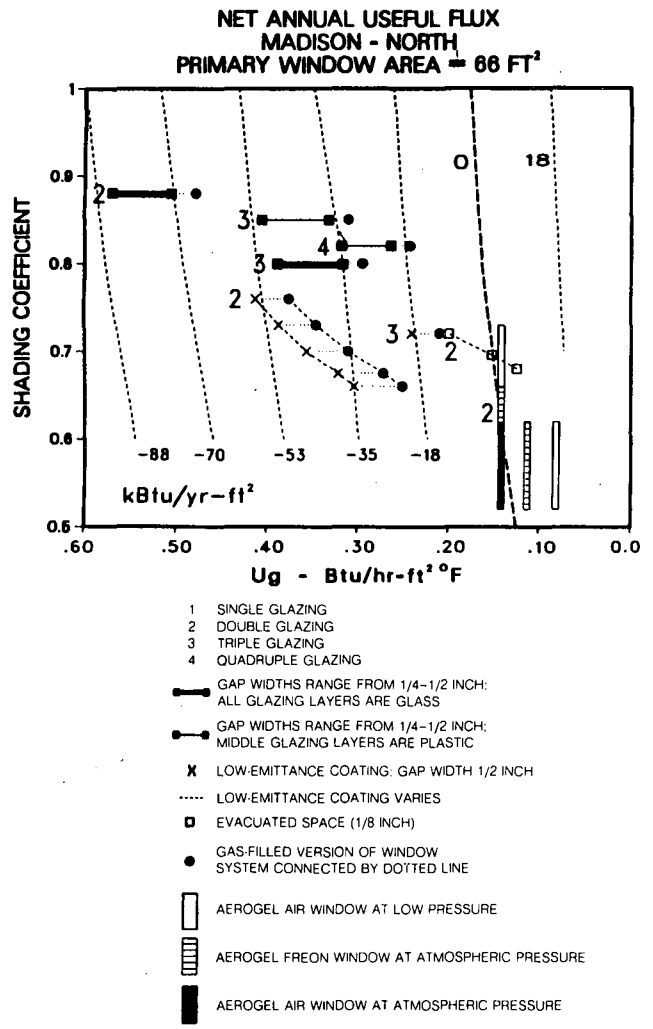

Figure 2. Simulation results for north zone, Madison, Wisconsin. (XBL 856-2870)

backscattering (RBS), in addition to complete optical characterization. RBS has proven particularly valuable in our efforts to remove impurities from the coatings. Figure 3 shows the small amount of chlorine remaining in the coating after adding H_2 to scavenge the bulk of the unwanted Cl in our CVD films.

Planned Activities for FY 1985

We will add reactive gas-handling capabilities to our sputtering system to produce TiN_xO_y films. The process parameters will be varied in an attempt to achieve the optimum optical properties predicted by our analytical models.

AEROGELS

Transparent silica aerogel is being developed at LBL because of its excellent thermal insulation properties for window glazing materials. It is an open cell porous solid containing a very high percentage of voids. Aerogel is transparent rather than translucent because the characteristic pore size is much smaller than the wavelength of light; therefore, it transmits rather than scatters light. A 1-inch-thick aerogel window has an R value of about 7, which can be increased to nearly R-20 by removing 90% of the air from the aerogel. The goals of this research are to improve the optical and thermal properties of aerogel, discover less expensive synthesis methods, develop methods to protect it from the environment, and develop a technology base for production of transparent aerogels.

Aerogel is prepared by mixing a metal alkoxide with water and alcohol along with suitable catalysts.

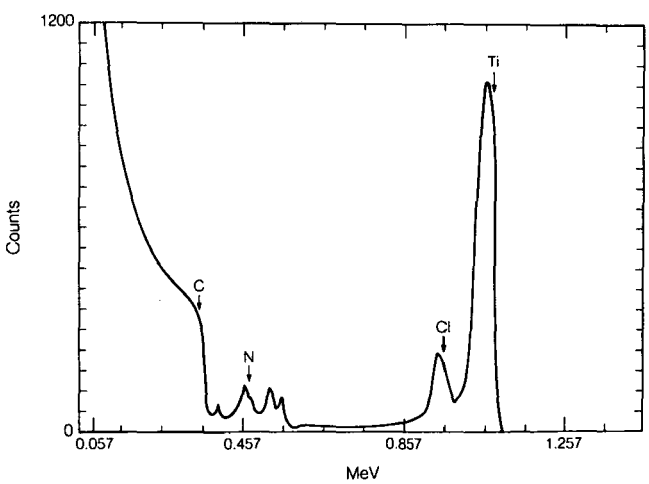

Figure 3. Rutherford backscattering spectrum for titanium oxynitride coating on glossy carbon substrate. (XBL 854-9799)

Water hydrolyzes the alkoxide compound to produce fine solid particles or polymers that link together to form alcogel, a transparent solid containing alcohol. To become useful as an insulator, the alcohol must be removed from the alcogel without damaging the silica matrix through the action of interfacial forces in the very fine pores. These interfacial forces can be eliminated by carrying out the solvent extraction under supercritical conditions. Researchers at LBL have been investigating both the preparation and drying of aerogel.

Accomplishments During FY 1985

Our efforts in 1985 have been concentrated on improving the two critical areas of synthesis of aerogels:

1. hydrolysis and condensation reaction of a less expensive alkoxide TEOS (tetraethylorthosilicate) than the toxic and expensive TMOS (tetramethylorthosilicate) normally used by others;
2. simplification of the drying process of the alcogels to achieve the aerogel without damage to the structure.

In addition, we have developed some unique techniques which allow us to study the microstructure of the gels by transmission electron microscopy and light scattering studies. They are discussed below. Progress in these three areas has significantly enhanced the prospects for large scale industrial preparation of aerogel for windows.

Alcogel Production from Low Toxicity Starting Material

Transparent silica aerogels for Cerenkov counters have been produced by hydrolysis and condensation of TMOS. Since TMOS is a very toxic starting material, the more desirable starting compound, TEOS, was used in the current work. Research in our laboratory led to the successful use of a base to catalyze TEOS.[2–4] Base catalysis of TEOS results in a more suitable material for window material than the acid catalysis method. We have improved the properties of the aerogel by exploring a wide range of process variables using the factorial design method.[2] Light scattering, optical transmission, and electron microscopy data were used to characterize the aerogels produced in our laboratory. Using these techniques we have established that the quality of the improved TEOS aerogels is comparable or better in transparency than those prepared from TMOS. The transmission spectrophotometer results confirming this are given in Fig. 4.

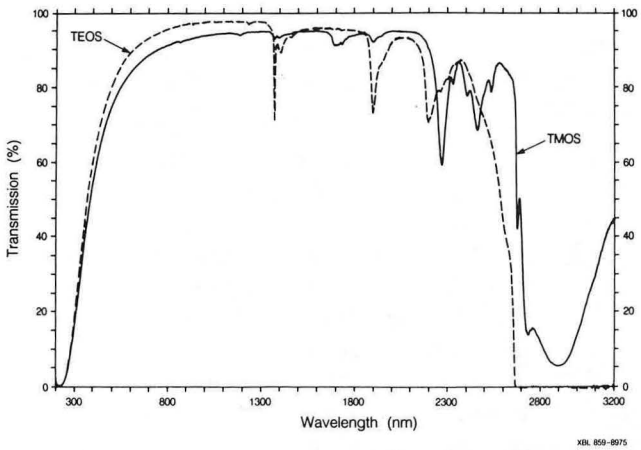

Figure 4. Transmission spectra of a 4-mm-thick sample of base catalyzed TMOS aerogel supercritically dried at 270°C and 110 bars (TMOS) and a 12-mm-thick base catalyzed TEOS aerogel sample supercritically dried by CO_2 but not heated to remove all adsorbed H_2O (TEOS). (XBL 859-8975)

Ambient Temperature Supercritical Drying

Alcogel is a low density open pore material containing a high fraction of voids filled with alcohol. In conventional supercritical drying, the alcohol is removed from the alcogel by slowly releasing the pressure in an autoclave after it has been heated above its critical pressure and temperature. Under these conditions, the interfacial tensions in the alcogel drop to zero. Typical conditions for supercritical drying of alcohol are $\geqslant$ 270°C and 1800 psi. The necessity to cycle pressure vessels to these temperatures makes the drying process expensive and time consuming. We have developed a solvent substitution process[5] in which alcohol is replaced by liquid CO_2, which permits drying of alcogels at $\leqslant$ 40°C and 1200 psi. We have improved the substitution and drying process to minimize shrinkage and damage to the structure. The shrinkage can be controlled to $\leqslant$ 5% of the initial dimensions. The reproducibility of the process is good, and the drying is achieved in less time per batch than the 2–3 days required by the high temperature process. Further efforts are in progress to reduce the shrinkage.

Gel Microstructure

We have developed a variety of sample preparation methods to overcome difficulties in the study of aerogel with electron microscopy.[6] Transmission electron microscope studies using these methods have provided excellent evidence of the physical gelation mechanism. Micrographs show a cross linked chained structure similar to that conceptualized previously by various workers (Fig. 4a). These sample preparation techniques for TEM studies are excellent for studying the microstructural details of gels and aerogels at various stages in the sol-gel process.

We have performed light scattering studies of acid and base catalyzed sol-gel systems. By studying the time evolution of the scattering intensity, we can differentiate gelation mechanisms between the two gels. Information from these experiments is helpful in formulating and controlling the desired properties of complex sol-gel systems.

Planned Activities for FY 1986

In FY 1986 we will explore the substitution of Freon 116 for alcohol to further reduce the supercritical drying conditions to $\leqslant$20°C and 430 psi. If successful, this substitution will lower the processing cost below that of the CO_2 method. Treatment of the gels to render them hydrophobic will be studied to improve the chemical stability of aerogel against weathering and moisture. The adhesion of aerogel to glass plates of the window will be examined to improve the mechanical stability and resiliency of the aerogels.

OPTICAL SWITCHING PROCESSES AND MATERIALS

Optical switching materials or devices can be used for energy-efficient windows and other passive solar applications. An optical shutter provides a large change in optical properties under the influence

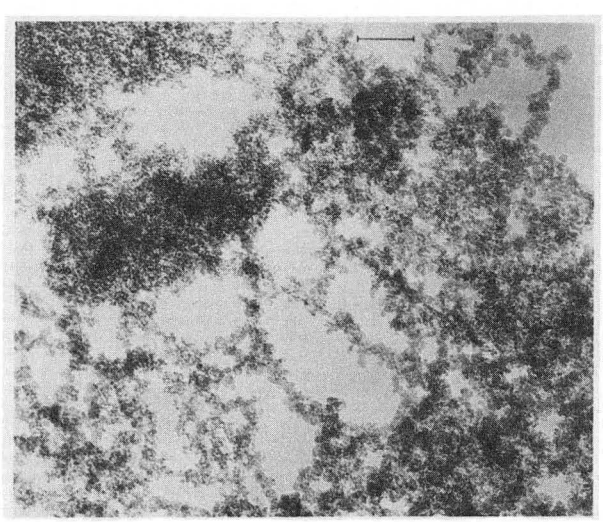

Figure 4a. Transmission electron micrograph of a base catalyzed TMOS aerogel flake after carbon coating. (XBB 859-7482)

of light, heat, an electric field, or their combination. The change can occur as a transformation from a material that is highly solar transmitting to one that reflects over part or all of the solar spectrum (Fig. 5). A less desirable alternative would be a material that switches from highly transmitting to highly absorbing since some of the absorbed energy would enter the building. An optical shutter coating would control the flow of visible light and/or solar heat gain through a building window, thus performing an energy management function. Depending upon design, such a coating could control glare, modulate daylight admittance, and limit solar heat gain to reduce cooling loads, prevent overheating, and improve thermal comfort. Initial results from energy simulation studies of office buildings suggest that the dynamic control attainable with optical shutter coatings provides substantial economic benefits by minimizing cooling and lighting energy use, reducing peak electricity demand, and potentially reducing the chiller and heating, ventilating, and air-conditioning (HVAC) system size.

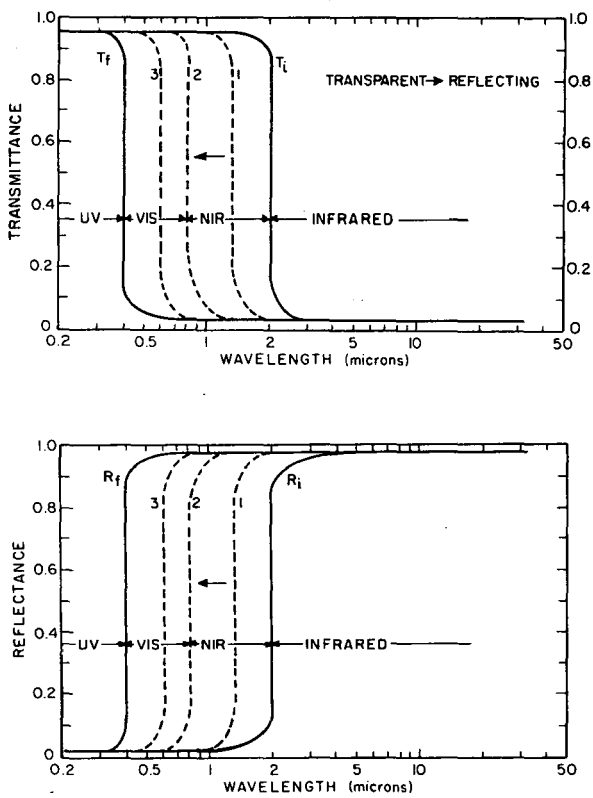

Figure 5. Idealized broadband spectral response for a solar optical shutter. This example ignores the effect of absorption and shows a highly transparent film transforming into a highly reflecting one. Such a shutter can control certain portions of the solar spectrum to provide or restrict both solar heating and lighting. (XBL 828-6452)

We consider materials that possess variable or reversible optical properties as potential candidates for an optical shutter. There are three classes of phenomena that may prove useful:

(1) Chromogenic materials, including electrochromic, photochromic, and thermochromic types.
(2) Physio-optic media, including mesogenic molecules or liquid crystals, and magneto-optic, electro-optic, and mechano-optic or deformable media.
(3) Electrodeposition, including reversible electrodeposition and electrophoresis.

Our research program focuses on electrochromic coatings because they offer the potential for active control (by an applied voltage) in response to building operating requirements and environmental conditions and because there is sufficient experience with optical displays and related applications to suggest that they would be the best candidates for glazing applications. The active control capability will allow the greatest range of potential benefits in terms of reducing cooling loads, providing daylighting savings, controlling peak electricity demand, and reducing HVAC size.

ELECTROCHROMIC DEVICES

Electrochromism is exhibited by many inorganic and organic materials.[7] An electrochromic material undergoes an intense color change when a colored compound is formed from an ion-insertion reaction induced by an instantaneous applied electric field. The reaction might follow:

$$MO_x + yA^+ + ye \rightleftarrows A_yMO_x \quad .$$

There are three categories of electrochromic materials: transition metal oxides, organic compounds, and intercalated materials. The materials that have attracted the most research interest are WO_3, MoO_3, and NiO_x films. With organic electrochromics, coloration of a liquid is achieved by an oxidation-reduction reaction, which may be coupled with a chemical reaction. Intercalated electrochromics are based on graphite and so are not useful for window applications.

A solid-state electrochromic device containing the elements shown in Fig. 6 can be fabricated: a transparent conductor, an electrochromic layer, an electrolyte or fast-ion conductor, a counter electrode, and a second transparent conductor. Many variations on this configuration are possible, although several of the approaches used for small electronic

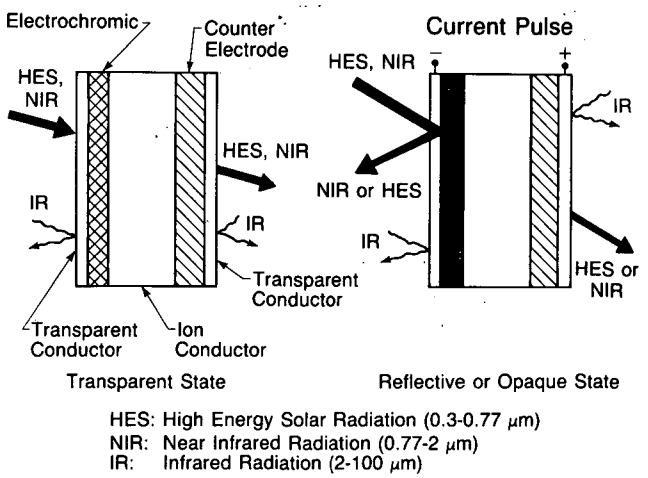

Figure 6. Schematic of an electrochromic optical switch shown in each of two states, transparent and colored. A current pulse causes an ion-based chemical reaction to take place in the electrochromic material (HES, high-energy solar; NIR, near-infrared; IR, infrared). (XBL 842-10105)

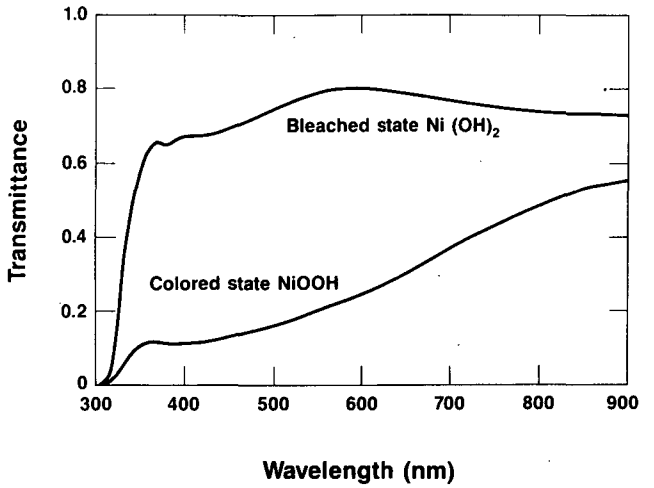

Figure 7. Transmission (near-normal) spectrum for nickel hydroxide in bleached and colored state. Conditions are IM-KOH electrolyte with 1 V applied potential. (XBL 852-6955)

displays cannot be scaled up successfully to the dimensions required for windows.

Accomplishments During FY 1984

Prior to 1984, a technical review of electrochromism revealed many possible materials that could be incorporated into solar glazings.[7] During 1984 our research focused on electrochromism in nickel oxide, which can be switched from transparent to bronze or dark gray, depending on impurities. We performed experiments on oxidized metal films and chemically deposited oxides on indium-tin-oxide coated glass. We obtained a normally transmitting film with solar transmittance (T_s) and visible transmittance (T_v) as follows: T_s (off) = 0.73, T_s (on) = 0.37, and T_v (off) = 0.75, T_v (on) = 0.24. The spectral response is shown in Fig. 7. In an electrochemical cell, 1 volt is required to switch the film. Besides spectrophotometry, voltammetry and Auger electron spectroscopy were performed on this film. These studies will help determine the active species in the electrochromic coloration reaction.

LBL continues to serve as scientific coordinator for the overall DOE-supported switching films program. Associated research was continued in 1984 by EIC Laboratories[8] and the Department of Electrical Engineering at Tufts University.[9] Electrochromic near-infrared reflectance modulation was demonstrated in polycrystalline WO_3 material.[10] Devices based on the configuration in Fig. 6 and with complementary electrochromic electrodes were made. Research by the Solar Energy Research Institute (SERI) has concentrated on devices based on amorphous WO_3 in the configuration: transparent conductor/WO_3/ion conductor/Au or indium-tin-oxide.[11]

Planned Activities for FY 1985

We will complete optical, chemical, and structural studies of electrochromic nickel oxide. We will compare the electrochromic response of sputter-prepared nickel oxide materials to the electrochemically prepared coatings. With our new reactive magnetron sputtering system, we will begin to survey and characterize electrochromism in other candidate materials such as titanium oxide. The objective of this work is to identify and characterize electrochromic materials with performance characteristics that are better than the commonly used WO_3 films.

OTHER SWITCHING FILM MECHANISMS

A number of other materials systems were reviewed to determine their suitability as optical switching materials. We continue to follow development of photochromic and thermochromic materials to determine if any may prove suitable to building applications. We also examined various physio-optic processes (i.e., liquid crystals, magneto-optic and electro-optic materials) as well as processes based on reversible electrodeposition and electrophoresis. Each approach has at least one attractive feature, but in general they appear less promising than the alternatives described above.

Accomplishments During FY 1984

An example of a device studied in FY 1984 is the dynamically light-scattering liquid crystal cell. It transforms from transparent to opaque white under applied potential; no polarizers are required. Its optical properties are T_s (off) = 0.82, T_s (on) = 0.77, T_v (off) = 0.83, T_v (on) = 0.20. Although the response of this device (Fig. 8) is promising as a broadband optical shutter, it suffers from excessive power requirements and lack of uniformity over large areas.

Planned Activities for FY 1985

We will continue to follow these novel approaches for optical switching mechanisms to determine if results in other fields have relevance to aperture requirements. We expect to obtain samples of photochromic plastics to determine their suitability for building applications.

MATERIALS FOR IMPROVED USE OF DAYLIGHT

The intensity and spatial distribution of daylight transmitted through windows and skylights must be controlled in order to reduce electric lighting requirements while maintaining occupant comfort. Conventional solutions rely on architectural elements and interior or exterior devices to control daylight admission and distribution. Greatly improved performance would result from materials or systems that could: (1) transmit maximum daylight with minimal cooling load impact (i.e., reject solar infrared radiation); (2) collect and distribute daylight beyond the perimeter zones in buildings; and (3) provide angular selectivity in accepting and redirecting incident light at the building envelope.

In earlier studies, we evaluated the performance of a variety of devices for daylight acceptance and control on the basis of their reflective and refractive optics. In 1982, we turned our attention to innovative optical materials and devices that showed the potential for replacing more complex mechanical systems. We reviewed the feasibility of approaches such as fiber-optics systems, hollow light guides, holographic coatings, selective-reflectance materials, and various scattering media. One promising approach that uses fluorescent concentrators to collect and redirect daylight is the subject of a patent disclosure.

LIGHT GUIDES

Accomplishments During FY 1984

In 1984, on the basis of the preceding year's review of potential systems for light guides, we focused on two promising areas. We predicted improved performance for hollow reflecting light pipes because of the availability of new low-cost materials of high reflectivity (more than 95%). Figure 9 shows the calculated transmission efficiency of this type of light guide as a function of aspect ratio (length/diameter) for R = 95%. Even for aspect ratios of 50 (e.g., L = 15 m, D = 0.3 m) the transmission has acceptable values at moderate concentration

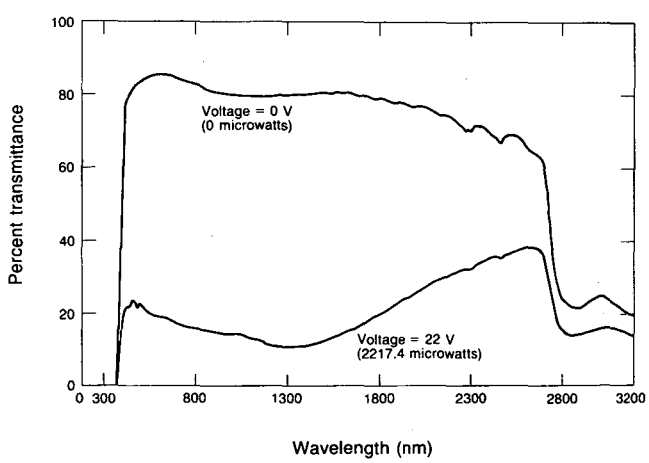

Figure 8. Spectral transmittance (near normal) for a dynamically scattering liquid crystal device. Response includes two glass cover plates and two transparent conductor electrode films. (XBL 852-7033)

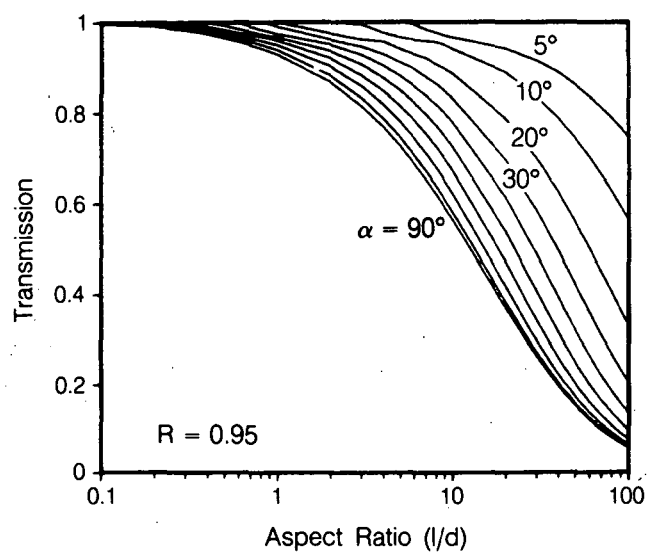

Figure 9. Transmission efficiency of a tubular light guide vs. aspect ratio (length/diameter); α is the half-angle of the concentrated sunlight and R is the inner surface reflectivity. (XBL 854-9798)

angles. We also investigated the performance of plastic optical fibers and evaluated the potential for improvement through further purification of the base polymer.

Planned Activities for FY 1985

We will continue our investigation of hollow reflecting light guides. Available reflecting materials will be completely characterized and the results used in improved analytical models. We will compare these model results with the actual performance of hollow prismatic light guides. Scale models of light guide elements will be tested in our sky simulator.

REFERENCES

1. Rubin, M. (1984), *Optical Constants and Bulk Optical Properties of Soda-Lime Silica Glasses for Windows*, LBL-13572, to be published in *Solar Energy Materials.*
2. Tewari, P.H., Hunt A.J., and Lofftus, K.D. (1985), "Structure and Chemistry of Sol-Gel Derived Transparent Silica Aerogels," in *Ultrastructure Processing of Ceramics, Glasses, and Composites*, presented at 2nd Ultrastructure Conference, Palm Coast, Florida, March 1, 1985.
3. Russo, R.E. and Hunt, A.J. (1985), "Comparison of Ethyl vs. Methyl Sol-Gels for Silica Aerogels using Polar Nephelometry," submitted to *J. Non-Crystalline Solids*; LBL-19693.
4. Tewari, P.H., Hunt A.J., and Lofftus, K.D. (1985), "Advances in Production of Transparent Silica Aerogels for Window Glazings," presented at the 1st International Conference on Aerogels, Wurzburg, West Germany, September 23–25, 1985.
5. Tewari, P.H., Hunt A.J., and Lofftus, K.D. (1985), "Ambient Temperature Supercritical Drying of Transparent Silica Aerogels," *Materials Letters 3*, p. 363.
6. Tewari, P.H., Hunt, A.J., Lieber, J., and Lofftus, K.D. (1985), "Microstructural Properties of Transparent Silica Aerogels," presented at the 1st International Conference on Aerogels, Wurzburg, West Germany, September 23–25, 1985.
7. Lampert, C.M. (1984),"Electrochromic Materials and Devices for Energy-Efficient Windows," *Solar Energy Mat. 11*, p. 1.
8. Rauh, D. and Cogan, S. (1984), "Materials for Electrochromic Windows," *Proceedings of SPIE 502*, p. 38.
9. Goldner, R.B., *et al.* (1984), "Optical Mobility Studies on Electrochromic Films for Variable Reflectivity Windows," *Proceedings of SPIE 502*, p. 54.
10. Goldner, R.B., *et al.* (1983), "High Near-Infrared Reflectivity Modulation with Polycrystalline Electrochromic WO_3 Films," *Appl. Phys. Lett. 43*, p. 1093.
11. Benson, D.K., Tracy, C.E., and Ruth, M.R. (1984), "Solid-State Electrochromic Switchable Window Glazings," *Proceedings of SPIE 502*, p. 46.

Active Solar Cooling*

M. Wahlig, J. Rasson, M. Warren, K. Dao, R. Armer, P. Brothers, and P.L. Chen

The purpose of this project is to make major contributions to the technology base necessary for solar energy to become a viable option for the cooling of buildings. This project has two major tasks: (1) research on improved absorption cycles for high efficiency active solar cooling and heating systems and (2) systems analysis of active solar cooling and heating systems to establish operating requirements, research needs, and thermal performance of current and advanced space conditioning systems.

Absorption Chiller Research

The objective of the research on absorption-cycle chillers is to achieve a significantly higher conversion efficiency than is possible in other approaches to solar cooling and heating of buildings. Being essentially heat pumps, absorption-cycle chillers can be used for heating as well as cooling if the refrigerant fluid does not freeze in the outdoor coil during heating applications. We restrict our fluid choices to those for which this heating option is available.

The absorption-cycle research program consists

*This work was supported by the Assistant Secretary for Conservation and Renewable Energy, Office of Solar Heat Technologies, Solar Buildings Technology Division of the U.S. Department of Energy under Contract No. DE-AC03-76SF00098.

of four phases, each successive phase leading closer to the final machine. The first phase was successfully completed some time ago.[1] By modifying a conventional gas-fired ammonia/water absorption chiller, we demonstrated the capability of our analysis techniques to predict accurately the performance of single-effect (i.e., single-stage) absorption-cycle chillers under operating conditions appropriate for solar-powered cooling.

In the second phase, a completely new solar-driven single-effect chiller was designed, fabricated, and tested, using the experience gained during the first phase. This new ammonia/water chiller had several unique features for recouping thermal and mechanical energy. The second phase was successfully completed[2] in FY 1982.

In the present, third phase, we are investigating the performance improvement obtained by adding a unique second stage to the single-effect chiller tested in the second phase. The concept of the resulting double-effect regenerative cycle (or cycle 2R) has been described previously.[3] Basically, with the addition of the second stage, the overall chiller efficiency increases continuously as a function of the inlet temperature from the solar collectors. This 2R chiller has been designed,[4] fabricated, and assembled; the debugging and testing was started in FY 1983 and was successfully completed in FY 1985.

In the fourth phase, a new concept in refrigeration-absorption cycles—one that should yield a still higher efficiency while requiring less heat-exchanger area, for a potentially lower cost—will be investigated. The basic concept of this single-effect regenerative cycle (which we call cycle 1R) has also been described previously.[5] The probability of successful development of the cycle 1R chiller has been greatly enhanced by our successful experience in developing the cycle 2R chiller.

Systems Analysis

The objectives of the systems analysis activities are: (1) to perform system simulation and analysis of active solar absorption and Rankine cooling/heating systems to establish the operating requirements and thermal performance of current and advanced space conditioning systems; (2) to use the results of these systems and economic analyses to determine future research needs for the solar cooling program and to determine where improvements can and must be made in thermal and electrical performance; and (3) to evaluate by computer simulation the impact of system controls and control strategies on annual energy savings for active solar cooling and heating systems. Previous work has focused on developing cost and performance goals for solar cooling systems.[6,7]

ACCOMPLISHMENTS DURING FY 1985

Absorption Chiller Research

Experimental testing of the 2R chiller was completed in FY 1985. The test results proved that the regenerative process is attainable and stable. Furthermore, the experimental performance results were ±5% of the theoretically predicted results. A full analysis and evaluation of the test results will continue into FY 1986.

Extensive testing of the vapor-driven multistage pump was conducted during FY 1985. The linkage between the drive side and the pump side was redesigned, resulting in improved piston alignment and reduction in friction forces. The pump piston seals were tested to determine the best seal design, i.e., a design that minimizes the leak across the piston with a low, acceptable level of piston friction.

Different seal materials were tested to determine the wear life in a specially designed testing apparatus. The test results showed that all materials tested in ammonia-water solution at room temperature exhibited unacceptable amounts of wear. Additional wear tests will continue as new materials are identified.

Meanwhile, another multistage pump design using an electric motor drive and plastic diaphram pumping elements was completed in FY 1985, as an alternative method of overcoming the seal problems of the vapor-driven pump. This design incorporates a radial configuration for the pistons to reduce the required parasitic power.

Systems Analysis

1. Comparison of Desiccant and Absorption Systems

In FY 1985 analysis was done to compare desiccant and advanced absorption solar cooling systems under comparable conditions.[8] To the extent possible, all cooling systems take advantage of the ability to reject heat directly to the atmosphere. Desiccant systems obtain their cooling effect from evaporative cooling and heat exchange. The advanced cycle desiccant systems have improved heat rejection capabilities. Advanced absorption cooling technology offers the possibility of chillers with thermal COP's of 1.55 or greater at design conditions. When evaporative cooling and heat exchange components

are added to an advanced absorption cooling system, the performance is enhanced further.

System coefficient of performance, system COP, the ratio of cooling effect delivered to heat input to regenerate the device, is calculated under different operating conditions. The heat input can be provided by solar or an auxiliary heat source (natural gas). The system coefficient of performance can be directly compared for different types of systems over the range of outdoor conditions relevant to the particular application.

In the ventilation mode desiccant cooling cycle, the inlet air stream is dried in a desiccant wheel and cooled by heat exchange with the return air stream. The supply air temperature is further reduced by evaporative cooling. The steady state heat and mass transfer of the desiccant wheel is modeled by analogy with heat transfer processes using heat and mass transfer effectivenesses. The cooling effect delivered is the difference between the enthalpy of the room and of the supply air. The thermal energy required to drive the system is the difference between the enthalpy leaving the heat exchanger and that leaving the heat source. Both moisture and heat are rejected from the desiccant wheel. The system thermal coefficient of performance is the ratio of the cooling effect delivered to the heat input required.

The advanced absorption cooling system is modeled including evaporative cooling, air-to-air heat exchanger, economizer cycle, and an evaporatively cooled condenser as shown in Fig. 1. An air-to-air heat exchanger transfers heat from the outside air stream (1) to the exhaust air stream (7). The cooled inlet air (2) is then mixed with return air from the room (5), based on a ratio of outdoor air, ROA, to determine the conditions of the mixed air

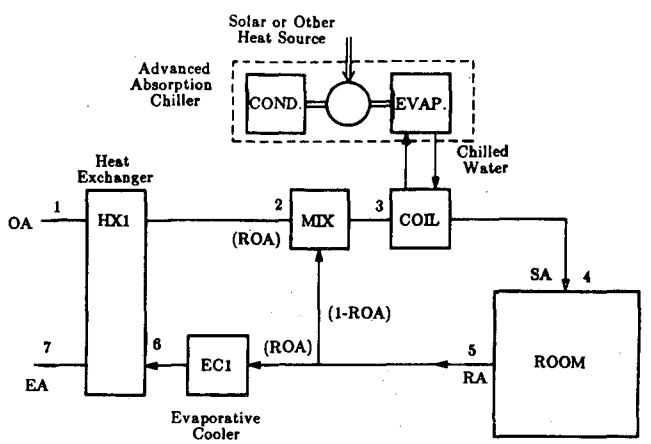

Figure 1. Schematic of a evaporatively cooled-closed cycle advanced-absorption system with evaporative cooling and air-to-air heat exchange. (XBL 864-1521)

(3) to the coil. The coil cools the air to the supply air state (4). The room return state (5) is assumed to be ARI conditions, as in the desiccant case. The room return air is evaporatively cooled (6). The output from the evaporative cooler is used in a sensible heat exchanger to cool the inlet air stream. The warm moist air stream (7) is exhausted. Outdoor air is also evaporatively cooled to cool the chiller condenser.

The thermal energy required to drive the system is determined by the thermal coefficient of performance of the advanced solar-fired absorption chiller operating at a condenser temperature given by the approach to the outdoor wet bulb temperature. For a system with a cooling coil, the system effectiveness, $\eta_{subsystem}$, can be defined as the ratio of the cooling effect delivered to the room to the enthalpy change across the coil. The application of heat exchange and evaporative cooling can greatly increase the system effectiveness, and improves the overall cooling effect delivered per unit of heat required. The chiller is modeled as an absorption chiller that can achieve a certain percentage of Carnot, where the performance depends on the chilled water temperature and condenser conditions. As we are considering the ultimate performance of such systems, we have assumed an efficiency of 0.70 of Carnot for the absorption chillers, consistent with the expected performance of the LBL cycle 1R chiller.

At low outside humidities indirect evaporative cooling can be an effective method of cooling. For this reason simulations were run using the evaporative cooling heat exchange, both with and without a desiccant wheel operating as a total enthalpy exchanger without a heat source for regeneration. Results of this analysis indicate that indirect evaporative cooling using either outdoor or return air is very effective. The use of the desiccant wheel does not improve the performance because moisture is transferred from the exhaust air to the inlet air streams.

Building cooling loads, calculated for a typical 930 m^2 (10,000 ft^2) office building using DOE2, have been analyzed. The hourly systems output file from DOE2 has been combined with the weather file to create a loads file with temperature, humidity, and heating and cooling loads for each of the 8760 hours of annual building operation. The hours of operation and the cooling loads are binned against outdoor temperature and humidity ratio to establish the annual range of operating conditions for the cooling system. By knowing the annual distribution of cooling loads encountered by the system over the year and the system COP over the range of operating con-

ditions, the heat input requirement can be calculated as a measure of annual system performance.

System coefficient of performance and the annual energy performance have been calculated under different operating conditions for open cycle desiccant and advanced absorption systems. The heat input can be provided by solar or an auxiliary heat source (natural gas). The system coefficient of performance can be directly compared for different types of systems over a range of outdoor temperatures and humidities where the bulk of the cooling demand occurs.

Results of analysis show that in Phoenix the seasonal system COP of advanced absorption systems with heat exchange and evaporative cooling is much larger than that of the ventilation mode desiccant system. In Phoenix, 48% of the cooling load occurs at low humidities where the entire cooling load can be met with indirect evaporative cooling. Almost all of the cooling load is Miami occurs at high humidities. In Miami with its greater latent loads, the two systems perform comparably.

The method can be extended to a wide range of desiccant and absorption cooling system configurations and control strategies. Advanced techniques of heat exchange and evaporative cooling that can benefit advanced desiccant systems will give a similar benefit to absorption systems. The ultimate solar application of these technologies will also be determined by other factors, including the coincidence of the solar resource with the cooling demand; the electrical parasitic power required to operate the systems; and the installed system cost. These issues are beyond the scope of this article.

2. Evaluation of Storage Options

Thermal storage is used in solar systems because there is a difference between the time at which energy is available as solar radiation and the time at which energy is required to meet a heating or cooling load. In solar heating systems solar radiation occurs in the daytime, while the greatest heating loads are at night. In solar cooling systems the solar radiation peaks at noon, while cooling loads typically peak around 3 or 4 pm. Storage is needed to bridge the gap between the noon supply of energy and the afternoon demand for cooling.

Different types of thermal storage may be used in a solar cooling system. Energy may be stored as "heat" on the hot side of the chiller, or it may be stored as coolth, on the cold side of the chiller. The storage may be sensible, in which the energy is stored as a change in temperature of the storage medium; or it may be latent, in which the energy is stored as a change in phase of the storage medium.

Computer simulation is used to determine the sensitivity to storage size and type of the annual performance of different storage configuration options.[9] Several issues are addressed: sensitivity of system performance to storage size and to load profile; sensitivity of hot-side sensible storage to storage stratification for both one and two tank systems; performance of hot-side latent storage; and the performance of cold-side storage. The study assumes careful design of solar cooling systems with the sizing of thermal storage based on the interaction between solar radiation and cooling load profiles for specific "design" days.[10] Chiller capacity is also taken into account. The annual performance of solar absorption cooling systems using different storage options is investigated using the simulation program TRNSYS.[11]

The system modeled is shown in Fig. 2. Evacuated tube collectors provide solar heated hot water to the storage device which in turn delivers hot water to the generator. The high performance evacuated tube collectors are modeled with performance data derived from the Sunmaster collector. The collector areas for the baseline system are chosen so that the high-solar fraction system has an annual solar fraction of 80%, and the medium solar fraction system has an annual solar fraction of 40%. The effect of other storage options on system performance is then measured by the change in annual solar fraction with respect to the annual solar fraction of the baseline system. Systems are simulated for an entire year using a 20-minute time step.

For low and medium (40%) solar fraction systems, the chiller is sized to use maximum output of the collectors. The remaining cooling load is provide by an electric backup chiller, as shown in Fig. 2, that operates when the solar system is unable to keep up with the load. For high solar fraction systems, the chiller is sized to meet the peak building load, and natural gas auxiliary backup is assumed.

The performance of systems with different storage options has been compared to the performance of a "state-of-the-art" baseline system that has a stratified hot-side water storage sized for a daily cycle (morning to afternoon).

The storage sizing is sensitive to the load distribution. Storage sizes for baseline systems operating seven days a week are significantly smaller than for comparable heating systems with the same collector areas. For systems which operate to meet 7-day loads with annual solar fractions of about 40%, there is little sensitivity of annual performance to storage size. For systems which have high (80%) annual solar fractions, multiple day storage can be beneficial in climates with variable summer weather. For sys-

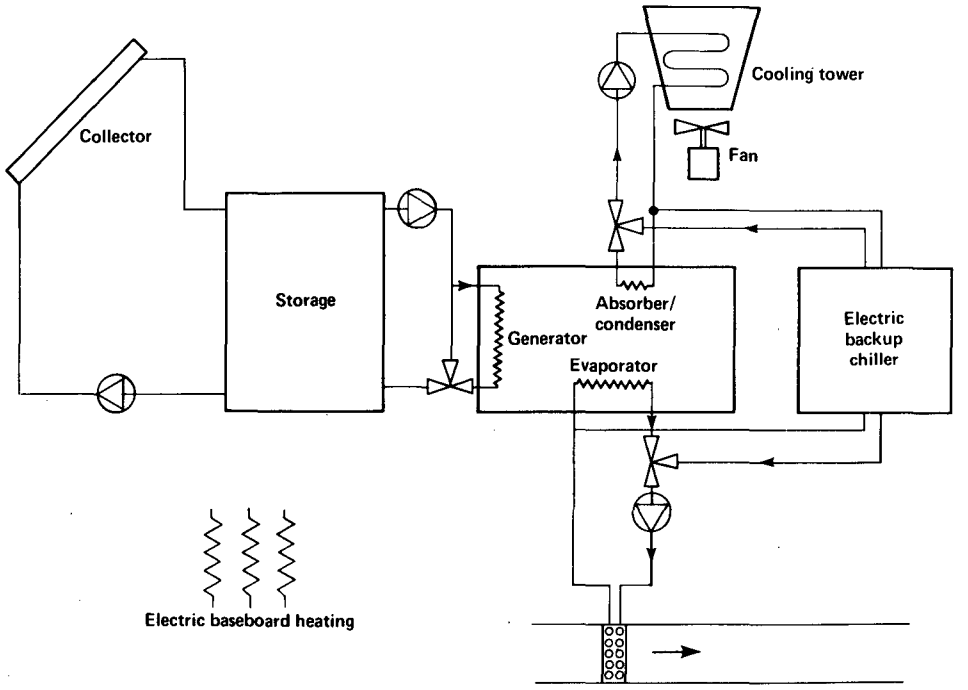

Figure 2. Active solar single-effect absorption cooling system. Medium solar fraction system uses a back-up electric chiller as shown. A high solar fraction system uses the solar chiller thermally fired and sized to meet the load so that no back-up chiller is necessary. (XBL 827-7251)

tems operating to meet 5-day (Monday-Friday) loads, the optimum storage is sized to store energy collected over the weekend. These systems have reduced collector areas (about 5/7) and much larger storage. Annual performance degrades with smaller storage and shows little or no improvement with larger storage.

For a properly sized cooling only system, stratification of hot-side storage has little effect on performance. Only when storage is significantly oversized will stratification play an important role. The use of two storage tanks to force stratification has no practical benefit for a system with high performance collectors.

The hot-side latent energy storage systems perform well when matched to chiller operating temperatures. Their future use depends on the cost of available phase change materials. The use of high temperature phase change materials with appropriate heat transfer fluids could eliminate the need for pressurized water storage for high temperature systems.

The use of cold-side storage by itself lowers the system performance significantly because of later starting times and earlier stopping times (when compared to the baseline system). The use of some hot-side storage can improve solar collection and can reduce the required chiller size, but is unlikely to improve performance above that of the baseline case.

This analysis has been done for today's state-of-the-art absorption technology that has a COP of about 0.7. Development of advanced solar fired absorption chillers gives the potential to achieve a COP of 1.55 at a firing temperature of 115 C (240 F).[5] Such improved chillers would require smaller collector areas to achieve the same amount of cooling rate and smaller hot-side storage volume to achieve the same amount of effective storage. Such systems would require significantly higher operating temperatures that would suggest the usefulness of hot-side latent storage; however, the sizing criteria and the conclusions of the analysis on the comparative advantage of different thermal storage options should remain unchanged.

3. Advanced Solar Cooling System Analysis

In FY 1985, detailed TRNSYS simulations were begun to establish solar cooling system performance using advanced chillers.[12] Both ideal chiller models (based on percentage of Carnot performance) and a performance-map chiller models (based on the characteristics of advanced cycles) were used. The results of the analysis using ideal chillers will be used to set upper bounds for performance and economics

of advanced absorption systems. Work on this analysis is continuing in FY 1986.

4. Advanced Absorption Cycle Analysis

LBL has continued work on modeling of high efficiency absorption chillers for solar cooling based on advanced cycles and working fluids.[13,14] In FY 1985 work on this project continued along three directions: 1) exploration into in-house program development and establishment of the requirements of a dedicated computer program that would model advanced chillers (like the 1R chiller under development at LBL) in sufficient detail to perform the machine design calculations; 2) exploration into the capabilities of packaged chemical process analysis programs, such as ASPEN and ASPEN-PLUS, for use in analysis of advanced-cycle chillers, thereby building on the developments in other industries; and 3) exploration into the capabilities of the analysis program developed by Gershon Grossman of Technion University in Israel for application to advanced-cycle analysis.

The basic computer program structure for the detailed analysis of advanced-absorption chillers was formulated. It consists of a combination of iterative and simultaneous solutions of the governing equations. The method was tested on a simpler single-effect cycle to test the methodology. The nonlinear set of equations was solved using the HYBRID solver from the National Physics Laboratory mathematical analysis package.

A review of chemical process simulation codes (flowsheet simulators) in common usage was also undertaken. Such programs have an extensive development history. ASPEN, Advanced System for Process Engineering, has been extensively developed at MIT under DOE support since 1977. It has been used with limited success in modeling a single-effect heat transformer problem.

Discussions begun in FY 1984 to establish a joint U.S./Israel research project to combine the research strengths of LBL and the TECHNION in the area of modeling, and analysis of advanced absorption cooling systems led to a joint agreement during FY 1985 between the U.S. DOE and the Ministry of Energy and Infrastructure of Israel (MOEI) on Simulation and Analysis of High Efficiency Absorption Systems for Solar Cooling. A project implementation plan was developed by LBL in August 1985.

This joint project allows us to take advantage of the Absorption Heat Pump Simulations and Studies Project that Gershon Grossman of TECHNION did for ORNL, involving the development of a simulation program to evaluate advanced absorption heat pumps for the DOE Conservation Program. The simulation program has been developed and is being tested for simple absorption systems and is being used to simulate absorption chillers under development at Carrier, Phillips, and Trane. The simulation program developed by Grossman at the Technion uses simultaneous solution of nonlinear algebraic equations. It is probable that this program will be capable of modeling closed-cycle absorption machines of moderate complexity. This program could probably also be used to model single-effect open-cycle systems.

Two computer code approaches for modeling advanced-cycle absorption chillers are being pursued. The first constitutes an extension of the Grossman computer code to model absorption-cycle chillers of moderate complexity. The second is the application of ASPEN or ASPEN-PLUS to complex closed-cycle absorption chillers. The TECHNION group will pursue the first approach in FY 1986; the LBL group will pursue the second approach. The Technion group will start developing component and system models for open-cycle cooling systems and will try to model the LBL 2R absorption cycle using slight modifications to their program. LBL will continue developing an iterative-solution model for complex absorption cycles.

PLANNED ACTIVITIES FOR FY 1986

Advanced Chiller Research

Completion of the analysis of the test results and documentation of the 2R chiller program will take place in FY 1986. The 2R chiller design and test results will be published in LBL reports and other scientific publications.

As part of the joint U.S.-Israel (LBL-Technion) project, LBL will continue the development of an analytical computer model capable of calculating performance of high efficiency absorption cycles such as the LBL 2R and 1R cycles and those being developed under DOE/Conservation sponsorship. Subroutines for these absorption-cycle models will be written as necessary, although it is anticipated that existing subroutines written for existing absorption models may be incorporated into these new, broader absorption models with only minor modifications. LBL will also acquire, as needed, available information on properties of working fluids and will share this information with Israeli researchers.

Systems Analysis

Comparative analysis of the performance of advanced absorption and desiccant solar cooling systems will continue during FY 1986. Performance will be calculated on an annual basis over a range of outdoor conditions. Better component models will be incorporated and used for the coil, evaporative coolers, condensers, etc. This effort will be coordinated with SERI researchers to achieve mutually agreed-upon comparative analysis techniques and system configurations. Work will also continue on TRNSYS simulation of advanced absorption cooling systems.

Models for regenerative evaporative cooling will be developed and applied to calculations of the performance of solar cooling systems. Building upon the concept proposed by Ian Maclaine-Cross, we will generate models for this component that can be incorporated into overall cooling systems analyses. These models will then be applied to performance improvement of conventional, absorption, and desiccant cooling systems. We will coordinate with SERI researchers on the model development and its applications.

REFERENCES

1. Dao, K., Simmons, M., Wolgast, R., and Wahlig, M. (1977), *Performance of an Experimental Solar-Driven Absorption Air Conditioner,* LBL-5911.
2. Dao, K., Rasson, J., and Wahlig, M. (1983), *Testing Results of an Ammonia-Water Absorption Air Conditioner Designed for Solar Cooling Applications,* LBL-16929 Draft.
3. Dao. K. (1978), *Conceptual Design of an Advanced Absorption Cycle: The Double-Effect Regenerative Absorption Refrigeration Cycle,* LBL-8405.
4. Dao, K., Wahlig, M., and Wali, E. (1980), *Development of Solar Driven Absorption Air Conditioners,* LBL-11175.
5. Dao, K. (1978), *A New Absorption Cycle: The Single-Effect Regenerative Absorption Refrigeration Cycle,* LBL-6879.
6. Warren, M.L. and Wahlig, M., (1983), "Methodology to Determine Cost and Performance Goals for Active Solar Cooling Systems," *ASME J. Sol. Energy Eng. 105,* p. 217.
7. Warren, M.L. and Wahlig, M. (1981), "Cost and Performance Goals for Commercial Active Solar Absorption Cooling Systems," presented at the Fourth Annual Technical Conference, ASME Solar Energy Division, Albuquerque, NM, April 26–30, 1982, and *ASME J. Sol. Energy Eng. 107,* (1985), p. 136.
8. Warren, M.L. and Wahlig, M. (1985), *Performance Comparison of Absorption and Desiccant Solar Cooling Systems,* LBL-20002, to be presented at the 1986 ASME Solar Energy Division Conference, Anaheim, CA, 14–17 1986.
9. Brothers, P.W. and Warren, M.L. (1985), *Thermal Energy Storage for Solar Absorption Cooling Systems,* LBL-19990, to be presented at the 1986 ASME Solar Energy Division Conference, Anaheim, CA, 14–17 April 1986,
10. Brothers, P.W. (1985), *The Design Day Approach for Sizing Solar Cooling Systems,* LBL-18988.
11. Solar Energy Laboratory (1981), *TRNSYS—A Transient Simulation Program,* Users Handbook, University of Wisconsin–Madison Report 38-11.
12. Warren, M.L. (1986), *Evaluation of Advanced Active Solar Closed Cycle Absorption Cooling Systems,* LBID-1090 Draft.
13. Warren, M.L., *et al.* (1984), *Development of a New Modeling Tool for Advanced Absorption Cycle Chillers,* LBID-18698.
14. Letter Report to DOE/HQ: Outlining the basic structure of computer code for modeling advanced-cycle absorption chillers, November 1985.

Biological Oxidations and Bioenergetic Studies on the Photochemical Conversion of Solar Energy*

L. Packer, R.J. Mehlhorn, I.V. Fry, A.E. Robinson, S. Belkin, E. Hrabeta, M. Huflejt, S. Spath, E. Tel-Or,† and G.A. Peschek‡

The Membrane Bioenergetics Group is concerned with understanding how membrane structures are involved in biological energy conversion in living systems. To this end, several microorganisms are under investigation.

1) *Halobacterium halobium,* an obligate halophile, synthesizes a unique protein (bacteriorhodopsin), which exists as a two-dimensional crystalline array in the outer membrane, whose sole function is the conversion of light energy to a transmembrane proton gradient. Studies on the isolated bacteriorhodopsin-containing membrane (purple membrane) by chemical modification,[1,2] and tryptic cleavage methods[3] are leading to a determination of amino acid residues involved in the proton translocation process, a stepping stone to elucidating the molecular events in this relatively simple biological pump.

2) Cyanobacteria (blue-green algae) are microorganisms which possess oxygenic photosynthesis similar to that of higher plants, as well as dark respiration similar to that of bacteria, yeast, and mammalian systems. In addition, strains of cyanobacteria, particularly filamentous varieties, are capable of fixing atmospheric nitrogen into ammonia, under aerobic conditions. Another unique feature of organisms of this class is their ability to adapt to extreme environmental conditions (salinity, toxic elements, restricted light regimes). Several lines of investigation using cyanobacteria are under consideration.

The first line of investigation exploits the ability of these organisms to grow under a range of salinities which presents an opportunity to alter the biochemistry of the cell by manipulating environmental conditions. Two organisms, *Synechococcus* 6311, a freshwater cyanobacterium which can grow in up to 0.6M NaCl, and *Agmenellum quadruplicatum,* a marine species which can grow in up to 2M NaCl, were used. The biochemical functions of respiration, photosynthesis, and the directing of photosynthate into osmoticum and cell storage products have been monitored using standard biochemical and novel magnetic resonance techniques (electron paramagnetic and nuclear magnetic resonance spectroscopies).

A second line of investigation deals with use of cyanobacteria as tools for technological and environmental problems. The technological problem involves the use of biological components in the NASA Closed Ecological Life Support Systems (CELSS) program as a regenerative life support subsystems for the revitalizaton of air, waste processing, and for the production of food for long-term space flight. Employment of photosynthetic systems (higher plants, green algae, and cyanobacteria) allows biomass production from relatively simple components which are readily recycled in a CELSS system.

The production of plant material in a closed system presents several problems. A primary consideration is that of the energy requirement for continuous operation, including illumination, temperature control, and various maintenance mechanisms. One way in which the energy demands can be lessened is by modifying the quality of the light used. Illumination of photosynthetic systems with white light (300–700 nm range) is wasteful, since photosynthetic organisms utilize only selected regions of the visible spectrum. Tailoring the emission profile of the light source to match that of the action spectrum of photosynthesis, or to select an "emission band" in a region of maximal absorption by some of the photosynthetic pigments would present an energy saving, especially if the selected "emission band" was in the blue region, when using fluorescent light sources.

A second concern is the probability of nitrogen loss from the closed system by the action of contaminating denitrifying bacteria, which degrade NO_3^- to N_2 gas, which is then lost from the biological system. Denitrification is most likely to occur irrespective of the method of waste processing due to the storage of human waste and non-food biomass (cellulose), which would result in an irreversible loss of fixed nitrogen.

The ability of certain strains of cyanobacteria to counter this loss by fixing atmospheric nitrogen back into ammonia makes them an attractive candidate for the CELSS program.

*This research was supported by the Office of Basic Energy Sciences of the U.S. Department of Energy under Contract No. DE-AC03-76SF00098, by the National Institutes of Health through the U.S. Department of Energy under Contract AS-04818, a NASA Interagency agreement A-14563c, and by the Kearny Foundation for Soil Science.

†On leave from the Department of Botany Faculty of Agriculture, The Hebrew University of Jerusalem, Rehovot, Isarel.

‡On leave from the Institut für Physikalische Chemie der Universität Wien IX, Wahringertrasse 42, Vienna, Austria.

The environmental problem is centered on using cyanobacteria for the removal of selenium and toxic compounds that have accumulated in the saline drainage waters on the west side of the San Joaquin Valley. Several species of cyanobacteria have been found with differing capabilities to withstand increased levels of selenate or selenite in the environment. Our research proposes to investigate the effect of selenate and selenite on the growth and metabolism of several species of cyanobacteria, the degree to which selenium compounds are accumulated, the oxidation state of the selenium compounds (species) within the cell, and how the accumulation affects the biology of the organism.

A third line of investigation deals with photooxidative stress, a process experienced by most oxygenic photosynthetic organisms under high light intensities. Chemical intermediates and enzymes involved in protective mechanisms against oxidative damage have been determined. In addition, a novel oximetric method using magnetic resonance techniques has been employed to monitor the intracellular oxygen concentration during photosynthesis/respiration cycles.

3) *Thiobacillus ferrooxidans,* an acidophilic chemolithotroph, utilizes the oxidation of ferrous ions to generate sufficient reductant to fix CO_2 into carbohydrate. Preliminary results have demonstrated a novel component in the electron transport chain of this organism, which may be the site of iron (II) oxidation.

ACCOMPLISHMENTS DURING FY 1985

Bacteriorhodopsin

In the past decade there have been varying reports of the stoichiometry of proton release from purple membrane in suspension and protons pumped after its incorporation into phospholipid vesicles. In an attempt to resolve the range of values observed, we have investigated the H^+/M_{412} ratio, measured in suspensions of purple membranes by the laser flash induced response of pH indicator dyes.[3] We have found this ratio to reflect the aggregation state of the membrane, assessed on the same preparations by quasi-elastic light scattering (QELS).[4] We have also found our measurements of proton release stoichiometry on retinal reconstituted white membrane suspensions to give much higher H^+/M_{412} ratios than the same measurements on purple membrane suspensions.

Using proton release figures for native and trypsin treated membrane preparations, the proton release activity of purple membranes declined from an initial value of 1.5 H^+/M_{412} to a value below 0.5 upon trypsin treatment. Retinal reconstituted white membrane, on the other hand, started with a much higher proton release stoichiometry, close to 4.0 H^+/M_{412}, and even after trypsin treatment it retained most of this activity. In summary, while purple membrane loses two-thirds of its activity, retinal reconstituted white membrane loses less than one-tenth of its activity.

While the absolute H^+/M_{412} figures presented here cannot be directly compared, due to surface charge considerations, the relative figures are most informative. One must remember that, on cleavage of the C-terminal tail by trypsin, the surface loses considerable negative charge, which will in turn increase the amount of deprotonated dye (hydroxycoumarin) in the interface region and so cause an increase in sensitivity of the dye to protons released into this region, decreasing any lowering of H^+/M_{412} stoichiometry upon trypsin treatment. We are confident, however, that our trypsin treatment procedure causes a similar extent of cleavage in both membrane preparations, so this increase in sensitivity should affect each of the samples equally. The fact is that the white membranes showed a much smaller decline in activity than the purple membranes. The reason for this decrease is that native purple membrane consists of a suspension of particles with homogeneous size distribution in a rather narrow range (around 260 nm), and upon trypsin treatment the membranes become extensively aggregated, with a QELS pattern more characteristic of a gel than of a suspension of particles. With the membranes stacked and confined, it is impossible for protons to be released into a region where they can be detected by the dye, or indeed by any other measurement technique. The light flash will still, however, generate M_{412} so that the observed ratio of H^+/M_{412} is apparently lower.

In the case of white membranes there is a quantitatively different effect. In the first place, white membrane patches are smaller (88 nm radius), even before trypsin treatment. Following treatment, they too aggregate, but to a much lesser extent than do purple membranes.

Cyanobacteria

Respiratory electron transport

In addition to oxygen evolving photosynthetic electron transport, cyanobacteria also possess, to a lesser degree, respiratory electron transport components. During the initial exposure of cells to a

saline environment, when photosynthetic electron flux was severely inhibited[5,6] respiratory electron transport was found to increase tenfold, concomitant with a build up of cellular carbohydrate.[6] Using low temperature electron paramagnetic resonance (EPR) spectroscopy to characterize components of the electron transport pathways,[7] Cu^{2+} signals arising from the terminal oxidase[7] were found to increase in salt grown cells,[6] demonstrating that the observed increase in endogenous whole cell respiration was due to elevated levels of the respiratory component (Cytochrome *c* oxidase) rather than an increase in substrate supply or enzyme activity.[6] The elevated respiratory activity, which maintains a trans-cytoplasmic membrane pH gradient, supplied the driving force for the removal of intracellular Na^+ levels in the high salt environment. Via a Na^+/H^+ antiporter, removal of intracellular Na^+ relieved the inhibition of cellular processes (particularly photosynthesis), which returned to normal levels.[6] However, the respiration rate did not decrease, maintaining the low cellular Na^+.

Effect of C-13 Enrichment on Detectability of Organic Solutes by NMR

This study showed that the detectability of organic solutes by nuclear magnetic resonance (NMR) spectroscopy can be significantly increased by providing cyanobacterial cells with bicarbonate enriched with C-13. Imposing high salinities during growth amplifies the concentration of the intracellular organic solute glucosyl-glycerol, thereby facilitating further its detection. NMR spectra were used to make reasonable quantitative estimates of intracellular solutes if the peaks were well resolved, unambiguously assigned, and if a peak height standard was included. The methodology, in combination with standard cell fractionation and biochemical analysis, permitted us to determine the conditions and time frame of glycogen and osmoregulant interconversion.[9]

The time course of glucosylglycerol accumulation in the light after upshock of the cells (sudden increase in salinity) was comparable to the time course of cell doubling, which is consistent with other studies of carbohydrate accumulation. The diversion of fixed carbon to the synthesis of glucosylglycerol can explain, in part, the marked reduction of cell growth rates observed in cells during the initial period following upshock.[9]

A downshock experiment indicated that depletion of the accumulated glucosylglycerol is very rapid and probably involves the incorporation into glycogen, a strategy that would conserve the cellular fixed carbon pool. However, no evidence for glycogen was observed, either by NMR or conventional chemical analyses.[9]

The upshock data also showed that there is conversion of glycogen to the osmotically active species glucosylglycerol in the light, but not in the dark. This was a surprising observation considering that the cell could fulfill a need for low molecular weight solutes, with a relatively low expenditure of energy. Previously it had been observed that cells of another cyanobacterium (*Synechococcus* 6311) take up salt during hypersaline shock and carry out metabolic processes in the light that enable them to recover from the effects of this high intracellular salinity. Thus, it would appear that the presence of organic "compatible solutes" is not a prerequisite for short-term cell survival either in the light or in the dark. During dark periods, however, these compounds may be required for energy production and different osmoregulatory mechanisms may be employed to compensate for the loss of organic osmoregulants to respiration.

Effects of Selenate Toxicity

The growth rates of laboratory cultures of *Synechococcus* 6311 were determined by measuring increments in cell density over a period of four days. Generation times were calculated during the early logarithmic growth phase. Cultures were subjected to a variety of sulfate and selenate concentrations in Kratz and Myers "C" medium under a light intensity of 50 $\mu Em^{-2}s^{-1}$, at 28°C and bubbled with air supplemented with 1% CO_2.

Near maximum growth rates were obtained with a minimum of 0.1 mM (14 ppm) of Na_2SO_4 in the growth medium. The minimum requirement for sulfate was determined in order to determine the sensitivity of the organism to selenate, since sulfate has been shown to have an antagonistic effect on selenate toxicity. Reproducibility of growth rates was determined using six independent replicates giving a value for the generation (cell doubling) time of 15.58 hours with a standard deviation of 0.50 hours. The reproducibility of the generation time permits a significant interpretation of even small changes in the growth rate.

The generation time (in the presence of 14 ppm and 1000 ppm Na_2SO_4) over a range of Na_2SeO_4 up to 5000 ppm was determined. Cells grown with minimal sulfate (14 ppm) showed sensitivity to selenate at 50 ppm, growth being totally inhibited at 100 ppm selenate. However, increasing the sulfate level to 1000 ppm facilitated cell growth in up to 5000 ppm selenate. Results obtained so far indicate

that it is the selenate/sulfate ratio which determines cell viability and growth, rather than absolute selenate concentration *per se.* When the selenate/sulfate ratio is greater than 1.0, growth inhibition and cell death occurred.

Growth of Cyanobacteria under Selected Light Regimes

Nostoc muscorum, a filamentous hetercystous nitrogen fixing blue-green algae, was grown under blue (400–500 nm) and white (300–700 nm) light at 150 $\mu Em^{-2}s^{-1}$. The cells grow readily under the blue light, even though the cell doubling time (generation time, G) increased by a factor of 2.5. Analysis of photosynthetic O_2 evolution and nitrogenase activity during growth under blue light reveals very little difference from those grown under white light when rates were calculated on a total protein basis. Calculation of rates (particularly photosynthesis) on a total chlorophyll basis revealed an apparent increase in photosynthetic rate. However, this reflected a decrease in total cell chlorophyll, a chromatic adaption to blue light. Analysis of cellular products after a seven-day growth period under blue and white light revealed that little change occurred in soluble sugars, glycogen, or lipids, while total protein decreases only by 10%. A component which does increase is cell wall material.[10]

In conclusion, the nitrogen fixing strain *Nostoc muscorum* is capable of growth under light at the blue end of the visible spectrum. One must evaluate whether the energy saving gained by employing blue photons outweigh the slower growth rate (and hence biomass production). However, if a system employing a continuous culture (kept at a fixed point in the exponential growth phase) for air revitalization, etc., then a slower growth rate may be advantageous, requiring less addition of growth medium to maintain the constant cell density.

Oxidative Damage

Nitrogenase, the enzyme responsible for the biological fixation of atmospheric N_2, is extremely oxygen-sensitive. One of the modes in which cyanobacteria "solved" the problem of N_2-fixation under aerobic conditions was the development of the heterocysts mentioned above. However, as with other nitrogenase containing microorganisms, the mechanisms by which these cells retain an oxygen-free internal environment is not completely understood. In addition, photooxidative damage to cell components occurs under high light, the mechanisms of protection against such damage are important factors in cell viability.

ESR oximetry for the measurement of intracellular O_2. We have recently developed an ESR technique which enables us to measure intracellular O_2 concentrations. We hope to utilize this method to gain a better understanding of the protection mechanisms against the toxic effects of O_2 to nitrogenase.

The technique is based upon the broadening effect dissolved O_2 has on the nitroxide spin-probes ESR signal. Photosynthetically generated oxygen, in a suspension of the cyanobacterim *Agmenellum quadruplicatum,* caused a broadening of the EPR signal by 0.5 G. The effect is even more pronounced when a higher derivative of the spectrum is examined. According to our calculations, this broadening is equivalent to O_2 concentration in the suspension of 2.5 mM.[11] Furthermore, by quenching the extracellular signal, it is possible to examine only the probe inside the cells, and by using the measured degree of broadening to calculate intracellular O_2 concentrations. Studies are presently underway to compare O_2 levels in non-N_2-fixing and some N_2-fixing cyanobacterial cells, as well as to establish the O_2-sensitivity of various photosynthetic activities.

Protective enzyme systems against oxyradical products. The mechanism for removal of inorganic and organic peroxides consists of a highly active ascorbate peroxidase acting in combination with a relatively low intracellular concentration of ascorbate (μmolar level) but which is regenerated by a large (mmolar level) concentration of reduced glutathione. The activities of ascorbate peroxidase observed in *N. muscorum* and *Synechococcus,* with an intracellular concentration of 20 to 100 μM ascorbate, were found to scavenge 60–230 nmoles $H_2O_2 \cdot$mg protein^{-1} min^{-1}. This rate is equivalent to 0.5–2.0 μmoles $H_2O_2 \cdot$mg chl^{-1}min^{-1} which approaches 30% of the photosynthetic electron transport rates and hence appears sufficient to scavenge relatively large amounts of H_2O_2 formed in the cells. The large pool of glutathione in the cells is used partially to regenerate the ascorbate by dehydroascorbate reductase while the steady state level of the glutathione disulphide is low and glutathione is maintained in the reduced form by glutathione reductase activity.[12] That the H_2O_2 removing system involves a cascade of reactions is also supported by studies of catalase. In *N. muscorum* and *Synechococcus* catalase has a very low affinity to H_2O_2 (unpublished results), and therefore is not as effective as ascorbate peroxidase in H_2O_2 removal.

Thiobacillus ferrooxidans

Studies on the electron transport chain of this

organism, using low temperature EPR spectroscopy, have revealed a novel component at g = 2.005, which is specifically reduced by Fe(II), and autooxidized specifically in the presence of sulfate ions. This ionic requirement is in agreement with the organism's ionic requirements for the formation of Jarosite deposits. Preliminary work places this novel component on the reduced end of the electron transport chain, and it is a likely candidate for the catalytic center responsible for the direct oxidation of Fe(II) to Fe(III) sulfate complexes. This line of research will be continued in FY 1986.

PLANNED ACTIVITIES FOR FY 1986

Cyanobacteria

Work with cyanobacteria will continue in several areas. The role of respiration, with emphasis on the removal of O_2 to facilitate the protection of the nitrogen fixing enzymes, will continue to be investigated. Components of the respiratory electron transport pathway in addition to the Cu^{2+} containing terminal oxidase will be investigated by EPR spectroscopy. Professor Peschek's group in Vienna, who have isolated outer membrane preparations with high oxidase activity, will make samples available for the determination of the Cu^{2+} containing oxidase and other electron transport components by EPR spectroscopy. The investigation of (photo)oxidative stress in several strains, both unicellular and filamentous will continue, using the standard biochemical and novel ESR oximetric techniques. Inactivation of cellular process by intracellular oxygen will be correlated with the levels of antioxidative enzymes and components within the cell to elucidate protective mechanisms. Two unique cyanobacteria, *Gloeothecae* (a unicellular aerobic nitrogen fixer) and *Gloeobacter* (a unicellular thylakoidless non-nitrogen fixer) will be investigated with respect to their antioxidative, electron transport, and photosynthetic electron transport pathways.

Thiobacillus ferrooxidans

Further characterization of electron transport components of this chemolithotroph will continue, particularly ionic requirements and the nature of the Jarosite deposits formed by the bacterial oxidation of $FeSO_4 \cdot 7H_2O$ at acid pH.

Halobacterium halobium

The role of specific amino acids in the structure and function of bacteriorhodopsin will be assessed by chemical modification, cleavage, and protein reconstitution techniques.

Recently we have been engaged in the selection and further characterization of carboxyl modifications which are region-specific. We propose to use these modifications in conjunction with chemical and proteolytic cleavage techniques to obtain and purify modified fragments of bacteriorhodopsin. Combinations of modified and unmodified fragments will be tested for the ability to reconstitute a native-like protein complex in the presence of the chromophore and native lipids. The products of the reassociation will be analyzed with respect to photocycle kinetics, M_{412} accumulation, light-induced protein release and spectroscopy. Further characterization of the tertiary and quaternary structure will be done by spectrapolarimetry and spectrofluorimetry.

The long-term goal is to develop a method by which the selectivity of amino acid modification can be enhanced by reconstitution of modified with unmodified fragments, so that the amino acids of particular helices can be studied, and the involvement of these residues in protein translocation can be determined.

REFERENCES

1. Takeda, K., Iwasa, T., Tokunaga, F., and Packer, L. (1985), "Tyrosine Residues Interacting with the Chromophore in Bacteriorhodopsin," *Biosci. Reports 5*, p. 615.
2. Sonnewald, II., Seltzer, S., Robinson, A.E., and Packer, L. (1985), "(Mesityl) bacteriorhodopsin. The Properties of an Analogue of the Purple Membrane Containing (Mesityl) Retinal as the Chromophore," *Photochem. Photobiol. 41*, p. 303.
3. Robinson, A.E., Hrabeta, E., and Packer, L. (1985), "Measurement of Proton/M_{412} Ratios in Suspensions of Purple and White Membranes from *Haloacterium halobium*," in *Ion Interactions of Biological Systems*, Plenum Press, New York.
4. LeFort-Tran, M., *et al.* (1985), "Stacking of Purple Membranes *in vitro*," in *Ion Interactions of Biological Systems*, Plenum Press, New York.
5. Packer, L., *et al.* (1985), "Some Insights into the Interaction of Water and Ions with the Bioenergetic System in Cyanobacteria," in *Proceedings of the International Workshop on Ion Interactions in Energy Transfer Systems*, Athens, Greece, 8–12 April 1985, sponsored by UNESCO and the Hellenic Biochemical and Biophysical Society, p. 99.

6. Fry, I.V., *et al.* (1985), "The Role of Respiration During the Adaptation of the Freshwater Cyanobacterium *Synechococcus* 6311 to Salinity," *Ach. Biochem. Biophys.*, in press.
7. Fry, I.V., Peschek, G.A., Huflejt, M., and Packer, L. (1985), "EPR Signals of Redox Active Copper in EDTA Washed Membranes of the Cyanobacterium *Synechococcus* 6311," *Biochem. Biophys. Res. Commun. 129,* p. 109.
8. Packer, L., Tel-Or, E., Mehlhorn, R.J., and Spath, S. (1985), "^{13}C NMR and ESR Studies of Osmoregulation in a Marine Cyanobacterium," *Amer. Soc. Plant Physiol. Abstr. 77,* p. 119.
9. Tel-Or, E., Spath, S. Mehlhorn, R.J., and Packer, L. (1985), "C-13 NMR Studies of Carbohydrates in a Marine Cyanobacterium," in preparation.
10. Packer, L., Fry, I.V., and Belkin, S. (1985), "Application of Photosynthetic N_2-Fixing Cyanobacteria to the CELSS Program," presented at the CELSS Meeting, Ames Research Center, Moffett Field, California, July 16–19, 1985.
11. Belkin, S., Mehlhorn, R.J., and Packer, L. (1985), "Determination of Dissolved Oxygen in Photosynthetic Systems by Intoxide Spin-Probe Broadening," submitted to *Archives of Biochemistry and Biophysics.*
12. Tel-Or, E., Huflejt, M., and Packer, L. (1985), "The Role of Glutathione and Ascorbate in Hydroperoxide Removal in Cyanobacteria," *Biochem. Biophys. Res. Commun. 132,* p. 533.

LBL Building 71 Solar Cooling Project*

F. Salter

This active solar cooling project is part of the Department of Energy's Solar in Federal Buildings Program. The program is intended to stimulate growth and technical improvements in solar technology through the installation and demonstration of a variety of commercially applicable solar energy systems in buildings owned or occupied by the federal government. The program provides technical and financial assistance through interagency agreements to federal agencies for design, acquisition, construction, and installation of solar heating and cooling equipment projects.

Building 71, which houses the Heavy Ion Linear Accelerator (HILAC), was chosen as the site for this demonstration project. The LBL Plant Engineering Department provides project engineering and contract administration. The LBL Active Solar Research Group provides technical assistance and review of the project.

Overall administration is provided by the San Francisco Operations Office of the Department of Energy (DOE/SAN). DOE/SAN has subcontracted technical management of the project to the Energy Technology Engineering Center (ETEC).

The Solar Cooling System provides substitute capacity for the existing Building 71 chilled water system with a solar-driven chiller installed next to and in parallel with the existing electric chillers. The system consists of roof-mounted collectors; storage tanks; a nominal 25-ton capacity lithium bromide chiller package; and associated pumps, piping, insulation, valves and fittings, controls, and instrumentation. The chiller package was supplied by Arkla Industries, Inc.

Table 1 summarizes the design parameters of the cooling system. The collector array uses Energy Design HP-250 evacuated-tube solar collectors.

ACCOMPLISHMENTS DURING FY 1985

Construction had been delayed for the first seven months of 1984 because of a lack of funds, with work resuming in August 1984. The solar loop was pressurized and 10 solar collectors were found to have leaks. Attempts to field-weld the solar collector stainless steel tubing were unsuccessful, and the entire tubing circuits were replaced with new copper fluid circuits for the damaged solar collectors.

Prior to acceptance tests, the construction subcontractor placed the solar loop in operation in November 1984 and operated the solar chiller for three days in December 1984. The solar loop was left operational until July 1985 when it was shut down by LBL because of excessive leakage from solar collectors and especially from silicone hose connections between solar collectors.

*This work was supported by the Assistant Secretary for Conservation and Renewable Energy, Office of Solar Heat Technologies, Solar Buildings Technology Division of the U.S. Department of Energy under Contract No. DE-AC03-76SF00098.

Table 1. Parameters of LBL Building 71 solar cooling system.

Chiller Capacity	25 tons (nominal)
Chiller COP	0.73
Average Operation	6 hr/day (at 22-ton loading)
Generator Entering-Water Temp.	185°F (adjustable 170°F to 200°F)
Exiting Chilled-Water Temp.	45°F
Entering Condenser-Water Temp.	80°F
Maximum Storage Temp.	250°F
Collector Area	5100 ft^2 (gross area)
Collector Type	evacuated tube (198 collector modules, with 7 tubes per module)
Storage Tank	2500 gallons
Thermal Ballast Tank	500 gallons
Expansion Tank	500 gallons

By January 1985 relatively little work remained to complete the project (aside from leakage problems), yet LBL was unable to expedite the subcontractor construction. Work continued at a very slow pace, especially after the subcontractor filed a $248,000 claim against LBL (claim was primarily against delays and problems associated with solar collector delivery and operation) in February 1985. LBL negotiated with the subcontractor during the spring and summer of 1985, eventually eliminating the claim.

The final inspection was held in September 1985. Acceptance tests were started in early November. The chiller failed during the course of the tests and the solar system was shut down.

LBL has since written to DOE recommending that the solar system be shut down permanently. This is based on the high cost of replacing the Arkla chiller ($48,000; Arkla, now owned by Preway, no longer manufactures or services solar chillers) and on major problems with the solar collectors. The solar collectors have had a high failure rate due to severe crimping at 180° bends within each evacuated tube and at tack welds on spacers between supply and return headers. Additionally, the silicone hose connections between solar collectors extrude beneath the hose clamps causing excessive leakage and need for repeated maintenance. LBL is concerned that all the solar collector stainless steel tubing circuits may eventually fail, possibly at an accelerated rate, especially with the potential for stress corrosion cracking of the stainless steel tubes. Eliminating leakage at solar collector connections would be extremely costly due to the high stagnation temperature (approximately 600°F), resulting thermal expansion, and narrow spacing between solar collectors. LBL is presently corresponding with Energy Design based on the above collector items.

Being a demonstration project, cost effectiveness was not one of the initial project requirements. At this point, the limited economic benefit of the project (savings of conventional fuel costs) makes it very difficult to justify the anticipated additional equipment costs and maintenance costs involved in proceeding to repair and operate the system.

PLANNED ACTIVITIES FOR FY 1986

Assuming that DOE accepts the LBL recommendation to discontinue operation of this system, this project will terminate in early FY 1986. The main outcome of the project has been increased experience with construction rather than with operation of solar cooling systems. Valuable information on use of stainless steel collectors (how not to do it!) will hopefully prevent the problems that surfaced here from re-occurring in future solar cooling and heating systems.

Solar Energy Conversion Using Microstructured Materials: Direct Radiant Heating of Small Particle Suspensions*

A.J. Hunt, J. Ayer, P. Hull, R. McLaughlin, F. Miller, J.E. Noring, R. Russo, and W. Yuen

The Solar Advanced Micromaterials Research and Development Group is investigating the use of microstructured materials for the conversion, control, and collection of solar energy. Current research is underway in four areas: (1) direct radiant heating of small-particle suspensions to produce useful fuels and chemicals, (2) radiant heating of small-particle suspensions to initiate reversible chemical reactions for thermal energy storage and regenerative electrochemical cells, (3) production of hydrogen from water, and (4) development of microporous optical materials for insulating windows and ceramics. This article describes research in the first area. Work in the second and third areas is reported in the Thermal Energy Storage section of the Chemical Process R&D Program (LBL-20201). The insulating windows and the ceramics research in the fourth area are described in the "Optical Materials Studies" and the "High Temperature Ceramics Development Using the Sol-Gel Process" articles of this chapter, respectively.

BRIEF HISTORY OF WORK PRIOR TO FY 1985

For the past seven years, we have been actively involved in developing solar thermal energy conversion systems using the principle of direct absorption of concentrated sunlight by a gas-particle mixture.[1-3] Small particles absorb sunlight concentrated by a field of mirrors or a parabolic dish to heat a gas to high temperature for electric power generation or industrial process heat. The concept was demonstrated experimentally by the design, construction, and successful solar test of an air-heating, 30 kW_t SPHER Receiver (SPHER is an acronym meaning *Small Particle Heat Exchange Receiver)* at the Georgia Institute of Technology Advanced Component Test Facility in FY 1982.[4] The solar tests confirmed the predictions that (1) small particles are effective solar absorbers, (2) high gas temperatures can be attained, and (3) the high temperature zone may be isolated from the surrounding walls. In two DOE-sponsored comparative evaluation studies of a number of advanced high temperature gas receivers the SPHER concept ranked first and second.[5,6]

Since FY 1983, we have been investigating the possibility of initiating high temperature chemical reactions by directly illuminating particle suspensions with concentrated sunlight. We call such a receiver STARR, an acronym meaning *Solar Thermally Activated Radiant Reactor,* in order to differentiate it from the strictly gas heating SPHER receiver. In this concept, the particles absorb sunlight to drive a chemical reaction.

In FY 1984, we made substantial progress in developing the STARR receiver technology. A survey of candidate chemical reactions was performed. Analytical models of the optical and heat transfer interactions in gas-particle mixtures were developed and improved, most notably an analytical expression to predict the conductive heat transfer between a particle of arbitrary size and the surrounding gas.[7] Experimental studies with entrained particles were carried out using a xenon arc lamp to simulate concentrated solar radiation. Reference 8 details these accomplishments.

ACCOMPLISHMENTS DURING FY 1985

Our research into STARR receiver technology was divided into four interrelated areas: (1) assessment of technical and economic potential of candidate chemical reactions, (2) calculation of optical properties of gas-particle mixtures for candidate small-particle materials, (3) continued development of an integrated solar thermal and fluid mechanical model of gas-particle mixtures in STARR receivers, and (4) experimental studies. The accomplishments in each of these areas will be discussed separately.

Assessment of Candidate Chemical Reactions

In FY 1984, we identified a large number of chemical reactions as candidates for the STARR receiver. In FY 1985, we evaluated these reactions using a set of technical and economic criteria. The technical criteria included process feasibility, efficient use of sunlight, adaptability to diurnal operation, and the availability of suitable particle materials. Economic criteria included cost competitiveness with similar products made using conventional energy sources, high product value, and plant location (to reduce transport costs for bulk products).

*This work was supported by the Solar Fuels and Chemicals Program managed by the San Francisco Operations Office, under the Assistant Secretary for Conservation and Renewable Energy, through the U.S. Department of Energy under Contract No. DE-AC03-76SF00098 and by the Solar Energy Research Institute.

Each candidate reaction was assigned to one of four categories dependent on the role of the particle in the process reaction:

1. *Particle as Gas Heater.* The particles absorb sunlight and heat the surrounding gas but do not participate in the process reaction.
2. *Particle as Feedstock.* The particle is the reactant for the process reaction; the gas acts solely as a carrier for the reacting solid material.
3. *Particle-Gas Reaction.* The particle undergoes a chemical reaction with the entrainment gas.
4. *Particle as Reaction Catalyst.* This is similar to the first category above except that the absorbing particle also acts as a catalyst or photocatalyst. Photocatalysis of high temperature reactions is an exciting and surprisingly little studied area that offers the potential of developing solar unique processes, that is, processes driven with solar energy that cannot be economically duplicated using conventional energy sources.

Chemical reactions worthy of further study were identified in each category. In gas heating applications, the thermal decomposition of hydrogen sulfide (H_2S) to hydrogen and sulfur ranked highest. It only requires 1/7 the energy per mole to produce hydrogen from H_2S as it does from water. In addition, H_2S is very plentiful and is an undesired byproduct of the natural gas and petrochemical industry. The absorbing particle may be carbon or a metal oxide.

Three reactions stand out in the category of the particle as feedstock. At present, elemental phosphorus is produced in electric arc furnaces by reacting phosphate ore with carbon and silica. The direct replacement of electrically derived heat by solar thermal heat produces an extremely attractive economic benefit. This may be accomplished by pelletizing the premixed feedstock and heating it to a high temperature with concentrated sunlight to initiate a reaction to release elemental phosphorus. Another interesting application of solar solids processing is provided by the Harteck process.[9] In the first step of this cycle, high pressure air is reacted with metal oxide particles to form a metal nitrate (the use of small particles may substantially enhance this reaction). In the second step, solar heat is used to decompose the metal nitrate particles to form NO_x and recover the metal oxide. The NO_x is then scrubbed with water to form nitric acid, an industrially important chemical. The net effect of this cycle is to fix atmospheric nitrogen with sunlight. The third reaction can be used in a thermochemical process to produce hydrogen and oxygen from water. In this reaction, magnetite (Fe_3O_4) particles are reduced by decomposition at high temperature to form FeO and release oxygen. In the second step of this thermochemical water splitting cycle, the FeO particles are oxidized to magnetite by low temperature steam to release hydrogen from water.

In the particle-gas reaction category, another type of water splitting reaction was identified in which both steps are solar driven. This involves the reaction of magnetite with water to form hematite (Fe_2O_3) and hydrogen. Since this reaction has a slightly positive free energy change it cannot occur spontaneously. However, magnetite is an excellent solar absorber which, under high radiant fluxes, may photo-reduce water adsorbed on its surface. The cycle is completed by the high temperature decomposition of hematite to reform magnetite.

In the particle as catalyst category, two reactions stand out. The photocatalyzed oxidation of nitrogen in air at moderately high temperatures (e.g., 1700 K) is a possibility. In the Wisconsin process (partly commercialized in the 1950's), temperatures in excess of 2500 K are required to thermally oxidize nitrogen, followed by a requirement for rapid quenching to temperatures below 1700 K to prevent decomposition of the nitric oxide. Driving this reaction photocatalytically at a temperature below 2000 K would overcome both of these stringent requirements. In another reaction, SO_3 decomposition forms the basis of several solar energy conversion processes, including multistep thermochemical hydrogen production and storage or transport cycles in which SO_2 and O_2 are recombined to produce heat. Iron oxides are used to catalyze SO_3 decomposition, and photocatalysis may play an important role in enhancing the dissociation.

In summary, several good candidates for STARR receiver application were identified. Among these candidates, we believe that the moderate temperature photo-oxidation of nitrogen in air, if it can be effected, would have the highest payoff for two reasons. First, the product, fixed nitrogen for fertilizers, is a very valuable commodity of world-wide usage that requires only air and water as primary feedstocks. Second, there is the potential for solar uniqueness, since this process would require solar photons to catalyze it.

Optical Properties Calculations

To design a STARR receiver it is necessary to understand the optical properties of absorbing parti-

cle suspensions. Computer codes utilizing the Mie calculation were developed to determine the absorption of *broad band* spectral radiation by gas-particle suspensions. Figure 1 illustrates the result of these calculations by showing the fraction of light absorbed by a particle suspension as a function of the product of particle mass loading and propagation distance.[10,11] Data are plotted for magnetite (Fe_3O_4), hematite (FeO_3), and cobalt oxide (Co_3O_4). These calculations were performed for light with the spectral characteristics of the xenon arc lamp used in our experiments; the particles are assumed to have a Gaussian size distribution with the mean particle diameter given for each curve. Note from this figure that the *product* of the particle mass loading and the propagation distance determines the overall absorption of the gas-particle mixture. This is important for STARR receiver design; i.e., the propagation distance is directly related to the receiver size, while the particle mass loading is generally related to the given application. Thus, there is an important coupling between the receiver size and the mass loading that must be considered in STARR receiver design studies.

Integrated Model of Gas-Particle Mixtures

To properly design a STARR receiver, it is important to understand the gas and particle temperatures, densities, and flows inside the receiver. To calculate these quantities requires development of a model to predict the effects of solar absorption and heat transfer within gas-particle mixtures, the fluid flow, and the chemical reactions. Since FY 1984, we have been working on versions of such a model that would include most major effects.[7,11-12]

To study possible chemical reactions carried out by STARR, we implemented the CHEMKIN computer codes at LBL. These state-of-the-art thermochemical codes were obtained from Sandia National Laboratories. This implementation will allow us to calculate chemical kinetics and equilibrium for complex reacting systems including the presence of condensed phase species.

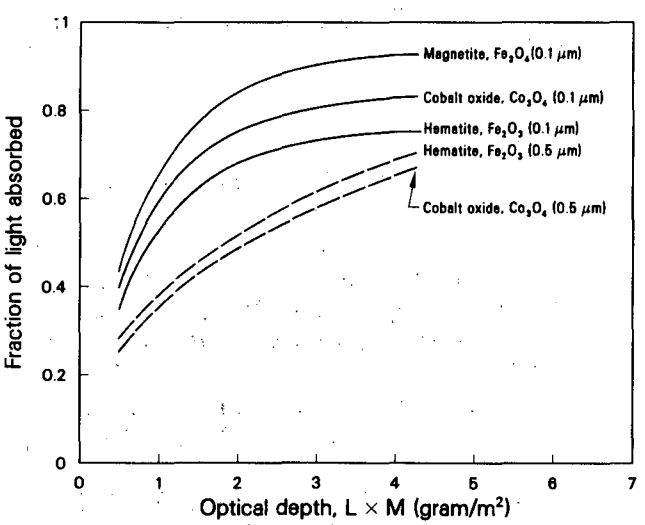

Figure 1. Fraction of the light absorbed from a xenon arc-lamp by a uniform gas-particle mixture as a function of the optical depth (the product of the mass of particles, per unit volume, and the path length). Each curve represents a specific particle. (XCG 862-7101)

Experimental Studies

Laboratory studies were used to validate our understanding of radiantly heated particle suspensions and to explore new ways of inducing chemical reactions with sunlight. Concentrated solar radiation is simulated in the laboratory using a high intensity xenon arc lamp mounted at one focus of an ellipsoidal reflector. The 2.2 kW xenon arc-image furnace is capable of delivering a peak flux of about 4000 kW/m^2 and a total radiant power to the focus of 520 watts. Several improvements were made to the solar simulator in FY 1985 to improve the alignment and reduce heat losses. The complete experimental system includes gas supplies, vortex particle entrainer, baffled optical attenuation tube, quartz reactor, dichotomous sampler, electronics, and instrumentation to measure temperature and flow. Particle composition is monitored off-line with an automatic x-ray diffractometer, and gas composition is monitored with a gas chromatograph.

The experimental system was used to investigate chemical reactions induced by radiant heating in the reactor system. Both oxidation and reduction of entrained particles were demonstrated. All the entrained particles were examined using Scanning Electron Microscopy (SEM). In addition to the metal oxides mentioned below, a beneficiated phosphate ore sample from Togo was examined for suitability for solar thermal processing (see Fig. 2).

An experiment was performed to oxidize powdered magnetite to hematite using air as the entraining gas. An important goal of this experiment was to assess how rapidly oxygen can diffuse into the magnetite particle. The results showed that over 70% of the magnetite particles smaller than 2.5 microns in size were converted to hematite in a few seconds in the reactor. This demonstrates an important advantage in using micron-sized particles to perform solid gas reactions where diffusion of a gas through the solid is necessary.

Powders of hematite, magnetite, cobalt oxide

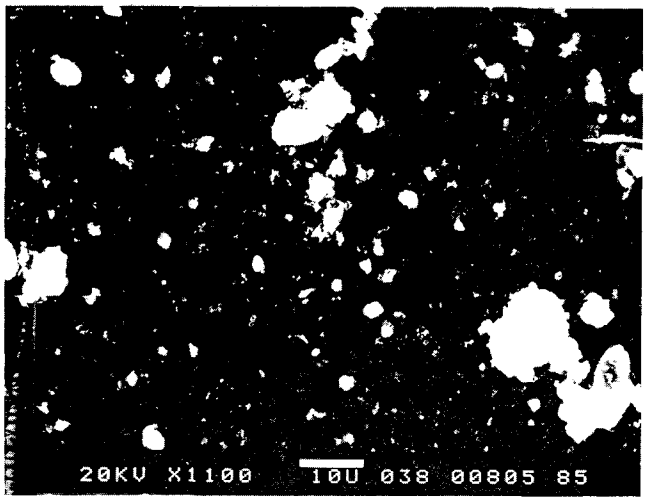

Figure 2. Scanning electron micrograph of beneficiated phosphate ore from Togo. (XBB 863-1734)

(CO_3O_4), copper oxide (CuO), zinc oxide (ZnO), and manganese dioxide (MnO_2) were separately entrained in argon and passed through the reactor to determine if they could be reduced by direct radiant decomposition (such reductions are important for hydrogen-producing multistep thermochemical cycles). Because of the limited size of the reactor, the particle suspensions were not sufficiently absorbing to reach the maximum theoretically attainable temperatures, and the resulting temperatures ranged from 1030 K to 1070 K. Significant reduction of copper oxide (CuO to Cu_2O) was demonstrated by x-ray diffraction measurements. The extent of conversion varied from 14% to 29%. Figure 3 gives the x-ray diffractometer measurements of the particle samples taken both before and after the solar simulator was turned on. As expected (because of the limited temperatures), hematite, magnetite, zinc oxide, and manganese dioxide did not show reduction. Cobalt oxide did show reduction in a first experiment, but no reduction in a subsequent experiment.

PLANNED ACTIVITIES FOR FY 1986

The research in direct radiant heating of small particle suspensions will continue in FY 1986 with support from SERI. The proposed work will concentrate on detecting and exploiting photolytic effects at high fluxes and temperatures to produce useful fuels and chemicals. Both experimental and analytical techniques will be used to explore radiantly induced chemical reactions. In particular, reactions involving the oxidation of nitrogen and the reforming of methane with carbon dioxide will be studied. Experiments using the solar facilities at Sandia National

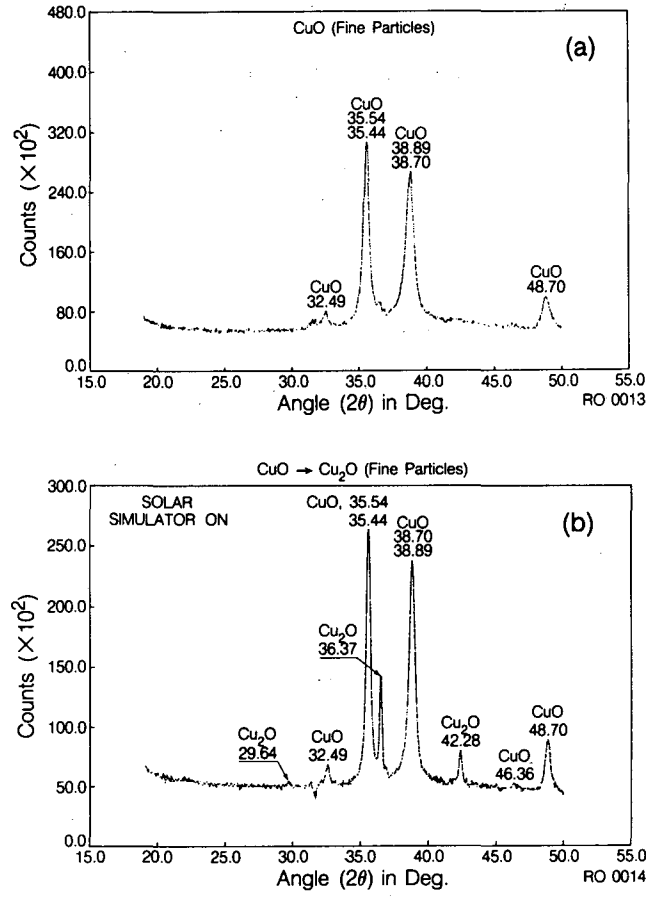

Figure 3. X-ray diffractometer measurements of copper oxide powder before and after solar simulator turned on. [(a) XBL 855-9323, (b) XBL 855-9325]

Laboratories in Albuquerque are planned for FY 1986 or FY 1987.

REFERENCES

1. Hunt, A.J. (1978), *Small Particle Heat Exchangers,* LBL-7841.
2. Hull, P.G. and Hunt, A.J. (1984), "A Reciprocating Solar Heated Engine Utilizing Direct Absorption by Small Particles," *Journal of Solar Energy Engineering 106,* p. 29, LBL-10622.
3. Hunt, A.J., Hansen, L., and Evans, D.B. (1984), "Solar Heat Receiver," U.S. Patent No. 4,499,893.
4. Hunt, A.J. and Brown, C.T. (1983), "Solar Test Results of an Advanced Direct Absorption High Temperature Gas Receiver (SPHER)," presented at the 1983 Solar World Congress, International Solar Energy Society, Perth, Australia, August 15–19; LBL-16497.

5. Drost, K. (1983), "Evaluation of Solar Air Heating Central Receiver Concepts," in *Proceedings of the 1982 American Section of the International Solar Energy Society*, Houston, TX, p. 293.
6. Boeing Aerospace Energy Systems (1985), "Small Central Receiver Brayton Cycle Study," Final Technical Report, SAND84-8189.
7. Yuen, W.W., Miller, F.J., and Hunt, A.J. (1986), "Heat Transfer Characteristics of a Gas-Particle Mixture Under Direct Radiant Heating," *International Communications in Heat and Mass Transfer 13*, p. 145; LBL-20289.
8. Hunt, A.J., *et al.* (1984), *Solar Radiant Heating of Gas-Particle Mixtures, FY 1984 Summary Report,* Final Report to DOE/SAN, LBL-20447.
9. Harteck, P. (1984), "Fixation of Nitrogen in the Presence of Water Vapor," U.S. Patent 4,426,367.
10. Hunt, A.J., *et al.* (1985), "Direct Radiant Heating of Particle Suspensions," in *Proceedings of the Solar Thermal Research Program Annual Conference*, Lakewood, Colorado, 20–22 February, p. 139; LBL-19388.
11. Hunt, A.J., *et al.* (1985), "Direct Radiant Heating of Particle Suspensions for the Production of Fuels and Chemicals Using Concentrated Sunlight," in *Proceedings of INTERSOL 85*, Montreal, Canada, 23–27 June, International Solar Energy Society, p. 1947; LBL-19842.
12. Hunt, A.J., *et al.* (1985), "Solar Radiant Processing of Gas-Particle Mixtures," in *ASME/AICHE Symposium Series*, Denver, Colorado, 4–8 August; LBL-19102.

High Temperature Ceramics Development Using the Sol-Gel Process*

A. Hunt, J. Lieber, K. Lofftus, and P. Tewari

The goal of this research is to develop advanced ceramics for high temperature applications based on microstructural fabrication techniques using sol-gel processing. In traditional ceramic preparation, the principal sources of unreliability in performance derive from the processing techniques and the state of the starting materials. It has been postulated by some research groups that uniform agglomerate-free fine *particles* can be used to produce more reliable and reproducible ceramics than those prepared traditionally from irregular shaped commercial powders. Other groups have suggested that controlling *pore* uniformity in green bodies (ceramic preforms before sintering) is the important factor and the particles do not necessarily have to be uniform. Evidence for improved performance in laboratory scale samples has been presented by proponents of both the "uniform particle" and "uniform pore" hypotheses.

*This work was supported by the Assistant Secretary for Conservation and Renewable Energy, Office of Energy Systems Research, Energy Conversion and Utilization Technology Division of the U.S. Department of Energy under Contract No. DE-AC03-76SF00098.

We are developing a high density sol-gel processing technique that offers the possibility of controlling both the uniformity of particle *and* pore sizes and thereby better control of the microstructure and reliability in the ceramic material. Work was initiated late in FY 1984 with a review of sol-gel preparation techniques for making metal oxide ceramics from alkoxide precursors.

ACCOMPLISHMENTS DURING FY 1985

Currently, the production of ceramics by sol-gel processing is carried out using two distinctly different processes. In one, hydrolysis of a metal alkoxide in alcohol leads to condensation and formation of a monolithic gel. This alcolgel is then air-dried slowly and sintered to obtain small samples of a ceramic or glassy material. In the second process, fine spherical metal oxide particles are produced by hydrolysis and condensation of metal alkoxides. The fine powders, without large agglomerates, are used to prepare ceramic "green bodies" that are subsequently sintered to produce experimental ceramic materials. We have been studying the monolithic approach because this technique offers a real possibility to control both particle and pore sizes as well as the interparticle bonding. In addition, this approach offers promise for producing multicomponent but homogeneous ceramics and glasses difficult to produce by conventional means.

The experimental research on monolithic gels at LBL was initiated by studying single component systems of silica. In the past, preparation of silica

alcogels was limited to rather low densities of solids. This occurred because of a solubility limit of the alkoxide in the alkoxide-water-alcohol ternary system. When this solubility limit is exceeded, phase separation or precipitation occurs; this sets an upper limit on the solid content in the alcogel. An important accomplishment of our research in FY 1985 was to find ways to overcome this solubility problem and allow the preparation of materials with much higher solid content, more suitable for ceramic applications.

In addition to the preparation of single component sol-gel solids, we have also synthesized the mixed oxide system SiO_2:Al_2O_3. Transmission Electron Microscopy (TEM) of this system shows that the Al_2O_3 particles are fine needles 5 nm diameter and 25–30 nm in length. The SiO_2 surrounds the Al_2O_3 needle. More definitive study to characterize the microstructure is in progress.

In addition to the synthesis work, we have developed several new techniques to study the evolution and details of gel microstructures. Special sample preparation methods were developed to overcome significant difficulties in stabilizing these very fine, electrically insulating, low thermal conductance materials for TEM studies. The kinetics of gelation were studied by following the intensity of scattered laser light. These studies and the resulting structural data help define the state of the starting material. By relating the properties of the starting material-microstructure with the final properties of the ceramics, not only a correlation between microstructural properties and final properties can be established, but one can tailor a ceramic property based on the starting microstructural properties.

PLANNED ACTIVITIES FOR FY 1986

The preparation of mixed oxide gels will be continued in FY 1986 with emphasis on obtaining very fine and homogeneous alcogels and ceramic precursors. The drying and sintering kinetics of the mixed oxide ceramics will be studied and their physical and mechanical characteristics will be measured. Further studies will be carried out to elucidate the relationship between the microstructural properties and the characteristics of the finished material.

ENERGY EFFICIENT BUILDINGS PROGRAM

INTRODUCTION

The importance of buildings in the U.S. economy is shown by the figures in Table 1. In 1983 our buildings sector used $155 billion worth of energy, mainly as electricity. Of the total annual U.S. electricity sales of $135 billion, most ($100 billion) went for operating the equipment and appliances in buildings.

To get a better feeling for the cost of energy in buildings, we note that the United States has 83 million occupied dwellings, with a total floor space of about 110 billion square feet, and another 50 billion square feet of nonresidential ("commercial") space. So every square foot costs about $1/year in energy services, with residential space costing a little less and commercial space a little more.

Table 1. U.S. energy expenses, 1983.[a]

Sector	Fuel [$\$10^9$]	Electricity [$\$10^9$]	Total [$\$10^9$]
Buildings	60	100	155
Residential	(40)	(55)	(90)
Commercial	(20)	(45)	(65)
Industry	65	35	100
Transport	150	0	150
Total	270	135	405

[a]Excluding federal subsidies and rounded to the nearest $5 billion.

Source: *State Energy Price and Expenditure Report,* 1983, DOE/EIA 0376(83) (February, 1986).

To update these costs to 1985 in 1985$ would raise the electricity costs, lower the fuel costs, and probably give a few percent total reduction. [Between 1980 and 1983 total energy bills rose 3% per year, electricity bills rose 6% per year, and the difference (fuel) dropped very slightly.]

In addition to the tabulated costs paid directly by customers in 1984, there were federal subsidies (11%) of $44 billion, bringing the energy total to about $450 billion, larger than all private and public expenditures for Health ($400 billion), Defense ($300 billion), Education ($200 billion), or farm income ($140 billion). For source of $44 billion energy subsidies see Heede, Morgan, and Ridley, "*The Hidden Costs of Energy,*" Center for Renewable Resources, Washington, DC 20036 (1985).

Since 1973 rising energy prices and awareness have remarkably reduced our energy bills. Our real GNP is up 30%, yet our primary[1] energy use is unchanged. If our energy efficiency were still frozen at 1973 levels, we would today be paying $526 billion annually instead of the $405 billion shown in Table 1; i.e., we are actually saving $121 billion each year, a very significant sum, comparable to our highly publicized national budget deficit.

In buildings the percentage savings are comparable. Since 1973 our stock of households has grown by 25% and commercial floor space has increased by 32%, yet primary energy use in buildings is up only 11 percent.[2] So energy use per square foot has fallen by 13%, and we are actually saving $22 billion per year.

So much for the past. Now, what of the future? How much more should we save? According to the SERI Solar/Conservation Study,[3] a "least-cost investment" scenario (one that maximizes life-cycle cost effectiveness) would halve our current energy use by the year 2000, and the same factor of one-half also applies to buildings as a sector. So, with optimal investments and design, our annual utility bill for buildings could drop from $155 billion to $75 billion.

The Energy Efficient Buildings Program at Lawrence Berkeley Laboratory was established to accelerate the capture of this $75 billion potential annual savings. In 1973 we spent about $7.5 million on this research, i.e., about $1 for every $10,000 of potential savings, or the equivalent of advancing the ultimate savings by 1 hour each year. In this chapter (as in earlier editions of the Annual Report), we describe contributions to science and technology leading to advancements measured not in hours, but in months, and in many cases in years.

Table 2 lists several examples of the remarkable successes of DOE-sponsored Buildings R&D projects, and we are pleased to point out that our EEB Program was responsible for the first two columns—Solid-state ballasts for fluorescent lights and Low-emissivity ("heat mirror") films for windows.

Table 2. Lead times and net savings[a] for successful DOE-sponsored buildings energy R&D projects.

	Solid state ballasts	Low-E window films	Residential absorption heat pump	Advanced electric heat pump	High efficiency refrigerator compressor	High efficiency refrigerator-freezer	Heat pump water heater
1. DOE project duration	1976–1980	1976–1990	1978–1988	1977–1986	1977–1981	1978–1983	1977–1982
2. Est. 50% penetration of sales	1995	2000	2001	1998	1990	1996	1995
3. Years by which DOE advanced commercialization	5 yr	5 yr	5 yr	2 yr	2 yr	2 yr	3 yr
4. Cost of conserved energy (CCE)[b]	2¢/kWh	$2/MBtu	$2.50/MBtu	$2.75/MBtu	1¢/kWh	3¢/kWh	3¢/kWh
5. Cost of DOE project	$3M	$2M	$6.8M	$2M	$1M	$0.8M	$0.7M
6. Net annual savings in 1985	$11M	$14M	$0M	$0M	$0.4M	$0.2M	$6.5M
7. Net annual savings at saturation (i.e., 10–15 years after 50% penetration)[c]	$5,000M	$3,000M	$2,400M	$2,500M	$1,100M	$850M	$3,000M
8. Cumulative net savings (line 7 × line 3)	$25,000M	$13,000M	$12,000M	$5,000M	$2,200M	$1,700M	$9,000M
9. DOE project ROI (return on investment, =line 8 ÷ line 5)	8,000:1	7,000:1	1,500:1	2,500:1	2,000:1	2,000:1	13,000:1

a. All dollar savings in energy costs are **net** of increased costs for purchase of the improved equipment (ballast, window, etc.).

b. For cost of conserved energy (CCE), we use a real discount rate d = 7%, and the useful life of the product: e.g., 10 years for ballasts, 20 years for windows. The CCE of low-E films, now still a novelty, is currently $4/MBtu, but as the market matures, we estimate that the CCE will drop to $2/MBtu.

c. Net annual savings at saturation are in 1985 dollars, uncorrected for growth in the building stock, changes in real energy costs, or discounted future values. We decided **not** to account explicitly for these three factors, since all three are uncertain and their combined impact probably small, as shown by the following calculation. To translate savings in 2000 or 2010 to 1985 terms, one multiplies by: $\exp[(g + e - d)T]$, with the following annual rates:

$$\left.\begin{array}{l} g = \text{growth rate of building sector (3\%)} \\ e = \text{real price escalation for electricity or fuel (1–2\%)} \\ d = \text{real discount rate (4–7\%)} \end{array}\right\} \quad g + e - d = (-3 \text{ to } +1\%)$$

T = years between 1985 and the est. saturation date, 20–25 years.

Source: "Federal R&D on Energy Efficiency; a White Paper," American Council for an Energy Efficient Economy, 1986, available from ACEEE, 1001 Connecticut Ave. NW, Suite 535, Washington, DC 20036, or LBL.

Several conclusions can be drawn from Table 2 (for more details, see the 1986 ACEEE White Paper cited below the table):

1. Gestation time, from initiation of research to 50% market penetration, is 25–30 years, even though the development was very cost effective and fairly obvious (indeed inevitable, eventually).
2. The payback times for the consumer are typically only 2–3 years. Put more precisely, line 4 shows that the cost of the conserved energy is typically 3 times cheaper than the current purchase price of energy.
3. The annual dollar savings to consumers are huge. Line 7 lists annual savings after the new technology saturates the market:
   a. For the high frequency ballasts, the savings are $5 billion per year, comparable with the output of 18 standard 1000 MW power plants. Related to the development of small solid-state high-frequency ballasts are the new compact fluorescent light bulbs, like the Phillips SL-18, which replace a 75-watt incandescent light for 18 watts. When they saturate high-use light sockets throughout the U.S. they will save another $5 billion, and another 18 power plants.
   b. For the low-emissivity window films, the annual fuel savings at saturation will be $3 billion, corresponding to about 1/5 the output of the entire Alaska pipeline.
4. The societal returns on the federal R&D costs are also huge—much greater than 1000 to 1 (line 9).

The Energy Efficient Buildings Program conducts theoretical and experimental research on various aspects of building technology that will permit such gains in energy efficiency without decreasing occupants' comfort or adversely affecting indoor air quality. To accomplish this goal, it has developed six major research groups whose findings and achievements are regularly reported in technical and scientific journals, presented at international conferences, and disseminated as Lawrence Berkeley Laboratory (LBL) reports. We also make available fact sheets on topics of interest to the building energy community, such as indoor air quality testing and blower door manufacturers. A brief overview of the scope and objectives of each group follows.

ENERGY PERFORMANCE OF BUILDINGS (EPB)

The Energy Performance of Buildings Group studies the flow of energy through all elements of a building. It tests air infiltration rates, studies thermal characteristics of structural elements, and develops models of the behavior of complete buildings. Research is conducted in the laboratory and in the field in single- and multifamily buildings. The group is investigating new techniques for measuring air leakage, using AC pressurization. The potential for savings in this area is great; the heat load associated with natural infiltration is about 2.5 quads per year, costing about $15 billion. It is estimated that it may be economic to reduce this by 25%.

The group developed the LBL infiltration model, which predicts the annual infiltration rate of a building from leakage area and weather data. It is possible, using this model, to predict the annual infiltration rate of a building from a single spot measurement with a blower door. The group developed a microcomputer program, CIRA (Computerized Instrumented Residential Audit), which is designed to speed up and improve the accuracy of residential audits of energy consumption.

The group has designed and tested a low-cost data acquisition system, the Energy Signature Monitor, a 16-channel, all-solid-state recorder, complete with sensors and user-friendly installation and analysis software, for residential, and possibly commercial, applications.

As lead lab for the multifamily sector in DOE's Retrofit Research program, the group conducts numerous projects in how to diagnose, monitor, analyze, and evaluate the energy conservation potential in multifamily buildings nationwide. A related series of projects focuses on the energy savings potential in public housing.

BUILDING VENTILATION AND INDOOR AIR QUALITY (BVIAQ)

An obvious way to improve the energy efficiency of a building—to lower air exchange rates by reducing air infiltration (whether natural or forced)—may have an undesirable side effect: because the indoor concentrations of air pollutants are reduced by the exchange of air with the outdoors, increasing airtightness may degrade indoor air quality. The goal of the BVIAQ Group is to investigate the factors affecting

indoor pollutant concentrations, including pollutant sources, ventilation rates, and removal processes, with particular attention to providing the scientific basis for the development of ventilation standards and system designs that promote energy efficiency while maintaining the comfort and health of building occupants. Activities in support of these goals include (1) development of new methodologies for measuring indoor pollutant concentrations; (2) laboratory studies of the emission and behavior of pollutants arising from building materials, soil, combustion appliances, and household products; and (3) field monitoring of indoor air quality in different types of buildings (primarily residences and office buildings) under a variety of ventilation conditions.

Closely related to this work is the investigation of strategies to control concentrations of indoor air pollutants without sacrificing energy efficiency. To this end, the BVIAQ Group performs laboratory and field tests of various control techniques, including ventilation systems that incorporate heat recuperation, as well as pollutant-specific removal techniques. A recuperation system can provide the necessary level of ventilation while recovering a substantial portion of the energy that would normally be lost in the exhaust air stream. The group has set up a laboratory for testing air-to-air heat exchangers and exhaust air heat pumps to provide independent data on these devices.

An interesting conclusion that can be drawn from the work of the BVIAQ Group is that the strongest influences on indoor concentrations are pollutant emission rates rather than ventilation rates. Indoor concentrations exceeding outdoor levels (and outdoor standards) occur whether buildings have been tightened or not. Throughout the building stock many houses have unacceptably high levels of radioactive radon gas, formaldehyde, and combustion products.

This finding means that substantial attention must be given to indoor air quality, independently of energy conservation measures, to limit the sources of contamination. Such efforts can reduce indoor pollutant concentrations (especially excessive levels), even while a modest reduction in air exchange rates occurs. To help determine the scale of the effort required, the group has developed a number of inexpensive passive samplers for the more common pollutants and tested them in field surveys.

BUILDING ENERGY SIMULATION (BES)

The Building Energy Simulation Group develops techniques to simulate the performance of buildings. Starting in 1978, the group developed a family of computer programs that simulate building energy performance, the most current version of which is known as DOE-2. These programs are now widely used by architects and engineers in the design of new buildings and in the retrofit of existing ones. DOE-2 is also used extensively by researchers and educators in building science. Each year a new version of DOE-2 and its documentation is produced, incorporating the most recent research results of projects at LBL and elsewhere, as well as capabilities to allow the study of new and emerging technologies. DOE-2 has become the standard against which other calculation procedures or programs are compared. It has been used to develop simplified approaches ranging from hand calculation methods or slide rules to microprocessor programs, ASHRAE handbook tables and procedures, and building codes in the U.S., France, and Singapore. DOE-2 is used by many hundreds of groups both in the U.S. and overseas.

The BES Group is also undertaking projects that are designed to lead to the production of the next generation of building performance simulation programs. The main efforts in the advanced simulation area at this time are the creation of a simulation "kernel" system and organization of the simulation development community to enhance collaboration. The kernel system will provide the basic tools and information to allow the BES and other groups to develop more advanced simulation programs. It will also provide a mechanism to facilitate exchange of research results and technology advances, and provide a basis for integrating performance simulation into computer-aided design (CAD) and expert system software. The organization of the simulation community through the creation of a professional society will enhance the exchange of information and allow more widespread dissemination of the new technologies into the design and research communities.

WINDOWS AND DAYLIGHTING

The Windows and Daylighting Group focuses on developing the technical basis for understanding the energy-related performance of windows. If the flow of heat and light through windows and skylights can be properly filtered and controlled, these building elements can outperform any insulated wall or roof component and provide net energy benefits to the building. At present the thermal cost of windows is estimated to be about $20 billion per year. The group's investigations are designed to develop the capability of accurately predicting net fenestration performance in residential and commercial buildings. Simulation studies, field measurements in a mobile field test facility, and building monitoring studies

help us to understand the complex tradeoffs in fenestration performance. The group develops analytical models and experimental procedures for determining the thermal and solar-optical properties of glazing materials; it also conducts materials-science studies to develop and characterize a new generation of thin-film coatings and other advanced optical technologies that may someday enhance the performance of conventional glazing materials. The first significant market penetration of windows incorporating high-transmittance low-emittance coatings (R3–R5 windows) occurred in 1984, 8 years after DOE support was initiated in this program. If they capture a large fraction of the market, as expected, they will ultimately save consumers $3 billion annually in heating bills.

In nonresidential buildings major reductions in electric energy use and peak electric demand can be achieved if the conflicts and tradeoffs between daylight savings and solar-gain-induced cooling loads can be understood. The DOE-2 building-energy analysis model has been modified to enable daylighting effects to be analyzed and is now being used for extensive parametric studies to determine total building energy use, peak electric demand, and HVAC loads as functions of climate, orientation, and window properties. LBL daylighting studies also employ both a unique 24-foot-diameter sky simulator for testing scale models under carefully controlled conditions and new experimental facilities for measuring the photometric and radiometric properties of complex fenestration systems.

Data from outdoor model tests and daylight availability studies are still being collected and analyzed. Results are used to validate and upgrade SUPERLITE, a powerful and versatile daylighting simulation model. Computational procedures for thermal performance are being validated with the Mobile Window Thermal Test facility (MoWITT), now collecting winter and summer performance data in Reno, Nevada, and Livermore, California. This unique facility combines the accuracy and control of laboratory testing with the realism and complexity of dynamic climatic effects; for the first time controlled measurement of the interaction between fenestration systems and a building HVAC system should be possible.

LIGHTING SYSTEMS

The research of the Lighting Systems Group is divided into three major categories: technical engineering, building applications, and impacts on health and visibility.

The technical engineering is concerned primarily with developing new concepts for efficiently converting electrical energy into visible light. Areas of interest include mechanisms for reducing the ultraviolet self-absorption in gas-discharge lamps and the excitation of plasma gas at ultrahigh frequency ranges (approximately 10^9 hertz). Both hold the promise of a more reliable and more efficient conversion of energy into light.

The building applications concentrate on the design of lighting systems, the effective use of lighting controls, and their interaction with a building's HVAC system.

Visibility impacts focus primarily on basic information needed to establish lighting conditions that enhance productivity in a cost-effective manner. It also seeks to determine any undesirable visual effects, such as excessive fatigue, associated with using modern office equipment such as visual display terminals in an advanced lighting environment.

Health impacts extend electric lighting research to a wider class of human activities. In specially designed experimental rooms, conditions can be varied, and nonsubjective responses to lighting variables can be measured by sensitive instrumentation.

Facilities for technical engineering are located at LBL; the productivity impacts program is located at the School of Optometry at Berkeley; and the health impacts program is located at the Medical Center on the San Francisco campus of the University of California.

The Lighting Group's successes include advancing the development of high-frequency solid-state "ballasts" for fluorescent lamps and the invention of a new high frequency surface wave lamp whose efficiency is more than 30% better than the common fluorescent lamp. A 2-year test of solid-state ballasts in a large office building showed an electricity savings of 40%. Scaled to the entire country, this represents an annual savings of $5 billion. The energy-efficient surface wave lamp promises to provide major reductions in energy use while considerably extending lamp life.

BUILDINGS ENERGY DATA (BED)

Without data on how buildings behave once built, even the best-designed energy conservation strategy can go astray. The Buildings Energy Data Group compiles and evaluates data on end uses of energy and on the costs and performance of energy-efficient technical measures. The BECA (Building Energy-use Compilation and Analysis) data base con-

tains separate elements for each major subset of buildings (efficient new houses, retrofitted buildings, etc.).

From these data BECA prepares estimates of least-cost technical potentials for improving energy efficiency in new and existing homes and commercial buildings, often as a cooperative effort with utilities, state agencies, or industry groups. Individual conservation (or solar) measures are catalogued in order of increasing cost per unit of energy saved. The results are supply curves (marginal cost curves) of saved energy. These are comparable to the supply curves for other market commodities and show the expected levels of production as a function of unit price.

RELATED RESEARCH

Closely related research on energy-efficient buildings and appliances is carried on in other programs of the Applied Science Division and is reported in other chapters of this Annual Report. Specifically the Energy Analysis chapter reviews building energy performance guidelines, appliance energy performance, rating systems for auditors and appraisers, and energy and peak-power modeling. The Solar Energy chapter summarizes the research of the Passive Solar Analysis and Design Group.

FUTURE RESEARCH

We are planning or proposing studies in the following topics:

Duct losses. In the U.S., fossil-fuel heating accounts for about 7 quads of energy annually, worth about $50 billion. As a very rough estimate, about half of this heat travels in warm-air distribution systems, where 10% of it is lost because of leaky ductwork—a loss of about $2 billion. We propose to study distribution losses and to set up a duct laboratory to investigate methods of improving distribution efficiencies and of fixing leaky ducts *in situ.*

Project RICH (Residential Integrated Cooling and Heating). As residential construction gets tighter, the need for mechanical ventilation to ensure adequate indoor air quality will increase. This ventilation air represents a heat source (or sink) approaching 1 kW of available power. Integrated HVAC systems that can recover this heat to condition internal air or displace domestic hot water demand could save up to $2 billion annually. Once a ventilation system has been integrated into the HVAC system, it becomes more practical to consider integrating other appliances (dryers, air conditioners, refrigerators, etc.) into a modular system that could save even more energy. We are currently trying to build a consensus of parties interested in this work and begin a unified research program.

Peak power reduction. For a typical summer-peaking utility, electricity for air conditioning systems accounts for at least 25% of the peak demand. This corresponds to the output of about 125 large (1000 MW) power plants. A very cost-effective method of reducing the peak is for commercial buildings to install thermal storage equipment. This allows chillers to be downsized and to be operated during off-peak periods. The cost of thermal storage appears to be about $200 per avoided kW, an attractive proposition compared with the typical cost of $1000 per kW for generation equipment. We have started to survey the use of thermal storage in commercial buildings in the U.S. and would like to carry out studies on the use of various methods of thermal storage such as water, ice, concrete, and phase-change materials to determine the optimal design of storage in commercial and residential buildings.

Responsive meters. At present a utility cannot bill a residential and small commercial customer for the instantaneous cost of providing electricity. Thus there is little incentive for consumers to reduce peak usage, since they do not know when it occurs or how much it costs. All that consumers see is an average price per kWh. If customers were billed for instantaneous cost, they would have an incentive to adopt cost-effective methods of reducing demand when the cost is highest. Such methods might include the use of thermal storage or the cycling of appliances during hours of high-priced energy. We would like to carry out a pilot study on the use of responsive meters (e.g., the British CALMU system), similar to studies we have already conducted on the use of controls for artificial lighting systems.

NOTES AND REFERENCES

1. There are two popular ways—"site" or end-use and "primary" or "resource" energy—to account for the energy associated with electricity. We prefer to use "primary" accounting, where 1 kWh sold—3414 Btu at the site—is equated with 11,500 Btu of fuel burned at the power plant. By "reflecting" this primary fuel, we find that 1 Btu of "electricity" and 1 Btu of fuel cost about the same—about $6/MBtu today; thus it is meaningful to add Btu's of primary electricity and Btu's of fuel and call them "primary energy."
2. *Overview of Building Energy Use and Report of Analyses–1985,* U.S. Department of Energy, DOE/CE-0140, October 1985, reprinted April 1986.

3. *A New Prosperity: Building A Sustainable Energy Future. The SERI Solar/Conservation Study,* Brick House Publishing, Andover, MA, 1981. The Buildings section of this comprehensive study was done by an LBL team.

Energy Performance of Buildings*

M.H. Sherman, J.T. Brunsell, P.G. Cleary, R.C. Diamond, D.J. Dickerhoff, J.B. Dickinson, H.E. Feustel, D. Hekmat, R.B. Kuelpmann, L.L. Lewicki, M.P. Modera, B.V. Smith, and R.F. Szydlowski

The Energy Performance of Buildings Group (EPB) carries out fundamental research into the ways energy is expended to maintain desirable conditions inside buildings. Our results form the basis of design and construction guidelines for new buildings and retrofit strategies for existing buildings. Our primary areas of research are air infiltration and retrofit research. In this article, the work carried out over the last year is split into four overlapping sections: 1) building energy retrofit research, 2) air infiltration, 3) air leakage, and 4) integrated ventilation. The emphasis in our work is on whole building performance. We collect, model, and analyze detailed data on the energy performance of buildings, including the micro-climate, the building's thermal characteristics, the mechanical systems, and the behavior of the occupants. Because of the multidisciplinary approach we work closely with other groups, both at the Laboratory and elsewhere.

BUILDING ENERGY RETROFIT RESEARCH (BERR)

While new buildings—both residential and commercial—are responding to higher energy prices and stricter energy codes by becoming more energy efficient, the existing stock represents a large area for energy conservation activity. Of the three buildings sectors, single-family, multifamily, and commercial, multifamily has had the least level of activity, and presents some of the greatest challenges. Over one quarter of the U.S. housing stock is in multifamily buildings. The Office of Technology Assessment estimates that while current levels of retrofit activity in multifamily buildings are likely to save 0.3 quads of energy (320 petajoules) by the year 2000, the *potential* savings are more than three times as much.[1] The reasons for this untapped energy savings are complex, and involve institutional as well as technological barriers. While we know something about the performance of retrofits in single-family houses, we have very little understanding of the interactions and performance of retrofits in multifamily buildings. The measured savings from retrofits in multifamily buildings are typically 25–50% less than the predicted savings, with a large spread around the mean.

The explanations for this wide divergence are usually hindered by the limitations of the available data. The Building Energy Retrofit Research project was initiated to address these problems in all three building sectors, Single-family, Multifamily, and Commercial. The Department of Energy has designated LBL as the primary lab for carrying out research in the multifamily sector. Several projects are being carried out in this area, including sector characterization and analysis, monitoring protocol development and demonstration, building diagnostics, occupant surveys, case studies, and technology transfer. In addition, special emphasis has been given to a sub-sector of multifamily buildings, specifically, federally-assisted housing.

Accomplishments During FY 1985

Our BERR work in the last year can be broken down into three areas: 1) Planning, 2) Retrofit monitoring and diagnostic demonstration, and 3) Utility data collection and analysis.

Two major planning documents were prepared this year, one dealing with multifamily retrofit research and the other with federally-assisted housing.[2,3] Both plans characterize the existing building stock, discuss barriers to retrofit activity, outline previous activities—private and public, and identify research needs. In addition, a cost benefit analysis using net present value was made for all of the multifamily research projects. The multifamily plan was done in conjunction with similar documents on the single-family and commercial sectors written by Oak Ridge National Laboratory (ORNL). Input on private sector activities was provided by Princeton University. The document has input from over forty organizations, and has had a preliminary review by a dozen organizations. The federally-assisted housing plan was done in-house, with input from several public housing authorities, as well as substantial review and comment from HUD.

Three main activities were undertaken in our retrofit monitoring and diagnostic demonstration work: 1) the development of a protocol for multifamily retrofit monitoring, including a survey of available equipment, 2) the demonstration of innovative diagnostics and evaluation of retrofits in a multifamily building in Minneapolis, and 3) the

*This work was funded by the Assistant Secretary for Conservation and Renewable Energy, Office of Building and Community Systems, Building Systems Division of the U.S. Department of Energy under Contract No. DE-AC03-76SF00098.

long-term monitoring of hot water retrofits in a public housing project in San Francisco.

The objective of the protocol is to provide a comprehensive standard for data collection and evaluation of retrofit performance.[4] Accompanying the development of the protocol is our work in documenting existing monitoring instrumentation. The first phase of gathering manufacturers' literature has been completed and a preliminary report was presented at the *Field Data Acquisition Workshop* in Dallas in October, 1985.[5]

The diagnostic demonstration project focused on a one-week investigation of a 7-unit apartment building in Minneapolis, working in conjunction with the Minneapolis Energy Office (see Fig. 1). The diagnostics involved using simultaneous measurements with six blower doors to investigate air leakage in the apartments—both between units and to the outside—and an evaluation of the building's ancient steam boiler, quantifying total energy losses (see Figs. 2 and 3). In addition, a short-term measurement using tracer-gas was made of a vent damper retrofit installed on the boiler.

The long-term monitoring of the hot-water system at Holly Courts (a complex of 10 buildings) is part of our collaborative work with the San Francisco Housing Authority. We are currently monitoring the hot water systems in four buildings (48 units total) to understand patterns of hot water use and the performance of the active solar retrofits. The residents were also interviewed to understand hot-water-use patterns and the effect of the residents on the performance of the retrofit.

The retrofit to the domestic hot water system involved installing a total of ninety-four 4 ft × 10 ft solar collector panels on the roofs of all ten buildings. The solar collectors were plumbed into storage tanks located in the boiler rooms in the basements of the buildings. The solar storage tanks were connected into the existing domestic hot water system for the building. Installation of the collectors began in November, 1984, and by January, 1985, the solar systems were operational in all ten buildings. By March, 1985, we installed the first of our monitoring systems (described below) in the boiler room in one of the buildings. In the next few months, three additional data loggers were installed in different buildings. A weather station was installed on the roof of

Figure 1. Exterior view of apartment building in Minneapolis, Minnesota, where building diagnostics were demonstrated. (XBB 8512-10273)

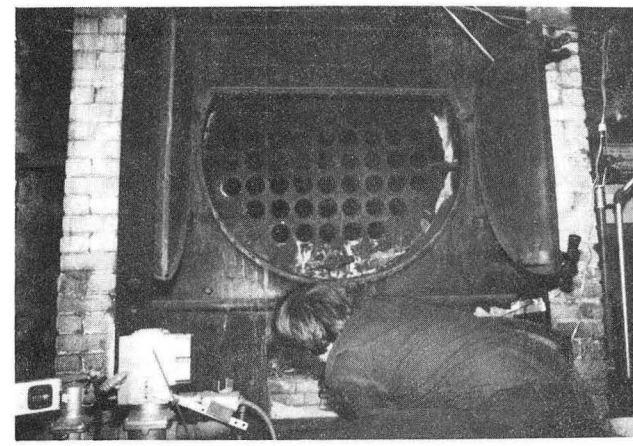

Figure 2. Large fire-tube boiler examined in multifamily case study. (XBB 8512-10277)

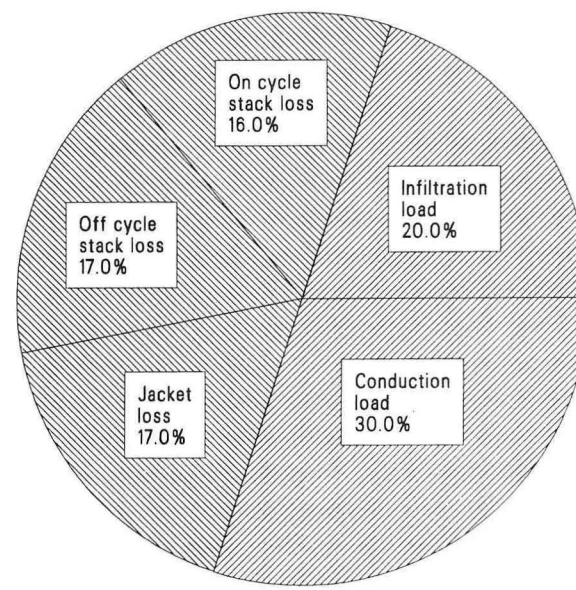

Figure 3. Boiler energy balance without stack damper. (XCG 853-106)

one of the buildings to collect local temperature, wind, and solar data.

The data acquisition system chosen for this project was the μMAC-5000. It is a programmable modular system that operates unattended in the boiler rooms at Holly Courts. Real time data for on-site weather, individual building domestic hot water use, and the contribution of the solar system are collected and converted to hourly averages. Data are stored in the system's memory and are transferred weekly to LBL by a telephone modem.

A total of thirteen sensors are used for each building, plus an additional four for the weather tower. The temperature sensors are all type T thermocouples, attached to the outer surface of the appropriate water pipes (using nylon wire ties and thermal contact grease) and insulated. The circulation pump for the solar system is monitored with a clamp-on ammeter. A water flow meter is installed in the domestic hot water supply line. It was important during this installation to minimize the disruption of the hot water service to the building residents. The only interruption required was roughly two hours at each building during the installation of the water flow meter.

The quantities calculated from the monitoring include the following:

- quantity of hot water used
- temperature of hot water delivered to occupants
- heat loss in building hot water pumped loop
- temperature of cold and solar preheat water supply
- operation time and average collection efficiency of the solar system

Six months of hot water data have been collected (with a data capture rate of 95%). Findings to date show high hot water use per household, different consumption patterns from those presented in the literature, and surprisingly close agreement between the measured hot water use and that calculated based on the occupants' reported usage patterns.

Our work in utility data collection and analysis has concentrated on federally-assisted housing, where we have been analyzing the performance of retrofits in public housing. Utility billing data along with information on building characteristics and retrofit strategy have been collected for over forty public housing projects. The study will attempt to determine the energy savings and cost-effectiveness of the conservation retrofits. Particular indicators include resource energy savings, the cost of conserved energy, and the internal rate of return. Preliminary results indicate that there is a wide variability in energy savings.

Planned Activities for FY 1986

Our monitoring work will include completion of the multifamily monitoring protocol and demonstration of its use on buildings in Minneapolis/St. Paul and Chicago. These measurements will be done in collaboration with the Energy Resource Center in St. Paul, the Minneapolis Energy Office and Minnesota Department of Energy and Economic Development, and the Center for Neighborhood Technology in Chicago. In addition to using the protocol to determine the performance of heating system retrofits, we will look at additional factors that affect retrofit adoption and performance, including moisture effects in sealed attics and behavioral effects. Limited diagnostics will also be performed on the heating systems. We currently plan to instrument four buildings, two in each city. We will also continue monitoring hot water use in one of the San Francisco public housing buildings.

The analysis work of utility bill data will continue with new retrofit data on the public housing projects. We will also collect and analyze baseline energy use from over 40,000 public housing units. We will calculate weather-corrected consumption levels for several years and compare them to estimates provided by an earlier study of estimated energy use in public housing.[6] We will also attempt to determine the influence of building and operating characteristics on variations in energy consumption.

In addition to our multifamily retrofit research we have some related projects in single-family housing. Some examples of these projects include the continuation of the warm room project and several of the infiltration projects described in the next article.

The warm-room retrofit is a response to a common problem: how to stay warm in a large, poorly insulated house during the coldest parts of winter. A traditional response is for residents to spend most of their time in one heated area of the house—usually the kitchen. In recent years the Institute for Human Development in Philadelphia has pioneered a variation in which the house is divided into warm and cool zones, the occupant controlling the temperature with a portable thermostat. In 1984 Kansas City was awarded a grant from the Urban Consortium to demonstrate the warm room approach, with LBL providing technical assistance. As part of our technical assistance we worked with city officials in selecting potential houses for the project. Twenty houses were audited and the residents were informed about

the warm-room approach. On the basis of the audits, we selected 5 houses as retrofit candidates and identified another 10 as controls. All residents were enthusiastic about the project, and pre-retrofit monitoring began.

Data were collected on the physical characteristics of the houses, additional gas meters were installed on the furnaces, blower door measurements were performed to determine leakage areas, and air quality measurements were taken to determine indoor levels of radon, nitrogen dioxide, and formaldehyde. In addition residents were asked about their daily activities to identify the most appropriate warm rooms. Residents have been reading their two gas meters every week and have been sending us the readings along with thermographs of their indoor temperatures. We used these data as input into a number of CIRA simulations of energy use in order to calculate the most cost-effective strategies for the retrofit.

AIR INFILTRATION

With improved insulation of the building shell, heat loss from ventilation—whether controlled or by infiltration—has become an even more important fraction of the building's overall heat loss. Infiltration is the flow of outside air driven by wind pressure and thermal buoyancy into the building. Unlike the equivalent loss for conduction, ventilation heat loss depends on wind speeds as well as the inside-outside temperature difference. We carry out research in three main areas: development of a simplified multizone model, multigas tracer measurements, and wind tunnel measurements of wind pressure distributions around buildings.

Multizone Model

Computer programs have been developed that calculate the energy consumption due to infiltration. A review showed that the majority of the programs found in the literature use an empirical power-law expression to relate air pressure to air flow and use Newton's method of iteration to solve the set of nonlinear equations.[7] These programs, which treat the true complexity of flows in a building by recognizing the effects of internal flow resistances, require extensive information about flow characteristics and pressure distribution. Therefore, simplified models have been developed. Most of these, including the LBL model,[8] simulate air infiltration of single-cell structures, such as single-family houses, under given weather conditions. A high percentage of existing buildings, however, have floor plans that are characterized more accurately as multichamber structures and cannot be treated by single-cell models. Most multicellular models in use are not available to the public or are written as research tools, rather than as tools for engineers and architects (see Fig. 4). A simplified multicell infiltration model capable of providing the same accuracy as the established single-cell models is therefore being developed at LBL.

To get accurate results from detailed computer models, the boundary conditions have to be well defined. One critical input parameter that needs further study is the wind pressure coefficient. The pressure distribution around the building can be determined either from measurements on full-scale buildings or on corresponding small-scale models in a boundary layer wind tunnel, our present method.

Accomplishments During FY 1985

Multizone Modeling

For purposes of modeling infiltration, buildings are classified as one of the following:

(a) row house (terrace house)
(b) detached house
(c) story-type house
(d) shaft-type house

These four basic categories reflect different permeability distributions of the building's envelope (which influences the wind effect) and different vertical flow resistances inside the building (which influences the stack effect).

The distinction between the four categories can be expressed by two permeability ratios. One param-

Comparison of Modelling Strategies

	advantage	disadvantage
single-cell	easy to handle few input data reasonable accuracy	only single cell no internal partitions no internal flows
detailed multi-cell	large buildings internal flows good accuracy	extensive input mainframe computer
simplified multi-cell	large buildings internal flows micro computer reduced input	reduced accuracy

Figure 4. Comparison of air infiltration modelling strategies. (XBL 858-3493)

eter, the envelope permeability ratio (epr) is used to describe the whole building for a given house type in categories a or b.[9]

The epr of row houses can be described by the average permeability ratio of the leeward side to the overall permeability of the building envelope of epr = 0.5, whereas the corresponding value for a detached house rises to epr = 0.75.

In the latest issue of the German standard, DIN 4701,[10] another parameter, the internal vertical permeability (ivp), was introduced to further differentiate construction types in categories c and d. For further considerations, it is useful to also introduce the ratio of the permeabilities from one floor to another and the overall permeability of the building envelope (vertical permeability ratio, or vpr). With regard to the thermal pressure distribution, two extremes exist: story-type buildings with no permeability between floors (vpr = 0) and shaft-type buildings with no air-flow resistance between the different stories (vpr = 1).

To describe the air-flow distribution for the different zones at the story level, we defined two more lumped parameters: the outside permeability ratio (opr) of the zone (which describes the influence on cross ventilation of the zone, cross ventilation being the portion of the air flow that exfiltrates out of the same zone where it infiltrates) and the inside permeability ratio (ipr) of the zone (which describes the stack influence of the zone).

In a previous study, the use of a detailed multizone infiltration model showed a strong relationship between the two latter ratios and the flow distribution in buildings.[11] With increasing values for opr and decreasing values for ipr, the zones become more wind-dominated. Consequently, increasing ipr in combination with decreasing opr shows the opposite effect.

With the two lumped parameters describing the flow for the whole building, we were able to describe the air flow through a multizone, multistory building with a very simple floor plan.[12] The use of the two lumped parameters describing the air flow through the zones will allow us to calculate the air flow through buildings with more complicated floor plans, too.

Multigas Tracer Measurements

To identify air movement into a building as well as its internal flows, we have developed a multigas tracer measurement system. The equipment can use up to four gases to measure four zones in a building. By using freons and sulfur hexafluoride as tracers, many different gases can be detected. Only minor hardware changes are necessary to expand the number of zones covered. The measurement equipment consists of a mass flow controller for each zone, a gas chromatograph with two columns, an electron capture detector (this detects all species that are electronegative), and a mechanism for sampling the different zones. A peristaltic pump draws sample gas from each zone into sampling bags for a 6-minute period; the content of the bags is analyzed, the bags are evacuated, and the sampling cycle continues.

Software development for the programs controlling the sampling and data acquisition has been finished. Our first tracer gas measurements took place in one unit of a 60-unit garden-apartment complex for the elderly in Oroville, California. In addition to the tracer concentration data for the different zones, weather data were recorded. Scale models of the test house and its surroundings have been built and initial smoke tests conducted to learn about flow characteristics of this housing. Measurements in multistory buildings showed air transport in vertical shafts and its distribution inside the building.

Wind Pressure Studies

To measure the wind pressure distribution on the surface of building models for different wind directions, a turntable for an existing wind tunnel in the Architecture Department at UC Berkeley was designed and built. A multiport valve connects up to 48 pressure taps on the model surface in a cycle with a single pressure transducer. Software to control the multiport valve and to help analyze the measurement data has been developed.

Pressure measurements in the wind tunnel have been carried out for the Oroville houses. Scale models of all the houses in which we did perform tracer gas measurements have been built (see Fig. 5). The measurements show a strong influence of the building's surrounding on the pressure coefficient distribution.

Planned Activities for FY 1986

Multizone Modeling

The use of the preliminary model is still somewhat limited. Our task is to incorporate the two lumped parameters which describe the air flow for the zones to be able to simulate buildings with more difficult floor plans. Therefore, a parameter study by using the detailed computer model will be carried out for a number of floor plans to find the minimum of input data needed to describe the air flow in the building.

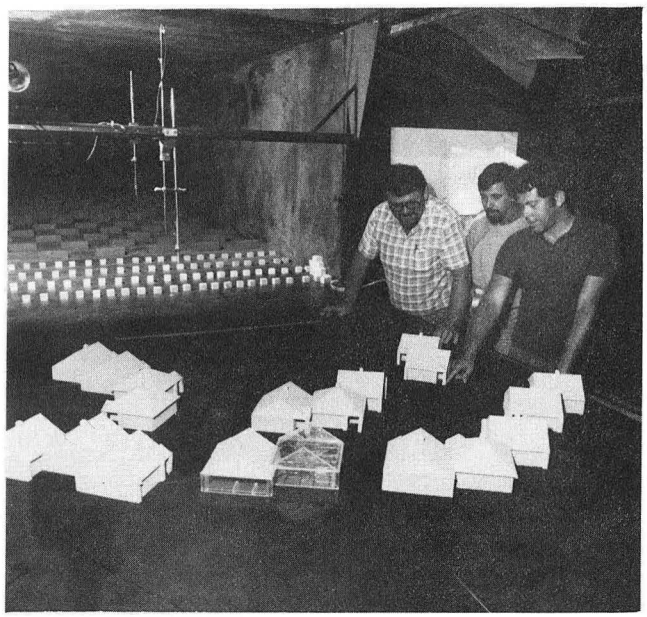

Figure 5. Wind tunnel measurements to determine pressure coefficients for the test house. (Surrounding buildings are included in the measurements.) (XBC 858-6285)

Multigas Tracer Measurements

As the collection cycle for the measurement system is very long (20 minutes for four chambers), real time comparison with the program was not possible. Therefore, the development of another measurement system is planned, using a residual gas analyzer to analyze the gas to overcome the long cycle time caused by the gas chromatograph. For more hardware reliability a new controller will be introduced and the necessary software will be developed.

Wind Pressure Studies

Pressure coefficient measurements will be carried out for a test building of the Ecole Polytechnique Federal de Lausanne for which tracer gas measurement and weather data have been collected. This test building contains nine zones on three different floors. It is shielded by adjacent buildings and pressure coefficient distribution is hard to predict. The wind tunnel measurements will help us to understand complicated flow pattern and will give us the necessary input data for our detailed computer model to simulate the internal flows. This will help us to validate both the detailed and the simplified model.

AIR LEAKAGE

The process of air flowing through a building envelope is called air leakage. Air leakage depends on the air tightness of the building as well as on the pressures driving the air flow. Air tightness is a property of the building alone and does not depend on the climate or other external properties. Typically, air tightness is quantified by the *Effective Leakage Area* (ELA), which is the amount of open area that would have the same air leakage as all of the leaks in a building under identical conditions. The measurement and study of air leakage allows us to: characterize the air tightness of buildings, better understand air flow through building envelopes, and estimate the effectiveness of retrofits on building ventilation.

Our air leakage research can be divided into three areas: leakage characterization, measurement techniques, and consensus standards. Our leakage characterization effort involves collecting and analyzing measured leakage data (primarily from North America) to determine the aggregate leakage behavior of residential buildings. The standard method for measuring building airtightness is called *fan pressurization*, and uses a device commonly known as a *blower door*. Over the last few years, we have developed a new method for measuring building airtightness, *AC Pressurization*, which allows us to determine the effective leakage area at low pressures, independent of wind effects. In addition, we are in the process of developing a technique for measuring air leakage in multifamily buildings. Finally, we are putting our experience to use in assisting the professional societies in the formation of consensus standards concerning the detection of leaks, the measurement of leakage area, and the specification of appropriate levels of airtightness in buildings.

Accomplishments During FY 1985

For the past three years we have been collecting and analyzing leakage data from fan pressurization measurements with the intent of determining aggregate leakage properties of building envelopes. One of the results of this effort in FY 84 was a compilation of over 500 leakage measurements that included house characterization data.[13] During FY 85 a version of this database was installed in-house on a micro-computer.

The new database is based on the data compiled at the University of Alberta, Edmonton, Canada, which was expanded both in quantity of measure-

ments and in depth of specification. Requests for new data were made to: researchers, government energy agencies, house doctor companies, the military, and any other parties that might have blower door data. The database now contains approximately 700 measurements. It is made up of five separate databases: a leakage database, which contains basic leakage information for quick reference; a leakage characteristics database, which contains complete information on the data analysis and detailed information about the measurement conditions; a house characteristics database, which contains a detailed description of each house, including its retrofit history; an address database; and a zipcode database, which contains climate information, including infiltration degree days and specific infiltration.

In late FY 84 we started a measurement program to examine seasonal changes in leakage area. The program involved measuring the leakage area and flow exponent of ten houses every month for a year. The data collected throughout FY 85 was compiled and analyzed to show the seasonal effects on leakage.[14] The monthly average leakage area for all of the houses is plotted in Fig. 6. While not all the houses showed seasonal variation, the Truckee houses had effective leakage areas up to 35% higher in the summer as compared to those measured in midwinter.

The measurement technique work in FY 85 was focused in two areas, multizone leakage measurement, and AC pressurization research. The multizone leakage measurements were made in a seven-unit apartment building in Minneapolis, Minnesota.

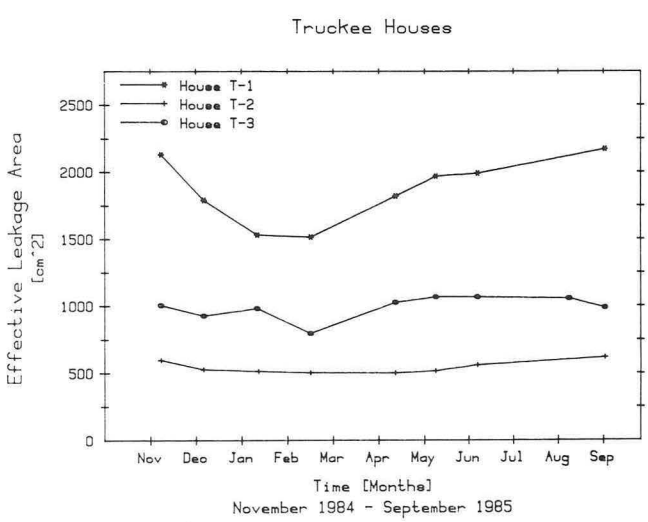

Figure 6. Seasonal leakage variation in three California houses. (XBL 8512-5237)

The measurement technique involved using six blower doors to pressurize the entire building to determine the total external leakage (see Fig. 7), as well as individual blower door tests to distinguish the leakage areas of different flow paths. The latter tests were made by testing individual apartments with and without simultaneous pressurization of adjacent apartments. These tests showed that only 40% of the leakage area of an individual apartment is in its exterior envelope, the majority of the leakage being to other apartments (see Fig. 8).

The major accomplishments for FY 85 in AC pressurization research were the design of a new field test prototype, and the filing of a patent application for the AC pressurization technique. The patent application, filed prior to the presentation of a technical paper describing AC pressurization, increased the probability that a commercial device will appear on the marketplace.

The new AC pressurization prototype is larger, sturdier and lighter than the first version (see Fig. 9). Because it displaces approximately 25% more volume it can provide our desired reference pressure

Figure 7. Air flow measurement in an apartment building in Minneapolis using six blower doors. (CBB 8512-10275)

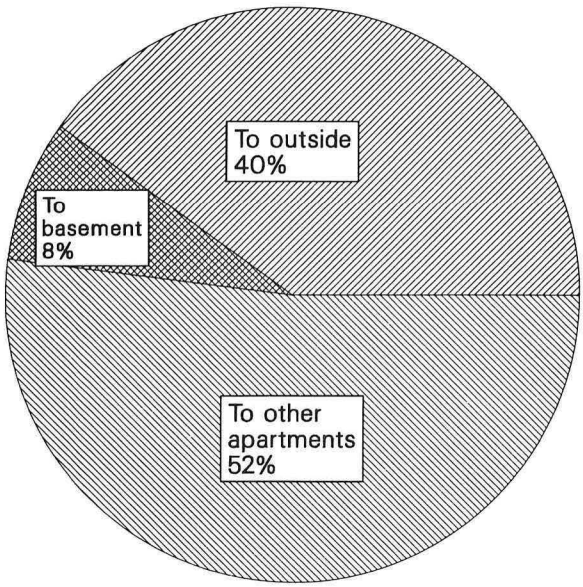

Figure 8. Leakage area of one apartment. (XCG 853-104)

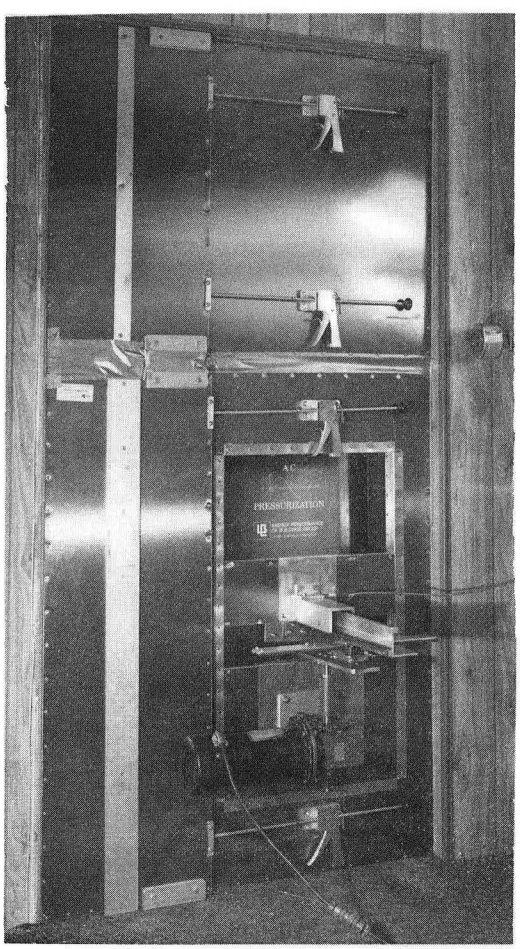

Figure 9. AC Pressurization. (CBB 862-997)

of 4 Pa at lower frequencies; because of the materials used and the quality of construction it can be operated at higher frequencies. The new device can thus be used to measure leaks over a wider frequency range, allowing a more careful examination of the large-area and high-volume leak effects. The FY 84 tests showed conclusively that AC pressurization did not measure the leakage area of fireplace chimneys (i.e., high-volume leaks). Tests in several houses also showed that as the size of a window opening was increased, after some point the incremental increase in leakage area could not be measured (large-area effect).

The lighter weight of the new device results from the choice of aluminum honeycomb, which is both lighter and stronger than plywood, as the structural material. This is particularly important for the piston, as the size of the motor required, as well as magnitude of the forces throughout the entire assembly, depends on the weight of the piston.

As part of our work with professional committees and organizations, we were primarily involved with two standard-writing organizations: the American Society for Testing and Materials (ASTM) and the American Society of Heating Refrigeration and Air-conditioning Engineers (ASHRAE). We are also the U.S. contact for the International Energy Agency's Annex V, the Air Infiltration Centre. The Centre maintains an extensive bibliography and distributes information to a large international audience including researchers throughout the U.S.

The main activity in ASTM during FY 85 has been the modification of Standard Test Method E 779, "Determining Air Leakage Rate by Fan Pressurization" to include improvements that have become apparent since its passage in 1981. The biggest single change has been the inclusion of the effective leakage area as part of the standard, including the calculation method. During FY 85 the task group responsible for the standard has forwarded the updated and revised version for approval; it is anticipated that the revisions will be formally approved by the society during FY 86.

In addition to measurement-related standards such as E779, we are working with ASHRAE on various energy-related standards. Specifically, we are heavily involved with standard project 119P, which is intended to promote energy conservation by setting maximum values for air leakage in detached, single-family, residential buildings. During FY 85 the standard project committee came to agreement on many of the substantial issues involved and produced an internal draft. Current thinking is that the standard will be climate-based, use effective leakage area divided by conditioned floor area as the quan-

tity of interest, and create a classification method for houses that is independent of the air tightness requirements.

Planned Activities for FY 1986

The leakage characterization work will continue and expand during FY 86. While continuing to collect measured leakage data, we will use our computerized database to: correlate leakage characteristics with other whole-house characteristics, examine the effects of climate on leakage, quantify the importance of duct leakage, and evaluate the effectiveness of various air leakage retrofits.

In the measurement area, further field tests will be made with the new prototype to examine the discrepancies between AC pressurization and DC pressurization. Because the size of leak that can be measured depends on the frequency at which the device operates, field and laboratory tests performed with the larger, lower-frequency prototype will better be able to quantify the effects of large leaks. The AC pressurization research in FY 86 will also include some theoretical research on periodic flows in cracks and orifices.

The standards work will also continue during FY 86. We expect that in FY 86 the revised ASTM E779 will become official and that the ASHRAE standard 119 will be available for public review. Other ASHRAE standards that are in the formation stage include one on calibration of fan pressurization units and one on methods of leak detection. The International Standards Organization (ISO) will begin the process of making an international fan pressurization standard in FY 86.

WASTE HEAT RECOVERY/INTEGRATED VENTILATION

The waste heat recovery/integrated ventilation project addresses the possibilities for energy management in single-family houses. As the insulation levels of houses are increasing, energy consumption for functions other than space conditioning represents a larger fraction of the total energy consumption. As the energy consumption for water heating, household appliances, and ventilation systems becomes relatively more important, the need to improve the efficiency in these areas also increases in importance. For many years there has been ongoing research on hot water systems, household appliance efficiency, and ventilation systems; however, there has been very little effort expended in trying to incorporate the resulting energy flows into an overall energy management strategy.

Integrated ventilation strategies are an important part of most waste heat recovery strategies, as conditioning of ventilation air represents approximately one-third of the space conditioning load of single-family residences. This fraction becomes even larger as the level of envelope insulation increases. Our research has concentrated on comparisons of infiltration (the predominant type of ventilation in the U.S.) with two mechanical ventilation systems with heat recovery: 1) two balanced fans with an air-to-air heat exchanger, and 2) an exhaust fan with a heat pump used to provide space heating or domestic hot water (DHW).

Accomplishments During FY 1985

The efforts in FY 85 on waste heat integration focused on integrated ventilation strategies, particularly on exhaust ventilation using a heat pump for domestic hot water. The model used for comparing different ventilation strategies was expanded and improved, using sensitivity runs to determine the importance of the assumptions used in our earlier comparisons. The effects of seasonal variations in supply water temperature and hot water demand were examined, as were the effects of DHW tank temperature and thermal stratification on COP and total heat delivered. It was found that average demand and supply water temperature provided results within 2% of one-year simulations that take into account seasonal variations. This result implies that we can save considerable computation time and cost. On the other hand, tank stratification was found to have an important impact on the total heat supplied by the heat pump. In addition, a new effective ventilation model was incorporated into the program. The average effective ventilation rate computed with this model uses the capacity of the room to compute an average exposure for constant pollutant sources.

Another part of the research in FY 85 was to reexamine the technique presently used for computing the total ventilation that occurs when mechanical ventilation and natural infiltration interact. The present technique, which is to add natural ventilation and unbalanced mechanical ventilation flows in quadrature, was compared against a true flow-balance model. The quadrature technique was found to provide estimates of the total flow within 10% of the actual values computed with the flow-balance model.

Planned Activities for FY 1986

There are three major activities planned for FY 86. The first activity is to use our new code, which includes the effective ventilation, flow addition model, and a stratified hot water tank model, to compare the economics of alternate ventilation strategies for different regions of the country. This will differ from previous activities of this sort in that it will include more detailed specification of hardware (both new and existing). The second activity is to use field data, both new and existing, to determine the energy and indoor air quality implications of leaky duct systems. This will include examinations of pressures inside duct systems, leakage measurements, and analysis of data in the air leakage database on duct leakage. The third activity, which depends upon completion of the first, is to evaluate more sophisticated cooling strategies, such as two-stage evaporative cooling, that require simulation of additional hardware, and more careful analysis of ventilation moisture flows.

REFERENCES

1. Office of Technology Assessment (1982), *Energy Efficiency of Buildings in Cities*, Government Printing Office, Washington, DC.
2. Diamond, R.C., *et al.* (1986), "Multiyear Plan for Multifamily Retrofit Research," to be published by DOE in 1986.
3. Ritschard, R.L., et al. (1985), *Multiyear Plan for Federally-Assisted Housing*, LBL-19683.
4. Szydlowski, R.F. (1986), "Protocol for Monitoring Multifamily Retrofits," to be published in 1986, Lawrence Berkeley Laboratory
5. Modera, M.P., Brunsell, J.T., and Diamond, R.C. (1986), "Improving Diagnostics and Energy Analysis for Multifamily Buildings," to be published in 1986, Lawrence Berkeley Laboratory.
6. Perkins & Will and the Ehrenkrantz Group (1980), *An Evaluation of the Physical Condition of the Public Housing Stock,* H-2850, Department of Housing and Urban Development.
7. Feustel, H.E. and Kendon, V.M. (1985), *Infiltration Models for Multicellular Structures—A Literature Survey*, LBL-17588.
8. Sherman, M.H. (1980), *Air Infiltration in Buildings,* LBL-10712.
9. Krischer, O. and Bec, H. (1957), "Die Durchlueftung von Raeumen durch Windangriff und der Waermebedarf fuer die Lueftung." VDI-Berichte 18, S. 29/56.
10. DIN 4701 "Regeln fuer die Berechnung des Waermebedarfs von Gebaeuden" Teil 1: Grundlagen der Berechnung (1983) Beuth Vertrieb Berlin.
11. Feustel, H.E. and Lenz, T.P. (1984), "Patterns of Infiltration in Multifamily Buildings," *Buildings and Environment 20;* LBL-17584.
12. Feustel, H.E. (1985), "Development of a Simplified Multizone Infiltration Model," in *Proceedings of the 6th AIC-Conference, Het Meerdal, Netherlands; LBL-19095.*
13. Sherman, M.H., Wilson, D.J., and Kiel, D.E. (1986), "Variability in Residential Air Leakage," to be published in an ASTM Special Technical Publication; LBL-17587.
14. Dickinson, J.B. and Feustel, H.E. (1986), *Seasonal Variation in Effective Leakage Area,* LBL-19337, to be published in 1986.

Building Ventilation and Indoor Air Quality*

D.T. Grimsrud, A.V. Nero, Jr., F. Abu-Jarad, R. Allen, M. Apte, J. Brown, S.R. Brown, J. Binenboym, W.J. Fisk, D. Froehlich, J.R. Girman, J. Harrison, A.T. Hodgson, K. Koshlap, J. McCann, B.A. Moed, R. Mowris, W.W. Nazaroff, T. Nuzum, B.S. Pedersen, R. Prill, K.L. Revzan, A. Robb, E. Saegebarth, G. Schiller, M. Schwehr, R.G. Sextro, H. Sokol, G.W. Traynor, B.H. Turk, S. Uno, and R. Young

Lawrence Berkeley Laboratory (LBL) carries out a broad program of work on indoor air quality in the context of its research on energy-efficient buildings and associated environmental effects. Efforts of the Buildings Ventilation and Indoor Air Quality Program include characterization of the emission of various pollutant classes from their respective sources, study of the effectiveness of ventilation in removing pollutants from indoor atmospheres, and examination of the nature and importance of chemical and physical reactions that can affect the occurrence and amount of airborne pollutants. The program has groups devoted specifically to three major pollutant classes: combustion products, arising from indoor appliances and other sources; radon and its daughters, arising from materials that contain radium, a naturally occurring radionuclide; and other organics, arising from a variety of building materials and consumer products. In addition, other groups study techniques for controlling airborne concentrations, develop devices for monitoring pollutants in buildings, and design or carry out field surveys of indoor air quality. Significant efforts are also devoted to assessment of the health effects of indoor pollutant exposures, and to the establishment of a numerical data base of pollutant concentration measurements in buildings.

*This work was supported by the Assistant Secretary for Conservation and Renewable Energy, Office of Buildings Energy Research and Development, Building Systems Division and by the Director, Office of Energy Research, Office of Health and Environmental Research, Human Health and Assessments Division and Pollutant Characterization and Safety Research Division of the U.S. Department of Energy under Contract No. DE-AC03-76SF00098; by the U.S. Environmental Protection Agency (EPA) through Interagency Agreement AD-89-F-2A-062 with DOE; by the Bonneville Power Administration, Portland, Oregon through Interagency Agreement DE-A179-83P12921; and by the Directorate for Health Sciences of the U.S. Consumer Product Safety Commission under Contract No. CPSC-IAG-81-1375.

The core of these efforts consists of research on the behavior of indoor air pollutants, specifically the influence on airborne concentrations of three classes of factors: source strengths or emission rates, ventilation rates or effectiveness, and reaction and transformation mechanisms. The work carried out by the individual groups is primarily experimental, consisting of fundamental—and often quite sophisticated—experiments on pollutant emission, transport, and removal, complemented by significant efforts advancing the theoretical framework within which results may be considered.

COMBUSTION POLLUTANT EXPOSURES

The pollutant emission rates of several new unvented combustion heating appliances were tested in FY 1985.[1] In addition, a new effort was initiated in FY 1985 to develop the groundwork for a macromodel of indoor combustion pollutant concentrations.[2] Overall, the thrust of the combustion-related research is shifting from the quantification of pollutant emission rates from a wide variety of indoor combustion sources to the overall evaluation of indoor exposures to combustion pollutants in U.S. residences.

Accomplishments During FY 1985

Pollutant Emissions from Unvented Combustion Space Heaters

By the end of FY 1985 we had conducted pollutant emission rate tests for all major unvented combustion space heating devices available in the U.S.[1,3,4] These appliances were unvented radiant, convective, and two-stage kerosene heaters, unvented infrared and convective natural gas heaters, and unvented infrared and convective propane heaters.

With regard to natural gas and propane unvented gas space heaters (UVGSHs), the following conclusions were made. For both infrared and convective heaters, no significant differences in emissions rates were observed between heaters with different fuel types (propane or natural gas). Carbon monoxide, nitrogen oxide, and nitrogen dioxide emission rates from infrared UVGSHs are stable with time and reproducible to within a few percent. CO emission rates from convective heaters are not as stable or reproducible and changes in emission rates with time of 50% were observed. The primary difference between infrared and convective heaters is the low NO_x emissions for infrared heaters. NO_x and NO_2 emission rates for infrared heaters are lower than those of convective heaters by a factor of approxi-

mately 10 for NO_x and 3 for NO_2. Changes in inlet pressure did not significantly alter emission rates. A slight increase in CO emission rates with decreased fuel consumption rates was observed in one heater. Finally, tuning was a factor in the CO emissions of some convective heaters, but was not a factor for other tunable convective heaters.

The CO and NO_2 emission rate results of the gas-fired space heaters are compared with the emission rate results of three types of kerosene heaters in Fig. 1. Clearly the multi-stage (actually two-stage) kerosene heater is a much improved product with regard to CO and NO_2 emissions relative to the other space heating appliances.

Groundwork for Developing a Macromodel of Indoor Combustion Pollutant Exposures

A macromodel of indoor combustion pollutant concentrations or exposures in U.S. residences must use a version of the indoor air pollution mass-balance equation as an integral part of the macromodel. A simple steady-state form of the mass-balance equation follows:

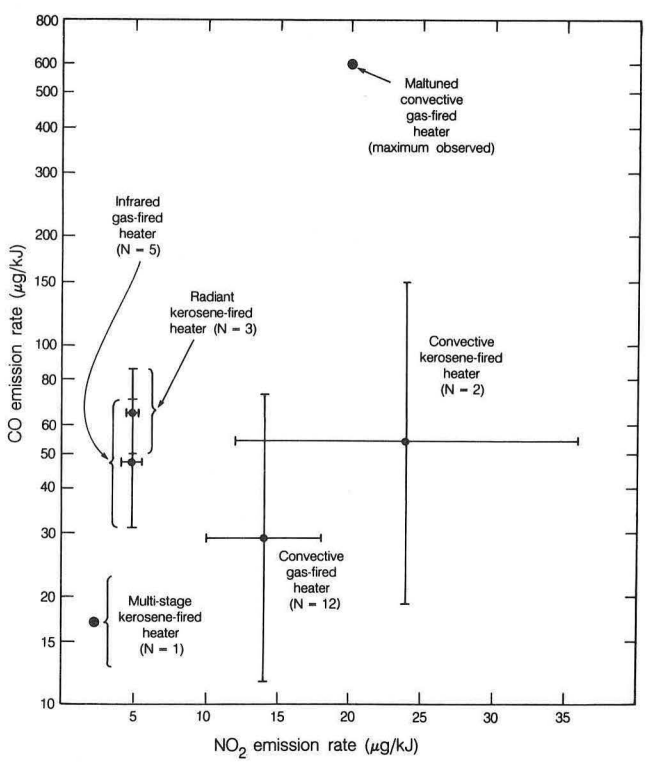

Figure 1. CO and NO_2 emission rates from well-tuned unvented gas-fired and kerosene-fired space heaters and the maximum observed for maltuned convective gas-fired space heaters. (XBL 851-9507)

$$C = \frac{PaC_o + S/V}{a + k} \qquad (1)$$

where:

C = pollutant concentration (ppm or $\mu g/m^3$);
P = fraction of the outdoor pollution that penetrates the building shell (dimensionless);
a = air exchange rate in air changes per hour (h^{-1});
C_o = outdoor pollutant concentration (ppm or $\mu g/m^3$);
S = indoor pollutant source strength (cm^3 or $\mu g/h$);
V = volume (m^3);
k = net rate of removal process other than air exchange (h^{-1}).

Figure 2 schematically shows how many factors combine to yield modeled indoor air pollution concentrations for unvented or partially vented combustion appliances. Conceptually, Fig. 2 represents an expanded form of Eq. 1. Throughout the remainder of this section, additional factors that may help to describe or model indoor combustion pollutant levels and that could be included in more complex versions of Eq. 1 will be explored.

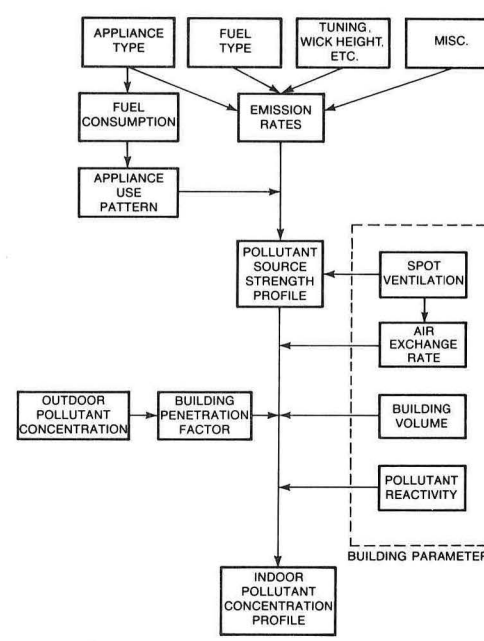

Figure 2. Schematic diagram of factors that affect indoor air pollution concentrations resulting from the use of an unvented or partially vented combustion appliance. (XBL 828-1054)

Many of the factors and quantities in Eq. 1 or Fig. 2 can be approximated by log-normal distributions.[4,5,6] Thus, it is useful to use the geometric standard deviation (GSD) as one measure of a parameter's relative importance in describing variations observed in indoor air pollution concentrations. In one regional study, the GSD's of combustion pollution source strengths (S) for kerosene-heater use and cigarette smoking were 2.9 and 3.1, respectively; the GSD of the outdoor pollutant concentration (C_o) was 1.7 for NO_2 and 1.8 for respirable suspended particles; the GSD for air exchange rates (a) was 1.8; the GSD of the house volumes (V) was 1.4; and the GSD for NO_2 reactivity (k) using an indirect measurement method was 2.4.[7] Therefore, the single largest factor influencing indoor combustion pollutant concentrations is the pollutant source strength. For NO_2, the indoor reactivity can also play a significant role in determining indoor air pollution concentrations. Outdoor pollutant concentrations were not useful in describing indoor concentrations in houses with relatively high indoor pollutant levels because the S/V term in Eq. 1 was much greater than the PaC_o term for such houses. Source strengths and NO_2 reactivity rates have received very little explicit attention in field monitoring studies, especially with regards to modeling, and future research efforts must address these important factors.

There are a wide variety of indoor combustion-pollutant sources, as shown in Table 1. Combustion sources can be categorized as smoking sources (i.e., cigarettes, cigars, and pipes) or combustion appliances. Combustion appliances can further be divided into three categories: unvented (e.g., portable kerosene heaters), partially vented, (e.g., gas ranges with range hoods), and vented (e.g., forced-air furnaces). A vented appliance is one that has a flue physically connected to the appliance that, under normal operating conditions, removes all, or almost all, of the pollution generated by the appliance.

An alternate and potentially useful way of categorizing combustion sources is by the force that drives the source usage. The use pattern of most of the sources listed on Table 1 is driven by the space heating requirements of the house, which do not affect other source use patterns, such as smoking and gas range use patterns. The usefulness of this type of categorization will be discussed later.

A very important factor that will affect macroassessments of population exposures to combustion pollutants is the market penetration of various sources. This critical parameter, although not discussed here, needs attention and the usefulness of existing surveys of market penetration conducted by utilities or other organizations needs exploring.

Table 1. Potential sources of indoor combustion pollutants.

Source	Type of Ventilation
1) Smoking (incl. pipes and cigars)	—
2) Unvented gas space heaters	Unvented
3) Portable kerosene space heaters	Unvented
4) Gas ranges without range hoods	Unvented
5) Gas ranges with range hoods	Mechanical ventilation
6) Wood stoves	Gravity flue
7) Coal stoves	Gravity flue
8) Forced-air furnace systems (gas, wood, coal, oil, etc.)	Gravity flue
9) Indoor gas water heaters	Gravity flue
10) Gas wall heaters	Gravity flue
11) Gas dryers	Gravity flue

Of all of the parameters in Eq. 1, the source strength is understood the least for U.S. houses. Modeling source strengths and extending the results to a variety of houses is not easy. Combustion source strengths depend upon a wide variety of factors. For example, the pollutant source strengths from unvented combustion appliances depend upon the appliance type, appliance use pattern, fuel type (including sulfur content), state of tune (or wick height for kerosene heaters), and other factors (see Fig. 2).

Of all the factors that significantly affect the strength of a combustion-related source, the least understood is the appliance use pattern and the force that drives the use pattern. Clearly, different sources or types of sources have different driving forces that affect their use pattern. Many use patterns are dependent upon the heating requirements of the house, others on the numbers of smokers, and others on the lifestyle of the occupants. Table 2 lists potential factors that can drive source usage. In Table 2, the source-driving factors fall into two gen-

Table 2. Potential factors for modeling combustion pollutant source strengths.

Factors Related to Space-Heating Sources (e.g., kerosene heaters, wood stoves, etc.)
— Meteorology (Indoor/Outdoor Temperature Differences)
— Insulation Level
— Volume
— Air Exchange Rate
— Other Sources of Heat
— Socio-Economic Factors
— Occupant Activity
Factors Related to Non-Space-Heating Sources (e.g., cigarettes, cooking stoves)
— Number of Occupants
— Home Volume
— Number of Smoking Occupants
— Socio-Economic Factors
— Occupant Activity

eral categories: those related to the heating requirements of the house, such as the house insulation level, and those not related to the heating requirements of the house, such as the number of smokers in the house. Source usage can also be influenced by socio-economic and other lifestyle factors. The development and validation of source usage models with inputs such as the outdoor temperature and house insulation level would greatly advance the current understanding of this subject.

It is neither feasible nor desirable to have models that account for all of the variation observed in indoor pollutant concentrations between houses. However, a model that is based on easily accessible data can be very useful for modeling exposures and for extrapolating results to larger populations. With the recent emphasis on energy conservation, large data bases are being created that contain house insulation levels and air exchange rates. Meteorological data, important to most existing air-exchange-rate models, are also widely available to assist in the modeling of space-heating appliance pollutant source strengths. Other sources of data on national or regional housing characteristics may also help in this effort.

There are many gaps in our knowledge of indoor combustion pollutant concentrations and the factors that affect them. With the development of a macromodel, information gaps can be identified and subsequent field studies can be designed to fill the gaps and test hypotheses that have been developed as part of the macromodel for indoor combustion pollutant exposures.

Planned Activities for FY 1986

The development of a macromodel for indoor combustion-pollutant exposure will continue in FY 1986. In addition, two studies started in FY 1985 will be completed. One study is aimed at quantifying organic emissions from kerosene space heaters. The other study is investigating the effectiveness of add-on catalytic devices for reducing pollutant emissions from kerosene space heaters.

ORGANIC CONTAMINANTS

The limited data on indoor/outdoor concentration ratios of volatile organic compounds (VOC) in residences, office and schools generally show that for many compounds, these ratios are greater than one and in many cases much greater than one.[8–11] These elevated ratios may result from the increased use of synthetic building materials, the introduction of new consumer products, and the development of construction practices which minimize ventilation. Considerably more data are needed on indoor concentrations and sources of VOC for even rudimentary assessments of population exposures and chronic health risks. Acute health problems, principally mucous membrane irritation, in some problem buildings have also been postulated to result from elevated indoor concentrations of VOC.

In FY 1985, our research efforts were directed toward (1) the fabrication of the air-handling system for an environmental chamber, (2) the characterization of methylene chloride emissions from consumer products including development of an exposure model, and (3) the validation of a multi-sorbent, thermally-desorbed sampler for VOC.

Accomplishments During FY 1985

Fabrication of the Environmental Chamber Air-Handling System

The design and construction of a 20-m^3 environmental chamber suitable for use in a wide variety of indoor air quality studies has already been described.[12] This past year we fabricated a more advanced air-handling system for the chamber. With the exception of the control system, the major components of the air-handling system for the chamber have been fabricated and installed in a loft adjacent to the chamber. In the order in which ventilation air passes through the single-pass system, the major components are: a variable speed blower; an air cleaning subsystem consisting of coarse filters, charcoal packs for scrubbing VOC, and HEPA filters; an

air-conditioning subsystem consisting of a pre-heater, a humidifier, chiller coils, and a final heater; and a volumetric flow monitoring system consisting of two turbine flowmeters mounted in parallel.

Standard components were used in the air-cleaning subsystem. However, to install the air-handling system in the limited space available and still create easy access for servicing, we had to design and fabricate housings and transitions for the components of both this subsystem and the air-conditioning subsystem.

The pre-heater and final heater, which are of our own designs, consist of two 3-kW and three 3-kW heating coils, respectively. The humidifier employs infrared heating of large pans of water coupled with dedicated mixing fans to insure uniformity of the humidification. The chiller coil has been installed in the air-handling system and a large chiller has been installed outside on the roof of the laboratory building. The chiller loop connecting the two components is not completed.

The volumetric flow rate of the ventilation air is monitored continuously by one of the two turbine flowmeters located just upstream of the chamber inlet. The smaller turbine flowmeter monitors ventilation rates from 0.5 to 3.0 air changes per hour with a precision of $\pm 3\%$; the larger flowmeter covers the range from 3.0 to 15 air changes per hour.

Methylene Chloride Emissions and Exposure from the Use of Consumer Products

A recently completed bioassay, which found methylene chloride (CH_2Cl_2) to be an animal carcinogen, has increased the concern about consumer exposure to this chemical.[13] To provide information on exposures sufficient to conduct a health risk assessment, CH_2Cl_2 source strengths and personal exposures were characterized in our 20-m^3 environmental chamber using typical applications of paint removers and aerosol finishes representative of the two major types of consumer products containing CH_2Cl_2. For each product, experiments were conducted at ventilation rates of ~0.5 and ~3 air changes per hour. Altogether, including duplicate experiments, a total of 10 experiments were performed.

Both the chamber concentration and the worker's breathing-zone concentration of CH_2Cl_2 were continuously monitored by infrared spectroscopy throughout each experiment. Figure 3 illustrates an experiment with a paint remover. In addition, the source strength of CH_2Cl_2 was determined from the product composition and the quantity of product used. Measured personal exposures resulting from the use of paint removers for work periods of ~90 min are listed in Table 3 and ranged from 1040 to 1200 ppm·h at the high ventilation rate and from 1970 to 2400 ppm·h at the low ventilation rate. Personal exposures from the use of aerosol finishes for work periods of 23 min or less ranged from 32 to 35 ppm·h for a single coat of a polyurethane finish and from 121 to 124 ppm·h for two coats of a metallic paint. Several occupational standards and guidelines for CH_2Cl_2 concentrations were exceeded during experiments with paint removers.

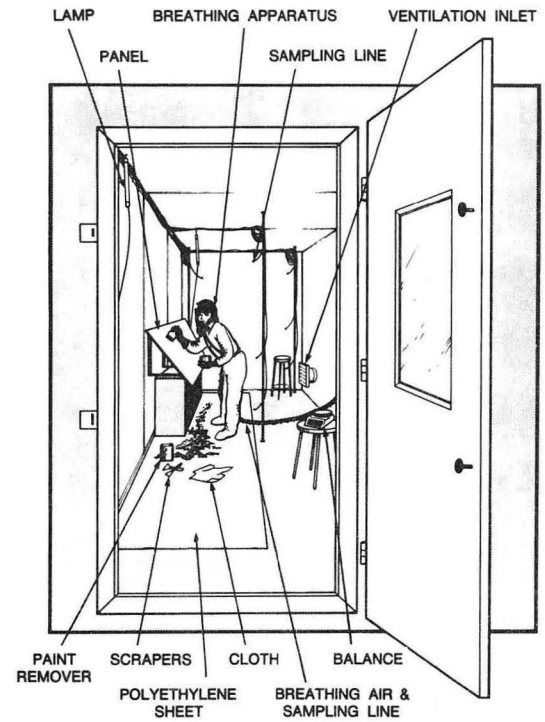

Figure 3. Lawrence Berkeley Laboratory's 20-m^3 environmental chamber setup for experiments with paint removers. For illustration, door with observation window is shown in open position and foreground sampling lines are omitted. Breathing-zone sampling line terminates at worker's right shoulder. (XBL 855-9537)

When chamber concentrations of CH_2Cl_2 were integrated over the work periods and compared to measured personal exposures, agreement was good at the low ventilation rate but differed by 21% at the high ventilation rate (Table 3). Temporal profiles of CH_2Cl_2 concentrations were calculated from the source strengths, the ventilation rates and the chamber volume using single-equation, mass-balance models. As illustrated in Figs. 4 and 5, these theoretical concentrations were in good agreement with measured concentrations. Exposure models based upon the concentration models were also developed and then evaluated by comparing theoreti-

Table 3. Measured personal and chamber exposures compared to theoretical exposures of CH_2Cl_2.

Product[a]	Exp.No.	Total Vent. Rate (h^{-1})	Work Period (min)	Mass used Product[b] (g)	Mass used CH_2Cl_2 (g)	Personal Exposure (ppm·h)	Chamber Exposure (ppm·h)	Theoretical Exposure[c] (ppm·h)
PR-A	1	3.19	90	316[d]	262[d]	1040	889	972
	5	0.62	86	325	270	1970	1970	1900
PR-B	2[e]	3.23	89	363	314	1120	921	1180
	3	3.20	91	389	337	1200	1010	1240
	4	0.63	88	385	333	2400	2350	2530
MP	6[e]	3.10	23	151	38.9	124	103	88.5
	7	3.12	21	161	41.6	121	103	85.7
	8	0.54	23	150	38.6	160	137	120
PF	10	3.11	10	72.8	19.6	31.6	23.9	31.2
	9	0.53	14	58.5	15.7	35.2	35.5	45.0

[a]PR = paint remover; MP = metallic paint; PF = polyurethane finish.
[b]Average density of paint removers was 1.18 g cm^{-3}.
[c]Calculated assuming a time-dependent source in a mass-balance model.
[d]Approximate value since some product was spilled during application.
[e]Duplicate experiments.

cal and measured exposures for the experiments. The exposure models appeared to have sufficient accuracy and precision for use in assessment of health risk from the use of consumer products containing CH_2Cl_2. A complete description of the study can be found in a recent report.[14]

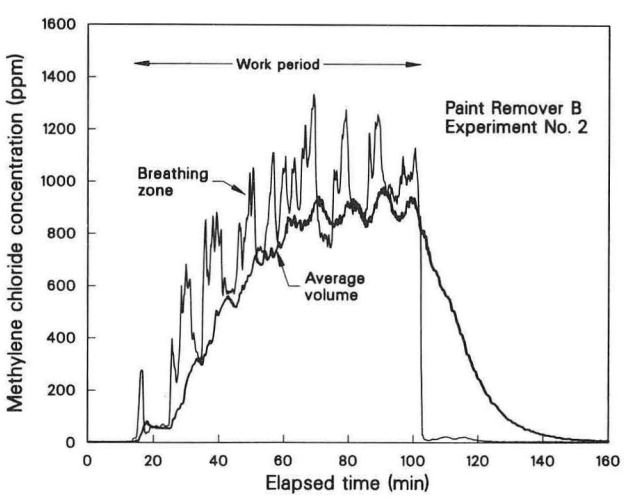

Figure 4. Temporal profiles of chamber and breathing-zone concentrations of CH_2Cl_2 during Experiment 2 with paint remover B at a ventilation rate of 3.23 air changes per hour. Duration of work period is shown above curves. At end of work period, breathing-zone sampling line was switched to laboratory air external to chamber. (XCG 861-7054)

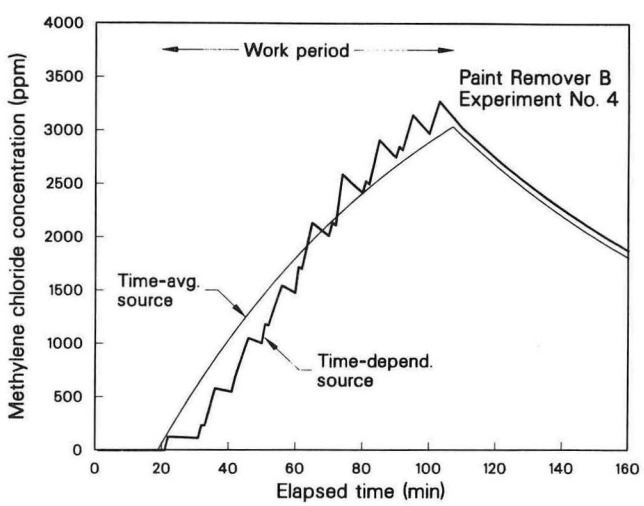

Figure 5. Temporal profiles of theoretical chamber concentration of CH_2Cl_2 for Experiment 2 with paint remover B at a ventilation rate of 3.23 air changes per hour. Concentrations were calculated using both time-dependent and time-averaged source strengths. Duration of work period is shown above curves. (XBG 861-7058)

Validation of a Multisorbent, Thermally Desorbed Sampler

Qualitative and quantitative methods for VOC which are rapid, reliable and relatively inexpensive are needed to survey a variety of buildings, to identify sources of potentially harmful compounds and to evaluate the efficacy of mitigation strategies. The present paucity of data on VOC concentrations can be largely attributed to the difficulty and expense of analysis for a wide range of VOC. Because most VOC occur at relatively low concentrations, a concentration step is generally required prior to chromatographic analysis, typically with a solid sorbent. However, no single sorbent is adequate for the wide range of VOC encountered.

An obvious solution for a generalized sampler for VOC is to use several complementary sorbent materials in series. One such sampler, containing glass beads, Tenax-TA, Ambersorb XE-340, and activated charcoal, is commercially available from Envirochem, Inc. for use in their sample concentrator/thermal desorption unit. We are evaluating this sampler, which was not previously validated for air sampling applications, and a modified version of it which omits the activated charcoal for the quantitative determination of a wide range of VOC simultaneously present in air at concentrations from a few nanograms to several micrograms per liter.

The solid sorbent sample concentrator/thermal desorption unit (Model 810A, Envirochem, Inc.) has been interfaced with a bench top capillary gas chromatograph/mass selective detector (Model 5970B, Hewlett Packard, Inc.). To achieve satisfactory chromatographic peak shape and separation for the lowest-boiling compounds, an on-column cryofocusing device which uses liquid nitrogen was developed for the oven of the gas chromatograph.

Optimal storage procedures for samplers have been determined. Upon complete thermal desorption, blank samplers are sealed with nylon caps with Teflon ferrules and placed in individual culture tubes with screw caps. These are then stored at $-10°C$. Air samplers are similarly stored prior to analysis.

A major component of the study is the determination of maximum sample volumes at standardized conditions for highly volatile compounds representative of a variety of chemical classes. The 20-m^3 environmental chamber has been employed for these experiments because it allows us to control experimental parameters while closely simulating real sampling situations. Triplicate samples have been collected at sample flowrates of $\sim 100\ cm^3\ min^{-1}$ regulated with electronic mass-flow controllers. The analytical precision and overall accuracy of the method is excellent as demonstrated in Table 4, which shows the results of analyses of chamber samples.

Breakthrough volumes have been determined for samplers containing Tenax and Ambersorb and compared to samplers containing Tenax alone. For this comparison, significant breakthrough has been defined as the loss of more than one percent of the mass of the compound entering the sampler. As shown in Table 4, the sampler with both Tenax and Ambersorb had significant breakthrough only for Freon-11. This is in contrast to the sampler with Tenax alone, for which case several compounds had breakthrough volumes of less than one liter.

Planned Activities for FY 1986

The control system for the environmental chamber will be completed and the performance of air-handling system will be evaluated. We will initiate a chamber study evaluating mitigation strategies for VOC emissions from realistic assemblies of building materials. The validation of the multisorbent sampling system will be completed by determining the effects of elevated humidity and competing compounds such as butane on breakthrough volumes. A field study to confirm the applicability of the exposure models developed for consumer products containing methylene chloride is underway and will examine the effects of variations in volume, ventilation patterns and rates and product use patterns.

CHARACTERIZING THE SOURCES OF RADON IN BUILDINGS

Radon and its immediate radioactive decay products are widespread contaminants in indoor air. The immediate parent of ^{222}Rn is ^{226}Ra, which is a ubiquitous constituent of crustal material, and is therefore present in soils and in building materials having rock- and soil-based components. The chemically inert radon gas, formed from the alpha decay of radium, can be transported through these materials by diffusive or convective flows and into the interior of homes.

While no national survey of indoor radon concentrations has been conducted, measurements from a variety of studies from around the United States indicate that indoor radon-222 concentrations in residences average $\sim 60\ Bq\ m^{-3}$ (1.6 pCi/L),† and

†The SI units for airborne concentration of radionuclides are $Bq\ m^{-3}$; the units in more common usage, until recently, have been pCi/L, where 1 pCi/L = 37 $Bq\ m^{-3}$.

Table 4. Measured and prepared concentrations of ten volatile organic compounds in a 20-m^3 environmental chamber are compared for a sampler containing Tenax-TA and Ambersorb XE-340. Breakthrough volumes for the same compounds with this sampler are also compared to those for a sampler containing only Tenax-TA.

Volatile Organic Compounds	Prepared Chamber Concentration (ng/L)	Measured Chamber Concentration[a] (ng/L)	Breakthrough Volume[b] Tenax-TA + Ambersorb XE-340 (L)	Tenax-TA (L)
Trichlorofluoro-methane (Freon-11)	277	330±4	<4	<0.5
n-Pentane	229	223±6	>10	<0.5
Methylene Chloride	240	228±5	8–10	<0.5
n-Hexane	238	246±8	>10	1–2
2-Butanone	218	218±7	>10	1–2
Chloroform	265	257±8	>10	1–2
Ethyl Acetate	241	246±6	>10	>4
1,1,1,-Trichloro-ethane	245	255±3	>10	<0.5
Benzene	239	256±8	>10	2–4
Pentanal	220	194±6	>10	0.5–1

[a]Average of three replicate samples ± standard deviation of measurement.

[b]Breakthrough is defined as the loss of more than one percent of the mass of the compound entering the sampler.

concentrations above 6000 Bq m^{-3} have been observed in some homes. Based on the distribution of these radon concentration data, the number of homes with indoor concentrations averaging above 300 Bq m^{-3} can be estimated to be 1 to 2% of the U.S. housing stock—approximately one to two million single-family dwellings. These data also show a geographical variation in indoor radon concentration, apparently due to regional differences in radon source strengths. The available dose-response data suggest that even average radon concentrations may produce several thousand cases of lung cancer per year in the U.S.[15]

The goals of the LBL radon research effort are to 1) provide a method of predicting or identifying those geographical areas where houses with high indoor radon concentrations might be found; 2) improve our understanding of the mechanisms for the production and transport of radon through soils and into buildings; and 3) develop or identify means of controlling high indoor radon concentrations. Studies on the behavior of the radon decay products—radon progeny—are described in the following section, **Particles and Radon Progeny**.

Accomplishments During FY 1985

There are five potential sources of radon: the soil surrounding the building, outdoor air, building materials, potable water, and natural gas. Of these, the first two are often the most significant, based on a comparison of the range of expected source strengths with the frequency distribution of entry rates that have been observed in single-family residences. This is illustrated in Fig. 6, where the observed entry rate is the product of the indoor radon concentration, C_i, and the air exchange rate, λ_V.

The solid line in Fig. 6 summarizes time-averaged data from 73 homes in several cities in which C_i and λ_V were measured simultaneously. The dashed line represents the entry rate distribution derived from the observed distribution of indoor radon concentrations and the distribution of measured air exchange rates from 578 houses. With the exception of the unattenuated soil flux, the strength of the other sources illustrated in Fig. 6 contribute only to the lower end of the entry rate distribution.[16] The importance of water as a potential source of

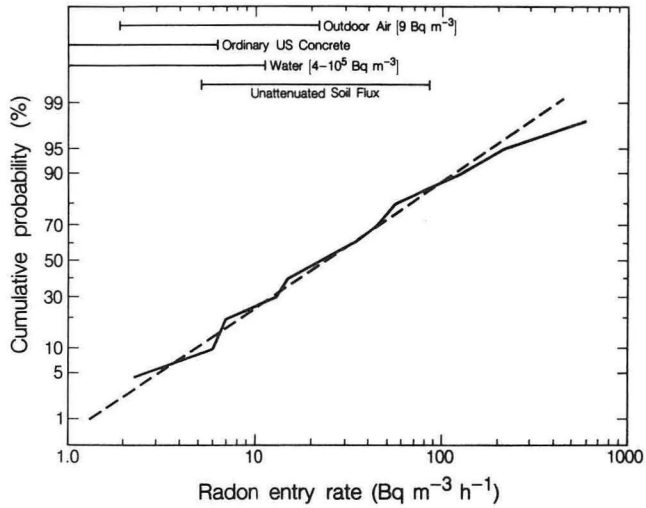

Figure 6. Cumulative frequency distribution for radon entry rates and a comparison with the range of source strengths from various radon sources. The range of source strengths at the top of the figure is based on an assumed single-story house with a 100 m^2 floor area, 2.4 m ceiling height, and 0.2 m thick concrete slab floor. References for data on these sources of indoor radon are given in Ref. 16. (XBL 858-9875)

indoor airborne radon varies with the source of the water. In some cases, high concentrations of radon dissolved in groundwater have been reported, and the resulting contributions to indoor air radon levels may be significant. A review of radon from potable water[5] was summarized in the FY 1984 Annual Report.[12]

The diffusive flux of radon from uncovered soil is, potentially, a significant source of radon, although a soil covering, such as a concrete slab floor, will substantially attenuate the radon flux from soil. On the other hand, it appears that convective flow of radon into building interiors may account for high radon entry rates. Bulk flow of gas from the soil into the building shell may occur through cracks or other openings in the building substructure driven by the slight negative pressure difference between the inside and outside of the building. Thus the nature of both the building substructure and the surrounding soil are important variables helping to determine the radon entry rates.

Factors Influencing Soil as a Source of Indoor Radon

In order to understand the influence of soil on indoor radon concentrations, a significant portion of our radon research effort has focussed on a) a review of important soil characteristics having a role in radon emanation, migration through soil and transport into buildings, b) the development of a framework for a geographically-based predictive capability, and c) an examination of relevant data and data sources for assessing the geographic variations in radon source strength.[17] The key elements in the production and migration of radon in soil and into buildings are shown schematically in Fig. 7. Two principal concepts are illustrated, radon availability, which is the amount of radon available for movement in the soil, and radon transport, which is the movement of radon through soil and into the building.

Important physical characteristics of soils include the size distributions of the soil grains and of the pores, and the soil moisture contents. The physical characteristics of representative soils are shown in Table 5. The grain size distribution is used to classify soil into three components, clay, silt or sand. The relative proportions of these components determine the basic soil texture, and therefore influence the fluid flow properties of soils. The void fraction of a soil is known as the porosity; these voids may be either air- or water-filled. The moisture content of soils also has an important influence on both radon emanation and migration. A well-drained soil often contains water in the smaller pore spaces and air in the larger pores. The presence of this capillary water increases the radon emanation fraction by absorbing the energy of the recoiling radon atom, formed in the alpha decay of its radium parent. Since most of the convective movement of air

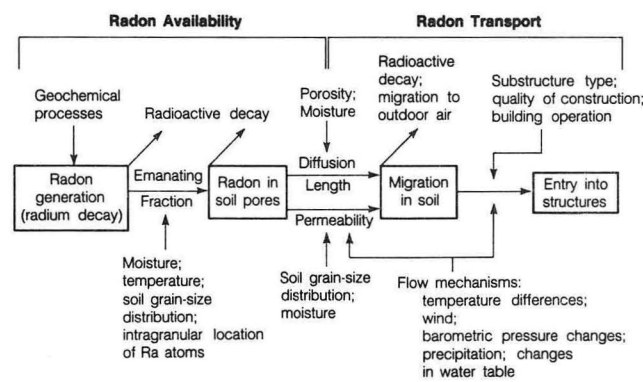

Figure 7. Schematic representation of radon production and migration in soil and its entry into buildings. The boxes illustrate the major states of radon in soil; the labels on the horizontal arrows connecting the boxes indicate a characteristic of the particular transition; parameters and processes that affect the rate of transition from one state to another are illustrated by the vertical arrows; and, finally, the diagonal arrows show the loss mechanisms for radon in soil. (XBL 8510-11933)

Table 5. Representative values of physical characteristics of soils.[a]

Texture class	Grain Size (μm)	Soil bulk density (g cm^{-3})	Porosity	Field Capacity Saturation[b] (%)
Sand	50–2000	1.44–1.58	0.40–0.46	15–20
Sandy loam		1.18–1.64	0.38–0.55	20–30
Loam		1.27–1.49	0.44–0.52	30–45
Silt	2–50		0.5	58
Silt loam		0.98–1.45	0.45–0.63	30–50
Clay loam		1.27–1.54	0.42–0.52	45–60
Silty clay loam		1.27–1.49	0.44–0.52	45–60
Silty clay				55–90
Clay	<2	1.18–1.54	0.42–0.56	55–90

[a]See Reference 17.

[b]Field capacity is defined as the fraction of the total pore volume that is filled with water after a soil has been throughly wetted and then drained for approximately two days.

through the soil occurs through the larger soil pores, the presence of this water does not increase the resistance to air flow. Thus, radon availability in soil appears to be greatest for moist soils.

Air permeability is one of the more important physical characteristics of soils that influences radon production and movement. In its simplest form, permeability is the relationship between the velocity of fluid flow through the medium and the applied pressure gradient, i.e., Darcy's law. Again, the moisture content of the soil influences the air permeability of the soil. This is illustrated by Fig. 8, where the value of the air permeability remains constant until water fills just over 40 percent of the pore space. As water content increases beyond this fraction, air permeability decreases dramatically.

The importance of soil permeability in understanding the sources of indoor radon arises from the range of permeability values for common soils, which can span over 10 orders of magnitude. At the upper end of this range, usually associated with large-grained soils, convective flow is the dominant transport process, and the potential radon entry rate into buildings increases correspondingly. At the

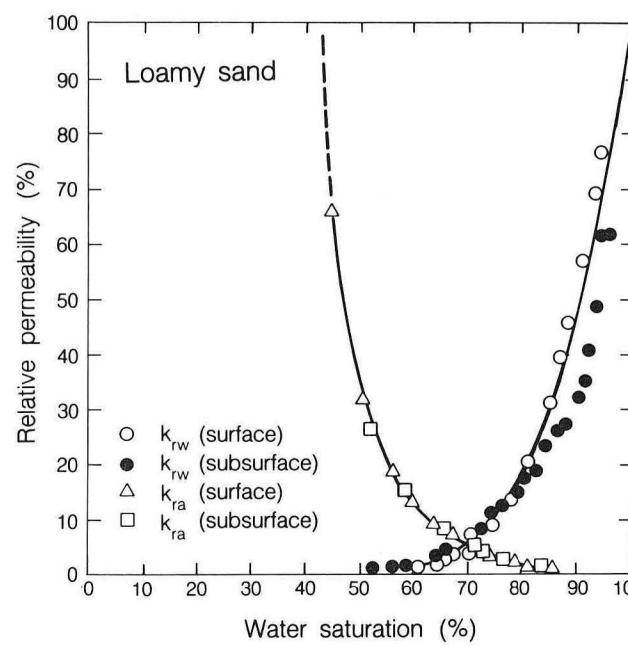

Figure 8. Relative permeability of loamy sand for air (k_{ra}) and water (k_{rw}) as a function of soil water saturation (from Ref. 18.). (XBL 8511-9030)

lower end of the permeability range, often associated with clayed soils, molecular diffusion is the more important radon transport process. Mathematically, a general transport equation for convective and diffusive flow for radon in soil can be derived, assuming the soil is isotropic:

$$\frac{\partial I_{Rn}}{\partial t} = D_e \nabla^2 I_{Rn}$$

$$+ \frac{k}{\epsilon \mu} \vec{\nabla} P \cdot \vec{\nabla} I_{Rn} + G - \lambda_{Rn} I_{Rn} \quad , \qquad (1)$$

where I_{Rn} is the activity concentration of radon in the soil pores, D_e is the effective diffusion coefficient, k is the intrinsic soil permeability, ϵ is the soil porosity, μ is the dynamic fluid viscosity, ∇P is the pressure gradient, G is the radon generation rate in the soil pores, and λ_{Rn} is the radon decay constant. The first term in this equation is transport due to diffusion, while the second describes convective flow.

In its most general form, this equation cannot be solved analytically. However, dimensionless analysis of this equation provides some very useful insights, as well as possible simplifications for its solution. Converting this equation into dimensionless form (see Ref. 17 for details) and choosing some typical values for pressure, porosity, viscosity and diffusivity, the intrinsic permeability then determines the relative importance of diffusion and convective transport. Thus in coarse textured soils, such as sands and gravels, the first term in equation 1 can be neglected, and convective flow dominates. In fine soils, with much smaller permeabilities, the second term can be neglected and diffusive transport is more important.

When the insights provided by analysis of the transport equations are combined with what is known about soil characteristics and the role of buildings in developing the driving forces for radon movement, a general predictive framework emerges. The utility of this approach in determining which geographic areas have potentially elevated indoor radon concentrations will depend upon the availability of data on soil characteristics. As noted earlier, some of the important soils data include air permeability of soils, radium content, soil moisture, and climatological factors. The availability of geographical data and/or indicator variables has been reviewed. Although air permeability has not been measured or estimated for most soils, two approaches may provide reasonable estimates. Water permeabilities of soils have been measured, and if a reasonable correlation between air and water permeabilities can be shown for a range of permeability values, then the extensive water permeability data for soils compiled by the Soil Conservation Service (SCS) may be extremely useful for geographically-based radon source strength assessments. Air permeability is also a function of soil texture and structure; data on both these parameters have also been compiled by the SCS.

As noted earlier, the radium content of the soil is another potentially important parameter in estimating the radon source potential of soils. Data covering most of the U.S. exist for shallow radium concentrations. These data were acquired by the National Airborne Radiometric Reconnaissance (NARR) survey, which employed aerial γ-spectrometry to measure concentrations of ^{40}K, ^{214}Bi (a radon-222 decay product) and ^{208}Tl (a radon-220 decay product) in the near-surface soil. The data tapes containing the complete data set have been processed at LBL, and the data gridded to approximately a one mile spacing along each flight line. From these average data several types of maps can be produced. One such map, a three-dimensional surface plot of shallow radium concentrations for a 1° by 2° quadrangle area, based on a least-squares approximation to the data, is illustrated in Fig. 9. Analysis of these data is also being used as part of a project to assess possible correlations between lung cancer data and surficial radium concentration (as a proxy for indoor radon concentration). See the section on **Risk Assessment** below.

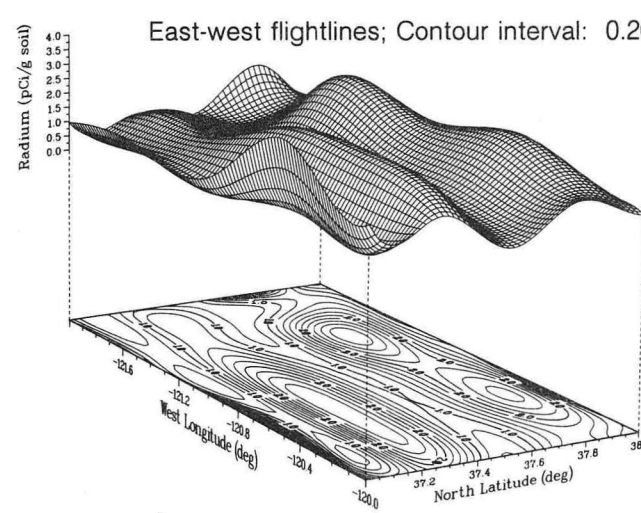

Figure 9. Surface mesh plot of values for radium concentration in the soil surface for the San Jose Quadrangle (1° latitude by 2° longitude). Data are from the NARR aerial radiometric survey. (XBL 862-494)

Planned Activities for FY 1986

Having developed a general framework for assessing the radon source potential based on geographic variables, future work will be directed toward 1) assessment of additional data bases, and 2) initiating experiments to verify some of the critical relationships, including the multiple role of soil moisture on radon availability. In addition, experimental work will focus on further examination of the coupling between the building substructure and the surrounding soil, and an evaluation of the correspondence between air and water permeabilities in soils of various textures. Finally, work will begin on the development of numerical models for radon movement in soil, based on the general transport equation discussed earlier.

PARTICLES AND RADON PROGENY

Particles are important indoor pollutants, with a number of indoor sources ranging from combustion processes to consumer product sprays. The physical and chemical composition of particles can be used to help identify the particle source. Because particles may themselves be toxic, or be carriers of adsorbed toxins, such as benzo(a)pyrene or radon progeny, their physical and chemical characteristics also help determine the health impacts associated with their inhalation.

Radon progeny, the radioactive decay products of radon, are also radioactive and are responsible for most of the health effects associated with radon. These airborne radionuclides interact with particles in the indoor air, and the specific alpha radiation dose to the lungs depends upon whether the radon progeny are attached or unattached to aerosols. Thus indoor particle concentrations are important determinants of radon progeny behavior.

Our present research efforts have focussed on 1) investigations to characterize the physical and chemical makeup of particles emitted by indoor sources, 2) further experiments to study the behavior of radon progeny under a variety of indoor environmental conditions, and 3) additional studies to model radon progeny behavior.

Accomplishments During FY 1985

Chemical and Physical Characteristics of Indoor Particles

In a previous collaboration with researchers at the California Department of Health Services, we began to investigate the chemical and physical nature of particles emitted from two sources, cigarette smoke and natural gas combustion. During the past year, this effort has been extended to several additional sources of particles, including cooking, an unvented kerosene heater, and several aerosol spray products.[19,20] One goal of this research has been to use the qualitative results to compare emissions from each source and to determine whether there are combinations of physical and chemical characteristics that can be used to identify individual particle sources uniquely.

Experiments were conducted in a 36-m^3 room within the Indoor Air Quality Research House for five of the six emission sources studied, including tobacco combustion, natural gas stove, cooking (frying hamburger), and two aerosol spray consumer products. Due to the high heat output of the sixth particle source, an unvented kerosene heater, experiments with this source were conducted in a 27-m^3 chamber which incorporated two copper solar collector panels to help absorb radiant energy from the heater. The chamber walls are uninsulated plasterboard, through which additional heat loss occurred, and the floor of this chamber is concrete, which provided an additional heat sink.

Individual sources were operated periodically for four to eight hours in order to provide the sampling quantities needed. Some of the mutagenicity experiments extended over two days to ensure that sufficient sample mass was available. A number of sampling procedures were used for both off-line and real-time measurements. The measurements, sampling procedures and analytic methods are summarized in Table 6. The real-time particle size analysis instrumentation, computer control and data logging have been described elsewhere.[21] In order to minimize infiltration of pollutants into the chambers due to the sampling flows, make-up air was supplied through a HEPA-filter and orifice-plate system at 230 to 300 L min^{-1}. Mixing fans mounted on the wall of the chambers with fan axes parallel to the walls were operated continuously to ensure that well-mixed conditions were maintained.

Tobacco smoke was generated using a cigarette smoking machine, modified to include an extinguishing mechanism. Emissions from natural gas combustion were produced by operating two burners of a cooking stove for 15 min. every half hour. Emissions from cooking were generated by frying 1.1 kg of hamburger in two cast-iron skillets for a 10 min. period, followed by a seven min. cooking period 3.5 hours later. Thus the total period of natural gas stove operation for cooking was a small fraction of that used to characterize emissions from the stove alone. The aerosol spray products, an

Table 6. Physical and chemical characterization measurements and methods.

Parameter Measured	Sampling Medium	Sampling Rate (L min^{-1})	Analytical Method
Airborne particle concentration	Continuous flow sampling	5	Condensation nucleus counter
Particle size distribution	Continuous flow sampling	5	Optical particle counter; Differential mobility analyzer
PAH composition of airborne particles	Teflon filter	8	High-pressure liquid chromatography
Elemental composition of airborne particles	Teflon filter	10	Energy dispersive X-ray spectrometry
Mutagenicity of airborne particles	Fiber glass	45	Modified Ames assay
Volatile organic compounds	Tenax tubes 50 mg per tube	0.5	gas chromatography/ mass spectrometry
Mutagenicity of gaseous compounds	Directly exposed *Salmonella* plates	0.5	Modified Ames assay

antiperspirant spray and a furniture dusting and polishing spray, were released remotely on a periodic basis until the spray cans were exhausted. Finally, emissions from the unvented kerosene heater were generated by a blue-flame, radiant model. This device was operated for four hour-on, hour-off cycles using a manual start-up, shut-down procedure, requiring entry into the chamber.

Real-time particle size distribution data are shown in Fig. 10 for each source. These measurements were made during or just after particle source operation. Figure 10a shows data for the experiment in which no source was operated but the chamber was operated normally, including supply of filtered air. The peak of the particle size distribution is ~0.2 μm, typical of outdoor particles that might have infiltrated into the chamber. Natural gas combustion, shown in Fig. 10b, produced large numbers of very small particles with diameters <0.01 μm. On the other hand, cooking hamburger produced significantly larger particles, as shown in Fig. 10c. Tobacco combustion resulted in the particle size distribution shown in Fig. 10d, with the peak near 0.15 μm. Particles from operation of the kerosene heater are peaked at very small sizes, ~0.02 μm (Fig. 10e), while the aerosol spray products yielded much larger particles with broad size distributions, as shown in Figs. 10f and 10g.

The results of the chemical and mutagenic tests are summarized in Table 7. The mutagenic analyses were done using a modified Ames test procedure. Particle samples were collected on filters, then extracted and tested using a microsuspension assay technique. In the case of particles, the *Salmonella typhimurium* strain TA98 was used, both with (w/ S9) and without (w/o S9) rat liver extract. A mutagenic response in the former case (w/ S9) indicates the presence of indirect-acting mutagens, whose metabolites are mutagenic, while in the later case (w/o S9), a mutagenic response represents the presence of direct-acting mutagens. In addition particle testing was also done using strain TA98NR, which is deficient in nitroreductase activity. Thus, a finding of mutagenic activity with TA98 but not TA98NR suggests the presence of nitroaromatic compounds. A complete discussion is provided in Ref. 20. Analysis of vapor phase mutagens was done by exposing the *Salmonella* plates directly to polluted air by drawing an airstream from the chamber and passing it through a dessicator-jar containing the plates. Strains TA98 and TA100 were used for these analyses. Particle phase mutagenicity results are shown in Fig. 11.

Since these experiments were conducted to provide sufficient amounts of sample, and not necessarily to replicate normal use patterns, the resulting

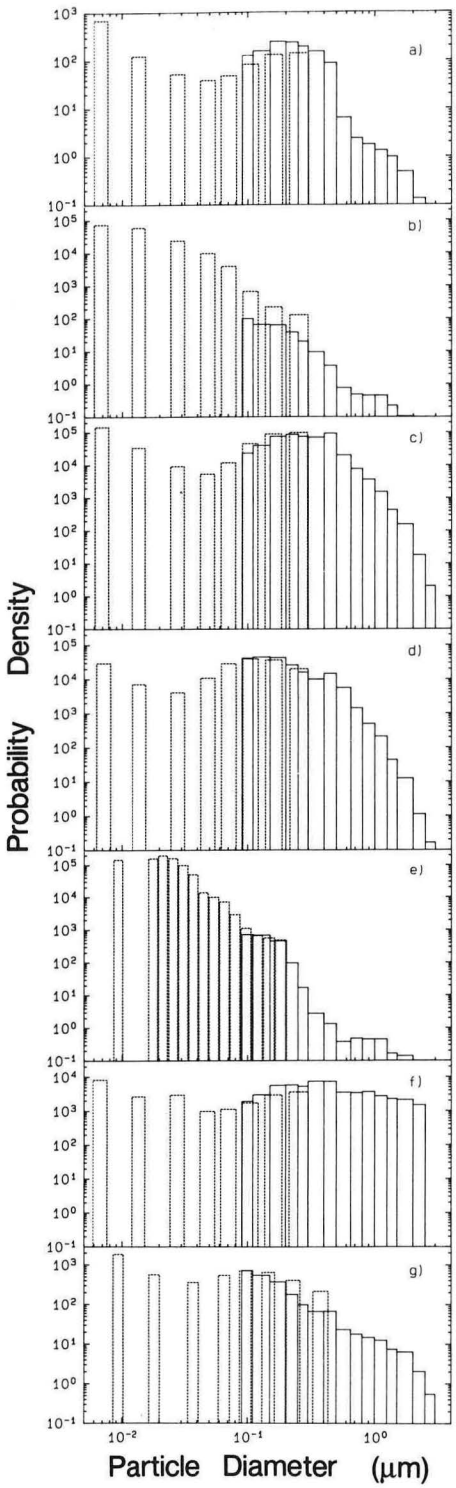

Figure 10. Particle size distribution data from the real-time measurement of particles from a) no source, b) natural-gas fired stove, c) frying hamburger, d) tobacco combustion, e) kerosene heater, f) antiperspirant aerosol spray, and f) dusting/polishing aerosol spray. (XBL 856-2716)

data aren't suitable for direct intercomparisons or for source strength determinations. Nevertheless, these data indicate that there are variations in the chemical and physical characteristics of particle emissions from different indoor sources that might provide unique source identifiers. It is also interesting to note that all the combustion sources tested contribute to mutagenicity, as measured by at least one of the modified Ames assays.

Radon Progeny Behavior and Air Circulation

The effects of air circulation on radon progeny concentrations under various initial particle concentrations have been investigated in a room-size chamber. In previous studies, air circulation alone produced only a small reduction in progeny concentrations in some experiments,[22] while in others larger reductions in airborne progeny concentrations have reported.[23]

The experiments were conducted in a 36-m^3 chamber at the Indoor Air Quality Research House. Real-time instrumentation was utilized to monitor particle concentration, particle size distributions, and airborne radon and radon progeny concentrations. Data logging and experimental control are provided by two dedicated computer systems. This instrumentation and control system are described elsewhere.[21,22] In addition to the airborne measurements, an array of CR-39 nuclear track detectors was placed on the walls, floor and ceiling of the test space in order to measure the deposition of radon progeny with and without air circulation and under differing conditions of particle concentration. Track detectors were also placed on both sides of the fan blades of the fan used for air circulation in the room. The results of the airborne measurements are reported here.

The experiments were conducted at three particle concentrations. In the first experiment, particle concentrations were initially reduced to less than 10 particles cm^{-3} using a portable HEPA-filter system placed in the room. After turning the filter system off, radon gas was injected into the test space to give an initial radon concentration $\sim$15000 Bq m^{-3}. Particle concentrations remained between 100 and 300 particles cm^{-3} during the course of the experiment. Initially the air circulation fan remained off for a five hour period, followed by a four-hour on period, and finally a five to six hour off period. The CR-39 detectors were replaced at the beginning of each time period. This protocol was used for all three experiments.

Table 7. Comparison of emission characteristics from several indoor sources.

Source	Elemental Composition	PAH[a]	Volatile Compounds[b]		Mutagenicity[c]
Gas stove	Si,S	—[d]	—	Particles:	TA98 (w/ and w/o S9)
					TA98NR (w/ and w/o S9)
				Vapors:	TA100 (w/ and w/o S9)
Frying hamburger	S,Cl	—	aldehydes,	Particles:	toxic to assay
			ketones,	Vapors:	TA98 (w/ S9)
			amines		TA100 (w/ and w/o S9)
Cigarette smoke	S,Cl,K	BKF,	alcohols,	Particles:	TA98 (w/ and w/o S9)
		BAP,	ketones		TA98NR (w/ and w/o S9)
		BGP,	halides	Vapors:	TA98 (w/ and w/o S9)
					TA100 (w/ and w/o S9)
Kerosene heater	Si,S,Cr	BKF,	—	Particles:	TA98 (w/ and w/o S9)
		BAP			TA98NR (w/ and w/o S9)
				Vapors:	TA100 (w/ S9)
Antiperspirant spray	Mg, Al, Si, Cl	—	alcohols, ketones, aldehydes		nonmutagenic
Dusting/Polishing spray	—	—	alcohol ketones, halides		nonmutagenic

[a]Polycyclic aromatic hydrocarbons: BKF: benzo(k)fluoranthene, BAP: benzo(a)pyrene, BGP: benzo(ghi)perylene.

[b]Excluding C_2–C_{12} alkanes and aromatic compounds, which were present in all samples.

[c]For particles, mutagenic tests are considered to be positive if the number of revertants measured in the sample is greater than a factor of two larger than the spontaneous revertants on a control plate. For the vapor phase, the tests are considered to be positive if the revertants measured in the sample are more than a factor of two larger than the spontaneous revertants on the control plates, *and* if the revertants on the sample also exceed by a factor of two the number of revertants measured simultaneously in air outside the test chamber.

[d]None detected.

The second experiment was conducted at moderate particle concentrations, averaging between 9000 and 20000 particles cm^{-3}. In this case, the gas range in the chamber was used periodically to add particles to the chamber air to compensate for the slow decay in particle concentrations. For the third experiment, particle concentrations were maintained between ~80000 to above 100000 particles cm^{-3} using tobacco combustion in a manually-operated cigarette smoking machine.

The effects of air circulation on radon progeny concentrations were seen quite clearly for the low and medium particle concentration experiments, while for the experiment done with high particle concentration no effect with air circulation was observed. At lower particle concentrations, a larger portion of the radon progeny remain unattached, and thus have a higher diffusivity than progeny attached to particles in the chamber air. The deposition rates of the unattached species are therefore much higher, and when the forced circulation fan is operating, the deposition rates are enhanced. In the case of high particle concentrations, almost all the progeny are attached to particles, reducing their deposition rate and concomitantly, reducing the effect of air circulation.

Planned Activities for FY 1986

Investigations of radon progeny behavior under a number of indoor environmental conditions will continue. Methods for direct measurement of unattached progeny will be improved. The experimental data will be compared with existing theoretical predictions of radon progeny behavior indoors.

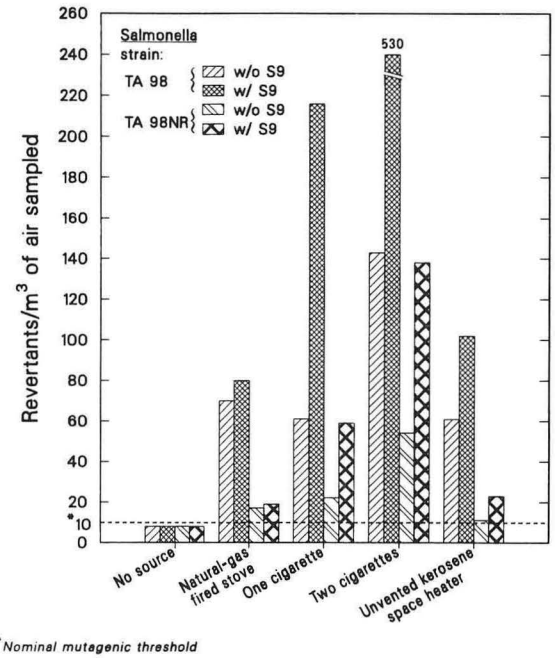

Figure 11. Particle-phase mutagenicity data from three indoor particle sources. The two aerosol sprays did not show any particle-phase mutagenicity and the particle extract from hamburger frying was toxic to the test bacteria; thus no mutagenicity assessment could be made. (XCG 855-266)

INDOOR AIR QUALITY CONTROL TECHNIQUES

Research on IAQ Control Techniques during FY 1985 focussed primarily on the following two topics: 1) multi-tracer measurement of ventilation rates, ages of air, and ventilation efficiencies in large mechanically-ventilated buildings, and 2) residential exhaust ventilation with heat-pump heat recovery. Our accomplishments during FY 1985 on these two topics and plans for FY 1986 are described below. In addition to these efforts, we collaborated with staff of the Radon and Field Survey Projects to plan investigations of radon mitigation techniques in twelve Pacific-Northwest houses. The results of these radon mitigation studies will be described in the FY 1986 Annual Report.

Accomplishments During FY 1985

Introduction: The efficiency of a ventilation process in removing indoor-generated pollutants and supplying or removing heat and moisture to and from a building, depends on numerous factors including: 1) the nominal air exchange rate; 2) the overall pattern of air flow between supply diffusers and exhaust registers; and 3) the spatial pattern (e.g., evenness) of outside air distribution throughout the building.

The nominal air exchange rate is simply the rate at which outside air enters the building divided by the indoor volume. A nominal time constant or turnover time can be computed by taking the inverse of the nominal air exchange rate.

The second factor, the overall airflow pattern, can, in theory, vary from one extreme, in which much of the air exiting the supply diffusers rapidly short circuits to the exhaust registers, to the other extreme, in which the flow between supply and exhaust approaches a piston-type displacement flow. Between these extremes is perfect mixing of the indoor air. In general, the efficiency of the ventilation process increases as short circuiting is reduced. The "nominal ventilation efficiency" is a performance parameter that characterizes the overall airflow pattern. The most unambiguous interpretation of this parameter is provided by an application of age distribution theory to ventilated buildings.[24] In this theory, the age of a parcel of air is the elapsed time since that parcel entered the building, and the nominal ventilation efficiency equals the turnover time (described above) divided by the mean age of all air parcels within the building. The nominal ventilation efficiency has a value of zero with complete short circuiting, a value of unity with complete mixing, and a theoretical upper limit of two for a perfect displacement flow.

The third factor, the spatial pattern of outside air distribution throughout the building, is indicated by the "local ventilation efficiency" which equals the turnover time, i.e., the age of all air within the building if the air were perfectly mixed, divided by the age of air at a specific point of interest. By comparing local ventilation efficiencies measured at different locations, the evenness of ventilation can be assessed.

Each of the performance parameters described above can be measured using transient tracer gas techniques. Two common transient techniques, the tracer decay and the tracer step up, are described in Refs. 24 and 25. Equations for analyzing the tracer gas data are also provided in these two references. The data analysis relies primarily on integrations of tracer gas concentrations, and the products of concentrations and time, with respect to time.

Experimental System

During FY 1985, we worked on development and checkout of a highly flexible experimental sys-

tem suitable for measuring ventilation rates, ages of air, and ventilation efficiencies in large buildings. This multi-tracer system will be used to study ventilation system performance and to assess the impacts of changes to ventilation systems. Some of these future studies will be conducted as part of more comprehensive investigations of ventilation and indoor air quality in large buildings.

The experimental system consists of six tracer gases and instrumentation for measuring tracer gas concentrations, stand-alone tracer gas injection systems, and stand-alone samplers. In buildings with six or fewer ventilation systems, the step up or constant injection rate technique[25] can be employed by injecting a different tracer gas into each ventilation system. The injection of each tracer gas will be controlled by a distinct stand-alone injection system placed in the building near the point of injection. The stand-alone samplers will also be placed at various locations within the building near to points where the time-history of tracer gas concentration is required. These samplers collect and store small air samples taken at different times during an experiment (e.g., every 15 minutes during a step up experiment). The concentration of each tracer gas in the samples can then be determined in the laboratory after completion of the experiment.

After preliminary experimentation with a number of potential tracers, a group of five halocarbons plus sulfur hexafluoride were selected. The chemical formula, chemical name, molecular weight, and boiling point of each tracer are provided in Table 8. In experiments, the peak concentrations of SF_6 and R-12B1 will be 200 ppb, and the peak concentration of the remaining tracers will be 1,000 ppb. Tracer gas concentrations are measured using a gas chromatograph with an electron capture detector and associated instrumentation.[25] Figure 12 shows a typical chromatogram and information for characterizing each peak.

To meet sampling requirements, we are designing a programmable stand-alone sampler that will collect small air samples for analysis at a later time in the laboratory. A preliminary design for a highly-automated and flexible sampler is described in Ref. 25.

The final component of the experimental system is a simple, stand-alone tracer injection system that is well-suited for the step-up tracer technique. The major components are depicted in Fig. 13. Experiments indicate that this system injects tracer at a highly stable rate (i.e., 2% maximum variation in injection rate during an experiment).

Results of Tests of System Performances: Two tests of the system, excluding the sampler, have been completed. Figure 14 illustrates the local ages of air measured simultaneously with each tracer gas in the well-mixed test space of a research house using both a tracer step-up and a tracer decay. Ideally, the data from each tracer gas should yield the same local age of air; the step-up and decay should give the same result; and all the ages of air calculated from tracer

Table 8. Selected properties of gaseous tracers.

Refrigerant Number	Chemical Name	Chemical Formula	Molecular Weight	Boiling Point (°C)
—	Sulfur Hexafluoride	SF_6	146.1	−64
13B1	Bromotri-fluoromethane	$CBrF_3$	148.9	−58
115	Chloropenta-fluoroethane	$CClF_2CF_3$	154.5	−39
12	Dichlorodi-fluoromethane	CCl_2F_2	120.9	−30
12B1	Bromochlorodi-fluoromethane	$CBrClF_2$	165.4	−4
114	1,2-dichloro-tetrafluoro-ethane	$CClF_2CClF_2$	170.9	+4

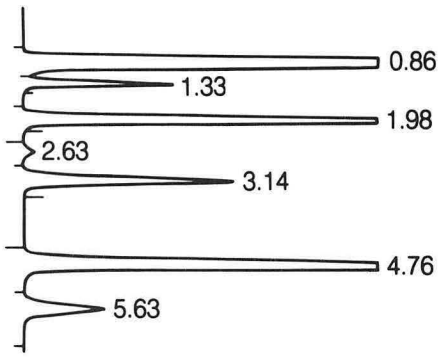

Retention Time (min)	Area	Component	Conc. (ppb)
0.86	1.9700E+07	Air	—
1.33	529140	SF_6	5
1.98	3098700	R–13B1	50
2.63	74651	R–115	50
3.14	1426800	R–12	50
4.76	7478000	R–12B1	50
5.63	657790	R–114	50

Figure 12. Sample chromatogram and table of data for characterization of peaks. (XBL 8512-5131)

gas data should equal the reference measurement of age of air (i.e., the inverse of the nominal air exchange rate) made with an orifice plate flow meter. The test results indicate a maximum deviation between tracer gases of 14% and a maximum deviation from the reference measurement of 17%.

The second test of system performance was conducted in an office building served by a single ventilation system. Both local and nominal ages of air

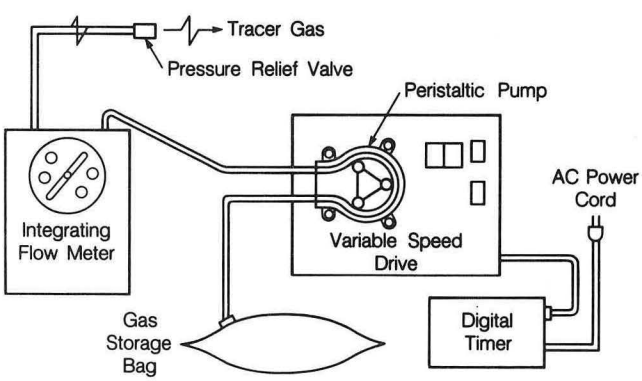

Figure 13. Schematic diagram of tracer gas injection system. (XBL 858-9898)

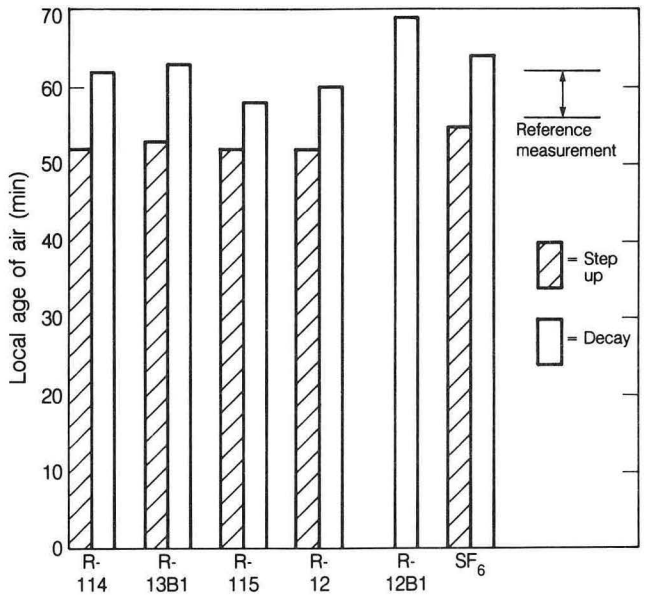

Figure 14. Local age of air based on tracer gas and reference measurements in the well-mixed test space of a research house. (XBL 8512-5130)

and ventilation efficiencies were computed from the data. The correspondence of the results from four of the tracer gases (R-13B1, R-115, R-12, and R-114) is quite good; however, the SF_6 and R-12B1 tracers yielded substantially different results especially for the mean age of air and nominal ventilation efficiency, which are difficult to measure accurately. We believe that the discrepancies with these two tracer gases may be due, in large part, to inaccuracy in our analysis of tracer gas concentrations and improved accuracy should be possible in the future.

Our FY 1985 efforts can be summarized as follows: 1) six tracer gases were selected and a suitable measurement technique was developed; 2) a stand-alone injection system was designed, fabricated, and tested (this system performs well); 3) a prototype stand-alone sampler was fabricated and tested (further evaluations are required); and 4) two tests of system performance (excluding the sampler) were completed with generally positive results.

Residential Exhaust Ventilation With Heat Recovery

Introduction: Controlled mechanical ventilation of residences is superior to uncontrolled ventilation from both indoor air quality and energy use perspectives. Controlled ventilation ensures a constant supply of fresh air to the building, permits convenient control of the ventilation rate, and allows air to be exhausted from areas with strong indoor pollutant sources. In addition, recovery of energy from the

exhaust air is possible when the ventilation is provided mechanically.

Balanced mechanical ventilation with heat recovery in an air-to-air heat exchanger is the only method available in the United States for providing controlled ventilation with heat recovery to residences. Another method that is being used in Europe is unbalanced, exhaust ventilation with heat recovery by a heat pump (see Fig. 15). With this latter type of ventilation system, air is exhausted mechanically from the residence but is not supplied mechanically. As a result, the building is depressurized slightly and outdoor air is drawn in through the building envelope. In a "leaky" building, the supply air enters the building through cracks and other incidental openings. In a tightly- sealed building, vent or slot systems are generally installed through the walls at appropriate locations to allow entry of the outdoor air.

Heat pumps designed to recover energy from an exhaust airstream are referred to as exhaust-air heat pumps. These heat pumps are ideally suited for heating the domestic hot water and can be used exclusively for this purpose. However, the amount of heat that can be extracted from the exhaust airstream by a heat pump is typically more than is required to meet hot water needs. Consequently, to maximize operation of the exhaust-air heat pump, a small fan coil can be utilized to supply heat to the indoor space from the hot water tank.

Packaged units for exhaust ventilation with heat recovery are available in Scandinavia. In addition, both a U.S. and Canadian manufacturer plan to market packaged units in the near future. Although this technique of ventilation with heat recovery appears promising, very few studies of system performance have been completed in Scandinavia and virtually no studies have been completed in the U.S. An examination of the suitability of this ventilation technology for U.S. housing is one of the efforts that was initiated in FY 1985.

FY 1985 Progress in Exhaust Ventilation Research: During FY 1985, we completed modifications to the existing computer model "TRNSYS" as required to simulate residential exhaust ventilation with heat recovery, and for purposes of comparison, to simulate balanced ventilation with air-to-air heat recovery and natural infiltration. The modified "TRNSYS" model simulates building loads, heating and cooling system operation, window opening, air infiltration and mechanical ventilation, hot water demands and storage, and operation of exhaust-air heat pumps, fan coils, and air-to-air heat exchangers.

An example of the results generated with the computer model is provided in Fig. 16, which shows the predicted total electricity usage in a highly-insulated, all-electric house located in Portland and ventilated by the different methods described above. The results indicate that exhaust ventilation with heat recovery is more energy efficient in this situation than natural ventilation or balanced ventilation with air-to-air heat recovery. The model also indicates that the ventilation rate is most stable in the case of exhaust ventilation.

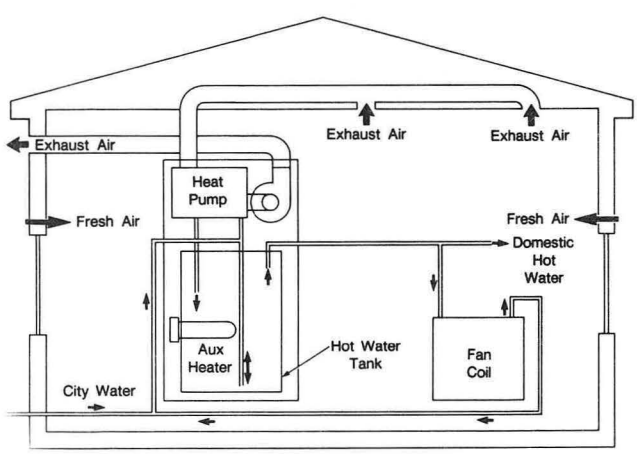

Figure 15. Schematic diagram of residential exhaust ventilation with heat pump heat recovery. (XBL 861-36)

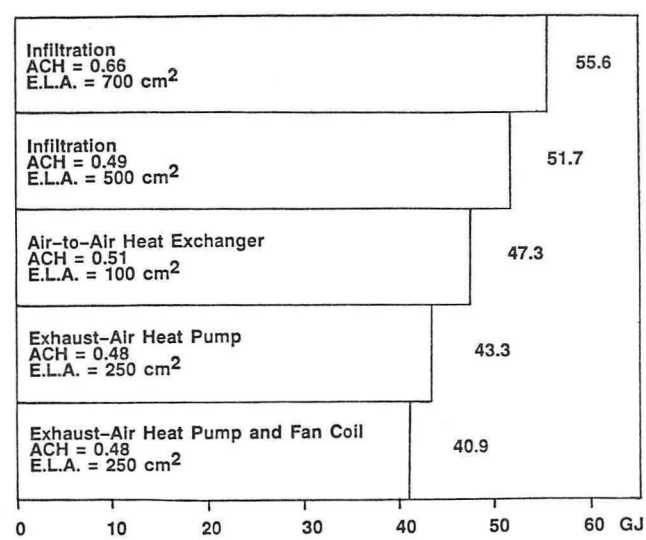

Figure 16. Predicted total electricity usage in a Portland-area, all-electric, 125 m^2 (1345 ft^2), highly insulated house (R38 ceiling, R28.5 walls, R31 floor) with four occupants and a total daily water demand of 300 kg (80 gal). The ACH value is an effective average air exchange rate for December 1 through February 28. E.L.A. = the effective leakage area of the building envelope. (XBL 861-37)

In addition to the computer modeling effort, during FY 1985 we initiated modifications to our experimental facility as required to study exhaust ventilation with heat recovery. Laboratory and field studies of this technology are required because of the highly limited amount of data on system performance that is available at the current time.

Planned Activities for FY 1986

Our research on the usage of multiple tracer gases to measure air exchange rates, ages of air, and ventilation efficiencies will continue during FY 1986. Major objectives are to complete development of the experimental system, to conduct additional tests as required to validate system performance, and to study ventilation in selected buildings.

Investigations of exhaust ventilation with heat recovery will also be continued in FY 1986. The output of the modified TRNSYS model and the results of a cost/benefit analysis will be documented in a publication. A numerical model will be developed and utilized to investigate the impact of exhaust ventilation on radon entry into residences. Finally, laboratory investigations of exhaust ventilation/heat recovery systems will be undertaken.

FIELD SURVEYS OF INDOOR AIR QUALITY

Three field studies examining indoor air quality funded by the Bonneville Power Administration (BPA) were in progress in FY 1985. The studies included (1) a comparison of new energy-efficient homes with new standard construction homes, (2) monitoring of existing single family dwellings undergoing weatherization to reduce energy consumption, and (3) a survey of 38 commercial and institutional buildings. All buildings were located in and around the Oregon cities of Portland and Salem; Spokane, Washington; and Coeur D'Alene, Idaho. Because of regulatory pressures from the Pacific Northwest Electric Power Planning Act, BPA instituted recommendations for energy conservation that have included methods for reducing the amount of outside air entering buildings. The studies examine whether concentrations of some indoor pollutants increase in response to the reduced ventilation and cause greater health-related risks.

Accomplishments During FY 1985

New Energy-Efficient Homes

Model Conservation Standards (MCS) for the construction of new energy-efficient houses include specifications calling for air infiltration packages leading to infiltration rates as low as 0.1 ach. These homes have air-to-air heat exchangers installed to raise the ventilation above 0.5 ach. Twenty-nine MCS homes were monitored along with 32 new homes, built according to standard construction practices, that served as controls. The goals of the study include comparing pollutant concentrations and installed ventilation rates in the two groups of houses along with an evaluation of pollutant source strengths.

Beginning in February, 1985 technicians visited each house to collect data on the structural characteristics, conduct a leakage area measurement with a blower door, and deploy passive pollutant and ventilation monitors. Passive samplers for formaldehyde (HCHO), water vapor (H_2O), and nitrogen dioxide (NO_2) were placed at two to five interior locations at each house and one outdoor location for a period of approximately seven days. These devices sample air by establishing a pollutant selective concentration gradient within a tube of known dimensions. The pollutant diffuses to and is collected on an adsorbent or chemically treated disc(s) at the capped end.[26–28] Upon analysis they provide a measure of the average pollutant concentrations in the sampled space during the period they were uncapped. Type SF Track-Etch passive radon (Rn) monitors were placed both with the other pollutant samplers and also in crawlspace and basement locations. The radon samplers were exposed for periods of approximately three months. Ventilation measurements were made with a passive perfluorocarbon tracer (PFT) injection and sampling system developed at Brookhaven National Laboratory to provide a time averaged ventilation rate during pollutant sampling.[29] Two sets were used: one for the seven day sampling period, the other for the longer radon sampling period. During the seven day period, occupants were asked to complete a daily log of house activities that would affect air quality.

Indoor water vapor concentrations were quite uniform in all houses regardless of the type of house

or the geographical region (see Table 9). Since outdoor concentrations were quite different between the regions, some other explanation such as similarity of indoor sources or buffering by house materials may account for the uniformity. Because of the small sample size, the observed differences in radon concentration between MCS and control homes are not statistically significant. Indoor radon concentrations generally are dominated by source variations rather than ventilation rate variations. As a result, the source strength differences overwhelm any differences in ventilation between the two groups of houses. The results for formaldehyde show an unusual regional variation, with all Spokane area homes having a geometric mean (median) of 60 ppb and all Portland area homes a geometric mean of 93 ppb. These differences are statistically significant at the 1% level. However, the concentration differences between MCS and control homes are *not* statistically different. The regional variations could be due to differences in local building materials or the amount of particle board and plywood used. Concentrations were above 100 ppb in 18 homes and above 200 ppb in three homes (the highest being 343 ppb). These levels exceed guidelines of 100 ppb promulgated by the EPA and ASHRAE 62-81 and may cause reactions in moderately sensitive individuals. Nitrogen dioxide was not a problem inside these homes since only one house contained a combustion heating appliance. Indoor levels were usually below those measured outdoors. The normalized leakage area, specific leakage area (SLA), shows that the MCS homes generally are tighter than the control group. Because of an extreme outlier in the Portland MCS group (14.99 cm^2m^{-2}), a nonparametric rank statistical test was used and determined that the differences in SLA between *all* groupings was significant at the 1% level. Once again a regional difference is obvious with the Spokane area homes being tighter than their Portland area counterparts. This is expected since

Table 9. New home data summary.

	Spokane			Portland			All Homes	
	MCS	Control	Total	MCS	Control	Total	MCS	Control
Number of Homes:	12	14	26	17	18	35	29	32
Radon ($pCiL^{-1}$):								
Mean	4.1	4.7	4.4	1.8	1.2	1.4	2.7	2.8
GM	1.9	3.5	2.6	1.3	1.0	1.1	1.5	1.7
GSD	3.8	2.2	3.0	2.2	2.2	2.1	2.8	2.8
Outside	—	—	0.5	—	—	0.5	—	—
Water Vapor (gkg^{-1}):								
Mean	6.29	6.39	6.34	6.81	6.80	6.80	6.59	6.62
SD	1.00	1.32	1.16	1.16	0.77	0.97	1.11	1.05
Outside	—	—	3.72	—	—	5.54	—	—
Nitrogen Dioxide (ppb):								
highest-indoor	—	—	7	—	—	7	7 (all)	
outdoor	—	—	22	—	—	19	22 (all)	
In ÷ Out (>10 ppb out)	—	—	0.22	—	—	0.24	0.23	0.24
Formaldehyde (ppb):								
Mean	64	65	65	120	98	109	97	84
GM	60	59	60	103	84	93	83	72
GSD	1.5	1.6	1.5	1.7	1.8	1.8	1.7	1.8
200 ppb> # > 100 ppb	0	1	1	7	7	14	7	8
# > 200 ppb	0	0	1	2	1	3	2	1
Specific Leakage Area (cm^2m^{-2}):								
Mean	1.26	3.13	2.26	3.60	4.81	4.22	2.63	4.08
SD	0.49	1.34	1.39	3.14	1.41	2.45	2.67	1.60

the Spokane area experiences an average 6835 heating degree days while Portland accumulates only 4792 heating degree days annually (65°F base). Therefore, in order to meet the MCS guidelines of a certain ventilation rate, homes in Spokane must be tighter. The tightness of the houses in this study can be compared with typical SLA values of four to ten for conventional housing in the United States. Note that the measured leakage areas do not account for the additional ventilation in the MCS homes supplied by the air-to-air heat exchangers. At this point the data indicate that pollutant levels are very similar in the MCS and control homes. This tends to support the hypothesis that while indoor air quality problems may be exacerbated by low ventilation rates, problems do not occur without a robust pollutant source. However, we are waiting on the analysis of the PFT ventilation samplers to complete the investigation of the effect of ventilation in indoor pollutant levels.

Existing Homes

From October 1984 through January 1985 one hundred existing homes built prior to 1980 were tested and screened for HCHO, H_2O, and Rn using mailed passive samplers (described above). Sixteen other homes were screened only for radon during a 30 minute visit by a technician using a continuous radon monitor. Forty eight of these homes with measurable levels of HCHO or Rn were then selected for more intensive monitoring to evaluate the effects of house tightening weatherization retrofits on the concentrations of these indoor air pollutants.

In the Phase I screening sample, 45 homes were located in the Spokane, WA–Coeur D'Alene, ID area and 71 homes were located north of Portland in Vancouver, WA. The use of mailed passive samplers was both effective and economical. Only three percent of all samplers were rendered useless; the total cost of monitoring each house was approximately $150. The majority of these homes had pollutant levels below most currently recommended guidelines and standards. Nitrogen dioxide concentrations averaged 6 ppb, and ranged from below detection (5 ppb) to 45 ppb, with approximately 98% below 16 ppb. Few homes had combustion appliances that would elevate these levels. Only one newly remodeled home had HCHO concentrations above 100 ppb (136 ppb), while 98% of the homes were below 80 ppb and the total group had a mean of 36 ppb. A plot of HCHO concentration vs. building age for all new and existing homes (Fig. 17) shows that levels tend to be lower in older homes.

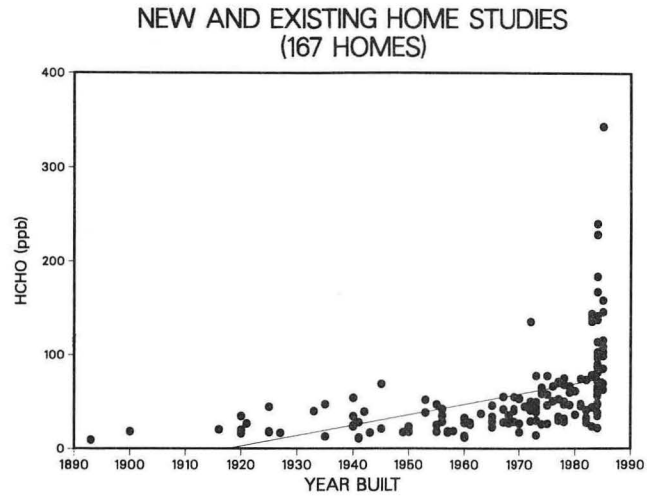

Figure 17. Indoor formaldehyde concentrations for 167 homes in the Pacific Northwest as a function of the age of the structures. Higher concentrations in newer homes could be due to a combination of greater use of UF-bonded wood products, higher outgassing rates for younger materials, and lower ventilation rates. (XBL 862-371)

Many factors could contribute to this: off-gassing of HCHO over time, less particle board and plywood in older buildings, and greater air leakage in older homes. The mean water vapor concentration was 6.15 gkg^{-1}, very similar to that measured in the new home study. Radon, however, appears to be a pollutant of concern in the Spokane River Valley area of Washington and Rathdrum Prairie of Idaho. While the average for a compilation of 552 U.S. residences is 1.6 $pCiL^{-1}$ and for 267 regional BPA employee homes is 1.4 $pCiL^{-1}$, the average heating season concentration for 46 new and existing homes in this area is 13.3 $pCiL^{-1}$.[15,30] Approximately 43% of these residences had concentrations above 8 $pCiL^{-1}$, the National Council on Radiation Protection and Measurements guideline. Concentrations were monitored in 14 of the 46 homes over the summer of 1985 using passive samplers and were observed to have declined by factors of up to 16 from heating season values. An examination of soils, domestic water supplies, and building materials strongly suggests that the high concentrations are due to the local subsurface soil composition and structure.

The more intensive monitoring of the 48 homes to be weatherized in Phase II began in December 1984. In each home, equipment was installed to monitor temperatures, windspeed and direction, and radon concentrations continuously. Passive monitors for pollutants and ventilation were also deployed along with instruments for making time-weighted average measurements of carbon monoxide

(CO) and respirable suspended particles (RSP). This equipment was operated for a 7–10 day period before and after each stage of weatherization, which could have included wall insulation and "house doctoring" along with caulking, weatherstripping and storm windows. Analysis of all data from this study continues and also waits on PFT ventilation rate measurements, so that effects of weatherization on infiltration and pollutant concentrations can be evaluated.

Figure 18 summarizes the preliminary findings of a separate four week controlled study of the interactive effects of air leakage reduction and conductive heat loss reduction on the pollutant levels generated by an unvented combustion heating source. Two identical units of a duplex in Oregon were used: one received staged weatherization of house-tightening followed by insulation, while the other was an unweatherized control. The figure shows the potential for reduced indoor air pollutant levels in homes with unvented combustion appliances resulting from increased R-values as a result of insulating during weatherization.

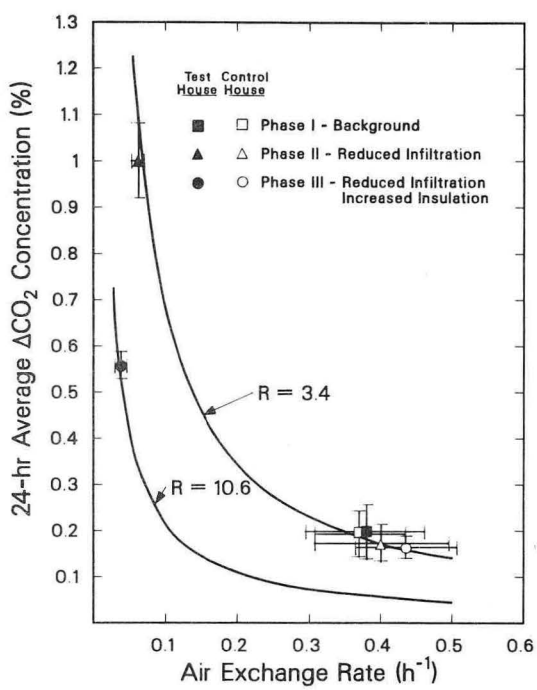

Figure 18. Effect of reduced infiltration house and reduced conductive losses resulting from house weatherization on indoor CO_2 concentrations in two dwellings with propane-fire space heaters. House tightening increases CO_2 concentrations while insulation retrofits reduces heating loads and therefore reduces CO_2 concentrations. (XCG 8411-13443)

Commercial and Institutional Buildings

A survey of 38 commercial and institutional buildings involved monitoring of ventilation rates and indoor air pollutant concentrations as detailed on Table 10. The objectives were to (1) inventory these parameters in non-residential, non-industrial facilities, (2) furnish data to assist in establishing energy conservation and ventilation guidelines and, (3) examine relationships between indoor air quality and ventilation rates. Field monitoring began in January, 1984 and continued into April, 1985. Two buildings were monitored twice for a total of 40 building assessments. Buildings ranged in age from 6 months to 90 years, in size from 9,300 to 369,000 sq. ft., and in occupancy from 25 to 2500 people. From 6 to 20 pollutant sampling sites were located in each building during the two week (10 working day) monitoring period. Sampling was started at the beginning of each working day and stopped at the end of occupancy for an accumulated minimum of 75 hours. Selected RSP filters were analyzed for up to 16 polycyclic aromatic hydrocarbons (PAH) including benzo(a)pyrene (BaP). Carbon dioxide (CO_2) was monitored at up to two locations for a one day period, while CO was sampled at up to seven locations for one 7–10 hour day. Twice daily observations of the ventilation system were recorded for use during a later tracer decay ventilation test. Data were also collected that describe building construction, materials, occupancy, smoking policies, and activities. Ventilation rates were measured in all buildings with a one time tracer dilution and decay test conducted over one 12-hour period during unoccupied hours. The ventilation systems were set up to mimic the conditions of the two week pollutant monitoring period, while a centrally located gas chromatograph with an electron capture detector monitored the decay of sulfur hexafluoride (SF_6) at up to nine building locations. The passive PFT system was also used to measure ventilation rates in 27 buildings. Samplers from this system were deployed along with the passive pollutant samplers for a three day period. Data from the analysis of these samplers are not yet available.

Table 11 presents a building average summary of all data collected. With the exception of RSP, most pollutant levels were quite low and often below the detection limits of our equipment. Formaldehyde reached the highest building average of 56 ppb in one six month old library. Individual site measurements ranged up to 75 ppb. Nitrogen dioxide averaged 18.1 ppb in all buildings and correlated most closely with outdoor concentrations whose source was primarily vehicular exhaust. Water vapor averaged 9.8 gkg^{-1} in one building, a level that could

Table 10. Air sampling instrumentation and analytical techniques.

Pollutant	Sampling Device	Analytical Techniques
HCHO	LBL Passive Diffusion Sampler	Spectrophotometric
H_2O	LBL Passive Diffusion Sampler	Gravimetric
Rn	Terradex Corp. Type SF Track Etch Sampler	Count number of alpha tracks on film, performed by Terradex Corp.
NO_2	Palmes' Passive Diffusion Sampler	Spectrophotometric
RSP	LBL Flow-Controlled Filtration Device with 3μ cut-point cyclone	Gravimetric
PAH	Same as RSP	HPLC, performed by McKesson Laboratory
CO_2	Horiba Model #APBA-210 CO_2 Detector	Non-dispersive Infrared Direct Reading
CO	LBL Constant-Flow Gas Collection Bag	General Electric Model 15EC53C01 Electrochemical Analyzer
Tracer	**Ventilation Measurement Device**	**Analytical Technique**
SF_6	Baseline Model 1030A Gas Chromatograph, Valco Electron Capture Detector Mod. 140B	Continuous Monitoring of Tracer Decay
Multiple	Source: Permeation Tubes	Brookhaven National Lab.
Perfluoro-carbons	Sampler: Passive Diffusion Adsorption Tubes	AIM System. Thermal Desorption and ECD/GC Analysis.

impair occupant comfort. Radon concentrations were elevated (7.8 $pCiL^{-1}$) in one building where air was drawn into the basement air handler through a three mile network of underground service tunnels. Otherwise, concentrations generally were low. Only six buildings averaged greater than the 2 ppm detection limit for CO. One individual site had an eight-hour average of 7 ppm, which is approaching the ASHRAE 62-1981 guideline of 9 ppm for a 10 hour average. At only one site, an elementary school classroom, did CO_2 exceed 1000 ppm (1300 ppm), while the average for all buildings was 499 ppm. RSP concentrations in smoking areas in 32 buildings had a geometric mean of 48 μgm^{-3} and ranged up to 308 μgm^{-3} at one site. In non-smoking areas, the geometric mean RSP was 16 μgm^{-3} and was lower than outdoor levels in 65% of the buildings. For comparison, the ASHRAE 62-1981 guideline is 75 μgm^{-3} for one year average exposure to total suspended particles (TSP). Both PAH and BaP were higher in smoking areas but were generally below a 2.2 ngm^{-3} average for BaP summarized from 121 United States ambient urban sites.[31] Building average ventilation rates ranged by a factor of 13 with a group average of 1.5 ach. Very poor correlation was noted between average building pollutant concentrations and measured outside air ventilation rates, implying that indoor air pollution in commercial buildings is dominated by factors other than ventilation (source strength, building volume, and other removal processes) (Fig. 19). Pollutant concentrations measured in two "problem" buildings with occupant complaints were below accepted guidelines. The cause of the complaints was not identified.

Table 11. Commercial and Institutional Building Summary.

	Mean	Standard Deviation	Range	Other/Comments
Building Use	—	—	—	6 schools 24 offices 3 libraries 5 multi-use
Age (yr)	23	—	0.5–90	—
Occupancy	526	—	25–2500	—
Height (stories)	5	—	underground-18	—
Area (ft^2)	94,250	—	9,300-369,000	—
No. HVAC Systems	5	—	0–32	—
HCHO (ppb)	below 36 ppb detection	—	BD-56	40[e]
$H_2O(gkg^{-1})$	6.6[a]	1.5	3.2–9.8	40[e]
NO_2 (ppb)	18.1[a]	8.4	BD (10)–43	33[e]
Rn ($pCiL^{-1}$)	0.8[b]	2.1	0.2–7.8	40[e]
CO (ppm)	below 2 ppm detection	—	BD–3.3	32[e]
CO_2 (ppm)	499[a]	102	337–840	39[e]
RSP (μg^{-3})	24[b]	2.0	BD[c]–67	40[e]
BaP (ng^{-3})	0.4[b]	2.7	BD[d]–4.90	29[e]
PAH (ng^{-3})	3.0[b]	3.9	BD[d]–45.49	29[e]
SF_6 Ventilation (ach)	1.5[a]	0.87	0.3–4.1	40[e]

[a]Arithmetic mean and standard deviation.

[b]Geometric mean and standard deviation.

[c]Detection limit based on minimum filter weight gain of 50 μg

[d]Detection limit based on analysis system sensitivities at time of analysis.

[e]Number of buildings included in summary.

Planned Activities for FY 1986

Analysis of the data from all three field studies will continue in FY 1986. Of primary importance is the necessity of integrating the perfluorocarbon tracer (PFT) ventilation results into the evaluation of the relationship between pollutant concentrations and ventilation rates.

In addition, 16 residences from this year's study identified as a having radon concentrations above 5.0 $pCiL^{-1}$ will be involved in a field evaluation of mitigation retrofits. Mitigation will be staged and includes sealing techniques, subsurface ventilation, house ventilation, and basement pressurization. Implementation, cost, and effectiveness will be investigated.

CONCENTRATION OF INDOOR POLLUTANTS DATA BASE

In the last decade, as many countries throughout the world have begun to pay serious attention to their energy policies, the importance of conserving energy in occupied buildings, both residential and commercial, has been increasingly acknowledged. As various energy-conserving measures have been proposed and implemented (particularly those that reduce ventilation), there has been a growing awareness that such measures, when combined with the presence of pollutant sources, can adversely change the air quality in the affected buildings, causing health and comfort problems for the occupants. Towards the end of identifying the sources of these

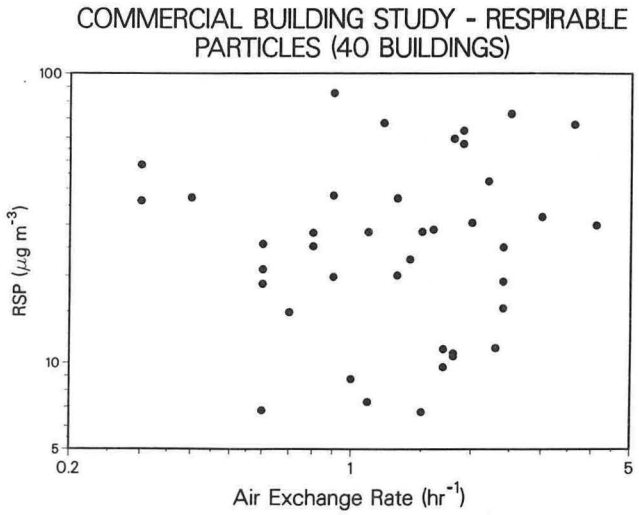

Figure 19. Scatter plot of average commercial indoor RSP concentrations and average building ventilation rates. Lack of observable correlation indicates that ventilation is not the most important parameter affecting indoor pollutant concentrations. (XBL 862-370)

problems and developing solutions to them, a significant amount of research has been carried out, mainly in Europe and North America, to monitor pollutant concentrations and other relevant parameters in a wide variety of building types and geographic locations.

Some of the results of this research have been published in journals or conference proceedings, some in internal reports, and some, for reasons of personnel shifts or program changes, have neither been formally collected nor published. The diversity of research sources and inaccessibility of some research results, combined with the rapid growth in the amount of research being carried out, has made it apparent that a centralized collection of these research results in an easily accessible form would greatly facilitate their exchange, evaluation, and analysis.

The goal of this project, therefore, is to create a computerized data base of those field studies devoted to monitoring indoor air quality in occupied buildings in the United States and Canada. (The term "data base" as used here means a collection of data files and command procedures which, together, comprise a data resource.) The Concentration of Indoor Pollutants data base (CIP data base) will contain research results, along with bibliographic references and information describing the experimental environment, and research procedures.

For a more detailed description of the CIP data base, see the 1984 Annual Report.

Accomplishments During FY 1985

The initial implementation of the CIP data base was completed in the Spring of 1985 and then reviewed by members of the project advisory committee and selected representatives of a number of gas and electric utilities. Each reviewer was asked to complete a questionnaire regarding the performance and usefulness of the data base. Based on this review process, modifications and enhancements to the CIP data base were carried out, and Version 2.0 of the Concentrations of Indoor Pollutants Data Base was released for general distribution in October. At that time the content of the bibliographic data base was 90% complete, with 192 entries, while the summary data base was 20% complete, with 20 entries. By the end of the year, both the bibliographic and summary data bases were 95% complete and current.

Planned Activities for FY 1986

During 1985 it became obvious that the data base needed to be converted from dBase II to dBase III for a number of reasons. Some of these were the increased power and flexibility of dBase III; the increasing number of potential users with dBase III; the decline in usage of 8-bit machines, which can't run dBase III; and the availability of a commercial compiler for dBase III to create a stand alone version of the CIP data base that would need neither dBase II or dBase III to run. Accordingly, work was begun on the conversion, and will be finished in the first quarter of 1986. There will then be a release of the new product as Version 3.0, along with the completed bibliographic and summary data bases.

The other major tasks for 1986 will be the continuing maintenance of the CIP data base and support of the user community. Maintaining the data base primarily consists of searching out and entering the results of new research. This includes monitoring the journals that publish research in indoor air quality, such as Environment International, Health Physics, the Journal of the Air Pollution Control Association, etc.; periodically searching the relevant electronic data bases, such as the Energy Data Base supported by the U.S. Department of Energy; and reviewing relevant conference proceedings. Periodically, updates containing the new entries to the CIP data base will be distributed to all users.

Support for the user community will consist of making the existence of the CIP data base known to as many potential users as possible; being available by phone and correspondence to aid users in utilizing the data base; and modifying the data base in response to user complaints and suggestions. A

newsletter will be distributed to all users on a regular basis, probably quarterly. It will address user needs, answer questions, and provide a communications medium for the user community.

The remote-access facility will become available in early 1986, allowing access to the CIP data base via the phone lines to remote users with a terminal and a modem. This facility will broaden the potential user community, and will be used as another communications medium with the user community.

RISK ASSESSMENT

The overall purpose of this work is to characterize indoor exposures to air pollutants and to examine their health implications. Considering the complexity of this question, the work has several manifestations. Exposure characterization and examination of health effects are the dominant part of the project. These efforts include 1) construction of an overall framework for examining exposures and health effects of indoor pollutants and 2) narrower studies of the three major pollutant classes to which the larger and broader efforts of LBL's Building Ventilation and Indoor Air Quality Program have been devoted: combustion products, radon and its decay products, and organic chemicals.

Accomplishments During FY 1985

Overall Framework for Assessing Exposures and Health Effects of Indoor Pollutants

Indoor pollutants fall into several pollutant classes, three of which—radon, combustion products, and organic compounds—can be characterized from similar scientific perspectives, in respect to both studying the behavior of the pollutants and estimating associated risks. However, in spite of these overall similarities, the nature of the exposures and health effects, as well as the character of the data that may be brought to bear on estimating these quantities, differ substantially. As a result, quantitative examination of a specific pollutant, pollutant class, or air pollution in general, requires careful attention to the specific behavior of pollutant(s) of interest and to the limited data that are available.

Considering our program's substantive experience with each of these pollutant classes, we have undertaken an effort to establish a consistent overall perspective for assessing the exposures and health risks of indoor pollutants. From the simplest point of view, of course, what is needed is information on pollutant concentrations during time spent indoors and on the risk factor expressing the relationship(s) between exposures and probability of associated health effects. The product of exposures and risk factors yield, the incidence or risk of the health effects induced. Unfortunately, the picture is complicated considerably by the need to consider multiple types of exposures and health effects and by the variable nature and reliability of the information available on both of these questions. The framework being developed will take this diversity into account, permitting an effective appreciation of the importance of indoor pollutants. This framework has already been applied to the case of lung cancer from ^{222}Rn decay products, where the exposure can be characterized by a relatively simple annual-average concentration and where the dose-response data for the health effect of interest is unusually strong.[15]

Related to the construction of this overall framework, we have also recently begun a logically subsidiary, but actually more substantial, effort developing a generalized approach for indoor exposure assessment *per se*, focusing for the present on exposures in homes. To some extent, the need for (and difficulty of) this effort would be circumvented by a large-scale national effort measuring all the pollutant concentrations (as well as influencing factors) in a statistical sample of U.S. homes. In the absence of results from such a survey, it is necessary to construct a surrogate that—within a consistent quantitative framework—makes the best possible use of presently available information. It is clear what the key elements in this surrogate are: 1) a data structure for describing U.S. housing and the associated factors that can influence indoor concentrations; 2) a capability for calculating indoor concentrations from the data contained in this structure; and 3) methods for sampling data in a way that is representative of the class of housing under consideration. The initial pollutant class for which the required computer programs will be developed is combustion products (see section on **Combustion Pollutant Exposures**). However, with the provision of analogous data for other pollutants, the same programs can treat classes of indoor pollutants. This exposure assessment framework will, we should note, not only provide improved understanding of exposures, but also indicate more clearly than heretofore possible what new or improved data are required and how survey efforts should be designed to obtain them.

Potential Risks from Exposure to Organic Carcinogens in Indoor Air

In FY 1985, progress was made in the area of assessing exposures of and potential risks from organic chemicals in indoor air. Increasing experi-

ence with so-called "complaint" or "sick" buildings suggests the occurrence of adverse effects on humans from exposure to organic chemicals in indoor air. However, except for a few cases involving such compounds as formaldehyde, chlordane, and pentachlorophenol, the complaints cannot be attributed with any certainty to individual chemicals. Furthermore, while the experience to date constitutes an important indicator of a potential problem, complaints are generally limited to acute or irritant effects, such as unpleasant odors, upper respiratory or eye irritation, or headaches. Thus complaints rarely serve as effective indicators of more life-threatening endpoints, such as cancer or reproductive effects, if only because individuals are not likely to be able to associate such toxic effects with the air inside the buildings they occupy.

These limitations on our experience with complaint buildings have so far precluded either: 1) assessment of the overall importance of organic chemicals indoors as a cause of any class of toxic effects or 2) identification of the most important contributors to such effects. Nonetheless, substantial data are available, primarily from other kinds of studies, on the toxic effects of many of the chemicals that occur indoors. Effective utilization of information from animal and human toxicology can help to narrow the focus of future studies by targeting high-risk chemicals and by identifying toxic effects to be examined in epidemiological studies. Such studies may include surveys in complaint (and control) buildings, as well as epidemiological studies designed to detect the association between particular chemicals and the more serious toxic effects, such as cancer and reproductive effects. Considering the many chemicals present in indoor air, at widely varying concentrations, and the limitations in sensitivity of epidemiological studies, success can only occur by targeting groups that are highly exposed to chemicals of particular concern. The full range of toxicological data should be brought to bear as a basis for indicating which chemicals (or chemical classes) are worthy of attention, as well as for indicating before hand the potential importance of various classes of effects.

In this study we have examined the current literature reporting concentrations of organic chemicals in indoor environments, and have constructed a nominal list of some 150 chemicals found indoors. We have then surveyed the known toxicological properties of these chemicals, relying primarily on results from animal studies. We have made rough estimates of the concentrations that might be expected to cause toxic effects in humans and have compared these to measured concentrations in indoor air as an approximate index of the significance of indoor exposures. The primary endpoints examined were carcinogenesis and reproductive effects, though some attention has also been given to other systemic toxic effects, and irritation.

As an example, for carcinogens we have calculated estimated risks from animal cancer test data and indoor air concentrations. The results of these calculations for 27 carcinogens found in indoor air are shown in Table 12. The values estimated for risk per unit exposure range over 4 orders of magnitude. This wide variation in the carcinogenic potential of carcinogens in indoor air is an important consideration underlying a study such as this. Thus, even though the evaluation of risks at indoor concentrations is complicated by fundamental limitations in the data on toxic effects, and by an incomplete framework within which to estimate the frequency or type of effects at low concentrations in humans relative to those at which toxicity is observed in animal experiments, the errors in the analysis are not likely to be as large as the very wide range of carcinogenic potency of the chemicals being evaluated. With such a wide range, even very rough approximations of risk may be useful.

As an example, consider the case of formaldehyde, which is commonly present in indoor air of non-complaint homes at concentrations averaging about 50 $\mu g/m^3$. Listed in Table 12 are three estimates of individual risk from lifetime exposure to this concentration. These estimates differ by a factor of 170. The higher estimates were calculated from risk estimates made by the Environmental Protection Agency (EPA) using a very conservative extrapolation model.[34] The lowest estimate was calculated from risk estimates made using an extrapolation model similar to the EPA's, but using less conservative assumptions and incorporating additional assumptions drawn from biological and pharmacological considerations, which result in considerably decreasing the estimated risk. Even though the difference in the lifetime risk estimates of these two models is roughly 150-fold, the fraction of total cancer risk attributed to formaldehyde is significant regardless of which model is used. Assessment of the importance of formaldehyde as an actual cause of human cancer will require the results of much more thorough investigations, but this simple analysis suggests that current emphasis on potential risks from chronic indoor exposures to formaldheyde is not inappropriate.

Inadequate data presently available on concentrations of chemicals in the indoor environment represent a major limitation of our analysis. For virtually no organic compounds (formaldehyde is to

Table 12. Estimates of carcinogenic risk from lifetime exposure to organic chemicals in indoor air.[a]

Chemical	Risk/Exposure[a] ($\mu g/m^3$) ($\times 10^{-5}$)	Exposure[b] ($\mu g/m^3$) MAX/MEAN or MEDIAN	Risk (Lifetime cancers per 10^5 people)
Aldrin	88	0.55/-	48/-
Benzene	>0.41	390/14	>160/>5.7
Benzo[a]pyrene	5.9	0.067/0.0071	0.4/0.042
Carbon tetrachloride	0.57	17/<1.4	9.7/<0.80
Chlordane	45	40/-	1800/-
Chloroform	1.4	47/<2.6	66/<3.6
Dibenz[a,h]anthracene	11	0.00050/0.00010	0.0055/0.0011
Dichlorvos	6.9[c]	10/-	69/-
Dieldrin	119	0.47/-	56/-
1,1,1-Trichloroethane	0.14[3]	1100/33	150/4.6
1,2-Dibromoethane	<13	<0.14/<0.14	<1.8/<1.8
1,1-Dichloroethane	0.059[d]	1.8/0.06	0.11/0.0035
1,2-Dichloroethane	<5.7	69/1.1	<390/<6.3
Ethanol	0.0035	390/130	1.4/0.46
Tetrachloroethylene	0.86	720/4.5	620/3.9
Trichloroethylene	0.16	180/<3.4	29<0.54
Formaldehyde	17[e](5.0) [~0.1][f]	125[7]/53[g]	2,100/900[5.3]
Heptachlor	<60	15/-	<900/-
Lindane	>5.4	50/0.18	>270/>0.97
Malathion	0.22[3]	2.0/-	0.44/-
Dichloromethane	(0.0180)	5000/<120	90/<2.2
Dimethylnitrosamine	278	0.8/-	222/-
N-Nitrosopyrrolidine	15	0.036/-	0.54/-
PCB's (Anrochlor 1260)	30	0.50/-	15/-
Di(2-ethylhexyl)phthalate	0.014[5]	230/60	3.2/0.84
Styrene	0.18	54/3.3	9.7/0.59
Vinylidene Chloride	3.0	420/2.7	1,300/8.1

[a]Estimates are based on the most potent TD50 reported by Gold, *et al.*[32] In parentheses are estimates from the Carcinogen Assessment Group at EPA (Anderson[33]). A "greater than" sign (>) indicates the TD50 was estimated from a dose-response that showed significant downward departure from linearity. A "less than" sign (<) indicates the TD50 was estimated from a dose-response that showed significant upward departure from linearity. All results were from experiments in either rats or mice.

[b]Data compiled from the published literature.

[c]The experiment used by Gold, *et al.*[32] to estimate the TD50 was classified negative by NCI/NTP or authors of a literature study.

[d]The experiment used by Gold, *et al.*[32] to estimate the TD50 was classified equivocal by the NCI/NTP.

[e]Gold, *et al.*[34]

[f]A much less conservative estimate than that of EPA, using the best estimate (instead of the upper 95% confidence limit value) and incorporating assumptions drawn from biochemical and pharmacological considerations (Starr[35]).

[g]At concentrations above 125 $\mu g/m^3$ the irritant effects of formaldehyde become noticeable to most people. We have, therefore, chosen this as the highest concentration that would be likely to occur chronically, even though much higher concentrations have been measured in non-complaint homes.

[h]In calculating a mean value, we have not included the relatively much higher concentrations reported in mobile homes.

some degree an exception) do we have sufficient direct information to state with much certainty what the frequency distribution of concentrations is, nor are we able to cite average exposures with any accuracy. Thus, in Table 12, risk from lifetime exposures to some carcinogens at high exposures (represented in the table by maximum values) may be quite significant (e.g., 10 carcinogens have lifetime risk values greater than 1 in a thousand cases of cancer). Though the absolute risk values shown represent only unlikely upper limits, since lifetime exposure to such high levels would not be expected to occur, this result does point out the importance of gaining a better understanding than we have now of the proportion of individuals exposed for extended periods to relatively high concentrations of these substances.

Other Pollutant-Specific Efforts

Part of the radon group's efforts over the past several years has involved examination of the aerial radiometric data accumulated as part of the National Uranium Resource Evaluation (NURE); the resulting information on surface radium concentrations may serve as a significant indicator of high indoor concentrations (see **Radon** section). Having obtained the entire NURE data set and loaded most of it into the LBL computer system, we have recently begun a collaboration with the Populations at Risk to Environmental Pollution project to examine potential correlations between the NURE data and U.S. health data that can be accessed through the LBL system. While the results of this examination may not provide unequivocal evidence on the relationship between (environmental) radon exposures and lung cancer rates, they would constitute the first systematic examination of such correlations, a substantial step beyond the limited and virtually anecdotal analyses performed to date.

In conjunction with the combustion emissions group, we have examined considerations in the design of field surveys to assess indoor exposures to combustion pollutants.[2] This represents a preliminary step in designing large scale assessments of indoor exposures to combustion pollutants via either field studies or modeling studies.

Planned Activities for FY 1986

We plan to continue our exposure and risk assessment efforts in combustion pollutant, radon and organic compounds. The new directions of this work will exemplify the type of analytical effort that is often neglected by the indoor air quality community, but without which we cannot hope to understand the significance of what we have done or choose effectively the path of future work.

REFERENCES

1. Traynor, G.W., *et al.* (1984), *Pollutant Emission Rates from Unvented Infrared and Convective Gas-Fired Space Heaters,* LBL-18258.
2. Traynor, G.W. (1985), "Field Monitoring Design Considerations for Assessing Indoor Exposures to Combustion Pollutants," accepted by *Atmos. Environ.*; LBL-19844.
3. Traynor, G.W., *et al.* (1983), "Pollutant Emissions from Portable Kerosene-Fired Space Heaters," *Environ. Sci. Technol. 17*, p. 369; Addendum in *Environ. Sci. Technol. 19*, p. 200.
4. Traynor, G.W., *et al.* (1985), "Indoor Air Pollution Due to Emissions from Unvented Gas-Fired Space Heaters,"
5. Nazaroff, W.W., Doyle, S.M., and Nero, A.V. (1985), "Potable Water as a Source of Airborne radon in U.S. Dwellings: A Review and Assessment," submitted to *Health Physics*; LBL-18154.
6. Traynor, G.W., Nitschke, I.A., and Clarke, W.A. (1985), "A Detailed Study of Thirty Houses with Indoor Combustion Sources," Paper 85-30A.3, in *Proceedings of the 78th Annual Air Pollution Control Association Meeting*, June 16–21, Detroit, MI. Air Pollution Control Association, Pittsburgh, PA.
7. Nitschke, I.A., *et al.* (1985), "Indoor Air Quality, Infiltration, and Ventilation in Residential Buildings," W.S. Fleming and Associates, 5802 Court Street Rd., Syracuse, NY 13206.
8. De Bortoli, M., *et al.* (1985), "Measurements of Indoor Air Quality and Comparison with Ambient Air," *Commission of the European Communities Report* EUR 1656 EN, Directorate-General for Science, Research and Development, Joint Research Centre, Ispra, Italy.
9. Hawthorne, A.R., *et al.* (1984), "An Indoor Air Quality Study of Forty East Tennessee Homes," Oak Ridge National Laboratory Report ORNL-5965, Oak Ridge, TN.
10. Lebret, E., *et al.* (1984) "Volatile Hydrocarbons in Dutch Homes" in *Proceedings of the 3rd International Conference on Indoor Air Quality and Climate*, August 20–24, 1984, Stockholm, Sweden, *4*, p. 169, Swedish Council for Building Research, Stockholm, Sweden.
11. Wallace, L.A., *et al.* (1985), "Personal Exposures, Indoor-Outdoor Relationships and Breath Levels for 355 Persons in New Jersey," *Atmos. Environ. 19*, p. 1651.

12. Grimsrud, D.T., *et al.* (1985), "Building Ventilation and Indoor Air Quality," in *FY 1984 Annual Report, Energy Efficient Buildings Program*, LBL-18753.
13. Report of the National Toxicology Program Board of Scientific Counselors Peer Review Panel, March 29, 1985, Research Triangle Park, NC.
14. Girman, J.R. and Hodgson, A.T. (1985), *Source Characterization and Personal Exposure to Methylene Chloride from Consumer Products,* LBL-20227.
15. Nero, A.V., Schwehr, M.B., Nazaroff, W.W., and Revzan, K.L. (1984), "Distribution of Airborne ^{222}Radon Concentrations in U.S. Homes," submitted to *Science*; LBL-18274.
16. Sextro, R.G. (1985), "Understanding the Origin of Radon Indoors—Building a Predictive Capability," submitted to *Atmospheric Environment*; LBL-20210.
17. Nazaroff, W.W., *et al.* (1985), *Factors Influencing Soil as a Source of Indoor Radon: A Framework for Geographically Assessing Radon Source Potentials,* LBL-20645.
18. Corey, A.T. (1957), "Measurement of Water and Air Permeability in Unsaturated Soil," *Soil Sci Soc Am. Proc. 21.*
19. Sexton, K, Webber, L.M., Hayward, S.B., and Sextro, R.G. (1985), "Characterization of Particle Composition, Organic Vapor Constituents, and Mutagenicity of Indoor Air Pollutant Emissions," submitted to *Environment International.*
20. Wang, Y.Y., *et al.* (1985) "Indoor Air Mutagens in Particle and Vapor Emissions from a Chamber Study," California Department of Health Services report CA/DOH/AIHL/R-290, Berkeley, CA; submitted to *Mutation Research.*
21. Offermann, F.J., *et al.* (1985), "Control of Respirable Particles in Indoor Air with Portable Air Cleaners," *Atmospheric Environment 19,* p. 1761.
22. Sextro, R.G., *et al.* (1984), "Evaluation of Indoor Aerosol Control Devices and Their Effects on Radon Progeny Concentrations," submitted to *Environment International*; LBL-17598.
23. Rudnick, S.N., Hinds, W.C., Maher, E.F., and First, M.W. (1985), "Effect of Plateout, Air Motion and Dust Removal on Radon decay Product Concentration in a Simulated Residence," *Health Physics 45,* p. 463.
24. Sandberg, M. and Sjoberg M. (1983), "The Use of Moments for Assessing Air Quality in Ventilated Rooms," *Building and Environment 18* (4), p. 181.
25. Fisk, W.J., *et al.* (1985), "Multi-Tracer System for Measuring Ventilation Rates and Ventilation Efficiencies in Large Mechanically-Ventilated Buildings," in *Proceedings of the 6th Air Infiltration Centre Conference,* Het Meerdal, Netherlands, September 16–19, 1985; *Air Infiltration Centre Conference,* Het Meerdal, Netherlands, September 16–19, 1985; LBL-20209.
26. Geisling, K.L., *et al.* (1982), "A Passive Sampling Device for Determining Formaldehyde in Indoor Air," *Environment International 8,* p. 153.
27. Girman, J.R., Allen, J.R., and Lee, A.Y. (1984), *A Passive Sampler for Water Vapor,* LBL-17599.
28. Palmes, E.D., Gunnison, A.F., DiMattio, J., and Tomzyk, C. (1976), "Personal Sampler for NO_2," *American Ind. Hygiene Assoc. J. 37,* p. 570.
29. Dietz, R.N., and Cote, E.A., "Air Infiltration in a Home Using a Convenient Perfluorocarbon Tracer Technique," *Environment International 8,* p. 419.
30. Thor, P.W. (1984), "BPA Radon Field Monitoring Study," in *Doing Better: Setting an Agenda for the Second Decade,* ACEEE 1984 Summer Study on Energy Efficiency in Buildings, Santa Cruz, CA, Vol. B, p. 283, American Council for an Energy Efficient Economy, Washington, D.C.
31. Baum, E.J. (1978), "Occurrence and Surveillance of Polycyclic Aromatic Hydrocarbons," in *Polycyclic Hydrocarbons and Cancer,* Vol. 1, Editors: H.V. Gelboin and P.O. Ts'o, Academic Press, N.Y., p. 45.
32. Gold, L.S., *et al.* (1984), "A Carcinogenic Potency Data-base of the Standardized Results of Animal Bioassays," *Envir. Hlth. Perspectives 58,* p. 9.
33. Anderson, E. (1983), "Quantitative Approaches in Use to Assess Cancer Risk," *Risk Analysis 3,* p. 277.
34. Gold, L.S., *et al.*, (1986), "Chronological Supplement to the Carcinogenic Potency Data-Base: Standardized Results of Animal Bioassays published through December, 1982," *Envir. Hlth. Perspectives,* in press.
35. Starr, T.B. (1985), "The Role of Assumptions and Mechanistic Data in Dose-Response," paper presented at Society for Risk Analysis Annual Meeting, Washington, DC.

Windows and Daylighting*

(This article, except for the section on Aerogels, has been reprinted from the FY 1984 Annual Report.)

S.E. Selkowitz, D. Arasteh, C. Conner, D.L. DiBartolomeo, A.J. Hunt, R.L. Johnson, H. Keller, J.D. Kessel, J.H. Klems, C.M. Lampert, J.G. Lieber, K.D. Lofftus, M. Navvab, E. Ne'eman, S. Nozaki, M.D. Rubin, M. Spitzglas, R. Sullivan, P. Tewari, N. Wen, and G.M. Wilde

Approximately 20% of annual energy consumption in the United States is for space conditioning of residential and commercial buildings. About 25% of this amount is required to offset heat loss and heat gain through windows. In other words 5% of our national energy consumption—3.5 quads annually, or the equivalent of 1.7 million barrels of oil per day—is tied to the energy-related performance of windows. Fenestration performance also directly affects peak electrical demand in buildings, sizing of the heating, ventilating, and air-conditioning (HVAC) system, and the thermal and visual comfort of building occupants.

The aim of the Windows and Daylighting Group is to develop a sound technical base for predicting the net energy performance of windows and skylights, including both thermal and daylighting aspects. This capability will be used to generate guidelines for optimal design and retrofit strategies in residential and commercial buildings and to assist in exploratory development of new high-performance materials and designs.

One of our program's strengths is its breadth and depth: we examine energy-related aspects of windows at the atomic and molecular level in our materials science studies at one extreme and perform field tests and *in-situ* experiments in large buildings at the other. We have developed, validated, and now use a unique and powerful set of interrelated computational tools and experimental facilities that enable us to address the major research issues in this field. A multidisciplinary team of scientists, engineers, and architects conducts these studies, in collaboration with researchers in industry and academia.

To be useful, the technical data developed by our program must be communicated to design professionals, to industry, and to other public and private interest groups. We publish our results and participate in all appropriate industrial, professional, and scientific meetings and societies, national and international, to ensure that our research results are widely disseminated and utilized.

Our work is organized into four major research areas:

- Optical materials studies
- Fenestration components and systems
  - —Thermal analysis
  - —Daylighting analysis
- Fenestration performance in buildings
  - —Simulation studies
  - —Field measurement facility
  - —Building monitoring
- Fenestration impact studies

Each of these areas is reviewed in the following sections.

OPTICAL MATERIALS STUDIES

Significant reductions in energy consumed by the building sector will come not only from better building design strategies but also from the development and introduction of new glazing materials. Since the inception of our program in 1976, identification, characterization, and exploratory development of promising new fenestration materials have been major activities. Research on new optical materials and on modifications of existing glazing materials is intended to create a technology base to assist industry with developing the next generation of advanced fenestration systems.

In addition to the research projects described below, the overall Optical Materials effort at LBL includes development of a multiyear research plan and scientific coordination of related DOE-funded research projects at universities, private sector firms, and other national laboratories.

Results of the DOE-supported program are made available to interested parties in the private sector. For example, an annual technical conference and industry forum is held each year in August in conjunction with a meeting of the International Society for Optical Engineering (SPIE). This meeting serves as a forum to review and discuss the direction of the overall DOE program as well as to report on recent technical progress. A joint international effort on glazing optical materials under the auspices of the International Energy Agency is being developed with our participation.

*This work was supported by the Assistant Secretary for Conservation and Renewable Energy, Office of Buildings Energy Research and Development, Building Systems Division; the Office of Solar Heat Technologies, Passive and Hybrid Solar Energy Division; and the Office of Energy Systems Research, Energy Conversion and Utilization Technology Program of the U.S. Department of Energy under Contract No. DE-AC03-76SF00098.

In 1976, when our program began, we identified the development of low-emittance ("low-E") coatings as a major program objective. DOE-supported research activities have helped the fenestration industry to accelerate market introduction of new high-performance window systems incorporating these coatings. Several small firms began offering commercial products in 1982, and in 1984 many of the largest glass and window manufacturers introduced "low-E" products. In the near term the use of low-E coatings in a conventional double-glazed window provides better thermal performance than triple glazing and makes a lighter and more compact window. In the long term this coating technology offers the potential to produce transparent windows having heat transfer values as low as those of insulating walls. On an annual basis such windows should outperform the best-insulated wall, even for a north orientation in a cold climate, since diffuse solar gain will offset some conductive losses. We initiated planning in late 1984 for a Low-E Window Roundtable, to be co-sponsored with the National Fenestration Council. We believe that the positive impact of this DOE-supported effort can serve as a model for the transfer and development of research findings in other optical materials areas.

GLASS AND PLASTIC SUBSTRATES

Accomplishments During FY 1984

To predict the optical properties of complex window systems incorporating thin-film coatings, the optical properties of the glass and plastic substrates must be accurately known. These properties have not been available in a complete and self-consistent form even for the most common varieties of glass used in windows, hence the need for this measurement effort. This year we completed work on standard clear glasses, glasses having absorbing additives, and high-purity glasses. Our results are summarized in a paper that includes a complete set of optical constants from the near ultraviolet through the little-studied far infrared for all common window glasses.[1] We also provide some spectrally and directionally averaged bulk properties for calculating solar and thermal radiative heat transfer through windows. Figure 1 shows the real and imaginary components of the complex index of refraction for a clear glass as determined by Kramers-Kronig analysis of reflection measured with a Fourier-transform spectrometer over the near-infrared and infrared spectrum.

Future measurements will be greatly simplified with our new spectrometer, which covers the ultraviolet to the near infrared. In addition to having optics that are far superior to those of our previous instrument, this system features completely automated operation and data collection. The instrument is installed and operating, although not all functions have been tested.

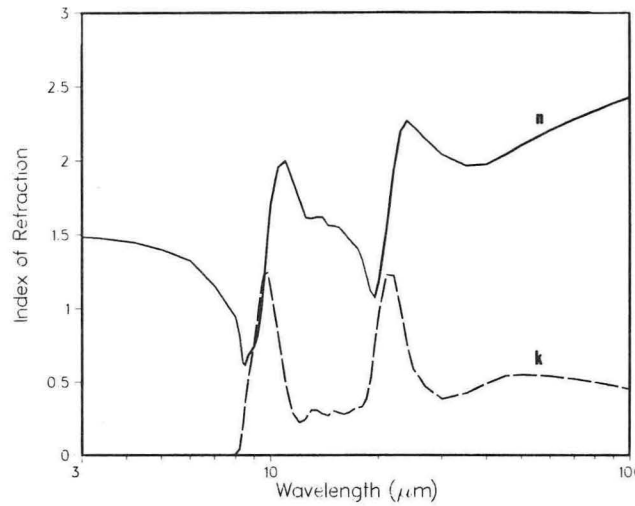

Figure 1. Real (n) and imaginary (k) parts of the complex index of refraction for soda-lime silica glass. (XBL 8412-5271)

Planned Activities for FY 1985

We will collect, organize, and catalogue our low-emissivity samples. These samples will be completely characterized as part of our participation in the Low-E Window Roundtable in August 1985. Our spectrometer will be fully functioning.

LOW-CONDUCTANCE, HIGH-TRANSMITTANCE GLAZINGS

An ideal glazing material for residences in cold climates would have good optical clarity, high solar transmittance to admit sunlight in winter, and low thermal conductance to reduce heating costs. Such windows would perform better than insulated walls on an annual basis, even in northern orientations in cold climates. Simulation results for a north-facing window in Madison, Wisconsin are shown in Fig. 2. Windows must have U-value and shading coefficient combinations that place them to the right of the "0" net heat transfer line if they are to provide net energy benefits. Two promising research activities are under way to develop the technical basis for such advanced windows.

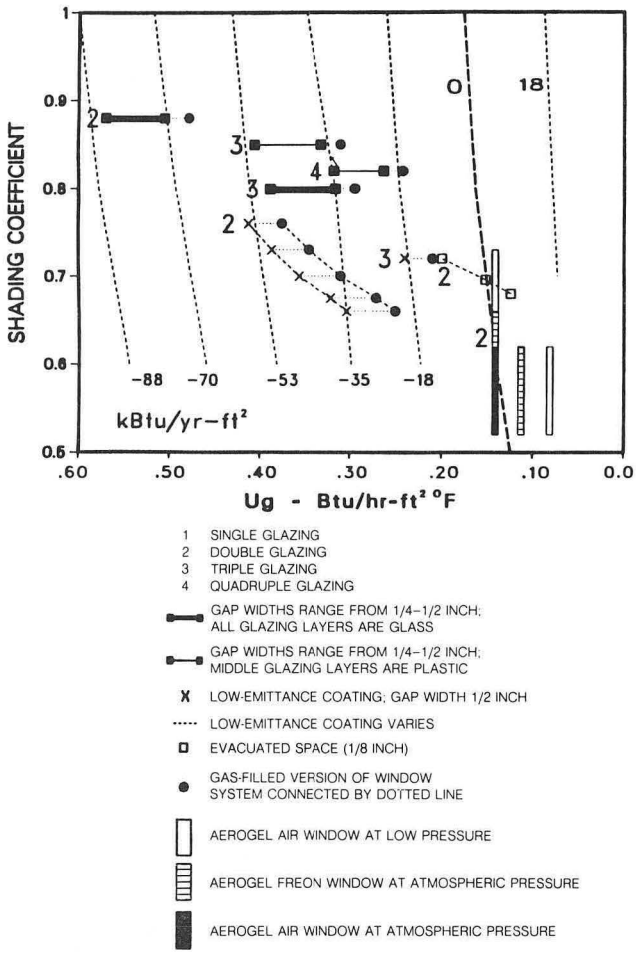

Figure 2. Simulation results for north-zone window, Madison, Wisconsin, showing net annual useful flux (primary window area = 66 ft^2). (XBL 856-2870)

Low-Emittance, Gradient-Index Coatings

Accomplishments During FY 1984

Since 1976 we have contributed to the development of window coatings that transmit sunlight but reflect in the thermal infrared, thus suppressing radiative heat transfer. Commercially available coatings based on metal-dielectric multilayer films have satisfactory optical properties but are not sufficiently durable to be used in nonsealed glazings. By producing a film having a continuously varying index of refraction to reduce reflection in the solar spectrum, we could use materials that are inherently more durable but less transparent than the metal films. Our analytical studies suggest that a gradient-index coating could improve solar transmittance by 25% without reducing emittance or durability.

We have begun by studying the titanium oxynitride (TiN_xO_y) system, producing these gradient-index coatings by plasma-assisted chemical vapor deposition (CVD). Better compositional control and durability have been achieved in a limited number of samples deposited by magnetron sputtering. We installed a new sputtering system and completed the first tests for homogeneous coatings. The coatings are being characterized by electron microscopy, Auger electron spectroscopy (AES), and Rutherford backscattering (RBS), in addition to complete optical characterization. RBS has proved particularly valuable in our efforts to remove impurities from the coatings. Figure 3 shows the small amount of chlorine remaining in the coating after adding H_2 to scavenge the bulk of the unwanted Cl in our CVD films.

Planned Activities for FY 1985

We will add reactive gas-handling capabilities to our sputtering system to produce TiN_xO_y films. The process parameters will be varied in an attempt to achieve the optimum optical properties predicted by our analytical models.

Aerogels

Transparent silica aerogel is being developed at LBL because of its excellent thermal insulation properties for window glazing materials. It is an open cell porous solid containing a very high percentage of voids. Aerogel is transparent rather than translucent because the characteristic pore size is much smaller than the wavelength of light; therefore, it transmits

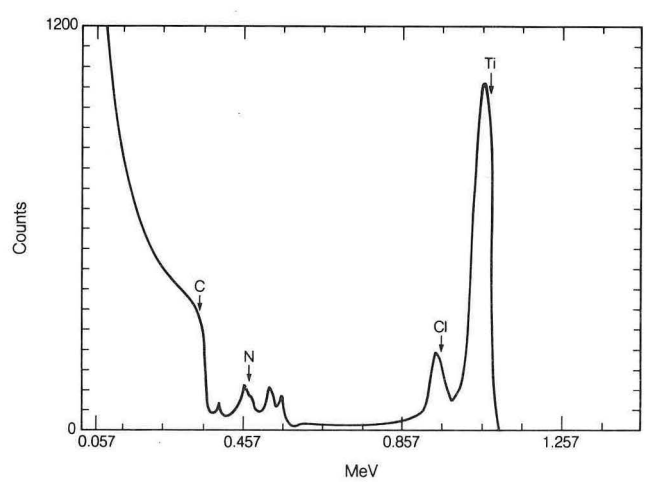

Figure 3. Rutherford backscattering spectrum for titanium oxynitride coating on glossy carbon substrate. (XBL 854-9799)

rather than scatters light. A 1-inch-thick aerogel window has an R value of about 7, which can be increased to nearly R-20 by removing 90% of the air from the aerogel. The goals of this research are to improve the optical and thermal properties of aerogel, discover less expensive synthesis methods, develop methods to protect it from the environment, and develop a technology base for production of transparent aerogels.

Aerogel is prepared by mixing a metal alkoxide with water and alcohol along with suitable catalysts. Water hydrolyzes the alkoxide compound to produce fine solid particles or polymers that link together to form alcogel, a transparent solid containing alcohol. To become useful as an insulator, the alcohol must be removed from the alcogel without damaging the silica matrix through the action of interfacial forces in the very fine pores. These interfacial forces can be eliminated by carrying out the solvent extraction under supercritical conditions. Researchers at LBL have been investigating both the preparation and drying of aerogel.

Accomplishments During FY 1985

Our efforts in 1985 have been concentrated on improving the two critical areas of synthesis of aerogels:

1. hydrolysis and condensation reaction of a less expensive alkoxide TEOS (tetraethylorthosilicate) than the toxic and expensive TMOS (tetramethylorthosilicate) normally used by others;
2. simplification of the drying process of the alcogels to achieve the aerogel without damage to the structure.

In addition, we have developed some unique techniques which allow us to study the microstructure of the gels by transmission electron microscopy and light scattering studies. They are discussed below. Progress in these three areas has significantly enhanced the prospects for large scale industrial preparation of aerogel for windows.

Alcogel Production from Low Toxicity Starting Material. Transparent silica aerogels for Cerenkov counters have been produced by hydrolysis and condensation of TMOS. Since TMOS is a very toxic starting material, the more desirable starting compound, TEOS, was used in the current work. Research in our laboratory led to the successful use of a base to catalyze TEOS.[2–4] Base catalysis of TEOS results in a more suitable material for window material than the acid catalysis method. We have improved the properties of the aerogel by exploring a wide range of process variables using the factorial design method.[2] Light scattering, optical transmission, and electron microscopy data were used to characterize the aerogels produced in our laboratory. Using these techniques we have established that the quality of the improved TEOS aerogels is comparable or better in transparency than those prepared from TMOS. The transmission spectrophotometer results confirming this are given in Fig. 4.

Ambient Temperature Supercritical Drying. Alcogel is a low density open pore material containing a high fraction of voids filled with alcohol. In conventional supercritical drying, the alcohol is removed from the alcogel by slowly releasing the pressure in an autoclave after it has been heated above its critical pressure and temperature. Under these conditions, the interfacial tensions in the alcogel drop to zero. Typical conditions for supercritical drying of alcohol are $\geqslant$ 270°C and 1800 psi. The necessity to cycle pressure vessels to these temperatures makes the drying process expensive and time consuming. We have developed a solvent substitution process[5] in which alcohol is replaced by liquid CO_2, which permits drying of alcogels at $\leqslant$ 40°C and 1200 psi. We have improved the substitution and drying process to minimize shrinkage and damage to the structure. The shrinkage can be controlled to $\leqslant$ 5% of the initial dimensions. The reproducibility of the process is good, and the drying is achieved in less time per batch than the 2–3 days required by the high temperature process. Further efforts are in progress to reduce the shrinkage.

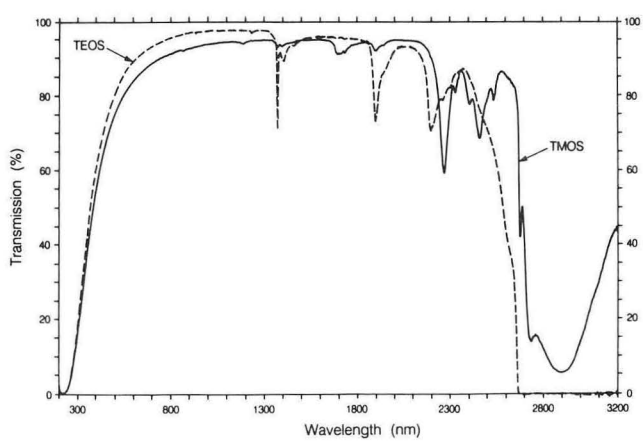

Figure 4. Transmission spectra of a 4-mm-thick sample of base catalyzed TMOS aerogel supercritically dried at 270°C and 110 bars (TMOS) and a 12-mm-thick base catalyzed TEOS aerogel sample supercritically dried by CO_2 but not heated to remove all adsorbed H_2O (TEOS). (XBL 859-8975)

Gel Microstructure. We have developed a variety of sample preparation methods to overcome difficulties in the study of aerogel with electron microscopy.[6] Transmission electron microscope studies using these methods have provided excellent evidence of the physical gelation mechanism. Micrographs show a cross linked chained structure similar to that conceptualized previously by various workers (Fig. 4a). These sample preparation techniques for TEM studies are excellent for studying the microstructural details of gels and aerogels at various stages in the sol-gel process.

We have performed light scattering studies of acid and base catalyzed sol-gel systems. By studying the time evolution of the scattering intensity, we can differentiate gelation mechanisms between the two gels. Information from these experiments is helpful in formulating and controlling the desired properties of complex sol-gel systems.

Planned Activities for FY 1986

In FY 1986 we will explore the substitution of Freon 116 for alcohol to further reduce the supercritical drying conditions to $\leqslant 20°C$ and 430 psi. If successful, this substitution will lower the processing cost below that of the CO_2 method. Treatment of the gels to render them hydrophobic will be studied to improve the chemical stability of aerogel against weathering and moisture. The adhesion of aerogel to glass plates of the window will be examined to improve the mechanical stability and resiliency of the aerogels.

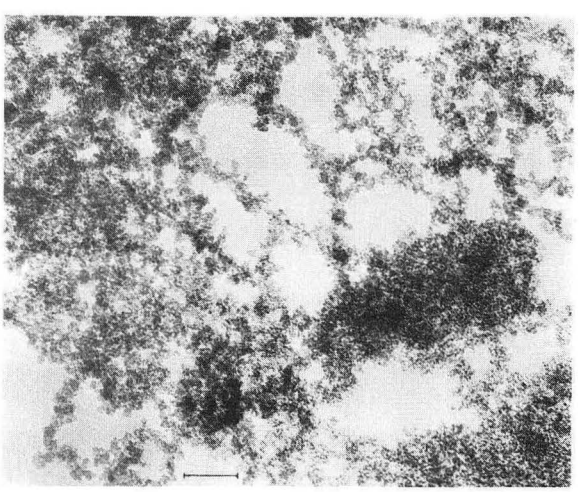

Figure 4a. Transmission electron micrograph of a base catalyzed TMOS aerogel flake after carbon coating. (XBB 859-7482)

OPTICAL SWITCHING PROCESSES AND MATERIALS

Optical switching materials or devices can be used for energy-efficient windows and other passive solar applications. An optical shutter provides a large change in optical properties under the influence of light, heat, an electric field, or their combination. The change can occur as a transformation from a material that is highly solar transmitting to one that reflects over part or all of the solar spectrum (Fig. 5). A less desirable alternative would be a material that switches from highly transmitting to highly absorbing since some of the absorbed energy would enter the building. An optical shutter coating would control the flow of visible light and/or solar heat gain through a building window, thus performing an energy management function. Depending upon design, such a coating could control glare, modulate daylight admittance, and limit solar heat gain to reduce cooling loads, prevent overheating, and improve thermal comfort. Initial results from energy

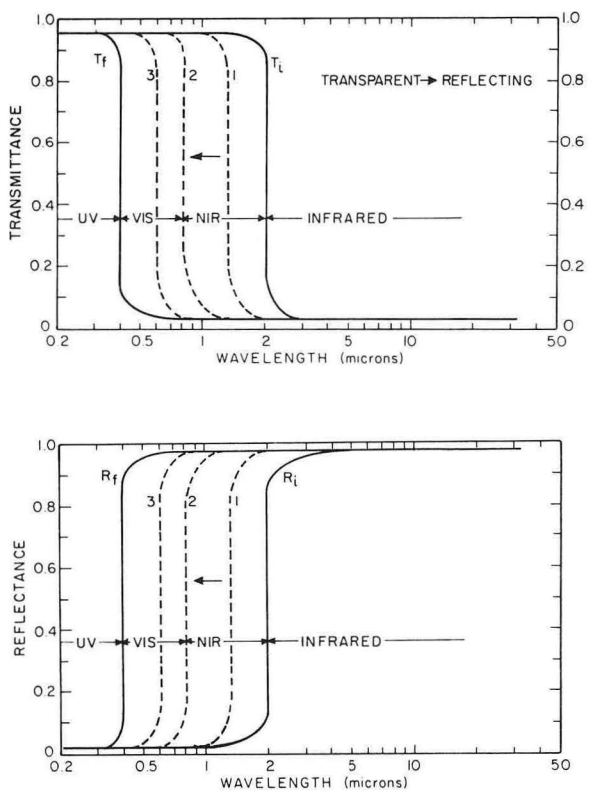

Figure 5. Idealized broadband spectral response for a solar optical shutter. This example ignores the effect of absorption and shows a highly transparent film transforming into a highly reflecting one. Such a shutter can control certain portions of the solar spectrum to provide or restrict both solar heating and lighting. (XBL 828-6452)

simulation studies of office buildings suggest that the dynamic control attainable with optical shutter coatings provides substantial economic benefits by minimizing cooling and lighting energy use, reducing peak electricity demand, and potentially reducing the HVAC system size.

We consider materials that possess variable or reversible optical properties as potential candidates for an optical shutter. There are three classes of phenomena that may prove useful:

(1) Chromogenic materials, including electrochromic, photochromic, and thermochromic types.
(2) Physio-optic media, including mesogenic molecules or liquid crystals, and magneto-optic, electro-optic, and mechano-optic or deformable media.
(3) Electrodeposition, including reversible electrodeposition and electrophoresis.

Our research program focuses on electrochromic coatings because they offer the potential for active control (by an applied voltage) in response to building operating requirements and environmental conditions and because there is sufficient experience with optical displays and related applications to suggest that they would be the best candidates for glazing applications. The active control capability will allow the greatest range of potential benefits in terms of reducing cooling loads, providing daylighting savings, controlling peak electricity demand, and reducing HVAC size.

Electrochromic Devices

Electrochromism is exhibited by many inorganic and organic materials.[7] An electrochromic material undergoes an intense color change when a colored compound is formed from an ion-insertion reaction induced by an instantaneous applied electric field. The reaction might follow:

$$MO_x + yA^+ + ye \rightleftarrows A_yMO_x \quad .$$

There are three categories of electrochromic materials: transition metal oxides, organic compounds, and intercalated materials. The materials that have attracted the most research interest are WO_3, MoO_3, and NiO_x films. With organic electrochromics, coloration of a liquid is achieved by an oxidation-reduction reaction, which may be coupled with a chemical reaction. Intercalated electrochromics are based on graphite and so are not useful for window applications.

A solid-state electrochromic device containing the elements shown in Fig. 6 can be fabricated: a transparent conductor, an electrochromic layer, an electrolyte or fast-ion conductor, a counter electrode, and a second transparent conductor. Many variations on this configuration are possible, although several of the approaches used for small electronic displays cannot be scaled up successfully to the dimensions required for windows.

Accomplishments During FY 1984

Prior to 1984 a technical review of electrochromism revealed many possible materials that could be incorporated into solar glazings.[7] During 1984 our research focused on electrochromism in nickel oxide, which can be switched from transparent to bronze or dark gray, depending on impurities. We performed experiments on oxidized metal films and chemically deposited oxides on indium-tin-oxide coated glass. We obtained a normally transmitting film with solar transmittance (T_s) and visible transmittance (T_v) as follows: T_s (off) = 0.73, T_s (on) = 0.37, T_v (off) = 0.75, and T_v (on) = 0.24. The spectral response is shown in Fig. 7. In an electrochemical cell 1 volt is required to switch the film. Besides spectrophotometry, voltammetry and Auger electron spectroscopy were performed on this film. These studies will help determine the active species in the electrochromic coloration reaction.

LBL continues to serve as scientific coordinator for the overall DOE-supported switching films program. Associated research was continued in 1984 by EIC Laboratories[8] and the Department of Electrical

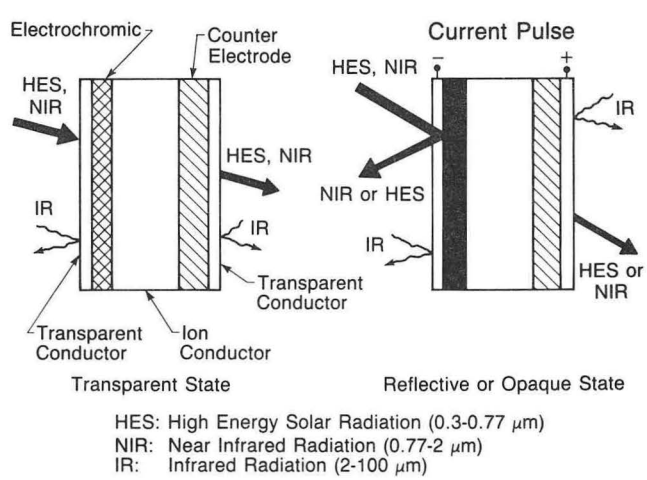

Figure 6. Schematic of an electrochromic optical switch shown in each of two states, transparent and colored. A current pulse causes an ion-based chemical reaction to take place in the electrochromic material. (XBL 842-10105)

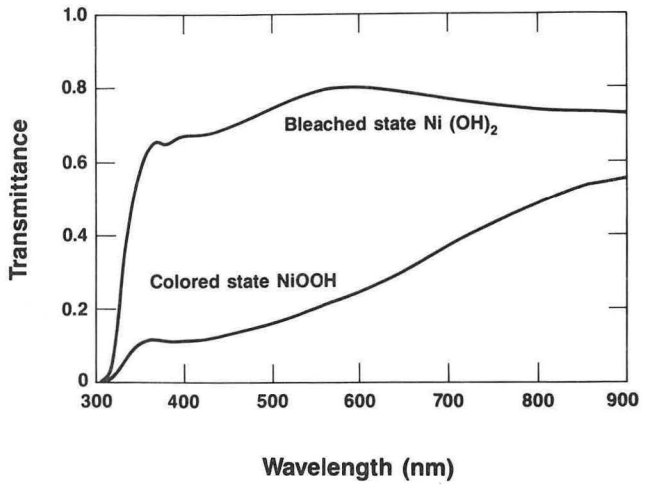

Figure 7. Transmission (near-normal) spectrum for nickel hydroxide in bleached and colored state. Conditions are IM-KOH electrolyte with 1 V applied potential. (XBL 852-6955)

Engineering at Tufts University.[9] Electrochromic near-infrared reflectance modulation was demonstrated in polycrystalline WO_3 material.[10] Devices based on the configuration in Fig. 6 and with complementary electrochromic electrodes were made. Research by the Solar Energy Research Institute (SERI) has concentrated on devices based on amorphous WO_3 in the configuration: transparent conductor/WO_3/ion conductor/Au or indium-tin-oxide.[11]

Planned Activities for FY 1985

We will complete optical, chemical, and structural studies of electrochromic nickel oxide. We will compare the electrochromic response of sputter-prepared nickel oxide materials to the electrochemically prepared coatings. With our new reactive magnetron sputtering system, we will begin to survey and characterize electrochromism in other candidate materials such as titanium oxide. The objective is to identify and characterize electrochromic materials with performance characteristics that are better than the commonly used WO_3 films.

Other Switching Film Mechanisms

A number of other materials systems were reviewed to determine their suitability as optical switching materials. We continue to follow development of photochromic and thermochromic materials to determine if any may prove suitable to building applications. We also examined various physio-optic processes (i.e., liquid crystals, magneto-optic and electro-optic materials) as well as processes based on reversible electrodeposition and electrophoresis. Each approach has at least one attractive feature, but in general they appear less promising than the alternatives described above.

Accomplishments During FY 1984

An example of a device studied in FY 1984 is the dynamically light-scattering liquid crystal cell. It transforms from transparent to opaque white under applied potential; no polarizers are required. Its optical properties are T_s (off) = 0.82, T_s (on) = 0.77, T_v (off) = 0.83, T_v (on) = 0.20. Although the response of this device (Fig. 8) is promising as a broadband optical shutter, it suffers from excessive power requirements and lack of uniformity over large areas.

Planned Activities for FY 1985

We will continue to follow these novel approaches for optical switching mechanisms to determine if results in other fields have relevance to aperture requirements. We expect to obtain samples of photochromic plastics to determine their suitability for building applications.

MATERIALS FOR IMPROVED USE OF DAYLIGHT

The intensity and spatial distribution of daylight transmitted through windows and skylights must be controlled in order to reduce electric lighting requirements while maintaining occupant comfort. Con-

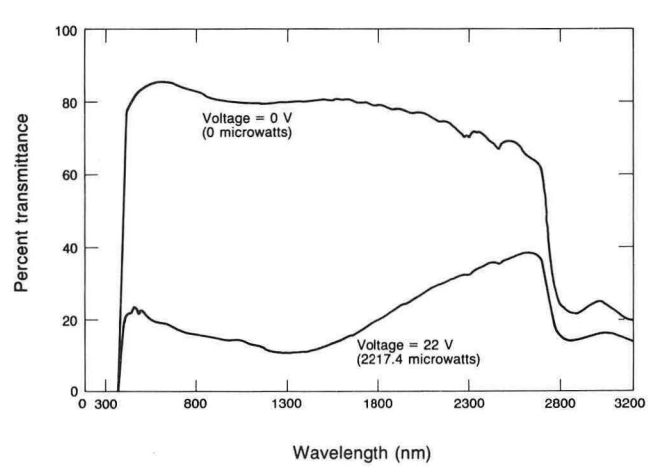

Figure 8. Spectral transmittance (near normal) for a dynamically scattering liquid crystal device. Response includes two glass cover plates and two transparent conductor electrode films. (XBL 852-7033)

ventional solutions rely on architectural elements and interior or exterior devices to control daylight admission and distribution. Greatly improved performance would result from materials or systems that could: (1) transmit maximum daylight with minimal cooling load impact (i.e., reject solar infrared radiation); (2) collect and distribute daylight beyond the perimeter zones in buildings; and (3) provide angular selectivity in accepting and redirecting incident light at the building envelope.

In earlier studies we evaluated the performance of a variety of devices for daylight acceptance and control on the basis of their reflective and refractive optics. In 1982 we turned our attention to innovative optical materials and devices that showed the potential for replacing more complex mechanical systems. We reviewed the feasibility of approaches such as fiber-optics systems, hollow light guides, holographic coatings, selective-reflectance materials, and various scattering media. One promising approach that uses fluorescent concentrators to collect and redirect daylight is the subject of a patent disclosure.

Light Guides

Accomplishments During FY 1984

In 1984, on the basis of the preceding year's review of potential systems for light guides, we focused on two promising areas. We predicted improved performance for hollow reflecting light pipes because of the availability of new low-cost materials of high reflectivity (more than 95%). Figure 9 shows the calculated transmission efficiency of this type of light guide as a function of aspect ratio (length/diameter) for R = 95%. Even for aspect ratios of 50 (e.g., L = 15 m, D = 0.3 m) the transmission has acceptable values at moderate concentration angles. We also investigated the performance of plastic optical fibers and evaluated the potential for improvement through further purification of the base polymer.

Planned Activities for FY 1985

We will continue our investigation of hollow reflecting light guides. Available reflecting materials will be completely characterized and the results used in improved analytical models. We will compare these model results with the actual performance of hollow prismatic light guides. Scale models of light guide elements will be tested in our sky simulator.

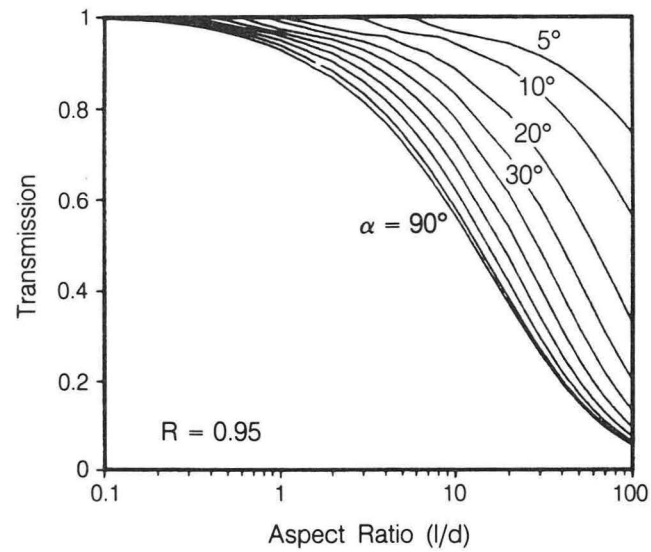

Figure 9. Transmission efficiency of a tubular light guide vs. aspect ratio (length/diameter). The parameter α is the half-angle of the concentrated sunlight. The inner surface reflectivity R is 0.95. (XBL 854-9798)

FENESTRATION COMPONENTS AND SYSTEMS

Research activities in this area are intended to develop and refine experimental techniques and analytical models for accurately determining the heat transfer and solar optical properties of fenestration components and systems. Many of the new algorithms and data sets are designed to be incorporated into hour-by-hour building energy simulation programs such as DOE-2.1. These new simulation capabilities will not only improve the accuracy of our predictions but will also allow us to predict the performance of new fenestration systems and novel architectural designs. Our overall plan for developing and implementing these new analysis capabilities in energy simulation models is shown schematically in Fig. 10.

THERMAL ANALYSIS

Accomplishments During FY 1984

We completed revisions to the fenestration chapter of the 1985 *ASHRAE Handbook of Fundamentals.* These include new tables on the properties of windows with (1) low-emittance coatings, (2) low-conductance gas-filled spaces, and (3) various convective and temperature-dependent boundary condi-

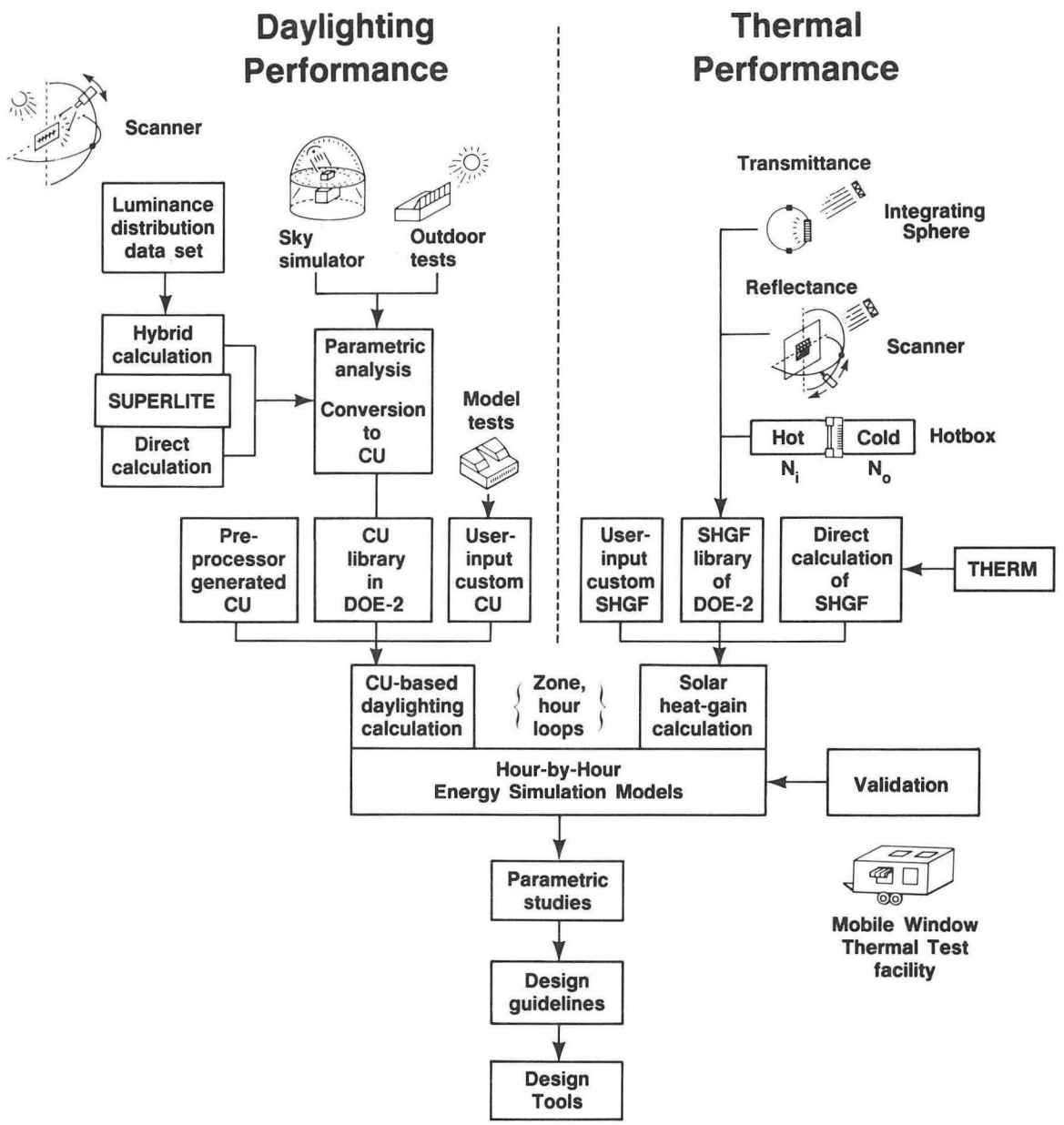

Figure 10. Schematic diagram of DOE-2.1 fenestration modeling capabilities under development. The new solar heat-gain model is shown on the right, the new illuminance model on the left. (XBL 8212-4972A)

tions. We also continued our participation in an International Energy Agency (IEA) task group (Annex XII) on windows and fenestration. We will jointly calculate the thermal properties and annual performance of several window systems and compare results from researchers in nine countries. One major objective is to better understand the accuracy and limitations of each calculation procedure and test method. We also participated in an International Standards Organization (ISO) work group on the thermal performance of fenestration.

Planned Activities for FY 1985

We will continue to participate in the IEA and ISO fenestration tasks. We will work with the ASHRAE Fenestration Committee to define the technical requirements for the next ASHRAE Hand-

book chapter update and will again work cooperatively with others to provide the required data. We will use our thermal analysis model, THERM, and experimental results to further investigate the effects of sealed glass edges and window sash and frame elements on overall conductance. We will also participate in DOE-cosponsored workshops on window U-value measurements and on low-emittance window systems.

SOLAR OPTICAL MODELS

Accomplishments During FY 1984

The solar optical properties of windows change with the sun's angle of incidence. For geometrically complex shading systems such as venetian blinds or egg-crate louvers, no adequate models exist to predict solar heat gain as a function of incidence angle. In addition, solar gain from ground-reflected sunlight and diffuse light from the sky cannot readily be calculated for complex shading systems. We are developing a new technique for determining solar heat gain through complex fenestration systems, a technique based on a standard series of laboratory measurements of the fenestration system's optical properties. Transmittance will be measured using a large integrating sphere with the window system mounted in a port and illuminated either with an electric light source or solar radiation.

In 1984 construction was completed on this 2-m-diameter sphere (Fig. 11). Preliminary results were obtained for shading devices, and comparisons with data from other sources were made. Sample results for several window-blind systems are shown in Fig. 12. For each sun position, total reflectance will be calculated by integrating measurements of bidirectional reflectance obtained from a radiance/luminance scanner. The design of this apparatus was completed in FY 1984, and major functional elements were assembled (Fig. 13) and tested.

Figure 11. The integrating sphere for measuring hemispherical transmittance of glazing materials and fenestration systems. (CBB 837-6399)

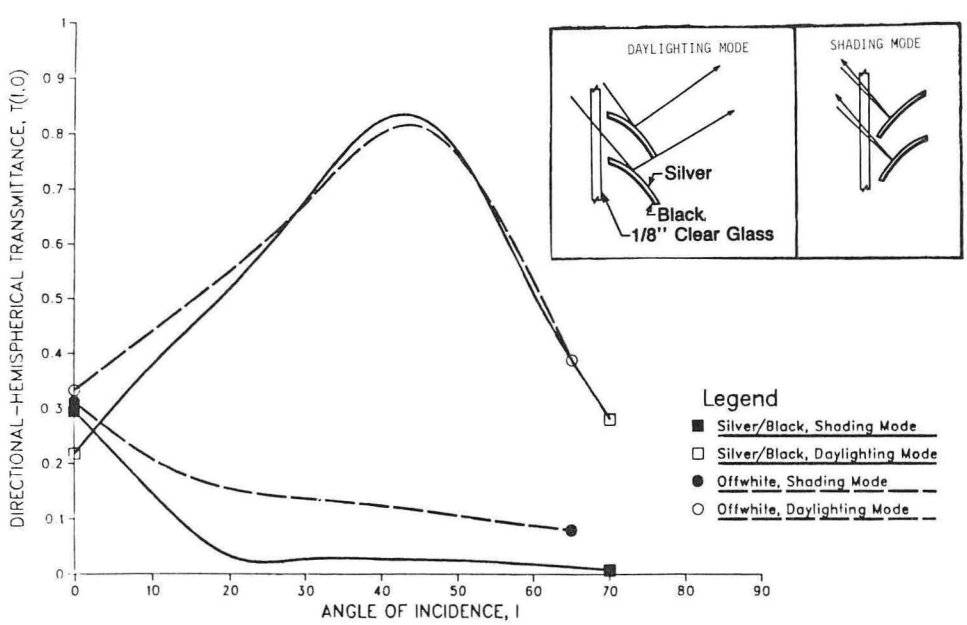

Figure 12. Measured transmittance of two venetian blinds with different surface treatments as a function of position and angle of incident light. (XBL 848-3341)

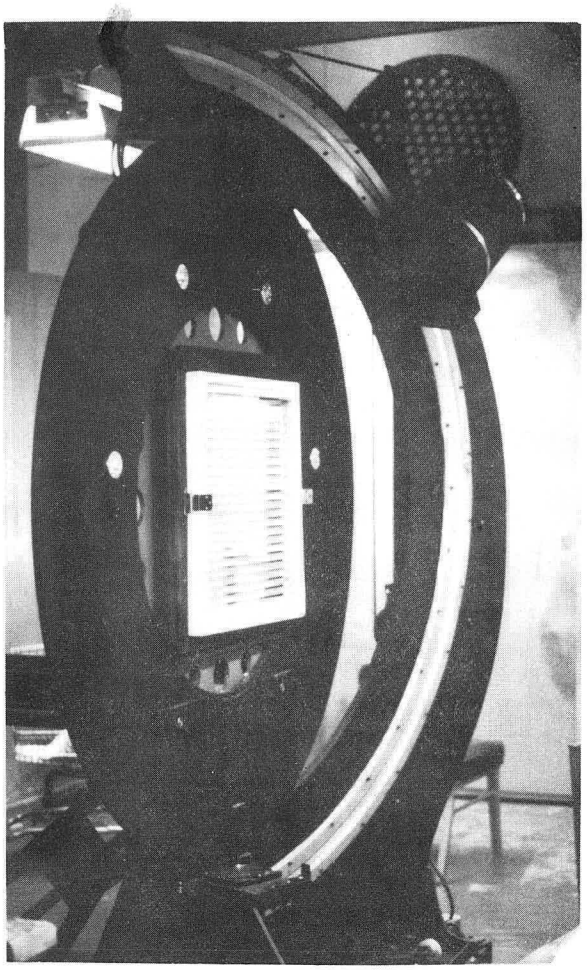

Figure 13. Scanning radiometer under construction. (CBB 852-1225)

Planned Activities for FY 1985

The major effort will be to complete initial development and testing of the radiance/luminance scanner to the point where we can begin to collect performance data. The integrating sphere and the scanner will then be used to determine the optical properties of shading systems. We will also complete initial development of the analysis procedures for determining the angle-dependent solar optical properties of multilayer fenestration systems based on the measured optical properties of each layer.

FENESTRATION LABORATORY

In 1977 we established the Fenestration Laboratory in the College of Environmental Design at the University of California, Berkeley, to support our research and development activities and to provide independent testing and evaluation of fenestration materials and devices. This facility enables us to evaluate both experimental prototypes and new devices being introduced to the market. In addition to the new integrating sphere and scanning radiometer described above, testing facilities include a calibrated hotbox for measuring window conductance and an air-leakage tester for measuring air flow across a window for a range of positive and negative pressure differentials. We have also developed capabilities for measuring the optical properties of glazing materials and coatings to fully characterize their performance. In FY 1984 the Fenestration Laboratory prepared sensors and instrumentation for the Mobile Window Thermal Test Facility and calibrated its heat-flow sensors, both described later in this article.

DAYLIGHTING ANALYSIS

To predict the energy consequences of daylighting strategies, one must be able to predict the daylight illuminance distribution pattern in a building from any window or skylight under all sun and sky conditions. Since no single approach provides the best solution, we use a variety of techniques to assess various aspects of daylighting performance.

The types and capabilities of the analysis and design tools required to evaluate the daylight performance of a building differ, depending on (1) the complexities of room and window geometries, (2) daylight utilization strategies in conjunction with electric lighting and building HVAC systems, and (3) the level of analytical accuracy required at a specific stage of design.

In previous years we developed several simplified daylighting design tools (e.g., the QUICKLITE program) that are now widely used in the architectural and lighting design communities. Last year we further developed our more advanced computational models (e.g., the SUPERLITE program) to expand the range of modeling capabilities and to improve computational accuracy. We also extended our analysis of daylight availability measurements and the photometric measurement capabilities of our Daylighting Laboratory.

Accomplishments During FY 1984

We continued to test and evaluate the SUPERLITE program, concentrating on the ability to model complex shading systems. Our approach is to define the daylight transmittance properties of the window and shading system as a candlepower distribution function that varies with the incidence angle of sunlight. Since we had only a limited data base of measured candlepower distributions, we used theoretical distributions that could be compared to results gen-

erated by other computational techniques. This comparison showed good agreement.

We tested a version of SUPERLITE with an electric lighting modeling capability and compared results with those from other computational models. The agreement was generally good. This new capability will allow us to study the combined effects of daylight and electric light in a room.

We developed an input processor that enables users to create an input file interactively by answering questions that appear on their terminal screens. This will be linked to a library of input room designs and a data base of photometric results. We also continued work on a user's manual for SUPERLITE that should facilitate its use by a wider audience.

Planned Activities for FY 1985

We will continue testing and validation of SUPERLITE's modeling of shading devices, using candlepower data sets measured by the luminance scanner.

We will release the SUPERLITE 1.0 program to users after completing the users' manual and continue further testing and modification of the program's capacity to analyze electric lighting systems.

We will then use SUPERLITE to produce the initial entries for a daylighting performance data base for various building and fenestration designs. The input and output processors will be extended so that parametric simulations can be routinely completed and results automatically entered into our performance data base.

COEFFICIENT-OF-UTILIZATION MODEL

Building energy analysis computer models must be able to properly predict the daylighting performance of complex design strategies commonly used by innovative architects. The models should either internally calculate the daylight illumination or be supplied with data precalculated by other illumination models or measured in scale models. The first approach, internal calculation of daylight illumination, is generally not practical for complex designs because of the significant computational cost and complexity required to obtain reasonably accurate answers. We are therefore developing a coefficient-of-utilization (CU) model that will be compatible with an hour-by-hour simulation model but still retain the flexibility and accuracy of more complex computational models.

Accomplishments During FY 1984

Our approach is to derive the CU model from regression analysis of a parametric series of daylighting analyses using SUPERLITE. We modified SUPERLITE to generate these parametric series and also modified the output to report the indoor illuminance level due to each external light source—the sun, sky, or ground.

We use a statistical computer software package to generate test regression equations for the sun, sky, and ground components with a limited number of generalized variables (e.g., location of window, window dimensions). Initial results suggest that good fits can be obtained with relatively simple regression expressions.

Planned Activities for FY 1985

We will expand the analytical effort to develop new CU models that can handle greater variation in room geometry and surface reflectance. After generating all equations, they will be thoroughly tested and validated. The final model will be documented as part of our efforts to formally publish results in FY 1986.

DAYLIGHTING MODELS FOR ENERGY SIMULATION PROGRAMS

As a result of collaborative efforts with the Building Energy Simulation (BES) Group over the past several years, we completed development and testing of an operational daylighting model in the DOE-2.1B program. This model enables us to determine the direct effects of daylighting on lighting electrical consumption, associated thermal loads, peak electric demand, and HVAC-system size requirements. The model can simulate, on an hourly basis, the use of simple operable shading systems by altering a window's solar optical properties in response to occupant requirements for thermal and visual comfort. Its output reports not only indicate average hourly and monthly savings for each zone but also provide several types of statistical summaries and frequency plots that enable us to examine the details of annual energy performance.

Accomplishments During FY 1984

We continued to test and use the new features in DOE-2.1B and enhancements in DOE-2.1C for fenestration studies. The 2.1C version of the program has the capability to replace a constant value (e.g., light

transmittance) with a function that can be dependent on many other factors. For example, the light transmittance could be a variable function of solar intensity and temperature. These user-generated "functional values" can be used to model complex designs with functions generated from scale model tests, or to assess the performance of new materials or designs with user-defined performance characteristics.

Planned Activities for FY 1985

Work will continue on the daylighting model for DOE-2.1D in conjunction with the BES group; it will be able to simulate more complicated sun-shading devices and more sophisticated daylighting solutions such as light shelves. These improvements will be based on the new coefficient-of-utilization model derived from SUPERLITE calculations or model tests. The new daylighting model should enable the program to simulate, without additional revisions, the performance of building designs of arbitrary complexity. A schematic of the planned procedure for calculating daylight illuminance and solar gain is shown in Fig. 10.

DAYLIGHT AVAILABILITY STUDIES

Accurate daylight availability models are necessary for many design and energy analysis simulations. In 1978 we began an availability measurement project to fill this need, as data were lacking for most U.S. locations. However, a generalized model of availability that is widely accepted has yet to be developed.

Accomplishments During FY 1984

We published three papers analyzing daylight availability data for San Francisco.[12–14] Analysis focused on the relationship of measured illuminance and irradiance to atmospheric parameters such as turbidity. A new functional relationship was developed to determine an illuminance turbidity for visible radiation analogous to the conventional turbidity terms used with solar radiation. We also developed new functional relationships for zenith luminance as a function of turbidity and found that our clear-sky luminance distribution data agree well with data from currently accepted European models. These results were published in the Technical Proceedings of the International Daylighting Conference.[15] (Sample results are shown in Fig. 14.)

To better coordinate research efforts on daylight availability, we have worked with the Florida Solar Energy Center (FSEC) to host review meetings

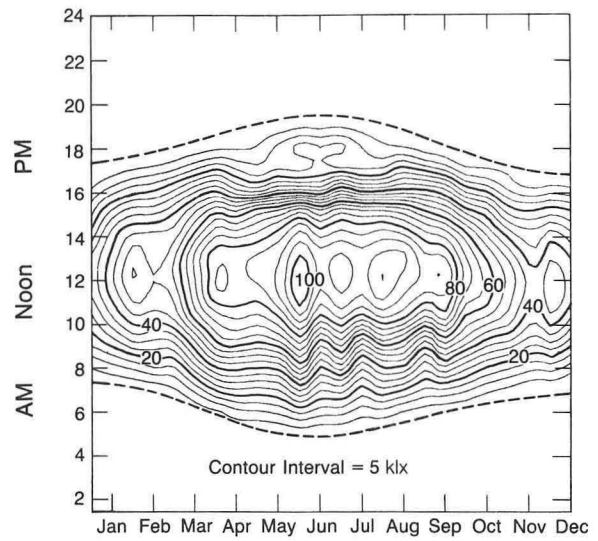

Figure 14. Isolux contours of global horizontal illuminance, based on four years of data measured in San Francisco. (XBL 845-10362)

attended by experts representing all the major groups undertaking daylight measurements in the United States and Canada. Topics included defining daylight measurement requirements, analysis procedures, sensor selection and calibration, and a standard format for presentation of data throughout the United States and Canada. We also initiated a three-way collaboration between LBL, FSEC, and Pacific Northwest Laboratories (PNL) to characterize luminance distributions under partly cloudy skies. For this study we will shift our availability measurement station from San Francisco to Berkeley and add new measurement techniques and instrumentation, including a scanning sky luminance mapper developed by PNL. Analysis of the data will be jointly undertaken by PNL, FSEC, and LBL.

Planned Activities in FY 1985

We will continue analysis of our existing data base and complete a study of the luminous efficacy of daylight and sunlight. The sky luminance scanner will be installed and become operational. Our new measurement capabilities should enable us to better understand topics requiring detailed measurements and to develop data for more standardized daylight availability models for designers in U.S. climates. The practical importance of errors in availability models on energy predictions is not well understood. An effort will be continued in FY 1985 to quantify these errors.

DAYLIGHT PHOTOMETRIC LABORATORY

The Sky Simulator

A 24-ft-diameter hemispherical sky simulator (Fig. 15) was designed and built on the University of California's Berkeley campus in 1979. In operation since 1980, it can simulate uniform, overcast, and clear-sky luminance distributions. Sky luminance distributions are reproduced on the underside of the hemisphere; light levels are then measured in a scale-model building at the center of the simulator. From these measurements we can accurately and reproducibly predict daylighting illuminance patterns in real buildings and thereby facilitate the design of energy-efficient buildings. The facility is used for research studies, for educational purposes, and on a limited basis by architects working on innovative daylighting designs.

Accomplishments During FY 1984

The sky-and-sun simulator were used to collect scale-model data on the daylighting performance of fenestration systems. In one study these data were compared with computer-model predictions for the identical room and fenestration designs. We also used the facility to study the daylighting performance of atria. These large glazed spaces are increasingly popular in office and retail buildings, but little information is available on their daylighting performance. A photograph of our reconfigurable atrium scale model is shown in Fig. 16. Our initial studies suggest that many common assumptions about the usable daylight in deep atria are overly optimistic and may lead to disappointing results.

Planned Activities for FY 1985

As part of our continuous upgrading of this facility, the sun simulator will be modified to provide a beam of more uniform cross section. The entire facility will be relamped and recalibrated so that the full dynamic range of possible sky luminance distributions can be precisely defined, in conjunction with the automated control-system software. We will also upgrade the illumination control system to provide more accurate luminance distributions. New amplifiers will be fabricated and installed to increase the precision of our photosensors in the upper light-level range and extend the lower range to measure illuminance as low as 0.1 lux. These efforts should significantly extend the efficiency and performance of the facility as a research and design tool.

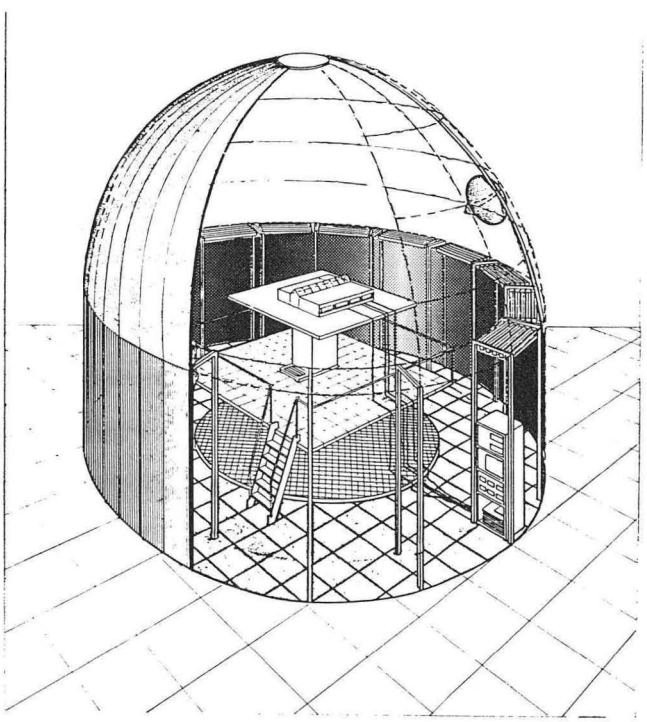

Figure 15. Schematic of 24-ft^2 diameter sky simulator with model on platform. (XBL 8412-5328)

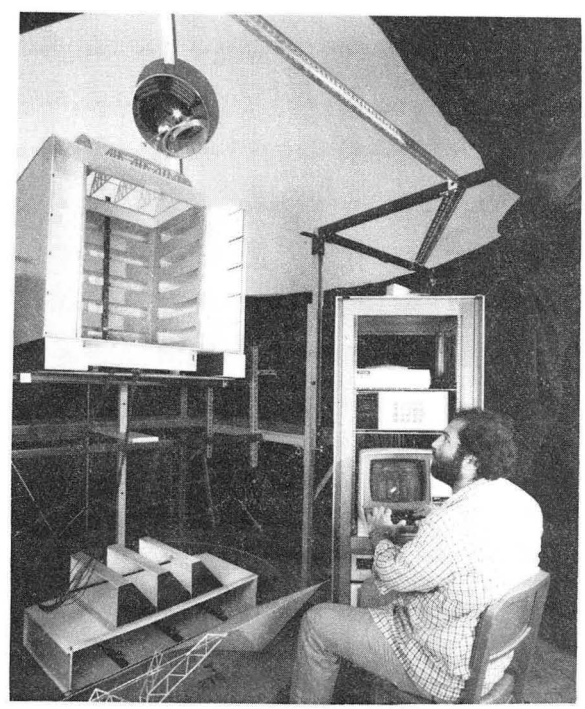

Figure 16. Interior of sky simulator showing reconfigurable scale model of a five-story atrium (with one side removed). (CBB 848-5926)

Outdoor Scale-Model Testing

In 1983 a 3000-ft^2 deck was constructed on the roof of Building 90 at LBL for model testing under outdoor sky conditions. We designed and built four platforms on this deck for scale models. The platforms can be oriented in different directions for simultaneous scale-model studies of the same design. We also installed a computerized data-acquisition system with 60 photometric sensors and appropriate data-collection software.

These facilities will be used to collect test data in parallel with our indoor model studies. Differences between the two sets of studies will help us understand how closely results from the standardized sky distributions in the simulator will predict results under real sky conditions. In FY 1984 there was little activity with the outdoor test facility, but in FY 1985 outdoor model tests will be carried out in conjunction with sky luminance measurements. The intent is to better understand the illuminance variability in interior spaces as a function of sky luminance distribution and the time-dependent variability under partly cloudy conditions.

Hemispherical and Bidirectional Visible Transmittance Testing

Accomplishments During FY 1984

The integrating sphere described in a preceding section (see Fig. 11) can also measure hemispherical visible transmittance of materials, devices, and building facades with an appropriate photometric sensor. Initial photometric measurements on a number of shading devices were made in conjunction with the thermal analysis testing described earlier. The sphere was also used to characterize the transmittance of 14 roof-glazing systems for atrium spaces.

The design and construction of the basic mechanical system of the luminance/radiance scanner was completed. The system will accept a 2 ft $\times$ 2 ft sample and scan at a maximum radius of about 6 ft. The system is driven by a series of stepper motors that at present are manually controlled.

Planned Activities for FY 1985

We expect to extend the calibration for the integrating sphere to include reflectance measurements and an improved assessment of measurement error. An improved collimated light source will also be designed and built.

Further research on the luminance scanner will center on development of the automated control system that will govern all aspects of the scanner operation and data acquisition. By the end of the year we expect to have the hardware installed and sufficient software operational so that limited data can be collected and analyzed.

DESIGN TOOLS

There is a continuing need to introduce improved daylighting design tools to potential users. In previous years the technical development of specific tools was undertaken by LBL staff and subcontractors. In FY 1984 increased emphasis was placed on documenting specific tools and distributing them to building industry professionals.

Accomplishments During FY 1984

New design tools for daylighting are beginning to be marketed by private-sector software firms, but it is difficult for a potential user to evaluate them. There is thus a need for photometric data and evaluation procedures to compare these tools. Initial steps were taken to develop the general procedure for comparisons and to establish a photometric data base derived from sky simulator measurements and SUPERLITE simulations.

To develop additional avenues of transferring daylighting research results to professionals, we contracted with Donald Prowler at the University of Pennsylvania to help initiate a daylighting research network of universities.

The plan for this network was reviewed by a group of practitioners and educators and was formalized as the Daylighting Network of North America (DNNA). An application process was initiated for two levels of network membership, Instructional Centers and Regional Centers. Regional Centers are intended to become nodes of daylighting research and dissemination activity for faculty and practitioner alike. The centers will make a concerted effort to plan and implement professional, educational, and design assistance programs.

The technical development of several daylighting design tools was completed during FY 1983. In FY 1984 the following design tools received additional testing, graphic development, packaging, and dissemination:

- *Clear Sky Protractors.* Developed with Harvey Bryan at the Massachusetts Institute of Technology (MIT), the protractors consist of a series of transparent overlays

that are placed over architectural plans and elevations to determine a window's daylight contribution at any point in a room.

- *MICROLITE 1.0.* This microcomputer-based program, a successor to QUICKLITE 1.0, can be used for daylighting analysis. A user-friendly version with color graphics for a microcomputer and a preliminary user's guide were completed by Harvey Bryan at MIT. The Designer's Software Exchange is distributing this package to educators and professionals.
- *SUPERLITE 1.0.* An extensive effort was launched to develop a graphically enhanced user's manual for this state-of-the-art mainframe computer model. Two draft versions of the manual were completed and reviewed. Final professional market evaluation is planned.
- *Daylighting Nomographs.* The completed manual and set of nomographs to estimate potential energy and peak-load savings in commercial buildings received additional professional distribution during FY 1984. More than 250 copies were selectively disseminated at engineering and architectural conferences and design tool workshops.
- *Advanced Envelope Design Tool.* As private firms have begun to develop and market simple microcomputer tools, we have turned our attention to the development of the next generation of more sophisticated tools based on advances in both hardware and software. We envision a tool that relies heavily on (1) imaging technologies to capture, store, manipulate, and present simulated environments as they are conceived and developed throughout the design process; (2) expert-systems software and design process studies to support the iterative and complex nature of building design; and (3) an array of information outputs to better communicate information between design team members and between the design team and the client. In 1984 we initiated a series of exploratory studies to better understand the requirements for such a tool. We also developed a working prototype of one useful element of this system, a self-calibrating photographic luminance camera that is described in more detail in the last part of this article.

Planned Activities for FY 1985

Additional technology transfer activities and specific dissemination pathways for daylighting research will be developed. A major emphasis will be placed on the further organizational development of the Daylighting Network as a focus for implementing daylighting research and information dissemination at a regional university-center level.

Final evaluation and dissemination of the SUPERLITE 1.0 User's Manual and program tape will be conducted during FY 1985.

Exploratory development of the Advanced Envelope Design Tool and several of its constituent elements will continue. The luminance camera will be tested and evaluated in a range of daylighted environments.

FENESTRATION PERFORMANCE IN BUILDINGS

Thermal and radiant energy flows through windows and skylights, unlike the flow through most other building-envelope components, can be managed so that these architectural elements provide net energy benefits to the building. Although heat loss and solar-gain-induced cooling loads must be minimized, solar gains in winter and useful daylight throughout the year reduce conventional energy requirements. Optimizing fenestration systems thus involves complex tradeoffs between competing requirements. Furthermore, since net energy use is a function of the interaction of the time-varying heat transfer through fenestration with the thermal and operational properties of the building, fenestration performance must be analyzed in the context of overall building performance if accurate conclusions are to be drawn. The optimum solutions do not depend on fenestration properties alone but may also be a sensitive function of climate, building type, orientation, and operating parameters. We examine fenestration performance in buildings from three complementary perspectives.

First, our *computer simulation studies* are designed to provide a better understanding of all aspects of optimizing fenestration design for energy performance and will lead to guidelines and analysis tools to assist the fenestration industry and the building design community. Our work originally focused on thermal performance in residential buildings but has shifted during the past 6 years to an emphasis on nonresidential buildings, including daylighting, peak-load management, and HVAC sizing issues.

As our second approach we have designed and built a heavily instrumented *Mobile Window Thermal Test (MoWiTT) Facility* to accurately measure the time-dependent HVAC load induced by fenestration under outdoor climate conditions. This facility tests the interaction of all climate parameters with a fenestration system installed in a room-like chamber, while eliminating or reducing many of the uncontrolled parameters one finds in complete buildings.

Some important performance issues, nevertheless, can be understood only by examining them in occupied buildings, so our third approach is direct measurement of fenestration performance as part of a *building monitoring program.* These three approaches, taken together, allow us to understand in detail the critical parameters that influence net fenestration performance in buildings.

SIMULATION STUDIES: NONRESIDENTIAL BUILDINGS

Most building simulation studies have focused on minimizing total energy consumption. Commercial and industrial customers, however, are generally billed for electricity on the basis of both energy consumption and peak electrical demand. A complete study of the cost effectiveness of fenestration systems, particularly daylighting strategies, must include their impact on peak electrical loads as well as on energy savings. Although the energy impact of daylighting has been under study by our group and others, there have been no prior detailed investigations of the impact of daylighting on peak loads.

Accomplishments During FY 1984

Over the past 2 years the energy performance of a five-zone prototypical office building has been simulated with DOE-2.1B for a wide range of glazing properties, window sizes, lighting loads, orientations, and climates. Both skylights and vertical fenestration were included. Initially we examined the impact of fenestration properties, including the effects of daylighting strategies, on office building energy performance and peak electrical demand. Lighting energy savings due to daylighting were examined for a range of fenestration properties and lighting control systems. Annual energy consumption of an office module was found to be sensitive to variations in the primary fenestration properties (U-value, shading coefficient, visible transmittance) as well as glazing area, orientation, climate, and operating strategy.

We conclude that, in almost all instances, it is possible to find a fenestration design strategy that outperforms a solid insulating wall or roof and that daylighting is almost always an essential component of the potential energy savings. If the installed electric lighting power density is high, the energy savings potential is large. However, if the electric lighting system is efficient and has low lighting power density, daylighting benefits will be smaller and may be negated by cooling loads from solar gain. We conclude that the net benefits of fenestration are highly dependent on the tradeoffs between daylighting savings and cooling loads resulting from solar gains. Visible transmittance properties, improved shading design, and window management will thus assume increasing importance for maximizing energy benefits from daylight.

A significant element of our studies has been a first attempt to quantify the impact of window-management strategies for controlling thermal comfort and glare from windows. Our studies in 1984 helped to identify three major technical factors that influence the daylighting/cooling balance. These are (1) the distribution of daylight in an interior space, relative to the lighting control sensor; (2) the luminous efficacy of transmitted daylight; and (3) the time-dependent variability in sunlight intensity based on climate conditions as well as hourly and seasonal patterns. Sample results from our simulation studies are shown in Figs. 17 and 18.

We continued our general studies on the peak-shaving potential of daylighting and completed a specific new analysis for West Coast climates as part of a study sponsored by Southern California Edison and Pacific Gas and Electric. Results show that—despite solar gains—daylighting can significantly reduce peak electrical demand during summer months. Parametric studies indicate that peak demand is a nonlinear function of glazing properties and window size for the daylighting case, but the relationship is almost linear in the nondaylighting case. The critical tradeoffs—between electric lighting reductions from daylighting and cooling load increases from solar gain—help determine the combination of window properties that minimize building peak loads. A breakdown of this load for a sample office building on the date of maximum demand is shown in Fig. 19 for both daylighted and nondaylighted cases. The economic implications of these results will depend on local utility rate structures. Figure 20 shows, as a function of installed lighting power density, conditions under which daylighted

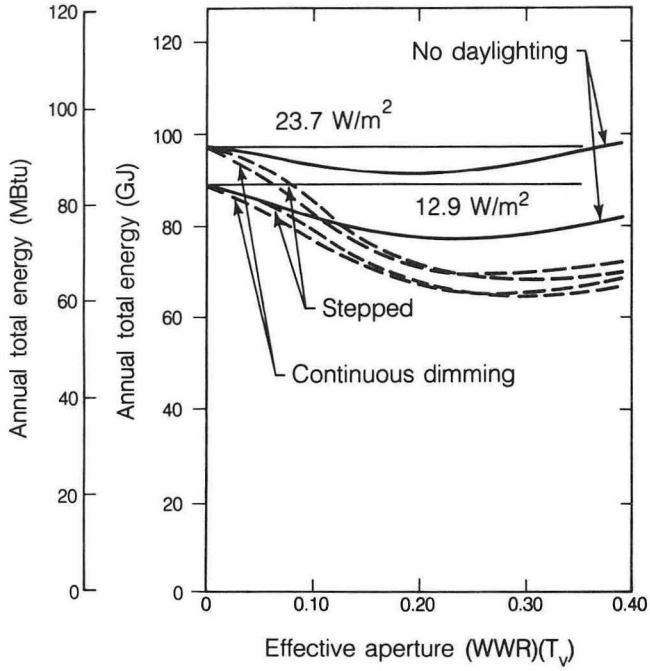

Figure 17. Energy consumption on the south zone of an office building in Madison, Wisconsin. The variation in annual energy use with window area and transmittance at two lighting power densities is shown for (1) an opaque exterior wall (thin horizontal lines), (2) a nondaylighted case, and (3) a daylighted case with two types of lighting controls. (XBL 847-9811)

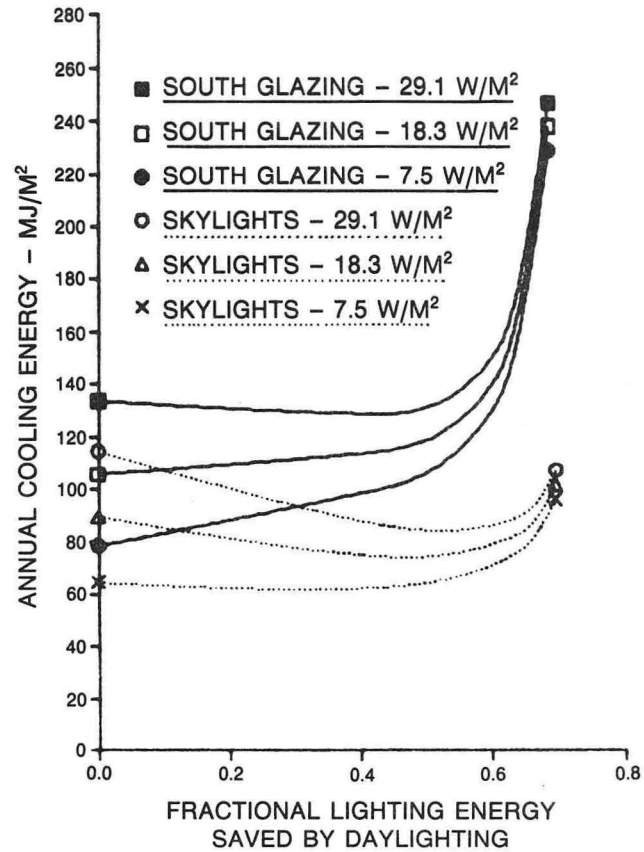

Figure 18. Cooling energy per unit floor area of daylighted space as a function of fractional electric lighting savings in Lake Charles, Louisiana. (XBL 856-2801)

offices with small or large windows may produce higher or lower peak demand than a nondaylighted space.

Energy effects with skylights follow similar patterns, with some noticeable differences. Daylighting benefits are maximized with relatively small ratios of skylight to roof areas (0.01–0.04). Because skylights provide more uniform daylight distribution, the cooling load impact of daylighting is less than with vertical fenestration. As effective aperture is increased beyond the minimum energy value, cooling loads rise rapidly to adversely affect net annual energy performance. Sample results for several climates are shown in Fig. 21. In FY 1984 these studies were extended to a wider range of climates, and additional sensitivity studies on key performance factors were completed.

The large number of DOE-2.1B parametric runs for window and skylight studies provided a data base large enough for multiple regression techniques to develop analytical expressions of energy requirements as functions of glazing parameters. This approach offers the potential for developing a generalized expression to accommodate climate variables. These simple expressions correlate well with DOE-2 results and offer the prospect of a design tool for easily assessing energy and cost trade-offs among fenestration options. The regression equations developed in our skylight studies have been adapted by the American Institute of Architects Foundation for a workbook on skylight design.

Simulations of advanced glazing materials having passive and active response functions indicate a large potential for these materials. The modeled performance compares favorably with conventionally managed windows and skylights, and automatic operation of the advanced glazings should be more reliable. Analysis in FY 1984 continued to examine the response of advanced glazing materials and the interaction of active fenestration control systems with building lighting and HVAC controls.

The DOE-2.1C program has new functional keyword features that allowed us to investigate the performance of optical switching materials. The shading coefficient and/or visible transmittance can be varied as an inverse function of incident solar radia-

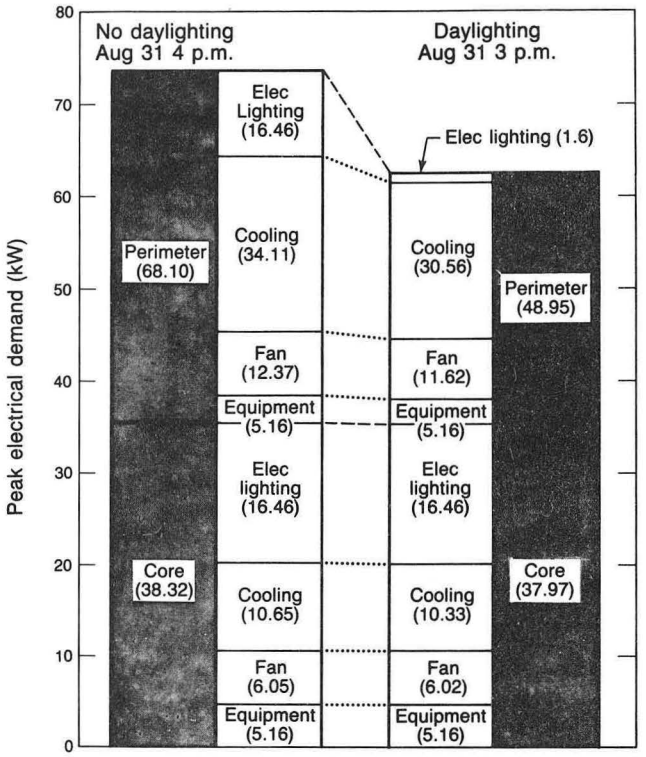

Figure 19. Peak electrical demand, broken down by end-use components, for an office building in Madison, Wisconsin. Nondaylighted (left) and daylighted cases are compared. Component breakdown is shown for the building's core (930 m^2) and perimeter (560 m^2) to reveal how daylighting can reduce peak demand in the outer zone. Numbers in parentheses indicate demand (W/m^2). Glazing area is 71% of floor-to-ceiling wall area; visible transmittance is 69%; lighting power density is 18.3 W/m^2. (XBL 8312-7444)

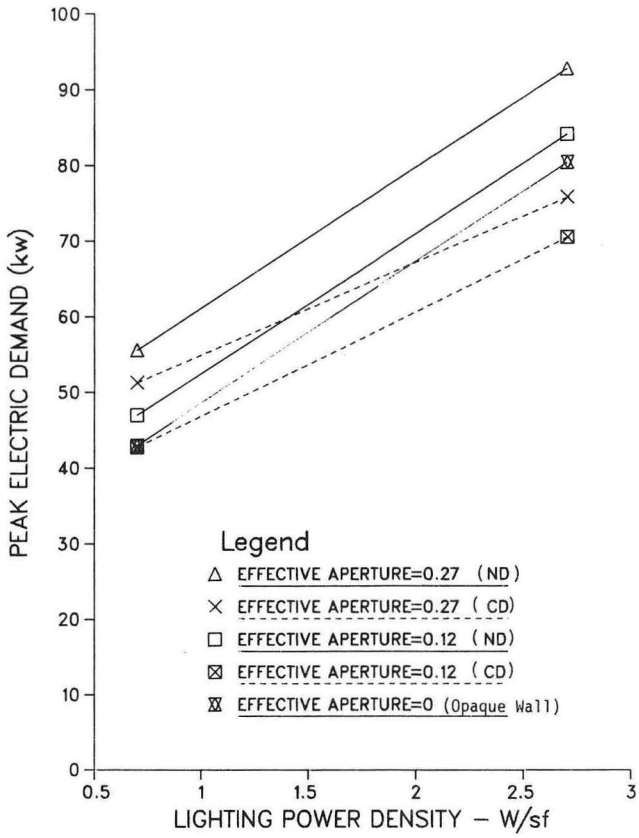

Figure 20. Peak electrical demand for an office module in Fresno as a function of installed electric lighting power density at two effective apertures in both daylighted (CD) and nondaylighted (ND) cases and an opaque wall. (XBL 856-2815)

tion, optical properties and setpoints can be altered, and the resulting effects of these still-hypothetical materials can be examined. Initial results suggest that simple control logic can provide performance equal to a conventionally operated window shade. We expect performance will improve with more sophisticated control logic. Electrically switched coatings could readily be made responsive to very sophisticated control algorithms to optimize energy, cooling loads, and costs. Since net cooling loads do not have an instantaneous relationship to transmitted solar gain due to time lags, "intelligent" anticipatory controls may prove to be beneficial. One control approach now being studied is to link the glazing transmittance to the daylight levels in the space so that excess light and solar gain are controlled. Sample simulation results are shown in Fig. 22. Ultimate control logic would integrate solar gain and daylight control with the operation of the building HVAC system. Simulations of this control mode will require additional modeling capabilities in DOE-2.

Planned Activities for FY 1985

Simulation studies to date have examined the energy impacts of many of the more important fenestration parameters within reasonable limits of design and have explored the potential of new optical materials. There are still important fenestration parameters to be studied, in particular shading devices for which adequate solar optical data do not exist. Optical properties of shading devices will be selectively measured in our laboratory and their annual performance simulated. We will also continue to look at variations in window-shade energy performance and management strategies, issues of daylight luminous efficacy, advanced glazing materi-

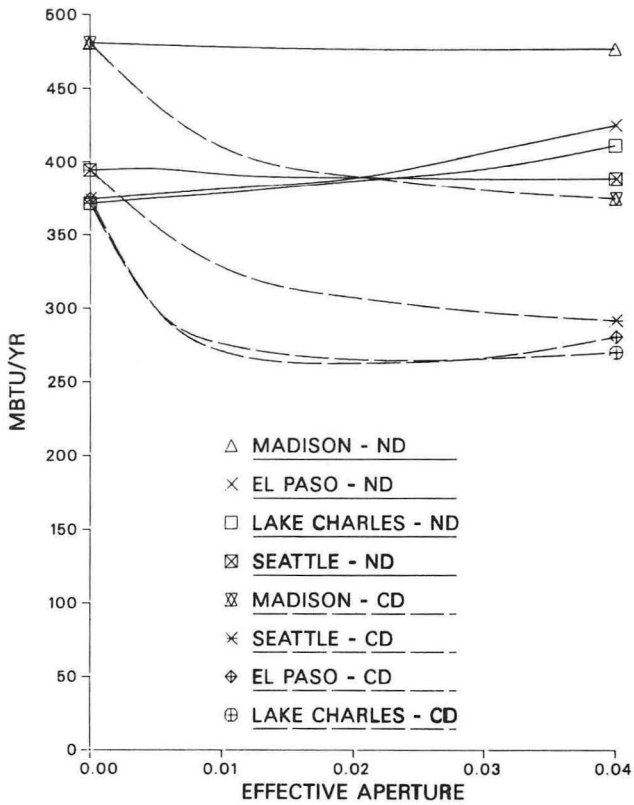

Figure 21. Energy consumption in a skylighted zone, showing variation in net annual consumption with effective aperture (skylight area and transmittance) for a non-daylighted (ND) and a continuously dimmed daylighted (CD) case in four climates. Installed lighting power density of 1.7 W/ft^2 provides 50 fc illumination. (XBL 8411-4635)

als, the effects of fenestration performance on HVAC, and the effects of various HVAC options on fenestration performance. The cost implications of fenestration design and daylighting as influenced by peak electrical demand, annual energy use, and chiller size will be examined.

Collaboration will continue with the Building Energy Simulation Group to develop improved window modeling capabilities. In particular development of improved exterior shading algorithms will be explored in conjunction with new measured data on solar shading devices.

SIMULATION STUDIES: RESIDENTIAL BUILDINGS

In previous residential simulation studies we examined the impacts of movable insulating systems on fenestration performance and compared them with the performance of several multiglazed insulating window alternatives. In FY 1983 we began to examine in more detail the tradeoffs between heat conductance and solar transmittance. The study uses the regression analysis techniques developed in our studies of commercial buildings and constitutes part of our contribution to the International Energy Agency cooperative study on fenestration performance.

Accomplishments During FY 1984

A full set of sensitivity analyses was completed to select the base case building design and its operational characteristics. Extensive sets of simulations were completed for two climate extremes: Madison, Wisconsin and Lake Charles, Louisiana. Using previously developed regression analysis techniques, we derived a set of simplified predictive equations for energy and cost performance. These equations were solved to directly predict fenestration properties that minimize cost and/or energy use. For a given climate, orientation, and window size, we developed graphic plots that allow one to quickly evaluate seasonal energy performance between many alternative existing or speculative fenestration systems (Fig. 23).

Planned Activities for FY 1985

One limitation of the simulation approach we have been developing is that a large set of simulations must be completed for each residential prototype in each climate. Initial studies conducted in FY 1984 suggest that it may be possible to extend results analytically between prototypes and climates. Efforts in FY 1985 will focus on developing the theoretical and analytical base for this approach and on testing its feasibility.

IN-SITU TESTING—FIELD VALIDATION

Net energy performance under actual conditions of use is the single piece of information most relevant to assessing the benefit to be derived from a window or window improvement. This is a dynamic property, essential for predicting the performance of managed window systems (windows having thermal and optical properties that can be manually or automatically changed by building occupants). Most laboratory testing facilities, however, are designed primarily to conduct steady-state measurements of static materials and devices. No experimental methodology exists for measuring the net performance of windows *in situ*.

In 1981 we began constructing a Mobile Window Thermal Test (MoWiTT) Facility to fill this experimental gap (Fig. 24); the facility will consist of one

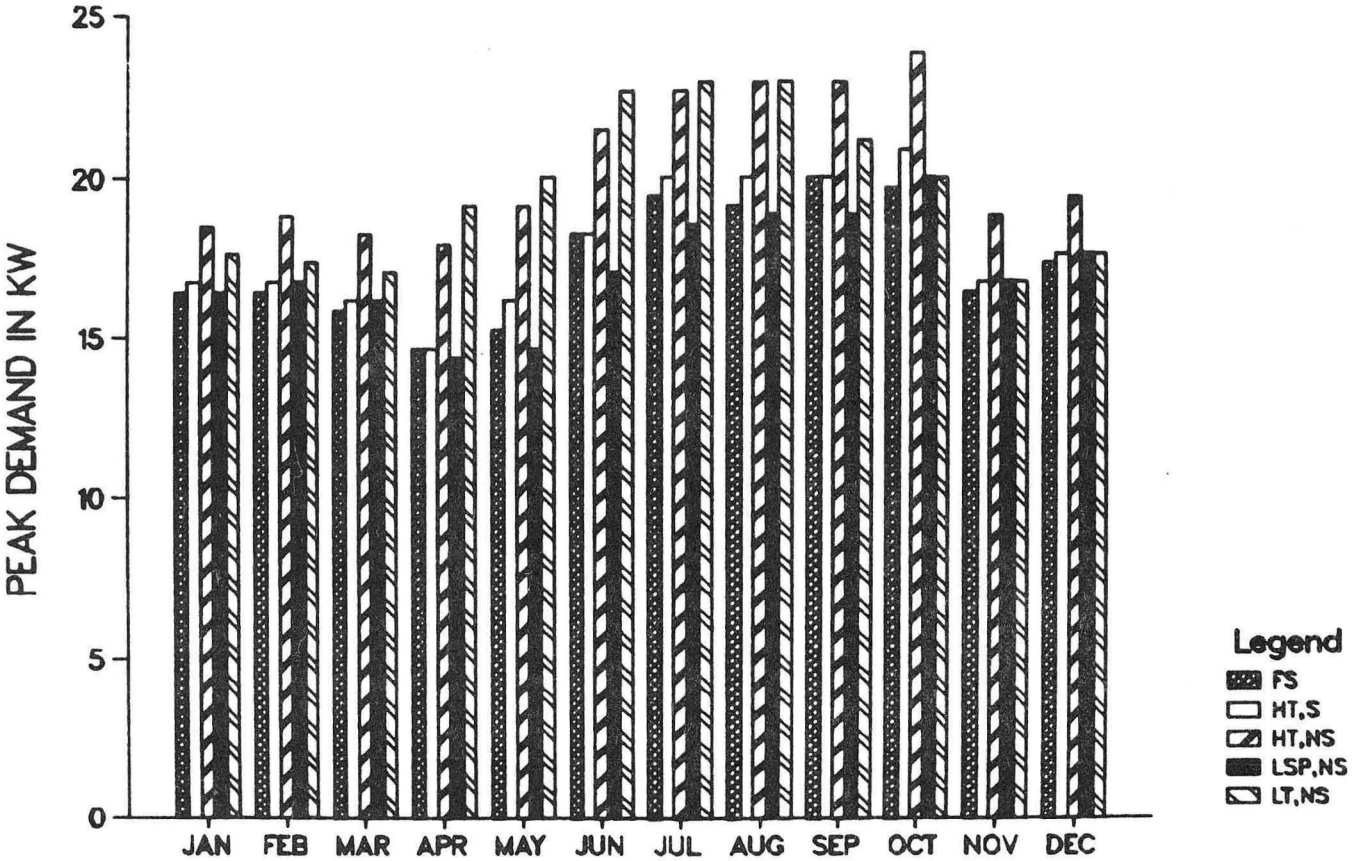

Figure 22. Monthly peak electric demand for an office building module in Madison, Wisconsin, comparing conventional glazings with two types of optical switching films. *FS*: electrochromic film with solar intensity control; *HT,S*: high-transmission glass with operable shading; *HT,NS*: high-transmittance glass without shading; *LSP,NS*: electrochromic film that maintains constant illuminance level; and *LT,NS*: low-transmission glass without shading. (XBL 856-2799)

or more measurement modules and an instrumented van. The measurement modules—each containing twin calorimeters surrounded by an air guard—will enable dynamic studies to be made of combined solar, infiltrative, conductive/convective, and radiative heat transfer as a function of window type and orientation.

An outgrowth of work on the MoWiTT facility was the development of a new heat-flow sensor. Instead of measuring the temperature difference with a deposited thermopile across a known thermal resistance (the usual method), this heat-flow sensor uses ac resistance thermometry. Such sensors can be made economically in sizes large enough to cover entire walls, and we have incorporated them into the MoWiTT facility.

In FY 1981 a successful 1-ft^2 prototype was built and tested, and larger units were built during FY 1982. In FY 1983 and FY 1984 these full-size units were calibrated with a large calibrated hotplate constructed at LBL for the purpose. Figure 25 shows the inside walls of a MoWiTT chamber completely covered with the sensors.

Accomplishments During FY 1984

The MoWiTT facility was readied for field deployment (Fig. 26). Basic construction was completed, and our efforts focused on calibration of all components and systems. Major accomplishments included the following:

- Tests of guard temperature-system capacity completed
- Guard air-handling system reconfigured to reduce air infiltration
- Air infiltration tests of both calorimeter chambers completed

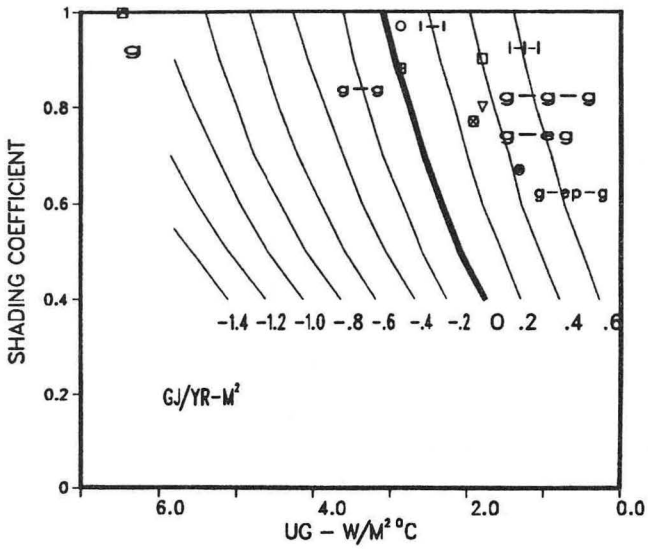

Figure 23. Net heating-season useful flux in Madison, Wisconsin, for a primary window area of 24.53 m^2 oriented due south. The performance of typical glazing systems is indicated in the table. (XBL 856-2800)

Glazing	U ($W/m^2°C$)	SC
g	6.46	1.0
g-g	2.87	0.88
g-g-g	1.8	0.8
g-eg	1.92	0.77
g-ep-g	1.32	0.67
l-l	2.87	0.97
l-l-l	1.80	0.9

g: 1/8 in. DS float glass
l: 1/8 in. low-iron sheet glass
e: low-emittance coating, e = 0.15
p: 4-mil polyester
All air gaps are 12.7 mm (1/2 in.)
U-value: standard ASHRAE winter conditions
SC: standard ASHRAE summer conditions

- Hotplate calibration of large-area heat-flow sensors for two chambers (83 m^2) completed
- Multiplexing and operation of wall-sized heat-flow sensor ensembles demonstrated

We meet twice each year with an industry advisory panel to review technical progress and discuss future plans.

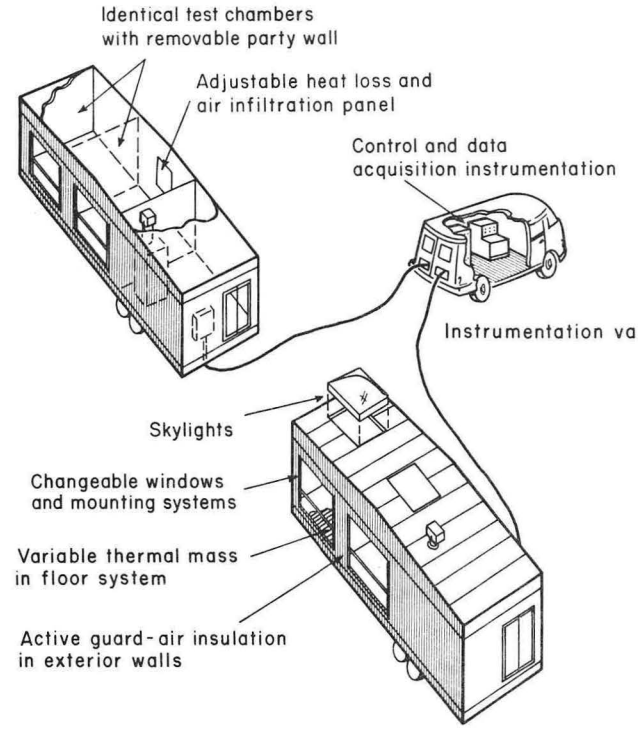

Figure 24. Schematic of Mobile Window Thermal Test (MoWiTT) Facility. One of the two double-module trailers has been built. (XBL 811-30)

Planned Activities for FY 1985

The accuracy of the calorimeters will be established by a series of redundant "closed-box" tests, and measurements on simple fenestration systems will be made. A "shakedown" period of operation will be conducted at a nearby field site in Livermore. After evaluation of these tests field operation will begin.

MONITORED BUILDINGS

Buildings are rarely built as designed and even less frequently operated as planned. It is well known that occupants can significantly alter energy consumption patterns in buildings. Thus, for energy performance to be accurately quantified, it is essential to monitor fenestration performance in occupied buildings. Our monitoring studies will provide results of critical importance to designers, building owners, and utility companies. In 1984, with support from Pacific Gas and Electric Company, we began to develop plans to monitor an award-winning 500,000-ft^2 office building that incorporates a number of innovative daylighting and fenestration systems. The objective is not only to better under-

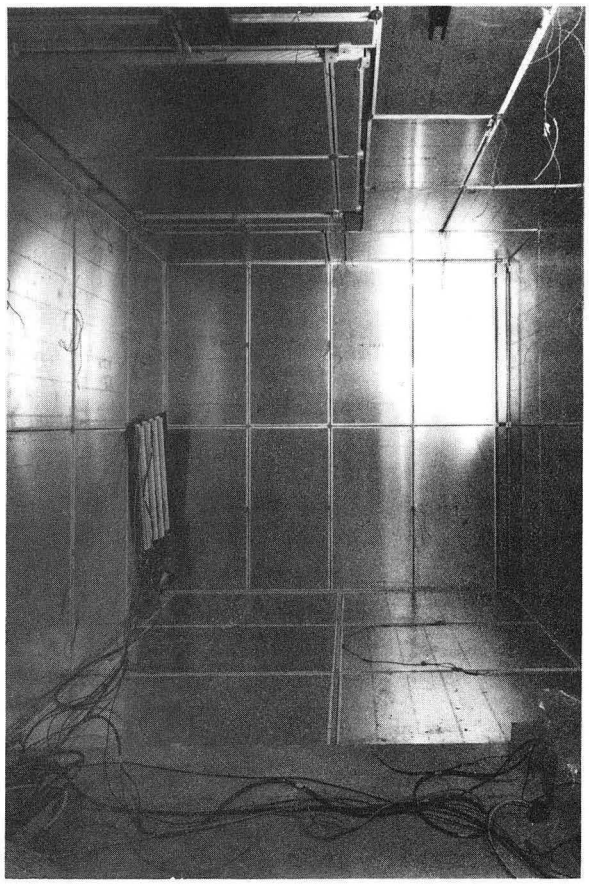

Figure 25. A MoWiTT calorimeter chamber completely instrumented with heat-flow sensors. Window will be mounted in far wall after calibration is complete. (CBB 838-7737)

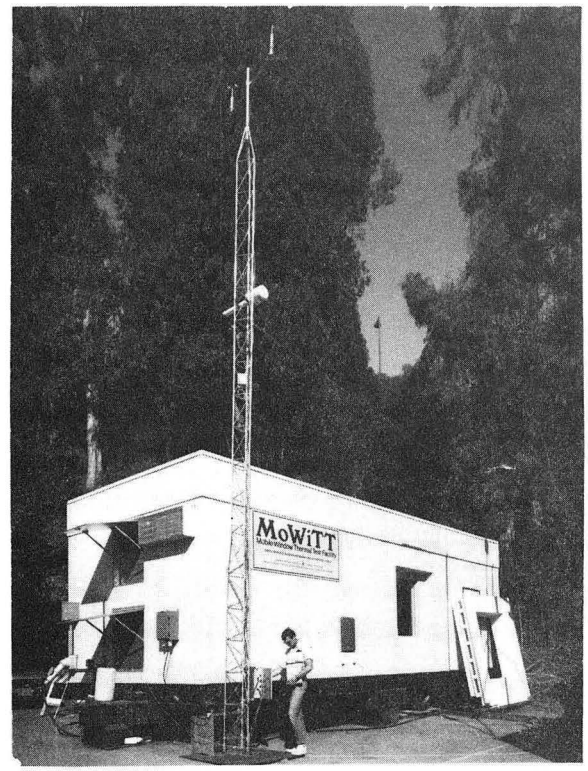

Figure 26. The MoWiTT Facility undergoing calibration and trial field test at LBL. Left chamber is fitted with a window; right chamber is undergoing a "sealed box" calibration test, after which it will be fitted with the frame system shown leaning against the wall. Left section of trailer contains chiller, fans, and pumps and the computerized data acquisition system that controls operation of the facility and records relevant data. (CBB 830-9555)

stand how the fenestration systems perform but also to develop a building monitoring approach that collects better data, useful for quantifying fenestration performance, at lower cost than has been possible before. We expect to complete the monitoring plan and begin deploying instrumentation in FY 1985. We also hope to identify other buildings with innovative fenestration systems that might become part of this monitoring program.

FENESTRATION IMPACT STUDIES

OCCUPANT RESPONSE TO FENESTRATION AND LIGHTING CONTROL SYSTEMS

In FY 1982, to study office-worker responses to lighting and fenestration controls, we developed a survey methodology that includes a written questionnaire and related physical measurements. The questionnaire asks each office worker to rate his or her responses to lighting and related thermal and acoustical conditions. Also included are demographics characterizing each worker (sex, age) and the worker's workplace (floor level, location, and type of office).

In FY 1983 we tested this methodology in two office buildings, one retrofitted, the other designed to be "energy-efficient." Preliminary analyses indicate that the surveys identified issues of concern to office workers but that additional responses regarding work tasks and organization are needed to quantify causal effects between worker responses and related environmental conditions.

Accomplishments During FY 1984

We completed analysis of survey results to date and published our findings for the retrofitted office building. We further refined the survey methodology

and conducted several walk-through surveys of buildings to better define key issues and select candidate buildings for future studies. A significant conclusion in our earlier surveys was the importance of quantifying the impact of daylight on the interior luminous environment. We therefore initiated a project to develop a luminance mapping capability for field studies of occupied buildings.

A survey and review of alternative imaging techniques was completed by Don Carner of Energy Conservation Associates, and a prototype photographic luminance camera was developed (Fig. 27). A 35-mm camera with a fisheye lens was modified to imprint an absolute optical density gradient scale on each exposure taken by the camera, so that an optical density map of the image can readily be converted into a luminance map, using an automated microdensitometer.

Planned Activities for FY 1985

Calibration of the camera will be completed, and a prototype system for digitizing the negatives and manipulating the resulting data to create the luminance maps will be implemented.

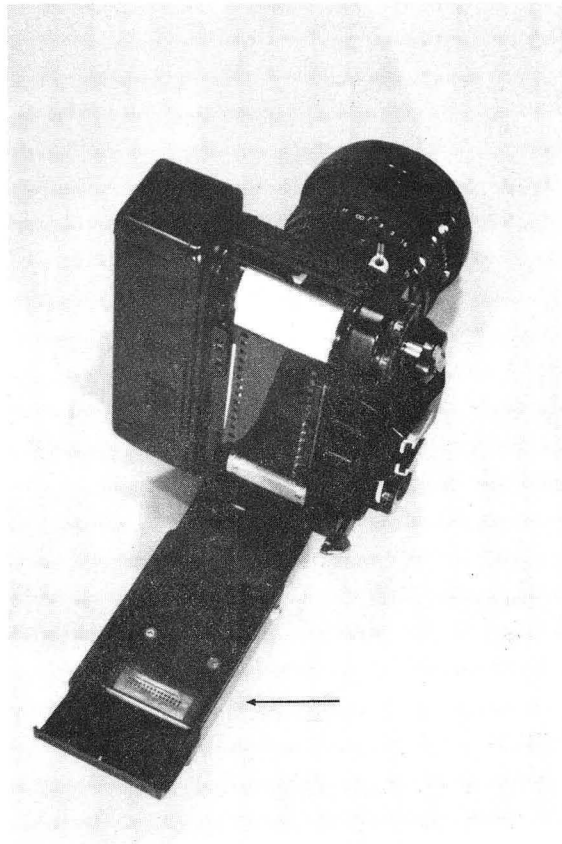

Figure 27. A prototype photographic luminance camera, with back opened to show panel for imprinting optical density scale (arrow). (CBB 857-5596)

REFERENCES

For additional references, see the Windows and Daylighting section of the Publications List.

1. Rubin, M. (1984), *Optical Constants and Bulk Optical Properties of Soda-Lime Silica Glasses for Windows*, LBL-13572, to be published in *Solar Energy Materials.*
2. Tewari, P.H., Hunt A.J., and Lofftus, K.D. (1985), "Structure and Chemistry of Sol-Gel Derived Transparent Silica Aerogels," in *Ultrastructure Processing of Ceramics, Glasses, and Composites*, presented at 2nd Ultrastructure Conference, Palm Coast, Florida, March 1, 1985.
3. Russo, R.E. and Hunt, A.J. (1985), "Comparison of Ethyl vs. Methyl Sol-Gels for Silica Aerogels using Polar Nephelometry," submitted to *J. Non-Crystalline Solids*; LBL-19693.
4. Tewari, P.H., Hunt A.J., and Lofftus, K.D. (1985), "Advances in Production of Transparent Silica Aerogels for Window Glazings," presented at the 1st International Conference on Aerogels, Wurzburg, West Germany, September 23–25, 1985.
5. Tewari, P.H., Hunt A.J., Lieber, J., and Lofftus, K.D. (1985), "Ambient Temperature Supercritical Drying of Transparent Silica Aerogels," *Materials Letters 3*, p. 363.
6. Tewari, P.H., Hunt, A.J., Lieber, J., and Lofftus, K.D. (1985), "Microstructural Properties of Transparent Silica Aerogels," presented at the 1st International Conference on Aerogels, Wurzburg, West Germany, September 23–25, 1985.
7. Lampert, C.M. (1984),"Electrochromic Materials and Devices for Energy-Efficient Windows," *Solar Energy Mat. 11*, p. 1.
8. Rauh, D. and Cogan, S. (1984), "Materials for Electrochromic Windows," *Proc. SPIE 502,* p. 38.
9. Goldner, R.B., *et al.* (1984), "Optical Mobility Studies on Electrochromic Films for Variable Reflectivity Windows," *Proc. SPIE 502*, p. 54.
10. Goldner, R.B., *et al.* (1983), "High Near-Infrared Reflectivity Modulation with Polycrystalline Electrochromic WO_3 Films," *Appl. Phys. Lett. 43*, p. 1093.

11. Benson, D.K., Tracy, C.E., and Ruth, M.R. (1984), "Solid-State Electrochromic Switchable Window Glazings," *Proc. SPIE 502*, p. 46.
12. Karayel, M., Navvab, M., Ne'eman, E., and Selkowitz, S. (1984), "Zenith Luminance and Sky Luminance Distributions for Daylighting Calculations," in Technical Proceedings of the 1983 International Daylighting Conference, Phoenix, AZ, February 16–18, 1983, J.W. Griffith and J.I. Yellot, Eds., *Energy and Buildings 6*, p. 283; LBL-15622.
13. Navvab, M., Karayel, M., Ne'eman, E., and Selkowitz, S. (1984), "Daylight Availability Data for San Francisco," in Technical Proceedings of the 1983 International Daylighting Conference, Phoenix, AZ, February 16–18, 1983, J.W. Griffith and J.I. Yellot, Eds., *Energy and Buildings 6*, p. 273; LBL-15623.
14. Navvab, M., Karayel, M., Ne'eman, E., and Selkowitz, S. (1984), "Analysis of Atmospheric Turbidity for Daylight Calculations," in Technical Proceedings of the 1983 International Daylighting Conference, Phoenix, AZ, February 16–18, 1983, J.W. Griffith and J.I. Yellot, Eds., *Energy and Buildings 6*, p. 293; LBL-17727.
15. Griffith, J.W. and Yellot, J.I., Eds. (1984), Technical Proceedings of the 1983 International Daylighting Conference, Phoenix, AZ, February 16–18, 1983, *Energy and Buildings 6*, Nos. 2–4.

Lighting Systems Research*

S.M. Berman, R.R. Verderber, R.D. Clear, D.D. Hollister, F. Li, D.J. Levy, O.C. Morse, F.M. Rubinstein, M.J. Siminovitch, G.J. Ward, and T.M. Zhou

We estimate that 50% of the electrical energy consumed by lighting, or about 12% of total national electrical energy sales, could be saved by gradually replacing existing lighting with energy-efficient lighting. This would amount to a yearly savings of some 220 billion kilowatt-hours of electricity.

The objective of the Department of Energy's National Lighting Program is to assist the lighting community (manufacturers, designers, and users) in achieving a more efficient lighting economy. The program, carried out at Lawrence Berkeley Laboratory (LBL), represents a unique partnership between a national laboratory–university complex and industry, facilitating technical advances, strengthening industry capabilities, and providing designers and the public with needed information.

To implement its objectives, the Lighting Program has divided its work into three major categories: engineering science, building applications, and impacts on human health and productivity.

The engineering science component undertakes research and development projects in lamp technology that are both long range and high risk. These are projects in which the lighting industry has an interest but does not pursue on its own and from which significant benefits could accrue to both the public and industry if the technical barriers were surmounted.

The building applications component undertakes research on the electromagnetic compatibility of high-frequency lighting with building functions, including machinery, computers, and other electrical and electronic systems as well as the interaction of lighting with building energy systems.

The impacts component examines relationships between workers and the physical lighting environment to ensure that energy-efficient technologies contribute to human productivity and health. These efforts are interdisciplinary, involving engineering, optometry, and medicine.

*This work was supported by the Assistant Secretary for Conservation and Renewable Energy, Office of Building and Community Systems, Building Equipment Division of the U.S. Department of Energy under Contract No. DE-AC03-76SF00098. Support was also received from the Electric Power Research Institute, Palo Alto, CA, and from the U.S. Naval Research and Development Center, Annapolis, MD.

Since its inception in 1976, the LBL Lighting Program has produced more than 105 reports and publications. These reports are available to the public and document research on subjects such as solid-state ballasts, operation of gas-discharge lamps at high frequency, daylight availability, energy-efficient fixtures, lighting control systems, and visibility and human productivity. Its internationally recognized interdisciplinary staff spans the fields of engineering, physics, architecture, optometry, and medicine and is involved in a variety of professional, technical, and governmental activities.

The Lighting Program combines the facilities and staff of LBL with those of the University of California College of Environmental Design and School of Optometry, both on the Berkeley campus, and the School of Medicine in San Francisco (UCSF). Because results are directed at enhancing the capabilities and long-term viability of the lighting industry and providing the design profession and the general public with needed information, the program is unique in the United States.

Described below are highlights of the accomplishments realized in FY 1985 by each of our three major efforts—engineering science, building applications, and health impacts—and activities planned for FY 1986. Publications and conference presentations of the past year may be found in the publications list at the end of this chapter.

ENGINEERING SCIENCE

The engineering science effort focuses on *advanced lamp technology* and light source development. To see what can be accomplished in this area, consider that today's fluorescent lamp has a luminous efficacy of approximately 80 lumens of light output per watt of electrical power input. Although this is nearly four times as efficient as an incandescent lamp, still greater efficacies are possible. White light can, theoretically, be produced at almost 450 lumens per watt. The advanced lamp technology program is working to supply the engineering science that will provide the basis for an efficacy of 200 lumens per watt within the next few years.

Two significant loss mechanisms have been isolated as targets of technical opportunity for achieving more efficient fluorescent lamps. The first application is to effect a reduction in the self-absorption of the ultraviolet (UV) radiation, a process that occurs within the lamp plasma before it strikes the phosphor-covered inner wall (the phosphor converts the UV radiation into visible light). The second is development of a more efficient phosphor matrix that will convert one energetic UV proton into two

visible photons. Reductions in self-absorption could provide a 30% improvement, while a two-photon phosphor could double lamp efficacy.

LBL is studying several ways of reducing the UV self-absorption. The first method is altering the isotopic composition of mercury. This element has seven stable isotopes, each with slightly different resonance UV emission spectra. Altering the naturally occurring isotopic composition can provide more escape channels for the resonance radiation, thereby reducing the probability of quenching collisions and increasing the amount of UV radiation reaching the phosphor. One possibility for isotope alteration—enrichment with ^{196}Hg—is being pursued in a joint effort by LBL and GTE Lighting. Should isotopic alterations prove economical, modified lamps would enter the market quickly, as lamps would simply be loaded with isotopically enriched rather than natural mercury, with other components remaining the same.

Another method of reducing UV self-absorption was recently discovered at LBL. It involves an applied magnetic field having a direction parallel to the main current. Axial magnetic field strengths of about 600 gauss can increase light emission by 6% to 10%. LBL and major firms in the lamp industry are studying practical ways to apply this technique.

To reduce the effects of energy loss in the phosphors requires altering the lamp's phosphor material. The materials used today convert each UV photon into at most one visible photon. Improving this conversion rate would increase the efficacy of low-pressure discharge lamps. Although the energetics are sufficient to permit the cascade conversion of a UV photon into two visible photons, this process must occur quickly, and the intermediate level in the cascade must be tuned carefully to ensure that both emitted photons are in the visible spectrum. LBL is studying phosphor chemistry to discover whether the two-photon phosphor is feasible. The lamp industry, long aware of the complexity of this problem and the extensive research effort required to provide solutions, is eagerly awaiting results.

A third mechanism developed at LBL uses a plasma excitation principle that allows for its excitation to be primarily near the inner lamp wall thereby reducing the UV transport distance and the likelihood of entrapment loss. This surface wave mode of operation occurs at high frequencies in the RF range between 100 and 1000 MHz and permits the lamp excitation without electrodes. This surface wave lamp shows better than 30% increased energy efficacy over fluorescents and operates without starting circuits and should be very long lasting because of the absence of electrode sputtering.

If these research directions at LBL come to full technological and commercial fruition, future fluorescent lamps should operate at high frequency and be isotopically enriched, magnetically loaded, and coated with a two-photon phosphor. Such lamps would have an efficacy of more than 200 lumens per watt, three times that of today's 60-cycle fluorescent.

Other lighting technology research concentrates on high-intensity discharge (HID) lamps, which could be made both more efficient and dimmable if operated without electrodes. High-frequency operation is required to excite the lamp plasma in an electrodeless mode; it may also permit lamps to function with just one or two metal halides and no mercury or sodium. Electrodeless operation would also enable the use of compounds that have desirable light output and color but that are excluded today because they would harm electrodes. Finally, an electrodeless lamp that could be dimmed without observable spectral changes would appeal to lighting designers. Table 1 summarizes these major targets of opportunity.

To address the lack of data on the plasma discharges, a program on plasma diagnostics has been initiated to measure electron and ion distribution in optically thin and thick plasmas.

Accomplishments During FY 1985

Mercury Absorption Studies

The mercury isotope separation study was conducted using the laboratory-scale photoionization reactor. This technique achieved a 47-fold enrichment of ^{196}Hg with the continuous flow process. The next step is design and construction of a pilot plant to produce this Hg isotope in sufficient quantity for filling lamps.

A simpler procedure was developed for obtaining a weighed amount of ^{201}Hg isotope in a lamp. The ^{201}Hg was amalgamated on a gold foil and weighed before and after the Hg was removed by heating. The second method to determine the amount of ^{201}Hg, pumping the Hg between two "cold" spots at opposite ends of the lamp, was found to be more accurate if the cold spots were inside the lamp. External cold spots gave erratic results.

Table 1. Targets of opportunity in lighting technology.

Technology	Comment	Total efficacy (lm/W)	Year entering market
Fluorescent lamps			
High-frequency operation		90	1980
Narrow-band phosphors		100	1983
Isotopically enriched	LBL/DOE	110	1988
Magnetically loaded	technical	135	1990
Two-photon phosphor	initiatives	200	1992
Gigahertz/electrodeless		230	1994
HID Lamps			
Today with (high-freq. ballast)			
400-W high-pressure sodium		(CRI-25) 100	1984
400-W metal halide		(CRI-66) 80	1984
400-W mercury vapor		50	1984
Electrodeless/high-freq.			
1000-W lamps	10–15% improvement		1989
Low-W lamps	30% improvement		1989
New gases	20–25% improvement		1990
Color-constant/dimmable	20–25% improvement		1993

Magnetic Enhancement

A Helmholtz coil system was constructed to measure the enhanced efficacy of a low-pressure discharge lamp immersed in an axial magnetic field. Figure 1 is a photograph of the system. The gas-discharge lamp is placed in a temperature-controlled integrating cylinder, which is surrounded by the 18-in. water-cooled Helmholtz coils. A photometer on the right side of the integrating cylinder measures the total light flux from the lamp. The power input to the lamp is measured over a range of magnetic fields from zero to 1000 gauss. The measured increase in lamp efficacy is from 3% to 7% at 800 gauss.

Surface-Wave Lamp

A second-generation surface-wave launcher with impedance matcher was designed and built. This new system permits instant starting of the lamp and assures perfect impedance matching once the lamp is ignited, which means that all of the r.f. power is delivered to the plasma with no reflected component. This is a requirement for improved efficiency. Using the surface-wave launcher resulted in a better than 30% gain in efficacy in a standard F15, T-8 fluorescent lamp (15 watt, 1 in. diameter, 18 in. long), operated at normal power input at 60 Hz.

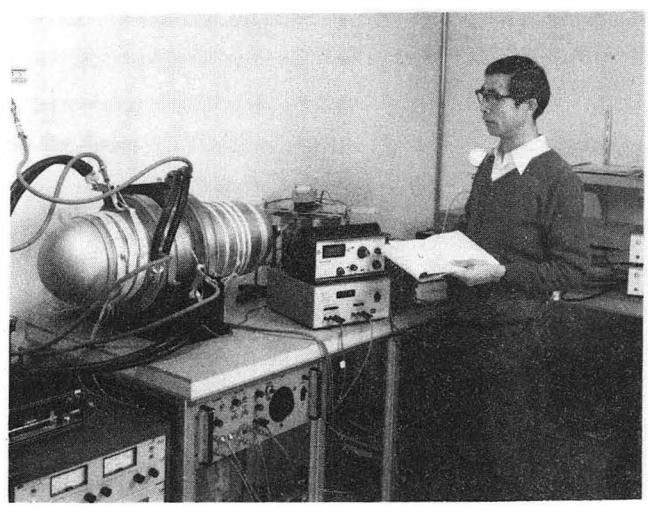

Figure 1. Photograph of the Helmholtz coil system (with test lamp in the integrating system) used to gather the total light flux of the lamp immersed in an axial magnetic field. (CBB 850-9876)

Electrodeless HID Lamp

Subcontractors have completed the first studies of the performance of new gases in electrodeless HID lamp systems. These gases could not be used in the past because of their corrosive interaction with the tungsten filament of lamps with electrodes. One lamp's efficacy was measured at 170 lumens per watt with a color rendering index (CRI) of 50. A lamp designed for optimum color rendition showed a CRI of 95 at an efficacy of 80 lumens per watt. These initial results indicate the vast improvements that can be realized with the electrodeless system. Notice in Table 1 that the 1000-watt high-pressure sodium lamp has an efficacy of 100 lumens per watt with a CRI of 25, while the metal-halide lamp with good color rendition has a CRI of 66 at 80 lm/W.

Diagnostics

To support the Lighting Program's lamp development efforts, we must characterize optically thick plasmas. We have set up spectroscopic equipment for measuring emission and absorption of the low- and high-pressure plasmas.

To study the metallic arc spectra, an electrodeless source assures the spectral purity of the plasma. The source can be operated at frequencies of 13.56 or 27.12 mHz at average power up to 1 kW.

The electrodeless light source can be filled with a variety of materials in the vacuum/filling/baking system.

Planned Activities for FY 1986

Mercury Absorption Studies

A lamp has been constructed and enriched with ^{201}Hg, increasing its concentration from its naturally occurring concentration of 15% to amounts ranging from 30% to 60%. Measurements on the lamp will be made to confirm the Richardson-Berman theory, which predicts that a maximum increase in lamp efficacy will occur in this isotope-concentration range. The result will have a significant bearing on the final method used to separate the Hg.

We are planning to complete detailed measurements of the ^{201}Hg-enriched low-pressure gas-discharge lamp. Measuring the amounts of Hg and isotope additions by two methods will assure the high degree of accuracy critical to selecting the Hg isotope for Hg isotope separation.

There are plans to consider an additional isotope separation process beyond the photochemical principles being worked on at GTE, which would utilize the AVLIS system at LLNL. The work in this area is dependent on the availability funds.

Magnetic Enhancement

LBL will systematically measure the lamps housed in the UV integrating cylinder to characterize the phenomenon of magnetic enhancement. The effect will be studied as a function of field intensity, lamp-wall temperature, gas fill, and input power. The angular distribution of the ultraviolet radiation will be examined to determine the extent of polarization. Finally, the change in the hyperfine structure will be studied with the high-resolution Jarrell-Ash spectrometer that has been put into commission.

Surface-Wave Lamp

The critical parameters influencing lamp efficacy including lamp diameter, length, and gas fill will be studied. We will continue investigating methods of screening lamps to contain the electromagnetic radiation. Initial measurements indicate that the levels a few feet from the lamps are negligible.

Electrodeless HID Lamp

The initial goal of this project was to develop a low-wattage, efficient HID lamp to replace the incandescent lamp. The effort to date has examined high-wattage, 400-watt lamps. A model of an electrodeless mercury-discharge HID lamp will be developed and used to determine the minimum wattage lamp feasible.

Diagnostics

The Lighting Program has described a technique to view and study slices of the plasma. The data can be analytically unfolded to determine the spatial distribution of mercury in the excited state through the plasma. A special precision-stepping motor mounted on an optical bench is required for scanning the plasma, and will be designed and constructed for conducting the measurements.

BUILDING APPLICATIONS

This component of the Lighting Program considers ways to apply energy-efficient lighting to buildings. Specific applications must take into account building type, location, type of work, schedule, climate, and other real-life factors that affect lighting criteria. The program therefore considers computer simulations of possible energy-efficient lighting with concomitant control systems, the effects of high-frequency lighting systems on the general electromag-

netic compatibility of buildings, and the interaction of lighting with a building's HVAC systems.

Accomplishments During FY 1985

CONTROLITE

The CONTROLITE program was completed. This computer program is designed to be compatible with an IBM PC and to determine the most cost-effective lighting control strategy to implement for a particular space. A two-day workshop presented the program to 50 participants, including controls manufacturers, lighting consultants, and architects. Discs and the documentation were given to the participants. Several errors were subsequently found by these participants and the final corrected program was made available. Over 100 copies have been requested and it appears that CONTROLITE will be a standard lighting program.

Advanced Lighting Design

The luminaire and lamp/ballast thermal testing chambers have been constructed and debugged. Some initial data show several important thermal features and advantages of the air-handling fixtures. We have presented papers and some preliminary results at the IES and IEEE/IAS meetings, and are now prepared to test various generic-type fixtures for the energy-efficient lighting layouts and the NBS program.

Figure 2 is a photograph of the luminaire thermal test chamber. The luminaire is placed in position and the room temperature and air flows can be varied. The rate of air flow is measured by an orifice in the tube shown in the figure. Figure 3 shows the dramatic increase in the light output when the minimum lamp wall temperature is decreased from 55°C to 40°C by an air flow of 50 cfm through the fixture.

An external cold spot inducer was devised based on the Peltier effect. Cursory experiments showed that supplying less than 0.5 watt to the device could save 6 to 10 watts for a 4-ft, F-40, fluorescent lamp, operated at an elevated temperature, which represents many typical installations. A patent disclosure has been filed and legal counsel has recommended applying for a patent. In FY 1986 LBL will develop concepts for practical use of this invention. About 40% of all fluorescent lighting installations are operated in this elevated mode. If widely used this device has the potential of saving 80 billion kWh annually.

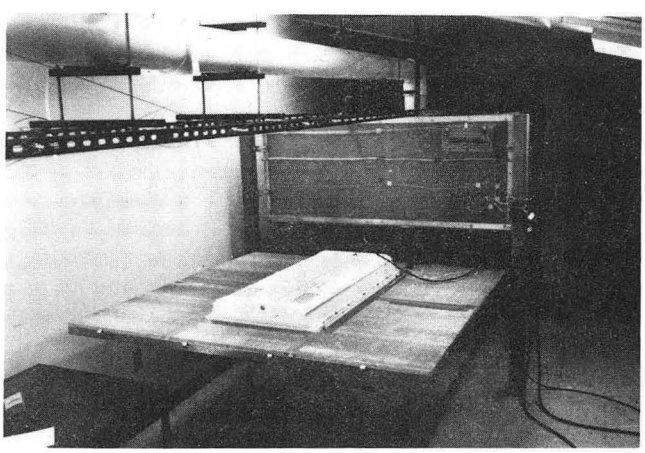

Figure 2. Photograph of the luminaire thermal test chamber for measuring thermal performance of fixtures. (CBB 855-4074)

Planned Activities for FY 1986

CONTROLITE

To further the use of lighting controls, we are preparing to write a chapter for the new Illuminating Engineering Society (IES) Handbook. This is the first time that a section has been devoted to lighting controls.

Advanced Lighting Design

We will use both the lamp/ballast integrating chamber and the luminaire thermal chamber to measure the thermal performance of four types of fixtures: open air, enclosed, air-handling, and parabolic. The data will be presented to NBS to help

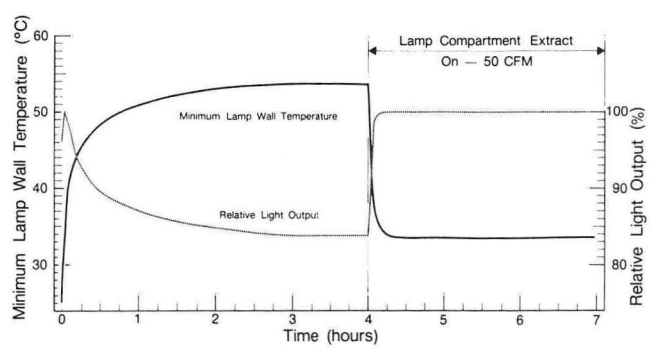

Figure 3. Plot of the minimum lamp-wall temperature (MLWT) and relative light output as a function of time for no air flow and a 50-cfm flow of air through the fixture. (XBL 858-3264)

their project determine the effect of lighting systems on the heating and cooling of spaces. In addition, we will present these techniques to NEMA to aid in setting up recommended testing standards, as well as establishing an explicit metric for the thermal performance of luminaires.

Optimization of Design Layouts

We are initiating our effort on dynamic lighting design. An open office space will be laid out and data from our luminaire test chamber and lamp/ballast integrating chamber will be input to determine the best energy-efficient system. The lighting will be evaluated with respect to economics as well as quality of illumination.

IMPACTS OF NEW LIGHTING TECHNIQUES ON PRODUCTIVITY AND HEALTH

The idea that lighting might negatively affect health has appeared often in the lay press in the past few years. Many factors have been implicated, but scientific data are lacking, especially to ascertain whether new energy-efficient technologies have adverse effects on human health and productivity.

Factors that may influence performance and productivity (as well as energy efficiency) may be associated with the lamp, the electronics and associated controls, the fixture, or the geometry and location of the lighting system. These lighting factors are: color variations; glare; intensity fluctuations; spectrum variations, including the ultraviolet region; electromagnetic fields generated by the lamp, ballast, or controls; and flicker, all of which could evoke a variety of human responses (behavioral, psychophysical, physiological, or biochemical).

Our research seeks to assure that new energy-efficient lighting technologies do not adversely affect human health and productivity. We are investigating whether any aspect of the new technologies can produce responses in humans. If they do, the effects will be characterized and the necessary changes in lighting technologies identified. Although subjective responses of workers provide some information, such responses are generally confounded by a mix of sociological factors and individual motivations; the investigations carried out by LBL use nonsubjective responses to establish cause and effect and ensure repeatability.

The impacts program is divided into three areas: (1) direct effects of lighting on the human autonomic system (carried out at UCSF), (2) interactions between lighting and visual display terminal operation that affect productivity or comfort (carried out at the UC School of Optometry), and (3) analysis of the general relationship between lighting and visual performance.

In the first area of this program, lamps to be evaluated include incandescent, cool-white fluorescent, full-spectrum fluorescent, high-pressure sodium, and metal halide. Human responses to exposure to various lighting conditions will be assessed by monitoring autonomic responses. Parameters to be monitored include heart rate, respiration rate, galvanic skin response, muscle strength, exercise tolerance, facial expression, and pupillary response. Behavioral measures to be used include memory (Wechsler Memory Scale and Sternberg's Memory Scanning Time), cognitive function (mental arithmetic), time estimation, and simple reaction time. Other behavioral tasks probably will be implemented.

Data-gathering and subject control are supervised by trained medical personnel. A national technical advisory committee oversees and reviews the project. First results of this effort concern the effects of visible-spectrum and low-frequency radiation on human muscle strength; as described below, they indicate that subjective psychological factors are the likely cause of reported effects.

Accomplishments During FY 1985

UCSF Program

Study I. Ten subjects who stated that they were bothered by fluorescent lighting were studied, using the maximal-strength forward shoulder flexion test. Each subject received 50 trials. To counterbalance the effects of fatigue in such a regime, the trials were conducted as a randomized sequence of paired 400-footcandle exposures to an incandescent and a cool-white fluorescent light. Over all subjects the mean difference in maximal muscle strength for the two lighting conditions was less than 0.2% of the usual strength. The standard distribution was 13 times the mean difference. A paired-t test showed that our results were likely due to chance ($p = 0.85$). Similarly, there was no statistical difference in the responses under the two lighting conditions ($p = 0.39$). Power analysis showed that 90% of the time we would have detected a difference in muscle strength of 4%. Since the effects of suggestion on maximal muscle strength have been reported to be about 10%, the effects of the lighting, as tested, are likely to be obscured by psychological effects.

Study II. The results of Study I are not in agreement with the popular writings of John Ott,[1] who

used "kinesiology testing" to support his claim that muscle weakness was caused by both cool-white fluorescent light and lack of electric-field shielding. Mr. Ott agreed to test the effect of shielding, double-blind, using his kinesiological evaluation of subjects' strength. On the unblinded tests the reported strength agreed with Mr. Ott's knowledge of grounding in 97% of the trials, but in the blinded condition the reported strengths agreed with grounding only 53% of the time (range 31–75%). The likelihood of obtaining such a difference by chance was less than one in 100,000. We conclude that blinding the kinesiology testing significantly alters the result, which in the unblinded case is susceptible to suggestion; any claims based on this methodology, unblinded, are suspect.

Study III. Experiments using infrared pupillometry to investigate visual reactions to high-pressure sodium and other HID lamps are under way. An important observation was recorded in the consensual pupillary flash reflex of subjects exposed to three types of light—incandescent, fluorescent, and high-pressure sodium (HPS). The results have shown a larger pupil diameter from HPS exposure compared with the other lights for the same levels of illumination. This initial result implies that, for equivalent visual acuity, higher illumination levels will be required with HPS lamps.

Visual Performance Program

In 1981 the International Commission on Illumination (CIE) released its publication CIE 19/2, *An Analytic Model for Describing the Influence of Lighting Parameters upon Visual Performance.* A review by LBL in FY 1982 of the original data used in the development of CIE 19/2 found serious errors, and in FY 1984 a fuller critique of the CIE 19/2 model of performance was completed. Statistical arguments show that the fitting parameters are not physically determined as was previously believed, and the curve fitting in CIE 19/2 does not constitute validation. Nevertheless, careful use of the material in CIE 19/2 could lead to better recommended light levels than the consensus of present practices put forth by the RQQ #6 committee of the Illuminating Engineering Society.

Interactions between Lighting and Visual Display Terminals

Besides studying the direct effects of lamps on humans, LBL is examining how lamp characteristics—in particular compound flicker—can affect workers using visual display terminals (VDTs). Compound flicker occurs when two independent light sources flicker at different rates that combine to produce a "beat." For example, light from a VDT with a refresh rate that differs slightly from its nominal 60 Hz will combine with standard fluorescent lighting flickering at 120 Hz to form a low-frequency beat. Experiments are being performed to ascertain the effects of beats in general, and the beat between VDTs and ambient lighting in particular, on the visual system.

Present results show that beats formed by independently modulated fluorescent luminaires cause subjects to exhibit frequency-specific declines in temporal contrast sensitivity and entrained pupillary oscillations when the flicker rates of the luminaires are below the critical fusion frequency (CFF). No evidence of these effects is found when the flicker rates are above CFF or when a VDT is viewed under flickering ambient illumination. High-frequency operation of the ambient lighting would eliminate any possible human response to these beats if they did cause a response of the visual system.

Planned Activities for FY 1986

UCSF Program

The health impacts work will continue; plans will be made to convene the advisory group to review the results comparing incandescent lamps with high-pressure sodium lamps. Work will continue to confirm the initial findings. One confounding variable could be the flicker modulation of the HPS illumination: the HPS has much deeper modulation than the incandescent or the fluorescent lamps. Experiments will be set up with the HPS lamps operated by high-frequency ballasts, thus eliminating any possibility of flicker. The outcome of these comparisons could be significant because the use of HPS is increasing, especially with new applications in the interior environment.

Visual Performance Program

The results of the CIE 19/2 study will be used to develop experimental measures that will produce additional data to improve the performance model. A program will be developed to evaluate the quality of illumination, determine methods, apply them to lighting design, and relate it to performance. Size effects on visibility will be included in the model.

UC Optometry Program

The video display work will continue attempts to relate effects of the beat frequency between the refresh rate of the screen and the ambient lighting. Further experiments are planned to explain the observations associated with the white and green screens and the different ambient lighting situations. The optometry laboratory will also corroborate the effect of HPS lighting which were initially observed at the UCSF School of Medicine.

REFERENCE

1. Ott, J.N. (1982), *Light, Radiation and You: How to Stay Healthy*, Devon-Adair Company, Greenwich, CT.

Buildings Energy Data*

J. Harris, A. Meier, H. Akbari, J. Busch, P. le Coniac, C. Conner, D. Connell, J. Eto, D. Flora, B. Gardiner, C. Goldman, K. Greely, S. Greenberg, M. Meal, E. Mills, A. Mitchell, O. de la Moriniere, M. Piette, R. Riley, A.H. Rosenfeld, D. Stein, A. Usibelli, and L. Wall

The Buildings Energy Data Group (BED) compiles, analyzes, and publishes *measured* energy performance data on efficient buildings and equipment. The group's goal is to improve energy efficiency in new and existing buildings by providing designers, owners, managers, policy-makers, and others with feedback on how well technical measures and operating strategies actually work to save energy or peak electric demand, and how this performance translates into net dollar savings. We provide information that will help these users make better-informed decisions on building design, operation, financing, energy demand forecasting, and public policy.

The core of BED's activity involves the development and updating of a data base series called BECA (Buildings Energy-Use Compilation and Analysis), and use of these data for comparative studies of measured building performance. BECA compilations include:

- New, low-energy homes (BECA-A)
- Retrofits of existing residential buildings (BECA-B)
- New, energy-efficient commercial buildings (BECA-CN)
- Retrofits of existing commercial buildings (BECA-CR)
- Efficient appliances and water heating systems (BECA-D)
- Comparisons of predicted and measured performance (BECA-V)
- Load management and thermal storage systems (BECA-LM)

Each compilation is independent, but all rely on a computerized data base management system (DATATRIEVE). The data bases can be queried to produce statistics on sets of buildings with similar features, location, function, etc. Data are obtained from a variety of published and unpublished sources, often with the help of collaborators within the research community, private industry, and utilities. Each new entry is carefully reviewed for data quality and consistency. We calculate normalized performance indices and then "echo" the results to our data suppliers, both to verify accuracy of the data and to provide the contributor with some immediate feedback, in the form of results that can be compared with other BECA buildings (or with performance predictions, baseline values, or standards).

The Buildings Energy Data Group is also active in three areas that complement the core compilation effort: development of energy performance indicators, primary data collection and analysis, and studies of conservation potential.

Unlike the dynamometer tests of automobile fuel efficiency (miles-per-gallon), there is no equivalent for buildings that can directly measure and compare their overall energy performance under consistent, controlled conditions. Instead, we must collect detailed information about the building's energy consumption, physical characteristics, and operating schedule, and use these data to extract standardized energy performance indicators. Development of these standard performance parameters is an important research goal of the group.

We often provide informal advice and guidance to data collectors, and, increasingly, participate directly in the analysis of primary data. In special circumstances, where we have identified significant data gaps, BED initiates small pilot projects to directly measure equipment or building energy performance.

The data compilations also provide a valuable data base from which to estimate the future potential for conservation. Studies of conservation potential begin by characterizing the technical performance and costs of series of conservation measures. We then calculate costs of conserved energy, and aggregate these measure-specific data into "supply curves of conserved energy" (or reduced peak power).

THE BECA BUILDING ENERGY-USE COMPILATIONS

Accomplishments During FY 1985

New, Low-Energy Homes

The data compilation for new, low-energy homes (BECA-A) contains over 350 entries. Design strategies include superinsulated, double-envelope, active

*This work was supported by the Assistant Secretary for Conservation and Renewable Energy, Office of Building and Community Systems, Building Systems Division of the U.S. Department of Energy under Contract No. DE-AC03-76SF00098, and by the Bonneville Power Administration, Pacific Gas and Electric Co., Southern California Edison Co., and the California Energy Commission.

and passive solar, earth sheltered, and combinations of these. Each BECA-A entry includes a building description, occupancy patterns, and measured energy consumption. For a growing percentage of houses we have submetered energy data by end-use and other detailed results of on-site monitoring.

During FY 85, we continued to refine our computerized procedure ("SUBMET") for calculating standardized heating energy performance parameters.[1] We first adjust for variations in inside temperatures and internal gains—the two major occupant-controlled variables. We then use regression techniques to estimate a balance temperature, k-value (response of heating load to changes in outside temperature), and average-season heating loads, based on measured energy consumption and outside temperatures. Houses with significant sources of unmetered heat, such as wood stoves, are excluded from the compilation. This normalization technique permits a more realistic comparison of buildings, but still leaves a large variation in performance, even among houses with similar designs. Results are shown in Fig. 1.

Compared with a base-case (estimated heating loads for typical new U.S. homes), the BECA-A houses tend to require only about 30–50 percent of the heating energy. The best of these houses use less energy for space heat than for water heating or major appliances—under $100/year, even in cold areas of the U.S. and Canada.[2]

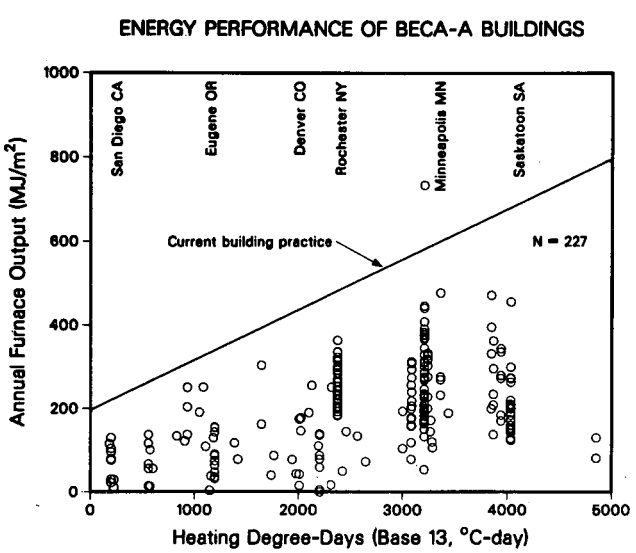

Figure 1. Thermal performance of 319 low-energy homes in the BECA-A compilation. Climate severity is approximated on the X-axis, in degree-days to base 13°C (rather than 18.3°C) to coincide with the average measured balance temperature. Energy consumption is expressed in terms of furnace output, as an indicator of building shell performance, without reflecting differences in heating system efficiency. The energy consumption plotted in the figure is based on the measured consumption, and then adjusted to standard operating conditions and system efficiencies. (XCG 848-13199)

In FY 85 we added about 50 data points to BECA-A, and began work on incorporating a large data set of well-monitored homes from the Pacific Northwest. The Bonneville Power Administration (BPA) selected our normalization technique for the analysis of data from the Residential Standards Demonstration Project.

Residential Retrofits

The compilation of measured energy savings from retrofits of residential buildings (BECA-B) now contains 90 single-family retrofit projects, representing over 50,000 homes, and 105 multifamily buildings, representing over 25,000 units. This year much of the data collection and analysis has focused on multifamily buildings, as summarized below.[3] We also participated in the data collection and analysis of five retrofitted public housing buildings in San Francisco.[4] Results on both single-family and multifamily retrofits are found in Ref. 5.

The most popular conservation measures in our sample of multifamily buildings involved HVAC system retrofits:

- heating system controls, such as outdoor resets, high-limit outdoor cutout, and aquastat,
- heating system equipment measures, such as new burners and vent dampers
- boiler replacements, and
- improved operations and maintenance practices.

The median cost of multifamily retrofits was $534/unit; costs were under $250/unit in 40 percent of the buildings. This suggests that many building owners confined their retrofit efforts to fairly low-cost measures, a pattern we find repeated in commercial (leased) buildings. For the multifamily sample, median annual energy savings were 11.7 MBtu/unit, or 16 percent of pre-retrofit energy use. Seventy percent of the projects saved between 10 and 30 percent.

Energy savings and cost-effectiveness are strongly influenced by the choice of retrofit strategies. We classified each building in the data base by retrofit strategy, and then calculated, for each group of projects, median values for energy savings, total cost, simple payback time, and internal rate of return (Table 1). Some interesting trends emerge when the

Table 1. Energy savings and cost-effectiveness of various retrofit strategies.[a]

Retrofit Strategy	Number of Projects [No. of Units]	Median Site Energy Savings [MBtu/unit-yr.]	Median Total Cost per Unit (1985 $)	Median SPT (years)	Median IRR (%)
Heating Controls	18 [5268]	6.5 ±2.6	48 ±58	1.2 ±0.5	95
System Packages[b]	13 [278]	20.3 ±4.9	177 ±146	1.9 ±1.0	47
System and Shell Packages	6 [138]	51.7 ±13.0	1141 ±358	2.2 ±1.6	50
EMCS[c]	4 [2858]	14.0 ±17.7	618 ±133	3.0 ±1.4	27
Shell Packages	14 [3397]	6.4 ±4.3	609 ±206	8.3 ±4.9	7
Distribution System Conversion[d]	7 [118]	23.7 ±12.5	780 ±1277	8.9 ±3.6	17
Window Measures	10 [11073]	11.0 ±1.2	1090 ±112	15.6 ±2.4	10
Solar DHW	6 [388]	2.3 ±3.6	568 ±21	36.5 ±57.0	0
Metering Conversion[e]	11 [2983]	10.6 ±4.4	228 ±5	1.4 ±0.3	57
Boiler Replacement & Controls	5 [568]	27.9 ±25.8	2191 ±1237	5.5 ±8.3	19
Boiler Replacement & Windows	7 [393]	21.0 ±5.3	2434 ±204	17.2 ±2.2	2

[a]Results given are median values plus standard error (se) of the sample median. Standard error of the sample median is computed from:

$$se[median(X)] = IQ(X)/N^{0.5}$$

where IQ is the interquartile range and N is the number of projects.

[b]"Packages" refers to sets of retrofit measures implemented at the same time, so that the savings attributable to individual retrofits cannot be determined. System packages are retrofits to space heat and hot water systems. Shell packages means that various envelope measures were implemented (e.g., insulation, caulking and weatherstripping, storm windows).

[c]EMCS refers to management control systems.

[d]At these projects, the heating distribution system was converted from steam to hot water.

[e]The category "Metering Conversion" includes conversion of electricity billing from master-metered to individual unit submetering and installation of tenant metering systems that divide total gas use in an apartment building on the basis of indicators that are proxies for the amount of heat delivered (e.g., number of hours that the thermostat calls for heat).

multifamily retrofit data are segmented in this fashion. For example, envelope measures (e.g., "shell" packages and window measures) tend to have much longer payback periods (over 8 years) than many of the heating system retrofits (under 2 years). Costs associated with HVAC system retrofits span a wide spectrum, ranging from $50 to $2400 per unit (high-cost HVAC retrofits typically include replacement of the existing heating plant). The most cost-effective retrofit strategies are not always those that produce the highest energy savings. For example, median energy savings were relatively small in buildings that installed heating system controls, although these measures proved to be exceptional investments, with a median payback time of just over one year.

Conversion to tenant submetering systems, although not strictly a technical efficiency measure, appeared economically attractive from the perspective of the building owner. Based on a sample of 10 low-rise Minnesota buildings, reduction in gas heating energy use (due to changes in occupant behavior) averaged 15–18 percent below pre-retrofit levels. Note that where submetering means that space heating costs are shifted from owner to tenant, this retrofit must be accompanied by a corresponding rent reduction to avoid significant increases in the tenants' total costs.

New, Energy-Efficient Commercial Buildings

The compilation of new, energy-efficient commercial buildings now includes 152 entries from the U.S. and abroad.[6] Most of the buildings are award winners, demonstration projects, or have been featured in case studies as energy-efficient buildings. About two-thirds of the buildings are offices. The average energy intensity for the BECA-CN offices is 66 kBtu/ft^2-yr (measured at the site), about half as much as the existing U.S. stock. A handful of the most efficient new buildings use only 20–30 kBtu/ft^2-yr (site).

We compare commercial building performance in terms of energy consumption, peak electric demand, operating conditions, energy costs, and building costs. These comparisons must consider services supplied by a building, such as computer centers, parking garages, and outdoor lights. Figure 2 shows the distribution of site energy use for office and school subsamples chosen to highlight such differences. For example, the offices with computer centers tend to have higher energy use than the other samples.

Over the past year we have placed increased emphasis on collecting and analyzing data on commercial building peak demand and electric load profiles; peak demand charges can represent 30–50 percent (or more) of total electricity costs for a large, new building. The "operating load factor" (OLF), or ratio of the average demand to the annual peak demand, represents a useful performance indicator. (Average demand is the annual electricity consumption (kWh/year) divided by 8760 hours/year.) Figure 3 shows the OLF for 32 all-electric offices in BECA-

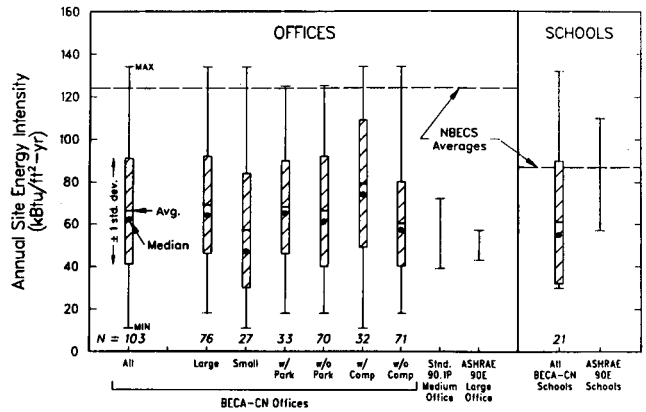

Figure 2. Annual site energy intensities for BECA-CN subsets. Maximum, minimum, average, and median values, and standard deviations are shown for 8 subsamples of BECA-CN offices and schools. ASHRAE Standard 90 simulation estimates, and NBECS averages for the U.S. stock (1979) are plotted for comparison. (XCG 861-7038)

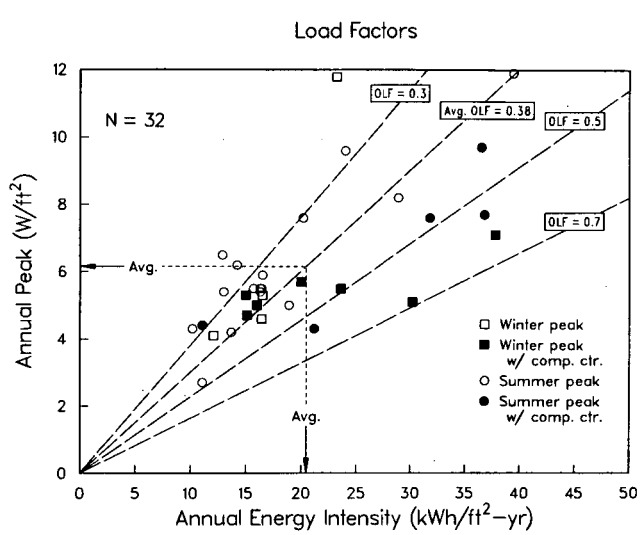

Figure 3. Operating load factor for all-electric buildings in BECA-CN. Operating load factor (OLF) is defined as the ratio between the buildings annual peak demand and electricity consumption. Lines of constant OLF, and the sample average (OLF = 0.38) are shown for comparison. Buildings with computer centers tend to have higher operating load factors. (XCG 8512-562)

CN. From a peak-shifting or shaving perspective, buildings with load management should have higher load factors. The buildings with computer centers have high load factors because of higher baseloads.

In 34 cases we have gathered data on predicted energy use prior to construction. Twenty-three of those buildings used more energy than predicted; however, the predicted consumptions were often based on less demanding conditions, or lower estimates of miscellaneous loads such as receptacles, exterior lighting, and computers. In some cases, the actual building did not include special energy features originally considered in design studies; in others, poor performance or changing operational requirements rendered some features unusable. One example was a night-time cooling system that could not be used as planned because the building was occupied twenty-four hours per day rather than the ten hours assumed in the design. High ventilation rates needed to flush the building were inconsistent with nighttime occupancy.

Commercial Retrofits

The compilation of measured energy savings from retrofits in nonresidential buildings (BECA-CR) includes over three hundred entries.[7] The median annual energy savings (in site energy) for the 94% of the buildings that saved site energy is 31 kBtu/ft^2-yr, or about 25%. The most common retrofits are measures that involve HVAC operations, maintenance, and lighting. The median retrofit cost is \$0.40/ft^2, resulting in a median payback time of only one year. We conclude that owners of many commercial buildings use very conservative investment criteria, and that actual investments seem to fall well short of the economic and technical potential. Table 2 shows the breakdown of median savings in the BECA-CR compilation, by building type.

Energy management in commercial buildings is often a continuing process, without clear "pre" and "post" periods. Our recent data collection has emphasized multi-year energy consumption records,

Table 2. BECA-CR summary. Summary of site energy savings from retrofits of commercial buildings that reduced energy use.[a]

Building Type	N	Savings (median)	Median Site Energy Savings (MJ/m^2-yr.)	(kBtu/ft^2-yr.)
Schools				
Elementary	82	27.7	345	30.4
Secondary	28	24.5	428	37.7
Colleges	13	44.5	1143	100.7
Offices				
Large	34	21.4	323	28.5
Small	13	20.8	370	32.6
Hospitals	6	26.4	1060	93.4
Retail	2	12.3	91	8.0
Hotels	5	14.4	480	42.3
Other				
Post Offices	92	24.0	318	28.0
Assembly	2	52.2	2141	188.6
Correctional	1	6.0	96	8.5
Other	14	23.6	268	23.6
TOTAL	292	24.6	350	30.8

[a]All averages are unweighted, i.e., each building's savings are weighted equally regardless of floorspace or energy usage.

in order to analyze long-term trends. Tracking buildings for several years can provide added insight into a building's energy performance, including the effects of successive retrofits or operational changes, the durability of savings, and the building's response to weather.

Residential Water Heating

In FY 85, we continued our compilation of measured energy performance of water heating systems (BECA-D). The compilation includes studies of new water heater performance (including heat pumps), retrofits (such as tank insulation), and baseline energy and water usage measurements. The compilation contains 75 entries, including measurements of over 11,000 water heaters.[8] In spite of the large number of water heating monitoring projects, few measured results include sufficient data on temperature, water usage, and heater/storage characteristics to make valid performance comparisons. Conclusions from the BECA-D data are summarized in Table 3.

Table 3. BECA-D summary. Measured energy performance data on residential water heating.

Item	Value[a]	Number of Households
Average Hot Water Use	17.7 gal/person-day (4.1)	273
Average Water Heating Electricity Use	4890 kWh/year (1483)	7115
Average Savings from Thermal Traps	340 kWh/year (158) 16 therms/year	74 1
Average Savings from Insulation Blankets	460 kWh/year (163) 11 therms/year (12)	79 25
Heat Pump Water Heater, Seasonal COP	1.98 (0.25)	500

[a]Numbers in parentheses are standard deviations.

Model Validation

The BECA-V compilation includes comparisons of building load predictions with measured energy performance. The data base contains over twenty-five studies, comprising about one hundred simulations of building energy use, performed with eighteen computer models. Complex or simplified methods of predicting building energy use play a central role not only in buildings research, but also in design and retrofit decisions, setting of efficiency standards, and the structuring of conservation programs. The success of these applications hinges to a large degree on the accuracy of model predictions. We find that prediction accuracy depends on several factors beyond the validity of the model's algorithms, most notably the quality of input data (or default assumptions) and the skills of model users.[9,10] With good quality data, many models can predict energy use of occupied buildings within 20% of the actual measured values.

Another aspect of model verification is inter-model comparisons. As part of a residential data analysis project funded by the Bonneville Power Administration, we compared results of three simplified heating load calculation methods with reference values produced by DOE-2, a state-of-the-art hourly simulation model.[11] We found that two of the models produced results reasonably consistent with DOE-2, except when modeling very tight, well-insulated houses. The third model consistently underestimated heating loads, compared with DOE-2. Inter-model comparisons of this sort can be a useful first step in planning (more costly) verification studies of predictions vs. measured data. They may also provide guidance in design of monitoring projects, concerning the choice of analytical models and the level of detail, accuracy, and duration for on-site data collection.

Planned Activities for FY 1986

Data collection and analysis for the BECA compilations will continue during FY 86, with special emphasis on detailed, submetered data; case studies of multiyear performance; refinement and validation of techniques for occupancy- and weather-normalization (particularly in larger, complex buildings); and more outreach and direct contacts with current and potential users of measured BECA data. The focus of activities will vary with the compilation.

For new, low energy homes (BECA-A), we will continue to investigate the performance contributions of specific components (glazing, reduced infiltration, efficient heating equipment), based on submetered data that will be available from the Pacific Northwest and other regions. The analysis of measured data on cooling will begin with the testing of performance parameters, first using "synthetic" (simulated) data. Economic analyses will focus on the incremental cost data from low-energy homes in the Pacific Northwest, plus an improved baseline analysis using national stock survey data. The data on low-energy buildings outside of the U.S. and Canada will be significantly expanded, as we obtain the results of several dozen monitored demonstration sites in France, Denmark, Sweden, and other European countries. Finally, we hope to expand our collection of performance data on "production" housing built for resale, but designed with energy-saving features—as opposed to custom-designed low-energy houses, or special demonstration projects. This will probably mean using whole-building data (perhaps supplemented with simplified, short-term test data), but aggregated across several houses of the same design in the same subdivision.

The residential retrofit data base (BECA-B) will continue to concentrate on multifamily buildings in FY 86, based on the more detailed data that will become available from the multifamily component of DOE's Buildings Energy Retrofit Research project. We will extend the savings calculation methods to accommodate end-use submetered data, indoor temperatures, and other changes in operating conditions. Over one hundred multifamily retrofits from Europe will be added to the compilation this coming year.

Up to now, the commercial buildings compilations (BECA-CN and BECA-CR) have depended largely on information which can be extracted from billing data. We believe that more detailed energy performance studies of occupied commercial buildings are needed. Monitoring of commercial buildings is already ten years behind the residential sector; only in 1984 did extensive submetering projects begin. As these data become available, future BECA efforts will focus on more detailed analyses of submetered data, for fewer buildings. As discussed below, we are currently testing techniques that are "intermediate" between billing data and continuous, multi-channel monitoring, especially the use of data that can be extracted from energy management systems already in place.

Our present compilations have shown that internal loads represent a major unknown factor in commercial buildings.[12] We will continue to investigate actual energy use for these loads, especially computers and electronic equipment. Detailed data of this sort will contribute to a better understanding of differences between predicted and measured energy use (or retrofit savings).

Even without more detailed data, cross-sectional comparison at the utility bill level should be of interest for buildings with standardized designs and similar functions, but located at different sites. We plan to assemble and analyze such data for efficient or retrofitted retail chains, banks, restaurants, etc. We are also collaborating with ASHRAE on a series of detailed, multiyear case studies of previous Energy Award winners.

Beginning with simulated data from the DOE-2 computer model, we are examining the weather-responsiveness of various commercial building types, in order to develop guidelines for weather-adjusting the energy use of these larger buildings. This is related to our continuing project with the Building Owners and Managers Association (BOMA), to refine and expand the energy section of their annual survey. Our participation consists of a series of investigations, principally with DOE-2 simulation data, to determine the key factors influencing commercial building energy consumption.

Given the importance of peak electric load management in commercial buildings, we will continue the BECA-LM compilation begun in FY 85. The emphasis will be on measured performance of thermal storage and energy management systems. Depending on data availability and staff resources, we hope to begin a new data compilation on retrofits and efficient new designs of industrial buildings (BECA-I).

Analysis of several multifamily retrofit projects will also contribute data on savings from water heating measures. We will continue to seek out measured data that permit comparisons of appliance performance in the field with laboratory test results.

PRIMARY DATA AND ANALYSIS

Accomplishments During FY 1985 and Planned Activities for FY 1986

The BECA compilations often reveal gaps in the data on measured performance of buildings and equipment, or a need to systematize methods of data collection, analysis, or comparison. In response, we occasionally undertake small, pilot monitoring projects to begin filling these data gaps and to test new approaches to data collection and analysis. Finally,

we work with other groups at LBL to develop standard measurement and analysis protocols, and informally advise people about to undertake a field monitoring project.

In past years we conducted small monitoring experiments on commercial, reach-in refrigerators and drinking water coolers, two end-uses that have been largely neglected in previous studies of commercial sector energy use and potential savings.[13,14] Even our limited monitoring suggested that, on a national basis, these two end-uses consume significant amounts of electricity—equivalent to 2.5 times the output of a 1000-MW baseload power plant. We found that both appliances could be designed to use thirty percent less electricity, with only small additional investments. This year we will participate in a BPA-sponsored study to test, in the laboratory and in actual homes, the performance of high-efficiency imported Japanese refrigerators. We will continue, at a low level, monitoring and data compilation on other poorly-documented appliances and equipment, including furnace accessories, refrigerated vending machines, and computer workstations.

A major new area of activity involves the use of in-place energy management systems (EMS) as sources of relatively low-cost performance monitoring data.[15] Compared with whole-building utility billing data, these systems in many cases can provide far more useful information on performance of building subsystems, energy consumption by end-use, and load profiles. Compared with a dedicated, on-site monitoring and data-logging system, extracting data from an existing EMS can be far more cost-effective. Use of an EMS offers two added advantages: the possibility of long-term tracking of building performance, and more direct feedback to help the building operator optimize control settings, maintenance schedules, and make other energy-related management decisions based on actual building conditions and responses. In FY 86 we will conduct a series of pilot studies to obtain practical experience with EMS-derived performance data at several commercial facilities.

CONSERVATION TECHNOLOGIES DATA AND POTENTIALS

Accomplishments During FY 1985

We have participated in several studies of the estimated technical and economic potential for conservation in the buildings sector.[16–21] In the past, such estimates were often based on engineering calculations or computer model predictions. Future studies will increasingly rely on measured data, as documented in the BECA data bases. For electricity end-uses, there will also be increased emphasis on peak demand savings and on load profile impacts in general, to make such "conservation technical potentials" studies more directly relevant to utility system "least-cost" energy planning decisions.[22]

In one recent study, we examined the maximum technically feasible potential for conservation in the residential sector of BPA's service area.[18] Over three hundred conservation measures were evaluated, using the LBL computer program, CPS 2.0. Each measure was ranked according to its "cost of conserved energy," and aggregated in the form of "supply curves of conserved energy." An example of a conservation supply curve is shown in Fig. 4. Our study found a technical potential for saving over 2800 billion kWh by the year 2000, a 42 percent reduction compared with BPA's "conventional" demand forecast.

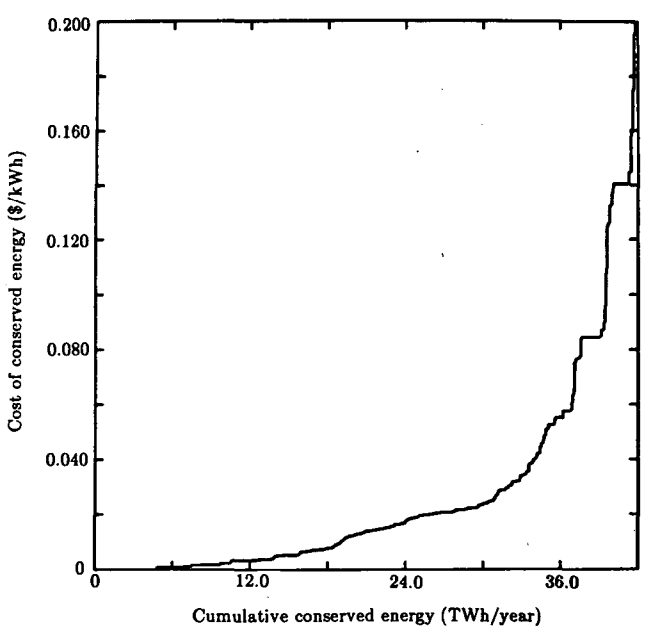

Figure 4. A supply curve of conserved energy for the residential sector in the Pacific Northwest, composed of many individual "steps." Each step represents a conservation measure applied to a subset of similar houses. The height of the step indicates the measure's cost-of-conserved-energy; the width represents the technical potential for savings if that measure were applied wherever feasible, throughout the stock. A measure is cost-effective if its cost-of-conserved-energy is less than a reference price (i.e., marginal or average cost). This supply curve shows that by the year 2000 there is a potential for saving 41.5 billion kWh at a cost of less than $0.15/kWh. This represents 42 percent of the forecasted residential electricity use in the region. (XBL 866-2322)

In another study we examined conservation technologies for new and existing commercial buildings in California.[18] The study analyzed technical performance, costs, and applicability of efficient technologies for air conditioning (including coolth storage), ventilation, refrigeration, motor efficiency, electric lighting, and daylighting. The study demonstrated that both existing and emerging technologies could significantly reduce energy use and peak power in California commercial buildings. However, we also concluded that installation of hardware does not, by itself, necessarily guarantee either energy savings or peak load reductions; a sustained effort at good building operation and management is also crucial. Indeed, carefully managed buildings **without** exceptional energy efficiency features will sometimes outperform those with "state-of-the-art" design but less continuing attention from the operator. We also found a number of areas with inadequate or poorly documented information, especially in terms of a technology's impact on electric load profiles. This again underscores the need for more detailed performance monitoring and analysis of occupied commercial buildings. The findings from this study were designed to be used not only by utility program planners and forecasters, but also by energy auditors in the field.

Planned Activities for FY 1986

The analysis of conservation and load-shaping potential will continue in FY 86, under a new Congressionally-mandated program to assist utilities and state regulatory agencies in developing data and analytical tools for "least-cost" energy services planning. Our efforts will focus on three areas:

- Updating the data base on residential and commercial technologies, with an emphasis on measured as opposed to calculated savings.
- Developing and testing the next generation of the CPS computer model for calculating conservation supply curves, to include a simplified micro-computer version, and capabilities for evaluating electric load-shaping impacts;
- Cooperative projects with selected utilities and states to apply these common models and data bases, using baseline stock and energy use data for specific utility service areas.

Several states have already indicated an interest in collaborating on least-cost studies, or have initiated projects of their own that can be enhanced by the national program through sharing of experience and data.

REFERENCES

1. Busch, J.F. (1986), "A Comparison of Building Thermal Performance Models Using Measured Data," *ASHRAE Transactions 92,* p. 2.
2. Busch, J.F. and Meier, A.K. (1985), "Monitored Performance of New, Low-Energy Homes: Updated Results from the BECA-A Database," presented at the 1985 ASME Solar Energy Division and ASES Engineering Division Annual Meeting, Knoxville, TN, March 25–29; LBL-18306.
3. C.A. Goldman and K.M. Greely (1986), Measured Energy Savings in Retrofitted Multifamily Buildings, presented at the 13th Annual Energy Technology Conference, Washington, DC, March 1986; LBL-20874.
4. Goldman, C.A. and Ritschard, R.L. (1986), "Energy Conservation in Public Housing: A Case Study of the San Francisco Housing Authority," *Energy and Buildings 9,* p. 1.
5. Goldman, C.A. (1986), "Measured Results of Energy Conservation Retrofits in Residential Buildings," *ASHRAE Transactions 92,* p. 1.
6. Piette, M. and Riley, R. (1986), "Energy Use and Peak Power for New Commercial Buildings from the BECA-CN Data Compilation: Key Findings and Issues," presented at the 13th Annual Energy Technology Conference, Washington, D.C., March 1986; LBL-20896.
7. Gardiner, B.L., Piette, M.A., and Harris, J.P. (1984), "Measured Results of Energy Conservation Retrofits in Non-Residential Buildings: An Update of the BECA-CR Data Base," presented at the ACEEE 1984 Summer Study on Energy Efficiency in Buildings, Santa Cruz, CA, August 14–22, 1984; LBL-17881.
8. Usibelli, A. (1984), "Monitored Energy Use of Residential Water Heaters (Buildings Energy–Use Compilation and Analysis: Part: D)," presented at the ACEEE 1984 Summer Study on Energy Efficiency in Buildings, Santa Cruz, CA, August 14–22, 1984; LBL-17873.
9. Wagner, B.S., "Comparisons of Predicted and Measured Energy Use in Occupied Buildings," *ASHRAE Transactions 90,* p. 2; LBL-17364.
10. Diamond, D., *et al.* (1985), "The DOE-2 Validation," *ASHRAE Journal,* November 1985.
11. Akbari, H., Conner, C., and Usibelli, A. (1985), "Residential Energy Simulations in the Pacific Northwest: A Comparison of Four Widely

Used Models," submitted to the ASHRAE 1986 summer meeting, Portland, Oregon; LBL-20221.

12. Gardiner, B.L. (1985), "The CAL-BECA Project Part 1: New California Nonresidential Buildings," prepared for the California Energy Commission and Universitywide Energy Research Group, April 1985.
13. Greenberg, S. and O'Regan, B. (1983), *Energy Efficiency in Commercial Food Service Refrigeration: An Assessment of Technical Potential and Data Needs,* LBL-16426.
14. Meier, A.K. (1984), *Measured Electricity Use of Drinking Fountains and Water Coolers,* LBL-17583.
15. Flora, D., Le Coniac, P., and Akbari, H. (1986), "Methods to Obtain Building Energy Performance Data: Are Energy Management Systems Promising Sources?" presented at the 13th Annual Energy Technology Conference, Washington, DC, March 1986; LBL-20897.
16. Meier, A., Wright, J., and Rosenfeld, A.H. (1983), *Saving Energy Through Greater Efficiency: The Potential for Conservation in California's Residential Sector,* University of California Press, Berkeley, CA; LBL-10738.
17. Solar Energy Research Institute (1981), *A New Prosperity: Building a Sustainable Energy Future,* Brick House Press, Andover, MA.
18. Usibelli, A., Gardiner, B., Luhrsen, W., and Meier, A. (1983), *A Residential Conservation Data Base for the Pacific Northwest,* prepared for the Bonneville Power Administration, Portland, OR; Final Report, LBL-17055, and Documentation and Appendixes, LBL-18107.
19. Usibelli, A., *et al.* (1984), "Commercial-Sector Conservation Technologies," prepared for Pacific Gas and Electric Company, San Francisco, CA and Southern California Edison Company, Rosemead, CA; LBL-18543.
20. Hunn, B.D., *et al.* (1985), "Electrical Energy Conservation and Peak Demand Reduction Potential for Buildings in Texas, Preliminary Results," presented at the Second Annual Symposium on Improving Building Energy Efficiency in Hot and Humid Climates, Sept. 24–26, 1985, Texas A&M University, College Station, TX.
21. Geller, H., Meier, A., and Rosenfeld, A.H. (1986), "A Conservation Power Plant (Project Merlin)," prepared for Pacific Gas and Electric Co. by the American Council for an Energy-Efficient Economy (ACEEE), Washington, DC.
22. Meier, A. and Usibelli, A. (1986), "Supply Curves of Conserved Energy: A Tool for Least-Cost Energy Analysis," presented at the 13th Annual Energy Technology Conference, Washington, D.C., March 1986; LBL-20894.

Building Energy Simulation*

J.J. Hirsch, B.E. Birdsall, W.F. Buhl, D.J. Connell, A.E. Erdem, D.J. Hopkins, K.H. Olson, and F.C. Winkelmann

The goal of the Building Energy Simulation Group (BESG) has been to create, test, document, and maintain a user-oriented, public-domain computer program that will enable architects and engineers to perform design studies of whole-building energy use under actual weather conditions. The development of this program, the current generation of which is known as DOE-2, has been guided by several objectives:

- The description of the building by the user should be in quasi-English so that the input can be easily understood by noncomputer scientists.
- When possible, calculations should be based upon well-established or proven algorithms, i.e., the calculational procedures should be acceptable to the engineering and research communities.
- The program should permit simulation of innovative as well as commonly available heating, ventilation, and air-conditioning (HVAC) equipment.
- The computer costs of the program should be minimal.
- The predicted energy use of a building should be acceptably close to measured values.

As can be seen in Fig. 1, DOE-2 is composed of two major segments: the Building Description Language (BDL) processor, which accepts quasi-English descriptions of building components, and the LOADS, SYSTEMS, PLANT, and ECONOMICS (LSPE) processor, which uses building descriptions to simulate building energy performance. Details of the development and structure of the DOE-2 program are available in past annual reports and other published material.[1-14]

The BESG is also undertaking projects that are designed to lead to the production of the next generation of building performance simulation programs. The main efforts in the advanced simulation area at this time are the creation of a simulation "kernel" system and organization of the simulation development community to enhance collaboration. The kernel system has three main components: software primitives, including a component model library and simulation tools; software harness to facilitate the construction of simulation programs by allowing general linkage of component models and support models; and a knowledge base, which will contain the rules of simulation development and use so as to allow, at a future time, the construction of expert systems for building performance simulation. These three aspects of the kernel system will provide the basic tools and information to allow the BESG and other groups to develop the simulation programs of the future. They will also provide a mechanism to facilitate exchange of research results and technology advances, and a basis for integrating performance simulation into CAD and expert system software.

ACCOMPLISHMENTS DURING FY 1985

The BESG maintains a research effort that continues to develop new versions of DOE-2. This ongoing research is divided into three parts. The first is the introduction of algorithm description techniques into the code. The second is the modeling of building envelope components and systems. The third is the simulation of HVAC equipment and associated control systems. Major new features of DOE-2.1C, which is the latest version completed and released to the public in 1985, are described below.

Functions

The DOE-2 simulation program consists of 9 modules with about 73000 lines of FORTRAN source code. Although, with regular BDL input a user can describe many simulation tasks, there are cases when standard capabilities are not enough. Examples of these might be: (1) treatment of building components such as windows with special properties; (2) use of different algorithms for some types of calculation; (3) computation of coefficients or intermediate values that are used in the regular simulation algorithms; (4) input of values that are not allowed by the standard BDL rules; (5) output of values that are intermediate results or are a combination of calculated values; or (6) quickly testing certain algorithms without modifying and recompiling the BDL and simulation programs. In order to allow these broader simulation capabilities we have implemented the "functions" feature in the DOE-2.1C LOADS program.

*This work was supported by the Assistant Secretary of Conservation and Renewable Energy, Office of Building and Community Systems, Building Systems Division of the U.S. Department of Energy under Contract No. DE-AC03-76SF00098.

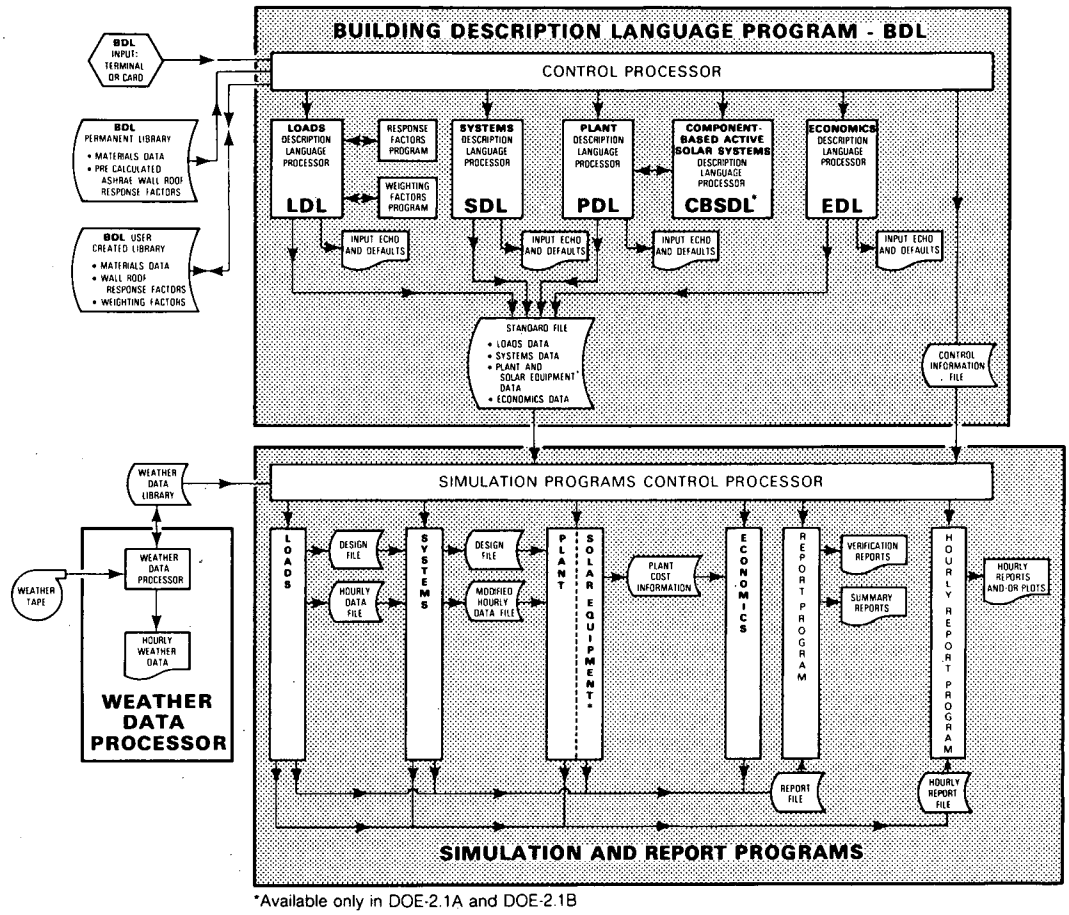

Figure 1. DOE-2 computer program configuration. (XBL 8010-2210B)

Using BDL, one writes in a subset of the FORTRAN language a subroutine that is similar to the ones in the LOADS simulation program. This subroutine has the capability of accessing and modifying all the variables that are used in the regular simulation modules. This newly added subroutine is triggered by BDL keywords in each component of the LOADS input. For example, if in the WINDOW command we say FUNCTION = (*FUNC1*, *FUNC2*), in the simulation phase every time the window calculations are done for that window the function FUNC1 will be triggered before the standard DOE-2 window computation, and FUNC2 will be triggered after the standard DOE-2 window computation. FUNC1 may be used to preset some of the constants and variables that are used in the regular DOE-2 algorithms. FUNC2 may be used to modify or completely recalculate the results that are computed by the regular DOE-2 algorithms.

The specifications of FUNC1 and FUNC2 follow the usual LOADS input. They start by using the ASSIGN statement to associate the simulation variables (that the function will use or alter) with the local function variables. This stage looks redundant, but is needed because some variables that are used in the simulation are pseudo-FORTRAN variables that may be more than 6 characters in length, and may contain embedded dashes. The ASSIGN statement also causes BDL to produce the necessary information to access these variables. Any variable inside the DOE-2 calculations can be accessed by an offset with respect to the beginning location of a labelled common block, or by a constant offset plus a base pointer with respect to the blank common block. With the ASSIGN statement, the local variable that will be used inside the function gets this access information.

Inside the computation section of the function, the local variables mentioned in the ASSIGN statement can be used in algebraic or logical expressions, or in I/O statements, just as in FORTRAN. These expressions are converted into sequential instruc-

tions to be evaluated at simulation time. The instructions are operator-operand pairs that include arithmetic, logical, I/O, and go to operations that are used in a general purpose computer.

In the simulation phase, whenever the FUNCTION keyword is used the following events take place. The appropriate function description block is accessed. By looking at the variables table, and using the access information in it, the values to be used in the function module are fetched from the DOE-2 simulation data structure into the local variables mentioned in the function. The next step involves the step by step execution of the instructions that define the arithmetic, logical, and I/O statements of the user input. After this, and before returning to the regular DOE-2 simulation stream, the values that were changed by the function are returned back to the DOE-2 simulation data-structure, again using the access information belonging to this function's variables table.

An example of an application of FUNCTIONS is given is Ref. 17, in which DOE-2 analyses are performed to evaluate innovative windows which use optical switching materials like electrochromics and photochromics for sun control.

Sunspace/Atrium Model

In a collaboration with the RAMSES group at the University of Paris-South, new capabilities have been added to DOE-2.1C to allow simulation of residential sunspaces (such as attached greenhouses) and commercial atria. This work was stimulated by the fact that sunspaces and atria are currently very popular architectural elements, and, being quite complex from a thermal point of view, require an accurate energy analysis to produce a design which is energy efficient and comfortable year-round.

The new algorithms allow simulation of different forms of heat transfer between the sunspace (or atrium) and adjacent rooms which could not be calculated with DOE-2.1B (see Fig. 2).

The calculation of beam solar radiation which passes through the sunspace into adjacent rooms is done by using the DOE-2 shadow routines to project the hourly-varying solar image of each exterior window onto the different interior surfaces in the sunspace. In this calculation external obstructions (such as overhangs and neighboring buildings) and internal obstructions are accounted for. Diffuse solar radiation incident on the interior surfaces of the sunspace is also calculated. This radiation, which is assumed to be uniformly distributed throughout the sunspace, originates by transmission through the exterior windows or by internal reflection of beam radiation.

The user can specify any of several different forms of convection between the sunspace and adjacent rooms. These include fan-forced or buoyancy-driven air circulation between upper and lower vents, free convection through a doorway opening, and for residential applications, use of a sunspace to preheat outside ventilation air. For commercial applications, the program allows return air from adjacent spaces to be passed into the sunspace, where, after mixing with the sunspace air, it is either exhausted or transferred back to the central air handling system.

The program makes available several mechanisms for controlling heat gain and loss from the sunspace and heat exchange with adjacent rooms: (1) Air flow between sunspace and adjacent rooms can be turned on and off via a time-clock schedule or by a controller which acts on the the sunspace-to-room temperature difference. (2) A venting algorithm allows outside air to be circulated through the sunspace to prevent overheating. The venting can either be fan-forced or natural. If forced, a fixed air-change rate is used. If natural, the program calculates the air-change rate from windspeed and inside-outside temperature difference using user-specified correlation coefficients. (3) For sun control, fixed obstructions such as fins and overhangs can be modeled, or movable shading devices can be deployed on exterior or interior glazing according to a time-of-year/time-of-day schedule. Alternatively, shades can be deployed whenever transmitted solar radiation exceeds a user-specified threshold value (which may vary seasonally or by time of day). More complex

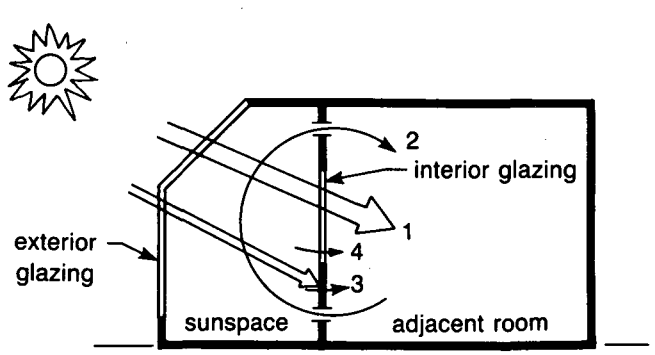

Figure 2. Cross section showing different forms of heat transfer between a sunspace and an adjacent room: (1) solar radiation passing from sunspace to room through interior glazing; (2) natural convection by thermocirculation through upper and lower vents; (3) delayed conduction through interior wall including effect of absorbed solar radiation; (4) conduction through interior glazing. (XBL 843-10167)

dynamic controls are possible with functional input (see previous section). (4) Conductive heat loss can be reduced by using movable insulation on sunspace exterior or interior windows. The insulation can be deployed according to a schedule or deployed whenever the outside temperature falls below a threshold value.

In order to track the large temperature swings that can occur in sunspaces, the venting and inter-zone convection calculation is done in small timesteps, ranging from 0.6 to 3 minutes depending on the sunspace heat capacity and load in a given hour. The conventional one-hour timestep used in DOE-2 was found to give unstable or unphysical results for the convection calculations, particularly when the temperature difference between sunspace and adjacent room was large at the beginning of an hour.

The interior walls in a sunspace are often fairly massive, so that the delay in the heat transfer by conduction through the wall can be important. The DOE-2.1B program was modified so that interior wall response factors are used in the SYSTEMS program to calculate delayed conduction taking into account time-varying space temperatures. This calculation also considers the interior sol-air effect, i.e., the effect of solar radiation absorbed on the sunspace side of an interior wall.

DOE-2 has a built-in routines which allow daylight illuminance levels in a sunspace to be calculated, although, due to the geometric complexity involved, the program cannot directly calculate illuminance levels in adjacent rooms due to daylight originating in the sunspace. However, functional input allows users to enter daylight factors, obtained from scale model measurements, which give room/sunspace illuminance ratios as a function of sky conditions. The program will then use these factors to determine hourly illuminance values and the corresponding reduction in electric lighting power for rooms with lighting control systems.

An important limitation of the sunspace model is that it does not account for air temperature stratification or in-room convective flows. We therefore caution against its use for multi-story atria unless the atrium air is well-mixed by the distribution system.

The French RAMSES group will validate the sunspace model against measurements of insulation, temperature, and inter-zone air flow for attached sunspaces on an apartment building near Paris. The program has been extensively tested in an energy analysis of the Pacific Museum of Flight in Seattle.[15] This building, which is currently under construction, contains a 48000 sq ft exhibition gallery with a 100% glazed roof through which sunlight can pass to adjacent rooms.

Sample results of the sunspace simulation are shown in Fig. 3, which is based on SYSTEMS hourly reports from the residential sunspace example in the DOE-2.1C Sample Run Book.[5]

Powered Induction Unit

The DOE-2 SYSTEMS program simulates a wide variety of secondary systems. Periodically new configurations appear on the market and are added to the DOE-2 simulation capabilities. The powered induction unit (PIU) has gained popularity in recent years, as designers have attempted to mitigate some of the perceived deficiencies of variable air volume (VAV) systems, and in addition to conserve energy by recovering excess heat from the building core. Consequently a model of the PIU system has been added to the DOE-2.1C SYSTEMS program.

The PIU system resembles the traditional VAV system with the addition, to the VAV terminal box, of a small fan or blower, which induces some amount of air from the plenum. The fan has two functions.

(1) Warm return air from the building core is sent into the plenum. The PIU fans draw this air from the plenum into the exterior zones requiring heat, thus conserving energy.

(2) The fan provides increased air movement when the VAV damper decreases primary air to the minimum, providing increased occupant comfort. In addition, primary air may be decreased below levels normally allowed in standard VAV systems, saving additional energy.

DOE-2 models two types of PIU boxes—series and parallel. In the series unit (Fig. 4) the fan draws air from both the primary (central system) and the secondary (plenum) air streams. The proportion of primary to secondary air is controlled by the VAV damper. The amount of secondary plus primary air is constant, and the fan runs all the time (when the central fan is on) at constant speed. In the parallel unit (Fig. 5) the fan draws air from the secondary air stream only. In addition, the operation of the fan is VAU intermittent—a thermostat set point regulates turning the fan on and off. When cooling is required, the fan is generally off, and the unit operates as a normal VAV. When the primary air damper is at minimum, the fan is on, and the operation is constant volume ventilating/heating. Thus

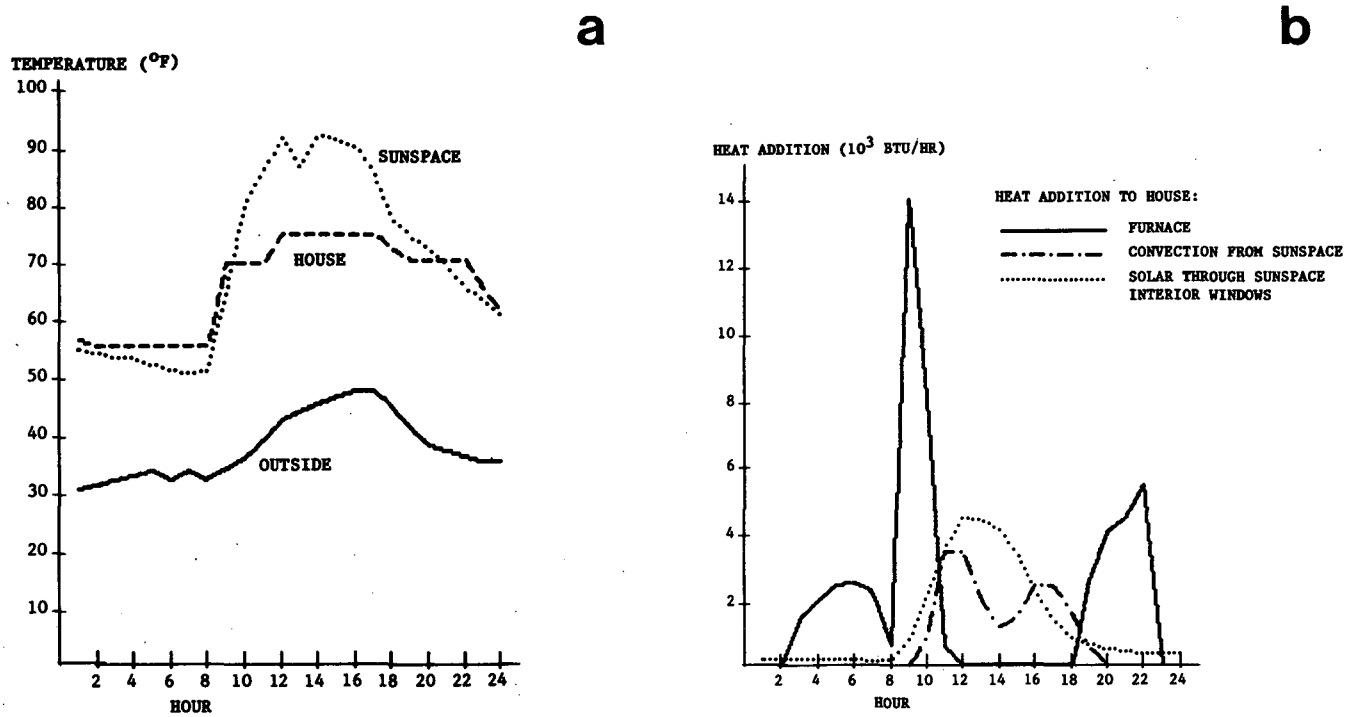

Figure 3. Sample hourly output for a clear January day in Chicago from a DOE-2.1C simulation of a house with a south-facing attached sunspace. The heating setpoint of the house is 70°F during the day and 55°F at night. Warm air from the sunspace is circulated to the house at 200 CFM whenever the sunspace-house temperature difference exceeds 4°F, and the house temperature is below 74°F. The sunspace is vented with outside air at 20 air changes per hour whenever the sunspace temperature exceeds 90°F. [(a) XBL 851-941 and (b) XBL 851-940]

the parallel unit does not supply a fixed air quantity to the zone under all conditions.

The capabilities of the PIU model are fairly broad. As in all DOE-2 system descriptions, the user gives a list of zones belonging to the system. In addition, for the PIU, one zone (the "induced-air-zone," usually the core zone) is denoted as a supplier of secondary air to the rest of the zones in the system. For each zone, the user can select the terminal unit as being constant volume, VAV, series PIU, or parallel PIU. The system can be simulated with any combination of terminal boxes in each zone. Reheat coils are also optional in each zone. When PIU boxes are selected, the user generally sizes the blowers. For parallel terminal units, the user supplies a set point temperature for the blower (which can be scheduled, to allow for setback). Normally the PIU fans operate in conjunction with the main

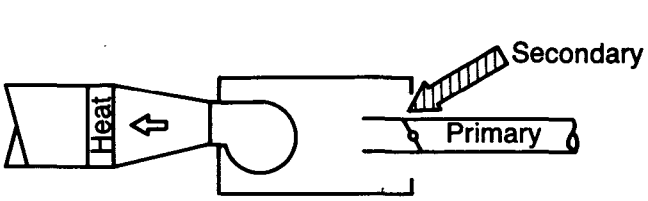

Figure 4. (XBL 843-10166)

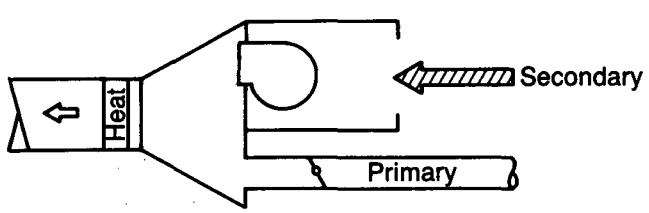

Figure 5. (XBL 843-10164)

system fan, but the user can decide to run the PIU fans independently at night and use the reheat coils to maintain a minimum temperature.

Two features of the PIU system have required changes in the DOE-2 simulation methods: the coupling of the "induced-air-zone" to the other zones, and the intermittent operation of the parallel PIU fan.

Normally DOE-2 models zones as being convectively independent, in order to avoid solving for all zone temperatures and extraction rates simultaneously. The exception has been plenums; air can be supplied from or returned through a plenum. In the case of a PIU system, however, air can be taken from one conditioned zone and supplied to other zones in the system. Since the zone temperatures and extraction rates are then strongly coupled, this situation would normally require iteration. DOE-2 avoids this by: (1) allowing only one zone to supply air; (2) simulating this zone first in each time step. Thus the temperature of the air coming from the induced-air-zone is known, and the rest of the zones are simulated independently. For each zone the program must keep track of the amount of primary air and secondary air required by each zone, and the amount of secondary air available from the induced-air-zone. If more secondary air is required than is available from the induced-air-zone, the additional air is assumed to come from the actual zone being simulated.

For each zone DOE-2 obtains the zone temperature and extraction rate by simultaneously solving the temperature deviation equation

$$\sum_{i=0}^{2} p_i \, (ER_{t-i\Delta} - \dot{Q}_{t-i\Delta}) = \sum_{i=0}^{3} g_i \, \Delta T_{t-i\Delta}$$

and the thermostat equation

$$ER_t = f(T_t) \; .$$

Here p and g are the coefficients of the room transfer functions, ER is the extraction rate, $\dot{Q}$ is the cooling load at constant temperature, ΔT is the difference between the constant temperature and the real room temperature, T_t. Normally $f(T_t)$ is assumed to be a piecewise linear function—the pieces being simply the heating action band, the dead band, and the cooling action band. The fan setpoint for parallel PIU's adds complexity by dividing either the cooling band or the dead band into two pieces (Fig. 6). If $f(T_t)$ were simply linear, ER_t and T_t could be obtained trivially. Since $f(T_t)$ is piecewise linear, and since the limits of each band (the capacities) are temperature

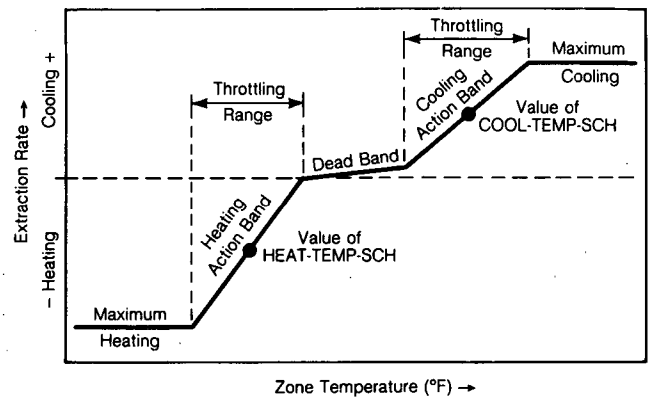

Figure 6. (XBL 825-600A)

dependent, DOE-2 employs a bracketing technique. An extraction rate (at the top or bottom of one of the bands) is assumed, and the temperature response is calculated. Depending on the temperature response, the endpoints are adjusted, the correct band is chosen, and the actual extraction rate and zone temperature are solved for. For the parallel PIU, extraction rates are also assumed for the fan on and for the fan off. Depending on the temperature response, the fan is assigned to be on, off, or a combination of the two for the time step.

Advanced Cogeneration Capabilities

Since its inception, the DOE-2 PLANT program has offered users the ability to study the performance of on-site electrical generation and cogeneration as part of a building's central plant. Recent changes in Federal and State laws, however, have granted small power producers and cogenerators additional flexibility in the operation of dispersed electrical generation facilities (PURPA). These changes permit easier access to electric utility grids for additional support on-site and, in addition, provide a regulated market for the sale of excess electrical energy. No longer must installations be sized to meet electrical peak demands, including the specification of redundant capacity, as in the days of the Total Energy Systems. Electricity may be both freely sold to and bought from the local grid.

The DOE-2.1C version of PLANT acknowledges these regulatory changes with an entirely reworked concept of electricity generators, and heat- and electricity-driven chillers, when operated in a cogeneration mode. When applied to reciprocating internal combustion engines (diesel and spark-ignition) and gas turbines, cogeneration refers to the sequential generation of electricity and the recovery of heat

for use in satisfying building thermal energy demands (heating and cooling). The new features have been used to study the economies of cogeneration in commercial buildings.[14]

The essence of the new concept is the explicit recognition of the energy value of both the cogeneration process-heat and electricity. Previously, the user was only permitted to schedule operation based on the electrical output of the prime movers. The associated heat recovered could only be used to the extent that a demand existed for thermal energy; any excess would be wasted. Now that the availability of a utility grid has loosened the requirement that operation be based solely on the on-site electrical needs, operation can be scheduled to eliminate wasted recovered thermal energy.

The user can now specify a cogeneration mode of operation that is based on either electrical or thermal loads. These features have been integrated with the existing command structure of PLANT to allow operation to be scheduled in either mode, during the course of a given day or on the basis of the magnitude of the load to be served. Thus the user can specify a cogeneration system that will track the thermal loads of a building, where these loads may consist of heating or cooling loads (if a heat-driven absorption chiller is available to accept recovered heat from the prime movers). In a thermal tracking mode with interconnection to a utility, both outputs of the prime movers will be fully used resulting in the most efficient use of energy from the electricity conversion process. At other times, when utility rates for purchase are high, operation can be scheduled for the full output of the generators in order to maximize sales of electricity to the utility. When utility rates for sale are high, operation can be scheduled to follow electrical loads, to minimize purchases from the utility. In addition, when both heat- and electricity-driven chillers are available to meet cooling loads, the output of the prime mover can be specified to balance loads between the two chillers. For example, increased electrical output will be accompanied by increased recovered thermal energy output. Both outputs can be used to satisfy cooling demands, and the loads on the two chillers will be allocated accordingly.

The implementation of these new cogeneration capabilities has required modifications to two aspects of the PLANT program: (a) equipment simulations; and (b) load allocations.

The equipment simulations for the prime movers (reciprocating internal combustion engine and gas turbine) and the chillers (absorption, centrifugal, reciprocating, and double-bundle) have been rewritten. The inputs and outputs of each type of equipment are now described with simple quadratic transfer functions. The coefficients to these equations remain user-definable, as before. The use of quadratic equations permits rapid determination of input values from output values, and vice versa, via the solution of the quadratic equation. This feature forms the cornerstone of the logic underlying the revised load allocation algorithms. Basically, these types of equipment are now no more than black boxes described by a handful of quadratic transfer functions.

The load allocation routines required several levels of modification. First, the original specification of prime mover equipment capacities had to be modified to include a rating for thermal output, as well as electrical output. Next, the user-input load allocation instructions for prime mover operation had to be similarly modified to permit load allocation on the basis of either thermal or electric loads. The allocation logic remains the same; only the nature of the loads being allocated has changed.

The major modification to the load allocation routines took place in the default allocation algorithms, which are used in conjunction with or in place of user-specified operation. The design of the PLANT program allows for varying levels of user-specified and default-optimized operation. For example, prime mover operation may be user specified on a daily/hourly basis, while chiller operation will be determined by the program. At an even higher level of generality, only a cogeneration mode (e.g., track thermal loads) need be specified by the user. The user-specified inputs for operation provide boundaries or constraints for the program's internal logic, which attempts to optimize the equipment operation. Generally the quadratic transfer functions are used to find the optimal operating point for each piece of equipment, and no iterations needed. For one situation, however—the determination of prime mover output when both heat- and electricity-driven chillers are present and a cooling load exists—an iterative solution was necessary.

Expanded Treatment of Energy Costs

The DOE-2.1C version of DOE-2 features greatly expanded capabilities for the treatment of energy costs. In the past decade, novel approaches for the billing of energy (electricity, in particular) have gained wide acceptance. Time-of-day prices, demand ratchets, and lifeline blocks are all increasingly familiar features of current and prospective rate schedules for energy. For dispersed producers of electricity,

Federal law permits several valuation options for the sale of electricity to the electric grid. All of these developments have been incorporated into DOE-2.1C.

The changes are symbolized by the movement of the energy cost commands from the PLANT program to the ECONOMICS program. In previous versions of DOE-2, energy costs were calculated by PLANT and life cycle costs by ECONOMICS. The energy cost calculations in PLANT could handle some simple block rate structures, but could not deal with time-of-day charges, demand ratchets, or complex block structures. In DOE-2.1C an hourly file containing plant loads, fuel demands, and generation is passed to ECONOMICS, allowing ECONOMICS to do all of the energy cost calculations, as well as the life cycle costs.

Rate structures of a number of utilities were analyzed and the structures were reduced to four basic components. These components correspond to four DOE-2 commands, each with its associated keywords and codewords. This discussion focuses on the concepts involved rather than the DOE-2 inputs.

The first component (corresponding to the ENERGY-COST command in DOE-2) identifies the type of energy being valued (fuel type and billing units) and describes the components of a monthly bill (minimum charges, fixed charges, and rate limitations). The first component also contains features for simplified rate structures (all consumption valued at one rate) and provides links to two of the other three components for more sophisticated rate structures.

The second component (SCHEDULE, DAY-CHARGE-SCHEDULE) describes how energy used in the hours of the monthly billing period is allocated into different billing categories. This component is used primarily to specify time-of-day rate structures (e.g., on-, off-, and shoulder-peak periods) and rates that vary by season (e.g., Winter versus Summer). This component is optional; the default is that all consumption during the month falls into the same billing category.

The third component (CHARGE-ASSIGNMENT) describes how the energy in a given billing category is actually billed. This component primarily describes block rate structures; many rate structures provide for successive tiers of use, each of which has a specific rate (dollars per unit of consumption) associated with it. Included in this category are lifeline rates, as well as declining block rates. In addition, some rate structures define the tier boundaries endogenously, based on demand (e.g., kWh/kW).

The fourth component (COST-PARAMETERS) is used only to describe features of electricity tariffs. These features include the specification of demand ratchets, and the PURPA mandated options for the sale of electricity to utilities. Demand ratchets are essentially hurdle levels of demand, which the demand charge can not fall below. They are typically based on a previously recorded level of demand, but can also appear as an average of previous high demands. In addition, the duration of demand ratchet can vary from 12 months down to 1 month, or can be restricted by season. The PURPA-mandated options permit sellers of electricity to choose one of two accounting conventions for the valuation of electricity sales. The first, called Net Sale, offsets purchases of electricity on-site and sells the excess at the utility's avoided cost rates. The second, called Simultaneous Buy/Sell, values all electricity generation at avoided cost, but bills on-site consumption at standard utility rates.

Advanced Simulation

The Building Energy Simulation Group, in collaboration with other institutions [(University of Strathclyde, Scotland; California State University, Fullerton, U.S.A.; University of Paris-South (CNRS), France; Chinese Academy of Sciences, Beijing, China; Centre Scientifique et Technique, France; and the Universite de Liege, Belgium] formulated a proposal for creating the software tools essential for the next generation of building energy simulation models. The intention of this project is not to develop a single new model but, instead, to provide a kernel system of highly-portable software modules and linking protocols which will enable groups in the public and private sectors to construct a variety of customized programs. The work plan has been developed in the context of the following guiding principles: (1) Researchers developing building performance simulation techniques can no longer afford to work as independent groups creating non-interchangeable software. Some mechanism must be found to give all developers access to the developments of others while retaining the flexibility to tailor a simulation system to individual needs. (2) As many energy sources become more expensive, and as improved efficiency technologies become more complex, designers of the future will be required to focus more critically on the intimate relationship between design and performance. This will require a quantum jump in the capability and accuracy of the energy simulation techniques now available. (3) The private sector of architectural and

engineering firms, HVAC equipment manufacturers, and CAD (Computer Aided Design) system vendors does not necessarily support the development of large public domain simulation codes. However, they *will* support developments of the kind proposed, which seek to create and order the building blocks of energy simulation. Private and public sector organizations can then use the resulting kernel system to construct customized simulation systems which embody an appropriate level of detail, offer wide ranging application potential, and use the most up-to-date techniques. (4) Increasingly, energy simulation models will form part of a building's operating system, allowing controls to be optimized in real time before being applied to the building. (5) The building design profession will increasingly rely on advanced CAD software packages. As systems possessing a drafting function proliferate, a demand will grow for explicit performance appraisal software. Designers will then come to rely on simulation techniques to test alternative hypotheses throughout the design stages and post occupancy. Indeed, CAD system integration is perhaps the most effective mechanism for market penetration of advanced energy analysis systems. (6) It is likely that, with the advent of powerful, integrated CAD systems, the design profession will seek to refine the building model and associated performance database beyond the construction phase. One possible scenario is that a client of the future will expect delivery of a computer-based model and performance database, in addition to the building itself. The information regarding building performance is then readily available for inspection. And, of course, the model can be used at any time as the basis for HVAC system maintenance, trouble shooting, and retrofits.

Each of these factors calls for the existence of a modular approach to energy simulation and, it could be argued, would be badly served if only free-standing, monolithic programs continue to be developed.

Existing simulation systems suffer to some extent from one or more of the following:

- The software structure is often extremely inflexible and unyielding. The program may have been conceived in a now-outdated machine environment—possibly batch oriented with card input. This means that the structure is monolithic, imposing extreme management and updating difficulties.
- To date it has not been possible to formulate a common approach to the simulation problem. Funding policy and the ever-present competition within and between the private and public sectors have served only to stifle inter-organization collaboration. The result is that each system has customized I/O procedures and unique internal structure. Physical models are different in each code, as are linking protocols, network representations, theoretical emphasis, and so on. This situation is obviously divisive and generates little confidence in the developments taking place.
- Often system authors are energy specialists, but have little formal training in modern software design and implementation techniques. The resulting software structure is inelegant, with the application knowledge inextricably bound to the source code. Contemporary software engineering favors the separation of the problem-specific knowledge from the basic software structure. This is a fundamental prerequisite of software system design which, if disregarded, can become a serious barrier to software evolution. For example, with existing systems it is often difficult to upgrade algorithms since this may require the detailed knowledge of data structures, internal memory, and possible side effects of one change on the rest of the software package. More elaborate modifications, such as substituting one numerical integration scheme for another, are at present intractable problems.
- In many of the currently available systems, the real world flowpaths have been oversimplified or omitted entirely and simultaneity of processes has not been addressed. An unsuspecting user is then left to struggle with the inadequacies of a model which has unacceptably degraded the all-important temporal and spatial couplings. These issues will certainly raise doubts about accuracy and flexibility and are the main focus in any validation exercise.
- And finally, among the research groups, there exists no clear statement on long term development objectives and task sharing required to accomplish these goals. As a result, many existing systems are not well tailored since each author organization has been forced to address every element of the problem: I/O, heat transfer theory, database design and management, solution techniques, software structure,

validation, documentation, etc. It is clear that no single organization can possess the necessary expertise in all areas. Each system is then promoted in a manner which implicitly undermines the development effort expended on its contemporaries. This is clearly an intolerable situation and one which serves only to fragment an already small development community.

Proposed Workplan

A model-creation system is proposed which consists of three main elements: (1) a public-domain library of *software primitives*; (2) a *software harness*, i.e. executive software for controlling how the primitives are linked into a modelling system, and (3) a *knowledge base*, which contains the rules for model construction. The characteristics of these elements and the tasks required to construct them are as follows.

(1) Software Primitives. Many useful models and techniques already exist within contemporary modeling systems, and much additional software continues to emerge as existing codes are extended or new developments pursued. The first task is to divide the useful, existing software into small, logically independent units called software primitives and place them within a central, public-domain library. Each library entry is then a small software module which performs a single task. The library entries will be independent in the sense that each primitive will have no "knowledge" of any overall data structure. The primitives will obtain data and return results in a standard way, by invoking special primitives which will fetch data from and return data to a central storage area. There will be no attempt to prescribe an overall modeling technology; instead, we hope to allow the free evolution of useful *software tools* for those concerned with developments in building energy simulation. Naturally, portability will be a necessary attribute for all of these tools.

The library will certainly have different types of entries: first principle, governing equation generators for building and system components; self-contained algorithmic approaches; data manipulators, software development and management tools, and simulation support modules. By accepting a high level of pluralism it is likely that a rich modeling base can be formed, entirely free of application assumptions. Many precedents already exist: the NAG, SLATEC, and SPSS libraries in the statistics and numerical analysis fields, GKS for computer graphics, the UNIX operating system and its software tools, and numerous other mathematical and structural (finite element) libraries.

Maintenance of the library will require some support software. Extracting, altering, and adding primitives to the library will require a simple database management system, for instance. It will be necessary to keep track of the history of the library—when a primitive was added or altered, and what the alteration was. This support software will be kept as simple as possible, and existing software will be used whenever possible.

Tasks:

- The required primitives must be identified and agreed upon.
- The standards for constructing a primitive must be considered and clearly defined.
- A proforma (or submittal form) must be drafted and tested to allow different groups to submit algorithms, theories, and procedures for transformation into a useful primitive.
- From the submitted proformas, the corresponding software tools must be generated, documented, and tested.
- The coordination of a regular publication is also necessary to inform the modeling community of the availability of new primitives as they emerge.

(2) Software Harness. The second stage addresses the development of harness or executive software which will allow primitives extracted from the library to be combined into an actual modeling system. This software will consist of a *data manager* used to define and control data traffic among the modules (primitives) and a *simulation controller* to control the sequence in which the modules (or groups of modules) will be executed. Creation of the software harness is analagous to the development of a computer operating system, such as UNIX, where the problems of concurrent processes and communication among processes have already been addressed. Using techniques from this field will facilitate the use of parallel processing at some future point in time. It will also permit the construction of any modeling approach (so long as the necessary software primitives exist), from the establishment and integration of matrix equations representing energy and fluid flow within buildings and their systems, to more pragmatic models which apply simplifications appropriate to the problem in hand.

It is important to note that the harness software is designed for use by model *developers* not by model users. It is an efficient way of building appropriate

models which can be easily improved as the underlying techniques are refined. Users would continue to use prescribed programs, the only difference being that their architecture would be highly modular and so easy to change.

Tasks:

- Supporting software must be created to allow the insertion of new primitives as free-standing entities.
- Data management routines must be devised to control information flow among software primitives.
- Simulation control routines will be developed to receive the flow-graph template and to trigger the operational primitives.
- Whole-building simulation systems must be devised, employing the software primitives and using existing programs as examples.
- Tests of the harness will be constructed and carried out at both the component and whole-building level.

(3) Knowledge Base. The third important stage consists of setting down the rules which govern model construction and use in a design, educational, or research context. This is essential if it is desired to move to so-called "expert" systems.

Concerning model construction, it would seem appropriate to set down the rules employed by some contemporary programs as a first step template. This would include those rules commonly applied to component models, as well as those applicable to overall solving strategies. Normal academic interchange would then serve to modify these templates or to create alternative approaches. Each participant can have his/her say, allowing the more effective templates to become prominent with time.

Model use is a different problem. A proper debate on the role of simulation in the building design process is long overdue. The intention here is to explain how existing and planned energy simulation systems work. This knowledge is required by those future developers who will construct expert systems in this application area. It is proposed not to develop decision-making software, but simply to organize a database of information in this one area.

Tasks:

- By inviting inputs from groups active in the field, it should be possible to create the software templates for some of the existing programs.
- National and/or international workshops would seem to be the appropriate mechanism to enable potential model users to set down their expectations of design appraisal by simulation.
- Additionally, the group of successful, seasoned users of existing software represents a source of knowledge that could be used for an expert system-based user interface.

The primitives library and software harness described above are illustrated schematically in Fig. 7.

International Association

To enhance collaboration and information exchange among individuals and organizations interested in building energy performance simulation, it is proposed that a new professional society be formed, tentatively called the International Association for Building Performance Simulation (IABPS). It is also the mission of IABPS to assist in the advancement of the field of building energy performance simulation by coordinating and conducting research which benefits model system developers or users and, specifically, to act as a repository and distribution point for the proposed prototype kernel system for the next generation of building energy simulation software.

During FY 1985, efforts were undertaken to organize the simulation community to form the above-mentioned association, as well as to begin work on the kernel system. The BESG also undertook specific technical projects to lay the groundwork

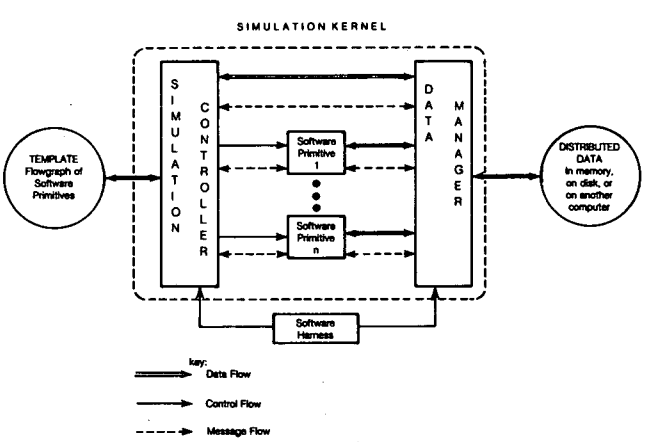

Figure 7. Proposed kernel system for creating building energy simulation models. (XBL 862-10304)

for the next generation of software. The major accomplishments during this period included:

(1) Numerous collaboration meetings were held, leading to the proposal for the next generation of building energy simulation software.

(2) Several current state-of-the-art building energy simulation programs were implemented on the BESG's ELXSI computer and a critical evaluation of the capabilities of these programs and their solution techniques and component algorithms was begun. The programs implemented include the following:

- ESP, which uses finite differencing to obtain a simultaneous solution of the coupled envelope and HVAC system heat flows. The implementation was done at LBL by J. A. Clarke, the program author, on leave from the ABACUS unit of the University of Strathclyde, Scotland. Also implemented were the ABACUS 3-D display programs BIBLE and VISTA.
- ASTEC, a program widely used in France for electric network analysis. Studies were done by J. Sornay of CSTB, France, while visiting LBL during FY1985.
- SPICE, an electric network analysis program developed at U.C. Berkeley.
- TRNSYS, the component-based system simulation program developed at the University of Wisconsin.
- HVACSIM+, a component-based system simulation program (recently developed by NBS) which uses variable-time-step, variable-order Gear algorithms for integrating systems of stiff, coupled differential equations.

(3) Lan-Chieh Huang, a mathematician on leave from the Chinese Academy of Sciences, began work on a new method for calculating unsteady, multi-dimensional natural convection in enclosures. The method, which is based on the Boussinesq approximation to the Navier-Stokes equations, uses exponentials to model the rapidly-varying flow in the boundary layer. This allows the heat flux at the walls to be calculated without using very fine gridding (and, therefore, large amounts of computer time) in the finite-difference solution.

(4) Work began on the use of ESP as a testbed for the implementation and evaluation of advanced simulation methods. The first technique to be investigated will be a "timestep controller" which will improve the accuracy of an energy calculation by dynamically changing the simulation timestep in response to variations in climatic variables, such as outside temperature or solar radiation, or building control variables such as thermostat setpoints.

Analysis Efforts for Others

An essential ingredient in the development of a computer program as large as DOE-2 is the ability to relate to the real needs of the program's users. Through involvement with studies such as those described below, the Building Energy Simulation Group gathers the information necessary to ensure this relevancy and usefulness.

A study[16] to compare BLAST (Building Loads Analysis and System Thermodynamics) and DOE-2 and their respective abilities to characterize the effects of thermal mass, wall position, and construction types was completed in FY 1985. The results indicate that DOE-2 and BLAST give similar results, and that DOE-2 agrees within a reasonable tolerance ($\pm 20\%$) with measured hourly data from test cells.

PLANNED ACTIVITIES FOR FY 1986

The DOE-2 program will be maintained and supported and its documentation clarified and supplemented as areas of confusion are uncovered. Several additions will also be made to supplement its capabilities. These include (1) continued effort to improve window and daylighting simulation in collaboration with the Windows and Daylighting Group, (2) an expanded user-library capability, (3) completion of the functional values specification to include SYSTEMS and, (4) the addition of new HVAC equipment and controls. We will also continue to carry out building energy performance studies.

During FY 1986, if, as expected, the developer and user communities agree, IABPS will be formed and begin to operate. It is expected that the "kernel" system concept will also be generally accepted and work will be contributed by many organizations. The BESG will begin work formulating methods of component model representation to allow convenient mathematical presentation of component

models and model reduction techniques; this will allow complex networks to be reduced to their minimum set of equations and solved in an optimum way. Work will also begin on design of the data structure and control flow for the software harness. The BESG will continue existing collaborations and continue efforts to form meaningful new collaborations.

REFERENCES

1. LBL Building Energy Simulation Group (1984), *DOE-2 Supplement, Version 2.1C,* LBL-8706 Rev. 4. Suppl.
2. LBL Building Energy Simulation Group (1984), *DOE-2 BDL Summary, Version 2.1C,* LBL-8688 Rev. 4.
3. LBL Building Energy Simulation Group (1981), *DOE-2 Users Guide, Version 2.1A,* LBL-8689 Rev. 3.
4. LBL Building Energy Analysis Group (1984), *DOE-2 Sample Run Book, Version 2.1C,* LBL-8678 Rev. 2.
5. LBL Building Energy Analysis Group and Group Q-11, Los Alamos National Laboratory (1984), *DOE-2 Reference Manual, Version 2.1C,* LBL-8706 Rev. 4.
6. Diamond, S.C. and Hunn, B.D. (1980), *The DOE-2 Verification Project: Phase 1 Results,* Los Alamos National Laboratory Publication LA-UR-80-357.
7. Schnurr, N.M., *et al.* (1979), *Applications of DOE-2 to Direct-Gain Passive Solar Systems: Implementation of a Weighting Factor Calculative Technique,* Los Alamos National Laboratory Publication LA-UR-79-2227.
8. Roschke, M.A., Hunn, B.D., and Diamond, S.C. (1978), *A Component Based Simulator for Solar Systems,* Los Alamos National Laboratory Publication LA-UR-78-1494.
9. Hirsch, J.J. (1982), *Simulation of HVAC Equipment in the DOE-2 Program,* LBL-14026.
10. Curtis, R.B. (1981), *The Theoretical Basis of the DOE-2 Building Energy-Use Analysis Program,* LBL-12300.
11. Building Energy Simulation Group (1985), *Overview of the DOE-2 Building Energy Analysis Computer Program,* LBL-19735.
12. Building Energy Simulation Group (LBL) and Group Q-11 (LANL), (1982), *DOE-2 Engineers Manual, Version 2.1A,* LBL-11353; Los Alamos National Laboratory Publication LA-8520-M.
13. Winkelmann, F.C. and Selkowitz, S. (1986), "Daylighting Simulation in the DOE-2 Building Energy Analysis Program," *Energy and Buildings 8, p. 271.*
14. Eto, J.H. (1984), *Commercial Building Cogeneration Opportunities,* LBL-18176.
15. Bazjanac, V. (1985), *Energy Performance of the Pacific Museum of Flight,* Berkeley, CA.
16. Birdsall, B. (1985), *A Comparison of DOE-2.1C Prediction with Thermal Mass Test Cell Measurements,* LBL-18981.

PUBLICATIONS LIST

This list of publications for the Energy Efficient Buildings Program covers the years 1982–1985. For earlier or more recent publications, please contact each group individually. This list is organized as follows:

- *Energy Efficient Buildings* (EEB)—general reports not specific to any group.
- *Buildings Energy Data* (BED)—reports on the compilation and analysis of building energy performance data.
- *Building Energy Simulation* (BES, including DOE-2)—reports concerning computer modeling and programming.
- *Energy Performance of Buildings*—reports specific to the energy performance of building envelopes.
- *Ventilation and Indoor Air Quality*—reports specific to building ventilation and indoor air quality.
- *Windows and Daylighting*—reports specific to the energy-efficient design of windows and use of daylighting.
- *Lighting Systems Research*—reports specific to the energy-efficient design of lighting systems, including daylighting.

Most reports have an LBL number and an EEB number, either of which may be used for ordering copies.

Energy Efficient Buildings (EEB)

1982

EEB 82-2, LBL-15182
Technology for Energy-Efficient Buildings, A. H. Rosenfeld, presented at the First U.S.–China Conference on Energy, Resources, and Environment, Beijing, China, November 7–12, 1982.

EEB 82-3, LBL-15183
Energy Efficiency in Chinese Apartment Buildings: Parametric Runs with the DOE-2 Computer Program, Y.J. Huang, M. Lokmanhekim, A.C. de Piedade, A.H. Rosenfeld, and D. Tseng. Presented at the First U.S.–China Conference on Energy, Resources, and Environment, Beijing, China, November 7–12, 1982.

1983

EEB 83-1, LBL-16064
Technology for Energy-Efficient Buildings—Progress and Potentials—Many Suggestions and Some Opportunities for Collaboration, A.H. Rosenfeld. Presented at the France-California Colloquium sponsored by AFME, Sophia Antipolis, France, May 16, 1983.

EEB 83-2, LBL-16074
Building Energy Rating Systems: Panel Summary, A.H. Rosenfeld and L. Schuck. Presented at ACEEE 1982 Summer Study on Energy-Efficient Buildings, Santa Cruz CA, August 22–28, 1982.

EEB 83-3, LBL-8913 (Rev.)
Storage of Heat and Coolth in Hollow-Core Concrete Slabs: Swedish Experience and Application to Large, American-Style Buildings, L.O. Anderson, K.G. Bernander, E. Isfält, and A. H. Rosenfeld. June 22, 1983.

LBL-15412 (Rev.),
The Assessment of Progress in Energy Efficient Buildings, L.W. Wall and A.H. Rosenfeld. Submitted to Proceedings of the Second International Congress on Building Energy Management, Ames, IA, May 30–June 3, 1983.

EEB 83-4, PUB-471
The Dollars and Sense of Conservation, Judith Goldhaber, 1983.

EEB 83-5, LBL-16813
Improving the Energy Efficiency of Residential Clothes Dryers. D. Hekmat and W.W. Fisk. July 1983.

1984

EEB 84-1, LBL-17553
Statement on the DOE FY '85 Conservation Budget Request for Buildings & Community Systems, testimony for Hearings on DOE Conservation & Solar Energy Budget for FY '85 by the U.S. House of Representatives, Subcommittee on Energy Conservation & Power of the Committee on Energy & Commerce, A.H. Rosenfeld, February 1984.

EEB 84-2
"Home Energy Ratings: A Promising Approach to Energy Conservation," A.H. Rosenfeld and L. Schuck, *Energy Conservation Bulletin* (a publication of the Energy Conservation Coalition), Vol. 3, No. 5, March–April 1984.

1985

EEB 85-1, LBL-19131
Saving Peak Power: At the Meter, Beyond the Meter, and at the Checkbook. A.H. Rosenfeld. Presented at the 1984 ACEEE Summer Study on Energy-Efficient Buildings, Santa Cruz CA, August 1984.

EEB 85-2, LBL-19135
Shifting Peak Power: At the Meter, Beyond the Meter, and at the Checkbook. A.H. Rosenfeld. Presented at the PG&E Energy Expo, Oakland CA, May 22, 1985. Published in the *Proceedings.* May 1984.

LBL-19448
The High Cost-Effectiveness of Cool Storage in New Commercial Buildings. O.de la Moriniere and A.H. Rosenfeld. Presented at ASHRAE Annual Meeting, Honolulu HI, June 1985. ASHRAE Transactions HI-85-15 No. 4.

EEB 85-5
Statement on the Least Cost Utility Planning Initiative. Testimony before the Subcommittee on Energy Development and Applications of the Committee on Science and Technol-

ogy, U.S. House of Representatives. Washington, D.C. September 26, 1985. A.H. Rosenfeld and M.D. Levine.

EEB 85-6, LBL-20506
Residential Energy Efficiency: Progress Since 1973 and Future Potential. A.H. Rosenfeld. Presented at the APS Short Course "Energy Sources: Conservation and Renewables." Washington, D.C. April 27–28, 1985. Published in AIP Conference Proceedings, No. 135.

EEB 85-7, LBL-20505
Energy Conservation in Large Buildings. A.H. Rosenfeld and D. Hafemeister. Presented at the APS Short Course "Energy Sources: Conservation and Renewables," Washington, D.C. April 27–28, 1985. AIP Conference Proceedings No. 135.

EEB 85-8, LBL-20507
Smart Meters and Spot Pricing: Experiments and Potential. A.H. Rosenfeld, D.A. Bulleit and R.A. Peddie. March 1986 Edition (Ed. R.H. Williams). November 1985.

EEB 85-9, LBL-20508
Electrical Energy Conservation and Peak Demand Reduction Potential for Buildings in Texas: Preliminary Results. B.D. Hunn, M.L. Baughman, S.C. Silver, A.H. Rosenfeld, and H. Akbari. Presented at the 2nd Annual Symposium, Improving Building Energy Efficiency in Hot and Humid Climates, Texas A&M University, College Station TX, September 24 –26, 1985. Published in the *Proceedings*, pp. 271-278.

EEB 85-10, LBL-20527
California Petroleum Violation Escrow Account (PVEA) Evaluation Report. A. Rosenfeld, J. Sathaye, and E. Vine. Consultant Report prepared for the California Energy Commission. March 15, 1985.

EEB 85-11, LBL-20525
Planning For Oil Overcharge Funds: The California Experience. E. Vine, J. Sathaye, and A. Rosenfeld. Submitted to *Energy*. January 1986.

Buildings Energy Data

1982

EEB-BED 82-01, LBL-14529
Thermal and Economic Performance of Low-Income Housing, R. Crenshaw, June 1982. Presented at PASSIVE '82, ASISES Conference, Knoxville, TN, August 29–September 3, 1982.

EEB-BED 82-02, LBL-14576,
Monitored Superinsulated and Solar Houses in North America: A Compilation and Economic Analysis, J.C. Ribot, J.G. Ingersoll, and A.H. Rosenfeld, June 1982. Presented at PASSIVE '82, ASISES Conference, Knoxville, TN, August 29–September 3, 1982.

EEB-BED 82-03, LBL-14111
Infiltration and Indoor Air Quality in a Sample of Passive Solar and Super Insulated Houses, B.S. Wagner and A.H. Rosenfeld, June 1982. Presented at PASSIVE '82, ASISES Conference, Knoxville, TN, August 29–September 3, 1982.

EEB-BED 82-04, LBL-14686
Supply Curves of Conserved Energy, A. Meier, Ph.D. Dissertation, May 1982.

EEB-BED 82-05, LBL-13385
"Building Energy Compilation and Analysis (BECA), Part B: Retrofit of Existing North American Residential Buildings," L. Wall, C.A. Goldman, A.H. Rosenfeld, and G.S. Dutt, *Energy and Buildings 5*, p. 151 (1983).

EEB-BED 82-07, LBL-14787
A Summary Report of Building Energy Compilation and Analysis (BECA)—Part B: Existing North American Residential Buildings, L.W. Wall, C.A. Goldman, and A.H. Rosenfeld, ACEEE 1982 Summer Study on Energy Efficient Buildings, Santa Cruz, CA, August 22–28, 1982.

EEB-BED 82-08, LBL-14788
Monitored Low-Energy Houses in North America and Europe: A Compilation and Economic Analysis, J.C. Ribot and A.H. Rosenfeld, ACEEE 1982 Summer Study on Energy Efficient Buildings, Santa Cruz, CA, August 22–28, 1982.

EEB-BED 82-09, LBL-14827
Building Energy Use Compilation and Analysis (BECA) Part C: Conservation Progress in Retrofitted Commercial Buildings, H. Ross and S. Whalen, ACEEE 1982 Summer Study on Energy Efficient Buildings, Santa Cruz, CA, August 22–28, 1982.

EEB-BED 82-10, LBL-14838
A Summary Report of Building Energy Compilation and Analysis (BECA) Part V: Validation of Energy Analysis Computer Programs, B.S. Wagner and A.H. Rosenfeld, ACEEE 1982 Summer Study on Energy Efficient Buildings, Santa Cruz, CA, August 22–28, 1982.

EEB-BED 82-11, LBL-14853
Instrumented Audits, R. Crenshaw, ACEEE 1982 Summer Study on Energy Energy Efficient Buildings, Santa Cruz, CA, August 22–28, 1982.

EEB-BED 82-12, LBL-14818
New Utility Strategies for Saving Energy in the Commercial Sector, S. Maves and J.P. Harris, ACEEE 1982 Summer Study on Energy Efficient Buildings, Santa Cruz, CA, August 22–28, 1982.

EEB-BED 82-13, LBL-14914
Technical Issues for Building Energy Use Labels, A.H. Rosenfeld and B.S. Wagner, ACEEE 1982 Summer Study on Energy Efficient Buildings, Santa Cruz, CA, August 22–28, 1982.

EEB-BED 82-14, LBL-14924
Purchasing Patterns of Energy-Efficient Refrigerators and Implied Consumer Discount Rates, A. Meier and J. Whittier, ACEEE 1982 Summer Study on Energy Efficient Buildings, Santa Cruz, CA, August 22–28, 1982.

EEB-BED 82-15, LBL-15083
Results of the Walnut Creek House Doctor Project, B.C. O'Regan, B.S. Wagner, and J.B. Dickinson, November 1982.

EEB-BED 82-16, LBL-15198
"The Cost of Conserved Energy as an Investment Statistic," A. Meier, October 1982. Published as "What Is the Cost to You of Conserved Energy?" *Harvard Business Review 61* (1), pp. 36–37 (January–February 1983).

EEB-BED 82-17, LBL-15375
A Summary Review of Building Energy Use Compilation and Analysis (BECA), Part C: Conservation Progress in Retrofitted Commercial Buildings, L.W. Wall and J. Flaherty, ACEEE 1982 Summer Study on Energy Efficient Buildings, Santa Cruz, CA, August 22–28, 1982.

EEB-BED 82-18, LBL-15374
Progress in Energy Efficient Buildings, L.W. Wall and A.H. Rosenfeld, December 1982. Presented at the Association of Energy Engineers, 5th Energy Audit Symposium and Productivity Exposition, Los Angeles, CA, February 17–18, 1983.

1983

EEB-BED 83-01, LBL-15635
Progress in Energy-Efficient Commercial Buildings as Assessed by the Data Base at LBL, L.W. Wall and A.H. Rosenfeld, January 1983. Presented at the Workshop on Designing and Managing Energy Conscious Commercial Buildings, Denver, CO, July 19–20, 1982.

EEB-BED 83-02, LBL-16121
Summary of International Data on Monitored Low-Energy Houses: A Compilation and Economic Analysis, J.C. Ribot, A.H. Rosenfeld, F. Flouquet, and W. Luhrsen. Presented at the 1983 International Conference on Earth Sheltered Buildings, Sydney, Australia, August 1–10, 1983. April 1983.

PUB-466
BECA Brochure: Buildings Energy Use Compilation and Analysis: Program Summary and Data Request, September 1983.

EEB BED 83-03, LBL-16669
Saving Energy in Real Houses: Results from LBL Residential Data Bases, C. Goldman, presented at the Working Conference on Families and Energy—Coping with Uncertainty, Michigan State University, October 9–11, 1983, September 1983.

EEB-BED 83-04, LBL-17088
Technical Performance and Cost-Effectiveness of Conservation Retrofits in Existing U.S. Residential Buildings: Analysis of the BECA-B Database, C. Goldman, Master's Thesis, October 1983.

EEB-BED 83-05, LBL-17055
A Residential Conservation Data Base for the Pacific Northwest, A. Usibelli, B. Gardiner, W. Luhrsen, and A. Meier. Prepared for the Bonneville Power Administration, Portland, OR, November 1983.

EEB-BED 83-06, LBL-18107
A Residential Conservation Data Base for the Pacific Northwest: Documentation and Appendixes, A. Usibelli, B. Gardiner, W. Luhrsen, and A. Meier. Prepared for the Bonneville Power Administration, Portland, OR, November 1983.

EEB-BED 83-07, LBL-16362
Residential Indoor Air Quality/Air Infiltration Study, B.S. Wagner, Masters Thesis, University of California at Berkeley, Energy and Resources Group, December 1982.

1984

EEB-BED 84-01, LBL-17583
Measured Electricity Use of Drinking Fountains and Water Coolers, A.K. Meier, April 1984.

EEB-BED 84-02, LBL-17364
Comparisons of Predicted and Measured Energy Use in Occupied Building, B.S. Wagner. Presented at the ASHRAE Annual Meeting in Kansas City, MO, June 17–20, 1984; *ASHRAE Trans. 90,* Part 2B, p. 232 (1984).

EEB-BED 84-03, LBL-17994
Energy Conservation in Public Housing: The San Francisco Experience, C.A. Goldman, R. Ritschard, and R. Atkielski, June 1984. Presented at ACEEE 1984 Summer Study on Energy Efficiency in Buildings, Santa Cruz, CA, August 14–22, 1984.

EEB-BED 84-03, LBL-17994Rev.
Energy Conservation in Public Housing: The San Francisco Housing Authority. C.A. Goldman and R. Ritschard. To be published in *Energy and Buildings.* April 1985.

EEB-BED 84-04, LBL-17926
Measured Energy Savings from Retrofitting Existing Residential Buildings: Updated Results from the BECA-B Project, C.A. Goldman, April 1984. Submitted to *Energy and Buildings.*

EEB-BED 84-05, LBL-18176
Commercial Building Cogeneration Opportunities. J.H. Eto. In *Proceedings* of Doing Better: Setting an Agenda for the Second Decade, New Commercial Buildings, pp. D-203-D-216, ACEEE 1984 Summer Study on Energy Efficient Buildings, Santa Cruz CA, August 14–22, 1984. August 1984.

EEB-BED 84 -06, LBL-16426
Energy Efficiency in Commercial Food Service Refrigeration: An Assessment of Technical Potential and Data Needs. B. O'Regan, S. Greenberg. July 1984.

1985

EEB-BED 85-01, LBL-18543
Commercial-Sector Conservation Technologies. A. Usibelli, S. Greenberg, M. Meal, A. Mitchell, R. Johnson, G. Sweitzer, F. Rubinstein, and D. Arasteh. February 1985.

EEB-BED 85-02, LBL-19244
The "CAL-BECA" Project, Part 1: New California Nonresidential Buildings. B. Gardiner. Prepared for the California Energy Commission, Sacramento CA, and the University-wide Energy Research Group, University of California, Berkeley CA. April 1985.

EEB-BED 85-03, LBL-19348
Monitored Energy Performance of New and Retrofitted Residential Buildings: Results from the "BECA" Data Base. J.P. Harris. Presented at the Conference on Energy Management and the Consumer, Versailles, France, April 1985. June 1985.

EEB-BED 85-04, LBL 19293
Energy-Efficient New Commercial Buildings in the Northwest Region: A Compilation of Measured Data. M.A. Piette, D. Flora and S. Crowder. May 1985.

EEB-BED 85-05, LBL-19212
Implications of Office Building Thermal Mass and Multi-Day Temperature Profiles for Cooling Strategies. J.H. Eto and G. Powell. To be published in *Proceedings of the 1985 ASME/AICHE National Heat Transfer Conference,* Denver, CO, August 4–7, 1985. August 1985.

EEB-BED 85-06, LBL-19413
Measured Energy Performance of Energy Efficient New Commercial Buildings: Results from the BECA-CN Data Compilation. M.A. Piette, L. Wall, and B. Gardiner. April 1985.

EEB-BED 85-07, LBL-19914
Characterizing the Effects of Weather on Commercial Building Energy Use. J.H. Eto. Presented at the Building Energy Simulation Conference, Seattle WA, August 21–22, 1985. August 1985.

EEB-BED 85-08, LBL 19912
Cooling Strategies Based on Indicators of Thermal Storage in Commercial Building Mass. J.H. Eto. Presented at the Second Annual Symposium on Improving Building Energy Efficiency in Hot and Humid Climates, Texas A&M University, College Station TX, September 24–26, 1985. September 1985.

Building Energy Simulation

1982

EEB-DOE-2 82-1, LBL-11353, LA-8520-M
DOE-2 Engineers Manual, Building Energy Analysis Group and Group-11, Los Alamos National Laboratory, November 1982.

EEB-DOE-2 82-2, LBL-14026
Simulation of HVAC Equipment in the DOE-2 Program, J.J. Hirsch. Presented at the International Conference on Systems Simulation in Buildings, Liege, Belgium, December 1982.

1983

EEB-DOE-2 83-1, LBL-15972
Technological and Economic Issues in Building Energy Use,

R.B. Curtis and J.M. Weingart. Presented at the Seminar on Energy Efficiency and Conservation, Lome, Togo, March 30–April 8, 1983.

EEB-DOE-2 83-2, LBL-16126
Optimal Cogeneration Systems for High-Rise Office Buildings, J.H. Eto. Presented at the 18th Intersociety Energy Conversion Engineering Conference, Orlando, FL, August 21–26, 1983.

EEB-DOE-2 83-3, LBL-11353 (III.2.9 only)
"Daylighting Calculation in DOE-2" (Chapter III.2.9 of the DOE-2 Engineers Manual), F.C. Winkelmann. May 1983.

EEB-DOE-2 83-4, LBL-8607 Rev. 3. Suppl.
DOE-2 Supplement, Building Simulation Group, January 1983.

EEB-DOE-2 83-5, LBL-8688 Rev. 3
DOE-2 BDL Summary, Building Energy Simulation Group, January 1983.

EEB-DOE-2 83-6, LBL-16645
Commercial Building Energy Performance Using Multiple Regression Techniques Analysis, R. Sullivan, R. Johnson, S. Nozaki, and S. Selkowitz. Presented at the ASHRAE Semi-Annual Conference, Kansas City, MO, June 24–28, 1984. October 1983.

EEB-DOE-2 83-7, LBL-16369
Multiple Regression Techniques Applied to Fenestration Effects on Commercial Building Energy Performance, R. Sullivan and S. Nozaki. Presented at the ASHRAE Winter Meeting, Atlanta, GA, January 1984. *ASHRAE Trans. 90,* Part 1A, p.116 (1984). June 1983.

1984

EEB-DOE-2 84-1, LBL-17459
Description of an Earth Contact Modeling Capability in the DOE-2.1B Energy Analysis Program, R. Sullivan, J. Bull, P. Davis, S. Nozaki and Z. Cumali. Presented at the ASHRAE Winter Meeting, Chicago, IL. January 27–31, 1985. June 1984.

EEB-DOE-2 84-2, LBL-16986
Issues in Building Maintenance and Building Energy Standards, R. Curtis. Presented at the ASEAN Conference on Energy Conservation in Buildings, Singapore, May 29–31, 1984. April 1984.

EEB-DOE-2 84-3, LBL-18046
DOE-2 Building Energy Analysis Program, R. Curtis, B. Birdsall, W.F. Buhl, E. Erdem, J.H. Eto, J.J. Hirsch, K. Olson, F.C. Winkelmann. Presented at the ASEAN Conference on Energy Conservation in Buildings, Singapore, May 29–31, 1984. April 1984.

EEB-DOE-2 84-4, LBL-18176
Commercial Building Cogeneration Opportunities. J.H. Eto. Presented at the ACEEE 1984 Summer Study, Santa Cruz, CA, August 1984; in Proceedings, Vol. D, Panels on New and Existing Commercial Buildings.

EEB-DOE-2 84-5, LBL-18508
Daylighting Simulation in the DOE-3 Building Energy Analysis Program, F.C. Winkelmann and S. Selkowitz, October 1984.

1985

EEB-DOE-2 85-1, LBL-18981
A Comparison of DOE-2.1C Predication with Thermal Mass Test Cell Measurements. B. Birdsall. January 1985.

EEB-DOE-2 85-2, LBL-19735
Overview of the DOE-2 Building Energy Analysis Program. Building Energy Simulation Group. June 1985.

Energy Performance of Buildings

1982

EEB-EPB, PUB-442
CIRA Reference Manual, Energy Performance of Buildings Group, May 1982.

EEB-EPB, PUB-448
CIRA Source Listings and Source Disks, Energy Performance of Buildings Group, July 1982.

EEB-EPB 82-4 LBL-12742
Results of the Bonneville Power Administration Weatherization and Tightening Projects at the Midway Substation Residential Community, J.B. Dickinson, D.T. Grimsrud, D.L. Krinkel, and R.D. Lipschutz, February 1982.

EEB-EPB 82-5 LBL-13949
Wind and Infiltration Interaction for Small Buildings, M.H. Sherman and D.T. Grimsrud. Presented at ASCE Annual Meeting, New Orleans, LA, October 23–29, 1982.

EEB-EPB 82-6, LBL-13678
A Comparison of Alternate Ventilation Strategies, M.H. Sherman and D.T. Grimsrud. Presented at the Third AIC Conference, London, September 1982.

EEB-EPB 82-7, LBL-14733
Infiltration and Leakage Measurements in New Houses Incorporating Energy Efficient Features, R.D. Lipschutz, J.B. Dickinson, and R.C. Diamond, ACEEE 1982 Summer Study on Energy Efficient Buildings, Santa Cruz, CA, August 22–28, 1982.

EEB-EPB 82-8, LBL-14734
Results of Recent Weatherization Retrofit Projects, J.B. Dickinson, R.D. Lipschutz, B. O'Regan, and B.S. Wagner, ACEEE 1982 Summer Study on Energy Efficient Buildings, Santa Cruz, CA, August 22–28, 1982.

EEB-EPB 82-9, LBL-14735
Component Leakage Testing in Residential Buildings, D.J. Dickerhoff, D.T. Grimsrud, and R.D. Lipschutz, ACEEE 1982 Summer Study on Energy Efficient Buildings, Santa Cruz, CA, August 22–28, 1982.

1983

EEB-EPB 83-1, LBL-15270
CIRA—A Microcomputer-Based Energy Analysis and Auditing Tool for Residential Applications, R.C. Sonderegger and J.D. Dixon. Presented at the Fourth International Symposium on the Use of Computers for Environmental Engineering Related to Buildings, Tokyo, Japan, March 30–April 1, 1983.

EEB-EPB 83-2, LBL-15473
Performance Calculations of Residential Cooling Systems for Simplified Energy Analysis, P-F. Brunello and R.C. Sonderegger. Submitted to *Energy and Buildings.*

EEB-EPB 83-3, LBL-15636
"A Detailed Examination of the LBL Infiltration Model using the Mobile Infiltration Test Unit," M.P. Modera, M. H. Sherman, and P. A. Levin. Presented at the ASHRAE Symposium, Washington, DC, June 26–30, 1983. *ASHRAE Trans. 89,* Part 2B, p. 157 (1983). July 1983.

EEB-EPB 83-4, LBL-15793
CIRA Economic Optimization Methodology, R.C. Sonderegger, P.G. Cleary, J-Y. Garnier, and J.D. Dixon. To be published in Proceedings of the ASHRAE/DOE Conference on the Thermal Performance of Exterior Envelopes of Buildings II, Las Vegas, NV, December 5–9, 1982. February 1983.

EEB-EPB 83-5, LBL-14925
Field Testing of Wind Cooling Effects on Navy Buildings, Pro-

ject Report, M.H. Sherman, D.J. Dickerhoff, and D.T. Grimsrud, May 1983.

EEB-EPB 83-6, LBL-16035
"Air Infiltration Research at the Lawrence Berkeley Laboratory," M.H. Sherman. *Air Infiltration Review 4* (4), pp. 4–5, May 1983.

EEB-EPB 83-7, LBL-16221
Component Leakage Areas in Residential Buildings, C. Reinhold and R. Sonderegger, July 1983. Presented at the 4th AIC Conference on Air Infiltration Reduction in Existing Buildings, Elm, Switzerland, September 26–28, 1983.

EEB-EPB 83-8, LBL-16644
Energy and Housing for the Elderly: Preliminary Observations, R.C. Diamond. Presented at the Working Conference on Families and Energy—Coping with Uncertainty, Michigan State University, October 9–11, 1983.

EEB-EPB 83-9, LBL-16657
Some Technical and Behavorial Aspects of Energy Use in a High-Rise Apartment Building, R.D. Lipschutz, R.C. Diamond, and R.C. Sonderegger. Presented at the Working Conference on Families and Energy—Coping with Uncertainty, Michigan State University, October 9–11, 1983.

EEB-EPB 83-10, LBL-16366
Energy Use in a High-Rise Apartment Building, September 1983. (Longer version of EEB-EPB 83-9).

EEB-EPB 83-11, LBL-16658
New Residential Building Construction in the United States, P.A. Levin. September 1983.

1984

EEB-EPB 84-01, LBL-17173
Technical Description: The Envelop Thermal Test Unit, M. Modera. Presented at the ASHRAE Symposium on Field Measurements of Heat Transfer in Building Envelopes, Chicago, IL, January 1985. January 1984.

EEP-EPB 84-02, LBL-16036
The Calculation of Natural Ventilation and Comfort, M. Sherman and S. Ashley. Presented at the ASHRAE 1984 Winter Meeting, Atlanta, GA, January–February 1984. January 1984.

EEB-EPB 84-03, LBL-15923
"A Simplified Model of Thermal Comfort," M. Sherman, *Energy and Buildings 8,* p. 37 (1985). January 1984.

EEB-EPB 84-04 LBL-17585
Description of ASHRAE's Proposed Air Tightness Standard, M. Sherman, in Proceedings of the 5th AIC Conference. October 1984.

EEB-EPB 84-05, LBL-17001
Comparison of Measured and Predicted Infiltration Using the LBL Infiltration Model, M. Sherman and M. Modera. Presented at the ASTM Symposium on Measured Air Leakage Performance of Buildings, Philadelphia, PA, April 1984. February 1985.

EEB-EPB 84-06, LBL-18062
Moisture Control by Attic Ventilation—An In-Situ Study, P. Cleary. To be presented at the ASHRAE 1985 Annual Conference, Honolulu, HI, June 1985. July 1984.

EEB-EPB 84-07, LBL-17590
Humidity in Attics—Sources and Control Methods, P. Cleary. Presented at the 1984 ACEEE Summer Study, Santa Cruz, CA, August 1984. July 1984.

EEB-EPB 84-08, LBL-17584
Air Infiltration in Multi-Family Buildings and its Dependency on Air Tightness, H. Feustel and F. Lenz. Submitted to *Energy and Buildings.* February 1985.

1985

EEB-EPB 85-01, LBL 17774
Seasonal Storage of Moisture in Roof Sheathing. P. Cleary and M. Sherman. Presented at the 1985 Symposium on Moisture and Humidity Measurement and Control in Science and Industry, Washington, D.C., April 15-19, 1985. December 1984.

EEB-EPB 85-02, LBL-17591
A Method to Predict the Hour-by-Hour Humidity Ratio of Attic Air. P. Cleary and R. Sonderegger. Presented at the American Society for Testing Materials, December 2-6, 1984, Dallas TX. December 1984.

EEB-EPB 85-03, LBL-18924
Current Research at Lawrence Berkeley Laboratory on Multizone Infiltration. H. Feustel. To be published in *Air Infiltration Review.* October 1984.

EEB-EPB 85-04, LBL 16924
A One-Channel Monitor for Wood Stove Heat Output: Project Report for the Hood River Conservation Program. M.P. Modera, B.S. Wagner, and J. Shelton. Presented at the 1984 American Society for an Energy Efficient Economy, Summer Study, Santa Cruz CA, August 14–22, 1984. February 1984.

EEB-EPB 85-05, LBL 17773
In-Situ Measurement of Wall Thermal Performance: Data Interpretation and Apparatus Design Recommendations. M.P. Modera, M.H. Sherman and S.G. deVinuesa. Presented at the American Society for Testing Materials Symposium on Thermal Insulation, Materials and Systems, Dallas TX. December 2–6, 1984. September 1984.

EEB-EPB 85-06, LBL 17587
Variability in Residential Air Leakage. M.H. Sherman, D.J. Wilson and D.E. Kiel. Presented at American Society for Testing Materials Symposium on Measured Air Leakage Performance of Buildings, Philadelphia PA, April 2–3, 1984. ASTM Special Technical Publication. April 1984.

EEB-EPB 85-07, LBL 17593
Energy Use Among the Low-Income Elderly: A Closer Look. R. C. Diamond. Presented at the 1984 American Society for an Energy Efficient Economy, Summer Study, Santa Cruz CA, August 14-22, 1984. July 1984.

EEB-EPB 85-08, LBL 17588
Infiltration Models for Multicellular Structures-A Literature Review. H.E. Feustel and V.M. Kendon. Published in *Energy and Buildings,* Vol. 8 No. 2, pp. 123-136, 1985. April 1985.

EEB-EPB 85-09, LBL 19040
The Prediction of Air Infiltration. M. Sherman and B. Dickinson. To be published in the Proceedings of the CLIMA 2000 Conference, August 25-30, 1985, Copenhagen, Denmark. July 1985.

EEB-EPB 85-10, LBL 20165
Building Energy Retrofit Research, Multifamily Sector. R. Diamond, C. Goldman, M. Modera, M. Rothkopf, M. Sherman, and E. Vine. August 1985.

EEB-EPB 85-11, LBL 14589
Temperature- and Wind-Induced Air Flow Patterns in a Staircase: Computer Modelling and Experimental Verification. H.E. Feustal, CH. Zuercher, R.C. Diamond, J.B. Dickinson, D.T. Grimsrud, and R. Lipschutz. Published in *Energy and Buildings,* 8, 1985. August 1985.

EEB-EPB 85-12, LBL 19571
Energy Impacts of Efficient Refrigerators in the Pacific Northwest. M. Sherman, M. Modera and D. Hekmat. April 1985.

EEB-EPB 85-13, LBL 18955
Ventilation and Infiltration. M. Modera and F. Peterson. To be published by the Royal Institute of Technology, Stockholm, Sweden. January 1985.

EEB-EPB 85-14, LBL 19095
Development of a Simplified Multizone Infiltration Model. H. Feustal. Published in the *Proceedings* of the 6th Air Infiltration Centre Conference, Het Meerdal, Netherlands, September 16-21, 1985. November 1985.

EEB-EPB 85-15, LBL 19776
Multizone Modeling and Air Leakage Analysis. M. Sherman. Published in the Proceedings of the 6th Air Infiltration Centre Conference, Het Meerdal, Netherlands, September 16-21, 1985. November 1985.

Ventilation and Indoor Air Quality

1982

EEB-Vent 80-14, LBL-10631
A Method for Estimating the Exhalation of Radon from Building Materials, J.G. Ingersoll, B.D. Stitt, and G.H. Zapalac, February 1982.

EEB-Vent 80-16, LBL-11771
"A Survey of Radionuclide Contents and Radon Emanation Rates in Building Materials in the United States," J.G. Ingersoll, *Health Physics 45,* p. 363 (1983).

EEB-Vent 80-20, LBID-625
Contaminant Control in the Built Environment: Formaldehyde and Radon, K. Alder and C.D. Hollowell, September 1982.

EEB-Vent 80-22, LBL-10775
"Radon and Its Daughters in Energy Efficient Buildings," A.V. Nero, M.L. Boegel, C.D. Hollowell, J.C. Ingersoll, W.W. Nazaroff, and K. Revzan, in *Natural Radiation Environment,* K.G. Vohrae *et al.*, Eds., Wiley Eastern, Ltd., New Delhi, India (1982).

EEB-Vent 82-2, LBL-13843
"Residential Air-to-Air Heat Exchangers: Performance, Energy Savings, and Economics," W.J. Fisk and I. Turiel, *Energy and Buildings 5,* p. 197 (1983). March 1982.

EEB-Vent 82-3, LBL-14027
Indoor Air Pollution from Portable Kerosene-Fired Space Heaters, Wood-Burning Stoves, and Wood-Burning Furnaces, G.W. Traynor, J.R. Allen, M.G. Apte, J.F. Dillworth, J.R. Girman, C.D. Hollowell, and J.F. Koonce. Presented at APCA Specialty Meeting: Residential Wood and Coal Combustion, Louisville, KY, March 1–2. March 1982.

EEB-Vent 82-4, LBID-501
A Carbon Monoxide Passive Monitor: A Research Need, J.R. Girman, G.W. Traynor, and C.D. Hollowell, March 1982.

EEB-Vent 82-5, LBL-14031
"Pollutant Emissions from Portable Kerosene-Fired Space Heaters," G.W. Traynor, J.R. Allen, M.G. Apte, J.R. Girman, and C.D. Hollowell, *Environ. Sci. Technol. 17,* p. 369 (1983). April 1982.

EEB-Vent 82-6, LBL-14448
Experimental and Predicted Overall Heat Transfer Coefficients for Four Residential Air-to-Air Heat Exchangers, R.A. Seban, A. Rostami, and M. Zarringhalam, May 1982.

EEB-Vent 82-7, LBL-14467
Exclusion List Methodology for Weatherization Program in the Pacific Northwest, A.V. Nero, I. Turiel, W.J. Fisk, J.R. Girman, and G.W. Traynor, August 1982.

EEB-Vent 82-9, LBL-13100
Residential Air-Leakage and Indoor Air Quality in Rochester, New York, F.J. Offermann, J.B. Dickinson, W.J. Fisk, D.T. Grimsrud, C.D. Hollowell, D.L. Krinkel, and G.D. Roseme, June 1982.

EEB-Vent 82-10, LBL-14616
Validation of a Passive Sampler for Determining Formaldehyde in Residential Air, A.T. Hodgson, K.L. Geisling, B. Remijn, and J.R. Girman, June 1982.

EEB-Vent 82-11, LBL-14784
"Energy Savings and Cost-Effectiveness of Heat Exchanger Use as an Indoor Air Quality Mitigation Measure in the BPA Weatherization Program," I. Turiel, W.J. Fisk, and M. Seedall, *Energy 8,* p. 323 (1983). July 1982.

EEB-Vent 82-12, LBL-14795
"Indoor Air Quality in Energy Efficient Residences," D.T. Grimsrud, R.D. Lipschutz, and J.R. Girman. Chapter 5 of *Indoor Air Quality,* P.J. Walsh and C.J. Dudney, Eds., CRC Press, Boca Raton, FL (1983). May 1983.

EEB-Vent 82-13, LBL-14907
"Optimizing the Total-Alpha Three-Count Technique for Measuring Concentrations of Radon Progeny in Residences," W.W. Nazaroff, *Health Physics 46,* p. 395 (1984). September 1982.

EEB-Vent 82-14, LBL-14358
Residential Air-to-Air Heat Exchangers: A Study of Ventilation Efficiencies, F.J. Offermann, W.J. Fisk, B. Pedersen, and K.L. Revzan, September 1982.

EEB-Vent 82-15, LBL-15376
"Ventilation Efficiencies of Wall- or Window-Mounted Residential Air-to-Air Heat Exchangers," F.J. Offermann, W.J. Fisk, D.T. Grimsrud, B. Pedersen, and K. L. Revzan. Presented at the 1983 ASHRAE Annual Meeting, June 26–30, Washington, DC. *ASHRAE Trans. 89,* Part 2B, p. 507. June 1982.

1983

EEB-Vent 83-1
Building Ventilation and Indoor Air Quality, 1982 Annual Report, D.T. Grimsrud, A.V. Nero *et al.*, January 1983.

EEB-Vent 83-2, LBL-15612
Indoor Air Pollution from Portable Kerosene-Fired Space Heaters, G.W. Traynor, M.G. Apte, J.F. Dillworth, and D.T. Grimsrud. Presented at Hazardous Heat: A Symposium on the Health & Safety of Kerosene Heaters, Hempstead, NY, November 8, 1982. February 1983.

EEB-Vent 83-3, LBL-15555
"Radon Daughter Carousel: An Automated Instrument for Measuring Indoor Concentration of ^{218}Po, ^{214}Pb, and ^{214}Bi," W.W. Nazaroff, *Rev. Sci. Instrum. 54,* p. 1227 (1983). March 1983.

EEB-Vent 83-4, LBL-15783
"Field Data Logger with EPROM Storage," A.W. Robb and W.W. Nazaroff. *Rev. Sci. Instrum. 54,* p. 1252 (1983). March 1983.

EEB-Vent 83-5, LBL-15907
Ventilation by Stratification and Displacement, E. Skaaret. Presented at the Second International Congress on Building Energy Management, Ames, IA, May 30–June 3, 1983. March 1983.

EEB-Vent 83-6, LBL-15878
Indoor Air Pollution Due to Emission from Unvented Gas-fired Space Heaters, G.W. Traynor *et al.* Presented at the Air Pollution Control Association 76th Annual Meeting, June 20–24, 1983. April 1983.

EEB-Vent 83-7, PUB-457
An Overview of Current Radon and Radon Daughter Research at LBL. February 1983.

EEB-Vent 83-8, LBL-15130
Indoor Air Pollution Due to Emissions from Unvented Gas-Fired Space Heaters: A Controlled Field Study, G.W. Traynor *et al.*, May 1983.

EEB-Vent 83-9, LBL-16155
Ventilation Effectiveness—A Guide to Efficient Ventilation, E. Skaaret and M. Mathisen. Presented at the ASHRAE Annual Meeting, June 26–30, 1983, Washington, DC. May 1983.

EEB-Vent 83-10, LBL-14959
Radon in Energy-Efficient Earth-Sheltered Structures, A.V. Nero. Presented at the 1983 International Conference on Earth Sheltered Buildings, Sydney, Australia. May 1983.

EEB-Vent 83-11, LBL-14574
Sources and Concentrations of Formaldehyde in Indoor Environments, J.R. Girman, K.L. Geisling, and A.T. Hodgson. Presented at the EPA National Symposium on Recent Advances in Pollutant Monitoring of Ambient Air and Stationary Sources, Raleigh, NC, May 3–6, 1983. June 1983.

EEB-Vent 83-12, LBL-16302
Laboratory Studies of The Temperature Dependence of the Palmes NO_2 Passive Sampler, J.R.Girman, A.T. Hodgson, B.K. Robison, and G.W. Traynor. Presented at the EPA National Symposium on Recent Advances in Pollutant Monitoring of Ambient Air and Stationary Sources, Raleigh, NC, May 3–6, 1983. June 1983.

EEB-Vent 83-13, LBL-16525
The Dependence of Indoor Pollutant Concentrations on Sources, Ventilation Rates, and Other Removal Factors. Indoor Air Quality Research: Current Status and Future Needs, A.V. Nero (D.T. Grimsrud co-author). Statement before a joint hearing of the Energy Development and Applications and Natural Resources Agriculture Research and Environment Subcommittees of the House Committee on Science and Technology, August 1983.

EEB-Vent 83-14, LBL-15839
Continuous Measurements of Radon Entry in a Single Family House, D.T. Grimsrud, W.W. Nazaroff, K.L. Revzan, and A.V. Nero. Presented at the Air Pollution Control Association 76th Annual Meeting, Atlanta, GA, June 19–24, 1983. Paper 83–9.8. June 1983.

EEB-Vent 83-15, LBL-16636
Characterizing the Source of Radon Indoors, A.V. Nero, and W.W. Nazaroff. Presented at the International Seminar on Indoor Exposure to Natural Radiation and Related Risk Agreement, Capri, Italy, October 3–5, 1983, and submitted to *Radiation Protection Dosimetry.* September 1983.

EEB-Vent 83-16, LBL-16595
"Time-Averaged Indoor Radon Concentrations and Infiltration Rates Sampled in Four U.S. Cities," S.M. Doyle, W.W. Nazaroff, and A.V. Nero, *Health Physics 47,* p. 579 (1984). October 1983.

EEB-Vent 83-17, LBL-17049
Manual on Indoor Air Quality, R.C. Diamond and D. Grimsrud, December 1983.

EEB-Vent 83-18, LBL-16637
Radon Entry into Houses Having a Crawl Space, W.W. Nazaroff and S.W. Doyle. Submitted to *Health Physics,* December 1983.

EEB-Vent 83-19, LBL-16783
Freezing in Residential Air-to-Air Heat Exchangers: An Experimental Study, W.F. Fisk, K.M. Archer, R.E. Chant, D. Hekmat, F. Offermann, and B.S. Pedersen, September 1983.

EEB-Vent 83-20, LBL-15693
Indoor Air Quality Audits for Commercial Buildings. D.T. Grimsrud, K. Geisling-Sobotka, J.F. Koonce and S.R. Schiller. February 1984.

EEB-Vent 83-21, LBL-17130
Emissions of Volatile Organic Compounds from Architectural Materials with Indoor Applications, A.T. Hodgson *et al.*, September 1983.

EEB-Vent 83-22, LBL-16659
Control of Respirable Particulates and Radon Progeny with Portable Air Cleaners, F.J. Offermann, R.G. Sextro, W.J. Fisk, W.W. Nazaroff, A.V. Nero, K. L. Revzan, and J. Yater. February 1984.

1984

EEB-Vent 84-01
Building Ventilation and Indoor Air Quality, 1983 Annual Report, D.T. Grimsrud, A.V. Nero, *et al.* January 1984.

EEB-Vent 84-02, LBL-16572
Radon Transport into A Single-Family House With A Basement, W.W. Nazaroff, H. Feustel, A.V. Nero, K.L. Revzan, D.T. Grimsrud, M.A. Essling, and R.E. Toohey. Submitted to *Atmospheric Environment.* January 1984.

EEB-Vent 84-03, LBL-16823
Transport of Radon from Soil into Residences, W.W. Nazaroff and A.V. Nero. In Proceedings of the 3rd International Conference on Indoor Air Quality and Climate, Stockholm, Sweden, August 20–24, 1984. February 1984.

EEB-Vent 84-04, LBL-17501
Improving the Energy Performance of Residential Clothes Dryers, D. Hekmat and W.J. Fisk. Presented at the 35th Annual International Appliance Technical Conference, Ohio State University, May 15–16, 1984. February 1984.

EEB-Vent 84-05, LBL-17603
Controlling Indoor Air Pollution From Tobacco Smoke: Models and Measurements, F.J. Offermann, J.R. Girman, and R.G. Sextro. In Proceedings of the 3rd International Conference on Indoor Air Quality and Climate, Stockholm, Sweden, August 20–24, 1984. July 1984.

EEB-Vent 84-06, LBL-16493
Indoor Air Quality Control Techniques: A Critical Review, W. Fisk, R. Spencer, D. Grimsrud, F. Offermann, B. Pedersen, and R. Sextro. March 1984.

EEB-Vent 84-07, LBL-17600
Indoor Air Pollution and Inter-Room Pollutant Transport Due to Unvented Kerosene-Fired Space Heaters, G.W. Traynor, M.G. Apte, A.R. Carruthers, J.F. Dillworth, D.T. Grimsrud, and W.T. Thompson. In Proceedings of the 3rd International Conference on Indoor Air Quality and Climate, Stockholm, Sweden, August 20–24, 1984. February 1984.

EEB-Vent 84-08, LBL-17599
A Passive Sampler for Water Vapor, J.R. Girman, J.R. Allen, and A.Y. Lee. In Proceedings of the 3rd International Conference on Indoor Air Quality and Climate, Stockholm, Sweden, August 20–24, 1984. February 1984.

EEB-Vent 84-09, LBL-17594
Volatile Organic Emissions from Adhesives with Indoor Applications, J.R. Girman, A.T. Hodgson, A.S. Newton, and A.W. Winkes. In Proceedings of the 3rd International Conference on Indoor Air Quality and Climate, Stockholm, Sweden, August 20–24, 1984. February 1984.

EEB-Vent 84-10, LBL-16822
Air Washing for the Control of Formaldehyde in Indoor Air. B.S. Pedersen and W.J. Fisk. In Proceedings of the 3rd International Conference on Indoor Air Quality and Climate, Stockholm, Sweden, August 20–24, February 1984.

EEB-Vent 84-12, LBL-17597
Ventilation for Control of Indoor Air Quality, W.J. Fisk. In Proceedings of the 3rd International Conference on Indoor Air Quality and Climate, Stockholm, Sweden, August 20–24, 1984. February 1984.

EEB-Vent 84-13, LBL-17598
Evaluation of Indoor Aerosol Control Devices and Their Effects on Radon Progeny Concentrations, R.G. Sextro, F.J. Offermann, W.W. Nazaroff, A.V. Nero, K.L. Revzan, and J. Yater. In Proceedings of the 3rd International Conference on Indoor Air Quality and Climate, Stockholm, Sweden, August 20–24, 1984. February 1984.

EEB-Vent 84-14, LBL-17601
Effectiveness of Local Ventilation in Removing Simulated Pollution from Point Sources, K.L. Revzan. In Proceedings of the 3rd International Conference on Indoor Air Quality and Climate, Stockholm, Sweden, August 20–24, 1984. February 1984.

EEB-Vent 84-15, LBL-17609
Radon Decay-Product Behavior Indoors: Numerical Modeling of Convection Effects, G.E. Schiller, A.V. Nero, K.L. Revzan, and C. Tien. In Proceedings of the APCA 77th Annual Meeting and Exhibition, San Francisco, June 24–29, 1984. March 1984.

EEB-Vent 84-16, LBID-842
Calibration and Intercomparison of Four Hygrometer Systems, D. Hekmat. November 1983.

EEB-Vent 84-17, LBL-17381
The Control of Formaldehyde in Indoor Air by Air Washing, B.S. Pedersen and W.J. Fisk. November 1983.

EEB-Vent 84-18, LBL-16701
Effectiveness of Local Ventilation in Removing Simulated Pollution from Point Sources, K.L. Revzan. To be submitted to *Energy and Buildings*. May 1984.

EEB-Vent 84-19, LBL-16955
Identifying Areas with Potential for High Indoor Radon Levels: Analysis of the National Airborne Radiometric Reconnaissance Data for California and the Pacific Northwest, B.A. Moed, W.W. Nazaroff, A.V. Nero, M.B. Schwehr, and A. Van Heuvelen. April 1984.

EEB-Vent 84-20, LBL-17939
Control of Respirable Particles in Indoor Air With Portable Air Cleaners, F.J. Offermann, R.G. Sextro, W.J. Fisk, D.T. Grimsrud, W.W. Nazaroff, A.V. Nero, K.L. Revzan, and J. Yater. Submitted to *Atmospheric Environment*. August 1984.

EEB-Vent 84-21, LBL-18024
"Performance of Residential Air-to-Air Heat Exchangers," W.J. Fisk, K.M. Archer, F.J. Offermann, R.E. Chant, D. Hekmat, and B.S. Pedersen. Presented at the ASHRAE Winter Meeting, Chicago, IL, January 27–30, 1985. *ASHRAE Trans. 91*, Part 1B, p. 159. November 1984.

EEB-Vent 84-22, LBL-18025
"Onset of Freezing in Residential Heat Exchangers," W.J. Fisk, K.M. Archer, F.J. Offermann, R.E. Chant, D. Hekmat, and B.S. Pedersen. Presented at the ASHRAE Winter Meeting, Chicago, IL, January 27–30, 1985. *ASHRAE Trans. 91*, Part 1B, p. 145. November 1984.

EEB-Vent 84-23, LBL-18139
Air Quality Issues in Ventilation Standards, A.V. Nero and D.T. Grimsrud. In Proceedings of the 5th AIC Conference, October 1–4, 1984, Reno, NV, Paper 8. July 1984.

EEB-Vent 84-24, LBL-18149
"Formaldehyde and Tracer Gas Transfer Between Airstreams in Enthalpy-Type Air-to-Air Heat Exchangers," W.J. Fisk, B.S. Pedersen, D. Hekmat, R.E. Chant, and H. Kaboli. Presented at the ASHRAE Winter Meeting, Chicago, IL, January 27-30, 1985. *ASHRAE Trans. 91*, Part 1B, p. 173. July 1984.

EEB-Vent 84-25, LBL-17600
Indoor Air Pollution and Inter-Room Pollutant Transport Due to Unvented Kerosene-Fired Space Heaters, G.W. Traynor, M.G. Apte, A.R. Carruthers, J.F. Dillworth, D.T. Grimsrud, and W.W. Thompson. Submitted to *Environmental Science and Technology*. July 1984.

EEB-Vent 84-26, LBL-18258
Pollutant Emission Rates From Unvented Infrared and Convective Gas-Fired Space Heaters, G.W. Traynor, M.G. Apte, A.R. Carruthers, J.F. Dillworth, and D.T. Grimsrud. March 1984.

EEB-Vent 84-27, LBL-18274
Distribution of Airborne ^{222}Radon Concentrations in U.S. Homes. A.V. Nero, M.B. Schwehr, W.W. Nazaroff, and K.L. Revzan. Submitted to *Science*. August 1984.

EEB-Vent 84-28, LBL-18321
Correction for External Mass-Transfer Resistance in Diffusive Sampling, P.P. Persoff and A.T. Hodgson. September 1984.

EEB-Vent 84-29, LBL-18374
Migration of Air in Soil and Into House Basements: A Source of Indoor Air Pollutants, W.W. Nazaroff, S.R. Lewis, S.M. Doyle, B.A. Moed, and A.V. Nero. Submitted to *Environmental Science and Technology*. September 1984.

EEB-Vent 84-30, LBL-18481
Radon Progeny Control with Portable Air Cleaners, R.G. Sextro, F.J. Offermann, W.W. Nazaroff, W.J. Fisk, D.T. Grimsrud, A.V. Nero, K. L. Revzan, and J. Yater. Submitted to *Atmospheric Environment*. November 1984.

EEB-Vent 84-31, LBL-18188
The Concentrations of Indoor Pollutants Data Base: A Status Report, S. R. Brown, R.A. Young, and D.T. Grimsrud. July 1984.

EEB-Vent 84-33, LBL 18274
Distribution of Airborne^{222} Radon Concentrations in U.S. Homes. A.V. Nero, M.B.Schwehr, W.W. Nazaroff and K.L. Revzan. November 1984.

1985

EEB-Vent 85-02, LBL 18875
Control of Indoor Pollutant Concentrations: Choosing a Strategy. W.J. Fisk. November 1984.

EEB-Vent 85-03, LBL 17599Rev.
A New Passive Sampler for Water Vapor. J.R. Girman, J.R. Allen, and A.Y. Lee. To be published in *Environment International*. November 1984.

EEB-Vent 85-04, LBL 17594
Volatile Organic Emissions from Adhesives with Indoor Applications. J. Girman, A.T. Hodgson, and A.S. Newton. Presented at the 3rd International Conference on Indoor Air Quality Control and Climate, Stockholm, Sweden, August 20-24, 1984. November 1984.

EEB-Vent 85-05, LBL 19346
Indoor Concentrations of Radon 222 and Its Daughters: Sources, Range, and Environmental Influences. A. Nero. Presented at the Seventh ORNL Life Sciences Symposium on Indoor Air and Human Health, Knoxville TN, October 29-31, 1984. To be published in *Proceedings*. April 1985.

EEB-Vent 85-06, LBL 17854
Indoor Air Pollution Due to Emissions from Wood-burning Stoves. G. Traynor, M. Apte, A. Carruthers, J. Dillworth, D. Grimsrud and L. Gundel. To be published in *Environmental Science and Technology*. April 1985.

EEB-Vent 85-07, LBL 18874
An Experimental Study of Air Washing for the Removal of Formaldehyde from Indoor Air. B.S. Pedersen and W.J. Fisk.

To be published in *Environment International.* November 1984.

EEB-Vent 85-08, LBL 19777
Bonneville Power Administration Indoor Air Quality Measurements in Northwest Residences: Status Report. B.H. Turk, D.T. Grimsrud, J. Harrison, R.J. Prill and K.L. Revzan. Published in *Proceedings* of Conference Conservation in Buildings: Northwest Perspective, Butte MT, May 1985. May 1985.

EEB-Vent 85-09, LBL 19869
Characterizing the Sources, Range, and Environmental Influences of Radon 222 and Its Decay Products. A.V. Nero, R.G. Sextro, S.M. Doyle, B.A. Moed, W.W. Nazaroff, K.L. Revzan and M.B. Schwehr. Published in *The Science of the Total Environment*, 45, pp. 233-244. June 1985.

EEB-Vent 85-10, LBL 19844
Field Monitoring Design Considerations for Assessing Indoor Exposures to Combustion Pollutants. G.W. Traynor. To be published in *Atmospheric Environment.* June 1985.

EEB-Vent 85-11, LBL 19915
Considerations in Evaluating Emissions from Consumer Products. J.R. Girman, A.T. Hodgson, M.L. Wind. Submitted to *Atmospheric Environment.* June 1985.

EEB-Vent 85-12, LBL 19726
Control of Indoor Radon and Radon Progeny Concentrations. R.G. Sextro. Presented at the ASHRAE Annual Meeting, Honolulu HI, June 1985. To be published in ASHRAE Transactions, 91, Part 2. May 1985.

EEB-Vent 85-13, LBL 20095
Discussion of Radon Transport into a Detached One-Story House with a Basement. W.W. Nazaroff. (Reply to T.W. D'Ottavio and R.B. Dietz.) Submitted to *Atmospheric Environment* July 1985.

EEB-Vent 85-15, LBL 20209
Multi-Tracer System for Measuring Ventilation Rates and Ventilation Efficiencies in Large Mechanically Ventilated Buildings. W.J. Fisk, J. Binenboym, H. Kaboli, D.T. Grimsrud, A.W. Robb, and B.J. Weber. Presented at the AIC Conference, Het Meerdal, Netherlands, September 16–19, 1985. September 1985.

Windows and Daylighting

1982

EEB-W 82-01, LBL-13753
"Durable Solar Optical Materials—The International Challenge," C.M. Lampert, *Proceedings of SPIE* (International Society for Optical Engineering) *324* (3) (1982). January 1982.

EEB-W 82-02, LBL-13756
"A Large-Area, High-Sensitivity Heat-Flow Sensor," J.H. Klems and D. DiBartolomeo, *Rev. Sci. Instrum. 53* (10), pp. 1609–1612 (1982). February 1982.

EEB-W 82-03, LBL-14250
"Advanced Heat-Mirror Films for Energy-Efficient Windows," C.M. Lampert, in *The Renewable Challenge*, Proceedings of the 1982 Annual Meeting of the American Section of the International Solar Energy Society (ASISES), Houston, TX, June 1–5, 1982. March 1982.

EEB-W 82-04, LBL-14369,
Energy Conservation through Interior Shading of Windows: An Analysis, Test and Evaluation of Reflective Venetian Blinds, R.L. Van Dyck and T.P. Konen, Stevens Institute of Technology, March 1982.

EEB-W 82-05, LBL-14462
"Transparent Silica Aerogels for Window Insulation," M. Rubin and C.M. Lampert, *Solar Energy Materials 7*(4), p. 393 (1983). June 1982.

EEB-W 82-06, LBL-14569
"The DOE-2 and SUPERLITE Daylighting Programs," S. Selkowitz, J. Kim, M. Navvab, and F. Winkelmann, June 1982. In *PASSIVE '82*, Proceedings of the Seventh National Passive Solar Conference, Knoxville, TN, August 29–September 3, 1982.

EEB-W 82-07, LBL-14590
"Advanced Optical Materials for Energy Efficiency and Solar Conversion," C.M. Lampert, in *Advanced Solar Materials* (Plenum, New York), 1983. June 1982.

EEB-W 82-08, LBID-560
Evaluation of Air-Flow Windows: Final Report, K. Brandle and R.F. Boehm, University of Utah, May 1981.

EEB-W 82-09, LBL-14694
"Solar Optical Materials for Innovative Window Design," C.M. Lampert, August 1982. To be published in *International Journal of Energy Research.*

EEB-W 82-10, LBL-14863
Design Tools for Daylighting Illumination and Energy Analysis, S. Selkowitz, July 1982. In Proceedings of the Workshop on Designing and Managing Energy-Conscious Commercial Buildings, Denver, CO, July 19–20, 1982.

EEB-W 82-11, LBL-15131
Advanced Optical and Thermal Technologies for Aperture Control, S. Selkowitz, C.M. Lampert, and M. Rubin, September 1982. In Proceedings of the Passive and Hybrid Solar Energy Update, Washington, DC, September 15–17, 1982.

EEB-W 82-12, LBL-15258
Transparent Heat-Mirror Materials and Deposition Technology, compiled by C.M. Lampert and S. Selkowitz, July 1982. Papers selected from the Proceedings of the International Society for Optical Engineering (SPIE) Conference on Optical Coatings for Energy Efficiency and Solar Applications and the Conference on Optical Thin Films, Los Angeles, CA, January 25–29, 1982.

EEB-W 82-13, LBL-14517
New Models for Analyzing the Thermal and Daylighting Performance of Fenestration, S. Selkowitz and F. Winkelmann. Presented at the ASHRAE/DOE Conference on the Thermal Performance of the Exterior Envelopes of Buildings II, Las Vegas, NV, December 6–9, 1982 (May 1982).

1983

EEB-W 83-01, LBL-15440
Windows for Accepting or Rejecting Solar Heat Gain: Final Report, University of Arizona, September 1982.

EEB-W 83-03, LBL-14509
Design and Construction of Large-Area Heat-Flow Sensors for Measuring Building Heat Flow, J.H. Klems. In Proceedings of the ASHRAE/DOE Conference on the Thermal Performance of the Exterior Envelopes of Buildings II, Las Vegas, NV, December 6–9, 1982. January 1983.

EEB-W 83-04, LBL-15622
"Zenith Luminance and Sky Luminance Distribution for Daylighting Calculations," M. Karayel, M. Navvab, E. Ne'eman, and S. Selkowitz. Presented at the International Daylighting Conference, Phoenix, AZ, February 16–18, 1983. *Energy and Buildings 6*, p. 183 (1984).

EEB-W 83-05, LBL-15623
"Daylight Availability Data for San Francisco," M. Navvab, M. Karayel, E. Ne'eman, and S. Selkowitz. Presented at the International Daylighting Conference, Phoenix, AZ, February 16–18, 1983. *Energy and Buildings 6*, p. 273 (1984).

EEB-W 83-06, LBL-15620
"The Impact of Daylighting on Peak Electrical Demand," U.S. Choi, R. Johnson, and S. Selkowitz. Presented at the International Daylighting Conference, Phoenix, AZ, February 16–18, 1983. *Energy and Buildings 6*, p. 387 (1984).

EEB-W 83-07, LBL-16154
New Tools for Analyzing the Thermal and Daylighting Performance of Fenestration in Multistory Buildings, S. Selkowitz. Presented at the International Symposium on the Design of Multistory Buildings for Physical and Environmental Performance, Sydney, Australia, June 1–3, 1983. May 1983.

EEB-W 83-08, LBL-16226
"Optical Films for Solar Energy Applications," C. Lampert. Presented at the session on Technology of Stratified Media of SPIE (the International Society for Optical Engineering) Conference, Los Angeles, CA, January 24–28, 1983. *Proc. SPIE 387*. May 1983.

EEB-W 83-09, LBL-15889
Impact of Fenestration on Energy Use and Peak Loads in Daylighted Commercial Buildings, S. Selkowitz, *et al.* Presented at Passive '83—The National Passive Solar Conference, Glorieta, NM, September 7–9, 1983.

EEB-W 83-10, LBL-16425
Daylight Availability as a Function of Atmospheric Conditions, E. Ne'eman and S. Selkowitz. Presented at the 5th Conference on Atmospheric Radiation, Baltimore, MD, October 31–November 4, 1983. July 1983.

EEB-W 83-11, LBL-15619
"A Comprehensive Approach to the Integration of Daylight and Electric Light in Buildings," E. Ne'eman. Presented at the International Daylighting Conference, Phoenix, AZ, February 16–18, 1983. *Energy and Buildings 6*, p. 97 (1984). August 1983.

EEB-W 83-12, LBL-16895
Advanced and Optical Thermal Technologies for Aperture Control, S. Selkowitz and C.M. Lampert. In Proceedings of the Passive and Hybrid Solar Energy Update, GPO, Washington, DC. November 1983.

EEB-W 83-13, LBL-16770
Building Envelope Thermal and Daylighting Analysis in Support of Recommendations to Upgrade ASHRAE/IES Standard 90: Vol. I—Parametric Study, Analysis, and Results, R. Johnson *et al.* Final Report to Batelle Pacific Northwest Laboratories. September 1983.

EEB-W 83-14, LBID-801
Building Envelope Thermal and Daylighting Analysis in Support of Recommendations to Upgrade ASHRAE/IES Standard 90: Vol. II—Data Base Definition and Procedural Guidelines, September 1983.

1984

EEB-W 84-01, LBL-17330
How Fenestration Can Significantly Affect Energy Use in Commercial Buildings, R. Johnson, S. Selkowitz, and R. Sullivan. Presented at the 11th Energy Technology Conference, March 19–21, 1984, Washington, DC. April 1984.

EEB-W 84-02, LBL-17429
Measurement of Fenestration Performance Under Realistic Conditions, J.H. Klems. Presented at Windows in Building Design and Maintenance, Gothenburg, Sweden, June 13–15, 1984. February 1984.

EEB-W 84-03, LBL-17476
Skylight Energy Performance and Design Optimization, D. Arasteh, R. Johnson, S. Selkowitz, and R. Sullivan. Presented at Windows in Building Design and Maintenance, Gothenburg, Sweden, June 13–15, 1984. February 1984.

EEB-W 84-04, LBL-17393
Electrochromic Materials for the Regulation of Solar Energy Transmission through Windows, C.M. Lampert. Invited Lecture at 2nd International Workshop on Physics of Semiconductor Devices, December 5–10, 1983, Delhi, India. February 1984.

EEB-W 84-05, LBL-17683
Obstacles to the Use of Exterior Fenestration and Daylighting Control Systems in the U.S. G. Sweitzer and R. Johnson. Presented at Windows in Building Design and Maintenance, Gothenburg, Sweden, June 13–15, 1984. March 1984.

EEB-W 84-06, LBL-17727
"Analysis of Atmospheric Turbidity for Daylight Calculations," M. Navvab, M. Karayel, E. Ne'eman, and S. Selkowitz, *Energy and Buildings 6*, p. 293 (1984). May 1983.

EEB-W 84-07, LBL-15628
"Office Worker Response to Lighting and Daylighting Issues in Workspace Environments: A Pilot Survey," E. Ne'eman, G. Sweitzer, and E. Vine. Presented at the International Daylighting Conference, Phoenix, AZ, February 16–18, 1983. *Energy and Buildings 6*, p. 159 (1984). March 1984.

EEB-W 84-08, LBL-16073
"Electrochromic Materials and Devices for Energy-Efficient Windows," C.M. Lampert, *Solar Energy Materials 11*, pp. 1–27 (1984). February 1984.

EEB-W 84-09, LBL-17920
Windows, Skylights, and Atria--Occupants' Visual/Subjective Comparison, E. Ne'eman and S. Selkowitz. Presented at the ASHRAE International Symposium on the Interface between the Building Envelope and HVAC Systems, Kansas City, MO, June 17–20, 1984. May 1984.

EEB-W 84-10, LBL-17943
Measurement of Fenestration Net Energy Performance: Considerations Leading to Development of the Mobile Window Thermal Test (MoWiTT) Facility, J.H. Klems. May 1984.

EEB-W 84-12, LBL-18002
Simple Phase-Sensitive Detector for Wheatstone Bridge Resistance Measurements, D. DiBartolomeo and J.H. Klems. Submitted to *Review of Scientific Instruments*. June 1984.

EEB-W 84-13, LBL-18087
Defining Daylighting from Windows in Terms of Candlepower Distribution Curves, M. Spitzglas. Presented at the IEEE/IAS 1984 Annual Meeting, Chicago, IL, September 30–October 4, 1984. June 1984.

EEB-W 84-14, LBL-18126
Peak Demand Savings from Daylighting in Commercial Buildings, S. Selkowitz, D. Arasteh, and R. Johnson. Presented at the 1984 ACEEE Summer Study, Santa Cruz, CA, August 14–21, 1984. July 1984.

EEB-W 84-15, LBL-18144
Measurement of Fenestration Net Energy Performance: Considerations Leading to Development of the Mobile Window Thermal Test (MoWiTT) Facility, J.H. Klems. Submitted to *Journal of Solar Energy Engineering*. August 1984.

EEB-W 84-16, LBL-15625
"Glazing Energy Performance and Design Optimization," R. Johnson, S. Selkowitz, S. Nozaki, C. Conner, and D. Arasteh, *Energy and Buildings 6*, p. 304 (1984). July 1984.

EEB-W 84-17, LBL-18198
Error Analysis of In-Situ Field Tests of Fenestration Net Energy Performance, J.H. Klems. Submitted to *Energy and Buildings*. August 1984.

EEB-W 84-19, LBL-18247
Analysis of Window Performance in a Single-Family Residence, S. Selkowitz and R. Sullivan. Presented at the 9th National Passive Solar Conference, Columbus, OH, September 24–26, 1984. August 1984.

EEB-W 84-20, LBL-18248
Daylighting Data for Atrium Design, M. Navvab and S. Selkowitz. Presented at the 9th National Passive Solar Conference, Columbus, OH, September 24–26, 1984. August 1984.

EEB-W 84-21, LBL-18299
A Literature Study on Electrochromic and Thermochromic Materials, Final Report, Honeywell Inc. August 1984.

EEB-W 84-22, LBL-17284
Integrating Sphere Measurements of Directional-Hemispherical Transmittance of Window Systems, J. Kessel and S. Selkowitz. Presented at the Illuminating Engineering Society Annual Technical Conference, St. Louis, MO, August 5–7, 1984. August 1984.

EEB-W 84-23, LBL-18607
Advanced Optical and Thermal Technologies for Aperture Control, S. Selkowitz, A. Hunt, C.M. Lampert, and M. Rubin. Presented at the 9th Passive and Hybrid Solar Energy Update, Washington, DC, September 5–7, 1984. September 1984.

EEB-W 84-24, LBL-18663
Influence of Windows on Building Energy Use, S. Selkowitz. Presented at Windows in Building Design and Maintenance, Gothenburg, Sweden, June 13–15, 1984. October 1984.

EEB-W 84-25, LBL-18245
High-Resolution Electron Microscopy Study, J. Mazur and C. Lampert. Presented at the 28th SPIE Annual International Technical Symposium, San Diego, CA, August 19–24, 1984. September 1984.

1985

EEB-W 85-01, LBL-17457
Energy Performance and Savings Potentials with Skylights. D. Arasteh, R. Johnson, S. Selkowitz, and R. Sullivan. Presented at the ASHRAE Winter Meeting, Chicago IL, January 27–30, 1985. To be published in ASHRAE Transactions, Vol. 91, Part. 1. December 1984.

EEB-W 85-02, LBL-18561
Energy Performance Analysis of Fenestration in a Single-Family Residence. R. Sullivan and S. Selkowitz. Presented at the ASHRAE Semi-Annual Meeting, Honolulu HI, June 23–27, 1985. December 1984.

EEB-W 85-03, LBL-19167
The Application of Daylighting Research Tools to Fenestration and Building Design Optimization. S. Selkowitz. Presented at Research and Design, Architectural Applications of Design and Technology Research, Los Angeles CA, March 14–18, 1985. February 1985.

EEB-W 85-04, LBL-19245
Residential Window Performance Analysis Using Regression Procedures. R. Sullivan and S. Selkowitz. Presented at CLIMA 2000, World Congress on Heating, Ventilating, and Air Conditioning, Copenhagen, Denmark, August 26–29, 1985. March 1985.

EEB-W 85-05, LBL-19304
Energy Reduction Implications with Fenestration. R. Johnson, D. Arasteh, and S. Selkowitz. Presented at CLIMA 2000, World Congress on Heating, Ventilating, and Air Conditioning, Copenhagen, Denmark, August 26–29, 1985. March 1985.

EEB-W 85-06, LBL-19383
Thermal Analysis of Buildings—Configuration Perturbations and Observed Climate Interface. R. Sullivan, Y.J. Huang, J. Bull, I. Turiel, R. Ritschard and S. Selkowitz. To be presented at the ASHRAE Semi-Annual Meeting, San Francisco CA, January 19–22, 1986. To be published in ASHRAE Transactions 1986, Vol. 92, Part. 1. April 1985.

EEB-W 85-07, LBL-19492
Prospects for Highly Insulating Window Systems. Presented at Conservation in Buildings: Northwest Perspective, sponsored by the National Center for Appropriate Technology, Butte MT, May 19–22, 1985. April 1985.

EEB-W 85-09, LBL-17286
Scale Model Measurements for a Daylighting Photometric Data Base. M. Spitzglas, M. Navvab, J. Kim, and S. Selkowitz. Presented at the Illuminating Engineering Society (IES) Annual Technical Conference, Detroit MI, July 21–24, 1985. To be published in the IES Journal. April 1985.

EEB-W 85-10, LBL-17456
The Effects of Skylight Parameters on Daylighting Energy Savings. D. Arasteh, R. Johnson, and S. Selkowitz. May 1985.

EEB-W 85-12, LBL-19734
Cooling Energy and Cost Savings with Daylighting in a Hot and Humid Climate. D. Arasteh, R. Johnson, S. Selkowitz, and D. Connell. Presented at the Second Annual Symposium on Improving Building Energy Efficiency in Hot and Humid Climates, Texas A&M University, College Station TX, September 24–26, 1985. July 1985.

EEB-W 85-13, LBL-20211
Chemical and Optical Properties of Electrochromic Nickel Oxide Films. C.M. Lampert, T.R. Omstead, and P.C. Yu. Presented at the SPIE's 29th Annual International Technical Symposium on Optical and Electro-Optical Engineering, San Diego CA, August 18–23, 1985. August 1985.

EEB-W 85-14, LBL-20079
Window Performance Analysis in a Single-Family Residence. R. Sullivan and S. Selkowitz. Presented at the Thermal Performance of the Exterior Envelopes of Buildings III, Clearwater Beach FL, Dec. 2–5, 1985. Published in the *Proceedings.* October 1985.

EEB-W 85-15, LBL-20080
Advanced Optical Materials for Daylighting in Office Buildings. R. Johnson, D. Connell, S. Selkowitz, and D. Arasteh. Presented at the Tenth National Passive Solar Conference, Raleigh NC, October 15–19, 1985. Published in the *Proceedings.*

Lighting Systems Research

1982

EEB-L 82-01, LBL-13889, *High-Intensity Discharge 400W Sodium Ballast: Phase II Final Report,* G. Felper, October 1981.

EEB-L 82-02, LBL-13894
A Computer Program for Analyzing the Energy Consumption of Automatically Controlled Lighting Systems: Final Report, The Lighting Group, Smith, Hinchman and Grylls Associates, Inc., January 1982.

EEB-L 82-03, LBL-13931
Relating Productivity to Visibility and Lighting, R. Clear and S. Berman, January 1982. Presented at the Public Works Canada Symposium, "The Integration of Visual Performance Criteria into the Illumination Design Process," Ottawa, Ontario, January 25–27, 1982.

EEB-L 82-04, LBL-14201
Energy Saving through Effective Lighting Control, D. Peterson and F. Rubinstein. Presented at the 9th Energy Technology

Conference and Exposition, Washington, DC, February 16–18, 1982.

EEB-L 82-05, LBL-19859
Energy Efficient Light Bulbs: The Magnetic Arc Spreading Fluorescent Lamp. Spellman High Voltage Electric Company. (Former LBID-525) November 1981.

EEB-L 82-06, LBL-14546
Energy-Efficient Incandescent Lamp: Final Report, Duro-Test Corporation, April 1982.

EEB-L 82-07, LBL-14596
Measurement of UV Radiation in a Low-Pressure Vapor-Discharge Tube with Mercury Isotopes, R.K. Sun, August 1982.

EEB-L 82-08, LBL-14561
The Measured Energy Savings from Two Lighting Control Strategies, F. Rubinstein and M. Karayel, June 1982. Presented at the IEEE Industry Applications Society 1982 Annual Meeting, San Francisco, CA, October 4–8, 1982.

EEB-L 82-09, LBL-15199
Proceedings of the Lighting-Electromagnetic Compatibility Conference, R. Verderber and S. Berman, Eds., September 1982.

EEB-L 82-10, LBL-15251
Integrated Circuit Control for Two-Lamp Electronic Ballast: Final Report, T. Kohler, November 1982.

EEB-L 82-11, LBL-15252
Energy-Efficient Compact Screw-In Fluorescent Lamp: Final Report, E.W. Morton, Westinghouse Electric Corp., November 1982.

1983

EEB-L 83-01, LBL-15631
"Photoelectric Control of Equi-Illumination Lighting Systems," F. Rubinstein. Presented at International Daylighting Conference, Phoenix, AZ, February 16–18, 1983. *Energy and Buildings 6,* p. 141 (1984).

EEB-L 83-02, LBL-15627
"Mutual Impacts of Lighting Controls and Daylighting Applications," R. Verderber and F. Rubinstein. Presented at the International Daylighting Conference, Phoenix, AZ, February 16–18, 1983. *Energy and Buildings 6,* p. 133 (1984). August 1983.

EEB-L 83-03, LBL-15964
Assessing Fluorescent Ballast/Lamp Systems, R. Verderber. To be published in *Electrical Consultant,* March–April 1984.

EEB-L 83-04, LBL-16225
Comparison of Technologies for New Energy-Efficient Lamps, R. Verderber and F. Rubinstein. Presented at the IEEE/IAS Annual Meeting, Mexico City, October 3–7, 1983.

EEB-L 83-05, LBL-16299
Experimental Studies Relating Environmental Lighting Flicker to Visual Fatigue in VDT Operators. S. Berman, D. Greenhouse, I. Bailey, and A. Bradley. Presented at the 20th Session of CIE (CIE Session 83), Amsterdam, Netherlands, August 31–September 8, 1983.

EEB-L 83-06, LBL-19860
Energy-Efficient HID Solid-State Ballast: Phase II Final Report. Jefferson Electric Division, Litton Industries, Inc. (Former LBID-770). June 1983.

EEB-L 83-07, LBL-16925
Test, Evaluation, and Report on Mercury Enrichment for Fluorescent Lamps: Final Report, GTE Lighting, October 1983.

EEB-L 83-08, LBL-15382
Field Study on Occupancy Scheduling as a Lighting Management Strategy, F. Rubinstein, M. Karayel and R. Verderber. Presented at the 1983 Annual IES Conference, Los Angeles CA, August 8–11, 1983, and to be published in *Lighting Design and Applications.*

EEB-L 83-09, LBL-17394
Experimental Studies of Enhanced Emittance by Zeeman Splitting of a Low-Pressure Mercury/Argon Discharge, D. Hollister and S.M. Berman. Presented at the Third International Symposium on the Science and Technology of Light Sources, Toulouse, France, April 1983. March 1983.

EEB-L 83-10, LBL-17433 Abs.
Theory of the Effects Magnetic Fields and Isotope Enrichment on the Radiant Emittance of the Hg-Ar Discharge, R.W. Richardson and S.M. Berman. Presented at the Third International Symposium on the Science and Technology of Light Sources, Toulouse, France, April 18–21, 1983. March 1983.

EEB-L 84-01, LBL-17196
High-Intensity Discharge (HID) Solid-State Ballast Program: Engineering Development Report (Phase II), Luminoptics Corp. December 1983.

1984

EEB-L 84-02, LBL-17444
CONTROLITE 1.0: Program Documentation, Final Report, Lighting Technologies. March 1984.

EEB-L 84-03, LBL-17285
Determining Lamp/Ballast System Performance with a Temperature Controlled Integrating Chamber, M. Siminovitch, F. Rubinstein, and R. Verderber, submitted to the Illuminating Engineering Society Annual Conference, St. Louis, MO, August 6–9, 1984. April 1984.

EEB-L 84-04, LBL-17846
Review of Lighting Control Equipment and Applications, R. Verderber. Presented at the Great PG&E Energy Expo, Oakland, CA, May 22–24, 1984. May 1984.

EEB-L 84-05, LBL-17929
Fluorescent Fixtures and Ballasts, R.R. Verderber. Presented at the Electric Power Research Institute (EPRI) Lighting and Utility Seminar, San Francisco, CA, May 21–22, 1984. May 1984.

EEB-L 84-06, LBL-17927
Development of Novel Lamps for Study of Enhanced Production of Resonance Radiation by Low-Density Mercury Discharges, Z.-X. Wang, D.D. Hollister, and S.M. Berman. Presented at the IEEE Industry Applications Society 1984 Annual Meeting, Chicago, IL, September 30–October 4, 1984. June 1984.

EEB-L 84-07, LBL-17967
Lighting Controls: The Role of Advanced Technology--Past, Present, and Future, R.R. Verderber and F.M. Rubinstein. Presented at the National Research Council of Canada's Lighting Control Symposium, Ottawa, Canada, June 28, 1984. May 1984.

EEB-L 84-08, LBL-18065
The Control of Daylight-Linked Lighting Systems, F. Rubinstein and G. Ward. Presented at the IEEE Industry Applications Society 1984 Annual Meeting, Chicago, IL, September 30–October 4, 1984. June 1984.

EEB-L 84-09, LBL-17998
Electromagnetic Interference from Fluorescent Lighting Operated with Solid-State Ballasts in Various Sites, M. G. Harms, L.P. Leung, and R.R. Verderber. Presented at the IEEE Industry Applications Society 1984 Annual Meeting, Chicago, IL, September 30–October 4, 1984. June 1984.

EEB-L 84-10, LBL-18114
New Lighting Technologies, Their Status and Impacts on Power Densities, R.R. Verderber and F.M. Rubinstein.

Presented at the ACEEE Summer Study, Santa Cruz, CA, August 14–21, 1984. July 1984.

EEB-L 84-11, LBL-16220
Fundamental Problems with Visual Performance Research Described in the CIE 19/2 Report, R. Clear and S. Berman. Submitted to the Illuminating Engineering Society 1983 Annual Conference. May 1983.

EEB-L 84-12, LBL-17763
Analysis of a Visual Performance Experiment, R. Clear and S. Berman. Presented at the Illuminating Engineering Society (IES) Annual Technical Conference, St. Louis, MO, August 6–9, 1984. July 1984.

EEB-L 84-13, LBL-18425
Quality Assurance Assessment of New Efficient Lighting Systems for Naval Ships: Final Report, R. Verderber. August 1984.

EEB-L 84-14, LBL-18683
An Experimental Methodology for Determining the System Performance of Fluorescent Lamp, Ballast, Fixture Combinations Operating Under Realistic Applications, M. Siminovitch, F. M. Rubinstein, and R.R. Verderber. November 1984.

1985

EEB-L 85-01, LBL-19035
Electrodeless HID Lamp Study: Final Report. J.M. Anderson, P.D. Johnson, C.E. Jones, and T.H. Rautenberg. January 1985.

EEB-L 85-02, LBL-19277
Lighting Research Program. S. Berman. Presented at the 12th Energy Technology Conference and Exposition, Washington, D.C., March 25–27, 1985. March 1985.

EEB-L 85-03, LBL-19423
Target Size, Visibility, and Roadway Performance. R. Clear and S. Berman. Presented at the Illuminating Engineering Society (IES) Annual Technical Conference, Detroit MI, July 21–24, 1985. To be published in the IES Journal. April 1985.

EEB-L 85-04, LBL-19168
A Luminaire/Plenum/HVAC Simulator. M.J. Siminovitch, F. M. Rubinstein, T.A. Clark, and R.R. Verderber. Presented at the Annual IEEE-IAS Conference in Toronto, Canada, October 6–11, 1985. July 1985.

EEB-L 85-05, LBL-19779
Effect of Filament Power Removal on a Fluorescent Lamp System. R.R. Verderber, O. Morse, and F.M. Rubinstein. Presented at the Annual IEEE-IAS Conference in Toronto, Canada, October 6–11, 1985. July 1985.

EEB-L 85-06, LBL-19778
Life of Fluorescent Lamps Operated at High Frequencies with Solid-State Ballasts. R.R. Verderber, O. Morse, and F.M. Rubinstein. Presented at the Annual IEEE-IAS Conference in Toronto, Canada, October 6-11, 1985. July 1985.

EEB-L 85-07, LBL-19474
Determining Optimum Sector Size for Automatic Lighting Controls. F. Rubinstein, R. Verderber, M. Karayel. Presented at the Illuminating Engineering Society Annual Technical Conference, Detroit MI, July 21–24, 1985. To be published in Journal of the IES. July 1985.

EEB-L 85-08, LBL-20119
Performance of Electronic Ballasts and Other New Lighting Equipment. R.R. Verderber and O. Morse. October 1985.

EEB-L 85-09, LBL-20614
Test, Evaluation, and Report on Mercury Enrichment for Fluorescent Lamps. J. Maya, M. Grossman, R. Lagushenko, R. Moskowitz. November 1985.

ENVIRONMENTAL RESEARCH PROGRAM

INTRODUCTION

The objective of the Environmental Research Program is to understand the formation, transformation, transport, and effects of energy-related pollutants on the environment. This multidisciplinary research program includes fundamental and applied research in physics, chemistry, engineering, and biology, as well as research on the development of advanced methods of measurement and analysis. The Program's Annual Report contains summaries of research performed during FY 1985 in the areas of Atmospheric Aerosol Research, Applied Physics and Laser Spectroscopy, Oil Shale Research, Combustion, Flue Gas Chemistry, Toxicological Effects on Biological Systems, and Trace Element Analysis.

The Atmospheric Aerosol Research group focused its studies on the formation, transformation, characterization, and effects of atmospheric aerosols. At present, the main research interests of the group concern the chemical processes that occur in haze, clouds, and fogs, and the role of particulate carbon in global climate modification. For their studies, the group developed novel analytical and research methods for characterizing particles, fog, and aerosol species. Aerosol research is performed in the laboratory and in the field. National and international cooperative studies constitute the principal emphasis of the field studies.

The Applied Physics and Laser Spectroscopy Research group applies advanced laser spectroscopy and condensed-matter physics to energy and environmental problems. Emphasis is on the development of physical methods, as opposed to conventional chemical analysis techniques. The ultrahigh sensitivity, narrow linewidth, and tunability of lasers and the minimal sample preparation required make it possible for group members to apply these techniques to the studies of surfaces and interfaces, amorphous photovoltaic semiconductors, and liquid crystals.

The Oil Shale project studies the environmental and waste-treatment problems that would arise from the tremendously large quantities of solid and liquid wastes that a commercial-scale shale oil industry would generate. A major task of the project is to delineate the potential problems of process wastewater and spent-shale codisposal, in particular the estimation of the types and quantities of uncontrollable air emissions that may result from such use of wastewaters (raw or treated). Its second major task is the development of economical approaches to the treatment of process wastewaters. Because of their high concentrations of organic and inorganic solutes, they present tremendous difficulties to any water management scheme that entails reuse or discharge. This research effort is conducted with the Sanitary Engineering and Environmental Health Research Laboratory of the University of California.

The Combustion Research group studies complex combustion processes by acquiring a fundamental understanding of the chemical and physical processes that determine combustion efficiency, emissions, and safety. Development of suitable analytical techniques for measuring intermediate and product species formed during the oxidation of fossil fuels and for characterizing turbulence has been a major effort. The characterization and understanding of turbulence and high-temperature chemistry are of high priority in this program. Areas of application that dominate these studies are engine research, pollutant abatement in utilities, fire control, and ignition phenomena.

The Scrubber Chemistry group is investigating the chemical character of pollutants generated by the combustion of fossil fuels to develop new, efficient strategies for pollutant emission control. Current research is directed toward understanding the kinetics and mechanisms of homogeneous and heterogeneous catalysis of the interactions of sulfur dioxide and nitrogen oxides, both among themselves and with other compounds. When this fundamental chemistry is understood, it will be applied to the development of an efficient, cost-effective scrubber for simultaneous desulfurization and denitrification of flue gases.

In Toxicological Effects on Biological Systems, the study of strongly chemically reactive compounds generated within cells during aerobic metabolism is of particular interest in attempting to understand cellular damage and repair. In particular, "active oxygen" species (including free radicals) that are

generated during the normal life span of cells have been implicated in many processes that result in altered cellular metabolism. The study of free radicals in mitochondrial membranes focuses primarily on oxygen radicals generated by mitochondria (the energy-generating organelles within cells) during respiration and their effects on biological membranes.

The main emphasis of the Trace Element Analysis group is the study of the relationship between massive repetitive life extinctions on the earth and asteroid (or other extraterrestrial) impacts. Studies of this relationship have concentrated on searches for unusually high iridium abundances in geochemical samples from rock layers known or expected to mark life-extinction horizons. Geochemical and other tests are made to determine if the iridium-rich rocks are of extraterrestrial origin and hence related to impacts. The nature of the sedimentation of the rocks, the worldwide extent of the extinction horizons, and the extent to which the extinctions are related to impacts are also studied.

The short reports that follow describe the program activities in FY 1985. For most of these reports, more detailed papers have been or will be published in appropriate scientific journals.

Estimates of Springtime Soot and Sulfur Fluxes Into the Arctic Troposphere: Implications to Source Regions*†

H. Rosen and A.D.A. Hansen

During winter and spring, the Arctic atmosphere contains significant concentrations of sulfur-[1] and carbon-containing[2] particles that may have been transported long distances from combustion sources at midlatitudes in Eurasia. The 1983 Arctic Gas and Aerosol Sampling Project (AGASP) explored the horizontal and vertical distributions of the haze throughout the western Arctic. (See Special Issue of *Geophysical Research Letters*, v. 11, 1984, for details.) One of the instruments on these flights was an aethalometer,[3] which can measure graphitic carbon concentrations on a real-time basis and which determined vertical profiles of graphitic particles in the Arctic troposphere.[4] In this report, we use these vertical profiles in conjunction with a box model calculation to make a first estimate of the fluxes of graphitic carbon, total carbon, and sulfur particles into the Arctic troposphere. These fluxes are compared with the fluxes of carbon and sulfur produced from fossil fuel combustion on a regional and global basis.

ACCOMPLISHMENTS DURING FY 1985

For the purposes of a box model calculation, we view the Arctic troposphere as a cylindrical volume with a radius extending from the North Pole to 70°N latitude and a height of 7 km, corresponding to the approximate level of the tropopause. For a conserved species like graphitic carbon that is not produced or destroyed in the atmosphere, the rate of change of the mass of particles within this box is equal to the flux of particles entering minus the flux leaving. This equation can be written as

$$\frac{dM(t)}{dt} = F_M - \frac{M(t)}{\tau}, \qquad (1)$$

where M(t) is the mass of the component with the box at time t; dM(t)/dt its rate of change; F_M is the input flux through all surfaces of the box; and $M(t)/\tau$ is the loss of mass, represented by an exponential decay with an effective residence time τ. This residence time includes both losses by deposition and by transport of air masses out of the Arctic basin. At equilibrium dM/dt = 0, and the input flux equals the decay rate:

$$F_M = \frac{M(t)}{\tau}. \qquad (2)$$

For nonequilibrium situations, the input flux can be greater or less than the decay rate. If the input flux at time t is less than $M(t)/\tau$, it had to be at least as large as this decay rate at some previous time. In other words, even for a nonequilibrium situation, Eq. (2) can be used to get a lower limit on the maximum input flux.

If one can estimate the mass of graphitic particles in the Arctic troposphere, then using Eq. (2), the input flux as a function of residence time can be determined. The mass of graphitic particles G is given by integrating the concentration as a function of altitude over the considered volume. The profiles of graphitic particles obtained during AGASP can be used to make an estimate of the concentrations during March and April, 1983. In this analysis we neglect the dependence of the graphitic concentrations on latitude and longitude and use an average vertical distribution obtained from the nine tropospheric AGASP flights to characterize the whole Arctic region. These flights were in the western Arctic, and therefore probably underrepresent the Arctic as a whole because the primary source regions appear to be in the eastern sector.[1] With these assumptions, we determine the average mass of graphitic particles in the Arctic troposphere during AGASP to be $G = 2.4 \times 10^{10}$ g $= 2.4 \times 10^4$ metric tons. Reliable total carbon determinations could not be obtained from the airborne filters on these flights. However, ground-level determinations have been made at the

*This work was supported by the Director, Office of Energy Research, Office of Basic Energy Sciences, Carbon Dioxide Research Division of the U.S. Department of Energy under Contract No. DE-AC03-76SF00098.

†Summary of paper published in *Atmospheric Environment 19*, pp. 2203–2207 (1985).

NOAA-GMCC station at Barrow, Alaska, and indicate that during March-April approximately 20% of the total carbon is graphitic.[5] Therefore, we assume that we can make an estimate of the total carbon in the Arctic from the ground-level measurements at Barrow by multiplying the graphitic component by 5, i.e., the estimated total particulate carbon mass is 1.2×10^5 tons. It is also possible to make an estimate of the total sulfur in the Arctic because we collected 20 airborne filters during AGASP, which we analyzed for sulfur and graphitic carbon contents. The sulfur-to-graphitic-carbon ratio for these filters is 3.3 ± 0.75. If we assume that the vertical profiles of sulfur and graphitic carbon are similar, then the total amount of particulate sulfur in the Arctic can be estimated by multiplying the graphitic mass by 3.3, i.e., the estimated particulate sulfur mass = 8×10^4 tons. This represents a lower limit on the total amount of sulfur in the Arctic because it does not include the gas-phase contribution.

These estimates of the mass of graphitic carbon, total carbon, and sulfur can be used in conjunction with Eq. (2) to estimate the input fluxes of each of these components into the Arctic troposphere. These estimates as a function of residence time are shown for total carbon and sulfur in Figs. 1 and 2. The shaded region in the figures represents a reasonable range of values for the residence time of particles in the Arctic atmosphere, from 1 week to 1 month.[1,6] This effective residence time includes the effects of deposition as well as transport of air out of the Arctic basin.

For comparing the fluxes shown in Figs. 1 and 2 with fluxes from source regions, we chose a residence time of 2 weeks, which will give fluxes within a factor of 2 of the extreme values of residence time. Recently, Marland *et al.*[7] have made estimates of fossil fuel burned as a function of latitude in 5° latitude bands. In Table 1 we compare the fluxes of graphitic carbon (F_G), total carbon (F_C), and sulfur (F_S) entering the Arctic to the carbon burned in various latitude ranges. It becomes immediately obvious from this table that sources between 70–90°N cannot account for these fluxes because the amount of carbon burned in this region is less than the flux of emitted particulate carbon. In other words, sources in the Arctic cannot account for the Arctic haze. In the latitude range 65–70°N, the fluxes are less than the carbon burned but are too large a fraction of it to be reasonable. Typical emission factors for soot as a fraction of the mass of carbonaceous fuel burned range from zero for complete combustion to ~4% for very dirty burning of soft coal. Significant source contributions in the 60–65°N latitude range are more

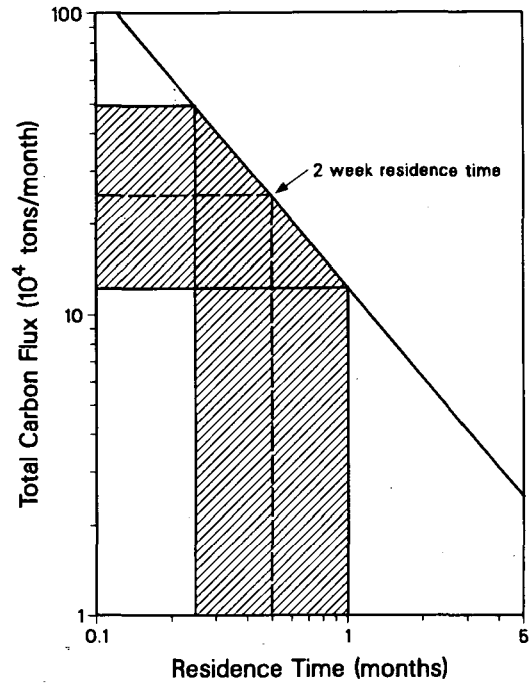

Figure 1. Estimated flux of total particulate carbon entering the Arctic troposphere as a function of residence time. The shaded area represents a range of residence times of 1 week to 4 weeks. (XCG 8410-13400)

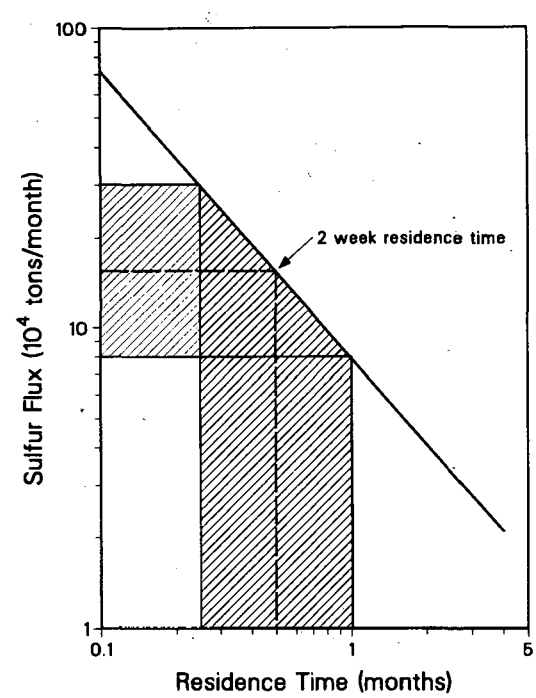

Figure 2. Estimated flux of sulfur entering the Arctic troposphere as a function of residence time. The shaded area represents a range of residence times of 1 week to 4 weeks. (XCG 8410-13402)

Table 1. Comparison of graphitic carbon total carbon, and sulfur fluxes to the amount of fuel burned at various latitudes.

Latitude	Carbon burned (tons month^{-1})	F_G as % of carbon burned	F_C as % of carbon burned	F_S as % carbon burned
75–90°N	1.5×10^3	3,200	16,300	10,600
70–75°N	5×10^4	98	490	320
65–70°N	7.6×10^5	6.4	32	21
60–65°N	3.3×10^6	1.5	7.4	4.8
55–60°N	2.5×10^7	0.2	1	0.6
50–55°N	7.1×10^7	0.07	0.35	0.2
45–50°N	5.3×10^7	0.09	0.45	0.3
0–45°N	2.3×10^8	0.02	0.1	0.07
Global	4.4×10^8	0.01	0.05	0.04

reasonable; however, it would still require extremely poor combustion of very high sulfur content fuels to fully account for the fluxes into the Arctic. Furthermore, it would require almost all the emissions from this region to be transported only in a northerly direction toward the Arctic with minimal deposition along the transport path. Major contributors to the Arctic haze in the 55–60° latitude band become more reasonable, but even here it would require very effective transport of source emissions to the Arctic. As one goes below 55°N latitude, the fluxes become a very reasonable fraction of the fuel burned, which is consistent with the midlatitude sources proposed on the basis of trace element analyses.[1]

The flux of sulfur, F_S, entering the Arctic can be compared with estimated sulfur emissions in various source regions.[8] These estimates are based on the sulfur content of the fuels and represent a maximum possible aerosol sulfur input into the atmosphere assuming complete conversion of SO_2 to particulate sulfur. Table 2 shows this comparison, with the Arctic sulfur flux shown as a percentage of the sulfur emissions from potential source regions. Individually, these fractions are large and could indicate that the Arctic haze is due to the combined input of several major source regions. On a global scale, these calculations estimate that 2.5% of the global sulfur emissions enter the Arctic, despite the fact that the Arctic is remote from major source regions and accounts for only ~6% of the northern hemisphere's surface area. These conclusions are preliminary because of uncertainties in the vertical and horizontal distribution of the Arctic haze and its residence time. However, they do indicate that the fluxes entering the Arctic are large, must be due to major combustion source regions, and have to be taken into account in the global sulfur and carbon budget.

PLANNED ACTIVITIES FOR FY 1986

During FY 1985 we also designed and constructed the second-generation aethalometer, incorporating greatly increased sensitivity as well as real-time data analysis and display. This instrument is scheduled for deployment on two major aircraft programs in FY 1986—AGASP-2, a more detailed study of Arctic haze, and WATOX 86 (Western Atlantic Ocean Experiment), which is part of an ongoing research program studying the flux of pollutants from the North American continent to the Atlantic ocean.

Table 2. Comparison of Arctic sulfur fluxes to sulfur emissions in various regions.[a]

Region	Sulfur emissions (tons month^{-1})	Arctic sulfur flux as % of emissions
Europe	2.5×10^6	6.4
Capitalist Europe	1.1×10^6	14.5
Socialist Europe	1.4×10^6	11.4
U.S.S.R.	1.1×10^6	14.5
U.S.A.	1.3×10^6	12.3
Canada	2.5×10^5	64.0
Global	6.6×10^6	2.4

[a]Sulfur emission data obtained from Moller (1984).

REFERENCES

1. Rahn, K.A. and McCaffrey, R.J. (1980), "On the Origin and Transport of the Winter Arctic Aerosol," *Ann. N.Y. Acad. Sci. 338*, p. 486.
2. Rosen, H. and Novakov, T. (1983), "Combustion-Generated Carbon Particles in the Arctic Atmosphere," *Nature 306*, p. 768.
3. Hansen, A.D.A., Rosen, H., and Novakov, T. (1982), "Real-Time Measurement of the Absorption Coefficient of Aerosol Particles," *Appl. Opt. 21*, p. 3060.
4. Hansen, A.D.A. and Rosen, H. (1984), "Vertical Distributions of Particulate Carbon, Sulfur, and Bromine in the Arctic Haze and Comparison with Ground-Level Measurements at Barrow, Alaska," *Geophys. Res. Lett. 11*, p. 381.
5. Rosen, H., Novakov, T., and Bodhaine, B.A. (1981), "Soot in the Arctic," *Atmospheric Environment 15*, p. 1371.
6. Raatz, W.E. and Shaw, G.E. (1983), "Long Range Tropospheric Transport of Pollution into the Alaskan Arctic," submitted to *J. Climate and Appl. Meteor.*
7. Marland, G., Rotty, R.M., and Treat, N.L. (1984), "CO_2 from Fossil Fuel Burning: Global Distributions of Emissions," submitted to *Tellus.*
8. Moller, D. (1984), "Estimation of the Global Man-Made Sulphur Emission," *Atmospheric Environment 18*, p. 19.

Horizontal Inhomogeneities in the Particulate Carbon Component of the Arctic Haze*†

A.D.A. Hansen and H. Rosen

The Arctic haze has been found to have a large carbonaceous component with submicron particles containing both organic compounds and microcrystalline graphitic forms.[1] This latter species is often termed "black carbon" due to its large optical absorption cross section. It can only be produced during incomplete combustion and is inert to transformation in the atmosphere. There are therefore no sources of black carbon within the atmosphere, making this material a good tracer for the evolution of a polluted air mass. Particulate black carbon was found through the Arctic troposphere during the Arctic Gas and Aerosol Sampling Project (AGASP) 1983 program in sufficient concentrations that its optical absorption may lead to a significant perturbation of the solar radiation balance.[2–4] We have previously reported results on the vertical distributions of aerosol black carbon in the Arctic haze, showing strong layering structure as well as significant concentrations at all altitudes in the troposphere.[5] In this report we present results from detailed analyses of portions of the flight tracks showing substantial horizontal variations of black carbon concentration, often (but not always) in conjunction with meteorological features.

ACCOMPLISHMENTS DURING FY 1985

Our installation aboard the AGASP WP-3D aircraft included the aethalometer, an instrument developed at Lawrence Berkeley Laboratory that measures the concentration of aerosol black carbon in real time.[6] We obtained a data set of black carbon concentrations averaged over 1-minute intervals and expressed in units of nanograms per geometric cubic meter. The estimated error on the measurements presented here is $\pm 0.09\ \mu g/m^3$. We then meshed these aethalometer data with the aircraft systems tape to give a data base containing average readings every minute for black carbon concentration, position and altitude, wind speed and direction, air temperature and relative humidity, etc. The periods of time during which all the above measurements were valid add to a total of approximately 70 hours of flying time north of 70° latitude. The flight patterns employed during the AGASP 1983 program included both rapid and gradual descents and ascents, as well as portions of level flight paths at various altitudes down to 30 m ASL. We scanned the data base to search for flight track portions that indicated a horizontal pass through a varying black carbon concentration. Details from three suitable events are presented in this report.

*This work was supported by the Director, Office of Energy Research, Office of Basic Energy Sciences, Carbon Dioxide Research Division of the U.S. Department of Energy under Contract No. DE-AC03-76SF00098.

†Summary of paper published in *Atmospheric Environment 19*, pp. 2175–2180 (1985).

Figure 1 shows data obtained during AGASP flight 9 over a period of approximately 35 minutes during which the aircraft flew in a constant northerly track at altitudes between 83 m and 91 m ASL. The track covered a distance of approximately 250 km from 75.5°N, 26.2°E to 78.2°N, 27.2°E, i.e., somewhat to the east of Spitzbergen. From 0 to 50 km on the track scale, the aircraft was over ocean with broken ice; from 50 km on, the surface was more or less continuous ice with leads. The air temperature had been steady at around 270 K before the ice was reached; it then gradually decreased to 265 K at the 200-km mark. During this time, the wind direction was steady at 200° to 210°, and the dew point was approximately constant at 261 K; i.e., the relative humidity increased from 60% to 80%. These data suggest that the aircraft was flying in a single moist air mass whose temperature was dropping. Conditions were noted as being overcast and visibly hazy. The black carbon concentration increased from about 0.2 $\mu g/m^3$ to a peak of 1.6 $\mu g/m^3$ at the 200-km mark. At this point, the observer's record states that snow flurries had started and continued for a few minutes until by the 250-km mark the aircraft had flown through a front into clear skies. The wind direction shifted by 55°, the air temperature fell by 5 K, and the dew point fell by 10°. The new air mass was colder and drier, and its black carbon concentration was down to about 0.25 $\mu g/m^3$.

Figure 2 shows 47 minutes of data from AGASP flight 3, encompassing almost a complete loop of length 130 km and height from 30 m to 1800 m altitude. The descent spiral was at 72.7°N, 156.8°W, and the ascent climb was at 71.5°N, 157.4°W. The low-level portion was a southerly track from about 200 km to 50 km north of Barrow. During this portion, the wind speed and direction were steady at 4.3 ±0.4 m/sec and 51 ±8° respectively, and the relative humidity was 75 ±5%. There was no clear evidence of a changing air mass. However, Fig. 2a shows that the average black carbon concentration

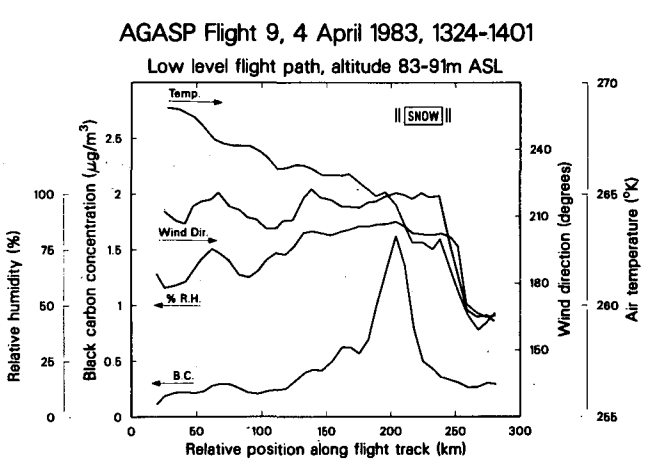

Figure 1. Data taken during low-level flight from 1324 to 1401 UT, 4 April 1983. Air temperature and wind direction scales are on the right-hand axis; relative humidity and aerosol black carbon concentration scales are on the left. The track was straight and northerly with the horizontal origin at 75.5°N, 26.2°E. The bar at upper right indicates the observation of snow flurries. (XCG 8411-13429)

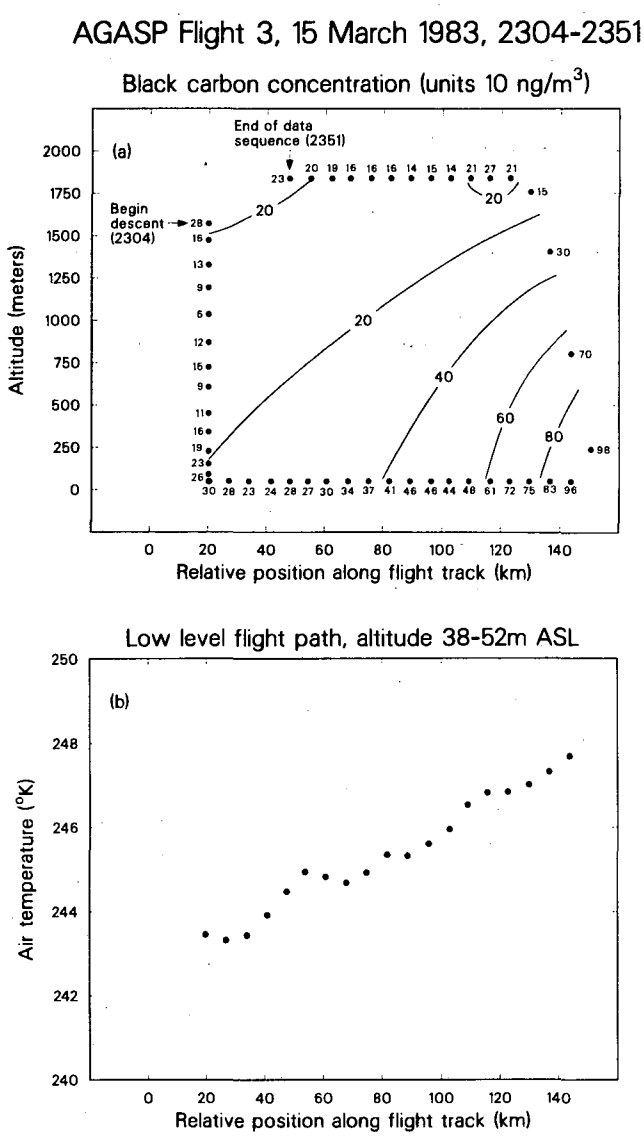

Figure 2. Data taken during loop flight pattern from 2304 to 2351 UT, 15 March 1983. The descent was a spiral at 72.7°N, 156.8°W; the level flight track was southerly. (a) Aerosol black carbon concentration vs. altitude and relative horizontal position. The contours are hypothetical, calculated by interpolation of the perimeter measurements. (b) Air temperature for the low-altitude flight track portion from 2317 to 2335 UT. (XCG 8411-13426A)

increased steadily from about 0.25 $\mu g/m^3$ to almost 1 $\mu g/m^3$ along the low-level track portion; and Fig. 2b shows that the air temperature increased by 4 K in the same period. The aircraft then climbed and essentially retraced its track at 1850 m altitude for altitude for about 100 km distance. We have constructed contours of aerosol black carbon concentration for the purposes of visualization, based on interpolation of the data points around the track perimeter. We emphasize that these are not measured contours; however, because there were neither sources nor sinks of aerosol black carbon within this perimeter, the implied continuity is reasonable. The data suggest a concentration of black carbon at low altitudes, with a maximum at some point beyond the 150-km track point. However, there was no evidence of precipitation nor crossing of an air mass boundary during the flight loop.

Figure 3 shows 51 minutes of data taken during AGASP flight 5. This track portion was a straight path from 71.8°N, 141.4°W to 74.0°N, 137.3°W over the Beaufort Sea during the flight from Anchorage, Alaska, to Thule Air Base, Greenland. The Canadian coast was from 100 to 400 km distant during this time. The flight profile was a descent to 30 m altitude followed by about 17 minutes of flying at low altitudes, after which the aircraft climbed to 1550 m ASL altitude. Figure 3b shows the air temperature and wind direction. There was a strong temperature inversion, with a 10 K fall between 700 m altitude and sea level. The wind direction shifted very little along the first 250 km of the track but then rapidly turned by 50° soon after the climb-out. At this time, although the air temperature showed little change, the dew point rose from 237 K to 252 K, indicating that the aircraft had entered a different air mass. The black carbon concentration was of the order of 0.2 $\mu g/m^3$ at high altitudes at the start of the sequence. This increased to 0.73 $\mu g/m^3$ at about 800 m altitude on the descent and then fell off rapidly to low values at low altitudes when the aircraft was within the surface temperature inversion air layer. Upon climbing, the black carbon concentration increased again to almost 1 $\mu g/m^3$ but then rapidly disappeared at the start of the level flight portion at the same time as the changing meteorological measurements indicated an air mass boundary. The constructed contours shown in the figure suggest a concentration maximum close to this point.

The data presented in Fig. 1 suggest the following situation, similar to one described by Raatz and Schnell[7] for another AGASP flight in the Norwegian Arctic. The aircraft was flying on a northerly track at a constant low altitude in a moist, polluted air mass. The black carbon concentration started increasing substantially at around the 150-km track mark but fell rapidly as soon as precipitation started. Shortly thereafter, the aircraft passed through a front into an air mass whose aerosol black carbon concentration was low. The removal of aerosols by precipitation is expected; however, there was no ongoing

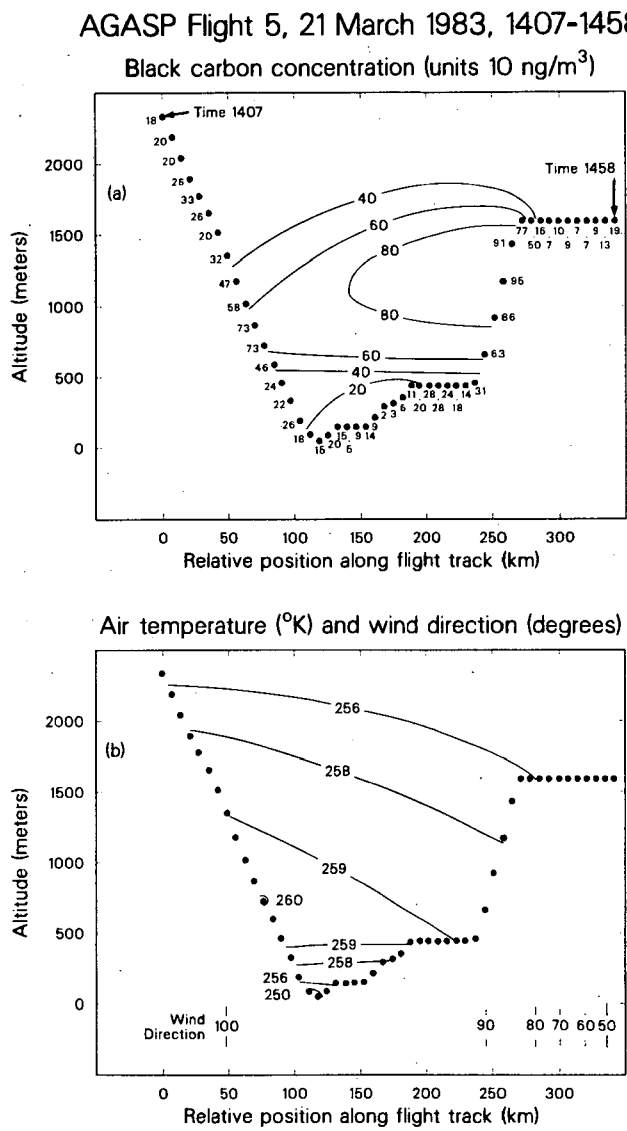

Figure 3. Data taken during descent/ascent flight pattern from 1407 to 1458 UT, 21 March 1983. The track was straight and northeasterly with the horizontal origin at 71.8°N, 141.4°W. (a) Aerosol black carbon concentration vs. altitude and horizontal position. (b) Air temperature and wind direction vs. altitude and position. In both figures the contours are estimated from the perimeter measurements and drawn for visualization purposes only. (XCG 8411-13430A)

meteorological activity to explain the five-fold change in black carbon concentration between the start of the track and the peak at the 200-km mark. Figure 2a shows a similar situation, in which the aerosol black carbon concentration increased four-fold within the same air mass. Here, the air temperature gradually rose (see Fig. 2b), but there was no clear evidence of recent meteorological activity or the approach of a front.

There may be several explanations for these observations. One is that the air masses were at one time uniformly polluted but that precipitation or other scavenging had occurred at some time in the past over only part of the air mass, removing aerosols from a portion of the flight track. Another is that the injection of carbonaceous aerosol into the air mass had been confined in an area at the source region and that these are plume edge profiles. However, this would require only a small amount of horizontal dispersion over the long transport paths (see Harris[8]) and imply a diffusion coefficient of the order of 10^9 cm^2/sec. At present, we cannot unambiguously identify either these or other possible mechanisms as explanation for the data.

The maximum instantaneous concentration of black carbon observed during the entire AGASP program was approximately 1.5 $\mu g/m^3$, which we shall take as a reasonable value for the maximum concentration likely to be found at the center of an inhomogeneity. If we assume that the flight track of Fig. 2a penetrated the edge of such a patch, we can estimate the size scale of the patch from the spacing of the contours. This suggests a horizontal scale of 50 to 100 km as the characteristic length over which the aerosol black carbon concentration changes by a factor of two. We must strongly emphasize that this distance represents a characteristic length on the basis of partial perimeter measurements, rather than an actual complete mapping. The data shown in Fig. 1 from the start of the track to the onset of precipitation also fit into this scale.

The data shown in Fig. 3 present a more complex situation. Figure 3b indicates a surface temperature inversion layer extending to about 400 m altitude and an air mass boundary at about 280 km on the track. The constructed contours in Fig. 3a show strong aerosol black carbon concentrations in the air above the surface layer but very low levels below the inversion, an observation in agreement with the expected weak coupling of these layers. The effect of the front at 280–300 km track is similar to that shown in Fig. 1: in the new air mass, the black carbon concentrations are low. The constructed contours indicate a very rapid change of aerosol black carbon concentration at the front and also show that the polluted air mass is resting on top of a clean surface temperature inversion layer. This contrasts with the situation often found in urban atmospheres, in which the emissions are trapped in the surface layer beneath the inversion. This observation in the Arctic may imply long-range transport of combustion emissions.[9–10]

PLANNED ACTIVITIES FOR FY 1986

The 1983 AGASP aircraft experiment demonstrated the value of measurements of aerosol black carbon from an airborne platform in real time. However, the instrument used during this program was still at the prototype stage. During FY 1985 we also designed and constructed the second-generation aethalometer, incorporating greatly increased sensitivity as well as real-time data analysis and display. This instrument is scheduled to be deployed on two major aircraft programs in FY 86—WATOX '86 (Western Atlantic Ocean Experiment) and AGASP-2, in which it will be used to indicate the presence of aerosol graphitic carbon as a tracer for combustion emissions in conjunction with airborne measurements of other pollutants.

REFERENCES

1. Rosen, H. and Novakov, T. (1983), "Combustion-Generated Carbon Particles in the Arctic Atmosphere," *Nature 306*, p. 768.
2. Shaw, G.E. and Stamnes, K. (1980), "Arctic Haze: Perturbation of the Polar Radiation Budget," *Ann. N.Y. Acad. Sci. 338*, p. 533.
3. Porch, W.M. and MacCracken, M.C. (1982), "Parametric Study of the Effects of Arctic Soot on Solar Radiation," *Atmos. Environ. 16*, p. 1365.
4. Valero, F.P.J., Ackerman, T.P. and Gore, W.J.Y. (1984), "The Absorption of Solar Radiation by the Arctic Atmosphere During the Haze Season and Its Effects on the Radiation Balance," *Geophys. Res. Lett. 11*, p. 465.
5. Hansen, A.D.A. and Rosen, H. (1984), "Vertical Distributions of Particulate Carbon, Sulfur and Bromine in the Arctic Haze and Comparison with Ground-Level Measurements at Barrow, Alaska," *Geophys. Res. Lett. 11*, p. 381.
6. Hansen, A.D.A., Rosen, H., and Novakov, T. (1982), "Real-Time Measurement of the Absorption Coefficient of Aerosol Particles," *Appl. Opt. 21*, p. 3060.
7. Raatz, W.E. and Schnell, R.C. (1984), Aerosol Distributions and an Arctic Aerosol Front Dur-

ing AGASP: Norwegian Arctic," *Geophys. Res. Lett. 11*, p. 373.
8. Harris, J.M. (1984), "Trajectories During AGASP," *Geophys. Res. Lett. 11*, p. 453.
9. Rahn, K.A. and McCaffrey, R.J. (1980), "On the Origin and Transport of the Winter Arctic Aerosol," *Ann. N.Y. Acad. Sci. 388*, p. 486.
10. Iversen, T. (1984), "On the Atmospheric Transport of Pollution to the Arctic," *Geophys. Res. Lett. 11*, p. 457.

Primary Oxidants—Results from Laboratory and Field Experiments*

W.H. Benner and T. Novakov

Chemical reactions that oxidize SO_2 dissolved in fog and rain droplets or in a layer of water that covers many particles in the troposphere are called heterogeneous-type reactions and are considered to be important in the formation of tropospheric sulfate. Because some of the reported[1] SO_2 oxidation reactions[2] are relatively slow at the concentrations of reactants found in the troposphere, long-range transport of pollutants is invoked to explain the concentrations of sulfate observed. Long-range transport supplies the reaction time necessary for the relatively slow reactions to produce the observed sulfate concentrations. In contrast, reactions that are much faster require respectively less reaction time to produce the same observed sulfate concentrations. The oxidation of dissolved SO_2 by dissolved H_2O_2 can be one of the fastest heterogeneous SO_2 oxidation reactions when enough H_2O_2 is available. In a recent publication,[1] we reported that incomplete combustion is a source of H_2O_2. Prior to this, it was generally assumed that gas-phase photochemical reactions produced all of the H_2O_2 found in the troposphere.

This report describes our continuing investigation of heterogeneous SO_2 oxidation reactions and focuses on the oxidation of SO_2 by gaseous oxidants produced during combustion of hydrocarbon fuels. It builds on work reported in previous annual reports[3,4] and summarizes experiments we conducted to determine how closely the heterogeneous oxidation of SO_2 is coupled to combustion emissions. The results presented here were also presented at a recent symposium on heterogeneous chemistry.[5]

*This work was supported by the Director, Office of Energy Research, Office of Health and Environmental Research, Physical and Technological Research Division of the U.S. Department of Energy under Contract No. DE-AC03-76SF00098 and by the National Science Foundation under Contract ATM 83-15442.

ACCOMPLISHMENTS DURING FY 1985

Filtered combustion gases from a laboratory diesel fuel burner and from two diesel-powered cars were individually sampled into several different aqueous solutions, using a technique described previously.[3] The solutions were H_2O, 1 mM H_2CO (pH = 5), 5 mM $CO_3^=$ (pH = 10), and a suspension of activated carbon in water. The H_2CO solution was used to quench the reactions between oxidants and S(IV) by converting the S(IV) to hydroxymethane sulfonate ion. The carbonate solution was used to quench the reaction between H_2O_2 and S(IV) by application of the fact that the rate constant for this reaction is 10^4 times slower at pH = 10 than at pH = 4.[1] The percent oxidized S, $SO_4^= \times 100\%/[S_{TOT}]$, in the samples was determined by ion chromatography, and the $[H_2O]$ was determined by a colorimetric technique.[6] No attempt was made to measure the amount of combustion water collected during sampling because the condensation of combustion water in the bubbler contributed a negligible dilution factor.

In a small diesel fuel burner, fuel and air were premixed and heated to $\approx$150°C before combustion. The fuel was introduced into the burner at $\approx$5 ml/min and, by adjusting the air flow rate, the air to fuel (A/F) ratio could be varied between 2 and 10. Optionally, a flame quencher (a water-cooled stainless steel surface) could be placed in the flame. The emissions from this burner were diluted with a large excess of air and only a small fraction of the diluted mixture was sampled through a bubbler. Exhaust gases from the diesel-powered cars were sampled directly without dilution. This sampling system was constructed from stainless steel and glass and was heated to preclude condensation of H_2O in the sampling tubes. Control experiments in which SO_2 and CO_2 from a cylinder were sampled simultaneously at concentrations and conditions similar to those present in the combustion streams and immediately analyzed showed the percent oxidized sulfur always to be less than 0.5% for samples collected in H_2CO, H_2O, and $CO_3^=$.

A set of field experiments was conducted by collaborators in Ljubljana, Yugoslavia, to see if detectable concentrations of primary oxidants could be detected in ambient air. The Ljubljana site was chosen because of an ongoing joint aerosol sampling project and because high levels of air pollution are commonly observed in winter due to poorly controlled coal burning. Filtered ambient air was bubbled through water for 3 hours, and H_2CO was then added to prevent oxidation of dissolved SO_2 by air (O_2). Later the samples were analyzed for percent oxidized sulfur.

Diesel Fuel Burner Experiments

The results of analysis of samples prepared by absorbing filtered diesel burner combustion gases into the three collection solutions is shown in the top half of Table 1. In these fuel burner experiments, a decrease in the A/F ratio increased the percent oxidized S. Thermal quenching of the flame also increased the percent oxidized S over that amount of S oxidized in nonquenched flame samples (Table 1).

Sampling filtered combustion gases into a suspension of an activated carbon (RB-1), suspension of which can catalytically oxidize dissolved SO_2, greatly increased the percent of oxidized SO_2. In these suspension experiments, a decrease in the A/F ratio from 10 to 2 also decreased the percent oxidized S, a finding that is opposite to that observed for unfiltered combustion gases collected in H_2O. The effect can be explained by the conversion of the normally hydrophilic RB-1 particles to hydrophobic ones as evidenced by their floating out of suspension. An A/F ratio of 2 caused more particles to become hydrophobic than did combustion gases from a flame having an A/F ratio of 10.

Combustion gas samples collected in H_2CO solutions showed a reproducible percent oxidized S, regardless of flame A/F ratio and thermal quenching. However, the 2% values observed for all samples of diesel fuel burner gases collected in H_2CO is above the 0.5% control value. This demonstrates that H_2CO chemically quenches the oxidation but not completely. Since H_2CO reduced the percent oxidized S, gas-phase oxidation of SO_2 before it is absorbed into water in these experiments can probably be discounted.

Much higher percentages of oxidized S were observed in filtered combustion gas samples collected in $CO_3^=$ solution. The cause for this can only be speculated at this time. The reaction between H_2O_2 and dissolved SO_2 at pH = 10 is many times slower than at the pH of the H_2O samples (pH = 3–4), so this increased oxidation can't be attributed to H_2O_2. NO_2^- is present in these samples, but the rate of reaction of NO_2^- with dissolved SO_2 also slows with increasing pH.[2] It suggests that a different oxidant may be involved. This finding could be of interest in materials damage studies of marble.

Diesel Car Experiments

The results of the analysis of samples prepared by absorbing filtered diesel car exhaust into the three collection solutions is shown in the bottom half of Table 1. In these experiments combustion conditions (i.e., A/F ratios) could not be varied; however, each car was made by a different manufacturer and maintained by separate owners.

The percent oxidized S in the H_2O samples was as large as 13 (diesel-2). H_2CO did not quench the oxidation of dissolved SO_2 in these samples as well as it did in the diesel fuel burner experiments.

Table 1.

	% S oxidized		
Conditions	H_2O	H_2CO	$CO_3^=$
Burner flame, not quenched, A/F = 2	4	2	27
Burner flame, not quenched, A/F = 10	2	2	
Burner flame, quenched, A/F = 2	9	2	
Burner flame, quenched, A/F = 10	3	2	
Diesel car 1	6	7	72
Diesel car 1 + 0.1 g/l RB-1	13		
Diesel car 2	13	9	40
Diesel car 2 + 0.1 g/l RB-1	25		

Again, samples collected in $CO_3^=$ solution showed much more oxidized S than did samples collected in H_2O. The speculation is also the same, i.e., an oxidant other than H_2O_2 was activated at this pH.

Repeated analysis of the samples over several hours showed that the percent S oxidized initially reflects only part of the chemistry that occurs in these samples. From Fig. 1 it can be seen that the exhaust gases from these two cars were very different in composition with respect to SO_2 oxidants. Starting first with the samples collected in H_2CO solution, little change in percent of oxidized S occurred with time. Although each car exhaust sample showed different initial percentages of oxidized S, the H_2CO allows only negligible S to be oxidized over the ensuing 2–3 hours. The same was observed for samples collected in $CO_3^=$ solution.

Samples that were not chemically quenched with H_2CO or $CO_3^=$ show large differences when diesel-1 and diesel-2 samples are compared. Exhaust from diesel-1 produced substances that continued to oxidize dissolved SO_2 while diesel-2 did not. By comparing H_2O samples of filtered combustion gases, diesel-1 produced a solution that continued to oxidize S, but this was not observed for diesel-2. In the water sample for diesel-1, 45% of the S was oxidized after 2 hours. Only differences in combustion for the two car engines can be invoked to explain these observations.

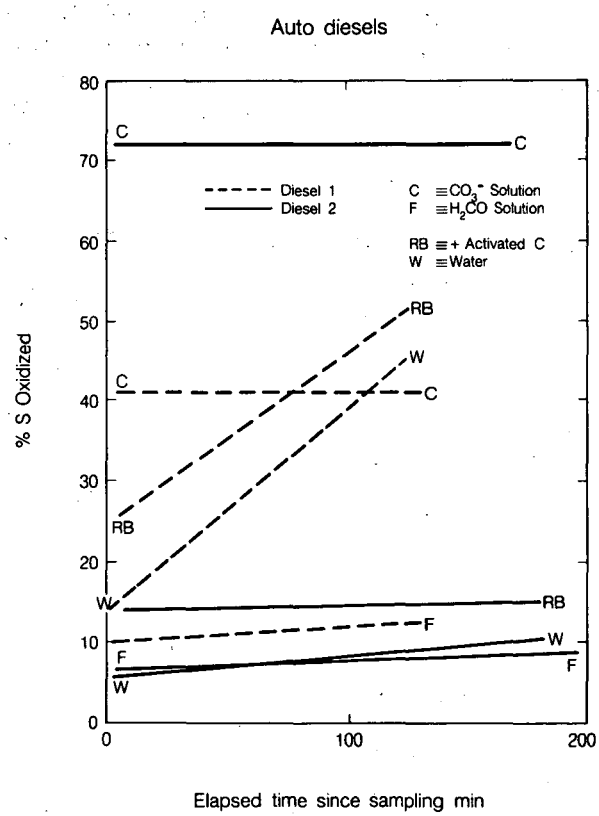

Figure 1. Oxidation of sulfur in bubbler samples. (XBL 859-11696)

Hydrogen Peroxide Sampling

Filtered exhaust samples collected from the laboratory diesel burner into H_2O, H_2CO, and $CO_3^=$ contained no detectable concentrations of H_2O_2 (H_2O_2 detection limit 10^{-8} M). All the filtered exhaust samples from the diesel cars, however, contained H_2O_2. The maximum H_2O_2 concentration was 5×10^{-6} M as compared to 1×10^{-4} M dissolved S. Comparison of collection solutions showed the highest H_2O_2 concentrations in the $CO_3^=$ solutions.

Field Experiments

Twenty samples of filtered ambient air were bubbled through H_2O and chemically quenched with H_2CO immediately after collection. Approximately 3 weeks later, these samples were analyzed at Technical University in Vienna and then reanalyzed 5 weeks later at LBL. Comparison of TUV and LBL analyses showed that a large increase in the percent S oxidized occurred between analyses. In some samples, no residual S(IV) was detected at LBL. Control experiments in which SO_2 alone was collected in H_2O and similarly quenched with H_2CO showed only 6% of the dissolved SO_2 to be oxidized after 3 months. Clearly the H_2CO quenching was not adequate for these samples. Extrapolation of the data backwards in time to sampling time indicated that as much as 20% of the dissolved S could have been oxidized initially; but because several of the extrapolations yielded negative percents, the results are questionable for assaying the presence of primary oxidants in this source-dominated air mass.

PLANNED ACTIVITIES FOR FY 1986

This work has demonstrated that the oxidation of SO_2 in tropospheric droplets can be closely connected with combustion efficiency. We have started to construct a fog chamber in which combustion H_2O in the presence of combustion gases is condensed on the combustion particles. Experiments will be conducted to determine the importance of rapid heterogeneous reactions in plumes. Studies at several field locations will be repeated.

REFERENCES

1. Benner, W.H. and Novakov, T. (1985), "Oxidation of SO_2 in Fog Droplets by Primary Oxidants," *Atmos. Environ. 19*, p. 1377.
2. Martin, L.R. (1984), "Kinetic Studies of Sulfite Oxidation in Aqueous Solution," in *SO_2, NO and NO_2 Oxidation Mechanisms*, J. Calvert, Ed., Butterworth, Boston, p. 63.
3. Benner, W.H., McKinney, P.M., and Novakov, T. (1983), "Evidence for Primary Oxidants of SO_2," in *Energy and Environment Division Annual Report, FY 1982*, LBL-15298, p. 3.
4. Benner, W.H. and Novakov, T. (1985), "Oxidation of SO_2 in Fog Droplets by Primary Oxidants," in *Applied Science Division Annual Report, FY 1984*, LBL-18754, p. 3.
5. Benner, W.H. and Novakov, T. (1985), "Primary Oxidants—Results from Field and Laboratory Studies," in *Proc. Symp. on Heterogeneous Processes in Source-Dominated Atmospheres*, p. 26, LBL-20261.
6. Madsen, B.C. and Kromis, M.S. (1984), "Flow Injection and Photometric Determination of Hydrogen Peroxide in Rainwater with N-Ethyl-N-(sulfopropyl)aniline Sodium Salt," *Anal. Chem. 56*, p. 2849.

Empirical Evidence for Heterogeneous SO_2 Oxidation in Ljubljana, Yugoslavia*

M. Bizjak,† V. Hudnik,† A.D.A. Hansen, and T. Novakov

Most previous work on sulfate aerosols was devoted either to SO_2 conversion during long-range transport or to sulfate formation in urban atmospheres where, because of the high degree of environmental regulations and controls, the pollutant concentrations are relatively low. Much less is known about sulfate chemistry in highly polluted source-dominated urban atmospheres, where scattered and usually inefficient small combustion furnaces are major sources of pollutants. Such atmospheres, because of high concentrations of both particles and gases, are more likely to provide conditions for heterogeneous reactions and therefore a greater probability for demonstrating their occurrence and inferring the contributions of local sources to aerosol sulfates. The research described in this report deals with certain aspects of heterogeneous formation of aerosol sulfate in Ljubljana, Yugoslavia. This location is well suited for such a study because of high pollutant concentrations, especially during the winter. Because relatively low-grade coal is burned in inefficient combustors, large soot concentrations are observed in the winter. During the relatively cold winters, inversions with characteristic pollution-induced urban fog occur almost daily.

ACCOMPLISHMENTS DURING FY 1985

Two kinds of 24-hour ground-level aerosol samples were collected in Ljubljana on two filters in parallel for different analyses. The filter materials used were quartz fiber (Pallflex type 2500 QAO, prefired for 6 hours at 700°C to remove combustible carbon) and cellulose membrane (Millipore type RATF, 1.2-μm pore size). Total samples, i.e., without size segregation, were collected during the 1981/82 sampling period. During the 1983/84 period, size-segregated 24-hour filter samples corresponding to cutoffs of < 0.3 μm and 2.0 μm were collected on the quartz afterfilters of two single-stage impactors. Two such units were used, producing one filter sample from which all particles of effective diameter greater than 0.3 μm have been excluded and another representing particles smaller than 2 μm. The impaction surfaces were greased to minimize particle bounce. The sampling was performed at the Hydrometeorological Institute in central Ljubljana. Meteorological data consisting of wind speed and direction, temperature, and relative humidity were collected at the site, as well as 24-hour average SO_2 concentrations by a conventional titration method.

The exposed quartz filters were analyzed for total carbon and sulfur by combustion followed by relative conductometric determination of SO_2 and CO_2

*The portion of this work done at LBL was supported by the Director, Office of Energy Research, Office of Health and Environmental Research, Physical and Technological Research Division of the U.S. Department of Energy under Contract No. DE-AC03-76SF00098 and by the National Science Foundation under Contract No. ATM-8315442. This work is a summary of LBL-20953, accepted for publication by *Atmospheric Enviroment*.

†Boris Kidrich Institute of Chemistry, Ljubljana, Yugoslavia.

at the B. Kidric Institute in Ljubljana. Portions of the same filters were also analyzed for total carbon at Lawrence Berkeley Laboratory by a combustion technique, and the Millipore filters were analyzed for sulfur and trace elements by x-ray fluorescence.

The seasonal pattern of pollutants in Ljubljana is illustrated in Fig. 1a and b, where biweekly SO_2 and particulate sulfur, S_p, concentrations are plotted as a function of time during the 1981/82 sampling season. The particulate sulfur to gaseous sulfur ratios, S_p/S_g, for this period are shown in Fig. 1c. This ratio, which can be viewed as a measure of SO_2-to-sulfate conversion, is about four times higher in the summer (~0.4) than in the winter (~0.1), indicating a different chemistry during the two seasons.

In the analysis of the data, we will also make use of another ratio: particulate sulfur to particulate carbon, S_p/C_p. In Ljubljana, as previously demonstrated,[1] total particulate carbon and soot concentrations are approximately equivalent. As a primary combustion-generated particulate pollutant, soot can be used as a conservative tracer for the products of incomplete combustion.[2] The S_p/C_p ratio can therefore be used to infer the relationship between secondary sulfates and primary source emissions. The S_p/C_p ratios for the 1981/82 sampling period are shown in Fig. 1d. The variations of these ratios are qualitatively similar to the variations of S_p/S_g ratios but with less pronounced maxima. Furthermore, there seems to be a clear difference in these ratios between Nov./Dec. and Jan./Feb., with the latter period having higher values.

The average 24-hour relative humidity was high, usually exceeding 80%, and the wind speed was generally low (< 1 m sec^{-1}) during both the Nov.-Dec. and Jan.-Feb. periods. The only drastic difference in meteorology corresponding to low and high S_p/C_p ratios was the ambient temperature. This is seen from Fig. 2, where S_p/C_p ratios, average daily relative humidity, and temperature are plotted for December 1981 and January 1982. This figure shows that the high S_p/C_p ratios during January correspond to periods with high humidity and persistent subzero temperatures. In our view, this observation represents the manifestation of a heterogeneous liquid-phase mechanism of SO_2 oxidation. Under conditions of high humidity and low wind speed, subzero temperatures would enhance condensation of water droplets on combustion nuclei and increase the solubility of SO_2. Such conditions are known to

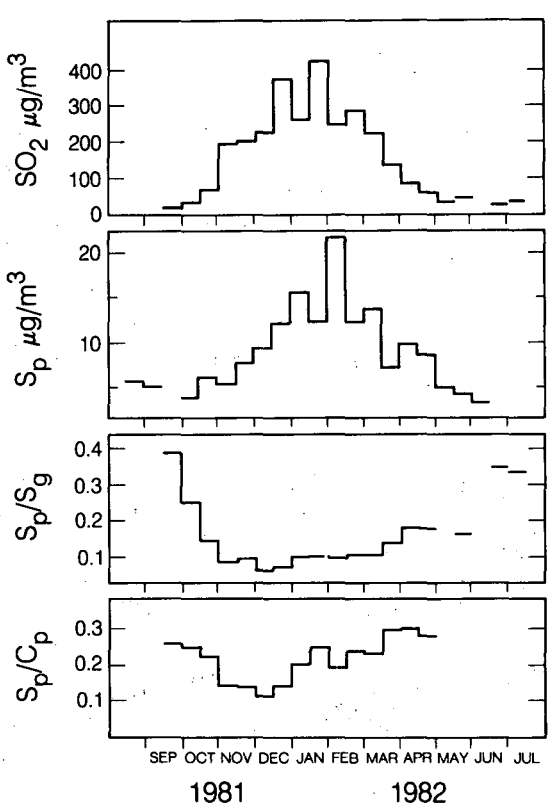

Figure 1. Biweekly concentrations of SO_2, particulate sulfur (S_p), particulate to gaseous sulfur ratios (S_p/S_g), and particulate sulfur to particulate carbon ratios (S_p/C_p) for the 1981–1982 sampling season. (XBL 8411-8924A)

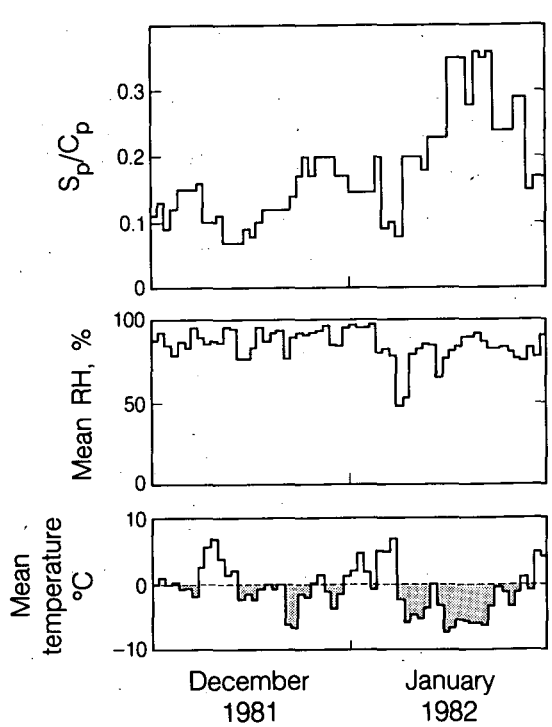

Figure 2. Dependence of the particulate sulfur to carbon ratio on mean relative humidity and ambient temperature. (XBL 859-12125)

favor the formation of urban fog, consisting of supercooled droplets.

The effect of high humidity and low ambient temperatures on enchanced sulfur formation observed from 1981/82 data has been confirmed during the winter of 1983/84 with size-segregated sampling. This is illustrated in Fig. 3, where S_p/C_p, and S_p/S_g ratios (for particle diameters < 2 μm), average temperature, relative humidity, and SO_2 concentrations for February 1984 are shown. The second half of the month showed a pronounced increase in the S_p/C_p and S_p/S_g ratios. It is clear from the figure that during this period the average daily temperatures were consistently below 0°C and that the increase in the S_p/C_p and S_p/S_g ratios occurred after the relative humidity exceeded approximately 65%. Such dependence on relative humidity has been shown to be characteristic of heterogeneous reactions.[3] It should be noted that during this period, the SO_2 concentration remained approximately constant, and therefore the apparent increase of the sulfate production is related entirely to the physical changes in the atmosphere, i.e., the liquid water content.

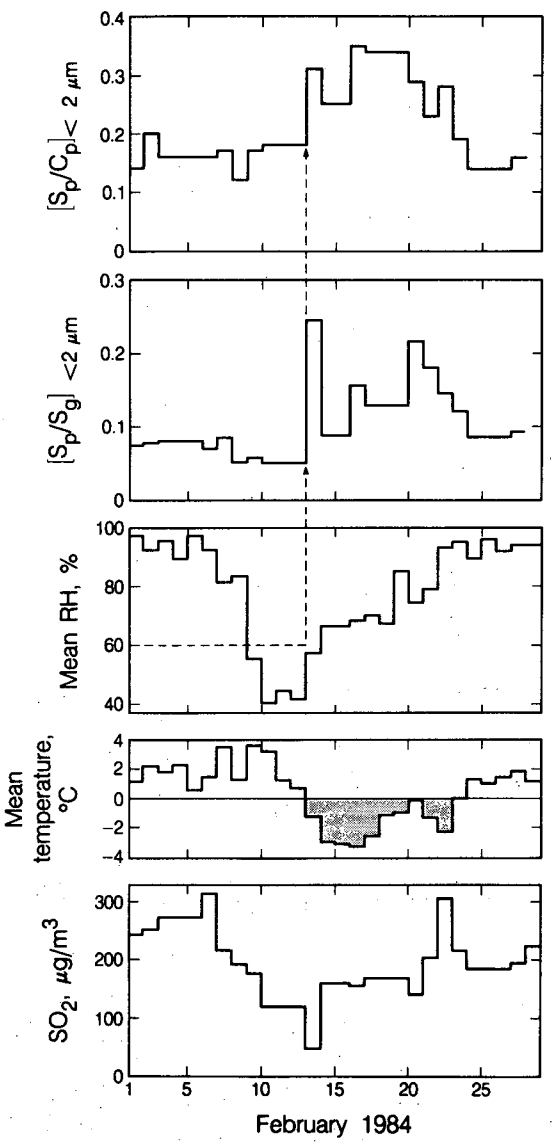

Figure 3. Dependence of particulate sulfur (S_p) to particulate carbon (C_p) and gaseous sulfur (S_g) ratios on mean daily relative humidity, temperature, and SO_2 concentration for February 1984. The data are for the < 2-μm size cut. An increase in S/C_p and S_p/S_g ratios is seen when the temperature is below 0°C and the relative humidity exceeds 60%. (XBL 859-12124)

The observations described thus far can be qualitatively explained as follows: Water may condense on soot (or other) particles in a plume, forming a layer of liquid water on the particle. The SO_2 in the plume will be dissolved in this layer and oxidized to sulfate by one or more oxidation mechanisms. If the ambient conditions, such as relative humidity and temperature, do not favor additional water condensation during transport to the receptor site, the entire oxidation would possibly occur in the first phases of plume development. The resulting sulfate concentration would be related to the volume of the original layer of condensed water and hence to soot concentration. However, if conditions favor additional condensation (e.g., high relative humidity and low temperature), particle-associated liquid water and its S(IV) content would continue to exist both in the plume and during transport, resulting in a S_p/C_p ratio greater than in conditions of low humidity.

PLANNED ACTIVITIES FOR FY 1986

We plan to continue aerosol sampling in Ljubljana using LBL-fabricated samplers that collect filters over preset time intervals of as little as 1/2 hour. These samples will allow a time-resolved analysis of the interrelationship of aerosol species and meteorological changes. In parallel with the aerosol sampling, we plan to collect bubbler samples to study oxidants that may be present in the gas phase.

REFERENCES

1. Bizjak, M., Hudnik, V., Gomiscek, S., Hansen, A. D. A., and Novakov, T. (1984), "Aerosol Studies in Ljubljana Under Conditions of Combustion-Derived Winter Pollution," *Sci. Total Environ. 336*, p. 377.
2. Novakov, T. (1981), "Microchemical Characterization of Aerosols," in *Nature, Aim and Methods of Microchemistry*, H. Malissa, M.

Grasserbauer, and R. Belcher, Eds., Springer-Verlag, New York, p. 141.
3. McMurry, P.H. and Wilson, J.C. (1983), "Droplet Phase (Heterogeneous) and Gas Phase (Homogeneous) Contributions to Secondary Ambient Aerosol Formation as a Function of Relative Humidity," *J. Geophys. Research 88*, p. 5101.

Kinetics of Soot-Catalyzed SO_2 Oxidation in Aqueous Systems*

L.A. Gundel, W.H. Benner, and T. Novakov

Because of its potential significance for atmospheric chemistry, oxidation of sulfur dioxide by carbon particles has received considerable attention, and assessments of its importance range from significant (under nonphotochemical conditions)[1] to negligible.[2] A recent review[3] using rate data obtained at LBL[4] concludes that this reaction can compete with H_2O_2 at pH < 6, only when the concentration of carbon exceeds 0.1 g l^{-1}. Such conditions frequently occur in polluted urban atmospheres.[5,6] Our earlier work[7] has shown that the differences in catalytic activity for different carbons could be ascribed to the capability of carbon surfaces to adsorb oxygen and that this adsorbed oxygen is the actual oxidant of dissolved SO_2. Fresh combustion carbon particles may therefore be more reactive than aged particles.

This report describes measurements of the reaction rate for two carbons that differ greatly in reactivity. The kinetic data are interpreted by a proposed mechanism for carbon-catalyzed oxidation. This complete kinetic information should help in assessing the importance of the conversion of SO_2 to $SO_4^=$. The results are used to estimate conversion rates for dissolved S(IV) under polluted atmospheric conditions.

ACCOMPLISHMENTS DURING FY 1985

Commercially available activated carbons Nuchar-SN (Westvaco) and RB1 (Norit) were used in this study. A sample of each carbon was ground overnight in an agate ball mill, washed in boiling de-ionized water, filtered, and dried at 100°C. Portions of each washed carbon were heated at 1000°C in N_2 for 15 minutes, cooled to room temperature, and exposed to room air for about half an hour before reaction. Earlier work[7] showed that this treatment cleaned the surface, decreased total oxygen content, and enhanced the catalytic reactivity. The purpose of heating in this experiment was preparation of carbons with reproducible oxidation behavior that would be more like freshly generated soot particles.

The oxidation rate of S(IV) was measured in aqueous slurries of these carbons. The S(IV) was prepared from $Na_2S_2O_5$ that hydrolyzes to HSO_3^- in solution. Before reaction, slurries of carbons were sonicated for 15 minutes to disperse and equilibrate the particles with dissolved air. The reaction began when 1.0 μl of the S(IV) solution was added from a syringe to 9.0 ml of suspended particles with continuous stirring. After mixing, the initial S(IV) concentration, $[S(IV)]_0$, was 3.8×10^{-4} M for all experiments; and the concentration of carbon particles was 1.0 g l^{-1}. To quench the reaction, 5.0 μl of formaldehyde was injected into the reaction mixture before filtration. The HCHO reacted with S(IV) to form hydroxymethane sulfonate, a stable adduct. The filtrate was analyzed by ion chromatography for S(IV) and $SO_4^=$. The filtered particles were dried, weighed, and extracted with water to measure levels of adsorbed $SO_4^=$. With this procedure we were able to study reaction times as short as 5 seconds; results obtained for times $\geqslant 1$ minute were indistinguishable from those obtained using filtration (i.e., without adding HCHO) to stop the reaction, as had been done in earlier studies.[7,8]

Figure 1 shows S(IV) and $SO_4^=$ concentrations as a function of time for Nuchar-SN. Figure 2 shows the data for RB1. The reaction has the same features as reported earlier[7,8]: an initial rapid drop in [S(IV)] followed by a slower step whose rate is constant and independent of [S(IV)]. For RB1, the first step accounts for the whole reaction. No second step was observed for the experimental conditions used.

The decrease in [S(IV)] was accompanied by a simultaneous increase in $[SO_4^=]$ concentration. For Nuchar, after 20 minutes the $[SO_4^=]$ in solution was about 40% of the decrease in [S(IV)] concentration. About half of this missing $[SO_4^=]$ was extracted with water from the filtered particles. After 20 minutes in contact with RB1, the [S(IV)] had dropped to zero,

*This work was supported by the Director, Office of Energy Research, Office of Health and Environmental Research, Physical and Technological Research Division of the U.S. Department of Energy, under Contract No. DE-AC03-76SF00098 and by the National Science Foundation under Contract No. ATM 83-15442.

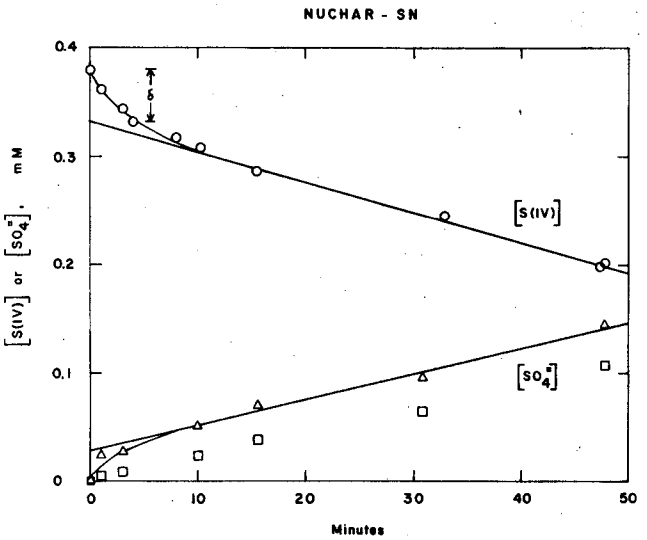

Figure 1. Kinetic data for Nuchar-SN. The circles represent [S(IV)] vs. time. The squares represent $[SO_4^=]$ in solution; the triangles correspond to the sum of $[SO_4^=]$ in solution and $[SO_4^=]$ extracted from the dried particles after reaction. The straight lines represent linear regression lines for t ≥ 10 minutes. (XBL 863-775)

and the $[SO_4^=]$ in solution was about 70% of the initial [S(IV)]. Here, about one-third of the missing sulfate was extracted from the particles. At this point we have no further data to indicate whether the missing sulfur was entirely adsorbed on the particles or partially present in solution as a species other

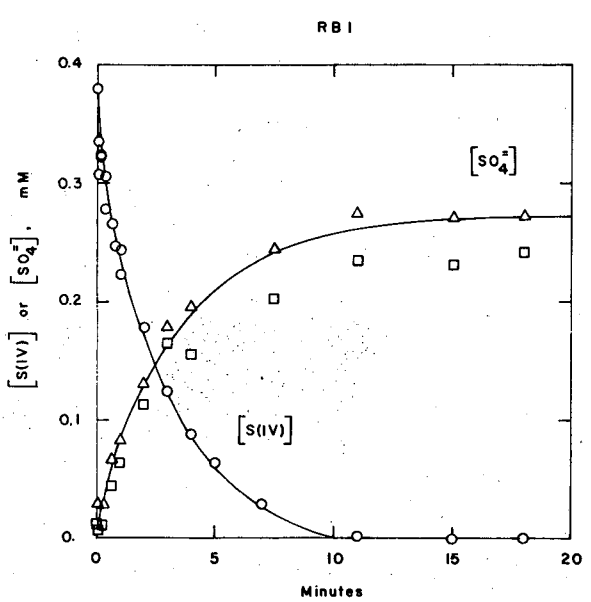

Figure 2. Kinetic data for RB1. The circles, squares, and triangles correspond to those in Fig. 1. (XBL 863-772)

than S(IV) or $SO_4^=$. These mass balance considerations are not taken into account in the subsequent discussion.

To interpret the kinetic data, we are extending the mechanism proposed by Brodzinsky *et al.*[8] These authors found that the slow part of the reaction could be explained as a sequence of three adsorption steps followed by the decomposition of the adsorbate to $SO_4^=$. These adsorption steps are formation of a surface oxygen species $Cx \cdot O_2$, which is in equilibrium with dissolved oxygen, and sequential adsorption of two S(IV) ions at the same site to form $Cx \cdot O_2 \cdot (S(IV))_2$. Two $SO_4^=$ ions diffuse away from the surface. The decomposition of $Cx \cdot O_2 \cdot (S(IV))_2$ is the rate-determining step. At equilibrium and at sufficiently high [S(IV)] the rate will be zero order in [S(IV)]. As the [S(IV)] drops, the rate will change to first order and then second order in [S(IV)].

For Nuchar-SN, when the initial concentration $[S(IV)]_o = 3.8 \times 10^{-4}$ M, the slow step has zero order dependence on [S(IV)]. The straight line in Fig. 1 can be represented by

$$[S(IV)]_z = [S(IV)]_o - \delta + k_z t, \qquad (1)$$

where $[S(IV)]_z$ is the S(IV) concentration attributable to this step and k_z is its rate constant.

The first step causes the decrease in [S(IV)] from $[S(IV)]_o$ to $[S(IV)]_z$. δ is the decrease in [S(IV)] due to the first step, defined as:

$$\delta + [S(IV)]_o - [S(IV)]_z \quad \text{at } t = 0. \qquad (2)$$

To investigate the first step, we have subtracted the contribution of the second, zero order step and plotted the logarithm of the difference ($[S(IV)] - [S(IV)]_z$) vs. time in Fig. 3. The straight line indicates that the first step has first order dependence on the difference between [S(IV)] and $[S(IV)]_z$. This means that the concentration of $Cx \cdot O_2 \cdot (S(IV))_2$ is higher during the rapid first step than it will be after the adsorption steps have reached equilibrium. This high $[Cx \cdot O_2 \cdot (S(IV))_2]$ could be due to either or both of these effects:

(a) The first step uses $Cx \cdot O_2$ that was formed from the gas-phase adsorption of oxygen before reactants mixed, and the initial $[Cx \cdot O_2]$ is higher than the equilibrium value.

(b) During the first step, the concentration of $Cx \cdot O_2 \cdot (S(IV))_2$ has not built up high enough to cause significant dissociation without reaction; i.e., before equilibrium is

established, the forward rate of the adsorption step to form $Cx \cdot O_2 \cdot (S(IV))_2$ is faster than the reverse rate to $Cx \cdot O_2 \cdot S(IV)$ and S(IV).

For RB1, Figs. 2 and 4 show that the reaction is first order in [S(IV)] throughout its course; i.e., there is no differentiation between the first and second step. This may mean that the third adsorption step never reaches equilibrium or that the reaction is so fast that the dissociation of $CxO_2 \cdot (S(IV))_2$ without reaction is unimportant. Either of these interpretations is consistent with first order dependence of the rate on [S(IV)].

Table 1 provides a summary of the rate data. The initial rate of reaction R_i, the first order rate constant k_1, and the zero order rate constant k_2 are given.

If carbon particles in polluted atmospheres have the range of activity represented by these two activated carbons, can this heterogeneous mechanism play an important role in atmospheric oxidation of SO_2 in water droplets containing soot? Using conditions representative of highly polluted urban atmospheres,[5] we have estimated the conversion time for [S(IV)] in two ways. First, $t_{0.95}$ represents the time necessary to reduce [S(IV)] from 3.80×10^{-4} M to 5% of this value, using

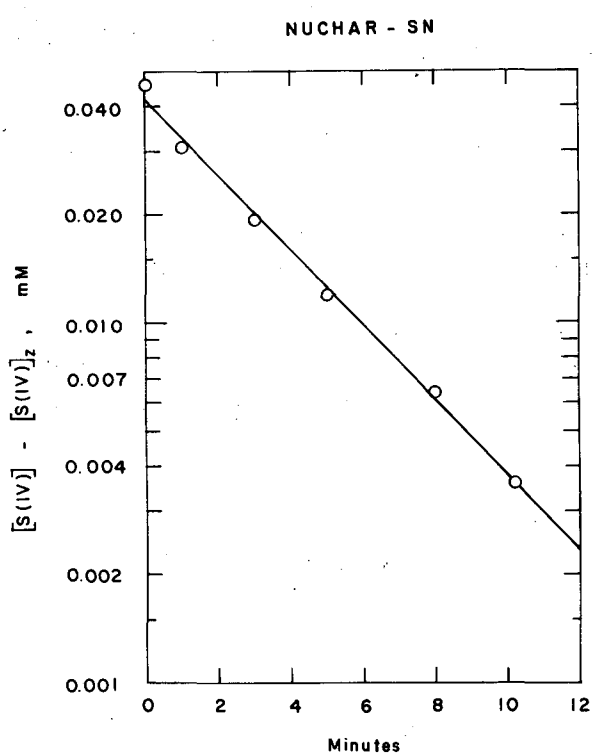

Figure 3. Semilogarithmic plot of the first step of the reaction for Nuchar-SN. (XBL 863-774)

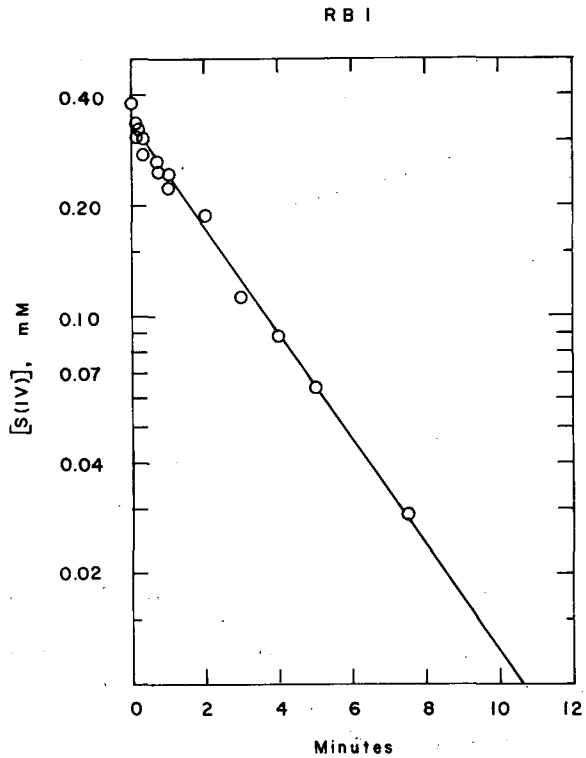

Figure 4. Semilogarithmic plot of the concentration of [S(IV)] vs. time for RB1. (XBL 863-773)

$$[S(IV)] = [S(IV)]_o - \delta(1 - \exp(-k_1 t)) + k_z t \quad (4)$$

for Nuchar-SN and RB1. For RB1 we used

$$[S(IV)] = [S(IV)]_o \exp(-k_1 t). \quad (5)$$

We also calculated the conversion time using the initial reaction rate R_i, the tangent to the curves of Figs. 1 and 2 at t = 0. This corresponds to the rate of reaction when the concentration of [S(IV)] is constant at its initial value, as occurs in water droplets that are in equilibrium with gaseous SO_2. The atmospheric conditions chosen are $[SO_2(g)] = 400\ \mu g\ m^{-3}$; $[C] = 100\ \mu g\ m^{-3}$; liquid water content (LWC) = $0.1\ g\ m^{-3}$; particulate sulfur to gaseous sulfur ratio, $S_p/S_g = 0.1$; and $[SO_4^{=}] = 6.25 \times 10^{-3}$ M. $[S(IV)] = 3.8 \times 10^{-4}$ M corresponds to the expected concentration at pH = 5 in equilibrium with $[SO_2(g)] = 400\ \mu g\ m^{-3}$.[9] R_i, $t_{0.95}$, and t_i are given in Table 1. For Nuchar-SN these times vary from 2 to 6 hours. For RB1 they are between 10 minutes and 1 hour. These results indicate that carbon could play a significant role in aqueous oxidation of SO_2 under such conditions.

Table 1. Rate data for oxidation of S(IV) in aqueous slurries of two activated carbons.

Carbon	R_i ($M\ g^{-1}s^{-1}$)	k_1 ($g^{-1}s^{-1}$)	k_2 ($M\ g^{-1}s^{-1}$)	$\frac{[SO_4^=]^a}{[S(IV)]_o-[S(IV)]}$	$t_{0.95}$[b]	t_i[c]
Nuchar-SN (1000°)	2.85×10^{-7}	4.00×10^{-3}	4.70×10^{-8}	0.44	1.9 hr	6.1 hr
RB1 (1000°)	1.85×10^{-6}	4.87×10^{-3}	—	0.62	10 min	56 min

[a] $[SO_4^=]/([S(IV)]_o - [S(IV)])$ is the fraction of the decrease in [S(IV)] that appears as $[SO_4^=]$ in solution for a reaction time of 20 minutes, when $[S(IV)] = 3.80 \times 10^{-4}$ M.

[b] $t_{0.95}$ is the time necessary to reduce [S(IV)] from its initial value of 3.80×10^{-4} M to 1.90×10^{-5} M, a reduction of 95%.

[c] t_i is the time necessary to produce $[SO_4^=] = 6.25 \times 10^{-3}$ M using the *initial* reaction rate. This assumes $[S(IV)] = 3.8 \times 10^{-4}$ M throughout the reaction, using ambient conditions reported in the text.

PLANNED ACTIVITIES FOR FY 1986

We will complete rate studies directed toward a better understanding of the reaction mechanism. The rate measurement will be extended to higher and lower initial concentrations of S(IV) · (10^{-3} to 10^{-5} M).

REFERENCES

1. Middleton, P. and Kiang, C.S. (1979), "The Relative Importance of Nitrate and Sulfate Aerosol Production Mechanisms in Urban Atmospheres," in *Nitrogenous Air Pollutants: Chemical and Biological Implications,* p. 269, D. Grosjean, Ed., Ann Arbor Science, Ann Arbor.
2. Harrison, R.M. and Pio, C.A. (1983), "Kinetics of SO_2 Oxidation over Carbonaceous Particles in the Presence of H_2O, NO_2, NH_3 and O_3<" *Atmos. Environ. 17*, p. 1261.
3. Calvert, J.G., *et al.* (1985), "Chemical Mechanisms of Acid Generation in the Troposphere," *Nature 317*, p. 27.
4. Chang, S.G., Toossi, R., and Novakov, T. (1981), "The Importance of Soot Particles and Nitrous Acid in Oxidizing SO_2 in Atmospheric Aqueous Droplets," *Atmos. Environ. 15*, p. 1287.
5. Bizjak, M., Hudnik, V., Hansen, A.D.A., and Novakov, T. (1986), *Evidence for Heterogeneous SO_2 Oxidation in Ljubljana, Yugoslavia,* LBL-20953 (submitted to *Atmospheric Environment*).
6. Dod, R.L., *et al.* (1986), *Sulfate and Carbonaceous Aerosols in Beijing, China,* LBL-20954 (submitted to *Atmospheric Environment*).
7. Gundel, L.A., Benner, W.H., and Novakov, T. (1985), "The Role of Surface Oxygen in S(IV) Oxidation by Different Carbons," in *Applied Science Division, Annual Report, FY 1984* (1985), LBL-18754, p. 8.
8. Brodzinsky, R., Chang, S.G., Markowitz, S.S., and Novakov, T. (1980), "Kinetics and Mechanism for the Catalytic Oxidation of Sulfur Dioxide on Carbon in Aqueous Suspensions," *J. Phys. Chem. 84*, p. 3354.
9. Martin, L.M. (1984), "Kinetic Studies of Sulfate Oxidation in Aqueous Solution," in *SO_2, NO and NO_2 Oxidation Mechanisms: Atmospheric Considerations,* p. 63, J.G. Calvert, Ed., Butterworth, Boston.

Sulfate and Carbonaceous Aerosols in Beijing, China*

R.L. Dod, R.D. Giauque, T. Novakov, W.H. Su,† Q.P. Zhang,†, and W.Z. Song†

Beijing air pollution is due principally to coal combustion with a relatively minor contribution from automotive sources. Coal is burned in a large number of individual furnaces and stoves as well as in a number of industrial plants. Because of the low height and large number of chimneys and stacks, the Beijing atmosphere, especially during cold periods, is dominated by local sources. Therefore, studies of pollutant chemistry at such a location may lead to a better understanding of the relation between secondary species such as aerosol sulfate and primary source emissions. Large urban centers such as Beijing, because of the lack of sufficient environmental controls and inefficient combustion technology, may contribute to atmospheric pollution disproportionately more than their per-capita energy consumption may suggest. Chemical characterization of such source-dominated atmospheres may also be useful in assessing their potential impact on the global environment.

ACCOMPLISHMENTS DURING FY 1985

Daily 24-hour filter samples of ambient aerosol particles (<12 μm diameter) were collected in a densely populated part of Beijing, using a sampler constructed at Lawrence Berkeley Laboratory. The sampling program was arranged to cover approximately three seasons—spring, summer, and winter. The spring samples were collected from March through the beginning of May, 1983. Summer samples were gathered during July, 1983; the winter samples, from the end of October, 1983, through February, 1984.

SO_2 measurements were made for a period each morning near the aerosol sampling site using a ThermoElectron Series 43 pulsed fluorescence monitor. In the absence of 24-hour averages, these were taken as estimates of the daily average SO_2 concentration. Total carbon was determined on the quartz filters by a combustion technique.[1] Temperature-programmed evolved gas analysis (EGA) was used to determine the primary carbon content.[2,3] Particulate sulfur and other trace element concentrations were measured on the cellulose ester filters by energy-dispersive x-ray fluorescence (XRF) spectrometry.[4]

A subset composed of 20% of the samples was analyzed by ion chromatography. Pieces of known area were taken from the quartz filters and extracted in water with sonication for 10 minutes. The extract was filtered and analyzed for anions using a Dionex System 12 ion chromatograph.

The agreement between sulfur concentrations determined by XRF on Millipore filters and sulfate on quartz filters determined by ion chromatography is shown in Fig. 1. The slope of the line is not significantly different from unity, with a correlation coefficient (r^2) of 0.98. This establishes not only that the sulfur in the aerosol particles is practically all in the form of sulfate but also that the parallel filter samples (on quartz and cellulose ester) do contain equivalent particle loadings and that artifact sulfate formation is not significant.

We have previously reported[5] that sulfate behavior in summer is different from that in winter. The summertime sulfate formation mechanism is more efficient, as evidenced by particulate to gaseous

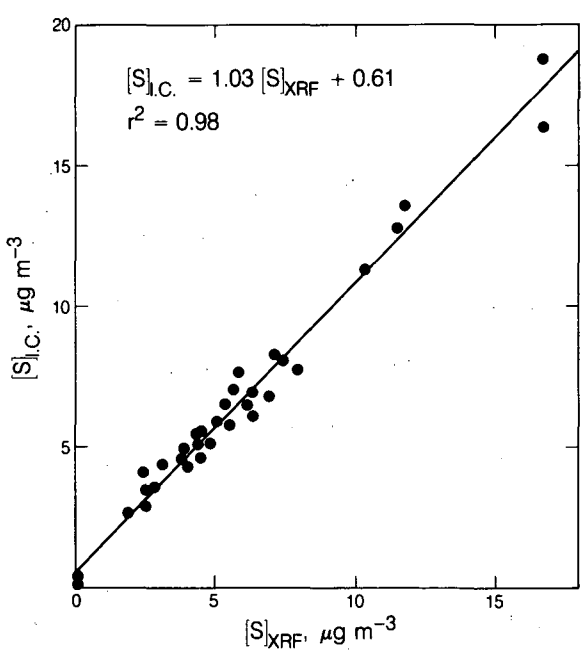

Figure 1. Particulate sulfate (as sulfur) determined by ion chromatography vs. total particulate sulfur determined by x-ray fluorescence for a representative set of samples—Beijing 1983/84. (XBL 859-8982)

*This work was supported by the Office of Energy Research, Office of Health and Environmental Research, Physical and Technological Research Division of the U.S. Department of Energy under Contract No. DE-AC03-76SF00098 and by the National Science Foundation under Contract No. ATM-8315442 and is a summary of a report submitted to *Atmospheric Environment* as LBL-20953.
†Institute of Environmental Chemistry, Academia Sinica, Beijing, People's Republic of China.

sulfur ratios twice those seen in winter. Nevertheless, the maximum absolute concentrations of sulfate are lower during the summer because the concentration of SO_2 available for oxidation is also low. Conversely, a relatively inefficient wintertime mechanism can produce high sulfate concentrations because the SO_2 concentrations are high.

An examination of supplementary meteorological information indicates that there may be a substantial increase in the S/C ratio when relative humidity exceeds 60%, suggesting that a heterogeneous aqueous process (or processes) is involved in the oxidation of SO_2. This finding is illustrated in Fig. 2, where the S/C ratios for the entire sampling period are plotted against the average 24-hour relative humidity. Qualitatively similar behavior has been observed in the United States by McMurry and Wilson.[6]

In Beijing during 1983/84, the relative humidities were markedly higher during summer than in winter or spring. Because high S/C ratios were also observed during summer, we conclude that the summertime SO_2 conversion mechanism could involve liquid water droplets as the medium in which the oxidation reaction takes place. During winter, low ambient humidity will limit both the aqueous-phase reaction time and the liquid water content. Such an explanation, although speculative, could explain the "quasi-primary" wintertime sulfate behavior.

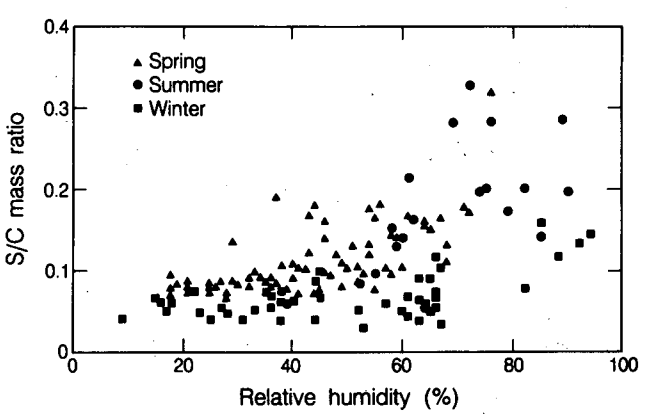

Figure 2. Particulate sulfur to carbon ratios as a function of daily mean relative humidity. (XBL 859-8983)

PLANNED ACTIVITIES FOR FY 1986

A new series of field experiments will be initiated to verify and expand on the results to date, collecting filter samples with better time resolution and with more complete meteorological and pollutant gas measurements.

REFERENCES

1. Huffman, E.W.D., Jr. (1977), "Performance of a New Automatic Carbon Dioxide Coulometer," *Microchem. J. 22*, p. 567.
2. Dod, R.L. and Novakov, T. (1982), "Application of Thermal Analysis and Photoelectron Spectroscopy for the Characterization of Particulate Matter," in *Industrial Applications of Surface Analysis,* L.A. Casper and C.J. Powell, Eds., American Chemical Society, Washington, DC, p. 397.
3. Novakov, T. (1981), "Microchemical Characterization of Aerosols," in *Nature, Aim and Methods of Microchemistry,* H. Malissa, M. Grasserbauer, and R. Belcher, Eds., Springer-Verlag, Vienna, p. 141.
4. Giauque, R.D., Garrett, R.B., and Goda, L.Y. (1979), "Determination of Trace Elements in Light Element Matrices by X-Ray Fluorescence Spectrometry with Incoherent Scattered Radiation as an Internal Standard," *Anal. Chem. 51*, p. 511.
5. Dod, R.L., Giauque, R.D., Novakov, T., and Su, W.H. (1985), "Aerosol Characterization in Beijing, China, 1983-1984," in *Applied Science Division Annual Report, FY 1984*, LBL-18754, p. 12.
6. McMurry, P.H. and Wilson, J.C. (1983), "Droplet Phase (Heterogeneous) and Gas Phase (Homogeneous) Contributions to Secondary Aerosol Formation," *J. Geophys. Res. 88*, p. 5101.

Size Fractionation of Black and Organic Particulate Carbon from Fires*

R.L. Dod, F. Mowrer, L.A. Gundel, R.B. Williamson, and T. Novakov

The concept of "nuclear winter" has been postulated with a number of assumptions regarding the smoke produced by post-nuclear secondary fires.[1] The general premise is that sufficient smoke may be generated and deposited in the stratosphere to cause a decrease in the incident solar energy reaching the earth's surface. Such a change in the net energy balance could potentially cause global cooling. Whether nuclear winter would occur in the aftermath of a nuclear exchange depends largely on the quantity of smoke generated, its distribution in the atmosphere, and the optical characteristics of the smoke produced.

Chemical kinetics during combustion are not understood in the detail necessary to predict smoke production. It has therefore been necessary to develop and use empirical methods to measure smoke generation.[2] Most of these methods have used optical techniques to quantify smoke production, with attenuation of light the principal measured parameter. None of the methods measured directly the size distribution or optical characteristics of smoke particles. A set of measurements of the black ("elemental") and organic carbon content of smoke particles from model forest fires has been reported.[3] The fuels were largely limited to pine needles, and no size segregation of the smoke particles was carried out.

We report here on a series of small-scale fire experiments that were conducted to measure as a function of particle size the black carbon, total carbon, and total mass of smoke particles produced in the burning of building materials such as those found in urban environments.

*This work was supported by the United States Department of Energy, Lawrence Berkeley Laboratory, under Contract No. DE-AC03-76SF00098 and Lawrence Livermore National Laboratory Director's Funds, under Contract No. W-7405-ENG-48.

ACCOMPLISHMENTS DURING FY 1985

Experimental Procedures

Sample Holders

Samples were tested in one of two orientations, depending on the nature of the product. The rigid building materials, including the Douglas fir, birch, and plywood samples, were tested in the parallel plate geometry; the flexible polyurethane samples were burned in the upward facing horizontal geometry.

The sample holder for the parallel plate geometry was adapted from the sample holder used for the proposed ASTM "Ease of Ignition" test apparatus.[4] The sample holders, constructed of brass bar stock, hold samples approximately 15 cm × 15 cm in face area. Two sample holders face each other across a 25.4-mm (1-in.) gap. Samples of varying thicknesses are accommodated and secured in the apparatus by four set screws at the back face of each holder that is used to hold test specimens in place. The specimen holders are bolted to the load cell platform.

Specimens tested in the horizontal orientation had their edges and bottom face wrapped in aluminum foil. These specimens were then placed on the load cell platform.

Burner

The source of ignition used for these experiments varied with the geometry being considered. The horizontal samples, which consisted solely of flexible polyurethane foam, were readily ignited by a match touched to the center of the exposed top sample face. The wood-based building materials tested in the parallel plate geometry were more difficult to ignite so a more severe ignition source, a methane burner, was used.

The methane burner consisted of a 13-mm (1/2-in.) stainless steel tube, which had 21 1.5-mm diameter holes bored along its length at intervals of about 6.5 mm. Methane from a gas cylinder was introduced into the tube at both ends to provide a flow rate of approximately 200 cm^3/s (25-SCFH). The burner tube was located centrally between the two sample holders at a distance of about 25-mm below the bottom of the two samples. The burner ports were located in the top of the tube so that the ignition flame extended up between the two samples. Smoke particle sampling was not conducted during the ignition phase.

Weight Loss Measurement Instrumentation

Mass loss measurements were made during each experiment. The samples and sample holders were placed on top of a weighing cell (Automatic Timing and Controls, Model 6005C, 1-lb dynamic range), which transmits a signal proportional to load to a chart recorder.

Exhaust System Assembly

The sample holder/weighing cell assembly was mounted on a platform, which was placed within a three-sided enclosure. This enclosure, constructed of sheet metal and measuring 0.91 m × 0.91 m × 1.22 m high (3 ft × 3 ft × 4 ft high), was topped by a pyramid-shaped reducer that terminated at the exhaust stack.

The exhaust stack was 100-mm (4-in.) diameter aluminum pipe. The length of the aluminum stack was 2.1 m. A 1.9-m length of 100-mm flexible duct connected the exhaust stack to the exhaust fan. This centrifugal blower produced flow rates of approximately 5.38 m^3/min (190 cfm) under test conditions, as determined by an orifice plate located in the aluminum stack.

Smoke Sampling Equipment

Smoke samples were taken from the exhaust duct approximately 3 m above the flame position. These samples were taken isokinetically through stainless steel probes at a rate of 14.2 liters/min (0.50 cfm).

One probe was connected to a 10-stage impactor for size fractionation of the smoke particles. The impactor (Pilat Mark 5 Source Test Cascade Impactor) (University of Washington) was fitted with aluminum foil collection plate inserts on the impaction plates. These inserts were cleaned before use by sonication in reagent grade acetone, followed by two rinses in the same solvent. The foils were then allowed to dry and equilibrate in a humidity-controlled atmosphere (51% R.H.) before their tare weights were determined. The afterfilter was quartz fiber (Pallflex 2500QAO) that had been fired in air at 800°C for 4 hours to remove all combustible carbon. The filters were humidity equilibrated as the foils before tare weights were determined. Following collection of a sample, the collection plate insert foils and afterfilter were removed from the impactor and returned to the humidity-controlled chamber. They were allowed to equilibrate for 24 hours before the weights were measured. The quartz and aluminum substrates used in this study are not optimum for mass determinations, but both are suitable for combustion carbon analyses. Replicate weighings showed that sample masses on the foils could be determined with a 1 σ error of 12 μg, and those on quartz with a 1 σ error of 20 μg.

The second sampling port was fitted with a filter stack unit composed of two stainless steel in-line 47-mm filter holders (Gelman Sciences Inc.). Each filter holder was loaded with a quartz fiber filter that had been treated as had the impactor afterfilter. Since we have shown that under ambient conditions the second (back-up) filter can contain carbon loadings equal to 10% of the loading (total) filter,[5] presumptively from adsorbed gaseous hydrocarbons, it was decided that this technique would allow a realistic correction for nonparticulate organic carbon in the filter samples.

Sample Analyses

The samples were analyzed by CO_2 evolved gas analysis, a thermal technique that has been shown to quantitatively determine the total carbon content of ambient aerosol particles. Additionally, the blackness of the sample was monitored for samples on quartz filters using the transmitted laser light intensity. This information was used to confirm the temperature at which CO_2 from the combustion of black carbon is evolved. We have further shown that for ambient and combustion source samples on quartz filters, black carbon can be determined by measurement of the change in laser light transmission as the sample is burned.[6] Black carbon from combustion sources has an extinction coefficient for visible light large enough to totally absorb incident light in less than 1 μm. To the extent that particles of black carbon exceed this physical (not aerodynamic) particle size, the content reported by this technique will be less than that actually present.

For each of the impactor and filter samples, total carbon was measured from the integrated area of the CO_2 thermogram, and black carbon was estimated from the area of the high temperature peak (Fig. 2). The high temperature peaks for these samples were identified as black carbon for the total filter and impactor afterfilter samples by the laser optical technique. For each of the thermograms, blank values were subtracted equal to either the CO_2 thermogram of a blank aluminum foil or the thermogram for the backup filter in the filter stack as appropriate. Solvent extraction followed by evolved gas analysis was carried out on some of the filter samples to confirm the black carbon determination.

The black carbon content of each of the filter samples was also calculated from the change in

transmission of incident laser light during the analysis. We applied an empirically determined relationship that we have determined for aerosol particles collected in ambient air and from combustion sources.[6]

Results

The summarized results from four test materials are shown in Figs. 1–4. For each particle size fraction, the total mass of collected smoke particles, as well as the total carbon and black carbon content of those particles, is shown. Organic carbon is in each example equal to the difference between total and black carbon. For each of the wood fuels, the preponderance of black carbon is present among the smallest size fraction collected, although organic carbon and noncarbon mass in the smoke particles may have a broader size distribution. Polyurethane foam also produced the majority of its black carbon smoke particles in the smallest size fractions, although it does show a broader size range for particles containing black carbon.

Agreement of the laser optical determined black carbon content with that determined by CO_2 evolved gas analysis is generally within 15% for the wood samples but differs by a factor of 2 for the polyurethane foam. The source of this relatively large disagreement may lie in the black carbon particle size distribution or in particle morphology. Assumptions regarding particle size and shape were made in the development of the laser transmission method; while these assumptions have proven valid for ambient particles and many combustion sources,

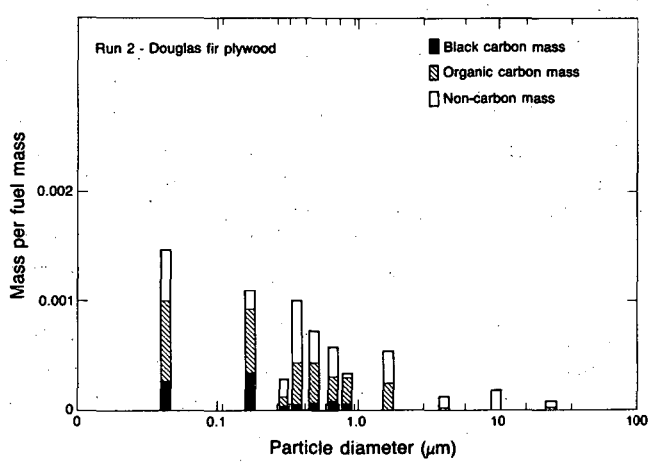

Figure 1. Smoke particle composition as a function of size. (XBL 8512-12819)

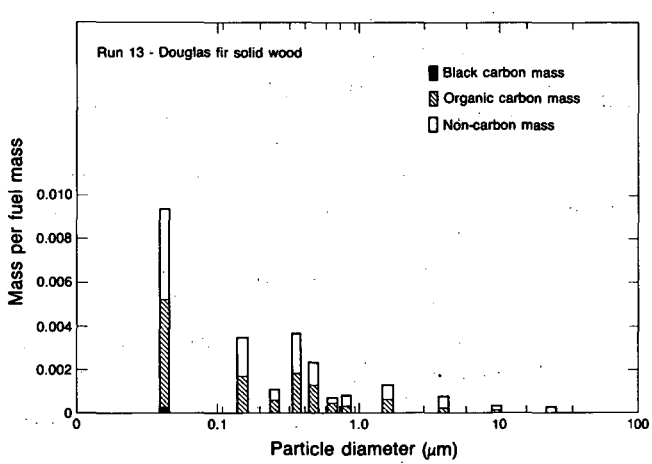

Figure 2. Smoke particle composition as a function of size. (XBL 8512-12820)

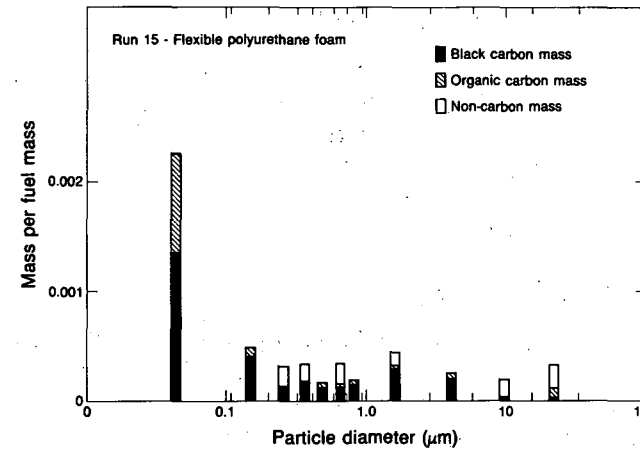

Figure 3. Smoke particle composition as a function of size. (XBL 8512-12821)

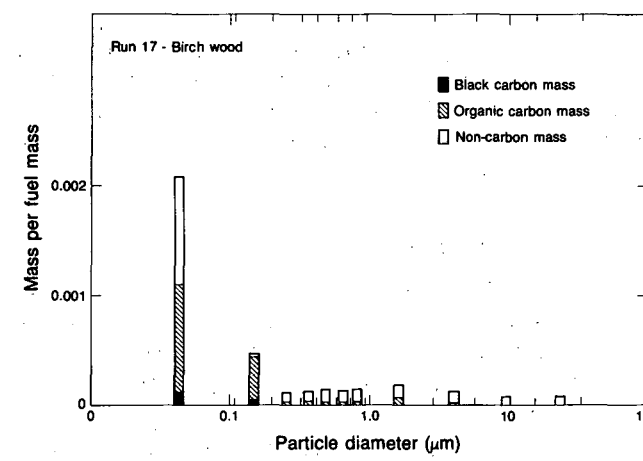

Figure 4. Smoke particle composition as a function of size. (XBL 8512-12822)

they may not hold for fuels such as polyurethane. Observation during individual tests are listed in Table 1.

Replicate combustion tests were carried out on all materials reported here, for a total of 18 test fires. Visual observations and weighings indicate that the results of these four tests are typical.

PLANNED ACTIVITIES FOR FY 1986

We intend to increase the size of our fires to test the transferability of our laboratory-scale results to larger conflagrations. We plan to control heat and oxygen at the fires to study smoke produced under conditions that might be found in a firestorm.

REFERENCES

1. Turco, R.P., *et al.* (1983), "Nuclear Winter: Global Consequences of Multiple Nuclear Explosions," *Science 222*, p. 1283.
2. Bard, S. and Pagni, P.J. (1981), "Carbon Particulate in Small Pool Fire Flames," *J. Heat Trans. 103*, p. 357.
3. Patterson, E.M. and McMahon, C.K. (1984), "Absorption Characteristics of Forest Fire Particulate Matter," *Atmos. Environ. 18*, p. 2541.
4. ASTM Committee E5. (1980), *Draft Standard Method of Test for Time to Ignition of Solid Materials by Flame Exposure.*
5. Dod, R., *et al.* (1980), "Investigation of Sampling Artifacts in Filtration Collection of Carbonaceous Aerosol Particles," LBL-10735, p. 8-35.
6. Gundel, L.A., Dod, R.L., Rosen, H., and Novakov, T. (1984), "The Relationship Between Optical Attenuation and Black Carbon Concentration for Ambient and Source Particles," *Sci. Total Environ. 36*, p. 197.

Table 1. Observations during individual tests.

Run 2 – Douglas fir plywood. The wood was ignited with a methane flame for 2 minutes prior to sampling. The wood burned with flaming for 4 minutes, followed by 2 minutes of smoldering combustion before sampling was terminated.

Run 13 – Douglas fir solid wood. After ignition with a methane flame, we found it difficult to maintain flaming combustion. Sampling was carried out for 4 minutes, followed by reignition using the methane burner. Sampling was then resumed for another 6 minutes. The particles were brown in appearance with evidence of liquid nature.

Run 15 – Flexible polyurethane foam. The foam ignited easily with a match at the center of the top surface of the sample. Flames then moved out in a circular pattern, melting and burning the foam. Sampling was for 6 minutes, the time required to completely burn the fuel.

Run 17 – Birch solid wood. Ignition was with methane and was repeated twice as the flame died. Sampling was not conducted during ignition periods. Total sampling period was 9 minutes, exclusively while wood flames were present.

APPLIED PHYSICS AND LASER SPECTROSCOPY RESEARCH*

(This article has been reprinted from the FY 1984 Annual Report.)

N.M. Amer,† S.-H. Chen, H. Dersch, A. Frova, R.W. Gerlach, W. Imler, M. Olmstead, A. Skumanich, D. Wei, and Z. Yasa

The research philosophy of our group is to develop and apply advanced laser spectroscopy and condensed-matter physics to energy-related problems. Lasers, with their high spectral purity and tunability, constitute an excellent probe of matter, and the advanced state of our knowledge of condensed-matter physics makes it possible to apply such knowledge to energy research. Areas of investigation that we are interested in include the development of novel laser spectroscopic techniques, the physics of photovoltaic semiconductors, semiconductor surfaces and interfaces, liquid crystals and their applications, and the detection of molecular and atomic species at the ultratrace level.

ACCOMPLISHMENTS DURING FY 1984

Laser Photothermal Measurements and Characterization

Laser photothermal spectroscopy employs the heating concomitant with the absorption of electromagnetic radiation to measure minute optical absorption coefficients (10^{-8}), to characterize nonradiative processes quantitatively, and to measure thermal properties of matter. This type of spectroscopy has been developed largely by our group here at LBL.

Spatially Resolved Photothermal Technique for the Investigation of Transport and Recombination in Semiconductors‡

The development of spatially resolved probes for the investigation of transport processes in semiconductors is of increasing interest. In principle, these methods should enable the study of such important phenomena as the interaction between macroscopic defects (e.g., dislocations) and carrier transport, as well as the fate of these carriers near interfaces. Typically, conventional methods integrate the measurement over the entire distance between the electrodes. Furthermore, the electrodes themselves may influence the results unless care is taken in configuring the experimental setup.

These limitations have motivated us to develop a noncontact, spatially resolved *in situ* probe of transport properties in semiconductors. The basic premise of the technique is the use of the heat associated with nonradiative processes (e.g., recombination of carriers) to deflect a focused laser probe beam (subgap energy) propagating *through* the semiconductor. The deflection of the probe beam is caused by a change in the refractive index of the sample, which is in turn governed by carrier diffusion and recombination (Fig. 1). A quantitative theory was developed to account for the observed signal.

The experimental setup employs the method of transverse photothermal deflection shown in Fig. 2. The sample used for our experiment was a *p*-doped Si ($\rho \approx 6\Omega\cdot$cm). One face of the crystal was mechanically polished and its surface treated with methanol to minimize surface recombination. The photocarriers were generated by an Ar^+ ion laser beam (5145

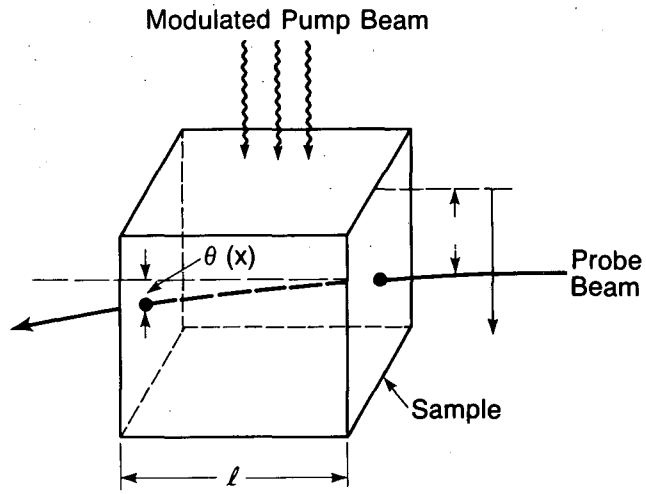

Figure 1. Principle of the scheme for spatially resolved photothermal detection of carrier transport and recombination in semiconductors. Such carrier processes govern the refractive index of semiconductors. A focused laser probe passing through a semiconductor sample will therefore be deflected by an angle, $\theta(x)$, that is governed by these processes. (XBL 8410-10944)

*Supported by the Director, Office of Energy Research, Office of Basic Energy Sciences, Materials Sciences Division of the U.S. Department of Energy under Contract No. DE-AC03-76SF00098, and by the Defense Advanced Research Projects Agency, Department of Defense under DARPA Contract No. 3343.

†Group Leader.

‡Complete version submitted to *Journal of Applied Physics*.

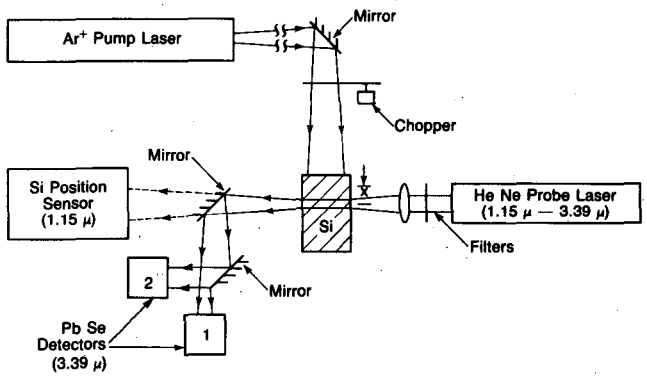

Figure 2. Experimental arrangement for deflection measurements. Two detection schemes are shown: for the 1.15 μ wavelength, a silicon position sensor was used; for the 3.39 μ wavelength, a mirror cutting the beam in two equal parts and two well-matched PbSe detectors were used. The signal was processed by a differential-phase-sensitive detector. (XBL 8410-10945)

Å), the maximum power density on the sample being ~500 mW/cm^2. This corresponds to a minority carrier density one order of magnitude smaller than that of the majority carriers. To probe the index of refraction gradient within the crystal, we used two different wavelengths (1.15 μ and 3.39 μ) from a HeNe laser focused to 30 μ. In the case of the 1.15 μ probe beam, the deflection was measured with a position-sensitive detector, while for the 3.39 μ beam two PbSe detectors were used, as shown in the figure. It should be pointed out that it is important to use an actual position-sensitive detector that gives good rejection of probe-beam intensity fluctuations. This is crucial for the 3.39 μ case where free-carrier absorption is significant.

The measurements were made at two probe-beam wavelengths: 1.15 μ and 3.39 μ. Before proceeding to describe the results, we note that the power dependence of the signal in the range of 30–500 mW/cm^2 was found to be linear within the experimental error.

Figure 3 shows the results obtained when the polished, methanol-treated face of the Si crystal was illuminated and the carrier transport probed at 1.15 μ. At this wavelength, the free-carrier dispersion is negligible, and one expects the $\partial T/\partial n$ term to be dominant. As can be seen, the two regions predicted by the theory are evident, and agreement with the theory is satisfactory.

It is interesting to note that by using the same set of parameters and varying the surface conditions of the Ar$^+$-illuminated surface (i.e., varying the surface recombination velocity s), we obtain good agreement between the theoretical predictions and the experimental results when the opposite unpolished and untreated face was illuminated (Fig. 4).

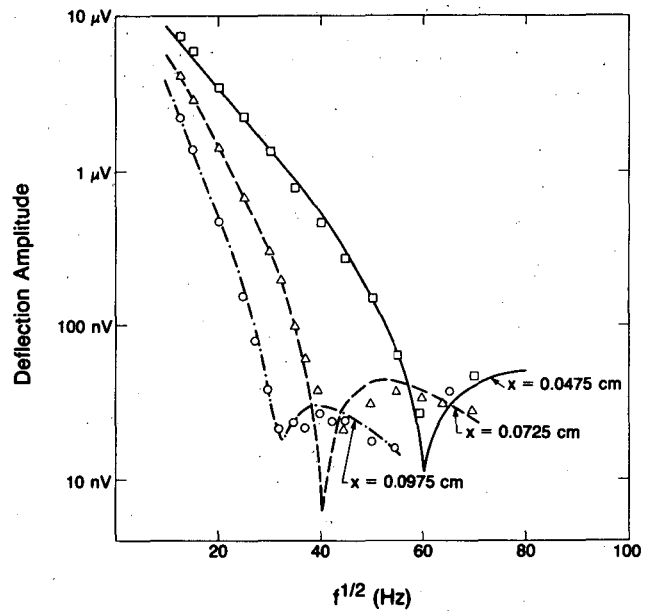

Figure 3. Comparison of the experimental measurements (points) with the theory (lines) for a well-polished treated surface of silicon crystal and a laser probe of 1.15 μ wavelength. (XBL 8410-10927)

To further test the theory, we probed the carrier transport with a 3.39 μ beam. At this wavelength,

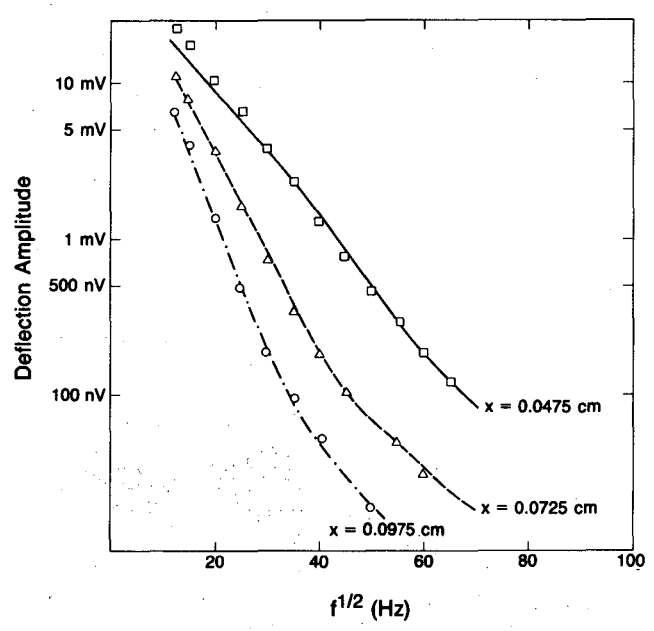

Figure 4. Comparison of the experimental measurements (points) with the theory (lines) for the unpolished surface of the Si crystal and a 1.15 μ laser probe. (XBL 8410-10924)

the free-carrier dispersion is not negligible. The free-carrier contribution (high frequency range) and the thermal contribution (low frequency range) are observed simultaneously. By using the preceding set of parameters to characterize the bulk and the illuminated surface, we obtain good agreement, as shown in Fig. 5.

*Photothermal Spectroscopy and Imaging of Gallium Arsenide**

The small rise in temperature associated with the absorption of electromagnetic radiation has provided the basis for a new spectroscopic tool generally known as photothermal spectroscopy. The advantages of this type of spectroscopy are its sensitivity and the relative ease with which it can be implemented.

The heating causes a change in the index of refraction of the medium surrounding the sample. This change is probed with a weak laser beam that is deflected as the index of refraction changes. Using phase-sensitive methods, the amplitude and the phase of the deflection can be readily measured with a position-sensitive detector (Fig. 6). Thus, by varying the wavelength of the optically exciting (pump) beam, the deflection of the probe beam is a measure

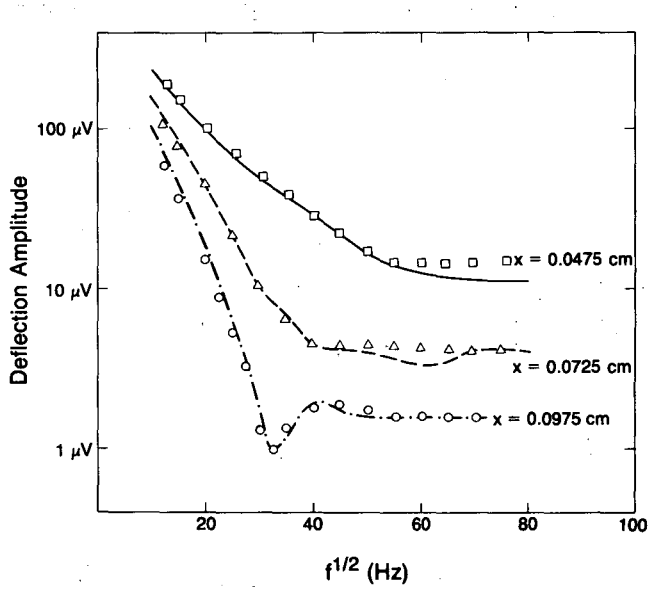

Figure 5. Comparison of the experimental measurements (points) with the theory (lines) for a well-polished treated surface and a 3.39 μ probe. (XBL 8410-10942)

*Complete version appeared in the *Proceedings of Third Conference on Semi-Insulating III–V Materials*, 1984.

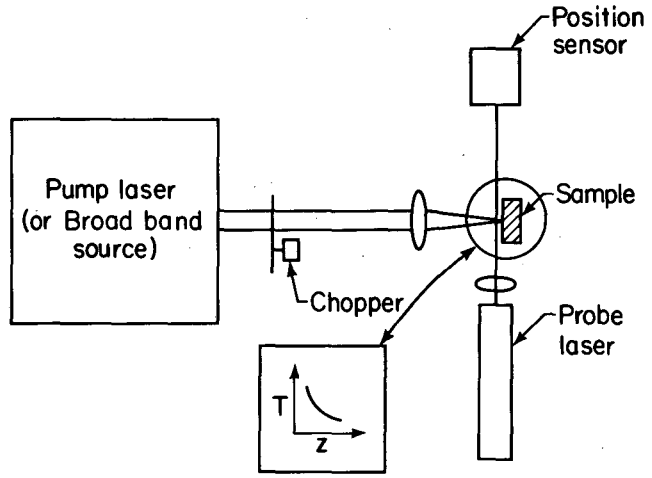

Figure 6. Schematic of experimental setup for photothermal deflection spectroscopy. (XBL 836-2666)

of the optical absorption. This type of spectroscopy is known as *photothermal deflection spectroscopy.*

The photothermal signal S is quantitatively related to the optical absorption coefficient in the following manner:

$$S = A[1 - \exp(-\alpha\ell)] \quad , \qquad (1)$$

where A is a constant that can be determined empirically, α is the optical absorption coefficient, and ℓ is the sample thickness.

Sensitivities of $\alpha\ell \approx 10^{-7}$ have been achieved, and the superiority of this technique in terms of sensitivity and flexibility has been demonstrated in a recent study of the optical properties of defects in amorphous semiconductors.

There exists a class of experimental conditions, however, for which photothermal deflection techniques are not suited in studying the optical and thermal properties of matter. Examples of such experiments are those that require vacuum and/or cryogenic temperatures. Such conditions are encountered in the study of surfaces and interfaces. Similar requirements exist for *in situ* and real-time characterization of thin-film semiconductors. These conditions motivated the use of optical heating in yet another manner. Since heating results in the expansion and buckling of the illuminated surface, a measurement of the surface displacement is a means of determining the optical and thermal properties of the illuminated solid. This small displacement can be detected in a variety of ways, the simplest of which is by reflecting a weak laser beam off the illuminated surface. As the surface is displaced upon being optically heated, the probe beam will be deflected from

its original reflection direction. This deflection is then detected with a position-sensitive detector (Fig. 7). Typically, $\alpha\ell$ of 10^{-6} are readily achievable. This version of photothermal spectroscopy is called *photothermal displacement spectroscopy.*

An important and characteristic parameter in photothermal spectroscopy is the thermal diffusion length L_{th}, which defines the depth from which the photothermal signal originates. L_{th}, which is also called the thermal wavelength, is given by:

$$L_{th} = (K_{th}/\omega\rho\, C)^{1/2} \quad , \qquad (2)$$

where K_{th} is the thermal conductivity of the sample, ω is the modulation frequency of the light, ρ is the density, and C is the heat capacity.

The modulation dependence of the thermal diffusion length is what is exploited to perform nondestructive depth profiling and imaging of solids. The higher the modulation frequency, the shorter the thermal length, and the closer to the surface the information is derived from. On the other hand, for low modulation frequencies, the photothermal signal is a probe of the bulk. Furthermore, by focusing the pump and probe beams, scanning microscopy can be performed. The achieved spatial resolution is a function of the size of the focal spot of the pump beam as well as the thermal diffusion length. Resolution to 1 micrometer has been attained.

We have performed scanning photothermal microscopy of semi-insulating LEC undoped GaAs wafers. The pump beam was an argon-ion laser focused to 1 micron on the wafer. The probe beam was a 0.5 mW HeNe laser. Both the deflection and the displacement schemes were used and yielded identical results. As can be seen (Fig. 8), both the phase and the amplitude of the photothermal signal exhibit small features that are due to the scattering of the thermal wave by thermal inhomogeneities in the wafer. By varying the modulation frequency, we were able to determine that these features lie on and near the surface. By analyzing the photothermal signal, using the theory we developed earlier, we were able to deduce that the inhomogeneities are arsenic-high inclusions. Our preliminary estimate of the degree of arsenic enhancement in these inclusions is approximately 14%, averaged over the 1-micron pump-beam diameter. To test the validity of our conclusion, scanned Auger spectroscopy (2-micron resolution) was performed on these inclusions. The Auger spectra verified our conclusion and gave an arsenic enhancement of 12%. Upon heating the wafers in a nitrogen atmosphere at 250°C, the arsenic-rich inclusions were no longer observed in the photothermal scans. This could be due to the arsenic diffusing into the matrix or evaporating out of the wafer.

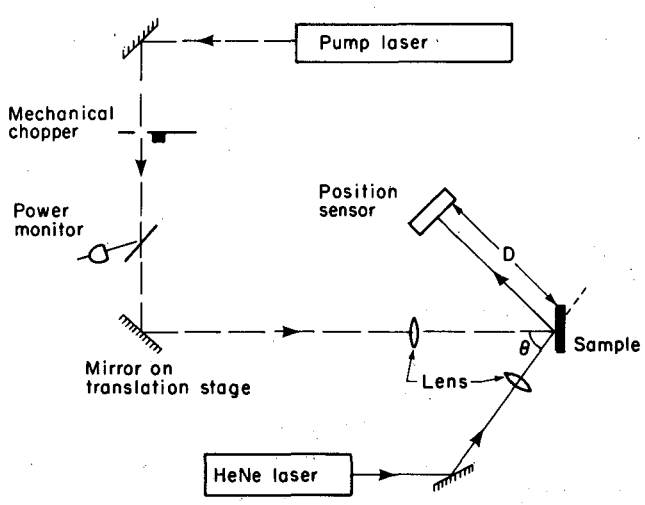

Figure 7. Schematic of experimental arrangement for photothermal displacement spectroscopy. (XBL 831-22)

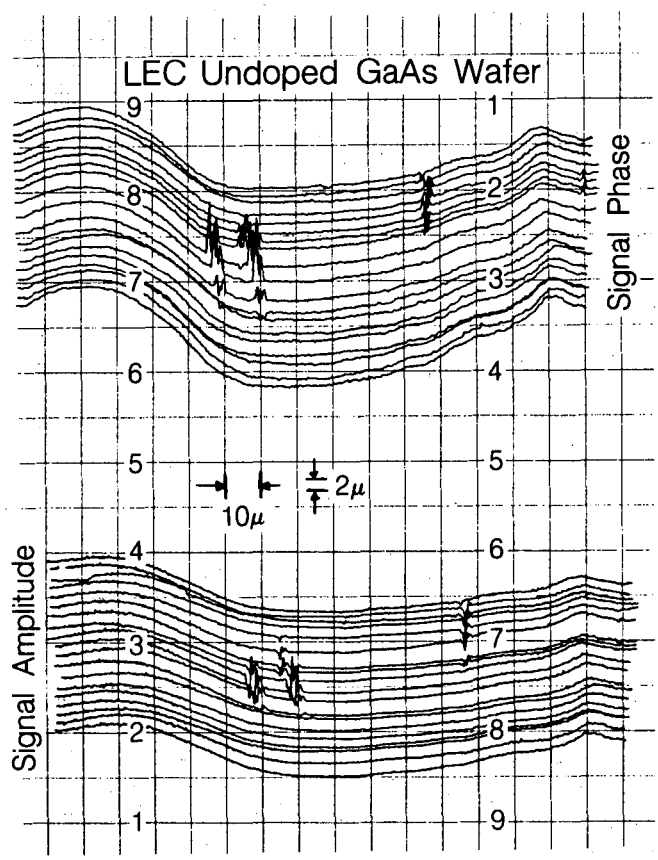

Figure 8. Spatially resolved photothermal scans of LEC undoped GaAs wafer. (XBL 845-1701)

We have also investigated the optical absorption spectra of undoped, chromium-doped, and silicon-doped GaAs crystals in the 0.5–1.5 eV range. In Fig. 9, we compare the photothermal deflection spectra of Cr- and Si-doped materials. As can be seen, the semi-insulating Cr-doped sample reproduces the main features obtained using conventional techniques. In addition, we observe a small peak at 0.5–0.6 eV, which we tentatively attribute to Fe impurities. The Si-doped sample exhibits a qualitatively different spectrum. The absorption coefficient does not drop at photon energies lower than 0.9 eV as is the case for the Cr-doped material. The spectra of two Si-doped n-GaAs samples are shown in Fig. 9. While both are from the same boule, sample A is from near the top of the boule, and sample B is from near the center. The larger thermal gradients and stresses expected near the top of the boule may account for the increased defect density in sample A.

In Fig. 10, we show the spectra of semi-insulating LEC GaAs and of the same material after being plastically deformed at 400°C. It is clear that the deformation increases the deep-level defect density. This is in agreement with results obtained by other methods such as electron spin resonance (ESR) and conventional infrared absorption.

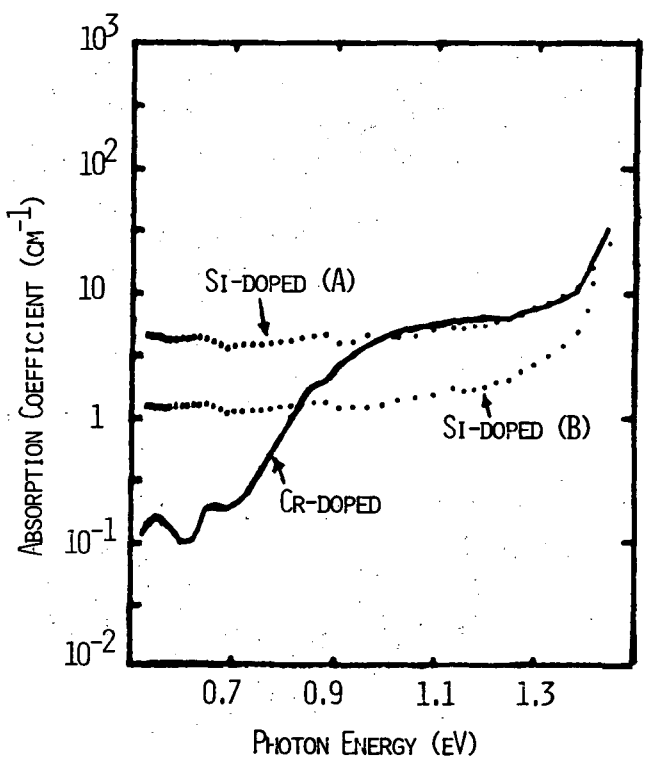

Figure 9. Photothermal absorption spectra of Cr- and Si-doped GaAs. (XBL 845-1702)

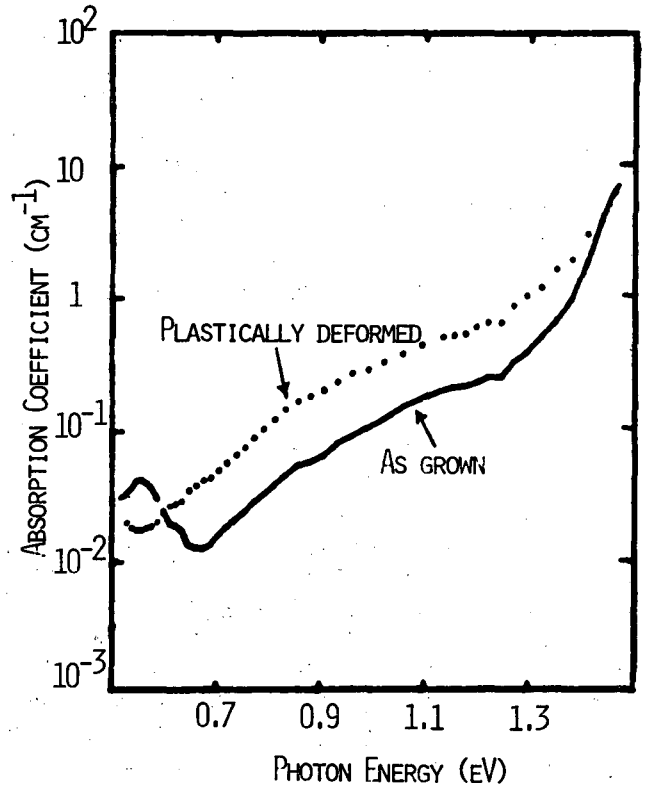

Figure 10. Photothermal absorption spectra of LEC semi-insulating as-grown and plastically deformed (at 400°C) GaAs. (XBL 845-1703)

*An Optical Approach to Thermopower and Conductivity Measurements in Thin-Film Semiconductors**

Conductivity and thermopower measurements are widely used to study the transport properties of semiconductors. The thermopower S is related to the Peltier coefficient Π, which, for conduction above a mobility edge E_c, may be written as:

$$ST = \Pi = \frac{kT}{e}\left[A + \ln\frac{N_0}{n}\right] . \qquad (3)$$

Since the quantities A and N_0 do not contain the mobility μ, the thermopower provides a measure of the carrier density n alone and is often applied to separate the product $n\mu$ in the conductivity $\sigma = en\mu$. Moreover, the sign of S directly gives the charge of the majority carriers.

A common problem with transport experiments is that properties of the metal contacts may influence the results. A current-voltage measurement reflects the conductivity only if the contact resistance is

*Complete version appeared in *Appl. Phys. Lett. 45*, p. 272 (1984).

much lower than the sample resistance. In the thermopower experiment, the metal contacts serve as reference for the thermovoltage, and contact properties are generally not considered to be a problem in the thermal equilibrium case, i.e., dark transport. In studying photoconductivity, however, thermopower measurements are much more difficult to perform because of the photovoltage, which may exceed the small thermovoltage. To understand the steady-state photoconductivity, it is essential to be able to distinguish between the effects due to change in carrier density and those due to changes in mobility. Photothermopower measurements are of particular importance in the case of hydrogenated amorphous silicon, since Hall effect data fail to give even the correct sign of the charge carriers. We have developed a technique to study transport properties that is based on the photothermal detection of Joule and Peltier heat generated by electrical currents. The method gives a spatially resolved profile of the conductivity along the film surface, thus allowing the detection of σ away from any metal contacts. The measurement of the Peltier heat rather than the thermovoltage avoids the influence of photovoltages on the signal. Preliminary results for the photo-Peltier coefficient of doped *a*-Si:H are presented.

All measurements were done on 1-micron-thick *a*-Si:H films deposited onto quartz substrates. An oscillating voltage, $U = U_0 \cos\omega t$ with frequency $f = 5$ to 10 Hz, is applied between two evaporated Al contacts in gap configuration with a spacing of 1 to 1.5 mm (Fig. 11). The heat generated by the current creates a temperature gradient perpendicular to the sample surface, which changes the index of refraction in the surrounding medium. This change is probed by a laser beam skimming the surface of the sample perpendicular to the current direction. To prevent changes in conductivity caused by the probe laser, an IR-laser ($\lambda = 3.39\ \mu$) is used, and the deflection is measured by a position-sensitive PbSe-detector. Both signals appearing at the reference frequency ($1f$ signal) and at twice the reference frequency ($2f$ signal) are monitored as the probe beam is scanned along the direction of the electric current (x direction). It has been demonstrated that the deflection is directly proportional to the heat generated within the interaction region between the probe laser and the sample. The Joule heat U^2/R (R = sample resistance) has a component oscillating at twice the reference frequency with amplitude $U_0^2/2R$. The differential Joule heat per unit length in the x direction is given by:

$$\frac{1}{\sigma}\left(\frac{U_0^2}{2R^2Q}\right),$$

where Q is a cross section of the sample. The $2f$ signal, therefore, provides a profile of the resistivity $1/\sigma$ along the x direction with a resolution determined by the beam diameter and the thermal diffusion length. Both quantities are on the order of 0.2 mm. The Peltier heat ΠI oscillates at the reference frequency with amplitude $\Pi \frac{U_0}{R}$ and appears centered and with opposite sign at each of the contacts.

In Fig. 12(a), the $2f$ signal, plotted as a function of x, is shown for a heavily phosphorous-doped sample. Both amplitude and phase are nearly constant, indicating that the conductivity is uniform throughout the sample. The strong decrease of the signal at both contacts shows that the contact resistance is negligible compared to the sample resistance. Furthermore, the time delay of the signal at the contacts, exhibited as a decreasing phase angle, indicates that the tail of the signal is caused by diffusing heat from the gap region rather than by contact properties. We found that the $2f$ signal is linear in the Joule heat over more than 3 orders of magnitude. This was verified both by varying the voltage at fixed resistance and by varying the resistance in photoconductive samples illuminated with different light intensities at fixed voltages. The minimum detectable signal corresponds to a total Joule heat of 10^{-5} W, which, for the given geometry and an electric field of 10^3 V/cm, corresponds to a lower limit of $10^{-6}\ \Omega^{-1}\text{cm}^{-1}$ for the conductivity.

The flat conductivity profile shown in Fig. 12(a) is not obtained in all samples. In Fig. 13, results for a sample with lower doping concentration are shown. It can be clearly seen that the major part of the Joule heat is generated at the contacts. It follows that the resistance of the film is much lower than indicated by a current-voltage measurement.

The magnitude and phase of the $1f$ signal of the heavily phosphorus-doped sample are plotted in Fig.

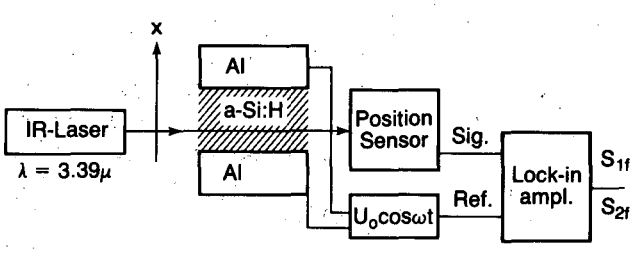

Figure 11. Experimental setup for thermopower and conductivity measurements on *a*-Si:H semiconducting thin film. (XBL 843-10190)

12(b). The signal has the predicted shape for the Peltier heat, with approximately symmetric peaks appearing at the contacts. The phase of the signal at the peak positions differs by 180°, indicating that the deposited heat has opposite signs at the contacts. Also shown is the phase of the $1f$ signal measured in a boron-doped sample, which at each contact is shifted by 180° with respect to the phosphorus-doped

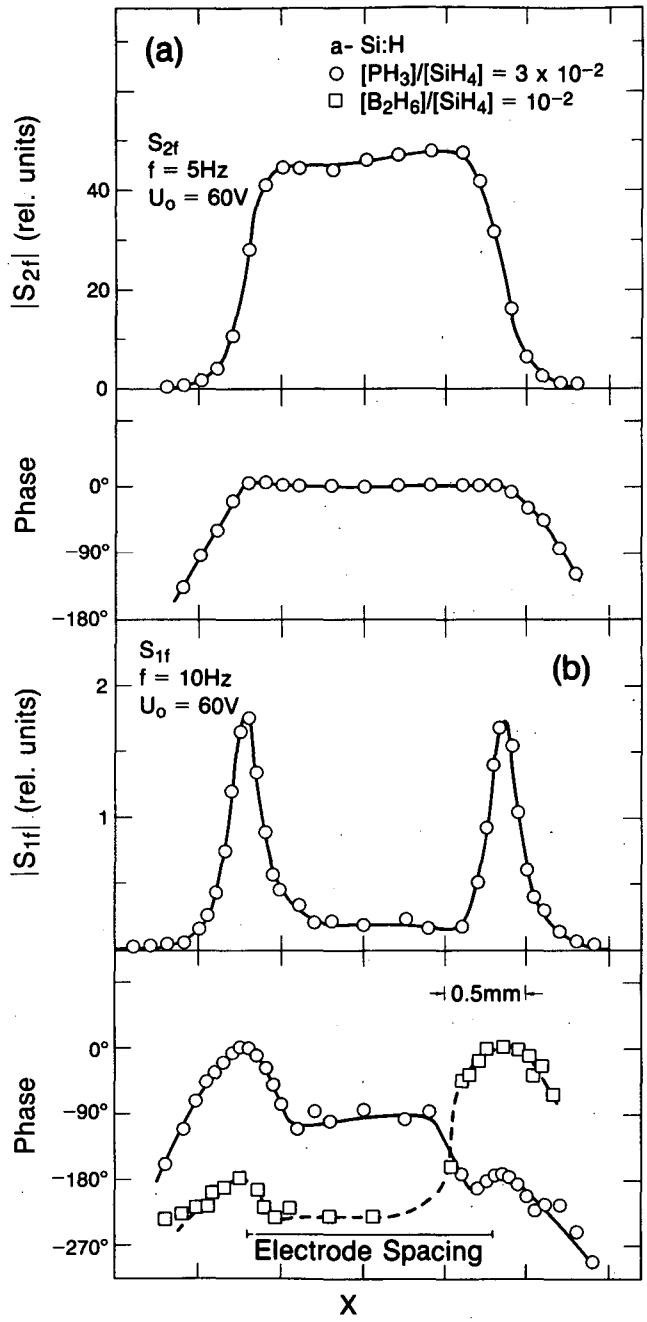

Figure 12. Magnitude and relative phase angle of (a) the $2f$ and (b) $1f$ signals for a heavily phosphorus-doped sample.
(XBL 843-10187)

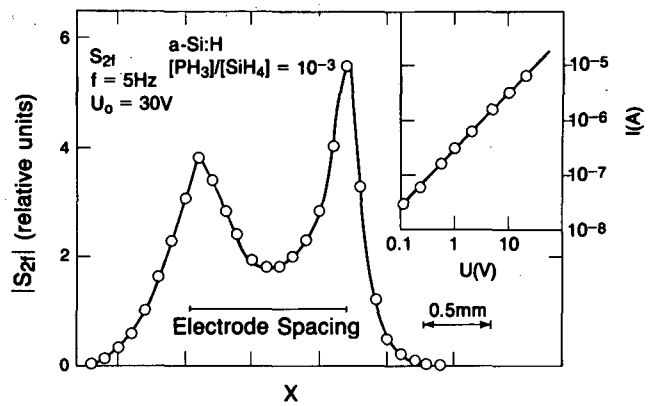

Figure 13. The $2f$ signal for a sample with non-ohmic contacts. Inset shows current-voltage characteristics.
(XBL 843-10184)

sample. This behavior reflects the change in sign of the Peltier coefficient as the conductivity is changed from n to p type. As in the case of the $2f$ signal, the phase decreases in the tails, which is attributed to heat diffusing from the peak position, leading to a time delay in the signal. The Peltier heat was found to be proportional to the current through the sample over more than 2 orders of magnitude. The Peltier coefficient Π can be calculated directly from the integrated $2f$ and $1f$ signals (S_{2f} and S_{1f}). These quantities are proportional to the total Joule heat $\left(\frac{U_0^2}{2R}\right)$ and Peltier heat $\left(\Pi \frac{U_0}{R}\right)$, respectively. To compare the signals quantitatively, we have chosen twice the frequency for S_{1f} than in the case of S_{2f} making sure that both quantities experience the same thermal relaxation. Dividing S_{1f} through S_{2f} and solving the equation for Π, we are left with:

$$\Pi = \frac{U_0}{2} \times \frac{S_{1f}}{S_{2f}} \quad . \tag{4}$$

Determining the sign of Π is equivalent to determining the phase angle, which corresponds to heating in phase with the applied voltage. This can easily be done by adding a dc-offset U_1 to the oscillating voltage $U_0 \cos\omega t$. Then, besides the signal from the Peltier heat, a second $1f$ signal due to the Joule heat appears with amplitude proportional to $(2U_1U_0)/R$. Comparing the phases of these two signals allows the determination of the sign of Π.

We have shown that the photothermal detection of electronic transport yields information about contact influences, macroscopic sample homogeneity, and Peltier coefficients of thin-film samples. Possible extensions of the method that are currently under

investigation include an ability to provide two-dimensional conductivity images of device structures and the separation of surface from bulk contributions to the conductivity.

*Heat Diffusion Solutions for the Nonresonant Spectrophone**

Most theoretical treatments of the nonresonant spectrophone have used as their starting point the standard inhomogeneous heat diffusion equation:

$$\rho_0 C_v \frac{\partial T'}{\partial t} = \kappa \nabla^2 T' + H \qquad (5)$$

where T' is the temperature disturbance, H is the heat released due to collisional deactivation of the optically excited molecules, ρ_0 is the density, C_v is the specific heat per unit mass at constant volume, and κ is the thermal conductivity. This equation neglects the work done on or by the gas in compression or expansion, respectively, and treats it as if it were a solid. A more proper equation of energy conservation for a gas, taking expansion and compression into account, is given by:

$$\rho_0 C_p \frac{\partial T'}{\partial t} = \kappa \nabla^2 T' + H + \frac{\partial p'}{\partial t} \qquad (6)$$

where p' is the pressure disturbance. When the cell dimensions are small compared to the acoustical wavelength, p' is constant throughout the cell, and, if one uses the ideal gas equation of state and the fact that the total mass of gas is conserved, one finds that p' is proportional to the volume integral of the temperature disturbance T'; if one assumes an $e^{-i\omega t}$ time dependence, one obtains the equation

$$\nabla^2 T' + \frac{i\omega\rho_0 C_p}{\kappa} T' - \frac{i\omega(\gamma - 1)\rho_0 C_p}{\gamma\kappa\pi R^2} \times \int_0^R T'(r')\, 2\pi r'\, dr' = -\frac{H}{\kappa}, \qquad (7)$$

where we have assumed an infinitely long cylindrical cell of radius R and assumed that H depends only on r, the radical coordinate, and neglected the microphone impedance correction.

*Complete version submitted for publication in *Journal of Applied Physics.*

We present here a general solution by a Green's function method and show that the pressure amplitude one obtains by integrating the temperature solution is:

$$p' = \frac{i(\gamma - 1)}{\pi R^2 \omega} \times \frac{\int_0^R H(r')\left[1 - \frac{I_0(kr')}{I_0(kR)}\right] 2\pi r'\, dr'}{1 + \left(\frac{2(\gamma - 1)}{\gamma k R}\right)\left(\frac{I_1(kR)}{I_0(kR)}\right)}, \qquad (8)$$

where $k = (-i\,\omega\rho_0 C_p/\kappa)^{1/2}$ and I_0 and I_1 are modified Bessel functions. We have also solved the heat diffusion Eq. (5) in the frequency domain for arbitrary $H(r)$ and obtained for the pressure:

$$p' = \frac{i(\gamma - 1)}{\pi R^2 \omega} \times \int_0^R H(r')\left[1 - \frac{I_0(k'r')}{I_0(k'R)}\right] 2\pi r' dr', \qquad (9)$$

where $k' = (-i\omega\rho_0 C_v/\kappa)^{1/2} = k/\sqrt{\gamma}$. The heat diffusion Eq. (5) tends to overestimate the temperature disturbance near the center of the cell and underestimate it near the walls, but these effects tend to cancel out in integrating to obtain the pressure, and thus it gives an excellent approximation for the pressure. In particular, both expressions (8) and (9) have identical limiting behavior at high and low frequencies. At low frequencies ($\omega << \kappa/\rho_0 C_p R^2$), both give

$$p' = \frac{p_0}{4\pi\kappa T_0} \int_0^R H(r')\left(1 - \frac{r'^2}{R^2}\right) 2\pi r'\, dr' \qquad (10)$$

At high frequencies ($\kappa/\rho_0 C_p R^2 << \omega << 3.83\, c/R$), both give

$$p' = \frac{i(\gamma - 1)}{\pi R^2 \omega} \int_0^R H(r')\, 2\pi r'\, dr'. \qquad (11)$$

Thus, the use of the heat diffusion equation for the photoacoustic effect in the nonresonant spectrophone is well justified; however, where the temperature and/or density solutions are needed, as in thermal lensing, photothermal deflection, etc., in finite-radius cells, the solution of Eq. (7) may be more appropriate.

*Photothermal Spectroscopy in Turbulent Media**

In the atmosphere, a propagating laser beam wanders due to the effect of turbulence. The larger turbulent eddies deflect the beam as a whole, and the smaller (<< beam diameter) turbulent eddies broaden the beam. Hence, after propagating in the atmosphere over a sufficient distance, a laser beam appears to have a long-term averaged diameter significantly greater than the short-term averaged beam spot that randomly wanders about a mean position with a frequency spectrum $\leqslant$ 1000 Hz.

In the application of photothermal deflection spectroscopy (PDS) for the measurement of small absorptions in the atmosphere, this turbulence-induced beam wander is the dominant source of noise because of the inherent sensitivity of the technique to variations in the beam position. A modulation scheme that minimizes this component of noise is considered to be the most effective solution. The following pulsed technique proved to be most effective with an $\alpha\ell \sim 10^{-4}$ detection level: In the typical geometry of a PDS experiment, a pulsed pump beam and a cw probe beam are used. The advantage of the high power of pulsed lasers is therefore available. The rapid thermalization following the pump absorption and the consequent stepwise deflection of the probe beam is detected by a lateral position sensor (LPS) with a bandwidth of ~100 Hz. Since the high-frequency signal from the LPS is independent of the low-frequency position of the probe beam, there is negligible influence from beam wandering on the signal detection process. Two samples are detected from the transient signal, at a separation of $\lesssim$10 μsec, one before and one after the pump pulse, and the process is repeated at the rate of the pump pulses for signal averaging. For times less than 100 μsec, turbulence is essentially stationary, so one can assume that there is no noise due to turbulence in the difference signal between the two samples. Note that the samples of the short-term-averaged probe beam are taken as it wanders on the LPS at low frequencies.

After each pump pulse, the imposed thermal gradient decays by heat diffusion. A pump repetition rate of $\leqslant$10 Hz allows sufficient diffusion. The primary effect of turbulence is to be observed in the overlap of the pump and probe beams. At each repetition of this process, the pump and probe beams have wandered to different positions (depending on the conditions of turbulence along the pathlength to the interaction region). Hence, the signal detected (the difference between the samples) is directly affected. However, the initial sample (before the pump pulse) yields information about the probe-beam position at the interaction region. Correlating this signal to the relative positions of the pump and probe at the interaction region, a normalization can be carried out. Since the pump beam also wanders, full correction is possible only if the pump-beam position is also monitored by a position sensor.

This technique accounts for the turbulence-induced beam wandering *before* the interaction region. The random deflections of the beam *after* the interaction region results in the loss of beam position information. The signal level before the pump pulse can only be correlated to the probe beam position at the interaction region probabilistically. This can be an important source of noise. An additional source of turbulence-induced noise is the variations in the beam diameters, which directly affect the signal. An analysis of these contributions of noise has been carried out in order to determine the smallest absorptions measurable under typical atmospheric conditions. Figure 14 shows a setup for a laboratory simulation. Experimental results have yielded a sensitivity of $\alpha\ell \sim 10^{-4}$.

Surfaces and Interfaces

Surfaces and interfaces play an increasingly important role in various technological applications.

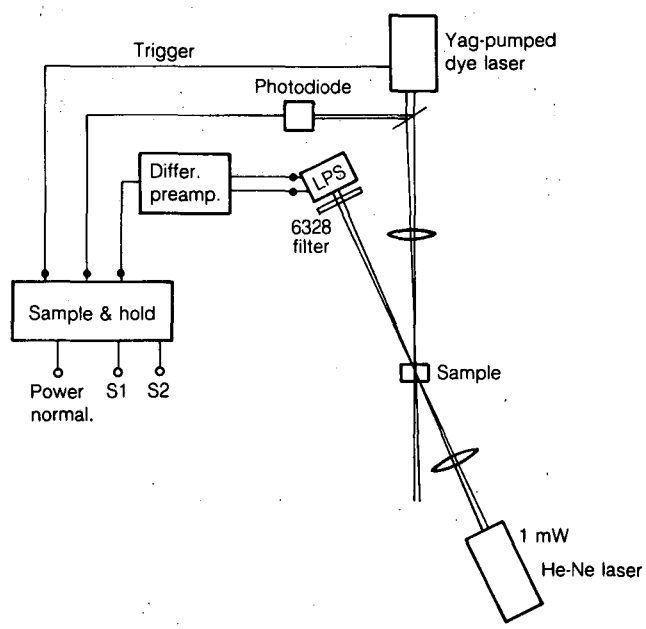

Figure 14. Experimental arrangement for a modulation scheme to minimize "noise" from atmosphere-caused beam wandering in photothermal deflection spectroscopy; LPS, lateral position sensor. (XBL 852-8815)

*Complete version to be submitted to *Applied Optics*.

Although the reactive nature of surfaces has been exploited for some time in processes such as catalysis, the exact nature and mechanisms responsible for their unique behavior remain to be ascertained. In this area of research, we employ photothermal spectroscopy to probe semiconductor surfaces and interfaces. Initially, our emphasis is on gaining a better understanding of the electronic properties of surface states through the investigation of their optical properties.

*Polarization and Temperature Dependence of Surface State Absorption in Si and Ge(111)**

The room temperature (111) cleavage faces of silicon and germanium are known to reconstruct to a metastable 2 × 1 unit cell, with period doubling along one of the three equivalent $<11\bar{2}>$ directions on the surface. The mechanism behind this doubling of the unit cell has been the subject of much inquiry, with numerous models proposed to explain the various experimental results. The polarization dependence of the surface optical absorption is a consequence of the overall symmetry of the dangling-bond orbitals and does not require exact knowledge of the atomic positions to allow comparison with a class of models. The angular dependence of the dipole matrix element is different for the various models, making the polarization-dependent dangling-bond absorption a crucial test of these models.

We have studied the (111)2×1 surface state absorption of both Si and Ge, using polarization-dependent photothermal displacement spectroscopy. In addition to investigating the room temperature cleaved surface, we have also monitored the temperature dependence of the surface absorption as it is changed during annealing of the Ge(111) surface from the 2×1 to the *c*-2×8 structure.

Polarization Dependence. The polarization-dependent dangling-bond absorption was measured using photothermal displacement spectroscopy. In brief, this involves the optical detection of the thermal expansion of a sample as it is heated by absorption of light. The change in slope of the surface due to local thermal expansion is detected through the deflection of a HeNe probe beam reflected from the sample. Among the advantages of this technique is the ability to measure surface absorption directly, without requiring a difference measurement between a clean and an oxidized surface.

Both Si and Ge (111)2×1 surfaces exhibit ~2% absorption of $[\bar{1}10]$ polarized light, peaked at ~0.46 eV for Si and ~0.50 eV for Ge. The polarization dependence of the absorption peaks for Si and Ge in single-domain regions are shown in Fig. 15. A $\cos^2\theta$ dependence with a maximum along $[\bar{1}10]$ can be seen for both Si and Ge. The silicon results are in agreement with recent polarization-dependent reflectivity measurements. There is no significant rotation of the pattern, with all measurements being within the experimental alignment error of $\sim \pm 5°$. The pattern was observed to change when areas of different or mixed domains were examined. It could always be fitted by:

$$\sum_{\beta_i=-1,0,1} a_i \cos^2\left(\theta + \beta_i \frac{2\pi}{3}\right) ,$$

with the a_i correlating to the observed LEED intensities of the different domains. Of the various models discussed below, this is consistent only with the π-bonded chain model for both materials. The surface absorption disappeared upon oxidation, as can be seen in Fig. 15.

Temperature Dependence. The Ge(111) surface converts from 2×1 to a *c*-2×8 structure upon mild annealing, and preliminary results of observing this phase transition via the polarization-dependent absorption as an order parameter are shown in Fig. 16. This particular cleave was not a single domain, but, by fitting the polarization dependence, it was determined that, at the measurement point, two domains were present in the ratio of ~12:1, with the primary absorption occurring for vertical polarization. The polarization of the incident light ($\kappa\omega$ = 0.48 eV) was alternated between vertical and horizontal during the annealing process, and the photothermal signal at the two polarizations is shown in Fig. 16(a). The spectrum and polarization dependence when half of the signal had been annealed away was indistinguishable from the original except in magnitude. The sample was then heated to 135°C, and as can be seen in Fig. 16, above ~105°C there was no significant polarization dependence. In the first cycle, the sample temperature was greater than 60°C, where the surface signal starts to diminish, for 40 minutes. In the second cycle, the time between the data points at 60°C and 105°C was 37 minutes.

Free carrier absorption can be seen contributing to the signal above room temperature. The surface

*Complete versions of this work appeared in *Phys. Rev. Lett. 52*, p. 1148 (1984); *Phys. Rev. B. 29*, p. 7048 (1984); and the *Proceedings of the 17th International Conference on the Physics of Semiconductors*, J.D. Chadi and W.A. Harrison, Eds. (Springer-Verlag, 1985).

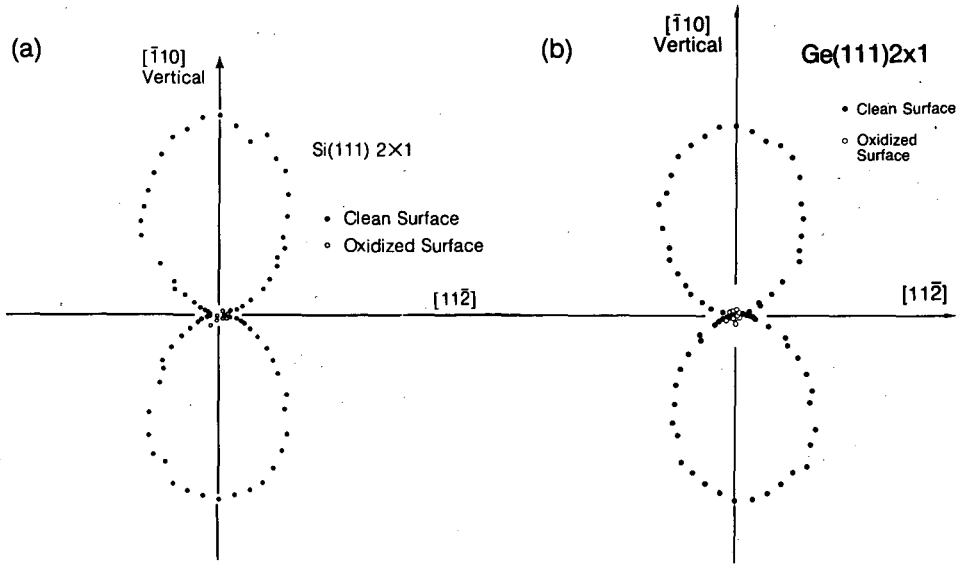

Figure 15. Polarization dependence of (111)2×1 peak absorption for (a) Si (0.46 eV) and (b) Ge (0.50 eV). [(a) XBL 8312-6936; (b) XBL 843-10183]

signal can be extracted as the difference between the absorption of light polarized parallel and perpendicular to [$\bar{1}$10], since the isotropic free carrier absorption adds equally to both polarizations [Fig. 16(b)]. It is also possible to separate surface and bulk contributions through the phase of the photothermal signal. The phase was observed to change smoothly from that of a surface absorption to the later arrival of the bulk signal between 60°C and 100°C. A vector separation of the two components was found to be consistent with the polarization data in Fig. 16.

The 135°C anneal resulted in a diffuse, "weak 8" LEED superstructure, and a subsequent 210°C anneal resulted in a sharp *c*-2×8 pattern. After the 210°C anneal, a small absorption at room temperature was detected at 0.48 eV. This absorption had a magnitude of ~0.06% and no polarization dependence. Although the signal-to-noise ratio was low, the phase seemed to indicate surface origin. If so, it would indicate that the *c*-2×8 structure has a small absorption at this energy. This is consistent with surface photovoltage (SPV) and photoconductivity (SPC) measurements, which find a signal at similar energies for the *c*-2×8 structure. The precise temperature dependence varies among cleaves, but the signal usually decays between 60°C and 130°C when the sample has been annealed just before cleavage. If the sample is not preannealed, the signal occasionally decays at 35°–60°C, and the resulting LEED pattern is 1×1, probably due to contamination.

The polarization-dependent optical absorption of cleaved Si and Ge (111)2×1 surfaces exhibit similar spectra, peaking at ~0.47 eV in Si and ~0.50 eV in Ge. This peak absorption has a strength of about 2-1/2% on flat, single-domain cleaves and is weaker on less homogeneous surfaces. The absorption is intrinsic to the 2×1 reconstruction and is the same as that previously seen with reflectivity, surface photovoltage, surface photoconductivity, and electron energy loss spectroscopies. The polarization dependence of this absorption was seen to follow $\sin^2\phi$, with maximum absorption parallel to [1$\bar{1}$0], and no absorption for light polarized along the period doubling [11$\bar{2}$] direction. This result was found to be consistent with only one of the many models proposed for these surfaces: a rebonded chain exhibiting a (1$\bar{1}$0) mirror plane. The size of the optical gap indicates a probable buckling of the π-bonded chain. This structural assignment is in agreement with data from a variety of other techniques as reported in the literature.

The polarization-dependent absorption is characteristic of the (111)2×1 surface and was used to probe the extent of the 2×1 phase during annealing and chemisorption. Monitoring of the absorption during a heating cycle similar to that in the stepwise annealing experiments showed additional decay in the 2×1 concentration upon reheating to a lower temperature than previously attained. This leads to the conclusion that the proximity of annealed

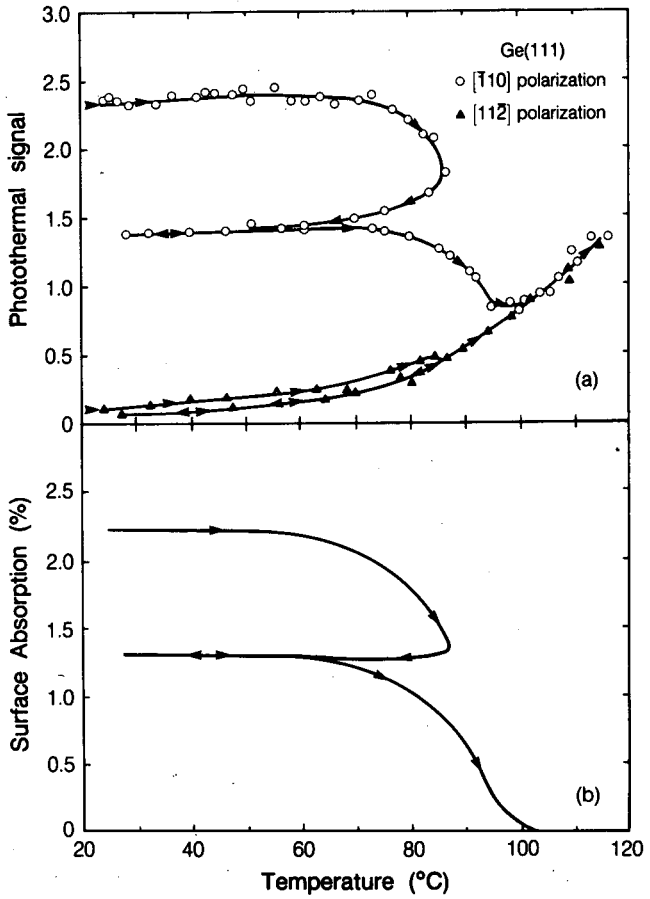

Figure 16. (a) Temperature dependence of photothermal signal from cleaved Ge(111). Sample is heated, cooled, and heated again. (b) Surface absorption. Difference between [$\bar{1}$10] and [11$\bar{2}$] signals in (a). (XBL 846-8488)

regions can lower the transition temperature of a given region of the surface. Preliminary experiments probing the temperature dependence of the surface optical energy gap showed little or no temperature dependence in the range of 300–450 K, contrary to the bulk gap dependence. This appears to support the buckled nature of the π-bonded chains, which would result in a strong interaction between the surface phonon and the dangling-bond states. Finally, these results have shown photothermal displacement spectroscopy to be a powerful new tool for surface studies, as well as for other applications that require remote sensing.

Amorphous Photovoltaic Semiconductors

Amorphous photovoltaic semiconductors, such as hydrogenated amorphous silicon (*a*-Si:H), hold promise for meeting Department of Energy cost and efficiency goals for thin-film solar cells prior to 1990. To achieve the higher conservation efficiencies required, it is necessary to better characterize the unique optical and transport properties of these materials. Photothermal spectroscopy can be used to elucidate the optical and electronic properties of *a*-Si:H. Of particular interest is the investigation of the optical properties near the so-called bandgap. By combining luminescence studies, photoconductivity, and optical absorption, a full and accurate characterization of the de-excitation of these photoexcited amorphous semiconductors can be achieved.

*The Effects of Dopants and Defects on Light-Induced Metastable States in Hydrogenated Amorphous Silicon**

An intriguing property of many amorphous semiconductors is that they exhibit metastable defect states. For both the chalcogenide glasses and *a*-Si:H, prolonged illumination creates defect states that disappear upon annealing. In the case of *a*-Si:H, these metastable states (Staebler-Wronski effect) alter various properties such as conductivity and luminescence. Yet, despite extensive research, they are still not well understood. Although silicon dangling-bond defects have been implicated, the question remains whether the apparent increase in the number of these defects is due to a shift in the Fermi level or to the creation of new defects upon illumination. Another significant issue is the connection between already existing (annealed-state) defects and dopants, and those defects induced by illumination. Using photothermal deflection spectroscopy (PDS), we have studied the optical absorption of the light-induced defects in *a*-Si:H. Since the measurement is insensitive to the position of the Fermi level, both the change in defect density due to illumination and the energy level of the defect can be determined.

Figure 17 shows that exposure to light enhances the gap-state absorption, whereas annealing restores the absorption to its original dark value. The enhancement is consistently reproducible when the illumination-anneal cycle is repeated several times. Previous work has demonstrated that the magnitude of gap-state absorption in *a*-Si:H provides a direct measure of the silicon dangling-bond-defect density, N_s. Using the same procedure for the change in optical absorption, we quantitatively determine the change in the defect density between the annealed and illuminated state, ΔN_s. For undoped material, ΔN_s is approximately $10^{16}\,\mathrm{cm}^{-3}$. By comparing the experimental absorption spectra with calculated spectra generated from density-of-states models, the defect energy level is determined to be ~1.25 eV

*Complete version to appear in *Physical Review B*.

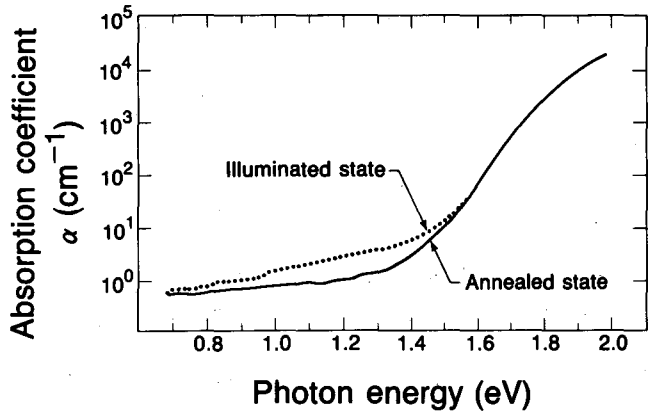

Figure 17. Effect of illumination on gap-state absorption of undoped *a*-Si:H. (XBL 847-10700)

below the conduction band. Since the energy of the defect and its cross section are identical to those measured for silicon dangling-bond defects, we conclude that the change in subgap absorption is due to silicon dangling-bond defects. Little or no change is seen in the exponential absorption (Urbach) edge.

Figure 18 shows that the light-induced defects scale with dopant concentration over a wide range of doping levels. The ratio $\Delta N_s/N_s$ is found to be independent of doping level to within a factor of 2. Thus, the effect is largest for high doping, unlike the case of conductivity changes. The fully compensated sample exhibited the least enhancement, $\lesssim 10^{15}$ cm^{-3} defects, which is an order of magnitude smaller than for the undoped material. For undoped material, the increase in defect density, ΔN_s, is constant to within a factor of 2 or 3, independent of the initial defect density, N_s, as seen in Fig. 19.

The results unambiguously show that the increase in defect density is not due simply to a shift in the Fermi level toward midgap upon illumination. A shift in the Fermi level, without any change in dangling bond defect density, results in less subgap absorption rather than the observed increase. Further, by successively increasing the dopant concentration, the Fermi level moves into the band tails so that after illumination it is still in a region of *smaller* dangling-bond density. Consequently, the effect should increase with increased doping, which is the opposite of what we observe. Since Fermi-level motion alone cannot account for the observed changes, we conclude that illumination creates new dangling-bond defects.

In terms of the mechanism for creating the dangling bonds, the results imply that the light-induced

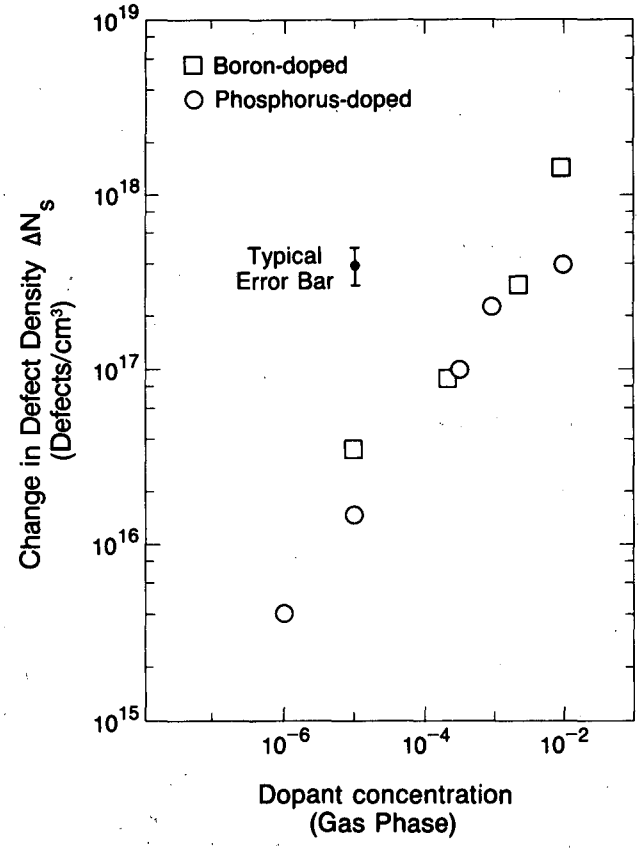

Figure 18. Dependence of the light-induced increase in defect density, ΔN_s, on dopant concentration. (XBL 836-2671)

defects do not result from breaking weak Si-Si bonds. One would expect ΔN_s to be relatively large for high-defect-density undoped material, which has substantial strain disorder (as evidenced by a broad Urbach edge) and consequently a large number of weak Si-Si bonds. Yet, for undoped material, ΔN_s is constant, *independent of disorder.*

Finally, there are several implications for solar cell fabrication. When air is let into the chamber during preparation, the cell exhibits an even larger efficiency drop after prolonged illumination, which again can be annealed away. The conclusion that light-induced defects are impurity-related is consistent with this observation. In addition, for *p-i-n* solar cells, illumination results in a fall-off in the blue response. Here, the doped outer layer will have the largest density of light-induced defects. Consequently, photons with short penetration depths will be strongly affected.

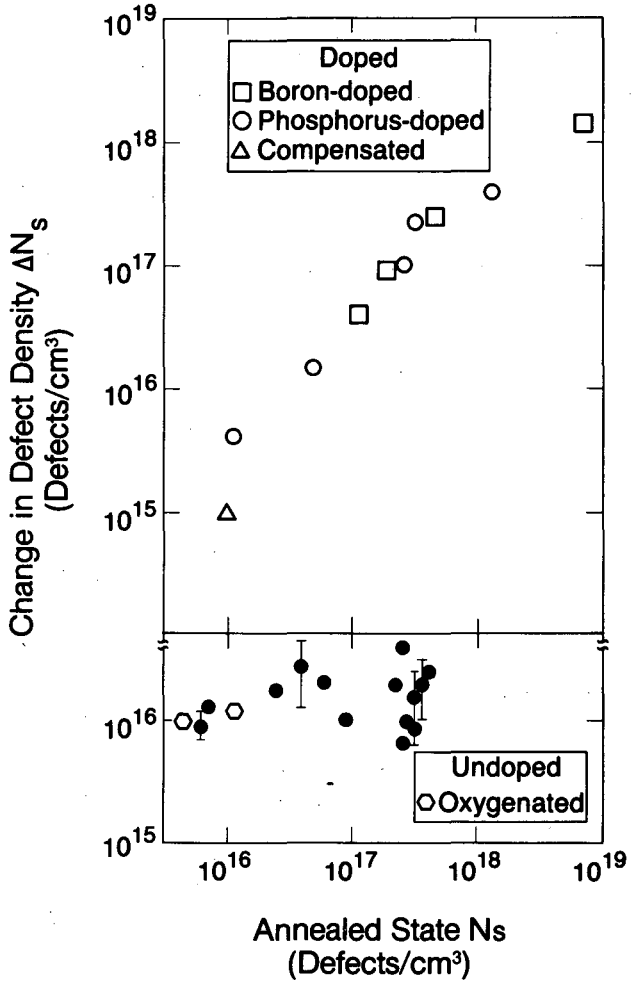

Figure 19. Dependence of the light-induced increase in defect density, ΔN_s on the initial defect density, N_s, for doped and undoped material. (XBL 847-10703)

*Urbach Edge and Gap States in Hydrogenated a-SiC and a-SiGe Alloys**

Considerable interest has developed recently in amorphous alloys based on hydrogenated amorphous silicon. Alloys with gaps smaller than *a*-Si:H—such as *a*-SiGe:H—are of interest in photovoltaic devices since they offer a better match to the solar spectrum (e.g., stacked cells). Alloys with gaps wider than *a*-Si:H—such as *a*-SiC:H or *a*-SiN:H—are also important in the construction of solar cells because they provide suitable window-layer materials. Moreover, *a*-SiC:H is promising for large-area white luminescence devices. Further interest in these alloys has resulted from the development of amorphous superstructures, which are developing into a major field of interest.

*Complete version to appear in *Solid State Communications.*

Most of these alloy phenomena are critically dependent on the spectral distribution of localized states—i.e., band tails and defect levels—inside the pseudogap of the alloy. For instance, the best SiGe alloys available to date have a density of dangling-bond defects that are a few times 10^{17} cm^{-3}. This results in a very poor photoconductive and luminescent behavior. Also, the SiC alloy, although exhibiting good room-temperature luminescence efficiency, shows a rapid drop in photoconductivity as the amount of carbon in the solid is gradually increased. Possible mechanisms behind this behavior include (1) the added compositional disorder of the alloy, which is reflected by a larger localized state density, and (2) the different energies and bond lengths of the elements, differences that can influence the formation of structural defects.

We investigated such effects when undoped *a*-Si:H, produced by glow discharge in silane, is increasingly mixed with either carbon or germanium.

The spectral distribution of the subgap states was determined by photothermal deflection spectroscopy (PDS), which allows detection of very weak optical absorption levels. The above-gap absorption was measured by direct transmission, using a Cary spectrophotometer. Typical absorption curves of the *a*-Si_xC_{1-x}:H alloys are shown in Fig. 20 for values of x between 1 and 0.77.

A remarkable result is that there is no appreciable variation in the density of defect states throughout the concentration range explored. This leads to two important conclusions: first, the presence of carbon has little effect on the existing structural defects, or on the bond passivation due to hydrogen; second, one can rule out the possibility that tail states are involved in the low-energy absorp-

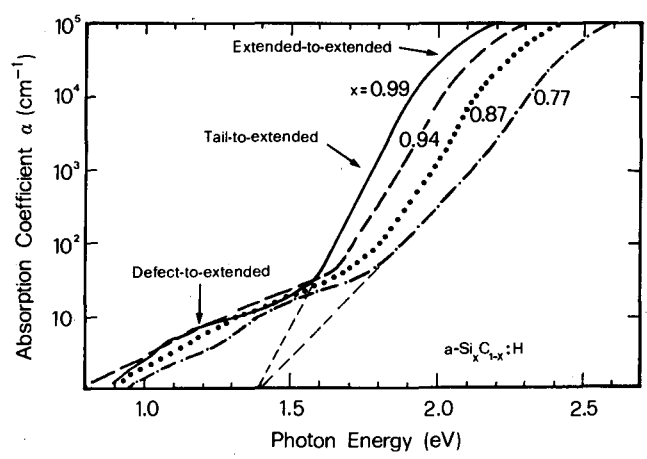

Figure 20. Absorption spectra of *a*-Si_xC_{1-x}:H alloys of different composition. (XBL 851-9704)

tion region because their increased density for larger C content would be reflected in stronger transition rates at those energies. The integrated absorption in the low-energy region is therefore a true measure of defect density.

Corresponding experimental results for the a-Si_xGe_{1-x}:H alloy are reported in Fig. 21. We shall stress only the significant differences. (1) The Urbach characteristic energy E_o increases with germanium content, but not as effectively as in a-SiC:H. Moreover, the tail is soon ill-defined for the reason discussed in (2) below, so that E_o is almost certainly overestimated. (2) The defect state density is higher than in a-SiC:H. It can be measured with some accuracy only for the lowest Ge content sample; its determination is otherwise made difficult by serious overlap with the Urbach tail. The values found are consistent with the silicon dangling-bond density found in the same samples by ESR. However, for $x \lesssim 0.60$, ESR predicts a higher density of Ge-related dangling bonds—10^{18} cm^{-3} and above. These states apparently are not optically active in the same energy range as Si dangling bonds but are closer to the gap. Figure 22 has been obtained by additively superimposing the Si and Ge dangling-bond spectra and the alloy bands. Because of their position in the upper half of the bandgap, above Fermi level, Ge dangling bonds can only be final states for transitions from the valence continuum. The minimum energy for these is about 1.1 eV, which already falls over the Urbach tail. This explains why in a-SiGe the latter is ill-defined for $x \leqslant 0.60$.

We now proceed to account for the Urbach tail broadening observed in the alloys in terms of compositional disorder. The appearance of an exponential tail below the fundamental threshold is due to

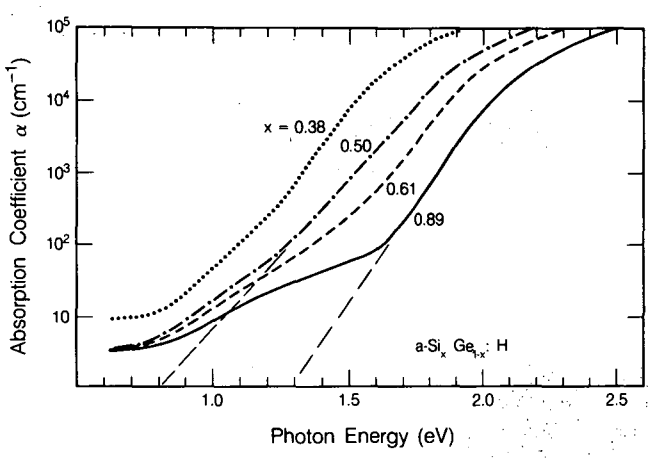

Figure 21. Absorption spectra of a-Si_xGe_{1-x}:H alloys.
(XBL 851-9705)

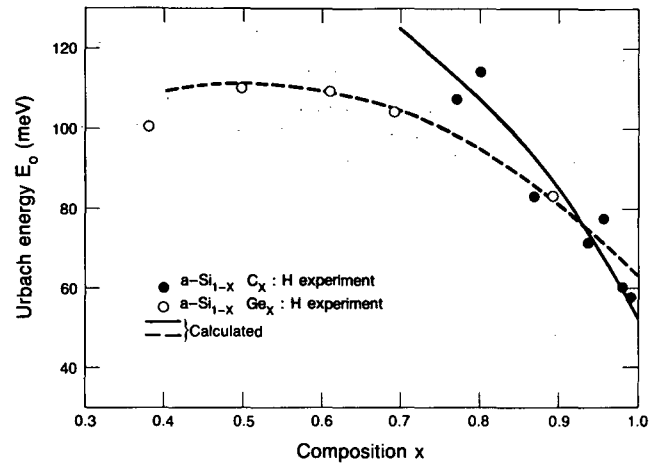

Figure 22. Urbach characteristic energy as deduced from PDS spectra and as calculated by a model assuming a Gaussian bandgap due to compositional disorder.
(XBL 8412-6457A)

the definition of local gap values over regions comparable to the phonon coherence length. The tail states are in a sense "pulled out" of the band continua. We extend the model to the alloys by taking a characteristic Urbach energy E_o that results from the sum of three contributions:

$$E_o = E_T + E_X + E_c$$

$$= K[\langle U^2\rangle_T + \langle U^2\rangle_X] + E_c \quad , \qquad (12)$$

where K is an appropriate quadratic deformation potential of the bandgap and the $\langle U^2\rangle$'s are the mean-square deviations of atoms from an ideally ordered configuration, respectively due to thermal and structural disorder. E_c is the added term from compositional disorder, due to potential fluctuations associated with the heterobonds. We take the $\langle U^2\rangle_T$ and $\langle U^2\rangle_X$ terms as constants; in other words, we assume that structural disorder and phonon effects are comparatively unaffected by the inclusion of carbon or germanium. A measure of the third term in Eq. (12) is then given by the gap spreading which stems from local fluctuations in the alloy composition. If these are Gaussian, as in the case of a-Si_xC_{1-x}:H, where the Si and C atoms are randomly distributed throughout the film without chemical ordering, Urbach tailing is expected. The probability of finding the local composition y in a cell containing n atoms for an alloy of given x, is:

$$P(y) \propto e^{-\frac{n(y-x)^2}{2x(1-x)}} \quad , \qquad (13)$$

whose full width at half maximum is:

$$\Delta = 2\,\frac{2\ln 2x(1-x)^{1/2}}{n} \quad . \qquad (14)$$

A measure of the bandgap spreading around $E_g(x)$ is given by:

$$\Delta E_g = \frac{dE_g}{dx}\,\Delta \quad ,$$

where (dE_g/dx) is the experimental x range. We assume $E \approx f\,\Delta\,E_g$, where f is a suitable coupling factor. We collect the prefactors into a single constant:

$$A = \frac{8\ln 2^{1/2}}{n} \quad ,$$

and try to fit the experimental data (Fig. 22) by means of the equation:

$$E_o = E_T + E_X + A[x(1-x)]^{1/2}\,\frac{dE_g}{dx} \quad . \qquad (15)$$

The best fitting is obtained for A = 0.106 for *a*-SiC and 0.192 for *a*-SiGe, and $E_T + E_X$ = 34 meV in both cases. If we take $f \approx 1$, i.e., the gap spreading does directly add to the Urbach energy, the A value gives $n \approx 150$ for the number of the sampled atoms in SiGe and $n \approx 490$ in SiC, which fit respectively in spheres of radii approximately 8 and 12 Å. These values are probably closer to the average localization length of the tail states than, for instance, to excitonic radii. The agreement of this model with the experimental data is particularly good.

Liquid Crystal Research

The liquid-crystalline state of matter is characterized by a spontaneous anisotropic order and by fluidity. The anisotropic order leads to anisotropy in the physical properties of the medium, and the fluidity makes it easily susceptible to external perturbations in the form of electric or magnetic fields, temperature, or pressure. In addition, we have demonstrated that certain gaseous organic pollutants change the liquid-crystalline structure. This change, which is readily detectable, was the basis for the development of a sensitive (10^{-6}) personal dosimeter for exposure to organic chemicals. Our current research focuses on the basic physics of the liquid-crystalline state to lay the groundwork for further applications of this class of materials.

*Two-Dimensional Phase Transition in Lyotropic Liquid Crystals**

The nature of phase transition in a monolayer of lecithin (DPPC) at the water-oil interface has been investigated using photon correlation spectroscopy (Fig. 23). We observe the following results:

Main Transition (LE/LC). The "main transition" is the large flat region shown in Fig. 24. We believe this region represents either a weak first-order or first-order phase transition. There clearly seems to be only one slope discontinuity, so the weak first-order transition seems more likely. This would be driven by chain melting and should not be of the Halperin-Nelson type because of the large entropy involved in the chain's degrees of freedom. The nearly zero slope is also consistent with a weak first-order transition. Presumably, the difference between air-water and oil-water isotherms is due to the size of the cooperative domains.

Second Phase Transition. We believe that we have also seen evidence of a second phase transition at lower areas. This may be related to the "pretransition" observed in bilayer stacks. This transition could possibly correspond to the elimination of a chain tilt in the region between the two transitions. It is also not likely to be of the Halperin-Nelson type since large viscosities are observed for pressures above the main (LE/LC) transition in lecithin monolayers.

We believe this is a real effect, since the flat region, the increase in transversal viscosity, and the decrease in slope all occur at the same region of the isotherm. Since the photon correlation is a local probe, a leak would not explain the increase in instrumental linewidth. Film collapse is unlikely because the size of the hysteresis indicates collapse did not occur until much later. Also, no evidence of a leak was observed during the course of the experiment. At very high pressures, above the second flat region, the high signal-to-noise ratio allowed rapid measurements, but total times of 5 minutes between points were still maintained since one could easily see that the film took ~3 minutes to "relax" to its final value.

*Complete version to be submitted to *Physical Review Letters*.

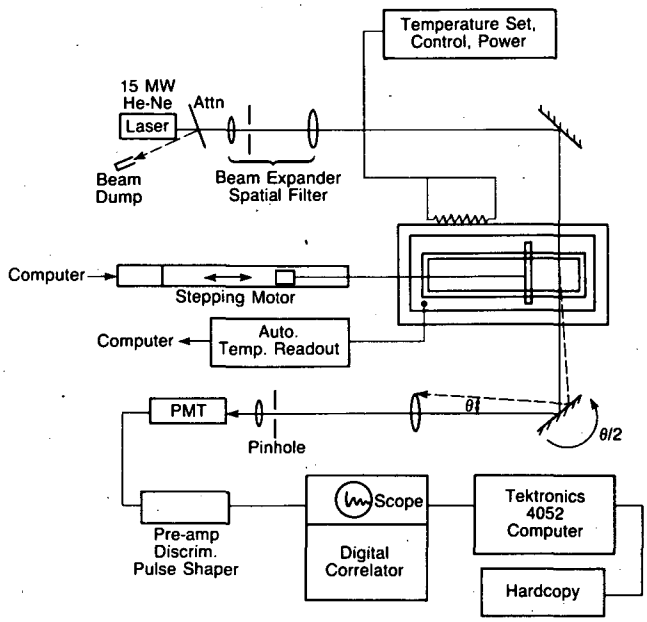

Figure 23. Experimental setup for a investigation of phase transition in a liquid-crystal monolayer (lecithin), using photon correlation spectroscopy. (XBL 846-10616)

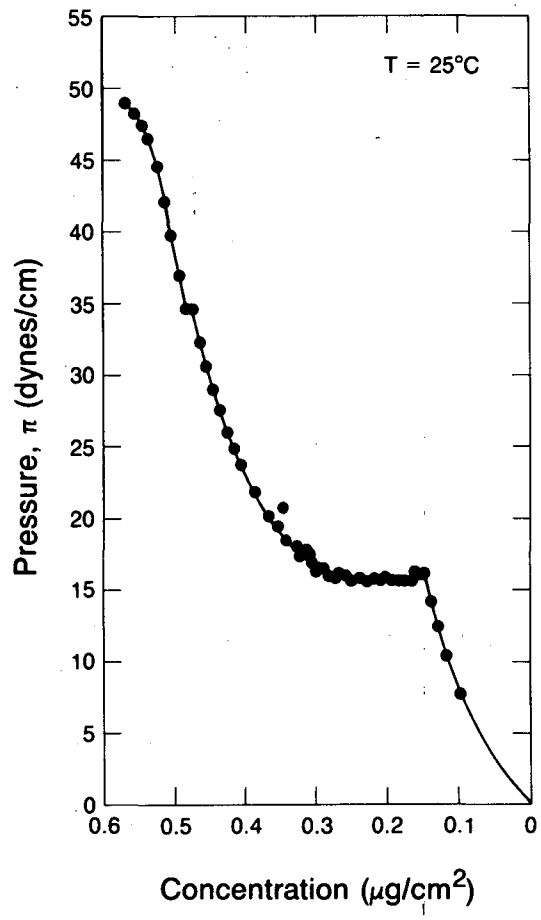

Figure 24. Lecithin (DPPC) isotherm at water-dodecane interface. (XBL 846-10640)

PLANNED ACTIVITIES FOR FY 1985

In laser spectroscopy, our goals will be to develop novel techniques and to exploit advanced applied physics concepts to the ultrasensitive measurements of minute optical absorption and vibrational spectra of gases, liquids, and solids. The emphasis will continue to be on unambiguous remote sensing of atmospheric constituents of laser photothermal spectroscopy and detection. Pulsed photothermal displacement spectroscopy will continue to be studied, and extensions of this technique for the study of liquids will be devised. Nonlinear photoacoustic and photothermal spectroscopy of gases will be initiated.

Research on amorphous semiconductors will focus on the physics of defects in hydrogenated amorphous silicon and germanium. The elucidation of the nature of the metastable photoinduced defects in amorphous silicon will continue to be of interest. A new research direction is the physics of photovoltaic devices.

Another relatively new activity is the investigation of the properties of semiconductor surfaces and interfaces. Processes at the liquid-semiconductor and gas-semiconductor interfaces will also be studied.

Finally, we will continue our research on laser physics and technology, with the goal of achieving widely tunable, high-average-power pulses a few femtoseconds wide. Another goal is to continue exploiting the waveguide laser configuration we have developed.

Treatment of an Oil Shale Retort Water by Stationary Fixed Biofilm*

J.B. Healy, Jr., G.W. Langlois, R.H. Sakaji, J.F. Thomas, and C.G. Daughton†

The process wastewaters from oil shale retorting originate from mineral dehydration, combustion, and input steam during pyrolysis of the embedded polymeric kerogen, a high-molecular-weight heterogeneous polymer. High concentrations of numerous organic and inorganic solutes are typically present. Although many of these compounds have been identified for a few waters (see references cited[1]), most have not. For the waters that have been studied only small portions of the spectrum of organic solutes have been found to be biodegradable during aerobic biological treatment.[1-3] Insufficient acclimated biomass, low individual-substrate concentrations, and chemical inhibition have been proposed as mechanisms responsible for the resistance of dissolved organic carbon (DOC) present in a range of process wastewaters.[1,2,4,5] All of these purported limitations could potentially be overcome by fixed-biofilm treatment (FBT), which has inherent advantages over homogeneous dispersed-growth systems.[6]

Few FBT studies that use small, lab-scale columns have been described in the literature,[7-9] and only two used actual industrial wastewater.[10,11] Several studies, however, were particularly relevant to retort water. With synthetic "wastewater" media, fixed biofilms are reported to be capable of removing low concentrations of aromatic compounds,[7-9] even in the presence of high ammonia concentrations.[10] These results suggest that the refractory aromatic amines present at low concentrations in ammonia-rich oil shale process waters could be removed in FBT reactors, especially when granular activated carbon (GAC) is used as a solid support.[12] We investigated the potential for FBT to remove a greater percentage of the organic solutes in Oxy-6 retort water (Occidental Oil Shale, Inc.) than has been reported for batch, dispersed-phase treatment.[1]

*This work was supported by the Assistant Secretary for Fossil Energy, Office of Oil Shale, Division of Oil, Gas, and Shale Technology of the U.S. Department of Energy under Contract No. DE-AC03-76SF00098.

†Sanitary Engineering and Environmental Health Research Laboratory, University of California (Berkeley), Richmond, CA 94804.

ACCOMPLISHMENTS DURING FY 1985

Removal of DOC from an oil shale retort water by stationary fixed-biofilm treatment was investigated using aerated, lab-scale columns operated on recycle mode.[13] The FBT columns were packed with one of four solid-support materials: (1) Calgon F-400 GAC, (2) spent shale, (3) raw shale, and (4) glass beads.

There are two major mechanisms by which fixed-biofilm columns can remove organic solutes from a wastewater: sorption onto the solid support and biodegradation. In practice it is difficult to determine the relative extents of these two processes for a complex waste because they occur simultaneously. Our initial objective was to pre-saturate the sorptive sites of the solid support so that any further DOC removals could be attributed to biological mechanisms. To ensure that the sorptive capacities of the columns had been exceeded, all columns were operated three times longer than the time estimated for saturation of the GAC, the support having the greatest sorptive capacity of the four packing materials. Removal of DOC by volatilization or sorption onto the pump tubing was less than 10% of the total DOC removed.

Sorption Equilibrium on GAC

A batch equilibrium experiment indicated that only three hours was required to reach 95% of sorptive equilibrium. Greater than 99% sorptive equilibrium was achieved between 15 and 24 hours; therefore the equilibrium time was assumed to be 24 hours. The sorptive equilibrium data were fitted to the Langmuir model for adsorption isotherms, and the sorptive capacity of GAC for the DOC in spent medium was determined to be 0.29 g/g.

Routine Operation of Columns

Hydraulic retention times of the columns after more than one year of operation under recycle mode were: glass beads, 1.4 hours; raw shale, 1.1 hours; GAC (fed raw medium), 0.8 hour. The hydraulic retention time for the GAC column that was fed spent medium and operated under single-pass mode was 0.2 hour. The above retention times appeared to be long enough to allow maximum biodegradation because doubling the retention times did not increase DOC removals.

Microbial growth in all of the columns and respective feed lines was extensive and most likely resulted from the high organic loading rate and presence of readily degradable fatty acids.[3] The development of thick biofilms occasionally caused clogging problems. Usually a simple disruption of the top portion of the column material was sufficient to reestablish flow. Clogging in the spent-shale column could not be remedied because the friable, combusted shale particles broke down into smaller sizes until they permanently clogged the passages. For this reason, the spent-shale column was abandoned.

Treatment of Raw Retort Water Medium

Fixed-biofilm treatment of raw medium effected limited removals of organic solutes. The percentage of DOC removed by the three columns ranged from 59% to 65% after 11 days of recycle operation (Table 1). The removals of DOC external to the fixed-biofilm columns (i.e., within the delivery and collection system) were less than 65 mg/L (5%). It is possible that biological removals were actually higher (approaching the total removal percentages of Table 1) because volatile and adsorbable compounds lost in the abiotic control system may have been biodegraded in the columns before being lost from the system. When external removal percentages were subtracted from total removal percentages in Table 1, the following minimum-biodegradation percentages (means) resulted: GAC/FBT, 60%; raw-shale/FBT, 56%; glass-beads/FBT, 54%; and batch shake flask, 52%. These corrected removals were biologically mediated because they were effected well after physical sorption removals had reached steady state. Although biological removals exceeded the 52% removal by 11-day batch cultures, a large portion of the DOC still resisted biodegradation.

The minimum-biodegradation percentages (means) were used for statistical comparisons. A one-way analysis of variance and subsequent significance testing showed that the GAC and raw-shale FBT columns removed significantly greater amounts of DOC than the batch culture ($P < 0.05$). In addition, the GAC column removed significantly greater amounts of DOC than the glass-beads and raw-shale columns ($P < 0.05$). There was no significant difference between the glass-beads colum and batch culture ($P > 0.05$). Removals by the raw-shale column were not statistically different from the removals by the glass-beads column ($P > 0.05$). DOC removals appeared to be synergistically enhanced when FBT was combined with a sorptive solid support, even when its sorptive sites were saturated (cp. GAC column versus glass-beads column).

As an indirect, rapid measure of organonitrogen compounds in the treated and untreated samples of raw media, headspaces were analyzed for the presence of these compounds. Many of the compounds were tentatively identified as simple alkylpyridines.[13] These were extensively removed by all of the FBT columns. These compounds did not disappear, however, from the headspace above an 11-day batch culture. Although a number of alkylpyridines are at least slowly biodegradable by acclimated cultures,[1] it was possible that some or all of the volatile alkylpyridines in the retort water medium were removed by volatilization or sorption onto the silicone tubing. Abiotic controls lost approximately the same amount of volatile organonitrogen compounds as the active

Table 1. Percentage of DOC removed from the hydrophilic (HpF) and lipophilic (LpF) fractions of raw retort water media by fixed-biofilm columns (operating under 11-day recycle mode) and by batch shake cultures.

Biological treatment conditions[a]	Percent DOC removed (n, rsd%)		
	HpF	LpF	Total
GAC[b]/fixed-biofilm	74 (4, 9.4)	57 (4, 19.8)	65 (14, 3.3)
Raw shale/fixed-biofilm	68 (3, 14.3)	56 (3, 22.6)	61 (11, 6.7)
Glass beads/fixed-biofilm	71 (4, 11.8)	50 (4, 28.0)	59 (14, 5.1)
Batch shake flask	71 (3, 2.9)	33 (3, 8.1)	52 (6, 5.1)

[a]Solid support material for fixed biofilms was previously saturated with organic solutes from raw retort-water media.

[b]GAC, granular activated carbon.

FBT columns. Retort-water medium treated with $HgCl_2$ and recycled for 11 days through an uninoculated glass-beads column produced a headspace (Fig. 1) that was typical of the headspaces obtained both for the FBT samples and for the abiotic control that excluded the glass-beads column. The total peak area for all peaks with retention times greater than 3 minutes decreased about 90% regardless of the type of FBT column or abiotic control conditions. The total removal of DOC by both abiotic controls was 5%.

A simple reverse-phase fractionation technique[1] indicated that raw Oxy-6 retort water contains roughly equal amounts of DOC in the polar (hydrophilic fraction; HpF) and nonpolar (lipophilic fraction; LpF) fractions, and as with batch culture, the majority of the DOC removed resided in the HpF (Table 1). The three FBT columns removed a similar amount of HpF-DOC as did batch culture (ca. 70%) (Table 1). In contrast, the increased total DOC removals by the FBT columns were at the expense of LpF-DOC; the columns removed 1.5 to 1.7 times as much DOC from the LpF (Table 1) as did the batch cultures. The percentage of LpF-DOC removed by the individual FBT columns increased in the same order as the percentage of total DOC removed (glass beads < raw shale < GAC). This same order also held for the relative decrease of the characteristic brownish color of the Oxy-6 retort water and UV absorbances. This color, in a variety of oil shale process wastewaters, is attributed to the presence of refractory aromatic amines in the LpF.[1]

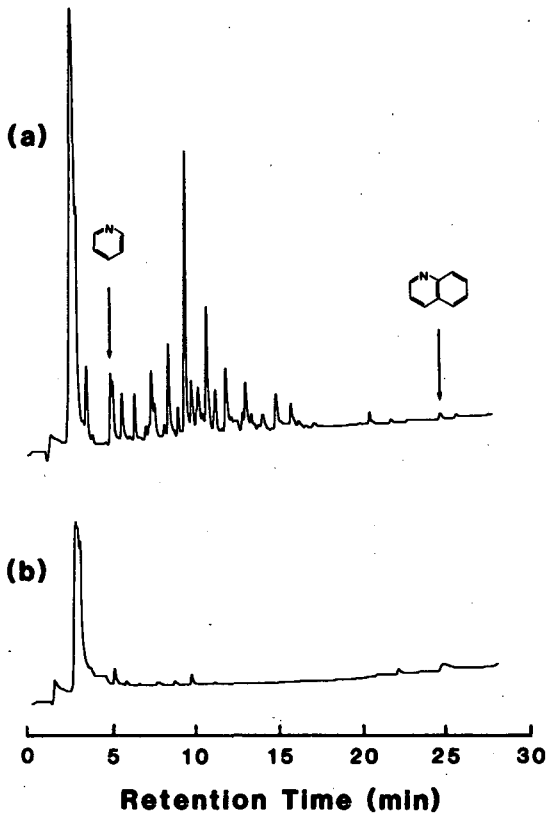

Figure 1. Gas chromatograms (flame thermionic, N-selective detection) of headspace over raw medium (Oxy-6 retort water) treated with 200 mg/L $HgCl_2$. Time 0, (a). After 11 days of recycle through glass-beads column, (b). Arrows mark positions of pyridine and quinoline, used for calculating retention indices. (XBL 8511-4771)

Despite abiotic losses of volatile nitrogenous compounds (Fig. 1), organic nitrogen measurements indicated that many less-volatile nitrogenous compounds (e.g., hydroxylated alkylpyridines and quinolines) remained after all of the biological treatments. Of the initial 88 mg/L of nonpolar organic nitrogen, 53 mg/L remained after treatment with the GAC column; 68 and 64 mg/L remained in the raw-shale and glass-beads columns, respectively. Batch shake cultures removed less than 5% of nonpolar organic nitrogen. Molar carbon-to-nitrogen ratios for the LpF fraction after any of the biotreatments ranged from 6 to 7, a range consistent with the presence of simple alkylpyridines and quinolines.

Even though the GAC-packed FBT column probably selected for a greater diversity of microbial niches, the column only increased the extent of DOC removal to 60% compared with 52% removals achievable in dispersed-phase batch cultures. The incomplete DOC removals and long treatment times in FBT columns suggest that FBT may be unsuitable for economic waste treatment. In addition, the FBT columns treating raw medium had the significant drawback of clogging.

Treatment of Spent Retort Water Medium

To avoid disruptions of the biofilm by clogging or from switching reservoirs in recycle mode, a GAC-packed FBT column was fed spent medium in single-pass mode. Since all of the readily degradable DOC in the spent water had been previously biooxidized during its production,[13] the remaining DOC was not expected to support a biofilm sufficiently thick to cause clogging. The spent medium was amended to 2% (vol/vol) with raw medium to provide about 10 mg/L of readily degradable fatty acids. This would meet the minimum requirements for a sparse biofilm. Bouwer and McCarty[7] supported a biofilm in the same size column with only 1 mg/L of acetate. The fatty acids could also have served as cosubstrates for organisms capable of degrading aromatic amines.

The GAC-packed FBT column fed spent medium was operated under single-pass mode for one year to ensure that the GAC sorptive sites had been completely saturated with spent-medium DOC. The adsorption capacity predicted by the Langmuir equation and a calculated first-order rate constant[13] were used to generate a theoretical breakthrough curve for the GAC spent-medium column. The effluent DOC concentration at breakthrough was defined to be 5% of the influent concentration, and the effluent concentration at exhaustion was defined to be 95% of the influent concentration.

The data collected during the first year of operation and the theoretical breakthrough curve for the GAC/spent-medium column are presented in Fig. 2. The volume of waste treated at exhaustion was 1.2 liters per gram of GAC. If biodegradation indeed were accounting for removal of a portion of the DOC, however, then saturation may have required a much longer time than estimated from the equilibrium data. Discrepancies have been observed[12] between observed saturation times and theoretical estimates. Furthermore, one research group believes that significant biodegradation did not occur in their GAC column until after saturation had first occurred.[9] Under our treatment conditions, 3.3 liters per gram of GAC were treated to ensure that saturation had indeed been achieved before DOC removals were attributed solely to biodegradation.

After one year of treatment under single-pass mode, the GAC-packed FBT column consistently removed, on average, 14% of the DOC from the spent medium (Fig.2). This removal was attributed to biodegradation because the replicate measurements were made well after sorptive removals had presumably reached a steady state. This contrasts with previous attempts to remove additional DOC from spent medium using batch cultures,[1] all of which have failed. Switching the GAC/spent-medium column to 11-day recycle mode after a year of single-pass operation did not significantly increase the DOC removal. Although this FBT column was able to remove some of the refractory material remaining after batch treatment of raw medium, the combined DOC removal (62%) remains as low as the removals by fixed-biofilm treatment in a single treatment step (Table 1).

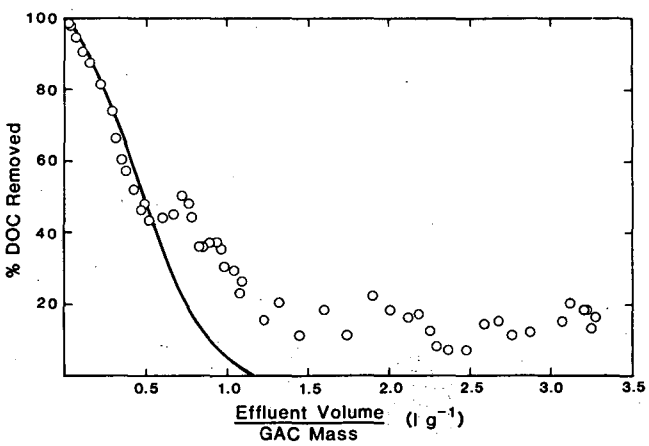

Figure 2. DOC removal from spent medium (Oxy-6 retort water) by a fixed-biofilm/GAC column operated under single-pass mode for one year; total cumulative volume of 150 liters of spent medium was treated by 44.8 grams of GAC. The theoretical removal of DOC by sorption (solid line) onto the GAC solid support was modeled from calculations made with data from adsorption isotherm experiments. (XBL 8511-4770)

REFERENCES

1. Healy, J.B., Jr., Langlois, G.W., and Daughton, C.G. (1985), "Biooxidation of Organic Solutes in Oil Shale Wastewaters," *Water Res. 19*, p. 1429.
2. Dobson, K.R., Stephenson, M., Greenfield, P.F., and Bell, P.R.F. (1985), "Identification and Treatability of Organics in Oil Shale Retort Water," *Water Res. 19*, p. 849.
3. Rogers, J.E., *et al.* (1981), "Microbiological Degradation of Organic Components in Oil Shale Retort Water: Organic Acids," *Appl. Envir. Microbiol. 42*, p. 830.
4. Healy, J.B., Jr., Jones, B.M., Langlois, G.W., and Daughton, C.G. (1983), "Biotreatment of Oil Shale Wastewaters," in *Sixteenth Oil Shale Symposium Proceedings*, J.H. Gary, Ed., Colorado School of Mines Press, Golden, CO, p. 498.
5. Jones, B.M., Sakaji, R.H., and Daughton, C.G. (1982), "Physicochemical Treatment Methods for Oil Shale Wastewater: Evaluation as Aids to Biooxidation," in *Fifteenth Oil Shale Symposium Proceedings*, J.H. Gary, Ed., Colorado School of Mines Press, Golden, CO, p. 581.
6. Stratton, R.G., Namkung, E., and Rittmann, B.E. (1983), "Secondary Utilization of Trace Organics by Biofilms on Porous Media," *J. Am. Water Works Assoc. 75*, p. 463.
7. Bouwer, E.J. and McCarty, P.L. (1982), "Removal of Trace Chlorinated Organic Compounds by Activated Carbon and Fixed-Film Bacteria," *Envir. Sci. Technol. 16*, p. 836.
8. Li, A.Y.L. and DiGiano, F.A. (1983), "Availability of Sorbed Substrate for Microbial Degradation on Granular Activated Carbon," *J. Wat. Pollut. Control Fed. 55*, p. 392.

9. Suidan, M.T., Siekerka, G.L., Kao, S.-W., and Pfeffer, J.T. (1983), "Anaerobic Filters for the Treatment of Coal Gasification Wastewater," *Biotechnol. Bioengng. 25*, p. 1581.

10. Lee, D.D., Scott, C.D., and Hancher, C.W. (1979), "Fluidized-Bed Bioreactor for Coal-Conversion Effluents," *J. Wat. Pollut. Control Fed. 51*, p. 974.

11. Suidan, M.T., Strubler, C.E., Kao, S.-W., and Pfeffer, J.T. (1983), "Treatment of Coal Gasification Wastewater with Anaerobic Filter Technology," *J. Wat. Pollut. Control Fed. 55*, p. 1263.

12. Ying, W.-C. and Weber, W.J., Jr. (1979), "Bio-Physicochemical Adsorption Model Systems for Wastewater Treatment," *J. Wat. Pollut. Control Fed. 51*, p. 2661.

13. Healy, J.B., Jr., Langlois, G.W., Sakaji, R.H., and Daughton, C.G. (1986), "Stationary Fixed-Biofilm Treatment of an Oil Shale Retort Water," LBL-19052.

Effect of Oil Shale Retort Water on Biooxidation of Aromatic Amines*

J.B. Healy, Jr., G.W. Langlois, J.F. Thomas, and C.G. Daughton†

Biooxidation would be one of the most cost-effective means of upgrading oil shale process wastewaters if a sufficient portion of dissolved organic carbon (DOC) were amenable to mineralization. In addition to large quantities of easily degradable aliphatic acids,[1] retort waters have been reported to contain numerous nitrogen heterocycles and other aromatic amines.[2–6] Several previous studies[7,8] have indicated that large numbers of aromatic amines, each present at a low part-per-million concentration, may be responsible for the resistance of a large portion of the DOC to biodegradation.

There is little published literature on simple aromatic amine catabolism. Of the studies, most have reported aromatic amines to be at least slowly biodegradable at relatively high concentrations in single-substrate systems.[9–14] Aromatic amines in retort water, however, may be refractory because of repression or inhibition of enzyme activity by high levels of the easily utilized nitrogen source, ammonia, or because of interactions of the numerous aromatic amine congeners.[7] Although some aromatic amines may be inherently recalcitrant,[12] no published literature exists regarding matrix effects that could cause normally biodegradable aromatic amines to resist biooxidation when present in a mixture.

The purpose of the work reported here was to determine the importance of inherent recalcitrance and inhibitory matrix effects on the resistance of multiple aromatic-amine substrates to biooxidation in retort water. For a simplified model system comprising a defined mixture of biodegradable aromatic amines at low concentrations, biodegradability was evaluated in the absence of high ammonia concentrations, and these results were compared with those obtained after adding a retort water containing ammonia.

ACCOMPLISHMENTS DURING FY 1985

To investigate possible causes of recalcitrance, we followed the disappearance of selected aromatic amines in both single- and mixed-substrate systems to model the more complex arrays found in retort waters. Before selecting individual compounds for the defined mixture, the biodegradability of each of 35 aromatic amines was evaluated in a series of batch, dispersed-phase cultures with each compound (100 mg/L) as the sole source of carbon, nitrogen, and energy. Although more than half of the compounds resisted biodegradation during the one to three months of incubation, we were able to demonstrate biodegradability for a sufficient number of the aromatic amines.

All cultures were incubated in 250-mL Erlenmeyer flasks at 30°C in the dark. Volatilization of aromatic amines was greatly reduced by capping the flasks with aluminum foil and by not agitating the culture fluid. Single-substrate cultures consisted of 33 mL of defined medium[15] containing 100 mg/L of the candidate aromatic amine. An inoculum was pooled from activated sludge (mixed-liquor suspended solids from the municipal sewage treat-

*This work was supported by the Assistant Secretary for Fossil Energy, Office of Oil Shale, Division of Oil, Gas, and Shale Technology of the U.S. Department of Energy under Contract No. DE-AC03-76SF00098.

†Sanitary Engineering and Environmental Health Research Laboratory, University of California (Berkeley), Richmond, CA 94804.

ment plant, Richmond, CA) and from a culture acclimated to nine oil shale wastewater media.[7]

Uninoculated media treated with 200 mg/L of the growth inhibitor, $HgCl_2$, served as the controls for detecting abiotic losses of DOC (e.g., volatilization). Losses of DOC measured in the controls were subtracted from the total removals in active cultures.

Cleavage of the heterocyclic and aromatic rings in single-substrate batch cultures was indicated by a reduction in UV absorbance. Only two to six days were required for original cultures to acclimate to aniline; 2-methylaniline; quinoline; pyridine; and 2- and 3-methyl-, 2- and 3-ethyl-, and 2- and 3-hydroxypyridine. Acclimation to 2-methylquinoline required a lag of 2 weeks before biodegradation began; mineralization occurred over the next 10 days. Excluding lag periods, each of these compounds was biodegraded in less than 2 weeks. Pyridine, quinoline, and aniline compounds substituted in the 4-position or those that contained more than one ring substitution were significantly more refractory than those substituted in the 2- or 3-positions.

Although original acclimation times for 2,4- and 2,6-dimethylpyridine were about one week, 5 weeks was needed for biodegradation of the initial 100 mg/L of substrate. After 3 weeks of acclimation, cultures required an additional 3 weeks to biodegrade 2,4,6-trimethylpyridine and 2-methylpyrazine. After 3 months of incubation in defined media, none of the other 20 aromatic amines was biodegraded. Some of these aromatic amines may be inherently refractory.

Time required for the biodegradation of an additional 100 mg/L of substrate by outgrown, acclimated cultures was much less than the time required for the original substrate dosage. For example, while 5 weeks was required for the biodegradation of more than 90% of the initial dose of 2,6-dimethylpyridine, only a few days were required for a second dose (Fig. 1). This increased rate can be attributed to the increased concentration of acclimated cells. Although greater cell numbers were observed with phase-contrast microscopy, the increase in cell numbers could not be quantified, because of predatory protozoa in the enrichment cultures.

Each of the 15 biodegradable aromatic amines was completely mineralized by the acclimated cultures as evidenced by DOC removals, which correlated with reductions in UV absorbance. These results agreed with those reported in the literature (Table 1). With the exceptions of cyanuric acid, 4-methyl- and 2,3,6-trimethyl-pyridine, and 3-methyl-, 4-methyl-, 2,4-dimethyl-, and *N*-methyl-aniline, the aromatic amines previously reported to be biodegradable were also mineralized in our defined media. In addition, we believe this is the first report of the biodegradability of 3-methyl- and 3-ethyl-pyridine; 2-methylquinoline; and 2-methylpyrazine.

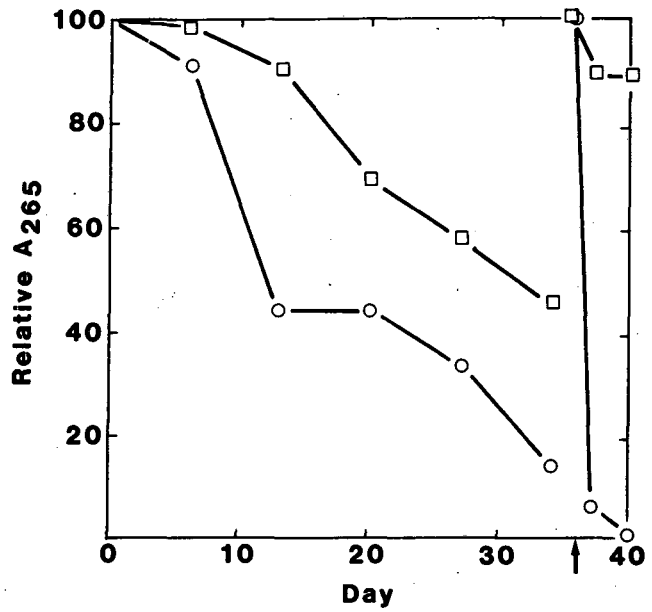

Figure 1. Relative disappearance (reduction in A_{265}) of 100 mg/L of 2,6-dimethylpyridine in an enrichment culture. Comparison of biodegradation (open circle) with abiotic losses from a $HgCl_2$-inhibited control (open square). Arrow indicates time of spike of an additional 100 mg/L of substrate. (XBL 8511-4769)

Of the 15 biodegradable aromatic amines, 12 had been previously studied as part of a defined mixture of 26 N-heterocycles.[16,7] These 12 N-heterocycles were used to make the multiple-substrate media containing the defined-mixture compounds. Acclimated cultures developed from a pool of the 12 individual enrichment cultures completely mineralized the mixture (92 mg/L) in less than a week. This behavior indicated that the individual substrates were degraded simultaneously by the mixed populations and that inhibitory interactions among the 12 component aromatic amines did not appear to be significant.

To determine the importance of inherent recalcitrance and inhibitory matrix effects on the resistance to biooxidation of multiple aromatic amine substrates in retort water, the defined mixture of 12 N-heterocycles was evaluated for its biodegradability in the presence and absence of Oxy-6 retort water. The total concentration of the defined mixture was increased to 332 mg/L so that these N-heterocycles could be easily detected above the endogenous DOC when added to 38% Oxy-6 retort water medium.[15] The behavior of this array of heterocycles in the

Table 1. Occurrence of aromatic amines in retort water and their biodegradability in defined media.

Chemical	Source[b]	Occurrence in retort water (literature reference)	Biodegradability[a]	
			Literature reference	This study
Aniline	1	+ (4)	+ (17,11)	+
2-Methylaniline	1	+ (4)	+ (11)	+
3-Methylaniline	1	+ (4)	+ (11)	−
4-Methylaniline	1	+ (4)	+ (11)	−
N-Methylaniline	1	+ (6)	+ (11)	−
2,4-Dimethylaniline	1	nr[c]	+ (17)	−
N-Ethylaniline	1	nr	nr	−
Pyridine	1	+ (4)	+ (12)	+
2-Methylpyridine	1	+ (4)	+ (12)	+
3-Methylpyridine	1	+ (4)	nr	+
4-Methylpyridine	1	+ (4)	+ (12)	−
2,4-Dimethylpyridine	1	+ (6)	+ (13)	+
2,6-Dimethylpyridine	1	+ (4)	+ (12)	+
2,3,6-Trimethylpyridine	2	nr	+ (12)	−
2,4,6-Trimethylpyridine	1	+ (4)	+ (13)	+
2-Ethylpyridine	2	+ (5)	+ (13)	+
3-Ethylpyridine	2	+ (3)	nr	+
4-Ethylpyridine	2	+ (2)	nr	−
3-Ethyl-4-methylpyridine	2	+ (5)	nr	−
4-Ethyl-3-methylpyridine	2	+ (5)	nr	−
5-Ethyl-2-methylpyridine	3	+ (5)	nr	−
2-*n*-Propylpyridine	2	nr	nr	−
4-tert-Butylpyridine	2	+ (3)	nr	−
2-Hydroxypyridine	4	+ (4)	+ (12)	+
3-Hydroxypyridine	4	+ (4)	+ (10)	+
2-Hydroxy-6-methylpyridine	4	+ (4)	nr	−
Quinoline	1	+ (4)	+ (9)	+
Isoquinoline	1	+ (4)	nr	−
8-Hydroxyquinoline	1	nr	nr	−
2-Methylquinoline	4	+ (4)	nr	+
4-Methylquinoline	4	+ (6)	nr	−
3,5-Dimethylpyrazole	1	+ (5)	nr	−
Benzimidazole	1	nr	nr	−
2-Methylpyrazine	1	nr	nr	+
Cyanuric acid	1	nr	+ (14)	−

[a]Biodegradability defined as the microbial cleavage of the ring structure.

[b]List of chemical suppliers: (1) Chem Service, West Chester, PA; (2) NOAH Chemical, Farmingdale, NY; (3) Fluka AG, Buchs, Switzerland; (4) Aldrich, Milwaukee, WI.

[c]nr, not reported.

absence of high ammonia in defined medium was then compared with its behavior in the retort water matrix.

These cultures were inoculated with 0.2 mL of either culture KY, which had been routinely maintained on 50% Oxy-6 retort-water medium, or culture RW-12, which was preadapted to 50% Oxy-6 retort water medium spiked with the defined mixture-12. Culture RW-12 was originally derived by combining culture KY with individual cultures acclimated to the 12 N-heterocycles.

Culture RW-12 biodegraded over 80% of the N-heterocycle mixture in defined medium (332 mg/L) in 3 weeks. Despite the threefold increase in total N-heterocycle concentration, the mixture was no more resistant to biooxidation than the same mixture at 92 mg/L.

The DOC removal from 38% Oxy-6 retort water by culture RW-12 was compared with the removal from the same retort water with the added (spiked) mixture of N-heterocycles (247 mg/L DOC). The major portion of biooxidation had ceased by day 21. After one week, 48% of the DOC in unspiked retort water was biooxidized. This was the same removal previously reported for culture KY,[7] which normally completes biooxidation of the readily degradable substrates (e.g., aliphatic acids) in 5 days and is incapable of further DOC removal. After three weeks, however, culture RW-12 had removed 55% of the DOC, indicating that these preadapted microorganisms were degrading additional solutes, perhaps aromatic amines to which culture KY was not adapted; in a parallel incubation with 38% Oxy-6 retort water, culture KY removed only 49% of the DOC by day 28.

Assuming that the readily degradable DOC in retort water medium was removed equally in the presence and absence of the N-heterocycle spike, the fate of the spike was isolated from the total removal of DOC by subtracting the DOC remaining for unspiked retort water from DOC remaining for spiked retort water. The resulting values indicated that the N-heterocycle spike was degraded slowly in the presence of retort water until degradation ceased at about 3 weeks. Only 32% of the spike was removed by culture RW-12. In contrast, the same culture removed 81% of the DOC from the spike when incubated in defined medium for the same time period.

Analysis of the N-heterocycle mixtures by high performance liquid chromatography (Fig. 2) allowed the monitoring of the fates of the individual aromatic amines. All 12 N-heterocycles were attacked via ring cleavage as indicated by the reduction in absorbance at 254 nm (cp. Fig. 2a,b). When

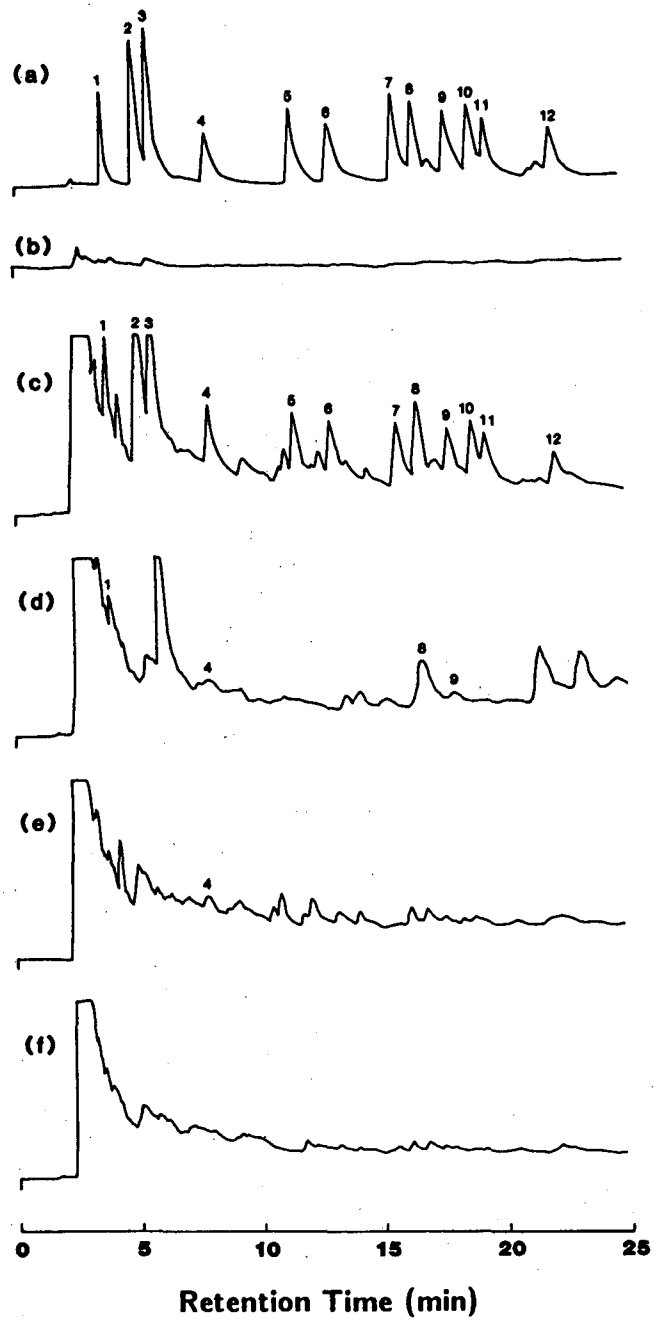

Figure 2. HPLC chromatograms of 12 aromatic amines in the presence and absence of Oxy-6 retort water at day 0 and at day 28 of incubation with culture RW-12. (a) aromatic amines in defined medium at day 0, and (b) day 28; (c) aromatic amines spiked in retort water at day 0, and (d) day 28; (e) unspiked retort water at day 0, and (f) day 28. Numbered-peak identification: (1) 2-hydroxypyridine, (2) 3-hydroxypyridine, (3) 2-methylpyrazine, (4) pyridine, (5) 2-methylpyridine, (6) 3-methylpyridine, (7) 2,6-dimethylpyridine, (8) 2-ethylpyridine, (9) 2,4-dimethylpyridine, (10) 3-ethylpyridine, (11) quinoline, and (12) 2,4,6-trimethylpyridine. (XBL 8511-4768)

spiked into Oxy-6 retort water, these 12 compounds were detectable above the endogenous levels of UV-absorbing compounds in the retort water (Fig. 2c). After 28 days, the majority of the spiked aromatic amines had been attacked (Fig. 2d). Only 2-ethylpyridine (peak 8) clearly remained above background levels. When compared with unspiked retort water (Fig. 2e), several new peaks appeared that may have been metabolites from the initial attack on the substrate spike; this would have accounted for some of the DOC that remained from the spike. Although this model substrate system contained no aromatic amines that were inherently recalcitrant, such compounds are expected to reside in the more complex array of aromatic amines present in retort water. Thus it appears that the retort water environment has inhibitory effects on the rate and extent of mineralization of normally biodegradable aromatic amines, most of which have been identified in retort waters.

Retort water that was not spiked with the N-heterocycle mixture generated numerous peaks (Fig. 2e) that were poorly separated under the HPLC conditions used. Some of these endogenous compounds, however, were definitely attacked (Fig. 2f). Total peak areas were reduced 52%, indicating that almost half of the endogenous aromatic compounds did not experience ring cleavage. The behavior of aromatic amines in spiked and unspiked retort water demonstrates the importance of inherent recalcitrance and inhibitory matrix effects on the resistance of the multiple aromatic-amine substrates to biooxidation in retort water and illustrates limitations likely to be experienced in the management of other complex industrial waste mixtures (e.g., leachates from hazardous waste dumps).

REFERENCES

1. Rogers, J.E., *et al.* (1981), "Microbiological Degradation of Organic Components in Oil Shale Retort Water: Organic Acids," *Appl. Envir. Microbiol. 42*, p. 830.
2. Dobson, K.R., Stephenson, M., Greenfield, P.F., and Bell, P.R.F. (1985), "Identification and Treatability of Organics in Oil Shale Retort Water," *Water Res. 19*, p. 849.
3. Hunter, L., Persoff, P., Thomas, J.F., and Daughton, C.G. (1985), "Identification and Correlation of Volatile Components in Retort Wastewaters," in *Applied Science Division Annual Report, FY 1984*, LBL-18754, p. 4–60.
4. Leenheer, J.A., Noyes, T.I., and Stuber, H.A. (1982), "Determination of Polar Organic Solutes in Oil-Shale Retort Water," *Envir. Sci. Technol. 16*, p. 714.
5. Pellizzari, E.D., *et al.* (1979), "Identification of Organic Components in Aqueous Effluents from Energy-Related Processes," in *Measurement of Organic Pollutants in Water and Wastewater*, C.E. Van Hall, Ed., American Society for Testing and Materials, Philadelphia, PA; ASTM STP 686, p. 256.
6. Raphaelian, L.A. and Harrison, W. (1981), "Organic Constituents in Process Water from the In-Situ Retorting of Oil from Oil-Shale Kerogen," Argonne National Laboratory report ANL/PAG-5.
7. Healy, J.B., Jr., Langlois, G.W., and Daughton, C.G. (1985), "Biooxidation of Organic Solutes in Oil Shale Wastewaters," *Water Res. 19*, p. 1429.
8. Jones, B.M., Sakaji, R.H., and Daughton, C.G. (1982), "Physicochemical Treatment Methods for Oil Shale Wastewater: Evaluation as Aids to Biooxidation," in *Fifteenth Oil Shale Symposium Proceedings*, J.H. Gary, Ed., Colorado School of Mines Press, Golden, CO, p. 581.
9. Grant, D.J.W. and Al-Najjar, T.R. (1976), "Degradation of Quinoline by a Soil Bacterium," *Microbios 15*, p. 177.
10. Khanna, M. and Shukla, O.P. (1977), "Microbial Metabolism of 3-Hydroxypyridine," *Indian J. Biochem. Biophys. 14*, p. 301.
11. Malaney, G.W. (1960), "Oxidative Abilities of Aniline-Acclimated Activated Sludge," *J. Wat. Pollut. Control Fed. 32*, p. 1300.
12. Naik, M.N., Jackson, R.B., Stokes, J., and Swaby, R.J. (1972), "Microbial Degradation and Phytotoxicity of Picloram and Other Substituted Pyridines," *Soil Biol. Biochem. 4*, p. 313.
13. Shukla, O.P. (1975), "Microbial Decomposition of 2-Ethylpyridine, 2,4-Lutidine, and 2,4,6-Collidine," *Indian J. Exp. Biol. 13*, p. 574.
14. Wolf, D.C. and Martin, J.P. (1975), "Microbial Decomposition of Ring-^{14}C Atrazine, Cyanuric Acid, and 2-Chloro-4,6-diamino-s-triazine," *J. Envir. Qual. 4*, p. 134.
15. Healy, J.B., Jr., Langlois, G.W., and Daughton, C.G. (1985), "Effect of Oil Shale Retort Water on Aromatic Amine Biooxidation," LBL-19819.
16. Healy, J.B., Jr., Jones, B.M., Langlois, G.W., and Daughton, C.G. (1983), "Biotreatment of Oil Shale Wastewaters," in *Sixteenth Oil Shale Symposium Proceedings*, J.H. Gary, Ed., Colorado School of Mines Press, Golden, CO, p. 498.
17. Baird, R., Carmona, L., and Jenkins, R.L. (1977), "Behavior of Benzidine and Other Aromatic Amines in Aerobic Wastewater Treatment," *J. Wat. Pollut. Control Fed. 49*, p. 1609.

Sunlight Reactions of Volatile Organonitrogen Emissions from Oil Shale Wastewaters*

E.R. Blatchley III, J.F. Thomas, and C.G. Daughton[†]

Oil shale developers anticipate the use of minimal upgrading for their process wastewaters (retort waters) prior to disposal. Most disposal schemes also involve temporary storage in ponds prior to disposal. For surface-retort processes, the retort waters would then be codisposed together with the solid wastes (spent shale). Codisposal will take place at elevated temperatures (probably above 65°C) because it will not be economically feasible to store spent shale long enough to allow cooling to ambient temperature. For pond storage and codisposal, the major transport process that will determine the immediate, short-term environmental disposition of organic solutes associated with these wastes will be volatilization.

Of several classes of organic compounds that could be emitted, a major one comprises organonitrogen species including heterocycles, aromatic amines, and nitriles. Nitrogenous compounds are of particular concern because (1) they crosscut the spectrum of compounds produced by most synfuel conversion processes, (2) they are particularly refractory to removal by conventional biotreatment and are therefore likely to undergo uncontrolled emissions and show high persistence, (3) they have extremely low odor thresholds and most are malodorous, (4) phototransformations present the possibility of formation of atmospheric NO_x, a known precursor to photochemical smog, and (5) these compounds are not currently regulated, mainly because they would be unique to the as-yet developed synfuels industry, and little is currently known about them. The problem of nuisance odor could be a major one since many areas of the U.S. are considering air-emission regulations based on smell. The Bay Area Air Quality Management District of San Francisco, for example, now enforces such regulations in the nine Bay Area counties.

*This work was supported by the Assistant Secretary for Fossil Energy, Office of Oil Shale, Division of Oil, Gas, and Shale Technology of the U.S. Department of Energy under Contract No. DE-AC03-76SF00098.

[†]Sanitary Engineering and Environmental Health Research Laboratory, University of California (Berkeley), Richmond, CA 94804.

The major chemical transformation processes that will determine the environmental fate of those compounds emitted to the atmosphere are all sunlight mediated. This project represents the first investigation of vapor-phase photoreactions of organonitrogen compounds (ONCs) emitted by retort waters. With a thorough understanding of the photochemistry, atmospheric lifetimes could be predicted and management practices could be designed to minimize associated hazards (such as toxic or nuisance photochemical products), or alternatively, to take advantage of reactions that serve to mineralize compounds that may otherwise be hazardous. It is noteworthy that the native air quality in the Western U.S. oil shale region is high. Any anthropogenic introduction of pollutants to the air could be significant. Compounds with sufficiently long lifetimes could be used, however, as tracers or indicators of pollution resulting from oil shale operations since their ambient, baseline concentrations are extremely low.

The photodecomposition of ONCs originating from a retort water was studied in an inert (N_2) atmosphere. The exclusion of molecular oxygen minimized the effects of indirect photoreaction, which could be substantial and will be the focus of future investigation. Only 3 of the 60 major ONCs that volatilized to the headspace were degraded as a result of photoreaction. It was possible that other compounds also photodegraded, but this could not be confirmed because of their relatively low concentrations in the retort water headspace.

ACCOMPLISHMENTS DURING FY 1985

The study was performed on static headspace of retort water samples since the headspace is representative of initial potential emissions. Gas condensate from Occidental Oil Shale Co.'s sixth experimental burn (Oxy-6 GC) was chosen for generation of headspace samples because of its high content of volatile components. Experiments were performed in an inert atmosphere of nitrogen gas to inhibit the formation of oxygen radicals and NO_x. This allowed for an evaluation of direct and photosensitized photoreactions; these would indicate minimum extents of *in-situ* photodecomposition. Future experiments will include the use of a more reactive atmosphere (e.g., air), in which radical induced reactions could also occur.

Headspace samples were generated under conditions that would make the headspace as concentrated as possible and which would also simulate expected codisposal conditions. To a 40-mL sample of Oxy-6 GC, 0.96 g of NaOH was added to increase the pH

from 8.8 to 11. This increased the concentrations of deprotonated (volatile) ONCs and also simulated the effect of alkali salts present in spent shale. This sample was then injected through a Teflon, septum-containing stopper used to seal a 2-L roundbottom flask that had previously been purged with N_2. Two 500-mL Pyrex gas-sampling tubes (GSTs) with Teflon stopcocks were then evacuated to 0.13 Pa and connected through a valved manifold to the 2-L roundbottom flask that had been equilibrated for 1 hour in a 65°C water bath. The valve was opened and the headspace allowed to equilibrate. Experimental samples and controls were produced by flushing the GSTs with N_2 into 2-L Tedlar gas-sampling bags, each equipped with a septum port; parallel experiments were performed in Pyrex GSTs by eliminating this last step. Tedlar is a poly(vinylfluoride) film similar in composition to Teflon. Tedlar was chosen because of its advantages over other container materials. Tedlar transmits tropospheric sunlight better than Pyrex glass, especially in the ultraviolet range, which is more intense at elevations such as those of the Western U.S. oil shale regions; it is less permeable to most gases than other polymeric materials; and the bags are relatively inexpensive and reuseable.

Bags containing the wastewater headspace were randomly divided into two groups: samples (to be exposed to sunlight) and controls (to be submitted to the same conditions, but without sunlight); controls were wrapped in aluminum foil. Both groups were placed on the roof of Building 112 at the U.C. Richmond Field Station from 7–15 May 1985. Time-course analyses of sample and control headspaces were performed using capillary gas chromatography (30-m fused-silica, KOH-deactivated Carbowax 20M column, programmed from 30°C to 220°C at 4°C/min) with flame ionization and flame thermionic (nitrogen/phosphorus) detectors (FID and NPD, respectively); the latter detector is highly selective for nitrogen and phosphorus compounds. Chromatographic data were recorded, stored, and manipulated using a computing integrator.

Chromatographic data (peak areas) from samples and controls at time zero were within approximately 10%, indicating that one headspace had been diluted slightly more than the other in the headspace transfer process. The data for the GSTs also indicated that leakage (presumably through the septum and stopcocks) was a dominant loss mechanism both for samples and controls. From this we concluded that the GSTs were not suitable for headspace containment over the period of irradiation. In contrast, leakage of headspace components through the walls of the Tedlar bags was minimal (Fig. 1). Losses of

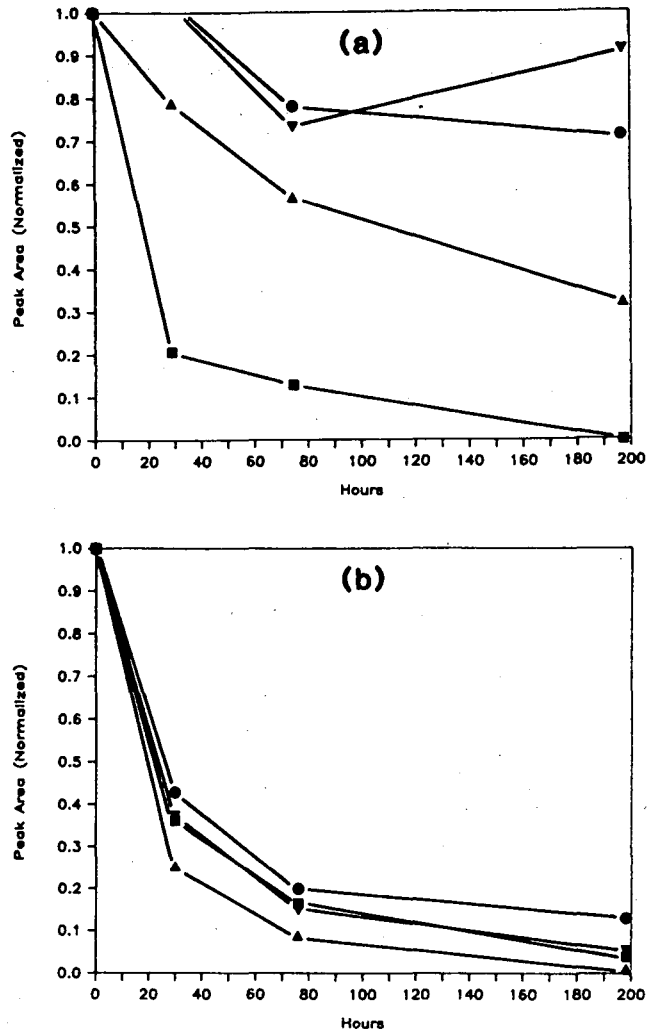

Figure 1. Normalized oil shale wastewater ONC peak areas as a function of time for Tedlar bags (a) and GSTs (b). Time-course headspace samples were analyzed by capillary gas chromatography. Resulting data were normalized with respect to time-zero peak areas. Data for four compounds are shown for each type of chamber: 2,6-dimethylpyridine (inverted triangle), pyridine (circle), C_3-pyridine isomer (triangle), aniline (square). (XBL 8511-4776)

headspace components because of sorption to the walls were found to be more significant but acceptable. Further investigation found these components to readily desorb when the headspace was expelled and replaced with N_2. This demonstrated that sorption was reversible and that cleaning the bags for reuse would be relatively easy.

There were 60 compounds present in the headspace in sufficient quantities to be resolved and detected under our gas chromatographic conditions. Of these, only three showed losses in the samples relative to the controls (Fig. 2). We attributed these losses to photoreactions. Possible mechanisms

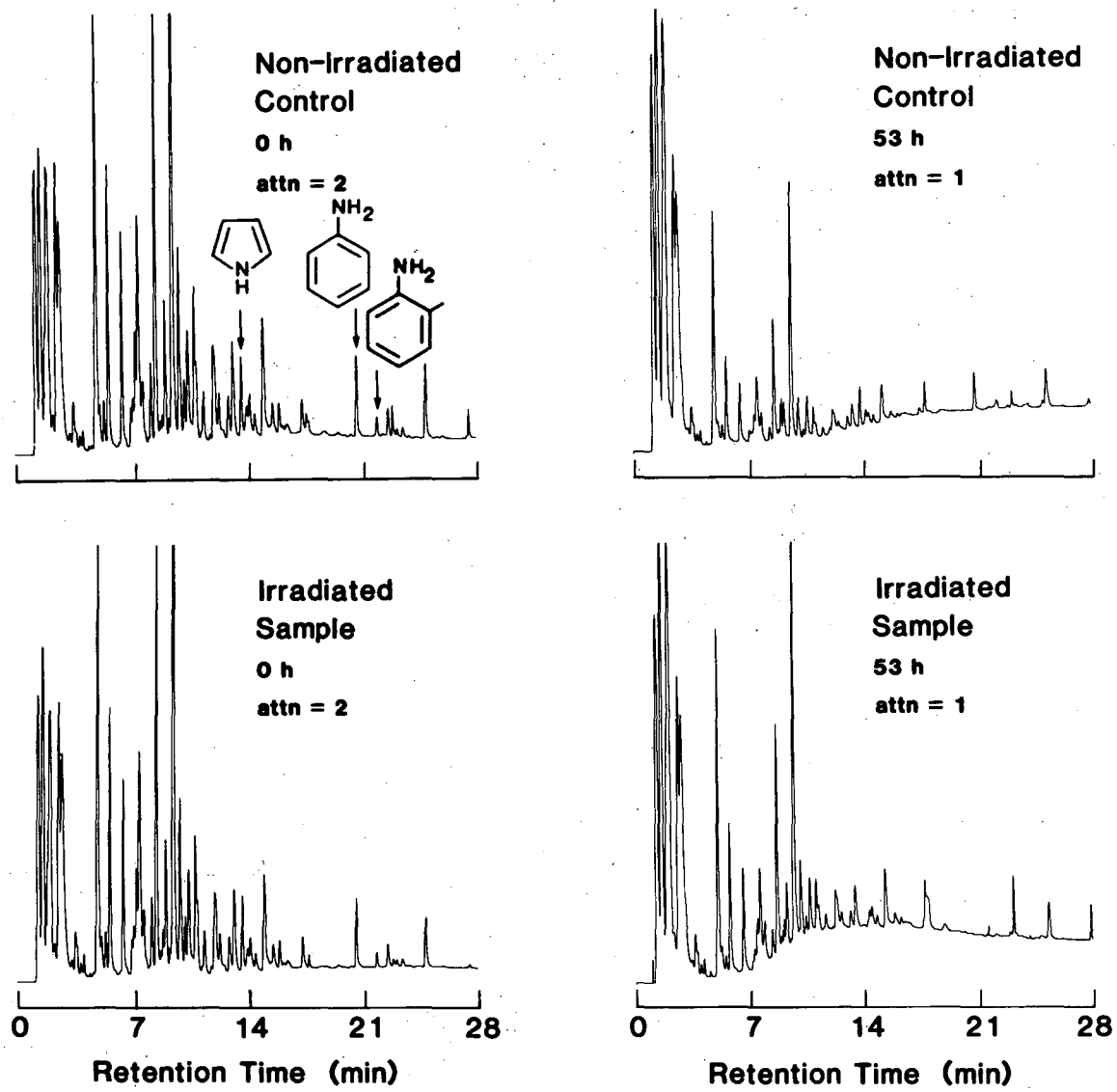

Figure 2. Oxy-6 gas condensate headspace chromatograms (flame ionization detection). Comparison of sunlight irradiated sample and non-irradiated control before and after 53 hours of exposure. Arrows indicate compounds that showed losses in the irradiated sample relative to the non-irradiated control after 53 hours. (XBL 855-2693A)

included reaction via direct absorption of radiation or by collision with other headspace components that had been electronically excited themselves by absorption of radiation. Analysis of Oxy-6 GC by gas chromatography/mass spectrometry indicated that these three compounds were aniline, pyrrole, and *o*-toluidine. These identifications were confirmed using a statistical retention-index matching technique on previously acquired gas chromatographic data from Oxy-6 GC.[1] Other headspace components (e.g., the other toluidine isomers) may have undergone similar reactions but were initially present at such low concentrations that other losses (e.g., sorption, leakage) made this difficult to confirm. No attempt was made to identify reaction products or quantify radiation.

Many of the components present in the retort water headspace are aliphatic pyridines. For example, of the 38 compounds identified in Oxy-6 GC headspace, 22 were alkyl pyridines.[1] None of these compounds underwent sufficient photodegradation to be detected in this experiment. This is significant

because the pyridines represent the majority of the ONCs present in Oxy-6 GC headspace, in part a result of their lower boiling points (higher volatilities) than other ONCs in the headspace. Their concentrations in retort waters are also higher than those of other ONCs.

These experiments were performed in an inert atmosphere. Irradiation in a more reactive atmosphere, such as air, would probably result in degradation of more compounds. Experiments performed on pure compounds in air support this hypothesis. The effects of sunlight exposure on pyridine, 2,4,6-trimethylpyridine, and quinoline in air were studied. A mass of pure compound less than that required to saturate the available headspace was placed in a 100-mL Pyrex volumetric flask. The flask was then stoppered by sliding a Teflon-backed silicone septum into the neck. Eight flasks were prepared for each compound. Four flasks from each group were wrapped in aluminum foil and used as controls. Headspace composition was monitored during the course of irradiation by extracting the headspace with pentane (injected through the septum) and analyzing the extract by gas chromatography. Extractions were performed in order to monitor the production of both volatile and nonvolatile reaction products. One pair of flasks was analyzed daily (one sample and one control). Resulting data indicated that 2,4,6-trimethylpyridine and quinoline photodegraded, while pyridine did not.

Reactions with atmospheric ozone may also prove to be important with respect to air quality. When ozone was injected into samples of Oxy-6 GC headspace, a "fog" formed immediately. Although the concentrations of ozone and organic components were much higher than could ever be expected to occur in the atmosphere, similar reactions could prove to be important in reducing atmospheric visibility.

PLANNED ACTIVITIES FOR FY 1986

To understand the behavior of emissions resulting from oil shale processes in general (not just those of Occidental's modified *in-situ* process), it will be necessary to perform similar experiments on retort water headspace samples from other processes. This work will be expanded to include emissions from wastewaters of other hydrocarbon extraction/conversion processes, such as coal gasification, tar sands extraction, and tertiary oil recovery.

To understand the importance of molecular oxygen on the photodegradation of volatile components, it will be necessary to perform experiments similar to those described, with the addition of air or O_2. Since it is possible that nitrogen oxides will be formed, headspace NO_x concentrations will be monitored using a chemiluminescent nitrogen detector.

REFERENCES

1. Hunter, L., Persoff, P., Thomas, J.F., and Daughton, C.G. (1985), "Identification and Correlation of Volatile Components in Retort Wastewaters," in *Applied Science Division Annual Report, FY 1984,* LBL-18754, p. 4–60.

Diffusivity of Nitrogen Heterocycles in Simulated Codisposed Oil Shale Wastes*

P. Persoff, J.F. Thomas, and C.G. Daughton†

Oil-shale retorting produces large amounts of solid and liquid wastes. For each barrel of shale oil recovered, approximately 0.4 barrels of retort water and 1.4 tons of spent shale are produced, both of which must be disposed of in an environmentally acceptable manner. Both the amounts and characteristics of these waste streams vary, depending on the retorting process and shale grade used. Retort wastewaters vary in quality, but all contain high concentrations of organic nitrogen,[1] largely in the form of nitrogen heterocycles (NHCs).[2,3] These compounds, because of their malodor and toxicity, could present nuisance or worker-health problems at oil shale development sites and environs if significant amounts were released to the atmosphere.

Considering the huge amounts of solid waste to be disposed of, the most feasible disposal option is compaction in landfills with eventual revegetation. Spent shale emerges from the retorting process at an

*This work was supported by the Assistant Secretary for Fossil Energy, Office of Oil Shale, Division of Oil, Gas, and Shale Technology of the U.S. Department of Energy under Contract No. DE-AC03-76SF00098.

†Sanitary Engineering and Environmental Health Research Laboratory, University of California (Berkeley), Richmond, CA 94804.

elevated temperature (typically 150 to 350°C). It must be cooled and then moisturized to promote compaction. Investigation of existing spent shale has shown that the optimum moisture level for compaction (permitting the densest and strongest compacted disposed material for a specified amount of compactive effort) is about 15 L of water per 100 kg of dry spent shale; this optimum level varies according to the process, but the figure cited is typical. This requirement for moisturizing water would be the largest demand for water imposed by a commercial oil shale development. In the semi-arid oil shale region of the western U.S., use of retort wastewater to satisfy the moisturizing-water requirement would be a prudent water conservation practice if it could be done in an environmentally sound manner. An immediate potential problem, however, would be release to the atmosphere of volatile NHCs (and other species) from warm, moisturized spent shale upon delivery to the dumpsite and before, during, and after compaction.

ACCOMPLISHMENTS DURING FY 1985

To estimate the rate at which volatile solutes are released from an oil shale waste codisposal pile, it is necessary to know the effective diffusivity of each compound in the codisposed waste. Effective diffusivity is defined[4] as the negative ratio of diffusive flux to the gradient of bulk concentration; others have used different definitions.[5,6] Under certain assumptions, the effective diffusivity can be calculated from the fractions of solute molecules that distribute to the solid, liquid, and gas phases. Knowing these distribution fractions, in turn, requires that both the Henry's Law constant for each solute and, if the solid phase adsorbs the solute, the adsorption isotherm for each solute be known. An expression to calculate the effective diffusivity has been reported previously,[4,7] as have sorption isotherms (Paraho spent shale and an aqueous solution of five NHCs).[8] This year a method to measure effective diffusivity of NHCs in simulated codisposed oil shale wastes was demonstrated. Effective diffusivity, D_e, was measured simultaneously for five NHCs in three porous media: water-saturated sand, unsaturated sand, and a simulated codisposed oil shale waste.

Apparatus and Methods

The aqueous phase for each of the three runs was the same. An aqueous solution of 5 NHCs (pyridine, pyrrole, and three methylpyridine isomers) was prepared. This solution was then diluted (10 in 11, vol/vol) with a pH 10 buffer (7.72 g boric acid and 6.88 g KOH per L) to produce final concentrations of solutes as shown in Table 1. The pH of the final solution was greater than 8, ensuring that each NHC was in its deprotonated (volatile) form.

The simulated codisposed oil shale waste consisted of Paraho spent shale, moisturized with the aqueous phase. The Paraho spent shale originated from Green River oil shale from the Anvil Points mine in Anvil Points, CO; this particular spent shale was retorted in run C-2, using the Paraho direct process, by Development Engineering, Inc., in the fall of 1979. This material contained 4.1 wt% mineral carbon (undecomposed carbonates) and 1.4 wt% organic carbon.[9] For our work, the −4 +8 mesh size fraction was separated by sieving. To prepare the sample of moisturized spent shale, 50 mL of the NHC aqueous phase was added to 323 g of the dry Paraho spent shale (−4 +8 mesh) in a polyethylene jar. The jar was then rotated on a jar mill for 20 min to uniformly distribute the liquid in the solid; in previous experiments, when water was added to spent shale particles and rotated for various times, the standard deviation of the moisture content (measured as weight loss on evaporation) was found to decrease with longer intervals of rotation up to 20 minutes, but not beyond. The solid/liquid admixture (342 g, assumed to consist of 296 g dry spent shale and 46 mL of the aqueous phase) was transferred to a diffusion cell (Fig. 1), forming a packed bed of moisturized spent-shale particles.

To prepare the sample of unsaturated sand, 50 mL of the buffered NHC solution was added to 606 g of 100-mesh reagent-grade sand in a polyethylene jar. The contents were mixed by rotating, and all of the combined material was transferred to the diffusion cell for sampling of diffusive emissions. For the sample of saturated sand, the diffusion cell was filled to approximately one-third with the buffered NHC solution, and sand was poured into the cell while shaking the cell. As the level of sand approached the liquid level, more liquid was added so that a saturated sand bed completely filled the cell, up to the air inlet holes.

The diffusion cell was a polyethylene jar modified by drilling four holes around its circumference at the level of the top of the sample. Polypropylene tubes (0.25-in. o.d.), which were inserted through these holes forming a gas-tight seal, were used to deliver air to flush the top surface of the sample and maintain the solute concentrations at zero at the top of the sample. The influent air was bubbled through two gas-washing bottles (in series) to saturate it with water and prevent evaporation of pore moisture from the sample. Evaporation would have caused advective solute transport, confounding measure-

Table 1. Effective diffusivity of NHCs in porous media.

NHC compound	Boiling point (°C)	Initial concentration in aqueous phase (mg/L)	Effective diffusivity ($cm^2/sec \times 10^{-7}$) Saturated sand	Unsaturated sand	Moisturized spent shale
Pyridine	115	22.3	100	10.6	0.24
Pyrrole	131	26.4	82	12	0.37
2-Methyl-pyridine	129	25.7	96	8.1	0.10
3-Methyl-pyridine	144	26.1	110	6.9	0.054
4-Methyl-pyridine	143	26.1	120	5.9	0.043
Experimental variables			Associated conditions		
Mass of sand or shale (g)			393	606	296
Volume of aqueous phase (mL)			86	50	46
Volume of air in pore space (mL) (by difference)			0	79	198
Cell volume (mL)			242	362	362
Cell depth (cm)			9	10	10

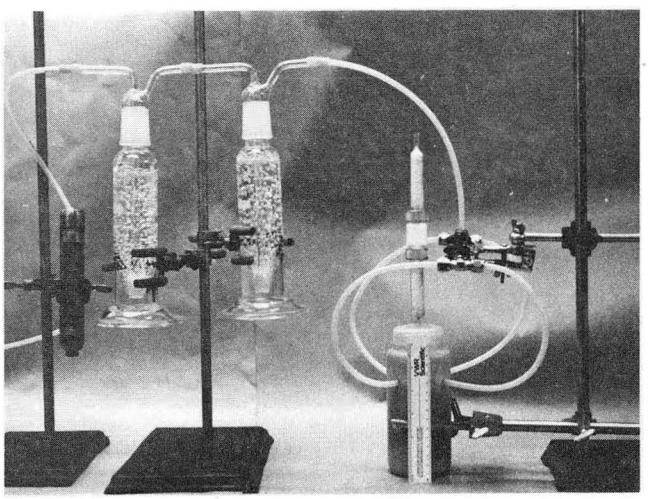

Figure 1. Experimental apparatus for measuring effective diffusivity of compounds in porous media. From left, air passes through a rotameter, two gas-washing bottles in series, then is divided equally into four tubes to sweep the surface of the sample in the diffusion cell. Air leaves the diffusion cell through two Tenax traps in series. (XBB 8511-9691)

ments of diffusive transport. During the runs, the water level dropped in the first bottle but not in the second, indicating that saturation was completed in the first bottle.

The effluent vapor phase, containing all species that volatilized from the packed bed, was passed through two adsorbent traps (Tenax) in series. The traps were 1/2-in. (o.d.) Pyrex tubes containing approximately 0.8 g of −60 +80 mesh Tenax GC (Alltech Associates, Deerfield, IL) retained between Pyrex wool plugs; both the Tenax and the Pyrex wool were pre-cleaned by Soxhlet extraction in methanol and followed by n-pentane and dried *in vacuo* for 4 hours at 110°C before filling the traps. The second trap in series was intended to detect breakthrough from the primary trap; no breakthrough was detected in any experiment. The pairs of Tenax traps were exposed for defined times, after which each trap was flushed with dry N_2 gas at a flow rate of 80 mL/min for 12 min to remove moisture from the traps; Tenax does not adsorb water. After exposure, each trap was placed in a Nutech 320 thermal desorber (Nutech Inc., Research Triangle

Park, NC) to transfer the adsorbed NHCs to a Hewlett-Packard 5840A gas chromatograph (GC) for separation and quantitation.

Each Tenax trap was heated to 280°C in helium (20 mL/min). The gas stream then passed through a cryotrap (a loop of 0.040-in. i.d. stainless steel tubing) maintained at −197°C, where desorbed species were "cryofocused." After 5 min of desorbing, the cryotrap was rapidly heated (<2 min) to 280°C, and the helium (20 mL/min) carried the re-vaporized species through a heated (200°C) 1/16-in. o.d. stainless-steel transfer line into the GC column (10-ft × 2-mm i.d. glass column, packed with 4% Carbowax 20M on 60–80 mesh Carbopack B, deactivated with 0.8% KOH). The transfer line and the glass GC column were connected by a zero-dead-volume reducing union, using a Vespel-and-graphite ferrule on the glass. After 5 min of transferring, the column temperature was increased from 50°C to 200°C at 30°C/min, then increased at 10°C/min to 220°C for isothermal operation for 22 min. Linear correlations ($r^2 > 0.99$) were established between peak-area response from flame ionization detection (FID) and mass of compound for each of the five NHCs by injection of aqueous standards; injection of aqueous standards onto the Tenax traps showed that recovery of spikes from the traps was quantitative.

Diffusivity Calculation

From the mass of each compound trapped during each sampling period, the flux of each species, J, was calculated. These data are plotted for moisturized spent shale (run 3) in Fig. 2, where C_o is the initial uniform bulk concentration of the solute in the diffusion cell and t represents the geometric mean of the starting and ending times of the sampling period. Similar plots (not shown) were drawn for saturated and unsaturated sand (runs 1 and 2, respectively).

A goal of this work was to determine whether diffusion in a packed bed of moisturized, adsorbent particles could be modeled as one-dimensional diffusion in a continuous, uniform medium with a constant or varying effective diffusivity, D_e. Diffusion in a uniform medium is expressed by Fick's second law:

$$\frac{\partial C}{\partial t} = D_e \frac{\partial^2 C}{\partial x^2} \quad , \qquad (1)$$

where

C	=	bulk concentration of solute (g/cm^3)
D_e	=	effective diffusivity (cm^2/sec)
t	=	time (sec)
x	=	distance (cm).

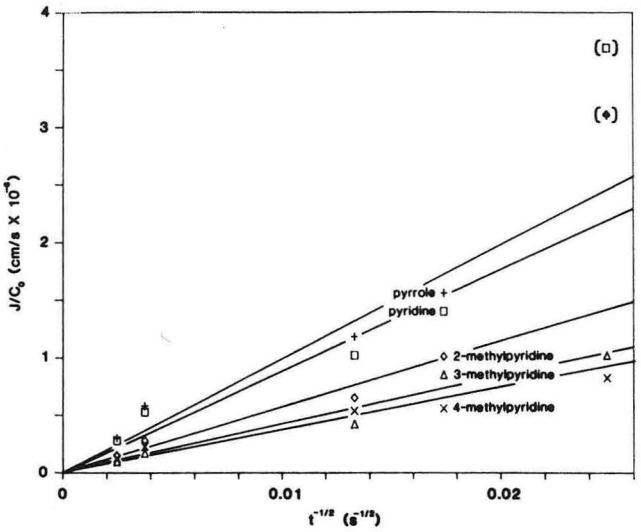

Figure 2. Plot of normalized flux (J/C_o) against inverse square root of time. Points in parentheses were not included in fitting the lines. Slopes of line are $(D_e/\pi)^{1/2}$. (XBL 8511-4777)

The boundary conditions (assuming 100% effective sweeping) are:

$$C = 0 \quad \text{at} \quad x = 0 \quad \text{for} \quad t \geqslant 0 \quad , \qquad (2)$$

$$\frac{\partial C}{\partial x} = 0 \quad \text{at} \quad x = L \quad , \qquad (3)$$

where L = depth of the diffusion cell (cm), and the initial condition is:

$$C = C_o \quad \text{everywhere at} \quad t = 0 \quad . \qquad (4)$$

For short times, the concentration at the bottom of the diffusion cell (i.e., x = L) remains at C_o. Under these conditions, the cell may be approximated by an infinitely deep cell, and boundary condition (3) is replaced by

$$\frac{\partial C}{\partial x} = 0 \quad \text{at} \quad x = \infty \quad . \qquad (5)$$

Equations (1) through (4) can be solved for C(x,t).[10] Evaluating $D_e \frac{\partial C}{\partial x}$ at x = 0 gives the diffusive flux J at x = 0. This is the flux measured in the experiment. A solution for J/C_o for the infinite-column approximation is:[11]

$$J/C_o = (D_e/\pi)^{1/2}\, t^{-1/2} \quad . \qquad (6)$$

The data for run 3 in Fig. 2 (and also for runs 1 and 2, not shown) were fitted by straight lines that were forced through the origin, as required by Eq. (6). This tentatively confirmed that all three systems behaved as one-dimensional diffusive systems with constant D_e. Values of effective diffusivity, calculated from the known initial concentrations of the five NHCs and the measured slopes, are shown in Table 1.

Phase Partitioning of Solutes

According to theory presented previously,[4,5] the effective diffusivity of a solute in a porous medium can be predicted from the distribution of solute molecules among the phases and a tortuosity factor for each phase that constitutes a diffusion path. Molecules that partition to the gas or liquid phases are available to transport by diffusion. Although molecules that partition to the solid phase participate in diffusional transport to a negligible degree (because solid-phase diffusion is much slower than diffusion in fluid phases), the solid phase serves as a reservoir of molecules that can replenish the fluid phases as they are depleted. Generally, the greater the proportion of solute molecules that partition to the solid phase, the lower will be the effective diffusivity.

Removal of pyridine and alkylpyridines from aqueous solution by sorption to the solid phase was detected for Paraho C-2 spent shale and for another carbonaceous spent shale, but was not found for two noncarbonaceous spent shales.[8] Sorption was greater for the more highly alkylated species. In control experiments, removal of pyridine and alkylpyridines from aqueous solution by sorption to the solid phase was not detected for either glass or sand.[8] This suggests that sorption from aqueous solution results from the activated-carbon-like char of carbonaceous spent shale. By contrast, in separate experiments, removal of vapor-phase pyridine from air to solid phases was detected for each of glass, sand, and carbonaceous and noncarbonaceous spent shales. This suggests that pyridine molecules can be removed from air either by affinity of the electronegative nitrogen to acid sites on the surface of sand or glass, or by affinity of the molecule to the char of carbonaceous spent shale. In an unsaturated system, where the solid surface is partly wet and partly dry, the water-air and water-solid partitioning coefficients would be insufficient to predict the partitioning of solutes among the three phases.

The values of effective diffusivity shown in Table 1 reflect the partitioning of solute molecules to the solid phase. In run 1 (saturated sand), all the solute molecules remained in the aqueous phase. The effective diffusivity would be expected to be close to the molecular diffusivity in water, reduced by a tortuosity factor; no reduction is required for porosity because the definition of effective diffusivity was based on bulk concentration rather than aqueous-phase concentration. The observed values were all close to 1×10^{-5} cm^2/sec, a typical value for molecular diffusivity in water for these compounds. This implies a tortuosity factor close to unity, which is reasonable for this situation.

In run 2 (unsaturated sand), the sand surface is believed to have been partly dry. Therefore, the pyridine molecules were distributed among all three phases. Distribution of pyridine molecules to the gas phase would increase the effective diffusivity (compared to run 1), while distribution to the solid phase would decrease it. More complex diffusion paths and isolated pockets of air or water would also decrease the effective diffusivity. Values of D_e measured in run 2 were smaller than those measured in run 1 by approximately one order of magnitude.

For run 3 (moisturized spent shale), D_e values were the lowest. This resulted from partitioning of NHCs to the solid phase from both the water and air phases. Higher values of effective diffusivity were associated with greater tendency of the solute to partition to the gas phase (i.e., lower boiling point) and with lesser tendency to sorb to the solid phase (i.e., greater polarity). This agrees with previous hypotheses.[4,7]

Graphical Determination of Diffusivity

The assumption used to calculate D_e—that in all three runs the diffusion cell could be approximated by an infinitely deep column—was confirmed by devising an alternative, graphical technique to find D_e from the experimental data. The method is described here because it is useful when the approximation of an infinitely deep column cannot be made.

This technique is based upon comparison of the experimental emission-rate data with a solution of Eq. (1)–(4) expressed in terms of dimensionless variables. The comparison is made by overlaying a plot of the experimental data on a plot of the dimensionless-variable solution, similar to the Theis method used in geohydrology.[12,13]

The length of the column, L, and the amount of each species originally present in the diffusion cell must be known. Define $f = f(t)$ as the cumulative fraction of material (originally present in the sample) emitted at any time. At time zero, f is zero, and at infinite time, f asymptotically approaches unity; df/dt is the fraction of material emitted per unit time

(sec^{-1}). The observed mass of each species trapped during each sampling interval is converted to an emission rate and expressed as df/dt. For each compound, these data are plotted (df/dt against t) on log-log paper. This plot is referred to as Fig. X. The auxiliary line, t(df/dt) = 1, must also be drawn on Fig. X.

The effective diffusivity, D_e, is found indirectly, by finding the characteristic time of the system, t_c, which is defined as L^2/D_e (sec). Dimensionless time, T, is the ratio t/t_c or tD_e/L^2.

Equations (1)–(4) can be solved[10] for C(x,t), and the solution can be manipulated to give f as a function of T. Differentiating f with respect to T gives df/dT, which is a dimensionless flux; this is plotted against T on log-log paper in Fig. 3. To be used, Fig. 3 must be enlarged so that its log cycles are the same length as those of the user's Fig. X. The auxiliary line, T(df/dT) = 1, is also drawn in Fig. 3. Note that Fig. X contains information about the one-dimensional diffusion cell in the experiment, and Fig. 3 contains information about an ideal one-dimensional diffusion cell. At small values of T (and therefore at small values of t), the curve df/dT versus T is asymptotic to the line df/dT = $(\pi^{-1/2})T^{-1/2}$, which can be shown to be equivalent to Eq. (6). For $T < 0.1$, the curve is quite close to the asymptotic line.

To find t_c, Fig. X must be overlain on the enlarged version of Fig. 3 such that the data points fall along the curve and the two auxiliary lines coincide. If both conditions cannot be met, the data are shown not to fit the model of Eqs. (1)–(4). When the superposition has been made, t_c is the ratio of any pair of values of t and T that correspond to each other. Figure 3 shows that the infinite-column approximation is valid for dimensionless times up to 0.1; therefore it was valid to use it for the experimental data presented here.

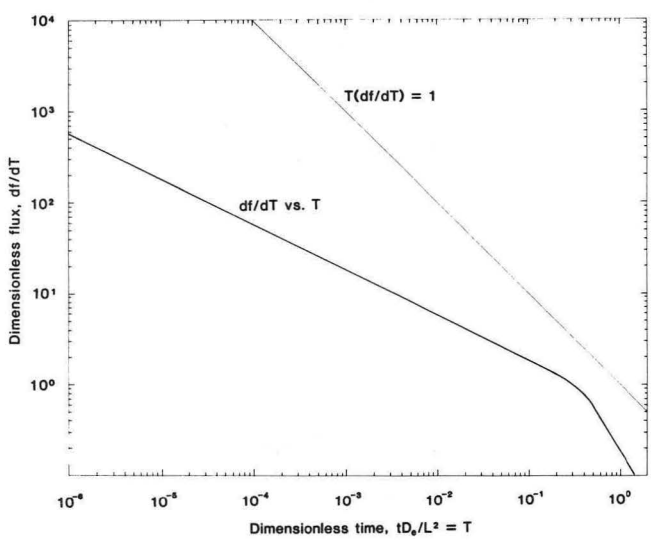

Figure 3. Plot of df/dT (dimensionless flux) against T (dimensionless time). Used for graphical interpretation of experimental data to find D_e. The auxiliary line, (df/dT) = 1, is also shown. (XBL 854-2163)

Conclusions

The results presented here show that sorption to the solid phase strongly influences the rate at which NHCs would be released from a codisposal pile. The moisture content could also be important. Moreover, it appears that the distribution of an NHC among the three phases of a codisposal pile would be determined not only by the amounts of water and air present, but also by the area of shale surface wetted by the water.

The trap-and-desorb technique used here could be applied to the measurement emissions from simulated codisposed wastes under conditions more closely resembling field conditions; by controlling the sample temperature and the humidity of the flushing air, water evaporation could be included in the experiment. A Proctor mold (a metal cylinder in which wastes are compacted to specified densities) fitted with air inlets and Tenax traps could be used as the diffusion cell for simulations of disposal of compacted material.

REFERENCES

1. Daughton, C.G., Jones, B.M., and Sakaji, R.H. (1985), "Organic Nitrogen Determination in Oil Shale Retort Waters," *Anal. Chem. 57*, p. 2326.
2. Hunter, L., Persoff, P., Thomas, J.F., and Daughton, C.G. (1985), "Identification and Correlation of Volatile Components in Retort Wastewaters," in *Applied Science Division Annual Report, FY 1984* , LBL-18754, p. 4–60.
3. Leenheer, J.A., Noyes, T.I., and Stuber H.A. (1982), "Determination of Polar Organic Solutes in Oil Shale Water," *Environ. Sci. Technol. 16*, p. 714.
4. Persoff, P., Hunter, L., and Daughton, C.G. (1984), "Atmospheric Emissions from Codisposed Oil Shale Wastes: a Preliminary Assessment," LBID-890.
5. Jury, W.A., Grover, R., Spencer, W.F., and Farmer, W.J. (1980), "Modelling Vapor Losses of Soil-Incorporated Triallate," *Soil Sci. Soc. Am. J. 44*, p. 445.

6. Thibodeaux, L.J. (1979), *Chemodynamics*, p. 335–341, John Wiley and Sons, New York.
7. Persoff, P., Hunter, L., Daughton, C.G., and Thomas, J.F. (1984), "Prediction of Atmospheric Emissions Resulting from Codisposal of Oil Shale Wastes," in *Applied Science Division Annual Report, FY 1983*, LBL-17073, p. 4–38.
8. Persoff, P., *et al.* (1985), "Removal of Nitrogen Heterocycles from Water by Sorption to Spent Oil Shale," *in Applied Science Division Annual Report, FY 1984*, LBL-18754, p. 4–63.
9. Heistand, R. (1980), letter to J.P. Fox, Development Engineering. Inc., Anvil Points, CO.
10. Crank, J. (1975), *The Mathematics of Diffusion*, 2nd ed., Clarendon Press, Oxford, UK.
11. Mayer, R., Letey, J., and Farmer, W.J. (1974) "Models for Predicting Volatilization of Soil-Incorporated Pesticides," *Soil Sci. Soc. Am. Proc. 38*, p. 563.
12. Freeze, R.A. and Cherry, J.A. (1979), *Groundwater*, p. 343, Prentice-Hall, Englewood Cliffs, NJ.
13. Todd, D.K. (1959), *Ground Water Hydrology*, p. 90, John Wiley and Sons, New York.

Flame Structure in Reacting Turbulent Boundary Layers*

R.K. Cheng, F. Robben, and L. Talbot

Combustion of premixed fuel lean mixtures embedded in a turbulent boundary layer over a strongly heated wall is an experimental configuration which is pertinent to many practical combustion situations. It is also suited for fundamental studies of turbulent combustion interactions since turbulent boundary layer is a classical flow configuration for fluid mechanics studies. Further, the heated turbulent boundary layer is capable of supporting combustion in fuel lean mixtures which otherwise cannot be studied in more conventional burners.

The overall objective of this program is to characterize experimentally the flow field of this reacting turbulent boundary layer using laser diagnostics techniques. The results are used for the development of theoretical turbulent combustion models. To study the changes in the turbulence properties due to combustion, measurements in isothermal and heated non-reacting turbulent boundary layers are also made. Previous investigations include the use of Rayleigh scattering for measuring density fluctuations in heated and reacting turbulent boundary layers[1] and two-component laser Doppler anemometry (LDA) for determining velocity statistics in the isothermal, heated, and reacting layers.[2] In FY 1985, a study of the spatial and temporal structures of the heated and reacting turbulent boundary layers using the two-point Rayleigh scattering technique has been completed.

ACCOMPLISHMENTS DURING FY 1985

The two-point Rayleigh technique[3] measures joint density statistics at two points separated by an adjustable distance. The results are deduced to obtain density spatial correlation coefficient at two points separated in three orthogonal directions, $R(\Delta x)$, $R(\Delta y)$, and $R(\Delta z)$. Here, Δx, Δy, and Δz represent respectively separation distances in the axial direction, x, the transverse direction normal to the heated wall , y, and spanwise direction parallel to the wall, z. Integration of the spatial correlations as functions of the separation distance gives the length scales of the density fluctuations l_x , l_y, and l_z. Also deduced are the space-time double correlations, $R(\Delta t,\Delta x,\Delta y)$, which is the correlation between the data obtained at the two points separated by Δx and Δy with a fixed time delay, Δt. The convection velocities of the thermal or combustion structures are given by correlating the optimum delay time of the space-time correlation with the separation distance. In addition, the orientations of the structures are shown by the locations on the Δx Δy plane where the optimum delay times become zero. The features of the thermal structures in the heated and reacting layers are compared with turbulence structures in isothermal turbulent boundary layer shown on visualization records.

The experimental conditions are free-stream velocity, U_∞, of 19 m/s; wall temperature , T_w, of 1000 K; and ethylene/air equivalence ratio $\phi = 0.35$. The separation distances range from 0.0 to 16.0 mm for Δz, 2.0 to 10.0 mm for Δy, and 2.0 to 50.0 mm for Δx. Figure 1 shows the longitudinal (axial) spatial correlation $R(\Delta x)$ obtained in the reacting layer at four transverse positions. Compared to the spanwise correlation $R(\Delta z)$ shown in FY 1984, the decay of $R(\Delta x)$ is more gradual than that shown for $R(\Delta z)$. The longitudinal length scale l_x is 9.0 mm compared to 4.4 mm for the spanwise length scale l_z. This shows that the thermal structures have a large aspect ratio (i.e., $l_x/l_z > 1$).

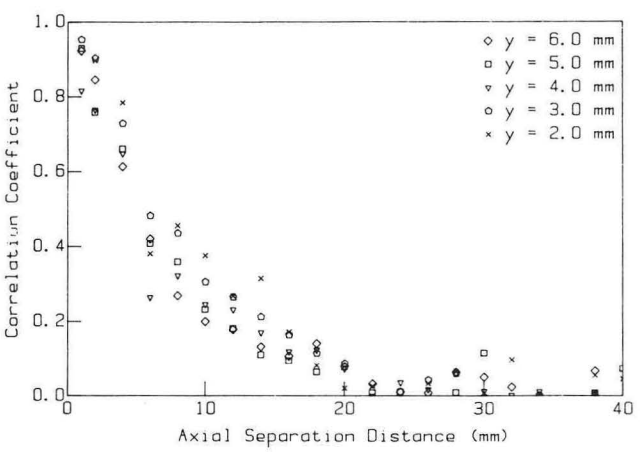

Figure 1. Longitudinal (axial) spatial correlation $R(\Delta x)$ obtained in the reacting layer at y = 2.0, 3.0, 4.0, and 5.0 mm above the heated wall. (XBL 862-455)

*This work was supported by the Director, Office of Energy Research, Office of Basic Energy Sciences, Chemical Sciences Division of the U.S. Department of Energy under Contract No. DE-AC03-76SF00098.

The space-time correlation $R(\Delta t,\Delta x,\Delta y)$ for the reacting layer with Δy fixed at 2.0 mm and various Δx are shown in Fig. 2. The optimum delay time t_0, which is shown by the maximum $R(\Delta t,\Delta x,\Delta y)$ for a fixed Δx and Δy, increases with increasing Δx. The convection velocity U_c for the thermal structures based on $\Delta x/t_0$ is close to the free stream velocity U_∞ . Also note that the optimum delay time for $\Delta x = 1.0$ and $\Delta y = 2.0$ is negative. This indicates that the thermal structures reach position 2 prior to position 1 (Fig. 3a). When Δx and Δy are both at 2.0 mm, t_0 becomes zero. As illustrated in Fig. 3b, this indicates that the thermal structures reach both positions at the same time. Since the two positions are located on an axis at 45° with respect to the wall, our results show that the orientations of the thermal structures are parallel to this 45° axis. Similar conclusions are drawn from the results obtained in the heated layer. Further, the convection velocity and the orientations of the thermal structures observed here are consistent with those observed for the turbulence structures in isothermal layers meaning that the transport of heat and reacting fronts in our flows are dominated by turbulence and with no apparent effects due to heat release.

PLANNED ACTIVITIES IN FY 1986

The diagnostic study of reacting turbulent boundary layer will be extended to include the use of ionization probes. The ionization probe measures the saturation ion current within the reaction fronts and therefore can be used as a flame front detector. One of the shortcomings of the Rayleigh technique for studying the reacting layer is that the measurement cannot distinguish between the heated non-reacting fluids from the reacting fluids. The use of two ionization probes will provide the correlations of the reaction front for comparison with the density correlations.

The technique for measuring velocity at two point separated in space will be developed for studying the reacting turbulent boundary layer. The velocity measurements will complement the density and ion current data. Since velocity space-time correlations in isothermal turbulent boundary layer are only available for the axial velocity component, our investigation will be the first study of transverse space-time correlation. Measurements in the heated and reacting layer will provide a more complete description of the effects of combustion in this flow.

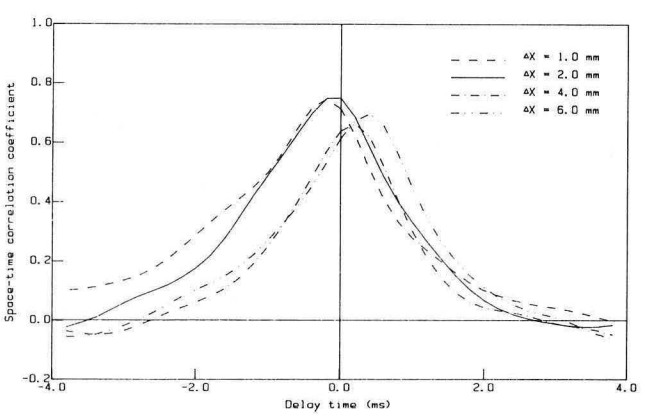

Figure 2. Space-time correlation coefficient $R(\Delta t, \Delta x, \Delta y)$ for the reacting layer with point y fixed at y = 2 mm and point 2 at 2 mm above and at various Δx. (XBL 862-456)

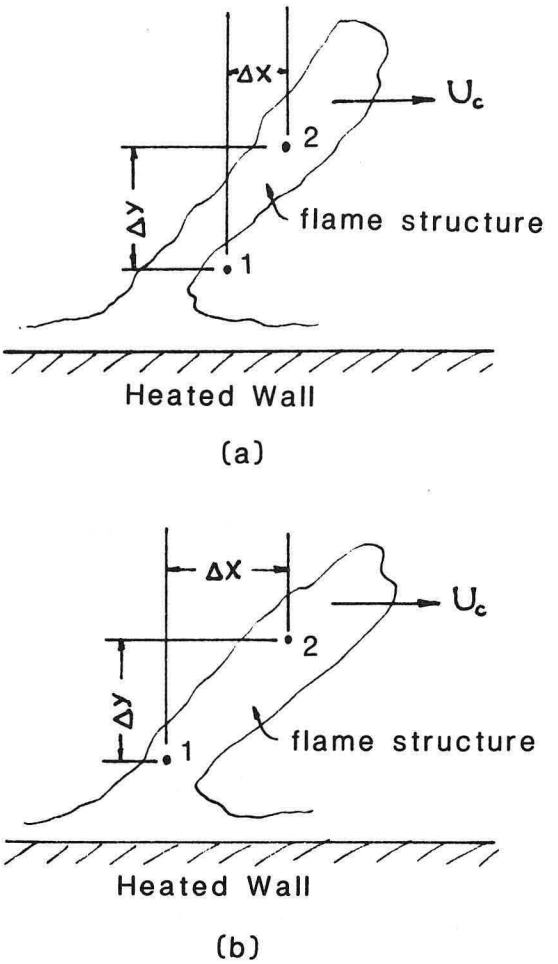

Figure 3. Schematics of the flame structures which would be consistent with the $R(\Delta t, \Delta x, \Delta y)$ results. (XBL 862-457)

REFERENCES

1. Ng, T.T., Cheng, R.K., Robben, F., and Talbot, L. (1982), "Combustion Turbulence Interaction in the Turbulent Boundary Layer Over a Hot Surface," *Nineteenth Symposium (International) on Combustion*, The Combustion Institute, p. 359.
2. Cheng, R.K. and Ng, T.T. (1985), "Conditional Reynolds Stress in a Strongly Heated Turbulent Boundary Layer with Premixed Combustion," to appear in *The Physics of Fluids.*
3. Namazian, M., Talbot, L., Robben, F., and Cheng, R.K. (1982), "Two-Point Rayleigh Scattering Measurements in a V-shaped Turbulent Flame," *Nineteenth Symposium (International) on Combustion,* The Combustion Institute, p. 487.

Intermittency and Conditional Velocity Statistics in Premixed Conical Turbulent Flames*

R.K. Cheng, I.G. Shepherd,† F. Robben, and L. Talbot

The overall goal of this program is to gain better physical understanding of the interaction between turbulence and combustion processes in premixed turbulent flames. The approach is to study the complex turbulent combustion flow field in simplified systems using laser diagnostic techniques. The results are used to compare with predictions of theoretical models. In FY 1985, we have initiated a study of premixed conical turbulent (large Bunsen type) flames. Although this flame configuration has been used in many experimental and theoretical studies the study of conditional velocities has been limited to one velocity component. Our study involves measuring conditional velocity statistics for two velocity components. The results are useful to investigate the difference or similarities between the flame processes in this flame and in the V-flames.

ACCOMPLISHMENTS DURING FY 1985

A schematic of the experimental setup is shown in Fig. 1. The burner is larger than ordinary laboratory model (5.0 cm diameter), and the turbulent flame is stabilized by a ring of pilot flames fitted at the burner exit. Incident turbulence was generated by perforated plate placed 5.0 cm upstream of the exit or at the entrance to the burner cylinder. Conditioned and unconditioned velocity statistics were measured by a two-component laser Doppler anemometry (LDA) system using the sampling technique described in Ref. 1. The intermittency was also obtained by monitoring the Mie scattering from silicon oil aerosol introduced into the flow. The intermittency data are needed to analyze the unconditioned velocity data to obtain the conditioned product velocities. Since intermittency is the probability of encountering the reactants, it can be interpreted as a measure of normalized mean density.

Results were obtained in six flames using either methane/air or ethylene/air mixtures of various concentration ratios. The mean velocity was varied from 3.0 to 8.0 m/s with the incident turbulence intensities ranging from 3 to 15%. Figure 2 shows the contours of the intermittency for a methane/air flame constructed based on three radial profiles at 50, 75, and 100 mm above the exit and a vertical profile along the centerline of the burner axis. As can be seen the flame brush thickness along the centerline is about 90 mm, compared to typical laminar flame thickness of 1 mm.

The conditioned reactant and unconditioned velocities were measured directly by LDA. The unconditioned product velocity was deduced from the unconditioned data using an analysis method described in Ref. 2. This method involves convoluting the velocity probability density functions and is more general than the method used in Ref. 1.

Typical conditioned and unconditioned profiles for the axial and radial velocity components are shown in Fig. 3. The profile of the radial velocity shows that the conditioned product velocities are higher than both the unconditioned and the conditioned reactant velocities. However, the axial velocities show little changes, and significant increases in the unconditioned turbulence intensities within the

*This work was supported by the Director, Office of Energy Research, Office of Basic Energy Sciences, Chemical Sciences Division of the U.S. Department of Energy under Contract No. DE-AC03-76SF00098.

†Department of Mechanical Engineering, University of California, Berkeley.

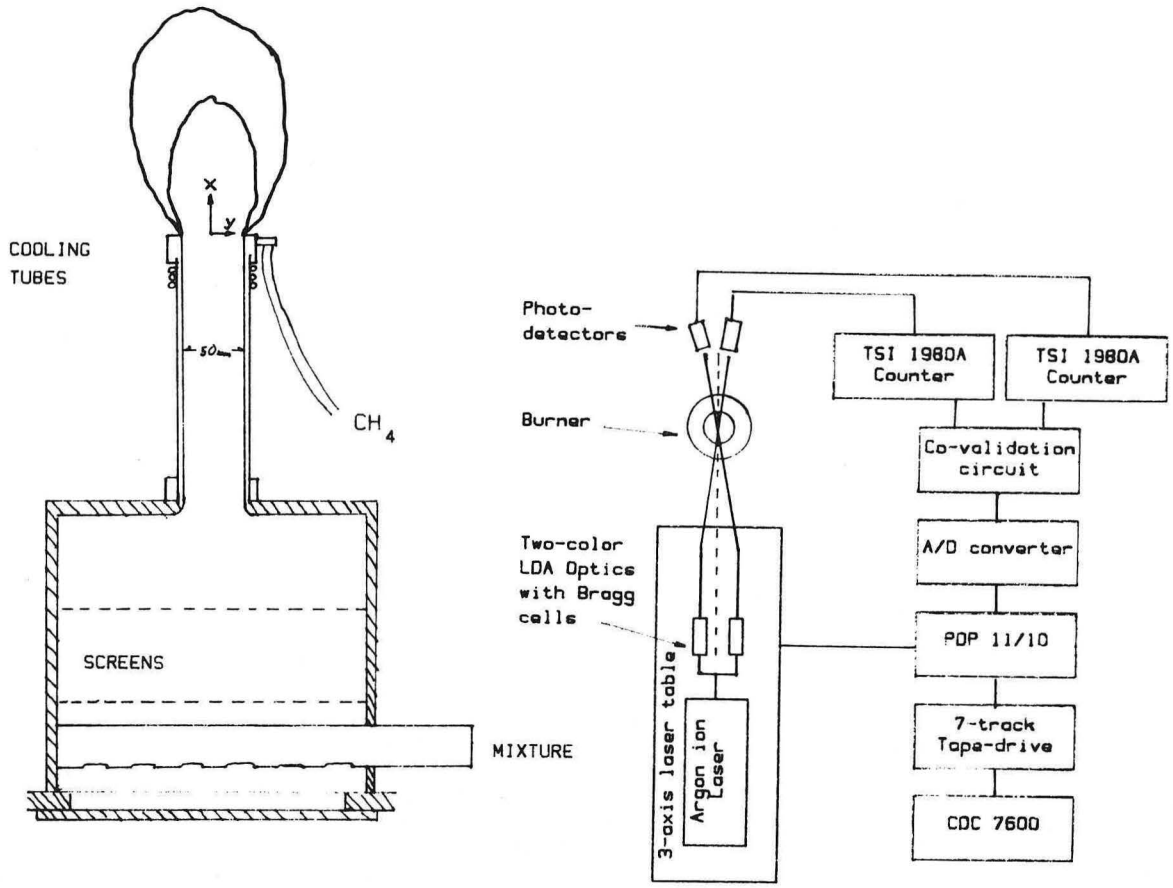

Figure 1. Schematic of the experimental setup. (XBL 862-463)

flame brush were only observed in flames with low incident turbulence (<5%).

The lack of observable increases in the unconditioned turbulence intensities can be explained by the reduction in the relative velocity between the products and the reactants ΔU. The magnitudes of the instantaneous relative velocity for a one-dimensional flame (i.e., the velocity jump across the flame front) Δu is often assumed to be $\Delta u = S_u (\tau - 1)$, where S_u is the local laminar burning velocity and τ is the reactant/product density ratio for the mixture. Since the Bunsen flame flow field is three-dimensional, the relative velocity Δu is reduced due to stream tube divergence. Therefore, the contributions to unconditioned velocity statistics, which are due mostly to the relative velocity, are also reduced.

PLANNED ACTIVITIES FOR FY 1986

Complete analysis of the data is expected to show the changes in ΔU with equivalence ratio and incident turbulence. Though the effect of stream tube divergence provides one of the explanations to the reduction of ΔU in conical flames, further study is needed to fully explain the significant reduction observed along the centerline. In FY 1986, measurement of the orientations of the flame fronts in conical flame will be initiated. Tomographic movies of the conical flame will be obtained and digitized. The distributions of the flame orientations will be correlated with the observed Δu for developing a kinematic model to describe the changes in flame generated turbulence.

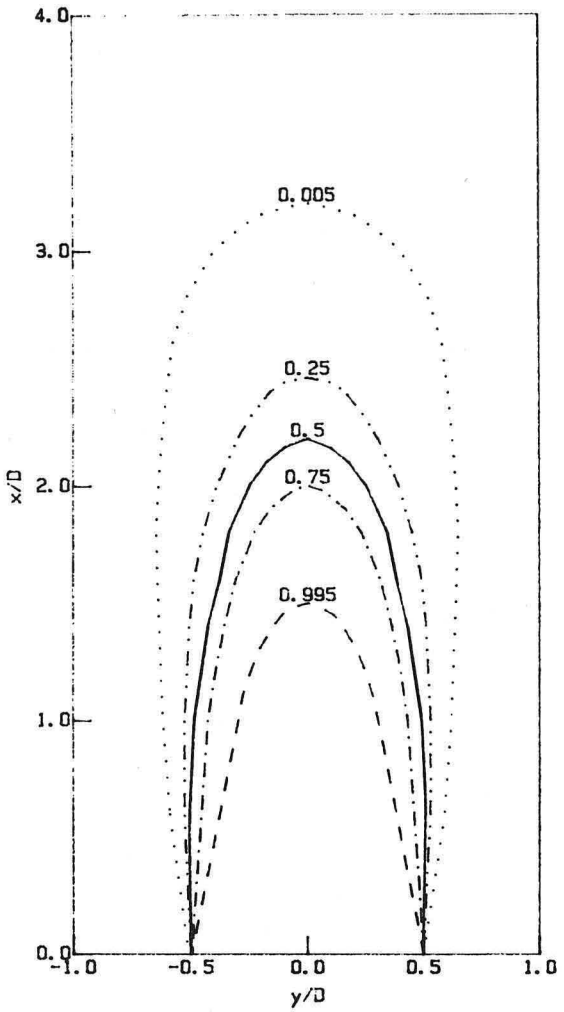

Figure 2. Contours of the intermittency measured in an ethylene/air turbulent conical flame with free stream velocity of 6.6 m/s, equivalence ratio of 0.6, and incident turbulence intensity of 10%. (XBL 862-464)

The initiation of a study in premixed turbulent flame enclosed in a flow channel is also planned. One of the main objectives is to determine whether or not many of the modeling assumptions regarding

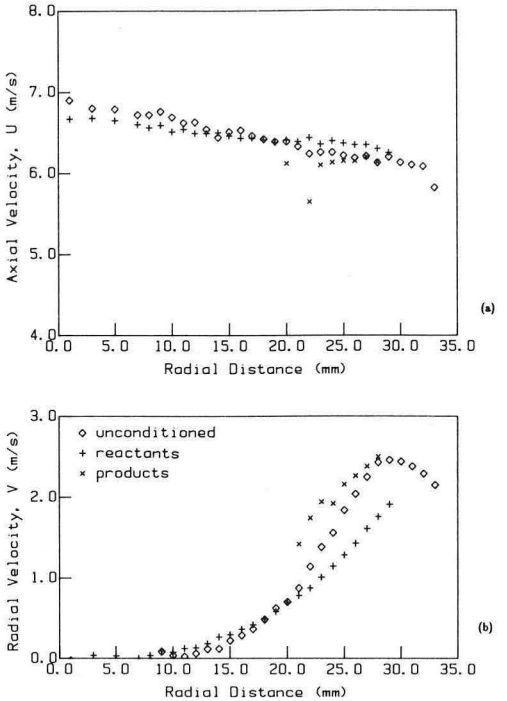

Figure 3. Radial profiles of the conditioned and unconditioned mean velocities for the flame of Fig. 1 at 50 mm above the burner exit. (XBL 862-465)

the behavior of the flame flow field with the constrain of the enclosure are justified. Measurement of the conditional velocities will provide further insight into the turbulence behavior in the enclosed burner.

REFERENCES

1. Cheng, R.K. (1984), "Conditional Sampling of Turbulence Intensities and Reynolds Stress in Premixed Flames," *Combustion Science and Technology 41,* p. 109.
2. Cheng, R.K. and Shepherd, I. G. (1986), "Intermittency and Conditioned Velocity Statistics in Premixed Conical Turbulence Flames," submitted to *Combustion Science and Technology.*

Spectral Behavior of Velocity Fluctuations in Premixed Turbulent Flames*

I. Gokalp,† I.G. Shepherd,‡ and R.K. Cheng

Although spectral analysis has been one of the principal means to to characterize fluid mechanical turbulence in non-reacting flows, experimental spectral information on fluctuating quantities in turbulent flames is scarce. A majority of the investigations of turbulent flames are focused on obtaining the statistical quantities such as the mean, variance, and correlation functions. The lack of spectral data may be due partly to the complexities inherent in the collection of reliable raw data suitable for spectral treatment. Another possible reason is that, at present, most theoretical models of turbulent combustion do not consider temporal scales. Since spectral data provide a great deal more information about the turbulent structures, attempts directed to obtaining them are worth pursuing. With the use of advanced laser optical techniques with sufficient spatial and temporal resolutions and the improved numerical techniques for the spectral analysis of both continuously and randomly sampled turbulent signals, the acquisition of spectral data is greatly facilitated.[1] In addition, development of recent numerical models which consider the length and time scales and the spectra[2-4] have generated more interest in the study of spectral behavior in turbulent flames. In FY 1985 we have initiated a study of the spectral behavior of velocity fluctuations in turbulent premixed V-flames.

ACCOMPLISHMENTS DURING FY 1985

Velocity spectra are calculated for two of the ethylene/air flames investigated in our earlier works. The velocity statistics have been reported in two papers,[5,6] but their spectral behavior has not been investigated. Particular attention is paid to the spectra of the velocity component closest to the normal of the turbulent flame brush. The experimental conditions are: Flame A with $U_\infty = 5.0$ m/s, $\phi = 0.8$, $u' = 5\%$ and Flame B with $U_\infty = 7.0$ m/s, $\phi = 0.75$, $u' = 7\%$. The equivalence ratio for the two flames is close and the main difference is in the turbulence intensities. For Flame B, the incident turbulence is more intense.

The spectral density distributions obtained for Flame A at x = 85 mm are compared in Fig. 1. Three spectra corresponding to the reactants, the flame zone (point of maximum rms fluctuation), and the products are shown. The rms fluctuation velocities are 0.3 m/s in the reactants and 1.2 m/s within the flame. The difference corresponds to an increase in energy level at all frequencies. The "wrinkled laminar flame" concept would predict increase in energy levels in the low frequency range. The spectra obtained at several height above the burner have the same features. The slopes of the reactant spectra are almost constant for different heights above the burner exit and are very close to the classical Komogoroff slope of $-5/3$, which indicates the presence of an inertia subrange. However, the spectra obtained within the flame and the product regions do not exhibit the $-5/3$ slope. The absence of the $-5/3$ slopes suggests that classical velocity spectral interpretation is not appropriate.

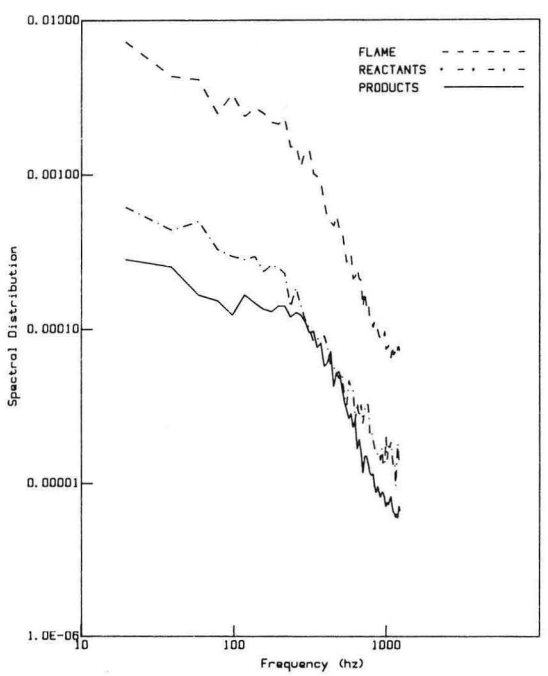

Figure 1. Frequency spectra for an ethylene/air turbulent V-flame with equivalence ratio of 0.8, free stream velocity of 5.0 m/s, and incident turbulent intensity of 5%. (XBL 862-458)

*This work was supported by the Director, Office of Energy Research, Office of Basic Energy Sciences, Chemical Sciences Division of the U.S. Department of Energy under Contract No. DE-AC03-76SF00098.

†Participating guest from CRCCHT-CNRS 45045 Orleans Cedex, France, sponsored by a NATO grant for international collaboration in research.

‡Dept. of Mechanical Engineering, University of California, Berkeley.

One aspect of the turbulent flame, which may provide the key for the interpretation of velocity spectra, is the dynamics of the wrinkled turbulent flame front. Within the flame brush, the stationary LDA probe measures intermittently velocities in the reactant and in the products. Since the two conditioned velocities are different, each passage of flame front across the measurement position results in a sudden jump in velocity. The velocity spectra then contain the effects due to the flame passage. The change in the spectral slopes may be due to this effect. Without the support of additional data, this remains a speculation at best. However, it emphasizes the need to study the analogy between velocity and scalar spectra.

Figure 2 shows the wave-number representation for the velocity spectra shown in Fig. 1. The main feature of the wave-number spectra is the shifting of the most energetic wave number (i.e., the wave number corresponding to the peak of the spectrum) toward a lower value in the flame and in the products. The shifting of the most energetic point of the product spectra to lower wave number is consistent with the dilatation effects and the increased viscosity which smears the small eddies to increase the mean size of the most energetic eddies.

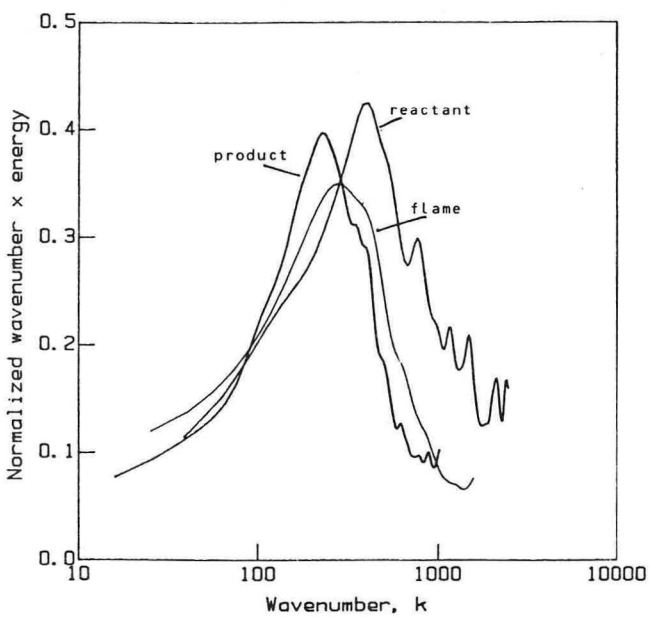

Figure 2. Normalized wave-number spectra corresponding to Fig. 1. (XBL 862-459)

PLANNED ACTIVITIES FOR FY 1986

Velocity spectra will be calculated for the data obtained in the conical flames. Since the velocity measurements for the conical flames are made for two velocity components, the spectra for the component normal to the flame brush will be studied. To further investigate the analogy between velocity and scalar spectra, the spectra for the intermittency will be calculated. Also the spectral dynamics of the flame front which can be deduced form the LARS data will be investigated. The results will be useful to identify the influence of the fluctuating flame on velocity statistics.

REFERENCES

1. Srekantaiah, D.V. and Coleman, H.W. (1984), "Turbulent Spectrum from Individual Realization Laser Velocimetry Data," *Experiments in Fluids 3*, p. 35.
2. Bray, K.N.C., Libby, P.A., and Moss, J.B. (1984), "Scalar Length Scale Variation in Premixed Turbulent Flames," *Twentieth (International) Symposium on Combustion,* The Combustion Institute, p. 421.
3. Bray, K.N.C., Libby, P.A., and Moss, J.B. (1984), "Flamlet Crossing Frequencies and Mean Reaction Rate in Premixed Turbulent Flames," *Combustion Science and Technology 41,* p. 143.
4. Kerstein, A.R. (1985), "Pair Exchange Model of Turbulent Premixed Flame Propagation," paper presented at the 1985 Fall Meeting of the Western States Section of the Combustion Institute, Davis, CA, Oct. 1985.
5. Cheng, R.K. and Ng, T.T. (1983), "Velocity Statistics in Premixed Turbulent Flames," *Combustion and Flame 52,* p. 185.
6. Cheng, R.K. and Ng, T.T. (1984), "On Defining the Turbulent Burning Velocity in Premixed V-Shaped Turbulent Flames," *Combustion and Flame 57,* p. 156.

Structure and Propagation of Turbulent Premixed Flames Stabilized in a Stagnation Flow*

P. Cho,† C.K. Law,† J.R. Hertzberg, and R.K. Cheng

Many configurations and methodologies have been adopted in the fundamental studies of structure and propagation of turbulent premixed flames. The most prevalent configurations for studying open and steady flames are the Bunsen-type conical flames and the V-flames stabilized by a rod. Although the two configurations are relevant to the burner geometries commonly found in practical combustors, comparison of the experimental results with predictions of theoretical turbulent combustion models is not straightforward. This is due in part to the fact that the flame brushs in both configurations are oblique to the approach flow. Since most of the turbulent combustion models (e.g., the model of Bray, Moss, and Libby[1]) are one dimensional, transformation of the results to the "flame coordinate" is necessary.

In view of the above considerations, we have initiated a study of premixed turbulent flame where the flame brush is locally normal to the approach flow and does not involve a recirculation region for stabilization. The methodology involves stabilizing a planar turbulent flame in a stagnation flow with incident turbulence generated by grid or perforated plate. This configuration has been adopted in previous studies of laminar flames,[2] although its application to turbulent flames has not been reported.

ACCOMPLISHMENTS DURING FY 1985

Figure 1 shows a schematic of the experimental setup. A uniform axisymmetrical flow of premixed methane/air mixture is provided by a 50 mm diameter nozzle. The exit velocity is varied from 3 to 6.7 m/s. Incident turbulence is generated by placing at 50 mm upstream of the nozzle exit either a square mesh grid or a perforated plate. The planar turbulent flame is stabilized by a solid brass 200 mm diameter circular stagnation plate. The surface facing the flow is convex (r = 460 mm) to allow LDA access close to the plate surface (Fig. 1). This arrangement enables measurements of the axial velocity component normal to the plate at 3.0 mm from the plate surface. Flow velocities are measured by a four-beam two-color LDA system with a 4.0 watt argon-ion laser. All four beams are shifted by Bragg cells and differential frequency of 5.0 MHz is used for both components for removal of directional ambiguity. The seeding is provided by refractory aluminum oxide particles of 0.3 μm introduced into the flow by a cyclone canister seeder.

The mean and rms centerline axial profiles for two of the thirty methane/air flames studied are compared in Fig. 2. Both mean axial velocity profiles exhibit the characteristic "hump-back" trend previously observed in laminar stagnation flames. The linear decrease of U, with decreasing distance from the wall, is due to the divergence of the stagnation flowfield. Flow acceleration due to combustion gives rise to the "hump." The rms fluctuation profiles show that within the flame zone, u′ increase to a peak of 0.8 m/s for the richer flame while the peak u′ is only slightly higher than the incident turbulence for the leaner flame. The corresponding v′ profiles show that the increase within the flame zone is only shown for the richer flame. But in both cases, v′ increases in the product zone while u′ decreases. The corresponding Reynolds stress profiles (not shown) do not indicate any changes through the flame zone. The same feature is found on all of the Reynolds stress profiles obtained for this study.

The point where the mean axial velocity profile deviates from linearly decay is the boundary of the turbulent flame brush. Since the flame brush is normal to the approach flow, the velocity at this point is by definition the turbulent burning velocity S_t. This concept is similar to that used for the determination of laminar flame speed in stagnation flow[1] and is consistent with the definition proposed by Cheng and Ng[3] for the determination of S_t in V-flames.

In Fig. 3, all of our results are compared with the results of Cheng and Ng[3] for ethylene/air V-flames, Smith and Gouldin[4] and Dandekar and Gouldin[5] for methane/air V-flames, Ballal and Lefebvre[6] for confined propane/air V-flames, and Abdel-Gayed and Bradley[7] for double expanding cylindrical hydrogen/air flames in the form of S_t/S_l versus u'/S_l. Our results are in excellent agreement with the results reported by others using different flame configurations.

*This work was a collaboration effort between U.C. Davis and LBL. The work at LBL was supported by the Director, Office of Energy Research, Office of Basic Energy Sciences, Chemical Sciences Division of the U.S. Department of Energy under Contract No. DE-AC03-76SF00098. The work at Davis was supported by the U.S. Air Force Office of Scientific Research under Grant No. 85-0147.

†Department of Mechanical Engineering, University of California, Davis, CA.

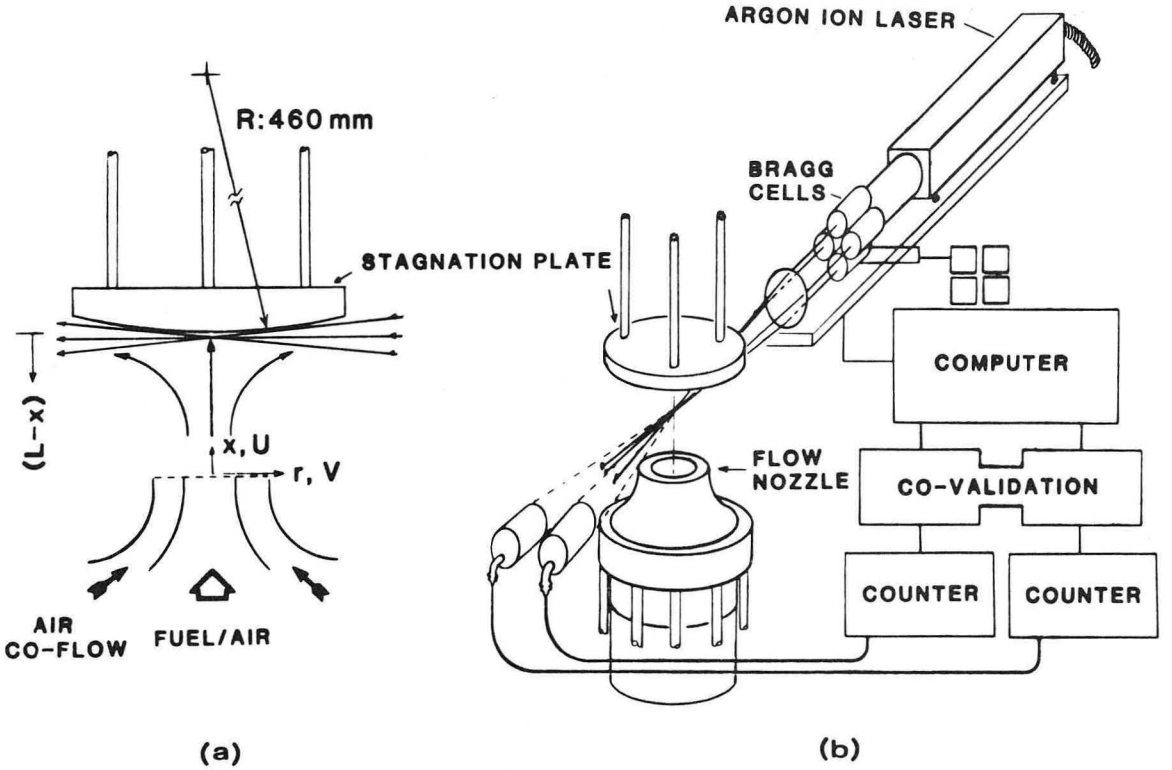

Figure 1. Schematic of the experimental setup. (XBL 862-452)

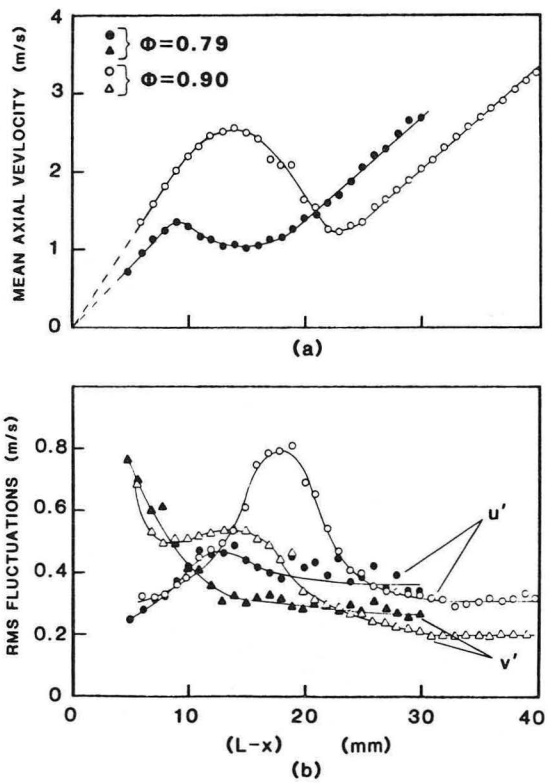

Figure 2. Velocity profiles of reacting flows, centerline traverse. (a) mean velocities; (b) rms fluctuations. (XBL 862-453)

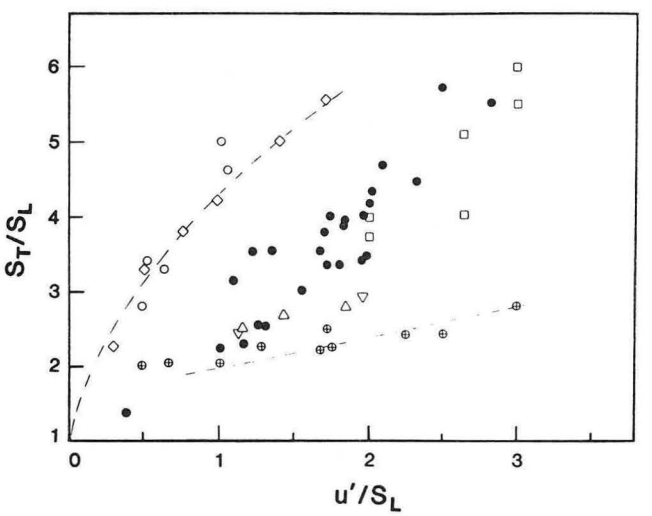

Figure 3. Correlation of turbulent flame speeds: Present work, propane/air, stagnation flow; Abdel-Gayed and Bradley, hydrogen/air bomb; Kleine, methane/air, cone; Ballal and Lefebvre, propane/air, confined V-flame; Cheng and Ng, ethylene/air, open V-flame; Dandekar and Gouldin, methane/air, open V-flame; Smith and Gouldin, ethylene/air, open V-flame. (XBL 862-454)

PLANNED ACTIVITIES FOR FY 1986

The study of turbulent stagnation flame will be extended to measurement of conditional velocities and scalar fluctuations. Ethylene and propane will be used as fuel. The scalar measurements will provide a more concise definition of the flame boundary for the determination of the turbulent flame speeds. The conditional velocities will be useful for studying flame-generated turbulence in this configuration where the flow field in the product zone is divergent.

REFERENCES

1. Bray, K.N.C., Moss, J.B., and Libby, P.A. (1985), "Unified Modeling Approach for Premixed Turbulent Combustion—Part I: General Formulation," *Combustion and Flame 61*, p. 87.
2. Wu, C.K. and Law, C.K. (1985), "On the Determination of Laminar Flame Speeds From Stretched Flames," *Twentieth Symposium (International) on Combustion*, The Combustion Institute, p. 1941.
3. Cheng, R.K. and Ng, T.T. (1984), "On Defining the Turbulence Burning Velocity in Premixed V-Shaped Turbulent Flames," *Combustion and Flame 57*, p. 155.
4. Smith, K.O. and Gouldin, F.C. (1979), "Turbulence Effects on Flame Speed and Flame Structure," *AIAA J. 171*, p. 1243.
5. Dandekar, K.V. and Gouldin, F.C. (1982), "Temperature and Velocity Measurements in Premixed Turbulent Flames," *AIAA J. 20*, p. 642.
6. Ballal, D.R. and Lefebvre, A.H. (1975), "The Structure and Propagation of Turbulent Flames," *Proc. Roy. Soc. London 344A*, p. 217.
7. Abdel-Gayed, R. and Bradley, D. (1977), "Dependence of Turbulent Burning Velocity to R.M.S. Turbulent Velocity," *Sixteenth Symposium (International) on Combustion*, The Combustion Institute, p. 1725.

Premixed Flame Stabilization on a Bluff Body*

J.R. Hertzberg and L. Talbot

In order to study the effects of fluid mechanics on combustion, the structure of a turbulent premixed flame stabilized on a bluff-body flameholder has been observed using Rayleigh scattering for single-point measurements of density. The region near the flame holder is the focus of this work. The intent is to observe the interaction of the recirculation zone and the developing flame in order to better understand the evolution of a flame sheet into a turbulent flame brush.

The combustor configuration for the laminar, premixed V-shaped flame consists of a vertical 5 cm diameter open jet of ethylene-air mixture with a square cross section rod flame holder transverse to the flow. Turbulence is generated by a wire grid of 1 mm elements and 5 mm spacing, placed 50 mm upstream of the flame holder, at the nozzle exit. The fuel-air jet is protected from shear with the stagnant surroundings by an annular air jet. Spatial coordinates are measured from the top center of the flameholder; Z is vertical, X is horizontal. Two conditions have been studied: (1) a very lean flame, close to being blown off the flame holder at 5.5 m/s, equivalence ratio $\phi = 0.54$ and (2) a slightly richer, well-stabilized flame at 5.5 m/s, $\phi = 0.63$.

ACCOMPLISHMENTS DURING FY 1985

Point measurements of density using laser Rayleigh scattering[1] have been made in a region beginning at 0.5 mm downstream of the flame holder and extending to 80 mm downstream.

Flame brush extent and position can be calculated from time-averaged profiles using the steepest gradient method, and is shown in Figs. 1 and 2. Figure 1 shows the growth of the flame zone with distance downstream. The well-stabilized flame shows a nearly constant rate of brush growth while the very lean case shows a much more rapid growth for the first 25 mm and then slows down for the rest of the observed region. Another important result is that both cases show an initial thickness of 1 mm. This could be due to a nearly laminar flame, moving slightly, or to the thickness of an as yet non-reacting shear flow with a temperature difference. Figure 2 shows the relative positions of the two brushes. It is

*This work was supported by the Air Force Office of Scientific Research under grant AFOSR 84-0124, through the U.S. Department of Energy under Contract No. DE-AC03-76SF00098.

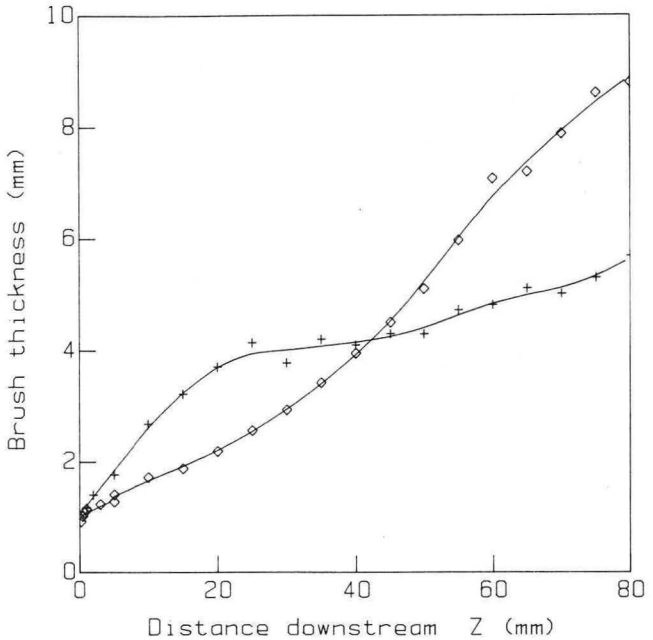

Figure 1. Flame thickness vs. distance downstream of flame holder. Well-stabilized case = diamond; very lean case = plus. (XBL 862-397)

interesting to note that the outer extent of the two coincide until approximately the same distance downstream that the slope of growth of the leaner case slackens. The inner extent of the leaner brush is closer to the centerline of the flow than the well-stabilized case, possibly indicating a narrower recirculation zone.

In order to examine the evolution of the structure of the brush with distance downstream the probability density function (pdf) of gas density at the center of the flame from each profile is shown in Fig. 3 for the richer case and in Fig. 4 for the leaner case. In both cases the pdf at Z = 5 mm is monomodal; that is, the stationary Rayleigh measurement volume sees an even distribution of densities, corresponding to gas temperatures ranging from room temperatures to burned gas temperatures, with nearly equal probability. Staying in the center of the flame and moving downstream, the distribution becomes bimodal: the measurement volume sees mostly burned or unburned, with very little in between. The difference between the two cases is that the well-stabilized case is noticeably bimodal by 20 mm downstream, while the lean case is just beginning to show signs of bimodality. This point, coupled with the fact that the lean case brush is twice as thick as the richer case, seems to indicate that the structure of the lean case at that position may be a thick laminar flame moving slightly, while the well-stabilized case shows a much thinner flame, flapping more rapidly. Unfor-

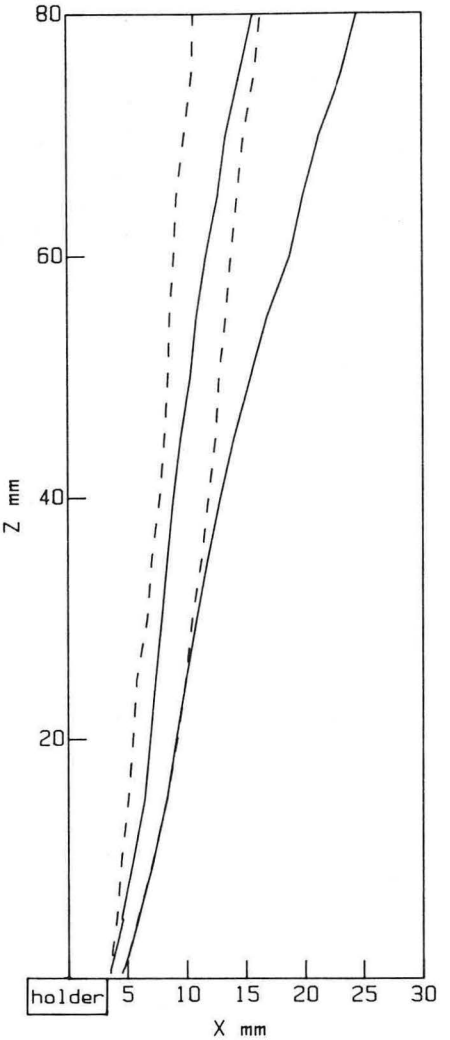

Figure 2. Flame brush position. Well-stabilized case = solid lines; very lean case = dashed line. (XBL 862-398)

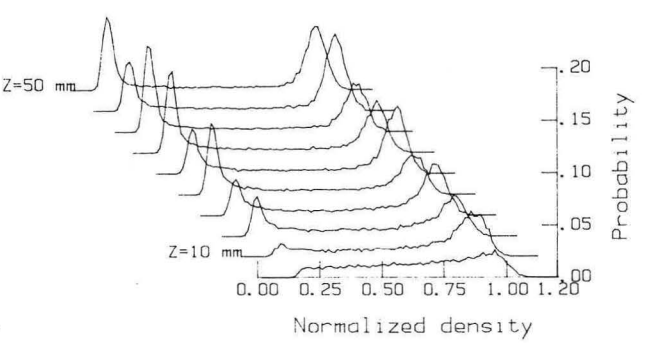

Figure 3. PDF of density at center of flame for well-stabilized case. (XBL 862-399)

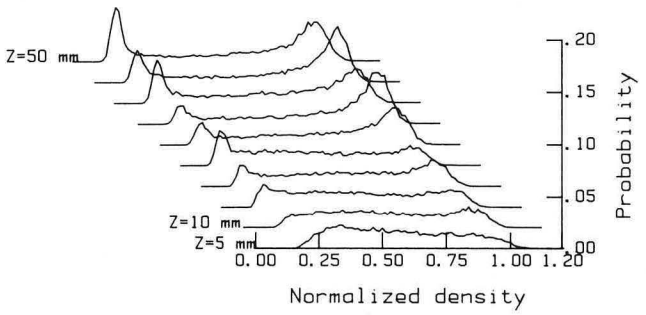

Figure 4. PDF of density at center of flame for very lean case. (XBL 862-400)

tunately, although it is true that the leaner flame will have a slightly thicker laminar flame, the magnitude of that difference is unlikely to be large enough to account for the data.

PLANNED ACTIVITIES FOR FY 1986

Laser doppler velocimetry measurements of reacting flow will be made in order to map the flow characteristics of the flame holder region in the well-stabilized and close to blow off cases. Ionization probe measurements will also be made to determine the flame stand off distance and how it changes with equivalence ratio.

REFERENCES

1. Namazian, M., et al. (1982), "Two-Point Rayleigh Scattering Measurements in a V-Shaped Flame," *Nineteenth Symposium (International) on Combustion,* The Combustion Institute, p. 487.

Fluid Dynamic Considerations in the Numerical Modeling of Flames*

M.Z. Pindera and L. Talbot

The objective of this investigation is to develop a deterministic numerical model of turbulent flame propagation in premixed reactants. The influence of the flame front on fluid dynamics of the surrounding gas is studied both for turbulent and non-turbulent conditions. The model is formulated for continuous flames of finite length such as the V-shaped configuration studied by Cheng[1] or for the stagnation point combustion studied by Wu and Law.[2] Compared to the statistical modeling approach used in many investigations where the change in flame turbulence is often used as input parameters, the present model is capable of predicting the turbulence phenomena.

ACCOMPLISHMENTS DURING FY 1985

The numerical model is based on the concept that the effects of flame exothermicity are manifested only through volumetric expansion which is confined to a narrow (in principle infinitesimally thin) flame region. The flame is thus taken as a collection of sources embedded in a flow of uniform density. The effects of pressure gradients at the flame front (the baroclinic term) are accounted for by adding vorticity to the flow on the burnt side. Magnitude of the vorticity can be found from conservation of momentum. Vorticity then is treated using the Lagrangian method of Chorin.[3] The dynamics of the flame itself are accounted for by computing the flame motion in two steps, as outlined by Ghoniem, *et al.*[4] First it propagates in the direction normal to itself at a specified flame speed, and then is advected by the motion of the gas. The theory and representative calculations have been reported in two papers (Pindera and Talbot[5–6]).

Comparisons of the numerical and experimental results are shown in Figs. 1–3. The experimental flame geometry is the turbulent premixed V-flame.[1] However, the calculations are obtained for a stationary flame without considering the effects of incident turbulence. Since the fluctuating flame is not expected to affect significantly the mean flow velocity, the overall features of the flow field can be compared. Figure 1 shows the mean axial velocity profiles at various axial positions reported by Cheng.[1] Figure 2 shows calculated velocity profiles for the same case when vorticity generation is not considered. As can be seen, the predicted velocity near $y = 0$ is much lower than the experimental value. Figure 3 shows the effects of including vorticity generation in the calculations. The comparison between

*This work was supported by the Director, Office of Energy Research, Office of Basic Energy Sciences, Chemical Sciences Division of the U.S. Department of Energy under Contract No. DE-AC03-76SF00098.

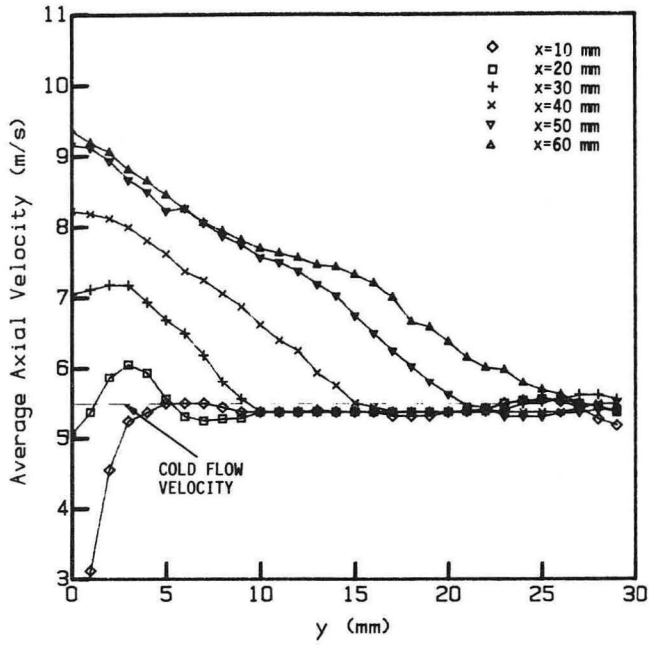

Figure 1. Measured average axial velocities. (XBL 862-421)

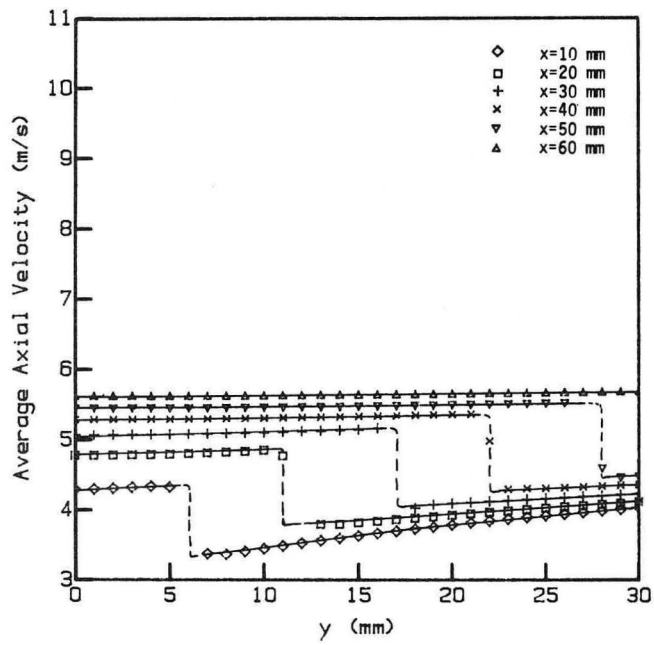

Figure 2. Calculated axial velocities; no vorticity. (XBL 862-422)

the experiments and theory is much improved. Our study shows that when the flame-produced vorticity is not considered in the model, as is common in models of this type (see, for example, Ghoniem, *et al.*,[4] Sethian,[7] Ashurst and Barr[8]), the results may be erroneous, since momentum is not conserved.

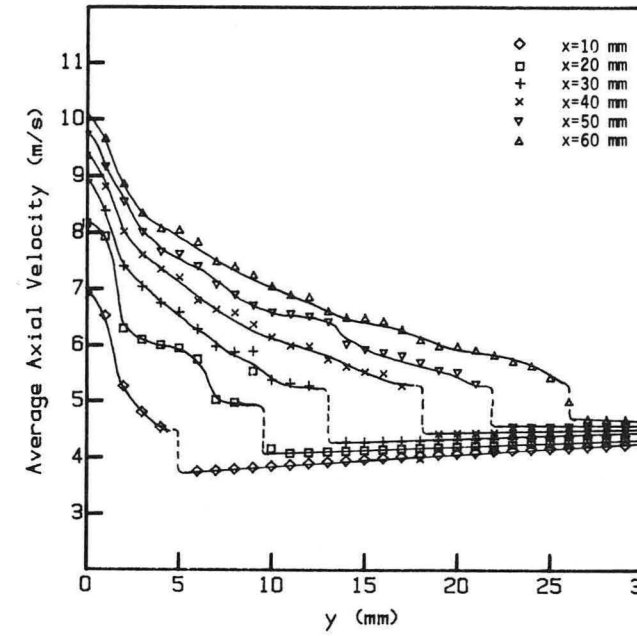

Figure 3. Calculated axial velocities; vorticity added. (XBL 862-423)

PLANNED ACTIVITIES FOR FY 1986

The model will be extended to include the interaction of the flame with the incident turbulent flow field. In particular the experimental work of Cheng[1] for the turbulent V-shaped flame geometry will be modeled. The algorithm will be generalized to consider the effects of nonuniform flame speed on the generation of vorticity. The experimental and predicted values of the mean velocities, the rms fluctuation intensities, and Reynolds stress will be compared.

REFERENCES

1. Cheng, R.K. (1984), "Conditional Sampling of Turbulence Intensities and Reynolds Stress in Premixed Flames," *Comb. Sci. and Tech 25*, p. 109.
2. Wu, C.K. and Law, C.K. (1984), "On the Determination of Laminar Flame Speeds from Stretched Flames," *Twentieth Symposium (International) on Combustion*, The Combustion Institute, p. 1941.
3. Chorin, A. J. (1973), "Numerical Study of Slightly Viscous Flow," *J. of Fluid Mech. 57*, p. 785.
4. Ghoniem, A.F., Chorin, A.J., and Oppenheim, A.K. (1982), "Numerical Modeling of Turbulent Flow in a Combustion Tunnel," *Phil. Trans. R. Soc. A 394*, p. 303.

5. Pindera, M.-Z. and Talbot, L. (1986), "Flame Induced Vorticity: Effects of Stretch," submitted to *Twenty-First Symposium (International) on Combustion*, The Combustion Institute.
6. Pindera, M.-Z. and Talbot, L. (1986), "Some Fluid Dynamic Considerations in the Modelling of Flames," submitted to *Combustion and Flame.*
7. Sethian, J. (1984), "Turbulent Combustion in Open and Closed Vessels," *J. Comp. Phys. 54,* p. 425.
8. Ashurst, W.T. and Barr, P.K. (1983), "Stochastic Calculation of Laminar Wrinkled Flame Propagation Via Vortex Dynamics," *Comb. Sci. and Tech. 34,* p. 227.

Linear Array for Rayleigh Scattering (LARS)*

I.G. Shepherd, G.L. Hubbard, W. Walker, III, F. Robben, and L. Talbot

The award of a Department of Defense Research Equipment Grant has made possible the development of a linear array for Rayleigh scattering system (LARS). This is a new space-time imaging technique which derives the gas density along a segment of a laser beam from the intensity of Rayleigh scattered light.

Previous two-point Rayleigh measurements made by this group[1,2] have been used to investigate the structure of premixed turbulent flame zones. These experiments have been used to develop a model[2,3] which predicts flame statistics from the probability density function of the flame front position. The new technique can determine the instantaneous flame front position directly and hence test some assumptions of the model. In addition it also makes possible the time resolved study of the flame front oscillations and the instantaneous flame profile.

ACCOMPLISHMENTS DURING FY 1985

This year the construction and testing of the LARS system have been completed and preliminary investigations commenced. The Rayleigh light scattered by a segment of a laser beam is imaged by means of collection optics and an image intensifier onto a 512 element Reticon array. The array is driven by a Microtex electronic data transfer system which is capable of a maximum 5 MHz pixel reading rate. The camera is interfaced by direct access memory to a PDP 11/73 computer which can store up to 2560 scan lines, i.e., 1.25 Mbytes of information. In order to deal with such large amounts of data an image processing system of the type used to analyze Landsat images has been incorporated into the computer. This system is manufactured by International Image Systems (I^2S) and is driven by a software package written and developed at U.C. Davis, and provides a sophisticated display as well as performing array computations very quickly. By such means systematic errors in the data, e.g., pixel-to-pixel sensitivity, may be readily removed from the data and carried out online. The camera system has a maximum line scan rate of 10 kHz and at a 1:1 optical magnification has a spatial resolution of 20 pixels/mm, adequate for the resolution of a flame front. A related system has been developed by Rajan, *et al.*[4] using, however, a pulsed laser which severely restricted the laser line sampling rates so that the time evolution of the flame front position could not be followed.

Preliminary experiments have been performed in a lean ($\phi = 0.6$), premixed V-shaped flame at 5 m/sec and inlet turbulence of 2%. Figure 1 is an iso-intensity contour in the space-time plane and shows the time history of the flame front position. The linear array was scanned at 3 kHz with a 1:1 magnification. From these data such information as the distribution of the magnitude of flame front excursions and the spectrum of flame front movement, Fig. 2, can be derived. By choosing a different iso-intensity contour, Fig. 3, a measure of the flame front thickness may be obtained. In this case the contour separation represents a 15% difference in light intensity.

PLANNED ACTIVITIES FOR FY 1986

There are two broad areas where the investigation of premixed turbulent flames studied by this

*This work was supported by the Air Force Office of Scientific Research under contract F-44620-76-C-0083, and additional equipment and facilities were provided by the Chemical Sciences Division of the U.S. Department of Energy under Contract No. DE-AC03-76SF00098.

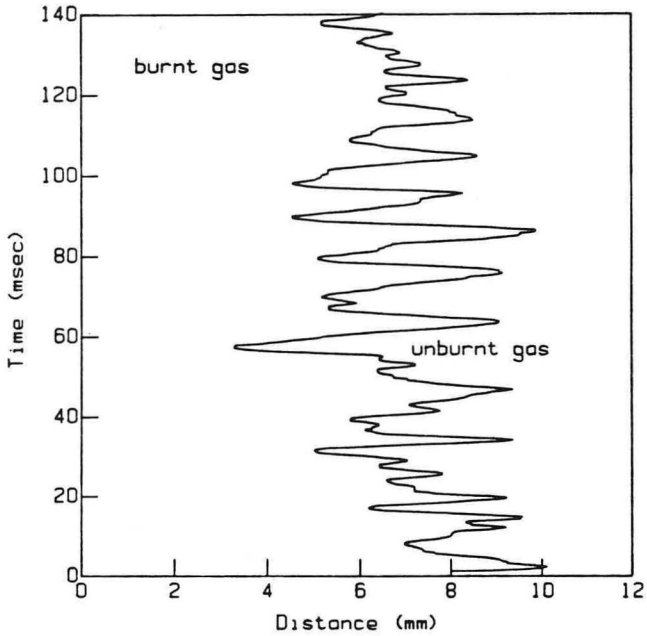

Figure 1. Flame front movement from iso-intensity contour. (XBL 862-460)

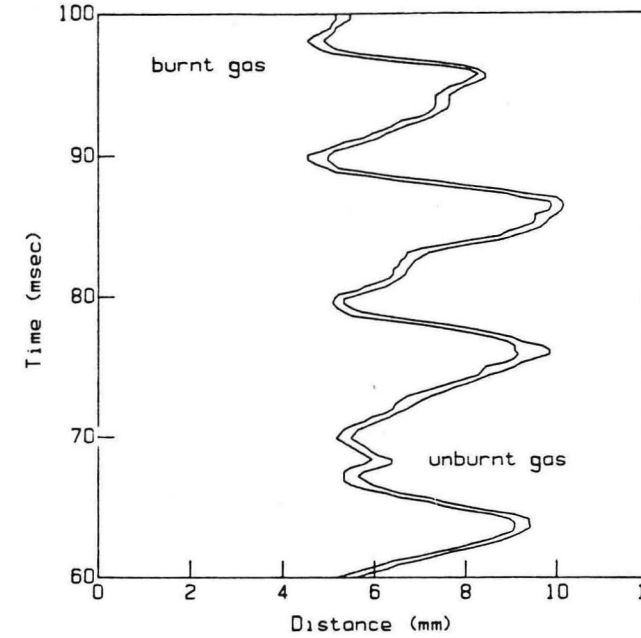

Figure 3. Two iso-intensity contours differing by 15% in light intensity. (XBL 862-462)

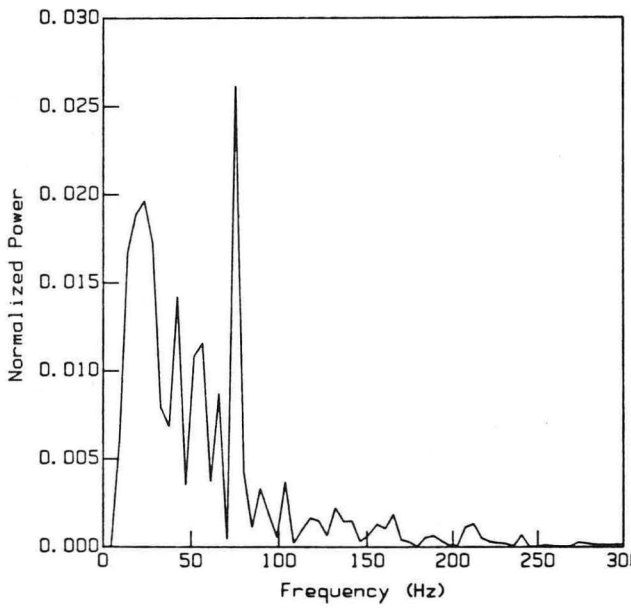

Figure 2. Spectrum of flame front oscillations. (XBL 862-461)

program is necessary: 1) the structure and evolution of the turbulent flame region and 2) the profile of the flame interface within the flame zone. LARS and laser tomography will be used to study these phenomena, and extensive use will be made of image processing techniques, at present under development, to reduce the data.

REFERENCES

1. Namazian, M., Talbot, L., Robben, F., and Cheng, R.K. (1982), "Two-point Rayleigh Scattering Measurements in a V-Shaped Turbulent Flame," *Nineteenth Symposium (International) on Combustion*, The Combustion Institute, p. 487.
2. Namazian, M., Talbot, L., and Robben, F. (1984), "Density Fluctuations in Premixed Turbulent Flames," *Twentieth Symposium (International) on Combustion*, The Combustion Institute, p. 411.
3. Namazian, M., Shepherd, I.G., and Talbot, L. (1986), "Characterization of Density Fluctuations in a Turbulent Premixed V-Shaped Flame," *Combustion and Flame.*
4. Rajan, S., Smith, J.R. and Rambach, G.D. (1984), "Internal Structure of a Turbulent Premixed Flame Using Rayleigh Scattering," *Combustion and Flame 57*, p. 95.

Theoretical Combustion Kinetics and Ignition Chemistry*

Nancy J. Brown, Ola Rashed, and Donald Lucas

Combustion chemistry consists of complex chain mechanisms involving radical species. Radicals occur in small concentrations throughout the flame due to their high reactivity, and as a consequence, are difficult to measure quantitatively. In the majority of flame systems, 100 or more elementary reactions are involved in the oxidation of fuel to CO_2, H_2O, and nitrogen or sulfur-containing pollutant species. The application of theoretical treatments of reactivity has been successful in predicting rate coefficients for several important reactions and for acquiring an understanding of the energetic factors which influence reactivity. Theories of reactivity are classified as being either dynamical or statistical, and our group has pursued the utilization of each of these to investigate reactivity and energy transfer in molecular systems important in high temperature combustion systems.

Understanding ignition phenomena in combustion systems operating over a range of pressures and temperatures, and which utilize a variety of fuel types, is a crucial step in achieving control over the combustion process. Controlling combustion will enable us to burn various fuels under conditions which maximize power output while minimizing pollutant emissions. Our research focusses upon understanding the chemistry of ignition processes. We have initiated combustion with laser photolysis to generate fixed concentrations of radicals to identify limiting requirements for ignition. Our experimental research is complemented by a modelling study which provides results useful for interpreting the experiments.

ACCOMPLISHMENTS DURING FY 1985

We have investigated energy transfer in the He_2 + OH system using the formalism of quasi-classical dynamics. Three basic approximations are employed: 1) the use of the Rashed-Brown[1] modification to the Schatz-Elgersma[2] analytical fit to the Walch-Dunning[3] ab initio potential surface, 2) treatment of the dynamics with classical mechanics, and 3) the use of Monte Carlo averaging techniques to sample the phase space of the system.

*This work was supported by the Director, Office of Basic Energy Sciences, Chemical Sciences Division of the U.S. Department of Energy under Contract No. DE-AC03-76SF00098.

Energy transfer is described in terms of changes in translational energy, and the rotational and vibrational energy in each molecule by subtracting relevant values of the initial energy from the final values. Angular momentum changes are determined in a similar fashion. Average values per collision of the various energy transfer quantities are computed for each ensemble of trajectories. Histograms of the various types of final energies in the system were computed, and state-to-state rotational and vibrational cross sections were determined. Further understanding of the energy transfer mechanism is gained through the use of correlation coefficients, which provide a measure of the relationship between two energy transfer quantities on a single collision basis.

Energy transfer is investigated as a function of translational temperature, the initial rotational energy in each molecule, and initial vibrational energy in each molecule. The translational temperatures considered are 300 to 4000 K, with the majority of the calculations performed at 1200 and 2000 K. The initial value of the rotational quantum number is in the range 0–6 for H_2 and 0–7 for OH. The initial value of the vibrational quantum number for each molecule is in the range 0–4.

The most important finding of our study can be summarized as follows:

1) The energy transfer mechanism is complex with ten types of energy transfer possible. Evidence was found for all types, and this indicates that energy transfer mechanisms in diatom-diatom collisions are far more complicated than those for atom-diatom collisions.

2) There is much more exchange between the translational degrees of freedom and He_2 vibration than OH vibration. Since translational energy is most effective in promoting reactivity in this system, and He_2 vibration couples strongly to it, this accounts for the greater effectiveness of He_2 vibration in promoting reactivity than OH vibration.

3) Translational energy is transferred to the rotational degrees of freedom of each molecule. There is greater propensity for the transfer of translation to OH rotation than He_2 rotation. This is illustrated by examining the rotational cross sections for both molecules as a function of temperature. The rotational cross sections in bohr^2 as a function of final rotational quantum number for various values of the translational temperature are plotted for H_2 in Fig. 1 and for OH in Fig. 2. For H_2, as the temperature is increased, the cross sections for lower final rotational states decrease while those for higher final rotational states increase. The OH rotational cross sections exhibit a maximum with respect to final rotational

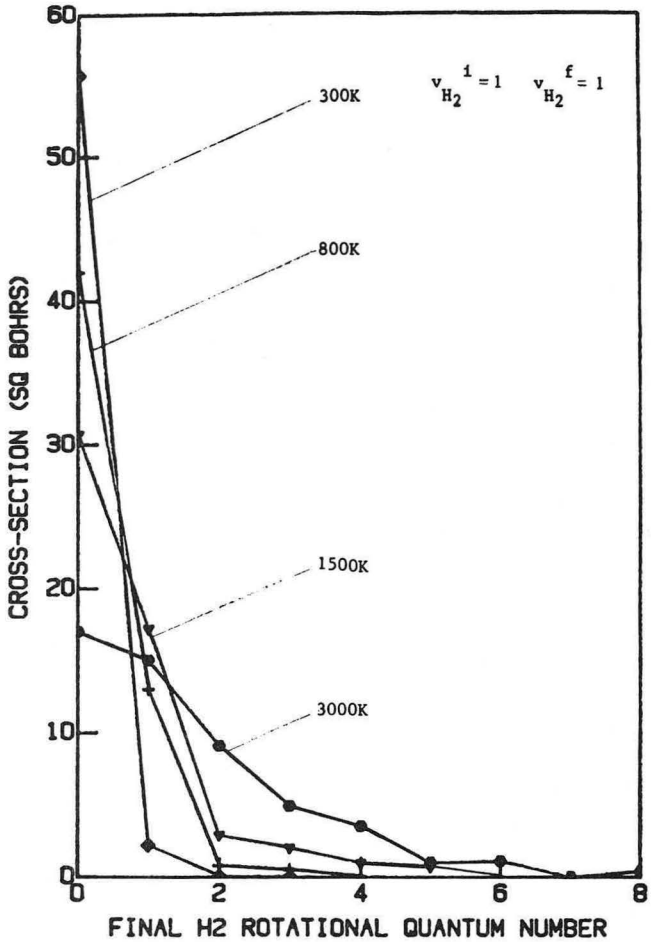

Figure 1. Rotational cross sections in bohr^2 for H_2 for no change in vibrational quantum number, as a function of H_2 final rotational quantum number for various values of the initial translational temperature in Kelvins. (XBL 863-994)

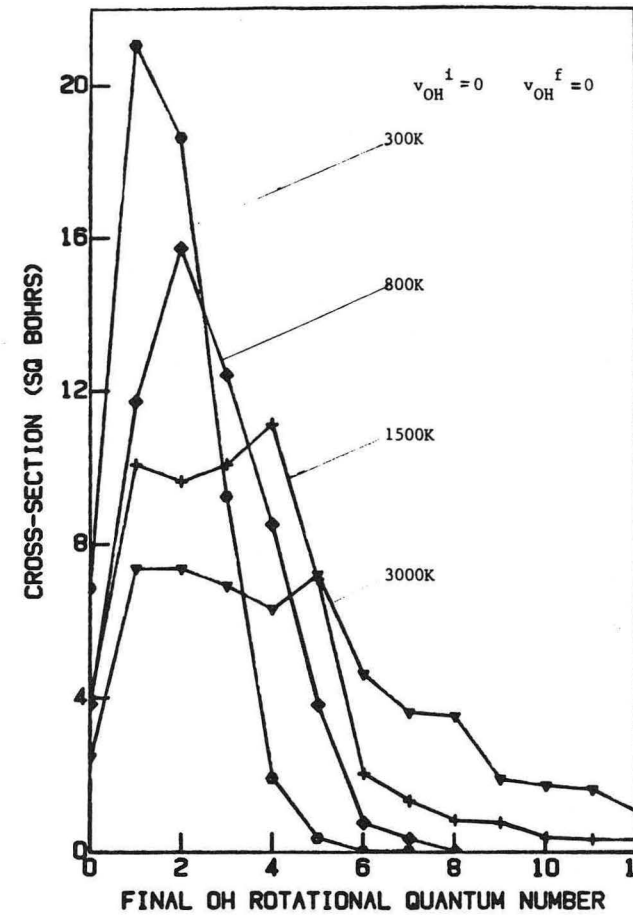

Figure 2. Rotational cross sections in bohr^2 for OH for no change in vibrational quantum number, as a function of OH final rotational quantum number for various values of the initial translational temperature in Kelvins. (XBL 863-993)

quantum number, the particular final rotational state associated with the maximum increases with temperature, and the number of cross sections with values close to the maximum value increases with temperature. The contrasting behavior of the He_2 and OH cross sections is a manifestation of the OH rotational degrees of freedom being more strongly coupled to the translational degree of freedom than H_2, since OH has a more asymmetric force field and is thus more amenable to rotational energy transfer.

4) Energy transfer does not depend strongly on the initial angular momentum in either molecule, which is consistent with our interpretation of the dependence of reactivity on reagent angular momentum.

5) Vibrational energy is transferred to translation, to the rotational degrees of freedom of the same molecule, and to the rotational and vibrational degrees of freedom of the other molecule. The OH molecule does not transfer vibrational energy as effectively as H_2. The H_2 vibrational deactivation associated with the v = 1 to v = 0 transition as a function of temperature follows the Landau-Teller relationship.

In a collaborative study with Dr. James A. Miller and Carmine Parish of Sandia National Laboratory, thermal rate coefficients for the two reactions

$$O + HCN \rightarrow NCO + H \qquad (1)$$

and

$$O + HCN \rightarrow NH + CO \qquad (2)$$

have been predicted. The reactions between O and HCN are the most important reaction steps in the conversion of fuel nitrogen to nitric oxide in

combustion systems. In our study of these reactions, we determined thermal rate coefficients suitable for comparison with experiment for various levels of theoretical approximations. Common to all treatments are the approximations that: 1) the Melius-Binkley calculations of the potential surface parameters using the BAC-MP4 technique provide suitable values of the transition state energies, frequencies, and geometries; 2) the RRKM or strong collision assumption is valid; and 3) the transition state approximation of no recrossing of the transition state dividing surface is valid. The various levels of theoretical approximation employed, each resulting in a thermal rate coefficient, were: 1) canonical theory, CT; 2) canonical theory with a Wigner tunneling correction, CTW; 3) microcanonical theory, MT; 4) microcanonical theory with angular momentum conservation, MJT; and 5) microcanonical theory with angular momentum conservation with one-dimensional tunneling, MJT-T. Barrier heights determined with the BAC-MP4 theory were also varied within the range of the stated error limits.

The reaction path was complex since the net reaction can take place on either of two potential energy surfaces, and both reactions involve the formation and destruction of intermediate complexes. The general formalism developed for obtaining thermal rate coefficients and the branching ratio, ($k_2/k_1 + k_2$), over a range of temperatures should be applicable to several reactive systems. Our theoretical results for the thermal rate coefficients determined using the basic BAC-MP4 parameters and modified parameters are compared with the experimental values of Perry and Melius,[4] Davies and Thrush,[5] and Lohr and Roth.[6] Figure 3 is an Arrhenius plot of the theoretically- and experimentally-determined rate coefficients over a range of temperatures. At high temperatures the available experimental results are predicted accurately by even the crudest theoretical treatment (CT), although the branching ratio predicted by theory is somewhat lower than the 20 to 30% determined experimentally. At lower temperatures the theoretical predictions using the basic BAC-MP4 parameters are too low. Adjustments of the BAC-MP4 barriers to values within their stated error limits lead to satisfactory agreement over the entire temperature range where experimental results are available (500 to 2500 K). The most important results of the investigation concern the dependence of the predictions on the level of approximation. At high temperatures, the rate coefficients calculated for reactions (1) and (2) are independent on the level of approximation. At low temperatures, the total rate coefficient, $k_1 + k_2$, which is dominated by k_1, is also relatively independent of the level of approximation,

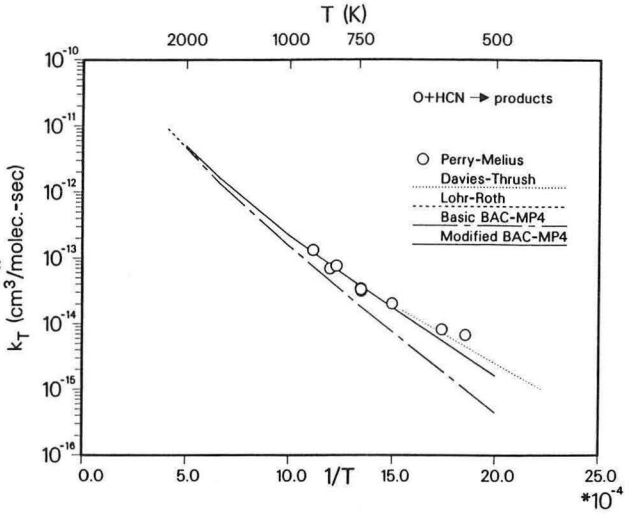

Figure 3. An Arrhenius plot (log k versus 1/T) of the theoretical predictions and experimental values of the thermal rate coefficient for the O + HCN reaction. (XBL 863-991)

and the branching ratio depends strongly on tunneling and on energy and angular momentum conservation. Each successive refinement in the theory produces larger values of k_2. The details of the theoretical treatments and the consequences of these are described in a paper[7] which summarizes the research.

The recent availability of high energy ultraviolet lasers provides new opportunities to study ignition. These lasers produce sufficient photons to initiate combustion by photolysis, and they place reactants in well-defined initial states in a much shorter time (approximately 20 ns) than that required for many chemical reactions important in combustion. We have studied ignition initiated by ozone photolysis at 248 nm using a Lamda Physik 200 EMG KrF excimer laser as a light source.

The ignition of ozone/fuel/oxygen mixtures in a constant volume cell was investigated using H_2, CH_4, and C_3H_8 as fuels. Ozone, the only significant absorber in this system, is photolyzed and produces oxygen atoms which initiate combustion. Light was focussed into heated and unheated aluminum cells with optical windows by MgF_2 or UV grade lenses of various focal lengths. Laser outputs were measured with a Gentec ED-500 joulemeter, and in typical experiments 350 to 400 mJ of light entered the reaction cell. Ozone was produced by passing oxygen through two thermo electron ozinators in series and trapped on silica gel cooled to dry ice-isopropanol mixtures. Ozone concentration in the reaction cell was monitored immediately before laser photolysis

by absorption using a deuterium lamp/monochromator/photomultiplier assembly. Initial gas pressures, measured with an MKS baratron, were in the range of 20 to 200 torr. Transient pressure measurements were made with a Kistler 211B piezotron flush-mounted in the cell wall, and a DEC/CAMAC microcomputer controlled timing and recorded the pressure data as previously described.[8] Spark schlieren photography was used to visualize the absorption and combustion events. Photographs were obtained using two 1.0 m focal length lenses and a knife edge stop, arranged in a U-shape because of space limitations.

A discretized, time-dependent absorption model was used to predict the spatial dependence of oxygen atoms produced by photolysis of ozone by focussed light. Modelling studies of constant volume hydrogen/oxygen/ozone combustion were performed using the CHEMKIN code with an appropriate driver routine. The appropriate conservation equations were solved to determine temperature, pressure, and species concentrations as a function of time. Induction time, defined as the time for the temperature to achieve one-half its total increase, was also computed. The model was verified for reliability by demonstrating concurrence with computational and experimental studies of ignition reported in the literature.[9]

Variation of the ozone partial pressure was the primary method for establishing ignition conditions. Combustion was confirmed by visual observation, pressure rise, and the appearance of water on the cell windows. Figure 4 is a plot of pressure versus time recorded for two ignition events in hydrogen/oxygen/ozone mixtures. Ignition occurs near the lens focus for the top trace and at the cell window for the bottom trace. The laser is fired at the time denoted by the arrow.

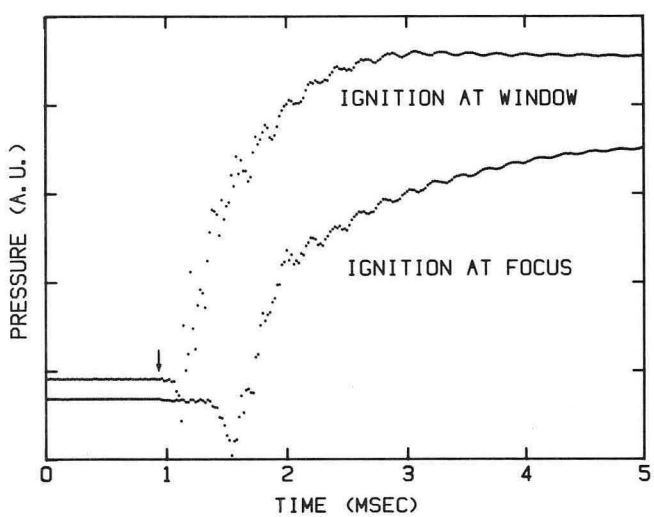

Figure 4. Pressure (arbitrary units) in laser ignited mixtures of hydrogen/oxygen/ozone as a function of time (msec). Ignition occurs near the focus for the top trace and at the window for the bottom trace. The laser is fired at the time denoted by the arrow. (XBL 861-31)

The use of a discretized, time-dependent Beer's Law model showed that photochemical ignition is sensitive to laser power, focal length of the lens, separation distance between the cell and lens, and ozone concentration, and that each of these factors affects the concentration of radicals available to initiate combustion. The system was quite sensitive to changing the initial ozone pressure, with a change of less than 4% in the partial pressure of ozone sufficient to change a no-burn case into a repeatable combustion event. The comparison of spark schlieren photographs, used to visualize ignition events and identify ignition sites with calculated radical concentrations, showed that absorption is a single photon process. The effects of equivalence ratio, pressure, and initial gas temperature were investigated, and temperature was the only variable having a significant effect. The modelling studies showed that ignition is not due entirely to thermal effects but is strongly dependent on the number and type of radicals present initially after photolysis. Hydrogen was the easiest fuel to ignite and methane was the least. The more specific results of the study are described in a paper recently submitted for publication.[10]

PLANNED ACTIVITIES FOR FY 1986

Energy transfer studies of H_2 + OH collisions will be completed. Isotope effects will be considered in both reactive and non-reactive collisions. Rate coefficient calculations for the $H_2 + OH \rightarrow H_2O + H$ reaction using a full Monte Carlo treatment of averaging over initial energy states will be completed and compared with those obtained using statistical theories. Isotope effects on reactivity will also be determined. Modelling studies of ignition will be continued for simple fuels. A new study utilizing and extending a statistical theory for the treatment of unimolecular reactions which occur along a reaction path with no barrier (loose transition state) will be initiated. Fabrication of a new molecular beam-mass spectrometer with a constant volume cell to support homogeneous combustion and a discharge flow reactor will be completed. This system will have the capability of monitoring combustion and reactivity on the microsecond time scale.

REFERENCES

1. Rashed, O. and Brown, N.J. (1985), "A Molecular Dynamics Study of the Reaction $H_2 + OH \rightarrow H_2O + H$," *J. Chem. Phys. 82*, p. 5506.
2. Schatz, G.C. and Elgersma, H. (1980), "A Quasi-Classical Trajectory Study of Product Vibrational Distributions in the $OH + H_2 \rightarrow H_2O + H$ Reaction," *Chem. Phys. Lett. 73*, p. 21.
3. Walch, S.P. and Dunning, T.H. (1980), " A Theoretical Study of the Potential Energy Surface for $OH + H_2$," *J. Chem. Phys. 72*, p. 1303.
4. Perry, R.A. and Melius, C.F. (1985), "The Rate and Mechanism of the Reaction of HCN with Oxygen Atoms over the Temperature Range 540–900 K," *Twentieth Symposium (Int.) on Combustion,* p. 639.
5. Davies, P.B. and Thrush, B.A. (1968), *Trans. Faraday Soc. 64*,
6. Roth, P., Lohr, R., and Hermanns, H.D. (1980), *Ber. Bunsenges. Phys. Chem. 84*, p. 835.
7. Miller, J.A., Parrish, C., and Brown, N.J. (1985), "A Statistical-Theoretical Rate Coefficient and Branching Ratio for the Reaction $O + HCN \rightarrow$ Products," accepted for publication in *J. Phys. Chem.*
8. Lucas, D., Peterson, R., Brown, N.J., and Oppenheim, A.K. (1985), "Molecular Beam Mass Spectrometer Sampling of Flash Ignited Combustion," *Twentieth Symposium (Int.) on Combustion,* p. 1205.
9. Dixon-Lewis, G. and Williams, D.J. (1977), "The Oxidation of Hydrogen and Carbon Monoxide," in *Comprehensive Chemical Kinetics*, Bamford and Tipper, Eds., Elsevier Scientific, Amsterdam, p. 1.
10. Lucas, D, Dunn-Rankin, D., Hom, K., and Brown, N.J. (1986), "Ignition by Excimer Laser Photolysis of Ozone," submitted to the *Twenty-First Symposium (Int.) on Combustion,* LBL-20871.

The Interaction of a Laminar Flame with its Self-Generated Flow During Constant Volume Combustion*

D. Dunn-Rankin and R.F. Sawyer

Flame propagation in tubes has been a subject of combustion research for more than a century,[1] and the formation of "tulip" flames during combustion in closed tubes has been recorded for nearly sixty years.[2–7] However, the cause of the tulip flame has eluded researchers. An example of the tulip flame phenomenon is shown in Fig. 1. The photograph is a sequence of frames extracted from a high-speed schlieren movie of a stoichiometric methane/air flame propagating in a closed rectangular duct (38 mm × 38 mm × 155 mm). The flame is initiated by a point igniter near one endwall of the combustion vessel. The tulip flame phenomenon is relatively insensitive to tube cross-section geometry, combustible mixture composition, and ignition source geometry.[7] Detailed descriptions of the development of tulip flames for many different experimental conditions are in the references mentioned above.

ACCOMPLISHMENTS DURING FY 1985

Historically, the tulip flame phenomenon has been attributed to a flame/pressure wave interaction,[3] or a flame instability.[8] Recently, however, the authors have used laser Doppler anemometry (LDA) to explore the possible role of combustion generated flow in tulip flame formation.[9] The present study extends the earlier exploratory work by providing a complete mapping of the flow field during the "tulip" formation. LDA measurements of the fluid velocity near the flame front suggest a fluid mechanical explanation for the formation of tulip flames.

The experimental apparatus (Fig. 2) consists of a laser Doppler anemometer, a high-speed schlieren cinematographic system, a closed combustion vessel, a spark ignition source, a gas mixing device, and a data-logging computer. A detailed description of the experimental apparatus and methodology can be found in an earlier report.[10]

The time history of the experimentally determined vector velocity field during the flame propagation is shown in Figs. 3a and b. The vectors with a dot at their origin represent negative velocity. The

*This work was supported by the Assistant Secretary for Conservation and Renewable Energy, Office of Energy Utilization Research of the U.S. Department of Energy under Contract No. DE-AC03-76SF00098.

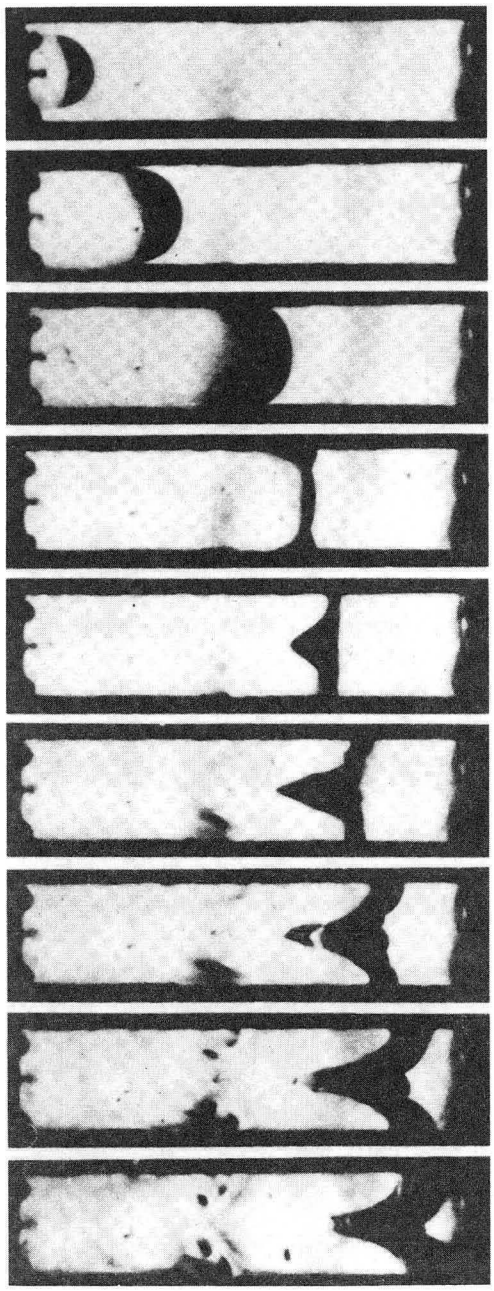

Figure 1. An example of the "tulip" flame formation. Stoichiometric methane/air flame initiated by a spark. Square cross-section vessel (38 mm × 38 mm × 155 mm). (XBB 866-4892)

flow field is assumed to have cylindrical symmetry except in the corners of the chamber. Individual frames from a high-speed schlieren movie of the flame propagation indicate the flame shape and location, and the solid line in the vector plots represents the flame location determined from LDA data rate reduction.

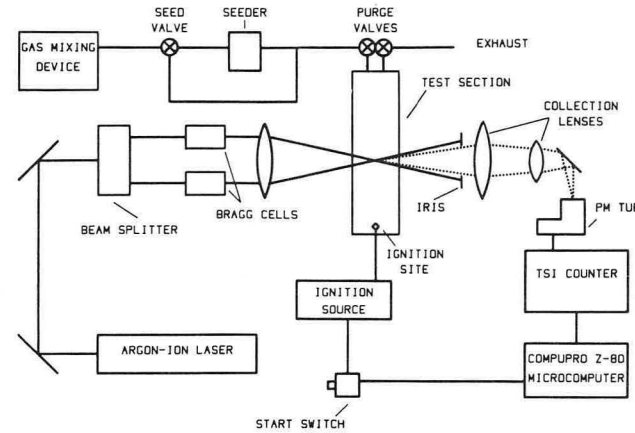

Figure 2. Schematic of experimental apparatus. (XBL 866-2379)

While the flame is convex toward the unburned gas (t < 15 ms), the entire flow field is positive. However, by the time the flame flattens (t = 20 ms), the burned gas flow field is entirely negative. At the same time, the unburned gas velocity has dropped to a very small, almost constant value. Previous studies have indicated that the decrease in unburned gas velocity is due primarily to a decrease in flame area.[10] The reversal of the direction of the burned gas motion and the decrease in unburned gas velocity occur very rapidly, which suggests that the "tulip" transition is a very rapid process. As the "tulip" continues to grow (t > 25 ms), a stagnation region develops in the burned gas behind the vertex of the tulip cusp. Furthermore, a small reverse flow appears in the unburned gas just within the confines of the tulip. This flow pattern and the tulip flame shape persist for the remainder of the combustion process, which indicates that the tulip configuration is a relatively stable flame shape in closed tube combustion.

PLANNED ACTIVITIES FOR FY 1986

Experimental observations will be compared with a theoretical model to identify and confirm the processes which control the flame folding process. The significance of combustion generated flow in engines will be investigated.

REFERENCES

1. Mallard, E. and LeChatlier, H. (1883), "Recherches Experimentales et Theoriques sur la Combustion des Melanges Gazeux Explosifs," *Annales Des Mines 8,* Series 4, p. 274 (in French).

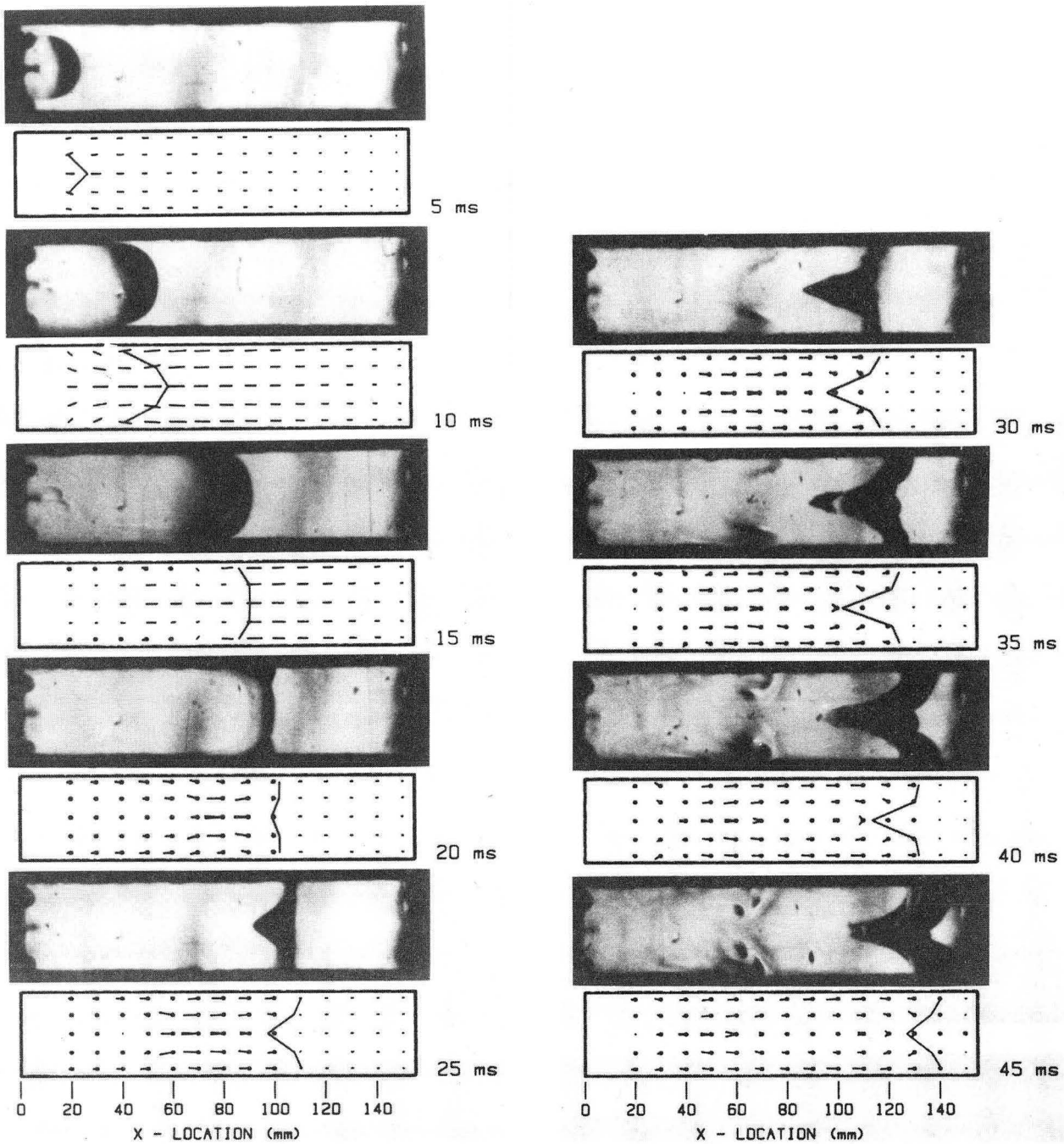

Figure 3. (a) Vector velocity field and flame shape during constant volume combustion. (b) Vector velocity field and flame shape during constant volume combustion. Stoichiometric methane/air flame. |(a) XBB 856-4521, (b) XBB 856-4522|

2. Ellis, O.C. de C. (1928), "Flame Movement in Gaseous Explosive Mixtures (Part 7)," *Fuel; a journal of fuel science 7,* p. 502.
3. Guenoche, H. (1964), "Flame Propagation in Tubes and Closed Vessels," in *Non-Steady Flame Propagation,* G.H. Markstein, Ed., Pergamon Press, New York.
4. Smith, O.I. (1977), "Lean Limit Combustion in an Expanding Chamber," LBL-6851; Ph.D. Thesis, College of Engineering, University of California, Berkeley.
5. Steinert, W.J., Dunn-Rankin, D., and Sawyer, R.F. (1982), "Influence of Chamber Length and Equivalence Ratio on Flame Propagation in a Constant Volume Duct," Western States Section/The Combustion Institute Paper No. 82-52; LBL-14965.
6. Wakai, K. and Shimizu, S. (1984), "Behavior of the Flame in a Closed Chamber," *Proceedings of JSME, 840-14* (October), p. 87 (In Japanese).
7. Dunn-Rankin, D. (1985), "The Interaction Between a Laminar Flame and Its Self-Generated Flow," LBL-19582; Ph.D. Thesis, College of Engineering, University of California, Berkeley.
8. Strehlow, R.A. (1984), *Combustion Fundmentals,* McGraw Hill, New York.
9. Dunn-Rankin, D., Cheng, R.K., and Sawyer, R.F. (1984), "LDA Study of Non-Steady Flame Propagation in a Constant Volume Duct," presented at the Second International Symposium on Applications of Laser Doppler Anemometry to Fluid Mechanics, July 2–4, Lisbon, Portugal; LBL-18150.
10. Dunn-Rankin, D. and Sawyer, R.F. (1985), "LDA Study of the Unburned Gas Motion Induced by Non-Steady Flame Propagation in a Constant Volume Duct," submitted to Joint Western-Central States Section/The Combustion Institute meeting, March 21–23, San Antonio, Texas. In preparation.

Compression Ignition of Coal Slurry Fuels*

D.D. Brehob and R.F. Sawyer

Most of the work on coal-fired diesel engines before 1945 was conducted by German industry using coal dust; see the review by Soehngen.[1] However, since that time most coal fueled diesel research and development has used coal slurries: various percentages of coal in oil, water, methanol, ethanol, or mixtures of the liquid carriers. The existing fuel storage and transportation infrastructure for diesel engines is designed for liquids. Thus, conversion to slurry usage would present fewer difficulties compared to pulverized coal. Coal slurries compared to dust give advantages in the areas of fuel handling, safety, and fuel injection control and reliability, with slight cost disadvantages and an ignitability disadvantage for coal/water slurry only. Coal slurried with water, methanol, and diesel No. 2 are the test fuels for this study. The slurries are evaluated using a 900 rpm, direct injection, square piston engine simulator (Fig. 1) operating for one combustion cycle per experiment.

A comprehensive summary of published work on diesel engine combustion of coal slurries is contained in the thesis by Brehob,[2] which extends an earlier review by Caton and Rosegay.[3] The engine tests described provide valuable information concerning engine modifications to enhance slurry combustion and to improve engine and injection system performance with slurries. The constant volume bomb studies of Siebers and Dyer[4] and the computer model studies of Bell and Caton[5] provide more fundamental information on coal slurry combustion under diesel engine conditions. Detailed information about the ignition characteristics of coal slurries under compression ignition conditions is not available currently. The objectives of this study are: 1) to establish engine conditions required for slurry combustion, and 2) to determine ignition delay characteristics of the three coal slurries tested.

*This work was supported by the Assistant Secretary for Conservation and Renewable Energy, Office of Advanced Energy Conversion Systems, Heat Engines Program of the U.S. Department of Energy under Contract No. DE-AC03-76SF00098.

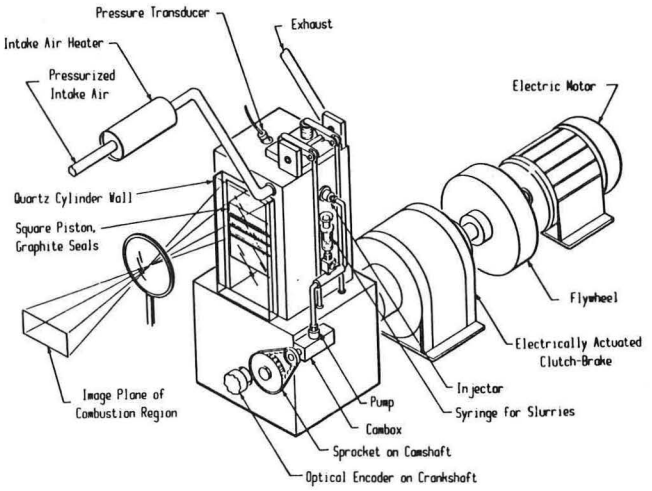

Figure 1. Square piston engine simulator. (XBL 8412-5422A)

ACCOMPLISHMENTS DURING FY 1985

Conditions for Ignition of Fuels

The longest ignition delays measured in the square piston engine simulator at 900 rpm are less than 10 msec (54 CAD) (crank angle degree). For injection at about 20° BTDC (before top dead center), ignition occurs as late as 35° ATDC (after top dead center). After this CAD, the lower temperatures and pressures from expansion do not permit substantial chemical activity. Ignition at 35° ATDC is not of practical significance; it does, however, provide information concerning the ignition characteristics of the fuels.

Neither pressure rise nor light emission is observed when injecting coal/water slurry into the maximum temperature and pressure conditions attainable in the square piston engine simulator in the current configuration: i.e., up to 22:1 CR (compression ratio), 150°C block temperature, and 250°C inlet temperature at IVC (intake valve closing). Thus, coal/water slurry does not compression ignite when injected into air at up to 1150 K and 52 atm in the nearly 10 msec available.

Henein and Elias[6] discuss using inlet air preheated to extend the cetane scale. Following the approach of Henein and Elias, to evaluate diesel No. 2, methanol, coal/oil, and coal/methanol slurries, the inlet air temperature is increased at constant injection timing until ignition is obtained. The measured minimum temperatures required for combustion at 16:1 CR (approximately 30 atm pressure for the injection timing of 20° BTDC) are:

Fuel	Temperature at IVC (K)	Temperature at injection (K)
Diesel No. 2	320	675
Coal/diesel	325	685
Methanol	450	825
Coal/methanol	360	725

The temperatures above are approximate due to the uncertainties in measurement and the unrepeatable nature of ignition near the limiting temperature.

The temperatures for coal/diesel ignition are nearly the same as those for diesel No. 2. Coal/methanol and methanol fuels both require higher temperatures than diesel fuel for ignition as expected due to the low cetane number of methanol. However, coal/methanol ignites at temperatures well below those required for neat methanol.

The autoignition of coal/methanol slurry at lower temperatures than neat methanol is due to either the coal or the additive package in the slurry. As mentioned above, coal addition to the liquid carrier increases the viscosity dramatically, causing the injected fuel droplets to be larger than with neat liquid fuel as shown in Fig. 2. Thus, any physical

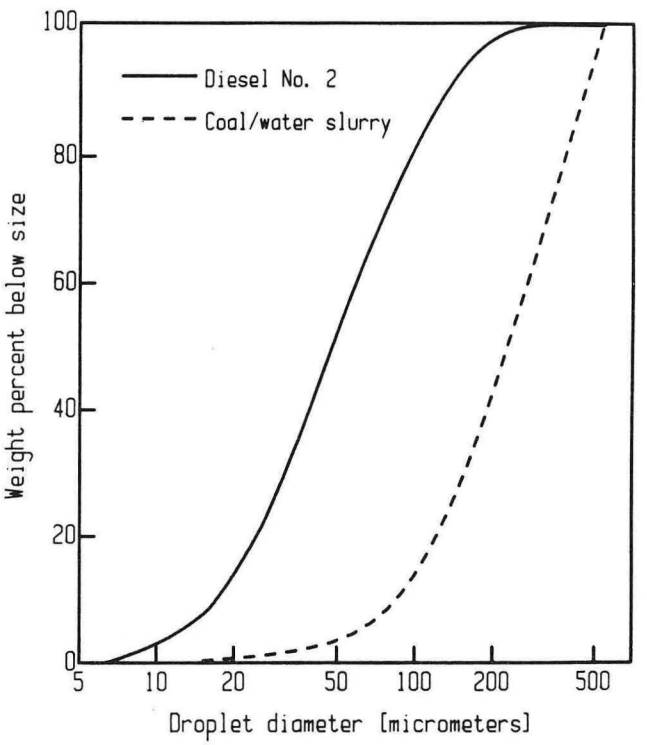

Figure 2. Fuel droplet size distributions for diesel No. 2 and coal/water slurry, from Nelson, *et al.*[7] (XBL 866-2377)

effect of the coal on the autoignition is most probably detrimental.

To investigate any chemical effects that the presence of coal might have on ignition, the volatile fraction must be characterized. Thurgood and Smoot[8] summarize data from 24 experiments in which the gaseous coal pyrolysis products are measured. Twenty of the reported experiments are conducted at rapid heating rates, i.e., greater than 10^4 K/sec. The products of devolatilization depend on coal type, heating rate, final temperature, and other factors. But average values of the components are: 3% CO_2, 15% CO, 53% H_2, 14% CH_4, 10% C_2H_6, and 5% of other C_2 molecules. The final temperatures of the coal in these experiments is 1000 K or higher. The fuel at the periphery of the spray cone injected into the square piston engine simulator experiences very high heating rates: on the order of 10^5 K/sec. However, when the coal/methanol is injected into 725 K air, the final fuel droplet temperature is below the maximum 800 K of the gas. This is significantly below the 1000 K reported by Thurgood and Smoot. Kimber and Gray[9] report that at 1050 K final temperature and a reaction time of 70 msec, less than 25% of the coal's volatile matter is removed. Therefore, it is unlikely that enough combustible gas is devolatilized during the approximately 5 msec before ignition. The more plausible explanation for the autoignition characteristics of coal/methanol is that the additive package contains chemicals that ignite more readily than methanol.

Ignition Delay

The end of the ignition delay is measured in two ways: emission of light from combustion and pressure rise compared to the motoring trace. The amount of light emitted from methanol combustion is much less than that emitted from the other fuels. To obtain adequate sensitivity from the photodiode, the gain is raised by a factor of five for methanol tests. At this high gain with engine block heating, the photodetector senses the infrared radiation from warm combustion chamber surfaces, giving erroneous ignition readings. Thus, only the pressure rise determination at start of combustion is used for methanol.

The diesel No. 2, methanol, coal/oil slurry, and coal/methanol slurry pressure delay results are shown in Fig. 3. Luminosity delay measurements are shown in Fig. 4 for the above fuels except for methanol. The following differences are significant at the 90% confidence level:

1) Coal/diesel has a lower activation temperature than diesel No. 2, coal/methanol, and

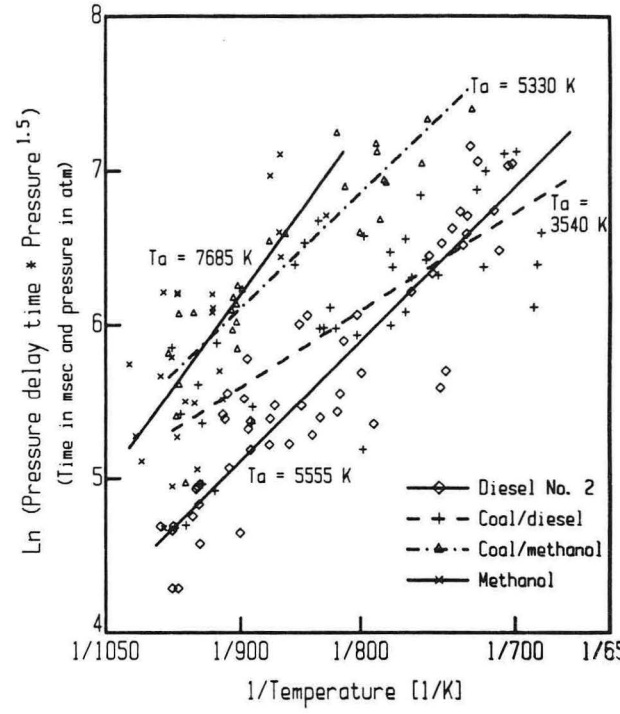

Figure 3. Temperature dependence of pressure defined ignition delay with pressure dependence to the 1.5 power for diesel No. 2, coal/diesel slurry, methanol, and coal/methanol slurry fuels in the square piston engine simulator. (XBL 866-2375)

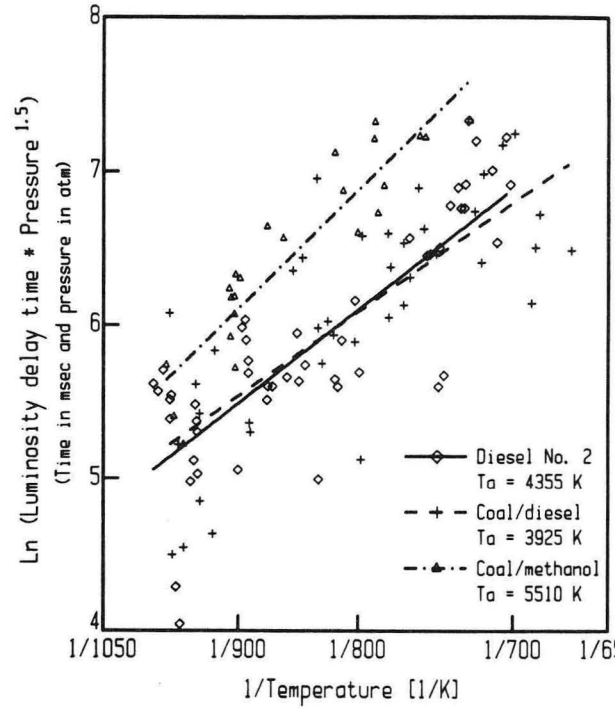

Figure 4. Temperature dependence of luminosity defined delay period with pressure dependence to the 1.5 power for diesel No. 2, coal/diesel slurry, and coal/methanol slurry in the square piston engine simulator. (XBL 866-2376)

methanol fuels by the pressure delay measurement.

2) Coal/diesel slurry has a lower activation temperature than coal/methanol when considering the luminosity delay.

No differences between the luminosity delay and pressure delay results are found within the measurement precision of these tests.

In both the luminosity and pressure delay analyses, the activation temperature for the coal slurry is lower than the neat fuel alone. The ignition delay interval is comprised of overlapping physical and chemical periods. El Wakil, *et al.*[10] present calculated physical delay times for a 20 micrometer decane droplet. They also report that physical delay times are proportional to the droplet diameter to the 1.75 power. From their findings, Fig. 5 is constructed. From Fig. 2, 10% of the mass of diesel fuel droplets is contained in droplets of less than 20 micrometers in diameter. In contrast, 10% of the mass of coal/oil droplets is found in 100 micrometers drop size or less. The physical delay for 20 micrometer droplets is almost negligible throughout the temperature range. However, at 100 micrometers, the physical delay interval is a sizable portion of the total delay period. Temperature plays a lesser role in determining the physical delay period than droplet diameter. Therefore, the lower T_a of coal/oil and coal/methanol slurry compared to the neat fuels may be due to a relatively long physical delay interval which is less sensitive to temperature than the chemical delay.

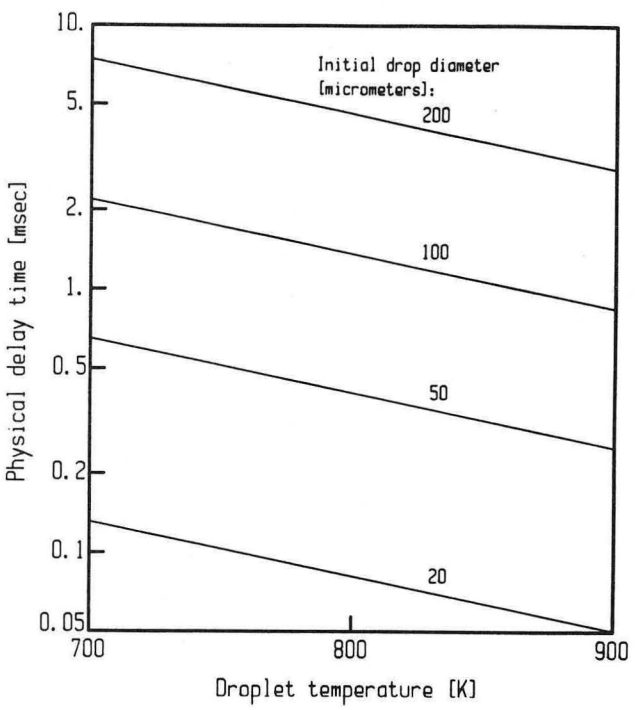

Figure 5. Physical delay time for decane droplets at varying droplet temperatures with drop diameter as a parameter. (Data taken from Fig. 7 of paper by El Wakil, *et al.*[10]). (XBL 866-2378)

Conclusions

1. Coal/methanol slurry ignites at significantly lower inlet temperatures than neat methanol: 360 K versus 450 K.
2. Coal/water slurry does not compression ignite at the conditions attainable in the square piston engine simulator.
3. Methanol compression ignition combustion emits low levels of light, making accurate luminosity delay measurements difficult.
4. The activation temperatures for the test fuels are:

Fuel	T_a (Lum) (K)	T_a (Pres) (K)
Diesel No. 2	4360	5560
Coal/diesel	3925	3540
Methanol	7685	—
Coal/methanol	5510	5330

The activation temperature for coal/diesel is lower than diesel and coal/methanol based on the pressure delay at the 90% confidence level.

5. The pressure and luminosity delay intervals are not different within the precision of the measurements in the square piston engine simulator.

PLANNED ACTIVITIES FOR FY 1986

This research has concluded and no further activities are planned.

REFERENCES

1. Soehngen, E.E. (1976), *Development of Coal-Burning Diesel Engines in Germany,* U.S. ERDA Report FE/WAPO/3387-1.

2. Brehob, D.D. (1985), *Compression Ignition Characteristics of Coal Slurries,* Ph.D. Thesis, University of California, Berkeley.
3. Caton, J.A. and Rosegay, K.H. (1983), "A Review and Comparison of Reciprocating Engine Operation Using Solid Fuels," SAE Paper 831362.
4. Siebers, D.L. and Dyer, T.M. (1985), "The Autoignition and Combustion of Coal-Water Slurry under Simulated Diesel Engine Conditions," ASME Paper 85-DGP-15.
5. Bell, S.R. and Caton, J.A. (1985), "Analytical Evaluations of Ignition Options for a Coal/Water Slurry Fueled Engine," Fall Meeting of the American Flame Research Committee, Livermore, CA, October 1985.
6. Henein, N.A. and Elias, N.Y. (1978), *SAE Transactions 87,* p. 2470.
7. Nelson, L.P., Seeker, W.R., and Zimperman, R.A. (1985), "The Atomization, Ignition, and Combustion Characteristics of Coal Slurry Fuels in Medium-Speed Diesel Engines," Paper 3-1A, presented at the Joint Technical Meeting of the Central and Western States Sections of the Combustion Institute, San Antonio, Texas, May, 1985.
8. Thurgood, J.R. and Smoot, L.D. (1979), *Pulverized-Coal Combustion and Gasification,* L.D. Smoot and D.T. Pratt, Eds., Plenum Press, p. 169.
9. Kimber, G.M. and Gray, M.D. (1967), *Combustion and Flame 11,* p. 260.
10. El Wakil, M.M., Myers, P.S., and Uyehara, O.A. (1956), *SAE Transactions 64,* p. 713.

Controlled Combustion*

N.J. Brown, J.A. Cavolowsky, C.F. Edwards, K. Hom, D. Lucas, A.K. Oppenheim, T.E. Parker, D.A. Rotman, R.F. Sawyer, and H.E. Stewart

The main purpose of the program is to acquire knowledge of the chemical and physical process that govern the evolution of exothermic energy in combustion systems and the effects of its deposition in the reacting medium. Basic problems one faces in this connection and the methodology adopted for their solution were described in the FY 1982 annual report.[1] The concepts put forth there were formulated comprehensively in a treatise on the Dynamic Features of Combustion published recently in the *Philosophical Transactions of the Royal Society.*[2] In current studies, particular emphasis was placed on further development of the molecular-beam mass-spectrometer technique in the measurement of the temperature profile with the concomitant life history of selected radicals as an indicator of the role they play in the initiation of the combustion process—a preamble to revealing their action in the control mechanism. In parallel to this effort, we continued our studies, carried out primarily by numerical analysis, of the fluid mechanical phenomena of turbulent flow under the influence of the exothermic energy deposition in the field.

ACCOMPLISHMENTS DURING FY 1985

Advances made last year pertain to the following three phases of our program:

1. Molecular beam sampling of plasma jets,
2. Shock tube and laser imaging apparatus,
3. Numerical analysis of the aero-thermo-chemico-dynamic features of combustion fields.

Progress made in each of them is reported here.

Molecular Beam Spectrometry

Possible effects of interaction between the plume and the sampling cone were investigated using laser schlieren photography.[3] According to our observations, in early stages the presence of the cone has negligible effect, and the plume front is not slowed by its presence in the field. At later times, when the front has advanced well past the cone, significant differences were quite evident. However, they were located primarily in the portion of the plume past the cone, whereas the sampled gas did not appear to be disturbed by the deflection of the plume occurring downstream of the sampling tip.

Temperatures in the plume were measured by means of a time-of-flight (TOF) technique we developed and verified previously.[4] Maximum tem-

*This work was supported by the Office of Energy Research, Basic Energy Science, Engineering, and Geosciences Division of the U.S. Department of Energy under Contract No. DE-AC03-76SF00098 and by the National Science Foundation under Grant CPE-8115163.

perature as high as 50,000 K was recorded 2 mm from the igniter, dropping to 2900 K at 4 mm and 1670 K at 8 mm.

Using continuous sampling, concentration of N atoms in the plume was measured as a function of time and distance from the igniter. Atom signals were averaged, normalized, and converted to mole fractions using ionization cross sections available in the literature. These results, displayed here in Fig. 1, represent the first direct measurement of radical species in a pulsed plasma jet igniter. As it was thus established, at the shortest separation distance of 2 mm the maximum concentration reached a maximum of 5%. Thereafter peak values dropped rapidly and smoothly to the practically undetectable level at a distance of about 14 mm. The measurements were found to be in reasonable agreement with equilibrium values computed for the temperature profile we established earlier by the TOF technique.

Concomitantly with these experiments, we carried out an exploratory investigation of the mechanism of plasma ignition by schlieren photography, using our square-piston engine simulator,[5] and completed a thermo-chemical analysis that revealed the influence of a quasi-equilibrium radical pool in the course of a thermal ignition process.[6]

Shock Tube

The experimental spray ignition studies at conditions encountered in an adiabatic diesel engine, reported last year,[7] were handicapped by a severely restricted optical accessibility afforded by the apparatus we used that consisted of a stainless steel vessel located in a high temperature furnace. In order to ameliorate the situation, a 40-ft. long, 5-in. I.D. shock tube was designed and fabricated. Its installation in our laboratory is nearing completion. Displayed in Fig. 2 is the driver section with the diaphragm system and the control console in front. Fig. 3 shows the driven section, while the test section is presented in Fig. 4. Compressed air to be maintained by design in the latter for at least 20 milliseconds should be at a pressure of up to 25 atmospheres within a temperature range of 600 to 900 K.

The program of studies to be carried out by the use of this apparatus consists, in turn, of high speed schlieren photography, quantitative holography, and laser-induced fluorescence imagery.

Numerical Analysis

Following the publication of studies reported in the FY 1984 annual report,[8–11] a concentrated effort was made by the Principal Investigator to bring to focus advances in the knowledge on turbulent combustion achieved as a consequence of their contribution. The result was presented in the plenary lecture at the Tenth International Colloquium on Dynamics of Explosions and Reactive Systems held in Berkeley on August 3–9, 1985.[12] In a nutshell, this can be expressed in terms of the following ten conjectures:

1. At Reynolds numbers encountered in most combustion chambers, the turbulent flow field is dominated by a large scale vortex structure.

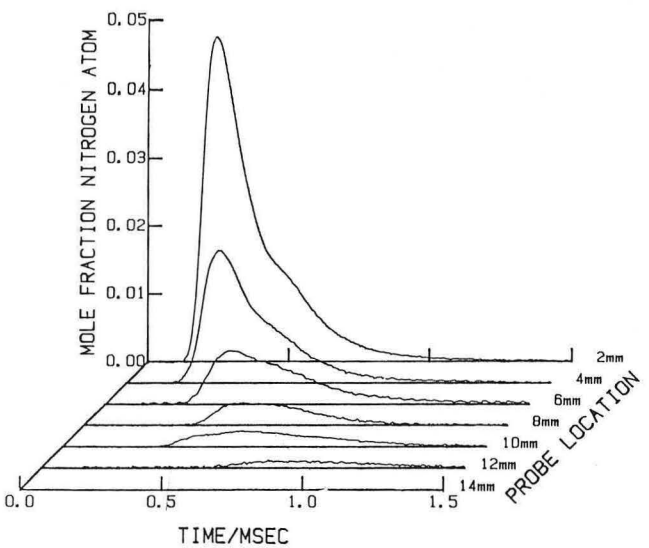

Figure 1. Nitrogen atom concentration as a function of time and distance from the injector tip. (XBL-862-673)

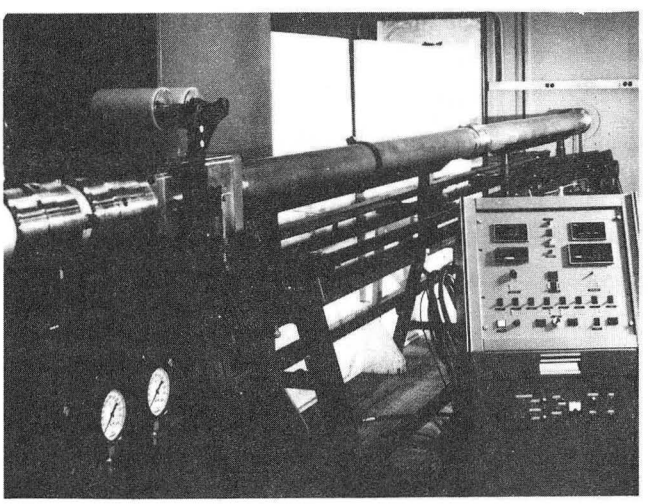

Figure 2. Shock tube driver section. (XBB 862-1156)

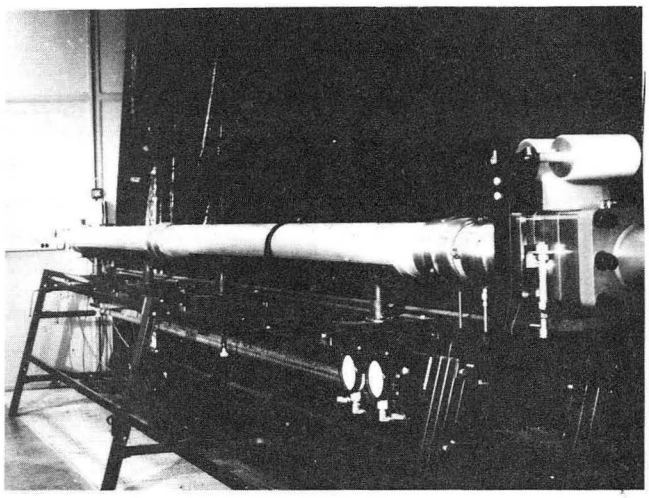

Figure 3. Shock tube driver section. (XBB 862-1157)

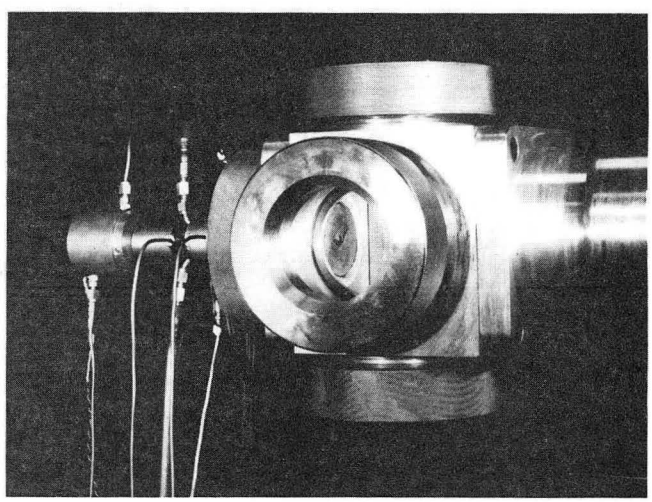

Figure 4. Shock tube test section. (XBB 862-1158)

2. In contrast to a laminar flame, turbulent flame front tends to be established along the particle path rather than across it.
3. Turbulent flame front is an interface—a contact boundary between the unburnt mixture and burnt gases incarcerated in the recirculation zone of a vortex, forming thus effectively its contour.
4. In general the flow field of the fresh mixture remains irrotational, whereas that of the burnt or burning gas is essentially rotational.
5. Although diffusion and reaction across the interface may be enhanced by local turbulence, the time of contact between unburnt and burnt gases is generally too short to attain steady state.
6. As a consequence, the interface forming the flame at the contour of a vortex encounters its subsequent neighbor before a diffusion-reaction wave can be fully developed, so that the process is completed within the recirculation zone.
7. Principal ports of entry for the unburnt mixture into the burnt gas regime are at the cusps between vortex contours.
8. Combustion is enhanced by both effects, the shortened contact time and the prolonged residence time, the former reducing diffusional losses while the latter enhances the progress of reaction.
9. Turbulent flow and combustion fields were treated at their threshold with inviscid flow, in direct contrast to the conventional approach concerned primarily with the intersection between laminar and turbulent flow regimes.
10. Our method of attack is of particular relevance to the technological aspects, while the conventional approach is of a more academic nature.

Of primary significance to the major purpose of our research program is the means we developed for ushering aerodynamics into the enclosure of a combustion chamber. A paper describing this achievement in the simplest possible case has been offered for presentation at the forthcoming Symposium (International) on Combustion to be held in Munich.[13] It concerns of highly idealized case of flame distortion, or stretch, taking place in the course of its propagation in a closed duct as a consequence of the flow field it created—the first time the controlling influence of a flow field generated by the combustion process in an enclosure has been revealed.

PLANNED ACTIVITIES FOR FY 1986

Continue measurements of concentration histories of chemical species involved in ignition of hydrocarbon-oxidizer mixtures and the concomitant temperature profiles by molecular beam mass spectroscopy.

Enhance the photographic study of the generation and formation of plasma jets by the use of the laser-powered high-speed schlieren system.

Develop further the numerical analysis of the aero-thermo-chemical-dynamic processes of combustion in enclosures with particular attention to those modeling conditions in internal combustion engines.

REFERENCES

1. Brown, N.J., *et al.* (1983), "Controlled Combustion," *Energy and Environment Division Annual Report*, FY 1982, LBL-15298, p. 4.
2. Oppenheim, A.K. (1985), "Dynamic Features of Combustion," *Phil. Trans. R. Soc. Lond. A 315*, p. 471.
3. Cavolowsky, J.A., Edwards, C.F., Oppenheim, A.K., and Lucas, D. (1986), "Pulsed Plasma Jet Igniters: Molecular Beam Measurements," *Combustion Science and Technology*, in press.
4. Lucas, D., Peterson, R., Brown, N.J., and Oppenheim, A.K. (1984), "Molecular Beam Mass Spectrometer Sampling of Flash-Ignited Combustion," *Twentieth Symposium (International) on Combustion*, The Combustion Institute, p. 1205.
5. Edwards, C.F., Stewart, H.E., and Oppenheim, A.K. (1985), "A Photographic Study of Plasma Ignition Systems," SAE Paper 850077, 10 pp.
6. Creighton, T.R. and Oppenheim, A.K. (1986), "Role of Radical Pool in Combustion," 10th International Colloquium on Dynamics of Explosives and Reactive Systems, *Progress of Astronautics and Aeronautics*, in press.
7. Parker, T.E., Forsha, M.D., Stewart, H.E., Hom, K., Sawyer, R.F., and Oppenheim, A.K. (1985), "Induction Period for Ignition of Fuel Sprays at High Temperatures and Pressures," SAE Paper 50087, 11 pp.
8. Brown, N.J., *et al.* (1985), "Controlled Combustion," *Applied Science Division Annual Report, FY 1984*, LBL-18754, p. 4.98.
9. Hsiao, C.-C., Ghoniem, A.F., Chorin, A.J., and Oppenheim, A.K. (1984), "Numerical Simulation of a Turbulent Flame Stabilized Behind a Rearward-Facing Step," *Twentieth Symposium (International) on Combustion*, The Combustion Institute, p. 495.
10. Ghoniem, A.F., Chen, D.-Y., and Oppenheim, A.K. (1984), "Formation and Inflammation of a Turbulent Jet," *AIAA J. 24*, p. 224.
11. Hsiao, C.-C., Ghoniem, A.F., and Oppenheim, A.K. (1986), "Numerical Modeling of Aerodynamic Features in Premixed Turbulent Combustion," N.A.S.A. Report, in press.
12. Oppenheim, A.K. (1986), "The Beauty of Combustion Fields and Their Aero-Thermo-Dynamic Significance," 10th International Colloquium on Dynamics of Explosions and Reactive Systems, *Progress in Astronautics and Aeronautics*, in press.
13. Rotman, D.A. and Oppenheim, A.K. (1986), "Aerothermodynamic Properties of Stretched Flames in Enclosures," to be presented at the 21st Symposium (International) on Combustion, Munich, August 3–8.

Reaction of Nitric Oxide with Ferrous Cysteine in Aqueous Solutions*

M.D. Tu and S.G. Chang

Japanese have developed a few flue gas simultaneous desulfurization and denitrification processes in the 70s and have shown that these wet processes are very efficient in SO_2 and NO_x removal (more than 85% for NO_x and 95% for SO_2). However, these wet processes have not reached the commercial stage yet because they are uncompetitive economically, according to cost evaluations.[1]

The most promising type of wet process developed so far is based on the addition of ferrous chelates in scrubbing liquors to enhance the absorption of NO by forming nitrosyl ferrous chelates in aqueous solutions. The nitrosyl ferrous chelates can then react with dissolved SO_2 to produce N_2, N_2O, dithionate, sulfate, and various N-S compounds using the type of chelates patented by the Japanese such as EDTA and NTA, while some ferrous chelates are oxidized by residual O_2 in flue gas and by intermediates produced in the system to ferric chelates, which are inactive. Therefore, this type of process requires regeneration of scrubbing liquors by removing dithionate, sulfate, and N-S compounds from the solutions and reduction of ferric chelates back to ferrous chelates.

ACCOMPLISHMENTS DURING FY 1985

We have recently developed new additives for combined removal of SO_2 and NO_x from flue gas.[2] The new additives include ferrous cysteine, alkalis, and borate. Employment of these new additives creates different and simpler scrubber chemistry compared to Japanese processes using ferrous chelates such as Fe^{2+}(EDTA). The production of dithionate and nitrogen-sulfur compounds can be suppressed or avoided by using these new additives. Ferric ions formed can be reduced by cysteine back to ferrous ions.

The reaction of ferrous cysteine with NO can behave differently depending on the molar ratio of cysteine to ferrous ion, $n_{cysteine}/n_{Fe^{2+}}$, and the pH of the solutions. We have performed experiments to determine the absorption capacity of NO in aqueous solutions containing ferrous cysteine complexes using a bench-scale gas absorber. Also, we have characterized the solid precipitates by means of a FTIR spectroscopy and elemental analysis, and gaseous products by a mass spectrometry.

Figure 1 shows the effect of pH on the absorption of NO when the reaction temperature is 55°C and $n_{cysteine}/n_{Fe^{2+}}$ is 4. The amount of NO absorbed per mole of Fe^{2+}, $n_{NO}/n_{Fe^{2+}}$, and per mole of cysteine, $n_{NO}/n_{cysteine}$, increases from 0.5 to 2.7 and 0.12 to 0.70, respectively, as the pH of the solution increases from 6 to 8. The $n_{NO}/n_{Fe^{2+}}$ and $n_{NO}/n_{cysteine}$ remain unchanged between pH 8 and 10. The effects of $n_{cysteine}/n_{Fe^{2+}}$ on $n_{NO}/n_{Fe^{2+}}$ and $n_{NO}/n_{cysteine}$ at pH 7 and 8 and 55°C are shown in Fig. 2. The $n_{NO}/n_{cysteine}$ decreases steadily from 0.57 to 0.24 as $n_{cysteine}/n_{Fe^{2+}}$ increases from 2 to 6 at pH 7. When pH is at 8, $n_{NO}/n_{cysteine}$ increases from 0.39 to 0.7 as $n_{cysteine}/n_{Fe^{2+}}$ increases from 2 to 4 and then gradually decreases to 0.64 at $n_{cysteine}/n_{Fe^{2+}}$ of 6. This same behavior was observed for $n_{NO}/n_{Fe^{2+}}$ in solutions at pH 7. The $n_{NO}/n_{Fe^{2+}}$ reaches the maximum value of 1.5 at $n_{cysteine}/n_{Fe^{2+}}$ of 4 and decreases slightly with increasing $n_{cysteine}/n_{Fe^{2+}}$ ratio. However, at pH 8, $n_{NO}/n_{Fe^{2+}}$ increases monotonously from 0.78 to 3.82 as $n_{cysteine}/n_{Fe^{2+}}$ increases from 2 to 6.

Varying the pH of the solution and the ratio of cysteine to Fe^{2+} not only affects the amount of NO absorbed but also changes the nature of the reaction products. Figure 3 shows the IR spectra of the precipitates obtained from the reaction of Fe^{2+} + 4 cysteine with NO at 55°C and different pHs. Also shown in Fig. 3 are the IR spectra of solid cysteine and cystine for comparison. It is obvious from these IR results that the nature of the solid is very different when the pH of solutions is changed from 7 to 10. The IR spectrum of precipitates at pH 7 shows several bands at 350(sh), 515(m), 920(w), 990(w), 1140(sh), 1255(m), 1265(m), 1310(m), 1430(m), and 1775(s) cm^{-1} in addition to all the bands of cystine. The band at 1775 cm^{-1} can be attributed to the M-NO stretching ν_{M-NO}. The relative intensity of this band decreases for solid precipitates obtained at pH 7.5, where the only other bands observed are those of cystine. The IR spectrum of solids at pH 8 shows different features than those at pH 7 and 7.5. The 1775 cm^{-1} ν_{M-NO} band disappears, neither does

*This work was supported by the Assistant Secretary for Fossil Energy, Office of Coal Utilization Systems, U.S. Department of Energy under Contract No. DE-AC03-76SF00098 through the Pittsburgh Energy Technology Center, Pittsburgh, PA.

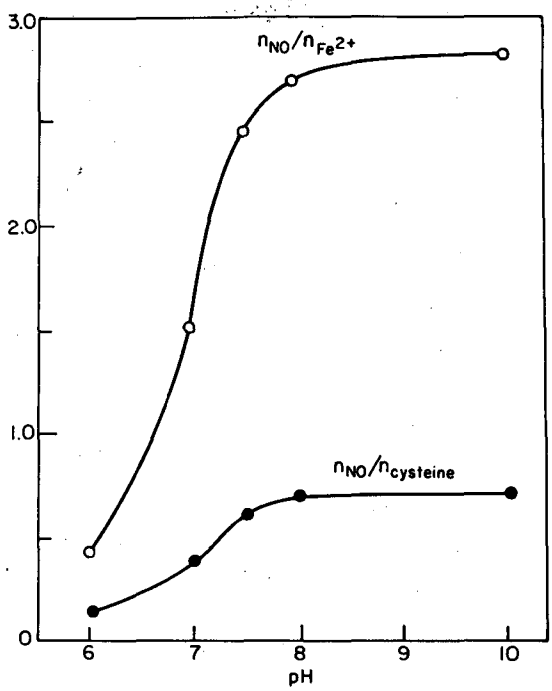

Figure 1. The effect of pH on the absorption of NO in aqueous solutions containing ferrous cysteine, with molar ratio of cysteine to ferrous ion of 4 and at 55°C. (XBL 863-7581)

those bands due to cystine, as observed in solids obtained at pH 7 and 7.5. However, the absence of the cystine bending bands, δ_s-NH_3^+ (1490 cm^{-1}), δ_{as}-NH_3^+ (1580 and 1620 cm^{-1}), and the stretching band, ν—-NH_3^+ (3030 cm^{-1}); and the presence of ν_s-NH_2 (3280 cm^{-1}) and ν_{as}-NH_2 (3350 cm^{-1} and 3370 cm^{-1}) indicate the bonding of the cystine amino group to the ferrous ion. The IR spectrum of solids at pH 10 resembles that of $Fe(OH)_2$ and/or $Fe(OH)_3$. The complete assignments of IR bands are in progress. The IR results are in good agreement with results of elemental analysis. Table 1 shows the n_{NO}/n_{Fe}^{2+} and $n_{cysteine}/n_{Fe}^{2+}$, obtained from elemental analysis, in the precipitates of reactions at pH 7 and 8 and 55°C. The solids at pH 7 contain two moles of NO per each mole of Fe^{2+} found, whereas, the solids at pH 8 does not contain NO at all.

The influence of $n_{cysteine}/n_{Fe}^{2+}$ on the nature of precipitates produced were studied. Figure 4 is the IR spectra of solids obtained at pH 7 and 55 °C. A strong band at 1775 cm^{-1} was observed for all ratio of $n_{cysteine}/n_{Fe}^{2+}$. Additional bands at 515, 990, 1255, 1265, 1310, and 1430 cm^{-1} appear for solids obtained when the ratio of $n_{cysteine}/n_{Fe}^{2+}$ is more than 3. Figure 5 shows IR spectra of the precipitates collected from the reaction at pH 8 and 55°C. There is no NO complex in the reaction products as evident from the absence of a band at 1775 cm^{-1}. Notice the increase in the intensity of the bands at 550, 849,

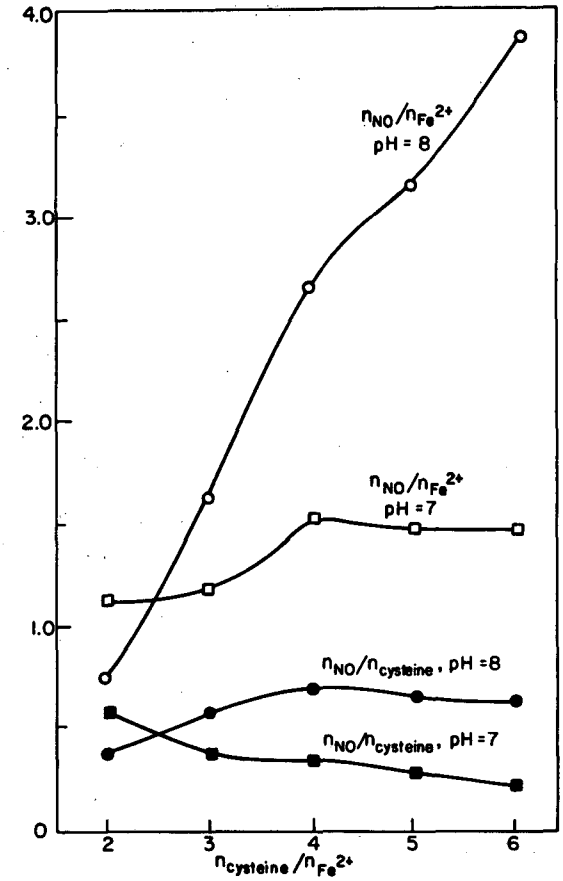

Figure 2. The effect of molar ratio of cysteine to ferrous ion on the absorption of NO in solutions at pH 7 and 8 and 55°C. (XBL 863-7582)

1125, 1300, 1340 cm^{-1}, as the $n_{cysteine}/n_{Fe}^{2+}$ increases from 2 to 6. Additional bands at 775 and 1470 cm^{-1} were observed for solids obtained when the ratio of $n_{cysteine}/n_{Fe}^{2+}$ were 4, 5 and 6; and two more bands at 455 and 870 cm^{-1} when the ratio is 5 and 6.

When the solid sample containing M-NO was subjected to heating (~ 155°C) or vacuum ($\leqslant 10^{-2}$ torr), NO would be released. Figure 6 shows the IR spectra of solids after heating at 155°C for 2 and 7 hours. Part of the NO was released after heating the solid sample for 2 hours, and all the NO had disappeared after heating for 7 hours. Analysis of the gaseous species evolved after heating showed mostly NO with a trace of N_2O. This again confirms that absorbed NO is present in the solid precipitates.

PLANNED ACTIVITIES FOR FY 1986

We will study the kinetics and mechanisms of the reaction of ferrous cysteine with NO and characterize the species produced in solid, liquid, and gas phases in order to make a mass balance for the reaction.

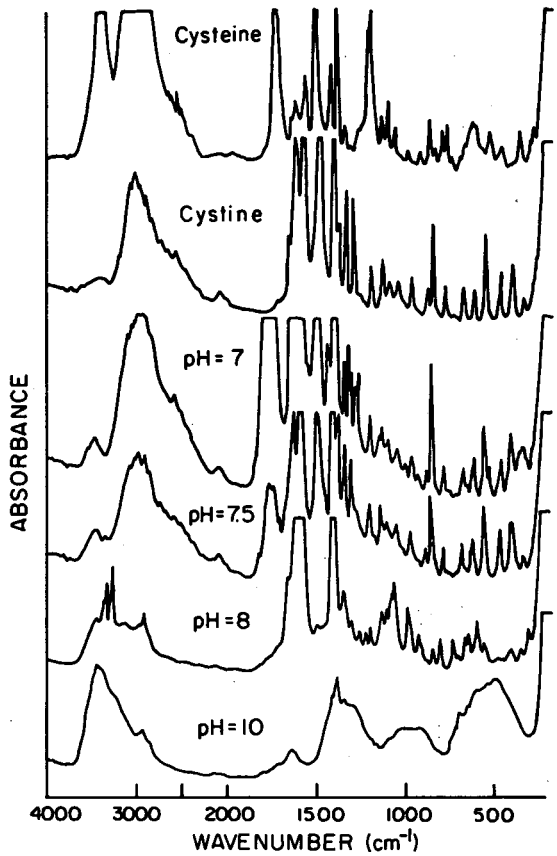

Figure 3. Infrared spectra of cysteine, cystine, and solid products of reaction Fe^{2+} + 4 cystine + NO at different pHs and 55°C. (XBL 863-7583)

Table 1. Chemical composition of the solid reaction products at pH 7 and 8 and 55°C.

$n_{cysteine}/n_{Fe}^{2+}$		2	3	4	5	6
pH 7	$\frac{n_{NO}}{n_{Fe}^{2+}}$	1.95	1.9	2.2	2.1	1.92
	$\frac{n_{cysteine}}{n_{Fe}^{2+}}$	3.0	2.0	2.0	4.3	2.0
pH 8	$\frac{n_{NO}}{n_{Fe}^{2+}}$	0	0	0	0	0
	$\frac{n_{cysteine}}{n_{Fe}^{2+}}$	1.73	2.07	2.14	2.83	3.42

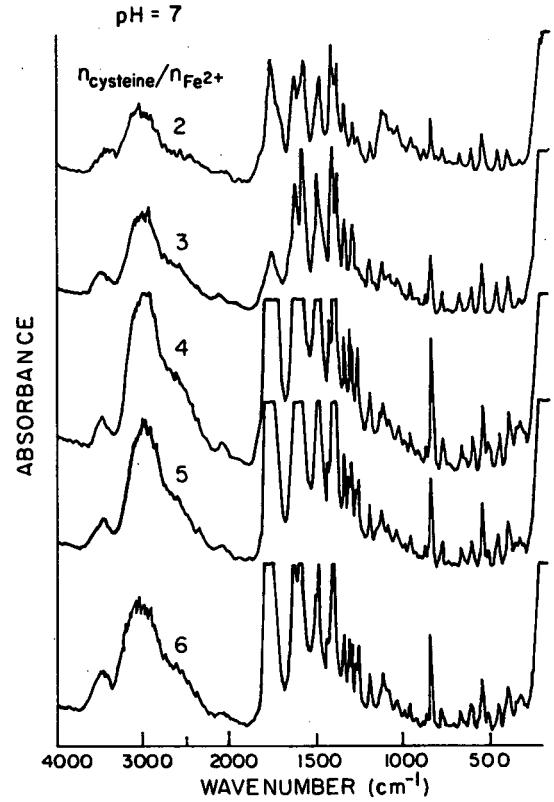

Figure 4. Infrared spectra of solid products from reactions of NO with ferrous cystine, with various molar ratio of cystine to ferrous ion at pH 7 and 55°C. (XBL 863-7584)

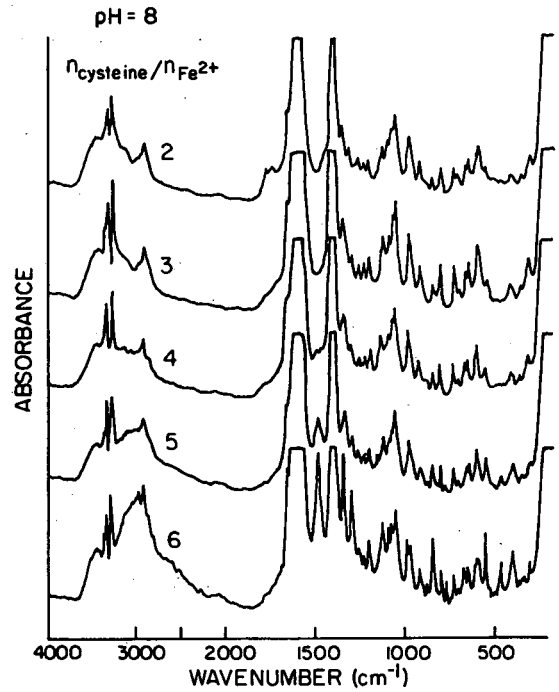

Figure 5. Infrared spectra of solid products from reaction of NO with ferrous cysteine, with various molar ratio of cystine to ferrous ion and at pH 8 and 55°C. (XBL 863-7585)

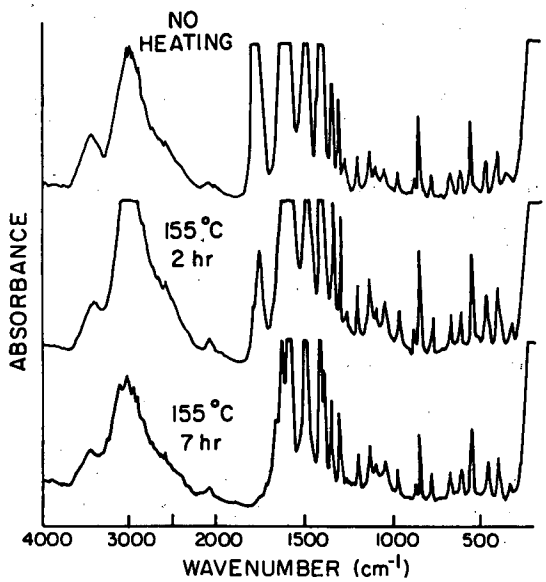

Figure 6. Infrared spectra showing the thermal stability (at 155°C) of solid products obtained from reaction Fe^{2+} + 4 cystine + NO at pH 7 and 55°C. (XBL 863-7586)

REFERENCES

1. Chang, S.G. (1986), "Technical Analyses of a Wet Process for Flue Gas Simultaneous Desulfurization and Denitrification," LBL-18835, to be published in *ACS Symposium Series.*
2. Chang, S.G. and Griffiths, E. (1986), "A Process for Combined Removal of SO_2 and NO_x from Flue Gas," LBL Patent Case No. IB-612.

Kinetics and Thermodynamics of the Reaction Between Cystine and Hydrogen Sulfide Ion*

D.K. Liu and S.G. Chang

We have recently discovered that a mixture of ferrous salts, cysteine, and alkalis (such as lime, limestone, trona, or sodium hydroxide) can be employed as additives in both wet and spray-drying systems to enhance removal efficiency of NO_x and SO_2 from flue gas. The employment of these additives creates different and simpler scrubber chemistry, compared to ferrous chelates such as Fe(II)EDTA or Fe(II)NTA used in several patented Japanese processes. Cysteine can coordinate to ferrous ion to form ferrous-cysteine complex which can efficiently bind and react with NO to form cystinatodinitrosyliron(II) salts. The cystinatodinitrosyliron(II) salt has low solubility and precipitates from neutral pH solutions. It can undergo thermal decomposition at $\geqslant$ 100°C to release NO and produce cystine, which is a dimer of cysteine. Also, cysteine can be oxidized to cystine in aqueous solutions by residual oxygen in flue gas. This oxidation is catalyzed by the presence of transition metal ions such as ferrous ion. Therefore, a cost-effective process to reduce cystine to cysteine for recycling in the scrubber system is very desirable. There are several methods available for reduction of naturally occurring amino acid cystine to cysteine. These methods include electro- and chemical reductions with sodium in liquid ammonia or zinc in HCl. However, these existing methods require the consumption of electric energy or relatively expensive chemical reagents and may not be cost-effective for large scale preparation in flue gas clean-up industry.

*This work was supported by the Assistant Secretary for Fossil Energy, Office of Coal Utilization Systems, U.S. Department of Energy under Contract No. DE-AC03-76SF00098 through the Pittsburgh Energy Technology Center, Pittsburgh, PA.

ACCOMPLISHMENTS DURING FY 1985

We have demonstrated that cystine (CySSCy) can be efficiently converted to cysteine (CySH) with HS^-/HSO_3^- under appropriate conditions.[1] Since little is known about the the kinetics and thermodynamics of the reaction of cystine with hydrogen sulfide ion, we decided to undertake a study of the following equilibria:

$$\text{CySSCy} + HS^- \underset{k_{-1}}{\overset{k_1}{\rightleftharpoons}} \text{CySH} + \text{CySS}^- \quad (1)$$

$$\text{CySS}^- + HS^- \underset{k_{-2}}{\overset{k_2}{\rightleftharpoons}} \text{CySH} + S_2^= \quad (2)$$

The results described here concern mainly with the first of these two reactions.

Equilibrium Constants

The equilibrium concentrations of cystine (CySSCy), cysteine (CySH), and thiacysteine ($CySS^-$) were determined quantitatively by an amino acid analyzer.[1] Assuming no competing reactions besides (1) and (2), we can then calculate the concentrations of HS^- and $S_2^=$ by mass balance. By keeping [CySSCy] = 2 mM and varying the concentrations of HS^-, we have obtained $K_1 = 0.30 \pm 0.06$ and $K_2 = 0.20 \pm 0.04$ at pH = 10 and 25°C.

Rate Constants

We have isolated the first equilibrium from the second in our determination of k_1 and k_{-1}. Our results below show this approximation to be justified.

In opposing reactions of second order represented by the following equation:

$$A + B \underset{k_{-1}}{\overset{k_1}{\rightleftharpoons}} C + D \qquad (3)$$

the rate of product formation (or the rate of disappearance of starting materials) has been shown[2] to be

$$\frac{dx}{dt} = \alpha + \beta x + \gamma x^2 \qquad (4)$$

where $\alpha = k_1A_oB_o$, $\beta = -k_1(A_o + B_o)$ and $\gamma = k_1 - k_{-1}$, if only A and B are present at the beginning of the reaction. Integrating we get

$$\int \frac{dx}{\alpha + \beta x + \gamma x^2} = \int dt \qquad (5)$$

There are more than one solution to this integral, depending on the relative values of k_1 and k_{-1}. For $k_1 < k_{-1}$ (which is this case), the solution is[3]

$$\tanh^{-1} \frac{2\gamma x + \beta}{q^{1/2}} = \frac{-q^{1/2}}{2} t + \Theta \qquad (6)$$

where $q = \beta^2 - 4\alpha\gamma$ and $\Theta = \tanh^{-1} \beta/q^{1/2}$ at t = 0 and x = 0. Therefore from the known starting concentrations of CySSCy and HS^-, the amount of cystine reacted at any given time (x) and the equilibrium constant K_1, we can obtain k_1 and k_{-1} from the following version of equation (6):

$$-\tanh^{-1}(ax - b) = ck_{-1}t - d \qquad (7)$$

where $a = 2\gamma/q^{1/2}$, $b = -\beta/q^{1/2}$, $c = q^{1/2}/2k_{-1}$, and $d = -\Theta$. By plotting $-\tanh^{-1}(ax-b)$ versus t, we can obtain k_{-1} from slope/c and k_1 from $0.30 \times k_{-1}$.

Figure 1 shows plots of equation (7) at different concentrations of HS^-. The fact that all the data fitted well as straight lines suggests that (i) the reactions first order with respect to both CySSCy and HS^-, i.e., $R_f = k_1[CySSCy][HS^-]$ and (ii) the first equilibrium can be separated from the second in the determination of k_1 and k_{-1}. From these plots we obtain $k_1 = 1.4 \pm 0.2\ M^{-1}\ min^{-1}$ and $k_{-1} = 4.6 \pm 0.6\ M^{-1}\ min^{-1}$ at pH = 10, $\mu = 0.16$ M and 25°C.

Temperature Dependence

The reaction between CySSCy and HS^- was studied at 25°C, 30°C, 35°C, and 40°C and the results are shown in Fig. 2a. By plotting log k_1 versus $1/T^0$ (Arrhenius plot), Fig. 2b, one obtains $E^* = 15.9$ kcal/mol.

Ionic Strength Dependence

The ionic strength (μ) dependence of the above reaction was also examined. Higher μ than 0.16 M was achieved by addition of NaCl whereas in the case of $\mu = 0.01$ M, the solution was not buffered by borate and the pH was adjusted to 10 by dropwise

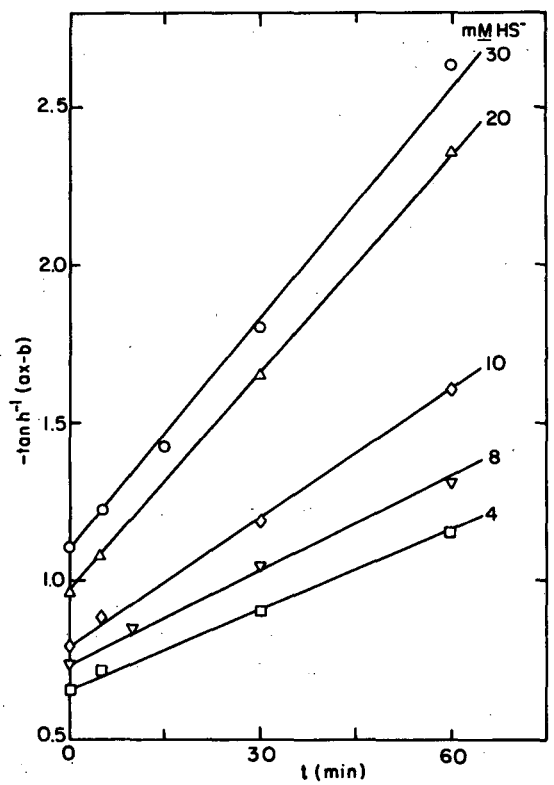

Figure 1. Dependence of the rate of reaction between CySSCy and HS^- on $[HS^-]$. All measurements were made at $T^0 = 25°C$, pH = 10, and $\mu = 0.16$ M. (XBL 863-7519)

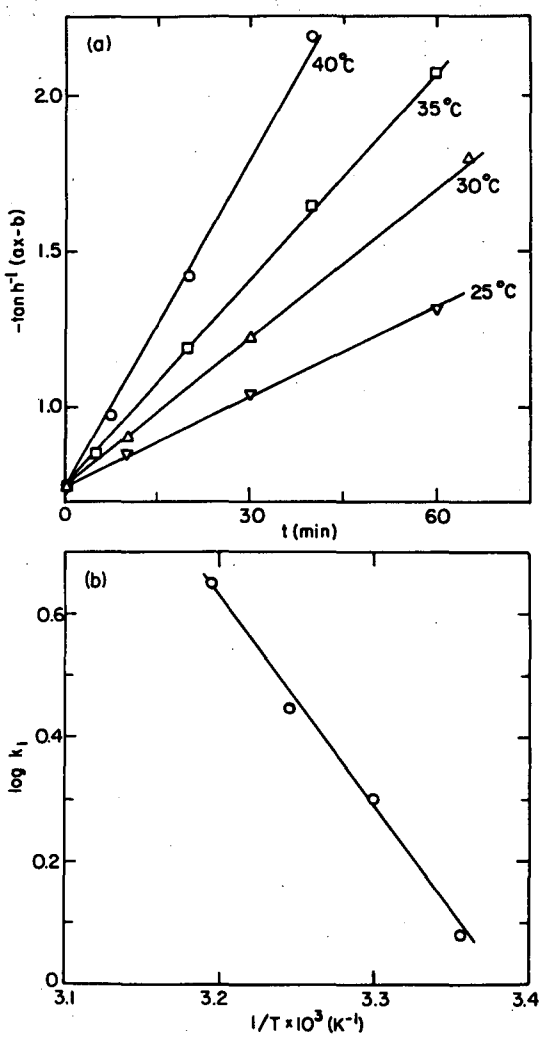

Figure 2. Temperature dependence of the rate of reaction between CySSCy and HS^-: (a) plot of $-\tanh^{-1}(ax-b)$ vs. t at different temperatures, pH = 10 and μ = 0.16 M; (b) plot of log k_1 vs. $1/T^0$ (Arrhenius plot) with slope = −3.47. (XBL 863-7521)

addition of 1N NaOH. The results are shown in Fig. 3a. Since in H_2O at 25°C

$$\log(k_1/k_1^0) = 1.02 z_A z_B \mu^{1/2} \quad (8)$$

a plot of log k_1 versus 1.02 $\mu^{1/2}$ (in the low ionic strength regime as demanded by the Debye-Hückel model) should yield a slope of $z_A z_B$ and an intercept of k_1^0, the rate constant k_1 at infinite dilution. Such a plot is shown in Fig. 3b, from which we obtain k_1^0 = 0.18 M^{-1} min^{-1} and $z_A z_B$ = 2.0. The later result suggests that CySSCy reacts as a dianion.

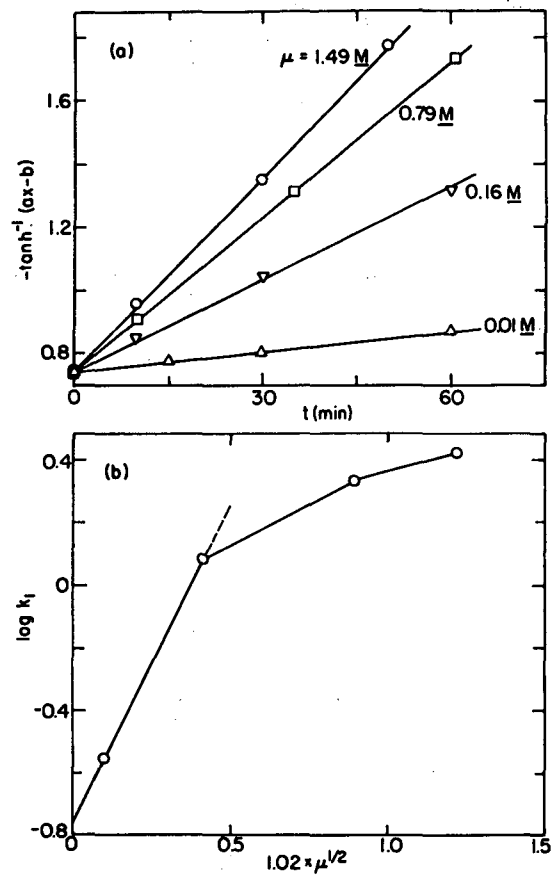

Figure 3. Ionic strength dependence of the rate of reaction between CySSCy and HS^-: (a) plot of $-\tanh^{-1}(ax-b)$ vs. t at different μ's, T^0 = 55°C and pH = 10; (b) plot of log k_1 vs. 1.02 $\mu^{1/2}$ with initial slope = 2.0. (XBL 863-7520)

PLANNED ACTIVITIES FOR FY 1986

Future work includes the pH dependence studies of this reaction and the study of kinetics and thermodynamics of reactions between $CySS^-$ and HS^- (Eq. 2) and between $CySSO_3^-$ and HS^-. The purpose of these studies is to obtain an optimum condition for the production of cysteine from cystine.

REFERENCES

1. Chang, S.G. and Liu, D.K. (1986), "A Process for Production of Cysteine from Cystine," LBL patent case no. IB-638, U.S. patent pending.
2. Benson, S.W. (1960), *The Foundations of Chemical Kinetics,* McGraw-Hill, Chap. 3.
3. *CRC Standard Mathematical Tables* (1968), 16th Edition, S.M. Selby, Ed., CRC Press.

Kinetics of the Reaction of Nitric Oxide with Sulfite and Bisulfite Ions in Aqueous Solution*

D. Littlejohn, K.Y. Hu, and S.G. Chang

There have been several studies[1-4] of the reaction of nitric oxide with dissolved sulfur dioxide, but there is disagreement about the kinetics of the system. An early study was done by Terres and Lichti,[1] who observed the decrease in pressure of nitric oxide in the presence of K_2SO_3, $KHSO_3$, and SO_2 H_2O. They were unable to obtain rate constants, but decided that a $(ONSO_3)^{2-}$ intermediate was involved and that the reaction between nitric oxide and bisulfite ion was first order in both species. Nunes and Powell[2] investigated the reaction of NO with SO_3^{2-} at pH 13–14 by observing the decrease in pressure of NO over the sulfite solution in a well-stirred reactor. The rate expression they obtained consisted of a sulfite dependent term and a sulfite independent term. Takeuchi, *et al.*[3] observed the loss of nitric oxide diluted with nitrogen after it either flowed over a sulfite solution surface or was bubbled through a sulfite solution. They found the reaction had second order dependence on nitric oxide and zero order dependence on sulfite concentration. Their results indicated the reaction was very fast. Martin, *et al.*[4] used a stopped-flow system to observe the reaction between dissolved nitric oxide and dissolved sulfur dioxide at pH $\leqslant 3$ by monitoring SO_2 H_2O at 280 mm. They found that the reaction was very slow and could only obtain an upper limit for the rate. In view of the disagreement of these studies, we decided to investigate the reaction system in an attempt to remove the ambiguity associated with it.

ACCOMPLISHMENTS DURING FY 1985

To avoid difficulties with the diffusion rate of nitric oxide influencing the observed rate or reaction, we decided to monitor the reaction of sulfite and bisulfite ions with dissolved nitric oxide rather than nitric oxide gas. A continuous-flow rapid-mixing system which could also be used in the stopped-flow mode was used for the experiments. Both tanks for the reactant solutions were filled with water and degassed by passing argon through them. Nitric oxide was then passed through one of the tanks until the solution was saturated. A lower flow of nitric oxide was passed through the solution during the experiments. The sulfite and/or bisulfite solution was prepared by weighing out reagent grade sodium sulfite and/or sodium metabisulfite. The pH of the solutions was adjusted by the addition of sodium hydroxide or hydrochloric acid, if necessary. After preparation, the two solutions were passed through flowmeters and a mixer and then into either a 1 cm or 5 cm pathlength UV cell. The cell was located in a temperature-controlled compartment in a Cary 219 spectrophotometer. The pH of the mixed solution was monitored with an in-line pH probe downstream of the cell.

Ackermann and Powell[5] found that the only product of the reaction of NO with SO_3^{2-} was N-nitrosohydroxylamine-N-sulfonate (NHAS), which has a strong UV absorption. NHAS was monitored in the wavelength range between 258 nm and 300 nm, where absorptions by other species would not interfere. The reaction was studied in two ways. In continuous-flow measurements, the flow rates of the reactants were stabilized and a spectrum of the reaction mixture was taken from 350 nm to 230 nm. In stopped-flow measurements, the flow rates of the reactants were stabilized and one wavelength where NHAS alone absorbed was monitored. The flow of the reactants was stopped abruptly and the change in NHAS concentration *vs* time was monitored. The results of the experiments at high pH conditions were analyzed to obtain a rate constant for NO + SO_3^{2-}. This rate constant was then used to correct low and intermediate pH experiments to obtain the rate constant for NO + HSO_3^-. The hydrolysis rate for NHAS was obtained from the stopped-flow experiments at low pH, and this was used to correct the low pH experiments for loss of the reaction product.

From the experiments in which the nitric oxide concentration was varied at constant sulfite concentration, it was found that the rate for NHAS production had first order dependence on nitric oxide concentration. Similarly, in experiments where SO_3^{2-} and HSO_3^- were varied with constant NO concentration, it was found that the rate for NHAS production had first order dependence on both SO_3^{2-} and HSO_3^-.

The pH of the mixed solution was varied from 4 to 10.5 to observe what influence the pH had on the rate. A plot of log k *vs* pH is shown in Fig. 1, where k is defined as

$$k = \frac{d[NHAS]/dt}{[NO]([HSO_3^-] + [SO_3^{2-}])} .$$

*This work was supported by the Assistant Secretary for Fossil Energy, Office of Coal Utilization Systems, U.S. Department of Energy under Contract No. DE-AC03-76SF00098 through the Pittsburgh Energy Technology Center, Pittsburgh, PA.

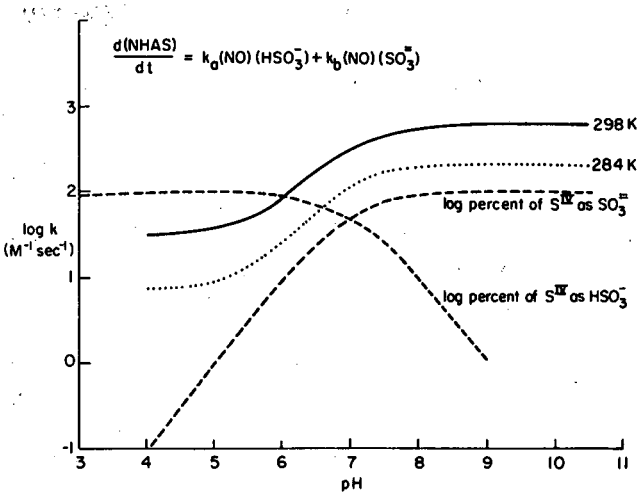

Figure 1. The pH dependence of the observed rate constant. (XBL 853-5938)

Also plotted as dashed lines are log percent of the total S(IV) oxide as HSO_3^- and SO_3^{2-}. The experimental curves indicate that both sulfite and bisulfite ions react with NO. If the reaction occurred only between SO_3^{2-} and NO, the experimentally obtained curve would be expected to follow the dashed line for SO_3^{2-}, rather than leveling out at lower pHs.

We also studied the temperature dependence of the reaction by putting the reactant tanks in a thermostatted bath, passing the reactant solutions through a second thermostatted bath just prior to mixing and regulating the temperature of the sample compartment. The curve of log k *vs* pH at 284 K is also shown in Fig. 1. Only the reaction of NO with SO_3^{2-} was studied at 323 K because of problems with the development of bubbles in the mixed solution which created unpredictable changes in the liquid volume between the mixer and the cell. The formation of the product can be expressed as

$$\frac{d[NHAS]}{dt} = k_a[NO][HSO_3^-] + k_b[NO][SO_3^{2-}].$$

The values for k_a and k_b are listed in Table 1. These values are plotted as log k *vs* 1/T in Fig. 2. For NO + SO_3^{2-}, a pre-exponential term of $A = 3.2 \times 10^{10}$ M^{-1} sec^{-1}, and an activation energy of $E_\alpha = 10.6$ kcal/mole are obtained where $k = Ae^{-E_a/RT}$. For NO

Table 1.

	k_a (M^{-1} sec^{-1})	k_b (M^{-1} sec^{-1})
284 K	7.5 ± 2	220 ± 35
298 K	32 ± 10	620 ± 100
323 K	–	2000 ± 500

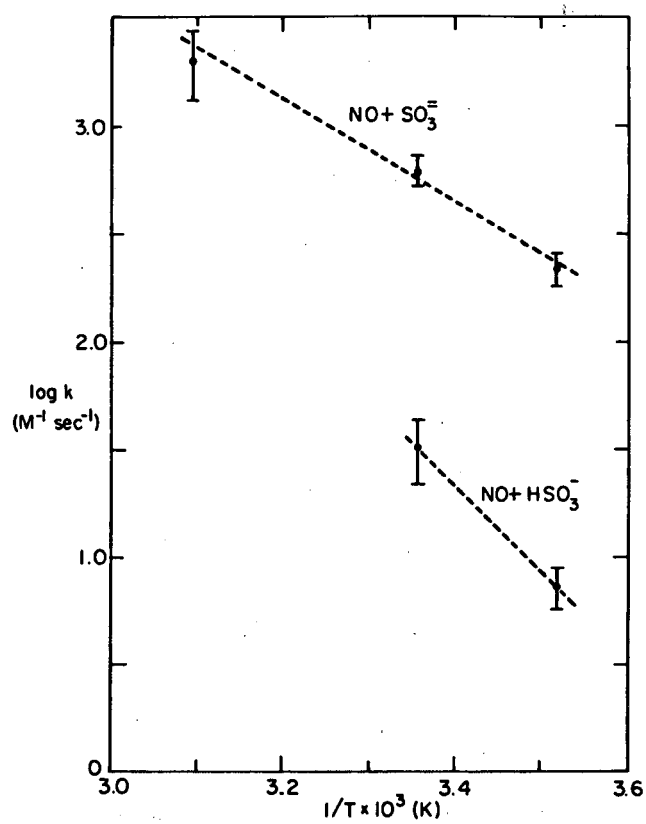

Figure 2. Arrhenius plot for NO + SO_3^{2-} and NO + HSO_3^-. (XBL 857-6393)

+ HSO_3^-, a pre-exponential term of 2.6×10^{14} M^{-1} sec^{-1} and an activation energy of 17.6 kcal/mole are obtained.

It was necessary to correct runs done at low pH for the hydrolysis of the NHAS product. Stopped-flow experiments were done at low pH conditions, and the NHAS concentration was monitored. The decaying absorbance curves obtained from these experiments were used to determine the hydrolysis rate constant for NHAS as a function of pH. Short intervals of the decay curve were used to calculate values of the rate constant. These values were averaged to obtain the hydrolysis rate constant. This is shown in Fig. 3, along with results obtained at higher pH conditions by Ackermann[6] and Seel and Winkler.[7] The latter used EDTA to bind any trace amounts of metal ions present in solution and obtained a lower hydrolysis rate constant than the former, suggesting the hydrolysis may be catalyzed by metal ions.

The first order dependence of the rate on both NO and SO_3^{2-}/HSO_3^- indicates the formation of an intermediate which rapidly reacts with a second NO to form the NHAS product. This is in agreement with what Terres and Lichti[1] and Nunes and Powell[2]

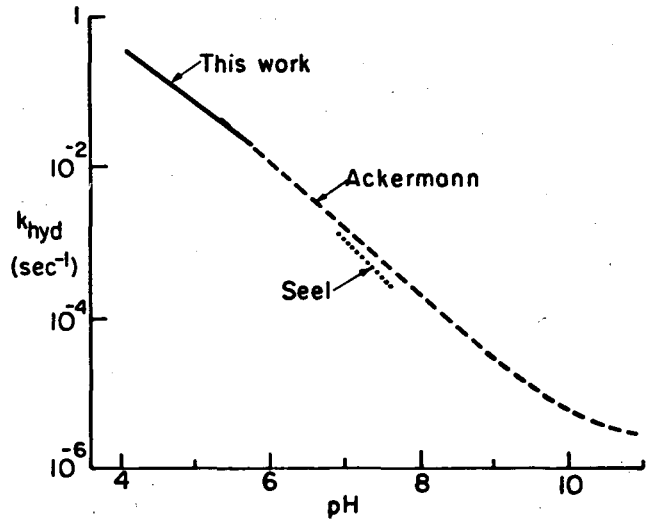

Figure 3. The pH dependence of the NHAS hydrolysis rate. (XBL 857-6394)

have observed. The following reaction scheme can explain our observations:

$$NO_{aq} + SO_3^{2-} \rightarrow (ONSO_3)^{2-}, \quad (1)$$

$$NO_{aq} + (ONSO_3)^{2-} \rightarrow {}^{-}ON(NO)SO_3^{-}, \quad (2)$$

$${}^{-}ON(NO)SO_3^{-} \xrightarrow{H^+} N_2O + SO_4^{2-}. \quad (3)$$

The reaction scheme also applies to HSO_3^-. Nunes and Powell's work with the reaction of NO with SO_3^{2-} and $SnCl_2$ in the presence of Cu(I) led them to believe that NO exists in two forms in aqueous solution, which they refer to as dissolved NO and hydrolyzed NO. They indicate that the dissolved form reacts more slowly than the hydrolyzed form. They propose the following reaction scheme for NO + SO_3^{2-}:

$$NO(gas) = NO(dissolved), \quad (4)$$

$$NO(dissolved) = NO(hydrolyzed), \quad (5)$$

$$NO(dissolved) + SO_3^{2-} \rightarrow (ONSO_3)^{2-}, \quad (6)$$

$$NO(hydrolyzed) + SO_3^{2-} \rightarrow (ONSO_3)^{2-}, \quad (7)$$

$$NO(unspecified) + (ONSO_3)^{2-} \rightarrow {}^{-}ON(NO)SO_3^{-}. \quad (8)$$

For the reaction of dissolved NO with SO_3^{2-} (reaction (6)), Nunes and Powell obtained $-d[NO]/dt = \frac{1}{2}\, d[NHAS]/dt = 0.45[NO][SO_3^{2-}]$ sec^{-1}, which is about three orders of magnitude slower than the rate we have obtained. From their temperature dependence, we calculate a pre-exponential term of $4.9 \times 10^5\ M^{-1}\ sec^{-1}$ and an activation energy of 8.2 kcal/mole for reaction (6). The activation energy is fairly close to the value we have obtained for reaction (2), 10.6 kcal/mole. They estimated that the rate constant for conversion of dissolved NO to hydrolyzed NO was about 0.14 sec^{-1} at 298 K.

Using the above rate constants, we modeled the stopped-flow experiments done with NO + SO_3^{2-} at 25°C in an attempt to determine if our results could validate their hypothesis that there are two forms of NO in solution. Since the hydrolyzed NO would react more quickly than the dissolved NO, the rate of NHAS formation should slow down as the hydrolyzed NO is consumed in a stopped-flow experiment. From the comparison of the calculations and the observed NHAS curves, we estimate that K_{eq} = [NO (hydrolyzed)]/[NO (dissolved)] is at least 10. There is considerable uncertainty in this value.

The only way we can reconcile their results with ours is to propose that the dissolution process for NO involves an intermediate which is formed directly from the gas phase and has a rate constant on the order of 0.1 sec^{-1} to form dissolved NO in aqueous solution. Without more information on the dissolution process, it is difficult to speculate about the chemistry associated with it.

PLANNED ACTIVITIES FOR FY 1986

The continuous-flow/stopped-flow apparatus used in this work is well-suited for studying rapid reactions in solution. Aqueous reactions involving dissolved nitrogen oxides and sulfur oxides may be studied in the future. A Raman spectrometer could be used as a detector instead of a UV-visible spectrometer. This would permit simultaneous observation of a number of species in the flowing solution.

REFERENCES

1. Terres, E. and Lichti, H. (1934), "Kinetische Untersuchung uber die Einwirkung von Stickoxyd auf Alkalisulfit, Alkalaibisulfit und schwelflige Saure in wahriger Losung," *Angew. Chem. 47*, p. 511.

2. Nunes, T.L. and Powell, R.E. (1970), "Kinetics of the Reaction of Nitric Oxide with Sulfite," *Inorg. Chem. 9*, p. 1916.
3. Takeuchi, H., Ando, M., and Kizawa, N. (1977), "Absorption of Nitrogen Oxides in Aqueous Sodium Sulfite and Bisulfite Solutions," *I & EC Process Des. & Dev. 16*, p. 303.
4. Martin, L.R., Damschen, D.E., and Judeikis, H.S. (1981), "The Reactions of Nitrogen Oxides with SO_2 in Aqueous Aerosols," *Atmos. Environ. 15*, p. 191.
5. Ackermann, M.N., Powell, R.E. (1967) "Air Oxidation of Hydroxylamine-N-Sulfonate," *Inorg. Chem. 6*, p. 1718.
6. Ackermann, M.N. (1966), "Alkaline Hydrolysis and Oxidation of Hydrolylamine-N-Sulfonate Ion," Ph.D. Thesis, University of California, Berkeley.
7. Seel, F. and Winkler, R. (1963), "Kinetik des saurekatalysierten Zerfalls des Nitrosohydroxylaminsulfonat-Ions," *Z. Naturforsch. 18a*, p. 155.

The Kinetics of Acid Hydrolysis of Nitridotrisulfate Ion*

David Littlejohn, Abigail R. Wizansky, and S.G. Chang

A number of nitrogen sulfonates are produced by reactions between bisulfite ions and nitrite ion in aqueous solution.[1] Thus, their chemistry is of interest in studies of aqueous aerosols in polluted air and in wet flue gas scrubbing systems. Some of the chemistry is shown in Fig. 1. While the hydrolysis reactions of hydroxyimidodisulfate (HIDS) and imidodisulfate (IDS) have been studied,[2,3] those of nitridotrisulfate (NTS) and hydroxylsulfamate (HSA) have not been thoroughly investigated. Sisler and Audrieth[4] observed the hydrolysis of NTS:

$$\mathrm{NTS} + \mathrm{H}^+ \rightarrow \mathrm{IDS} + \mathrm{HSO_4}^- . \qquad (1)$$

They found that it occurred much more quickly than the hydrolysis of IDS. No quantitative information was obtained.

ACCOMPLISHMENTS DURING FY 1985

We have studied the hydrolysis of NTS over a temperature range of 283 K to 333 K, a pH range of 4 to 7, and an ionic strength range of 0.05 to 1.0. The potassium salt of NTS was prepared by the method of Sisler and Audrieth,[4] and the purity was checked by Raman spectroscopy and ion chromatography. Experiments were done by dissolving the NTS salt in a slightly alkaline solution and then mixing with a acidic buffer solution to initiate hydrolysis. Buffers used included acetate, oxalate, phosphate, phthalate, malonate, and succinate solutions. Sodium chloride was used to adjust the ionic strength of the solutions. The hydrolysis was monitored by measuring the concentrations of the reaction products, IDS and SO_4^{2-}, by ion chromatography.[5] The products could not be measured simultaneously. Sulfate was usually monitored because ion chromatographic detection of SO_4^{2-} is linear over a wider concentration range than IDS.

The dependence of the rate of the hydrolysis reaction on the concentrations of NTS and H^+ was checked. Using buffers to maintain the solutions at pH 5, runs were made in which the NTS concentration was varied from 10^{-3} M to 10^{-2} M. A plot of $\log_{10}$ [NTS] *vs* $\log_{10}$ (rate) is shown in Fig. 2. The slope for the line is 1.07 ± 0.10, indicating first-

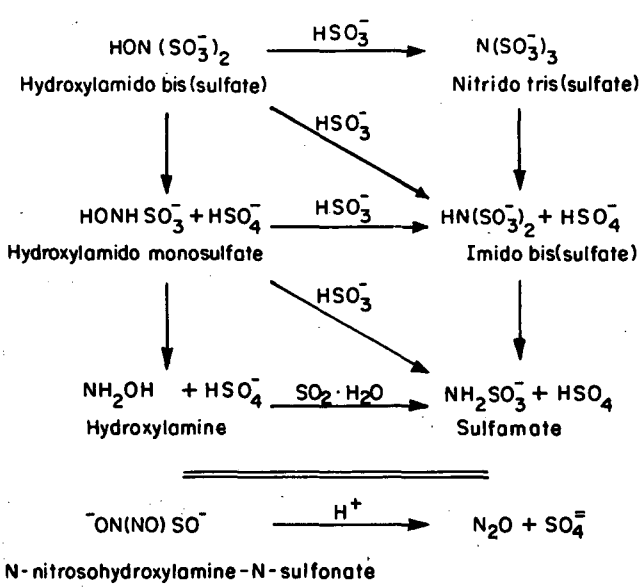

Figure 1. Reactions involving nitrogen sulfonates. (XBL 854-6046)

*This work was supported by the Assistant Secretary for Fossil Energy, Office of Coal Utilization Systems, U.S. Department of Energy under Contract No. DE-AC03-76SF00098 through the Pittsburgh Energy Technology Center, Pittsburgh, PA.

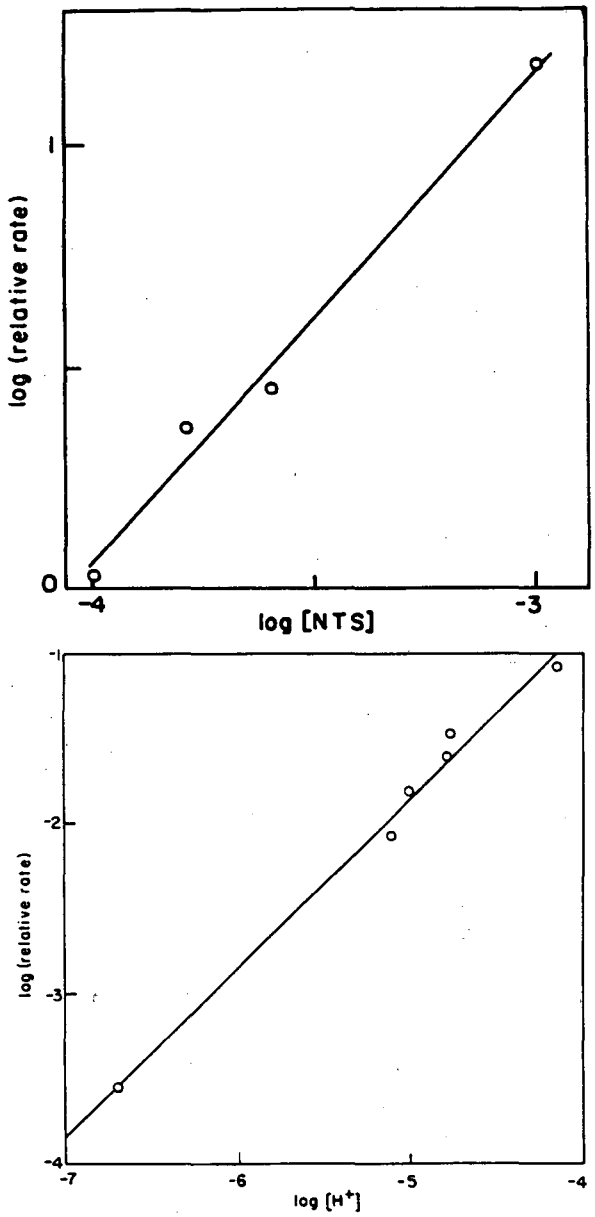

Figure 2. Rate dependence on $[H^+]$ and [NTS]. (XBL 863-1165)

order dependence on NTS concentration. The hydrogen ion dependence was done with solutions of 2.5×10^{-3} M NTS at pH 4 to 7. A plot of $\log_{10}$ (rate) *vs* pH is shown in Fig. 2. The slope of the line is 0.92 ± 0.09, indicating the hydrolysis reaction also has first-order dependence on H^+.

The temperature dependence of the hydrolysis reaction was studied by immersing the reaction mixtures in controlled-temperature water baths. The reaction was studied at 283 K, 298 K, 313 K, and 333 K. The rate constant was calculated using the expression

$$-\frac{d(NTS)}{dt} = k(H^+)(NTS).$$

Most runs were done with initial NTS concentrations of 2.5×10^{-3} M and ionic strengths of μ = 0.05. The rate constants obtained at these conditions are:

T =	283 K	k = 3.03 ± 0.17	$M^{-1}\,sec^{-1}$
	298 K	k = 12.7 ± 2.0	
	313 K	k = 70 ± 18	
	333 K	k = 227 ± 12 .	

An Arrhenius plot of these values is shown on Fig. 3. If the rate constant is expressed as k = A exp (−Ea/RT) where R is the gas constant and T is the absolute temperature, then values of A = 1.5 ± 0.7 $\times 10^{13}$ $L\,mol^{-1}\,sec^{-1}$ and E_a = 16.5 ± .3 kcal/mole. Both the pre-exponential factor and the activation energy are similar to those of the acid-catalyzed HIDS hydrolysis.[1]

The effect of ionic strength on the hydrolysis reaction was investigated by adding sodium chloride and/or changing the buffer concentration. The ionic strength was varied from μ = 0.08 to μ = 1.0. All runs were done with an NTS concentration of 2.5×10^{-3} M. All of these runs were done in the pH range of 4.8 to 5.2. A plot of log k *vs* $\mu^{1/2}$ is shown in Fig. 4. The slope of the plot should be equal to the product of charges of the reacting ions.[6] The slope of this plot is about −1, suggesting that it is the 1− form of NTS reacting with H+ to form IDS. The ionization constants for NTS are not known. It is estimated the pK_as are fairly low.[4]

Solutions of NTS in the range of pH 8 to 10 exhibit little or no deterioration over a period of

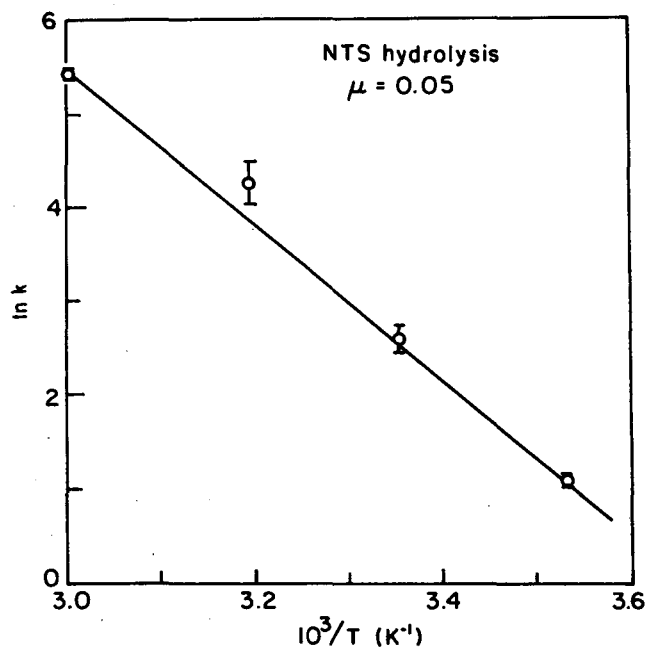

Figure 3. Arrhenius plot for the hydrolysis of NTS. (XBL 863-7576)

many days. This indicates that the uncatalyzed hydrolysis reaction is insignificant compared to the acid-catalyzed reaction.

PLANNED ACTIVITIES FOR FY 1986

Another of the nitrogen sulfonates shown in Fig. 1, HSA, is known to hydrolyze in acidic solutions, and its hydrolysis kinetics have not been studied. The method used to study the hydrolysis of NTS should readily lend itself to the study of the hydrolysis of HSA. We plan to study this reaction in FY 1986.

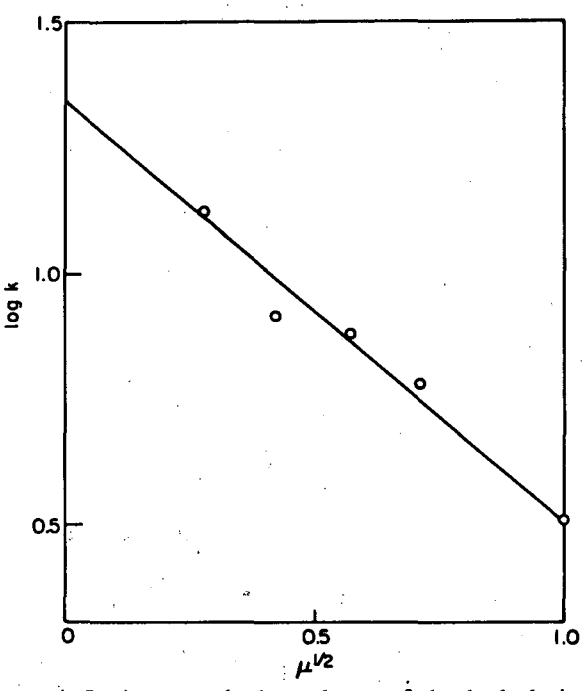

Figure 4. Ionic strength dependence of the hydrolysis of NTS. (XBL 863-7575)

REFERENCES

1. Chang, S.G., Littlejohn, D., and Lin, N.H. (1982), "Kinetics of Reactions is a Wet Flue Gas Simultaneous Desulfurization and Denitrification System," in *Flue Gas Desulfurization*, ACS Symposium Series No. 188, American Chemical Society, Washington, D.C., p. 127.
2. Naiditch, S. and Yost, D.M. (1941), "The Rate and Mechanism of the Hydrolysis of Hydroxylamine Disulfonate Ion," *J. Am. Chem. Soc. 63*, p. 2123.
3. Doyle, G.J. and Davidson, N. (1949), "The Kinetics of the Acid-Catalyzed Hydrolysis of Amine Disulfonate Ion; The Third Ionization Constant of Amine Disulfonic Acid," *J. Am. Chem. Soc. 71*, p. 3491.
4. Sisler, H. and Audrieth, L.F. (1938), "Potassium Nitrilosulfonate," *J. Am. Chem. Soc. 60*, p. 1947.
5. Littlejohn, D. and Chang, S.G. (1986), *Determination of Nitrogen-Sulfur Compounds by Ion Chromatography" Anal. Chem. 58*, p. 158.
6. Olson, A.R. and Simonson, T.R. (1949), "Rates of Ionic Reactions in Aqueous Solutions," *J. Chem. Phys. 17*, p. 1167.

Determination of Nitrogen-Sulfur Compounds by Ion Chromatography*

D. Littlejohn and S.G. Chang

A number of nitrogen-sulfur compounds can form in aqueous solutions of nitrogen oxyanions and sulfur oxyanions.[1,2] Conditions suitable for their formation exist in wet flue gas scrubbers and aqueous aerosols in polluted air. The nitrogen sulfonates of interest include hydroxyimidodisulfate (HIDS), hydroxysulfamate (HSA), nitridotrisulfate (NTS), imidodisulfate (IDS), and N-nitroso-hydroxylamine-N-sulfonate (NHAS).

Three techniques have been previously described for the determination of some of these compounds. The gravimetric and iodometric technique developed by Sato, *et al.*[3] requires a series of treatments of a sample to obtain the amounts of HIDS, NTS, and IDS present. They gave no method for HSA or NHAS determination. Oblath[4] used a method where HIDS was oxidized to nitrosodisulfonate ($ON(SO_3^-)_2$), and colorimetry was done to determine nitrosodisulfonate. This technique also involves a number of steps. Raman spectrometry permits simultaneous determination of all of the compounds listed above and requires a very small sample volume.[5] It eliminates the need for extensive manipulation of the sample. The major limitation of Raman spectrometry is lack of sensitivity. Samples with low concentrations (0.001–0.01 M) of the compounds of interest require very long data aquisition times. Determination of these compounds by ion chromatography has been found to combine high sensitivity and rapid measurement times.

*This work was supported by the Assistant Secretary for Fossil Energy, Office of Coal Utilization Systems, U.S. Department of Energy under Contract No. DE-AC03-76SF00098 through the Pittsburgh Energy Technology Center, Pittsburgh, PA.

ACCOMPLISHMENTS DURING FY 1985

A Dionex 2010i ion chromatograph equipped with a Dionex AG4 guard column, a Dionex AS4 anion separation column, and a Dionex anion fiber suppressor was used in the determinations. For determination of HSA and sulfamate, 1.5 mM bicarbonate eluent was used with a flow rate of 2.0 mL/min at a pressure of 700–800 psi. For determination of HIDS, IDS, and NHAS, the AG4 column alone was used as the separation column with 12 mM or 18 mM carbonate eluents. The flow rate was 1.5 mL/min at a pressure of 200–300 psi. A 50 μL sample loop volume was used. For conductivity suppression, 0.025 N H_2SO_4 was used with a flow rate of 2.5–3.5 mL/min for the 1.5 mM eluent and a flow rate of 5–7 mL/min for the 12 mM and 18 mM eluents.

The NTS and IDS for standard solutions were synthesized by the procedure given by Sisler and Audrieth.[6] HIDS was prepared by the method of Rollefson and Oldershaw.[7] HSA was prepared by the method given by Oblath.[4] The potassium salts of the above compounds were stored in a vacuum desiccator at 5°C until solutions were needed. Solutions of these compounds were treated with sufficient concentrated NaOH to make the solutions alkaline. NHAS solutions were prepared on a vacuum line just prior to use, following the method of Nunes and Powell.[8]

An ion chromatogram of a mixture of IDS, HIDS, and NHAS is shown in the bottom half of Fig. 1. The chromatogram was recorded on the 10 μS scale. The peak present at $\Delta t \approx 1$ min is due to sulfate impurity. An ion chromatogram of a mixture of sulfamate and HSA is shown in the top half of Fig. 1. This chromatogram was also recorded on the 10 μS scale.

It was not possible to make determinations of NTS with the column used in these studies because it is very strongly retained on the column. In the alkaline conditions of carbonate and bicarbonate eluents, NTS has a 3− charge. HSA and sulfamate have 1− charges and will pass through the 5 cm guard column and 25 cm separation column in a few minutes using a low concentration eluent. IDS, HIDS, and NHAS have 2− charges and require a high concentration eluent to pass through the 5 cm guard column alone in a few minutes.

To transport a compound with a 3− charge through a column with this type of ion exchange resin in a reasonable time would require an excessively high eluent concentration. A resin that would work well with NTS would be unlikely to separate the other compounds. It may be possible to analyze NTS by using a column with a more hydrophobic resin or by MPIC (Mobile Phase Ion Chromatography).

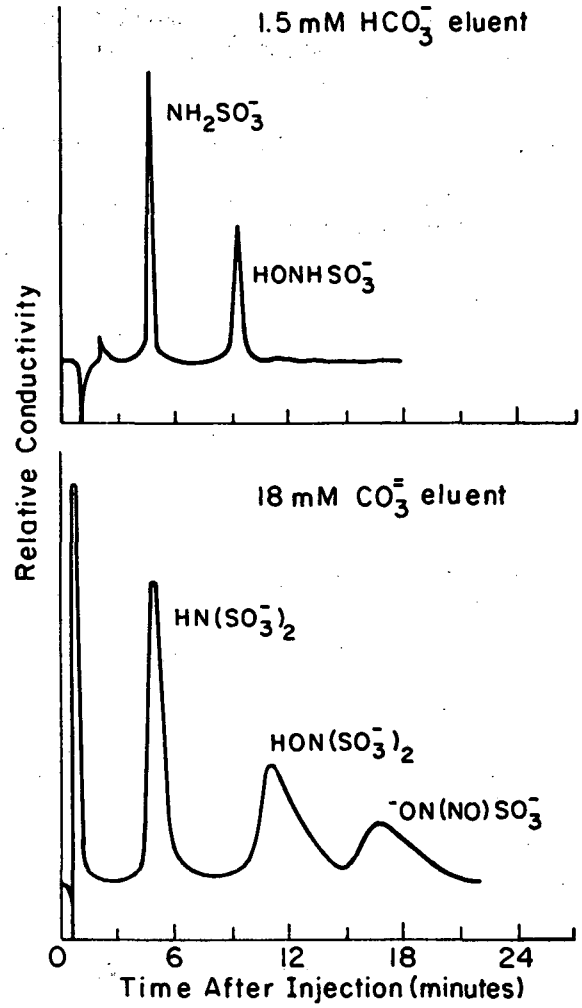

Figure 1. (Top) Ion chromatogram of sulfamate and hydroxysulfamate. (Bottom) Ion chromatogram of imidodisulfate, hydroxyimidodisulfate, and N-nitrosohydroxylamine-N-sulfonate. (XBL 854-6043)

These compounds can hydrolyze in aqueous solutions under acidic conditions. Generally, they are stable in alkaline solutions, although NHAS and HSA are susceptible to attack by oxygen.[9] There is considerable variation in the rates of hydrolysis for these compounds. For a given pH and nitrogen sulfonate concentration, the relative hydrolysis rates, in increasing order, are: HSA, IDS, HIDS, NTS, and NHAS. Since NTS hydrolyzes much more easily than IDS, it can be converted into IDS for measurement by ion chromatography. A sample can be run on the ion chromatograph to determine IDS, acidified to pH 2–3 and allowed to stand 5–10 minutes, and run again to measure the increase in IDS concentration. Tests done with standard solutions indi-

cate this is a quantitative method. The hydrolysis of IDS is sufficiently slow under these conditions that it does not affect the results.[10]

It was found that determinations of nitrogen-sulfur compounds in samples were best done by comparison with standard solutions. Ion chromatograms of dilutions of freshly prepared alkaline solutions of the compounds were run either prior to or following chromatograms of solutions containing unknown amounts of the compounds. This minimized the influence of variations in the ion chromatograph operating parameters. The linearity of the ion chromatograph's response to the compounds was checked by measuring the peak heights obtained from a range of sample concentrations. The highest concentrations injected were 1×10^{-3} M. Figure 2 shows a plot of peak height *vs* concentration for HSA and sulfamate. Both HSA and sulfamate significantly deviate from linearity above 2×10^{-4} M. The peaks become broader and shorter than what would be expected from extrapolation of the peak heights obtained at lower concentration. Figure 3 shows a plot of peak height *vs* concentration for IDS, HIDS, and NHAS. IDS deviated from linear response above 2×10^{-4} M concentration, while HIDS, and NHAS exhibited good linearity up to 6×10^{-4} M concentration. All compounds exhibited broadening of the peaks at the highest concentrations

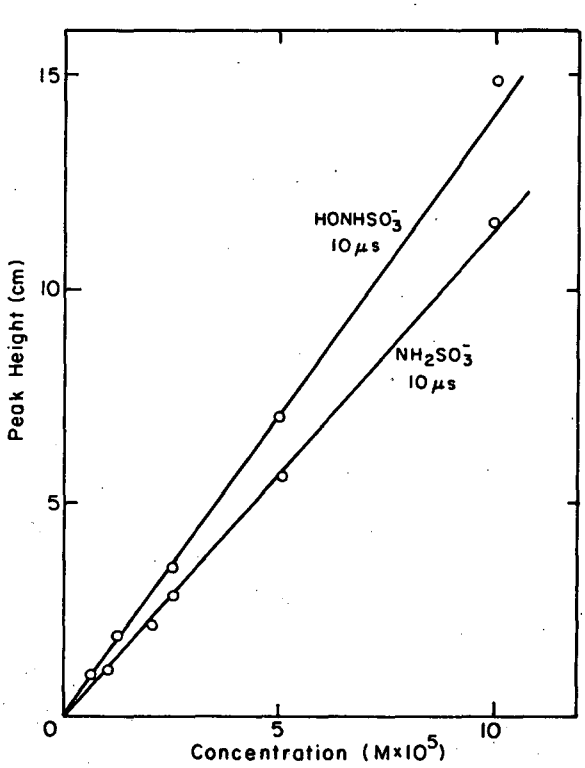

Figure 2. Calibration curve for sulfamate and hydroxysulfamate. (XBL 854-6044)

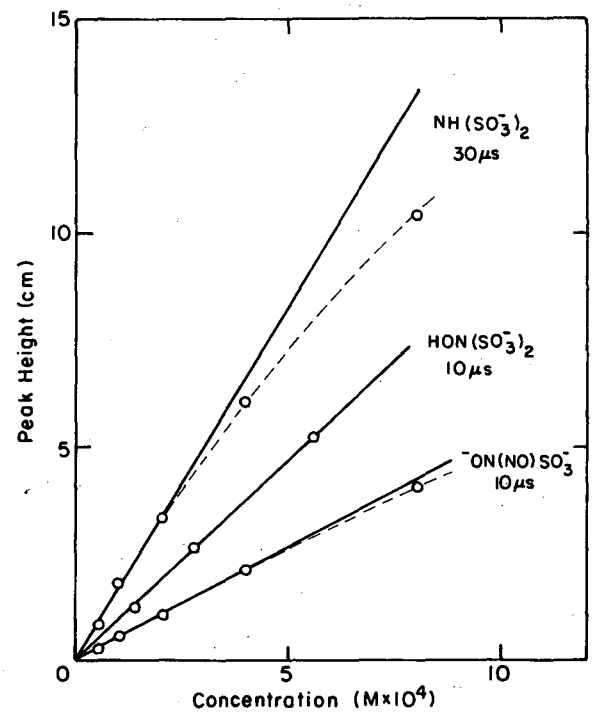

Figure 3. Calibration curve for imidodisulfate, hydroxyimidodisulfate, and N-nitrosohydroxylamine-N-sulfonate. (XBL 854-6045)

tested. Also, when the AG4 column alone was used, reduction in the compounds' retention time was noted at high concentrations ($\sim 1 \times 10^{-3}$ M).

Detection limits for the compounds were obtained where the detection limit was defined as the concentration that generated a peak with a height twice that of the background noise. The detection limits obtained are as follows: HSA : 0.5×10^{-6} M, sulfamate : 0.6×10^{-6} M, IDS : 1.4×10^{-6} M, HIDS : 7.4×10^{-6} M, NHAS : 12×10^{-6} M. As the retention time of a compound increases, the peak broadens and decreases in height. Thus, it is advantageous to have as short a retention time as possible within the limitations of obtaining separation between the peaks of chromatogram.

A number of flue gas scrubbing liquors have been analyzed by the method discussed above. Table 1 lists the range of concentrations observed for seven anions found in several scrubbing liquor samples from typical closed-loop lime-limestone scrubbers. The samples were in the pH range of 6 to 8.5. No HSA was found in the samples, presumably because oxidation would occur rapidly enough to eliminate it from the samples before analysis.

PLANNED ACTIVITIES FOR FY 1986

There are a number of other nitrogen-sulfur compounds that have similar structure to those stu-

Table 1.

Anion	Range of Concentration
Cl^-	$3.0 - 3.6 \times 10^{-2}$ M
NO_3^-	$1.8 - 4.2 \times 10^{-3}$ M
$SO_4^=$	$3.2 - 4.2 \times 10^{-2}$ M
$S_2O_3^=$	$0 - 3.2 \times 10^{-3}$ M
IDS	$0.7 - 3.3 \times 10^{-3}$ M
HIDS	$0.3 - 0.8 \times 10^{-3}$ M
NTS	$0 - 1.3 \times 10^{-3}$ M

died. Ion chromatography may be a suitable technique to study these compounds also. We plan to attempt to detect some of these compounds by ion chromatography.

REFERENCES

1. Oblath, S.B., Markowitz, S.S., Novakov, T., and Chang, S.G. (1982), "Kinetics of the Initial Reaction of Nitrite Ion in Bisulfite Solutions," *J. Phys. Chem. 86*, p. 4853.
2. Chang, S.G., Littlejohn, D., and Lin, N.H. (1982), "Kinetics of Reactions in a Wet Flue Gas Simultaneous Desulfurization and Denitrification System," *ACS Symp. Ser. No. 188*, American Chemical Society, Washington, DC.
3. Sato, T., Matani, S., and Okabe, T. (1979), "Oxidation of Sodium Sulfite with Nitrogen Dioxide," *ACS/CSJ Chemical Congress*, Honolulu, HI.
4. Oblath, S.B. (1981), "Kinetics of the Reduction of Nitrite Ion by Sulfur Dioxide in Aqueous Solution," Ph.D. Thesis, University of California, Berkeley.
5. Littlejohn, D. and Chang, S.G. (1984), "Identification of Species in a Wet Flue Gas Desulfurization and Denitrification System by Laser Raman Spectroscopy," *Environ. Sci. Tech. 18* p. 305.
6. Sisler, H. and Audrieth, L.F. (1938), "Potassium Nitrilosulfonate," *J. Am. Chem. Soc. 60* p. 1947.
7. Rollefson, G.K. and Oldershaw, C.F. (1932), "The Reduction of Nitrites to Hydroxylamine by Sulfites," *J. Am. Chem. Soc. 54*, p. 977.
8. Nunes, T.L. and Powell, R.E. (1970), "Kinetics of the Reaction of Nitric Oxide with Sulfite," *Inorg. Chem. 9*, p. 1917.
9. Ackermann, M.N. and Powell, R.E. (1967), "Air Oxidation of Hydroxylamine-N-Sulfonate," *Inorg. Chem. 6*, p. 1718.
10. Doyle, G.J. and Davidson, N. (1949), "The Kinetics of the Acid-Catalyzed Hydrolysis of Amine Disulfonate Ion; The Third Ionization Constant of Amine Disulfonic Acid," *J. Am. Chem. Soc. 71*, p. 3491.

Investigation of the Reaction of Oxygen with Bisulfite Ion in Aqueous Solutions Using a High-Pressure Stopped-Flow Technique*

D. Littlejohn, K.Y. Hu, and S.G. Chang

The oxidation of aqueous bisulfite ion by molecular oxygen has been under investigation for many years, and the reaction process is still poorly understood,[1-3] although it is known the main products are SO_4^{2-} and H^+:

$$O_2 + 2HSO_3^- \rightarrow 2SO_4^{2-} + 2H^+$$

*This work was supported by the Electric Power Research Institute, Palo Alto, CA, through the U.S. Department of Energy under Contract No. DE-AC03-76SF00098.

The reaction is very important in wet flue-gas desulfurization processes. It would be highly desirable to be able to control the reaction in wet scrubbing systems so that the degree of oxidation is no larger than that desired. Trace concentrations of transition metal ions have been reported to significantly affect the rate of oxidation, as well as the reaction products.

ACCOMPLISHMENTS DURING FY 1985

We have investigated the reaction by using a high-pressure, rapid-mixing flow system in conjunction with a laser Raman spectrometer. Use of higher-than-atmospheric pressures raises the dissolved oxygen concentration to where it can be more readily observed by Raman spectroscopy. Besides dissolved oxygen, use of Raman spectroscopy permits observation of all important species in the reaction system: HSO_3^-, SO_4^{2-}, SO_2H_2O, HSO_4^-, and $S_2O_6^{2-}$. ClO_4^- is added to the reaction mixture as a

reference ion so that quantitative measurements can be made. The positions of the Raman peaks of these compounds and their relative strengths are listed in Table 1. The hydrogen ion concentration can be obtained from the concentrations of HSO_3^- and SO_2H_2O and the equilibrium between them:

$$SO_2H_2O = HSO_3^- + H^+ \quad K_1 = 0.0139\ M$$

(Ref. 4)

In addition to this equilibrium, there are several others in this system that are important. They are:

$$HSO_4^- = SO_4^{2-} + H^+ \quad K_2 = 0.0103\ M$$

(Ref. 1)

$$2HSO_3^- = S_2O_5^{2-} + H_2O \quad K_3 = 0.088\ M$$

(Ref. 5)

$$HSO_3^- = SO_3^{2-} + H^+ \quad K_4 = 1 \times 10^{-7}\ M$$

(Ref. 6)

$$SO_2\,(g) = SO_2\ H_2O \quad H_1 = 1.5\ M\ atm^{-1}$$

(Ref. 7)

$$O_2\,(g) = O_2\,(aq) \quad H_2 = 1.25 \times 10^{-3}\ M\ atm^{-1}$$

(Ref. 7)

These equilibria are used in determining the concentrations of these species in the reaction system.

A number of experiments have been done with dissolved oxygen concentrations ranging from 8×10^{-3} to 4×10^{-2} M (after mixing) and bisulfite concentrations ranging from 0.06 to 0.4 M (after mixing). The pH of the solution immediately after mixing is in the range of 3.5 to 4. The experiments are performed by obtaining a stable flow of the reactants and abruptly stopping the flow while monitoring one compound with the Raman spectrometer. The behavior of the compounds is observed for a period of time after the flow is stopped. The process is repeated until all species have been observed. The reacted solution is scanned with the Raman spectrometer to determine the concentrations of the compounds present at the end of reaction.

Table 1.

Compound	Raman Peak	R.S.E.[a]
$S_2O_5^{2-}$	235 cm^{-1}	0.15
$S_2O_6^{2-}$	710	0.47
ClO_4^-	934	1.06
SO_4^{2-}	981	1.00
HSO_3^-	1023	0.12
	1055	0.16
HSO_4^-	1050	0.050
X	~ 1090	~ 0.5
$S_2O_6^{2-}$	1092	1.48
SO_2H_2O	1152	0.94
O_2	1550	0.38

[a]R.S.E. (Relative Scattering Efficiency) = $\frac{\text{compound peak height/compound molarity}}{981\ cm^{-1}\ SO_4^{2-}\ \text{peak height}/SO_4^{2-}\ \text{molarity}}$

Metal ions can be added to the reactant solutions to observe their effect on the reaction system. To date, runs have been made with Fe(II) and Mn(II) added to the bisulfite solution.

Most of the experiments done have involved conditions where the bisulfite concentration is in excess of the oxygen concentration. Initial $[O_2]$ to $[HSO_3^-]$ ratios have ranged from 0.02 to 0.4. The results we have obtained allow us to divide the experiments into two groups: those where all the oxygen is consumed very shortly after mixing and those where some oxygen exists for a longer time (on the order of 50 seconds or more). The boundary between the two conditions occurs at $[O_2]$:$[HSO_3^-]$ of about 0.07. Results obtained within each group tend to be similar. The cause of this apparent bimodal behavior is under investigation.

A rapid initial drop in oxygen concentration was observed in almost all the experiments done. A concurrent drop in the bisulfite concentration was also seen. The stoichiometry of the rapidly reacting O_2 to HSO_3^- was about 1 to 2, the same as that for the oxidation reaction.

The curves of concentration *vs* time for O_2, HSO_3^-, $SO_2\ H_2O$, and $(SO_4^{2-} + HSO_4^-)$ obtained from the experiments can be used to develop mass balances for sulfur and oxygen for the experimental runs. The oxygen mass balance using $[O_2] + 2 \times [(SO_4^{2-} + HSO_4^-)]$ shows a dip shortly after the flow is stopped with a gradual return to the original level. The sulfur mass balance using $[HSO_3^-] + [SO_2\ H_2O] + [(SO_4^{2-} + HSO_4^-)]$ shows a similar dip after the flow is stopped. These are shown in Fig. 1 for run 39. These curves are indicative of an intermediate formed from bisulfite and oxygen and decaying into sulfate and hydrogen ion.

While attempting to observe dithionate ion, $S_2O_6^{2-}$, at 1092 cm^{-1}, a curve was obtained that was similar to that which would be expected of the intermediate suggested by the mass balance plots for oxygen and sulfur. Checking nearby wavenumber positions indicated that the signal maximum was at ~ 1090 cm^{-1}, rather than at 1092 cm^{-1}, the $S_2O_6^{2-}$ maximum. The curve for the intermediate is shown in Fig. 2 for run 39, which had conditions where all

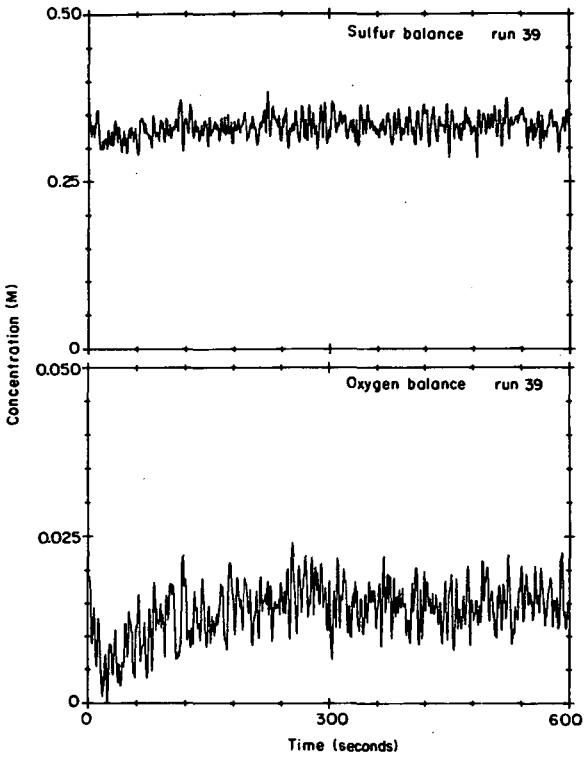

Figure 1. Upper curve—sum of the concentrations of sulfur-containing species in the reaction system *vs* time. Lower curve—sum of concentrations of oxygen-containing species in the reaction system *vs* time. (XBL 863-7579)

of the oxygen was consumed rapidly. By adjusting the height of the curve to flatten the oxygen and sulfur mass balance curves when added to them, the relative scattering efficiency for the intermediate can be estimated to be 0.5. It is listed in Table 1 as "X." The decay rate of the intermediate after its maximum agrees well with the formation rate of (SO_4^{2-} + HSO_4^-), as would be expected. The maximum concentration of the intermediate is reached approximately 10 to 30 seconds after the flow is stopped in the experiments.

PLANNED ACTIVITIES FOR FY 1986

The formation of the observed intermediate, either from the reactants or another intermediate, should show some dependence on reactant concentrations and trace amounts of metal ions. Because of the limited signal-to-noise ratio for the data we can obtain by stopped-flow techniques, it is difficult to calculate quantitative results for the decay of O_2 and HSO_3^- and the growth of the 1090 cm^{-1} intermediate on a short time scale. This is the information needed to deduce the oxygen and bisulfite ion dependence on the reaction rate and needed to observe the possible catalytic effects of metal ions. Also, doing mass balance measurements for sulfur and oxygen

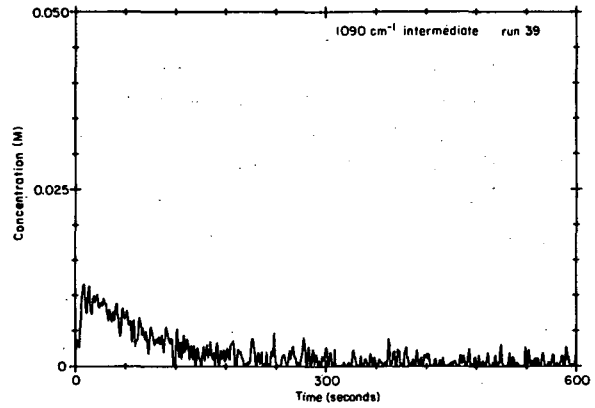

Figure 2. Plot of the 1090 cm^{-1} signal *vs* time. Concentration was calculated assuming one O_2 is equivalent to one intermediate molecule. (XBL 863-7580)

on a short time scale would indicate whether there is another intermediate coupling the reactants to the 1090 cm^{-1} intermediate.

This problem can be overcome by doing continuous flow experiments that would permit long-term observation of the reacting solution at a given time after mixing. The time delay between mixing and observation can be varied by changing the flow rate and the volume between the mixer and the observation cell. We plan to begin such experiments in the near future.

REFERENCES

1. Huss, A., Lim, P.K., and Eckert, C.A. (1982), "Oxidation of Aqueous Sulfur Dioxide. 1. Homogeneous Manganese (II) and Iron (II) Catalysis at Low pH," *J. Phys. Chem. 86*, p. 4224.
2. Huss, A., Lim, P.K., and Eckert, C.A. (1982), "Oxidation of Aqueous Sulfur Dioxide. 2. High-Pressure Studies and Proposed Reaction Mechanisms," *J. Phys. Chem. 86*, p. 4229.
3. Lim, P.K., Huss, A., and Eckert, C.A. (1982), "Oxidation of Aqueous Sulfur Dioxide. 3. The Effects of Chelating Agents and Phenolic Antioxidants," *J.Phys. Chem. 86*, p. 4233.
4. Huss, A. and Eckert, C.A. (1977), "Equilibria and Ion Activities of Sulfur Dioxide Solutions," *J. Phys. Chem. 81*, p. 2268.
5. Connick, R.E., Tam, T.M., and von Deuster, E. (1982), "Equilibrium Constant for the Dimerization of Bisulfite Ion to Form $S_2O_5^{2-}$," *Inorg. Chem. 21*, p. 103.
6. Rhee, J.S. and Dasgupta, P.K. (1985), "The Second Dissociation Constant of SO_2H_2O," *J. Phys. Chem. 89*, p. 1799.
7. *Lange's Handbook of Chemistry* (1973), John A. Dean, Ed., 11th edition, p. 10–5.

Asymmetry of the Inner Mitochondrial Membrane*

R.J. Mehlhorn, J. Maguire, J. Lang, and L. Packer

Mitochondria are often referred to as the "powerhouses" of aerobic cells, because they are the sites within the cells where oxidative metabolism converts foodstuffs to energy-rich adenosine triphosphate (ATP), which is the common currency for energy-consuming reactions in the cell. This project is seeking to determine how the asymmetric structure of the inner mitochondrial membrane is related to energy conversion of respiratory substrates to ion gradients and ATP synthesis. The release of free radical molecules from the membrane, a process that promotes oxidative damage and may contribute to mammalian aging, is also being studied. Our approach uses nitroxide spin probes to specifically probe aqueous and membrane domains, and the basic electron spin resonance (ESR) methodology is being validated in a variety of membrane systems. We have developed ESR procedures for specifically observing spin probes inside of cells and membrane vesicles, including treatment of cells or membrane vesicles with impermeable paramagnetic ion complexes to eradicate the ESR signal of probes in the external aqueous phase. Transmembrane concentrations gradients of hydrophobic ions sensitive to electrical potentials, or of weak acids and amines sensitive to pH gradients, are measured by comparing ESR signals prior and subsequent to treatment with the paramagnetic complexes and related to electrochemical gradients. The intracellular environment can also be studied selectively by the use of spin labeled pH-responsive groups or hydrophobic ions, which can be induced to accumulate inside cells or membrane vesicles by imposing electrochemical potentials. These studies of bioenergetics phenomena have thus enabled us to elaborate procedures for selectively probing internal and external environments of membrane enclosed domains. This has set the stage for studying free radical production and reactions in each of these environments. Irreversible loss of the nitroxide spectrum is related to reactions with biological free radicals. Supportive evidence for free radical formation is being sought with the complementary ESR technique of spin trapping, and this approach is applied to the detection of free radicals in several biological systems. We are also using low temperature electron paramagenetic resonance (EPR) to study the structure of purified mitochondrial electron transport complex II and the mechanism of its production of superoxide radicals.

*This work was supported by the National Institutes of Health (AG-04818) through the U.S. Department of Energy under Contract No. DE-AC03-76SF00098.

ACCOMPLISHMENTS DURING FY 1985

Free Radical Studies

ESR schemes for free radical detection: A procedure for detecting free radical species in biological environments has been described.[1] The method consists of monitoring the loss of ESR signal in a free radical-generating environment such as the respiring mitochondrial membrane and characterizing the reaction products, primarily by chromatographic methods. The significance of this assay is that it allows for the detection of free radical reactions within the membrane interior. We have noted that the lipid spin probes which are deeply imbedded in the mitochondrial membrane, e.g., the stearic acid nitroxides, suffer a very slow spin signal loss relative to aqueous spin probes unless free radical processes are inititated within the membrane and thus they are especially effective for the detection of free radical reactions in these domains. On the other hand, the occurrence of free radical processes in the aqueous mitochondrial regions is amenable to study with conventional nitrone spin traps, although the resulting adducts are so unstable that they do not accumulate significantly and therefore require high concentrations of spin trapping agents to elicit an ESR-detectable signal.

Review of the free radical theory of aging: We have reviewed the status of the free radical theory of aging.[2] The purpose of writing this review was twofold: (1) to compile the data which appear to support or contradict the theory and (2) to identify research directions that are most likely to make a significant impact on aging research. One specific objective in producing this review was to identify critical research areas that can benefit from our ESR approach for free radical detection. Although the free radical theory of aging was proposed several decades ago the involvement of radicals in the aging

process remains obscure. A diagram encompassing current understanding of free radical processes in mammals and indicating how such radicals might contribute to aging is shown in Fig. 1.

Considerable progress has been made in detecting oxygen free radicals in biological environments, and such radicals are now known to be generated during a variety of metabolic processes. The failure to achieve substantial lifespan extensions with antioxidants casts doubt on the validity of the theory as originally formulated. Further doubts about the theory arise from studies with cultured cell aging models, which fail to exhibit an expected sensitivity

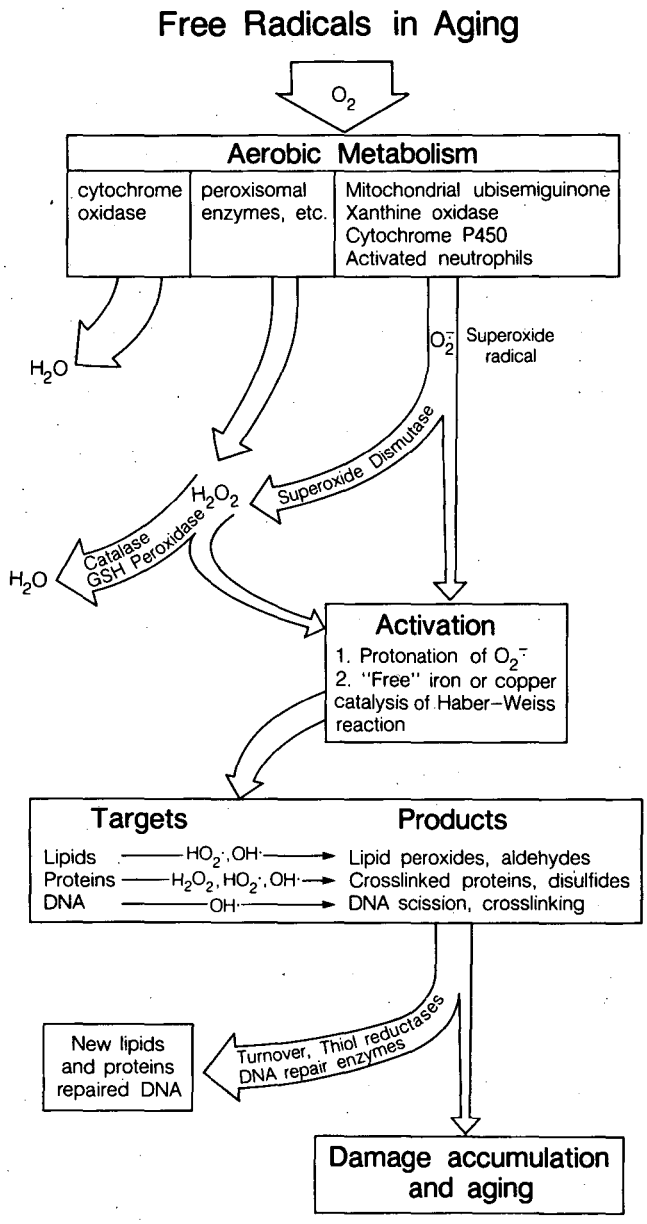

Figure 1. Scheme of free radical reactions in aerobic cells and how they contribute to aging. GSH refers to glutathione. (XBL 855-8893)

to the oxygen concentration in their growth environments. Only one nutritional manipulation, caloric restriction, is known to exert substantial life-extending effects; however its relationship to free radicals has not been resolved. Thus, present knowledge does not argue for a predominant role of free radicals in aging. However, compelling evidence exists for the involvement of free radicals in life-shortening diseases, including autoimmunity, cancer, atherosclerosis, and Parkinson's disease. Further studies of the effects of normally-occurring free radicals are warranted; quantitative data on damage associated with these species may reveal that previous analyses failed to identify critical cellular targets.

Free radical production during the metabolism of diethylstilbestrol: We have found that horseradish peroxidase or prostaglandin H synthase (PGS)-catalyzed oxidation of diethylstibestrol (DES) in the presence of the spin trap 5,5-dimethyl-1-pyrroline-N-oxide (DMPO) caused the generation of an ESR signal indicative of a free radical intermediate (a_N = 14.9 G, a_H = 18.3 G).[3,4] The identity of the trapped radical could not be identified on the basis of published hyperfine coupling constants but the observation that horseradish peroxidasecatalyzed oxidation of 1-naphthol produced an identical ESR signal suggests that the radical was either a phenoxy or phenoxy-derived radical. During horseradish peroxidase-catalyzed oxidation of diethylstilbestrol in the presence of glutathione the thiol reduced the diethylstibestrol radical to generate a thiyl radical, as shown by a thiol-dependent oxygen uptake during horseradish peroxidase-catalyzed oxidation of diethylstilbestrol and the observation of an ESR signal consistent with DMPO-glutathionyl radical adduct formation. A DES analog devoid of free hydroxyl groups, namely diethylstilbestrol dipropionate, did not produce an ESR signal above control levels during horseradish peroxidase-catalyzed metabolism in the presence of 5,5-dimethylpyrroline-N-oxide. We concluded that free radicals are formed during peroxidatic metabolism of diethylstilbestrol and must be considered as possible determinants of the genotoxic activity of this compound.

Metal and metalloid interactions with membranes: A review of how trace metals and metalloids in the environment may exert destructive biological effects has been written.[5] In part this work was motivated by a recognition that transition metal ions like copper and iron may play a critical role in promoting metabolically initiated free radical chains by participating in a Fenton reaction. The interaction of metal(loid)s with membranes can be particularly significant. To the extent that membranes prevent the entry of these species into cells, they will inhibit

damaging effects. However, many interactions with membranes can result in direct damage, or, more seriously, can lead to an amplification of toxicity. Direct damage can include structural alteration such as a disruption of vital lipid-protein associations or introduction of new surface charges. More substantial damage can occur when metals or metalloids act catalytically to impair membrane function, e.g., by providing ion conductance pathways or by promoting free radical reactions which may cause massive oxidation of membrane lipids. Recognition of factors involved in the interaction of metal(loid) compounds with membranes is useful for predicting toxic effects of such compounds in biological environments.

Studies of free radical generation and oxidative damage in mitochondria: We have discussed evidence, including data from our laboratory, that oxygen radicals derived from mitochondria play a major role in cellular damage.[6] In this paper we described detection schemes for mitochondrial radicals, which are being developed with ESR spin probe techniques, and which are designed to elucidate the pathways of oxidative damage. We also considered the activities of mitochondrial electron transport and isolated electron transport complexes in superoxide radical generation, transition metal catalysis of free radical formation and evidence for the formation of thiyl radicals, and their possible involvement in oxidative damage. We concluded with a comprehensive hypothesis for the production and fate of mitochondrial oxygen radicals.

Mutagenicity of nitroxide free radicals: We have found that stable nitroxides increase the number of revertants in the Salmonella typhimurium tester strain, TA 104.[7] (The Salmonella mutagenesis assay system is widely used for detecting potential carcinogens.) The observed mutagenicity was more pronounced with the piperidine nitroxide Tempol, than with the pyrrolidine nitroxide PCAOL. Mutagenicity was dramatically increased in the presence of a superoxide radical generating system, xanthine oxidase/hypoxanthine. The nitroxide mutagenicity was suppressed in TA 104 cells that contained the regulon against oxidative stress, OxyR, suggesting that the mutagenic effect is due to an oxidation mechanism that occurs frequently in aerobic cells. A plausible mechanism of mutagenesis was suggested to be the thiol oxidation product sulfenyl hydroperoxide. The enhancement of the nitroxide mutagenicity by exogenous xanthine oxidase appears to rule out a significant role for a direct attack of the nitroxide on DNA radicals in the mutagenic effect.

Superoxide production by an isolated mitochondrial electron transport complex: We have obtained data that purified mitochondrial electron transport complex II generates superoxide radicals in the absence of ubiquinone.[8] Although the rate of superoxide radical production is about 2% of the rate seen with the enzyme when the artificial dye phenazine methosulfate is used as an electron acceptor, our measurement of a finite rate contradicts earlier literature reports that this complex does not produce superoxide.

Bioenergetics Studies

ESR probe studies of transmembrane proton movements: Procedures for using nitroxide spin probes to kinetically study proton gradients have been described.[9] Membrane proton pumps, like bacteriorhodopsin, generate electrochemical potentials that can be measured with a combination of probes responsive to transmembrane electrical and pH gradients. We described how nitroxide spin probes are employed to study permeability of halobacterial envelope vesicle and erythrocyte membranes to spin labeled weakly polar molecules, ions, amines, and weak acids. Weakly polar spin probes with fewer than two hydrogen bonding residues permeate most membranes too rapidly to measure with available stop-flow ESR techniques (half-time for uptake less than 100 msec). One of these nitroxides, 4-oxo-2,2,6,6-tetramethyl piperidine-N-oxyl (TEMPONE), has been used to measure volume changes in many envelope and cell preparations and permeates at least one cell (the red cell) appreciably more rapidly than water does. The permeability of amine and carboxyl spin labels is also high when the probes are predominantly in their uncharged states. However, under typical physiological conditions where these species exist predominantly in their charged forms, the permeabilities of these probes may be imposing rate limitations on measurements of proton fluxes. This limitation can be overcome by working with nitroxides whose pK_a's are similar to those of the membrane suspensions under study. Hydrophobic spin-labeled cations with point but not delocalized charge centers enter halobacterial envelope vesicles in response to light-induced transmembrane electrical potentials. However, in no case that we have examined is the permeability of permanently charged cationic nitroxides fast enough to respond to electrical membrane energization phenomena in the subsecond time domain. Amphiphilic cationic spin probes, which are analogues of the widely-used cationic detergent cetyl-trimethyl ammonium bromide (CTAB), bind extensively to the halobacterial membrane yet do not partition into non-polar organic solvents, and thus would not be considered

to be hydrophobic ions. These amphiphiles exhibit significant rates of membrane permeation but do not accumulate in response to electrical potentials, suggesting that they diffuse across the membrane in conjunction with anions. We have emphasized that ion pairing may well occur with many other membrane-binding probes and must be controlled for accurate and meaningful measurements of proton gradients.

ESR studies of light-dependent volume changes in cell envelope vesicles from Halobacterium halobium: The measurement of volume changes can provide information about solute fluxes, including ionic currents, across biological membranes. This potential application of the ESR technique was developed in illuminated cell envelope vesicles from *H. halobium,* an experimental system that has proven to be a useful model system for perfecting several ESR assays of bioenergetics parameters.[10] We demonstrated light-driven swelling in vesicles containing halorhodopsin (a proposed inward-directed chloride pump) and shrinking in vesicles containing bacteriorhodopsin, (an outward-directed proton pump which functions in these vesicles in combination with a proton/sodium antiporter). Swelling of the halorhodopsin vesicles was not inhibited by uncouplers or by gramicidin, whereas shrinking of the bacteriorhodopsin vesicles was inhibited by these ionophores. Vesicles from a strain which contains both pigments, R1, showed relatively small volume changes with illumination. This study established procedures for using the ESR volume measurement technique for obtaining fundamental insights into mechanisms of ion pumping across energy-transducing membranes.

Surface potential measurements of mitochondrial membranes: Measurements of the surface potential of the inner mitochondrial membrane using electron paramagnetic probes have been described.[11] The first stage of this research consisted of characterizing the permeability of our nitroxide probes used for these measurements. It had been suggested by other workers that the Cat_n probes used for such studies were too permeable to be useful for surface potential work. We have found that the probes do indeed cross the inner mitochondrial membrane at an appreciable rate at room temperature, but that rapid mixing procedures can be used to overcome this difficulty. The problem of probe reduction and destruction was discussed, and kinetic analysis of the decrease of ESR signal intensity, inferred from double integration of the spectra, was used to correct for this phenomenon. Data were presented on the permeability of the mitochondrial membrane to cationic, amphiphilic spin probes designated Cat_n. The uptake of these probes was compared to that of a freely permeable phosphonium ion probe. The repartitioning of the Cat_n probes upon energization of mitochondria with ATP was interpreted in terms of a decrease of about 15 millivolts in the surface potential of the inner mitochondrial membrane upon energization. Conflicting interpretations of spin probe data about mitochondrial surface potentials in the literature were also reviewed, and misinterpretations of data were identified.

PLANNED ACTIVITIES FOR FY 1986

Evidence will be sought for the hypothesis that biological oxidative damage associated with normal aerobic metabolism is due primarily to mitochondrial superoxide free radicals in a process that involves thiols and transition metal ions. This hypothesis provides an explanation for the marginal effects of antioxidants in retarding aging rates, without discarding the primary concept of the "free radical theory of aging," i.e., that metabolically generated free radicals cause aging. To test the postulate that mitochondrial superoxide plays a predominant role in cell damage, superoxide production of several subcellular fractions will be compared. Mitochondrial superoxide production will be quantitated within and outside of the mitochondria, thus defining the effect of the asymmetric structure of the membrane on superoxide production. Data on the membrane sidedness of superoxide release and on non-mitochondrial sources will provide valuable data about the relative contributions of the extramitochondrial and intramitochondrial compartments to the total cellular superoxide burden. Lipid peroxidation will be compared with thiol oxidation to estimate how these two potentially major targets of superoxide radicals are affected by superoxide released from mitochondria. Electron spin resonance tools for the detection and characterization of free radical species will play an integral part in the studies; they will be supported by HPLC analyses of oxidation products, including thiol and lipid derivatives. The animal model will consist of controlled age groups of Fischer 344 rats.

REFERENCES AND BIBLIOGRAPHY

1. Mehlhorn, R.J. and Packer, L. (1984), "ESR Spin Destruction Methods for Radical Detection," *Methods Enzymol. 105*, p. 215.
2. Mehlhorn, R.J. and Cole, G. (1985), "The Free Radical Theory of Aging: A Critical Review," *Adv. Free Radical Biology & Medicine 1,* p. 165.
3. Ross, D., Mehlhorn, R.J., Moldeus, P., and Smith, M. (1986), "Metabolism of Diethylstilbestrol by Horseradish Peroxidase and Prostaglandin Synthase: Generation of Free Radicals

and Their Interaction with Glutathione," *J. Biol. Chem. 260,* p. 16210.

4. Ross, D., Mehlhorn, R.J., Moldeus, P., and Smith, M.T. (1986), "Metabolism of Diethylstilbestrol by Horseradish Peroxidase and Prostaglandin Synthase Evidence for a Free Radical Intermediate," in *Proceedings of the 3rd International Symposium on Biological Reactive Intermediates,* R. Snyder, Ed, Plenum Press, in press.
5. Mehlhorn, R.J. (1986), "The Interaction of Metals and Metalloids with Biomembranes," to be published as a Dahlem Workshop Book, Springer Verlag, in press.
6. Mehlhorn, R.J., Maguire, J.J., Hartzog, G., and Packer, L. (1986), "Oxygen Radicals and Cancer: Free Radical Generation and Oxidative Damage in Mitochondria," in *Biomembranes in Cancer Cells,* T. Galeotti, A. Cittadini, G. Neri, and S. Papa, Eds, Elsevier Science, Amsterdam, p. 223.
7. Sies, H. and Mehlhorn, R.J. (1986), "Mutagenicity of Nitroxide Free Radicals," submitted to *Arch. Biochem. Biophys.*
8. Maguire, J.J., Mehlhorn, R.J., Akrell, B.A.C., and Packer, L. (1986), "Superoxide Production by Mitochondrial Complex II," submitted to *Arch. Biochem. Biophys.*
9. Mehlhorn, R.J., *et al.* (1986), "Measurement of Transmembrane Proton Movements with Nitroxide Spin Probes," *Methods Enzymol.,* in press.
10. Mehlhorn, R.J., Schobert, B. Packer, L., and Lanyi, J. (1985), "ESR Studies of Light-Dependent Volume Changes in Cell Envelope Vesicles from Halobacterium Halobium," *Biochim. Biophys. Acta. 809,* p. 66.
11. Hartzog, G., Mehlhorn, R.J., and Packer, L. (1986), "A Reevaluation of Mitochondrial Surface Potentials," in *Ion Interactions in Energy Transport Systems,* S. Papa, G. Papageorgiou, and J. Barker, Eds, Plenum Press, in press.

Ackrell, B.A.C., Maguire, J.J., Dallman, P., and Kearney, E.B. (1984), "Effect of Iron Deficiency on Succinate and NADH-Ubiquinone Oxidoreductases in Skeletal Muscle Mitochondria," *J. Biol. Chem. 259,* p. 10053

Ackrell, B.A.C., Cochran, B., Larson, K., Maguire, J.J., and Kearney, E.B. (1985), "Lack of Assembly of Succinate and NADH-Ubiquinone Oxidoreductases in Iron-Deficient Rat Skeletal Muscle Mitochondria," in *Flavins and Flavoproteins,* R.C. Bray, P.C. Engel, and S.G. Mayhew, Eds, Walter de Gruyter, Berlin, N.Y., in press.

Ball, M.C., Mehlhorn, R.J., Terry, N., and Packer, L., (1985), "Electron Spin Resonance Studies of Ionic Permeability Properties of Thylakoid Membranes of Beta Vulgaris and Avicennia Germinans," *Plant Physiol. 78,* p. 1.

Hederstedt, L., Maguire, J.J., Waring, A.J., and Ohnishi, A.J. (1985), "Characterization by EPR and Studies on Subunit Location and Assembly of the Iron-Sulfur Clusters of Bacillus Subtilis Succinate Dehydrogenase," *J. Biol. Chem. 260,* p. 5554.

Lomax, T.L. and Mehlhorn, R.J. (1986), "Determination of Plant Membrane Vesicle Volume and pH Gradient Using Electron Spin Resonance Spectroscopy," *Biochim. Biophys. Acta. 821,* p. 106.

Lomax, T.L., Mehlhorn, R.J., and Briggs, W.R. (1985), "Quantitation of [^{14}C] IAA Uptake by Plant Membrane Vesicles Using ESR Volume and ΔpH Determinations," *Proc. Natl. Acad. Sci. USA. 82,* p. 6541.

Maguire, J.J., *et al.* (1986), "Electron Paramagnetic Resonance Studies of Succinate Dehydrogenase II. Evidence for Detection of the Tetranuclear Cluster S-2 in Succinate Ubiquinone Reductase and Reconstitutively Active Enzyme," *J. Biol. Chem. 260,* p. 10909.

Melandri B.A., Mehlhorn, R.J., and Packer, L. (1984), "Light-Induced Proton Gradients and Internal Volumes in Chromatophores of Rhodospeudomonas Sphaeroides," *Arch. Biochem. Biophys. 235,* p. 95.

Packer, L. and Mehlorn, R.J. (1986), "Modification and Spin Labeling Studies of Membrane Bioenergetics," in *Recent Advances in Biological Membrane Studies: Structure and Biogenesis, Oxidations and Energetics,* L. Packer. Ed, in press.

Poole, R.J., Mehlorn, R.J., and Packer, L. (1985), "A Study of Transport in Tonoplast Vesicles Using Spin-Labelled Probes," in *Biochemistry and Function of Vacuolar Adenosine-Triphosphatase in Fungi and Plants,* B.P. Martin, Ed, p. 114.

Impacts of Large Extraterrestrial Bodies and Mass Extinctions*

F. Asaro, Helen V. Michel, W. Alvarez, and L.W. Alvarez

Studies of the extinction of species and the ages of craters in the last 250 million years (MY) have suggested they each have a periodicity of 26–28 MY. Extraterrestrial causes have been hypothesized for these effects, and the best developed theory suggests that a companion star to our Sun, nicknamed Nemesis, orbits the Sun with the same period. Other hypotheses of the source of the perturbation of the comet cloud are a planet X orbiting the Sun and the periodic movement of the solar system through the Galactic center. At the time of Nemesis' closest approach, comets from the outer fringes of the solar system are injected into the inner part and a small number of these can impact on the Earth. The more energetic impacts would raise a huge dust cloud that contained the vaporized comet debris. This cloud would be distributed all around the Earth and settle in a few months. Evidence for the impacts would appear world wide as single or multiple Ir and other geochemical anomalies and be repeated about every 26–28 MY. Such evidence for single impacts has been amply demonstrated for the 66 MY old Cretaceous-Tertiary boundary,[1] and to a lesser extent for the 39 MY old horizon in the terminal Eocene.[2] One exciting ramification is that multiple impacts during a comet shower could produce what appear to be gradual (10^5) year extinctions.

The purpose of this project is test the validity of the Nemesis and other models for the periodic extinctions of species by a detailed stratigraphic study for iridium and other geochemical or mineralogical anomalies in rock strata associated with minor and mass extinctions. To accomplish these studies it is necessary to test many thousands of samples, and previous techniques are inadequate.

*This work was supported by the Director, Office of Energy Research, Office of Basic Energy Sciences, Engineering and Geosciences Division of the U.S. Department of Energy under Contract No. DE-AC03-76SF00098 and the National Aeronautics and Space Administration Ames Research Center under Contract No. A-71683B. Support was also received from the Murdock Charitable Trust.

As a byproduct of this effort we would also determine the usefulness of Ir and other geochemical anomalies (associated with bolide impacts) as time markers by finding: a) What mineral phases or fossil forms are likely to contain the above anomalies in marine and non-marine environments, b) How far and in what direction are the above anomalies likely to migrate from the position of initial deposition (and thus influence the validity of a geochemical anomaly horizon as a high-precision worldwide time marker), and c) How likely are the above anomalies to disappear from the sedimentary record.

As another byproduct we would attempt to determine and demonstrate the usefulness of each geochemical anomaly horizon as a worldwide time marker.

ACCOMPLISHMENTS DURING FY 1985

An Iridium Coincidence Spectrometer, which can measure by neutron activation analysis (without any chemical separation) iridium contents of rocks 500 times faster than was previously possible without labor-intensive chemical separations, has been built and tested. It is 100 times faster than analyses previously made by us at LBL which involved high volume carrier-free radiochemical separations, and it is 10 to 100 times cheaper to operate than the cost of analyses elsewhere which necessitates rather complete radiochemical separations of iridium.

The spectrometer is very reliable in that interference corrections from irradiated elements other than iridium are nearly negligible. Also the possibility of contamination due to the use of iridium carrier in chemical separations is eliminated.

To register an iridium event, the spectrometer requires that two nuclear gamma-rays characteristic of the isotope ^{192}Ir be detected nearly simultaneously (i.e., in coincidence) in two Ge solid state crystals. Two other isotopes, ^{46}Sc and ^{60}Co, each have two high energy gamma rays in coincidence, which can scatter out of the Ge crystals and leave residues of energy which would appear to be coincident gamma-rays of ^{192}Ir. Two large tanks of mineral-oil-based scintillator completely surround the germanium detectors, detect the scattered radiations, and veto nearly all of the unwanted coincidences seen by the germanium. The resulting background from irradiated rock samples which count 40,000

counts per second in each germanium detector is only 2–3 coincidences per hour. Although this background is usually not significant, it is always measured and considered.

The sensitivity of the spectrometer at the 95% confidence level for rock samples of the type we normally expect to measure is 50 parts-per-trillion of iridium in a 7 min count. This performance is possible through the cooperation of the staff of the University of Missouri Research Reactor Facility in Columbia, Missouri.

About 5000 samples have been collected for a detailed search for geochemical anomalies related to impacts with particular emphasis on rocks 90–95 MY old from the Italian Apennine mountains and the Western interior United States. This level has many extinctions and corresponds to the next older extinction horizon (in the predicted ~27 MY cycle) before the 39 and 66 MY old horizons where worldwide iridium anomalies have already been detected.

The iridium anomaly in ~39 MY old rock strata has now been seen in a deep sea core taken from near New Zealand. This is the most southerly region that this anomaly has been seen, and it confirms its worldwide distribution.

PLANNED ACTIVITIES FOR FY 1986

Detailed studies will be made of the 250 MY old Permian-Triassic boundary in China[3] in collaboration with Chinese scientists. Studies of this boundary in India will be made with Canadian scientists. This boundary is of particular interest because the largest mass extinction known in the geological record took place in that time region. Eighty to ninety percent of the good rock sections from that time are in China with a few others in Russia, Iran, and India.

Detailed studies of the fine structure of iridium anomalies at extinction horizons will be made to determine if there are indications of clustering of comet impacts on the Earth.

REFERENCES

1. Michel, H.V., Asaro, F., Alvarez, W., and Alvarez, L.W. (1985), "Elemental Profile of Iridium and Other Elements Near the Cretaceous-Tertiary Boundary in Hole 577B," Deep Sea Drilling Project Initial Report DSDP Vol. 86, p. 533.
2. Alvarez, W., Asaro, F., Michel, H.V., and Alvarez, W. (1982), "Iridium Anomaly Approximately Synchronous with Terminal Eocene Extinctions," *Science 216*, p. 8.
3. Asaro, F., *et al.* (1985), "Geochemical Study of the Permian-Triassic Boundary in the Meishan, Tangshan and Watchapo Mountain Sections in the People's Republic of China," in Abstracts with Program, Conference on Rare Events in Geology, Gwatt, Switzerland, May 20–22, 1985.

Studies of Source of Lithic Artifacts and Trade Routes by Elemental Analysis*

F.H. Stross, F. Asaro, and H.V. Michel

X-ray fluorescence analyses (XRF) and neutron activation analyses (NAA) were used in studies to determine patterns of distribution of artifacts made from obsidian. The studies were carried out in collaboration with the academic institutions who funded the projects.

*This work was supported by the University of Texas, San Antonio, and the University of Colorado, Boulder, and by the U.S. Department of Energy under Contract No. DE-AC03-76SF00098.

ACCOMPLISHMENTS DURING FY 1985

Wild Cane Cay Project

This project was carried out in collaboration with Heather McKillop from the University of California at Santa Barbara and was jointly funded by the Social Sciences and Humanities Research Council of Canada and U.C., Santa Barbara, with Ms. McKillop as the principal investigator. It is to study the role of coastal areas in the development of prehistoric, complex societies. Specifically, Wild Cane Cay, an island off the mouth of the Deep River in southern Belize, was chosen for study as an example of coastal commerce in Maya territory during Classic and Postclassic periods (ca 4th century A.D. to the Conquest).

One hundred obsidian artifacts were studied. They were mostly scrapers or knives, including

bifaces and stemmed blades, and also cores (residual rock from the manufacture of blades from boulders).

Preliminary analysis of the artifacts by XRF indicated that 78 specimens came from deposits related to the volcano Ixtepeque; 17 specimens matched the important El Chayal source, farther to the west-(northwest), and one specimen matched the "representative Rio Pixcaya" composition, a large deposit yet farther west. All these sources are located in the highlands of Guatemala, southwest of Wild Cane Cay. Three specimens came from one source of unknown location, which was designated "Source Z." One specimen was unassigned. The four specimens last mentioned bear a general resemblance to Guatemala Highland obsidian patterns, but do not closely match any of those known to us. The results are presented in Table 1. All of the source assignments are considered to be tentative until they are confirmed by NAA on selected samples.

It is of interest that an earlier study,[1] made in collaboration with Professor N. Hammond (Rutgers University), involved 23 obsidian artifacts from Wild Cane Cay, of which 19 came from Ixtepeque and four from El Chayal, a proportion very similar to that found for the present, larger sampling by McKillop.

Belize River Trade Project

This study of artifacts from Belize (formerly British Honduras in Central America) has been carried out in collaboration with Dr. Anabel Ford from the University of California, Santa Barbara. Procurement sources for obsidian artifacts found in the inhabited Peten area, dating from the first millenium A.D., during the period of Mayan florescence shifted from the western to the eastern obsidian sources in the Guatemala Highlands. The habitations were

Table 1. Preliminary XRF Results on Wild Cane Cay Obsidian Samples (McKillop, *et al.*, unpublished data) Site 32/179-1.

No. of Samples	Ba (ppm)[a]	Zr (ppm)[b]	Rb/Zr	Sr/Zr
		Matching Ixtepeque Source		
78	1034 ± 46	176 ± 7	.58 ± .02	.90 ± .02
Reference[b]	1030 ± 27	175 ± 2	.57 ± .01	.90 ± .02
		Matching El Chayal Source		
17	923 ± 48	119 ± 4	1.30 ± .07	1.31 ± .03
Reference[b]	915 ± 24	117 ± 3	1.24 ± .04	1.29 ± .04
		Matching Rio Pixcaya Source		
1	1010 ± 22	117 ± 1	.96 ± .01	1.65 ± .01
Reference[b]	1105 ± 32	115 ± 3	1.01 ± .05	1.65 ± .06
		Unknown Source Z		
3	909 ± 52	99 ± 3	1.62 ± .05	1.49 ± .02
		Unassigned Artifact (Sample 8143-Y)		
1	966 ± 30	139 ± 4	1.37 ± .06	1.47 ± .06

[a]Errors are root-mean-square deviations for groups and estimated counting errors for single samples.

[b]Reference source data are from Asaro, *et al.*, *Am. Antiquity 43*, 436 (1978); Stross *et al.*, *Am. Antiquity 48*, 323 (1983); and Asaro, *et al.*, unpublished data.

directly or indirectly connected with the important center of Tikal, centrally located in the vast jungle area of the Peten, and the changes in obsidian procurement are of significance because they presumably reflect political events such as changes in the power structures, trade monopolies, military actions, and migrations. A manuscript was prepared for publication.

Other studies of the Belize River region (Colha, Pulltrouser Swamp, Cerros) carried out in collaboration with Professor Tom Hester of the University of Texas of San Antonio have also shown that most of the obsidian originated from the Guatemalan Highlands. These studies in Belize are significantly changing certain aspects of Mayan history, both in very early times (before the beginning of the Christian era) and in the post-classic (after the tenth century A.D.) to and including the Conquest.

PLANNED ACTIVITIES FOR FY 1986

Belize River Trade Project

Several continuing studies are concerned with the movement of obsidian raw material and artifacts between the Peten area—specifically the centers of Tikal and Yaxha—and Moho Cay, a small island at the mouth of the Belize River, which apparently was used as a trans-shipment point between coastal and inland trade for a long time. The Belize River itself was used in the shipment as far inland as it was navigable or convenient, probably to a point near the present-day Benque Viejo (site of Xunantunich) at the Guatemala-Belize border; the goods were then carried overland to or from points west in the Peten.

The area of the presumed portage point, including the site of el Pilar, has been excavated by BRASS (the Belize River Archaeological Settlement Survey, organized by the University of California, Santa Barbara), and a relatively high density of obsidian artifacts has been observed here. Analysis of these artifacts leading to the determination of the sources of obsidian, coupled with dating of the strata in which they were found, is expected to shed light on the important features of trade in that region.

Colossi of Memnon Project

Analytical studies of the Colossi of Memnon, well-known quartzite monuments located in the Plain of Thebes in Upper Egypt, have revealed[2] that the Roman reconstruction of the northern statue, and consequently the prior damage to the monument, had been far more extensive than hitherto supposed and included the entire rear portion of the pedestal of the statue. Speculation on how the damage had been brought about included the setting of great fires around the monuments, to spall and weaken the stone.

The technique of thermoluminescence (TL) is capable of measuring the length of time elapsed since certain materials, including clay and quartzite, were last subjected to temperatures exceeding ca 500°C. It has been possible to engage the collaboration of a team of French scholars expert in the application of TL to quartzite (including Professor M. Schvoerer, pioneer in this technique) for performing some measurements on Colossi samples available to us. By this study it may be possible to determine if great fires were indeed set around the Colossi in historic times. This would provide information on how, and possibly by whom, the defacement observed today (and already in Roman times) had been brought about, and thus reveal some highly relevant background relating to hitherto unknown history involving these monuments.

REFERENCES

1. Stross, F.H., *et al.* (1978), "Mayan Obsidian: Source Correlation for Southern Belize Artifacts," *Archaeometry 20*(1), p. 89.
2. Bowman, H., *et al.* (1984), "The Northern Colossus of Memnon: New Slants," *Archaeometry 26*(2), p. 218.

ENERGY ANALYSIS PROGRAM

INTRODUCTION

The Energy Analysis Program is engaged in interdisciplinary activities in which analysts from different fields work together on issues of national significance. The Program's emphases on economics, public policy, and behavioral science distinguish it from other LBL activities. At the same time, however, engineering and technical analyses underlie its economic and policy studies, a foundation that distinguishes its work from that of most other analysis groups working on public policy issues. Virtually all of the Program's research and analysis is quantitative, and much of the research staff is engaged in developing and applying mathematical models.

At present, the work of the Energy Analysis Program emphasizes the study of energy use in buildings. This subject has been stressed for a number of reasons; one of the most important is the strong research effort within the Applied Science Division on energy conservation in buildings (especially the Energy Efficient Buildings and Solar Energy programs). The Energy Analysis Program provides a rigorous and extensive analytical and economic capability that complements the more technical pursuits of other groups in the Division involved in building energy research. The Program will continue to emphasize analysis of energy use and efficiency in buildings, and it is also applying techniques to other important national and international energy and resource policy issues.

The work of the program during fiscal year 1985 can be divided into the following groups of projects:

(1) Engineering and technical residential energy studies, including simulation studies and analysis of results of program survey data.

(2) Economic modeling, including studies of regulatory policies to reduce energy use of appliances and of heating and cooling equipment; studies of market behavior; development of models to valuate hourly and peak effects of conservation programs for residences; residential energy demand forecasting; analysis of the effects of energy conservation programs on electric and gas utilities; and analysis of governmental policies on transferring natural resources to the private sector for development.

(3) International studies of the structure and determinants of energy demand in developed and less developed countries.

The projects described in the following pages provide a solid start to a systematic analysis of the issues studied. Most of them will continue to expand and evolve. They can be expected to deepen our understanding of energy use and energy conservation in buildings. In addition, the Program is striving to expand its work to encompass other key energy and resource policy issues. In particular, international energy issues, critical energy price and supply questions, key resource and environmental issues, conservation program evaluations, and electric utility analyses are likely to constitute some of the new initiatives of the Program over the next few years.

Simplified Calculations of Energy Use in Residences*

R. Ritschard, Y. Huang, and J. Bull

Over the past five years, the Energy Analysis Program has compiled a comprehensive residential database using the DOE-2.1 computer program for five single-family prototypes (one-story, two-story, split-level, and end-unit and mid-unit townhouses), and two multi-family building types (end-unit and mid-unit apartments) with three foundation conditions (slab-on-grade, unheated basement, and ventilated crawl space) in 45 U.S. climates.

For each prototype building, foundation type, and location, we did a parametric set of 18 to 20 simulations to evaluate the energy impacts of typical conservation measures, such as ceiling, wall and foundation insulation, different window glazings and areas, and varying infiltration rates. The complete database consists of both base case parametric simulations and an equal number of DOE-2 runs for sensitivity analyses of optional measures including added south windows, reflective and heat-absorbing glazings, thermal mass, night insulation, whole-house fans, attached sunspaces, and night temperature setbacks. We used the single-family portion of this database to develop the DOE-sponsored energy slide rules and PEAR, a microcomputer version of the database.[1,2]

This article, which summarizes a more detailed LBL report,[3] describes simplified methods for estimating energy use in typical houses. In particular, we explain the *delta (Δ) load* format developed for the residential slide rules, and a more refined *component load* approach that has been incorporated into the PEAR microcomputer program.

*This work was supported by the Assistant Secretary for Conservation and Renewable Energy, Office of Buildings and Community Systems, Building Systems Division (Architectural and Engineering Systems Branch) of the U.S. Department of Energy under Contract No. DE-AC03-76SF00098.

ACCOMPLISHMENTS DURING FY 1985

Determination of Δ Loads

The DOE-2 database provides annual heating and cooling loads for selected packages of conservation measures in a prototype house for any of the 45 climate locations. We define Δ loads as the change in loads due to the addition of conservation measures. We have calculated them by comparing simulations in the database differing by only a single measure. We derive cumulative Δ loads for each component, e.g., ceilings or walls, by summing individual Δ loads for the same component. These cumulative Δ loads are actually composite values that assume all building components are being tightened simultaneously. For example, the Δ load for R-0 to R-38 ceiling is the sum of the Δ load from R-0 to R-19 ceiling on an uninsulated house, plus the Δ load from R-19 to R-38 ceilings on a moderately insulated house. For typical conservation packages, this procedure produces the most accurate Δ loads and minimizes interactions between different building components.

The Δ load approach is a convenient and easy to understand format for presenting the data. For each prototype and location, we have transformed the database into a series of Δ loads spanning the conservation measure simulated. For the energy slide rules, we show the Δ loads as linear distances on a series of tabs (see Fig. 1). By aligning the tabs, the user can calculate the total building load for any combination of measures by subtracting in analog fashion the Δ loads from a worst case base house. The Δ loads format gives an accurate representation of the database, but lacks flexibility for extending that data to building geometries and component characteristics different from those assumed in generating the database. Therefore, we analyzed this data further using linear regression procedures to establish the relationship between key building characteristics and component loads.

Determination of Component Loads

The Δ loads and base loads described above are prototype specific. They ignore changing surface-to-

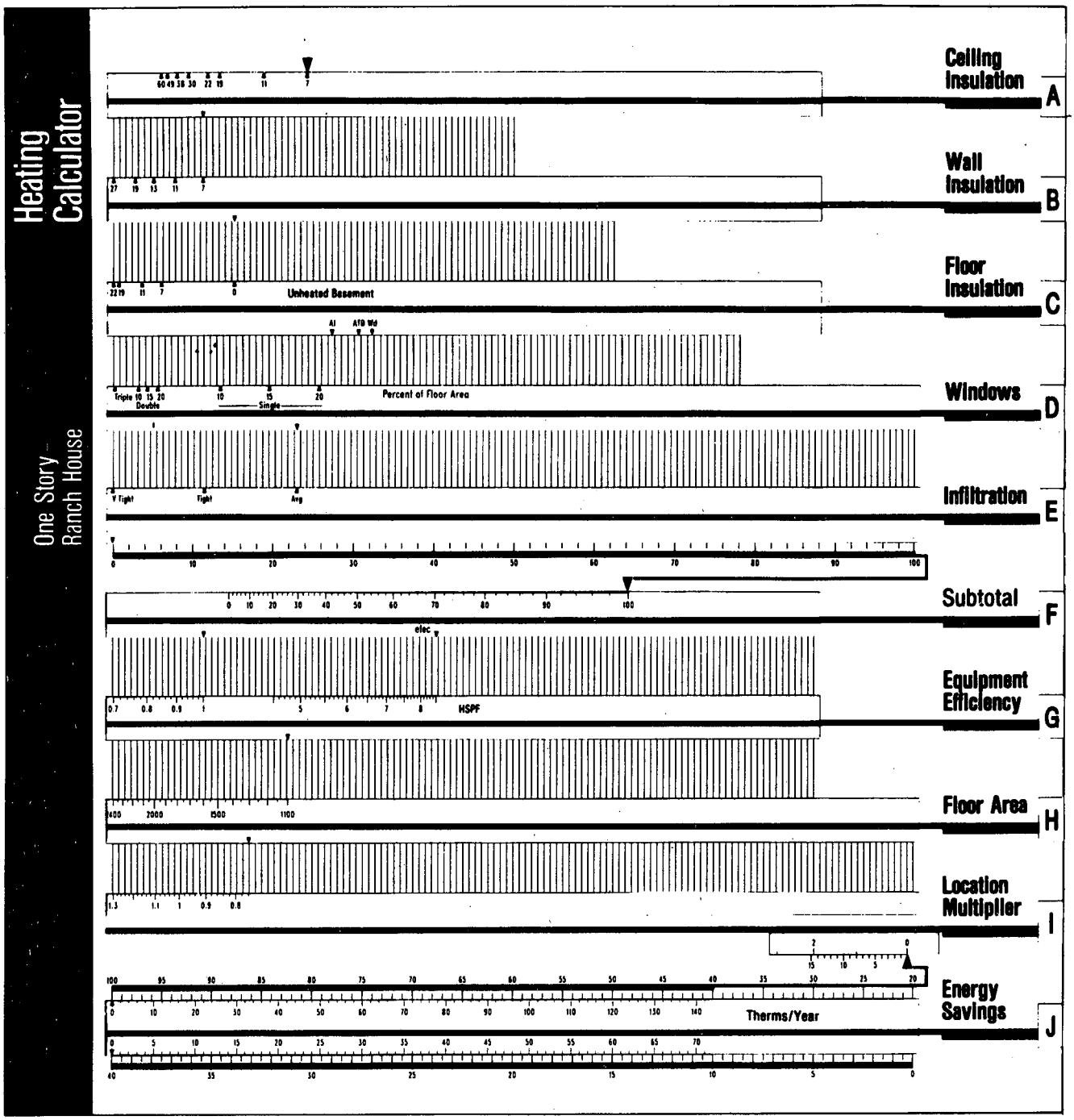

Figure 1. Heating calculator for one-story ranch house. (XBL 8312-2463)

volume ratios for varying sizes within one building prototype. This may, in turn, cause significant errors in estimating the Δ loads for houses where the ratios of wall-to-roof, window-to-wall, etc. differ significantly from those of the prototype house, leading to serious difficulties when the data are used for assessing tradeoffs between conservation options in homes differing substantially from the prototype.

To increase the flexibility of the database in handling different measures and prototypical designs, we developed the concept of component loads. We define *component loads* as the net annual contribution of each building component to the heating or cooling loads of the building. We have calculated them from regressions correlating the Δ loads to key physical parameters terms associated with the various building components. For insulation measures, we have regressed them against either ceiling or wall conductivity or total foundation conductance (as Btu/hr·ft^2·°F). For infiltration, we have regressed against air changes per hour; and for windows, against window area. As an example, Figures 2a and b show the relationship between heating or cooling Δ loads and ceiling conductance for a one-story ranch house in Washington, D.C.

Where the regression line meets the y-axis (y-intercept) the component loads can be assumed to be zero (i.e., zero conductance for the ceiling, etc.). We base the component loads for the simulated measures on the magnitude of difference (i.e., Δ loads) from the y-intercept (indicated on the right-hand scale of Figs. 2a and 2b). To facilitate scaling, we have normalized the component loads either per square foot (for ceiling, walls, and windows), per perimeter foot (for foundations), or per cubic foot (for infiltration). Since component loads correspond to the net loads for each component, they can be scaled by the actual amounts of ceiling, foundation, window, etc., thus making the database relatively prototype-free. The functional form of the regression equations also makes it easy to interpolate component loads for intermediate building design conditions using either adjacent component loads or general regression equations to describe the entire range.

There are two additional terms used in the component loads calculations, the *residual load* and the

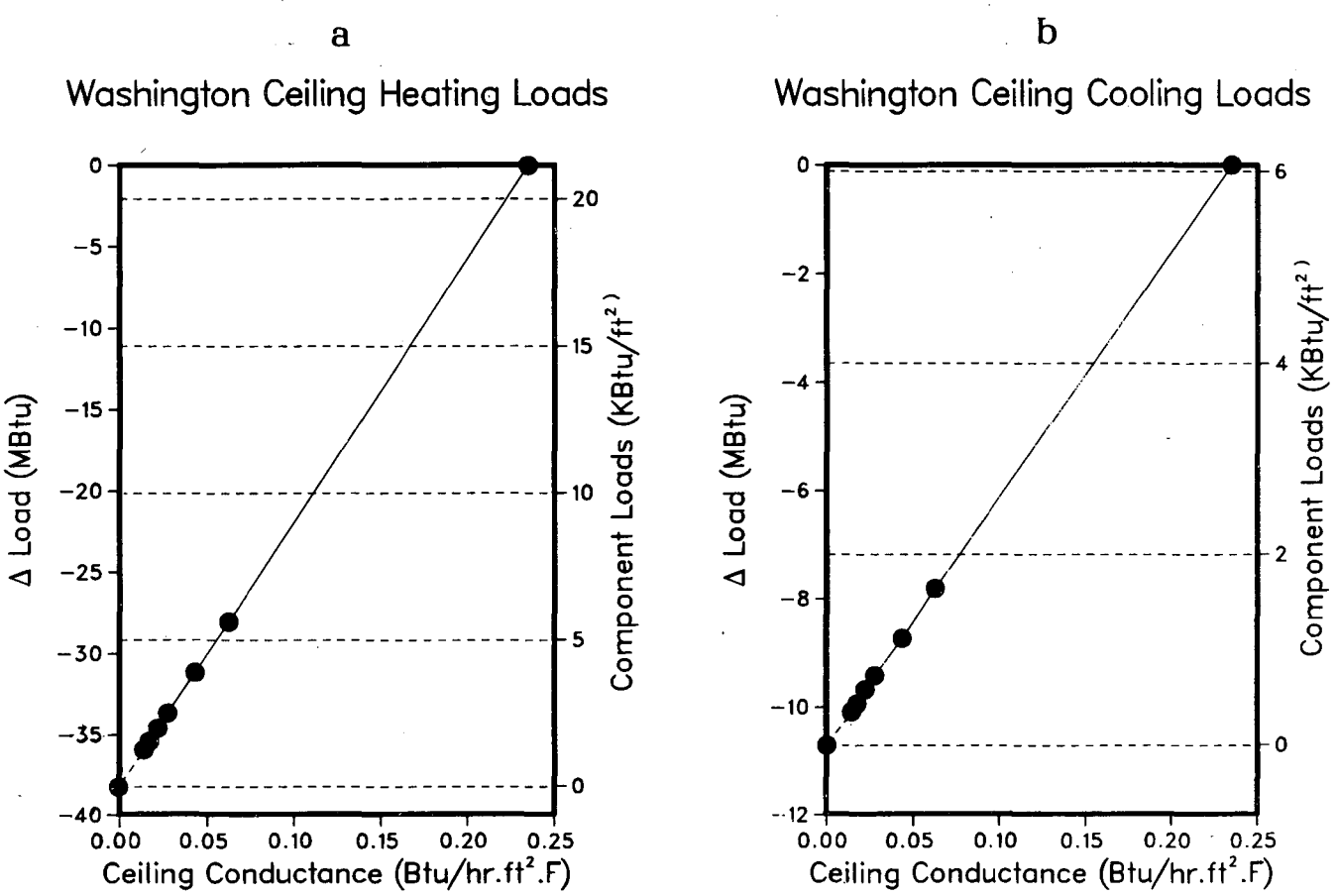

Figure 2. Ceiling heating (a) and cooling (b) loads in Washington, D.C. (XBL 8512-5192)

floor area adjustment. The residual load is the difference between the sum of the component loads and the total loads from the actual DOE-2 database. It represents the net effect of internal loads and interactions ignored in the component-by-component regression analysis. Since we held internal loads constant for each of the database simulations, we did not do component regressions for them. The predominant influence of internal loads on the residuals is evident in that they are always negative for heating and positive for cooling loads. The floor area adjustment is a secondary correction based on DOE-2 sensitivity analysis for each prototype with varying house sizes while keeping the aspect ratios and ceiling heights constant. Using the component loads approach, we develop a set of regression equations to calculate different floor areas (between 1000 ft^2 and 3000 ft^2) for the various building prototypes.

The component loads calculation requires a series of simple calculations that are too complex to incorporate into a mechanical slide rule, but are ideally suited for the microcomputer. We have incorporated this format into PEAR.[2] The component loads approach allows PEAR to adjust for different roof areas, wall areas and heights, perimeter lengths, and window areas to the point where the geometries of the original prototypes are of only incidental concern. At the same time, the regression equations allow PEAR to interpolate for intermediate component conditions.

Conclusions

The residential energy database developed in support of several DOE-sponsored programs provides benchmark numbers for determining the energy savings potential of typical conservation measures. Although databases are inherently less flexible than actual simulation programs, we describe a procedure to extend the database with good accuracy to the range of parametric options and designs found in typical houses. The procedure, which is based on the relationship between building component loads and key physical parameters, results in a set of regression equations that allow us to extend the simulation results to buildings with different geometries, conservation measures, and physical characteristics from those of the base case building prototype.

The results of our regression analysis also make it possible to compress the size of the data set, and to use it in novel ways. For example, if the relationship between the component loads and conductivities is known, it is easy to calculate the exact R-value necessary to achieve a certain reduction in load. We believe that the component loads approach, using simple linear regression equations, provides a accurate estimation of energy savings for typical residential conservation measures. The regression equations, which can be used in microcomputer programs like PEAR, extend the flexibility of the base case data. Results generated by such an approach lend themselves well to setting thermal performance levels for residential energy guidelines or building standards.

PLANNED ACTIVITIES DURING FY 1986

In FY 1986, we plan to extend the component loads approach in the following ways:

1. Investigate the relationships between total, component, and Δ loads for the 45 climate regions and building-related climate parameters, such as degree-days, latent enthalpy hours, heating and cooling insulation hours, etc. When we find reliable climate determinants, we can reduce the 45 geographical sets of data and develop extrapolation procedures to extend the data to other locations.
2. Identify the relationship between component loads for different prototype buildings, e.g., one-story versus two-story, detached versus attached, and single-family versus multi-family. Secondary terms may be added so that a single database can include all typical residential house types. This work includes additional analysis on the effects of internal loads, shading, and different surface-to-volume ratios on various component loads.
3. Expand and modify, if necessary, the simplified calculation procedure for heavy mass construction and for superinsulated houses.
4. Evaluate the relationship of window conductance, window sash, transmission, emissivity, and shading coefficients to window component loads. This analysis requires expanding the existing database to cover the parameters mentioned. The goal of this effort is a simplified calculation method that will allow users to choose any combination of window characteristics and shading assumptions.

REFERENCES

1. Huang, Y.J., *et al.* (1985), *Methodology and Assumptions for the Evaluation of Heating and Cooling Energy Requirements in New Single-Family Residential Buildings,* LBL-16342.

2. Ritschard, *et al.* (1985), *PEAR: A Microcomputer Program for Residential Energy Analysis,* LBL-20355.

3. Huang, Y.J., Ritschard, R., and Bull, J. (1985), *Simplified Calculations of Energy Use in Residences Using a Large DOE-2 Database,* LBL-20107.

Survey of Low-Rise Multi-Family Building Practices*

P. Albrand, I. Turiel, R. Ritschard, and D. Wilson

The Building Energy Analysis Group at Lawrence Berkeley Laboratory (LBL) has been studying energy use in new low-rise multi-family buildings. The major objectives of this research are to: 1) gain a better understanding of the major determinants of energy use and power demand in multi-family residences, 2) evaluate the cost-effectiveness of conservation measures in various climates, and 3) transfer this information to builders of such housing and other interested parties. The research includes collection of data on energy use and building characteristics of new multi-family buildings, development of prototypical buildings, computer simulation, and energy and economic analysis.

Although multi-family dwellings accounted for about 38% (665,000 units)[1] of all new residential units built in 1984, there is surprisingly little published information on building characteristics available. Therefore, in order to satisfy a need for such data, we organized and convened a panel of builders of multi-family residences from across the country. With guidance provided by panel members, we produced a survey instrument especially designed to collect information on multi-family building characteristics.

*This work was supported by the Assistant Secretary for Conservation and Renewable Energy, Office of Buildings and Community Systems, Buildings Systems Division (Architectural and Engineering Branch), of the U.S. Department of Energy under Contract No. DE-AC03-76SF00098.

Our preliminary findings covered a small number of multi-family buildings. Thus, the results were not generalized nor considered as statistically representative of new multi-family housing. However, we compare our survey results to previous studies, and to previous assumptions about multi-family prototypes, and identify several major research issues for the multi-family sector, such as developing new prototypical buildings and performing energy and economic analyses.

We first collected data on multi-family buildings from four major sources of information.[1-4] Multi-family housing includes all buildings with two or more living units. For the existing U.S. housing stock, multi-family buildings make up more than 26% of all residential units (see Table 1),[2] and about one third of all new residential units built each year are in multi-family buildings.[3] Most new multi-family units were built in the South and West. Three states (California, Florida and Texas) account for approximately 45% of all new units in buildings with five or more units, and seventy-five percent of all multi-family units built each year are in buildings with more than four units.[4] Although a major decrease in construction occurred in the residential

Table 1. Existing housing stock.[a]

	No. of units (millions)	% of total Units	Average heated floor space (ft^2)
Single family detached	53.8	64.2	1717
Single family attached	3.9	4.6	1535
2–4 units	10.1	12.1	1137
>4 units	12.2	14.6	795
Mobile homes	3.8	4.5	860
Total Residential	83.8	–	–

[a]1982 Residential Energy Consumption Survey: Housing Characteristics DOE/EIA-0314 (82), August 1984.

sector between 1979 and 1982, this did not affect the construction of multi-family units to the same extent as single-family units.

Multi-family housing consume more than 20% of the energy used by residential buildings, or more than 1.9 Quads out of a total of 9.5 Quads for all residential buildings.[2] Electricity is the dominant heating source for newly constructed multi-family housing units (see Fig. 1).[3] More than twice as many new units use electric heat as all the other fuels combined. During the last decade, the use of natural gas and oil for heating has decreased somewhat. In 1983, 89% of newly constructed multi-family units were air-conditioned.[3] In that same year, electric heat pumps were installed in 28% of new multi-family units.[3] Thirty-three of the 39 respondents in the NAHB survey[4] stated that individual heating ventilation and air conditioning systems (rather than central systems), would be chosen for new garden apartment projects over the next 3–5 years.

Low-rise buildings (1–3 stories) account for 86% of all new multi-family units[3] and thus represent most new multi-family housing. The average size of new multi-family units has varied between 900 and 1000 square feet over the last few years. Approximately two-thirds of these units are occupied by renters and the majority of those are individually metered.[3] Thus, there is little financial incentive for builders of such units to implement energy conservation measures.

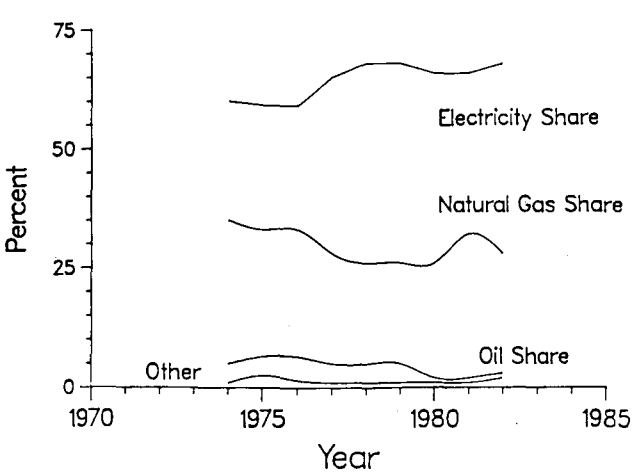

Figure 1. Heating fuel mix in multi-family units.
(XBL 862-447)

ACCOMPLISHMENTS DURING FY 1985

We developed a detailed 50-item survey instrument, recommended by the panel we organized, and sent it to 28 various builders across the U.S. The questions focused on building components, construction elements, typical architectural features, and space conditioning systems. There were two purposes in gathering these data: 1) to identify trends in multi-family construction characteristics and equipment use, and 2) to use these data to develop input to a building computer simulation program (DOE-2).

We achieved an overall 50% response rate, with 7 responses coming from the top 20 U.S. builders.* We attempted to contact builders in all typical U.S. climate regions, but concentrated our efforts in California, Texas and Florida. We decided not to weight our results (for percentage of builders and percentage of units), because of very consistent answers of the respondents. The survey respondents indicated that most of the buildings they constructed ranged from one story to four stories. Two- and three-story buildings represent almost 70% of the total, and over 80% are three stories and less.

Regarding the building envelope, our survey found that wall framing is generally 2×4 studs 16″ on center (O.C.), with plywood sheathing and interior drywall. The exterior wall is generally insulated (95%), with either fiberglass and a polyethylene vapor barrier, or rigid polyurethane insulation. Ten percent of the respondents report placing radiant barriers in the attic walls.

Ninety-five percent of the time, roofs are reported to be wood-frame, using wood rafters, with 1/2″ plywood sheathing covered by 1/8″ asphalt shingles or spanish tiles. Some of the builders use prefabricated roof structure, such as trusses and panels. Roofs are reported peaked 90% of the time, and of a medium-light color. All ceilings are reported insulated: either with fiberglass or rigid batts.

The most prevalent type of floor, reported in 45% of the survey responses, consists of 2×10 joists with slab-on-grade, basement and crawl space with a prevalence of slab foundations due to the extensive coverage of warm regions of the country (California, Texas and Florida).

*"Building Design & Construction," December, 1983.

The slabs, when they are insulated, have either insulation under the slab, or more commonly, perimeter insulation with an R-8 to R-10 value. The crawl spaces usually have insulation both under the floor and on the walls (R-19) and a polyethylene vapor barrier on the ground. Basement foundations appear generally to be used as garage space.

Eighty percent of the respondents reported they use regular window glass, with only 20% of them using tinted glass (typically in luxurious condominiums). The windows are generally equally distributed among the different orientations of the building, with an average window area of 10–12% of the floor area. No builders in the survey incorporated movable window insulation.

While passive solar strategies are not a prime consideration, 90% of the respondents in our survey are employing insulation and infiltration reduction (weatherstripping, caulking) and 20% are reported to use vapor barriers as a means to reduce energy consumption.

Our survey found that 95% of the apartments are reported to have individual heating and cooling systems. The type of installed equipment varies (see Table 2), but it should be noted that 57% are electrically heated. Natural ventilation (when the outdoor temperature allows it), and air conditioning remain the two major methods of cooling. The type of installed equipment varies, but it should be noted that 57% is electrically heated. The average seasonal energy efficiency ratio (SEER) of the air conditioners for the cooling systems is 8.25.

Typical appliances purchased and installed in the final installation of a typical multi-family building as reported in our survey are: ranges, electrical dishwashers, furnaces, water heaters, refrigerators, and garbage disposers.

The results of our multi-family survey, summarized in Table 3, are generally consistent with national data obtained from the Department of Housing and Urban Development. Locations with warm climates (California, Florida, Texas) are well represented by our respondents.

Table 2. Cooling equipment.

Type of equipment	Survey results (%)
Heat Pump	22.9
Air Conditioner	45.4
Other	31.6

Table 3. Summary of survey results.

GENERAL CHARACTERISTICS

Low-rise (1–3 stories) account for most new construction (75% are 2–3 stories).

Almost 90% of the buildings are rectangular in shape.

Average unit floor area equals 964 ft^2.

Typically, there are 12″ to 24″ overhangs on the eaves.

CONSTRUCTION CHARACTERISTICS

Walls

- 90% of the buildings have wood frame roof and wall construction.
- Wall insulation in 90% of the buildings varies from R-11 to R-19.
- Party wall insulation in 60% of the building varies from R-8 to R-13.

Floors/Ceilings

- Three types of floors are used: Slab-on-grade (70%) crawl-space (25%), basement (5%)
- Floor insulation in 42% of the buildings varies from R-8 to R-19.
- Ceiling insulation in the buildings varies from R-19 to R-33.

Windows

- Equal number of single and double glazing.
- Use of aluminum sash (53%) and wood sash 947%).
- Few special features: Reflective glazing, movable insulation, solar film.
- Window areas average 10 to 15% of the floor area of the building.

Infiltration

- Use of weatherstripping and caulk (90%).

Systems

- Individual heating and cooling systems (90–100%).
- Increasing use of heat pump (25.8%).
- Important use of air conditioner (46%).
- Use of temperature thermostat (20%).

PLANNED ACTIVITIES FOR FY 1986

The data obtained from both LBL and HUD surveys showed that the overwhelming majority of new units are in buildings with three or fewer stories. This supports our decision to study first low-rise multi-family buildings. Our initial assumptions used to model a two-story apartment building prototype[5]

appear to be valid. However, our survey results identified a need for a new 3-story prototype (26% of the respondents in our survey are building 3-story garden apartments). From the survey results, we also identified three major research topics that warrant further attention. They are internal loads patterns of multi-family buildings, building peak loads and space conditioning system type selection.

From our survey (and other studies), we found that most new low-rise multi-family construction is in hot locations and that almost all units in these areas use air conditioners for cooling. Therefore, it is important to study methods of reducing cooling energy use and peak demand in such buildings. The total building peak load in low-rise multi-family buildings could be lowered through improved design of a multi-zone building, by understanding the effect of orientation, by the use of thermal mass, by the optimum location of windows, and by the use of shading. Peak load reductions or shifts in loads to off-peak time, could lead to both consumer and utility company savings, if the utility company concerned uses off-peak rates. For example, San Diego Gas & Electric's costs for electricity drop from 11 cents/kWh during peak time to 7 cents/kWh during off-peak time. Utility company savings result from a lessened need to generate costly peak energy.

In order to study methods of reducing cooling energy use and peak power demand, we first need to improve our understanding of internal loads in multi-family buildings. The number of persons occupying a zone, the appliances used, and the lighting schedules determine the daily profile of internal loads within that zone. These load profiles for each zone are more difficult to determine in a multi-zone building such as a multi-family building, because the different zones are occupied independently of each other. In FY 86, we plan to gather measured data from existing building and test the sensitivity of different internal loads schedule in the simulation model.

Our survey results show that almost all space conditioning systems in new low-rise multi-family buildings are individual in nature. However, it may be more energy efficient to use central systems in some climates. The differences in heating and cooling loads for individual zones at any given moment of time can significantly affect the energy efficiency of a central HVAC system. We plan to study the use of individual space conditioning systems versus central or multi-zone systems, the use of new systems such as heat pumps, and the size and efficiency of the equipment versus the energy use.

Although our preliminary survey results are consistent with the earlier assumptions we made concerning low-rise multi-family construction characteristics, we need to determine whether these results hold for a larger database of new multi-family buildings and how construction characteristics vary with climate. Additionally, it is important to gather data on appliance saturations and use and occupancy patterns in order to determine better internal loads schedules. This will allow us to study more accurately strategies for reduction of cooling energy use and peak power demand in low-rise multi-family buildings.

REFERENCES

1. Energy Information Administration, Washington, D.C. (1984), "1982 Residential Energy Consumption Survey," DOE/EIA-0314 (82).
2. Energy Information Administration, Washington, D.C. (1983), "Consumption and Expenditures, April 1981 through March 1982," DOE/EIA/0321.
3. Department of Housing and Urban Development, Washington, D.C. (1984), "Characteristics of New Housing," C25-83-13.
4. National Housing Development, Houston (1985), "National Council of the Multi-family Housing Industry."
5. Turiel, I., *et al.* (1985), *Low-Rise Multi-Family Housing Prototype Development & Preliminary Energy Analysis,* LBL-18823.

Energy and Economic Analysis of Conservation Measures for Low Rise Multi-Family Housing

I. Turiel, P. Albrand, and R. Ritschard

The Building Energy Analysis Group at Lawrence Berkeley Laboratory is studying energy use in new multi-family buildings. Multi-family units account for about 35% of all new residential units constructed each year. The principal objectives of this research are to gain a better understanding of the major determinants of energy use in multi-family residences and the cost-effectiveness of conservation measures in various climates and to transfer this information to builders of such housing. The research includes collection of data on energy use and building characteristics of multi-family buildings, development of prototypical buildings, and energy and economic analyses.

The present research project on multi-family housing focuses on new construction. Since low-rise buildings with more than four units account for most of the new construction and most of the energy use in the new multi-family housing sector, we analyzed this type of structure. Additionally, since much of the new construction is in the Sun Belt (i.e., South and West), we emphasized methods of reducing cooling energy use.

ACCOMPLISHMENTS DURING FY 1985

We began our research by collecting data on multi-family housing. We are interested in both energy use and construction characteristics data. Since the availability of such data is limited, we met with builders of multi-family residences and developed a questionnaire to gather additional information. We have analyzed the responses we have received to date (see preceding annual report article by Albrand, *et al.*). When this analysis is complete, we will develop new prototypical buildings. We developed the prototypical building used for the analyses described in this report with information obtained from discussions with builders and from data on new single-family housing construction. A preliminary analysis of early questionnaire returns indicates that our initial building characteristics assumptions are reasonable.

The parametric analyses described below were carried out with the computer program DOE-2.[1] We performed many simulations to determine the heating and cooling loads for each apartment within our prototypical building in different climates. We tabulated the reductions in space conditioning loads achieved by employing various conservation measures. We expressed the results for average end- and mid-units so that these average units could serve as building blocks for most other multi-family designs. That is, the heating and cooling load reductions we calculated for average end- and mid-units in the six-unit, two-story prototypical building can be used for similar units in other larger two-story buildings.

Our initial prototype is a two-story building consisting of six 1200 ft^2 apartment units. We also performed some simulations for floor space areas ranging from 900 to 2000 ft,[2] allowing heating and cooling load reductions for a 1200 ft^2 apartment unit to be scaled upwards to a 2000 ft^2 unit or downwards to a 900 ft^2 unit. This prototype is representative of most two-story buildings with six or more units since the middle and end units in this six-plex will behave thermally like any similar units in a larger two-story building. We assumed a two foot fixed overhang on all four sides of the building. We performed simulations with window area for each unit equal to 10%, 15%, and 20% of the unit floor area. We modelled three types of foundations (ventilated crawl space, slab-on-grade, and unheated basement). Party walls between units are composed of four layers of gypsum board and R-11 insulation. We assumed the cooling setpoint to be 78°F and the heating setpoint to be 70°F with a nighttime setback to 60°F. Sensible internal loads are 53,100 Btu per day. We modelled infiltration to average 0.7 air changes per hour during the winter. A detailed description of the building construction characteristics and operating conditions can be found elsewhere.[2]

Using the prototype described above, we performed a number of sensitivity analyses with the DOE-2.1 computer program. These include studies of: ceiling insulation, wall insulation, foundation types with variable insulation, infiltration rate, window area, glazing type (number of glazings and reflective/absorptive glazing), floor area, roof solar absorptivity, movable nighttime insulation, thermostat setback, and building orientation. We simulated the building prototype with six separate zones, one for each apartment. Heating and cooling loads are obtained for each of the six zones. In order to reduce the quantity of data presented, we calculated the heating and cooling loads for average mid- and

*This work was supported by the Assistant Secretary for Conservation and Renewable Energy, Office of Buildings and Community Systems, Buildings Systems Division (Architectural and Engineering Branch) of the U.S. Department of Energy under Contract No. DE-AC03-76SF00098.

end-apartment units. That is, the loads in the two mid-units and the four end-units are separately averaged and the results are presented separately for each. Therefore, these average results are applicable to two-story buildings only. Expressing the results as loads for average mid- and end-units, allows one to calculate the loads for other larger two-story buildings by using the results of this analysis for a six-unit building. The number of mid- and end-units are multiplied by the average mid and end loads, respectively and the two products are summed to give the total load for the larger building. We carried out many of the parametric studies for 45 climatically representative locations throughout the United States. In some cases, we performed simulations for 11 locations and developed regression equations to extrapolate the results to all 45 locations.

An example of the type of analysis we have carried out is the estimation of the effect of reflective glazing on cooling and heating energy use and on the cost of space conditioning. A detailed description of this analysis and also one of movable insulation can be found in another report.[3] We simulated the use of reflective glazing on all windows for the prototypical building described above in 11 locations. The reflectance for this glazing was 45% compared to the assumption of 6% for clear single-pane glass. We correlated changes in heating and cooling loads to average (of four cardinal directions) vertical insulation during the heating and cooling periods, respectively, obtaining the equations shown below.

Delta Heating Load (MBtu/ft^2) =

$$1.64 \times 10^{-3} + 2.0\times10^{-4} \cdot z \qquad (1)$$

Delta Cooling Load (MBtu/ft^2) =

$$2.71 \times 10^{-3} + 2.7\times10^{-4} \cdot y \qquad (2)$$

where

z = solar insulation (kBtu/ft^2) during the hours when there is a heating load,

y = solar insulation (kBtu/ft^2) during the hours when there is a cooling load.

Figure 1 illustrates the linear relationship between the delta cooling load and the average vertical insulation during the cooling period. We also performed similar analyses for double- and triple-pane windows and for delta heating loads. The correlation coefficients achieved with this regression analysis range from 0.95 to 0.99. We use the regression equations to predict heating and cooling load changes in other locations where the amount of vertical insulation is known but for which no computer simulations have been performed.

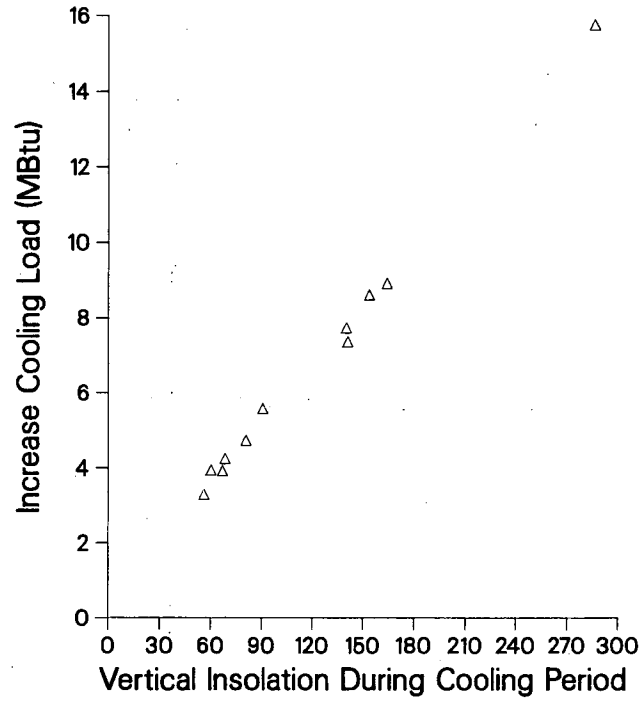

Figure 1. The effect of reflective glazing on cooling load plotted for eleven locations as a function of average vertical insolation (kBtu/ft^2) during the cooling period. (XBL 851-992)

We have also assessed the cost effectiveness of using reflective glazing. Figure 2 shows on a map of the United States the change in the annual cost of space conditioning (1985$/yr) for 100 ft^2 of reflective single-pane glass relative to the single-pane glass described for the base case end unit apartment. It is important to note that the values shown on the map are approximate for locations between the 45 cities for which we calculated space conditioning costs. We assumed a gas space heating system with a seasonal COP of 0.7 and an electrical cooling system with a seasonal COP of 2.4 (SEER = 8.2). We assumed the costs of electricity and natural gas were $0.08/kWh and $0.50/therm, respectively, for all locations.

The cost savings are substantial (30–80$/yr) in climates with warm summers and mild winters; e.g., in southwestern and southern parts of the U.S. these savings would be proportionally higher for apart-

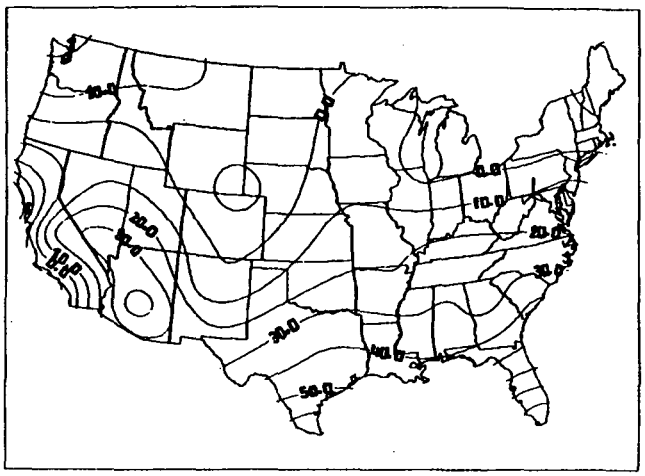

GAS SPACE HEATING

Figure 2. The impact of reflective glazing on the annual cost ($985) of space conditioning a 1200 ft^2 end-unit apartment with 100 ft^2 of single-pane windows is shown on a map of the U.S. The cost changes are for an apartment heating with natural gas and cooled with an electric air conditioner. (XBL 8512-5070)

ments with more than 100 ft^2 of window area. The savings moderate as one moves north to cooler locations. In the Pacific Northwest and parts of California, Idaho, Montana and Nevada, space conditioning costs increase with the use of reflective glazing. The additional capital cost of reflective glazing is approximately $4.00 per square foot.[4] The map should be used to determine which regions of the U.S. are likely to have reasonably short (<10 yrs) simple payback periods for the use of reflective glazing. The simple payback period is obtained by dividing the additional capital cost of reflective glazing by the annual dollar savings shown on the map. Therefore, the simple payback period is 5–13 years for an end-unit apartment with gas space heating in the southwestern or southern parts of the U.S. Electrically heated residences will have longer payback periods.

PLANNED ACTIVITIES FOR FY 1986

Using computer simulations, we have quantified reduced space conditioning loads that result from added thermal insulation, nighttime thermostat setback, decreased infiltration, and proper choice of orientation and glazing. We plan to perform additional cost-benefit analyses to determine the cost-effectiveness of specific measures in various locations. Local fuel prices and other heating and cooling equipment types will be incorporated into the economic analyses. We are developing a microcomputer program that will allow such calculations to be made in an easy to use and inexpensive manner. In the next phase of our work, we will analyze additions. Local fuel prices and other heating and cooling equipment types will be incorporated into the economic analyses. We are developing a microcomputer program that will allow such calculations to be made in an easy to use and inexpensive manner. In the next phase of our work, we will analyze additions. Local fuel prices and other heating and cooling equipment types will be incorporated into the economic analyses. We are developing a microcomputer program that will allow such calculations to be made in an easy to use and inexpensive manner. In the next phase of our work, we will analyze additional conservation measures (e.g., external shading) and additional prototypical low-rise apartments. We also plan to develop a three-story prototype in order to broaden our coverage of low-rise multifamily housing. With the addition of this prototype, we will be able to apply the building block approach to almost any low-rise multi-family building.

REFERENCES

1. DOE-2 Reference Manual, Parts 1 and 2 (Version 2.1B) (1980), U.S. Department of Commerce, National Technical Information Service, Springfield, VA 22161
2. Turiel, I., Ritschard, R., Wilson, D., and Albrand, P. (1985), *Low Rise Multi-Family Housing: Prototype Development and Preliminary Energy Analysis,* LBL-18823.
3. Turiel, I., *et al.* (1985), *Parametric Analysis of Impact of Reflective Glazing and Movable Window Insulation on Heating and Cooling Loads and Space Conditioning Costs in Residential Buildings,* LBL-20217.
4. Means Construction Cost Data (1984), Robert Snow Means Company, Inc., Kingston, MA 02364.

Potential for Wind Induced Ventilation in Residences*

S.J. Byrne, R.L. Ritschard, and D.M. Foley

Wind induced ventilation of buildings can be a significant means of increasing occupant comfort and reducing cooling energy consumption in hot climates. In FY 85, the Building Energy Analysis Group began investigating the magnitude of this savings and how buildings might be better designed to enhance it. This paper describes the first phase of that work—the development of a simple graphic tool that enables a building designer to evaluate the potential for wind induced ventilation cooling in several climate zones. The graphic format is similar to conventional "wind roses" that are currently used by designers, but with the additional effects of human comfort and building cooling load taken into account.

This design tool allows the user to determine: (1) the human comfort level when the interior wind speed is at various fractions of the available exterior wind speed, (2) the building cooling load for those ambient conditions that are uncomfortable, and (3) the direction the wind is blowing from when mechanical cooling is required to maintain comfort.

Thus, the results indicate the potential savings from inducing various ventilation air flow rates as well as the orientation of building openings that will minimize the annual cooling load. Local weather patterns, such as strong northerly winds, combined with lower air temperature during brief storms (in which case mechanical cooling could be unnecessary) are automatically accounted for and are weighted by the frequency of occurrence.

ACCOMPLISHMENTS DURING FY 1985

In order to properly size and orient building openings to take advantage of ventilation cooling, a designer must be aware of local wind speed and direction as well as coincident ambient dry bulb and relative humidity. The designer must then determine the impact of the combination of wind speed, temperature and humidity on human comfort and the resulting effect on the building cooling load.

The research on this project was organized to solve these problems and was composed of three parts: (1) analysis of long term weather data, especially coincident wind speed and direction, dry bulb temperature and relative humidity, (2) mathematical modeling of the effects of wind speed on human comfort under conditions of high temperature and humidity, and (3) development of a simplified model of residential building cooling load that correlates with data from DOE-2 simulations.

Analysis of Weather Data

Summary information on wind direction, frequency, and prevailing wind speed is available as "wind rose" plots[1] of conditions at local weather stations. Although this information has traditionally been used as an indication of average local wind conditions, its usefulness in building design is very limited. Wind rose plots (see example in Fig. 1) indicate frequency of wind blowing in each of 16 directions and wind speed is given for the prevailing wind direction. This provides a designer with no information on coincident temperature and humidity, which must be used to determine whether ventilation is beneficial. Although it is possible to use monthly wind roses together with monthly average weather data,[2] the designer is at best, left with a rough estimate that indicates little about the effect on human comfort and building cooling loads.

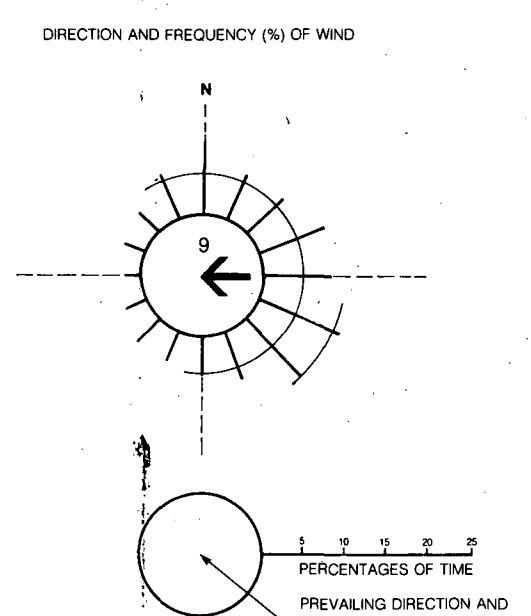

Figure 1. Annual wind roses for Miami. (XBL 859-3897)

*This work was supported by the Assistant Secretary for Conservation and Renewable Energy, Office of Building Energy Research and Development, Buildings Systems Division of the U.S. Department of Energy under Contract No. DE-AC03-76SF00098.

Hourly weather data are available in a variety of formats and can be obtained for multiple, contiguous years[3] or for a single, average year.[4–6] For this analysis, we chose to analyze long term (approximately 12 contiguous years) data for each location, because the methods for determining "average" years emphasize average temperature and solar radiation but not wind speed or direction. We used data from years prior to 1965, when reporting frequency was changed from hourly to once every three hours at most locations. Available weather tapes begin during mid 1952 through early 1953, thus yielding approximately 12 years of hourly data for each location. Our summarized results, therefore, represent average potential for wind induced ventilation cooling and may not be exactly the same for any specific year.

Because this analysis is intended to show the benefit of ventilation cooling in buildings, the wind speed measured at the local weather station (usually a nearby airport) was translated to what could be expected at the building site, accounting for: (1) the difference in height between the wind tower at the weather station and a typical building height, and (2) the difference in terrain between a typical weather station and a typical residential building site.[7]

In this work, we converted the weather station wind speed to a height of 3 meters in a suburban area. The wind direction was unchanged from the measured value. This represents the available wind speed and direction for ventilation cooling of most single family houses. Local obstructions (e.g., large, nearby buildings, trees or hills) might reduce the wind speed or alter the direction and should be accounted for in the actual building design.

Mathematical Modeling of Human Comfort

To be acceptable to its occupants, a built environment must provide thermal comfort. Achieving thermal comfort depends on both environmental and personal factors, some subject to the occupants' control, and others not. The important environmental determinants of thermal comfort are temperature, humidity, radiation and air movement, while important personal factors are clothing and activity level.

Because thermal comfort and discomfort are subjective sensations, it is difficult to predict the effects of any combination of environmental and personal factors. However, sensations of comfort or discomfort correlate with physiological quantities which can be measured or calculated (e.g., skin temperature, body core temperature, rates of sweating and breathing, etc.). Reported thermal sensations from human test subjects have been compared with physiological measurements, and from these data, researchers have been able to develop mathematical models and computer algorithms to predict the response of a person to a given thermal environment, taking into account that person's clothing and activity level.

Three of the most widely used comfort algorithms are the Fanger Comfort Model, developed by P.O. Fanger of the Technical University of Denmark,[8] the Pierce Two Node Model, developed by A.P. Gagge and colleagues at the J.B. Pierce Foundation,[9] and the KSU Two Node Model, developed by N.Z. Azer and colleagues at Kansas State University.[10] A comparison of the three algorithms is given by Berglund.[11] For the work which led to this paper, we used a modified version of the Pierce Two Node Model.

Humans regulate their heat exchange with the environment in order to maintain, within a very close tolerance, the temperature of their body core. The Pierce model describes this heat exchange process by modeling the human body as two discrete compartments: an inner core and an outer skin. The core, which is assumed to be of uniform temperature, is modeled as the source of all metabolic heat production. To maintain a constant core temperature, all of the metabolic heat and work must be transferred to the surroundings. In the model, the core transfers energy directly to the environment through respiration and work. The remaining metabolic heat is transferred to the skin compartment, both passively by conduction and actively by the controlled flow of blood from the core to the skin. The skin gives off heat to the environment through convection, radiation, evaporation of sweat and diffusion of water vapor through the skin.

From the values of physiological variables calculated in the model, the discomfort index can be determined. In the version of the Pierce model that we used, the discomfort index, DISC, is calculated by:

$$\mathrm{DISC} = 5.0 \cdot \frac{\dfrac{(0.68 \cdot E_{rsw}) + E_{dif}}{E_{max}} - P_{wet}}{1.0 - P_{wet}} \qquad (4)$$

where:

E_{max} = maximum rate of evaporation of sweat (W/m^2),
= $(P_{sk} - P_a)/[1/h_{cl} + 1/(16.5h_c)]$;
P_{sk} = saturation vapor pressure at skin temperature (kPa);
P_a = partial vapor pressure at air temperature (kPa);

h_{cl} = moisture conductance of clothing (W/m^2kPa),
= $115 / I_{clo}$;
I_{clo} = thermal resistance of clothing (clo);
h_c = convective heat transfer coefficient (W/m^2K),
= $8.6 \cdot V^{0.56}$;
V = air velocity (m/s);
P_{wet} = fraction of skin wettedness (dimensionless),
= $0.08 \cdot ACT / 58.2 - 0.02$;
ACT = metabolic heat from activity (W/m^2).

Each of the environmental determinants of thermal comfort has some influence on the discomfort index. In our work, we assumed that the mean radiant temperature of the building is equal to the dry bulb temperature, which is often the case for light weight residential construction. We also assumed the occupants are not directly exposed to solar radiation. Therefore, the influence of radiation in the model was negligible.

We tested the sensitivity of the model to temperature, humidity, air movement, activity level and clothing. Figure 2 shows the discomfort index (DISC) as a function of dry bulb temperature, relative humidity and wind speed. The rate of increase in DISC with temperature is significantly higher at 80% RH than at 20% RH. Likewise, the impact of wind speed on comfort is greater at higher humidity and temperature levels. Thus, a combination of increasing temperature and humidity affects comfort more than either parameter alone and the use of wind to provide occupant comfort is more significant in hot-humid climates than in hot-arid climates. A similar parametric analysis was made to determine the sensitivity of the model to activity level and clothing. Increasing the activity level increases metabolic heat production (met), and thus, at high ambient temperatures, increases thermal discomfort. The rate of increase of discomfort with activity level is greater when the amount of clothing (clo) value is greater, because clothing acts as an impedance to heat dissipation.

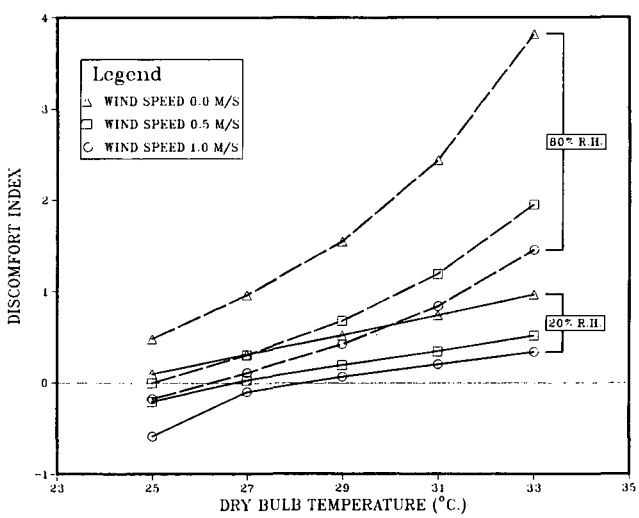

Figure 2. Discomfort index (DISC) as a function of dry bulb temperature, relative humidity and wind speed. (XBL 859-3884)

In our work, we assumed a clo value of 0.5, corresponding to light clothing suitable for office or home in a warm climate. We set the activity level at 1.1 met, representing a person working at a desk, reading or watching television.[12] Further, we set the maximum acceptable interior wind speed to 1.0 m/s, since any wind above that speed is likely to cause papers to rustle and may be irritating to occupants. We set the discomfort index at which a person is likely to turn on an air conditioner to 0.5.

Estimating Building Cooling Load

A reliable indicator for building cooling loads should recognize latent as well as sensible cooling loads. Data from a LBL data base of DOE-2.1A loads for a typical 1-story residential prototype in 45 U.S. locations showed latent percentages varying from 5% for an uninsulated house in arid Phoenix to 35% for a moderately well-insulated house in Miami. Therefore, climate parameters based only on temperature differences, such as cooling degree days or degree hours, can be substantially in error for estimating cooling loads. This was confirmed in comparisons made between the cooling loads and degree hour data for the same locations.

To incorporate the effects of latent cooling, we used the concept of cooling enthalpy hours. Enthalpy hours define the amount of energy that must be removed from the air each hour to lower ambient air conditions to a reference condition defined by dry bulb temperature *as well as* humidity ratio. Cooling enthalpy hours can be further divided into sensible and latent components. The sensible component is proportional to cooling degree days and is useful for estimating sensible loads using standard $UA\Delta T$ calculations. The latent component can be related to latent cooling loads for a given infiltration rate.

On a psychometric chart, cooling enthalpy appears as the difference in enthalpy between the ambient air condition and the reference point. Latent enthalpy is the enthalpy reduction necessary

to lower humidity ratios to the reference level, keeping the dry bulb temperature fixed. Sensible enthalpy is the additional enthalpy reduction necessary to lower the dry bulb temperature to the base temperature, keeping the humidity ratio constant. Therefore, latent enthalpy corresponds to a vertical movement, and sensible enthalpy to a horizontal movement on the psychometric chart. The total change in enthalpy times the number of hours that condition exists equals the number of enthalpy hours.

The reference dry bulb temperature for calculating enthalpy hours is interpreted, similar to cooling degree days, as the balance point or threshold ambient temperature above which mechanical cooling will be required to maintain the indoor temperature specified by the thermostat set point. Because of solar gain, we used reference temperatures of 18°C for the daytime, and 24°C for the nighttime hours. We calculated the balance point temperatures assuming a typical 143 m^2 prototype house with 0.30 $W/m^2°C$ ceilings, 0.52 $W/m^2°C$ walls, and 0.5 ach infiltration. More details on the prototype house and operating conditions as well as the LBL data base are given by Huang.[13]

The reference humidity ratio is more difficult to define, since cooling controls in residential systems generally respond only to indoor temperature and not to humidity. For this study, we chose a humidity ratio of 0.0116 (kg of moisture/kg of dry air), corresponding to the upper limit of the human comfort zone.[12] This humidity ratio is chosen on the assumption that a properly sized air conditioner will maintain indoor comfort by keeping the humidity ratio below this level. Latent loads from the LBL residential data base correlate well with latent enthalpy hours at 0.0116 base humidity ratio.

We imposed two conditions on the calculations: (1) latent enthalpy hours are not counted when sensible enthalpy hours are nonpositive; and (2) negative latent enthalpy hours are set to zero. The first condition assumes that the air conditioner will be off because the ambient air is cool, even though it has more enthalphy content than the reference point. The second condition assumes that typical residential cooling systems do not humidify even though ambient air conditions may be hot and dry.

The relationship of sensible and latent enthalpy hours to cooling loads for a particular house depends on its total conductance and infiltration rate. For this study, we assume an average summer infiltration rate of 0.5 ach (air changes/hour) for a prototype 1-story house with a volume of 348.9 m^3. The latent load (kJ) is estimated from latent enthalpy hours by:

$$Q_{lat} = HH_{lat} \cdot V \cdot \rho \qquad (6)$$

where:

HH_{lat} = latent enthalpy hours (kJ-h/kg dry air);
V = volumetric air change rate (348.9 $m^3/h \cdot 0.5$);
ρ = density of air (1.2 kg/m^3);
or:
$Q_{lat} = HH_{lat} \cdot 209$ kg/h.

The sensible load (kJ) is estimated from sensible enthalpy hours by:

$$Q_{sen} = (HH_{sen} \cdot V \cdot \rho) + (HH_{sen} \cdot UA) \qquad (7)$$

where:

HH_{sen} = sensible enthalpy hours (kJ-h/kg dry air);
V, ρ = same as for Q_{lat} above;
UA = building conductance,
= 1055 kJ/h-°C;
or:
$Q_{sen} = (HH_{sen} \cdot 209) + (HH_{sen} \cdot 1055)$
$= HH_{sen} \cdot 1264$ kg/h.

The estimated total cooling load (kJ) is then:

$$Q_{total} = (HH_{lat} \cdot 209) + (HH_{sen} \cdot 1264) \qquad (8)$$

The predicted cooling load using this model was compared to a large data base of DOE-2.1A simulations in 45 cities. The resulting high correlation coefficient indicates an accurate estimation of both the latent and the sensible fractions of the total annual cooling load.

Applications

An example of the resulting plot of building cooling load versus wind speed and direction is shown in Fig. 3. The center of each plot represents zero cooling load and the outerost circle is the maximum cooling load (shown as Q_{max}) while the wind is blowing in any single direction. Thus, the scale on each plot varies so that the resolution can be kept as large as possible. The contour lines represent the building cooling load at various percentages of the outside wind speed. The outermost (solid) contour line is for the case of no ventilation; the next (dashed) contour line inward is the cooling load with 20% of the outside wind speed available for ventila-

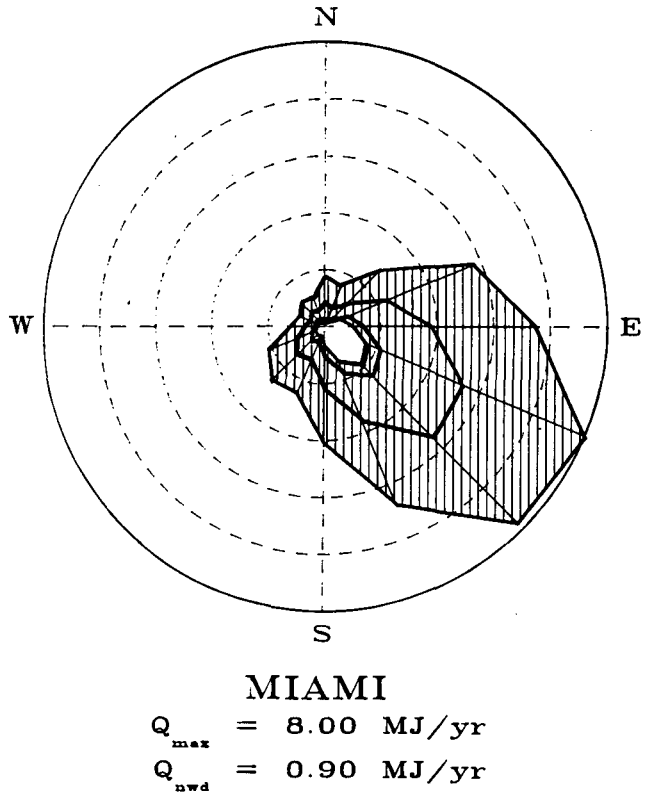

Figure 3. Plot of building cooling load versus wind speed and direction. (XBL 859-3889)

tion. Contour lines alternate between solid and dashed lines and are plotted for 0%, 20%, 40%, 60%, and 100% of the outside wind speed. In addition to the cooling load while the wind is blowing, there is a load during periods of no wind (shown as Q_{nwd}) that should be accounted for in any annual energy calculations.

The primary usefulness of these plots is in the ability of a designer to assess quickly the potential benefit of ventilation cooling and the impact that it will have on orientation of a single building or an entire subdivision. This can be accomplished early in the design process to ensure that subsequent design decisions do not conflict with the ventilation scheme.

Figure 4 shows total cooling load, as a function of interior wind speed, for several cities. The hot-humid climates show a significant reduction in annual cooling load up to high fractions of the outside wind speed, while most of the potential savings in hot-arid climates is realized at lower wind speed fractions. This indicates the importance of properly designing buildings in hot-humid climates to induce natural ventilation.

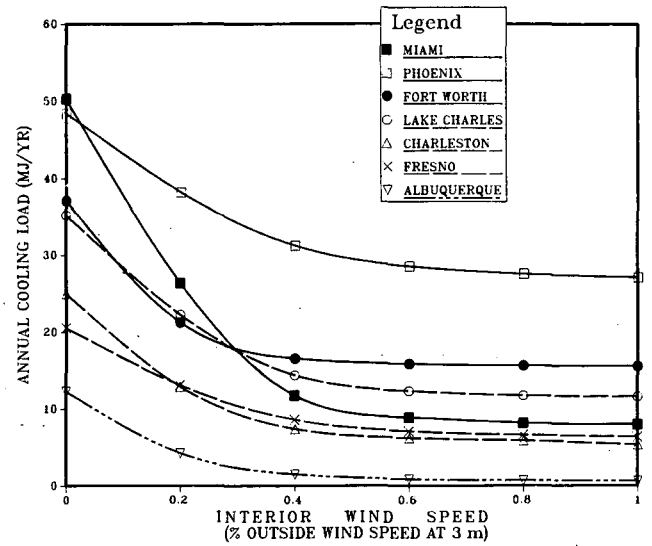

Figure 4. Total cooling load as a function of interior wind speed. (XBL 859-3883)

It is important to note that these plots account only for the impact of ventilation on cooling load and a building designed for minimal energy consumption should also account for the effects of solar gain. It may be necessary to design ventilation openings that are well shaded from direct solar radiation in order to prevent the additional solar gain from offsetting the benefits of ventilation.

PLANNED ACTIVITIES FOR FY 1986

In this paper, we do not propose the means by which any particular ventilation rate can be induced in a building. Continuing research in this area will utilize air flow simulation models and a wind tunnel to explore design alternatives that enhance the natural ventilation of buildings. This work will be started in FY 86 with wind tunnel studies of ventilation design strategies. Long term results of this project will be simplified design guidelines and mathematical models to predict air flow rates in arbitrary building shapes.

REFERENCES

1. U.S. Department of Commerce, National Oceanic and Atmospheric Administration (1980), *Climates of the United States,* Ashville, North Carolina.
2. U.S. Department of Commerce, National Oceanic and Atmospheric Administration (1981), *Local Climatological Data: Annual Summaries for 1981,* Ashville, North Carolina.

3. U.S. Department of Commerce, National Oceanic and Atmospheric Administration (1978), *SOLMET Volume 1: User's Manual,* Ashville, North Carolina.
4. Hall, I.J. (1985), "Generation of Typical Meterological Years for 26 SOLMET Stations," *ASHRAE Transactions,* v. 85, part 2.
5. North Atlantic Treaty Organization (1977), "Test Reference Year (TRY) Final Report," Rational Use of Energy Pilot Study, Report #NATO/CCMS-60.
6. Crow, L.W. (1981), "Development of Hourly Data for Weather Year for Energy Calculations (WYEC)," *ASHRAE Journal,* October, 1981.
7. Sherman, M.H. and Grimsrud, D.T. (1980), *Measurement of Infiltration Using Fan Pressurization and Weather Data,* LBL-10852.
8. Fanger, P.O. (1970), *Thermal Comfort: Analysis and Applications in Environmental Engineering,* Danish Technical Press, Copenhagen, Denmark.
9. Gagge, A.P., Stolwijk, J., and Nishi, Y. (1971), "An Effective Temperature Scale Based on a Simple Model of Human Physiological Regulatory Response," *ASHRAE Transactions,* v. 77, part 2.
10. Azer, N.Z. and Hsu, S. (1977), "The Prediction of Thermal Sensation from a Simple Model of the Physiological Regulatory Response," *ASHRAE Transactions,* v. 83, part 1.
11. Berglund, L. (1978), "Mathematical Models for Predicting the Thermal Response of Building Occupants," *ASHRAE Transactions,* v. 84, part 1.
12. American Society of Heating, Refrigerating, and Air-Conditioning Engineers (1985), *ASHRAE Handbook: Fundamentals,* Atlanta, Georgia.
13. Huang, Y.J., *et al.* (1985), *Affordable Housing through Energy Conservation, Technical Support Document,* LBL-16342.

Residential Prototype Loads Comparisons*

R. Sullivan, Y.J. Huang, R. Ritschard, I. Turiel, and J. Bull

ACCOMPLISHMENTS DURING FY 1985

The Building Energy Analysis Group at Lawrence Berkeley Laboratory has been extensively involved in investigating residential energy use in prototypical houses in the United States. This research has centered on evaluating the influence of various energy conservation measures such as exterior surface insulation, glazing type and conductance, infiltration levels, use of night setback, etc. One of the more recent projects has been the definition and development of a very large data base constructed from numerous DOE-2 building energy simulations of five residential prototypes.

*This work was supported by the Assistant Secretary for Conservation and Renewable Energy, Office of Buildings Energy Research and Development, Building Equipment Division of the U.S. Department of Energy under Contract No. DE-AC03-76SF00098.

The original purpose for the data base was the development of simplified energy analysis tools capable of accurately estimating the energy savings associated with particular conservation measures.[1-3] These tools were designed for use by non-technical groups such as home builders, home buyers, and others in the building industry. The availability of such a large number of building energy simulations permits a more detailed analysis of a broad spectrum of residential building design issues. The work reported here is related to such an analysis with emphasis on the relationship among building prototypes and configurations and their variation with geographic location.

A thermal load comparison of five residential prototypes was accomplished along with a discussion of the implications associated with varying configuration parameters and geographic locations. A data base constructed from DOE-2.1A computer simulations for five building models (one-story ranch, two-story, split-level, middle-unit townhouse, and end-unit townhouse) with a climate base of 17 locations was used for the analysis. Also investigated were the differences associated with three floor types: slab-on-grade, basement, and ventilated crawl space. Results indicate that the thermal loads of various prototypes are proportional to each other in a manner that is independent of geographic location.

In addition, percent heating and cooling load changes for a particular prototype resulting from implementation of a conservation measure are also approximately constant with location. An analysis of multiple-regression-derived algebraic formulas established conditions for exact or approximate linear independence of a building's heat gain or loss components. Procedures were also defined for the simplification of future parametric studies of the thermal analysis of buildings using a methodology that incorporated the observations reported.

Intra- and Inter-Prototype Thermal Load Relationships

Reference 4 described the development of a proportional relationship between residential building thermal loads for varying configuration parameters. Through the use of numerous building energy simulations using both the DOE-2.1 and BLAST energy analysis computer programs, it was shown that the form of the relationship was independent of climatic location and covered a broad spectrum of those variables. The study concentrated on the relationship prevalent among varying configurations of the same basic prototype residence. A second study,[5] concentrated on the relationship that exists across prototypes, which of course leads to much more general conclusions regarding the significance of the results.

Figures 1 and 2 represent the basis for investigation of the proportionality expressed by the figures, i.e., the linear relationship associated with configuration changes as a function of geographic location. Thermal load values due to implementation of specific conservation measures are shown for the

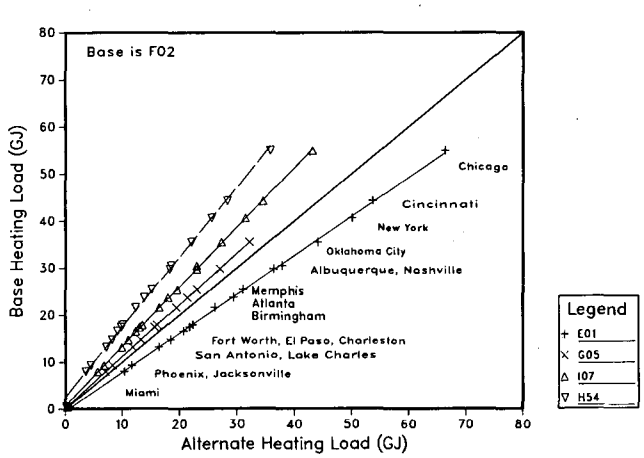

Figure 1. Residential heating load comparison for various configurations and geographic locations (TRY) using DOE-2.1A for a one-zone (143 m^2), ranch style, slab-on-grade house showing the effects of envelope conductance and infiltration. (XBL 8512-4977)

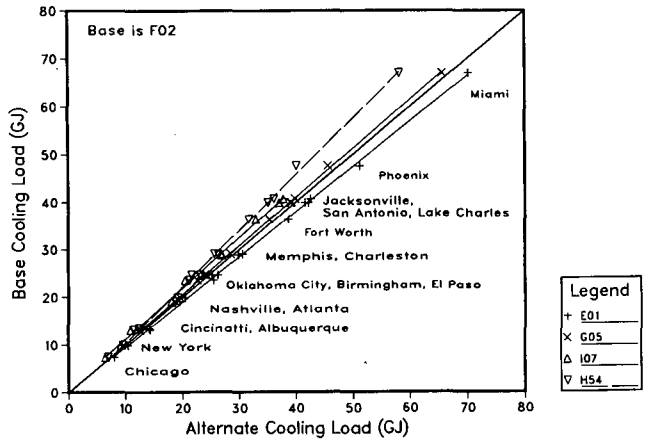

Figure 2. Residential cooling load comparison for various configurations and geographic locations (TRY) using DOE-2.1A for a one-zone (143 m^2), ranch style, slab-on-grade house showing the effects of envelope conductance and infiltration. (XBL 8512-4975)

slab-on-grade, ranch prototype using configuration F02 as a base. The slopes of the curves on these figures are presented on Table 1. They correspond to

Table 1. Heating and Cooling Load Ratios for Five Residential Prototypes and Four Configurations (Slab-On-Grade Floor) Using F02 as a Base Load (Alternate Configuration)/Load (Base Configuration F02)

Prototype	Configuration	Heating	Cooling
Ranch	E01	1.22	1.06
	G05	.91	.98
	I07	.77	.92
	H54	.61	.88
Two-story	E01	1.25	1.06
	G05	.88	.97
	I07	.76	.92
	H54	.59	.87
Split-level	E01	1.27	1.06
	G05	.89	.97
	I07	.75	.91
	H54	.59	.88
End-townhouse	E01	1.33	1.06
	G05	.88	.97
	I07	.74	.93
	H54	.57	.90
Mid-townhouse	E01	1.39	1.06
	G05	.93	.99
	I07	.76	.94
	H54	.56	.91

the ratios of the alternate loads to the base loads. Data for the complete set of five prototypes using the slab-on-grade floor are shown in the table. Although the intercepts on the figures do not go exactly through the origin, the approximate relationship between configurations can be ascertained using only the slopes.

The base configuration, F02, corresponds to R=19 (3.34) roof insulation, R=11 (1.94) wall insulation, an equivalent floor U-value of 0.4 (0.69), double-pane glass, and 0.7 air-changes per hour of infiltration. Configuration E01 shows the change in load when using single-pane glass. Heating load increases from a low of about 22% of the base level for the ranch style house to a high of 39% for the mid-townhouse. The cooling load increases by 6% for all prototypes. G05 indicates the effect of increased wall insulation, R=19 (3.34). Almost no change in cooling is apparent; however, there is a 12% reduction in heating for those prototypes with a large percentage of wall surface area. Configuration I07 has increased roof, wall, and glass resistance values, and therefore a significant reduction in load is apparent for all prototypes, particularly heating. The percent change in heating is about equivalent to that resulting from a switch from single pane to double pane glass. H54 shows the largest reduction in thermal load with the decreases varying from 39% to 44% for heating and 9% to 13% for cooling. The H54 values are a result of both increased roof and wall insulation (R=30 and R=19), and a decrease in the average infiltration rate to 0.4 air-changes per hour.

The significance of Figures 1 and 2 is that the slopes or percent increase or decrease in load are approximately the same regardless of geographic location. Surprisingly, the same type of proportionality results when comparing the various prototypes. For example, Figures 3 and 4 present results for configuration F02 for all five prototypes for the slab-on-grade floor for seventeen climate locations. The base prototype values, which are presented along the vertical axis, represent the one-story ranch. Load values for the other four prototypes are along the horizontal axis. Heating and cooling correlate with house size; i.e., the largest load is associated with the largest surface area and/or largest floor area. Heating, in particular, is well behaved because of the strong influence of house conductivity. The two-story has the largest loads followed by the split-level, ranch, and end- and mid-townhouses. Using the slopes of Figures 3 and 4, one can quickly obtain an estimate of inter-prototype relationships similar to the data contained in Table 1.

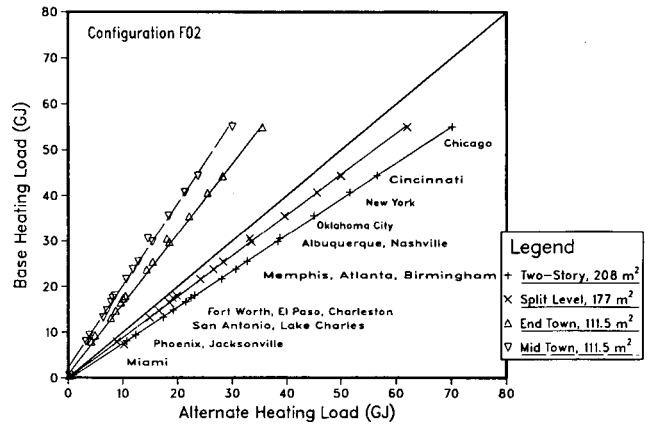

Figure 3. Residential heating load comparison for various prototypes and geographic locations (TRY) using DOE-2.1A. The base prototype is a one-zone (143 m^2), ranch style, slab-on-grade house. (XBL 8512-4974)

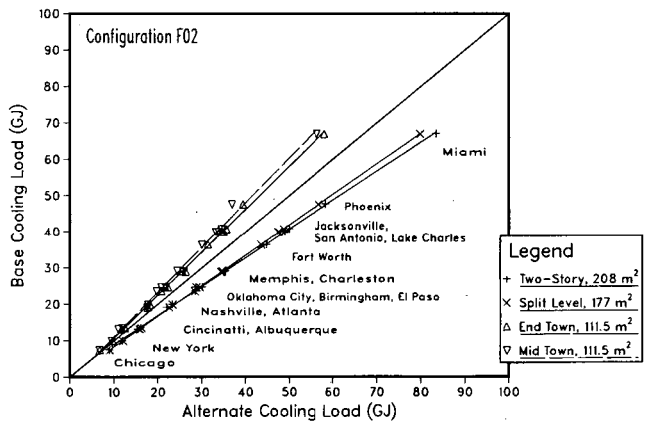

Figure 4. Residential cooling load comparison for various prototypes and geographic locations (TRY) using DOE-2.1A. The base prototype is a one-zone (143 m^2), ranch style, slab-on-grade house. (XBL 8512-4976)

Theoretical Considerations

The studies reported in Refs. 6–8 detailed the use of multiple regression procedures to generate simplified algebraic expressions relating building configuration parameters to the heating and cooling thermal load and/or energy use. Although various building models were used in each analysis, it was shown that a very convenient and compact equation form could be used to accurately predict load or energy. The equation presented below contains the major components contributing to building thermal

loads, namely: envelope conductance, solar gains, internal gains, and infiltration.

$$Q_{ij} = \alpha_i C_j + \beta_i S_j + \gamma_i L_j + \delta_i I_j \qquad (1)$$

where

$\alpha,\beta,\gamma,\delta$ = regression coefficients
C = envelope conductance
S = solar gain
L = internal gain
I = infiltration level
i = geographic location
j = configuration

The regression coefficients represent the climate dependent effect and also contain conversion factors to insure proper units. Each of the other terms is related to a particular configuration variable. This expression does not contain all load producing items; for example, natural ventilation could be an additional term. However, those items generally deemed necessary for adequate building energy analysis studies are included.

The convenient separation of variables provided by equation (1) permits an analysis of the influence of each component and also provides a method of showing under what conditions the (Q) values of two configurations are linearly related and climate independent. It is easily seen from the nature of this basic expression that the change in a component of (Q) is proportional to the change in a particular configuration variable. However, the linearity to be dealt with is the total heating or cooling load or energy, which can be expressed as:

$$\frac{(Q_{b2} - Q_{a2})}{(Q_{b1} - Q_{a1})} = \frac{(Q_{c2} - Q_{a2})}{(Q_{c1} - Q_{a1})} = \frac{(Q_{c2} - Q_{b2})}{(Q_{c1} - Q_{b1})} \qquad (2)$$

where a, b, and c refer to specific weather locations and 1 and 2 to different configurations. This form is used rather than a direct ratio, for example (Q_{b2}/Q_{b1}), since the intercept does not necessarily go through the origin. For equation (2) to be true, the variables α, β, γ, and δ must be related to a specific weather parameter (X_i) in the following fashion:

$$\phi_i = m_\phi X_i + k_\phi \qquad (3)$$

where (ϕ) represents the regression coefficient and (m) and (k) are slope and intercept values that define the functional dependence on the climate variable (X_i). This statement implies that each coefficient, or those which dominate, must be linearly related to the same weather parameter.

Such a condition is easily seen when one considers the heating requirement. For example, envelope conduction and infiltration, which are both temperature driven, are usually the largest components of the heating load; thus, heating degree hours can be representative of (X_i). Actually, the solar and internal gain terms also correlate with heating degree days, but not in as linear a fashion as the conduction and infiltration (see Ref. 6). The cooling load is somewhat more complicated than heating because of the influence of solar radiation and humidity as well as temperature. Reference 9 has shown, however, that the cooling load can be linearily related to cooling degree hours that are calculated considering not only outside air temperature but also humidity ratio.

Conclusions

a. The heating and cooling loads of one residential prototype appear to be linearily related to the loads of various prototypes regardless of geographic location provided levels of house conductivity, solar transmission, internal gains, and infiltration levels are not extremely different for each prototype. This is also true for the per unit floor area thermal loads.
b. Heating load/floor area correlates well with residential surface area to volume ratio. A unique characteristic curve relating these parameters can be defined as a function of prototype configuration properties and geographic location.
c. Percent heating load changes resulting from a conservation measure for a particular prototype also seem to be uniform throughout all climate locations. This implies, for example, that a 20% change in Chicago due to, say, wall insulation, would also be a 20% change in Phoenix.
d. Percent cooling changes due to conservation measures are not as uniform as heating changes throughout the climate range. However, the difference in values from location to location is not dramatic—on the order of a few percent.
e. Each prototype yields different percent distributions of the effect of a particular conservation measure. This conclusion is obvious when one considers the components contributing to a buildings thermal load.
f. Per unit floor area, the mid-townhouse yields the smallest heating load, followed by the end-townhouse, two-story, and split level. The ranch style house results in the largest heating load. The cooling load per unit floor area is lowest with the two-story, followed by the

split-level, ranch, and mid- and end-townhouses.

g. The slab-on-grade floor type, for a given prototype, results in the smallest heating and cooling loads when compared to the basement and crawl space floors. The basement yields the largest loads. However, if one considers the basement floor area in a per unit floor area comparison, basement prototype heating and cooling loads per unit floor area are the lowest.

h. A comparison of the thermal loads of many residential prototypes and configurations can be made based on the tabular load ratios. The documented linearities insure that the relationships defined will be quite accurate.

PLANNED ACTIVITIES FOR FY 1986

It is anticipated that the intra- and inter-prototype thermal load comparisons will continue through the next fiscal year. The results presented are representative of annual residential heating and cooling loads, but they do not relate to the individual incremental component loads which are of importance to decisions related to cost-benefit analysis. Additional analysis will be accomplished by investigating the thermal loads at the component level.

The results discussed have implications in regards to future parametric studies involving the thermal analysis of buildings. Understanding the characteristics of building parameters in varying geographic locations is greatly simplified through definition of a procedure utilizing the linearity reported. Such procedures will be defined and used on all subsequent studies.

Continued investigation of the theoretical considerations and specific definition of the weather variables, particularly those associated with cooling, that define the observed proportionality will continue to be analyzed.

REFERENCES

1. Huang, Y.J., *et al.* (1984) "Affordable housing through energy conservation, a guide to designing and constructing energy efficient homes." Technical Support Document Number US DOE/CS 20524-6, Applied Science Division, LBL.
2. Huang, Y.J., Ritschard, R., and Bull, J. (1985), *Simplified calculations of energy use in residences using a large DOE-2 database,* LBL-20107.
3. Ritschard, R., *et al.* (1985), *PEAR: A microcomputer program for residential energy analysis,* LBL-20355.
4. Sullivan, *et al.* (1985), *Thermal analysis of building—configuration perturbations and observed climate interface,* LBL-19383.
5. Sullivan, R., *et al.* (1985), *Residential prototype thermal load comparisons and variations with geographic location,* LBL-20051.
6. Johnson, R., *et al.* (1983), *Building envelope thermal and daylighting analysis in support of recommendations to upgrade ASHRAE/IES Standard 90,* LBL-16770.
7. Sullivan, R. and Selkowitz, S. (1984), *Energy performance analysis of fenestration in a single family residence,* LBL-18561.
8. Turiel, I., Boschen, D., Seedal, M., and Levine, M. (1984), "Simplified energy analysis methodology for commercial buildings," *Energy and Buildings 6*, p. 67.
9. Huang, Y.J. and Bull, J. (1985), *Correlation of residential energy use to climate parameters,* LBL-19437.

Federally-Assisted Housing: Plans and Preliminary Analysis*

R. Ritschard, C. Goldman,† E. Vine, R. Diamond,‡ E. Mills, and K. Greely

The potential for energy and cost savings in federally-assisted housing is great.[1] The financial, institutional, technical, and social barriers, however, are also tremendous. There is an indisputable need to reduce long-term energy costs through cost-effective retrofit measures. Investment in such options will maintain and improve the federal housing stock, will reduce energy consumption, will improve tenant comfort levels, and, most importantly, will save federal dollars.

In FY 1985, the Department of Energy initiated at LBL a research effort on federally assisted housing. The major emphasis was placed on publicly supported housing because of the availability of data and because a great conservation potential had been identified.[1,2]

Public housing authorities (PHAs) have begun in recent years to address their need to contain rising energy costs through various retrofit projects funded by the U.S. Department of Housing and Urban Development (HUD), by utility companies, or by the local housing authorities themselves using HUD operating funds. However, actual measured data on energy usage or data on the performance of energy saving measures are virtually nonexistent. Thus, many local PHAs are forced to make decisions about conservation investment strategies without a sound technical basis. The goal of this study is to characterize the existing public housing building stock and energy use patterns, to describe barriers to retrofit activity, and to conduct research that addresses these conservation barriers.

ACCOMPLISHMENTS DURING FY 1985

In FY 1985, we completed a major planning effort. The planning document[3] provides a profile of the existing data on energy use patterns and conservation in public housing. It also contains a description of the physical characteristics of existing buildings and the conservation potential. Finally, it identifies the various technical, informational, economic, behavioral, and institutional barriers that hinder the efforts of local housing authorities and HUD to promote energy conservation. Table 1 summarizes these barriers to conservation.

We also identified a set of research needs that can help overcome existing barriers to conservation in public housing (see Table 2). For each topic, we developed a brief research agenda for pursuit by DOE over the next few years. In addition, we suggest that improvements in existing information transfer mechanisms are needed to help eliminate certain barriers.

Table 1. Summary of barriers to conservation in public housing.

Technical
• Little technical analysis of retrofit actions already taken.
• Decisions made without adequate technical information.
• Conditions of housing may make retrofits impossible.
Informational
• Lack of knowledge about building stock.
• Lack of data on energy use pattens.
• No network for exchange of information.
• Availability and quality of information varies.
Economic, Behavioral and Institutional
• Tenants seldom included in retrofit process.
• No incentive for tenants to conserve energy.
• Cost-effective investments not always implemented.

Table 2. Summary of research needs in public housing.

• Detailed monitoring of retrofit performance.
• Analyze existing retrofit performance data.
• Characterize building stock and energy use trends.
• Evaluate financing and subsidy policy alternatives.
• Develop simplified audit and analysis methods.
• Analyze trends towards individual metering.
• Evaluate energy audits and audit procedures.
• Evaluate tenant incentive programs.
• Develop information dissemination strategies.

*This work is supported by the Assistant Secretary for Conservation and Renewable Energy, Office of Buildings and Community Systems, Building Systems Division of the U.S. Department of Energy under Contract No. DE-AC03-76SF00098.

†Buildings Energy Data Group of the Energy Efficient Buildings Program.

‡Energy Performance of Buildings Group of the Energy Efficient Buildings Program.

In FY 85, we initiated work on two of these research topics: retrofit performance monitoring and analysis of existing retrofit data. We also conducted a preliminary analysis of the impact of existing HUD funding policies on energy conservation activities of the San Francisco Housing Authority. (Presented as a separate Annual Report article.)

Retrofit Performance Monitoring

The objective of this research is to evaluate the installation and performance of a specific retrofit measure (e.g., solar hot water systems) in actual public housing buildings and to assess the effects of the retrofit on the building occupants. By March 1985, we had installed monitoring systems (i.e., data loggers) on four of the ten buildings at Holly Courts, a 118-unit public housing project in San Francisco. The data loggers have been collecting data on the temperatures and flows in the solar hot water system since that time. In addition, we interviewed members of 42 households about their hot water and energy consuming behavior. We present a more detailed account of the occupant behavior portion of this study in an accompanying Annual Report article ("Occupant Behavior in Public Housing").

Analysis of Existing Retrofit Data

Over the last decade, HUD and many local housing authorities have sponsored major retrofit projects in response to the "energy crisis," but little analysis has been performed to quantify the results. We initiated a project last year to evaluate systematically existing utility billing data on past and current retrofit activities at selected public housing sites in order to determine how effective these retrofits had been. In FY 85, we compiled data on 41 retrofit measures at 36 public housing projects. A more detailed description of this work is presented in an accompanying Annual Report article ("Measured Energy Savings From Conservation Retrofits in Public Housing Projects").

PLANNED ACTIVITIES FOR FY 1986

In FY 1986, we will continue the retrofit performance monitoring at one of the Holly Courts buildings and complete the analysis of existing retrofit data. We will also initiate a baseline energy use analysis.

Retrofit Performance Monitoring

We will complete the analysis of energy use, hot water demand patterns, and solar system performance, and conduct a follow-on tenant survey. At the end of FY 1986, we plan to have a better understanding of the variation in performance of the retrofits and variation in domestic hot water usage in the overall context of a whole-building system. We also expect to determine whether the results of this case study can be extended to other buildings, including public housing projects in San Francisco and in other parts of the country and to multi-family buildings in general.

Analysis of Existing Retrofit Data

We will complete the analysis of 41 retrofit measures and prepare a final report that will be circulated to DOE, HUD, and local housing authorities for their review. In addition, we will gather additional data, if available, in areas that are currently not included, such as projects that have implemented shell measures and projects in the South and Midwest, etc. The results of this analysis will provide cost/savings estimates for various retrofit measures that can be compared to similar results from the private sector. The findings should also be useful to HUD's conservation programs by providing some information on what retrofit measures from our sample worked.

Baseline Energy Use Analysis

Our literature search and survey of local housing authorities led to the conclusion that an analysis of baseline energy use data from selected multi-family buildings is needed. This effort includes collecting data on building characteristics and energy use, analyzing the energy use data to adjust for weather and occupant effects, and estimating the influence of building and operating conditions on variations in energy consumption. The results of this analysis can provide useful information in support of developing simplified energy analysis methods for multi-family housing. This research addresses the apparent lack of accurate energy use estimates for multi-family units in both the private and public sectors. The baseline analysis will also be of particular interest to HUD policymakers, who could use the results to estimate Allowable Utility Expense Levels for local PHAs and Utility Allowances for the public housing tenants.

REFERENCES

1. Ritschard, R. and Dickey, D. (1984), "Energy Conservation in Public Housing: It Can Work," *Energy Systems and Policy 8*(3), pp. 269–291.

2. Perkins & Will and Ehrenkrantz Group (1980), "An Evaluation of the Physical Condition of Public Housing Stock," HUD Report No. H2850, U.S. Department of Housing and Urban Development, Washington, D.C.

3. Ritschard, R., et al. (1985), *Federally-Assisted Housing: Characteristics and Research Needs for Multi-year Plan FY 1986–1989,* LBL-19683.

Measured Energy Savings from Conservation Retrofits in Public Housing Projects*

C. Goldman,† K. Greely,† and R. Ritschard

During the last decade, the U.S. Department of Housing and Urban Development (HUD) and local public housing authorities (PHAs) have initiated major conservation programs. Our review of energy conservation work in public housing indicated that in spite of major retrofit activity, little documented information is available on the energy savings from retrofits.[1] This article, which summarizes a more detailed LBL report,[2] describes a project that is part of DOE's long-term program to improve energy efficiency in federally-assisted housing. The objectives of this project are: 1) summarize measured data available on previous HUD conservation initiatives, 2) develop a consistent analytic framework to use in determining energy savings and cost-effectiveness of conservation retrofits, 3) discuss factors that are correlated with high or low energy savings, and 4) provide recommendations on cost-effective retrofit strategies based on measured data.

In this article, we describe sources for retrofit data in public housing and discuss problems encountered during the data compilation process. In addition, we outline the methods that we will use in FY 86 to determine energy savings and cost-effectiveness. We also discuss preliminary results from projects with sufficient data, including distribution of retrofit costs, frequency of specific types of measures, and the physical and demographic characteristics of the included projects.

*This work was supported by the Assistant Secretary for Conservation and Renewable Energy, Office of Buildings and Community Systems, Building Systems Division of the U.S. Department of Energy under Contract No. DE-AC03-76SF00098.

†Buildings Energy Data Group of the Energy Efficient Buildings Program.

ACCOMPLISHMENTS DURING FY 1985

We obtained information on retrofit projects from PHAs, HUD regional offices, and consultants who worked for local PHAs. The data collected typically included metered energy consumption, installed retrofit measures and their cost, the price of the space heating fuel the winter after retrofit, and a brief description of the physical characteristics of the buildings (e.g., conditioned floor area, building and heating system types). We designed a database management system that stores information on project building characteristics and historical energy use and that includes data fields that specifically interface with reporting forms filed with HUD by local public housing authorities (HUD-51466B and HUD-51885).

In 1980, HUD awarded $23 million to 47 PHAs for modernizing oil heating systems and another $5 million to 61 PHAs to install and test innovative energy conservation and solar measures. Comprehensive evaluations were available from only three of 61 PHAs (Trenton, NJ, Greeneville, TN, and St. Paul, MN)[3–5] that participated in the innovative energy grants program. We contacted the Office of Public Housing in HUD for information on the results of retrofit efforts in 14 other PHAs that had received grants. HUD responded that eight of these 14 had not reported any results and that one PHA had never carried out the retrofit and provided LBL with brief progress reports from the remaining five PHAs. Ironically, as of February 1985, two of the five PHAs that submitted progress reports did not include energy use data because of delays in installing the retrofits; hence savings from the retrofits are still not known. Our experience with innovative energy grant recipients illustrates some of the difficulties in obtaining measured data on the results of conservation activities. Moreover, it indicates that, except for a few PHAs, a serious evaluation has not been conducted of HUD's early conservation initiatives.

LBL has also contacted many local PHAs directly in an effort to determine the scope of their

recent retrofit activity, to discover whether evaluations of previous efforts had taken place, and to learn of their plans for future retrofits. The response to this mail survey was particularly encouraging (29 large PHAs, or nearly 40%, returned completed questionnaires). Over the last year, we contacted 10 other PHAs through telephone surveys. From this group, we have received information on building stock characteristics, heating system specifications, fuel types, and maintenance problems in addition to energy retrofit activities. The survey indicates that various retrofits had already been implemented at nearly all PHAs surveyed. Conservation measures/practices include boiler plant modernization, hot water flow restrictors, "shell" weatherization measures (weatherstripping/caulking, insulation, and window replacements), tenant education, meter conversions, lighting retrofits, and solar systems installation. With few exceptions, PHAs have conducted only preliminary analyses of the effectiveness of these measures; typically, LBL still must perform the energy and economic analysis. The survey has so far yielded usable data on 25 projects—14 projects managed by the New York City Housing Authority and 11 projects operated by the San Francisco Housing Authority.

Results

At present, we have compiled data on 36 housing projects that have installed retrofits. The overwhelming majority of projects are centrally heated (89%), and most heat with oil (54%), followed by natural gas (37%). Of the projects with central heating systems, 31% heat with hot water while 38% have steam distribution systems. Roughly half of the projects are low-rise buildings (4 stories or fewer) while 47% are high-rise complexes (Fig. 1). Families occupy 58% of the housing projects, while 22% contain senior units. Almost all projects are master-metered, which typically means that tenants do not pay their space heating and hot water costs directly. There is a large variation in the number of units in each project, ranging from a project with single-family dwellings to 1000-unit apartment complexes with several buildings. Our sample has a distinct regional bias, as the buildings are concentrated principally in the New York–New Jersey area and California. To some extent, this bias replicates the concentration of public housing units in the Northeast corridor. Retrofit data are needed for the Midwest and South, however.

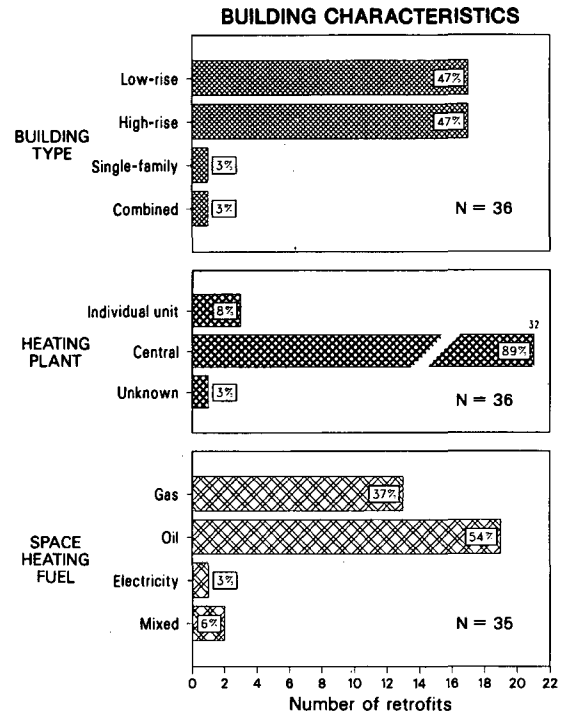

Figure 1. Selected characteristics of projects in the database. Note the bias towards centrally-heated, oil-fueled buildings. (XCG 858-382)

Conservation Strategies

Most retrofits are directed towards improving energy efficiency in the two largest end use areas (measured as a percentage of site energy consumption): space heating and domestic hot water. Figure 2 is a histogram of the frequency with which various retrofit measures were installed in the 36 projects. In most cases, more than one measure was installed at each project. The median first cost is approximately $550/unit for the 38 projects. Many authorities confined their retrofit efforts to low-cost measures. For example, retrofitting existing heating systems with improved controls was the most common measure, with first costs ranging from $100–450/unit. Examples of retrofits included in this category are thermostatic radiator vents, boiler aquastats, outdoor resets, and cutouts. Retrofits to reduce domestic hot water use were also frequently implemented. The San Francisco Housing Authority installed solar domestic hot water systems at six projects, and wrapped hot water tanks at two other pro-

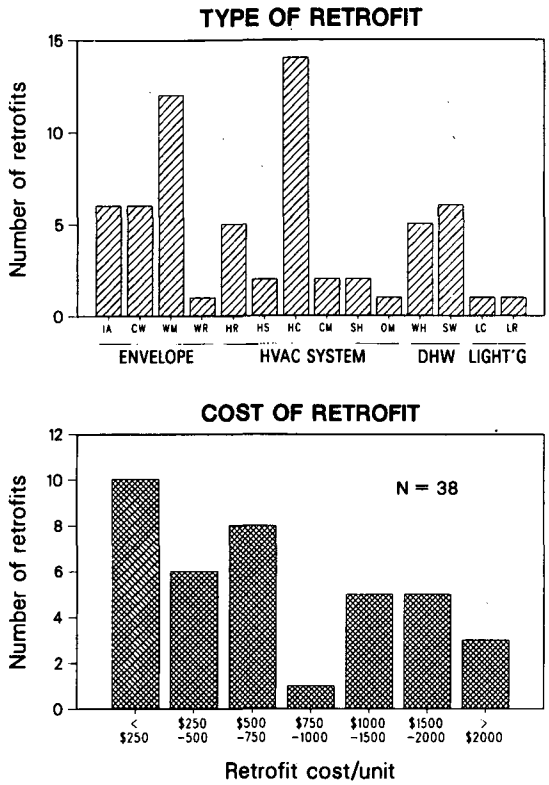

Figure 2. Retrofit characteristics. "Type of Measures" refers to measures implemented singly or in combination with other retrofits. Therefore, the number of retrofits shown here is greater than the number of analyzed retrofits. "Cost of Retrofits" is the initial cost, in 1985 dollars. Retrofit Codes: AI = Attic Insulation, CW = Caulk & Weatherstrip, WM = Window Measures, WR = Window Replacement, HR = Heating System Controls, CM = Computerized Heating Control System, SH = Solar Space Heat, OM = Operations and Maintenance, WH = Water Heater, SW = Solar Domestic Hot Water, LC = Lighting Controls, LR = Lighting Replacement. (XCG 858-380)

jects, while several Northeast housing authorities installed separate domestic hot water boilers. Window measures were also extremely popular. For example, the New York City Housing Authority installed double-glazed thermal-break aluminum windows in nine apartment complexes. This retrofit was fairly expensive, averaging $1070/unit in the nine buildings. Several local authorities indicated that window retrofits were favored by tenants because of their high visibility, i.e., they tend to improve building appearance and security. Several of the retrofit strategies, e.g. the solar retrofits, had particularly high initial capital costs; hence, at these projects, we will be taking a close look at cost-effectiveness as well as the energy savings levels, particularly given that existing tax credits (which will soon expire) improve the attractiveness of these investments.

Conclusion

During FY 85, we gained first-hand experience with problems that make it difficult to determine energy savings attributable to conservation measures. These include: 1) absence of good record-keeping, 2) limited contact between local public housing authorities and the buildings research community, and 3) little awareness of the potential benefits to the PHA of evaluation. We hope this study, when completed, will at a minimum summarize measured data on retrofit efforts in public housing. Optimally, it will provide recommendations on what conservation measures work best for specific building and heating system types. In addition, we hope the database management system and analytic methods that we are utilizing will serve as an example to HUD and local public housing authorities of the feasibility and importance of developing an energy management accounting system that incorporates historical energy use and occupancy, weather, key building characteristics, and economic data in order to track energy use patterns and determine energy savings and cost-effectiveness.

PLANNED ACTIVITIES FOR FY 1986

In FY 86, we will obtain and report results from the energy and economic analyses and target further data collection efforts in areas that are currently under-represented. We will focus on data collection in the following areas:

- projects located in the South and Midwest,
- projects that have implemented shell measures (e.g., attic and wall insulation, infiltration-reduction),
- retrofit efforts in buildings with individual apartment heating units or that heat with gas or electricity.

REFERENCES

1. Ritschard, R.L. and Dickey D. (1984), "Energy Conservation in Public Housing: It Can Work," *Energy Systems and Policy 8*(3), p. 269.
2. Goldman C.A., Greely K., and Ritschard R.L. (1985), "Measured Energy Savings from Conservation Retrofits: Status Report," for the U.S. Department of Energy, Building Systems Division.

3. Gold, C. (1982), "The Page Homes Demonstration Project for the Application of Computers to Energy Conservation in Public Housing Authority Projects," Bumblebee Energy Systems Inc., Trenton, NJ.
4. Solar Applications Branch, Tennessee Valley Authority (1984), "Greeneville Passive Solar Retrofit Demonstration," TVA/OP/ECR-84/62, TVA, Knoxville, TN.
5. Patten, C., Sherman M., and Shapiro, B. (1982), "Case Studies of Successful Energy Conservation Programs in PHA'S: St. Paul, Minnesota," Council of Large Public Housing Authorities, Boston, MA.

Impact of HUD Subsidy Policy on Retrofit Savings for Public Housing Authorities*

E. Mills and R. Ritschard

The cost-effectiveness of energy conservation retrofits in the public housing sector must be viewed from a special financial perspective. Rather than attributing costs and benefits to a single party, it is necessary to determine cost-effectiveness for two actors—the U.S. Department of Housing and Urban Development (HUD) and the public housing authority (PHA). Our calculations show that actual savings can be negative for the housing authority, even for retrofits with very short payback periods according to the single party model. The exact distribution of benefits is determined by the HUD subsidy framework—the Performance Funding System (PFS). Under the PFS, the housing authority retains roughly one and one-half years of utility expense savings over the life of the retrofit. Key policy questions center around the influence such a sharing of savings may have on the choice made at the housing authority level of whether to invest in conservation, and if an expanding "pie" could be enjoyed by all actors under an alternative allocation of costs and benefits.

This work is a follow-on to our analysis of energy savings using actual pre- and post-retrofit PHA utility data normalized to long-term average weather conditions. The financial results discussed here differ significantly from ones based on the simple payback time and presented in a previous report.[1]

ACCOMPLISHMENTS DURING FY 1985

Modeling the PFS

We developed a micro-computer spreadsheet to model the allocation of costs and benefits of retrofit activity between HUD and the PHA, based on the subsidy system rules. The subsidy for PHA utility expenditures, known as the "Allowable Utility Expense Level," is the product of expected consumption and price for each fuel. Consumption is estimated by calculating an average based on three previous years of utility billing data. This estimate is reviewed at year-end and compared to the actual energy use levels. HUD recaptures any savings resulting from lower than expected *prices* or reimburses the PHA for additional energy expenditures resulting from price increases. More importantly, if *consumption* changes, HUD and the PHA share the difference between estimated and actual consumption on a 50/50 basis. As a result, during the years following the installation of a retrofit the subsidy decreases along with the rolling base. By year six the subsidy is completely adjusted; i.e., HUD recaptures all of the energy savings. The PHA retains roughly one and one-half years of the lifetime energy savings. Table 1 illustrates the year-by-year distribution of retrofit energy savings.

The ultimate distribution of energy savings also depends on how the retrofit and associated maintenance costs are paid for. Energy improvements are ordinarily capitalized with HUD Modernization Funds. In rare cases, a housing authority will pay for the retrofit with general operating subsidies (intended for non-energy applications) or will con-

*This work was supported by the Assistant Secretary for Conservation and Renewable Energy, Office of Building and Community Systems, Buildings Systems Division of the U.S. Department of Energy under Contract No. DE-AC03-76SF00098.

Table 1. Annual distribution of HUD/PHA energy savings under the Performance Funding System. We assume that the retrofit is installed in the middle of year one.

Year	PHA % share	HUD % share
0	—	—
1	25.0	25.0
2	50.0	50.0
3	33.5	66.5
4	16.5	83.5
5	0.0	100.0

tract with an Energy Service Company (ESCO) to finance the project. Many retrofits also have substantial associated maintenance costs or savings, for which the housing authority is not compensated.

Methodology

Using the PFS treatment of savings and costs, we can determine the net present values (NPVs) of costs and savings, over the life of a retrofit, for HUD and the PHA. We begin with *measured* energy savings, from analysis of housing authority monthly utility bills, and normalize consumption for differences in weather conditions and, when possible, changes in occupancy before and after the retrofit. We use local energy prices, reported by the PHA, to compute the dollar savings in year one and apply DOE residential price escalation forecasts to estimate the effect of future price changes.[2] We then distribute the annual savings between HUD and the PHA according to the factors developed in Table I. The retrofit cost is deducted from the present value of HUD's energy savings if the retrofits are paid for by HUD under its Modernization program and from the housing authority savings if the PHA pays for the retrofit out of general operating subsidies. The present value of any associated maintenance costs, over the retrofit lifetime, is deducted from the PHA's energy savings.

Case Studies

We completed an analysis of the impact of the PFS on a retrofit project undertaken in 1982 by the San Francisco Housing Authority (SFHA). The Authority insulated and weatherized a number of multi-family, low-rise buildings utilizing a zero-interest loan program available through their local utility. We analyzed utility bills for 1827 dwelling units distributed in five projects and calculated gas savings from three years of utility bills, two years before and one year after the retrofit. The simple payback time for the measures was 2.2 years, under the assumption that one party finances the retrofit and retains the savings. However, the PFS methodology shows that the actual net present value of the retrofit savings and costs is −$78,600 (−$43/dwelling unit) for the Authority and $1,426,900 ($781/dwelling unit) for HUD.

The negative savings occurred because the San Francisco Housing Authority capitalized the retrofit with their general operating subsidies rather than Modernization Funds intended for conservation investments. Although the PHA obtained a zero-interest loan, the present value of eight years of payments exceeded that of their energy savings. Figure 1 illustrates the resulting distribution of gas savings between HUD and the PHA and the relative size of the loan annuity.

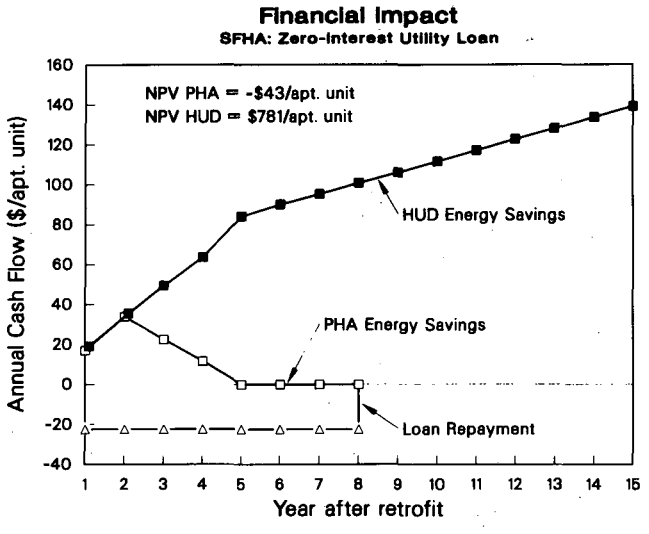

Figure 1. Allocation of energy and cost savings from a retrofit package that includes attic insulation, water heater retrofits, caulking/weatherstripping, thermostat clocks, and heating controls under the Performance Funding System. The present value of the loan payments is subtracted from the PHA energy savings in the net present value (NPV) calculation because the funds are diverted from general operating subsidies. (XCG 865-7232A)

Conclusions

Given the characteristics of the Performance Funding System, cost evaluation methods such as the simple payback time can not capture the differences in benefits for HUD and the PHA. Energy savings may be insufficient to balance capital costs paid by the authority. The project we analyzed had a simple payback time of only 2.2 years, and yet produced *negative* savings for the PHA and substantial positive savings for HUD because the authority paid for retrofits with general operating subsidies. Following is a list of preliminary findings derived from the case study and from examination of the subsidy system rules.

- A one and one-half year payback time is required if the PHA finances the retrofit out of general operating subsidies.
- Negative savings can result for the authority if the retrofit requires new maintenance expenditures for which the authority receives no subsidy supplement.
- An authority has little or no incentive to insure that savings persist beyond year five. It may in fact be profitable for them to let maintenance programs lapse once HUD has recaptured the yearly energy savings.
- If a retrofit fails to save energy, savings degrade with time, or savings are negative, HUD experiences a greater loss than the PHA.
- It is difficult for the PHA to contract with private sector energy service companies (who are normally compensated from the energy savings) because HUD recaptures most of the savings.

PLANNED ACTIVITIES FOR FY 1986

Our next step is to develop the model further to reflect various innovative conservation investment strategies. We will develop prototypical spreadsheets, using LOTUS 1-2-3, to represent these strategies and compare their relative financial impacts. The spreadsheets will be useful to PHAs interested in planning future retrofit projects and evaluating previous ones. They will assist policymakers in analyzing the quantitative impact of alternative utility subsidy options.

REFERENCES

1. Goldman, C.A. and Ritschard, R.L. (1984), *Energy Conservation in Public Housing: A Case Study of the San Francisco Housing Authority*, LBL-17994.
2. U.S. Department of Energy (1985), *Energy Prices and Discount Factors for Life-cycle Cost Analysis*, prepared by the National Bureau of Standards, NBSIR85-3273.

Analysis of Occupant Behavior and Energy and Hot Water Consumption in Public Housing*

E. Vine and R. Diamond

Lawrence Berkeley Laboratory has been involved in the analysis of energy-related issues in public housing since the early 1980s. The principal objective of this research has been to understand how energy is used in public housing by analyzing baseline energy use, energy conservation retrofits, and tenant behavior. In the past year, the Energy Analysis Program and the Energy Performance of Buildings Group (of the Energy Efficient Buildings Program) focused their research on tenant behavior as part of a research project that was monitoring the performance of a domestic hot water retrofit at a public housing project in San Francisco (see the other Building Energy Analysis articles in this report).

ACCOMPLISHMENTS DURING FY 1985

A key activity of DOE's Building Energy Retrofit Research project is to improve the energy efficiency of the nation's public housing stock. During the past year, a research plan was drawn up that identified short-term research needed to meet this ambitious and important goal.[2] One of the research areas identified in the plan was the need to conduct retrofit performance monitoring. The purpose of the retrofit monitoring is to evaluate the installation and perfor-

*This work was supported by the Assistant Secretary for Conservation and Renewable Energy, Office of Buildings and Community Systems, Systems Analysis Division of the U.S. Department of Energy under contract DE-AC03-76SF00098.

mance of specific retrofits, and to assess the effects of the building occupants. Our review of energy conservation work in public housing also indicates that, in spite of major retrofit activity, little effort had been made to evaluate the effect of such activity. Previous evaluations relied almost exclusively on whole-building utility billing data or on engineering estimates.[3] These data do not permit analysis of the significant factors that affect retrofit performance, nor can they explain differences between predicted and actual energy savings. Detailed monitoring of public housing buildings, however, allows us to characterize the energy savings more fully, evaluating the installation and performance of the retrofits, as well as the effect of building occupants.

In October 1984, we began a hot water retrofit monitoring project in conjunction with the Housing Authority of San Francisco. The housing project selected for this study was Holly Courts. The goal of the project was to evaluate the performance of a solar domestic hot water retrofit, looking not only at the performance of the system (the supply side), but also at the hot water usage patterns of the residents (the demand side). This is one of the first detailed evaluations of a hot water retrofit in a multifamily building; the results will thus have important applications for sectors besides the public housing stock.

Holly Courts, California's first public housing project (1939), is located in south-central San Francisco. While the climate can be cool and foggy at anytime of year, the sun shines on an average of 66% of the daylight hours. San Francisco has 3080 annual heating degree days (base 65°F) and 39 cooling degree days (base 65°F). Half of the units have a southern exposure. The 118 apartments are located in ten two-story, bungalow-style buildings, and the project has 48 one-bedroom units, 60 two-bedroom, and 10 three-bedroom units, housing over 350 residents. The average apartment size is 794 ft^2. The buildings have concrete construction and originally were uninsulated. However, blown-in insulation (R-19) was installed between the roof deck and the second story ceiling in September, 1982. The original wood casement windows were replaced in the early seventies with single-pane aluminum-frame windows. The apartments are individually heated with a free-standing gas heater; domestic hot water is provided by gas-fired central boilers in each building. The tenants are billed directly for their gas usage (for space heating and cooking) and for electricity. The Housing Authority pays for the gas for the domestic hot water. The average energy consumption per unit in 1984–85 was 210 kWh per month for electricity, and 21 therms per month for gas. Average monthly domestic hot water gas consumption per unit is about 32 therms, larger than the gas use for space heating.

The retrofit to the domestic hot water system involved installing a total of ninety-four 4 ft × 10 ft solar collector panels on the roofs of the ten buildings. The solar collectors were plumbed into storage tanks located in the boiler rooms in the basements of the buildings. The solar storage tanks were connected into the existing domestic hot water system for the building. Installation began in November, 1984, and by January, 1985, the solar systems were operational in all ten buildings. By March, 1985, the first of our monitoring systems were installed in the boiler room in one of the buildings at Holly Courts. In the next few months, we installed three additional data loggers in different buildings. We installed a weather station on the roof of one of the buildings to collect local temperature, wind, and solar data.

The data acquisition system was a flexible, programmable, modular system that operates unattended in the boiler rooms at Holly Courts. Real time data for site weather conditions, individual building domestic hot water use, and the contribution of the solar system were collected and converted to hourly averages. Data were stored in the system's memory and were transferred weekly to LBL by a phone modem. We calculated the following quantities from the monitoring: quantity of hot water used, temperature of hot water delivered to occupants, heat loss in building hot water pumped loop, temperature of cold and solar preheat water supply, and operation time and average collection efficiency of the solar system.

Table 1 shows the domestic hot water consumption for the individual buildings from April to July, 1985.

The average household consumption, 88 gallons/day, appears to be higher than any of the average values given in the literature. In the coming

Table 1. Holly Courts hot water consumption.

Bldg.	Units	People[a]	Gal/day[b]	Gal/unit/day
D	9	19	755	84
E	15	35	1346	90
F	15	46	1447	96
G	9	21	678	75
TOTAL	48	121	4226	88

[a]Estimated from 87% of units surveyed.

[b]Average from 4/85–7/85.

year, we plan to examine the literature in greater detail to compare our domestic hot water usage pattern with those reported in other studies.

We conducted a survey of the occupants of Holly Courts in order to obtain information to:

1. describe daily domestic hot water use profiles,
2. examine how hot water use profiles affect the performance of the solar system,
3. examine how the solar hot water retrofit affects hot water use profiles,
4. compare occupant-reported hot water usage with actual hot water usage,
5. compare hot water use and energy consumption.

We conducted the survey in May of 1985, five months after the solar retrofits were installed. We completed interviews at 42 of the 48 units (88% response rate) in the four buildings being monitored. The interviews, conducted in English and Spanish, took approximately 20 minutes each. We asked residents about their daily hot water use in the bathroom and kitchen, their satisfaction with their hot water, their awareness of the solar system, their attitudes towards conservation, and standard demographic variables.

Respondents in our survey were typically not married, female, about 45 years old, and had less than high school education (Tables 2 and 3). Almost 40% of the sample was black, 32% were white, and 25% Hispanic. Over one-half the sample were unemployed or retired with only 12% working full-time, typically in a service occupation. In general, the population was stable with relatively little turnover in household composition from the previous year and with relatively long tenancy in the public housing complex.

Table 2. Holly Courts occupant profile.

	Avg.	S.D.[a]	Range	No.
Number of years lived in Holly Courts	9.5	6.7	1–28	42
Number of years lived in same apt.	8.2	6.6	1–23	42
Age of respondent (years)	45.5	16.7	21–82	40
Education of tenant (years)	10.6	4.0	0–17	40
Avg. household size (people)	2.6	1.6	1–9	42

[a]S.D. = standard deviation.

Table 3. Holly Courts frequencies.

Sex of respondent (N = 42)	7.1%	Male
	92.9%	Female
Ethnicity of respondent (N = 41)	4.9%	Asian American
	39.0%	Black
	31.7%	Caucasian
	24.4%	Hispanic
Marital status of respondent (N = 42)	40.5%	Single
	7.1%	Married
	28.6%	Separated
	23.8%	Other
Employment status of respondent (N = 41)	12.2%	Working full time
	22.2%	Working part time
	14.6%	Retired
	48.8%	Unemployed
Occupational status of respondent (N = 11)	18.2%	Professional
	9.1%	Craft
	72.7%	Service
Changes in the number of people occupying a unit in the last year (N = 39)	25.6%	Yes
	74.4%	No

Hot water consumption varies greatly over a daily cycle. A typical daily profile shows peaks in the morning and evening indicating family bathing practices, peaks around meal times for cooking and dish washing, and scattered peaks throughout the day for clothes washing. For example, the average daily hot water consumption for a one week period in Building D, a nine-unit building, varied between 30 and 40 gallons per hour, with peak rates exceeding 150 gallons per hour.

We used the survey data to reconstruct the end use breakdown for the daily profiles by combining their reported frequency of use with standard usage factors. The largest daily hot water use (43% of total) was for bathing and showering, which was split evenly between the morning and evening periods. Clothes washing was the next largest user (30%), and occurred during the morning, afternoon, and evening periods, with the greatest usage in the morning. The third main hot water use was for dish washing (26%), and followed the same pattern as clothes washing.

We combined the reported data on time and frequency of hot water use to form an average daily

profile, which was compared to the measured average daily profile (Fig. 1). (We added the average measured nighttime flow to the reported data to account for leaking faucets.) The profiles are remarkably close, giving support to the reliability of the occupant reported data. Interestingly, the profiles in no way resembled the standard profile for average daily consumption reported in the literature and widely used for calculating collector sizes, and estimating performance of retrofits.

Not only are the usage patterns at Holly Courts unusual, but the absolute water consumption is higher than usual. This raises the question of whether this is an anomaly, or whether the results can be extended to other buildings, including other public housing projects in San Francisco and elsewhere, and to multifamily buildings in general.

PLANNED ACTIVITIES FOR FY 1986

Our findings so far indicate that evaluation of retrofits is difficult and that even such straightforward questions as energy savings and costs are hidden by a complex interaction of physical, institutional, and behavioral issues. While we have a better understanding of the whole system, there are still important questions to answer, including the following:

1. What is the variation (seasonal, weekly, weekday/weekend, daily) in performance of retrofits?
2. What is the variation (seasonal, weekly, weekday/weekend, daily) in domestic hot water usage?
3. How does domestic hot water usage compare with energy consumption?
4. What are the sociodemographic differences between high and low water consumers?
5. Why do Holly Courts' daily profiles differ from those reported in the literature?
6. How can we explain differences in water usage between different buildings—e.g., different boilers, circulation losses, etc?
7. How does occupant-reported behavior compare with actual usage?
8. What additional retrofits would be appropriate and cost-effective for these buildings?
9. How generalizable are the results from this study to other public housing and multifamily housing projects (in San Francisco and elsewhere)?

We hope to derive answers to these questions from analysis of data we have collected, and other existing data, literature reviews, and, possibly, another survey of Holly Courts.

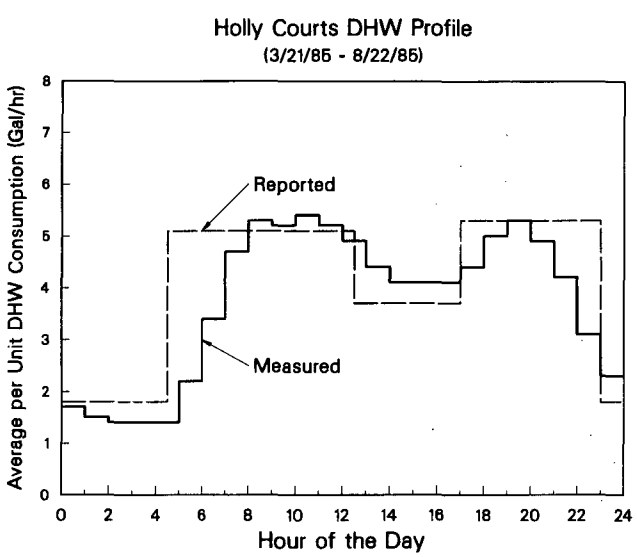

Figure 1. Comparison of reported and measured domestic hot water consumption by time-of-day. (XCG 8512-552)

REFERENCES

1. Ritschard, R., *et al.* (1985), *Multi-Year Research Plan for Federally-Assisted Housing,* LBL-19683.
2. Perkins & Will and Ehrenkrantz Group (1980), *An Evaluation of the Physical Condition of the Public Housing Stock*, H-2850 Department of Housing and Urban Development, Washington, D.C.

Home Energy Rating Tool: Follow-On Analysis*

R. Ritschard, C. Hsui, and Y.J. Huang

During FY 1984, we initiated an effort for the California Energy Commission (CEC) to develop a simplified energy rating tool for existing houses as part of a Home Rating and Labeling Demonstration Project. The major goals of this work are: (1) to develop and field-test a simple and reliable tool for estimating the energy efficiency of typical existing homes and to assign ratings to them, and (2) to explore various delivery mechanisms for promoting the use of the rating tool. The CEC selected three areas of the state to test three delivery mechanisms. The City of Roseville will implement a program in which the city, as an electric utility, will offer the home rating and labeling service. As the model for a utility-focused delivery mechanism, Roseville will conduct a certified audit of homes and deliver the appropriate rating label. The City of Pasadena will operate a program very similar to that of Roseville but, as the model for the government-focused delivery mechanism, will use city building officials to certify a home's rating and provide labels. Finally, the County of Marin will test the rating program through realtors. Trained realtors operating within the county will market the rating and labeling service and, with some assistance from the county, provide audits and labels on their own.

The follow-on work described here illustrates the feasibility of translating complex technical information, which result from a series of parametric simulations using a state-of-the-art computer code (DOE-2.1), into a simplified format ("slide rule") that can be used by a non-technical audience. If the rating tool in combination with the delivery mechanisms being tested should prove successful, it may have applicability to other areas in California as well as to other parts of the country.

ACCOMPLISHMENTS DURING FY 1985

During FY 1985, we completed a final version of the home energy rating tool for each of three California climate zones: Zone 3 (Marin), Zone 9 (Pasadena), and Zone 12 (Roseville). All values used in the rating tool, with the exception of those for domestic hot water, are based on DOE-2.1A simulations. (Test runs with DOE-2.1B showed insignificant differences in total loads.) The domestic hot water values used on the rating tool are calculated using standard CEC procedures. During the first part of the analysis, we compared consecutive DOE-2 runs to determine the Δ heating and cooling loads for each conservation measure (e.g., R-30 ceiling compared to R-19 ceiling, etc.) while holding other parameters constant. We performed these DOE-2 simulations on the one-story and two-story prototypes for various thermal integrities (ceiling, wall and floor insulation, different infiltration levels) and window measures (i.e., window area, number of panes, type of window sash, shaded and unshaded) in the three climate zones.

After developing a database of Δ heating and cooling loads, we regressed these Δ loads against Δ steady-state conductances to calculate the component loads for each individual building component. We used this analytical approach to develop an energy calculating slide rule for new site-built, single-family houses in support of a Department of Energy program.[1] In our previous work, we showed that this method is reliable and allows one to recompose DOE-2 energy budgets for any particular combination of conservation measures within the database to a high degree of accuracy (within 8% for heating and 12% for cooling). We describe the methodology in greater detail elsewhere.[2] These component loads, with a few minor modifications, are converted into heating and cooling normalized units, which appear on the rating tool.

Figure 1 shows the draft rating tool for climate zone 3. To use the rating tool, one follows a series of sequential steps indicated by the heavy lines on the rating tool sleeve. First, the user aligns each of the six tabs (A-F_N) to the appropriate level of conservation for the ceiling, walls, floor, infiltration, window area (including total south window area), window sash type, glazing levels (i.e., single-, double-, or triple-pane), and presence or absence of thermal mass. The thermal mass side of Tabs E and F (i.e., E_M and F_M) are used only for houses where over half of the floor area (or an equivalent amount of wall area) has exposed concrete or tile that is in the path of direct sunlight. Tabs A_1 through D_1 are used for one-story houses, while the reverse sides of each tab, which are labeled A_2, etc., are used for two-story buildings.

The user computes an energy rating by adding the numbers for both heating and cooling that appear in the small windows to the left of the six

*This work was funded by the California Energy Commission under Contract No. 400-83-009, with facilities support provided by the U.S. Department of Energy under Contract No. DE-AC03-76SF00098.

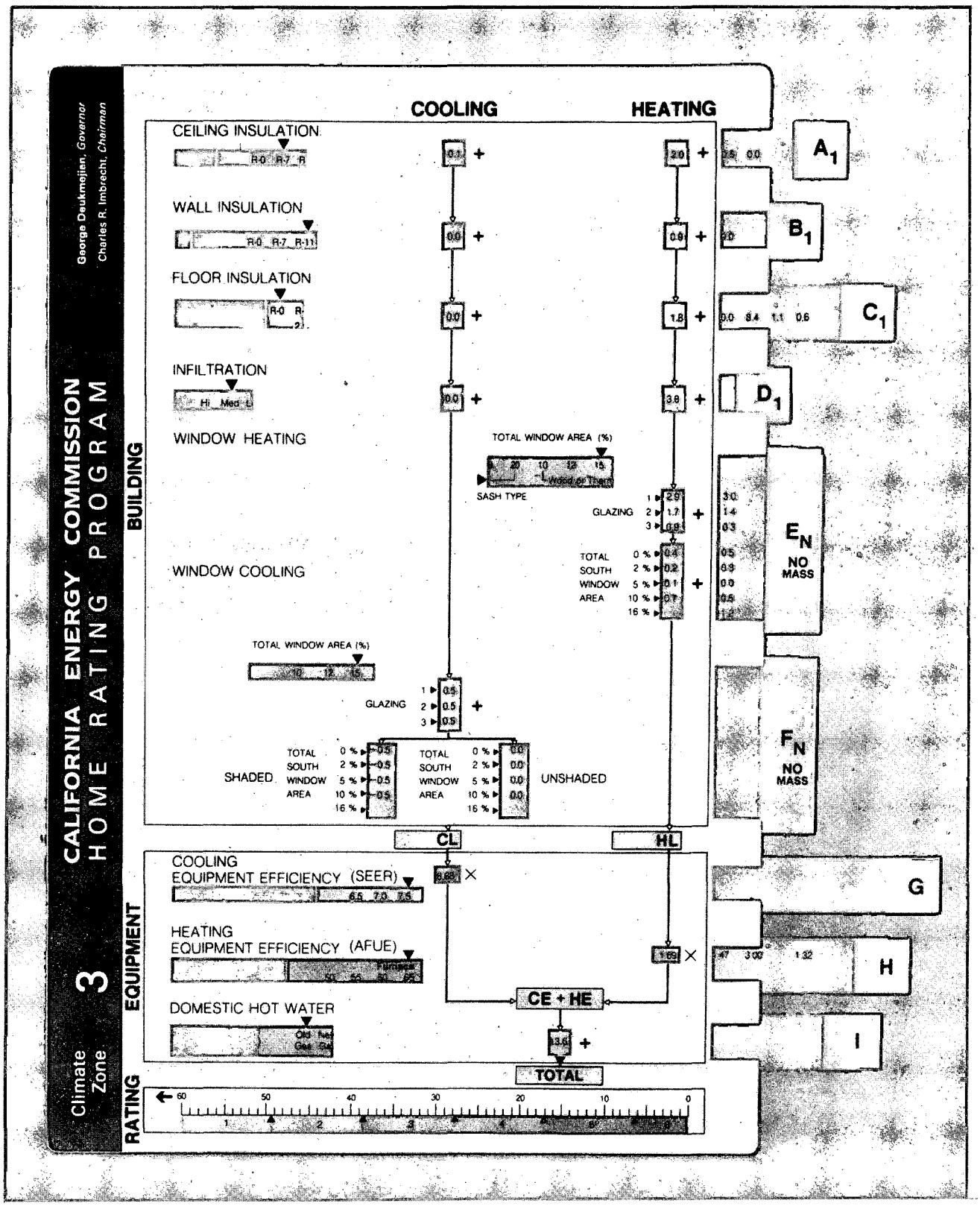

Figure 1. Draft rating tool for climate Zone 3. (CBB 8512-10177)

tabs. The sum of these values represents the heating and cooling load of the house. One then converts the loads into energies by multiplying them by the appropriate heating and cooling equipment efficiencies from windows adjacent to Tabs G and H. Finally, the domestic hot water system (including solar) is considered on Tab I, and the calculated value is added to the heating and cooling energy use to produce a final house energy usage (in the Total window). The user can then get credit for additional energy conservation features, such as setback thermostats, low-flow shower heads, and outlet gaskets, by subtracting the estimated savings (available on a supplemental form) from the total energy use calculated on the rating tool. This final value is converted into a energy rating scale on the tool that ranges from 1 (poorest) to 6 (best). The scale was set using the energy budget for a house that met the 1978 new building standard as a "3," and a current Title 24 house (1982 new building standard) as a "5." All rating are scaled linearly from these two benchmarks. Because of the differences in their climates, there are different rating tools for each demonstration city.

Due to printing delays at the CEC, the demonstration period did not begin until the end of FY 1985. At that time, the County of Marin withdrew its participation in the program because of an unwillingness on the part of the realtors to assume responsibility for rating properties that they would later market. The demonstration phase, however, will continue in the other two communities during most of 1986, and a follow-on evaluation program will be initiated.

PLANNED ACTIVITIES FOR FY 1986

In FY 1986, we will prepare a report that documents the technical assumptions and methodology used to develop the rating tools for the three demonstration areas. In that report, we will describe the prototype buildings and modeling assumptions used in the computer simulations and compare them to the analysis used to generate the California Title 24 budgets. Next fiscal year, we will also extend our analysis to the other 13 California climate zones. We will complete our analysis of all 16 climate zones using DOE-2.1C, the most up-to-date version of the program, which will then be available. We anticipate that after the demonstration period has been completed, we will make modifications to the rating tool format, if necessary, and produce a complete set of rating tools for all of the climate zones.

An important aspect of the CEC Program is to evaluate the process of rating and labeling houses. Next year we will determine the effectiveness of the delivery mechanisms used during the demonstration projects in the Cities of Pasadena and Roseville. The goal of this evaluation is to determine the usefulness of the home rating system to homeowners, lenders, project proponents, and others in the building industry. To meet the goals of the process evaluation, we plan to:

1. Identify and recommend solutions to technical and delivery problems identified during the demonstration phase.
2. Review, on-site, a sample of labeling conducted by each pilot demonstration city.
3. Identify any additional training that may be required and the specific target audience (i.e., local government staff, local utility staff, etc.).
4. Compare delivery mechanisms utilized in CEC demonstration projects and identify strengths and weaknesses of each approach.
5. Identify other potential users and uses for the home rating system.

REFERENCES

1. Huang, Y.J., *et al.* (1985), *Methodology and Assumptions for the Evaluation of Heating and Cooling Energy Requirements in New Single-Family Residential Buildings,* LBL-16342.
2. Huang, Y.J, Ritschard, R., and Bull, J. (1985), *Simplified Calculations of Energy Use in Residences Using a Large DOE-2 Database,* LBL-20107.

Performance of Daylighting Systems in Commercial Buildings in Hot Climates: Singapore Case Study*

M. Levine and I. Turiel

The term daylighting encompasses various strategies for using light from outside a building to replace artificial interior lighting. It is potentially a powerful way to reduce building energy use in hot, sunny locations.[1] Although modern interest in daylighting is now almost ten years old, it has not been extensively applied.[2] This lack of implementation persists in spite of the substantial potential benefits from reduced energy use and equipment costs that are possible, especially in commercial buildings.

Often architects are not familiar with the concept of daylighting, and even when they are aware of its advantages, methods of evaluating the benefits of various daylighting configurations are not widely available and are complex.[3] Consequently, choosing an optimal daylighting strategy is beyond the reach of most practicing building designers.

The long run objective of this research is to develop a tool that can promote wider use of daylighting in commercial buildings at a specific location, Singapore. This tool should simplify the task of choosing an optimal daylighting strategy by permitting building designers to estimate and compare the potential reductions in energy use that would result from various daylighting approaches. Later the algorithm will be incorporated in a microcomputer program and made available to Singapore's architects and building engineers.

ACCOMPLISHMENTS DURING FY 1985

Methodology

Our general approach is to model the effects of daylighting in a reference Singapore office building and then use physical understanding to generalize the results obtained from a small set of simulation runs. We began simulating the energy performance of a typical Singapore office building. We used the DOE-2.1B program to simulate energy use.[4,5] We augmented hourly weather data for 1979 obtained from the National Climatic Center with measurements of Singapore's direct and diffuse solar radiation.[6] Figure 1 is a schematic of the floor plan of the reference building used. The full building has ten stories with a total conditioned area of 5250 m^2. We assumed the 100 m^2 of unconditioned interior zone on each floor to be thermally isolated from the remainder of the building.

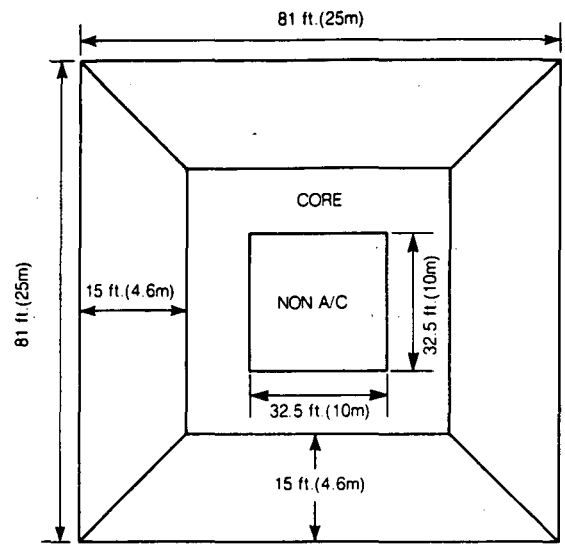

Figure 1. Schematic of typical floor of Singapore reference building: ten floors, 5,500 ft^2 of conditioned space/floor. (XBL 8512-5193)

This building represents a favorable design for daylighting because it has a large perimeter zone that can benefit from daylighting and a small core zone that cannot. However, the techniques developed in the present research can be accurately applied to various building designs.

To perform a large series of parametric studies easily, we used a single-floor module prepared by other researchers at Lawrence Berkeley Laboratory for an extensive study of daylighting in various U.S. locations.[7] Figure 2 shows two views of this module. The module can be viewed as a typical floor of a multi-story building. We applied results from the analysis of the module to the full building shown in Fig. 1.

The analysis of daylighting systems involved simulating photosensors at 5 and 10 m from the windows to measure interior lighting levels, control systems that adjust the artificial lighting levels within the perimeter zone of the building in response to light from outside the building, and internal shades or curtains to reduce glare. We did not consider more sophisticated or complex systems that might

*This work was supported by the U.S. Agency for International Development, through the U.S. Department of Energy under Contract No. DE-AC03-76SF00098.

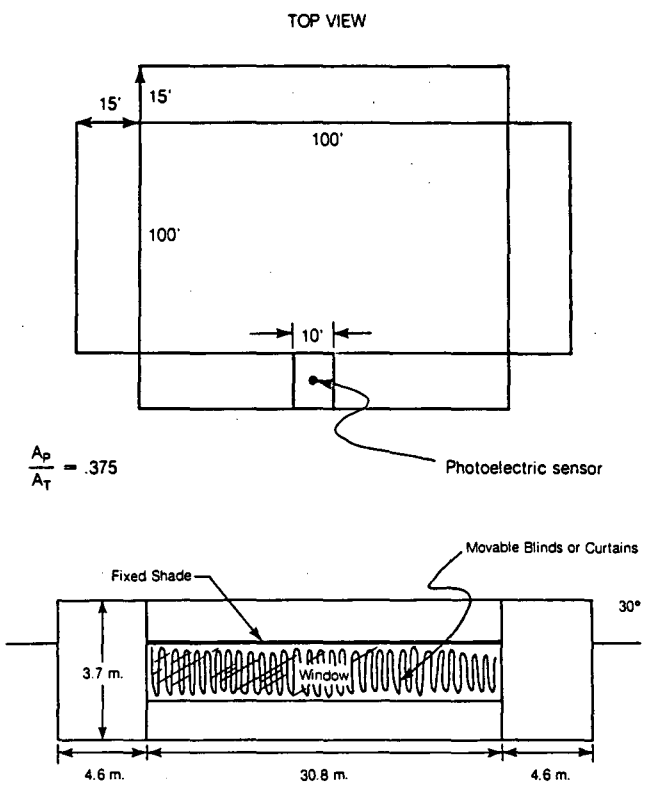

Figure 2. Module run to provide data for full DOE-2 analysis of reference office building. [(top) XBL 8512-5194, (bottom) XBL 8512-5195]

further increase energy savings or improve the quality of lighting, for example, "light shelves," automatic shading devices. Such additions are not likely to change the effectiveness of daylighting systems significantly in most applications.

Major Issues in the Analysis of Daylighting

The effects of daylighting depend on the characteristics of the external environment and of the building itself. For our purposes, the external environment is defined by the hourly weather data. Several characteristics of Singapore's sunshine are particularly relevant to daylighting possibilities. Although lying near the equator, Singapore does not receive intense solar radiation. High cloud density throughout the year limits the shine hours to 30 to 50 percent of daylight hours. Further, the high moisture content of the air creates a condition in which the diffuse component of solar radiation falling on a horizontal surface accounts for about 43 percent of the total radiation on an average day. Approximately 70 percent of the radiation on the vertical walls is diffuse. The high proportion of diffuse radiation in Singapore improves the performance of daylighting systems, as diffuse radiation provides usable light with relatively little glare.

A number of variables that are subject to the control of the building designer affect the performance of and energy savings resulting from daylighting systems. These include:

1. the window area (expressed for our purposes as window-to-wall ratio, WWR),
2. the amount of visible radiation transmitted through glass (TVIS),*
3. the area of the building that is in the perimeter zone (i.e., near windows),
4. the external shading of windows,
5. the lighting power (in W/m^2),
6. lighting level (in lx) in the perimeter zone of the building,
7. the type of controls used to reduce artificial lighting in the perimeter zone (specifically continuous or step controls), and
8. the methods of controlling glare problems introduced by daylighting (internal curtains, blinds, or shades).

Table 1 shows qualitatively how these eight parameters could be expected to affect lighting, cooling, and total energy use in a building. As the table shows, the direction of the net effect on total energy use is unclear for the key daylighting parameters. In this study we attempted to access all these relationships quantitatively. We then found ways to optimize use of daylighting techniques in a reference building by computer simulation. Later, we generalized these results in such a way that they could be applied to other Singapore office buildings.

The product of the window area of a building and the visible transmittance through the window material is a measure of the amount of visible radiation that is available to replace artificial light in the building. Window area divided by total envelope area is termed the window to wall ratio of a building (WWR). Thus, in a daylighted building the amount of lighting energy saved increases as the product of

*The passage of radiation through materials is impeded differently at different areas of the spectrum. The shading coefficient (SC) measures the fraction of total radiation that passes through a material, whereas the TVIS refers only to the visible part of the spectrum.

Table 1. Importance of eight factors on building energy use in a daylighted building.

Parameter[a]	Cooling	Lighting	Total
1. WWR	+	−	?
2. TVIS	+	−	?
3. Perimeter area	0	−	−
4. External shade	−	+	?
5. Light power	+	+	+
6. Light level	+	+	+
7. Continuous controls	−	−	−
8. Glare control	−	+	?

[a]An increase in each parameter causes an increase (+), decrease (−), or no change (0), in cooling, lighting, and total energy use in the building.

WWR and TVIS increases, and, in general, the savings rise asymptotically towards a maximum. However, because of the greater solar gain, increasing WWR × TVIS has the opposite effect on the cooling energy requirements of a building; thus, the overall effect on the total energy requirement of the building is indeterminate.

Figure 3 shows the effect of WWR × TVIS on the lighting energy requirements in the perimeter zone at three lighting levels: low, medium, and high. The building has continuous dimming controls, a lighting power of 16.2 W/m^2, and no external shading or window setback. As expected, the lighting energy use decreases as the product of WWR × TVIS increases, but the savings reach their potential maximum at moderate levels of WWR × TVIS. It is worth noting that a 45–65 percent reduction in lighting energy is achieved at the low value of WWR × TVIS of 0.12, the higher percentage savings being attained at lower lighting levels. A value of WWR × TVIS equal to 0.12 could, for example, correspond to a building with dark gray tinted single pane windows (shading coefficient = 0.44) that occupy 40 percent of the wall space. The upper bound of savings is just over 70 percent, and the difference between the various lighting levels becomes less significant as this value is approached. Figure 3 makes clear that large savings can be made easily by raising either WWR or TVIS, but that diminishing returns rapidly set in after WWR × TVIS reaches 0.12 to 0.15.

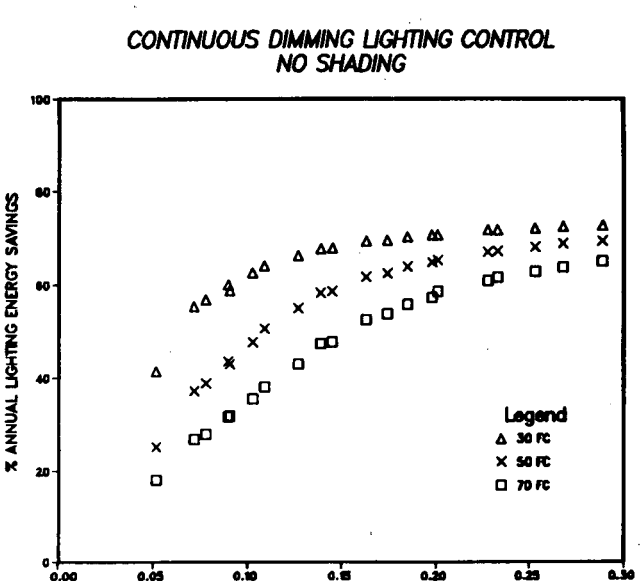

Figure 3. Effect of WWR × TVIS on lighting energy requirements in the perimeter zone. (XBL 8512-5196)

Figure 4 shows the effects of WWR and TVIS on the total energy use of the building. This simulation is based on a building with no external shading or window setback, continuous dimming controls, a medium illumination level, and a lighting power of 16 W/m^2. Also relevant to the interpretation of the results in Figure 4 is the fact that the perimeter area in the reference building constitutes 72 percent of the conditioned space. As we note later, the lighting savings as a fraction of total building energy use is directly proportional to the fraction of the conditioned and lighted space in the perimeter zone. Figure 4 illustrates the total reduction in energy use that can be expected to result from daylighting. We note that the lighting energy is continuously reduced as WWR × TVIS increases. However, the cooling and fan energy requirements increase with an increase in WWR × TVIS. Furthermore, cooling and fan energy requirements grow virtually linearly, whereas lighting energy savings flatten out. Thus, the energy requirements for this building reach a minimum at a WWR × TVIS of about 0.11, compared to the initial value of WWR × TVIS of about 0.14 in the reference building. This is close to the optimal configuration for daylighting in the reference building, yielding reductions in total energy use of 18.5 percent.

In summary, in the building studied, total energy use is minimized by adopting a WWR × TVIS of 0.11. However, at any given value of WWR × TVIS the percentage energy savings resulting from daylighting is close to 20 percent.

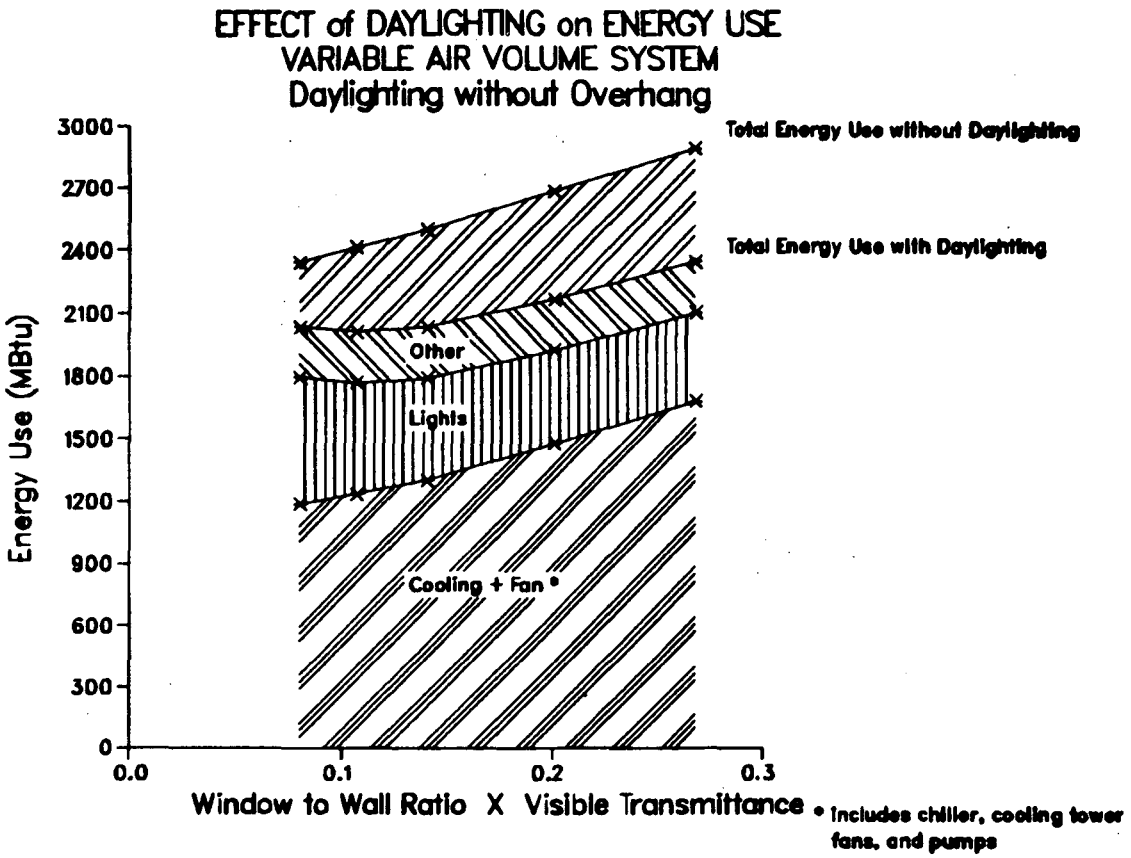

Figure 4. Effect of WWR × TVIS in total building energy use. (XBL 8512-5197)

CONCLUSIONS

The central assertion of this work is that it is possible to estimate the effects of the major design parameters on the performance of daylighting in commercial buildings in Singapore with a high degree of accuracy. The approach to building a model that obtains these estimates has been the use of results of DOE-2.1B simulations combined with a physical understanding of the factors affecting cooling and lighting energy requirements of buildings. The climate of Singapore simplifies the problem considerably, because of the relative constancy of solar gain and other climatic parameters throughout the workday and year.

We believe that the approach outlined in this paper has the potential for yielding accurate assessments of the impacts of daylighting in Singapore and other regions with hot climates. We further believe that this approach, when written for a microcomputer with proper graphical output and optimization routines, will provide architects and building engineers with a valuable tool for evaluating daylighting.

Finally, although the issue has not been directly addressed in this paper it is important to note that the potential savings from daylighting also include the possible benefits of reducing the peak load on the entire electricity system.[8]

PLANNED ACTIVITIES FOR FY 1986

Continuing research on daylighting in Singapore will extend the current work by developing a microcomputer code for assessing daylighting impacts and will analyze impacts of daylighting on the peak power requirements of the Singapore electrical system. In later years, we will extend the daylighting research to other members of ASEAN.

REFERENCES

1. Ne'eman, E. and Shrifteilig, D. (1982), "Daylighting of Buildings in a Hot Climate," *Energy and Buildings, 4*(3), pp. 195–204.
2. Rosenfeld, A.H. and Selkowitz, S. (1982), "Beam Daylighting: An Alternative Illumination Technique," *Energy and Buildings 1*(1), pp. 43–50.

3. Ander, G.D. and Maeda, B.T. (1984), "Simplified Daylighting Energy Savings for Non-Daylighting Building Energy Simulation Programs," *Energy and Buildings, 6*(3), pp. 221–228.
4. Building Energy Simulation Group (1985), *Overview of the DOE-2 Building Energy Analysis Program,* LBL-19735.
5. Turiel, I., Curtis, R., and Levine, M. (1984), "Parametric Energy Analysis in Support of Singapore Energy Conservation Standards for Commercial Buildings," *Proceedings of the ASEAN Conference on Energy Conservation in Buildings,* 29–31 May 1984, pp. 195–265, Development and Building Control Division, Public Works Department, Ministry of National Development, Republic of Singapore.
6. The climatic measurements and data analysis were performed by Professor K.R. Rao of the National University of Singapore.
7. Steve Selkowitz and collaborators at Lawrence Berkeley Laboratory have performed a series of studies as part of the analysis of ASHRAE standards. Selkowitz and collaborators have also developed nomograms that permit the assessment of effects of design parameters on lighting energy use (but not cooling energy) in commercial buildings. The nomogram approach provided an important input to the approach described in this paper.
8. Choi, U.S. Johnson, R., and Selkowitz, S. (1984), "The Impact of Daylighting on Peak Electrical Demand," *Energy and Buildings, 6*(4), pp. 387–399.

Estimation of Energy Intensity by End Use for Commercial Buildings Using Conditional Demand Analysis*

I. Turiel, P. Craig, M. Levine, J. McMahon, G. McCollister,† and B. Hesterberg†

Despite a widespread application in the residential sector, the statistical technique known as conditional demand analysis has seen scant application in the commercial sector, due in large part to the greater diversity of commercial customers. This report describes the results of a study to estimate the energy intensities of major end-uses in commercial buildings in the service area of the Pacific Gas and Electric Company (PG&E).[1] We applied the conditional demand analysis technique to PG&E's 1982 Energy Use Survey data base to produce estimates of electricity and natural gas consumption per square foot for seven end uses consisting of space heating, air conditioning, lighting, water heating, cooking, refrigeration, and miscellaneous use. We provided these estimates for offices, food stores, restaurants, retail buildings, hotels and motels, hospitals, schools, warehouses, and miscellaneous buildings. The results of this study will be used for forecasting electricity use in the commercial sector.

*This work was supported by the Pacific Gas and Electric Company, through the U.S. Department of Energy under Contract No. DE-AC03-76SF00098.

†QED Research, Inc.

ACCOMPLISHMENTS DURING FY 1985

Methodology and Data

We used conditional demand analysis to model a customer's billed energy consumption as a function of building and business characteristics, climatic factors, and the stock of energy-using equipment. The technique requires high-quality data to obtain statistically significant estimates of average energy use per equipment type. Unfortunately, high-quality data are difficult to obtain for the commercial sector, and, as a result, this technique has seen very little application in the commercial sector. The lack of high-quality data is due to several factors. First, the diversity of customers is much greater in the commercial sector. Office buildings, for example, vary greatly in size. In some offices, windows open; in others, they do not. Some commercial buildings are occupied by diverse businesses; for example, a restaurant, a bank, and offices may occupy a large building.

Second, commercial buildings often have several electric or natural gas accounts. Conditional demand analysis depends heavily on complete billing data that are matched precisely with local weather data and with the characteristics of the building and occupants using the energy. It is difficult to design a data collection strategy that will properly match billing data with building and customer characteristics for a high percentage of possible circumstances.

Third, it is more difficult to measure the characteristics of energy-using equipment in the commer-

cial sector. For example, asking a household how many refrigerators it owns is more informative than asking the same question of a commercial customer, because, in that sector, energy use by refrigeration equipment is more variable from customer to customer.

To overcome these problems, several unique methodologies were designed for data collection and analysis. First, PG&E initiated an effort to design a data collection framework under which a customer's billing data could be matched to data obtained from a survey. This strategy matches multiple gas and electric accounts for each building by using name and address information. This forms a population of buildings from which a sample can be drawn and surveyed. In 1982, PG&E mailed questionnaires to such a sample and followed up by phone for customers who did not respond. Over 5,000 useful responses were returned to PG&E.

Second, this information was processed under PG&E's direction to remove inconsistent responses. The special characteristics of the commercial customers were considered in conducting this review. Third, we conducted the conditional demand analysis separately for buildings of different types. For example, the diversity among food stores is much less than that among all commercial buildings. Fourth, two techniques were designed for specifying the conditional demand equations for heating and air conditioning. In one, we used previous research experience and a knowledge of building physics, and, in the other, the weather sensitivity of each building was modeled separately. We tested both techniques in the conditional demand analysis and reported the results for the one yielding the best statistical fit (see Tables 1 and 2 below). These approaches were required because energy requirements for these end-uses depend on a complicated array of building and operating characteristics.

Annual Estimates of EUI's

The statistical results of this study include annual estimates of energy consumption per square foot for major end-uses in nine business types. We formed the business types by grouping buildings with similar business activities and energy-using equipment. We report the estimates for electric end-uses in Table 1 and for natural gas end-uses in Table 2. These estimates represent energy consumption per square foot of floor space (EUI's) that is served by that end-use. Floor space in buildings or parts of buildings that is not served by that end-use is not included in the computations used to derive the estimates.

These estimates do not indicate the amount of energy consumed by these end-uses or the relative percentages of energy consumed by each end-use. To derive these types of estimates, the energy consumption rates in this report must be multiplied by the number of square feet served by each end-use

Table 1. Energy utilization intensities—electricity (kWh/ft^2/year).

Building Type	Air Conditioning	Space Heating	Water Heating	Lighting	Refrigeration	Cooking	Ventilation	Miscellaneous
Offices	4.3	1.7	1.7	8.6	2.0	1.3	n.e.	0.2
Restaurants	7.4	4.1	6.6	6.8	16.0	17.9	n.e.	2.2
Retail	3.6	0.8	0.4	5.1	2.2	0.4	n.e.	3.7
Food Stores	2.0	1.4	0.9	14.2	24.1	1.2	n.e.	1.5
Warehouses	5.9	2.6	1.7	2.1	6.6	0.6	n.e.	0.1
Schools	2.1	0.5	0.4	2.0	1.4	0.6	0.6	2.0
Hospitals	4.7	1.3	3.2	7.4	1.9	1.5	3.0	0.9
Hotels/Motels	3.2	1.3	0.6	3.3	4.6	2.9	n.e.	2.6
Miscellaneous	6.2	2.9	n.e.[a]	3.9	4.0	1.8	0.5	2.0

[a]n.e. = not estimated.

Table 2. Energy utilization intensities—natural gas (kBtu/ft^2/year).

Building Type	Space Heating	Water Heating	Cooking	Clothes Dryers	Pools	Air Conditioning	Miscellaneous
Offices	26	9	n.e.[a]	n.e.	n.e.	n.e.	1
Restaurants	21	14	259	77	109	n.e.	n.e.
Retail	12	25	n.e.	148	n.e.	n.e.	3
Food Stores	34	2	49	n.e.	n.e.	n.e.	n.e.
Warehouses	37	11	33	33	n.e.	n.e.	2
Schools	35	5	1	n.e.	8	n.e.	1
Hospitals	75	75	41	n.e.	28	21	n.e.
Hotels/Motels	20	46	47	19	7	n.e.	n.e.
Miscellaneous	28	14	11	14	88	n.e.	2

[a]n.e. = not estimated.

and by the saturation of each end-use. Separate estimates of ventilation were possible for only three building types. For other building types, ventilation is contained primarily in the air conditioning or miscellaneous category.

The results in Table 1 indicate that combined air conditioning and ventilation intensity is highest in hospitals, restaurants, and buildings in the miscellaneous category, but lowest in food stores. Figure 1 plots the results for air conditioning. Schools are often closed during the summer, and refrigeration equipment in food stores draws heat from the building, reducing space cooling requirements. The electric space and water heating estimates are generally low relative to gas space and water heating, since electricity will most likely be chosen when these end-uses are not expected to be used very intensely. The highest estimates of electric space and water heating were found in restaurants. The lighting category includes both indoor and outdoor types of lighting. Lighting intensity is especially high in food stores, hospitals, restaurants, and retail stores. In food stores, lighting in refrigeration and freezer units is probably responsible for higher electricity consumption, whereas in hospitals, continuous operating hours is probably the reason. The refrigeration category includes both freezers and refrigerators. The energy intensity of refrigeration is high in food stores because of the high density of display units, many without doors. Refrigeration is also high in restaurants, where units are opened frequently and are often located in hot kitchens. Naturally, cooking use is very intense in restaurants. Ventilation was difficult to distinguish from the refrigeration end-use.

The results indicate that space heating use reaches extremes for two building types. It is very low in retail buildings and very high in hospitals. Long operating hours and strict temperature control are responsible for high space heating use in hospitals. Water heating use is also very high in hospitals, due to the need for extreme cleanliness and the domestic needs of the patients. Use of hot water is also high in hotels and motels. Water heating use is low in offices. Some use can be attributed to cafeterias, to hand washing in restrooms, and use by

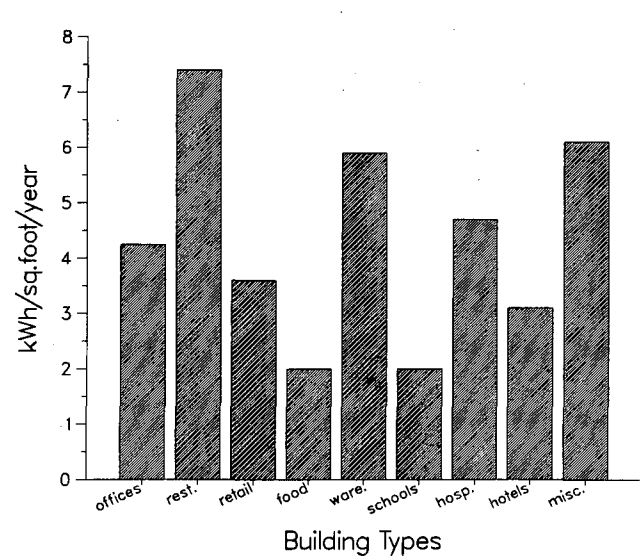

Figure 1. Energy utilization intensities—air conditioning. (XBL 8512-5199)

other business types in office buildings, such as restaurants. Also, schools and food stores use only small amounts of hot water. Cooking use is, of course, very high in restaurants and the food store category, which includes bakeries. It is also high in hotels and motels, which often house restaurants, and in hospitals, where three meals are cooked for patients each day. Use for clothes dryers is high in the retail and restaurant categories because these business types have laundries, and in hotels and motels for washing linen. Natural gas use for air conditioning was significant in only one building type, hospitals.

PLANNED ACTIVITIES FOR FY 1986

We plan to extend our FY 1985 research in several directions. These include a calculation of energy consumption by end use incorporating equipment saturations, and the stratification of EUI's by building age, climate zone, and building size. We also plan to gather data to improve our confidence in two of the EUI's: electric space heating and electric cooking. Finally, we will compare two methods of specifying seasonal energy consumption for space heating and air conditioning. These are the engineering approach and the statistical approach, which involve regressing monthly energy use on heating and cooling degree days.

REFERENCES

1. McCollister, G., *et al.* (1985), "Energy Utilization Intensities for Major End-Uses in the Commercial Sector," Draft Report to PG&E.

ECONOMIC STUDIES

The LBL Residential Energy Demand Forecasting Model*

J.E. McMahon and P. Chan

Computer models for projecting residential energy consumption at the end-use level have been in existence since the 1970's. The ORNL Engineering-Economic Model of Residential Energy Use[1] combines engineering information (costs and efficiencies of products available for purchase) and economic formulations (elasticities of demand separated into fuel choice, efficiency choice, and usage decisions) to provide simulations of future energy consumption at the end-use level. This approach attempts to consider the problem at a sufficient level of disaggregation to utilize engineering information as well as the important economic determinants of market behavior. The LBL Residential Energy Model[2] (see Fig. 1), has been developed as the next generation of computer model to provide

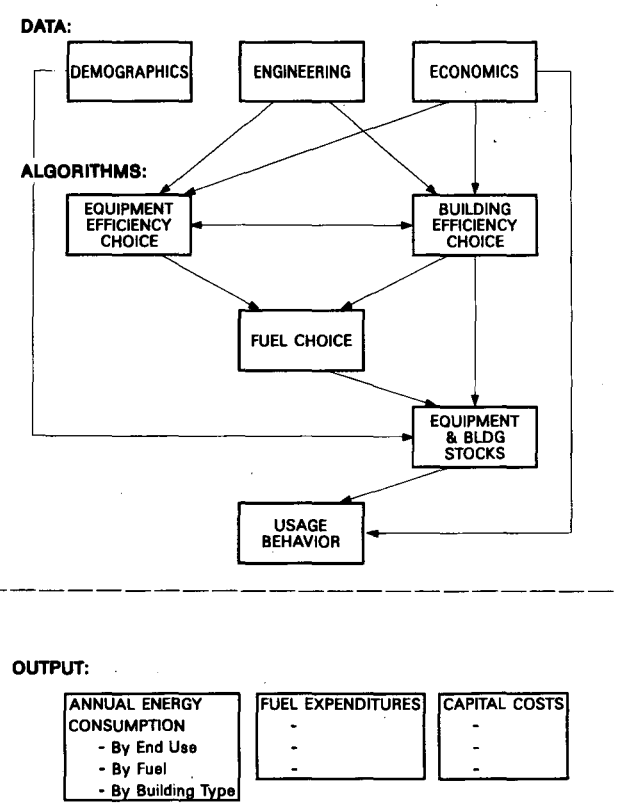

Figure 1. Logic diagram showing major components of LBL Residential Energy Model. (XCG 8412-13510)

*This work was supported by the Assistant Secretary for Conservation and Renewable Energy, Office of Buildings Energy Research and Development, Building Equipment Division of the U.S. Department of Energy under Contract No. DE-AC03-76SF00098.

improved policy analysis at the end-use level. The major improvements to our prior models include:

- representation of recent equipment efficiency trends;
- new techniques for forecasting future appliance efficiencies and annual appliance replacements; and
- extension of the model to include heat-pump space-conditioning systems.

The resulting forecasts agree more closely with recently reported energy consumption and provide lower estimates of future energy consumption.

ACCOMPLISHMENTS DURING FY 1985

During the past year we have made improvements in both the data and the model specifications.

Data

We have updated the data used by the model in several ways:

1. Housing starts/stocks. The 1980 Census gives higher estimates of the housing stocks than previous surveys, and shows an increase in the fraction of dwelling units in multifamily dwellings, at the expense of single family houses. At the same time, the construction forecast has been revised downward.
2. Energy cost projections. The last decade has seen dramatic changes in expectations regarding energy costs. For that reason, the assumed energy price projections have been altered repeatedly to keep abreast of changes in the market.
3. Income projections. The expected increases in real income were previously based on per capita estimates. The older estimates were optimistic, and have not been borne out by recent experience. In addition, we have changed the definition of the input variable to income per household. Currently, we assume 1.2 percent/year real growth in income per household after 1985.
4. Engineering Analysis. We developed a new aggregation procedure for combining data for various classes of products, e.g., manual defrost and frost-free refrigerators. We designed this method to extract as much information as possible, yet simplify the representation to a single curve for each product type.
5. Recent efficiency trends. We have included in the model the significant changes in design that have been reported by trade associations. Projections of future efficiencies are based upon the observed efficiencies and an analysis of the decision processes in the market since 1972.
6. Projected floor area per house. The older projections, extrapolating from historic trends, predicted in the year 2000 floor area per new house 20 percent above 1977 average house size. In view of the recent cessation of the trend toward larger houses, we have assumed that floor area per new house (within each house type) remains constant. Of course, the average floor area across the entire housing stock will continue to change, reflecting changes in the composition of the stock, e.g., the percent of all households that are single family.

Model Specification Changes

We made several key changes in the method of projecting future energy consumption in recent years:

1. Efficiency of new appliances. The improvements to the model are:
   1) Recognize the initial difference between the efficiency of a new appliance and the one it replaces.
   2) Include data on recent efficiency trends (through 1981 for many products) and begin projection after the last year of available data on efficiency of new units.
   3) Replace the algorithm for forecasting future appliance efficiencies. The new approach is based on a detailed analysis of market behavior over the last 10 years. We have replaced the market behavior algorithm. The original formulation was theoretical, since data on appliance efficiencies were not available. Recent work at LBL[3] using data made available during the Department of Energy analysis of proposed Consumer Product Efficiency Standards[4] (CPES) indicates that the original formulation, assuming an inverse relationship between energy price and unit energy consumption, forecasts higher efficiency improvements than observed in the market in the past 10 years. Appliance efficiencies have improved, but not by as much as had been forecast. What

appears to be relatively constant is the discount rate implicit in the market's appliance efficiency choice. On the whole, the tradeoff between operating cost and purchase cost by purchasers of appliances has not changed over time. Increases in energy costs have been reflected in the operating costs of appliances, and efficiencies (and presumably purchase costs) have increased. But, in most cases, the efficiency increases have only kept pace with rising energy costs, and do not yet indicate any change in the market decision-making process toward placing more emphasis on energy conservation. The details of the analysis of market behavior regarding efficiency choice are reported elsewhere.[3]

2. Construction practices in new houses. Just as new appliances are more efficient than those already in use, new houses are constructed in such a way as to reduce their space conditioning energy requirements relative to old houses. While measured data on the energy consumption of new houses are more difficult to obtain, the characteristics of new houses are known from national surveys. We used a physical model of heat transfer in a house (DOE-2.1 Building Energy Analysis Program[5]) to determine the annual energy consumptions for heating and for cooling, based on the characteristics of the house. Just as in the treatment of appliance efficiency, the new distinction made for thermal integrity is that the average new house has different characteristics and, therefore, different energy consumption from the average house already in existence.

3. Appliance retirements. The original formulation used an exponential retirement function, equivalent to retiring each year a constant percentage of the existing appliances of each age. We found data on retirement functions that give the percent of appliances that retire during each year after original purchase. The use of a vintaging approach achieves two purposes: 1) it eliminates the erroneous early retirement of young appliances (retirements in early years of the projection are therefore lower in the new method); 2) it captures the wave-like rise and fall of replacement sales, reflecting the aging of units purchased during peak economic and housing construction periods.

4. Energy use of retiring appliances. The old method accounted for the energy use of retiring appliances by retiring the energy use of the average unit in stock at the time. This was inaccurate, since units of several ages retire in any given year and the older retirees are likely to consume more energy (be less efficient) than newer models. In the new model, the retirees retain the unit energy consumption appropriate for their vintage. This change decreases the estimated energy consumption in future years. Since the greater portion of retiring appliances are older than the average appliance in stock, the new method assigns lower efficiencies to the retirees. As a consequence, the average efficiency of surviving appliances is higher than before.

5. Appliance price deflators. Another new feature is the ability to adjust the real purchase price of equipment each year of the forecast. Changes in the real price per unit may occur as technologies for the manufacture of a product evolve, or as economies of scale are realized. Different changes in the real price over time may be applied to different products and fuel types.

6. Explicit treatment of heat pumps. The old model subsumed heat pumps under electric central space heating and central air conditioning. The market shares of heat pumps were determined indirectly, using an old formulation to forecast the saturation of electric central space heating systems. The model has been revised to consider heat pumps as an explicit technology option for heating and cooling, and the new market share elasticities are under development.

7. Distribution of efficiencies. Early analyses of appliance efficiency standards assumed the 1978 distribution (number of shipments in each range of efficiencies) to be static for all time. We calculated the average efficiency in the presence of CPES exogenously by applying the CPES level to the 1978 distribution. Thus, the average efficiency in the presence of standards was assumed to be constant in all future years, unless exceeded by the average efficiency in the base case.

   The LBL model moves the 1978 distribution of efficiencies each year in the standards case so that the average efficiency agrees with the base case projection. The distribution is expressed in efficiencies as a fraction of the average, so that broadening of the distribution also occurs. To obtain the average efficiency in the standards case, all shipments with efficiencies less than the standard are assumed to be upgraded to the standard. Those with efficiencies at or above the standard are unaffected. We calcu-

late the shipment-weighted average from the adjusted distribution.

The new method has the advantages that: 1) the distribution of efficiencies changes in a way consistent with the change in the average efficiency; 2) the effect of the standard level diminishes with time, as the base case efficiencies move to or beyond the standards. Whereas in the old model the efficiency level in the standards case was a function of the standard level and of the 1978 distribution of efficiencies, the efficiency level in the new method is a function of the standard level and a distribution that changes (toward more efficient products) over time; 3) standards can be applied to individual classes of appliances. The change, while permitting analysis of standards affecting only some classes of appliances, does not alter the assumption of constant market shares of each class within an appliance type. For example, the fraction of new refrigerators that are top-mount, automatic-defrost remains constant over time. The framework could encompass a forecast of market shares by class, but we are aware of no such credible forecasts at this time.

8. Purchase cost/energy use formulation. The old model used a 3-parameter fit to the data from the Engineering Analysis[6] to obtain the continuous function of purchase cost to unit energy consumption. In work at LBL during the summer and fall of 1982, it became clear that the old formulation could lead to ambiguous results. Similar curve fits could be obtained, having different values for two of the three parameters. Since these parameters were important for calculating life cycle costs and aggregate implicit discount rates, the ambiguity was a problem.

   The solution in the new method is to use a 2-parameter formulation, which provides unambiguous values for the two parameters and provides good fits to the data points. Consequently, the shape of the purchase cost/energy use curves changed slightly for some products.

9. Twelve end uses. The old model considered only nine end uses, including the regulated products. The new model considers total residential energy consumption, composed of 12 end uses: central space heating, room space heating, room air conditioners, central air conditioners, heat pumps, water heaters, refrigerators, freezers, ranges and ovens, dryers, lighting, and miscellaneous. (The new end uses are heat pumps, lighting, and miscellaneous.) Lighting and miscellaneous had been considered in even older versions of the old model, but to the exclusion of dryers and room space heaters, since the total number of end uses had been fixed. Separating heat pumps from central air conditioners eliminates the overcounting of savings for a policy applied only to non-heat-pump air conditioners, and permits consideration of different standard levels for heat pumps and conventional central air conditioners.

   Another important change involves reformatting the inputs, such that one set of inputs is defined for use with all end uses (such as housing starts), while additional sets of input are defined specific to each end use. The new model has been generalized so that it is now easy to analyze subsets or the full set of end uses, as desired.

10. Graphical output. We added the capability of obtaining graphical output for most of the key outputs. The pictorial presentation, as opposed to tabular, facilitates analysis of large amounts of data, and is particularly useful when analyzing trends over time or the difference between two scenarios. Among the graphs that can be produced are: total residential energy consumption over time, fuel prices over time, efficiency trends over time, and residential purchases of appliances by type over time. Some graphs illustrate the difference between two sets of results, usually a base case and a policy case: energy savings over time, net present benefit by end use (bar graph), efficiency of new units over time, and percent energy savings by end use by house type over time.

PLANNED ACTIVITIES FOR FY 1986

We will incorporate the results of a new analysis of market share elasticities (see D. Wood, *et al., Market Share Elasticites of Home Heating and Cooling Systems* in this volume). By replacing the current algorithm, we will greatly improve the forecast of the penetration of heat pumps into the space heating/cooling market. In addition, we will capture the influence of choosing central air conditioning on the selection of a heating system. Also, we will introduce competition between room and central heating systems as a function of the operating and equipment costs of the alternatives.

We will increase the level of detail in two areas: efficiency forecasts and regional differences. First, rather than forecasting the average efficiency for a product, the forecast will consider each class. For

example, frost-free top-mount refrigerators will be treated as distinct from manual-defrost refrigerators. This will permit a direct comparison of the forecast with actual designs of appliances, making better use of the detailed engineering information in the data base.

Second, we will expand the data base for the USA to treat separate regions. The model will then recognize the differences in climate and energy prices in different parts of the country. In the process, we will update the data base using the 1980 Census and other recent sources.

Finally, we will separate the effects of efficiency changes and equipment capacity (e.g., the size of refrigerators or air conditioners) on energy consumption per unit.

REFERENCES

1. Hirst, E. and Carney, J. (1978), "The ORNL Engineering-Economic Model of Residential Energy Use," Oak Ridge National Laboratory, ORNL/CON-24.
2. McMahon, J. (1985), "The LBL Residential Energy Model: An Improved Policy Analysis Tool," (submitted to *Energy Systems and Policy*); LBL-18622.
3. Ruderman, H., Levine, M., and McMahon, J. (1984), *The Behavior of the Market for Energy Efficiency in the Purchase of Appliances and Home Heating and Cooling Equipment*, LBL-15304.
4. U.S. Department of Energy, Assistant Secretary, Conservation and Renewable Energy, Test and Evaluation Branch (1982), *Consumer Products Efficiency Standards Economic Analysis Document*, DOE/CE-0029, Washington, D.C.
5. Building Energy Simulation Group (1985), *DOE-2 Reference Manual*, LBL-8706, Rev. 4.
6. U.S. Department of Energy, Assistant Secretary, Conservation and Renewable Energy, Test and Evaluation Branch (1983), *Consumer Products Efficiency Standards Engineering Analysis Document*, DOE/CE-0030, Washington, D.C.

Economic Impacts of Residential Conservation Programs on Electric Utilities*

E. Kahn, C. Pignone, J. Eto, J. McMahon, and M.D. Levine

Conservation programs mandated by the federal government will have economic impacts on electric utilities that may or may not be favorable to those utilities. The impact depends upon local circumstances such as the rate structure, the utility's marginal costs, and the nature of local utility regulation. To understand how these factors interact, it is necessary to model the hourly demand changes associated with particular conservation programs. Methods of economic valuation must then be developed to reflect the gains and losses associated with load shape changes.

This article describes two case studies of residential conservation programs involving utilities with substantially different marginal costs. These cases, Detroit Edison and Pacific Gas and Electric, illustrate the economic method used to estimate economic impacts. The impacts of conservation programs are unfavorable in the former case, but quite favorable in the latter.

ACCOMPLISHMENTS DURING FY 1985

Most economic analyses of conservation programs focus on the consumer perspective. It is equally important, however, to characterize the impact of conservation programs on utility earnings. To estimate these effects, we modified an accounting measure known as earnings before interest and taxes (EBIT) to include the changes in utility investment associated with particular conservation programs.

EBIT is simply the difference between revenues and costs. The economic value of marginal load changes is the difference between marginal revenues and marginal costs. Investment costs must be considered along with operating costs. Depending upon circumstances, the relevant investment costs may be for peaking turbines or baseload facilities.

The marginal revenues associated with conservation programs are specific to particular rate

*This work was supported by the Assistant Secretary for Conservation and Renewable Energy, Office of Buildings Energy Research and Development, Building Systems Division of the U.S. Department of Energy, under Contract No. DE-AC03-76SF00098.

schedules. Where a utility has more than one residential tariff, the conservation impact must be estimated for each rate classification. Our analysis is conducted using the LBL Residential Energy Model[1] applied at the rate class level. This means forecasting electricity sales for each tariff class with and without the conservation program. Since the LBL model is quite data-intensive, the base-case forecast (made with limited data) commonly involves some adjustment to achieve correspondence with utility estimates.

Once the quantity change associated with conservation programs has been estimated, it must be applied to the sales frequency distribution in a way that will account for the nonlinearity of the revenue response. It is necessary to know the distribution of sales over the rate tiers because tariff schedules typically have price distinctions based on the quantity consumed.[2] Marginal revenue is determined by changes in the entire sales distribution induced by conservation programs. We adopted the block-adjustment method to model these changes. Figure 1 illustrates the procedure.

Figure 1 shows two distributions, o and n. Suppose n represents the sales distribution after conservation, o the distribution before conservation, and $B_{1,o}$ = 340 kWh/month, the consumption level above which the electricity price changes from p_1 to p_2. If we know only the distribution o, its mean value μ_o, and the mean value μ_n of n, we estimate the fraction of sales below $B_{1,o}$ for the distribution n as follows. We know that n will have a larger fraction of sales below $B_{1,o}$ than o. Instead of estimating the change for the curve o to the curve n, we increase the quantity of electricity for which p_1 will be the price. This is done by defining a new price boundary, $B_{1,n}$, which is greater than $B_{1,o}$ by the ratio μ_o/μ_n. The fraction of sales at p_1 is then read off curve o at the point $B_{1,n}$. In Fig. 1, this point is labeled a.

The error of this procedure is measured by comparing point a with point b, both projected to the vertical axis. Point b is just the intersection of $B_{1,o}$ with the curve n. In this case, the block adjustment method predicts too small a fraction of sales at price p_1. The revenue impact of this error depends upon whether $p_2 > p_1$. If it is, then the block adjustment method overestimates revenue. For the purposes of case study analysis, the block adjustment method must be used until a superior alternative is developed.

Marginal costs present a different problem. Here, it is necessary to aggregate all effects up to the system level, taking due account of the diversity of load profiles across individual users. We use the LBL Hourly Demand Model[3] to perform this aggregation. Figure 2 illustrates the kind of result that comes from testing particular conservation programs. This figure shows hourly residential loads for a projected peak day in 1996. The largest load impact shown here results from a mandated efficiency standard for central air conditioners that would require a seasonal energy efficiency ratio (SEER) of 12 by 1987.

Once load impacts have been aggregated from rate classes and spread over the hours of the year, they are then valued at the utility's marginal cost.

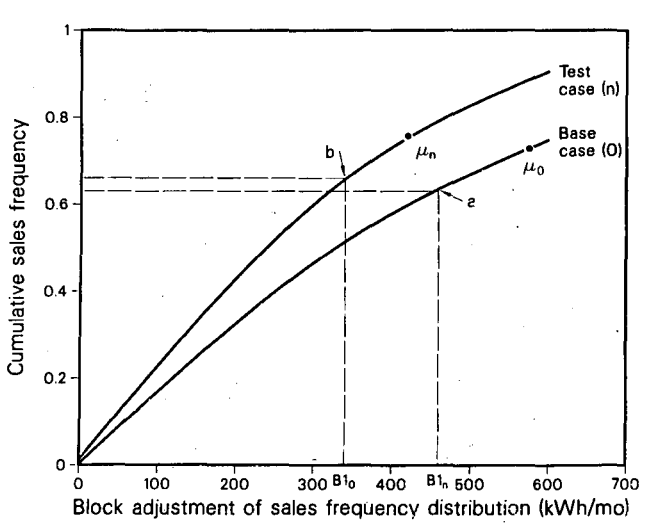

Figure 1. Cumulative sales frequency of electricity vs. block adjustment of sales frequency distribution. (XCG 844-13045)

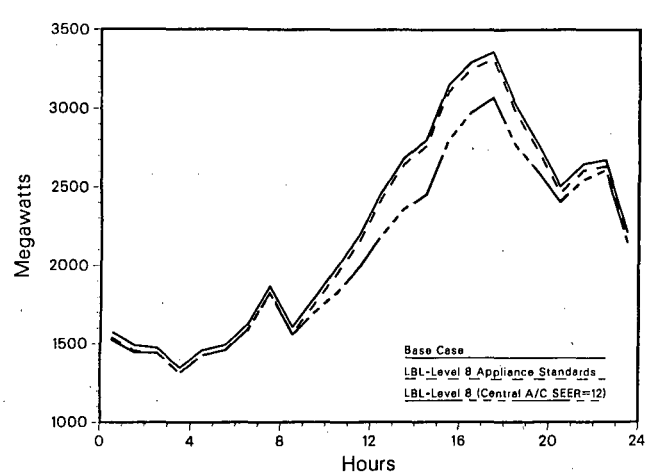

Figure 2. Projected Pacific Gas and Electric Company residential hourly load profiles for a peak summer day in 1996 (base case and two conservation scenarios). (XCG 848-13191)

Marginal cost has two components, capacity and energy. Capacity costs are typically concentrated in those hours of the year where the utility system loss-of-load probability is greatest. Simulations of Pacific Gas and Electric Company (PG&E), for example, show that the highest 10% of the load hours in July and August typically account for over 95% of the annual system reliability risk. Therefore, only these hours have capacity value.

Marginal energy costs are also estimated by system simulation methods. Typically, these methods involve load aggregation techniques that suppress the chronological sequence of loads.[4] The simulated result is summarized in the form of a load duration curve resembling Fig. 3. The monotonically declining curve represents the number of hours in the simulated period for which the system load is at a given level. Because the loads are sorted by magnitude, chronological features are lost. The supply system is dispatched to serve loads in economic order. Figure 3 shows the order in which Detroit Edison plants would serve projected 1988 loads. The plants with lowest operating costs serve the base load. These are placed at the bottom of the load duration curve (LDC). Plants that intersect the LDC are marginal producers.

Figure 3 shows how the average marginal cost over a given period can be calculated as a weighted average of the marginal costs of the plants intersecting the LDC. The appropriate weights are the marginal fractions, which are shown at the top of Fig. 3. They represent the fraction of hours for which a given plant is the marginal producer. This is the vertical projection of the points at which that plant intersects the LDC.

Applying marginal energy-cost results to a particular conservation program requires an estimate of how to translate load impacts from the hourly demand model to the more aggregated level of the LDCs. For case study purposes, we make relatively simple assumptions that result in proxies that are easy to use.

Case study results are described in detail elsewhere.[5,6] The results for Detroit Edison (DECO) are uniformly negative. Because of substantial excess capacity, DECO has low marginal costs. Therefore, the benefits of conservation in terms of the value of avoided energy production are small. There is no benefit in avoided capacity costs. The case of PG&E is more complex. This utility has high capacity costs. While its marginal energy cost is higher than DECO's, it is still less than marginal revenue. The net result of these effects depends upon the particular conservation program.

Figure 4 shows results for a conservation program corresponding to one of the two for which the effects are illustrated in Fig. 2. The positive net gain of this program is due principally to the capacity value associated with high-efficiency central air conditioners. Other programs without this component show much smaller benefits.

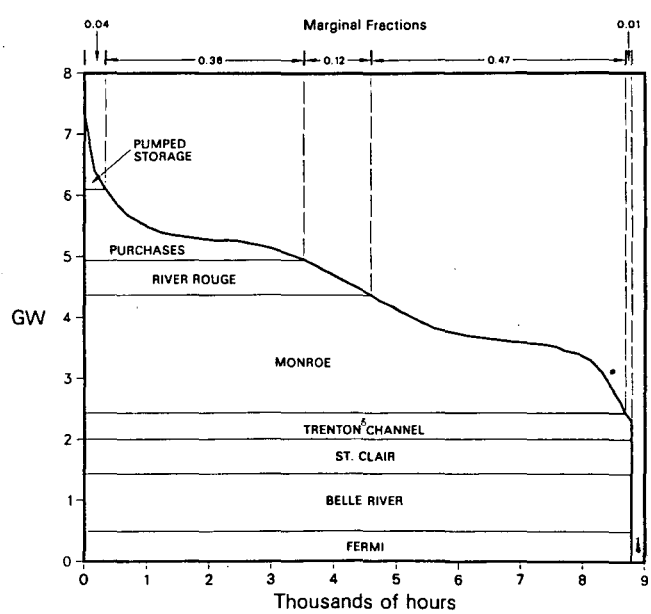

Figure 3. Fully dispatched load duration curve for Detroit Edison Company, 1988 projection. (XCG 844-13046)

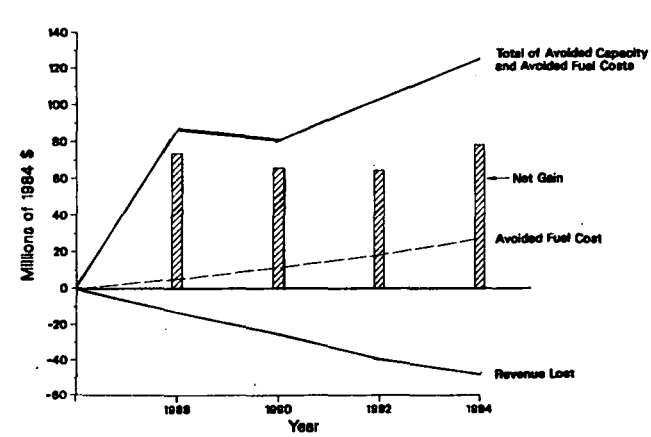

Figure 4. Economic impacts of central air conditioner standards (SEER = 12) on PG&E. (XBL 851-985)

PLANNED ACTIVITIES FOR FY 1986

We will complete case studies of the financial impacts of appliance efficiency standards on the Nevada Power Company and the Texas Power & Light Service Territory of the Texas Utilities Electric Company. The Nevada Power Company study will feature independent simulations of avoided production costs.

We will also perform detailed analyses of the techniques and models available for direct integration of load shape changes into traditional supply planning models.

REFERENCES

1. McMahon, J. (1984), *The LBL Residential Energy Model*, LBL-18622.
2. Liittschwager, J. (1971), "Mathematical Models for Public Utility Rate Revisions," *Management Science 17*, p. B339.
3. Verzhbinsky, G., Vine, E., Ruderman, H., and Levine, M. (1983), *The Hourly and Peak Demand Model: Description and Validation*, LBL-17784.
4. Bloom, J. (1984), "Generation Cost Curves Including Energy Storage," *IEEE Trans. on Power Apparatus and Systems, PAS-103*, p. 1725.
5. Pignone, C. (1984), *Financial Impact on Utilities of Load Shape Changes: Stage I Technical Report—The Detroit Edison Company*, LBL-19750.
6. Eto, J., McMahon, J., and Chan, P. (1984), *Financial Impact on Utilities of Load Shape Changes: Stage II Technical Report—The Pacific Gas and Electric Company*, LBL-19751.

Regional Analysis of the Economic and Institutional Environment for New and Enhanced Utility Programs*

W. Yen-Wood, E. Kahn, and M. Levine

The advent of increasing marginal costs and slower growth in the 1970's along with a proactive regulatory environment has spurred utilities to explore alternatives to traditional planning methods. "Least-Cost Planning" and "Demand-Side Management" strategies, emphasizing the need to optimize the cost and timing of electricity supply and demand, are emerging as credible alternatives to conventional supply planning focusing on construction of large-scale central station power plants. In this context, the objective of the Utility Overview Study is to provide conservation policy makers with an estimate of *where* and *when* investor-owned utilities (IOUs) will be interested in promoting energy conservation as an alternative to importing power or constructing new power plants for meeting future energy demand. The project began in FY 1984 with the identification of Energy Supply/Demand Balance and Cost, Ratemaking, and Political/Institutional Environment as three key factors relevant to utility decision-making concerning energy conservation programs. The initial Overview Study database included 85 IOUs representing 70% of total generation in the U.S. Due to the complexity of the utility planning environment (geographical boundaries of electric utilities may be defined by their service areas, investment in generation capacity, or power exchange agreements) as well as data availability considerations, we have incorporated several levels of analysis in the Overview Study. Table 1 presents the selected Utility Overview Study indicators by North American Electric Reliability Council (NERC) Region, DOE Electric Region, State, Utility, and annual data. We present the findings of the Overview Study at the level of DOE Electric Regions because these subregions approximate the flow of energy transfers among power pools within the NERC Regions.

*This work was supported by the Assistant Secretary for Conservation and Renewable Energy, Office of Building Energy Research and Development, Buildings Systems Division of the U.S. Department of Energy under Contract No. DE-AC03-76SF00098.

Table 1

UTILITY OVERVIEW STUDY INDICATORS								
Factor/Indicator	NERC Region	Annual Data	Electric Subregion	Annual Data	State	Annual Data	Utility	Annual Data
I. Energy Supply/Demand Balance Factor								
POG	•	1984			•	1983		
PLCC	•	1982,83	•	1983	•	1982	•	1982
GROWTH	•	1983-92,1984-93	•	1984-93				
YEARS	•	1982,83	•	1983	•	1982	•	1982
PAC	•	1982			•	1982	•	1982
SUR/DEF, SHORT	•	1984-93	•	1984-93				
RYN, SubRYN,	•	1984-93	•	1984-93				
II. Ratemaking Factor								
RATES	•	1982			•	1982		
RES							•	1983
COM							•	1983
IND							•	1983
FARM							•	1983
CWIP	•	1982,84			•	1982,84	•	1982-84
III. Institutional Factor								
INSUL	•	1981			•	1981	•	1981
AUDIT	•	1981			•	1981	•	1981
SOLAR	•	1981			•	1981	•	1981
COGEN	•	1981			•	1981	•	1981
LOAD	•	1981			•	1981	•	1981
OTHER	•	1981			•	1981	•	1981
INVEST	•	1985			•	1985		
ASSESS	•	1985			•	1985		
INCENT	•	1985			•	1985		
OPTION	•	1985			•	1985		
STAT	•	1985			•	1985		

LEGEND

POG - Percent Oil/Gas
PLCC - Percent Low-Cost Capacity
GROWTH - Average Annual Growth Rate
YEARS - Years Until Expensive Energy is Needed
SUR/DEF - Regional Capacity Surplus/Deficit
SHORT - Subregional Capacity Surplus/Deficit
RYN - Regional Years to Need for New Capacity
SubRYN - Subregional Years to Need for New Capacity
RATES - Inverted Rate Structure
RES - Inverted Rate Structure - Residential Sector
COM - Inverted Rate Structure - Commercial Sector
IND - Inverted Rate Structure - Industrial Sector
FARM - Inverted Rate Structure - Farm Sector
CWIP - Construction Work in Progress

INSUL - Incentive for Insulation
AUDIT - Incentive for Energy Audit
SOLAR - Incentive for Solar Application
COGEN - Incentive for Cogeneration
LOAD - Incentive for Load Management
OTHER - Other Conservation Incentives Potential
INVEST - Utilities Required to Invest in all Cost-Effective Energy Conservation Prior to New Energy Resources
ASSESS - State Conducted Assessment of Conservation Resource Plans
INCENT - Commission Offers Conservation/Load Management Incentives
OPTION - Demand-Options Included in Required Utility Resource Plans
STAT - State has Statutory Authority to Require Utility Investment in Conservation and Load Management

XBL 863-777

ACCOMPLISHMENTS DURING FY 1985

Preliminary selection of indicators for the Utility Overview Study was carried in FY 1984 at the NERC Region, State, and Utility level. In FY 1985, we proceeded with the development of the Need for New Capacity indicator at the regional and subregional level, an update of the Regional Potential Low-Cost Capacity indicator, and extension of this analysis to the level of Electric Regions. We also adopted a new set of rate structure and institutional indicators based on newly available data. The results for indicators are compiled in a final report.[1]

Background Note on the NERC Regions and DOE Electric Regions (Subregions)

The NERC was formed by the electric utility industry in 1968 after the Northeast blackout to promote the reliability and adequacy of power supply in the United States and Canada. NERC has nine regional councils comprising nearly all the electric utilities in North America. Both NERC and DOE have defined subregions to support smaller area analyses of power supplies. NERC Subregions and DOE Electric Regions were designated in accordance with historic associations among neighboring utilities, contractual and informal power pools, and practical system operating considerations. Figure 1 shows the location of NERC Regions and DOE Electric Regions. Some States may belong to more than one NERC Region or Electric Region. Three interconnected transmission networks provide for the distribution of electricity in the U.S.: The Eastern Interconnected System (EIS), the Western Interconnected System (WIS), and the Texas Interconnected System. Cooperation among utilities within interconnected systems may take place through sale of bulk power, power pools, wheeling, and joint projects.

Regional Indicators of Potential for New and Enhanced Energy Conservation Programs

The economic impact of energy conservation on electric utilities consists of changes in projected revenue resulting from lost sales and avoided costs. In the short run, if conservation reduces peak demand, it will increase the profitability of total electricity sales by lowering average production costs. In the long run, conservation may involve load shape changes that shift the balance between peak and base load generation. Average production costs will decline if peak generation declines more than base load.

We consider marginal energy cost of baseload generation to be the most influential factor determining the near-term potential for conservation among investor-owned utilities operating in an environment of increasing marginal costs. Need for new generating capacity will reinforce the potential for conservation in regions where there is no low-cost energy, and promote consideration of strategic conservation programs where there are temporary surpluses. Active interest in conservation by public service commissions together with a favorable ratemaking environment will encourage the early adoption of conservation programs.

Of the indicators defined to analyze the energy supply/demand balance, the ratemaking context, and the political/and institutional environment, we consider the six that best characterize the conditions under which utilities will be favorable to energy conservation are: (1) High Oil Backout Potential, (2) Little or No Marginal Low-Cost Base Power, (3) Relatively High Growth, (4) Early Need for New Capacity, (5) High Risk for New Power Plants (Low CWIP), and (6) Favorable Institutional Environment.

Figure 2(a) thru 2(f) highlights the results for these indicators by State and Electric Regions.

High Oil Backout Potential

Following the 1973 Oil Crisis, utilities have embarked upon programs to use less expensive coal and nuclear fuels in order to decrease dependence on more expensive oil and natural gas. Possible shortages of critical fuels and increasing marginal costs may prompt utilities in Regions heavily dependent on oil and gas to consider conservation as an important aspect of their demand-side strategy.

Figure 2(a) shows percent of oil/gas generation to total thermal generation among the states in 1984.[3] It should be noted that in 1984, actual oil and gas capability accounts for a greater proportion of generating capacity than that reflected by data on generation because of the gradual shift in fuel sources. At the regional level, oil and gas fired generation is expected to account for the largest share (40%–60%) of total generation in the (NPCC—Rhode Island, Massachusetts, Connecticut, New York) and Southwest (ERCOT—Texas, SPP—Louisiana, Oklahoma); between 10–20% in the West (WSCC—primarily California) and the Mid-Atlantic States (MACC—New Jersey); and about 7% in the Southeast (SERC—primarily Florida). This pattern of fuel consumption among regions is expected to

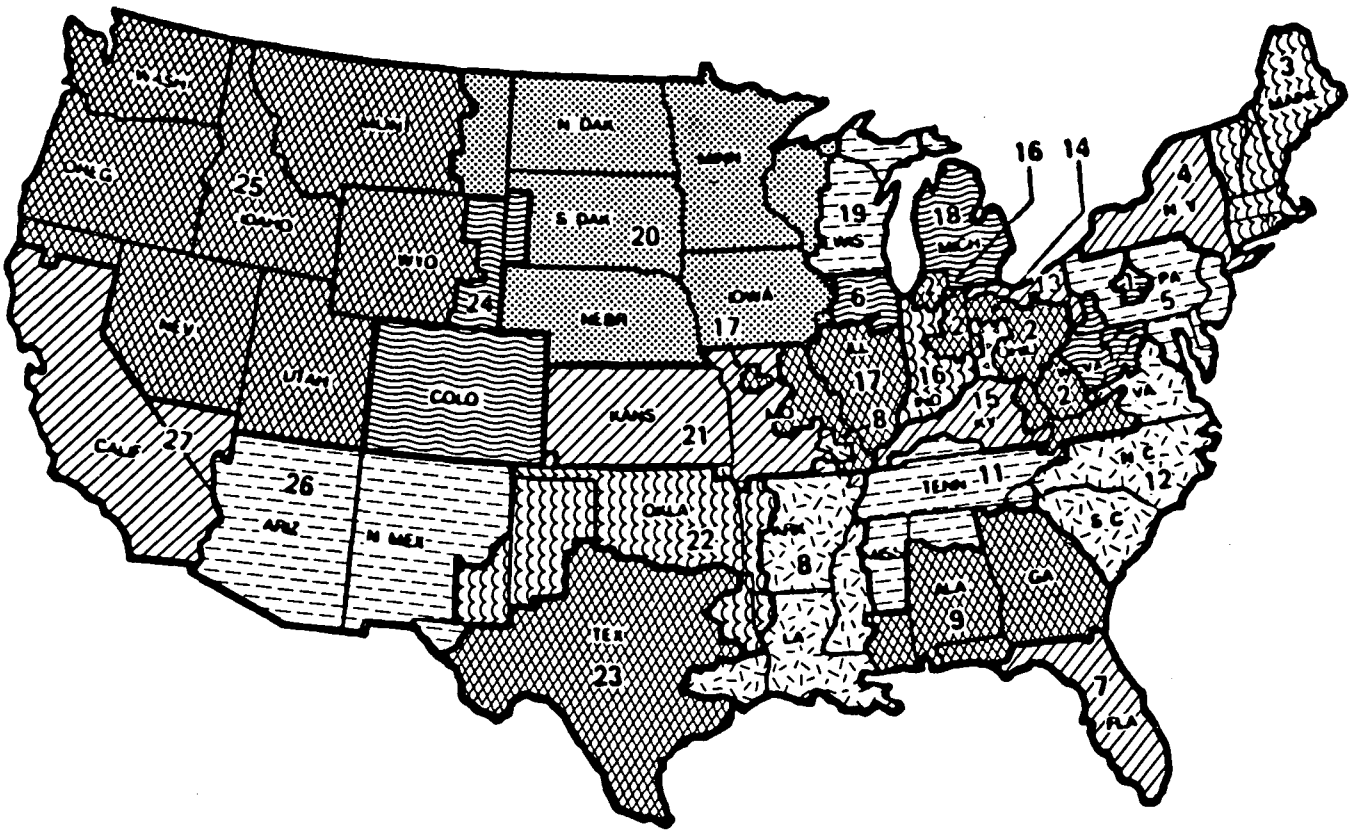

RELIABILITY COUNCIL/Electric Region

ECAR

1. APS (Allegheny Power System)
2. WOIM (West Virginia-Ohio-Indiana-Michigan System)
13. WPANCO (Western Pennsylvania-North Central Ohio Group)
14. CDH (Cincinnati-Dayton-Hamilton Group)
15. KY (Kentucky Group)
16. IND (Indiana Group)
18. LMS (Lower Michigan Systems)

ERCOT

23. No Subregions

MAAC

5. No Subregions

MAIN

6. CECO (Commonwealth Edison Company)
17. SCIM (South Central Illinois-East Missouri Group)
19. WIUM (Wisconsin-Upper Michigan Systems Group)

MAPP

20. No Subregion

NPCC

3. NEPOOL (New England Power Pool)
4. NYPP (New York Power Pool)

SERC

7. FCG (Florida Electric Power Coordinating Group)
9. SOCO (Southern Company Group)
11. TVA (Tennessee Valley Authority)
12. VACAR (Virginia-Carolinas Group)

SPP

8. MSGS (Middle South-Gulf States Group)
21. MOKN (Missouri-Kansas Group)
22. OKLA (Oklahoma Group)

WSCC

24. RMPA (Rocky Mountain Power Area)
25. NWPP (Northwest Power Pool Area)
26. AZNM (Arizona-New Mexico Power Area)
27. CASN (California-Southern Nevada Power Area)

Figure 1. NERC regions and DOE Electric regions. (XBL 8510-11733)

a) High Oil/Gas Backout (POG)

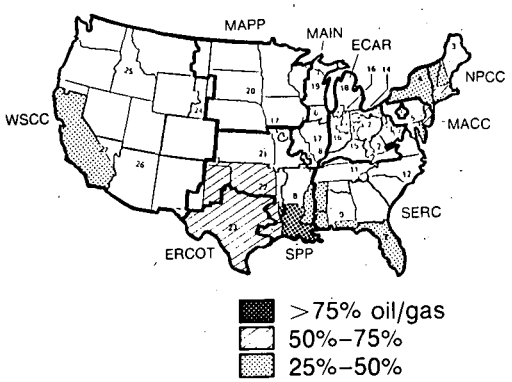

Source: 1984 State data

b) Little or No Marginal Low-Cost Power (Projected 1986 Estimate for YEARS)

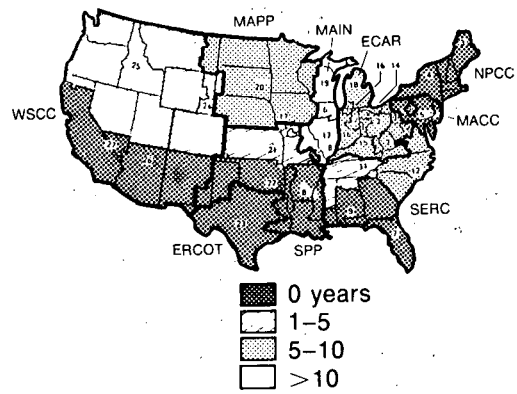

Source: DOE, 1984 Subregional data

c) Relatively High Growth 1984-1993 (GROWTH)

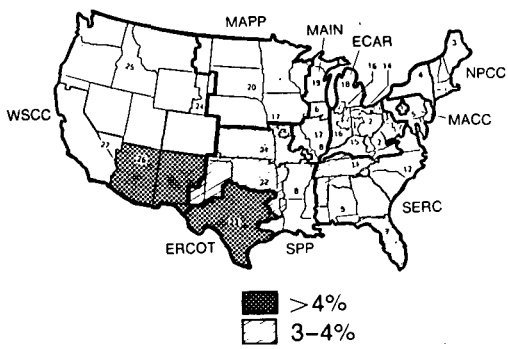

Source: NERC, 1984 Subregional data

d) Early Need for New Capacity – Case II (SubRYN-2)

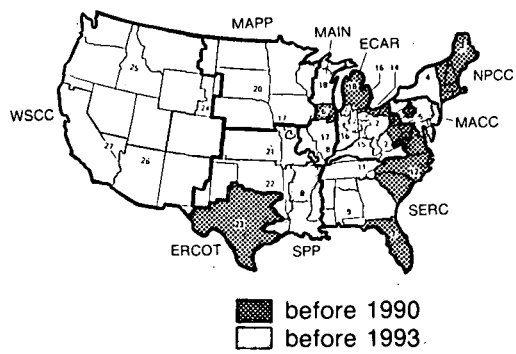

Source: DOE, 1984 Subregional data

e) High Risk for New Power Plants (Low or No CWIP)

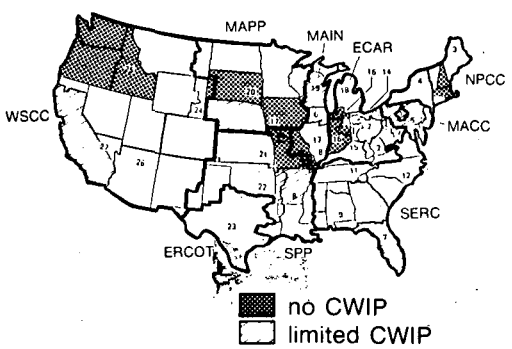

Source: NARUC, 1984 State data

f) Institutions Favor Conservation

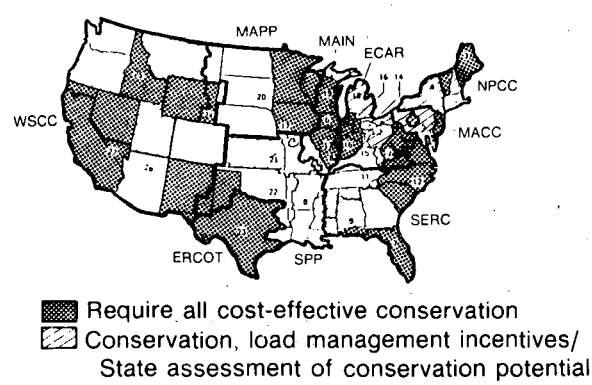

Source: Schneider Survey, 1985 State data

Figure 2. Selected indicators of potential for new and enhanced electric utility conservation programs. (XBL 862-9106)

remain about the same during 1984–1993 because of the projected slowdown in capacity additions.[4]

Little or No Marginal Low-Cost Base Power

We define Potential Low-Cost Capacity (PLCC) as the potential to produce energy from all inexpensive generating facilities (hydro, nuclear, coal and imports*) in excess of that needed to meet the utility's total demand. Utilities with excess low-cost marginal power have a near-term incentive to increase revenues because the primary cost associated with selling an addition kWh is fuel cost, which is usually lower than the average cost of electricity. They are unlikely to favor energy conservation because increase sales represent an opportunity to generate additional profits. In an environment of increasing marginal cost, utilities with little or no available cheap power will tend to favor conservation.

Where PLCC > 0, we estimate the number of years (YEARS) until the available low-cost energy is used up given the average (1984–1993) growth rate projected for the region and subregion. We believe that utilities will consider conservation as an option for meeting electricity demand so long as the supply of low-cost marginal energy is less than ten years, the time needed for construction and licensing of new coal and nuclear power plants.

Figure 2(b) is a map of the 1986 YEARS estimate at the Electric Region (subregional) level. Based on 1983 data, the subregions projected to have no low-cost power in 1986 are located in:

ERCOT (Electric Region 23, Texas),
MAAC (Electric Region 5, Pennsylvania, New Jersey, Maryland),
NPCC (the New England States),

and portions of:

WSCC (Electric Region 25—Northwest Power Pool, Electric Region 26—the Arizona–New Mexico Group,
Electric Region 27–California–Southern Nevada Group),
SPP (Electric Region 8, Middle South Utilities/Gulf States Utilities Group, and Electric Region 22, Oklahoma Group)
SERC (primarily Electric Region 7, Florida Coordinating Group, and Electric Region 9, the Southern Company Group).

The subregions projected to have 1 to 5 years of low-cost power available are located in:

SERC—Electric Region 11, The Tennessee Valley Authority Group,
SPP—Electric Region 21, Missouri–Kansas Group,
WSCC (Electric Region 24, Rocky Mountain Power Pool).

Given the growth rates in these regions, surplus cheap power is expected to be fully utilized by 1990.

Electric Regions located in ECAR and MAPP are projected to have between 5 and 10 years of surplus low-cost energy. Their interest in conservation may depend on the availability of other least-cost options for meeting projected demand.

The economic environment for conservation is unfavorable in the three Electric Regions located in MAIN. Electric Region 6—the Commonwealth Edison Co., Electric Region 17—the Illinois– Missouri Group, and Electric Region 19—the Wisconsin–Upper Michigan Systems Group are all projected to have greater than 10 Years of surplus cheap power in 1986. However, surplus low-cost power in the MAIN Reliability Council area is projected to decrease from 12 years to less than 10 years by 1990.

Relatively High Growth

The rate of growth of electricity demand plays a significant role in utility decision-making, as it influences electricity production, the type and quantity of fuel consumed, capacity expansion, reliability, financing, and end-use electricity prices. Lower than expected demand growth exerts upward pressures on electricity prices as new plants come on line. Higher than expected rates of electricity demand increase the need for capacity required to ensure reliable electricity supplies.

Figure 2(c) shows the subregions where projected 1984–93 average annual net energy growth rates are greater than 3%.[5] The subregions with relatively high electricity demand growth (>4%) are WSCC (Electric Region 26—Arizona–New Mexico) and ERCOT (Electric Region 23—Texas). SPP (Electric Region 21 and 22, Missouri–Kansas and Oklahoma Groups), and SERC (Electric Region 7 and 11, Florida Coordinating Group and Tennessee Valley Authority Group) have projected average electricity demand growth rates between 3% and 4%.

*We assume in general imports will be lower-than-average cost power. Formally, PLCC is expressed as:

$PLCC = |(C + N + H + NP) - T)|/ T$, where
C = Coal Capacity$_i$ (MW) · 8760 hr · 0.65 (capacity factor),
N = Nuclear generation (MWh)
H = Nuclear generation (MWh)
NP = Net purchases (MWh)
T = Total Net Generation.

Early Need for New Capacity

We focused on data for years where adjusted reserves at the subregional level are less than 5% as the most favorable case for conservation.* Regional and subregional surplus/deficit (SUR/DEF, SHORT) at time of summer and winter peak is computed as capability (MW) in excess of or needed to meet a 5% reserve margin.[6] Based on the demand growth rate in the region and subregion, we estimated the Years Until New Capacity is Needed (RYN, SubRYN) for when surpluses will be used up.

We examine two cases of projected capacity additions. Case I is our analyses of when and where new capacity is needed based on DOE regional data for planned capability 1983–1992.

Under Case I, need for new capacity in the later half of the 1980's is projected for:

ECAR (Electric Regions 1, 13, 14, 18),
MAIN (Electric Region 6),
NPCC (Electric Region 3), and
SERC (Electric Regions 11, 12);

and in the early 1990's for:

MAPP (Electric Region 20), and
ERCOT (Electric Region 23).

Figure 2(d) shows the timing of need for new capacity† among the Electric Regions under Case II. In Case II, planned capability is adjusted for nuclear power plants not in operation or likely to be canceled.‡ The near term consequences of such reductions in planned capacity may be less reliable electricity supplies, power purchases, higher utility oil and natural gas consumption, and/or higher electricity prices. Projected shortages deepen for all affected regions in Case I and are expected to occur earlier for ERCOT (1989) and MAAC (1990). Several of these NERC Regions may need to institute conservation programs or plan for new capacity or purchases (provided adequate transmission facilities are available) at some peak periods during the coming decade if the predicted conditions actually occur.

*DOE defines Adjusted Reserve as: Planned Capability − (Outages + Scheduled Maintenance + Other Unavailability) − Peak. An adjusted reserve margin of 5%–7% is consider sufficient to ensure reliability. This is roughly equivalent to capacity margins of 15%–20% used by the industry.

†We present the earlier of summer or winter estimates.

‡We considered the following nuclear power plants as likely to be canceled: Midland 2 (ECAR), South Texas 2 (ERCOT), TMI-1 (1985 only), TMI-2, Limerick 2 (MAAC), Seabrook 2 (NPCC), and Grand Gulf 2 (SPP).

High Risk for New Power Plants (Low CWIP)

Given the lengthening construction period for new power plants, utilities are increasingly advocating the partial or total inclusion of financing costs in the rate base *as they occur* to improve their cash flow during the construction period. Concurrent ratebasing of construction financing costs is generally referred to as CWIP—Construction Work in Progress. If the full cost of financing new power plant construction is allowed in the rate base, the long-term attractiveness of conservation compared with new construction as a way of balancing supply and demand will decline because this treatment of financing costs reduces the economic disincentive for building unnecessary capacity. Figure 2(e) shows the location of states that disallowed or limited CWIP in 1984[7]:

NPCC (New Hampshire, Massachusetts, Connecticut, and Rhode Island)
WSCC (Washington, Oregon, Idaho, California),
MAPP (S. Dakota, Nebraska, Iowa),
SPP (Missouri, Arkansas),
ECAR (Indiana),
MACC (Pennsylvania),
and SERC (Florida).

It is important to keep in mind that regulatory policy is this area is volatile; state public service commissions may expand or contract allowance of CWIP based on their evaluation of both the need for new capacity and a utility's financial condition.

Favorable Political/Institutional Environment

In FY 85, we updated the indicators for the Political/Institutional Factor with the results from a recent survey of public service commissions conducted by the Office of Congresswoman Claudine Schneider.[8,9] We consider the requirement of conservation investments as the most favorable indicator of regulatory interest in energy conservation, followed by the existence of state conservation, load management incentives, and/or assessments of conservation potential. Nineteen states require utilities to demonstrate that they are acquiring all cost-effective conservation and load management before investing in new energy sources. Eleven states have instituted either conservation or level management incentives, and 28 states have conducted independent assessments of conservation potential.

Figure 2(f) shows the states with the most favorable environment for conservation. They are located in:

ECAR (Indiana, Michigan, Ohio);
ERCOT (Texas),
MACC (New Jersey, Pennsylvania, Maryland);
MAIN (Wisconsin, Illinois, Michigan);
MAPP (Iowa, Minnesota);
NPCC (Maine, Vermont, Delaware, New Hampshire, Connecticut, Massachusetts, New York);
SERC (Virginia, North Carolina, South Carolina, Florida, Alabama, Mississippi);
SPP (Kansas, Texas); and
WSCC (California, Nevada, Idaho, Wyoming, Oregon, Montana, New Mexico).

Combining the Selected Indicators

Table 2 summarizes the result of the six indicators for the NERC regions. "No Low-Cost Power" and "Early Need for New Capacity" are weighted as key indicators of merit in the composite rating of "Favorable to Conservation."

There is a clear need now to consider conservation in Group A: Texas (ERCOT—Electric Region 23), the mid-Atlantic (MAAC—Electric Region 5), the Northeast (NPCC—Electric Region 3 and 4), Florida (SERC—Electric Region 7), the Mid-South (SPP—Electric Region 8), and the West (WSCC—Electric Regions 25, 26, and 27) are areas that have regions with no surplus low-cost capacity. Also, on economic grounds, the potential for conservation is good in Group B, regions with 1–5 years of cheap energy, which includes SERC—Electric Regions 9 and 11 (Southerm Compny and TVA), SPP—Electric Regions 21 (Missouri–Kansas) and 22 (Oklahoma), and WSCC—Electric Regions 24 (Rocky Mountain).

Group C represents regions that are borderline favorable to conservation. They include Electric Regions in ECAR (1, 13, 14, 16, 18), MAPP (20), and SERC (12) that have an estimated 5 to 10 years of surplus low-cost energy. Some Electric Regions in ECAR and SERC are expected to need additional new capacity by the early 1990s. Utilities in these areas may consider appropriate "least-cost" capacity-enhancing alternatives along with conservation research at this time.

Utilities within regions belonging to Group D are considered unlikely to implement conservation programs in the near term. The availability of CWIP in Electric Regions 2 and 15 (ECAR), combined with an expected 5 to 10 years surplus of low-cost energy, would also make conservation a less competitive option in the long term compared with construction of small power plants. There may be some tension between the institutional environment and economic reality for Electric Regions in MAIN. For 1986, Electric Regions 6, 17, 19 in MAIN are projected to have greater than 10 years of low-cost surplus energy. PUCs in these regions seem to favor conservation, whereas the economics of excess low-cost capacity would tend to push utilities to promote greater sales in the short term. Utility interest in conservation for MAIN may become more favorable after the 1990s when the region will have less than 10 years of surplus low-cost power and a need for new capacity to ensure reliability of power supply.

Limitations of the Study

The purpose of our regional analysis is to segment the market for energy conservation among investor-owned utilities having different system characteristics to support DOE policy and program planning efforts. Selected indicators focused on key economic measures of avoided costs, and provide a qualitative review of the ratemaking and institutional environment. At the next step of implementation, actual design and selection of conservation programs, will require careful examination of program costs/benefits at the utility level.

PLANNED ACTIVITIES FOR FY 1986

Although the work on this study was completed during the past fiscal year, related research is continuing. Two new LBL utility case studies—Texas Power and Light and Nevada Power—are in process to examine the effect of appliance standards on utility revenues. Two computer models developed to analyze generation expansion (EGEAS) and load management alternatives (LMSTM) are being evaluated to determine through hands-on experience the application of these models in comparing supply and demand-side options. A third project, jointly funded by PG&E and DOE, examines methodological issues associated with demand-side management programs for a large utility. When completed, these studies will provide useful information for the development of conservation programs and Least-Cost initiatives.

REFERENCES

1. Yen-Wood, W., Kahn, E., Levine, M. (1985), *Utility Overview Study Final Report, FY 1985* LBL-21056, *Forthcoming.*
2. Federal Energy Regulatory Commission (1971), *Power Pooling in the United States, FERC-0049, (Washington, D.C.).* Edison Electric Institute (1984), Table 22–Generation by Fuel, Total Electric Utility Industry (by State and Kind of Fuel), p. 31.

Table 2

FAVORABLE TO CONSERVATION - 1986

NERC Reliability Region	DOE Electricity Region	Identification	High Oil Backout	No Low-Cost Power	High Demand Growth	Early Need for Cap	No/Low CWIP	Favorable Inst.	Composite Rating
ECAR	1	Allegheny Power Systems (APS)		~		+		+	C
	2	W. Va-Ohio-Ind-Mich Systems (WOIM)		~				+	D
	13	W. Pa-No. Central Ohio (WPANCO)		~		+		+	C
	14	Cincinnati-Dayton-Hamilton (CDH)		~	+		+	+	C
	15	Kentucky Group (KY)		~				+	D
	16	Indiana Group		~		+	+	+	C
	18	Lower Michigan Systems		~	+	+		+	C
ERCOT	23	Texas Interconnected Systems Group (TIS)	+	+	+	+		+	A
MACC	5	Pennsylvania-New Jersey-Maryland Interconnection (PJM)		+		+			A
MAIN	6	Commonwealth Edison Co. (CECO)				+		+	D
	17	Illinois-Missouri Group (ILLMO)						+	D
	19	Wisconsin-Upper Michigan Systems Group (WUMS)				+		+	D
MAPP	20	Mid-Continent Area Power Pool		~			+	+	C
NPCC	3	New England Power Pool (NEPOOL)	~	+		+	+	+	A
	4	New York Power Pool (NYPP)	~	+			+	+	A
SERC	7	Florida Coordinating Group (FCG)	~	+	+	+		+	A
	9	Southern Company Group (SOCO)		+					B
	11	Tennessee Valley Authority Group (TVA)		+	+	+			B
	12	Virginia-Carolina Group (VACAR)		~		+		+	C
SPP	8	Middle South Utilities/Gulf States Utilities Group (MSGS)	+	+		+	+	~	A
	21	Missouri-Kansas Group (MOKAN)		+	+		+	+	B
	22	Oklahoma Group (OKLA)	+	+	+			+	B
WSCC	24	Rocky Mountain Power Pool (RMPP)		+				~	B
	25	Northwest Power Pool (NWPP)		+				+	A
	26	Arizona-New Mexico Group (AZNM)		+	+			+	A
	27	California-So. Nevada (CASN)	+	+			+	+	A

Indicators: + - Very Favorable; + - Favorable; ~ - Borderline Favorable

Capacity Rating: A - Very Favorable; B - Favorable; C - Borderline Favorable; D - Unfavorable

Source: LBL Report LBL -21056

Note: To derive the composite rating, we assigned the following numerical weights and scales to selected indicators. Scales for each indicator are shown in parenthesis, in the order for "very favorable," "favorable," and "borderline favorable."

1. High Oil Backout = 1, (3, 2, 1)
2. No Low-Cost Power = 5, (5, 3, 1)
3. High Demand Growth = 1, (3, 2, 1)
4. Early Need for New Capacity = 1.5, (3, 2, 1)
5. No/Low CWIP = 1, (3, 2, 1)
6. Favorable Institutional Environment = 1, (3, 2, 1)

For the composite rating, Very Favorable is A = > 27; Favorable is B = 18 to 26; Borderline Favorable is C = 9 to 17; Unfavorable is D = 0 to 8.

XBL 862-443

3. Edison Electric Institute (1984), *Statistical Yearbook of the Electric Utility Industry/1983,* Washington, D.C. Table 22–Generation by Fuel, Total Electric Utility Industry (by State and Kind of Fuel), p. 31.
4. Energy Information Administration (1985), *Annual Outlook for U.S. Electric Power 1985,* DOE/EIA-0474(85).
5. North American Electric Reliability Council (1984), *Electric Power Supply & Demand, 1984–1993,* Table 1–Net Energy for Load, p. 9.
6. Department of Energy (1984), *Electric Power Supply and Demand for the Contiguous United States 1984–1993,* DOE/IE-0003, pp. 8, 30–32, and Tables ER1–ER27.
7. National Association of Utility Regulatory Commissioners (1983), *1983 Report of the Ad Hoc Committee on Energy Conservation,* Washington, D.C.
8. Markowitz, P. (1985), Personal Communication with Winifred Yen-Wood, November 4, 1985.
9. Schneider, Claudine (1985), "Survey Results of Regulatory Utility Commissions' Electrical Resource Planning and Conservation Activities."

Energy Efficiency Choice in the Purchase of Residential Appliances*

H. Ruderman, M.D. Levine, and J.E. McMahon

This study provides a quantitative analysis of the behavior of the market for the purchase of energy efficiency in residential appliances and heating and cooling equipment. Accurate forecasts of residential energy use require quantitative assessments of market decisions about energy efficiency. The results of our investigation of market behavior can lead to a better understanding of the barriers to investment in energy conservation. Understanding market behavior over time is a prerequisite to an evaluation of the need for and the importance of policies to promote energy efficiency.

The importance of such an analysis to DOE's assessment of its proposed Consumer Products Efficiency Standards relates to its use in forecasting the behavior of the market. Most of the direct impacts of standards (energy savings, net present benefit, and cost of proposed standards) depend critically on the degree to which higher efficiency would be incorporated into new products in the absence of standards. The research will lead to improvements in the methodology and data in the base-case residential energy forecast, thereby improving estimates of the impacts of the standards.

*This work was supported by the Assistant Secretary for Conservation and Renewable Energy, Office of Buildings Energy Research and Development, Building Equipment Division of the U.S. Department of Energy under Contract No. DE-AC03-76SF00098.

In this study, we examine the historical efficiency choices for eight consumer products: gas central space heaters, oil central space heaters, room air conditioners, central air conditioners, electric water heaters, gas water heaters, refrigerators, and freezers. These products were selected because (1) they account for a major part of residential energy consumption, (2) data on efficiency and costs are readily available, and (3) they are under consideration by DOE for efficiency standards.

We characterize the behavior of the market for these eight products by a single quantity, which we call an aggregate market discount rate. The aggregate market discount rate quantifies the behavior of the market as a whole with respect to energy efficiency decisions. Choices by individual purchasers are constrained by the decisions made by the manufacturers of appliances, the wholesalers or retailers who distribute them, and third-party appliance installers such as builders or plumbers. The value of the discount rate reflects the actions of all these decision makers. It is determined empirically from data on the efficiency and cost of appliances purchased between 1972 and 1980. By examining the historical behavior of the market discount rate, we can better understand the factors that influence efficiency choice. Furthermore, the market discount rate can be used as a parameter in forecasting future residential energy consumption. A paper on this work will appear in *The Energy Journal;* it is also available as an LBL report.[1]

ACCOMPLISHMENTS DURING FY 1985

Most of the work for this study was completed during FY 1983 and was described in the previous

annual report. During FY 1985, effort focused on four aspects of the study: (1) calculating payback periods as well as aggregate market discount rates; (2) recalculating discount rates based on monthly compounding rather than annual compounding; (3) examining aggregation bias in the estimation of payback periods; and (4) completing a paper for publication in a refereed journal. This article will discuss the first three aspects.

Payback Period Calculation

The simple payback period is defined as the time needed to recoup an initial investment in energy efficiency. Numerically, the payback period is equal to the increase in purchase cost divided by the decrease in annual operating cost. Assuming the operating costs change only because fuel use decreases, we have:

$$\text{Payback} = \frac{\Delta PC}{FP \cdot \Delta E} = \frac{-1}{FP}\frac{dPC}{dE} \quad , \qquad (1)$$

where PC is the purchase cost, FP is the fuel price, and E is the annual energy consumption. For a continuous cost-efficiency curve, the payback period is the present worth factor.

The purchase cost versus energy use relationship that we used was an exponential curve of the form:

$$E = E_\infty + (E_o - E_\infty)\exp[-A(C-1)] \quad . \qquad (2)$$

where:

- $C = PC/PC_o$,
- E = annual unit energy consumption (UEC),
- E_o = highest UEC,
- E_∞ = minimum UEC attainable at infinite purchase cost,
- PC = purchase cost corresponding to E,
- PC_o = purchase cost corresponding to E_o,

and A is a parameter determined from the shape of the curve. Using this expression, the simple payback period is:

$$\text{Payback} = \frac{PC_o}{A \cdot FP \cdot TI}\frac{1}{(E - E_\infty)} \quad , \qquad (3)$$

where we have included a factor TI to account for the possibility that the thermal integrity of the structure may change with time.*

*This factor is defined as the relative energy use at different levels of thermal integrity; hence, TI decreases with better insulation and lower air infiltration.

Presenting this study's results in terms of a payback period has some advantages. First, the concept is simpler than that of an aggregate market discount rate and may be closer to what consumers use to make decisions. Second, the payback period does not depend on assumptions about appliance lifetimes and compounding periods. This point will be discussed in more detail below. Finally, discount rates are nonlinear functions of the measured parameters; hence, their values can be very sensitive to small changes in the measurements.

Average payback periods during the years 1972–1980 for the eight appliances are presented in Table 1. Except for air conditioners, the market required an average payback of less than 3 years for an investment in improved appliance efficiency, and for electric water heaters and freezers, the requirement was less than 1 year. Most of the payback periods appear to be stable over time. This supports our previous conclusions that the market for energy efficiency is not working well and that it has not shown much improvement over the past 10 years despite rapid increases in energy prices and increased awareness of energy conservation.

Table 1. Payback period (in years) for appliances, 1972–1980.

Appliance	1972	1978	1980
Gas central space heater	2.98	2.38	2.21
Oil central space heater	2.33	1.70	1.18
Room air conditioner	5.11	4.77	5.25
Central air conditioner	4.96	4.16	5.18
Electric water heater	0.48	0.41	0.41
Gas water heater	1.50	1.07	0.98
Refrigerator	1.35	1.45	1.69
Freezer	0.60	0.67	0.72

Monthly Discounting

The most common method for evaluating discount rates is to take the time period as 1 year. However, this will underestimate the discount rate when the payback period is shorter than 1 year. Since fuel and electricity bills are paid monthly, we chose a one-month time period for evaluating the market discount rate. It is calculated by solving the following equation for the discount rate r, given a present worth factor or payback period:

$$PWF = \sum_{t=1}^{N}\frac{1}{(1+r)^t} = \frac{1}{r}\left[1 - \frac{1}{(1+r)^N}\right] \quad . \qquad (4)$$

The appliance lifetime N in this equation is expressed in months. An exact calculation would take into account the monthly variation in energy use by each appliance and the month in which it was bought. Since these data are not available, we average over 1 year so that the monthly energy use is one-twelfth of the annual. In presenting our results, we calculate an annualized discount rate $\bar{r}$ from the monthly discount rate r, using the relationship:

$$1 + \bar{r} = (1 + r)^{12} \quad .$$

The revised annualized discount rates shown in Table 2 are higher than those calculated previously for a period of 1 year. The difference is largest for appliances with short payback periods. Although the values are different, our original qualitative results—that market discount rates for most appliances are higher than those expected under perfect market conditions—still hold. These results support the viewpoint that market forces alone are not enough to eliminate the substantial economic inefficiencies in appliance energy use.

Aggregation Bias

In calculating the payback period and market discount rate, we assume that all consumers will have an average energy use corresponding to the sales-weighted efficiency factor (SWEF). If, in fact, there is a distribution of energy consumption due to differences in efficiency choice or usage, the average market payback period of these users may be different from that calculated from the average energy use. We investigate this aggregation bias in two cases: one in which there is a distribution in energy use and a second in which there is a distribution in appliance efficiency. In the first case, the average payback period is greater than that calculated from the average energy use (and the discount rate is less). In the second case, the direction of the aggregation bias depends on the ratio of average efficiency to the maximum efficiency corresponding to E_∞. The amount of bias depends on the width of the energy and efficiency distributions.

To estimate the magnitude of the aggregation bias, we used data on the distribution of efficiency of central air conditioners in 1980 published by the Air-Conditioning and Refrigeration Institute.[2] The average efficiency (SEER) was 7.76, with a standard deviation of about 10%. This gives an aggregation bias of about 1%. Biases of this size are small compared to the uncertainties caused by measurement error in the SWEF and other data used to calculate the payback period.

Table 2. Aggregate market discount rates (in percent) for appliances, 1972–1980.

Appliance	1972	1978	1980
Gas central space heater	39	51	56
Oil central space heater	52	78	127
Room air conditioner	20	22	19
Central air conditioner	19	25	18
Electric water heater	587	825	816
Gas water heater	91	146	166
Refrigerator	105	96	78
Freezer	379	307	270

PLANNED ACTIVITIES FOR FY 1986

Work during FY 1986 on consumer behavior will concentrate on collecting data on individual purchases of appliances. We will follow up on a TRENDEX survey of refrigerator purchases to get information on the model bought, from which information we can determine its capacity and efficiency. On the basis of these data, we will develop an econometric model of refrigerator purchases relating capacity and efficiency choice to household characteristics such as family size and income.

REFERENCES

1. Ruderman, H., Levine, M.D., and McMahon J.E. (1984), *The Behavior of the Market for Energy Efficiency in the Purchase of Appliances and Home Heating and Cooling Equipment*, LBL-15304.
2. Air-Conditioning and Refrigeration Institute (1983), *Comparative Study of Energy Efficiency Ratios*, Arlington, VA.

An Investigation of the Reasons for the Rapid Market Penetration of Electric Heat Pumps in the Residential Sector*

Mark D. Levine

Imagine the task of an analyst in 1973 whose job it was to predict the sales of heat pumps in residential buildings in the United States. Such an analyst would be aware of the reputation of heat pumps for unreliability. If the analyst were old enough, he might remember the experience with heat pumps in Florida during the 1940's, in which the high failure rate and low reliability of the product virtually destroyed a potentially lucrative market. The analyst would note that the sales of heat pumps had remained relatively constant for many years, at about 2 percent of the total residential market. The analyst would perform economic calculations, and conclude from these calculations that heat pumps were not nearly competitive with gas heat systems and central air conditioners. He would check with manufacturers and discover that no major breakthroughs had occurred in heat pump systems.

The conclusion from this information would be inescapable: heat pumps would probably continue to serve its small market niche. However, there would be no reason to suppose they would increase their market share significantly in the near future (the next ten or fifteen years). A good analyst, working in a position of responsibility, could easily have staked his reputation on such a forecast. If he had done so, he would have been wrong. Starting in 1973, sales of heat pumps in the residential market began a slow ascent, increased again in 1974, and showed dramatic increases in 1975, 1976, and 1977. By 1977, the small market niche had grown to almost eight times the sales in 1972. Relatively constant sales through 1980 gave way to another large increase in 1981. By 1981, sales of heat pumps were more than ten times the 1972 levels; they commanded 20 percent of the total residential space heating market and 50 percent of the electric heating market.

*This work was supported by the Assistant Secretary for Conservation and Renewable Energy, Office of Buildings Energy Research and Development, Building Equipment Division of the U.S. Department of Energy under Contract No. DE-AC03-76SF00098.

ACCOMPLISHMENTS DURING FY 1985

The basic issue addressed by this study was: how can we account for the rapid and seemingly unexpected sales of heat pumps in the United States during the past decade? Are the factors that caused this dramatic increase in market acceptance likely to continue? What basis can be used to forecast future heat pump sales in the residential sector? From the experience of the past decade, what factors are most likely to influence the marketability of heat pumps?

Approach

The first step of the analysis consisted of a series of telephone interviews with individuals in various regions of the United States who were involved in and knowledgeable about the factors affecting heat pump sales. We chose nine locations for which heat pump sales were relatively high (greater than 30 percent of the residential heating market in 1979), with the idea of identifying the causes of high sales.† These nine "case studies" were: Phoenix, Arizona; Philadelphia, Pennsylvania; Tennessee Valley; state of Iowa; portions of the state of Kentucky; state of Maryland; southern and central Indiana; Cincinnati, Ohio; and northeast Ohio.

The second step—carried out at the same time as the case studies— involved the collection of all national (and, where possible, regional) data relevant to the forecasting of heat pump sales. This included: estimates of heat pump performance in different climates; cost of fuels and competing heating and cooling systems; national and regional sales data; and related information. These data provide the standard information base for forecasting. As we have noted, this is the information that—taken alone—served to mislead our hypothetical analyst forecasting heat pump sales in 1972. As we will observe, the current economic data without the information from the case studies fail to explain the phenomenal growth in heat pump sales in the United States.

The third step in the analysis involved the development of analytic techniques to forecast future heat pump sales in the United States. The approach is a mixed estimation technique involving both the use of a discrete choice and an enginnering-economic model. The forecasting uses data concerning both the traditional economic factors and the market factors identified in the case studies of heat pump sales.

†One location, Philadelphia, Pennsylvania, was in a state with lower than 30 percent saturation of heat pumps. It was included because the city represented an example of several factors likely to increase the market for heat pumps in the future.

We have presently completed a first effort on the first two steps. As noted, nine case studies have been carried out and the generally available economic data relevant to sales forecasts have been gathered.

Results

Interpretation of the Rapid Increase in Heat Pump Sales during the Mid-1970's

Sales of heat pumps had been steady from 1963 through 1971. Total U.S. sales were between 76,000 and 88,000 for all but one of these years—97,000 heat pumps were sold in the United States in 1969. Annual sales to the residential sector were virtually constant from 1966 through 1971 (ranging between 60,000 and 68,000), having increased from 49,000 in 1963. Residential sales increased to 80,000 in 1972, but this increase was due to high levels of residential construction in that year rather than to any basic change in the market for heat pumps.

Thus, it was reasonable to conclude that the heat pump industry had achieved a comfortable albeit small niche in the market and expected to see little change in its activities after 1972.

The shock of the oil embargo had some impact on heat pump sales. Total sales grew 20 percent in 1973, almost 20 percent in 1974, and another 20 percent in 1975. The primary effect of the oil embargo and OPEC price increases was on the price and availability of liquid fuels. Heat pumps were not competing strongly in those regions (especially the Northeast) in which fuel oil was a major fuel for space heating. Both gas and electricity prices were rising from 1973–1975, but electric heat pumps were not nearly competitive on a life-cycle cost basis as was gas heating at that time. Furthermore, the higher first cost of electric heat pumps *vis a vis* gas furnaces was a further disincentive to the purchase of heat pumps.

We thus interpret the increase in sales of electric heat pumps in the 1973–1975 period as largely due to effective marketing strategies that recognized the substantial concern about *future* availability and cost of fossil fuels that had permeated large segments of American society. A mature and stable industry had demonstrated the reliability of heat pumps throughout the 1960's. Thus, having a product with a proved track record, the industry was able to benefit from changing perceptions among potential customers.

Had no other developments in fuel availability and cost taken place after 1975, it is unclear whether heat pumps would have continued to increase sales, maintained its market position, or lost sales to competing space conditioning systems. The economics in 1975 was not favorable to heat pumps in competition with gas furnaces. However, the industry had built up into marketing activities and could probably maintain its roughly 5 percent penetration of the residential space heating market. Thus, a good guess is that, had events in the U.S. energy system not radically changed in 1975, annual sales of heat pumps might have reached another plateau at between 150,000 and 200,000 units after 1975.

However, events did change; 1975 saw a shortage of natural gas, starting in several regions of the United States and spreading to very large parts of the nation. The reasons for this shortage need not concern us here, although it is interesting to note that many analysts have concluded that it was largely a result of the U.S. government policies (low, regulated natural gas prices) and could probably have been avoided.

The gas shortage was addressed by giving residential customers who already had gas hookups priority rights (i.e., high allocations) to natural gas. Industrial and electric utility users of gas were restricted and new gas hookups in the residential sector were severely curtailed. Given the shortage of natural gas, public policy dictated that the residential consumer already dependent on gas for space heating suffer the minimum curtailments, as there was no alternative source of heat.

These developments profoundly affected the market for heat pumps in the United States. In vast areas of the country, heat pumps were no longer competing with gas furnaces in new residential construction. The main competition was electric resistance heating (either electric furnaces or strip heating). The economics of heat pumps had turned around, virtually overnight. In many, if not most, parts of the country the heat pumps suddenly became the most economic space conditioning system.

Adding to the attractiveness of heat pumps during the natural gas shortage was the steadily increasing demand for central air conditioning. This phenomenon, largely due to higher income levels and the benefits of air conditioning in hot areas, had been in progress for many years. (Annual sales of unitary air conditioning grew steadily from somewhat under 500,000 in 1962 to between 2.3 and 2.8 million for every year but one from 1972 through 1981). The demand for air conditioning is clearly beneficial to the sales of heat pumps: the economic attractiveness is increased, as the piping, ductwork,

and chiller are paid for in the purchase of the central air conditioners. The relatively high saturation of heat pumps in new houses in the southern portion of the United States, where the sales of central air conditioning systems are highest, is not surprising considering the relative economic advantage of heat pumps when central air conditioning is in any case desired.

The natural gas shortage persisted from 1975 through 1978. Large areas of the United States suffered restrictions in new gas hookups as late as 1978, when the shortages were finally ending. With this background, the rapid increase in heat pump sales during 1975 and 1978 is not surprising. Total sales increased from 139,000 in 1974 to 160,000 in 1975, 325,000 in 1976, 494,000 in 1977, and 572,000 in 1978.*

Presumably the relatively low increase in sales in 1975 is accounted for by the necessity for the industry to increase productive capacity. However, the industry was able to scale up production very rapidly. Sales in 1978 were over 350 percent of the levels of just three years earlier. They were 700 percent of the sales in 1972, just six years earlier.

An important issue confronting the industry after 1978 was whether—in the absence of a natural gas shortage and, as became clearer in later years, the absence of an apparent threat of future shortages—heat pumps could maintain their market share. The sales data for 1979 through 1981 show that heat pump sales remain high. Sales were 640, 447, and 540 thousand units in these three years. The drop in sales in 1980 is due to the low number of housing starts in that year. From 1975 to the present, heat pumps have captured a very consistent 25 percent of the space heating market in new houses. The end of the natural gas shortage shows no influence on the saturation of heat pumps in the 1975–1981 period.

This overview at the national level gives considerable insight into some of the factors responsible for the success of heat pumps in U.S. markets. However, it does not capture the whole story. Numerous forces are at work that strongly influence the market for heat pumps. To understand the factors affecting future markets, we need to understand these forces. We now turn to the information gained in the nine case studies.

*Most of the sales were in the residential market. In 1978, 485 thousand out of 572,000 heat pumps were sold to the residential sector.

Results of Case Studied: Success in the Market Past Natural Gas Shortages

Table 1 summarizes the information gained in the case studies. In all of these cases, sales of heat pumps were high from 1975 through 1978 and have remained high after the end of the natural gas shortage through the present. In this paper, we are able only to summarize the major reasons for the continued success of heat pumps in those markets after the natural gas shortage had abated throughout most of the nation.

Phoenix, Arizona presents an interesting case, with applicability in many other urban areas that have experienced rapid growth in surrounding suburbs. The moratorium on new gas hookups extended from 1976 through 1979 in Phoenix. During this time, urban development was rapid, with the urban area spreading outward from the center. The result of this growth with no new gas hookups was a ring around many parts of the city which is not penetrated by gas mains. Most new housing

Table 1. Summary of heat pump case studies.

	Historical Gas Permit Moratorium	Gas Distribution Costs
Phoenix, Arizona	Recent	High
Philadelphia, Pennsylvania	Now	Low
Tennessee Valley	Recent	High
Kentucky (Except Owensboro Area)	Recent	High
Maryland	Recent	High
Indiana (Southern & Central)	Recent	High
Cincinnati, Ohio	Recent	Low
Northeast Ohio	Recent	Low

developments are presently several miles from existing gas mains. Thus, the cost of new gas hookups is very high. (The charge for a gas hookup is between $300 and $800, depending on the size and location of the new housing development.) As a result of these new economic considerations, the vast majority of new houses in the Phoenix area are expected to have heat pumps.

Philadelphia, Pennsylvania is a case of a persistent gas shortage combined with a utility, Philadelphia Electric Company (PECO), that has marketed heat pumps effectively. For various reasons, gas availability (and new residential gas hookups) did not materialize in the area as quickly after the shortage as in other parts of the country. Because Philadelphia is not a rapidly growing urban area like Phoenix, this did not give a long-term advantage to heat pumps. Nonetheless, it did permit heat pumps to gain a solid and continuing position in the market. PECO has sound economic reasons to promote heat pump sales: a surplus of generating capacity and a high summer peak (providing an incentive to increase winter demand). The utility has combined an extensive heat pump marketing activity with a special winter heating rate that is 3 cents per kilowatt hour below summer rates. For customers who install or replace a central air conditioner, heat pumps are very attractive under these conditions. The utility is particularly eager to see add-on heat pumps using existing gas or oil furnaces as backup systems, as this configuration improves the electric load factor (but causes peaking problems for the gas utilities). As a result of these circumstances, heat pumps capture about 50 percent of the new residential heating market in the PECO service area.

Tennessee has three factors favoring heat pumps:

(1) memory of severe impacts of the gas shortage;
(2) a Federal electricity generating entity, the Tennessee Valley Authority (TVA) eager to promote heat pumps for many of the same reasons as PECO;
(3) low electricity rates, because of low-cost TVA power.

Furthermore, the climate in the TVA area (extending beyond the state of Tennessee) has sufficient cooling loads to provide markets for air conditioning and heating loads to justify the use of a heat pump in winter. Even without special winter heating rates, the economics in the TVA area are relatively favorable to heat pumps.

Iowa illustrates another situation favorable to heat pumps. The state is primarily rural, and natural gas is not available in rural areas. Thus, electric heat pumps compete with high priced propane fuel. Heat pumps have a competitive advantage against propane in addition to providing air conditioning.

The remaining case studies are not discussed in this paper, as they represent various combinations of factors identified in the first four case studies. It is important to recognize that the various factors influencing the market for heat pumps in these case studies are found, albeit in different combinations and of differing importance, throughout the United States. (The major exception to this statement is the colder (northern) portion of the United States, where the performance of commercially available heat pumps has not yet made them widely marketable).

Prospects for the Future

At first glance, it is somewhat surprising that residential heat pumps have been able to maintain their substantial market share after 1976, when the natural gas shortage in the United States ended. Because of higher first costs, heat pumps do not have favorable economics when compared with gas furnaces in almost all regions of the United States. (If a house does not need central air conditioning, then heat pumps are very expensive compared to gas furnaces. However, because of higher first costs of heat pumps compared with gas furnace/central air conditioning systems and the relative costs of electricity and natural gas for heating, the annualized cost of a heat pump system is higher in most parts of the country than that of a gas furnace/air conditioning system.)

Nonetheless, for the factors identified above, we believe it is likely that heat pumps will retain their market share. We believe the rural areas and suburban areas without gas mains, like Phoenix, will continue to be growing markets. We are convinced that those electric utilities which stand to benefit from heat pump sales will be an important instrument for marketing heat pumps, both through direct marketing programs and preferential rates, where permitted by regulatory agencies. The importance of these utility programs should not be underestimated, as the utilities have been potent actors in the space conditioning market. (We estimate that as many as one third of U.S. utilities would clearly benefit from increased sales of heat pumps.) Central air conditioning sales are expected to remain strong. Furthermore, the sales of heat pumps over the past decade will open up a large replacement market for heat pumps.

When we combine these market factors with a heat pump industry that has a strong marketing apparatus of its own, we conclude that the industry

is likely to hold (or possibly increase slightly) its share over the next five to ten years, in the absence of surprises in the price and availability of energy. Over the longer term, the higher price escalation of natural gas will eventually benefit heat pumps, if costs and efficiency improvements of heat pumps and gas furnaces are comparable.

PLANNED ACTIVITIES FOR FY 1986

In FY 1986, we will expand the case studies, gather more quantified data in a number of additional regions, and then commence the modeling during the current and next fiscal years. The challenge facing this work is to do better than the hypothetical analyst in 1972, who was totally misled by historical data on heat pump sales. A major issue is whether rigorous modeling is able to give more credible answers about future sales of heat pumps than we can do at present, given the information from the case studies and the national data. In any case, we are convinced that a meaningful model of heat pump penetration needs to properly account for many factors—in addition to the direct economic data—that influence sales of heat pumps. The exercise we are involved in is thus a serious effort to build a model that departs from (or, from another point of view, extends) the traditional economic approaches to forecasting the market penetration of products.

Validation of the LBL Residential Hourly Demand Model*

H. Ruderman, G. Verzhbinsky, and M.D. Levine

For the past few years, we have been developing a model of hourly and peak residential electricity demand in utility service areas. The model enables us to examine the effects of various energy conservation policies on utility load shapes. Changes in peak load and load factor can affect the financial picture of an electric utility by reducing or increasing the need for new generating capacity. Knowing how conservation policies affect electricity sales and load shapes is crucial for understanding whether utilities will support the policies and assist in their widespread adoption. Application of the model to two utility service areas is described in another article ("Economic Impacts of Residential Conservation Programs on Electric Utilities") in this report.

The model operates by disaggregating projections of annual residential electricity consumption for 12 end uses to each hour of the year. The disaggregation is accomplished with the aid of hourly load profiles for the temperature-insensitive end uses and by fraction-in-use matrices for the temperature-sensitive end uses. The latter contain data on the fraction of the installed appliance capacity in use for each hour of the day, versus temperature or a temperature-humidity index. At present, the annual consumption projections are provided by the ORNL/LBL Residential Energy Use Model.[1,2] Because of the high level of disaggregation in both the hourly and annual consumption models, utility and government policies targeted at specific appliances and building characteristics can be evaluated. Details of the construction, operation, and validation of the residential hourly and peak load model may be found in an LBL report.[3]

ACCOMPLISHMENTS DURING FY 1985

Work this year was primarily directed toward (1) adding a new heat pump module, (2) calibrating and validating the model, and (3) completing the documentation.

New Heat Pump Module

This year, we wrote a new module to calculate heat pump loads in the heating mode. The key part of this effort was an analysis of the difference in performance of heat pumps and electric resistance heaters. Using the DOE-2 program, we simulated hourly electricity loads in residential buildings heated by heat pumps or resistance heaters in four locations: Detroit; Washington, DC; Phoenix; and Minneapolis. For each location, we recorded the heat pump electricity demand for heating for each hour of the year in a matrix by hour of the day and outdoor dry-bulb temperature. Each element in the

*This work was supported by the Assistant Secretary for Conservation and Renewable Energy, Office of Buildings Energy Research and Development, Building Equipment Division of the U.S. Department of Energy under Contract No. DE-AC03-76SF00098.

matrix represented the average heat pump demand for the corresponding hour and temperature. We constructed a similar set of matrices for the operation of electric resistance heaters under the same conditions. Dividing each element in the heat pump matrix by the corresponding element of the resistance heater matrix gives a matrix of heat pump efficiencies.

In examining these efficiency matrices, we noticed that they were nearly the same for all locations, except for missing elements in the warmer locations that represented combinations of temperature and hour of day that did not occur. Furthermore, there was little diurnal variation in the efficiency. Thus, we concluded that the average heat pump efficiency depended only on temperature. A code was incorporated in the peak load model to construct the heat pump fraction-in-use matrix by multiplying elements of the corresponding electric resistance fraction-in-use matrix by the heat pump efficiency at that temperature.

The heat pump module was tested by simulating a winter peaking utility based on data from the Detroit Edison Company (DECO). DECO was changed from a summer to a winter peaking utility by increasing the saturation and market penetration of electric heating systems relative to gas and oil systems. With these changes, the peak residential load occurred in January. We compared projections of annual energy use and peak load for space heating for two cases: (1) all-electric heating was supplied by resistance heaters operating at 100% efficiency, and (2) 10% of the electric heating systems were heat pumps with an average coefficient of performance (COP) of 1.88.

The results showed both qualitative and quantitative agreement with what would be expected if heat pumps were substituted for electric resistance heaters. The average COP of heat pumps was higher than the COP at peak load because peaks occur during periods of low outdoor temperature. The average COP calculated from the ratio of annual energy use was 1.89. The peak load COP of 1.13 calculated from the ratio of peak loads was slightly different from the value of 1.11 calculated from the DOE-2 simulations of resistance heaters and heat pumps discussed above. This small discrepancy is due to the normalization to annual energy consumption in the model. We believe these results demonstrate that the module is operating correctly, but the final test will be to compare heat pump loads with measured utility data when they become available.

Model Validation

A major effort took place during this year to validate the LBL residential hourly and peak demand model, using data from DECO. We compared historical residential loads in the service area with the loads calculated by the model. This allowed us to calibrate the model to account for some of the residual demand diversity not included in the original matrices. We used the Detroit Edison service area because this utility provided us with the most complete set of data.

Before comparing the simulated loads with actual measurements, we made adjustments to the data in the ORNL/LBL and peak load models. First, to estimate building thermal integrities, we compared utility data on annual energy consumption for space conditioning with results from the DOE-2 energy model for single-family detached houses. Second, we modified the fraction-in-use matrices for several end uses in order to match the observed daily load shapes.

The data provided by DECO for annual heating and cooling requirements of existing single-family homes are used in the ORNL/LBL and hourly load models. However, DECO did not have data on the heating and cooling requirements of new houses. We used the relative values obtained from DOE-2 simulations, scaled to the data for existing houses, to obtain the annual energy requirements of new houses. We then calculated the ratio of energy consumption for new and existing houses from DOE-2 heating and cooling loads to obtain the thermal integrity factors needed in the ORNL/LBL model.

We made some adjustments to the original fraction-in-use matrices to get better agreement with the historical load shapes. For example, the hourly load curve for freezers contained an obvious typographical error. In another instance, the original curve for clothes dryers showed a sharp dip in energy use during the evening. There seemed to be no obvious explanation for this result, so we increased the load during these hours to give a smooth variation. Another problem was that the load curve for cooking peaked between 6 and 7 a.m. and again between 4 and 5 p.m. Better agreement with measured load shapes was obtained when the cooking curve was shifted 1 hour later.

The most significant change was made in the shape of the miscellaneous load. The original data for this load shape came from single-family homes in Southern California, where the miscellaneous load

varied by more than a factor of 20 from its minimum in the middle of the night to its maximum at 9 p.m. We believe the miscellaneous load varies greatly between service areas because of differences in the mix of appliances that contribute to this component of demand, so that the Southern California data are naturally different from data from residences in the DECO service area. For example, electric swimming pool heaters are commonplace in Southern California, whereas electric blowers on gas furnaces are important in Detroit. Additional research is needed to characterize this end use properly. It may be necessary to further disaggregate the miscellaneous load to reproduce accurately its time and temperature dependence in the model. As a first approximation, we used flat summer and winter miscellaneous loads (taken at the average of the daily load curves). These gave good fits to the hourly load shapes, so we made no further adjustment.

Figure 1 compares the annual residential electricity sales for 1977–1982 in the DECO service area with the results of the ORNL/LBL model. The model results have been corrected for year-to-year differences in weather. We derived unit energy consumptions for space conditioning equipment from DOE-2 runs using a Temperature Reference Year (TRY) tape. We adjusted space heating and cooling annual electricity use for actual weather in proportion to heating and cooling degree days, respectively. The calculated residential sales are about 1% lower than the actual sales over the 6-year period, which gives us confidence that the ORNL/LBL model is responding properly to changes in housing stock, appliance saturation and efficiency, and economic conditions.

A direct comparison of simulated peak residential loads with actual loads was not possible because DECO reports the residential load on the system peak day rather than on the residential peak day. Figure 2 compares the calculated and actual maximum residential load on the system peak day during the period 1977–1982. Except for 1981, the two agree to within 10%. The 1981 point was calculated using a temperature of 98°F from a weather tape for that year. Detroit Edison, however, claims the maximum temperature on the peak day was 92°F, which would bring the calculated load down to about 2400 MW, closer to the actual value of 2185 MW. We are investigating the possibility that we used the wrong weather tape in the calculations for 1981.

Figure 3 shows a comparison of the hourly loads that occurred on the peak days of each month during 1982 with the predictions of the hourly load model after the adjustments described above were made. The agreement is quite good for most months. There appears to be some tendency for the evening peak to be too short and for the early morning minimum to be too low. Because the agreement of the hourly load shape is good over the whole year, we believe the model can accurately forecast load-duration curves as well as peak residential loads.

The largest discrepancy occurs on May 18th, when the temperature exceeded 80°F for the entire afternoon. That the model predicted a load much larger than the actual load may be due two factors, one technical and one behavioral, that it does not capture. First, the model calculates the air condi-

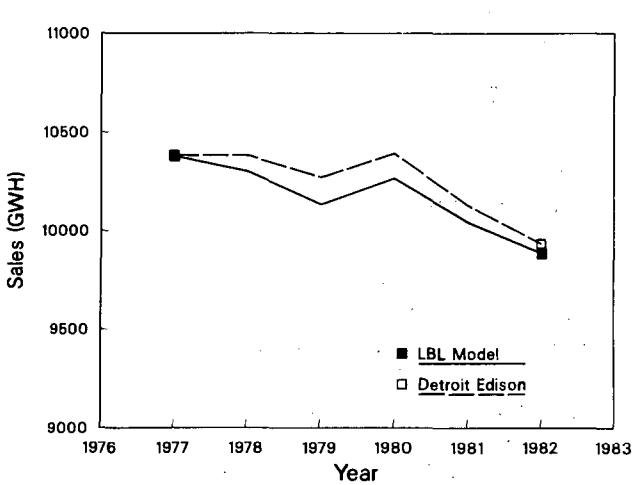

Figure 1. Comparison of annual residential electricity sales, 1977–1982, in Detroit Edison service area with results of the ORNL/LBL Residential Energy Use Model. (XCG 851-7)

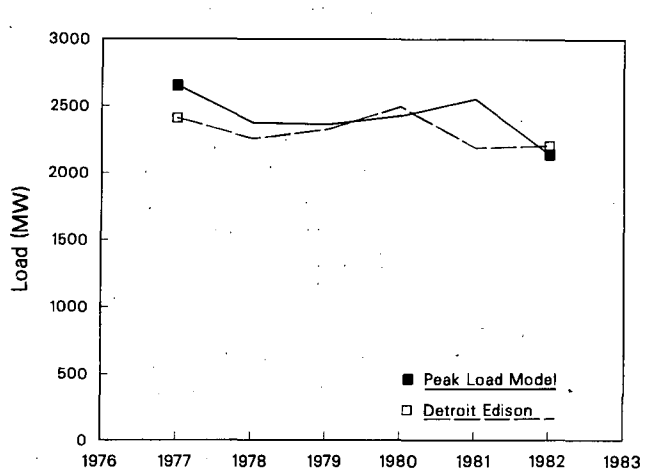

Figure 2. Comparison of the calculated and actual maximum residential loads on DECO's system peak day for each year of the period 1977–1982. (XCG 851-8)

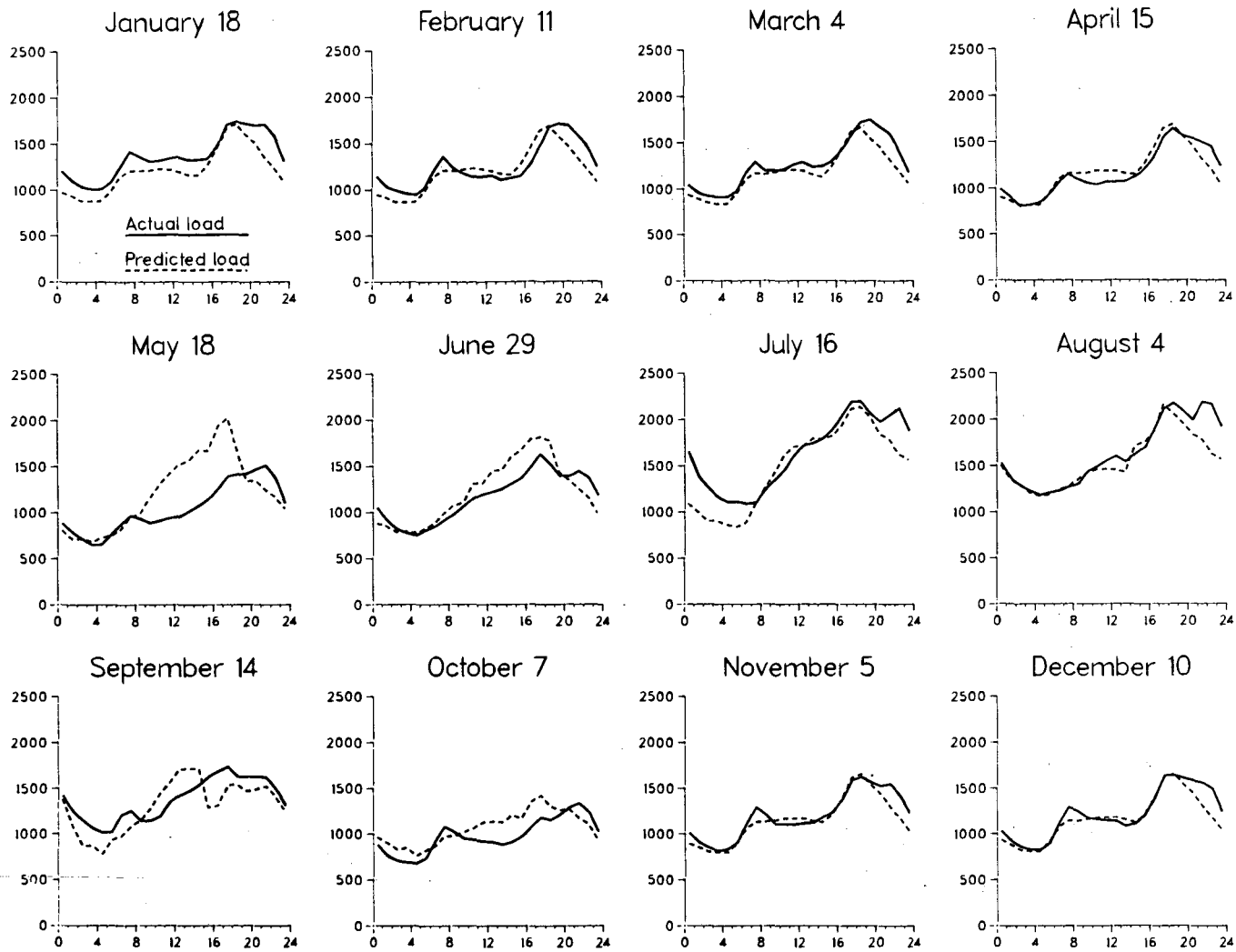

Figure 3. Hourly DECO loads (in MW) on monthly peak days of 1982, compared with predictions of the LBL hourly load model. (XCG 851-6)

tioner load based on the current temperature; it does not explicitly take into account thermal lags. Rather, thermal lags are implicit in the data used in constructing the fraction-in-use matrices. If the days preceding May 18th had lower temperatures so that the heat stored in buildings did not increase as is typical during summer months, then the model, because its matrices are based on typical summer days, would predict too high an air conditioning load. The behavioral explanation is that people do not run air conditioners as much on the first warm day of the year as they would in midsummer, especially if some effort is needed to get them operating after they have been turned off for the winter.

PLANNED ACTIVITIES FOR FY 1986

With the installation of the new heat pump module and the validation of the model, emphasis has shifted from developing the model to applying it to specific utilities. However, we will continue with a low-level effort to correct deficiencies and improve the quality of the fraction-in-use matrices based on our experience in using the model.

With additional funding, we will add the capability to assess the effects of load management and time-of-day pricing on residential load shapes. This task involves building two new modules integrated with the existing module. One, the load manage-

ment module, will modify the fraction-in-use matrices and hourly load profiles on the basis of information about the nature and impacts of specific utility load management programs. The other, a time-of-day pricing module, is more complex, as it involves the assessment of all available data on elasticities of electricity demand as a function of time of day and weather conditions.

The inclusion of time-of-day pricing and load management will yield a model of more general applicability to virtually all major end-use management programs utilities are likely to undertake. The main benefit of performing this work is that its completion will give the model the ability to address a much greater range of utility programs affecting residential loads.

REFERENCES

1. Hirst, E. and Carney, J. (1978), *The ORNL Engineering-Economic Model of Residential Energy Use,* Oak Ridge National Laboratory Report ORNL/CON-24, Oak Ridge, TN.
2. McMahon, J.E. (1984), *The LBL Residential Energy Model,* LBL-18622.
3. Verzhbinsky, G., Ruderman, H., and Levine, M.D. (1985), *The Residential Hourly and Peak Demand Model: Description and Validation,* LBL-18698 (in press).

Market Share Elasticities of Home Heating and Cooling Systems*

David Wood, Henry Ruderman, and James E. McMahon

Concern over future energy demand has prompted several researchers to develop predictive computer models of national energy use. A significant factor in such models is the efficiency of home appliances, in particular space heating and cooling equipment, which account for the largest components of residential energy consumption. An example is the Oak Ridge Residential Energy Demand Forecasting Model,[1] which LBL has modified substantially to create the LBL Residential Energy Model (LBL-REM).[2]

These models require accurate estimates of how the market shares of various fuels (electricity, gas, or oil) or technologies (centralized vs. decentralized systems) change in response to changes in the economy. Thus, estimates of own- and cross-elasticities of market share (with respect to capital costs, operating costs, and income) are commonly found as inputs to the modeling effort. This article describes a new method of developing such estimates.

The unique features of our approach[3] are: 1) the derivation of aggregate market share elasticities from individual household data; 2) the linkage of space heating to air conditioning choice; 3) explicit treatment of individual technologies, including heat pumps; and 4) the direct calculation of new market shares due to changes in the explanatory variables, without carrying out an integration. The first three of these features derive from the corresponding aspects of a study[4] by Electric Power Research Institute (EPRI) which we take as a starting point for our work. The last feature is a direct consequence of the manner in which we develop the elasticities, and is exploited in LBL-REM to provide forecasts of future fuel and technology choices by households. Combining these elasticities with existing techniques for forecasting efficiency choice, thermal integrity of the building shell, and usage behavior results in substantial improvement of the forecasting model.

The study by EPRI has two important features which improve upon previous studies of fuel type market share in residential space heating:

1) It uses a database of individual households and actual technology choices to estimate the coefficients of an equation relating the probability of selecting among different space heating technologies to household and geographic characteristics. The average of these probabilities over all households can be taken as the predicted market share of that technology. Summing over technologies of a given fuel type provides an estimate of the market share of that fuel. Almost all previous studies of fuel

*This work was supported by the Assistant Secretary for Conservation and Renewable Energy, Office of Building and Community Systems, Building Equipment Division of the U.S. Department of Energy under Contract No. DE-AC03-76SF00098.

type market share rely on state-level aggregated data, which introduce bias in to the estimates.

2) Each household's choice of heating technology is modeled jointly with the choice of central cooling. Since the cost of heating system chosen (central or non-central) depends highly on the presence of central air conditioning, it seems unwise to model the two choices independently. Statistical cross-tabulations verify that heating system choice is correlated with cooling choice. The EPRI study is the first to model that linkage explicitly.

ACCOMPLISHMENTS DURING FY 1985

Calculation of Market Share Elasticities

Like most previous studies, our method starts from regression equations. (We use slightly modified versions of the coefficients estimated by EPRI.[5] The classical approach to finding elasticities from such equations requires calculating analytic derivatives of market share and using those derivatives (at the mean values of the independent variables) in the formula for the elasticity. This approach has two defects: 1) McFadden and Reid[6] have shown that using only the mean values neglects the variation of the independent variables and thereby introduces bias in the elasticities, and 2) given the technology-specific choices and the nested logit formulation used in the EPRI report, calculating market share derivatives of interest analytically turns out to be so time-consuming as to be judged unprofitable (given the first defect). Instead, we use a "simulation" approach.

We perturb slightly the economic factor for which we want elasticities (e.g., price of electricity, capital cost of a gas furnace, etc.). For each household in the database, we calculate the new probability under the perturbed conditions of choosing each technology from the regression equation, and determine the change in probability. These changes in probabilities are averaged across households, giving an estimate of the change in market share due to the change in that economic factor. Dividing by the relative size of the perturbation and the original market share gives the appropriate arc elasticity, as a function of the perturbation size. These estimates are approximately quadratic in the perturbation size.

We calculate the arc elasticity as a function of perturbation size for thirteen perturbations (ranging from −33% to +50%) and fit a least-squares quadratic curve to the data. The intercept of this curve (equivalent to a perturbation size approaching a limit of zero) is taken as our value for the point elasticity. A summary of our own-elasticity results can be found in Table 1.

Table 1. Market share own-elasticities for space conditioning equipment.

Equipment	Capital Cost	Energy Cost	Income
Gas Central Heater	−0.38	−0.53	0.07
Gas Non-Central Heater	−1.50	−0.23	−0.57
Oil Central Heater	−1.21	−1.21	−0.30
Oil Non-Central Heater	−1.46	−0.90	−0.59
Electric Central Heater	−0.61	−1.16	−0.15
Electric Non-Central Heater	−0.85	−0.90	−0.26
Central Air Conditioner	−0.20	−0.34	0.30
Heat Pump	−1.77	−0.30	0.38

Modifications to LBL-REM

The LBL Residential Energy Model (LBL-REM) calculates the market shares of each of eight technologies or technology groups, shown in Table 2, below. Note that central electric systems and non-central electric systems together compose the category "conventional electric," and heat pumps are distinct from this grouping. Note also that central air conditioning is possible in combination with any of the other technologies (indeed, it is necessary with heat pumps), rather than being an alternative to them. For the work reported in this article we calculated the arc elasticity as a function of perturbation size for each of these technology groups with respect to a number of explanatory variables. Specifically, we use elasticities of market share with respect to changes in 1) the operating cost of each of the eight technologies, 2) the capital cost of each of the eight technologies, and 3) household income.

As explained in the section above, we can use the quadratic relationship between arc elasticity and perturbation size to estimate new market shares directly, as the consequence of simultaneous changes in a variety of explanatory variables. For perturbations smaller than or equal to +50%, we use the

Table 2. Technology groups

Heating Systems	Cooling Systems
Gas Systems	
1. central gas	
2. non-central gas	
Oil Systems	
3. central oil	
4. non-central oil	
Conventional Electric Systems	Conventional Electric Systems
5. central electric	8. central air conditioning
6. non-central electric	
Non-Conventional Electric Systems	
7. heat pumps (includes central cooling)	

parameters of the quadratic curve estimated on the data. For perturbations greater than +50% (up to +400%), we fit both an exponential and linear model to the data, and select coefficients from the better-fitting model.†

The model stores values for household income and the capital and operating costs of each of the technologies in the "base year" of the simulation (currently, 1977). Operating costs are calculated by the expression

$$OC = \frac{\text{(fuel price)(usage)(thermal integrity)}}{\text{(equipment efficiency)}}.$$

Next we describe a new algorithm for use by LBL-REM in estimating new market shares.

LBL-REM Algorithm for Estimating New Market Shares

The following steps for estimating the market shares of space-heating technologies are carried out for each year of a projection:

1) Calculate "current year" values for:
   a) household income;
   b) the capital cost of eight technologies;
   c) the operating cost of eight technologies, given the new fuel prices, efficiencies, thermal integrity, etc.
2) For household income, capital cost, and operating cost of the eight technologies, calculate:

$$\delta = \frac{\text{new value} - \text{base value}}{\text{base value}}.$$

   Call these δ_{inc}, δ_{CC}, and δ_{OC}, respectively.
3) Use these seventeen values of δ (one income effect, eight capital cost effects, and eight operating cost effects) to find the new market shares of each technology. (See Page 5-74.)
   Note that each of the seventeen values of δ must be tested for $\delta \leq 0.5$, and the appropriate linear or exponential expression substituted for the quadratic relationship above when the test is not met.

With this procedure, we are treating the effect of simultaneous changes in all the explanatory variables (income, eight capital costs, and eight operating costs) as being additive in their individual effects. This is accomplished only by a) neglecting all terms of order δ^3 or higher, which seems reasonable if the different perturbations are "small," and b) neglecting cross-product terms of order δ^2, which seems somewhat less defensible.

We can reduce this error somewhat (at least for operating costs) by using the following argument:

†More specifically, we solve two equations: $y = a + b\delta$ and $y = ae^{b\delta}$ for the value of the elasticity at the two endpoints of the range $\delta = 0.5$ to 4.0. To insure continuity with the range where $\delta \leq 0.5$, the left endpoint is solved not for the calculated elasticity itself, but rather for the fitted value of the quadratic curve derived on the data where $\delta \leq 0.5$. For each of these two equations, the quality of the fit to selected data points in the range can be compared by finding the multiple-r-squared value for each equation. The better-fitting equation is then used to predict new market shares when perturbations are in the range $\delta = 0.5$ to 4.0.

$$MS_{new} = MS_{old}[\ 1 + (\text{income effects}) + (\text{capital cost effects}) + (\text{operating cost effects})\ ]$$

$$= MS_{old}[\ 1 + \delta_{inc}(a_{0,inc} + a_{1,inc}\delta_{inc} + a_{2,inc}\delta_{inc}^2) +$$

$$\left.\begin{array}{l}\delta_{CC}(a_{0,CC} + a_{1,CC}\delta_{CC} + a_{2,CC}\delta_{CC}^2) + \\ \delta_{OC}(a_{0,OC} + a_{1,OC}\delta_{OC} + a_{2,OC}\delta_{OC}^2)\end{array}\right\}\ \text{terms in first of eight technologies}$$

$$+ \ \ldots \ +$$

$$\left.\begin{array}{l}\delta_{CC}(a_{0,CC} + a_{1,CC}\delta_{CC} + a_{2,CC}\delta_{CC}^2) + \\ \delta_{OC}(a_{0,OC} + a_{1,OC}\delta_{OC} + a_{2,OC}\delta_{OC}^2)\ ]\end{array}\right\}\ \text{terms in last of eight technologies}$$

Some portion of the change in market share of any given technology is due to simultaneous changes in operating cost of all the other systems. And some portion of the (different) changes in the operating cost of all systems using a given fuel is due to the (common) change in fuel price. If we can capture that portion of the change, we could apply the perturbation δ associated with it against an elasticity that was calculated with respect to fuel price, i.e, with respect to simultaneous changes in the operating cost of all the technologies using that fuel. Essentially, we want to find δ_{fuel} and δ_{tech} such that:

$$\delta_{OC} = \delta_{fuel} + \delta_{tech}$$

where *fuel* refers to new fuel prices (and is common to all technologies using that fuel) and *tech* refers to technology-specific changes in efficiency, usage, etc.

That portion of the change due to changing fuel prices is used in conjunction with an elasticity calculated by perturbing the operating cost of all technologies using that fuel. As such, it is free of any error caused by neglecting the second-order terms in the product of various perturbation sizes for various operating costs. Only the technology-specific changes δ_{tech} carry that error. However, this procedure of dividing δ_{OC} into two parts carries its own error.

We are essentially obliged to trade off between these two sources of error. If we treat the effect of simultaneous changes in several variables as being additive in their individual effects, we make an error due to neglect of some second-order terms. Breaking up the change in operating cost into two parts (in the calculation $\delta_{OC} = \delta_{fuel} + \delta_{tech}$), avoids that error for the "fuel price" portion of the change. Unfortunately, this calculation also requires that we neglect a different second-order term, this time in the product $\delta_{fuel} \cdot \delta_{tech}$.

There seems to be no practical way out of this dilemma. Treating multiple effects other than additively leads to the requirement of calculating elasticities in all possible combinations of variables that might be perturbed, a combinatorial problem that is unpleasant to contemplate, let alone carry out. Otherwise, we wish to choose a procedure which will make the neglected terms as small as possible. In the procedure we propose to use (which ignores the common fuel price effects), the neglected terms are second-order products like $\delta_{1,OC} \cdot \delta_{2,OC}$, where $\delta_{i,OC}$ refers to the perturbation in operating cost of the ith technology, and perturbations are the net of changes in fuel prices, efficiencies, etc. In the alternative procedure (capturing the common fuel price effects), the neglected terms are products like $\delta_{fuel} \cdot \delta_{tech}$.

Clearly, for economic scenarios in which the operating costs of technologies in a particular fuel type tend to move together (i.e., the change in fuel price dominates the technology-specific changes) δ_{tech} will be small relative to δ_{fuel} and their product will be small. If the scenario involves large technology-specific changes above and beyond the fuel price effects, then their product will be (relatively) large. In particular, if fuel prices tend to increase and technology efficiencies improve correspondingly, then the net change in operating costs $\delta_{i,OC}$ may be very small, while δ_{fuel} and δ_{tech} will be large and opposite in sign. For this scenario, the main algorithm will be neglecting terms in the product $\delta_{1,OC} \cdot \delta_{2,OC}$, while the alternative algorithm will neglect the product $\delta_{fuel} \cdot \delta_{tech}$. The main algorithm will be superior. (We note in passing that in scenarios where fuel prices do not change, both algorithms will produce the same results.)

We believe that scenarios of rising fuel prices and efficiencies are more typical of those planned for modeling with LBL-REM, and so we prefer to use the main algorithm. We also intend to produce a

working version using the alternative algorithm, in order to test the significance of the different estimating procedures.

PLANNED ACTIVITIES FOR FY 1986

These elasticities, and the improved algorithm for calculating new market shares, are being incorporated into LBL-REM and will be used in our ongoing analysis of appliance efficiency standards. Further work includes understanding the role of aggregated and disaggregated modeling in the estimation of market share elasticities.

REFERENCES

1. Hirst, E. and Carney, J. (1978), "The ORNL Engineering-Economic Model of Residential Energy Use," Oak Ridge National Laboratory, ORNL/CON-24.
2. McMahon, J. (1985), "The LBL Residential Energy Model: An Improved Policy Analysis Tool," (submitted to *Energy Systems and Policy*); LBL-18622.
3. Wood, D., Ruderman, H., and McMahon, J. (1985), *Market Share Elasticities for Fuel and Technology Choice in Home Heating and Cooling,* LBL-20090.
4. Electric Power Research Institute (1984), "Household Appliance Choice: Revision of REEPS Behavioral Models," EPRI EA-3409.
5. Wood, D. (1985), *A Review of Assumptions and Analysis in EPRI Report EA-3409: Household Appliance Choice: Revision of REEPS Behavioral Models,* LBL-20332.
6. McFadden, D. and Reid, F. (1975), "Aggregate Travel Demand Forecasting From Disaggregated Behavioral Models," National Academy of Science, National Research Council, Transportation Research Board, *Record,* No. 534, Washington, D.C.

Utility Load Shape Impacts of Residential Energy Conservation Measures*

H. Ruderman, P. Chan, and M.D. Levine

The role of utilities in supplying electricity is changing rapidly. No longer are utilities required only to deliver kilowatt-hours to the consumer; now they are expected to supply a broad range of energy services. Utilities across the country have offered rebates for more efficient appliances and granted low- and even zero-interest loans to weatherize their customer's houses. They have been required to implement federal programs—such as the Residential Conservation Service, which provides energy audits for houses—and a wide variety of demand-side programs initiated by public utility or service commissions. Such programs to reduce demand growth affect utility plans for constructing new generating capacity and influence the financial outlook of many companies.

The purpose of this study is to evaluate a variety of measures to reduce household electricity demand in terms of their impacts on annual consumption and load shapes and to compare them across service areas. Load shape change is an important aspect of the assessment of demand-side programs, and one that has received little attention to date. It is the interplay of these two types of effects, combined with the economics of supply and the structure of rates of

*This work was supported by the Assistant Secretary for Conservation and Renewable Energy, Office of Buildings Energy Research and Development, Building Systems Division of the U.S. Department of Energy under Contract No. DE-AC03-76SF00098.

the utility, that results in economic impacts on utilities. Because of the lack of peak charges in most residential rates, most utilities sell peak residential power at prices lower than costs. (The loss is made up in sales of baseload power, either in the residential sector or elsewhere.) Thus, residential conservation programs that reduce peak power more than baseload are, in most cases, desirable for utilities. A much more complete characterization of the economic impacts of demand-side programs can be found in another report.[1]

Using different words, the significance of this study is that it looks at the key issue of the load shape impact of utility conservation programs in considerable detail. The absence of such analysis among utilities for many (or most) of their conservation programs has led to an underestimation of the benefits of those programs that have a favorable impact on load shapes (and, conversely, an overestimation of benefits of programs with unfavorable impacts on load shapes). This study is intended to perform the detailed calculations to estimate load shape impacts for a variety of conservation measures in three locations, as a first step to developing an agenda of conservation programs that are well-suited to particular utilities.

ACCOMPLISHMENTS DURING FY 1985

Methodology

We have developed a methodology for calculating changes in annual electricity consumption and hourly loads in the residential sector resulting from the implementation of one or more energy conservation measures in a utility service area. We used the methodology to evaluate various measures in three service areas with differing load characteristics. We evaluated the measures by comparing their impacts on electricity sales and on peak summer and winter loads. The measures were ranked on the basis of a figure-of-merit related to their ability to reduce peak loads relative to electricity consumption.

We considered five measures to improve the thermal integrity of residential structures:

(1) increasing ceiling insulation;
(2) increasing wall insulation;
(3) installing basement and perimeter insulation;
(4) triple glazing; and
(5) decreasing the air infiltration rate.

A second set of measures involved replacing existing appliances with high efficiency models: central air conditioners with a seasonal energy efficiency ratio (SEER) of 14.0, room air conditioners with a energy efficiency ratio (EER) of 11.5, and refrigerators with an energy factor (EF) of 8.7. In addition, we looked at four combinations of measures. One was to bring all houses in the service area up to current (1981) construction practice and current appliance efficiency levels. The others were to convert all houses to passive solar at three levels of thermal integrity and appliance efficiencies.

To examine the effects of these measures, we chose three utilities that differed widely in their climatic conditions and appliance saturations and other household characteristics. The characteristics of the three service areas are summarized in Table 1.

The Detroit Edison Company (DECO) is representative of utilities located in colder climates with long heating seasons. Normally, DECO is a summer peaking utility because most houses in Detroit use gas heaters. To examine more carefully the effects of conservation measures that affect heating loads, we converted DECO to a winter peaking utility by increasing the saturation of electric space heaters from a few percent to nearly fifty percent. Virginia Electric Power Company (VEPCO) is representative of hot and humid climates with large cooling loads. Sixty-five percent of the households

Table 1. Characteristics of utility service areas, 1981.

	Utility Service Area		
	DECO	PG&E	VEPCO
Financial			
Median Family Income ($1000)	21.0	21.7	19.9
Electricity Price (1975 $/MBtu)	$3.56	$3.26	$3.54
Customers			
Residential Customers (1000)	1599	2468	1239
Saturations			
Electric Space Heat (%)	48.6	12.8	26.3
Central Air Conditioner (%)	21.6	15.1	38.3
Room Air Conditioner (%)	31.0	8.9	26.5
Climate			
Heating Degree Days (65°F)	6551	3664	4247
Cooling Degree Days (75°F)	213	526	501
Annual Heating Hours	4810	3912	4515
Annual Cooling Hours	955	1220	1970
Energy and Load			
Residential Sales (GWh)	18,544	14,381	13,478
Summer Peak Load (MW)	3076	3070	3747
Winter Peak Load (MW)	7804	2347	3275

have air conditioners and run them for an average of 2000 hours per year. The climatic conditions in the Pacific Gas and Electric Company (PG&E) service area are less extreme than in the other two. It has a low air conditioner saturation and a relatively short heating season.

We determined the effects of an energy conservation program on hourly load shapes in three stages. First, we calculated the changes in heating and cooling loads in an individual building incorporating the conservation measure. Second, we assumed that the annual energy consumption by end use was calculated for a case in which all homes in the service area incorporated the particular measure. Finally, we disaggregated the annual energy consumption for each end use by hour of the year using hourly load profiles. We compared these results to a base case that did not include the conservation measure. In this way, we were able to determine the percentage changes in annual electricity consumption and winter and summer peak loads.

Our results on the changes in annual electricity consumption and in the hourly load shapes on the peak summer and winter days were derived as follows. First, we compared the effects of the conservation measures within a single utility service area. In addition, we ranked the measures according to a figure of merit based on their relative effect on base and peak load. Then we compared the conservation measures across the three service areas, pointing out the the differences in their effectiveness. Tables 2, 3, and 4 summarize the savings in energy and peak power produced by various means.

An important parameter in utility planning is the system load factor, defined as the ratio of average load to annual peak load for the entire service area. The smaller the load factor, the more load has to be satisfied by expensive fossil-fuel-burning peaking generators. The figure of merit we have chosen to rank the conservation measures is the ratio of the change in peak load resulting from the implementation of the measure in all residential buildings in the

Table 2. Savings from conservation measures—Detroit Edison Company.

		Summer Peak Day			Winter Peak Day		
Conservation Measure	Percent Annual Energy	Percent Peak Load	Figure of Merit[a]	Rank	Percent Peak Load	Figure of Merit[a]	Rank
Ceiling Insulation R-27 to R-38	2.69	1.23	0.46	6	4.33	1.61	3
Wall Insulation R-11 to R-19	2.47	0.75	0.31	7	3.50	1.42	4
Basement Insulation None to R-10	9.50	−1.78	−0.19	8	11.39	1.20	5
Triple Glazing	2.66	1.44	0.54	5	4.29	1.61	2
Low Infiltration 0.7 to 0.4 ACH	7.82	5.43	0.69	4	14.77	1.89	1
Room Air Conditioner EER 6.72 to 11.5	0.56	6.16	11.07	2			
Central Air Conditioner SEER 7.06 to 14.0	1.01	15.09	14.92	1			
Refrigerator EF 4.95 to 8.7	4.45	3.82	0.86	3	0.62	0.14	6
Current Practice	12.94	3.72	0.29		14.03	1.08	
Current Practice with Night Setback	12.75	3.72	0.29		9.26	0.73	
Passive Solar stock practice	5.88	2.28	0.39		6.89	1.17	
Passive Solar current practice	17.78	6.29	0.35		22.37	1.26	
Passive Solar best available	31.09	32.08	1.03		44.54	1.43	

[a]Ratio of percent peak load savings to percent annual energy savings.

Table 3. Savings from conservation measures—Pacific Gas and Electric Company.

Conservation Measure	Percent Annual Energy	Summer Peak Day: Percent Peak Load	Summer Peak Day: Figure of Merit[a]	Summer Peak Day: Rank	Winter Peak Day: Percent Peak Load	Winter Peak Day: Figure of Merit[a]	Winter Peak Day: Rank
Ceiling Insulation R-19 to R-38	0.81	1.92	2.37	5	1.05	1.30	5
Wall Insulation R-11 to R-19	1.17	2.83	2.41	4	2.24	1.90	3
Perimeter Insulation None to R-10	1.32	0.51	0.39	8	2.08	1.58	4
Triple Glazing	1.15	3.20	2.78	3	2.55	2.21	2
Low Infiltration 0.7 to 0.4 ACH	0.89	1.81	2.04	6	2.48	2.79	1
Room Air Conditioner EER 6.72 to 11.5	0.30	2.87	9.57	1			
Central Air Conditioner SEER 7.06 to 14.0	1.46	13.70	9.40	2			
Refrigerator EF 4.95 to 8.7	9.93	6.43	0.65	7	7.31	0.74	6
Current Practice	6.62	8.78	1.33		6.69	1.01	
Current Practice with Night Setback	6.60	8.78	1.33		6.61	1.00	
Passive Solar stock practice	2.00	6.20	3.10		4.27	2.14	
Passive Solar current practice	8.58	13.29	1.55		10.71	1.25	
Passive Solar best available	16.99	31.48	1.85		19.45	1.14	

[a]Ratio of percent peak load savings to percent annual energy savings.

service area to the change in annual electricity consumption. If the system peak occurs at the same time as the residential peak, there is a direct relationship between our figure of merit and the effect of the conservation measure in the system load factor. In any case, the figure of merit is useful as an indicator of relative effect of the measure on peak and base load.

Impacts on Electricity Consumption and Load Shape

The results to date can be summarized by the following points:

- Air conditioner efficiency improvements are the most effective measures for increasing summer system load factors.
- Reducing the air infiltration rate is the most effective measure for reducing winter peak loads.
- Bringing all houses in the service areas up to current practice would result in significant savings in energy and winter peak power.
- Refrigerator efficiency improvements are more suitable for reducing base load.
- Adding insulation in the basement can adversely affect summer peak loads.
- Night setback of thermostats during the winter has little effect on overall electricity demand and only a small effect on winter peak power.

In interpreting results, it is important to note the assumptions made in doing the calculations. We are

interested in making comparisons of effectiveness among conservation measures and between service areas. To do this, we have examined a hypothetical case in which the conservation measures are applied to all residential buildings in the service area. Thus, our results can be interpreted as the maximum potential savings resulting from implementing the measure. Our values of percent energy and peak power savings depend on the saturation of the conservation measure. The figure of merit is less dependent on both the appliance saturation and the level of implementation of the conservation measure.

In the case of Detroit Edison, we performed a set of computer simulations in which we increased the saturation of electric space heating to nearly fifty percent to emphasize the effects on winter peak loads. Our results on energy and peak power—for winter cases—therefore apply to a hypothetical utility having a winter peak due to electric space heating rather than to Detroit Edison itself. The figure of merit applies to Detroit Edison as well as to the hypothetical utility.

Interutility Comparison

An examination of the load shapes for the peak winter day in the three service areas shows that demand is reduced during all hours of the day by the thermal integrity measures. Demand reduction during the summer varies among service areas and among the various measures. Air conditioning in the PG&E service area is a major portion of the residential load between 9 am and 9 pm. In the DECO and VEPCO service areas, the air conditioning load extends well into the night. One might expect that PG&E would show the highest air conditioner figure of merit, but in fact DECO has the highest because its cooling season is the shortest.

Table 4. Savings from conservation measures—Virginia Electric Power Company.

		Summer Peak Day			Winter Peak Day		
Conservation Measure	Percent Annual Energy	Percent Peak Load	Figure of Merit[a]	Rank	Percent Peak Load	Figure of Merit[a]	Rank
Ceiling Insulation R-24 to R-38	1.36	2.88	2.13	3	2.37	1.75	3
Wall Insulation R-12 to R-19	0.97	1.34	1.39	6	1.72	1.78	2
Basement Insulation None to R-10	2.72	1.51	0.55	7	3.98	1.46	5
Triple Glazing	3.12	5.48	1.76	4	5.00	1.60	4
Low Infiltration 0.7 to 0.4 ACH	2.22	3.44	1.55	5	4.86	2.19	1
Room Air Conditioner EER 6.72 to 11.5	0.89	3.61	4.06	2			
Central Air Conditioner SEER 7.06 to 14.0	3.08	19.28	6.26	1			
Refrigerator EF 4.95 to 8.7	5.22	2.68	0.51	8	2.39	0.46	6
Current Practice	9.10	13.65	1.50		11.12	1.22	
Current Practice with Night Setback	9.01	13.65	1.51		10.62	1.18	
Passive Solar stock practice	4.34	8.70	2.00		7.15	1.65	
Passive Solar current practice	11.19	18.94	1.69		13.74	1.23	
Passive Solar best available	19.17	39.66	2.07		20.95	1.09	

[a]Ratio of percent peak load savings to percent annual energy savings.

PG&E has a smaller space conditioning load than the other two utilities, so it shows the lowest annual energy savings due to the thermal integrity measures. This is also reflected in the fact that refrigerator improvements provide the largest energy savings in its service area. For a winter peaking utility, reducing the air infiltration rate is the best way to reduce load factor. Triple glazing is also effective for DECO and PG&E, while wall and ceiling insulation helps for VEPCO. The pattern for the summer peak is less consistent. However, increasing the basement insulation could adversely effect the system load factor in some service areas.

In all three service areas, bringing houses up to current practice would reduce the winter peak load and electricity demand. These effects are largest in the DECO service area. Although night setback changes the daily load shape during the winter, it has no impact on overall electricity demand and very little on the winter peak.

Passive solar construction practices by themselves (e.g., just moving all the windows to the south wall, adding thermal mass, etc.) have relatively small savings. However, combining them with thermal integrity and appliance efficiency improvements results in substantial energy and peak power reductions. It is interesting to note that the effects are roughly linear: if you add the savings due to current practice to those due to passive solar, you get fairly close to the passive solar with current practice savings.

The effects of passive solar construction differ among the service areas. In a winter peaking utility, such as our modified Detroit Edison, the major impact is the reduction of winter peak load. In a utility with a large air conditioning saturation, such as VEPCO, it is summer peak load that shows the largest reduction. Promoting passive solar housing appears to be a good way for a utility to ameliorate its load growth problems.

PLANNED ACTIVITIES FOR FY 1986

Most of the analysis on this project was completed during FY 1985. During FY 1986, we will be evaluating alternative formulations for the figure of merit to select the one that best characterizes the financial impacts on a utility. We will write a paper to be submitted to a referenced journal.

REFERENCES

1. Kahn, E., *et al.* (1985), "The Effect of Conservation Programs on Electric Utility Earnings: Results of Two Case Studies," submitted to *Energy Policy.*

Impacts of Proposed Changes in the Federal Tax Code on Renewable Energy and Cogeneration Projects*

E. Kahn and C. Goldman

The development of certain cogeneration and renewable energy technologies has been influenced by favorable federal and state legislation enacted in the late 1970's. The legislation provided subsidies for either the investment in, or output from, specific renewable technologies. In addition, the Public Utilities Regulatory Policies Act of 1978 (PURPA) created a market for electricity from such projects by requiring utilities to purchase their output at avoided cost. As a direct result of these policies, several renewable energy technologies and industrial cogeneration have experienced accelerated development. The status of current renewable energy incentives changes significantly at the end of 1985 as all renewable energy investment tax credits expire. Key provisions of the *President's Tax Proposals to the Congress for Fairness, Growth, and Simplicity* also affect renewable energy and cogeneration projects.[1] The most significant provisions are:

- repeal of 10 percent investment tax credit
- lower corporate and individual tax rates
- replacement of accelerated cost recovery system (ACRS) with capital cost recovery system (CCRS)
- non-deductibility of state taxes on federal income tax returns
- institute an alternative minimum tax for corporations

*This work was supported by the Assistant Secretary for Policy, Safety, and Environment, Office of Policy Integration, Policy Planning and Analysis Division of the U.S. Department of Energy under Contract No. DE-AC03-76SF00098.

This article discusses the impact of the President's Tax Proposals and the scheduled expiration of energy investment tax credits on eight selected energy projects.

ACCOMPLISHMENTS DURING FY 1985

Methodology

Projects were selected that were representative of the best technologies currently available and that had high expected returns under current tax law.[2] They are actual projects either in operation or in the advanced development stage. We attempted to simulate the criteria investors would use when deciding to undertake renewable energy or conservation projects. Spread sheets of project revenue, cost, and tax data were developed for each project. Cash flows were projected out to 1997, the last year for which we have a reliable forecast of electricity prices (as indicated by utility standard offers to purchase electricity at fixed prices). We then estimated the investor's after-tax internal rate of return (IRR) under several scenarios:

- current law (before December 31, 1985)
- current law (after 1985) and
- the President's Tax Proposals.

The internal rate of return is calculated from the after-tax net equity cash flows (ATNEC) in each year. ATNEC includes pre-tax income plus depreciation plus any tax savings (or liability) minus equity funds and debt principal repayment. By convention, negative taxes are assumed to be tax savings to investors from net operating losses generated by the project. By analyzing changes in the profitability of these projects, we were able to develop an initial assessment of how currently scheduled and proposed revisions in tax law will affect the development of these and similar renewable energy and cogeneration projects.

Results

The impact of the President's Tax Proposals on the investor's leveraged rate of return is shown in Table 1. Uniformly, the President's Tax Proposal lowers these returns. However, returns on cogeneration projects are still quite favorable (24–26 percent) and the President's Proposal tends to reinforce its emergence as the dominant small power technology.

After December 1985, with the expiration of the energy tax credits (ETC), very high investor rates of return disappear for wind turbines, small hydro, geothermal and wood-fired electricity. The effect is most dramatic for wind-turbines and small hydro. With interest rates at 14 percent, the equity returns on these projects fall to a level that is unlikely to attract much capital. Although returns are much lower under the President's proposal, the yearly cash flows are less variable than under current law (see Fig. 1.) The repeal of the alternative fuels production credit (AFPC) has a very adverse impact on the landfill gas recovery project, as evidenced by the drop in the rate of return from 27.5 to 8.8 percent. This project is analyzed on an all-equity basis. The sponsor's minimum return requirement is 15 percent on this basis; hence the project is no longer viable. Geothermal and wood-electric projects are still financially viable under current law after 1985.

Rates of return on equity for the five renewable energy technologies are in the 7 to 15 percent range under the President's proposal. It is unlikely that

Table 1. Rate of return on equity for selected projects.[a]

	Geothermal[b]	Gas-fired Cogeneration	Coal-fired Cogeneration	Landfill Gas[c]	Wind	Small Hydro	Wood-Electric
Current Law	0.391 (0.54)	0.412	0.402	0.275	0.472	0.274	0.260
Current Law after Dec. 31, 1985	0.226 (0.33)	0.412	0.402	0.088[d]	0.140	0.144	0.195
President's Tax Proposal	0.093 (0.17)	0.242	0.265	0.097	0.122	0.072	0.148

[a]The geothermal, cogeneration, and landfill gas projects are corporate-financed, whereas the wind, small hydroelectric, and electricity from wood waste projects are financed by limited partnerships.

[b]IRR in parentheses is for geothermal project without transmission costs.

[c]All equity.

[d]Assumes Alternate Fuels Production Credit (AFPC) is repealed.

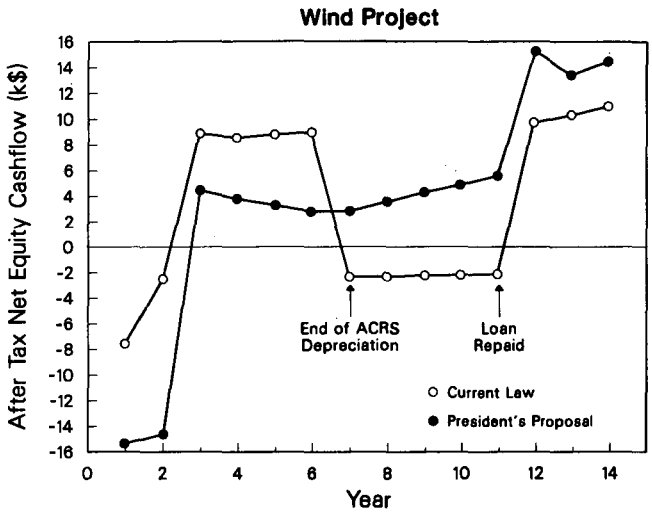

Figure 1. After tax net equity cash flows until 1997 for a wind turbine project under current law and the President's proposal. (XCG 8510-474)

projects with such returns could attract capital since the IRR on equity is at or below the cost of debt. However, a geothermal project unburdened by the need to provide transmission facilities would fare somewhat better.

The analysis of selected projects gives a characterization of the change in returns associated with various tax regimes. These changes do not constitute a forecast of the market for such projects. In this study, we developed a methodology that illustrates how results from a financial analysis of representative projects can be extended to develop a forecasting approach to the market for renewable technologies and cogeneration. We assumed that investment will occur if a project meets the "hurdle rate," some specified minimum rate of return target. The hurdle rate must be greater than the cost of debt to compensate for the added risk. We believe that the hurdle rate lies somewhere between 15 and 20 percent return on equity capital. We then attempted to estimate and quantify endogenous project variability (e.g., distribution of technical and cost characteristics) and exogenous sources of risk (e.g., deviations of input fuel costs or output product prices from their expected level) in order to develop a distribution of returns on a family of similar projects.

We applied this approach to two of our typical projects, wind turbine generators and large-scale gas-fired cogeneration. The single most uncertain variable associated with wind turbine technology is its technical performance. How much output can wind turbine machines produce? The distribution of technical characteristics, which is of most interest for gas turbine cogenerators, does not involve performance uncertainties, but rather capital cost and sizing issues. These applications occur in industrial process activities, where the precise mix of power production to steam use can be quite variable. The coefficient of variation is lower for the cogeneration project than the wind turbine project, which suggests that the returns for these type of projects are less variable.

PLANNED ACTIVITIES FOR FY 1986

Although work on this was completed during the past fiscal year, related research in the following areas is necessary in order to translate change in investor returns on selected projects into a forecast of the market for such projects:

- analysis of the distribution of technical characteristics
- a national survey of avoided cost prices
- examination of issues related to technical progress
- analysis of the sensitivity of the results to macro-economic factors (e.g., interest rates).

Improved forecasting capability does not depend equally on all these efforts. The most important issue is the availability and analysis of market data on the nature of projects within a given technology. We plan to pursue these research areas in FY 86 depending on funding availability.

REFERENCES

1. U.S. Department of Treasury (1985), *The President's Tax Proposals to the Congress for Fairness, Growth, and Simplicity*, Washington, D.C.
2. Kahn, E. and Goldman, C.A. (1985), *Impact of Tax Reform on Renewable Energy and Cogeneration Projects*, LBL-20620.

A Decade of U.S. Energy Policy*

M. Levine and P. Craig†

In 1965, a high level governmental committee reported that "no grounds exist for serious concern that the Nation is using up any of its stocks of fossil fuel too rapidly; rather, there is the suspicion that we are using them up too slowly...rather than fearing a future day when fossil-fuel resources will be largely exhausted..., we are concerned for the day when the value of untapped fossil-fuel resources might have tumbled...and the nation will regret that it did not make greater use of these stocks when they were still precious."[1]

At about the same time warnings were appearing that U.S. oil and gas production would soon peak.[2] At the time few took them seriously. Yet the predictions have since turned out to be remarkably prescient. U.S. natural gas production peaked in 1973 and had been dropping since. Oil production in the contiguous United States peaked in 1970, and it too is declining. More recently oil from the North Slope of Alaska has come on stream, thus holding total U.S. production roughly constant in recent years. These developments provided the best support in the early 1970's for the idea that the United States and possibly the world were entering a period of decline in the growth of oil supply over the long term.

In December 1973, in the middle of the Organization of Arab Petroleum Exporting Countries (OAPEC) embargo and only months after the Yom Kippur war of September 1973, the Nixon Administration issued the "Dixy Lee Ray" report on energy R&D. The report, commissioned in the summer of 1973, included a figure showing oil imports to the United States—then about 6 million barrels per day (mmbpd)—dropping to zero by 1980.[3] President Nixon stated that "by the end of the decade we will have developed the potential to meet our own energy needs without relying on any foreign energy sources."[4] Events proved otherwise. Imports increased to more than 8 mmbpd, then dropped due to conservation and a slumping economy (though hardly at all due to the new supply technologies which were the dominant focus of the Ray report) to about 3 mmbpd. Today, total self-sufficiency is neither in sight nor a national goal.

The year 1973 is remembered primarily for the oil embargo and the "seven day war" between Israel and Egypt. This was also the year, however, in which the Texas Railroad Commission—responsible for allocating ("pro-rationing") oil production among Texas producers, found that even at 100% production it was no longer possible to meet national demand. Thus, in 1973, it became technically possible for foreign producers to dominate world oil prices. That this possibility existed in 1973 was known to some. That the shift of power to OPEC could occur so rapidly was a surprise to almost everyone—probably including the OPEC nations themselves.

Energy policy in the 1970's was characterized by remarkable complexity, with innumerable twists and turns of policy, attitudes, and beliefs. In 1973, the nation became aware of its growing energy vulnerability. Crash efforts were mounted to develop new energy technologies. Legislation was passed in abundance. An army of people (including ourselves) became instant energy experts. The federal energy establishment was constantly being reorganized. Despite the continuing confusion, most participants felt themselves a part of an important process having vital implications for the nation's future.

By 1981, much of this feeling had dissipated as oil supply was more than ample to meet demand, oil prices eased, and energy issues receded from national prominence. In the course of a short decade the energy problem was transformed (in the public consciousness) from a minor issue concerning a few experts to a major national crisis threatening the Nation and then to one of many issues of some but not overwhelming importance.

ACCOMPLISHMENTS DURING FY 1985

Our aim in this study was to review some of the critical events in the evolution of U.S. energy policy during this eventful "energy decade". While it is too early to write a balanced history of the decade, it is possible to learn a few lessons about the formulation of public policy in response to rapid and distressing changes in price and availability of critical resources. We have chosen to focus on four major areas: (1) institutional change, (2) regulation, energy prices, and allocation policies, (3) energy conservation, and (4) research and development. Each of these areas engages many important aspects of energy policy decisions. A more detailed discussion of the issues presented here is presented elsewhere.[5]

*This work was supported by the Assistant Secretary for Conservation and Renewable Energy, Office of Buildings Energy Research and Development, Building Systems Division of the U.S. Department of Energy under Contract No. DE-AC03-76SF00098.

†Department of Applied Science, University of California, Davis, CA 95616.

New Institutions of Government

The embargo and subsequent energy price escalation combined with growing fears of shortages to produce what became a long series of energy "czars" and governmental re-organizations. The Federal Energy Office (FEO) was created to manage the shortage and, after the embargo, to administer price controls. The Atomic Energy Commission (AEC) became the Energy Research and Development Administration (ERDA) under the Energy Reorganization Act of 1974; AEC regulatory functions were assigned to the Nuclear Regulatory Commission (NRC); in 1974 the FEO became the Federal Energy Administration (FEA), the change signifying increasing importance and "permanence" within the federal government. The FEA absorbed the Federal Power Commission (FPC), the agency that had administered natural gas price regulations. New energy programs in solar energy and conservation were started in the National Science Foundation, while older programs in coal housed in the Department of Interior grew in size. All these were moved to ERDA.

As the decade progressed and the national sensitivity to the implications of oil shortage grew, the idea of ERDA, devoted to research and development, grew obsolete. A Cabinet level Department of Energy (DOE) was proposed and approved (Department of Energy Organization Act, 1977). DOE was the product of a national sense of crisis. This new entity brought together staff from many institutional backgrounds, with many persuasions. From the outset the DOE was engulfed in continuing controversy, relating to both its objectives and its managerial competence. Contributing to its problems was an inability to draw upon or to build a national constituency. Among the many problems faced by DOE were the self-induced problem of defining success in virtually every program in terms of "barrels per day of oil delivered." Goal-oriented criteria for success are helpful in virtually any project. The DOE failed to recognize that a goal specified in terms of product delivered is inappropriate to a government agency that cannot itself produce the oil. This type of goal is even more inappropriate when one is often dealing with research and development projects, where the intrinsic nature of the problems renders the goal of product delivery virtually meaningless.

Philosophically opposed to DOE's objectives, the Reagan presidential campaign identified the agency as a candidate for abolition. Today DOE still survives, but internal morale has suffered greatly, and the promise of the organization for national leadership has (for the time being at least) vanished.

Legislation

Energy legislation enacted in the energy decade ultimately included incentives for virtually all energy supply and conservation technologies. There was something for everyone, yet the incentives were not well balanced. The prevailing view was that competition would lead to the best of them flourishing, while the losers would fall by the wayside.

The problem was that incentives, once introduced, are hard to remove. The intangible drilling expenses long enjoyed by the oil and gas business provided a subsidy to that sector not enjoyed by solar. Since political factors made it impossible to remove the existing subsidy, the compromise was new subsidies. By way of example, lobbying by solar groups led to incentives for active solar systems. As chance would have it, Congress at the time was not interested in conservation incentives. Since no one could come up with a good way to distinguish passive solar devices from conservation, only active solar was included—a singularly poor decision from a cost-effectiveness perspective.

The chaos in energy regulation was captured by former FPC Commissioner William O. Doub (1976): "...energy policy making literally resembles a Rube Goldberg production with an abundance of action and few real results...the cost of complying with federal regulations represents about $14 billion annually".[6] A similar gloomy conclusion characterized the government's energy production incentives: "We feel secure in concluding that both past and present energy policy has not had the objective of promoting a more efficient use of our scarce energy resources."[7] And, in a generally optimistic report on the eventual prospects for a synfuel industry in the U.S., Perry and Landsbert (1981) express reservations about the ability of the government to induce this new industry: "This program will either become part of the everyday economy, or it will fail."[8]

These quotations hint at some of the dilemmas posed for the nation in attempting to deal with the "crisis" following the OAPEC embargo. In the largest sense the debate was over the allocation of increasingly scarce resources—the root stuff of economics. Rapid price rises induced by an emergent monopoly and shortages induced in large part from poor allocation programs imposed by our own government led to new incentives, and to new winners and losers. Many of the government regulations were designed to minimize adverse impacts on special groups (e.g., low income weatherization programs and lifeline utility rates intended to protect low income persons from fast-changing energy prices). Other policies encouraged new technologies on grounds that government investment would speed

their entry into the market place. Some (the windfall oil profits tax) were designed to capture some of the unanticipated gains to those who happened to own oil.

The laws with the most profound effects on energy during the decade were those that continued or extended energy price regulations. We thus turn to the subject of price regulation.

Energy Price Regulations

Throughout most of the decade, the federal government regulated oil and natural gas prices. State utility commissions regulated electricity prices. Coal and uranium prices were not regulated.

Oil price regulations originated in the following ways: (1) the Cost of Living Council was in the early 1970's regulating prices throughout the economy in an effort to control inflation; oil, like many other products, was price-controlled and (2) the embargo and subsequent control of world oil prices by a functioning cartel motivated the government to continue price controls on oil long after control on other products were removed.

It is easy to understand the motivations of the government—the rapid increases in oil prices in 1974, combined with the government commitment to reduce inflation and the widespread belief that oil prices greatly contributed to inflation, resulted in oil price controls that became increasingly complex at the decade progressed. Strong political currents also supported price controls; the oil companies were widely seen as gaining enormous profits from the operations of the OPEC cartel. There were powerful popular pressures to keep prices of oil products as low as possible. For example, John Sawhill, Administrator of the Federal Energy Administration under President Ford, was forced to resign his position because of his support for a five cent per gallon gasoline tax. (In 1983, a five cent per gallon tax on gasoline was enacted into law with little controversy or notice.)

Toward the end of the Carter Administration, legislation was passed that gradually phased out oil price controls. A windfall profits tax was included in the political compromise that effected oil price decontrol. The Reagan Administration has taken steps to hasten the process of full decontrol of oil prices set in motion in the previous Administration.

Natural gas price regulation persisted throughout the decade (with the exception of the intrastate market, where prices were unregulated). While there was interest in deregulating prices, the influence of interest groups that benefited from the price controls (especially consumers and pipeline companies that were not vertically integrated) was sufficient to maintain the controls.

The consequences of the price controls were particularly visible for natural gas. A significant shortage in natural gas persisted from 1975 through 1978 throughout large parts of the country. The shortage is not surprising, since the price of natural gas in the interstate market was far lower than that of competing fuels. Partially in response to the shortage, the Federal Power Commission in the late 1970's tripled the price of new gas contracts in the regulated interstate market. There was relatively little outcry at this very large price increase since the price on new contracts could be folded into existing contracts to yield a much smaller increase in average gas prices. Adding transport costs and profits to the selling price of natural gas still left it much lower in price than competing fuels.

The Natural Gas Policy Act (NGPA), passed in 1978, continues gas price regulation until 1985 (or later, for some types of natural gas). The objective of the Act is to allow higher natural gas prices both to achieve greater parity with competing fuels and to spur development of new gas reserves. The NGPA coincided with and contributed to the end to the natural gas shortages. Although the Reagan Administration favors natural gas price deregulation, it has not accelerated the NGPA schedule.

Electricity prices continue to be regulated at the state level. There is little support for deregulation (although reform of the regulatory process is much desired by many groups), primarily because electric utilities are recognized to be a natural monopoly for which price regulation is appropriate.

Important changes have occurred in the areas of wheeling and of marginal cost pricing. The Public Utilities Regulatory Policies Act (PURPA, 1978) requires utilities to wheel power at reasonable prices. PURPA also requires utilities to calculate marginal prices for electricity as a function of time of day, season, and reliability and to pay marginal costs for electricity to any supplier who wishes to sell it. This part of the legislation has had a significant effect on the sources of electricity supply in California, creating a substantial role for small power producers. The chief planning executive of one major utility, Pacific Gas and Electric Company, has gone on record that his company is, for planning purposes, assuming that all additional generation capacity needs will be met by purchases from external sources during the next twenty years.

Lessons Learned

Price regulation that keeps prices down reduces supplies and encourages demand, creating substantial potential for shortages and fostering inefficient and uneconomic allocation and use of energy resources.

The energy decade has, in our judgment, provided very strong evidence of the disadvantages of energy price regulations. While we feel the government has a legitimate role in protecting the population (and groups within the public) from serious shocks outside their control, energy price regulations are not the means to achieve these ends.

Nonetheless, price deregulation remains a complex issue. An important technical issue—the treatment of existing gas supply contracts—is a complicated matter that will be difficult to deal with.

Most analyses of energy price regulation do not discuss issues of economic and monopoly rents accruing to producers. It is a major political issue. At times, substantial portions of the public have accused the oil companies of causing shortages and/or higher prices. Although the evidence does not support this view, the notion that the oil companies have benefited from OPEC is defensible: any major economic actor will attempt to gain from a new and changing economic environment. The more serious analytic issue is the degree to which the public should capture a portion of the economic and monopoly rents derived from oil and gas production. Congress clearly decided that such public capture of these rents was appropriate in passing the Windfall Profits Tax in 1980. Although the Windfall Profits Tax was strongly opposed by the oil industry prior to its passage, it appears to have worked relatively smoothly in the past few years.

In short, energy price deregulation is likely to cause a far more efficient allocation and use of energy resources than regulated prices. Other things being equal, it is also more likely to encourage development of new supplies.

Energy Conservation

During the energy decade conservation grew from nonexistent to a pervasive part of the federal effort. Programs covered virtually every aspect of the economy. A partial listing included:

- mandatory fuel economy standards for automobiles and light trucks, which established progressively tighter fleet average fuel economy requirements for new vehicles from 1978 to 1985
- building energy performance standards for new buildings, designed to reduce energy use for heating and cooling in all new buildings
- residential conservation service, requiring utilities to provide low-cost (subsidized) energy audits for houses
- solar and energy conservation tax credits
- mandatory minimum energy efficiency standards for consumer products (household appliances and heating and cooling systems); energy labels for these products
- funds to support a wide range of state and local activities to reduce wasteful energy use, including support for state energy commissions, energy extension services at universities, and related activities
- grants for low income weatherization, to provide subsidies for residential conservation investments among low income groups
- schools and hospitals program, to provide support for energy conserving capital investments in these institutions
- a federal energy management program that established criteria for energy conservation measures in all federal buildings
- some (albeit limited) consumer information programs about energy conservation
- targets for reductions in energy use in industry

So long as the Nation had a goal of energy independence to protect the public from potentially enormous economic shocks, the actions to reduce demand were easily justified as the easiest and most cost-effective measures in the short run to reduce energy supply pressures.

Energy conservation has proven remarkably successful. One measure is the ratio of economic output to energy input. The Energy to GNP ratio has fallen each year since 1975. The dramatic reduction of energy demand growth during the decade has resulted in reduced vulnerability to the Nation.

A major change in perceptions about energy conservation and the economy took place during the decade. Early in the decade, there was widespread belief that energy and economic growth were inextricably linked: a 3% growth in the economy meant a 3% growth in energy demand. It is now widely recognized that increased efficiency in energy use means that the economy can grow at a rate considerably greater than that of energy demand. Rather than being seen as a threat to the economy, energy conservation is now widely recognized as a means of improving economic performance as well as providing protection from future energy difficulties.

Research and Development During the Energy Decade

The rapid rise in R&D expenditures on energy during the energy decade (up until 1981) diversified R&D activities away from the prior overwhelming emphasis on nuclear energy. The budgets reflect the objective of ERDA (as stated by its two major planning documents, ERDA 48 and ERDA 76) to support a diverse array of projects with the intention that sufficient numbers would succeed and thereby provide protection particularly against vulnerable oil supplies.

The degree of success of the federal R&D is mixed, at best. Judged from the perspective of the Dixy Lee Ray report, and major later planning documents such as ERDA-48 and ERDA-76, achievements are very disappointing. The investment in new energy technologies have not succeeded in establishing new major sources of energy for the country. The expectations that the federal research, development, and demonstration (RD&D) activities would produce in the middle or late 1980's commercial technologies to support new, large, and viable industries were not realized. Technologies to convert coal into liquid and gaseous fuel forms, to extract and process shale oil and possible tar sands, to develop a viable breeder reactor (to assure a virtually inexhaustible source of uranium for electricity), to convert wastes into liquid or gaseous fuels, and to provide solar energy for space heating, industrial process heat, and electricity were seen in the early 1970's as candidates for widespread commercial success in the 1980's.

It is now clear that none of these technologies had a chance for widespread commercial application within a short time. Many of the programs were oversold. R&D contributed very little to increasing energy supplies during the decade. Some key R&D projects did hasten the ability to reduce demand growth by speeding up commercialization of cost-effective energy conserving end use technologies (e.g., energy efficient lighting systems, improved heat pumps and other heating systems).

Much of the RD&D budget was devoted to very large-scale demonstration programs. The large increases in the budgets necessitated some ways of spending money in large chunks. The demonstration programs met this need admirably. They also made fine "pork barrel" projects. Large facilities can be spread around the country, an approach taken for coal conversion facilities.

The research on environmental, safety, and health aspects of energy technologies did achieve some successes during the decade: a considerably improved understanding of measures to improve the safety of nuclear power plants (or, from a different perspective, a recognition of the inadequacies of current design in ensuring safety); increased knowledge about indoor air quality (IAQ) and some control measures; advances in reducing environmental problems of fossil fuel conversion.

The federal budget for energy R&D demonstrate the rapid change in research priorities that has taken place since 1980. Conservation and solar energy research have been slashed to 15 to 20% of fiscal year 1980 levels; fossil energy research is less than 40% of 1980 levels; energy research (high-energy physics and basic research support) has increased by more than 20% in nominal dollars; and nuclear energy and defense-related research have grown very rapidly. Since 1980, the federal involvement in energy R&D has shifted back towards the priorities of the vintage AEC days. Figure 1 displays this vividly. The current budget represents a compromise between the proposals of the Reagan Administration, which had originally committed itself to dismantling DOE and eliminating the conservation and solar—and possibly the fossil fuel—research programs altogether, and Congress, which has acceded only partially to the Administration budget requests and has preserved at least a skeleton of these programs.

Thus, we have seen two dramatic shifts in R&D priorities during a single decade. The approach of

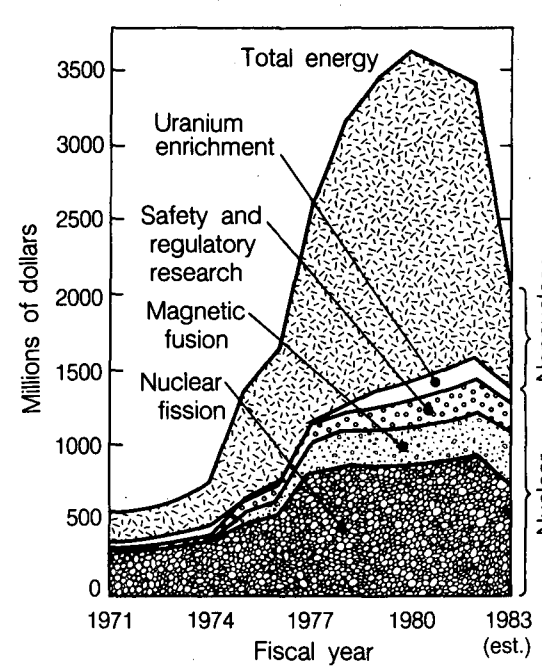

Figure 1. Federal energy R&D expenditures (1971–1983). (XBL 8411-9000)

the 1970's, in which the federal government became involved in virtually all aspects of R&D, has been replaced by a program of greatly enhanced weapons and nuclear energy research, somewhat expanded basic research, and tremendous cuts in research on conservation, solar, environment, and fossil fuels.

Lessons Learned

A major misconception that guided the federal research program during most of the energy decade was the assumption that energy R&D could solve the Nation's energy programs in a short period of time. Not only was the program oversold—to Congress and to the American people—but the overselling led to poorly designed research activities. The government acted as if it believed that it could achieve commercialization of new energy technologies by spending large sums of money. Perhaps the experience of the AEC contributed to this misconception: the federal government had been a major factor in the "creation" of the nuclear power industry and its efforts were crucial in achieving commercialization of nuclear power plant.

In the absence of very large subsidies, new energy technologies can not achieve commercial acceptance until they are cost effective. This is obvious, but was often ignored throughout the energy decade. The demonstration plants to convert coal to liquid or gaseous fuels, the Barstow thermal solar electricity facility, oil shale projects, and the Clinch River Breeder reactor were premature. The technologies are not ready to compete in the market; they do not yield sufficient nonmarket benefits to justify large expenditures on full-scale demonstrations; and they are so unlikely to be picked up by the private sector that the federal expenditures for demonstrations cannot, in our judgment, be justified.

While the government cannot commercialize a technology before it is ready, federal research can be essential to carrying out longer term research to identify new and promising technologies and overcome important technical problems; to treat environmental, safety, and health issues that will not be dealt with by the private sector; and to support small-scale demonstration projects that will enhance the viability of energy technologies that are close to being economic, particularly in risk-sharing ventures with the private sector.

Conclusions

In reviewing the energy decade, we generally found more mistakes than successes. Those who believed in the need for government involvement generally found themselves chastened, while those who believed in R&D were discouraged by the failure of our governmental processes to provide consistent support. For the time being at least, a variety of factors have reduced many of the once "insuperable" energy problems confronting the Nation to manageable size. The same uncertainty in events and factors outside our control will—with certainty—cause unexpected changes in the U.S. energy system, affecting the population in important ways. We do not presume to know what these unexpected changes will be. The energy decade provides a useful basis for assessing a governmental role that can best cope with an uncertain future.

From this complex web of history we would draw some conclusions about government involvement in the management of a critical mineral, during times of real or potential disruption:

- Research and development with a long time to payoff is important for the national good, yet hard for industry to support. There is a continuing need for government to become involved, and to remain involved.
- Government policy to foster energy conservation can provide near- and longer-term economic benefits.
- Government involvement in the energy pricing system and in allocations has been cause for a long series of problems. While there are certainly occasions where such involvement is important—as when there is a prospect for a long term shortage—the major lesson learned is that the problems involved in government intervention are far larger than many people believed, and that the costs of intervention can be substantial.
- The government role is a complex one—as energy is a complex problem. In the face of great uncertainties, considerable care is required to avoid counterproductive actions that respond to immediate political pressures.

PLANNED ACTIVITIES FOR FY 1986

None.

REFERENCES

1. Energy Study Group (1965), "Energy R&D and National Policy," quoted in "The Clouded Crystal Ball" section of *The New Yorker*, May 1977.
2. Hubbert, M.K. (1969), "Energy Resources" in *Resources and Man, A Report of the Committee on Resources and Man*, National Research Council, W.H. Freeman and Co., San Francisco, CA.
3. U.S. Atomic Energy Commission (1973), *The Nation's Energy Future: A Report to Richard M. Nixon, President of the United States.* Submitted by Dixy Lee Ray, Chairman, United States Atomic Energy Commission. December 1, 1973. U.S. Government Printing Office Stock Number 5210-00363.
4. Starr, C. (1979), "Energy and Power," reprinted from *Scientific American* in *Energy*, W.H. Freeman and Co., San Francisco, CA.
5. Levine, M.D. and Graig, P.P. (1985), "A Decade of United States Energy Policy," *Ann. Rev. Energy 10*, pp 557–587.
6. Doub, W.O. (1976), "Energy Regulation: A Quagmire for Energy Policy," *Ann. Rev. Energy*, V1, pp. 715–725.
7. Kalt, J.P. and Stillman, R.S. (1980), "The Role of Government Incentives in Energy Production: An Historical Overview," *Ann. Rev. Energy*, V5, pp. 1–32.
8. Perry, H. and Landsberg, H.H. (1981), "Factors in the Development of a Major U.S. Synthetic Fuels Industry," *Ann. Rev. Energy*, V6, pp. 233–266.

Analysis of Federal Energy Efficiency Standards for Appliances*

M.D. Levine, P. Chan, J.E. McMahon, and H. Ruderman

In 1978, Congress required the U.S. Department of Energy (DOE) to develop and promulgate minimum energy efficiency standards for all major residential appliances and heating and cooling equipment. Lawrence Berkeley Laboratory's Energy Analysis Program has been deeply involved in the analysis of these standards. The major responsibility of the LBL team has been to assess the benefits and costs of standards to the consumer and to estimate the reductions in energy use that could result from them. DOE decided not to set any standards for appliances. This rulemaking was overturned by a U.S. Circuit Court decision. LBL is now responsible for carrying out over the next several years a reevaluation of the original standards to provide guidance when DOE reissues standards in 1988.

*This work was supported by the Assistant Secretary for Conservation and Renewable Energy, Office of Buildings, Energy Research and Development, Building Systems Division of the U.S. Department of Energy under Contract No. DE-AC03-76SF00098.

ACCOMPLISHMENTS DURING FY 1985

Methodology

Our basic approach to evaluating impacts of appliance standards is to estimate the differences between a base-case forecast (i.e., the expected energy efficiency and other parameters when no federal standards are promulgated) and a standards case forecast, in which the energy efficiency and related variables are determined or influenced by the federal policy. If the efficiency of new appliances, appliance usage, first costs, and operating costs were precisely known over the time horizon of the study (as they cannot be) for both the base case and the standards case, then the direct economic impact of the standards on appliance purchasers—the difference between the two cases—would also be exactly known.

Figure 1 presents an overview of the research methodology. The general categories of data required are shown at the left: socioeconomic data for energy forecasting (e.g., projections of housing starts); economic data (demand elasticities); economic forecasts (energy prices); and the economics of appliance efficiency improvements. The model used to project the base and standards cases is a version of the Oak Ridge Residential Energy Demand Forecasting Model (ORNL).[1] This model has been substantially improved for the purpose of analyzing standards.[2] The results of the analysis,

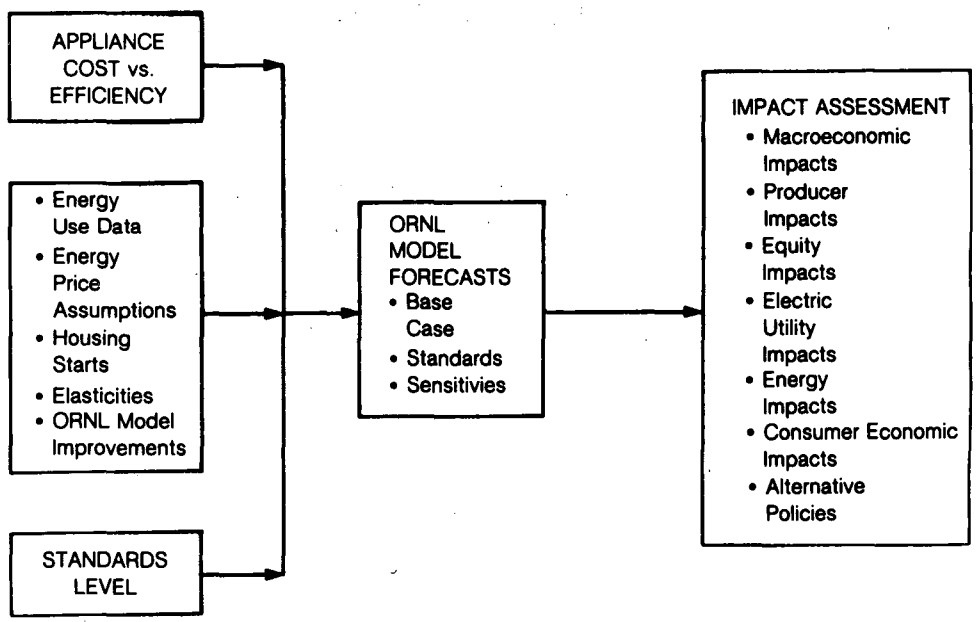

Figure 1. Overview of research methodology. (XBL 845-1963)

shown at the right in Fig. 1, provide direct measures of the impact of standards on appliance purchasers and on the nation: change in energy use as a function of time, change in the life-cycle cost of the appliance over time, net present benefit or cost of the standards to the consumer, and changes in shipments of products resulting from the standards. Impacts on manufacturers and on different groups of consumers cannot be evaluated directly from the model and the data. However, the analysis of direct economic impacts can be combined with other data to obtain estimates of these impacts.

The analysis requires a great deal of data disaggregated by appliance type. Only from such disaggregation can we estimate the retirement rates of individual appliances, the direct and cross price (between fuels) elasticities for energy by end use, and the cost of efficiency improvements for each appliance type.

Key Issues

Some of the most important issues in the analysis of appliance efficiency standards involve the following questions:

- What is the nature of the market for energy efficiency in residential appliances?
- What are the likely impacts of standards on consumers, manufacturers, other interest groups, and the U.S. economy?
- How will the impacts on appliance purchasers vary among income groups and among regions of the country?
- How do the estimated impacts vary with different products, and why? Should a government policy set different criteria for different appliances? If so, on what basis?
- What are the most important sources of uncertainty in estimates of the impacts of standards? How can such uncertainty be dealt with to improve the quality of public policy analysis?
- If standards are promulgated, might their effects be reduced (or even eliminated) by increased usage of the more efficient products? What is the implication of such a "usage elasticity" on the analysis of policy?
- How does the interaction among end uses effect our estimates of energy savings and economic impacts?
- What is the effect on other conservation investments (e.g., thermal integrity)?
- How accurate are the underlying data on cost versus efficiency improvements for the appliances? How can one account for future technological improvements?

Results

Under various plausible assumptions, the analysis projected estimates of energy savings from

the standards that ranged between 11 and 19 quads over a 20-year time horizon, with an expected value of 13 to 15 quads. While 14 quads amount to only about 5% of aggregate residential energy demand over the 20-year period, the impact on energy demand *growth* is dramatic. Figure 2 shows projected residential energy demand with and without standards. The standards originally contemplated by DOE were designed to be within present technological capabilities and to be below life-cycle cost minimums at current fuel prices; if they were to be introduced in 1986, overall residential energy demand growth would be reduced to zero for a decade. Because the legislation provided for updates to the standards, the process could lead to level residential energy demand for two decades or longer. (Other policies or higher-than-expected energy prices could result in declining residential energy demand.)

The total economic impact on consumers is significant. Absent periodic updates to and tightening of the minimum efficiency standards, energy demand is reduced by almost 0.5 quads per year within 6 or 7 years of implementation. At a cost to the consumer of $6 per million Btu, this is a reduction in fuel costs of $3 billion per year. The estimated net present benefit of minimum efficiency standards (fuel cost savings discounted at 10% real, minus the increased first cost of more efficient appliances) is $12 billion, with a range between $10 billion and $16 billion under various alternative assumptions.

Figure 3 shows the estimated energy savings and net benefits of the standards for the six products that consume the largest amounts of energy. Water heaters and refrigerators yield the greatest potential

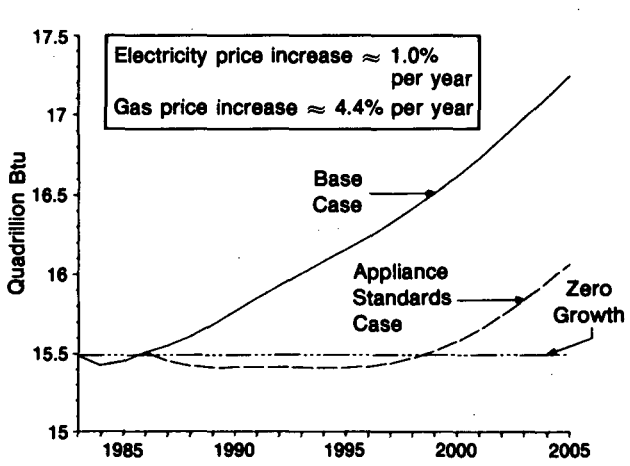

Figure 2. Residential energy demand forecasts. (XBL 845-1966)

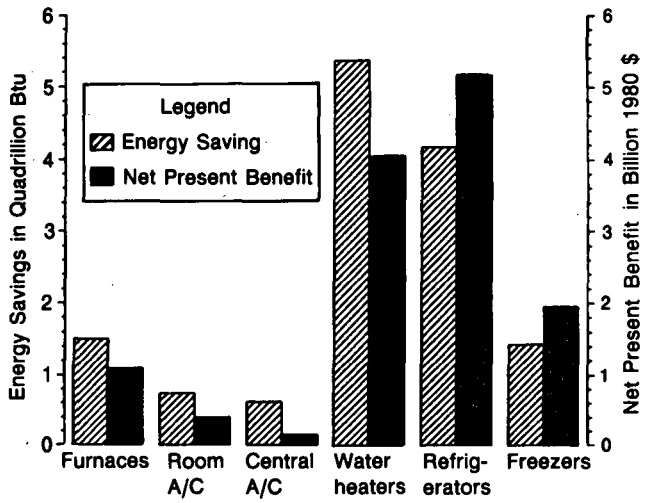

Figure 3. Energy savings and net present benefit of proposed federal standards, by product. (XBL 845-1965)

energy savings. The net benefits are also greatest for these two products, both because the energy savings are largest and because the increased first cost of efficiency improvements are low. Room air conditioners and freezers also yield high net benefits per unit of energy saved.

Standards are estimated to have relatively little impact on furnaces. The major reason is that DOE originally proposed relatively low standards that would have yielded little improvement in energy efficiency over that expected without standards. Since then, condensing furnaces with efficiencies substantially higher than the trial standards have been introduced and are currently selling well. Thus, a tighter minimum standard for furnaces could show substantial energy savings; uncertainty in costs have until recently made the estimation of net benefits speculative.

Central air conditioners show significant energy savings; however, the net benefits are not nearly so great per dollar invested, nor are the unit energy savings as much, as for other products. This is because it is assumed that measures to reduce energy use are added incrementally to existing central air conditioner models, making efficiency improvements relatively expensive. If a full redesign of central air conditioners (and other products) were evaluated, the cost of efficiency improvements could conceivably be different (and lower) than the incremental approach.

Figure 4 shows the projected annual energy savings for several of the most important variables for which we performed sensitivity analyses. The reference or base case assumes a real price escalation

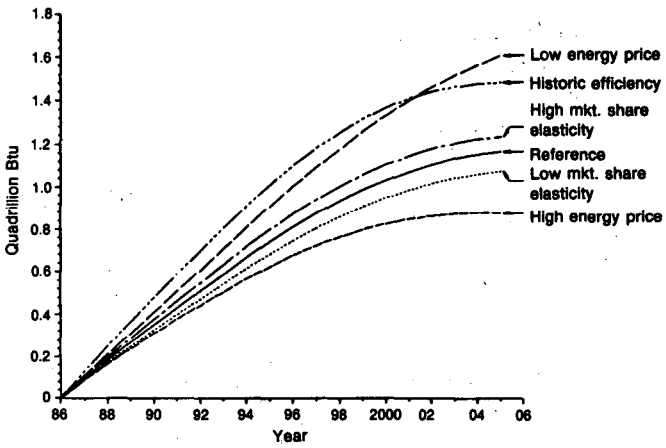

Figure 4. Projections of annual savings in residential energy use under proposed standards for appliance energy efficiency, using various base-case assumptions. (XBL 845-1964)

averaging 4.4% per year for natural gas and 1.0% per year for electricity over a 20-year period. The low energy price forecast assumes real energy price increases of 1.6% per year for natural gas and no increase for electricity. The high energy price forecast is for annual real price increases of 6.1% and 2.0%. The forecast labeled "historic efficiency" does not consider energy prices explicitly; rather, it assumes that, for each appliance, the efficiency improvements of the past decade will continue. The two remaining cases (high and low market share elasticities) make different assumptions about market response to higher energy prices (in terms of the energy efficiency of new product purchases). The results of research conducted to date suggest that the reference case with a constant discount rate may best approximate reality. (This research is discussed in a preceding article on energy efficiency choice by Ruderman *et al.*)

PLANNED ACTIVITIES FOR FY 1986

The reanalysis of appliance efficiency standards will take place over the next two years. Current work at LBL involves (1) improvements to the energy demand forecasting model (particularly in treating various classes of appliances such as frost-free and partially automatic refrigerators); (2) systematic analyses of the strengths and weaknesses of the energy demand model; (3) analysis of energy demand and usage elasticities to improve forecasting results; (4) studies of aggregation issues such as effects of regional climates and fuel prices, and average consumer income; (5) updating market share elasticities for space conditioning equipment choice; (6) improvements in forecasting efficiencies of new appliances; (7) analysis of manufacturers' decisions regarding the energy efficiency of new product lines; and (8) collection and analysis of data on appliance purchases.

Subcontracting will emphasize improved data on the distribution of energy efficiency of appliances sold both nationally and by region of the nation and a preliminary reassessment of trade-offs between cost and energy efficiency in appliances.

REFERENCES

1. Hirst, E. and Carney, J. (1978), *The ORNL Engineering-Economic Model of Residential Energy Use,* Oak Ridge National Laboratory, ORNL/CON-24.
2. McMahon, J.E. (1986), "The LBL Residential Energy Model: An Improved Policy Analysis Tool," submitted to *Energy Systems and Policy*; LBL-18622.

Modeling the Demand for Household Appliances and Energy*

H. Ruderman

The National Energy Conservation Policy Act (NECPA) of 1978 required the U.S. Department of Energy to promulgate minimum energy-efficiency standards for 13 types of consumer products. Standards would be imposed if they were technologically feasible and economically justified. After a considerable amount of technical and economic analysis, DOE decided in 1983 that standards were not justified for any of the products. A Federal Circuit Court overturned DOE's no standards rulemaking in a decision issued in July 1985. NEPCA required DOE to conduct a reanalysis of the appliance standards within five years of their issuance to determine if they should be amended. The Court placed a deadline of August 1988 for a new rulemaking. DOE asked the Energy Analysis Program at LBL to manage the appliance standards reanalysis.

As a first step in the reanalysis, LBL assembled a panel of experts to (1) review the previous standards analysis, (2) recommend changes needed for the reanalysis, and (3) formulate a research agenda to accomplish these changes. This Appliance Standards Analytic Review Group (ASARG) met four times between October 1983 and October 1984 and wrote a report on their findings and recommendations. The ASARG recommended a restructuring of the analysis to better address the legislative requirements and major issues raised concerning the previous analysis. The proposed structure consists of four integrated components (engineering analysis, consumer analysis, manufacturer analysis, and impact analysis) having consistent input, output and assumptions.

The consumer analysis uses models to forecast expenditures for appliances and energy, the number of appliances sold, and the amount of energy they consume. The primary component of the consumer analysis forecasting model is the consumer demand model, which determines the response of households to changes in income, energy prices, equipment costs, and appliance efficiencies. The development of the consumer demand model will take place in four stages: (1) model formulation, (2) data collection, (3) parameter estimation, and (4) testing and validation. When these stages have been completed it can be integrated with the other components of the forecasting model.

During FY–85, the main emphasis of our effort on consumer demand modeling was on the first stage, formulating the model. Some preliminary work was done on evaluating methods of collecting data and estimating the parameters of the model from an existing data set. This article presents an overview of the components of the consumer demand model. A more detailed description of the proposed model may be found in a draft LBL report.[1]

ACCOMPLISHMENTS DURING FY 1985

The consumer analysis addresses the legislative requirements to forecast the economic impacts on consumers and the energy savings resulting from the imposition of standards. In addition, it provides data to the manufacturing and impact analyses. These data include yearly forecasts of appliance sales, equipment costs, efficiency choice, energy consumption, and energy costs. To perform these calculations, we must model the response of consumers to changes in demographic, economic and technological factors. The consumer demand model is thus a critical component in the analysis.

Consumer behavior has a short and a long run component, both of which have to be considered. In the short run, a household can change the amount of service provided by the appliance. Over the long run, a household can replace its stock of energy-using appliances or alter the thermal integrity of the residence. The purpose of the consumer demand model is to calculate household energy use and appliance acquisitions, taking into account these long and short term decisions. Of particular importance for the analysis of standards are the fuel, technology, and efficiency choices.

The consumer demand model has two major components, an appliance utilization model and a technology choice model, which are shown in Fig. 1. The appliance utilization model is used to forecast the short-term response to changes in energy price, income, and appliance and housing characteristics. It also forecasts the longer term capacity, efficiency and thermal integrity changes. The technology choice model simulates household decisions on the acquisition of new or replacement appliances. Included in this model are decisions on fuel, type of equipment, and appliance class.

*This work was supported by the Assistant Secretary for Conservation and Renewable Energy, Office of Building Energy Research and Development, Building Equipment Division of the U.S. Department of Energy under Contract No. DE-AC03-76SF00098.

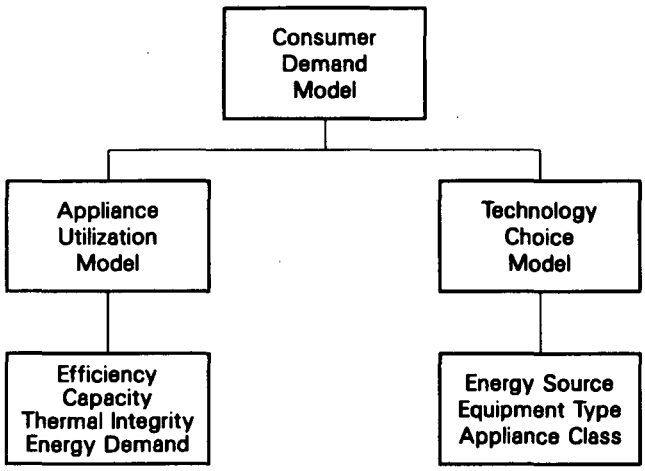

Figure 1. Components of the consumer demand model. (XCG 8511-541)

Consumer demand models will be constructed for the 11 appliance types listed in Table 1. Within each type there may be several classes of appliance. We will discuss the different types under four categories: (1) space conditioning, (2) water heating, (3) refrigeration, and (4) other appliances.

Short-Run Appliance Utilization Decisions

Our approach to modeling end-use energy demand is to consider both the engineering and the economic determinants of demand. We explicitly take into account the engineering factors which cannot be affected by the household in the short run. These are the efficiency and capacity of the appliance and, for space conditioning end uses, the thermal integrity of the residence and weather conditions. Given these engineering constraints, the household decides how much the appliance is used. The utilization decision depends on energy prices and household income as well as the engineering factors. Other factors, such as house size, family size, or occupancy, can influence the demand for certain end uses.

Table 1. Appliance types used in the consumer demand model.

Space Conditioning	
Central Space Heaters	Central Air Conditioners
Home Heating Equipment	Room Air Conditioners
Heat Pumps	
Water Heating	
Gas Water Heaters	Electric Water Heaters
Refrigeration	
Refrigerator/Freezers	Freezers
Other Appliances	
Clothes Dryers	Kitchen Ranges and Ovens

The energy demand model is of the form:

$$E = \frac{C}{e} \cdot \left[\frac{W}{\theta} \right] \cdot h. \tag{1}$$

This is an engineering model which relates the annual energy consumption E by an appliance to its capacity C, efficiency e, and annual utilization h. For space conditioning end uses, there is an additional factor $[W/\theta]$, where W is a measure of the weather and θ is a measure of the thermal integrity of the residence. The economic behavior is in the utilization factor

$$h = h(p, Y, e, C, [\theta,] Z) \tag{2}$$

which depends on energy price p, household income Y, and other household and appliance characteristics Z. This separation of the engineering determinants of energy demand from the short-term behavioral determinants will enable us to study them individually.

Long-Run Capital Stock Decisions

Household decisions regarding capital stock affect energy demand in the long run. These decisions are made when an appliance is purchased for a new home or when it is a retrofit or replacement for a previously owned appliance. The new and retrofit choices are modeled separately because they are made by different agents and have different determinants.

In addition to modeling the household's choice of fuel and technology to provide the end-use service, we have equations for the capacity and efficiency choices because of their strong influence on energy consumption. For space conditioning end uses, we also model decisions about dwelling thermal integrity. Equations for the capital costs of the appliances and thermal integrity are part of the model. Some factors that influence these long-run decisions are climate, house and family size, appliance availability constraints, family income, and energy prices and their anticipated escalation rates.

The model contains long-run capital choice equations for efficiency, capacity, and thermal integrity.

$$e = e(p_o, Y_o, [\theta,] C, K_a, W, Z). \quad (3)$$

$$C = C(p_o, Y_o, [\theta,] K_a, W, Z). \quad (4)$$

$$\theta = \theta(p_o, Y_o, K_\theta, W, Z). \quad (5)$$

Capital costs for purchasing and installing the appliance and the thermal integrity improvements are denoted by K_a and K_θ, respectively. The energy price and income variables have been subscripted to indicate that capital decisions are made at an different time than the utilization decision. We may also want adjust these variables for anticipated price and income escalation. Note that the thermal integrity choice is independent of capacity and efficiency, while the capacity decision is independent of efficiency. This is to ensure there will be no identification problem in estimating these equations.

Two additional equations for capital costs are included in the model.

$$K_a = K_a(e, C, Z) \ . \quad (6)$$

$$K_\theta = K_\theta(\theta, Z) \ . \quad (7)$$

They serve as constraints on the capital choice equations. They can be estimated independently of the other equations using data on appliance prices and the cost of thermal integrity improvements. It may be possible to use engineering equations for the capital costs (e.g., cost versus efficiency curves). The capital costs for some end uses should include installation costs.

As a first approximation, we will assume that the equations for h, C and e are of constant elasticity form. Whether we have to consider more complex forms is an empirical question that will have to be answered by looking at the data. The energy demand and capacity and efficiency choice equations under this assumption are

$$E = A p^{\beta_1} Y^{\beta_2} e^{\beta_3 - 1} C^{\beta_4 + 1} Z_1^{\beta_5} \ , \quad (8)$$

$$e = \bar{B} p^{\gamma_1} Y^{\gamma_2} C^{\gamma_3} Z_1^{\gamma_4} Z_2^{\gamma_5} \ , \quad (9)$$

and

$$C = \bar{C} p^{\epsilon_1} Y^{\epsilon_2} Z_1^{\epsilon_3} Z_2^{\epsilon_4} \ . \quad (10)$$

In these equations, p is the energy price, Y is the household income, Z_1 and Z_2 are sets of household and appliance attributes, and $\beta_1 \cdots \beta_5$, $\gamma_1 \cdots \gamma_5$, $\epsilon_1 \cdots \epsilon_4$ are parameters to be determined. For space heating and cooling, Z_1 and Z_2 will contain variables for climate and thermal integrity. The purchase price of the appliance K is also assumed to have a constant elasticity form

$$K = K_o e^{\alpha_1} C^{\alpha_2} Z_2^{\alpha_3}. \quad (11)$$

Technology Choice

Technology choice includes decisions about energy source (gas, oil or electricity), type of equipment (room or central air conditioner), and appliance class (top, side or bottom mounted freezer, with or without automatic defrost). Since these represent qualitatively different, non-overlapping sets of possibilities, some form of discrete choice model is appropriate.

The discrete choice model is based on the assumption that consumers choose the appliance that maximizes a weighted sum of the consumer and appliance attributes. In addition, there is a disturbance term representing omitted variables or truly random consumer behavior. (This is known as a random utility model.) The weights are the unknown parameters to be estimated, and they may depend on the appliance and the consumer. These assumptions, along with an assumption about the distribution of the disturbance terms, lead to some form of the multinomial logit distribution. The simplest form of the model is

$$P_{ij} = \frac{\exp(\sum_k \beta_{kj} x_{kij})}{\sum_i \exp(\sum_k \beta_{kj} x_{kij})} \quad (12)$$

where P_{ij} is the probability that household j makes choice i, x_{kij} is the kth attribute which may depend on i and j, and β_{jk} is the unknown weight for the kth attribute. More complex nested logit forms that include correlations between end uses are employed in our technology choice model. As an example of a nested logit model, we now describe our model of space conditioning.

Because of their interdependencies, the choice of space heating and cooling technologies will be be modeled jointly. For new residences, we will use a discrete choice model with three levels of decision making. At the highest level is the decision on heating system configuration—should there be a central system, a non-central system, or none at all. The next level of decision is whether or not to install air conditioning. The third level is the choice of space

heating system. An example of a decision tree for space conditioning technology choice is shown in Table 2.

The decisions to install a space heating system and whether it is to be central or non-central are made at the time the residence is constructed, usually by the builder. Factors that influence this decision are the size of the building, the climate, the cost of pipes or ducts, and possibly the income of potential occupants. In this type of model, the costs of the heating and cooling equipment affect the decision indirectly through their influence on the lower level decisions.

The second decision, whether or not to have air conditioning, depends on climate, equipment cost, and family income. For central air conditioners, this decision is often made by the builder, whereas for room air conditioners it is made by the occupants. The room air conditioner decision includes the number of units installed, which depends on house and family size.

The space heating technology choices shown in the last column of Table 2 are meant to be representative. The technologies eventually included will be selected after the appliance classes for the central and non-central heating systems have been determined. They will also depend on the amount of effort we want to expend on data collection. At the least, we have to distinguish four fuel types—gas, oil, electricity and other. Space heating technology choice depends on capital and installation costs, maintenance costs, fuel prices, and income. For non-central systems, the decision includes the number of units installed, which depends on house or family size.

Table 2. Example of a decision tree for space conditioning technology.

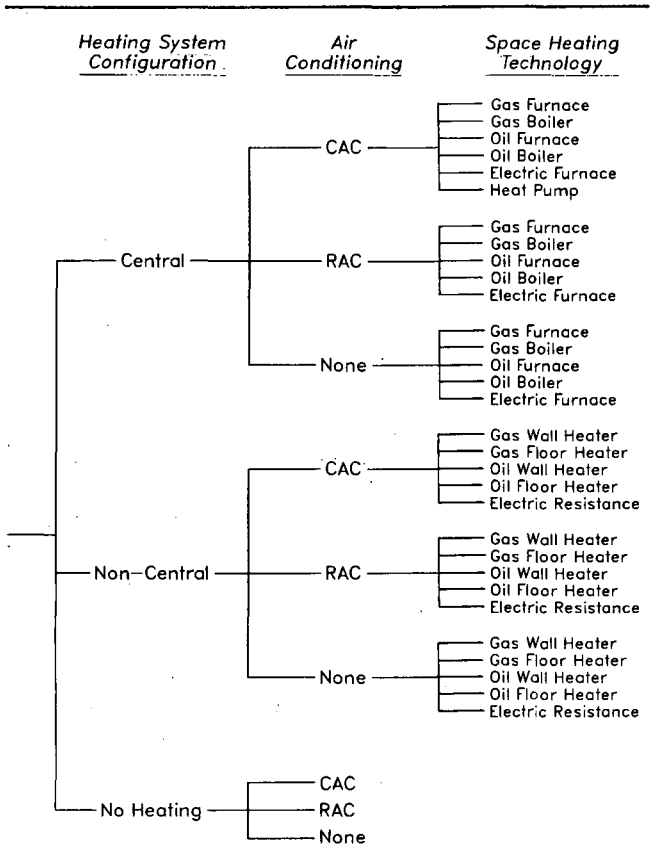

The formulation of the consumer demand model allowed us to identify the data requirements for estimating the parameters of the appliance utilization and technology choice models. We evaluated existing data sources for the relevant information. There were no sources that contained national household data on appliance efficiency and capacity choice. We decided to use a national survey of appliance purchases by a market research organization and add our own questions to determine the actual appliance that was bought and at what price. This will enable us to obtain a broad range of information on the purchase decisions, including consumer attitudes, perceptions and the purchase process.

As a test of the space conditioning model we made preliminary fits of the appliance utilization model and the technology choice model to data from the annual housing survey. These data were compiled by Cambridge Systematics, Inc. (CSI) for the REEPS Model.[2] CSI assumes efficiencies for various appliances and calculates energy consumption and capital cost (which depends on capacity) using a simplified thermal load model. We made additional calculations under different assumptions about efficiency choice, e.g., minimizing life-cycle costs. Our fits were able to distinguish among these different models of behavior.

PLANNED ACTIVITIES FOR FY 1986

Additional work will be done on the model formulation stage during next fiscal year. Of especial interest will be an attempt to incorporate market behavior variables in the consumer demand model. These would include consumer's perceptions of the attributes of the product (brand name, reliability, price, energy use, and other features) as well as information on the process the consumer went through in making the purchase.

A major effort will be to begin the data collection for refrigerators and possibly at least one other appliance. This will involve adding our own questions to the market research questionnaire. The first step will be to determine the brand name and model

number so we can identify the efficiency and capacity of the model purchased. We will also ask the purchase cost. These are the primary data we need to estimate the technology choice and some of the appliance utilization equations. In addition to the data from the survey, we need to collect additional information on household energy consumption (from utility bills) and weather data to be able to estimate the appliance utilization equation. If the data collection proceeds as planned, the third stage, parameter estimation, will begin.

REFERENCES

1. Ruderman, H. (1985), "A Consumer Demand Model for Analyzing the Effects of Efficiency Standards on Appliance Choice and Residential Energy Consumption," Draft LBL-19589.
2. Cambridge Systematics, Inc. (1984), "Household Appliance Choice: Revision of the REEPS Behavioral Models," EPRI EA-3409.

Planning for Oil Overcharge Funds: The California Experience*

E. Vine, J. Sathaye, and A. Rosenfeld†

Within the next few years, states will be receiving some of the largest amounts of funds ($3–5 billion) ever released by the U.S. government to be spent on energy conservation and renewable energy programs and projects. The source of these funds is the Petroleum Violation Escrow Account (PVEA). In anticipation of these funds, a PVEA planning process was developed in California to assist the Governor and the State Legislature in allocating the PVEA money. The California Energy Commission selected the Lawrence Berkeley Laboratory (LBL) to evaluate energy projects proposed by state agencies and those generated from public workshops.[1] The evaluation process lasted eight months, from July 1984 to March 1985. We review the evaluation process undertaken in California and present the evaluations of ten energy programs as examples.

ACCOMPLISHMENTS DURING FY 1985

The PVEA is derived from judgements against oil companies (and negotiated settlements with them) stemming from legal actions by the federal government for price overcharges during the period September 1973 to January 1981. The federal government is in the process of collecting and disbursing oil company profits resulting from the violations of federal price regulations. Monies collected and not yet disbursed are held in a Department of Energy (DOE) escrow account.

Decisions at the federal level on how to disburse PVEA funds have been made through a series of court cases, out-of-court settlements between DOE and the oil companies, and one directive from Congress (the Warner Amendment). The most frequently used forms of disbursement have been direct payment to identifiable injured parties (generally larger users, such as utilities) and supplemental funding for state energy programs. Under DOE's Subpart V process (generally used for out-of-court settlements), direct payments to injured parties are made first, with the residual going to the states. Because of the way the entitlements program operated, crude oil overcharges were spread approximately equally among all refiners. For this reason, distributions of PVEA funds from crude oil cases to the states are made according to the percentage of refined petroleum products consumed in each state.

As of November 1985, the federal government has distributed approximately $800 million: $82 million through the Chevron consent order, $200 million through the Warner Amendment, and the remainder through direct payments to injured parties that could be identified by DOE. Two cases pending before the courts, the Exxon and Stripper Well cases, have the potential of providing significantly greater PVEA funds to the states.

The Warner Amendment (Public Law 97-377, or Section 155 of the Further Continuing Appropriations Act, 1983) restricted the use of most of the PVEA funds to supplement current levels of funding in the following five existing programs: Weatherization Assistance Program, Low-Income Home Energy Assistance Program, Energy Extension Service Pro-

*This work was supported by the California Energy Commission through the U.S. Department of Energy under Contract No. DE-AC03-76SF00098.

†Energy Efficient Buildings Program.

gram, Institutional Conservation (Schools and Hospitals) Program, and the State Energy Conservation Program. The mechanism and guidelines for the disbursement of future funds are not entirely clear and may be different from those under the Warner Amendment. However, the appellate court decision on the Exxon case (now under appeal to the U.S. Supreme Court) will use the Warner Amendment restrictions for disbursing these funds.

Figure 1 presents the evaluation process undertaken in this project. In 1983, in anticipation of oil overcharge funds, the California State Legislature directed the California Energy Commission (CEC), in cooperation with two other state agencies, to define a scope and select a contractor for studying the energy conservation potential for all possible uses of PVEA funds (California Budget Act of 1983).

The CEC began the evaluation process to assure the broadest possible participation by state agencies and the general public in developing ideas for expenditure of PVEA funds. The actual development of proposals and evaluation criteria was undertaken by an advisory committee to the CEC (the PVEA Working Group) composed of representatives from sixteen state agencies. These agencies represented a wide range of views and concerns related to energy. At the beginning of the process, we organized an evaluation team (the LBL Evaluation Team) to assist in the development of evaluation criteria and in the evaluation of state agency proposals and projects proposed in the public workshops. This team was composed of thirteen individuals from LBL and the University of California (Berkeley and Davis campuses) and four private consultants who had considerable knowledge and expertise in energy conservation and renewable energy sources.

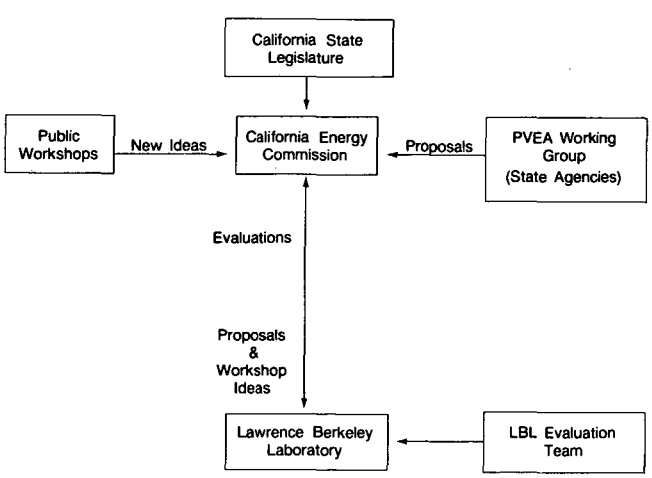

Figure 1. Flowchart of PVEA evaluation process. (XBL 8512-5035)

One of the principal objectives of the evaluation process was to ensure an objective and consistent evaluation of all proposals. One mechanism for achieving this objective was to have all agencies respond to the same criteria, information requests, and assumptions for developing their proposals. The PVEA Working Group first developed evaluation criteria and included a set of instructions for preparing proposals. It agreed to emphasize proposals for generic statewide programs under which actual projects would be selected later through competitive processes. LBL evaluators studied the resulting proposals and often requested additional information from the proposing agencies to develop better and more complete proposals. Members of the LBL Evaluation Team also received explanations and clarifications of these additional information requests. Thus, the evaluation process was an iterative process: evaluators received and evaluated proposals from state agencies, requested additional information and modifications or clarifications to existing data, received additional information, and completed their evaluations of the proposals.

The PVEA Working Group met during a period of more than eight months and considered more than 200 proposals. Proposals that appeared to be premature or unworkable were withdrawn. Several agencies worked together to develop joint proposals and eliminate duplication. Ultimately, 73 PVEA proposals were submitted to LBL for evaluation.

During this period, the CEC conducted a series of statewide workshops for the general public to encourage their participation in the PVEA planning process and the development of their own proposals. The public workshops generated close to 550 proposals from local governments, constituent organizations, and members of the general public. In reviewing the public workshop ideas, we concentrated on identifying important energy opportunities that were missed by the state agency proposals. Based on this review, new proposals were formulated and, in some instances, agencies expanded their proposals to accomodate new ideas. LBL evaluated the public workshop suggestions and allocated the great majority of them to state agency proposals or other public proposals. Drawing from 57 ideas received at public workshops, LBL prepared and evaluated ten new proposals. In sum, a total of 83 agency and public workshop proposals were submitted to LBL for detailed evaluation.

We evaluated the proposals according to sixteen criteria (Table 1). We compared the proposals with

Table 1. Evaluation criteria.

1. Projected energy savings or production, over time
2. Projected direct non-energy benefits, over time
3. Projected cost, over time
4. Cost-effectiveness (societal and leveraged)
5. Leverage of private funds
6. Conformance with U.S. Department of Energy rules
7. Level of expansion over current efforts
8. Monitoring and feedback provisions
9. Minimum level of effort for project to be viable
10. Other programs serving the same clients simultaneously
11. Level of programmatic or technological innovation
12. Plans to continue the project after PVEA funding
13. Likelihood of continued financial obligation beyond PVEA
14. Low-income impacts
15. Environmental impacts
16. Job development

one another based on these criteria, but they were not given an overall ranking. The information collected in response to these criteria was intended to be used by the governor and the state legislature for developing their own priority list of projects to be funded.

The evaluation report examined the criteria in greater depth.[2] However, four criteria deserve special attention. First, in examining cost-effectiveness, we made great efforts to reduce the energy benefits and project costs from each proposal into comparable benefit-cost ratios. We calculated the benefit-cost ratios by discounting future energy benefits and project costs back to their present value (we used a real discount rate of 6%). This adjusts the results to account for the time value of money; for example, at a real discount rate of 6%, a dollar today is worth 1.34 times the dollar amount to be received five years from now. The societal energy benefit-cost ratio includes all costs to implement energy savings measures—both PVEA and participant shares. This ratio indicates the return per dollar spent from the standpoint of the entire economy. The leveraged energy benefit-cost ratio includes only the PVEA-funded costs. This ratio indicates the benefits per dollar of PVEA funds expended.

Second, we made monitoring and feedback provisions an important criterion because many existing energy conservation programs are being implemented without any knowledge of their energy savings and cost-effectiveness. Accordingly, this criterion served as a stimulus for agencies to include monitoring and feedback provisions in their proposal so that better data would be available for managing the programs and conducting program and project evaluations.

Third, the advent of PVEA funds represents an opportunity for state agencies and the general public to develop new and innovative energy programs. Accordingly, the criterion of programmatic or technological innovation served as a stimulus for the development of proposals different from traditional energy programs and projects. In addition, in one of our reports to the state agencies during the initial development of the proposals,[2] we provided innovative energy projects and ideas from nineteen other states.

Fourth, the low-income population was considered to be in need of special assistance based on data indicating that low-income people bear a proportionately greater burden of rising energy costs than other income groups. Accordingly, we prepared a report on the energy characteristics of low-income households in California so that state agencies would attempt to develop programs and projects targeted to low-income groups.[3]

The detailed evaluations of each proposal included information on the above criteria and additional proposal features, such as the kinds of organizations involved in the actual delivery of services ("service providers": e.g., utility companies, industries, state agencies, local governments, schools, consumer groups, and contractors) and the groups that would use the services ("target end users": e.g., low-income households, schools, residential sector, state agencies, businesses, transportation sector, local governments, and agricultural sector).

After preparing detailed evaluations, we provided summary evaluations of each proposal and a large table briefly describing the key characteristics of the proposals that would be relevant for decision-makers. Table 2 of this report presents an excerpt from this table showing ten proposals chosen to illustrate the criteria mentioned above.

Table 2 characterizes each proposal in successive columns, with the following information: (1) title of proposal, (2) service provider, (3) target end-user, (4) new/expansion (whether the proposal is a new idea, or an expansion of an existing project or program), (5) program duration (in years), (6) societal energy benefit-cost ratio, (7) leveraged energy benefit-cost ratio, (8) energy benefits, (9) PVEA funds, (10) matching funds, and (11) participant costs. For the last six characteristics (6–11), categories from "very

Table 2. Example of summary table.

Proposal	Service Provider	Target User	New/[a] Expn.	Program Duration (Yr)	Benefit/Cost[b,c] Societal	Benefit/Cost[b,c] Leveraged	Energy[c] Saved	Cost (M$)[c] PVEA	Cost (M$)[c] Matching	Cost (M$)[c] Participant[d]
1. Energy program for low-income/ underserved clients	Contractor Local govt.	Low-income Resid.	Exp.	3	M	H	L	5.77(M)	0.18(M)	20.3(H)
2. Irrigation of agricultural land	State	Agric.	New	3	M	M	VL	0.3(VL)	0.07(L)	None
3. Revolving loan fund	State	Business Agric.	New	10	M	H	H	30.0(H)	0.8(M)	127(VH)
4. Fuel efficient fleet maintenance	Local govt.	State Local govt. Transp.	Exp.	3	H	H	M	1.5(L)	0.06(L)	None
5. K-12 energy management centers	County School	Schools	Exp.	3	H	H	M	5.3(M)	0.06(L)	2.1(M)
6. Telecommuting/telework project	Contractor	State Local govt. Business	New	2	L	L	U	3.2(M)	0.03(VL)	None
7. Cogeneration in university and college facilities	State	State	Exp.	3	M	VH	L	1.1(L)	0.18(M)	None
8. Transit bus remanufacturing	Local govt.	Transp.	New	3	L	L	VL	8.0(M)	1.0(M)	None
9. Transportation system management for local government	Local govt.	Transp.	Exp.	5	H	H	M	20.0(H)	None	2.5(M)
10. Home energy rating system	Local govt.	Resid.	Exp.	4	H	H	H	4.0(M)	U	36.0(H)

[a]New idea or expansion of existing project.

[b]Definitions of benefit/cost ratios: Societal ratio = Net energy benefits/(PVEA costs + all other costs); Leveraged ratio = Net energy benefits/PVEA costs.

[c]VL–Very Low, L–Low, M–Medium, H–High, VH–Very High, U–Unknown, Resid.–Residential, Transp.–Transportation, Agric.–Agriculture.

[d]Participant is the same as target user.

low" to "very high" were constructed using the data from the summary evaluations. The projects were grouped into approximate thirds (low, medium, and high). The extreme groups are then subdivided at logical breakpoints (very low and low, very high and high). For benefit-cost ratios, we eliminated the "very low" category in order to identify all projects below 1.00 (a standard economic criterion) as "low." It is important to note that the boundaries between groups are only rough approximations and are used primarily to distinguish groups of proposals (rather than one proposal from another). Hence, in certain instances, adjacent ratings are extremely close and, in light of the uncertainties in quantitative estimates, the differences may be overstated.

In general, we found that certain types of proposals had higher benefit-cost ratios than others due to the nature of their program. For example, energy education/information programs that focused on changing people's behavior typically had minimal costs (especially, if the program infrastructure was already in place) and large benefits spread over time. In contrast, capital intensive projects (e.g., bus remanufacturing) had high initial costs and moderate benefits spread over time. Such projects often had small benefit-cost ratios.

In summary, the process of evaluating energy proposals in California in anticipation of large amounts of oil overcharge funds was characterized by several distinctive features. First, this was the first time in California that all state agencies with energy conservation and renewable energy interests came together to express their views and priorities for developing energy programs. As a result of this interaction, agencies were able to coordinate some of their current programs and to cooperate in joint ven-

tures in the planning and possible utilization of the oil overcharge funds.

Second, the general public was able to suggest ideas through public workshops for the allocation of these funds. They were given the opportunity to comment on proposals, and the process was used to develop and evaluate these proposals. The public generated over 500 ideas for proposals.

Third, the evaluation was an iterative process in which the evaluators and the proposers were in close contact with one another in the development and final evaluation of the proposals. This was not an evaluation in the classical sense in which a proposal (or program or project) is submitted and the evaluation is conducted on the final product. In the PVEA evaluation, proposals changed as a result of initial evaluations, and the evaluations changed as the proposals evolved. We believe this iterative process resulted in better proposals and evaluations with minimal loss in objectivity.

Finally, we included in the evaluation criteria certain unusual items (feedback and monitoring provisions, low-income impacts, and programmatic/technological innovations) that we believe are important in proposals. We introduced these items to stimulate agencies to consider them in the development of their proposals for this evaluation and in future program development. We also wrote reports on innovative projects in other states and on energy use and low-income households to emphasize the importance of these criteria.[2,3]

While the evaluation process has been completed, the impact of the Evaluation Report continues. Major new PVEA funds available to California will be allocated by the Governor and the State Legislature through the state's budget process. The regular budget process will be assisted by the PVEA planning process implemented through the California Energy Commission (CEC) and by the Governor's PVEA Task Force (composed of eight representatives of the state's main agencies). Using the evaluations contained in this report, the Governor's PVEA Task Force has already developed a plan of expenditure for these funds. The detail of those decisions was incorporated into a series of budget change letters submitted to the Legislature on March 1, 1985.

California state agencies have also used this report in funding several of their projects with existing PVEA funds and in exploring potential programs and projects suggested in the report. Other states are also examining the report to determine how they should determine their distribution of oil overcharge funds.

In conclusion, the evaluation process appears to be having a positive impact on how state agencies spend oil overcharge funds to promote the use of energy conservation and renewable sources of energy.

PLANNED ACTIVITIES FOR FY 1986

None. The project has been completed.

ACKNOWLEDGEMENTS

We would like to thank Paul Gertner, Kent Smith, and Don Wallace of the California Energy Commission for their assistance in the evaluation process. We are especially grateful for the work conducted by the LBL Evaluation Team. Finally, we express our gratitude to Mike Rothkopf for his editorial comments and to the support staff of the Applied Science Division for their help in preparing the Evaluation Report.

REFERENCES

1. California Energy Commission (1985), *California's Petroleum Violation Escrow Account (PVEA) Evaluation Report* (P110-85-001), and *Technical Support Document* (P100-85-001A), Sacramento, CA.
2. Vine, E. (1985), *State Survey of Innovative Energy Programs and Projects,* LBL-19126.
3. Vine, E. and Gold, S. (1985), *Low-Income Households and Energy Use in California,* LBL-19127.

Policy Analysis of Natural Resource Sale Mechanisms*

M. Rothkopf, D. Wood, and C. Bart McGuire

Each year, the federal and state governments transfer natural resources worth billions of dollars to the private sector for development. These resources include oil, gas, coal, timber, and minerals such as uranium. Many transfer mechanisms are used, including claim staking, lotteries, and many different kinds of auctions. Auction mechanisms used include oral and sealed bidding for lump sums, unit prices, royalty percentages, or profit shares. In addition, there are many different rules and practices that affect the conduct and results of natural resource auctions. Among these rules are restrictions on joint bidding by potential competitors, choice of bid variables, restrictions (such as minimums) on acceptable bids, and criteria for rejecting all bids. The state or federal government in choosing its rules have several objectives; these may include increasing government revenue, the economic efficiency of the transfer and resource development process, fairness, and avoiding the appearance of unfairness.

The general purpose of the research reported here is the analysis of policy issues related to the design of resource transfer mechanisms and the development of tools to support such analyses. One particular objective has been the development of a simulation model to analyze a particular form of auction used by the U.S. Forest Service to sell logging rights in national forests of the western United States. Another particular objective has been an analysis of two issues related to federal coal leasing: the use of negotiations instead of auctions for "captive" coal tracts and the impact of changed rail rates on Bureau of Land Management (BLM) leasing revenue.

ACCOMPLISHMENTS DURING FY 1985

Unit-Price Auction Simulation

Currently, the Forest Service logging rights auction is a progressive oral auction in which bids are vectors of unit prices for each marketable species of tree on a tract. The total amount of a bid is the inner product of the bid vector with a vector of Forest Service estimates of the quantities of each marketable species. The whole tract is awarded to the high bidder figures on this basis, but the payment by the winner is made at the time the trees are cut and is based upon the actual, not estimated, quantity harvested. Bidders have discovered that they can profit by "unbalancing" or "skewing" their bids to take advantage of perceived Forest Service estimating errors—especially an overestimate of a minor species. The Forest Service has been criticized for sales in which this occurred,[1] and is considering rule changes to limit skewed bidding.[2,3] The bidding literature contains insightful analysis of how bidders can best bid in such unit-price auctions,[4,5] but only a little analysis of how bid takers can best manage them.[6]

Our unit-price auction simulator models the quantity and value estimating processes of the seller and of each bidder, and each bidder's strategy choice. It performs a Monte Carlo simulation of the auction to evaluate a variety of measures of auction performance, including the probability that at least one acceptable bid is received, the expected revenue received by the seller, and the probability that each bidder (including each less efficient one) wins. These simulations can be repreated for various sets of auction rules to estimate the effects of rule changes.

Several kinds of bidding strategies can be treated by the model. The model will handle bidders who skew their bids in the manner suggested by Stark[4] and those who do not skew their bids. The model characterizes a bidder's strategy in terms of two factors: the maximum fraction of his or her tool value estimate the bidder is willing to bid (if competing bids make this necessary) and, for skewing bidders, the additional fraction of the estimated additional profit from skewing that the bidder would "give back" in the form of further bid increases (again, if competing bids make this necessary). Bidders' strategies characterized in terms of these two fractions may either be prespecified or be classified as "optimal." For bidders with "optimal" strategies, the model adjusts the two fractions that compose the strategy so that (within tolerances) no further adjustments could increase that bidder's expected profit. If there are two or more bidders with "optimal" strategies, then the strategies of each must be adjusted to find (to within tolerances) a Nash equilibrium set of strategies in which no optimizing bidder can unilaterally improve his or her own expected profit.

Stark's original work on skewed bidding[4] showed that the optimal pattern in skewing bids is the solution of a linear programming problem and, furthermore, that in certain situations the optimal pattern

*This work was supported by the U.S. Department of Interior, Bureau of Land Management, and the U.S. Department of Energy under Contract No. DE-AC03-76SF00098.

of skewing could be determined without resorting to iterative calculations (such as the simplex method). We have used this result and extended our ability to obtain essentially noniterative solutions to two additional kinds of constraints, including those proposed by the U.S. Forest Service.[2,3]

Finding optimal or equilibrium strategies is computationally difficult because each evaluation of the objective functions of the bidders for a given set of strategies requires a Monte Carlo simulation. Such evaluations involve a substantial computational effort, one that increases as the square of the required precision.

We have used three methods for equilibrium calculations. The first method involves running a set of Monte Carlo simulations in a pattern suggested by experimental design considerations, fitting quadratic surfaces to the results, finding the equilibrium on the quadratic surfaces, and iterating with a new pattern centered around this point. This method is related to an approach discussed by Glad and Goldstein.[7] The second approach is specialized, applying only to situations in which all optimizing bidders are identical for strategic purposes. It looks for symmetric sets of equilibrium strategies by varying one bidder's strategy and using the results to make a damped adjustment of all bidders' strategies. The third method is more general, applying to both symmetric and asymmetric auctions. It determines each bidder's best strategic response for several fixed values of the opponents' strategies, and fits functional forms to these values. We find the equilibrium strategies by locating the intersection of these functions.

Of the three methods, the third is generally superior, and was used to produce most of our results. The first approach is the most direct, but our problem seems to require strong curvature of the fitted surfaces or unreasonably good initial guesses for convergences. The second method (when it can be used) converges quite quickly for reasonably good initial guesses, but provides no direct way to estimate the uncertainty of the equilibrium except by replicating the entire algorithm. This replication, if required, would make it more costly than the third method. Versions of all three methods have been implemented on the CDC 7600 and/or LBL's MIDAS parallel processor computer.

The second and third approaches both require finding a bidder's "best response strategy" to opponents' fixed strategies. We have tried two approaches to this subproblem: an iterative application of simplex search[8] and a fairly straightforward application of classical response surface methodology. Of these, the second method has been more useful.

Use of the simulator has lead us to the following preliminary conclusions:

(1) For some auction conditions, near-optimal strategies for a bidder (given the strategy of his competitors) cover a wide range of "givebacks" of anticipated profits from skewing. Hence, little is lost by assuming that "giveback" is arbitrarily fixed rather than optimized. This significantly eases the calculation burden of finding equilibrium strategies. Fig. 1 illustrates this.

(2) To the extend that equilibrium strategies can be relied upon, it appears that if there are two or more optimizing bidders (who are also skewing bidders and who value the timber equally), then much of the apparent revenue gain by winning bidders who skew will be competed away. Fig. 2 illustrates this.

(3) In these auctions, symmetric equilibrium bidding strategies are more aggressive with few bidders. Unlike sealed-bid, first-price auctions, this is true in comparing two-bidder auctions with three-bidder auctions. In addition, at equilibrium, expected government revenue increases and the expected profit of the winning bidder decreases with the number of symmetric bidders. Fig. 3 illustrates this.

(4) When there is only one skewing bidder, the effect of skewing on government revenue can be severe. Table 1 illustrates this.

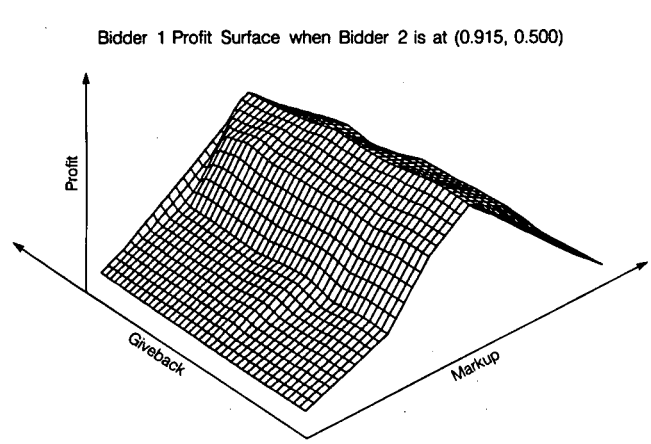

Figure 1. An example of a surface fitted to simulation results that illustrate the common situation in which "giveback" strategy does not significantly affect a bidder's expected profit. (XCG 854-9810)

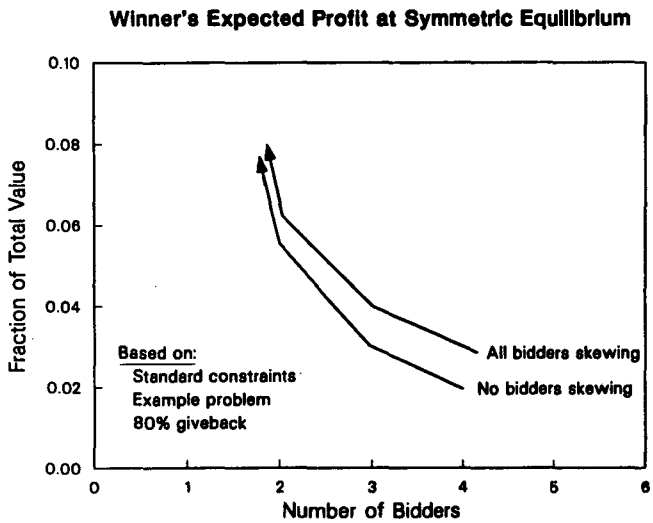

Figure 2. At symmetric equilibrium, much of the apparent extra profits from skewing are competed away. (XCG 854-184)

Analysis of Captive Coal Lease Negotiations

The Commission Fair Market Value Policy for Federal Coal Leasing made many recommendations.[9] One of the difficult but common problems it dealt with is the "captive tract" situation in which a coal tract is of substantial value to only one private party.

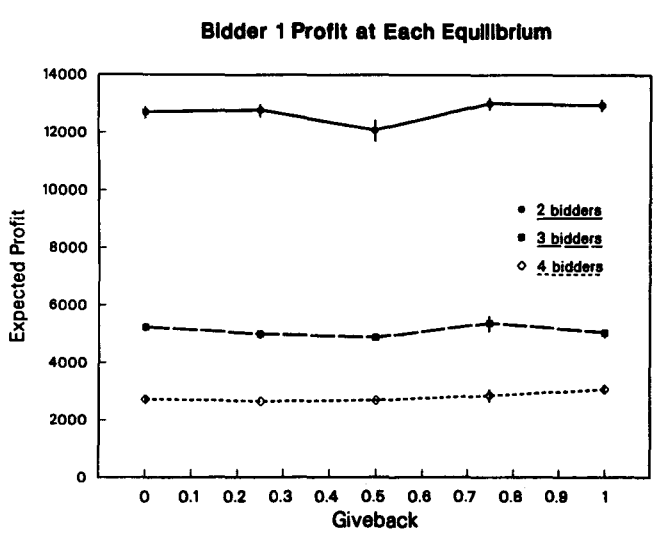

Figure 3. This figure shows the expected profits at equilibrium of bidders in symmetric action. As the number of bidders increase, the expected profit of each bidder falls by a greater factor; hence, profit paid by the government decreases. This figure also shows again the unimportance of the "giveback" part of bidder strategy. (XBL 854-185)

Table 1. One skewing bidder—one non-skewing bidder.

Constraints	Lower Markup[a] at Equilibrium
None	~0.25[b]
"Standard"	~0.625[b]
"Tight"	~0.875

[a]Since this is a second price auction, the lower markup largely determines the price.

[b]Equilibrium unstable—also, values below ~0.65 are extrapolations into a region with <1% of auctions won by lower bidder.

In such a situation, the government is unlikely to obtain more than one competitive bid. Furthermore, the value of the tract is likely to be difficult to estimate. Such situations prompted the Commission to recommend that the government consider negotiations as an alternative to competitive sales.[9] We have analyzed negotiations as an alternative to competitive sales and identified a number of situations in which negotiations of an appropriate kind are advantageous. In this analysis, we have considered various criteria including economic efficiency, government revenue, fairness, the appearance of fairness, and administrative workability.

Our analysis, currently in the form of a draft report,[10] draws upon such parts of bedding theory and bargaining theory as are relevant. It notes the advantages of negotiating exchanged under existing regulations that leave the government with economically logical potential runnable tracts. It also notes the advantages of negotiating shares for the "cooperative leasing" by auction of such tracts. Each of these procedures when usable, will reduce the valuation issues determined by nonmarket mechanisms by converting "captive" tracts into competitive tracts.

For other "captive" tracts, the report finds that there are significant potential advantages to lease negotiations provided that:

1. all negotiations are tentative, subject to "validation" of their one bidder nature in a post-negotiation formal sale procedure (we find that post-negotiation "validation" has clear advantages over pre-negotiation "validation.")
2. the government gains leverage in its negotiations by negotiating on more leases than

it will conclude, using whenever possible one of the "round-robin" negotiation procedures we describe,

3. government employees and not independent agents negotiate for the government, and
4. negotiations are narrowly confined to the amount of the lease bonus.

The report also suggests that the government may wish to consider the use of final-offer arbitration on leases, such as "bypasses," on which both the government and the only interested private party have high interest in an agreement being reached. Fig. 4 shows a potential decision sequence for selecting a mechanism for a coal lease sale.

The report analyzes requiring the use of economic evaluation models in the negotiating process and the use of negotiation fees. While economic evaluation models may well be useful, the report points out some serious problems associated with *requiring* that negotiations conducted be solely in terms of discussing inputs to such a model. The report also raises concerns about the use of negotiation fees. If such fees are used in spite of these concerns, the report notes advantages to the fees being neither refundable nor creditable against a lease bonus.

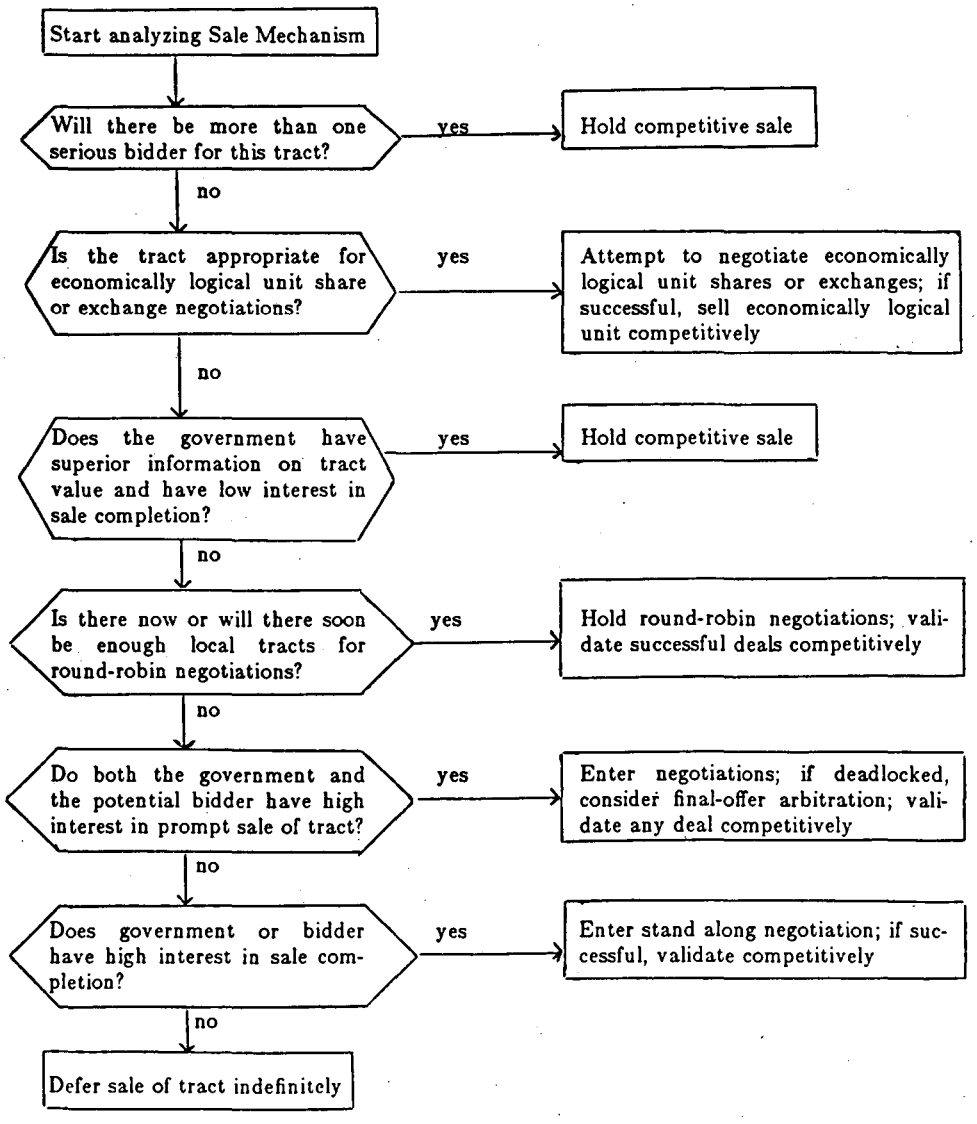

Figure 4. Potential decision sequence for selecting a sale mechanism for a coal tract. (XBL 862-442)

Effect on Government Revenue of Higher Coal Prices

In support of the BLM's responsibility with respect to the management of federal coal, we performed a theoretical economic analysis of the long run effect on federal revenue of an increase in coal prices such as one that would be caused by a reduction in railroad charges for transporting coal. We derived the formulas for two elasticities. The first of these, ϵ_Q, is the elasticity of the quantity of coal produced with respect to the price of "upstream"—i.e., preshipment—coal. The second elasticity, ϵ_R, is the elasticity of the residual value upstream coal with respect to price. These elasticities are given by

$$\epsilon_Q = \epsilon_s \epsilon_d / (\epsilon_d - \epsilon_s)$$

and

$$\epsilon_{Rr} = (\epsilon_s + 1)\epsilon_d / (\epsilon_d - \epsilon_s),$$

where ϵ_s is the price elasticity of coal supply and ϵ_d is price elasticity of coal demand.

The first of these elasticities, where combined with the direct effect of the price increase, gives the total long run effect on government and *ad velorum* royalties. The second, when combined with an analysis of the ability of the government to capture residual value in lease sale bonuses, gives the effect on government revenue from such bonuses. We reviewed the various bidding models of bonus capture and concluded that for the conditions faced by the Bureau of Land Management a reasonable estimate of the percentage of residual value captured by the government as a function of the number of serious bidders was 15%, 60% and 75% for 1, 2 and 3 bidder sales, respectively. We have documented our analysis in a memorandum.[11]

PLANNED ACTIVITIES FOR FY 1985

We plan to complete a paper on our Forest Service auction simulation, analyze future issues related to the sale of Federal coal tracts, and survey the uses of bidding to sell natural resources by the State of California. We also hope to analyze the sale of "options to lease" instead of leases for coal tracts.

REFERENCES

1. General Accounting Office (1983), "Skewed Bidding Presents Costly Problems for the Forest Service Timber Sales Program," GRAD/RCED-83-37, February 9, Washington, DC.
2. U.S. Forest Service (1983), "National Forest Timber Sales; Control of Skewed Bidding; Procedures," *Federal Register 48* (128), pp. 30417–30420.
3. U.S. Forest Service (1984), "National Forest Timber Sales; Control of Skewed Bidding; Procedures," *Federal Register 49* (137), pp. 28748–28749.
4. Stark, R.M. (1974), "Unbalanced Highway Contract Tendering," *Operational Research Quarterly 25*, p. 373.
5. Deikman, J.E., Mayer, R.H., Jr., and Stark, R.M. (1981), "Coping with Uncertainty in Unit Price Contracting," Preprint 81-541, ASCE Meeting, October 1981, St. Louis, MO.
6. Rothkopf, M.H (1983), *Comment on Proposed Policy on Procedures for Control of Skewed Bidding in National Forest Timber Sales,* LBL-16571.
7. Glad, T. and Goldstein, A. (1977), "Optimization of Functions Whose Values are Subject to Small Errors," *BIT 17*, p. 160.
8. Nelder, J.A. and Mead, R. (1965), "A Simplex Method for Function Minimization," *Computer J. 7*, p. 308.
9. Commission on Fair Market Value Policy for Federal Coal Leasing (1984), D.F. Linowes, Chairman, *Report of the Commission,* February, 1984.
10. Rothkopf, M.H. and McGuire, C.B. (1985), "Assessment of Negotiation Options for Coal-Lease Sales," Draft Report, Lawrence Berkeley Laboratory.
11. Rothkopf, M.H. (1985), "Government Capture of Higher Coal Prices," memorandum.

A Natural Gas Policy Model*

T.J. Teisberg,† B.A. Miller,† and M.H. Rothkopf

Natural gas supply in the U.S. has recently undergone major changes in regulatory environment, and further changes are being contemplated. Furthermore, there is a contract structure between gas producers, gas pipelines, and gas customers that, in part, predates current regulations and poses potential problems for further regulatory changes. To help analyze the effects of various regulatory policies, we have constructed an initial version of a "conceptual" linear programming model. The model is concerned with the "short run" behavior (i.e., behavior under given contracts) of individual pipelines. It is designed to help answer questions such as

(1) Do pipelines have incentives to shut-in low cost gas and produce high cost gas when gas is in surplus and there are take-or-pay obligations on the high cost gas?
(2) How are pipelines' decisions about shutting-in production affected by the existence of pipeline affiliated gas supply?
(3) Why do pipelines resist proposals for contract carriage, and does the level of resistance depend upon the source and destination of the transported gas?
(4) How do alternative pipeline rate designs affect efficiency in natural gas markets?
(5) What is the effect of old gas price decontrol, with and without renegotiation of high cost gas contracts

Such a model can take as exogenous burner tip gas demand and wellhead gas supply conditions. However, in order to be useful it must incorporate a number of potentially inconvenient aspects of the situations faced by pipelines including:

(1) A pipeline transportation network with capacity constraints on links in the network.
(2) Gas storage at nodes on the pipeline network.
(3) Gas supply available from contracts with differing prices and differing take-or-pay requirements.
(4) Explicit representation of gas supply from pipeline affiliated sources.
(5) Explicit representation of non-system (transportation) gas.
(6) Gas demand markets with differing price elasticities of demand.
(7) Seasonality of demand.
(8) Capacity to vary the pipeline rate structure.

ACCOMPLISHMENTS DURING FY 1985

This project was initiated during FY 1985. We identified the problem defined above and the need for a model with the features listed above. We then reviewed the following models to determine their suitability for answering the policy questions in which DOE was interested:

(1) Energy Information Administration, Gas Analysis Modeling System (GAMS), DOE/EIA-0450/1, August 1984.
(2) ICF, Inc., Updated Natural Gas Forecasts using Two-Market Model, September 1982.
(3) Decision Focus, Inc., A Regional Model of the United States Natural Gas Production, Transmission, Distribution and Consumption System, September 1984.
(4) Beltramo, M.A., Manne, A.S., and Weyant, J.P., A North American Gas Trade Model: GTM, September 1984.

The first model, GAMS, is a very large scale computer model. It consists of 4000 lines of FORTRAN code, and it requires 30 minutes of CPU time on a mainframe computer to execute. GAMS is so large because it simulates the gas market from the exploration for new gas reserves to the consumption choices of gas consumers, and the impact of macroeconomic variables on those choices. Exploration decisions, for example, are modeled as the solution of a linear program, and pipeline gas acquisition decisions are modeled as the solution of a dynamic program.

Because GAMS is so large and detailed, it was judged to be unsuitable as a conceptual model for understanding pipeline behavior. Also, for all of its detail, GAMS does not include some of the specific features mentioned above. These features are gas storage activities, an explicit representation of pipeline affiliated gas supply, and an explicit distinction between system gas and non-system gas (i.e., transportation gas).

The second model is the ICF Two-Market model. In scope, it is similar to GAMS, since it simulates the gas market from the exploration for

*This work was supported by the Policy, Planning and Analysis Office of the U.S. Department of Energy under Contract No. DE-AC03-76SF00098.

†Applied Decision Analysis, Inc.

new gas to the consumption choices of gas consumers. Although the ICF model is considerably smaller than GAMS, it was still judged unsuitable as a conceptual model of pipeline behavior because of its large scope and because it does not incorporate certain features mentioned above. Features not incorporated include seasonality of demand, gas storage, a detailed pipeline transportation network, contract take-or-pay provisions, pipeline affiliated gas supply, and an explicit distinction between system and non-system gas.

The third model, created by DFI, is essentially a network representation of the US natural gas market, where the network structure is derived from a map of major natural gas pipelines. The model is solved by equilibrating supply and demand at nodes of the network. Transportation between nodes of the network adds a simple markup to the cost of gas at the originating node.

The national scope of the DFI model is neither necessary nor desirable in a conceptual model intended to develop understanding of pipeline behavior. Furthermore, a number of features listed above are not available in the DFI model. These include seasonality of natural gas demand, storage of gas, pipeline affiliated gas supply, and supply contracts which set take-or-pay quantities and prices for each supply node, explicit representation of non-system gas transportation, and alternative pipeline rate structures.

The fourth model is the Gas Trade Model (GTM). Like the DFI model, GTM is a network model of the US natural gas market, with particular emphasis on the role of Canadian and Mexican natural gas imports in the US market. Also, like the DFI model, GTM does not offer a number of important features. These include seasonality of natural gas demand, storage of gas, pipeline affiliated gas supply, and supply contracts which set take-or-pay quantities and prices for each supply node, non-system gas transportation, and alternative pipeline rate structures.

After this review, we designed a new model to answer the policy questions of DOE's Office of Economic Analysis and to incorporate the features listed above, which DOE wished to be included in the model. This model is a linear programming model, which we will refer to as the One Pipeline LP.

The One Pipeline LP explicitly focuses on pipeline decision making within a transportation network, and over the course of an annual cycle of demand. Specifically, the pipeline decides (1) how much system gas to take from supply regions/categories for delivery to demand regions/classes, (2) how much non-system gas to transport, (3) how much gas to store/withdraw at any location. and (4) how much gas to pre-pay (as required by take-or-pay provisions) at each supply region/category. The model is formulated as a pipeline profit maximization linear programming problem. All of the features listed above are included in the One Pipeline LP model.

The One-Pipeline LP is capable of simulating a range of situations including the following:

1. "Current situation," with surplus gas, prepayment of low cost gas, and production of high cost gas.
2. Possible tendency for pipelines to shut-in non-affiliated gas, while producing affiliated gas.
3. Varying degrees of pipeline willingness to transport gas on a contract basis, depending upon the profit from such carriage, and the extent to which such carriage relieves take-or-pay, or serves demand otherwise served by pipeline system supply.
4. Effect of alternative pipeline rate designs.
5. Effect of old gas price decontrol, with or without contract renegotiation.

The details of the initial prototype One Pipeline LP model and illustrative results obtained from it are contained in a report written by Teisberg.[1] This prototype model has been applied so far using hypothetical data only. However, there still appear to be a number of insights that can be derived from these results. Perhaps the three most important insights are the following:

First, the incentive for pipelines to product affiliated supply rather than non-affiliated supply appears to be very strong; in all of the cases modeled so far affiliated supply is produced to the capacity limit. In reality, it may not be politically possible for a pipeline to arbitrarily produce its own gas in preference to others' gas. However, the results here suggest that pipelines will favor production of their own gas to the maximum extent possible.

The second important insight from the model concerns the relationship between the pipeline's gas production choices (and hence its weighted average cost of gas) and (1) the elasticity of demand, (2) the extent to which fixed cost is recovered through unit charges, and (3) the cost of pre-paying gas. Specifically, a pipeline will tend to produce the lower cost gas and shut-in the higher cost gas if (1) its demand is more elastic, (2) its fixed costs are relatively heavily loaded into unit prices, and (3) the pipeline does not perceive a high cost to pre-paying gas. Since two of these last three factors are directly influ-

enced by regulatory policy, it may be advisable for regulators to consider the possible implications of regulation on a pipeline's choice of which gas to produce and which to shut-in.

The third important insight from the model concerns decontrol. The illustrative results reported above indicate that if decontrol means an increase in the cost of oil gas, then decontrol may reduce welfare. This is possible because decontrol without price reduction raises average gas costs above market clearing prices, thereby reducing throughput and consumer welfare. However, there are at least two important qualifications of this conclusions. First, it is possible that decontrol of old gas would put sufficient pressure on pipelines that they would seek and obtain substantial price concessions on high cost gas supplies. Second, the results here take no account of possible welfare gains from increased recovery from price decontrolled old gas fields.

PLANNED ACTIVITIES FOR FY 1986

During FY 1986 we expect to expand the model, further document it, and apply it to a specific pipeline. An initial extension will be improving the ability of the model to handle the effects of purchased gas cost adjustment regulations.

REFERENCES

1. Teisberg, T.J. (1985), "Study on the Development of a Natural Gas Policy Model," Phase 1 Report ADA-85-2051 to Lawrence Berkeley Laboratory, Applied Decision Analysis, Inc.

INTERNATIONAL ENERGY STUDIES

Residential Energy Use in Industrialized Countries*

Lee Schipper, Andrea Ketoff, Stephen Meyers, Peter Goering, and Dianne Hawk

For several years, the International Energy Studies Group at LBL has been following residential energy use and its underlying structure in the major Organization for Economic Corporation and Development (OECD) countries. Recently this work was expanded to include the services sector. The goals of the work are to 1) establish a data base on energy use in homes and buildings in OECD countries; 2) analyze the components of changes in energy use since 1973, particularly the permanence of these changes; 3) extend this analysis through econometric work; 4) analyze the relationship between government conservation programs, and actual savings in the residential sector; and 5) evaluate techniques or policies from overseas that may be applied in the United States.

Since official data covering these sectors are almost non-existent, the group has gathered information on every aspect of energy use from numerous private and government sources. Thus, we collected and analyzed data on the building stocks, heating fuel choices, unit consumption, electric and gas appliances, prices, incomes, conservation programs, and other components of residential energy use. These results are summarized in recent reviews,[1,2] whereas our groundwork is published in a variety of other papers.[3–8]

ACCOMPLISHMENTS DURING FY 1985

Our work led us to examine total energy consumption by fuel and end-use for the period 1960–1983, with an emphasis on the period after the 1973 oil price shock. In most countries (Canada, U.S., W. Germany, France, Sweden, Denmark, UK), energy use declined through 1975 due to reductions in space heating intensities. Primary energy use continued to grow because of increased electric appliance ownership and, in the case of Canada, Norway, and Sweden, because of the growing popularity of electric heating. The second oil shock (1979) unleashed a torrent of energy conservation activity. These conservation efforts continued to influence residential energy use through 1983. Oil use per home fell dramatically in every country as a result of reductions in space heating intensity and increased use of wood or electricity as a secondary fuel. Electricity use per home for appliances virtually ceased

*This work was supported by the Assistant Secretary for Conservation and Renewable Energy, Office of Building Energy Research and Development, Building and Community Systems Division of the U.S. Department of Energy under Contract No. DE-AC03-76SF00098. The project also received support from the Swedish Council for Building Research, Stockholm.

to grow as newer, more efficient appliances entered the stock. Gas use per home stopped growing in countries where saturation growth continued to be strong, e.g., France, Germany, and Holland, and declined markedly in the U.S. and Canada.

The continued increase in electricity use for space heating—most notable in Norway and Sweden but also important in France, Canada, and the U.S.—accounted for much of the increase in primary energy use per dwelling, although, electric heating in each country became more efficient as new homes with tight shells entered the stock.

The Decline in Oil Use

The decline in residential energy consumption was driven primarily by curtailed oil use. We examined home oil consumption in great detail.[9,10] For six major OECD countries (Canada, Denmark, France, Norway, Sweden, and the U.S.), home oil use decreased between 31% and 55% during the period 1972/3–1983. In W. Germany, oil consumption did not decline this dramatically: W. Germany consumed 13% less oil in 1983 than it did in 1972. Together these countries achieved an oil savings of about 1.2 million barrels per day [59 million tons of oil equivalent (MToe) per year]. One-third of these savings were induced by reductions in the number of homes heated with oil; the remainder resulted from reductions in oil use per oil heated home. During this period, however, the size of these homes and the penetration of central heating throughout the housing stock increased significantly; hence, these figures underestimate the real conservation efforts made to date. For Canada, France, Norway, and the U.S., we estimate that between 50% and 65% of the savings in oil use per household arose from technical measures and should be permanent; the rest resulted from short term changes in behavior. Denmark, Germany, and Sweden represent the extremes in this analysis. Because of the great increase in the number of oil-heated homes in Germany, the permanent reduction in oil use from lower intensities was outweighted by growth in consumption due to changes in structure. In Denmark, only 25% of the oil savings should be considered permanent; in contrast, we estimate that over three-quarters of the savings in Sweden arose from permanent measures. If heating oil supplies were interrupted today, or if prices suddenly shot up, the Swedes would be in the best position to reduce consumption. Most users in other countries would be hard pressed to make great cuts in the very short term.

Oil is on its way out of the residential market. The share of oil in final residential energy use fell from between 53% and 71% (Canada, Denmark, France, Germany, Sweden) in 1972/3 to as little as 24% in Canada, 36% in Sweden and 40% in France by 1983. Germany and Denmark have remained somewhat more dependent on oil: 47% of residential energy use in Germany is based on oil and 52% in Denmark. Shares in the U.S. and Norway have always been lower than in the above-mentioned countries—13% and 18%, respectively.

Just as increases in the price of heating oil influenced oil use in 1973 and in 1979, it is likely that recent price drops will affect oil demand. Although data are preliminary, it appears that, as a result, conservation incentives have diminished. After 1982, oil use per oil heated home did not decline as much as in previous years and may actually have increased slightly in a few countries. While there is some indication that oil users may be losing interest in reducing their oil bills, momentum for conversions to other fuels is strong in every country.

The Oil Substitutes

By 1983 the near term effects of the 1979/80 price shock appeared to have worn off, and consumers appear to have gained a permanent awareness of the economic benefits of efficient energy use. Gas, electricity, and district heating continue to fight for the heating market abandoned by oil. This year we have initiated two studies concerning fuel substitution. One focuses on the substitution of electricity for oil and the other traces the transition to gas from various other fuels.

We have analyzed the emergence of electricity as a primary energy source in the sector. The past 25 years fall into four periods punctuated by changes in world oil prices that affect all aspects of energy supply and demand: the period prior to the 1973 Oil Crisis, the proceeding years up to the second round of oil price increases (1973–1979), the following period of increasing oil prices (1979–1982), and the last three years, which have been marked by more stable oil prices and diminishing concerns over energy in many countries. Growth in electricity use can be attributed to different factors in each of these four periods. Prior to 1973, electricity consumption increased due to appliance saturation in most countries. In response to the dramatic oil price increases in 1973, new homes were equipped with electric space and water heaters rather than oil-fired equipment. In addition some homeowners converted from oil-fired to electric space and water heating. After the second oil price shock in 1979, and throughout the following years of increasing oil prices, the growth in electricity consumption was due

primarily to conversions. Finally, in recent years growth in electricity consumption has slowed, and in some cases consumption has actually declined. This trend can be explained by three factors: increased appliance efficiency, greatly improved thermal integrity of building shells, and increased electricity prices.

Many other aspects of electricity use need to be investigated and compared on an international basis. These areas include, for example, appliance saturation in low vs. high income countries; distribution of consumption over various end-uses; consumption per capita, per dwelling, and per unit; policy initiatives and their effects; and the behavior of households with either primary or secondary electric heating equipment (what are the most common fuel combinations in households with both systems; how is the secondary system used?).

In order to undertake a systematic treatment of information in the energy market and to make forecasts of future gas consumption, we are developing a formal model of gas demand in the residential sector (see description in following article). The rapid expansion of gas networks in the European countries has motivated conversion from heating oil in both apartments and homes. Analysis based on historical data indicates that intensity of gas use for space heating appears to be falling slowly but steadily in Holland, the United Kingdom, and the U.S.—the three countries with the greatest dependence on gas.

Conservation Policies

What role have policies played in all of these changes? Very few policies governing energy use in existing homes have been enacted. Building codes have been implemented for new buildings in most OECD countries. Usually these codes do not go beyond the practices already adopted by builders for economic reasons. Only in the U.S. do changes in building practices lag behind what appears to be economical.

In Sweden,[11] a complex system of building codes linked to financial support for builders and buyers (in place since the early 1960s) clearly stimulated the building industry to produce far more efficient homes than anywhere else. The extra costs incurred were automatically financed through normal home-financing channels. This led to practices that were on average better than what was required by codes. The Swedish building code required R values of 19 for walls and 25 for roofs. In 1983, the average R value in Sweden was 25 for walls and 40 for roofs. Similarly, through the retrofit grant program in Sweden, administered by a key group that was in place long before 1973, nearly 2/3 of the stock of single-family dwellings and half the apartments have been insulated or subjected to various other conservation techniques. These figures have not been matched in any other country.

In other OECD countries, the impact of policies is not clear. This is because energy savings came about through rapid reductions in energy intensities for heating fuels, principally oil. Denmark, W. Germany, France, and the U.S. are important examples. In Holland, the reduction in gas heating use has been gradual. In this country, the National Insulation Program, which will eventually reach most of the eligible dwellings, is responsible for this decline in consumption.

The impact of government policies is being felt more in the 1980's than in the previous decade. In Denmark and France, programs in the mid-1980s appear to be replacing the "quick and dirty" savings won in 1979/1981 with more permanent savings through the provision of better building shells and equipment. In our judgement, these programs are substantially increasing the rate of investment in retrofit measures by enabling households to improve comfort at a low cost. Thus we find that while conservation programs and policies had only a minor effect in the 1970s, they are bearing fruit in the 1980s in most European countries. In all these countries, new homes heated by gas or electricity and new electric appliances are considerably more efficient than the older ones. This was accomplished without strict codes/standards in place. The U.S. appears to have achieved less improvement in appliance efficiency than other countries.

Promising Foreign Technologies

Our work has uncovered several new technologies that may benefit the United States. One of the most impressive is the exhaust-air heat pump for domestic hot water heating. The device currently outfits half of the new single-family dwellings stock in Sweden.[11] This small device uses the stream of 20°C air from the house ventilation system (active ventilation is necessary in very tight houses) to provide roughly half of the energy required for domestic hot water. If the home uses a hydronic space heating system, surplus heat from the heat pump can also heat the home. Other promising technologies from Europe include bivalent (two-fueled) heat pumps—promoted in France, condensing gas furnaces, and multi-fuel boilers that use oil (or gas), wood, or electricity, depending on which is most advantageous to use. Finally, electric appliances have become more efficient in every country, judging from catalogues

from the major manufacturers (Philips, Electrolux, Mitsubushi). Equally important, the market has absorbed these devices, perhaps to a greater extent in Denmark, Germany, and Japan than in the U.S. Indeed, many observers await an invasion of very efficient appliances from Japan. High electricity prices and government guidelines have stimulated technical developments in Japan.

Perhaps the most dramatic technology, however, is the wooden house itself.[11] Factory crafted houses from Sweden (with some from Norway and Denmark as well) have the best thermal performance of any production houses in the world, at minimal extra cost. In our study[11] we found that houses built in Sweden in the late 1970s and early 1980s generally performed as expected. We also found that with the exchange rates of 1984/5, these houses could be profitably exported to the U.S. More importantly, the Swedish factory crafting techniques could make low-cost thermal comfort available in new U.S. homes. As of May, 1985, the construction of nearly 300 Swedish homes was planned in the U.S. (mostly in the East), and an advanced home from Denmark had recently been assembled at the Brookhaven National Laboratory.

PLANNED ACTIVITIES FOR FY 1986

During 1986, we will be following these developments carefully to see whether falling oil prices will lead to less interest in efficient home energy use, or whether the events of the 1970s and the knowledge gained from experimenting with new ways of saving energy, coupled with today's incentive programs for energy savings, will lead to even more reductions in the cost of basic comforts and energy services. We will also analyze trends in natural gas and electricity use and extend this analysis through econometric work. Based on the results of these studies, we will develop possible scenarios for future energy use in OECD countries.

REFERENCES

1. Schipper, L., Kahane, A., Ketoff, A. (1985), "Explaining Residential Energy Use by International Bottom-Up Comparisons," *Ann. Rev. En. 10*, Palo Alto: Ann. Revs. Inc.
2. Schipper, L. and Ketoff, A. (1985), "Residential Energy Use in the OECD. The Bottom Up Approach," *Energy Journal* (in press).
3. Schipper, L. (1984), "Residential Energy Use and Conservation in Sweden," *Energy and Buildings 6*, p. 11.
4. Schipper, L. (1984), *Internationella Jamforelse av Bostadernas Energiforbrukning.* (International Comparison of Residential Energy Use), R 131:84. Stockholm: Swedish Council for Building Research.
5. Meyers, S. and Schipper, L. (1984), "Energy in American Homes: Changes and Prospects," Energy, The International Journal XX, 1984.
6. Schipper, L. (1983), "Residential Energy Use and Conservation In Denmark," *Energy Policy* (December).
7. Schipper, L. and Ketoff, A. (1983), "Home Energy Use in the OECD: How Much Have We Saved?" *Energy Policy* (June).
8. Schipper, L., Ketoff, A., and Meyers, S. (1981), *International Residential Energy Use: Indicators of End Use and Conservation, LBL-11703.*
9. Schipper, L. and Ketoff, A. (1985), "Oil Conservation: Permanent or Reversible? The Example of Homes in the OECD," *Economia delle Fonti di Energia 25.*
10. Schipper, L. and Ketoff, A. (1985), "Residential Oil Conservation in the OECD: Permanent or Reversible?" *Science*, December 6, 1985.
11. Schipper, L., *et al.* (1985), *Coming in from the Cold: Energy Efficient Swedish Housing for the U.S.*, Washington, DC: Seven Locks Press, Cabin John, Maryland.

Energy Use in the Service Sector: An International Perspective*

Lee Schipper, Steven Meyers, and Andrea N. Ketoff

The service sector has become more important in recent years because it has shown the strongest growth, particularly in the use of electricity. In FY 1984, the International Energy Studies Group of the Energy Analysis Program began an international compilation and analysis of data concerning energy use in the service sector. Our first publication, containing data and analysis on the structural setting for service sector energy consumption and on trends in service sector energy consumption between 1970 and 1982 for eight industrial countries, appeared in FY 1985.[1]

ACCOMPLISHMENTS DURING FY 1985

Commercial sector *delivered* energy consumption has either declined or grown slowly since 1971/72 in the eight countries for which we have reliable time-series data —Canada, Denmark, France, Germany, Norway, Sweden, the UK, and the U.S. (see Table 1). Denmark has seen the largest decline (8%), while Sweden has seen the biggest (but still modest) increase (7%). Delivered energy consumption *per capita* has fallen or stayed the same in all eight countries. All indications are that commercial sector energy use grew faster than the residential sector before 1971/72; after this time both sectors grew more slowly, but commercial still outpaced residential, or at least contracted more slowly.

Part of the decline in delivered energy consumption may be attributable to structural changes that lead to the use of fuels that are more energy-efficient in terms of delivered energy. Here we refer to district heat and electricity, which, unlike oil and gas, do not have combustion losses when used at the building site. Counting primary energy shows all of the energy resources that go into district heat and electricity production for the commercial sector. Since electricity production in particular has high energy losses, increasing use of electricity in the commercial sector has led to growth in primary energy consumption. This growth ranged from 1.3% per year in Denmark and 2.4% per year in Sweden to 4.5% per year in electricity-intensive Norway.

The result of differing growth rates has been considerable shift in the shares of the fuels used in the commercial sector. Oil accounted for between 55% (Denmark) and 72% (France) of total delivered energy consumption in the early 1970s. By 1982, the oil share had fallen to between 37% (Denmark) and 47% (France). In Canada and the U.S., where the oil shares in the early 1970s were 33% and 25%, respectively, substantial drops in the oil share occurred as well.

The electricity share of total delivered energy consumption has grown to over 25% in all of the countries: from 16% to 33% in Denmark, from 16% to 29% in France, from 14% to 26% in Germany,

Table 1. Average annual growth rates in service sector energy consumption (%).[a]

	CANADA 1973–81	DENMARK 1972–82	FRANCE 1974–82	GERMANY 1971–83	NORWAY 1972–82	SWEDEN 1972–82	UK 1970–80	USA 1971–82
Delivered Energy								
Total	0.6	−0.9	−0.9	0.0	1.8	0.7	0.3	0.4
Per capita	−0.7	−1.1	−1.3	0.0	1.4	−0.4	0.2	−0.6
Primary Energy								
Total	0.9	1.3	1.4	1.5	4.5	2.4	1.2	1.8
Per capita	−0.4	1.0	0.9	1.5	4.1	2.2	1.1	0.8

[a]First and last years had roughly similar climate.

*This work was supported by the Assistant Secretary for Conservation and Renewable Energy, Office of Building Energy Research and Development, Buildings Systems Division of the U.S. Department of Energy under Contract No. DE-AC03-76SF00098.

from 25 to 38% in Sweden, from 23% to 35% in the U.S., and from 29% to 34% in Canada. Gas consumption has taken on a major share of total delivered energy consumption in France (22% in 1982), Germany (21% in 1982), and the UK (31% in 1980) and has risen to nearly half of total consumption in Canada and stayed at that level in the U.S.

On a per capita basis, commercial sector energy consumption (Table 2) is some 50–100% higher in the U.S. and Canada than in the European countries, which are roughly in the same range, once the colder Swedish climate is taken into account. This finding does not account for differences in the amount of commercial sector floor area per capita. The accuracy and comparability of floor area estimates among countries is difficult to assess. Using the estimates available to us, we found that the greater level of floor area per capita in the U.S. explains some of the difference in per capita energy use. Energy use per square meter of floor area remains considerably higher in the U.S., however. This may in part be attributable to the nearly universal use of air conditioning in the U.S.

Two important indicators for the service sector are energy and electricity consumption per employee (Table 3). We found that delivered energy consumption per employee was lower in 1982 than in 1970 in each of the eight countries. This was due in part to growing penetration of electricity in the heating market. Electricity consumption per employee increased in every country between 1970 and 1982. The increase was particularly great in Denmark, France, and Germany. The increase in electricity intensity slowed in most cases after 1978.

International Workshop

In FY 1985, an international workshop on energy use in the service sector sponsored by the Electric Power Research Institute and co-organized by the International Energy Studies group brought together participants from 10 countries. The topics discussed during the course of the meeting included overviews of consumption trends, data collection and analysis, models and forecasting, and new technologies in buildings. A proceedings is in preparation.

PLANNED ACTIVITIES FOR FY 1986

We will update our data base and further analyze service sector energy use. We will examine the sector in more detail, looking at energy use and structure in subsectors. We will present equipment/fuel choices in new buildings where data permit.

REFERENCES

1. Schipper, L., Meyers, S., and Ketoff, A. (1985), *Energy Use in the Service Sector: An International Perspective,* LBL-19443 (in press, *Energy Policy*).

Table 2. Service sector buildings energy consumption.[a]

	CANADA 1982	DENMARK 1982	FRANCE 1983	GERMANY 1982	NORWAY 1982	SWEDEN 1982	UK 1980	USA 1979
DELIVERED ENERGY								
Total (PJ)	743	69	547	765	64	150	706	5540
Per capita (GJ)	30	14	10	12	16	18	13	25
per sq m (MJ)	1895[b]	870	793	765	1290	1120	—	1325
Primary Energy								
Total (PJ)	1197	120	893	1155	144	270	1209	9620
Per capita (GJ)	48	23	16	19	35	32	22	43
Per sq m (MJ)	3024[b]	1500	1295	1120	2870	2015	—	2300
Climate Index	107.8	94.8	99.1	95.8	98.2	100.7	99.8	102.7
DD Normal (18°C)	4581	3122	2450	3116	4069	4010	2917	2600

[a]Probably includes some non-buildings energy consumption in Canada, Denmark, and Germany. Residential consumption has been removed from U.S. data.

[b]1981.

Table 3. Commercial sector energy and electricity intensity (GJ per service sector employee[a]).

	CANADA	DENMARK	FRANCE	GERMANY	NORWAY	SWEDEN	UK	USA
				Delivered Energy				
1970	139	—	—	84	61[b]	65	56[b]	118
1971	137[b]	—	—	85[b]	66[b]	64[b]	52	117[b]
1972	150	57	—	91	61[b]	65	52[b]	116
1973	125	—	58[b]	94	55[b]	66[b]	51[b]	115
1974	122	—	56[b]	87	54[b]	60	48	108
1975	109[b]	49	50[b]	87	53[b]	62	47	103
1976	119	57[b]	51[b]	91[b]	54[b]	68	49	107
1977	117[b]	56	52[b]	87	55[b]	66[b]	51	102[b]
1978	115	54[b]	53[b]	92	53[b]	66	51[b]	100
1979	109[b]	54	52[b]	94	55[b]	65	52	99
1980	103	49	50[b]	84	53[b]	62	49	94[b]
1981	99	47[b]	49[b]	79[b]	54[b]	58	49	90
1982	102	46	48[b]	74	53[b]	55[b]	49	90[b]
				Electricity				
1970	30.2	—	—	11.5	18.7[b]	13.2	10.3[b]	26.4
1971	31.2[b]	—	—	12.1[b]	21.9[b]	14.8[b]	10.5	27.4[b]
1972	35.1	9.4	—	13.3	22.5[b]	16.2	10.7[b]	28.7
1973	36.5	—	9.2[b]	14.0	23.2[b]	17.1[b]	11.2[b]	30.0
1974	36.1	—	9.7[b]	14.4	26.5[b]	16.1	10.1	28.8
1975	34.7[b]	10.5	10.1[b]	15.1	26.3[b]	17.1	10.7	30.0
1976	36.9	12.0[b]	10.8[b]	16.2[b]	26.5[b]	18.7	11.0	30.5
1977	38.8[b]	12.9	11.4[b]	17.0	28.0[b]	18.8[b]	11.6	30.7[b]
1978	33.5	14.5[b]	12.1[b]	17.9	27.6[b]	19.7	12.1[b]	30.6
1979	34.3[b]	15.7	12.5[b]	18.2	29.8[b]	19.8	12.5	30.4
1980	32.8	14.8	12.9[b]	18.1	30.0[b]	20.5	12.4	30.7[b]
1981	31.1	14.7[b]	13.5[b]	18.9[b]	32.4[b]	20.3	12.8	32.2
1982	33.0	15.4	14.0[b]	19.2	34.5[b]	21.3[b]	12.8	32.4[b]

[a]Source for employees: OECD Labour Force Statistics (Services includes major divisions 6–9 and 0 of the ISIC).

[b]Years of weather within 2 index points of heating degree-day normal. (French and Norwegian consumption data were weather-normalized by the source.) Annual fluctuations in cooling degree-days affect Canadian and U.S. electricity data.

Energy Consumption and Structure of the U.S. Residential Sector*

S. Meyers

Investigation of energy consumption by the U.S. residential sector has been part of the international research on residential energy use by the International Energy Studies Group for several years.[1] In FY 1985, we began to put together a comprehensive overview of both the trends in U.S. residential energy consumption in the 1970–1984 period and the chief structural factors shaping those trends. The basis of our approach is the belief that changes in energy consumption must be looked at in the context of changes in the structural setting for that consumption. Under structural setting we include information on households and housing, penetration of various end uses, the efficiency of equipment, and conservation measures undertaken by households.

ACCOMPLISHMENTS DURING FY 1985

We assembled and compared data from a variety of governmental and non-governmental sources during FY 1985. We worked with data tapes from the Residential Energy Consumption Surveys of the Energy Information Administration in order to gather additional detail. We have focused on trends with respect to the structural setting and energy consumption for the residential sector as a whole, for natural gas, for electricity, for oil, and for other fuels. The key findings from our sector overview are described below.

The Structural Setting

The physical setting for U.S. residential energy use has changed substantially since 1970. The number of households in the U.S. grew from around 64.5 million in 1970 to around 85.4 million in 1984. The combined result of additions and losses is that nearly 26% of the 1983 occupied housing stock was built after 1969.

The average number of persons per household fell from 3.06 in 1970 to 2.72 in 1983. (The median number fell from 2.74 to 2.32.) This means that there is lower demand per household for certain purposes (especially water heating and clothes washing/drying). The percentage of 1-person households rose from 18% in 1970 to 22% in 1983, while the percentage of 2-person households rose from 30% to 32%. Along with the increased participation of wives in the labor force, this has probably resulted in more homes being left empty (and at lower indoor winter temperature) today than in the early 1970s.

The average U.S. household is located in a slightly warmer climate today than in 1970. A lower percentage of households lived in single-family houses in 1983 (68.1%) than in 1970 (71.4%). This trend means that a lower percentage of homes have all walls and ceiling exposed to the weather.

The average home today is better insulated and has lower air infiltration than in 1970. This is due to both retrofitting of older homes and addition of more energy-conserving new homes. There has been an increase in the percentage of single-family homes with storm windows (from 45% to 52%) and in the percentage with attic/roof insulation (from 71% to 78%). Slight increase is evident in the percentage of homes with storm doors. There has been considerable retrofit activity on single-family houses and mobile homes, particularly in the 1979–81 period.

The introduction of new housing into the stock has resulted in improvement in the average thermal integrity of U.S. homes.[†] Data from surveys conducted by the National Association of Home Builders (NAHB) provide evidence of considerable increase since 1973 in the average level of ceiling and floor insulation and in the installation of double and triple window glazing in newly-constructed single-family houses. Data for low-rise multi-family housing, which accounts for 60–85% of all new multi-family housing, show little increase in insulation levels but some increase in the use of double and triple glazing since 1976. Measurements of air infiltration rates suggest that recently constructed homes have lower values than older homes.

The three main trends with respect to energy-using equipment that have affected the level of total energy consumption are the increased electrification of space heating, water heating, and cooking; growth in appliance holdings; and improved energy efficiency of new appliances. The penetration of electricity as main space heating fuel rose from 8% in 1970 to 19% in 1983. The penetration of air-conditioners grew substantially from 37% in 1970 to 59% in 1983.

The major appliances in the average U.S. home today are more energy-efficient than in 1970. New

*This work was supported by the Assistant Secretary for Conservation and Renewable Energy, Office of Building Energy Research and Development, Building and Community Systems Division of the U.S. Department of Energy under Contract No. DE-AC03-76SF00098.

[†]Homes built after 1969 accounted for 23% of the 1982 stock of single-family houses, 31% of the 1982 stock of multi-family units, and 73% of the 1982 stock of mobile homes, according to RECS.

refrigerators and freezers in 1984 were on average 60–70% more efficient than in 1972. Central air-conditioners were 30% more efficient, while room air conditioners were 25% more efficient. Gas space and water heaters were around 15% more efficient.

Survey data on energy-conserving behavior by U.S. households provide evidence of considerable change in heating practices. The most important change has been a major reduction in winter indoor temperatures. The percentage of households keeping the thermostat at 70°F or higher when someone was at home during the daytime fell from around 85% in 1973 to around 46% in 1981 (the first year RECS collected such information). The percentage of households keeping the thermostat at 70°F or higher during sleeping hours fell from around 51% in 1973 to around 22% in 1981. The RECS data suggest that daytime temperatures crept upward from 1981 to 1982. The percentage of households using small room heaters (electric and kerosene) and wood stoves increased between 1978 and 1982.

Energy Consumption

Primary energy consumption accounted for by the U.S. residential sector, adjusted to approximate normal weather, was 5% higher in 1984 than in 1973 (see Table 1). Delivered energy consumption, adjusted to approximate normal weather, was 9% lower in 1984 than in the peak year of 1973. Useful energy consumption (approximate combustion losses removed) was 5% lower in 1984 than in the peak year of 1973.

The time-series for primary energy shows a drop in 1974 followed by a period of increase up until 1979, and some decline through 1983, 1984 saw a substantial increase due largely to growth in electricity consumption. The time-series for delivered energy shows a larger drop in 1974 followed by several years of very modest increase, gradual decline in 1978–79 followed by a large decline in 1980, and modest decline in 1981–82, followed by a large drop in 1983; 1984 saw the first increase since

Table 1. U.S. residential energy consumption adjusted to approximate normal weather (quadrillion Btu).[a]

	Gas	Oil	LPG	Elec.	Coal	Wood	Total Delivered[b]	Elec. Losses	Total Primary[b]	Total Useful[c]
1970	4.98	2.35	0.34	1.59	0.15	0.40	9.61	3.86	13.47	6.81
1971	5.20	2.42	0.35	1.71	0.14	0.38	10.01	4.14	14.15	7.11
1972	5.19	2.41	0.36	1.86	0.11	0.38	10.12	4.47	14.59	7.24
1973	5.22	2.56	0.37	1.99	0.11	0.35	10.43	4.77	15.20	7.48
1974	5.07	2.30	0.38	2.02	0.11	0.37	10.07	4.93	15.00	7.26
1975	5.16	2.26	0.38	2.02	0.09	0.43	10.13	4.88	15.01	7.30
1976	5.12	2.30	0.38	2.12	0.08	0.48	10.24	5.11	15.35	7.41
1977	5.01	2.35	0.38	2.21	0.09	0.54	10.31	5.34	15.65	7.49
1978	4.90	2.18	0.38	2.28	0.09	0.62	10.14	5.58	15.72	7.40
1979	4.96	1.95	0.36	2.38	0.07	0.73	10.09	5.75	15.84	7.41
1980	4.82	1.58	0.33	2.43	0.06	0.86	9.65	5.91	15.56	7.14
1981	4.78	1.43	0.31	2.51	0.07	0.87	9.54	5.98	15.52	7.10
1982	4.75	1.35	0.30	2.52	0.08	0.94	9.47	6.05	15.51	7.06
1983	4.50	1.23	0.35	2.54	0.08	0.93	9.17	6.09	15.26	6.87
1984	4.70	1.25	0.35[d]	2.66	0.08[d]	0.93[d]	9.51	6.38[d]	15.89	7.13

[a]No adjustment has been made to LPG, coal, and wood due to the somewhat uncertain accuracy of the data.

[b]Includes 50% of wood consumption.

[c]Excludes estimated combustion losses: 35% of delivered energy for gas, oil, LPG, and coal, 65% of delivered energy for wood.

[d]Estimate.

1977. The time-series for useful energy shows a trend similar to that of delivered energy, except that the decline is slightly less after 1977. This decline is smaller because part of the decline in delivered energy is attributable to the increased penetration of electricity in the heating market.

Average energy consumption per household, counted as primary energy, adjusted to approximate normal weather, was 15% lower in 1984 than in 1973 (see Table 2). Counted as delivered energy, it was 26% lower in 1984 than in the peak year of 1973. Counted as useful energy, it was 23% lower in 1984 than in the peak year of 1973.

Table 2. U.S. residential energy consumption per household adjusted to approximate normal weather (million Btu).[a]

	Primary Energy	Delivered Energy	Useful Energy
1970	209	149	106
1971	215	152	108
1972	215	149	107
1973	219	150	108
1974	211	142	102
1975	208	140	101
1976	208	138	100
1977	208	137	100
1978	204	131	96
1979	202	129	94
1980	193	119	88
1981	188	116	86
1982	186	113	85
1983[b]	182	109	82
1984	186	111	83

Source: Table 1; Current Population Series (for household numbers).[c]

[a]No adjustment has been made to LPG, wood, and coal.

[b]The CPS number of households for 1983 seems low, given the known additions to the stock. This means that the values given for consumption per household may be slightly overstated.

[c]Published data on households from the CPS for the 1970–79 period reflect the undercounting of the 1970 census (estimated at about 1.1 million households). To correct for this, 1.1 million households have been added to the CPS estimate for each year in this period.

The time-series for primary energy shows a drop in 1974 followed by a period of stability up until 1978, gradual decline in 1978–79 followed by a large drop in 1980, and gradual decline in 1981–82 (see Table 2). 1984 saw the first increase since 1973. The time-series for delivered energy shows a drop in 1974 followed by several years of slight decline, declines in 1978–79 followed by a large decline in 1980, and steady decline in the 1981–83 period. Here too, 1984 saw the first increase since 1973. The time-series for useful energy shows a trend similar to that of delivered energy, except that the decline is slightly less after 1973.

The shares of the fuels in total residential delivered energy consumption have changed as follows (based on Table 1):

	1970	1977	1984
		(percent)	
Gas	52	49	49
Electricity	17	21	28
Oil	24	23	13
LPG	4	4	4
Wood	2	3	5

PLANNED ACTIVITIES FOR FY 1986

We will complete the full report of the project early in FY 1986. We will then produce a condensed version of the full report. We will do additional work on the U.S. residential sector as needed in the context of other International Energy Studies projects.

REFERENCES

1. Meyers, S. (1984), "Energy in American Homes: Changes and Prospects," *Energy,* Vol. 9, No. 6.

Residential Demand for Natural Gas: A Dynamic, Discrete-Continuous Choice Approach*

Oystein Olsen † *and Sarita Bartlett*

We are developing a model as a part of an ongoing project for analyzing gas demand for space heating in the *residential sector* in Western Europe. We are using a *discrete-continuous dynamic choice model.* A reasonable interpretation of this approach is that households' decisions on energy consumption are carried out in two steps. In the first step households have to choose between a limited (discrete) number of fuel systems or technologies. Given this technology choice, a (continuous) decision is made on how intensively the equipment should be utilized. In the short run households can change energy consumption only by varying the intensity in applying the installed equipment, while in a longer time perspective changes in prices and other variables can motivate consumers to convert to another fuel system. Formally, the technology choice involves comparisons of levels of indirect utility attached to the various fuel systems. Consistent with the theory of consumer behavior, we use equations describing gas use per household derived from the indirect utility functions by using *Roy's identity.*

ACCOMPLISHMENTS DURING FY 1985

The technology decision in the present model is a *dynamic, discrete choice.* This is an extension of the traditional (static) approach for analyzing behaviour involving limited dependent variables. In this dynamic version the choice probabilities are, at each point of time, dependent on the technology choice previously made. Assuming that the stochastic (unknown) terms influencing individuals' utility are independently distributed over fuel alternatives and develop over time according to an extremal process (assuming explicitly a structure of autocorrelation in the disturbance terms), time paths for "state probabilities" (frequencies for various technologies) and the transition between alternatives can be described as a Markov process. The transition probabilities are functions of the explanatory variables (fuel prices, conversion costs, income level and socio-economic variables) specified in the indirect utility functions and thus include parameters which are to be estimated. The expressions for the transition probabilities reveal that this dynamic structure may be interpreted as a modified Multi-Nomial Logit (MNL) model.

The dynamic version of the discrete/continuous choice model is particularly relevant when analyzing the demand for natural gas. In this market, significant conversions from other fuels have taken place, and a large part of the potential for future increase in gas consumption, especially in Europe, is believed to consist of conversions. It is therefore important that the model allows for transition from one technology to another, as opposed to the static MNL model, which is probably best suited for modeling investment decisions, or choices, that are irreversible.

We are preparing to estimate the dynamic discrete-continuous choice model from data on energy use in various European countries, differentiated by end use and type of fuel, the number of dwellings and the choice of fuel system and other "structural" and economic variables collected in a database by the International Energy Studies Group at Lawrence Berkeley Laboratory. The model thus applies directly information on how energy consumption is related to the dwelling stock, dwelling size etc. This distinguishes the present approach from most other studies of energy demand. In the first stage of the project, we are modeling only the energy use for *space heating* in the residential sector. This is, however, by far the most important end use, absorbing more than 75 percent of total energy consumption by households in the countries included in this study. Furthermore, it is probably close to realistic to simplify the analyzes and assume that the primary fuel choice is the technology decision for space heating and that this is done separately from choice of fuel system for hot water heating and cooking.

A significant characteristic of the present analysis is that we do not model the demand for housing services or dwellings. The dwelling stock is given exogenously by the model user in order to determine the development of total gas consumption.

PLANNED ACTIVITIES FOR 1986

During the coming year we plan to complete data preparation and model estimation and to report our results.

*This work was supported by the Norwegian Central Bureau of Statistics, Oslo, through the U.S. Department of Energy under Contract No. DE-AC03-76SF00098.

†Oystein Olsen of that Bureau is a visiting research fellow at the Lawrence Berkeley Laboratory.

Changes in the Patterns of Oil Use in Latin America

Andre Ghirardi, Peter Goering, and Andrea Ketoff

Despite efforts to develop alternative energy sources, all less developed countries (LDCs) in Latin America still rely heavily on petroleum products. On a worldwide basis, the share of petroleum use is higher in LDCs than in industrialized economies, and LDCs account for most of the net growth in world petroleum demand.

There are wide differences in the behavior of oil demand among LDCs. While the oil importers (or non-exporters) managed some degree of reduction in their oil intensities through substitution and conservation, the oil-exporters generally increased their petroleum intensity.

Although for different reasons, oil substitution and energy conservation are equally important to importers and exporters alike. The predicament of the oil importers is that their purchases of foreign energy sources cost much more now than ten years ago and, in most cases, consume most of their foreign exchange earnings, thus hindering their ability to pay their mounting foreign debt. In the exporting countries, oil invariably accounts for most of the government's income and is the most important source of foreign exchange. While the exporters want to sell as much oil as possible to finance development, their production is limited by world demand, as well as by the size of their reserves.

Among the exporters, Mexico and Venezuela find themselves in financial difficulties despite the richess of their oil reserves. The contraction in oil demand caused by the worldwide recession of the early 1980s severely cut down these countries' incomes. Many exporters are compensating by lowering their prices and producing more, adding much uncertainty to the immediate future of the world oil market.

After four years of nearly complete stagnation, many economies show signs of recovery. For LDCs, this recovery represents renewed opportunity for growth, increased exports, and possible alleviation of their debt burden.

The possibility of renewed economic growth raises new questions about oil demand. Much of the urban and industrial development taking place in LDCs will contribute to increase demand for petroleum products for industrial processes, urban transportation, and household use. In light of the substantial reduction in petroleum demand achieved by many LDCs during the last decade, two of the main questions on the future of the petroleum market in those countries are: What are the components of the reduction in oil use in LDCs, and where is the reduction likely to be reversed? We examine changes in the composition of economic output, energy conservation and fuel substitution to provide elements that will help answer these questions.

This analysis is based on a sectoral disaggregation of energy use. It associates the trends in energy demand with the observed changes in the levels of sectoral activity. We generally limit the scope of our work to the study of commercial fuels, but we do examine the use of wood for cooking in the residential sector and its potential replacement with LPG and other commercial energy forms.

This study analyzes Argentina, Brazil, Mexico and Venezuela. These countries account for more than 75 percent of the energy and oil use in Latin America and also produce more than 84 percent of the region's GDP.

ACCOMPLISHMENTS DURING FY 1985

During FY 1985, we attempted to quantify the "*oil backout*" in Latin America. We investigated its nature within the main economic sectors and the patterns of oil use among different groups of countries. The assessment of the changes in the Latin-American oil market is based on the sectoral analyses summarized below.

Sectoral Behavior of Petroleum Intensity

The present configuration of the structure of energy demand in Latin America shows signs of some of the adjustments described above and of the severe economic recession, which, despite some isolated improvements in performance, has not been totally overcome.

Between 1981 and 1983, the aggregate petroleum use in the region declined noticeably. Although that

*This work was supported by the Office of Policy, Planning and Analysis, the Assistant Secretary for Fossil Energy, Office of Planning and Environment, and the Assistant Secretary for International Affairs and Energy Emergencies, Office of International Energy Analysis, of the U.S. Department of Energy under Contract No. DE-AC03-76SF00098; by grants from the Exxon Corp. (and Esso Eastern), the Standard Oil Company of Ohio, Chevron Inc., and Statoil of Norway. The project also received assistance from Scallop Corp., NY.

coincides with a recessionary period, the reduction in petroleum use went beyond the effects of low economic activity. There was widespread substitution away from petroleum-based fuels, resulting in a reduction of petroleum intensity, some of which is likely to prevail, even in a healthy economy.

In order to assess the extent of this *oil backout* in the region, we calculated, for each country, how much petroleum would have been used in 1983 if the economies had been operating with the same petroleum intensity they had in 1978. We define *savings* as the difference between what would have been necessary and what was actually consumed.

The results show savings of 20 million TOE, which, while impressive, were unevenly distributed. Brazil and Argentina did in fact achieve overall reduction in the oil intensity of their economy. Venezuela's oil intensity increased, despite some effective substitution of natural gas for fuel oil in industry. The petroleum intensity in Mexico remained virtually unchanged. That is, while the non-exporting countries combined to save approximately 19 million TOE with respect to 1978 levels, the levels of savings in the exporting countries were marginal or nil.

Seventy-eight percent of the reduction in oil use was achieved in Brazil, primarily in transportation and industry. In transportation, Brazil curbed gasoline demand through use of alcohol fuels and, until recently, mandated conservation. In industry there was substitution for fuel oil, mostly with electricity and coal.

The savings achieved in Argentina were nearly evenly split between industry and power generation. The predominant trend in industry was the substitution of natural gas for fuel oil. In power generation both natural gas and hydroelectricity increased their share relative to petroleum fuels. There was virtually no reduction of oil intensity in the transportation sector in Argentina.

Industry

The process of industrialization in Latin America took place at high growth rates during the 1970s, until it was halted by the oil price increase of 1979. Nevertheless, before the recession of the late 1970s and early 1980s, a number of the regional developing economies brought many industrial activities up to the level of international competition. This process is mostly noticeable in the basic and more energy-intensive industries: iron and steel, aluminum, chemicals, cement, and paper.

Production of these items is being transferred to those developing countries that have adopted modern technologies and have the competitive advantage of lower labor costs (than the industrialized economies) and proximity to the raw materials. In most countries included in this study, the relative share of basic industries with respect to total GDP shows a pronounced increase during the 1970s.

The four Latin-American countries analyzed here produced a net petroleum savings of 10.3 million TOE in 1983, with respect to 1978 levels.† Those savings correspond to 37 percent of the combined industrial use of petroleum in those four countries in 1978.

Most of the savings were achieved in Brazil, which is the largest oil importer among LDCs. Smaller savings were achieved by Mexico and Argentina, while Venezuela increased its industrial oil intensity.

The nature of the changes in the patterns of oil use are closely related to the availability of resources in each country. In Argentina and Mexico, the reduction in use of petroleum products in industry is mostly caused by increased use of natural gas. Brazil, besides needing to import most of its petroleum, did not have large natural gas reserves (that has changed now) and managed to reduce oil use mostly through mandated conservation (by limiting the amount of fuel oil made available to each industry) and by subsidizing the use of domestic energy sources such as coal, charcoal, and, most of all, hydroelectricity. Despite a slight increase in the oil intensity of its industry since 1978, Venezuela also promoted large-scale substitution of natural gas for oil in industry.

In all four countries, there were successful efforts to reduce the oil intensity of the cement industry, through substitution with coal (Brazil) or natural gas (Argentina, Venezuela, Mexico). In many cases, there may be complete substitution of petroleum products for cement production. In the countries that are well endowed with natural gas, use of fuel oil in the cement industry could be entirely eliminated.

Large reductions in oil intensity can continue to be realized in the steel industry, as newer and more efficient plants (especially direct reduction) replace old ones. The sector is also increasing its electrification, as the direct-reduction furnaces are coupled with electric-arc steelmaking.

More than any other sector, industrial activity has shown contrasting features in its structure of

†These savings are measured at end-use levels. The primary savings would be higher, and would vary according to each country's efficiency of refining and use.

energy use. On one hand, the emergence of the basic industries tends to make the whole sector more energy intensive. On the other hand, higher oil prices have provided the necessary incentive for fuel substitution and conservation. The evidence collected suggests that future industrial output will be at least as energy intensive as it is now (based on the increasing share of the energy-intensive industries) but less intensive in petroleum products, due especially to substitution with natural gas. Other forms of substitution, of the kind found in Brazil, are neither capital intensive nor cost effective at current world oil prices. Therefore they are likely to be reversed in the presence of abundant and inexpensive fuel oil.

Transportation

While energy use in the industrial sector has shown a fairly high degree of adaptation to changes in energy prices, the transportation sector appears to be less flexible. Except in the Brazilian market, it is less amenable to fuel substitution.

There are clear differences in the nature of adjustment observed in the two major classes of vehicles: a) automobiles and b) trucks and buses.

The predominant feature in the automobile fleet in the countries studied is the nearly continuous increase of the number of cars per capita, a consequence of rising incomes and, in many cases, of the ample availability and declining real prices of domestically produced vehicles.

That trend is strong in all of Latin America, where the car fleet grew at an average yearly rate of 9.7% between 1970 and 1983, which is far in excess of the 2.5% growth rate of population during the same period. Although the growth in car ownership was clearly disrupted by the recent recession, there is no indication of saturation of the automobile market. On the contrary, in face of the high inflation rates prevailing most everywhere in the developing world, the purchase of durable goods (especially cars) is seen as one of the most available shelters against currency devaluation.

The ownership of cars is much higher in Latin America than in LDCs on other continents. At 50 cars per 1000, it is nearly four times higher than in Asian LDCs (13 per 1000). This is due to a higher level of urbanization, to the greater distance between urban centers, and to a development process designed to rely on motor vehicles.

Although the purchase and use of cars in the studied countries were somewhat dampened by the recent decline in real incomes, there is evidence that automobile use is concentrated in the higher income strata and, therefore, is only weakly affected by the country's overall economic situation.

The energy intensity of the car fleets in different countries covers a wide range. At the high end is Venezuela, where fuel consumption is around 4000 liters per car per year. At the low end there is Brazil, with a specific consumption below 1400 liters per car per year. The difference is largely due to the composition of the car fleet: in Venezuela, nearly half of the cars still have eight cylinders, consuming an average 5000 liters per year, while in Brazil the higher price of imported petroleum has, for many years, led to the production of smaller and more efficient vehicles. Also contributing to the lower gasoline intensity in Brazil is the large availability of alcohol made from biomass as an alternative to gasoline for automobiles.

Fuel use in freight transport differs from that of automobiles in that there is, to a greater extent, the possibility of substitution between gasoline and diesel oil. In many of the countries studied, changes in domestic pricing policies have caused an increased dieselization of the truck fleet. As the international price of oil increased during the 1970s, some governments chose to pass most of the price increase to gasoline, in order to allow for a more gradual increase in the price of diesel and avoid passing the full impact of higher energy prices to the costs of the products shipped by truck. That type of policy was followed in Argentina and Brazil. In the countries that adopted that kind of pricing policy, the diesel truck fleet has outgrown the gasoline units since 1978, and the use of diesel oil has increased with respect to that of gasoline.

That pattern of pricing and substitution, however, is found only among the non-exporters of petroleum. The oil-exporting countries have not, in many cases, brought the domestic price of fuels up to the opportunity cost of petroleum, therefore providing no incentive for conservation or substitution. The differences in pricing policy are clearly reflected in the structure of fuel use. In Argentina and Brazil, energy use in transportation is evenly divided between gasoline and diesel. By contrast, gasoline accounts for 60 percent of transportation energy use in Mexico and a high 80 percent in Venezuela, where most of the smaller trucks and buses run on gasoline.

Freight and passenger transport also differ in their response to overall economic conditions. Some of the countries studied showed a decline in the fuel intensity of the transportation sector during the recession years. That is mostly due to the low levels of industrial activity, which, in turn, reduce demand for freight transport.

The transportation sector is, by nature, so dependent on liquid fuels that pricing policies alone are unlikely to produce permanent declines in the aggregate petroleum intensity of the sector. Any rapid reduction in the intensity of use of gasoline and diesel would require, besides a coherent pricing policy, measures to encourage the production of smaller and more efficient cars, as well as better vehicle maintenance. In Brazil, much of the reduction in gasoline use was achieved through mandated conservation, by requiring that gasoline stations remain close on weekends. In the absence of such measures specifically aimed at improving vehicle efficiency, most countries will continue to consume at the levels presently observed.

Residential

In contrast with the savings sometimes observed in other sectors, the petroleum intensity of household energy use has increased in all the countries studied. This characteristic of residential energy use is due mostly to two factors: a) urban population growth and b) fuel substitution. Due to its direct dependence on the rate of (urban) population growth, energy use in the residential sector is largely independent from each country's overall economic performance. Typically, residential energy use in the countries studied has grown at an average yearly rate around 3 or 4 percent, even in the presence of economic recession.

Growth of urban population has far exceeded that of the total population. In Latin America, urban population increased at an average yearly rate of 4 percent between 1960 and 1984, while the rate for total population was 2.5 percent.

Urbanization is accompanied by a decline in the convenient availability of wood and its replacement with LPG for cooking, as well as the substitution of electricity for kerosene used for lighting. The effects of that process are clearly seen in the rising use of LPG and electricity per household.

This pattern of substitution is often accompanied by a decline in total energy use, most of it due to the higher efficiency of LPG with respect to wood. The actual amount of wood used in the residential sector is largely unknown. Better estimates are necessary in order to assess more accurately the process of deforestation, as well as to gauge the potential expansion of demand for LPG as the process of urbanization progresses. Few countries provide estimates of the amount of wood used in the residential sector; those estimates that exist are subject to significant imprecision because the use of wood takes place primarily in the rural areas, in a dispersed form, with no register of the amounts actually gathered. The existing estimates are of the *delivered* energy; that is, they do not take into account the efficiency of use, which is typically low, in the range of 5–15%.

Power Generation

The differences in energy use between exporters and non-exporters observed in the industrial and transportation sectors are not present in the power generation sector. In this case, the fuel use patterns are dictated primarily by two factors: the price of fuel oil and the availability and cost of alternative domestic fuels.

The higher petroleum prices enhanced the competitiveness of hydroelectricity and natural gas, both of which increased their participation in electricity generation for the region as a whole. Natural gas, which was gaining a higher share of the power-generation market even before the 1978–79 increase in the price of oil, expanded its market share at a faster rate, especially in Argentina and Venezuela. In Brazil, most of the discoveries of new gas reserves are quite recent, and that fuel has had no impact on electricity generation so far. The country continues to rely almost exclusively on hydroelectricity, as it has done for more that three decades.

Despite the more prominent role of non-petroleum fuels, there is evidence that the declining price of petroleum and the existence of surpluses of fuel oil (true for all four countries) are having an impact. Hydroelectric projects, which are highly capital intensive and require several years of construction work, have been delayed in Argentina and Venezuela. In fact, there has been an increase in the use of petroleum products for power generation in Venezuela since 1979, caused by the existence of surpluses of fuel oil and diesel.

Both coal and nuclear power should continue to play a marginal role in electricity generation in the region. There is no evidence of higher use of coal in power plants in any of the countries studied. Although the region possesses substantial deposits of high-grade coal, their exploration has been deferred, and a higher priority has been given to the development of petroleum and natural gas reserves. The emphasis given to nuclear programs in Brazil and Argentina in the 1970s has subsided. The prospect for participation of nuclear power in electricity generation has been weakened by the high cost of the technology, safety problems, and the availability of domestic alternatives.

PLANNED ACTIVITIES FOR FY 1986

During the next fiscal year, we expect to pursue the following activities.

Integrated Assessment: Following the completion of summary profiles for four countries (Argentina, Brazil, Mexico, and Venezuela), we will produce an integrated assessment of the structure of energy demand for the region, emphasizing the changes in end-use patterns caused by the price changes of 1978–79.

Study of Oil-Exporting Countries: In the last three years, government agencies in Mexico and Venezuela have shown a growing interest in conservation and substitution policies, especially in order to promote a more rational use of their petroleum resources. Whereas most of the oil-importing LDCs made policy adjustments in response to the price increase of 1978–79, the oil exporters are contemplating conservation policies in response to a financial crisis which started in 1982. Slack demand for oil and declining prices have reduced the inflow of foreign exchange in those two countries and have contributed to produce a massive external debt. We intend to conduct a study of the balance between the domestic petroleum market in Mexico and Venezuela and the volume of petroleum exports necessary to finance their economic development.

Colombia: We will expand the sample of countries studied by writing a country profile for Colombia. We will also add that country to our data base, collecting and organizing the information on energy demand and the structure of economic activity.

Outlook for Oil and Energy Demand in Asia*

Jayant A. Sathaye and Melchor Guererro

During the past two years, the International Energy Studies Group at the Lawrence Berkeley Laboratory has analyzed in detail energy demand patterns in 13 developing countries that account for most of the increase in world oil demand.† In 1983 the Asian countries in the study used 293.8 MTOE of commercial energy, of which 135.5 MTOE were oil products. But the intensity of oil use in these countries changed; if the 1978 patterns had held through 1983, oil use in East and South East Asia would have been 23.0 MTOE higher than it actually was, but in S. Asia, changing intensities led to much smaller oil savings (Figs. 1, 2, and 3). *For all these countries, oil use will increase in the future,* because of economic growth, even if oil intensities or shares continue to fall.

Because of many differences in the economies, the near term outlook for oil and energy demand is different for East and South East Asia than for South Asia. The long run outlook, however, is similar across Asia. The near term outlook calls for substitution and improved demand management in most of the countries in East and South East Asia. This means that the share of oil in energy demand in this region will decline, but the total demand for oil will increase, even if economies grow at a slower pace than the average annual growth rates of 5% to 10% in the 1970s. In the long run, oil demand may increase after the potential for substitution is exhausted.

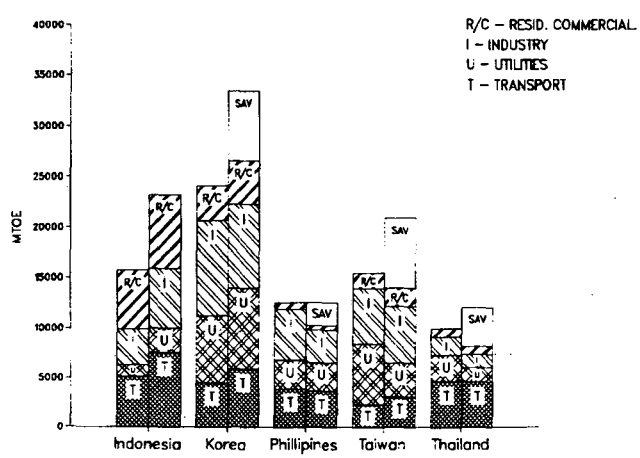

Figure 1. Oil backout in Asia, 1978 vs. 1982–83, by sector. (XBL 862-445)

*This work was supported by Contributions from Exxon Corporation (and Esso Eastern), the Standard Oil Company of Ohio, Chevron Inc., and Statoil of Norway through the U.S. Department of Energy under Contract No. DE-AC03-76SF00098. The project also received assistance from Scallop Corp., NY.

†These are Argentina, Brazil, Mexico and Venezuela in S. America, and Bangladesh, India, and Pakistan (S. Asia) Indonesia, Malaysia, Philippines, and Thailand (S.E. Asia), and Korea and Taiwan (E. Asia) in Asia.

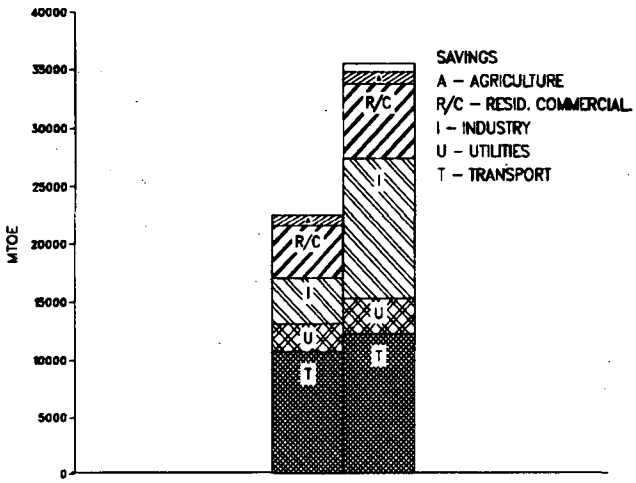

Figure 2. Total oil backout in India, 1978 vs. 1983, by sector. (XBL 862-444)

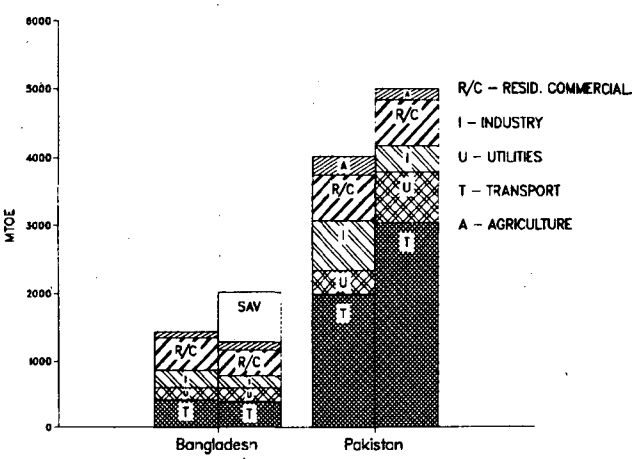

Figure 3. Total oil backout in Bangladesh and Pakistan, 1978 vs. 1983, by sector. (XBL 862-446)

ACCOMPLISHMENTS DURING FY 1985

In FY 85, we addressed the quantification of the oil backout in the Asian countries since 1978. We wrote country reports highlighting the nature of oil use in each of the four major sectors—industry, power, transport and households.[1-9] These reports describe the structural changes prompted by each country's desire to reduce the demand for oil. The changes varied between sectors from substitution, primarily in the industrial sector, to reduced, and perhaps more efficient, use of oil in the transport sector.

We set up a data base for each of the nine Asian countries. It contains information and data on both energy use and economic and structural activity for each sector, from as far back as 1970 to 1983 or 1984. The data base is in standard IBM PC format.

Background

Economic development in Asia has been rapid in the past two decades. Even after the first oil price increase, economic development did not slow and was accompanied by an increase in both the share and absolute level of oil use. After the second oil price increase, economic development slowed in most oil importing developing countries (OIDCs) in East Asia (gross domestic product declined in Korea in 1980–81). This was accompanied by a decline in the share of oil use, as most countries scrambled to find substitutes for oil and to manage energy consumption more effectively. The South Asian countries, however, were relatively insulated from this world recession and were further assisted by transfer payments from their own nationals working in the Middle East. Their economies continued to grow, as did their demand for oil and energy, at annual growth rates of around 5%. Thus the energy and economic development of South Asia and East or South East Asia differed after 1978.

In South Asia, oil is used for the most essential needs, yet there is still room for improved management of its use. This may not occur unless the price of middle distillates, the major petroleum products in use, is increased to provide an incentive for improved use. Nevertheless the population base is enormous. The outlook is, therefore, for annual growth in oil and energy consumption to exceed 5%. This translates into increases in oil demand in excess of 50,000 BPD annually. In the rest of Asia the growth rates may be lower, but the total volumes are as high or higher.

Industry

Industry in Asian countries accounts for over 50% of the modern or "commercial" energy use. Prior to the first oil price increase, much of industry in East and South East Asia was powered by oil, which was inexpensive, convenient to use, and easily available on the world market. Only in South Asia did the economies rely extensively on energy from sources other than oil. The result was that after 1978, the most oil-dependent countries in E. and S.E. Asia had to move rapidly away from oil. These countries reduced the intensity of oil and energy use through energy management, something at which

South Korea was particularly successful. Most S.E. and E. Asian countries also employed alternative domestic or imported fuels, such as coal, natural gas, and nuclear fuel, for power generation.

Korea, Taiwan, and the Philippines, however, do not have easy access to natural gas. Much of the substitution away from oil is limited to the use of coal in cement and steel plants. In Indonesia, Malaysia, Pakistan, Bangladesh and Thailand, on the other hand, domestic natural gas is likely to provide most of the future industrial energy use and even fuel homes. Most power plants in East and South East Asian countries are expected to continue the switch from oil to coal, natural gas, hydro, geothermal and nuclear energy. This substitution should be completed by 1987–88. The share of oil would then reach its lowest point unless the price of oil rises to make further improved management of its use more attractive. Barring this possibility, the share and absolute use should increase. If the oil price increases further, the oil share would decline, but absolute oil consumption still may increase.

Transport

The demand for fuels in the transport sector is driven by the need for personal transport, which is being met by increasing numbers of autos and motorcycles, and by expansion of bus and train services. The first two modes drive gasoline demand, while the latter two, combined with trucks, as well as rail freight, drive diesel demand. The ownership of cars is extremely low, e.g., around 1 to 2 per thousand persons in South Asia, and that of motorcycles is high in most of Asia compared to that in Latin America. These numbers will rise. The rapid increase in car ownership, brought about by liberalized granting of licenses for their manufacture in Korea and India, is a preliminary indication of this trend. In the short run, the growth in freight transport aided by the subsidized price of diesel compared to the international price and the high gasoline price would ensure that diesel demand continues to grow rapidly. This has already caused a mismatch between the refinery supply mix and the demand slate. In the long run, however, acquisition of cars and motorcycles will drive gasoline demand in these countries ahead of that for diesel.

Households

In households, demand for fuels is driven primarily by the need for cooking, lighting and comfort. In the lower income South Asian countries, cooking and lighting needs predominate. In South Asia and Indonesia, traditional fuels supply as much as 80% of the household energy needs. The level of use is sensitive to the price of kerosene, their petroleum substitute, which together with LPG forms the bulk of commercial fuels used for cooking. Lighting and comfort needs in cities are met through the use of electricity, and in rural areas through the use of kerosene for lighting and occasionally for refrigeration, but the overall level of electrification is very low. The demand for kerosene and LPG is likely to increase as more households move away from traditional fuels in these countries. The use of electricity is also spreading rapidly as households acquire appliances to meet new services, such as refrigeration and air-conditioning. In middle-income countries, such as Taiwan (and Singapore, which we have also examined), about a quarter of the homes had air-conditioners by 1983. Saturation of refrigerators was close to 90%. Korea and the larger cities of the other Asian countries are approaching these levels. As this development spreads to the remaining Asian countries, however, demand for all forms of energy for households, and a parallel increase for electric power and even some oil products or gas for the growing commercial sectors of these countries, will push energy and oil demand upwards even more.

Conclusion

The economies in Asia are younger than those in Latin America and hold potential for continued rapid economic growth in the coming decade. Meeting the energy needs of these economies will be a critical to maintaining healthy rates of economic development and the social stability that this development assures. The middle-income countries in the region are determined to diversify their mix of energy supplies and to institute measures to better manage their use of energy. Their demand for oil will still increase in the long run with economic growth.

The lower income countries in this region, along with Indonesia, have large populations, which are perennially short of electricity and kerosene for household use.[‡] If the rural consumer were to consume as much kerosene as his urban counterpart in India, 11.6 liters per capita in 1978–79, it would add 62,000 BPD to consumption of petroleum products. Similar figures would result from an increase in

[‡]Estimates for India suggest that economic growth *rates* would rise by as much as 30% in the short run, if adequate power were available for industry.

automobile use. Despite the low level of personal consumption, the large population base combined with the promise offered by recent rapid economic growth rates may lead to unsustainable consumption of oil in the near future. Thus, the low levels of use today in S. Asia and much of S.E. Asia, coupled to large populations, pose just as imposing a challenge on the world's energy markets as does the continued expansion of the more mature economies of N. Asia. Meeting this challenge is a major task for the energy industries and concerned governments in the Asia-Pacific Region.

PLANNED ACTIVITIES FOR FY 1986

During the past year, the work on this region focused on background energy-economy reports on each of the nine study countries and an analysis of the backout of oil during the period after 1978. The work this year will focus on examining the reasons for the expected upturn in the demand for oil, the magnitude and feasibility of this upturn, the ability of the economies to sustain the increasing demand for oil and the policies that might be adopted for its management. Additionally, the work will focus on studying new countries, including those in the Middle-East and Africa, whose patterns of demand and economic development are significantly different from those studied thus far.

REFERENCES

1. Sathaye, J. (1985), *Changes in Modern Energy Demand in Bangladesh, India and Pakistan: A Comparison*, LBL-21008.
2. Sathaye, J. and Meyers, S. (1985), "Transportation and Home Energy Use in Cities of Developing Countries," submitted to *The Energy Journal.*
3. Sathaye, J. and Meyers, S. (1985), "Changes in Oil Demand in Oil-Importing Developing Countries: The Case of the Philippines," accepted by *The Energy Journal.*
4. Sathaye, J. and Meyers, S. (1985), Energy Use in Cities of the Developing Countries, *Annual Review of Energy*, Annual Review, Inc., Palo Alto, CA.
5. Pignone, C. (1984), *Indonesia Country Report* (unpublished).
6. Schipper, L., Sathaye, J., and Meyers, S. (1984), *Energy Demand in The Developing Countries: Toward a Better Understanding.* Energy Research Group Manuscript Reports, ERG MR2e, International Development Research Center, Ottawa, Canada.
7. Sanchez, D. and Sathaye, J. (1984), *Energy Planning in the Republic of Liberia,* Report of Mission Sept. 1983 to DTCD, United Nations, New York.
8. IES Group Reports: Thailand, Sept. 1984.
9. IES Group Reports: Taiwan, Sept. 1984.

Changing Energy Use Patterns in Mexico*

Andrea N. Ketoff, Andre Ghirardi, and Peter Goering

The objective of this study is to assess the structure of energy demand in Mexico and its evolution during the last decade. This analysis is to be integrated with a larger comparative study of patterns of energy demand in 15 countries of Latin America and Asia.

The results of the assessment indicate that the efficiency of energy use in Mexico is rather low (in comparison with the other countries studied so far) and that the current climate of economic recession may provide the opportunity and the incentive for the definition of demand-oriented energy policies.

As in the other studies in this series, the following analysis uses a bottom-up approach, that is, characterizing the patterns of energy use according to changes in *structure* (e.g., number of cars, tons of steel) and *intensity* (i.e., unit consumption). This approach provides a better understanding of the factors that determine energy demand, highlighting the characteristics of specific sectors. It also provides the basis for inter-country comparisons of energy use indicators, thus helping the assessment of future energy demand for regions or groups of countries.

*This work was supported by the Assistant Secretary for International Affairs of the U.S. Department of Energy under Contract No. DE-AC03-76SF00098; by grants from the Exxon Corp., the Standard Oil Company of Ohio, Chevron Inc., Shell, USA, and Statoil of Norway. The project also received assistance from Scallop Corp., NY.

ACCOMPLISHMENTS DURING FY 1985

In FY 1985, this project compiled a consistent set of data on energy demand and sectoral structure and produced a summary assessment of the relationship between sectoral energy use and economic growth in Mexico during the last 10 years. The compilation of data, although not yet complete, has already produced a body of information that is unique in the uniformity with which it treats each of the main sectors of the economy and in the consistency with which it presents the hypothesis used to generate estimates of individual data points. There are no other sources containing that type of information that have been both validated by cross-checking sources and condensed into parallel time series.

Summary Assessment of Energy-Use Patterns

Oil accounts for more than 70% of Mexico's commercial energy use. The dependence on oil has been increasing gradually as petroleum resources have been the basis for the country's economic growth, both as a source of energy and, after 1977, as a source of foreign exchange.

The perception of an abundance of domestic fuel resources and the resulting low energy prices have served as a disincentive to the exploration of non-petroleum energy sources as well as to the pursuit of higher efficiency in the use of energy. As a result, there has been a decline in the efficiency of energy use, most noticeably in the period of growth ranging from the mid-1970s until 1981.

The drop in international oil prices and in OECD oil demand during the 1982 recession hit Mexico particularly hard, since 75% of government revenues were generated by oil exports, primarily to the United States. The current economic reality of oil revenues drained by the debt service payments and of continuing recession is motivating a growing interest in energy conservation and in a demand-oriented energy policy.

The discovery of vast oil reserves in the mid-seventies in the Bay of Campeche brought about an upturn in the Mexican economy. Within a period of five years, proven petroleum reserves increased from 6 to 72 billion barrels, production tripled, and oil exports increased ten-fold, reaching 600 million barrels per year and replacing agriculture as the country's main source of foreign exchange.[1]

In the presence of these changes, aggregate energy demand indicators showed a steady growth between 1970 and 1981.

Some of the main characteristics of that growth period were:

- Energy use per capita increased 80% between 1970 and 1982 and leveled off in the two following years.
- The use of *energy* relative to gross domestic product increased 36% in the same period.
- The use of *oil* relative to GDP increased 49%.

Despite the increase in the overall energy-intensity of the economy in recent years, there is no sign of that the increase was directly related to the increase in petroleum revenues, contrarily to what we observed in Venezuela. Also in contrast to most other major Latin-American economies, there is no evidence of substantial fuel substitution.

In order to understand the implications of the trends identified above, we must look at the underlying structure of energy use in the country. Table 1 shows a disaggregation of energy use in 1983, by fuels and by major end-use sectors.

Industrial Energy Use

Industrial energy use is dominated by three sectors: Iron & Steel (27%), Chemicals (11%), and Cement (9%). Combined with three other sectors—Sugar, Paper & Pulp, and Glass, these industries account for 61% of total commercial energy demand of the sector in 1981. Bagasse, used exclusively in the sugar industry, represents another 7% of total industrial energy use.

The energy and petroleum intensities of the industrial sector varied only slightly (less than 10%) between 1970 and 1981. There was, however, a remarkable drop in natural gas intensity of the sector (−20% since 1970), in contrast with the sharp increase registered in other Latin-American countries, most noticeably Argentina and Venezuela. Although many industries (e.g., cement production) are equipped with dual-firing capability, the price difference still favors the use of fuel oil over natural gas.

The level of efficiency of industrial processes is uneven among subsectors, influenced by the quality of the imported technology as well as by the age of the production plants. The energy-intensity of cement production is comparable with the levels observed in OECD countries, but the same is not true for the sugar or the paper industry, two of the largest energy users in the sector. Comparisons of specific consumption (energy/tonne) of the principal energy-intensive processes with those of other developing as well as industrialized countries suggest that, although Mexico does not have the worst per-

Table 1. MEXICO—Fuel distribution by sectors, 1983.

	Industry	Non-Energy	Res.-Comm.	Agricult.	Transport.	TOTAL
OIL, 10^{12} kcal	61.15	48.84	68.47	1.62	262.67	442.75
—, % of sec.	25.6	42.3	41.3	29.8	99.8	56.2
—, % of fuel	(13.8)	(11.0)	(15.5)	(0.4)	(59.3)	(100)
NAT. GAS, 10^{12} kcal	93.51	66.53	6.25	—	—	166.29
—, % of sec.	39.2	57.7	3.8			21.1
—, % of fuel	(56.2)	(40.0)	(3.8)			(100)
COAL, 10^{12} kcal	38.19	—	—	—	—	38.19
—, % of sec.	16.0					4.8
—, % of fuel	(100)					(100)
WOOD,BAGASSE, 10^{12} kcal	15.47	—	72.16	—	—	87.63
—, % of sec.	6.5		43.6			11.1
—, % of fuel	(17.7)		(82.3)			(100)
ELECTRICITY, 10^{12} kcal	30.42	—	18.75	3.82	0.45	53.44
—, % of sec.	12.7		11.3	70.2	0.2	6.8
—, % of fuel	(56.9)		(35.1)	(7.2)	(0.8)	(100)
TOTAL, 10^{12} kcal	238.74	115.37	165.63	5.44	263.12	788.30
—, % of sec.	100	100	100	100	100	100
—, % of fuel	(30.3)	(14.6)	(21.0)	(0.7)	(33.4)	(100)

Source: CFE.

formance in energy use per unit of output, much can be done to improve the energy productivity.

The steel industry is the most energy-intensive sector in the Mexican industry. In 1981, steel accounted for over 27% of industrial energy use. Steel production has grown strongly in the last 15 years, going from 3.9 million tons in 1970 to a maximum of 7.7 million tons in 1981. The period of recession that started in 1982 resulted in lower production in 1982 and 1983. By 1984 there were indications of a possible recovery, as output increased to 7.5 million tons in 1984.

The chemical industry, led by basic organic chemicals, experienced high growth throughout the 1970s and early 1980s, with output increasing at an yearly average of 15 percent. Availability of cheap natural gas as a feedstock has pushed the petrochemical subsector to even higher growth rates. In 1981, natural gas accounted for 57% of the purchased energy used in the chemical industry and oil another 28%. Purchased electricity was about 8% and cogeneration another 5%. Since most of the chemical industry plant is fairly new, energy intensities in it are closer to world standards than they are in other sectors. A high percentage of the energy used in the industry is for process heat, suggesting the possibility of efficiency improvements through cogeneration.

Cement output grew steadily from the 1950s until the current recessionary period, while the petroleum intensity of this sector declined over 20% since 1968 due to modernization. At the same time electricity use has increased, but electrical energy intensity is still only 10% of petroleum intensity. The trend of petroleum substitution by electricity is likely to continue in the near future. Growth in future cement production, as with steel production, will be closely linked with economic development.

Transportation

Transportation uses more energy than any other sector (40% of total). That share is still increasing, driven by the growth of the vehicle fleet, which is driven, in turn, by growth in car ownership per capita. This indicator grew 9% per year from 1970 to 1981 but stagnated in the following years, as a consequence of declining personal incomes.

Gasoline consumption per car (~3000 liters/car) is among the highest in Latin America. Although information about the last 3 years is still sketchy, there is indication that as incomes declined and gasoline prices reached international levels, the use of private cars, and gasoline use per car, was reduced markedly. The price increase also resulted in an

unexpected growth in the illegal use of LPG in cars. LPG prices are kept artificially low, since that fuel is meant primarily for cooking.

Gasoline is used in almost 100% of private cars (no diesel cars are sold) and in part of the truck and bus fleet, despite the considerable price difference, particularly until 1981. There is evidence that some substitution of diesel for gasoline occurred in the 1970s. However, the share of gasoline in the total energy supply of the sector is still in excess of 60 percent, compared to 50 percent in Argentina and Brasil.

The Residential Sector

Energy demand in the residential sector shows large growth potential, due to the high rates of growth of population and urbanization in Mexico. That is particularly true for cooking fuels, since they represent the largest share of household energy use. While electrification is relatively high (more than 80% of households), one-third of Mexican families still rely on wood as the main fuel for cooking.

Residential electricity use per capita is currently 180 kWh/year (23 percent lower than in Brasil), although it increased almost 60% between 1970 and 1983. About two-thirds of the population lives in areas where no heating or cooling is needed. Air conditioning is diffused principally in the dry Northern regions, where subsidized electricity prices during the summer months (since 1973) have led to a 230% increase in electricity demand per customer between 1973 and 1980.[2]

The increasing levels of appliance ownership will be one of the main forces driving electricity demand. Refrigerators are the most rapidly diffusing energy-using devices in Mexican homes, although their saturation remained under 30% in 1984. The existence of a large market for electrical appliances also presents an opportunity for the effective implementation of conservation policies, possibly through the establishment of standards for appliance efficiency.

Wherever gas is used for cooking, LPG is generally the fuel of choice. The use of natural gas remains limited to the few urban areas served by the gas network, and its widespread distribution is restrained by the fact that the housing stock consists mainly of one or two story homes, which increases the cost of distribution networks.

The Petroleum Industry

Although for purposes of comparison with other countries this study is aimed primarily at final energy demand, it should be noted that the Mexican petroleum industry presents a better opportunity for energy conservation than any other sector of the local economy. There is evidence that the overall efficiency of the oil industry has been declining in recent years, reaching levels much below those of most oil-exporting countries.[3] The probable causes are to be found in poor integration and maintenance of the refining system, as well as the internal pricing structure within the oil industry: products are transferred at no cost within Pemex, and accurate accounting has been established only in recent years.

Pemex has launched a plan for energy saving, particularly focused on natural gas. This calls for better combustion control and maintenance. In 1984, the first phase of this plan—including reductions in flared gas in fields—has produced savings estimated at 1.2 MTOE (Million Tons of Oil Equivalent).[4]

Electricity Generation

Electricity generation increased nearly threefold between 1970 and 1983. Annual growth continued at 8–10 per cent per year until 1983, when it was reduced to 2%.

Thermal generating capacity has grown faster than hydroelectric generation during the last decade. The contribution of hydroelectric plants, which provided more than half of total electricity generated in 1971, dropped to 37% by 1982. Unlike all other Latin-American countries, hydroelectric generation in Mexico is not expected to grow considerably, due to the high capital costs and the limited number of unexploited sites for large dams.

Despite the existence of dual-firing capability developed to guarantee the use of the natural gas associated with oil deposits, the natural gas share of thermal generation dropped from 40 to 18 percent between 1970 and 1984. That appears to have been caused mostly by the difference in price and the existence of surpluses of fuel oil.[4,5]

Coal and geothermal sites have been developed as alternatives in recent years, although they have not resulted in major changes in the overall structure of electricity generation. Geothermal capacity is expected to reach 600 MW by 1990, coal 1200 MW. Construction of more than one of the many nuclear power plants planned in the late seventies nows appears highly unlikely because of the increasing costs and the difficulties in procuring foreign exchange.

PLANNED ACTIVITIES FOR FY 1986

During the next fiscal year, we expect to examine the opportunities for improving energy efficiency in

the Mexican Public Sector, in collaboration with the Mexican Department of Energy (SEMIP). This sector is important to Mexico's ability to make better use of its resources and to have oil available for export. We will analyze the patterns of energy use in the state-owned industries—the energy sector (oil and electricity), the public transportation system, and the government buildings. This study will help identify the areas and conditions for cooperation in the areas of technology transfer and policy formulation.

REFERENCES AND BIBLIOGRAPHY

1. Petroleos Mexicanos (1984), *Anuario Estadistico 1983,* Mexico.
2. Comision Federal de Electricidad (1982), *Evolucion de las Tarifas de Energia Electrica en Mexico, 1962–1980,* Mexico.
3. Petroleos Mexicanos, 1980 to 1984, *Memoria de Labores.* Mexico.
4. Petroleos Mexicanos (1985), *Evolucion de la offerta y demanda de Energia en 1984,* Mexico.
5. Comision Federal de Electricidad (1983), *Estadisticas 1965–1982, Mexico.*

Schipper, L., Sathaye, J., and Meyers, S. (1984), "Energy Demand in The Developing Countries: Toward a Better Understanding," Energy Research Group Manuscript Reports, ERG MR2e, The Energy Research Group, P.O. Box 8500, Ottawa K1G 3H9, Canada.

Ghirardi, A. (1985) "Trends of Energy Use in Brasil: Is Self-Sufficiency in Sight?" *Journal of Energy and Development 10* (173), p. 2.

Ghirardi, A. and Ketoff, A. (1985), "The Structure of Energy Demand in Argentina," submitted to *Energy Policy.*

Poder Ejecutivo Federal (1984), *Programa Nacional de Energeticos 1984–1988,* Mexico.

Schutz, F. (1984), *Uso Efficiente de la Energia en Mexico,* IIE, Mexico.

Petroleos Mexicanos, CEE (1985), *Perfiles Economicos Internacionales: Consumo de Energia en la Industria Siderurgica, Mexico.*

Residential Energy Use in LDCs: Guidelines for the Analysis of Low-Income African Countries*

Gianfranco Rizzo,† Andrea Ketoff, and Andre Ghirardi

There is much concern today about the impact of higher energy costs on the economies of the oil-importing Less Developed Countries (LDCs), particularly the low-income countries whose development is further restrained by the increasing burden of providing energy resources.

In these countries, energy demand is typically dominated by the residential sector, which sometimes accounts for as much as seventy percent of national energy use. Most of the demand in this sector is met with non-commercial fuels (fuelwood and charcoal), but as urbanization increases and lifestyle improves these traditional fuels are replaced by commercial sources, namely kerosene, LPG, and electricity.

ACCOMPLISHMENTS DURING FY 1985

In order to illustrate the patterns of energy use and fuel substitution in Africa, we have studied a sample of eleven countries, selected according to the level of economic development and the availability of information.

*This work was supported by the Italian National Research Council (CNR) under Grant No. 215.17/07 through the U.S. Department of Energy under Contract No. DE-AC03-76SF00098.

†Gianfranco Rizzo—from IEREN/CNR (Istituto per l'Edilizia ed il Risparmio Energetico), Palermo, Italy—is a Visiting Researcher Fellow at the Lawrence Berkeley Laboratory.

In most LDCs, the lack of reliable data is a severe limitation to the scope and accuracy of analyses of residential energy markets and to the adoption of demand-oriented policies. While there is usually some record of transactions involving commercial fuels, the use of non-commercial fuels is often gauged by means of broad estimations of the various forms of biomass collected by each household. More precise estimates of the use of these non-commercial fuels can only be generated by local surveys of the fuel-gathering activities.

There are few complete surveys of household energy use in African countries, but a number of small-scale studies have started to produce some information on the profile of energy use in that sector. In their review of studies on West African countries, Kahane and Lwakabamba address some of the problems created by the diversity of these studies, and the difficulties to achieve consistent international comparisons that will help understanding the determinants of residential energy demand.[1]

For this study, we selected countries for which some sectoral data had been already collected or estimated in previous studies.[2–4] These are: Angola, Botswana, Kenya, Lesotho, Malawi, Mozambique, Sierra Leone, Swaziland, Tanzania, Zambia, and Zimbabwe. All these countries are in South and East Africa, except for Sierra Leone, which was selected here because of the extensive data-gathering performed there.

Three main features emerge from the analysis of residential energy demand in these countries and appear to be typical of most low-income LDCs: the high share of residential energy use; the small (but growing) use of commercial fuels; and the predominance of cooking as the most energy-intensive activity.

The high share of residential energy use, over the total national consumption, is evident in all cases. If we include non-commercial energy sources in the accounting, household primary energy use is over 50% of total national consumption in all but one (Swaziland) of the countries studied, reaching 75% in Mozambique, Lesotho, and Sierra Leone (Table 1). Unlike the LDCs in other regions of the world (e.g., Latin America), there is relatively little fuel use in industry and transportation. In most of the countries studied, the level of industrialization is low, and the use of trucks, buses and automobiles is limited by the poor infrastructure of road transport.

Clearly, the residential sector should be the focus of demand-oriented policies, not only because of the threat of deforestation and biomass-fuel shortage, but also because that sector will continue to be the main determinant of fuel consumption in the immediate future.[5,6]

The second characteristic, the high use of non-commercial fuels, is closely linked with the demographic concentration in rural areas. Whereas the use of oil, gas and electricity is growing steadily in urban areas, three-quarters (or more) of the population lives in rural areas, where energy is supplied almost exclusively by fuelwood and agricultural residues. Nowhere in the region studied is the use of commercial energy more than 20 percent of the total, with the average being around 10 percent (Table 1).

Even in urban dwellings, the share of non-commercial fuels varies between 60 and 90 per cent, except for Lesotho and Swaziland, where coal is widely used for heating, covering as much as 50% of urban demand.

Although the use of kerosene and electricity has become more frequent with increasing urbanization, wood-burning backup systems are still kept in use. A typical example of that pattern of fuel use is found in Sierra Leone, where fuelwood remains as a secondary energy source in all urban households that use charcoal or kerosene as their principal cooking fuel (50% of the dwellings).[2]

A recent survey in that country shows that the use of fuelwood for cooking is entirely discontinued only in households that cook with LPG. The survey results also show a clear pattern of fuel substitution as a function of household income. As incomes grow, so does the use of LPG and electricity, replacing fuelwood, charcoal, and kerosene. If the above findings are representative of the typical patterns of fuel substitution, they would have important policy implications. They show that only LPG provides complete displacement of fuelwood for cooking, that is, the problem of deforestation by wood gathering would not be eliminated by promoting higher use of kerosene (or charcoal).

Finally, there is the issue of the predominance of cooking as the most fuel-consuming task in households. Its share of total use in the countries studied ranges from 20 to 90 percent, with the higher values generally observed in rural areas (Table 1).

It should be kept in mind, however, that the label "cooking" really encompasses a number of functions in African households, including water heating and space heating, when needed.[7] The most widely used form of cooking, in both rural and urban areas, is the open-fire burning of fuelwood, although charcoal and kerosene are *also* used in higher income urban households (electric hot water supplements these fuels for water heating in the high income urban households).

Table 1. Household energy use in African countries.

	Angola 1980	Botswana 1980	Kenya 1980	Lesotho 1980	Malawi 1980	Mozambique 1980	SierraLeone 1982	Swaziland 1980	Tanzania 1980	Zambia 1980	Zimbabwe 1980
Population, 10^6	7.10	1.00	15.90	1.30	6.10	12.10	3.35	0.63	18.70	5.80	7.40
Urban pop, %	21.1	13.4	...	9.4	7.3	7.8	25.0	14.7	7.3	42.0	22.7
GNP/cap (US Doll.)[a]	470	910	420	420	230	230	280[b]	680	280	560	630
Total E. Use, PJ	105	22	332	24	165	282	46	24	439	150	244
Urban E. Use, %	11.8	9.1	10.8	11.1	7.3	4.2	22.6	10.0	4.5	20.5	8.9
Non-Comm.Fuels, %	74.3	54.6	71.7	75.0	91.0	88.0	78.8	62.5	90.4	57.4	51.3
Resid. E. Use, PJ	59	11	194	18	68	215	32	5	285	73	112
(Resid./Tot., %)	(56.2)	(50.0)	(58.4)	(75.0)	(41.2)	(76.2)	(68.1)	(20.8)	(64.9)	(48.6)	(45.9)
Comm.Fuels, %	3.4	9.1	5.1	11.1	0.7	1.4	4.2	20.0	1.4	4.1	4.4
— Oil, %	*2.6*	*4.2*	*4.0*	*4.9*	*0.4*	*1.0*	*3.5*	*4.8*	*1.1*	*1.0*	*1.0*
— Elec, %	*0.8*	*2.6*	*1.1*	*0.4*	*0.3*	*0.4*	*0.7*	*3.6*	*0.3*	*3.1*	*3.0*
— Coal, %	—	*2.3*	—	*5.8*	—	—	—	*11.6*	—	—	*0.4*
Non-Comm. Fuels, %	96.6	90.9	94.9	88.9	99.3	98.6	95.8	80.0	98.6	95.9	96.6
— Fuelwood, %	*84.2*	*90.1*	*79.0*	*54.5*	*92.6*	*89.8*	*89.1*	*75.9*	*92.8*	*76.9*	*95.0*
— Charcoal, %	*8.5*	—	*11.3*	—	*2.5*	*0.5*	*6.5*	—	*3.0*	*17.4*	—
— Other Biomass, %	*3.9*	*0.8*	*4.6*	*34.4*	*4.2*	*8.3*	*0.2*	*4.1*	*2.8*	*1.6*	*0.6*
Comm. Urban, %	21.4	34.8	26.8	83.4	9.7	15.3	11.7	89.0	20.8	12.6	39.5
— Oil, %	*14.6*	*10.6*	*17.1*	*23.9*	*4.6*	*10.0*	*9.1*	*20.5*	*14.3*	*3.2*	*5.2*
— Elec, %	*6.8*	*12.1*	*9.7*	*4.9*	*5.1*	*5.3*	*2.6*	*24.6*	*6.5*	*9.4*	*33.0*
— Coal, %	—	*12.1*	—	*54.6*	—	—	—	*43.9*	—	—	*1.3*
Non-Comm. Urban, %	78.6	65.2	73.2	16.6	90.3	84.7	88.3	11.0	79.2	87.4	60.5
— Fuelwood, %	—	*65.2*	*14.1*	*16.6*	*48.4*	*75.8*	*78.3*	*11.0*	*43.0*	*16.7*	*60.5*
— Charcoal, %	*78.6*	—	*59.1*	—	*41.9*	*8.9*	*10.0*	—	*36.2*	*70.7*	—
Comm in Rural, %	1.2	0.6	2.4	5.2	0.1	0.6	2.0	5.4	0.5	1.7	1.0
Urban Resid. E. Use:											
— Cooking+HW, %	88.5	54.5	78.0	18.2	41.3	53.8	79.6	19.2	38.3	70.5	30.4
— Lighting, %	7.7	10.6	10.3	4.9	4.8	6.8	9.2	20.5	11.8	3.9	6.1
— Heating and other, %	3.8	34.9	11.7	76.9	53.9	39.4	11.2	60.3	49.9	25.6	63.5

[a] From World Bank.

[b] 1980 figure.

Due to their prevalence, woodstoves are the primary target of any policy aimed at improving energy use efficiency, as demonstrated by several pilot projects and programs initiated by local and international agencies.

PLANNED ACTIVITIES FOR FY 1986

Comprehensive surveys of appliance saturation and efficiency are usually an impossible task for poor countries with dispersed population. With such quality of data, many of the available modeling tools cannot be applied effectively for policy purposes. Using international comparisons we were able to characterize the factors that are common to the countries sampled, although the detail of information and its reliability is often uneven.

With new support from DOE for 1986, we plan to expand our study to other African countries and to extend our analysis to the other sectors. The literature surveyed allows preliminary estimation of the fuel distribution by principal sectors. In order to perform comprehensive analyses and scenarios, as well as to carry out effective energy planning, statistics on energy use need to be more disaggregated and integrated with economic and price data.

We will carry out this integration in cooperation with other international research institutions (including the Italian National Research Council) and with the direct collaboration of local expert and government authorities.

REFERENCES

1. A. Kahane and S. Lwakabamba (1985), "Energy in West Africa: A Literature Survey," International Energy Study Group Report to Energy Research Group, International Development Research Centre (IDRC), Ottawa, Canada, March 1985.

2. Davidson, O.R. (1985), "Energy Use Patterns in Sierra Leone," Final report to the International Development Research Centre (IDRC), Ottawa, Canada, April 1985.
3. Schipper, L., *et al.* (1982), "Energy Conversion in Kenya's Modern Sector," discussion paper from Center for Energy Policy Research Resources for the Future, Washington, DC, May 1982.
4. Energy for Development (1983), Proceedings of the Regional Workshop in Eastern and Southern Africa, Volume II, Arusha, Tanzania, April 4–13, 1983.
5. Leach, G., Jarass, L., Hoffmann, L., Obermair, G. (1985), "Energy and Development: A Comparison of 13 Countries," Final report sponsored by the Commission of the European Communities, Directorate General for Energy, March 1985.
6. Wood, Energy and Household, Perspectives on Rural Kenya (1984), Edited by Barnes, C., Ensminger, J., O'Keefe, P., Report No. 6 of the series "Energy, Environment and Development in Africa," "The Beijer Institute" and "The Scandinavian Institute of African Studies.
7. Baldwin, S., Geller, H., Dutt, G., Ravindranath, N.H. (1985), "Improved Woodburning Cookstoves: Signs of Success," The Center for Energy and Environmental Studies, PU/CEES Report No. 184 Princeton University, July 1985.

Transport Energy Use in Cities of the Less Developed Countries*

Jayant Sathaye and Stephen Meyers

The International Energy Studies Group has been studying the use of energy in the urban areas of Less Developed Countries (LDCs) countries for the last several years. The changes in energy-using capital stock (dwellings, vehicles, appliances) are similar in urban areas of most LDCs. The more advanced LDCs thus provide a clue to the future development of cities in less advanced countries. Since the use of modern fuels is concentrated in the urban area, changes in structure can be used as a guide to future demand for modern fuels in the LDCs.

In FY 1984, we reviewed the use of energy in homes and for transportation in the cities of LDCs. In FY 1985 we expanded the review of transportation energy use to look in more detail at the transportation sector and the potential for growth in this sector. Most of the information we gathered concerns transportation of people rather than goods.

*This work was supported in part by the International Development Research Centre, Ottawa, Canada; in part by the Office of Policy, Planning and Analysis, U.S. Department of Energy, under Contract No. DE-AC03-76SF00098; and in part by grants from the Exxon Corporation, Chevron, CONOCO, Shell Oil Co., and Statoil of Norway.

ACCOMPLISHMENTS DURING FY 1985

A number of transport options (modes) are in use in cities of LDCs. Walking, bicycles, and cycle rickshaws are common forms of transportation. In China, for example, government policy and low income combine to restrict transportation mainly to walking and bicycles (Table 1).[1]

Mass transport is popular and exists in many forms. Along with large buses, smaller private buses and shared taxis are common. The most common form of private transportation is the motorcycle. Ownership of motorcycles has grown rapidly in many places (Table 2).

Members of higher-income households are more likely to own or have access to, and travel by, car. In Malaysia, 40% of the surveyed households reported the car as their mode of travel to work.[2] Among the poor households, very few people used a car, but in the wealthiest group, over 90% did so.

The most distinctive feature of the transportation sector in LDC cities is the rapid growth in use of automobiles. Automobile ownership in develop-

Table 1. Frequency of trips (percent).

	Walking	Bus/Trolley Car	Bicycle	Other
Shanghai	43.2	38.5	13.2	7.8
Tianjin	42.6	10.3	44.5	2.6
Xuzhou	46.5	6.2	44.6	2.7

Source: Yushi and Guangrong (1985).

Table 2. Motor vehicle registration per thousand persons.

	1970		1982	
	Cars	M/Cycles	Cars	M/Cycles
USA	436.4	13.8	540.9	26.0
Argentina	70.6	—	114.9	—
Venezuela	56.1	—	97.1	
Brazil	28.7	—	64.9	—
Taiwan	3.4	47.7	32.4	278.7
Korea	1.9	—	7.8	10.4
India	1.3	1.1	1.5	3.5

Source: Country specific transportation and population statistics.

Table 3. Urban car ownership.

	Population thousands (1970)	Income per capita (1970 US$)	Number of autos per 1000 Population (1970)
Seoul	5536	440	6.3
Calcutta	7402	270	13.0
Bombay	5792	390	13.5
Jakarta	4312	325	18.0
Bangkok	3090	525	49.7
Sao Paulo	8400	785	62.3
Beunos Aires	8400	1800	73.9
Mexico City	8600	1275	78.3
London	10547	2550	222.0

Source: World Bank (1975).

ing countries is much lower than in developed countries, but has grown rapidly since 1970 (Table 2).

Rapid growth in ownership of cars and motorcycles can occur if economic conditions permit. Per capita ownership of cars in Taiwan increased by almost ten-fold during a period of rapid economic growth from 1970 to 1982. In India, the three-fold increase in per capita ownership of motorcycles was primarily due to the government policy of liberalizing the granting of licenses for the manufacture of motorcycles.

Increase in private rather than business car ownership has driven the rapid increase in ownership of cars, though the use of business cars remains common. The share of private cars in Korea and Taiwan increased from 53 and 58 percent in 1970 to 76 and 88 percent, respectively, in 1982.

The level of automobile ownership depends heavily on income (Table 3). Ownership increases with income, unless restrained by government policy to limit imports of automobiles, as in Seoul, Bombay and Calcutta, or by heavy tax on imported cars, as in Jakarta.[3] It is much higher in Latin America than in Asia, even at the same average income level. This may be due in part to government policies limiting or heavily taxing the import of cars. The higher population density in Asia may also encourage the use of motorcycles and public transport. Additionally, the fact that Latin American countries have enjoyed higher incomes for a relatively longer time period may contribute to their higher level of car ownership. Malaysia has had a low population density, a good network of roads, a relatively high per capita income for a long time period, and a relatively unrestricted government policy, all of which have stimulated private vehicle ownership. As a result, car ownership in Malaysia at 74 cars per thousand persons (1982) was very close to that in Latin America.

Within a country, energy use in personal transportation varies enormously among income groups. This is because of the large increase in energy use that comes with automobile ownership. A 1974 survey of household energy use in Hong Kong found a forty-fold increase in per capita energy use for transportation between the lowest and highest income groups.[4] Most of this increase was accounted for by use of gasoline and diesel fuel for private use.

The growing use of cars has an important effect on energy use, since cars use considerably more energy per passenger-kilometer than other transport modes. Energy efficiencies calculated for Hong Kong show the automobile to be 10 to 15 times more energy intensive than buses.[4] In three Latin American countries, automobile transportation is responsible for 65–75% of energy used in passenger transportation, but carry only 25–35% of the total volume of traffic.[5]

The operating efficiency of cars—expressed in terms of amount of fuel use per distance travelled—has been improving in most developing countries. The degree of improvement depends on whether cars are imported, assembled, or manufactured domestically. Those that assemble or manufacture their own cars tend to lag behind. For example, the Ambassador, the most popular model of car produced in India, is of 1960s vintage and has a fuel consumption more than twice that of a comparably sized Japanese or German car (Table 4).[6] In Taiwan, the fuel consumption is between these two extremes, since the cars assembled are of a more recent vintage.

Table 4. Gas mileage of new cars (liters/100 km).

India Ambassador	Taiwan	Japan Corolla	Japan Civic	Germany Rabbit
13.6	8.5[a]	6.0	6.4	6.0

Source: World Bank (1985) and Chang (1985).
[a]Estimate based on data in Chang (1985).

Gains in gas mileage have been achieved through smaller size and improved vehicle characteristics. An estimate for passenger cars in Taiwan was that halving the displacement results in a 45% decrease in fuel consumption per passenger-km.[7] These gains have been partly offset by the growing number of air-conditioned vehicles in some developing countries. On the average, fuel consumption per passenger kilometer is 12% higher for air-conditioned cars than for non air-conditioned cars.

The impact of growing automobile use depends on how well the capacity is utilized. Traffic conditions also affect energy consumption. Congestion, which has become severe in many LDC cities, leads to slower travel and less efficient operation of fuel-powered vehicles. Average trip length is affected by particular features of the urban landscape, such as the degree of urban sprawl. Average trip lengths in Nairobi were reported to be 1.5 to 2.8 miles.[8] Comparable figures for Mexico City, which is larger than Nairobi, were 3.5 to 6.0 miles.[9] Automobile ownership encourages the taking of longer trips: the average car trip in Nairobi was almost twice as long as the average foot or bicycle trip.

Per capita ownership of cars in LCDs is still low compared to that in developed countries, but it has grown rapidly. The growing use of private automobiles in LDC cities brings with it a large increase in per capita energy use for transport. If households are at a point where automobile ownership is a possibility, moderate increases in household income may lead to substantial growth in the consumption of transport fuels. The price and availability of automobiles, the ability of people to purchase them, and the existence and adequacy of alternatives to private automobile use, will be major determining factors of energy use in urban passenger transportation.

PLANNED ACTIVITIES FOR FY 1986

During the coming year, we plan to expand our studies to the industrial sector.

REFERENCES

1. Yushi, M. and Guangrong, H. (1985), *China's Transport and Its Energy Use*, unpublished draft, IDRC, Ottawa, Canada.
2. Socio-Economic Research Unit (1981), *The Use of Energy and Attitudes towards Energy Conservation among Urban Households*, Kuala Lumpur.
3. World Bank (1975), *Urban Transport, Sector Policy Paper*, Washington D.C.
4. Newcombe, K. (1975), Energy Use in Hong Kong: Sector End Use Analysis, *Urban Ecology 1*, pp. 285–309.
5. Inter-American Development Bank (1982), "The Impact of Energy Costs on Transportation in Latin America," Inter-American Development Bank, Washington, D.C.
6. World Bank (1985), "Energy Use in the Transport Sector in India," unpublished draft.
7. Chang, C.J., Tzeng, G.H., and Chang, S.H. (1985), "Characteristics of Fuel Consumption in Highway Transportation Sector in Taiwan," paper presented at the Seventh Annual International Conference, Bonn, W. Germany.
8. McGranahan, G., *et al.* (1979), "Patterns of Urban Household Energy Use in Developing Countries: The Case of Nairobi," Institute for Energy Research, SUNY, Stony Brook, New York.
9. McGranahan, G. and Taylor, M. (1977), "Urban Energy Use Patterns in Developing Countries: A Preliminary Study of Mexico City," SUNY, Stony Brook, New York.

Energy Conservation Measures and Policies for Commercial Buildings for the Association of Southeast Asian Nations (ASEAN)*

M. Levine and I. Turiel

Energy use in commercial buildings is a significant portion of energy demand within the five present ASEAN† member countries. To the extent that expenditures on energy for space conditioning, lighting, and other uses can be reduced without loss of amenity and without compromising the functions which the energy fulfills, the ASEAN nations will benefit economically from measures to conserve energy. These benefits will accrue both to the nations as a whole in the form of reduced oil imports, improved balance of payments, and lower costs in the modern sector as well as to the individual building owners and occupants.

ACCOMPLISHMENTS DURING FY 1985

To assess the impacts of energy conservation in buildings on the economies of the ASEAN member countries, we needed to estimate (1) total energy use of commercial buildings for each country, (2) the cost of the energy used in the commercial sector, and (3) the potential for cost-effective measures to reduce energy use.

Table 1 shows the estimated energy use of the five ASEAN countries for the latest year available, an approximate projection to 1982 to place all on a common basis, the amount of electricity used within commercial buildings, and the total cost of the electrical energy use in buildings. Many of the numbers in Table 1 are estimates, but they are likely to be within 10 or 15 percent of the actual consumption.

The first observation from Table 1 is that buildings consume a significant portion of total electricity in the ASEAN countries. Counting only the electricity for the commercial sector, 26 percent of electricity in ASEAN is used in commercial buildings. If one assumes that about 15 percent of industrial electricity use is space conditioning and lighting industrial buildings, then the estimate of energy use in ASEAN commercial buildings increases to 32 percent of total electricity production. This varies from a high of 50 percent of electricity use for buildings in Singapore to a low of 21 percent of electricity use for buildings in Thailand. These estimates are shown for each of the ASEAN countries in Table 2.

All countries in ASEAN generate almost all of their electricity from oil. If one assumes (for the sake of simplicity) that the cost of a kilowatt hour of electricity is about $0.10 (U.S. currency), then the total annual expenditure for electricity for buildings in ASEAN is between $1.5 and $1.9 billion. (The higher estimate accounts for electricity use in industrial buildings.)

The implications of these estimated expenditures for policies to conserve energy in buildings are sub-

Table 1. Energy use in ASEAN countries.[a]

Country	Energy Use per Capita (1980) (mmBtu/yr)	Total Electricity (1980) (GWh/yr)	Electricity in Commercial Buildings (GWh/yr)
Indonesia	6.8	7,000	2600
Malaysia	21.4	8,470	2510
Philippines	11.3	19,400	4770
Singapore	72.6	6,670	3330
Thailand	11.7	15,900	1800

[a]Sources: Total energy use is derived from "Asian Energy Problems: An Asian Development Bank Survey," Praeger, 1982. The total use includes only commercially sold fuels. Many ASEAN countries use considerable quantities of non-commercial fuels, so comparisons among the countries should be made with care. Population data are from "The World Almanac," Newspaper Enterprise Association, 1984. Total electricity production data and electricity use in commercial buildings are derived from (1) "Energy Planning for Development in Indonesia," Energy/Development International, 1981 and "Renewable Energy Technology and Services—Prospects for a Strong USA/Indonesian Trade Relationship," Jerome Weingart and Associates, 1981; (2) "31st. Annual Report of the National Electricity Board of the States of Malaya;" (3) "Ministry of Energy Report for 1982," Philippines Ministry of Energy; (4) "Energy Conservation in Singapore," Lee Ek Tieng, in Energy—the International Journal, 1983; and (5) "Electric Power in Thailand 1981," Thai National Energy Administration.

*This work was supported by the U.S. Agency for International Development through the U.S. Department of Energy under Contract No. DE-AC03-76SF00098.

†The Association of Southeast Asian Nations consists of Brunei, Indonesia, Malaysia, the Philippines, Singapore, and Thailand. Brunei was accepted as the sixth member of ASEAN after the bulk of the study was completed. Therefore, it was not possible to include Brunei in this report.

Table 2. Electricity use in ASEAN commercial buildings.

Country	Electricity Use in Commercial Buildings (GWh/yr)[a]	Percentage of Total Electricity Use in Nation	Annual Cost in $ Millions (at $0.10 per kWh)
Indonesia	2600/2700	38.6	270
Malaysia	2510/3070	36.2	307
Philippines	4770/6170	31.8	617
Singapore	3330/3330	50.0	333
Thailand	1800/3350	21.1	335
TOTAL	5,000/18,600	Avg: 32.4	1860

[a]Two figures are presented for electricity use in commercial buildings. The first represents the total use in commercial buildings others than those associated with industrial activities. This number includes the portion of transmission losses in each of the countries appropriately allocated to the commercial sector. The second estimate includes commercial buildings serving the industrial sector. This is derived by assuming that 15 percent of industrial electricity use goes for space conditioning, lighting, and related uses in buildings. The percentage of total electricity use estimates are derived from the latter electricity use (including industrial buildings).

Table 3. Commercial building energy use, trade balance, and oil imports in the three ASEAN countries oil importing countries.[a]

Country	Cost of Oil Imports for Electricity for Commercial Buildings[a] ($ millions)	Balance of Trade Deficit ($millions)	Cost/ Trade Definit
Philippines	340	2800	0.121
Singapore	180	7400	0.024
Thailand	185	2900	0.064

[a]Imported oil is assumed to cost $31/barrel. The source of the balance of trade deficits is "The World Handbook," 1984. The balance of trade deficit data are for 1981.

stantial. If, as we suggest later in this report, ASEAN countries could reduce energy use in buildings by 15 percent in the near term and as much as 40 percent in the longer term, then the total annual reduction in energy costs for ASEAN would be $280 million (near term) and $750 million (longer term). The estimated savings do not take into consideration the growth of the commercial sector. Electricity demand has grown rapidly during the past years among all ASEAN countries and is expected to continue to grow. Electricity use in buildings has also increased, as the ASEAN economies have spurred construction.

It is worth stressing that these reductions in energy costs ($280 to $750 million) are annual savings. Because such a large percentage of electricity is generated from oil, a large portion of the savings will go to reducing imports (with the exception of Indonesia), thus having an impact on balance of payments. Table 3 compares the near-term savings in oil costs to the ASEAN countries that import oil (Philippines, Singapore, and Thailand) with total deficits in trade balance. (A price of imported oil of $31 per barrel is used for the calculation.) It is evident from this table that the 15 percent near-term reduction of energy use by commercial buildings can contribute to a reduction in balance of payments deficits among the three oil importing ASEAN countries.

Thus, a basic conclusion is that energy conservation in ASEAN buildings can make significant contributions to the ASEAN economies.

High Priority Conservation Measures

To gain an overview of the potential for reducing energy use in commercial buildings in ASEAN, it is useful to understand how energy is currently used. This permits the assignment of priorities for revisions to the energy standards.

A hypothetical commercial office building was simulated using the DOE-2 computer code.[1-3] Typical building operating profiles and hourly weather data for Singapore were used in the simulation. Thus, the results are directly applicable to Singapore. However, because the weather in most ASEAN cities is hot and humid most of the year, the results give a qualitative feeling for the sources of commercial building energy use throughout ASEAN.

The total energy use of the hypothetical office building was estimated to be 540 kBtu (158 kWh) per square meter per year; 53 percent of the energy is used for air conditioning (cooling and air movement); 38 percent of the energy is for lighting. The remainder is for miscellaneous equipment.

The largest sources of the cooling loads are solar radiation through windows (28 percent), lights (22 percent), and ventilation (16 percent). Occupants contribute 13 percent of the cooling loads. Walls contribute only 10 percent and glass conductance, 5 percent.

It is useful to look at individual components to understand their contribution to total building energy use. The most important is lighting. As noted, the electricity to operate lights is 38 percent of total energy use. However, lights contribute to the

cooling load as well. When this contribution is accounted for, lights consume 51 percent of the total energy use of the office building.[‡]

Windows are also an important component. Through their impact on cooling loads, they contribute about 13 percent to the total energy use of the building (for a hypothetical building conforming to OTTV requirements). Of equal or greater importance, they have the potential to reduce the amount of artificial lighting required by the building. Thus, windows have a considerably greater potential for reducing energy use than their 13 percent contribution to total energy use suggests.

Of the remaining 36 percent of the energy use of a hypothetical building, the contributions come from miscellaneous equipment (9 percent), ventilation (8 percent), occupants (7 percent), and walls (5 percent).

Because of the variability of miscellaneous equipment, energy savings for equipment have not been analyzed. Ventilation levels are presently set in most codes. The issue of maintaining proper ventilation levels (not too low for health reasons; not too high for energy reasons) is treated as a maintenance problem, discussed below. Loads due to people are not subject to control. Walls contribute little to total building energy use. Because the temperature is above interior comfort conditions day and night for almost the entire year, cooling of the building at night yields little reduction in energy use in Singapore. The potential for designing buildings to take advantage of night cooling in other parts of ASEAN needs to be explored.

Equipment energy efficiency is a final important energy saving measure. Present practice for new buildings in Singapore appears to be good (based on discussions with Singapore professionals). We have no data as yet on building practice in the other ASEAN countries. Equipment in most existing buildings, however, is not adequately maintained: the major concern of building managers is in the comfort of the occupants. Ventilation rates are often higher than necessary. Cooling equipment, fans, and pumps are permitted to degrade in efficiency so long as comfort conditions can be met. Considerable energy savings are likely if policies relating to the maintenance of equipment are adopted and carried out. Policies to establish good maintenance practices in buildings have been given little attention; they deserve much more.

[‡]The assumption is made that the lighting power is 20 watts/square meter. If the actual lighting power is 16 watts/square meter, the total contribution of lighting to energy use (including its effect on cooling) is reduced to 45 percent of the total.

This brief discussion suggests that the following three areas deserve priority attention in considering commercial building energy conservation policies in ASEAN: lighting, windows (especially to encourage the use of daylight), and equipment maintenance. The analysis completed for Singapore suggests a 15 to 20 percent reduction in energy use is cost-effective and possible in the near term and a reduction of up to 40 percent may be possible in the longer term, considering measures affecting lighting, windows, and equipment maintenance. We anticipate that similar magnitudes of savings can occur throughout ASEAN, although the specific measures and the cost-effectiveness is likely to vary with location.

In short, the economic potential of energy conservation in commercial buildings throughout ASEAN is substantial.

Alternative Policy Approaches

There are numerous approaches to realizing the potential for cost-effective conservation in ASEAN commercial buildings. It is premature at this point in the study to provide recommendations regarding the most desirable approaches. However, a description of the alternatives does give a sense of the options available.

The choices range from purely informational to mandatory standards with enforcement. For many countries, it is useful to approach conservation policies in an evolutionary manner, beginning with information and developing over time a set of requirements that can be followed and are accepted without a great deal of difficulty. Thus, we have itemized the policies in different steps, recognizing that different nations have designers and builders who are at different stages of awareness and implementation of energy conservation in buildings. We also recognize that political and economic considerations will play an important role in determining which steps might be omitted, what emphasis to give to different policies, and how far it is reasonable to pursue energy conservation policies for commercial buildings.

Step 1: Modest Information Campaign

This involves making widely available to the building community information packages about the most effective (and presumably most cost-effective) ways of achieving energy conservation in new and existing commercial buildings.

Step 2: Government Buildings Program

The government can set an example by retrofitting existing buildings and requiring new buildings to

be energy conserving. This can take the form of taking measures that will ensure that most government-owned buildings are energy efficient or by choosing a select number of buildings that are made to be very energy efficient.

Step 3: Development of Tools to Evaluate Conservation Measures

A tool is needed for practitioners that is reasonably accurate but relatively simple to use. There are several relatively simple computer codes (running on microcomputers) available in the United States for evaluating commercial building energy use. These tools need to be tested in ASEAN climates against more complex computer tools before they should be made available within ASEAN.

Step 4: Energy Labels

A system that is gaining favorable attention in several countries (notably France and the United States) involves labeling buildings to indicate their expected energy performance. The building labels would provide sufficient information that the owner, occupants, and prospective purchasers could readily determine if the building in energy conserving, average, or the building equivalent of a "gas guzzler." Such labels are presently used for automobiles and most major household appliances in the United States.

Step 5: Component Standards

Many countries throughout the world have adopted the component standards put forward by the American Society of Heating, Refrigeration, and Air Conditioning Engineers (ASHRAE) for various building components (e.g., lighting, wall insulation, heating and cooling equipment). These standards may be optional, mandatory (but without enforcement), or mandatory (with enforcement).

Step 6: Implementation of Mandatory Standards

The choice of methods for the implementation of energy conservation standards in ASEAN (if some member countries choose to adopt standards) is not a simple one. The work accomplished to date—involving considerable quantitative assessment of energy conservation measures in an office building in Singapore—provides new insight into policy approaches. The findings of the analysis suggest that it may be possible to develop relatively simple but accurate equations that will allow (1) a performance approach not suffering from the complexity of previous efforts to permit tradeoffs among all major conservation measures and (2) a microcomputer code that will facilitate the implementation of such an approach. It should be noted that this approach is likely to work in Singapore, where one does not need to be concerned about heating and where the climate is not variable. Whether a simplified but accurate performance approach is possible in other ASEAN climates requires considerable additional research.

Specific Measures to Reduce Commercial Building Energy Use in ASEAN: Lessons from the Singapore Analysis

We list here the most important findings of the analysis of measures to reduce energy use in commercial buildings in Singapore.

- The Desirability of Reducing Lighting Levels
- Daylighting
- Maintenance of Building Equipment
- Alternative Approaches to Implementing Policies to Reduce Energy Use in Commercial Buildings

Conclusions and Recommendations

We have already noted the substantial energy conservation opportunities for commercial buildings in ASEAN. It is worth repeating some earlier figures: ASEAN has the potential of reducing its energy costs by as much as $280 million per year in the near term and $750 million per year in the longer term. These estimates underscore the potential economic benefits of effective energy conservation policies applied to commercial buildings.

Achieving these large energy savings depends on policies adopted by the ASEAN countries. We have made no recommendation on one particular policy approach. Each country should evaluate the different approaches to decide which are most appropriate to their economic and political environment.

PLANNED ACTIVITIES FOR FY 1986

In FY 1986, we intend to extend our analysis of energy conservation in ASEAN buildings, including the following efforts:

- Apply the approach used in Singapore to other ASEAN countries. This involves a comprehensive analysis of impacts of conservation measures in commercial buildings using the DOE-2.1B computer code. It requires the ASEAN participants to gather detailed solar radiation data and participate in the project in other key ways.

- Transfer the DOE-2.1B computer code to those ASEAN countries desirous of using it for the analysis of energy performance of buildings.
- Work with the ASEAN government policy community to understand appropriate energy conservation policy approaches which the technical analysis can support; work with the government, research, and buildings communities to support demonstrations of advanced conservation measures with high potential payoffs within ASEAN.
- Develop a microcomputer program for the implementation of conservation policies, with initial work on this program beginning in Singapore.

REFERENCES

1. Turiel, I., Curtis, R., and Levine, M. (1984), "Parametric Energy Analysis in Support of Singapore Energy Conservation Standards for Commercial Buildings," *Proceedings of the ASEAN Conference on Energy Conservation in Buildings*, Singapore, May 29–31, 1984, p. 195.
2. Building Energy Simulation Group (1985), *Overview of the DOE-2 Building Energy Analysis Program*, LBL-19735.
3. Levine, M., Turiel, I., and Curtis R. (1984), "Toward A Practical Daylighting Analysis Tool for Singapore," *Proceedings of the ASEAN Conference on Energy Conservation in Buildings*, Singapore, May 29–31, 1984, p. 277.

This report was done with support from the Department of Energy. Any conclusions or opinions expressed in this report represent solely those of the author(s) and not necessarily those of The Regents of the University of California, the Lawrence Berkeley Laboratory or the Department of Energy.
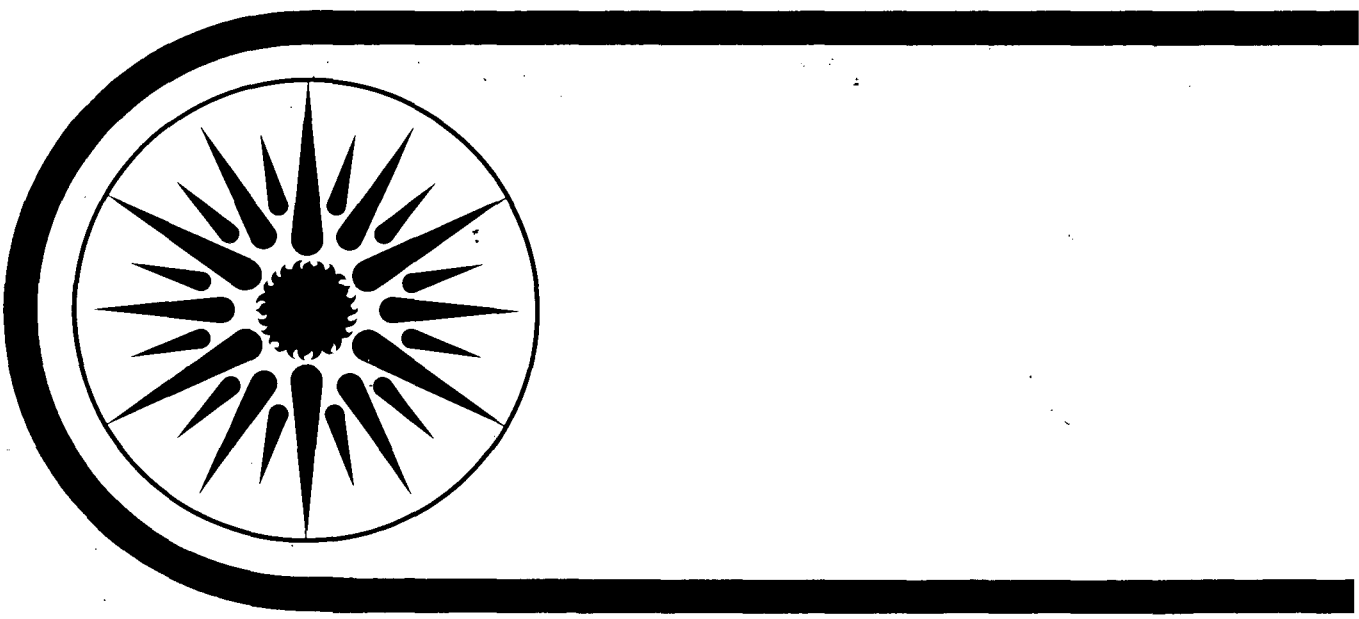
Reference to a company or product name does not imply approval or recommendation of the product by the University of California or the U.S. Department of Energy to the exclusion of others that may be suitable.